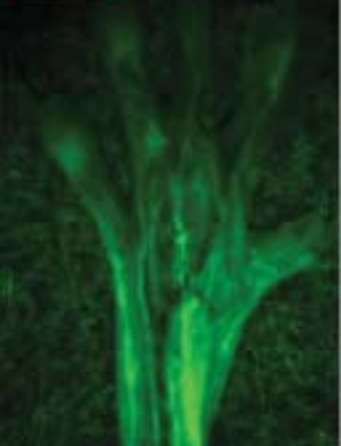
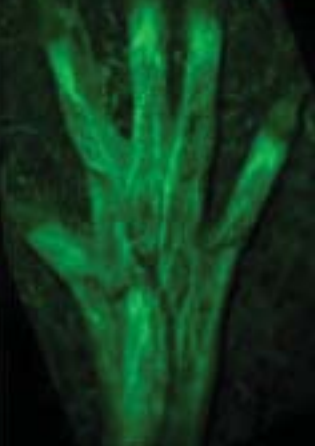


修復再生医学による神経系難治性疾患の治療 に向けた横断的トランスレーショナル研究

平成 18 年度、平成 19 年度私立大学学術研究高度化推進事業
(学術フロンティア推進事業) 研究成果報告書

<p>解剖学第 1 解剖学第 2 生理学第 2 医化学 薬理学 微生物学 衛生学 附属生命医学 研究所</p>	<p>修復</p> 	<p>再生</p> 	<p>心療内科 神経内科 脳神経外科 整形外科 眼科 耳鼻咽喉科 麻酔科 救急医学科</p>
<p>大阪医大麻酔科・稲田病院</p>			

関西医科大学

Kansai Medical University



平成 20 年 11 月

はじめに

日本で約 1,700 万人が慢性痛に罹患し、慢性痛患者の 77%は慢性痛の治療に満足していないことが最近の大規模調査で明らかにされています。慢性痛は鎮痛薬、理学療法などの保存療法が取られていますが、身体的、心因的、社会的要因が複雑に絡み合うため、特に神経因性疼痛は有効な治療法がなく難治性であると考えられてきました。慢性痛は二足歩行を獲得した人類に不可避の運動器系（骨、関節、筋肉、神経など）疾患で、研究代表者らの最近の基礎研究から、慢性痛の原因が運動器系に属する末梢組織上の感覚受容器にあり、その原因を除くことにより治ると考えるに至りました。平成 17 年、本学術フロンティア推進事の共同研究機関の 1 つ、稲田病院の稲田有史博士は、150 年前から現在に至るまで治らないとされてきた神経損傷によるカウザルギー患者の激痛を人工神経を用いた神経再生で治すことに世界で初めて成功し、国内外で注目を集めています。関西医科大学は、平成 13 年度より学術フロンティア推進事業の支援を受け、再生医学難病治療センターが開設され、骨髄に含まれる多様な幹細胞の「再生能」を利用して白血病や自己免疫疾患などの難病に対し新しい治療法の開発研究を行い、また、内耳や網膜などの感覚器の再生にも取り組み、着実に成果を上げてきました。本学のブレインメディカルサービス、総合リハビリテーションセンターでは、他大学でも少ない科を超えた共同診療体制やコメディカルとの協力体制があり、感覚・運動器系の疾患に対して総合的に対処し、豊富な診療実績を有しています。関西医科大学は、平成 18 年 1 月に最新の機器設備を備えた枚方病院を開院し、骨髄移植をはじめとする高度先進医療を推進しています。本事業では、1) 平成 13 年度からの事業を継続発展させるため、2) 滝井キャンパスにある基礎医学講座、附属生命医学研究所の基礎研究の成果を附属滝井病院のブレインメディカルサービスの診療・治療に活かすため、3) 神経系難治性疾患に焦点をあてた研究を推進するため、ブレインメディカルリサーチセンターを組織しました。

本研究組織の特徴は、遺伝子導入や幹細胞による「再生能」に加えて、神経系の「可塑性」や「自己修復能」に焦点を当て、その正常な機能を維持・修復させることを目標として、関西医科大学の基礎部門と臨床部門が連携してトランスレーショナル研究を推進することにあります。さらに本事業は専門性の異なる大阪医科大学麻酔科と神経再生にすぐれた実績を有する稲田病院との共同プロジェクトではありますが、今後その他の施設とも連携して地域に密着したネットワークが構築できる発展性を有しています。高齢化社会を迎える日本にあつて、感覚・運動器系の機能の維持・修復は医療・介護費の軽減という医療経済の観点だけでなく、患者個々の QOL の向上からも重要な意義があります。

本報告書は、本事業が 3 年目を迎え、5 年プロジェクトをより実りのあるものにするために、平成 18、19 年度の研究活動の概要をまとめたものです。

平成 20 年 11 月

神経細胞の再生におけるトランスレーショナル研究

2005年(平成17年)7月2日 土曜日

脊髄損傷に自分の骨髄細胞

事故で首を打って半身不遂になる脊髄損傷の患者に、自身の骨髄細胞を培養して移植する日本で初めての再生医療について、関西医科大学(大阪府守口市)は1日、医学倫理委員会の審議を経て実施を承認した。損傷した脊髄に細胞が到達すれば、神経が再生して歩きの回復が期待される可能性がある。今後2年間で20人を自費で治療する方針という。

関西医大が承認

責任者の中谷勇典教授(救急医学)によると、脊髄損傷を起こした直後の患者から骨髄を採取し、間質細胞と呼ばれる細胞を分離して培養。増やした間質細胞を細胞膜から脊髄細胞に似た細胞膜を被せたネズミの変種では、細胞を移植したネズミの方が足の動きがよくなった。損傷部分に生じた空洞も小さくなった。グループは「移植した細胞から何らかの要素が伸びて神経の再生が促進されたと考えられる」と説明する。ただしサルのを使った実験は動物実験の面から実施していない。サルの脳脊髄液に細胞を注入し、異常が起きないことは確認している。

この再生医療について、中谷教授はこの程度、効果があるかはわからない」としている。患者の同意を取る際に適度な期待をさせることのないよう、新聞や文書の表現などは慎重にしているという。

国内では交通事故やスポーツ事故などで毎年約5千人が脊髄損傷を起こしているといわれるが、有効な治療はない。計画は、4年10月いったん承認を受けたが、安全面と倫理面から検査を追加、再審議していた。

骨髄細胞移植で脊髄損傷を再生

交通事故などで脊髄を損傷した患者に、自分の骨髄の細胞を移植して神経細胞の再生を促す治療の臨床試験が、関西医科大学大森井病院(大阪府守口市)で始まった。骨髄細胞を使った脊髄損傷の治療は世界でも例がないという。研究グループの鈴木雅久・京都大助教授(形成外科)が13日、岡山大学で発表された。

臨床試験を開始

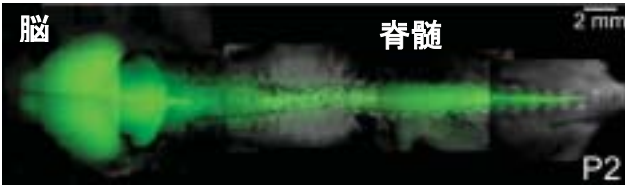
関西医大 四肢マヒの30代男性

事故直後、救命救急センターに運ばれた重度の脊髄損傷患者が対象。骨折治療用の腰の骨を取る際に同時に骨髄液を採取、間質細胞と呼ばれる成分を培養して増やし、患者の腰から脊髄内に注射する。移植した細胞が損傷部にまで移動し、神経幹細胞の増殖・再生を促す効果をねらっている。23例の治療を目指す。昨年7月に同医科大で計画が承認された。

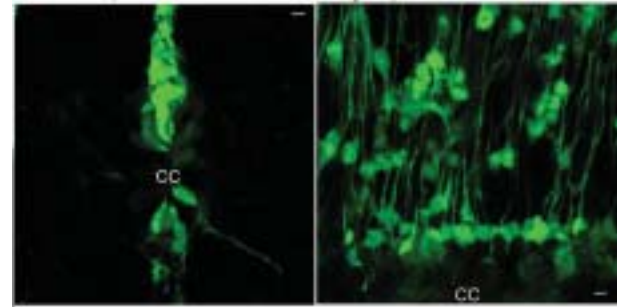
関西医大が承認され、中谷勇典教授(救急医学)らの研究グループが準備を進めていた。マヒで、十分な説明と同意の後に治療を実施した。今のところ、状態は安定しているという。

移植から1か月後に外傷委員会を含む検討会で安全性を確認し、3か月後、6か月後に運動や知覚機能をチェックする。鈴木助教授は「安全性を最優先に慎重に進めていきたい」と話している。

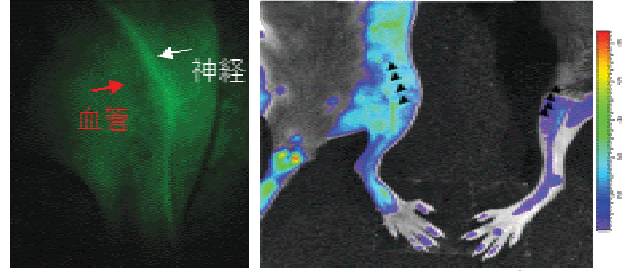
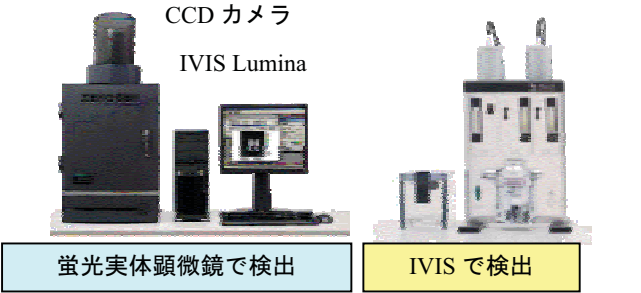
骨髄液 ↓ 骨髄細胞 ↓ 移植 ↓ 脊髄損傷の神経再生治療



生後2日目の神経幹 (nestin 陽性) 細胞の分布
山口正洋東京大学准教授との共同研究



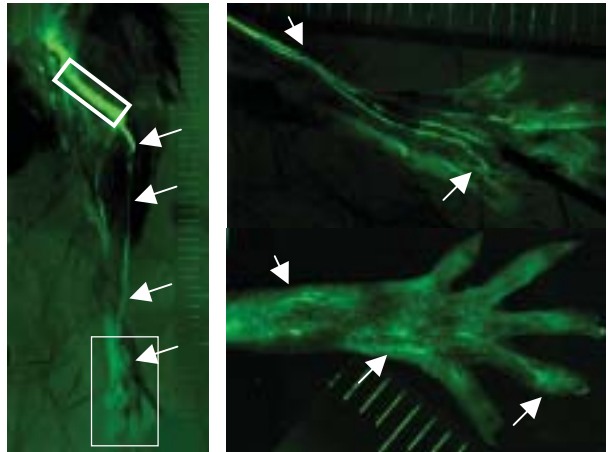
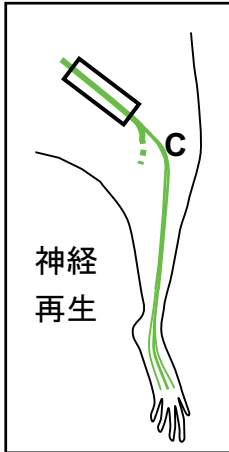
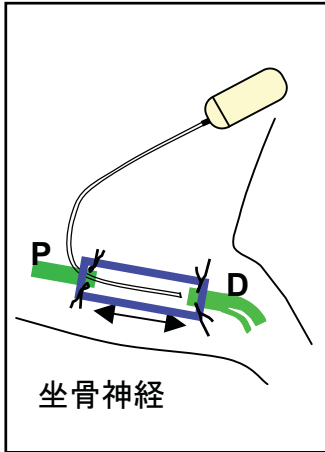
脊髄中心管(CC)付近での nestin 陽性細胞の局在



読売新聞 2006.4.11 掲載

in vivo イメージングシステム

末梢神経の再生におけるトランスレーショナル研究



神経が特異的に光る Thy1-YFP マウスを用いた末梢神経の再生モデルの確立

医療ルネサンス 末梢神経の再生治療 ①

取り戻せた自然な笑顔

「笑顔を取り戻せた」と、笑顔で話す患者さん。手術後、舌の感覚が戻り、食事や会話に支障がなくなった。末梢神経再生治療の効果を実感された。

末梢神経再生治療の成果を伝える記事。患者の笑顔が中心。

医療ルネサンス 末梢神経の再生治療 ②

親知らず抜歯 舌神経切断

親知らずの抜歯に伴って舌の神経が切断された。末梢神経再生治療により、舌の感覚が回復し、食事や会話に支障がなくなった。

親知らず抜歯と舌神経切断に関する記事。患者の回復を伝える。

医療ルネサンス 末梢神経の再生治療 ③

損傷部切断後に結合

神経損傷部の切断後に、末梢神経再生治療により神経が結合し、感覚が回復した。

神経損傷部の切断と結合に関する記事。患者の回復を伝える。

医療ルネサンス 末梢神経の再生治療 ④

血流回復で痛み消える

末梢神経再生治療により血流が回復し、痛みが解消された。

血流回復と痛み解消に関する記事。患者の回復を伝える。

事業概要

大学名：関西医科大学

研究組織名：ブレインメディカルリサーチセンター

研究プロジェクト名：修復再生医学による神経系難治性疾患の治療に向けた横断的トランスレーショナル研究

研究代表者名：伊藤誠二（関西医科大学 医学研究科先端医療学専攻 教授）

ブレインメディカルリサーチセンター設置工事：

滝井キャンパス2号館6階にブレインメディカルリサーチセンターを設置した。工事は第1期を平成18年度、第2期を平成19年度の2年間で、第1期は共同利用施設の設置工事を平成18年11月に着工し、平成19年3月に完工した。工事面積は165 m²である。第2期は平成19年度6月着工、同年10月に完工し工事面積は197 m²で、臨床医学・機能系研究室、形態系研究室、モデル動物部門研究室、共同利用研究施設が設置された。

研究装置・設備・研究費の支出状況：

《施設》

施設の名称	整備年度	研究施設面積	事業経費	補助金
ブレインメディカル リサーチセンター	平成18年度	m ² 165	千円 30,975	千円 15,487
	平成19年度	197	37,065	15,752

《装置・設備》

装置・設備の名称	整備年度	物品名	事業経費	補助金額
in vivo イメージング システム	平成18年度	リアルタイム in vivo イメージングシステム	千円	千円
		動物飼育システム	44,995	22,497
		バイオハザード対策用 キャビネット		

《研究費》

年度	物品費	通信運搬費	印刷製本費	旅費交通費
平成18年度	33,465,675	0	0	430,080
平成19年度	58,971,110	80,275	241,500	277,690
年度	人件費	業務委託費	雑費	合計(円)
平成18年度	0	105,300	1,886,995	35,888,050
平成19年度	82,454	192,226	1,803,805	61,649,060

研究プロジェクト参加研究者数：事業推進者 20 名、研究分担者 48 名

研究プロジェクトに参加する部門、事業推進担当者と研究課題

部門区分	事業推進者	申請時の課題名
【 基礎・社会医学系部門 】		
解剖学第一	山田 久夫	自己修復力を応用した中枢神経の再生と機能温存
解剖学第二	杉本 哲夫	神経疾患モデル動物を用いる機能性分子の探索
生理学第二	中村 加枝	
医化学	伊藤 誠二	慢性痛の発生・維持機構の解明とその修復・再生にむけた基礎研究
薬理学	中邨 智之	グルタミン酸受容体刺激による神経変性の分子機構と薬理的防御
微生物学	藤澤 順一	修復・再生過程における組織幹細胞の in vivo で追跡可能な解析系の開発
衛生学	菌田 精昭	ヒト骨髄及び臍帯血由来未分化組織幹細胞の同定と細胞移植・再生医療への応用
分子遺伝学部門	木梨 達雄	神経系の再構築・機能修復における細胞接着分子の役割
生体情報部門	松田 達志	
モデル動物部門	李 成一	
【 臨床医学系部門 】		
心療内科学	中井 吉英	慢性疼痛発症の予測因子に関する研究
神経内科学	日下 博文	神経・筋難病疾患における変性機序の解明と神経・筋再生医療の検討
脳神経外科学	河本 圭司	脳血管障害後の運動機能修復・再生に向けた臨床応用研究
整形外科	飯田 寛和	運動器系疾患の診断・治療の基礎となる臨床研究
眼科学	高橋 寛治	網膜神経節細胞の細胞死抑制と神経細胞の再生
耳鼻咽喉科学	友田 幸一	内耳有毛細胞の再生と機能回復に関する研究
麻酔科学	新宮 興	ペインクリニックにおける急性痛の慢性痛への移行予防のための臨床研究
救急医学科	中谷 壽男	急性期脊髄損傷に対する培養自家骨髄間質細胞による脊髄再生治療
【 共同研究機関 】		
大阪医科大学 麻酔科	南 敏明	帯状疱疹後神経痛の機能分子の探索と臨床研究
稲田病院院長	稲田 有史	コラーゲンをを用いる神経再生の基礎研究と臨床応用

平成 19 年度に生理学第 2、附属生命医学研究所生体情報部門、モデル動物部門が新たに加わり、基礎系 7 講座、臨床系 8 講座、附属生命医学研究所 3 部門、2 共同研究機関で事業を推進している。

研究活動の概要

20世紀初頭に神経生理学者の Santiago Ramon y Cajal が「成体哺乳類の中樞神経系は、一度損傷を受けると二度と再生しない」と述べて以来、長年、神経系は再生しないということが信じられてきた。1990年代になると、神経幹細胞がヒトをはじめとして成体脳で見つかり、神経系を再生させる再生医療が現実性をおび、再生医療研究が盛んになった。神経系の再生には脳梗塞、パーキンソン病、脊髄損傷など臨床応用が期待される細胞体を含む神経細胞の再生と主に末梢神経系で見られる軸索の再生がある。関西医科大学では、自己骨髄細胞移植における脊髄損傷の治療の臨床試験を実施するだけでなく、難病モデルの治療にむけた骨髄内骨髄移植の研究を通じて、臨床基礎研究が活発に行われ、神経系においても骨髄細胞やヒト臍帯血を網膜の網膜細胞への分化 (*Stem Cells* **20**, 279-283, 2002; *Acta Neurobiol. Exp.* **67**, 359-365, 2007)、また、遺伝子導入による内耳の有毛細胞の再生 (*Nat. Med.* **11**:1271-1276, 2005)、など臨床応用にむけた臨床基礎研究に従事する研究者の育成がなされてきた。末梢神経系は修復・再生能力の高い組織である。稲田病院の稲田有史博士は、150年前から現在に至るまで治らないとされてきた神経損傷によるカウザルギー患者の激痛を人工神経を用いた神経再生で治すことに世界で初めて成功した (*Neurosurgery* **55**, 640-646, 2004; *Pain* **117**, 251-258, 2005)。医療ルネサンス (p. 3) で紹介された画期的な成果をあげるためには、難治性慢性疼痛の患者の手術適応の評価が重要である。疼痛など疾病の慢性化には、心因的、社会的、行動学的な要因が関与する。神経修復・再生による治療可能な対象疾患神経系難治性疾患の患者の診療に日々携わる臨床現場で、画期的とはいえなくとも、有効な治療成績をえるには、神経修復・再生による治療可能な対象疾患の類型化、標準化が必要である。

本プロジェクトでは、

(1) 臨床系分野では、神経修復・再生による治療可能な対象疾患の標準化と幹細胞の臨床応用にむけた動物実験

(2) 基礎系分野では、神経系の修復・再生機構、変性機構の解明とその予防に関する基礎研究、組織幹細胞の同定と評価系の確立

を3年間の到達目標に掲げ、

1) 難治性慢性疼痛のトランスレーショナル研究

1. 心療内科は慢性疼痛患者の心理学的特性、行動学的特性による分類
2. 生理学第2では、報酬とコスト・嫌悪感情の神経メカニズム
3. 麻酔科は癌性疼痛、大阪医科大学麻酔科は帯状疱疹後神経痛に対するくも膜下ステロイド投与の臨床研究
4. 稲田病院は神経再生による難治性疼痛患者の治療
5. 医化学は慢性痛の発症・維持機構と末梢神経再生の基礎研究

2) 神経系の修復・再生機構、変性機構とその予防に関する基礎研究と臨床応用にむけた動物実験

1. 神経内科は筋萎縮性側索硬化症の病態の解明と治療に向けた動物実験

2. 脳神経外科は治療に向けた脊髄損傷、脳梗塞モデルの動物実験
3. 眼科は緑内障治療に向けた神経節細胞の細胞保護に関する基礎実験
4. 薬理学ではアルツハイマー病における変性機構とその予防の基礎研究
5. 分子遺伝学は神経系の修復・再生、変性機構におけるニューロン・グリアの細胞移動の基礎研究

3) 組織幹細胞の同定と評価系の確立と治療に向けた動物実験

1. 解剖学第1では、大脳皮質での神経幹・前駆細胞の存在と細胞新生を誘導する条件、因子の探索、その過程に関する基礎研究
2. 解剖学第2では、神経再生に関与する機能分子探索の新技術の開発
3. 微生物は修復・再生過程における造血幹細胞、組織幹細胞の関与を追跡できるウイルスベクターの開発と *in vivo* イメージング装置を用いた体内動態解析
4. 衛生学はヒト骨髄及び臍帯血中に存在する臓器・組織幹細胞同定とその幹細胞特性の解明
5. 整形外科は椎間板再生における骨髄細胞の効果と移植の基礎実験
6. 耳鼻咽喉科は遺伝子導入による内耳有毛細胞の再生の臨床応用研究
7. 救急医学科は骨髄間質細胞を用いた急性期脊髄損傷治療

と事業推進担当者の個々の領域で事業を推進した。

本プロジェクトでは、

1. 大阪医科大学麻酔科と医化学は帯状疱疹後神経痛患者のくも膜下ステロイド投与前後の脳脊髄液から疼痛マーカーの探索
2. 大阪医科大学麻酔科と医化学は鎮痛薬に向けたアクロメリン酸誘導体の鎮痛薬の創薬にむけた基礎研究
3. 稲田病院と医化学は神経因性疼痛患者手術のサンプルから疼痛マーカーの探索

など、すでに部門を越えたトランスレーショナル研究がスタートしている。

慢性疼痛でのトランスレーショナル研究をプロトタイプとして、組織幹細胞や蛍光タンパクを発現したマウスの提供、蛍光タンパクを発現する細胞、マウスの作製を通じて基礎と臨床の関連講座が連携して横断的トランスレーショナル研究を行うことにより、神経修復・再生の恩恵を受ける対象疾患の標準化と基礎研究からその適用範囲を拡大することを目指す。

濱田彰前附属滝井病院病院長の諮問により、ブレインメディカルセンター設置準備委員会（栗本 匡久委員長）が、平成18年11月から平成19年10月まで計7回の委員会を開催し、平成19年10月12日に高橋伯夫病院長に第1次答申書（p. 75）を提出した。その後、平成19年11月に交代した日下博文委員長のもと、4回開催され、第1回答申書と香里病院開設に伴う附属滝井病院再編を見据えて、具体的な議論を重ねて、平成20年5月26日に高橋伯夫病院長に構造（施設）・設備関係書類を添付した第2次答申書（p. 73）が提出された。関西医大の中長期経営ビジョンにブレインメディカルセンター設置が組み入れられ、ブレインメディカルリサーチセンターと連携できることを期待する。

シンポジウム、セミナー、情報公開

学術フロンティア推進事業キックオフシンポジウムが平成18年8月25日（金）滝井キャンパスで開催された。日置紘士郎前学長、伊藤誠二センター長について、宮崎東洋順天堂大学名誉教授、共同研究機関の稲田有史病院長、中西重忠京都大学名誉教授によりプログラム（右に掲載）に従って講演が行われた。神経系難治性疾患の1つ神経因性疼痛をテーマとして、宮崎先生の臨床現場におけるペインクリニックの現状とペインセンターあり方、稲田先生の神経再生による神経因性疼痛の最新の治療方法、脳科学の機能分子からシステムへの基礎研究の展開が臨床の問題の解決へのさらなる展開という、まさに本事業がめざす修復再生医学を用いたトランスレーショナル研究の方向性を明示が示された有意義なシンポジウムであった。

それ以降、本プロジェクトのトランスレーショナル研究を推進するために、大学院講義と連携して、ブレインメディカルリサーチセンターセミナーを随時開催し、事業推進担当者、研究者間の意見交換、意思疎通の場として連携を強めている。

また、平成19年2月3日にブレインメディカルリサーチセンターの医化学、整形外科、神経内科、心療内科、麻酔科が「痛みの基礎と臨床」のテーマで、市民公開講座を開催した。2008年6月26日付けの読売新聞の医療ルネッサンスに「高齢者の痛み④」（中井吉英教授）、2008年9月8日から11日付けの同シリーズに「末梢神経の再生①～④」（稲田有史病院長）の記事が掲載された。ブレインメディカルリサーチセンターのホームページ（<http://www2.kmu.ac.jp/bmrc/>）を作成して、患者、一般社会に研究成果、一般知識の普及に努めている。

学術フロンティア推進事業キックオフシンポジウム

日時：平成18年8月25日(金) 18:00～17:00
場 所：関西医科大学中野館5階講義室

--- プログラム ---

18:00～14:10
日置 紘士郎 関西医科大学学長
「学術フロンティア推進事業開始にあたって
---ブレインメディカルリサーチセンターの建設について---

14:10～14:30
伊藤 誠二 研究先主
「本学がフロンティア推進事業から学ぼうとする」

14:30～15:10
宮崎 東洋 朝倉聖人大学名誉教授
「日本におけるPain Managementの現状とペインセンターのあり方」

15:10～15:50
稲田 有史 稲田有史病院長
「学術フロンティア推進事業と科学研究
---痛みの基礎と臨床の現状について---

16:00～17:00
中西 重忠 大阪バイオサイエンス研究所長
京都大学大学院研究科名誉教授
「分子生物学に開いたペイン管理のシステム構築」

主催：関西医科大学フロンティア推進事業推進センター
共催：日本脳神経学会
協賛：日本神経学会(日本ペインクリニック学会)
http://www3.kmu.ac.jp/bmrc/kickoff.html
連絡先：関西医科大学広報課 電話 060-6993-9425

関西医科大学
第9回 市民公開講座

2月3日(土)

午後1時～午後4時30分
場 所：関西医科大学中野館5階講義室
本席4席 無料招待

＜「痛みのメカニズム」＞ 伊藤誠二
＜「ペインクリニックについて」＞ 宮崎東洋
＜「痛みの基礎と臨床」＞ 稲田有史
＜「痛みの基礎と臨床」＞ 中西重忠
＜「痛みの基礎と臨床」＞ 伊藤誠二

医療ルネッサンス 高齢者の痛み

ストレスで胃腸機能異常

胃腸の健康は生活習慣から始まる。ストレスが胃腸機能を低下させ、消化器疾患の原因となる。ストレスが胃腸機能を低下させ、消化器疾患の原因となる。ストレスが胃腸機能を低下させ、消化器疾患の原因となる。

ブレインメディカルリサーチセンター関連セミナー

2006年8月25日	学術フロンティア推進事業キックオフシンポジウム	
	1. 関西医科大学 日置 紘士郎学長 2. 関西医科大学 伊藤 誠二研究代表者 3. 順天堂大学 宮崎 東洋名誉教授 4. 稲田病院 稲田 有史病院長 5. 大阪バイオサイエンス研究所 中西 重忠所長	学術フロンティア推進事業開始にあたって 本学術フロンティア推進事業がめざすもの 日本における Multidisciplinary Pain Clinic の現状 とペインセンターのあり方 難治性疼痛への再生医療の応用 分子脳科学に携わってー機能分子からシステム へー
2006年9月8日 (医化学担当)	米国国立衛生研究所、NIDDK John A. Hanover 部長	Clues to Diabetes susceptibility: calcium-triggered nuclear entry and the hexosamine signaling pathway
2006年11月7日 (医化学担当)	京都大学再生医科学研究所 臓器再建応用分野 中村 達雄准教授	In situ tissue engineering とその臨床応用
2007年2月3日 (ブレインメディカルリサーチセンター担当)	関西医科大学第9回市民公開講座ー日本に1700万人いる慢性痛をめぐるー	
	1. 医化学講座 伊藤 誠二教授 2. 整形外科科学講座 赤木 繁夫助教授 3. 神経内科学講座 伊東 秀文助教授 4. 麻酔科学講座 田口 仁士助教授 5. 心療内科学講座 福永 幹彦助教授	痛みのメカニズム 腰痛について 頭痛について ペインクリニックについて 胸痛、腹痛、舌痛などについて
2007年6月1日 (医化学担当)	京都大学大学院薬学研究科 医療薬科学専攻 佐治 英郎教授	分子イメージング：概要と臨床診断・医薬品開発 への応用
2007年7月20日 (解剖学第2担当)	自然科学研究機構生理学研究所 水野 昇所長	神経路の形態学的研究方法の展開ー”情”の神経 路を中心にー
2007年9月21日 (医化学担当)	奈良先端科学技術大学院大学バイオ サイエンス研究科 稲垣 直之准教授	神経細胞が極性を獲得するしくみの解析
2007年11月22日 (ブレインメディカルリサーチセンター担当)	第44回日本臨床生理学会シンポジウム「疼痛の臨床生理とペインクリニック」	
	1. 関西医科大学麻酔科学 田口 仁士准教授 2. 大阪医科大学麻酔科学 南 敏明教授 3. 兵庫医科大学疼痛制御科学・ペインクリ ニック部 村川 和重教授 4. 関西医科大学医化学 伊藤 誠二教授	癌性疼痛のくも膜下ステロイド投与による治療 帯状疱疹後神経痛に対するくも膜下局所麻酔薬 およびステロイド注入療法 難治性疼痛に対する脊髄刺激療法について 難治性疼痛の発症機構と診断・治療のバイオマ ーカーの探索
2007年12月4日 (医化学担当)	九州大学大学院医学研究院 統合生理学 古江 秀昌助教	GABA を介した痛みの周辺抑制と痛覚伝達系の 異常
2008年2月28日 (麻酔科担当)	大阪大学大学院医学系研究科 疼痛医学講座 柴田 政彦教授	臨床データに基づく CRPS 判定指標の作成
2008年3月15日 (分子遺伝学担当)	1. 名古屋大学大学院医学系研究科 宮田 卓樹教授 2. 京都大学工学研究科 合成生物化学専攻 岡田 峰陽准教授 3. 千葉大学大学院医学研究院 免疫細胞 移動イメージング 中山 俊憲教授 4. 京都大学大学院医学研究 神経細胞薬理 石崎 敏理助教 5. 大阪バイオサイエンス研究所 分子生物学部門 橋本 茂研究員 6. 自然科学研究機構生理学研究所 脳機能計測センター 根本 知己准教授	神経前駆細胞の三次元的営み：「個」の極性化・ 細胞周期随伴的核移動による「集団」の偽重層化 2光子顕微鏡による生体内免疫細胞移動 アレルギー性気道炎症の生体内免疫細胞移動イ メージング Rho シグナルによる細胞接着・移動とその生理的 意義 乳癌の浸潤形質獲得過程における Arf6 の活性化 機序 2光子顕微鏡による生体 in vivo イメージング
2008年3月21日 (神経内科担当)	徳島大学ヘルスバイオサイエンス研究部 感覚情報医学講座 梶 龍児教授	基底核疾患 Up date
2008年5月9日 (薬理学担当)	理化学研究所分子イメージング 研究プログラム矢野恒夫コーディネーター	マイクロドーズ臨床試験と PET の応用例
2008年7月31日 (心療内科担当)	愛知医科大学 学際的痛みセンター 牛田 享宏教授	運動器の慢性痛と学際的アプローチ

平成 18, 19 年度の研究活動報告

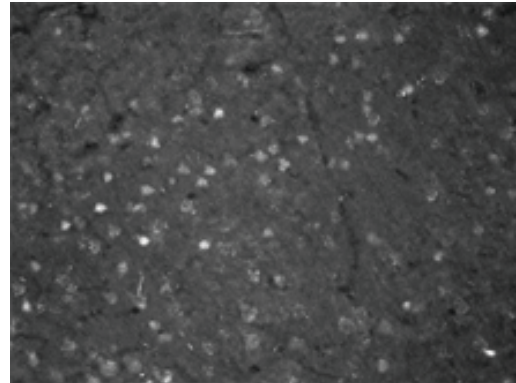
研究成果報告書

研究課題名	幹細胞による神経再生		
(英文)	Regeneration of neural tissues developing the intrinsic stem/progenitor cells		
事業推進者	山田 久夫	E-mail	yamada@takii.kmu.ac.jp
所属・職名	医学研究科・神経機能再生医学（解剖学第1）講座・教授		
研究分担者名	若林 毅俊、森 徹自、高森 康晴、北宅 弘太郎		
キーワード	神経系幹前駆細胞、ウィルスベクター、lamin、BrdU、細胞新生、細胞更新		
<p>1. 概要</p> <p>脳内に潜んでいる幹前駆細胞を賦活して組織再生を促し、再生医療に応用しうる方策を考案するトランスレーショナルリサーチをおこなう。</p> <p>2. 研究の背景と目的</p> <p>脳をはじめとする神経組織は、元来再生が不可能とされてきた。しかし近年、脳内にも幹・前駆細胞が存在することが明らかとなっているほか、障害後の脳に骨髄由来細胞などを付加した場合に一種の再生様所見が得られることも分かっている。われわれは既知のもの以外に、脳内のいたるところに幹前駆細胞の性質をもった新たな細胞の存在することを明らかにし、その細胞の生存過程を追究しつつ、神経系細胞の細胞更新・新生・分化・細胞死について、一連の基礎研究を展開している。このような基礎研究から得られた成果はトランスレーショナルに再生医療に応用されうるが、その際課題となる点は、細胞新生を促す条件の確立、新生した細胞をニューロンに分化させる方策・組織再構築を誘導させる因子の探索、その過程を追究するための標識法・マーカーの探索、などである。本研究計画では、特にその3点についての研究をおこなう。</p> <p>3. 研究方法</p> <p>ラットおよびマウスを用いた研究で、基本的には組織細胞化学法・分子形態学的手法を用い、必要に応じて分子生物学的手法を併用する。</p> <p>(1) 標識法・マーカーの探索：</p> <p style="padding-left: 20px;">ウィルスを用いた標識、BrdU 摂取</p> <p style="padding-left: 20px;">その他 各細胞種固有・各分化段階マーカーの探索</p> <p>(2) 細胞新生を促す条件の確立：</p> <p style="padding-left: 20px;">皮埋め込み電極からの電気刺激</p> <p style="padding-left: 20px;">麻酔下に脳表面への KCl 滴下</p> <p style="padding-left: 20px;">Pentylene tetrazole (PTZ) 腹腔内投与による癲癇様発作誘導など</p> <p>(3) 新生した細胞をニューロンに分化させる方策・組織再構築を誘導させる因子の探索：</p> <p style="padding-left: 20px;">細胞新生誘導後の長期観察による新規因子の探索</p> <p style="padding-left: 20px;">リンパ球やサイトカイン／成長因子類の探索</p> <p style="padding-left: 20px;">病態脳の利用した解析など</p> <p>4. これまでの成果</p> <p>(1) レトロウィルス・レンチウイルスを用いた分裂細胞の標識法については、ベクターを改変し、培養細胞に感染させてみたところ、従来より効率よく標識することができた。ニューロン系各分化段階、グリア系各分化段階における 核膜タンパク質ラミンのアイソタイプ発現について検索した実験では、未分化な幹細胞から分化が進むにつれ、lamin A/C は発現</p>			

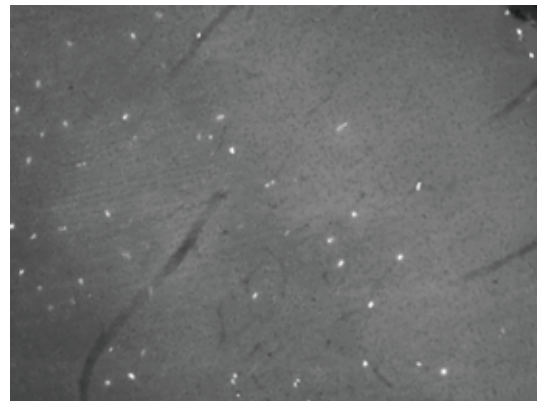
が減少したのち元に戻るのに比し、**lamin B1** では増加したのち減少、分化しきった細胞では **lamin B2** が最も発現量が多いという所見が得られ、分化度を表すマーカーとして使用できることが判明した。

(2) 終脳皮質の過剰興奮が細胞新生を促すことを既に報告しているが、皮下埋め込み電極からの電気刺激、麻酔下に脳表面への **KCl** 滴下、**pentylene tetrazole (PTZ)** 腹腔内投与による癲癇様発作誘導、にて過剰興奮させたところ、皮下埋め込み電極による電気刺激ではほとんど効果がなかった。**KCl** 滴下は効果があったが、より簡便な方法として、**PTZ** 投与方法が考えられた。本投与をおこなったラットに、**c-fos** 発現細胞、**BrdU** 摂取細胞、**Ki67** 陽性細胞などの増加が観察された。次年度で詳細な条件設定をおこなう。

写真は **PTZ 60 mg/kg** を 1 回腹腔投与した 2 時間後の終脳皮質体性感覚野で、多数の **c-fos** 陽性ニューロンが見られる。



写真は、麻酔下終脳表面に **KCl 2 M** を滴下、2 日後の終脳皮質体性感覚野で **BrdU** を摂取した細胞が多数認められる。



6. これまでの発表論文

(1) 発表論文

1. Wakabayashi, T., Kosaka, J., Mori, T., Takamori, Y. & Yamada, H.
Doublecortin expression continues into adulthood in horizontal cells in the rat retina.
Neurosci. Lett. **442**, 249-252 (2008).
2. Cui, Y., Kataoka, Y., Inui, T., Mochizuki, T., Onoe, H., Matsumura, K., Urade, Y., Yamada, H. & Watanabe, Y.
Up-regulated neuronal COX-2 expression after cortical spreading depression is involved in non-REM sleep induction in rats.
J. Neurosci. Res. **86**, 929-936 (2008).
3. Ikeura, T., Kataoka, Y., Wakabayashi, T., Mori, T., Takamori, Y., Takamido, S., Okazaki, K. &

Yamada, H.

Effects of sensory denervation by neonatal capsaicin administration on experimental pancreatitis induced by dibutyltin dichloride.

Med. Mol. Morphol. **40**, 141-149 (2007).

4. Mochizuki-Oda, N., Kusuno, T., Hanada, T., Tominaga, M., Tominaga, T., Suzuki, M., Yamada, H. & Yamada, H.

Thermo-sensitive receptor protein: Role of TRPVs in control of body temperature under heat radiation.

AIP. Conf. Proc. **902**, 62-64 (2007).

5. Takamori, Y., Tamura, Y., Kataoka, Y., Cui, Y., Seo, S., Kanazawa, T., Kurokawa, K. & Yamada, H.
Differential expression of nuclear lamin, the major component of nuclear lamina, during neurogenesis in two germinal regions of adult rat brain.

Eur. J. Neurosci. **25**, 1653-1662 (2007).

6. Tamura, Y., Kataoka, Y., Cui, Y., Takamori, Y., Watanabe, Y. & Yamada, H.

Multi-directional differentiation of doublecortin- and NG2-immunopositive progenitor cells in the adult rat neocortex in vivo.

Eur. J. Neurosci. **25**, 3489-3498 (2007).

7. Tamura, Y., Kataoka, Y., Cui, Y., Takamori, Y., Watanabe, Y. & Yamada, H.

Intracellular translocation of glutathione S-transferase pi during oligodendrocyte differentiation in adult rat cerebral cortex in vivo.

Neuroscience **148**, 535-540 (2007).

8. 森徹自、若林毅俊、高森康晴、山田久夫 : Cre-LoxP 遺伝子改変システムの応用.

脳 **21** **10**, 91-96 (2007).

9. 森徹自、若林毅俊、高森康晴、山田久夫 : Cre-LoxP 遺伝子改変システムの改良.

脳 **21** **9**, 479-484 (2006).

10. Takamido, S., Kataoka, Y., Tanano, A., Cui, Y., Ikeura, T., Shimatani, M., Kubota, Y., Okazaki, K. & Yamada, H.

Intrapancreatic axonal hyperbranching of dorsal root ganglia neurons in chronic pancreatitis model rats and its relation to pancreatic pain.

Pancreas **33**, 268-279 (2006).

11. Yamada, M., Nakao, S., Sakamoto, S., Takamori, Y., Tamura, Y., Mochizuki-Oda, N., Kataoka, Y., Yamada, H. & Shingu, K.

Propofol acts at the sigma-1 receptor and inhibits pentazocine-induced c-Fos expression in the mouse posterior cingulate and retrosplenial cortices.

Acta. Anaesthesiol. Scand. **50**, 875-881 (2006).

12. Kataoka, Y., Tamura, Y., Takamori, Y., Cui, Y. & Yamada, H.

Perineuronal germinal cells in the rat cerebral cortex.

Med. Mol. Morphol. **39**, 28-32 (2006).

7. これまでの成果の情報公開

ホームページ : 解剖学第一講座 = <http://www3.kmu.ac.jp/anat1/>

Differential expression of nuclear lamin, the major component of nuclear lamina, during neurogenesis in two germinal regions of adult rat brain

Yasuharu Takamori,¹ Yasuhisa Tamura,¹ Yosky Kataoka,¹ Yilong Cui,¹ Saori Seo,^{1,2} Takenori Kanazawa,^{1,2} Kiyoshi Kurokawa³ and Hisao Yamada¹

¹Department of Anatomy and Cell Science, Kansai Medical University, 10–15 Fumizono-cho, Moriguchi, Osaka 570–8506, Japan

²Medical student for elective research course, Kansai Medical University, 10–15 Fumizono-cho, Moriguchi, Osaka 570–8506, Japan

³Department of Anatomy, Shiga University of Medical Science, Seta-Tsukinowa-cho, Otsu, Shiga 520–2192, Japan

Keywords: adult, neurogenesis, neuronal differentiation, rat brain

Abstract

Lamins are major structural proteins of the nuclear envelope. Three lamin subtypes, A/C, B1 and B2, predominate in mammalian somatic cells. While the expression levels of lamins in several tissues are known to change during cell differentiation, lamin expression is poorly understood in the nervous system. To investigate the expression of lamins during neuronal differentiation in the mammalian adult brain, we performed immunohistochemical studies on lamins A/C, B1 and B2 in two neurogenic regions of rat brain: the subgranular zone of the dentate gyrus and the subventricular zone of the lateral ventricle. In particular, three types of cells were analysed using confocal microscopy: GFAP-positive cells as primary progenitor (stem) cells, PSA-NCAM-positive cells as subsequent neuronal progenitor cells, and NeuN-positive mature neurons. GFAP-positive cells possessed lamin A/C (++) and B2 (++) and B1 (+), PSA-NCAM-positive cells possessed lamin A/C (–), B1 (+++) and B2 (+), and mature neurons possessed lamin A/C (++) and B2 (+++), in both neurogenic regions. These observations showed that the compositions of expressing lamin subtypes are distinct in particular differentiation stages during neurogenesis in the adult rat brain. Our results suggest that the alteration of nuclear lamina structure is coupled with the progression of neuronal differentiation.

Introduction

Lamins are type-V intermediate-filament proteins that form a nuclear lamina, a filamentous meshwork underlying the inner nuclear membrane, and have diverse functions including structural support for the nuclear envelope, organization of chromatin and regulation of gene expression (Gruenbaum *et al.*, 2005). Lamins are subdivided into A-type and B-type based on sequence homology, and three lamin genes (*LMNA*, *LMNB1* and *LMNB2*) have been characterized in mammals. *LMNA* encodes four A-type lamins (lamin A, AΔ10, C and C2) generated by alternative splicing. *LMNB1* encodes lamin B1 and *LMNB2* encodes lamins B2 and B3 (Östlund & Worman, 2003; Broers *et al.*, 2004).

Lamins A, B1 and B2, and C are major subtypes in mammalian somatic cells, but the expression pattern is reported to depend on cell differentiation states in some organs (Mounkes & Stewart, 2004). In mouse development, lamin A/C is not observed in early developmental stages but appears as the organogenesis and tissue differentiation progress: lamin A/C appears in muscle cells of the trunk or head at embryonic day 12 when myogenesis begins, in epidermis at embryonic day 15 when stratification begins and in other tissues such as heart, liver or lung after birth (Stewart & Burke, 1987; Röber *et al.*, 1989). In adult tissues, lamin A/C is not observed in immature cells but is observed in final differentiated cells. Lamin B1 is expressed

abundantly in immature cells but faintly in final differentiated cells in muscle and epithelial cells of skin, bronchus and colon (Cance *et al.*, 1992; Broers *et al.*, 1997). The induction of lamin A/C expression following cell differentiation is also observed in several cells *in vitro* (Lebel *et al.*, 1987; Gaustad *et al.*, 2004; Constantinescu *et al.*, 2006). These reports suggest that lamin expression is regulated during cell differentiation.

In the development of mouse brain, lamin A/C is first observed at postnatal day 5 while B-type lamins are observed through all developmental stages (Röber *et al.*, 1989). This observation suggests that expression of lamin A/C varies during neuronal differentiation. However, those observations did not distinguish between cell types, i.e. neurons and glial cells. Moreover, B-type lamins were not distinguished into lamin B1 and B2 in that study.

Although it was classically seen as a nonregenerative tissue, the adult mammalian central nervous system retains the potential for cell renewal, cell proliferation and neurogenesis (Temple, 2001; Tamura *et al.*, 2004; Kataoka *et al.*, 2006). Two neurogenic regions are well studied in adult mammals: the subgranular zone (SGZ) of hippocampal dentate gyrus and the subventricular zone (SVZ), the latter providing neuronal progenitor cells to the olfactory bulb through the rostral migratory stream (RMS; Altman & Das, 1965; Altman, 1969). In both regions, primary neuronal progenitor cells (stem cells) are glial fibrillary acidic protein (GFAP)-positive (Doetsch *et al.*, 1999; Seri *et al.*, 2001), while later neuronal progenitor cells are polysialylated neural cell adhesion molecule (PSA-NCAM)-positive (Seki & Arai, 1991; Bonfanti & Theodosis, 1994; Rousselot *et al.*, 1995). In the

Correspondence: Dr H. Yamada, as above.

E-mail: yamada@takii.kmu.ac.jp

Received 20 September 2006, revised 19 January 2007, accepted 30 January 2007

present study, we investigated changes in expression patterns of lamins A/C, B1 and B2 during the distinctive neurogenic stages by simultaneous immunohistochemical observations of the lamin subtypes and relevant differentiation marker proteins in the cells of both neurogenic regions of adult rats, by using a confocal laser microscope.

Materials and methods

Animals

Adult Sprague–Dawley rats (8 weeks old, male and female; Nippon SLC, Hamamatsu, Japan) were used for all the experiments. All experimental protocols were approved by the animal ethics Committee of Kansai Medical University and were performed in accordance with the Principles of Laboratory Animal Care (NIH publication no. 85–23, revised 1985).

Tissue preparation

We used two fixation procedures based on the immunohistochemical conditions suitable for primary antibodies.

For methanol and acetone fixation, animals were killed by cervical dislocation under deep anaesthesia with diethyl ether. Brains were dissected and snap-frozen with CO₂ gas. Coronal or sagittal sections (10 µm thickness) were cut using a cryostat (Leica, Vienna, Austria), collected on glass slides and air-dried at room temperature for 1 h. Subsequently, they were fixed in cold methanol (–20 °C for 10 min) followed by three dips in acetone (4 °C, three dips 5 s each) and air-dried for 5 min.

Some specimens were prepared by the formaldehyde fixation method. Animals were transcardially perfused with 0.1 M phosphate-buffered saline (PBS) at pH 7.4 under deep anaesthesia with diethyl ether, followed by a fixative containing 4% formaldehyde and 0.2% picric acid in 0.1 M phosphate buffer (pH 7.4). Brains were quickly dissected and incubated for 24 h in the same fixative at 4 °C. After fixation, brains were cryoprotected in 10% sucrose solution for 24 h followed by incubation in 20% sucrose solution for 24 h. Brains then were snap-frozen with CO₂ gas and coronal or sagittal sections (30 µm thickness) were prepared using a cryostat. These sections were stored at 4 °C in PBS and used for free-floating immunohistochemistry.

Immunohistochemistry

Primary antibodies are summarized in Table 1. Because most of the anti-lamin antibodies are not effective on formaldehyde-fixed slices (Senda *et al.*, 2005), we preferentially used methanol- and acetone-

fixed slices to visualize nuclear lamins. The subtype specificities for anti-lamin monoclonal antibodies has been reported previously (Table 1). Polyclonal anti-lamin B1 antibody (C-20) was effective with formaldehyde fixation (Kataoka *et al.*, 2006) and the staining pattern was similar to that of monoclonal anti-lamin B1 antibody with methanol–acetone fixation. Because the anti-PSA-NCAM antibody was effective in formaldehyde fixation but not in methanol–acetone fixation, polyclonal anti-lamin B1 antibody was used for multilabelled immunostaining.

Sections were rinsed in PBS with 0.03% Triton X-100 and incubated with primary antibodies (Table 1) at 4 °C for 24 h. Sections were then rinsed in PBS with 0.03% Triton X-100 three times and incubated with Cy2-, Cy3- or Cy5-labelled donkey secondary antibodies specific to appropriate animal species (Jackson Immuno-Research, West Grove, PA, USA; 1 : 200) at 4 °C for 3 h. Sections were then rinsed in PBS with 0.03% Triton X-100 three times and mounted with medium containing 100 mM DTT, 5 µg/mL Hoechst dye 33258 (Nacalai Tesuque Inc., Kyoto, Japan), 50% glycerol and PBS at pH 7.4. Some sections were counterstained with TOPRO-3 (Molecular Probes, Eugene, OR, USA; 1 : 1000) for nucleic acid detection. Fluorescently immunolabelled sections were observed with a confocal laser microscope (model LSM510-META; Carl Zeiss, Oberkochen, Germany). Some images were reconstructed digitally with Adobe Photoshop. For all results, the level of immunoreactivity observed is indicated as follows: +++, highly positive; ++, positive; +, weakly positive; –, negative.

Results

Lamin subtypes in germinal zone of dentate gyrus

Formaldehyde-fixed brain sections were employed in immunostaining for lamin B1 with the polyclonal antibody, and methanol- and acetone-fixed sections were employed for lamin B1 with the monoclonal antibody, lamins A/C and B2. For all of these immunohistochemical stainings, nuclear envelopes were visualized not only in neurons but also in non-neuronal cells, such as glial cells and endothelial cells (Fig. 1). Similar staining patterns for lamin B1 were observed for both formaldehyde fixation and methanol–acetone fixation (data not shown). Immunostaining patterns for polyclonal anti-lamin A/C antibody and monoclonal anti-lamin A/C antibody were identical, and those using two monoclonal antibodies against lamin B2 were also identical (data not shown). In the pyramidal neurons at the CA1–CA3 region and granule neurons at the dentate gyrus, intense immunoreactivities for lamin A/C and B2 were detected (Fig. 1A and C). On the other hand, immunoreactivity for lamin B1 was generally weak in these regions; immunoreactivity

TABLE 1. List of antibodies used in this study

Antigen	Animal	Antibody type	Clone name	Supplier	Dilution	Fixation	Reference
Lamin A/C	Mouse	mAb	131C3	Chemicon International Inc.	1 : 100	M/A	Pugh <i>et al.</i> (1997)
Lamin A/C	Rabbit	pAb	H-110	Santa Cruz Biotechnology	1 : 100	M/A	
Lamin B1	Mouse	mAb	119D5-F1	Chemicon International Inc.	1 : 100	M/A	Machiels <i>et al.</i> (1995)
Lamin B1	Goat	pAb	C-20	Santa Cruz Biotechnology	1 : 100	F	
Lamin B2	Mouse	mAb	LN43	Chemicon International Inc.	1 : 100	M/A	Bridger <i>et al.</i> (1993)
Lamin B2	Mouse	mAb	E-3	Zymed Laboratories	1 : 100	M/A	Lehner <i>et al.</i> , 1986
GFAP	Rabbit	pAb		Sigma	1 : 500	M/A	
PSA-NCAM	Mouse	mAb	2–2B	Chemicon International Inc.	1 : 100	F	
NeuN	Mouse	mAb		Chemicon International Inc.	1 : 100	F	

F, formaldehyde; M/A, methanol–acetone; mAb, monoclonal antibody; pAb, polyclonal antibody.

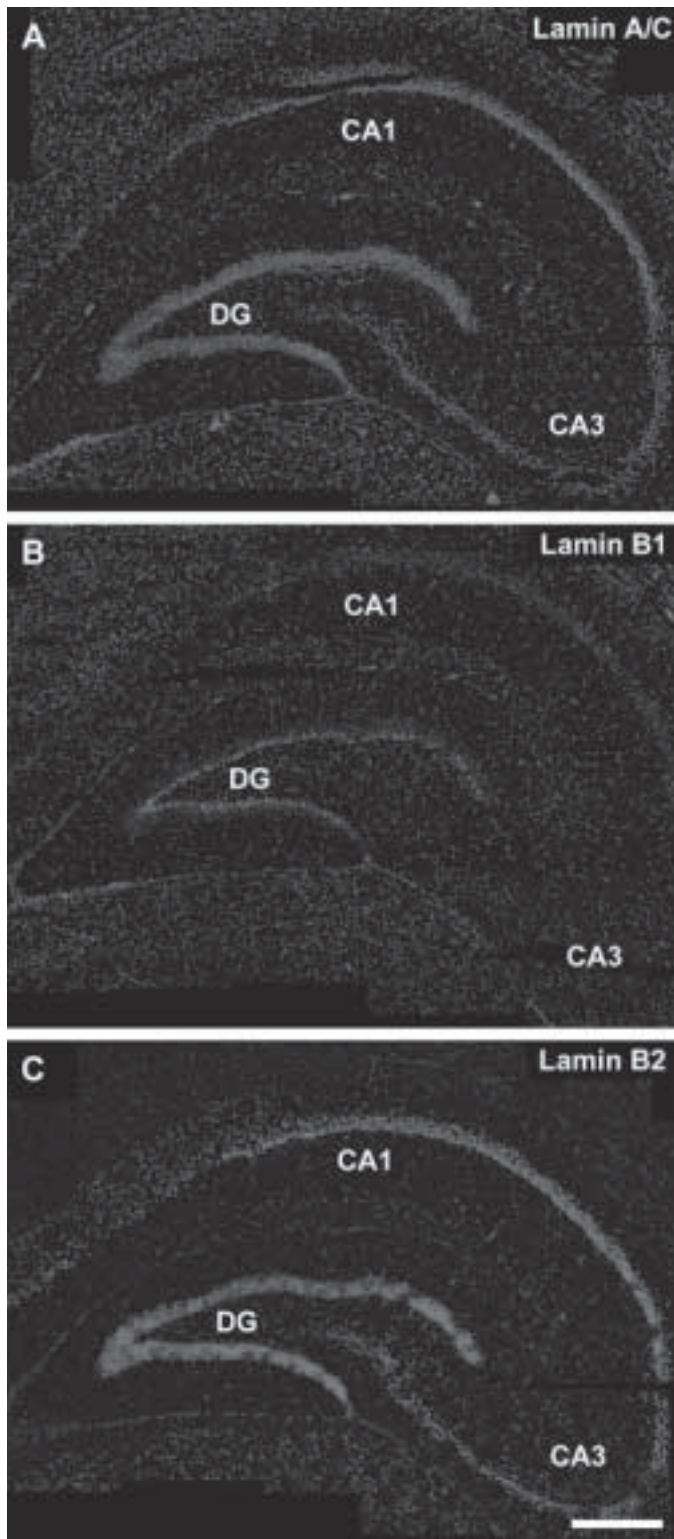


FIG. 1. Photomicrographs showing immunofluorescence images of hippocampus treated with anti-lamin antibodies. Specimens were fixed with methanol-acetone and stained with antibodies against (A) lamin A/C, (B) lamin B1 and (C) lamin B2. Images were digitally reconstructed. DG, dentate gyrus. Scale bar, 0.5 mm.

was modestly intense only in cells located on the inner ridge of the dentate gyrus, which is known to be involved in neurogenesis (Fig. 1B).

Multiple immunostainings for the lamins, NeuN (a marker protein for mature neurons) and the polysialic acid of PSA-NCAM (a marker protein for progenitor cells) were performed in formaldehyde-fixed brain sections (Fig. 2). The granule cell layer (GCL) of the dentate gyrus was mainly composed of NeuN-positive neurons (Fig. 2C). Besides mature neurons, both GFAP-positive and PSA-NCAM-positive progenitor cells have previously been observed in the dentate gyrus (Seki & Arai, 1991; Seri *et al.*, 2001; Seri *et al.*, 2004). Here, PSA-NCAM-positive progenitor cells were observed in and around the SGZ, and showed intense lamin B1-immunoreactivity in their nuclear envelopes compared with NeuN-positive mature granule neurons (Fig. 2A–F, small and large arrowheads). PSA-NCAM-positive progenitor cells were distinguished into two types based on morphologic features. The first type showed a small cell body and an oval- or polygonal-shaped nucleus with diameters of $\sim 8 \mu\text{m}$ (Fig. 2A–C, small arrowheads). These cells showed no obvious processes, formed cell clusters and resided in the SGZ. This cell type is consistent with previously reported neuronal progenitor cells in early stages (Seri *et al.*, 2004). The second type had a large cell body and an oval-shaped nucleus with a vertical axis, perpendicular to the GCL, with diameters of $\sim 13 \mu\text{m}$, similar to those of mature granule neurons (Fig. 2D–F, large arrowheads). These cells showed long vertical processes that traversed the GCL, and they resided solely between the GCL and the SGZ. Such cells are consistent with previously reported neuronal progenitor cells in late stages (Seri *et al.*, 2004).

In methanol- and acetone-fixed sections, multiple immunostainings revealed that granule neurons residing in the GCL showed intense lamin A/C immunoreactivity compared with lamin B1 (Fig. 2H and I). However, clustering small cells identified as the first type of progenitor cell, and intensively immunopositive for lamin B1 (small arrowheads in Fig. 2A–C), showed weak or no lamin A/C immunoreactivity (Fig. 2G–I, small arrowheads). Cells with larger nuclei that resided solely between the GCL and SGZ and were identified as the second type of progenitor cell (large arrowheads in Fig. 2D–F) showed intense immunoreactivities for both lamins B1 and A/C (Fig. 2G–I, large arrowheads). Double immunostaining for lamin A/C and lamin B2 indicated that almost all the cells that were intensively immunopositive for lamin A/C also showed intensive immunoreactivity for lamin B2, suggesting that mature granule neurons and second-type progenitor cells potently expressed lamin B2 (Fig. 2J and L). The clustering small cells (first-type progenitor cells), which were observed to be weakly positive or negative for lamin A/C, also showed weak lamin B2 immunoreactivity (Fig. 2J–L, small arrowheads).

We then examined the existence of each lamin subtype in GFAP-positive progenitor cells in the SGZ of the dentate gyrus in methanol- and acetone-fixed sections. GFAP-positive progenitor cells having long radial processes were observed in the SGZ (Fig. 3B, D and F, arrowheads). These cells are identical to previously reported primary neuronal progenitor cells called radial astrocytes, which are distinguished from horizontal astrocytes based on morphologic features (Seri *et al.*, 2001; Seri *et al.*, 2004). Authentic astrocytes also showed GFAP immunoreactivity and existed in the GCL of the dentate gyrus, but their radial processes were not as long (data not shown). Radial astrocytes showed intensive immunoreactivities for lamin A/C (Fig. 3A and B, arrowheads), for lamin B1 (Fig. 3C and D, arrowheads) and for lamin B2 (Fig. 3E and F, arrowheads). The lamin A/C immunoreactivity in radial astrocytes was similar to that observed in mature granule neurons (Fig. 3A and B, arrowheads). Lamin B1 immunoreactivity was more intense than that observed in mature granule neurons but weaker than that observed in first-type PSA-NCAM-positive progenitor cells (Fig. 3C and D, arrowheads).

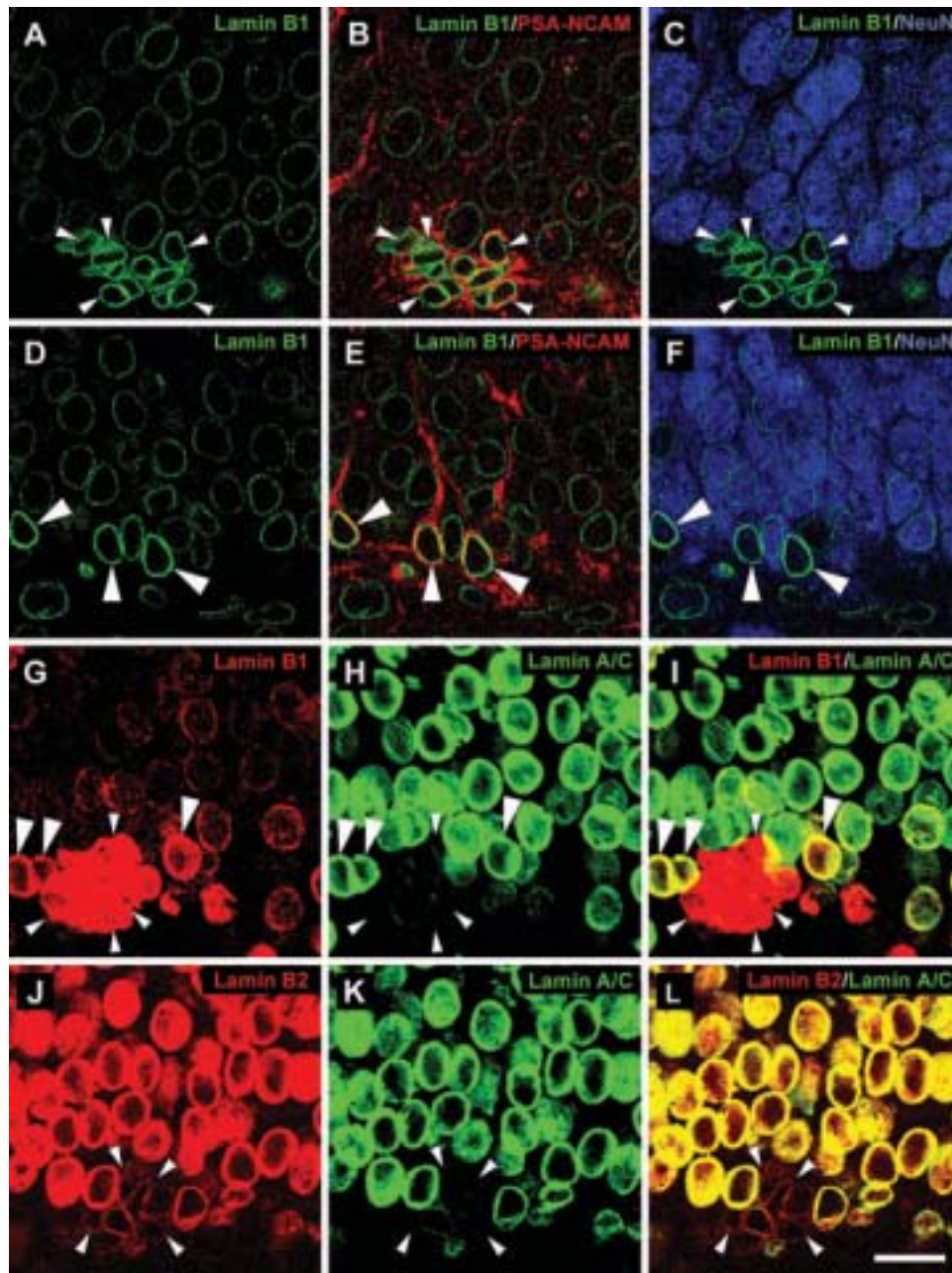


FIG. 2. Photomicrographs showing immunofluorescence images of dentate gyrus. (A–F) Specimens were fixed with formaldehyde and triple-labelled with antibodies against lamin B1 (green), PSA-NCAM (red) and NeuN (blue). Small arrowheads indicate the clustering small PSA-NCAM-positive cells. Large arrowheads indicate large PSA-NCAM-positive cells that have long protruding processes. (G–I) Specimens were fixed with methanol–acetone and double-labelled with antibodies against lamin A/C (green) and lamin B1 (red). Large arrowheads indicate double-immunoreactive cells. Small arrowheads indicate clustering small cells. (J–L) Specimens were fixed with methanol–acetone and double-labelled with antibodies against lamin B2 (red) and lamin A/C (green). Small arrowheads indicate clustering small cells. Scale bar, 20 μm .

Lamin B2 immunoreactivity was weaker than that of mature granule neurons but more intense than that of first-type PSA-NCAM-positive progenitor cells (Fig. 3E and F, arrowheads). No differences between male and female were observed in any of these lamin expression patterns.

Lamin subtypes in the SVZ

The SVZ exists beneath the ependymal cell layer of the lateral wall of the lateral ventricle. In the SVZ, there are GFAP-positive neural stem

cells and PSA-NCAM-positive neuronal progenitor cells (Bonfanti & Theodosis, 1994; Rousselot *et al.*, 1995; Doetsch *et al.*, 1999). Multiple immunostainings for lamin B1 and PSA-NCAM were performed in formaldehyde-fixed brain sections (Fig. 4A–C). PSA-NCAM-positive cells formed clusters under the ependymal layer and showed intense lamin B1 immunoreactivity in their nuclear envelopes compared with ependymal cells (Fig. 4A–C, small arrowheads). These cells are consistent with previously reported neuronal progenitor cells (Doetsch *et al.*, 1999). Some PSA-NCAM-negative cells also showed intense lamin B1 immunoreactivity, but these cells were observed

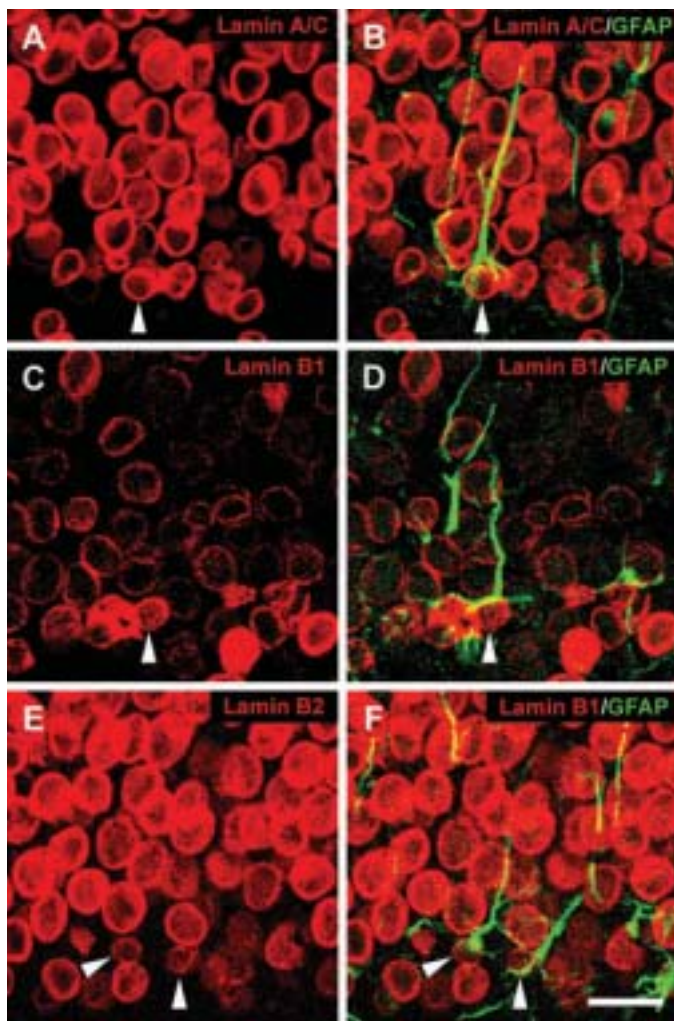


FIG. 3. Photomicrographs showing immunofluorescence images of dentate gyrus. (A and B) Specimens were double-labelled with antibodies against lamin A/C (red) and GFAP (green). (C and D) Specimens were double-labelled with antibodies against lamin B1 (red) and GFAP (green). (E and F) Specimens were double-labelled with antibodies against lamin B2 (red) and GFAP (green). All specimens were fixed with methanol–acetone. Arrowheads indicate GFAP-positive cells, which have long radial processes. Scale bar, 20 μ m.

outside the cluster of PSA-NCAM-positive cells (Fig. 4A–C, large arrowheads).

In methanol- and acetone-fixed sections, multiple immunostainings revealed that clustering cells which were identified as neuronal progenitor cells and were intensively immunopositive for lamin B1 (arrowheads in Fig. 4A–C) showed weak or no lamin A/C immunoreactivity (Fig. 4D–F, arrowheads). Double immunostaining for lamin A/C and lamin B2 indicated that clustering progenitor cells, which were weakly positive or negative for lamin A/C, showed weak lamin B2-immunoreactivity (Fig. 4G–I, arrowheads).

We next examined the existence of each lamin subtype in GFAP-positive neural stem cells in the SVZ in methanol- and acetone-fixed sections. GFAP-positive cells were observed under the ependymal layer of the lateral wall of the lateral ventricle (Fig. 5B, E and H, large arrowheads). These cells are identical to previously reported neural stem cells, based on their immunoreactivity and location (Doetsch *et al.*, 1999). GFAP-positive cells located in the SVZ showed intense immunoreactivities for lamin A/C (Fig. 5A–C large arrowheads)

compared with those of clustering progenitor cells, which were negative for lamin A/C (Fig. 5A–C small arrowheads). GFAP-positive cells showed immunoreactivities for lamin B1; the intensity was heterogeneous (Fig. 5D–F, large arrowheads), but also generally weaker than that of clustering progenitor cells (Fig. 5D–F, small arrowheads). The GFAP-positive cells also showed intense lamin B2 immunoreactivity (Fig. 5G–I, large arrowheads) that was more intense than that of clustering progenitor cells (Fig. 5G–I, small arrowheads).

Lamin subtypes in migrating cells within the glial tubes (RMS) and the olfactory bulb

Multiple immunostainings for lamin B1 and GFAP were performed in methanol- and acetone-fixed brain sagittal sections (Fig. 6A and B). GFAP-positive cells were observed from the lateral ventricle to the olfactory bulb (Fig. 6B). This structure is consistent with the previously reported glial tube, which provides for the migration of PSA-NCAM-positive progenitor cells through the RMS (Lois *et al.*, 1996; Peretto *et al.*, 1997). Cells intensely positive for lamin B1 were observed in the anterior side of the lateral ventricle, as well as the glial tube and the core of the olfactory bulb (Fig. 6A).

In the RMS, multiple immunostainings for lamin B1 and PSA-NCAM were performed in formaldehyde-fixed brain sections (Fig. 6C and D). PSA-NCAM-positive cells showed intense lamin B1 immunoreactivity like that found in the SVZ (Fig. 6C–E). These cells were lamin A/C-negative and weakly lamin B2-positive, as in the SVZ (data not shown).

In the olfactory bulb, multiple immunostainings for lamin B1, PSA-NCAM and NeuN were performed in formaldehyde-fixed brain sections (Fig. 6F–I). Both PSA-NCAM-positive progenitor cells and NeuN-positive mature neurons were observed (Fig. 6F–I). PSA-NCAM-positive cells showed no NeuN immunoreactivity, and NeuN-positive cells showed no PSA-NCAM immunoreactivity, respectively (Fig. 6F–I). The PSA-NCAM-positive cells showed intense lamin B1 immunoreactivity (Fig. 6F–I arrowheads) compared with NeuN-positive neurons. No difference between male and female was observed in any of these lamin expression patterns.

Discussion

In the present study, we have demonstrated that the composition of nuclear lamin is altered during neuronal differentiation in the two neurogenic regions (the SGZ and the SVZ) of adult rat brain; lamin A/C (++) , B1 (++) and B2 (++) in GFAP-positive primary progenitor (stem) cells, A/C (–), B1 (+++) and B2 (+) in PSA-NCAM-positive subsequent neuronal progenitor cells, and A/C (++) , B1 (+) and B2 (+++) in NeuN-positive mature neurons (Fig. 7A and B). In dentate gyrus, the late stage of PSA-NCAM-positive progenitor cells possess lamin A/C (+), B1 (++) and B2 (++) (Fig. 7A). Lamin A/C and lamin B2 expression was reduced, but lamin B1 expression was induced at the particular stage of neuronal differentiation that is immunoreactive for PSA-NCAM.

We used two fixation methods, formaldehyde fixation and methanol–acetone fixation. Most antibodies against the lamins were functional only in methanol–acetone fixation but not in formaldehyde fixation (Senda *et al.*, 2005). PSA-NCAM, however, could be immunodetected only in formaldehyde fixation but not in methanol–acetone fixation. Consequently, we could not perform multiimmunodetection of PSA-NCAM and the lamins without lamin B1.

In the dentate gyrus, the primary neuronal progenitor cells were previously identified as GFAP-positive cells that have long radial

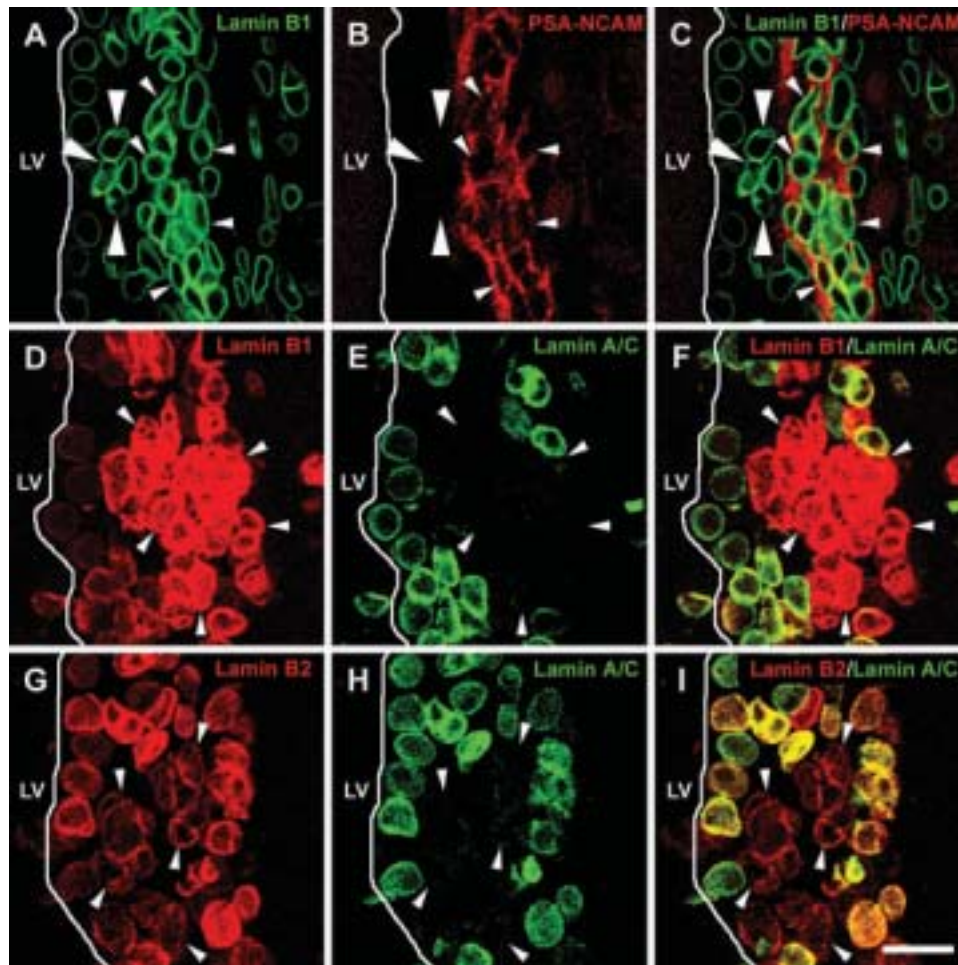


FIG. 4. Photomicrographs showing immunofluorescence images of the SVZ. (A–C) Specimens were fixed with formaldehyde and double-labelled with antibodies against lamin B1 (green) and PSA-NCAM (red). (D–F) Specimens were fixed with methanol–acetone and double-labelled with antibodies against lamin B1 (red) and lamin A/C (green). (G–I) Specimens were fixed with methanol–acetone and double-labelled with antibodies against lamin B2 (red) and lamin A/C (green). Arrowheads indicate the cluster of progenitor cells. The apical surface of the ependymal cell layer is lined with white. LV, lateral ventricle. Scale bar, 20 μ m.

processes and reside in the SGZ, and were named radial astrocytes or type 1 cells (Seri *et al.*, 2001; Filippov *et al.*, 2003; Kempermann *et al.*, 2004; Seri *et al.*, 2004). We distinguished these cells from authentic astrocytes or horizontal astrocytes by such features (Seri *et al.*, 2004). These cells moderately expressed lamins A/C, B1 and B2 (Fig. 3A–F), and they differentiate into transient neuronal progenitor cells that are PSA-NCAM-positive (Seki & Arai, 1991; Seri *et al.*, 2001). PSA-NCAM-positive cells are also called D cells and can be subdivided into three types based on differentiation steps and morphological features (Seri *et al.*, 2004). D1 cells are mitotic, have morphological characteristics such as small cell bodies and no obvious process, and form cell clusters. D1 cells mature into D2 cells, which are postmitotic and have short protruding processes. D2 cells further mature into D3 cells, which have prominent, frequently vertical, branched processes and show more morphologic similarity to granule neurons (Seri *et al.*, 2004). In the present study, we distinguished small and large cell bodies in PSA-NCAM-positive cells in formaldehyde-fixed sections (Fig. 2A–F). The small PSA-NCAM-positive cells were morphologically identical to D1 cells (Seri *et al.*, 2004). In methanol–acetone fixation we distinguished these cell types by morphological features and localization (Fig. 2G–L). These cells showed intense immunoreactivity for lamin B1 (Fig. 2A–C), but showed no immunoreactivity for lamin A/C and

weak immunoreactivity for lamin B2 (Fig. 2G–L). Large PSA-NCAM-positive cells, which had long vertical processes and were located between the SGZ and the GCL, were identical to D2 or D3 cells (Seri *et al.*, 2004). These cells showed intense immunoreactivities for lamin B1 (Fig. 2D–I) and lamin A/C (Fig. 2G–I). Mature granule neurons showed intense immunoreactivities for lamins A/C and B2, and weak immunoreactivity for lamin B1 (Fig. 3), like those observed in other mature neurons including pyramidal neurons in the hippocampal CA1–CA3 region (Fig. 1). While intensely visible in the CA1 region, the immunoreactivities for lamins A/C and B2 in the CA3 region seemed to be lower under the low magnification (Fig. 1). However, the immunoreactivities for each lamin in the CA1 and CA3 pyramidal neurons were confirmed to be identical under magnified view (data not shown). The apparent difference between CA1 and CA3 under low magnification was due to the larger cell size and lower density of nuclei in the CA3 region than the CA1 region. The expression pattern for lamin subtypes in the course of neuronal differentiation in dentate gyrus is summarized in Fig. 7A.

In the SVZ, the primary neuronal stem cells were previously identified as GFAP-positive cells, are located beneath ependymal cells and are called SVZ astrocytes or B cells. These cells mature into intermediate progenitor cells named C cells, which are highly proliferative and express neither GFAP nor PSA-NCAM. These

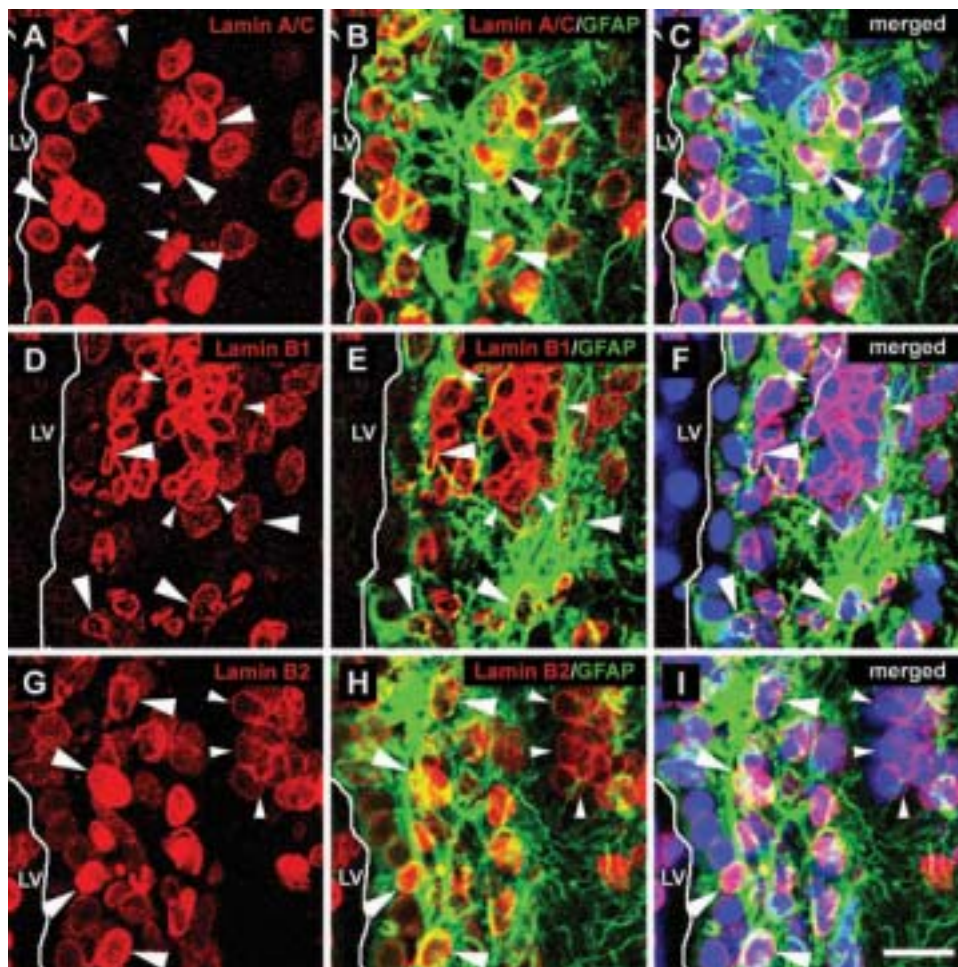


FIG. 5. Photomicrographs showing immunofluorescence images of the SVZ. (A–C) Specimens were triple-labelled with antibodies against lamin A/C (red), GFAP (green) and TOPRO-3 (blue). (D–F) Specimens were triple-labelled with antibodies against lamin B1 (red), GFAP (green) and TOPRO-3 (blue). (G–I) Specimens were triple-labelled with antibodies against lamin B2 (red), GFAP (green) and TOPRO-3 (blue). Specimens were fixed with methanol–acetone. Arrowheads indicate GFAP-positive cells. The apical surface of the ependymal cell layer is lined with white. LV, lateral ventricle. Scale bar, 20 μ m.

intermediate progenitor cells mature into subsequent progenitor cells, which are named A cells and are immunoreactive for PSA-NCAM (Doetsch *et al.*, 1999). The PSA-NCAM-positive cells assemble into chains that are contained within the glial tubes, migrate to the olfactory bulb through the RMS and differentiate into granule and periglomerular inhibitory neurons (Luskin, 1993; Bonfanti & Theodosis, 1994; Lois *et al.*, 1996). In the present study, we detected moderate immunoreactivities for lamins A/C, B1 and B2 in the GFAP-positive stem cells (Fig. 5), which were located beneath ependymal cells and the surrounding clusters of PSA-NCAM-positive cells with their processes. We observed heterogeneous immunoreactivities for lamin B1 in GFAP-positive cells (Fig. 5D–F large arrowheads), which may indicate that this population of GFAP-positive cells is heterogeneous and includes stem cells and authentic astrocytes (Garcia *et al.*, 2004). PSA-NCAM-positive cells showed intense immunoreactivity for lamin B1 but showed no or weak immunoreactivities for lamins A/C and B2 in the SVZ and the RMS (Figs 4 and 6C–E). In the SVZ, we found PSA-NCAM-negative cells that showed intense lamin B1 immunoreactivity (Fig. 4A–C, small arrowheads). As these cells resided outside the cell cluster of PSA-NCAM-positive cells, they were thought to be GFAP-positive stem cells or C cells. In the olfactory bulb, NeuN-positive mature neurons showed weak lamin B1 immunoreactivity compared with PSA-

NCAM-positive cells (Fig. 6). The expression pattern for lamin subtypes in the course of neuronal differentiation in the SVZ, the RMS and the olfactory bulb is summarized in Fig. 7B. The alteration of each lamin subtype is revealed to be consistent in the two neurogenic regions of adult mammalian brain.

Lamin expression is believed to be related to cell differentiation. Lamin A/C was not observed in undifferentiated states, but was induced following progression of differentiation *in vitro*, e.g. mouse embryonal carcinoma cell differentiation (Lebel *et al.*, 1987), the differentiation from human adipose tissue stem cells into cardiomyocyte (Gaustad *et al.*, 2004) and, most recently, the differentiation from human embryonic stem cells into neuronal and cardiomyocyte lineages (Constantinescu *et al.*, 2006). In mouse development, lamin A/C is not observed in early developmental stages but is observed once cell differentiation begins (Schatten *et al.*, 1985; Stewart & Burke, 1987; Röber *et al.*, 1989). In adult mammalian tissues, lamin A/C is not observed in undifferentiated or proliferative cells, but is observed in differentiated or nonproliferative cells. On the other hand, lamin B1 is abundantly expressed in undifferentiated cells but is absent or only faintly observed in differentiated cells in several tissues, such as muscles, testis and epithelial cells of skin, bronchus and colon (Röber *et al.*, 1990; Cance *et al.*, 1992; Ausma *et al.*, 1996; Coates *et al.*, 1996; Broers *et al.*, 1997; Jansen *et al.*, 1997; Machiels

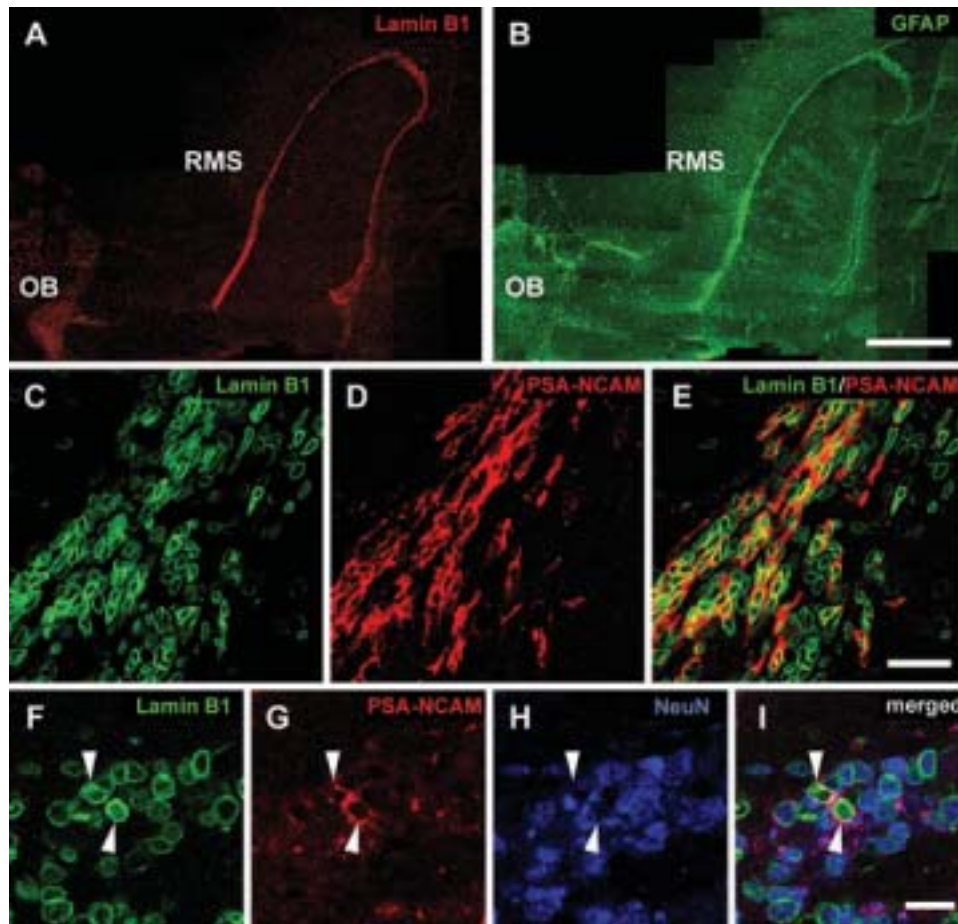


FIG. 6. Photomicrographs showing immunofluorescence images of rostral migratory stream (RMS) and olfactory bulb (OB). (A and B) Photomicrographs showing immunofluorescence images of brain sagittal section. Specimens were fixed with methanol–acetone and double-labelled with antibodies against lamin B1 (red) and GFAP (green). (C–E) Photomicrographs showing immunofluorescence images of RMS. Specimens were fixed with formaldehyde and double-labelled with antibodies against lamin B1 (green) and PSA-NCAM (red). (F–I) Photomicrographs showing immunofluorescence images of olfactory bulb. Specimens were fixed with formaldehyde and triple-labelled with antibodies against lamin B1 (green), PSA-NCAM (red) and NeuN (blue). Arrowheads indicate PSA-NCAM-positive NeuN-negative cells. Scale bars, 1 mm (A and B), 30 μ m (C–E), 20 μ m (F–I).

et al., 1997; Manilal *et al.*, 1999; Venables *et al.*, 2001; Tilli *et al.*, 2003). These reports nicely complement our observation that lamin A/C is not expressed in PSA-NCAM-positive progenitor cells but is expressed in mature neurons, while lamin B1 is expressed at high levels in PSA-NCAM-positive progenitor cells but at low levels in mature neurons in two adult neurogenic regions (Fig. 7).

In the mouse brain, lamin A/C first appears in a minority of cells at postnatal day 5 and is present in almost all cells at postnatal day 15. B-type lamins, on the other hand, are present through all developmental stages (Röber *et al.*, 1989). This report, however, did not distinguish neuronal cells from the other cells and did not distinguish between lamin B1 and B2. The existence of A-type and B-type lamins in adult human cerebellum was reported previously (Cance *et al.*, 1992). The authors of that study reported that B-type lamins were immunopositive in all cells in cerebellum, but these antibodies were not specific to lamin B1 or B2 alone. Their observations, however, support our results that lamin B1 and B2 are present in mature neurons (Fig. 7). Moreover, they reported that lamin A/C was present in the neurons in granular layer or white matter, while the cells in the molecular layer as well as Purkinje cells had a reduced or absent level of lamin A/C (Cance *et al.*, 1992). In the present study, we demonstrated that lamin A/C was present in all mature neurons in adult rat neurogenic regions and the hippocampus, that nearly mature

neurons also showed intense immunoreactivity for lamin A/C (Fig. 1), but that some neurons showed weak immunoreactivity in other brain regions (data not shown). These different observations are thought to depend on the specific antibodies used, brain regions studied or detection techniques employed.

In this paper, we have demonstrated that an alteration of lamin subtypes occurs during neuronal differentiation. We hypothesize that this switching of lamin subtypes alters the structure of nuclear lamina and the state of nuclear proteins that associate with nuclear lamina. As the expression of lamin A/C is specifically down-regulated in progenitor cells that express PSA-NCAM during neuronal differentiation, lamin A/C may participate in particular functions in GFAP-positive progenitor (stem) cells and mature neurons. Lamin A/C might regulate the expression of genes, as demonstrated by observations that lamin A/C can interact with transcription factors such as MOK2, a Krüppel/TFIIIA-related zinc finger protein expressed preferentially in brain and testis (Dreuillet *et al.*, 2002), sterol response element binding protein 1, which is involved in adipocyte differentiation (Lloyd *et al.*, 2002), and retinoblastoma protein, which is involved in cell-cycle arrest and cell differentiation (Ozaki *et al.*, 1994; Johnson *et al.*, 2004; Nitta *et al.*, 2006). As expressions of lamins B1 and B2 are regulated distinctly during neuronal differentiation, they may participate in some independent cellular functions. It

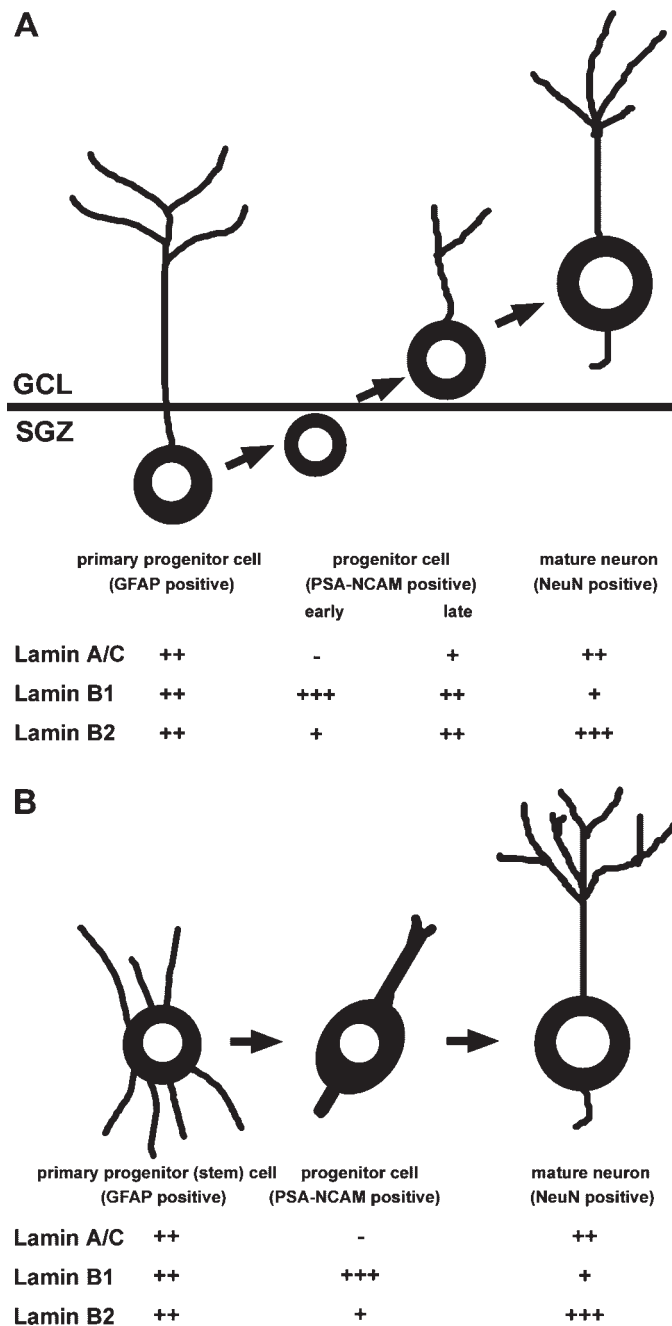


FIG. 7. Summary of expression pattern of nuclear lamin during adult neurogenesis in (A) dentate gyrus and (B) subventricular zone. (A and B) In these two neurogenic regions in mammalian brain, GFAP-positive primary neuronal progenitor or stem cells differentiate into PSA-NCAM-positive subsequent progenitor cells, and finally differentiate into NeuN-positive mature neurons. (A) In dentate gyrus, the late stage of PSA-NCAM-positive progenitor cells shows an intermediate expression pattern. The composition of lamin subtypes in nuclear lamina is altered in the course of neuronal differentiation in mammalian adult brain. The levels of immunoreactivity are indicated as follows: +++, highly positive; ++, positive; +, weakly positive; -, negative.

has been reported that mice with a mutant form of *LMNB1*, the gene encoding lamin B1 protein, showed developmental defects in lung and bone, and the fibroblasts from mutant embryos exhibited impaired adipocyte differentiation and an increased occurrence of polyploidy (Vergnes *et al.*, 2004). This previous report and our observations indicate that lamin B1 might play important functions during cellular

proliferation or the differentiation process. Our results imply that alteration of nuclear lamina is coupled with the progression of neuronal differentiation, but it is not clear whether switching of lamin expression is necessary for neuronal differentiation. To determine the functional relevance of lamin for neuronal differentiation further analyses are needed, such as overexpression or down-regulation of lamin subtypes at particular differentiation stages.

As lamins are predominantly localized to the inner nuclear membrane, they are useful for precisely determining the positions of cell nuclei in brain (Kataoka *et al.*, 2006). Moreover, as the composition of lamin subtypes is altered during differentiation in neuronal cells it can be said that lamins have a unique property that may be suitable for monitoring the cell differentiation process. Recently, we have observed that NG2-positive cells, which were previously reported as oligodendrocyte-progenitor cells (Dawson *et al.*, 2000; Horner *et al.*, 2002; Nishiyama *et al.*, 2002), have intense lamin B1 immunoreactivity compared with mature oligodendrocytes, and this is consistent with that observed for neuronal cells (Yasuharu Takamori, unpublished observation). It was previously proposed that lamin A/C could be used as a marker for cell differentiation in several systems *in vitro* (Gaustad *et al.*, 2004; Constantinescu *et al.*, 2006). Indeed, it is difficult to use lamins solely as markers to distinguish cell types and populations in the brain *in vivo* because lamins are present not only in neuronal cells but also in glial and endothelial cells (Fig. 1). However, by combining them with other cell markers or distinguishing the neuronal and glial cell nuclei on the basis of size and morphology, lamins might become useful molecules for the study of neuronal differentiation.

Acknowledgements

This work was supported in part by research grants from Kansai Medical University.

Abbreviations

GCL, granule cell layer; GFAP, glial fibrillary acidic protein; PBS, phosphate-buffered saline; PSA-NCAM, polysialylated neural cell adhesion molecule; RMS, rostral migratory stream; SGZ, subgranular zone; SVZ, subventricular zone.

References

- Altman, J. (1969) Autoradiographic and histological studies of postnatal neurogenesis. IV. Cell proliferation and migration in the anterior forebrain, with special reference to persisting neurogenesis in the olfactory bulb. *J. Comp. Neurol.*, **137**, 433–457.
- Altman, J. & Das, G.D. (1965) Autoradiographic and histological evidence of postnatal hippocampal neurogenesis in rats. *J. Comp. Neurol.*, **124**, 319–335.
- Ausma, J., van Eys, G.J., Broers, J.L., Thone, F., Flameng, W., Ramaekers, F.C. & Borgers, M. (1996) Nuclear lamin expression in chronic hibernating myocardium in man. *J. Mol. Cell. Cardiol.*, **28**, 1297–1305.
- Bonfanti, L. & Theodosis, D.T. (1994) Expression of polysialylated neural cell adhesion molecule by proliferating cells in the subependymal layer of the adult rat, in its rostral extension and in the olfactory bulb. *Neuroscience*, **62**, 291–305.
- Bridger, J.M., Kill, I.R., O'Farrell, M. & Hutchison, C.J. (1993) Internal lamin structures within G1 nuclei of human dermal fibroblasts. *J. Cell Sci.*, **104**, 297–306.
- Broers, J.L., Hutchison, C.J. & Ramaekers, F.C. (2004) Laminopathies. *J. Pathol.*, **204**, 478–488.
- Broers, J.L., Machiels, B.M., Kuijpers, H.J., Smedts, F., van den Kieboom, R., Raymond, Y. & Ramaekers, F.C. (1997) A- and B-type lamins are differentially expressed in normal human tissues. *Histochem. Cel. Biol.*, **107**, 505–517.

- Cance, W.G., Chaudhary, N., Worman, H.J., Blobel, G. & Cordon-Cardo, C. (1992) Expression of the nuclear lamins in normal and neoplastic human tissues. *J. Exp. Clin. Cancer Res.*, **11**, 233–246.
- Coates, P.J., Hobbs, R.C., Crocker, J., Rowlands, D.C., Murray, P., Quinlan, R. & Hall, P.A. (1996) Identification of the antigen recognized by the monoclonal antibody BU31 as lamins A and C. *J. Pathol.*, **178**, 21–29.
- Constantinescu, D., Gray, H.L., Sammak, P.J., Schatten, G.P. & Csoka, A.B. (2006) Lamin A/C expression is a marker of mouse and human embryonic stem cell differentiation. *Stem Cells*, **24**, 177–185.
- Dawson, M.R., Levine, J.M. & Reynolds, R. (2000) NG2-expressing cells in the central nervous system: are they oligodendroglial progenitors? *J. Neurosci. Res.*, **61**, 471–479.
- Doetsch, F., Caille, I., Lim, D.A., Garcia-Verdugo, J.M. & Alvarez-Buylla, A. (1999) Subventricular zone astrocytes are neural stem cells in the adult mammalian brain. *Cell*, **97**, 703–716.
- Dreuillet, C., Tillit, J., Kress, M. & Emoult-Lange, M. (2002) In vivo and in vitro interaction between human transcription factor MOK2 and nuclear lamin A/C. *Nucl. Acids Res.*, **30**, 4634–4642.
- Filippov, V., Kronenberg, G., Pivneva, T., Reuter, K., Steiner, B., Wang, L.P., Yamaguchi, M., Kettenmann, H. & Kempermann, G. (2003) Subpopulation of nestin-expressing progenitor cells in the adult murine hippocampus shows electrophysiological and morphological characteristics of astrocytes. *Mol. Cell Neurosci.*, **23**, 373–382.
- Garcia, A.D., Doan, N.B., Imura, T., Bush, T.G. & Sofroniew, M.V. (2004) GFAP-expressing progenitors are the principal source of constitutive neurogenesis in adult mouse forebrain. *Nat. Neurosci.*, **7**, 1233–1241.
- Gaustad, K.G., Boquest, A.C., Anderson, B.E., Gerdes, A.M. & Collas, P. (2004) Differentiation of human adipose tissue stem cells using extracts of rat cardiomyocytes. *Biochem. Biophys. Res. Commun.*, **314**, 420–427.
- Gruenbaum, Y., Margalit, A., Goldman, R.D., Shumaker, D.K. & Wilson, K.L. (2005) The nuclear lamina comes of age. *Nat. Rev. Mol. Cell Biol.*, **6**, 21–31.
- Horner, P.J., Thallmair, M. & Gage, F.H. (2002) Defining the NG2-expressing cell of the adult CNS. *J. Neurocytol.*, **31**, 469–480.
- Jansen, M.P., Machiels, B.M., Hopman, A.H., Broers, J.L., Bot, F.J., Arends, J.W., Ramaekers, F.C. & Schouten, H.C. (1997) Comparison of A and B-type lamin expression in reactive lymph nodes and nodular sclerosing Hodgkin's disease. *Histopathology*, **31**, 304–312.
- Johnson, B.R., Nitta, R.T., Frock, R.L., Mounkes, L., Barbie, D.A., Stewart, C.L., Harlow, E. & Kennedy, B.K. (2004) A-type lamins regulate retinoblastoma protein function by promoting subnuclear localization and preventing proteasomal degradation. *Proc. Natl Acad. Sci. USA*, **101**, 9677–9682.
- Kataoka, Y., Tamura, Y., Takamori, Y., Cui, Y. & Yamada, H. (2006) Perineuronal germinal cells in the rat cerebral cortex. *Med. Mol. Morph.*, **39**, 28–32.
- Kempermann, G., Jessberger, S., Steiner, B. & Kronenberg, G. (2004) Milestones of neuronal development in the adult hippocampus. *Trends Neurosci.*, **27**, 447–452.
- Lebel, S., Lampron, C., Royal, A. & Raymond, Y. (1987) Lamins A and C appear during retinoic acid-induced differentiation of mouse embryonal carcinoma cells. *J. Cell Biol.*, **105**, 1099–1104.
- Lehner, C.F., Kurer, V., Eppenberger, H.M. & Nigg, E.A. (1986) The nuclear lamin protein family in higher vertebrates. Identification of quantitatively minor lamin proteins by monoclonal antibodies. *J. Biol. Chem.*, **261**, 13293–13301.
- Lloyd, D.J., Trembath, R.C. & Shackleton, S. (2002) A novel interaction between lamin A and SREBP1: implications for partial lipodystrophy and other laminopathies. *Hum. Mol. Genet.*, **11**, 769–777.
- Lois, C., Garcia-Verdugo, J.M. & Alvarez-Buylla, A. (1996) Chain migration of neuronal precursors. *Science*, **271**, 978–981.
- Luskin, M.B. (1993) Restricted proliferation and migration of postnatally generated neurons derived from the forebrain subventricular zone. *Neuron*, **11**, 173–189.
- Machiels, B.M., Broers, J.L., Raymond, Y., de Ley, L., Kuijpers, H.J., Caberg, N.E. & Ramaekers, F.C. (1995) Abnormal A-type lamin organization in a human lung carcinoma cell line. *Eur. J. Cell Biol.*, **67**, 328–335.
- Machiels, B.M., Ramaekers, F.C., Kuijpers, H.J., Groenewoud, J.S., Oosterhuis, J.W. & Looijenga, L.H. (1997) Nuclear lamin expression in normal testis and testicular germ cell tumours of adolescents and adults. *J. Pathol.*, **182**, 197–204.
- Manilal, S., Sewry, C.A., Pereboev, A., Man, N., Gobbi, P., Hawkes, S., Love, D.R. & Morris, G.E. (1999) Distribution of emerin and lamins in the heart and implications for Emery-Dreifuss muscular dystrophy. *Hum. Mol. Genet.*, **8**, 353–359.
- Mounkes, L. & Stewart, C.L. (2004) Structural organization and functions of the nucleus in development, aging, and disease. *Curr. Top. Dev. Biol.*, **61**, 191–228.
- Nishiyama, A., Watanabe, M., Yang, Z. & Bu, J. (2002) Identity, distribution, and development of polydendrocytes: NG2-expressing glial cells. *J. Neurocytol.*, **31**, 437–455.
- Nitta, R.T., Jameson, S.A., Kudlow, B.A., Conlan, L.A. & Kennedy, B.K. (2006) Stabilization of the retinoblastoma protein by A-type nuclear lamins is required for INK4A-mediated cell cycle arrest. *Mol. Cell Biol.*, **26**, 5360–5372.
- Östlund, C. & Worman, H.J. (2003) Nuclear envelope proteins and neuromuscular diseases. *Muscle Nerve*, **27**, 393–406.
- Ozaki, T., Saijo, M., Murakami, K., Enomoto, H., Taya, Y. & Sakiyama, S. (1994) Complex formation between lamin A and the retinoblastoma gene product: identification of the domain on lamin A required for its interaction. *Oncogene*, **9**, 2649–2653.
- Peretto, P., Merighi, A., Fasolo, A. & Bonfanti, L. (1997) Glial tubes in the rostral migratory stream of the adult rat. *Brain Res. Bull.*, **42**, 9–21.
- Pugh, G.E., Coates, P.J., Lane, E.B., Raymond, Y. & Quinlan, R.A. (1997) Distinct nuclear assembly pathways for lamins A and C lead to their increase during quiescence in Swiss 3T3 cells. *J. Cell Sci.*, **110**, 2483–2493.
- Röber, R.A., Sauter, H., Weber, K. & Osborn, M. (1990) Cells of the cellular immune and hemopoietic system of the mouse lack lamins A/C: distinction versus other somatic cells. *J. Cell Sci.*, **95**, 587–598.
- Röber, R.A., Weber, K. & Osborn, M. (1989) Differential timing of nuclear lamin A/C expression in the various organs of the mouse embryo and the young animal: a developmental study. *Development*, **105**, 365–378.
- Rousselot, P., Lois, C. & Alvarez-Buylla, A. (1995) Embryonic (PSA) N-CAM reveals chains of migrating neuroblasts between the lateral ventricle and the olfactory bulb of adult mice. *J. Comp. Neurol.*, **351**, 351–361.
- Schatten, G., Maul, G.G., Schatten, H., Chaly, N., Simerly, C., Balczon, R. & Brown, D.L. (1985) Nuclear lamins and peripheral nuclear antigens during fertilization and embryogenesis in mice and sea urchins. *Proc. Natl Acad. Sci. USA*, **82**, 4727–4731.
- Seki, T. & Arai, Y. (1991) The persistent expression of a highly polysialylated NCAM in the dentate gyrus of the adult rat. *Neurosci. Res.*, **12**, 503–513.
- Senda, T., Iizuka-Kogo, A. & Shimomura, A. (2005) Visualization of the nuclear lamina in mouse anterior pituitary cells and immunocytochemical detection of lamin A/C by quick-freeze freeze-substitution electron microscopy. *J. Histochem. Cytochem.*, **53**, 497–507.
- Seri, B., Garcia-Verdugo, J.M., Collado-Morente, L., McEwen, B.S. & Alvarez-Buylla, A. (2004) Cell types, lineage, and architecture of the germinal zone in the adult dentate gyrus. *J. Comp. Neurol.*, **478**, 359–378.
- Seri, B., Garcia-Verdugo, J.M., McEwen, B.S. & Alvarez-Buylla, A. (2001) Astrocytes give rise to new neurons in the adult mammalian hippocampus. *J. Neurosci.*, **21**, 7153–7160.
- Stewart, C. & Burke, B. (1987) Teratocarcinoma stem cells and early mouse embryos contain only a single major lamin polypeptide closely resembling lamin B. *Cell*, **51**, 383–392.
- Tamura, Y., Kataoka, Y., Cui, Y. & Yamada, H. (2004) Cellular proliferation in the cerebral cortex following neural excitation in rats. *Neurosci. Res.*, **50**, 129–133.
- Temple, S. (2001) The development of neural stem cells. *Nature*, **414**, 112–117.
- Tilli, C.M., Ramaekers, F.C., Broers, J.L., Hutchison, C.J. & Neumann, H.A. (2003) Lamin expression in normal human skin, actinic keratosis, squamous cell carcinoma and basal cell carcinoma. *Br. J. Dermatol.*, **148**, 102–109.
- Venables, R.S., McLean, S., Luny, D., Moteleb, E., Morley, S., Quinlan, R.A., Lane, E.B. & Hutchison, C.J. (2001) Expression of individual lamins in basal cell carcinomas of the skin. *Br. J. Cancer*, **84**, 512–519.
- Vergnes, L., Peterfy, M., Bergo, M.O., Young, S.G. & Reue, K. (2004) Lamin B1 is required for mouse development and nuclear integrity. *Proc. Natl Acad. Sci. USA*, **101**, 10428–10433.

Multi-directional differentiation of doublecortin- and NG2-immunopositive progenitor cells in the adult rat neocortex *in vivo*

Yasuhisa Tamura,^{1,2,3} Yosky Kataoka,^{1,2,3} Yilong Cui,^{1,2,3} Yasuharu Takamori,¹ Yasuyoshi Watanabe^{2,3} and Hisao Yamada¹

¹Department of Anatomy and Cell Science, KMU 21C COE Project, Kansai Medical University, 10–15 Fumizono-cho, Moriguchi, Osaka 570-8506, Japan

²Molecular Imaging Research Program, RIKEN Frontier Research System, 6-7-3 Minatojima minamimachi, Chuo-ku, Kobe, Hyogo 650-0047, Japan

³Department of Physiology, Osaka City University Graduate School of Medicine, 1-4-3 Asahimachi, Abeno-ku, Osaka 545-8585, Japan

Keywords: BrdU, cerebral cortex, gliogenesis, neural progenitor cells, neurogenesis

Abstract

In the adult mammalian brain, multipotent stem or progenitor cells involved in reproduction of neurons and glial cells have been well investigated only in very restricted regions; the subventricular zone of the lateral ventricle and the dentate gyrus in the hippocampal formation. In the neocortex, a series of *in vitro* studies has suggested the possible existence of neural progenitor cells possessing neurogenic and/or gliogenic potential in adult mammals. However, the cellular properties of the cortical progenitor cells *in vivo* have not been fully elucidated. Using 5'-bromodeoxyuridine labeling and immunohistochemical analysis of cell differentiation markers, we found that a subpopulation of NG2-immunopositive cells co-expressing doublecortin (DCX), an immature neuron marker, ubiquitously reside in the adult rat neocortex. Furthermore, these cells are the major population of proliferating cells in the region. The DCX(+)/NG2(+) cells reproduced the same daughter cells, or differentiated into DCX(+)/NG2(-) (approximately 1%) or DCX(-)/NG2(+) (approximately 10%) cells within 2 weeks after cell division. The DCX(+)/NG2(-) cells were also immunopositive for TUC-4, a neuronal lineage marker, suggesting that these cells were committed to neuronal cell differentiation, whereas the DCX(-)/NG2(+) cells showed faint immunoreactivity for glutathione S-transferase (GST)-pi, an oligodendrocyte lineage marker, in the cytoplasm, suggesting glial cell lineage, and thereafter the cells differentiated into NG2(-)/GST-pi(+) mature oligodendrocytes after a further 2 weeks. These findings indicate that DCX(+)/NG2(+) cells ubiquitously exist as 'multipotent progenitor cells' in the neocortex of adult rats.

Introduction

In adult mammals, continuous reproduction of neurons is known in two restricted regions: the subventricular zone (SVZ) of the lateral ventricle and the subgranular zone of the hippocampal dentate gyrus (Cameron *et al.*, 1993; Lois & Alvarez-Buylla, 1993). These neurogenic regions contain neural progenitor cells that possess proliferative potential including self-reproduction, and can generate a wide variety of neural cells including neurons, astrocytes and oligodendrocytes, *in vitro* (Morshead *et al.*, 1994; Gage *et al.*, 1995; Gritti *et al.*, 1999). The neural progenitor cells in the neurogenic regions *in vivo* include glial fibrillary acidic protein-immunopositive [GFAP(+)] cells and the polysialyated form of neural cell adhesion molecule-immunopositive [PSA-NCAM(+)] cells, which are derived from GFAP(+) cells (Doetsch *et al.*, 1999, 2002; Seri *et al.*, 2001).

Some neural progenitor cells in the SVZ have also been reported to express NG2 chondroitin sulfate proteoglycan (Belachew *et al.*, 2003).

Observations that cells isolated from the adult rat cerebral cortex self-renewed and generated both neurons and glial cells under cultured conditions have implied that the cerebral cortex also includes neural progenitor cells (Palmer *et al.*, 1999). However, very little is known about the cellular properties of cortical progenitor cells *in vivo*. Recently, NG2(+) cells isolated from the cerebral gray matter of early postnatal mice were shown to form neurospheres and gave rise to neurons, as well as astrocytes and oligodendrocytes *in vitro* (Belachew *et al.*, 2003). Moreover, NG2(+) cells were found to be the major proliferating cell population in the cerebral cortex of adult rats *in vivo* (Dawson *et al.*, 2003; Tamura *et al.*, 2004). These reports indicate that NG2(+) cells may be a candidate for neural progenitor cells in the adult cortex. However, it remains unclear whether all NG2(+) cells are cortical progenitor cells and whether the cells have multipotent activities *in vivo*. Indeed, it has been reported that only a small fraction of cortical NG2(+) cells isolated from early postnatal mice

Correspondence: Dr Y. Kataoka, as above.³

E-mail: kataokay@med.osaka-cu.ac.jp

Received 10 August 2006, revised 20 April 2007, accepted 7 May 2007

are immunopositive for Tuj1 and HuC/D, markers for immature neurons (Chittajallu *et al.*, 2004). Moreover, different subtypes of NG2(+) cells have been identified in the gray matter of adult rodent brain on the basis of morphological criteria (Nishiyama *et al.*, 1999) and physiological properties (Chittajallu *et al.*, 2004). These observations suggest that NG2(+) cells are composed of heterogeneous cellular populations.

In the present study, we identified progenitor cells that express doublecortin (DCX), an immature neuron marker, among NG2(+) cells in the neocortex of adult rats *in vivo*. Furthermore, we examined whether these cells have multipotent activity by tracing their differentiation.

Materials and methods

Animals and BrdU injections

Adult male Wistar rats (SLC, Hamamatsu, Japan; 250–350 g body weight) were used. All experimental protocols were approved by the Ethics Committee on Animal Care and Use, Kansai Medical University, and were performed in accordance with the Principles of Laboratory Animal Care (NIH publication no. 85-23, revised 1985). For labeling of proliferating cells, adult rats ($n = 15$) were intraperitoneally injected with 5-bromodeoxyuridine (BrdU) at 50 mg/kg body weight. Each animal underwent a single injection of BrdU.

Immunohistochemistry

Animals were deeply anesthetized with diethyl ether and perfused transcardially with 4% formaldehyde buffered with 0.1 M phosphate-buffered saline (PBS; pH 7.4) at 2 h ($n = 5$), 14 days ($n = 5$) and 28 days ($n = 5$) after injection of BrdU (Sigma, St Louis, MO, USA). Brains were removed, postfixed overnight at 4 °C in 4% formaldehyde buffered with 0.1 M PBS and then immersed in 20% (w/v) sucrose solution. Coronal brain sections (30 μ m thickness) were prepared using a cryostat and collected as free-floating sections. For detection of BrdU incorporation, brain sections were preincubated in 50% formamide/2 \times standard sodium citrate (SSC) for 2 h at 65 °C, incubated in 2 N HCl for 30 min at 37 °C, rinsed in 0.1 M boric acid (pH 8.5) for 10 min at 25 °C, and then washed with 0.3% Triton X-100 in PBS (PBST). For multiplex-immunostaining, coronal sections were incubated with several primary antibodies for 12–36 h at 4 °C. The primary antibodies used in this study were: monoclonal rat anti-BrdU IgG (1 : 10, Oxford Biotechnology, Oxford, UK); polyclonal rabbit anti-Ki67 IgG (1 : 1000, Novocastra, Newcastle, UK); polyclonal goat anti-DCX (C-18) IgG (1 : 100, Santa Cruz Biotechnology, Santa Cruz, USA); monoclonal mouse anti-PSA-NCAM IgM (1 : 200, Chemicon, Temecula, CA, USA); polyclonal rabbit anti-TUC-4 protein IgG (1 : 1000, Chemicon); monoclonal mouse anti-neuronal nuclei (NeuN) IgG (1 : 200, Chemicon); monoclonal mouse anti-NG2 IgG (1 : 200, Chemicon); polyclonal rabbit anti-NG2 IgG (1 : 200, Chemicon); polyclonal rabbit anti-glutathione S-transferase (GST)-pi IgG (1 : 500, Medical & Biological Laboratories, Nagoya, Japan); monoclonal mouse anti-oligodendrocytes (clone RIP) IgG (1 : 20 000, Chemicon); and polyclonal rabbit anti-GFAP IgG (1 : 100, Sigma). After washing for 30 min (three washes of 10 min each) with PBST, brain sections were incubated in the appropriate secondary antibodies conjugated with either Cy2, Cy3 or Cy5 (1 : 200, Jackson ImmunoResearch, West Grove, PA, USA) for 4 h at 4 °C and washed with PBST for 30 min. Some of the staining sections were mounted with solution containing TO-PRO3 (1 : 1000,

Molecular Probes, Eugene, OR, USA) and then examined using a confocal laser microscope (LSM510META Ver. 3.2; Carl Zeiss).

Cell counting procedure

Coronal brain sections (30 μ m thickness) were randomly selected from 2.30 mm to 3.80 mm posterior to the bregma from each animal. Confocal images were captured at 1- μ m intervals along the Z-axis (depth) from each section and were reconstructed into three-dimensional images. The percentages of cells expressing each cellular marker among all BrdU-labeled cells were evaluated in the neocortical parenchyma, including the motor cortex, somatosensory cortex and auditory cortex of both hemispheres of three coronal sections from each animal. The proportion of DCX(+) cells in the neocortical NG2(+) cells was estimated in 12 square areas (150 \times 150 μ m), which were randomly selected in the neocortical areas described above from each hemisphere. Vascular cells, including endothelial and perivascular cells, which were defined as cells having crescent or narrow nuclei located along the wall of the blood vessels, were omitted from analysis. Data from each animal were averaged.

Results

NG2-immunopositive [NG2(+)] cells were abundantly observed in all cortical layers in the adult rat neocortex (Fig. 1A). Some were closely attached to the somata of the NeuN(+) neurons (perineuronal territory, Kataoka *et al.*, 2006; arrowhead in Fig. 1B). We investigated whether neocortical cells express immature neuron markers by immunofluorescent staining for neuronal-lineage markers (PSA-NCAM and DCX). The studies revealed that many DCX(+) cells existed throughout the neocortex (Fig. 1C), although none of the cortical cells was immunopositive for PSA-NCAM within the neocortex (data not shown). The majority of DCX(+) cortical cells were found in the perineuronal territory of NeuN(+) neurons, and the multiple processes of these cells appeared to wrap around the cell bodies of the neurons (Fig. 1D), as did some of the NG2(+) cells (arrowhead in Fig. 1B). In order to investigate the coexistence of DCX and NG2 in these cells, we then performed triple immunofluorescent staining of DCX, NG2 and TO-PRO3, a DNA/RNA marker contained abundantly in neuronal somata. The study clearly revealed that such NG2(+) cells in the perineuronal territory had positive immunoreactivity for DCX (arrowheads in Fig. 2A–D), and that DCX(-)/NG2(+) cells were also observed in the cortex (arrows in Fig. 2A–D) but not in the perineuronal territory. As shown in Fig. 2G, cell pairs consisting of a DCX(+)/NG2(+) cell (arrowhead) and a DCX(-)/NG2(+) cell (arrow) were observed, suggesting that these distinctive cells originated from identical cells. Cell counting studies showed that $63 \pm 3\%$ (mean \pm SD, $n = 2938$ cells from five animals) of neocortical NG2(+) cells were immunopositive for DCX. The cell densities of DCX(+)/NG2(+) cells were 70 ± 7 cells/mm² (mean \pm SD, $n = 5$ animals) in the motor cortex (M1 and M2 defined by Paxinos & Watson, 1998), 75 ± 7 cells/mm² in the somatosensory cortex (S1BF and S1Tr) and 68 ± 5 cells/mm² in the auditory cortex (Au1, Au and AuD). These results indicate that two subtypes of NG2(+) cells exist in the neocortex, based on the presence or absence of DCX co-expression. DCX(+)/NG2(-) cells were also very occasionally observed in the adult rat neocortex (asterisk in Fig. 2H–L).

It has been reported that immature neuron markers such as PSA-NCAM and DCX are expressed only in cells observed in the entorhinal and piriform cortex (Seki & Arai, 1991; Nacher *et al.*, 2001), and that the majority of DCX-expressing cells are

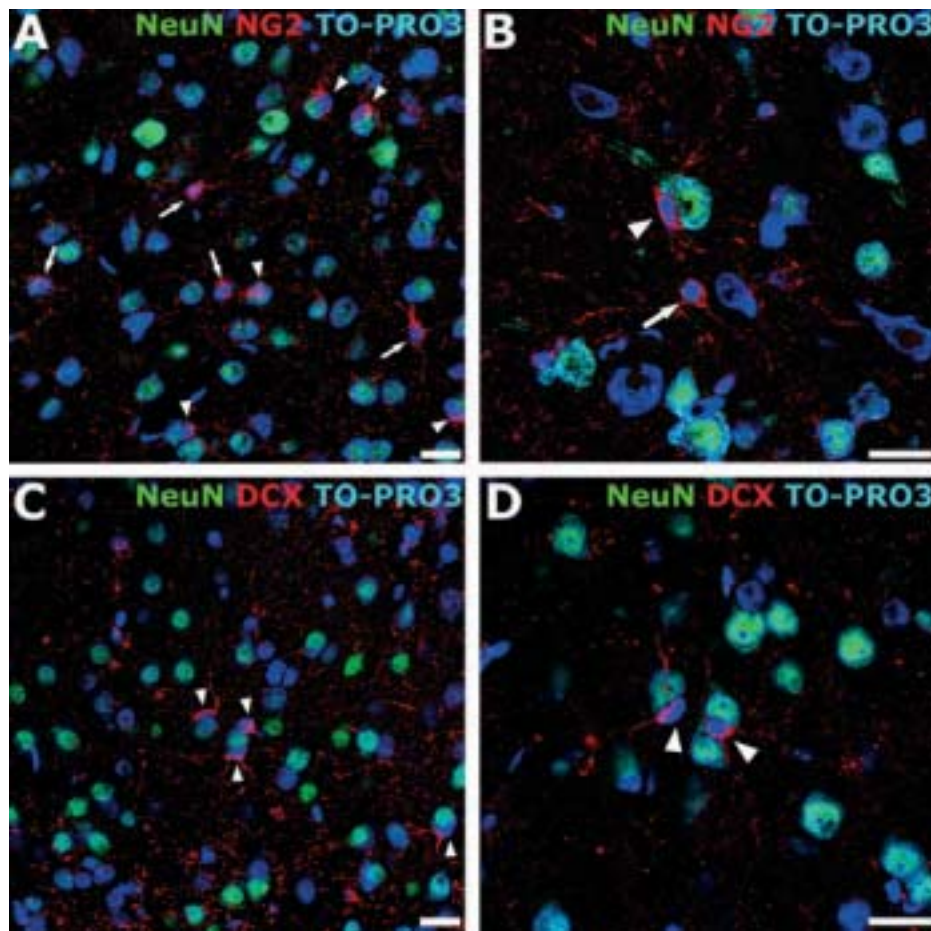


FIG. 1. The existence of NG2- or doublecortin (DCX)-positive cells in the neocortex of adult rats. (A) NG2(+) cells (red) were abundantly present in the neocortex. (B) An NG2(+) cell (arrowhead) close to NeuN(+) neuronal soma (green) and NG2(+) cell (arrow) out of the perineuronal territory. (C and D) DCX(+) cells (red) located in the perineuronal territory of NeuN(+) neurons (green). All cell nuclei and neuronal somata were stained with TO-PRO3. Scale bars: 20 μ m.

immunopositive for PSA-NCAM in these areas of adult rats (Nacher *et al.*, 2001). In the present study, we found DCX(+) cells throughout all layers of the neocortex including the motor cortex, somatosensory cortex and auditory cortex, in addition to the entorhinal cortex and piriform cortex. Triple staining revealed that the cortical DCX(+)/NG2(+) cells were not immunopositive for PSA-NCAM; Fig. 3 shows that PSA-NCAM was observed only in DCX(+)/NG2(-) cells (arrows), but not in DCX(+)/NG2(+) cells (arrowheads) in the piriform cortex. These observations indicate that DCX(+)/NG2(+) cells ubiquitously observed in the adult cortex and DCX(+)/PSA-NCAM(+) cells in the piriform cortex are distinct cell populations.

NG2(+) cells have been reported to be the major population of proliferating cells in the cerebral cortex of adult rats, based on analysis of BrdU-incorporated cell nuclei 2 h after BrdU injection (Dawson *et al.*, 2003; Dayer *et al.*, 2005; Kataoka *et al.*, 2006). In the present study, we determined whether cortical proliferating cells are DCX(+)/NG2(+) cells or DCX(-)/NG2(+) cells by triple staining for NG2, DCX and BrdU using the same BrdU labeling method (Table 1). Almost all the BrdU-incorporated cells ($94.2 \pm 1.8\%$; $n = 5$ animals) were DCX(+)/NG2(+) cells (Fig. 4A–D), while none of the DCX(-)/NG2(+) cells or DCX(+)/NG2(-) cells showed BrdU incorporation at 2 h after BrdU injection (Table 1). We also confirmed that almost all the Ki67-positive cells were DCX(+)/NG2(+) cells (data not shown), indicating that these cells are the major cell population entering the cell cycle. The remaining proliferating cells

were microglia showing immunoreactivity for OX-42 (data not shown).

We investigated cellular differentiation after proliferation of DCX(+)/NG2(+) cells in the adult neocortex by multiple immunodetection of cell differentiation markers and BrdU at various time points after BrdU injection. At 14 days after BrdU injection, approximately 80% ($79.5 \pm 3.8\%$), 10% ($9.5 \pm 3.4\%$) and 1% ($0.61 \pm 0.44\%$) of BrdU-labeled cells (1168 cells from five animals) were DCX(+)/NG2(+) (small arrow in Fig. 4E), DCX(-)/NG2(+) (big arrow in Fig. 4H) and DCX(+)/NG2(-) cells (arrowheads in Fig. 4E and I), respectively (Table 1). These results indicate that DCX(+)/NG2(+) cells may produce both DCX(+)/NG2(-) and DCX(-)/NG2(+) cells in addition to the reproduction of DCX(+)/NG2(+) cells. We performed other multiple immunohistochemical staining analyses of these cells to determine whether the cells were committed to the neuronal or glial cell lineage. TUC-4, a neuronal lineage marker (Seki, 2002), was found in all DCX(+)/NG2(-) cells ($n = 11$ cells at 14–28 days after BrdU injection; arrowhead in Fig. 5), but not in DCX(+)/NG2(+) or DCX(-)/NG2(+) cells, suggesting that the DCX(+)/NG2(-) cells were committed to the neuronal cell lineage after generation of the cells from DCX(+)/NG2(+) cells. We were unable to detect mature neuronal markers, including NeuN, γ -aminobutyric acid (GABA) or GAD-67, in BrdU-incorporated cells at 14 and 28 days after BrdU injection.

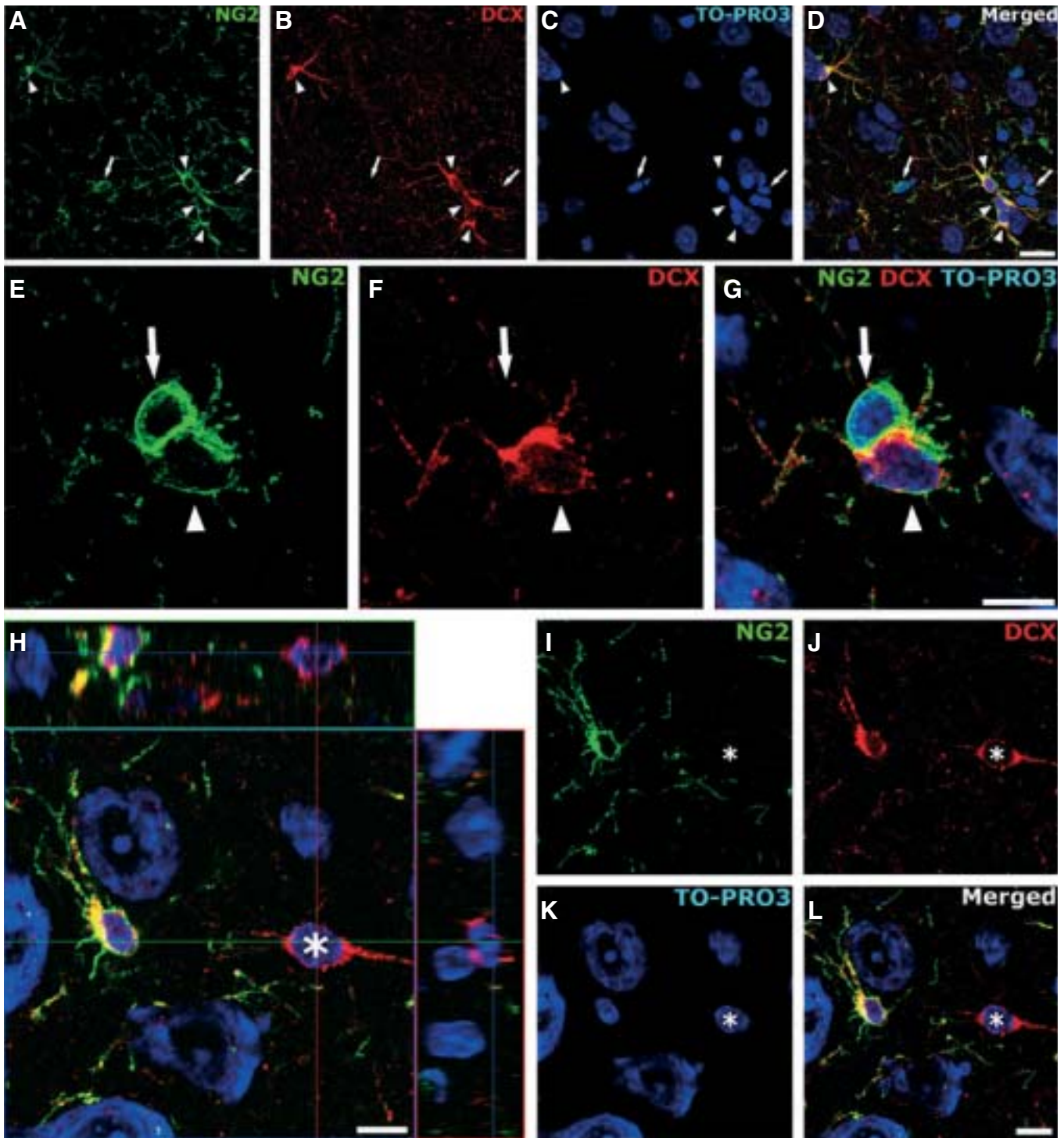


FIG. 2. Two subtypes of NG2(+) cells were distinguished with triple staining for NG2 (green), doublecortin (DCX; red) and TO-PRO3 (blue) in the neocortex. Arrowheads, DCX(+)/NG2(+) cells (yellow in D and G); arrows, DCX(-)/NG2(+) cells; asterisks, an NG2(-)/DCX(+) cell. Scale bars: 20 μ m (A–D); 10 μ m (E–L).

In order to examine differentiation of DCX(+)/NG2(+) cells into the glial lineage, we performed triple immunohistochemistry for BrdU, NG2 and GST-pi, an oligodendrocyte lineage marker, or for BrdU, DCX and GST-pi. At 14 days after BrdU injection, a portion of BrdU(+)/NG2(+) cells started to show faint immunoreactivity for GST-pi in the cytoplasm (Fig. 6A–D). GST-pi immunoreactivity was detected in all DCX(-)/NG2(+) cells found in this study, but not in

BrdU(+)/NG2(-) and BrdU(+)/DCX(+) cells. These findings suggested that only DCX(-)/NG2(+) cells were committed to the oligodendrocyte lineage at that time point. Furthermore, among the BrdU-labeled cells at Day 28, potent GST-pi immunoreactivity was observed only in DCX(-)/NG2(-) cells (Fig. 6E–H), and was faint in DCX(-)/NG2(+) cells, but not at all present in any DCX(+) cells (Table 1). Immunohistochemical staining for RIP (Friedman *et al.*,

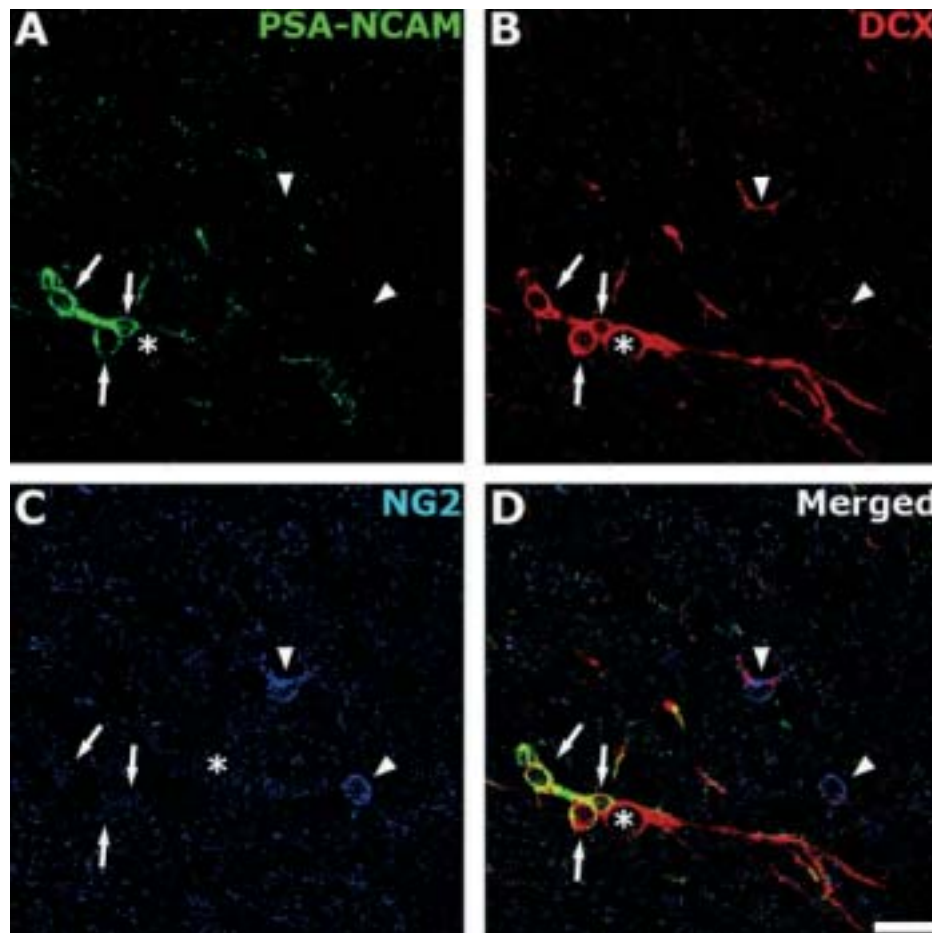


FIG. 3. Doublecortin (DCX)(+)/NG2(+) cells were a different population from DCX(+)/polysialyated form of neural cell adhesion molecule (PSA-NCAM)(+) cells in the piriform cortex. (A–D) Triple immunohistochemistry for PSA-NCAM (green), DCX (red) and NG2 (blue) in the piriform cortex. Arrowheads, DCX(+)/NG2(+) cells not immunopositive for PSA-NCAM; arrows, DCX(+)/PSA-NCAM(+) cells not immunopositive for NG2. Asterisks, DCX(+) cell not immunopositive for NG2 nor PSA-NCAM (referred to in Nacher *et al.*, 2001). Scale bar: 20 μ m.

TABLE 1. Percentages of cells immunopositive for various cell differentiation markers in all BrdU-labeled cells

	BrdU-labeled cells immunopositive for each marker after injection of BrdU (%)		
	After 2 h	After 14 days	After 28 days
DCX(+)/NG2(+)	94.2 \pm 1.8 (450/479)	79.5 \pm 3.8 (932/1168)	69.4 \pm 3.2 (584/843)
DCX(+)/NG2(-)	0 (0/479)	0.61 \pm 0.44 (7/1168)	0.52 \pm 0.69 (4/843)
DCX(-)/NG2(+)	0 (0/479)	9.5 \pm 3.4 (112/1168)	11.0 \pm 1.8 (95/843)
NG2(+)/GST-pi(+)	0 (0/213)	10.2 \pm 2.6 (52/519)	12.4 \pm 2.8 (48/373)
NG2(-)/GST-pi(+)	0 (0/213)	0 (0/519)	9.2 \pm 1.2 (35/373)

Data are presented as mean \pm SEM (%), $n = 5$ animals at each time point. The number of positive cells for each marker/number of BrdU-labeled cells is given in parentheses. DCX, doublecortin; GST, glutathione S-transferase.

1989), another mature oligodendrocyte marker, revealed that this immunoreactivity was detected in most of the DCX(-)/NG2(-)/GST-pi(+) cells (Fig. 6I–K).

Discussion

In the present study, we have provided novel evidence that the adult rat neocortex ubiquitously possesses DCX(+)/NG2(+) cells and that these cells are the major population of cortical cells involved in cell

reproduction. The DCX(+)/NG2(+) cells differentiate into two kinds of cell lineages [DCX(+)/NG2(-) cells and DCX(-)/NG2(+) cells] at 14–28 days after mitosis, as well as undergoing reproduction into identical cells. DCX(+)/NG2(-) cells were immunoreactive for TUC-4, a neuronal lineage marker, whereas DCX(-)/NG2(+) cells started to co-express an oligodendrocyte marker GST-pi. Furthermore, the NG2(+)/GST-pi(+) cells differentiated into new mature oligodendrocytes at 28 days. These results indicate that the DCX(+)/NG2(+) cells serve as cortical progenitor cells, retaining the potential to produce neuronal lineage cells and oligodendrocytes in the neocortex (Fig. 7).

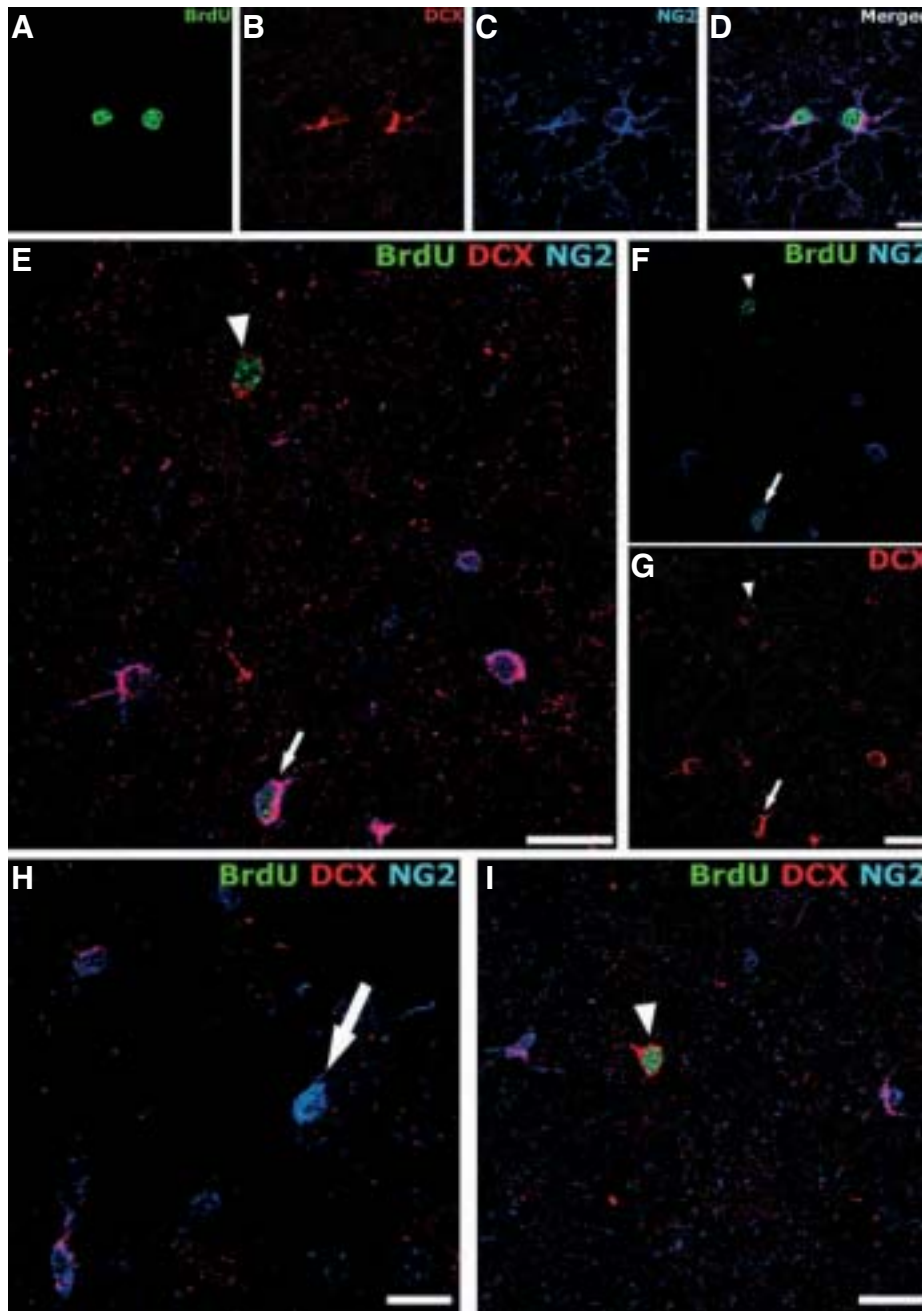


FIG. 4. (A–D) 5'-Bromodeoxyuridine (BrdU)-incorporated nuclei (green) in NG2(+)/doublecortin (DCX)(+) cells in the neocortex at 2 h after BrdU injection: (red), DCX; (blue), NG2. (E–I) Multi-differentiation of BrdU-labeled NG2(+)/DCX(+) cells in the neocortex at 14 days after BrdU injection: BrdU (green), DCX (red) and NG2 (blue). Arrowheads in (E–G), BrdU-labeled DCX(+)/NG2(-) cells; (E–G) indicate the same area. Small arrows in (E–G), a BrdU-labeled DCX(+)/NG2(+) cell. Big arrow in (H), a BrdU-labeled DCX(-)/NG2(+) cell. Scale bars: 10 μm (A–D); 20 μm (E–I).

Two subtypes of NG2-positive cells in the neocortex of adult rats

It has been known that NG2(+) cells abundantly and broadly exist in the cerebral cortex of adult rats. We observed that $1.2 \pm 0.4\%$ and $1.8 \pm 0.7\%$ of NG2(+) cells (813 cells and 946 cells from five animals) in the neocortex were immunoreactive for BrdU and Ki67, respectively, 2 h after BrdU injection. The findings suggested that few cortical NG2(+) cells are involved in the cell cycle, and are supported by a previous report that only 1.5% of all NG2-positive cells are labeled with BrdU 2 h after BrdU injection (Dawson *et al.*, 2003). In the spinal cord of adult rats, two subtypes of NG2-positive cells were

argued based on their response to experimental demyelination (Keirstead *et al.*, 1998). Thus, we assumed that two distinct populations of NG2(+) cells were also present in the adult cortex, and confirmed this finding based on co-expression of DCX (Fig. 2). Proliferative activity was observed only in the DCX(+)/NG2(+) cells, but not in the DCX(-)/NG2(+) cells (Fig. 4D). Furthermore, we confirmed that none of the DCX(+)/NG2(+) cells in the neocortex was immunopositive for GFAP or nestin. Our previous studies showed that the majority of proliferating cells are located close to the neuronal somata (the perineuronal territory) in the cerebral cortex of adult rats (Kataoka *et al.*, 2006). Indeed, in the present study, most of the

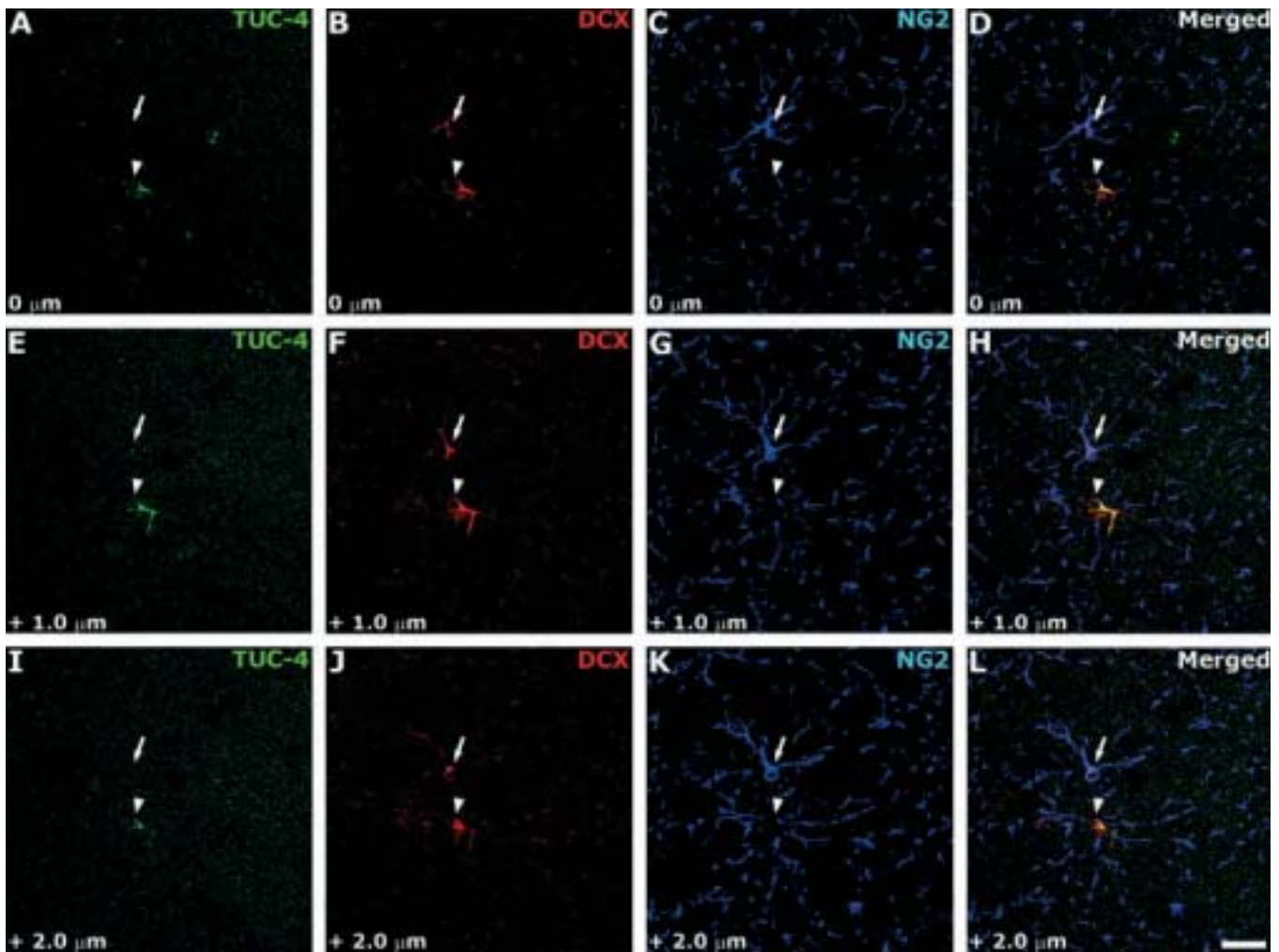


FIG. 5. A neuronal lineage marker (TUC-4)-expressing doublecortin (DCX)(+)/NG2(-) cells. Sequential confocal images (0 to +2 μm ; A–D, 0 μm ; E–H, +1.0 μm ; I–L, +2.0 μm) captured at 1- μm intervals for TUC-4 (green), DCX (red) and NG2 (blue). Arrowheads, DCX(+)/NG2(-) cells immunopositive for TUC-4; arrows, DCX(+)/NG2(+) cells not immunopositive for TUC-4. Scale bar: 20 μm .

DCX(+)/NG2(+) cells were observed in the perineuronal territory, and many DCX(-)/NG2(+) cells were outside this area (data not shown). These findings suggest that the DCX(+)/NG2(+) cells are 'cortical progenitor cells' in the neocortex.

Existence of DCX(+) cells in the adult neocortex

In the present study, we observed that the DCX(+)/NG2(+) cells exist throughout the neocortex of adult rats under physiological conditions (Fig. 2). However, previous studies in adult rats have reported that DCX(+) cells are observed only in cortical layers II or III of the piriform cortex, and in layer II of the entorhinal, perirhinal and insular cortex (Nacher *et al.*, 2001, 2004), but not in the neocortex more dorsal to these regions (Jin *et al.*, 2003; Yang *et al.*, 2004; Dayer *et al.*, 2005). Indeed, the intensity of DCX immunoreactivity in the DCX(+)/NG2(+) cells observed in the present study was weaker than that in the previously reported DCX(+) cells in the piriform cortex (Fig. 3D). Thus, we could barely immunodetect DCX in the DCX(+)/NG2(+) cells at lower magnifications using a confocal laser-scanning microscope; however, we were able to successfully detect them at higher magnifications, i.e. $\times 40$ or $\times 63$ at the objective lens. Furthermore, we confirmed the expression of DCX in the neocortex

using Western blot analysis; a single 40-kDa band of DCX protein (Brown *et al.*, 2003) was detected in tissue homogenates prepared from the parietal cortical tissue as well as piriform cortex (data not shown).

Cellular differentiation of the DCX(+)/NG2(+) cells

In the current study, we showed that DCX(+)/NG2(-) cells are generated from DCX(+)/NG2(+) cells in the neocortex of adult rats using BrdU-labeling methods (Fig. 4 and Table 1), and that all the DCX(+)/NG2(-) cells contain TUC-4 (Fig. 5). In the dentate gyrus of the hippocampus, it has been shown that a subset of NG2(+) cells can differentiate into GABAergic neurons, upregulating the expression of TOAD-64 (referred to as TUC-4) and downregulating the expression of NG2 (Belachew *et al.*, 2003). We confirmed that the NG2(+) cells in the dentate gyrus were also immunoreactive for DCX (data not shown). Furthermore, DCX-expressing NG2(+) progenitor cells are also observed in the anterior SVZ, and these cells differentiate into GABAergic interneurons in the olfactory bulb. Such NG2(+) cells of these neurogenic regions differentiate into GABAergic interneurons following downregulation of the NG2 expression (Aguirre & Gallo, 2004). The possibility exists that the DCX(+)/NG2(+) cells in the

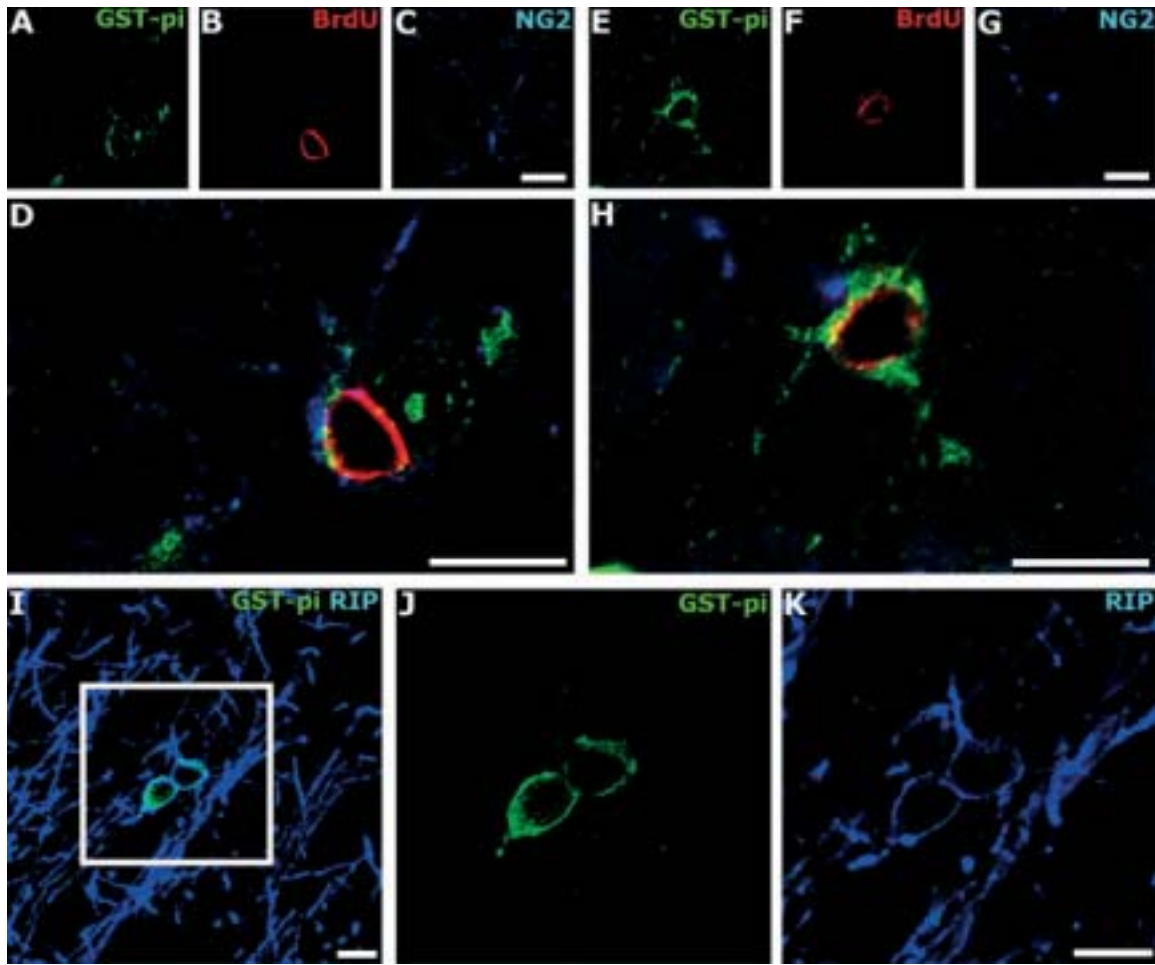


FIG. 6. Glial lineage markers expressing DCX(-)/NG2(+) cells. (A–D) A 5'-bromodeoxyuridine (BrdU)-labeled NG2(+)/glutathione S-transferase (GST)-pi(+) cell in the neocortex at 14 days after BrdU injection. (E–H) A BrdU-labeled NG2(-)/GST-pi(+) cell in the neocortex at 28 days after BrdU injection: GST-pi (green), BrdU (red) and NG2 (blue). (I–K) Two GST-pi(+)/RIP(+) cells in the neocortex, GST-pi (green) and RIP (blue). (G and K) Magnified views of the area indicated by a white square in (I). Scale bars: 10 μm.

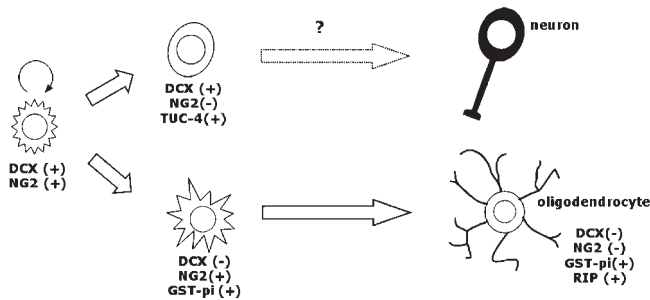


FIG. 7. Schematic representation of a hypothetical differentiation model of doublecortin (DCX)(+)/NG2(+) cells in the adult neocortex. DCX(+)/NG2(+) cells reproduce the identical cells, DCX(+)/NG2(-) cells and DCX(+)/NG2(-) cells. In the neuronal lineage, newly generated DCX(+)/NG2(-) cells show TUC-4 immunoreactivity. In the oligodendrocyte differentiation, newly generated DCX(-)/NG2(+) cells show glutathione S-transferase (GST)-pi immunoreactivity, and the cells further differentiate into mature oligodendrocytes immunopositive for GST-pi and RIP. During oligodendrocyte differentiation, the expression of NG2 is downregulated, whereas that of cytoplasmic GST-pi is upregulated.

adult neocortex also differentiate into GABAergic interneurons with downregulation of NG2 expression. In the present study, we were able to demonstrate that neocortical DCX(+)/NG2(+) cells have the

potential to give rise to DCX(+)/NG2(-) cells committed to neuronal lineage cells, but found that none of the cells indicated immunohistochemical characteristics of mature GABAergic neurons. Under such a low-stimulative environment as in the present experiment, rodent neocortex might not need to generate new neurons. In fact, it has been reported that neurogenesis occurs in the cerebral cortex of adult mice under pathological conditions (Magavi *et al.*, 2000). Furthermore, in the present study we were unable to determine the fates and functions of newly generated DCX(+)/NG2(-) cells in the neocortex. Although those cells were not immunohistochemically mature neurons, such neuronal lineage cells might have physiological functions even at immature stages. A subpopulation of immature cells in the cortex has been reported to show physiological properties, including ion channel expression profiles and depolarization-induced multiple spikes (Chittajallu *et al.*, 2004).

At 2 h after BrdU injection, a small number of dividing cells were OX-42(+) microglia. Thus, we cannot rule out the possibility that the DCX(+)/NG2(-) cells were generated from the microglia *in situ* in the neocortex. However, until now microglia has not been reported to give rise to neurons or other glial cells, including astrocytes, oligodendrocytes and NG2(+) glial progenitor cells in the adult brain under physiological conditions. Indeed, we observed that none of the OX-42(+) cells was immunoreactive for NG2 and/or DCX in the

neocortex. The origin of the newly generated DCX(+)/NG2(-) cells may be related to BrdU(+)/DCX(+) cells originating in the SVZ migrating into the neocortex under pathological conditions, as shown by Magavi *et al.* (2000). In the neonatal brain, newly generated DCX(+) cells have also been reported to migrate from the SVZ to the cerebral cortex (Suzuki & Goldman, 2003; Fagel *et al.*, 2006). The vast majority of the DCX(+) young neurons migrating from the SVZ have been known to express PSA-NCAM (Doetsch *et al.*, 1997, 1999; Fagel *et al.*, 2006). However, the newly generated DCX(+)/NG2(-) cells observed in the present study were not immunopositive for PSA-NCAM (data not shown). Based on these findings we suggest that the DCX(+)/NG2(-) cells were likely derived from the DCX(+)/NG2(+) cells *in situ* in the neocortical parenchyma.

Dawson *et al.* (2003) suggested that cortical NG2(+) cells can generate new oligodendrocytes, by finding BrdU-labeled cells expressing 2',3'-cyclic nucleotide 3'-phosphodiesterase (CNPase), an oligodendrocyte marker. However, that study did not trace the differentiation between NG2-expressing cells and CNPase-expressing mature oligodendrocytes, and could not show that NG2(+) cells were on the identical cell lineage path of mature oligodendrocytes. In the present study, using GST-pi, an oligodendrocyte lineage marker, we were able to trace every stage of oligodendrocyte differentiation by NG2(+)/GST-pi(+) cells from DCX(+)/NG2(+) progenitor cells to NG2(-)/GST-pi(+) mature oligodendrocytes (Fig. 6A–H and Table 1). The NG2(-)/GST-pi(+) cells were confirmed to be mature oligodendrocytes by observation of immunoreactivity for RIP, a mature oligodendrocyte marker (Fig. 6I). These results are in agreement with previous reports indicating maturation of oligodendrocytes following the downregulation of NG2 expression (Nishiyama *et al.*, 1996) and the progressive expression of RIP (Friedman *et al.*, 1989). We have provided the first evidence that cortical NG2(+) cells co-expressing a neuronal marker reproduce mature oligodendrocytes.

It has been reported that NG2(+) cells may give rise to GFAP(+) astrocytes in the cerebral cortex of adult rats (Dawson *et al.*, 2003). In the present study, BrdU-labeled GFAP(+) astrocytes were infrequently found in the adult neocortex at 28 days after BrdU injection (less than 1%, 2/456 cells from five animals). Thus, perineuronal DCX(+)/NG2(+) cells might differentiate into astrocytes as well as oligodendrocytes and neurons. We previously demonstrated that neural excitation stimulates cellular proliferation of the perineuronal cells (Tamura *et al.*, 2004; Kataoka *et al.*, 2006), and such an excitation facilitates the production of GFAP(+) astrocytes (unpublished observation). These observations suggest that local neural activity controls the production rates of astrocytes, oligodendrocytes and neurons by regulating the proliferation rate and the direction of the differentiation of the DCX(+)/NG2(+) cells.

Acknowledgements

This work was supported in part by Special Coordination Funds for Promoting Science and Technology from the Ministry of Education, Culture, Sports, Science and Technology, Japan to Y.K., by a consignment expense from the Molecular Imaging Program on 'Research Base for Exploring New Drugs' from the Ministry of Education, Culture, Sports, Science and Technology to Y.W., and by a Grant-in-Aid for Scientific Research from the Japan Society for Promotion of Science to Y.K. and H.Y.

Abbreviations

BrdU, 5'-bromodeoxyuridine; CNPase, 2',3'-cyclic nucleotide 3'-phosphodiesterase; DCX, doublecortin; GABA, γ -aminobutyric acid; GFAP, glial fibrillary acidic protein; GST, glutathione S-transferase; PBS, phosphate-buffered saline; PBST, 0.3% Triton X-100 in PBS; PSA-NCAM, polysialated form of neural cell adhesion molecule; SVZ, subventricular zone.

References

- Aguirre, A. & Gallo, V. (2004) Postnatal neurogenesis and gliogenesis in the olfactory bulb from NG2-expressing progenitors of the subventricular zone. *J. Neurosci.*, **24**, 10530–10541.
- Belachew, S., Chittajallu, R., Aguirre, A.A., Yuan, X., Kirby, M., Anderson, S. & Gallo, V. (2003) Postnatal NG2 proteoglycan-expressing progenitor cells are intrinsically multipotent and generate functional neurons. *J. Cell Biol.*, **161**, 169–186.
- Brown, J.P., Couillard-Despres, S., Cooper-Kuhn, C.M., Winkler, J., Aigner, L. & Kuhn, H.G. (2003) Transient expression of doublecortin during adult neurogenesis. *J. Comp. Neurol.*, **467**, 1–10.
- Cameron, H.A., Woolley, C.S., McEwen, B.S. & Gould, E. (1993) Differentiation of newly born neurons and glia in the dentate gyrus of the adult rat. *Neuroscience*, **56**, 337–344.
- Chittajallu, R., Aguirre, A. & Gallo, V. (2004) NG2-positive cells in the mouse white and grey matter display distinct physiological properties. *J. Physiol.*, **561**, 109–122.
- Dawson, M.R., Polito, A., Levine, J.M. & Reynolds, R. (2003) NG2-expressing glial progenitor cells: an abundant and widespread population of cycling cells in the adult rat CNS. *Mol. Cell. Neurosci.*, **24**, 476–488.
- Dayer, A.G., Cleaver, K.M., Abouantoun, T. & Cameron, H.A. (2005) New GABAergic interneurons in the adult neocortex and striatum are generated from different precursors. *J. Cell Biol.*, **168**, 415–427.
- Doetsch, F., Caille, I., Lim, D.A., Garcia-Verdugo, J.M. & Alvarez-Buylla, A. (1999) Subventricular zone astrocytes are neural stem cells in the adult mammalian brain. *Cell*, **97**, 703–716.
- Doetsch, F., Garcia-Verdugo, J.M. & Alvarez-Buylla, A. (1997) Cellular composition and three-dimensional organization of the subventricular germinal zone in the adult mammalian brain. *J. Neurosci.*, **17**, 5046–5061.
- Doetsch, F., Petreanu, L., Caille, I., Garcia-Verdugo, J.M. & Alvarez-Buylla, A. (2002) EGF converts transit-amplifying neurogenic precursors in the adult brain into multipotent stem cells. *Neuron*, **36**, 1021–1034.
- Fagel, D.M., Ganat, Y., Silbereis, J., Ebbitt, T., Stewart, W., Zhang, H., Ment, L.R. & Vaccarino, F.M. (2006) Cortical neurogenesis enhanced by chronic perinatal hypoxia. *Exp. Neurol.*, **199**, 77–91.
- Friedman, B., Hockfield, S., Black, J.A., Woodruff, K.A. & Waxman, S.G. (1989) *In situ* demonstration of mature oligodendrocytes and their processes: an immunocytochemical study with a new monoclonal antibody, rip. *Glia*, **2**, 380–390.
- Gage, F.H., Coates, P.W., Palmer, T.D., Kuhn, H.G., Fisher, L.J., Suhonen, J.O., Peterson, D.A., Suhr, S.T. & Ray, J. (1995) Survival and differentiation of adult neuronal progenitor cells transplanted to the adult brain. *Proc. Natl Acad. Sci. USA*, **92**, 11879–11883.
- Gritti, A., Frolichsthal-Schoeller, P., Galli, R., Parati, E.A., Cova, L., Pagano, S.F., Bjornson, C.R. & Vescovi, A.L. (1999) Epidermal and fibroblast growth factors behave as mitogenic regulators for a single multipotent stem cell-like population from the subventricular region of the adult mouse forebrain. *J. Neurosci.*, **19**, 3287–3297.
- Jin, K., Sun, Y., Xie, L., Peel, A., Mao, X.O., Bateur, S. & Greenberg, D.A. (2003) Directed migration of neuronal precursors into the ischemic cerebral cortex and striatum. *Mol. Cell. Neurosci.*, **24**, 171–189.
- Kataoka, Y., Tamura, Y., Takamori, Y., Cui, Y. & Yamada, H. (2006) Perineuronal germinal cells in the rat cerebral cortex. *Med. Mol. Morphol.*, **39**, 28–32.
- Keirstead, H.S., Levine, J.M. & Blakemore, W.F. (1998) Response of the oligodendrocyte progenitor cell population (defined by NG2 labelling) to demyelination of the adult spinal cord. *Glia*, **22**, 161–170.
- Lois, C. & Alvarez-Buylla, A. (1993) Proliferating subventricular zone cells in the adult mammalian forebrain can differentiate into neurons and glia. *Proc. Natl Acad. Sci. USA*, **90**, 2074–2077.
- Magavi, S.S., Leavitt, B.R. & Macklis, J.D. (2000) Induction of neurogenesis in the neocortex of adult mice. *Nature*, **405**, 951–955.
- Morshead, C.M., Reynolds, B.A., Craig, C.G., McBurney, M.W., Staines, W.A., Morassutti, D., Weiss, S. & van der Kooy, D. (1994) Neural stem cells in the adult mammalian forebrain: a relatively quiescent subpopulation of subependymal cells. *Neuron*, **13**, 1071–1082.
- Nacher, J., Crespo, C. & McEwen, B.S. (2001) Doublecortin expression in the adult rat telencephalon. *Eur. J. Neurosci.*, **14**, 629–644.
- Nacher, J., Pham, K., Gil-Fernandez, V. & McEwen, B.S. (2004) Chronic restraint stress and chronic corticosterone treatment modulate differentially the expression of molecules related to structural plasticity in the adult rat piriform cortex. *Neuroscience*, **126**, 503–509.

- Nishiyama, A., Chang, A. & Trapp, B.D. (1999) NG2+ glial cells: a novel glial cell population in the adult brain. *J. Neuropathol. Exp. Neurol.*, **58**, 1113–1124.
- Nishiyama, A., Lin, X.H., Giese, N., Heldin, C.H. & Stallcup, W.B. (1996) Interaction between NG2 proteoglycan and PDGF alpha-receptor on O2A progenitor cells is required for optimal response to PDGF. *J. Neurosci. Res.*, **43**, 315–330.
- Palmer, T.D., Markakis, E.A., Willhoite, A.R., Safar, F. & Gage, F.H. (1999) Fibroblast growth factor-2 activates a latent neurogenic program in neural stem cells from diverse regions of the adult CNS. *J. Neurosci.*, **19**, 8487–8497.
- Paxinos, G. & Watson, C. (1998) *The Rat Brain in Stereotaxic Coordinates*, 4th Edn. Academic Press, San Diego.
- Seki, T. (2002) Expression patterns of immature neuronal markers PSA-NCAM, CRMP-4 and NeuroD in the hippocampus of young adult and aged rodents. *J. Neurosci. Res.*, **70**, 327–334.
- Seki, T. & Arai, Y. (1991) Expression of highly polysialylated NCAM in the neocortex and piriform cortex of the developing and the adult rat. *Anat. Embryol. (Berl.)*, **184**, 395–401.
- Seri, B., Garcia-Verdugo, J.M., McEwen, B.S. & Alvarez-Buylla, A. (2001) Astrocytes give rise to new neurons in the adult mammalian hippocampus. *J. Neurosci.*, **21**, 7153–7160.
- Suzuki, S.O. & Goldman, J.E. (2003) Multiple cell populations in the early postnatal subventricular zone take distinct migratory pathways: a dynamic study of glial and neuronal progenitor migration. *J. Neurosci.*, **23**, 4240–4250.
- Tamura, Y., Kataoka, Y., Cui, Y. & Yamada, H. (2004) Cellular proliferation in the cerebral cortex following neural excitation in rats. *Neurosci. Res.*, **50**, 129–133.
- Yang, H.K., Sundholm-Peters, N.L., Goings, G.E., Walker, A.S., Hyland, K. & Szele, F.G. (2004) Distribution of doublecortin expressing cells near the lateral ventricles in the adult mouse brain. *J. Neurosci. Res.*, **76**, 282–295.

INTRACELLULAR TRANSLOCATION OF GLUTATHIONE S-TRANSFERASE PI DURING OLIGODENDROCYTE DIFFERENTIATION IN ADULT RAT CEREBRAL CORTEX *IN VIVO*

Y. TAMURA,^{a,b,c} Y. KATAOKA,^{a,b,c*} Y. CUI,^{a,b,c}
Y. TAKAMORI,^a Y. WATANABE^{b,c} AND H. YAMADA^a

^aDepartment of Anatomy and Cell Science, KMU 21C COE Project, Kansai Medical University, 10-15 Fumizono-cho, Moriguchi, Osaka 570-8506, Japan

^bMolecular Imaging Research Program, Frontier Research System, RIKEN, 6-7-3 Minatojima minamimachi, Chuo-ku, Kobe 650-0047, Japan

^cDepartment of Physiology, Osaka City University Graduate School of Medicine, 1-4-3 Asahimachi, Abeno-ku, Osaka 545-8585, Japan

Abstract—Glutathione S-transferase (GST)-pi is a cytosolic isoenzyme used as a marker for mature oligodendrocytes in the mammalian brain. However, the cellular properties of GST-pi-immunoreactive [GST-pi (+)] cells in adult brain are not completely understood. We immunohistochemically demonstrated the existence of two subtypes of GST-pi (+) cells in the cerebral cortex of adult rats: one subtype exhibited GST-pi in the cytoplasm (C-type cells), while the other did mainly in the nucleus (N-type cells). The GST-pi (+) C-type cells were also immunopositive for 2',3'-cyclic nucleotide 3'-phosphodiesterase and RIP, indicating that they were mature oligodendrocytes, while the GST-pi (+) N-type cells expressed NG2, indicating that they were oligodendrocyte progenitor cells. Furthermore, observation of the fate of newly-generated cells by 5-bromodeoxyuridine-labeling revealed that the GST-pi (+) N-type cells differentiated into C-type cells. These findings indicate translocation of GST-pi from the nucleus to the cytoplasm during oligodendrocyte maturation. © 2007 IBRO. Published by Elsevier Ltd. All rights reserved.

Key words: oligodendrocyte progenitor cells, NG2, CNPase, RIP, BrdU.

Glutathione S-transferases (GSTs) are phase II detoxification enzymes that catalyze the conjugation of various xenobiotic and endogenous electrophiles with reduced glutathione. The mammalian GSTs consist of eight distinct classes (alpha, mu, pi, theta, sigma, kappa, zeta, and omega) separable on the basis of their biological properties (Mannervik et al., 1985; Meyer et al., 1991; Meyer and Thomas, 1995; Pemble et al., 1996; Board et al., 1997, 2000). The GST isoenzymes are widely expressed and

*Correspondence to: Y. Kataoka, Department of Physiology, Osaka City University Graduate School of Medicine, 1-4-3 Asahimachi, Abeno-ku, Osaka 545-8585, Japan. Tel: +81-6-6645-3711; fax: +81-6-6645-3712.

E-mail address: kataokay@med.osaka-cu.ac.jp (Y. Kataoka).

Abbreviations: BrdU, 5-bromodeoxyuridine; CNPase, 2',3'-cyclic nucleotide 3'-phosphodiesterase; GST, glutathione S-transferase; PBS, phosphate-buffered saline; PBST, 0.3% Triton X-100 in phosphate-buffered saline.

0306-4522/07\$30.00+0.00 © 2007 IBRO. Published by Elsevier Ltd. All rights reserved.
doi:10.1016/j.neuroscience.2007.06.026

distributed among several types of tissue including the brain (Theodore et al., 1985; Li et al., 1986; Abramovitz and Listowsky, 1987). Three GST isoenzymes (alpha, mu, and pi) have been observed in neurons and glial cells in the brain: GST-alpha is expressed in the nuclei of neurons of the rat brain (Johnson et al., 1993); GST-mu is expressed in glial fibrillary acidic protein (GFAP)-immunopositive astrocytes, but in neither neurons nor oligodendrocytes in rat brain (Abramovitz et al., 1988; Cammer and Zhang, 1992); and GST-pi is found in the cytoplasm of mature oligodendrocytes, which are immunopositive for 2',3'-cyclic nucleotide 3'-phosphodiesterase (CNPase), in rodent cerebral cortex (Cammer et al., 1989; Tansey and Cammer, 1991). Of these three GSTs, GST-pi has been used as a specific marker protein for mature oligodendrocytes in the mammalian adult brain (Tanaka et al., 2003; Mason et al., 2004; Gotts and Chesselet, 2005). However, it was recently reported that glial cells containing GST-pi protein in both the cytoplasm and nucleus were observed in the gray and white matter of normal human brain (Terrier et al., 1990). Thus, the properties of these GST-pi (+) cells have yet to be determined.

In the present study, we investigated the properties of GST-pi (+) C-type cells and GST (+) N-type cells using several specific markers of the oligodendrocyte lineage, including differentiation state-specific markers. Furthermore, cell differentiation processes in this lineage were observed using a flash labeling method with 5-bromodeoxyuridine (BrdU).

EXPERIMENTAL PROCEDURES

Animals and BrdU injections

Adult male Wistar rats (SLC, Hamamatsu, Japan; 250–350 g body weight) were used. All experimental protocols were approved by the Ethics Committee on Animal Care and Use of Kansai Medical University and were performed in accordance with the Principles of Laboratory Animal Care (NIH Publication No. 85-23, revised 1985). Every effort was made to minimize the number of animals used and their suffering. In order to label proliferating cells, rats ($n=9$) were intraperitoneally injected with BrdU diluted with saline (50 mg/kg body weight).

Histochemistry

Animals were deeply anesthetized with diethyl ether and perfused transcardially with 4% formaldehyde buffered with 0.1 M phosphate-buffered saline (PBS; pH 7.4) 2 h, 14 days, and 28 days after BrdU injection. The brains were removed, post-fixed in 4% formaldehyde buffered with 0.1 M PBS overnight at 4 °C, and then immersed in 20% (w/v) sucrose solution. Coronal brain sections

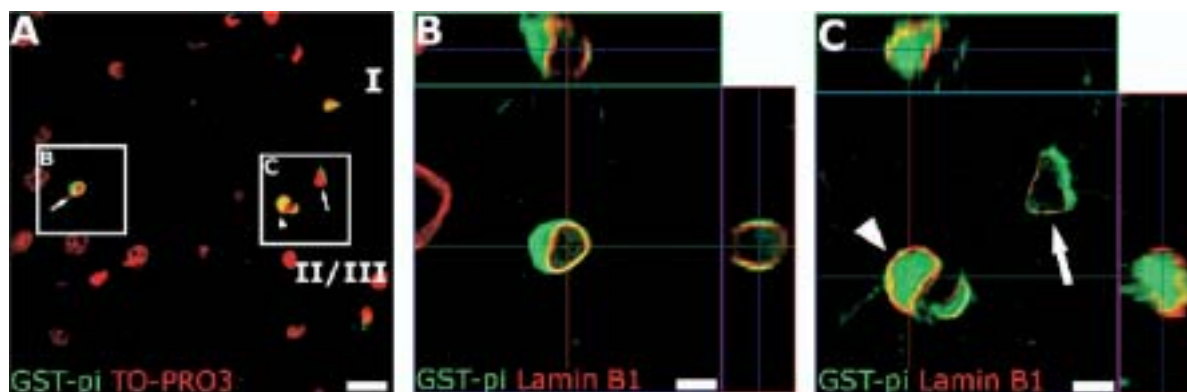


Fig. 1. Two subtypes of GST-pi (+) cells in cerebral cortex. (A) Double staining for GST-pi (green) and TO-PRO3 (red) in cortical layers I and II–III of somatosensory cortex reveals two subtypes of GST-pi (+) cells; arrows indicate cytoplasmic GST-pi (+) cells, while the arrowhead indicates a nuclear GST-pi (+) cell on the image of a single z-slice. (B, C) Single-z-slice images with ortho-images of confocal z-stacks (upper and right panels in B and C) of GST-pi (+) cells in the areas indicated by boxes in A. Double-immunostaining for GST-pi (green) and lamin B1 (red) reveals that GST-pi (+) cells include both GST-pi (+) C-type cells, which exhibit immunoreactivity for GST-pi in the cytoplasm (B, and arrow in C), and a GST-pi (+) N-type cell, which exhibits immunoreactivity mainly within the nucleus (arrowhead in C). Scale bars=20 μm in (A); 5 μm (B, C).

(30- μm thickness, 0.26 mm to 3.80 mm posterior to bregma) were prepared using a cryostat and collected as free-floating sections.

For detection of BrdU incorporation, brain sections were pre-incubated in 50% formamide/2 \times saline–sodium citrate buffer for 2 h at 65 $^{\circ}\text{C}$, incubated in 2 N HCl for 30 min at 37 $^{\circ}\text{C}$, rinsed in 0.1 M boric acid (pH 8.5) for 10 min at 25 $^{\circ}\text{C}$, and then washed with 0.3% Triton X-100 in phosphate-buffered saline (PBST), as described previously (Tamura et al., 2004). For multiplex-immunostaining, brain sections were incubated with several primary antibodies at 4 $^{\circ}\text{C}$ for 12–36 h. The primary antibodies used in this study were as follows: monoclonal mouse anti-GST-pi IgG (1:1000, BD Biosciences, San Jose, CA, USA), polyclonal rabbit anti-GST-pi IgG (1:500, Medical and Biological Laboratories, Nagoya, Japan), monoclonal rat anti-BrdU IgG (1:10, Oxford Biotechnology, Oxford, UK), polyclonal rabbit anti-Ki67 IgG (1:1000, Novocastra, Newcastle, UK), monoclonal mouse anti-NG2 IgG (1:200, Chemicon, Temecula, CA, USA), polyclonal rabbit anti-NG2 IgG (1:200, Chemicon), monoclonal mouse anti-CNPase IgG (1:20,000, Sigma, Taufkirchen, Germany), monoclonal mouse anti-oligodendrocytes (clone RIP) IgG (1:20,000, Chemicon), and polyclonal goat anti-lamin B1 IgG (1:100, Santa Cruz Biotechnology, Santa Cruz, CA, USA). After washing with PBST for 30 min, brain sections were incubated with secondary antibodies conjugated with Cy2, Cy3, or Cy5 (1:200, Jackson ImmunoResearch, West Grove, PA, USA) for 4 h at 4 $^{\circ}\text{C}$ and washed with PBST for 30 min. The sections were mounted with TO-PRO3-containing solution (Molecular Probes, Eugene, OR, USA) and examined using a confocal laser microscope (LSM510META Ver. 3.2; Carl Zeiss, Oberkochen, Germany).

Cell counting procedure

Two brain sections were randomly selected from each animal. The number of cells expressing each oligodendrocyte lineage marker among GST-pi (+) cells was counted in 72 square areas (150 $\mu\text{m} \times 150 \mu\text{m}$, 12 square areas in each hemisphere) randomly positioned in layers I–VI of cerebral cortex (motor cortex, M1 and M2; somatosensory cortex, S1BF, S1DZ, S1FL, S1HL, and S1Tr; and auditory cortex, Au1, AuD, and AuV; as defined by Paxinos and Watson, 1998). The number of cells expressing each cellular marker among all BrdU-labeled cells was counted in the same area of each animal. Data from each animal were averaged.

RESULTS

Two subtypes of GST-pi (+) cells

GST-pi (+) cells were widely present throughout layers I–VI of cerebral cortex of adult rats. Double staining for GST-pi and TO-PRO3, a DNA marker, which allows visualization of all cells, especially the nuclei, revealed two different types of GST-pi (+) cells on the basis of intracellular distribution of GST-pi immunoreactivity: cells exhibiting GST-pi immunoreactivity in the cytoplasm (C-type cells, arrows in Fig. 1A) and those exhibiting immunoreactivity in the nucleus (N-type cells, arrowhead in Fig. 1A). In order to visualize the nuclear membrane, immunohistochemical staining for lamin B1, a nuclear envelope protein (Kataoka et al., 2006; Takamori et al., 2007), was performed. Confocal z-series analysis of double-immunofluorescence staining for GST-pi and lamin B1 clearly showed that the C-type cells contained GST-pi mainly in the cytoplasm and little within the nucleus (Fig. 1B and arrow in Fig. 1C), while N-type cells contained this protein mainly in the nucleus and in small amounts in the cytoplasm, especially around the nucleus (arrowhead in Fig. 1C).

Expression of GST-pi in oligodendrocyte-lineage cells

To examine the features of GST-pi (+) C-type and N-type cells in the cerebral cortex, we performed double-immunofluorescence staining using mature oligodendrocyte cell markers (CNPase and RIP). All the cells immunopositive for CNPase were GST-pi (+) cells (arrows in Fig. 2A). However, GST-pi (+) cells without CNPase were also observed (arrowheads in Fig. 2A). Cell counting revealed that $72.6 \pm 2.8\%$ (mean \pm S.D., $n = 1389$ cells from three animals) and $72.4 \pm 1.5\%$ (mean \pm S.D., $n = 1338$ cells from three animals) of GST-pi (+) cells were CNPase (+) and RIP (+), respectively. The distribution of CNPase (+) cells was very similar to that of RIP (+) cells. The antigen recognized with the RIP antibody has recently been iden-

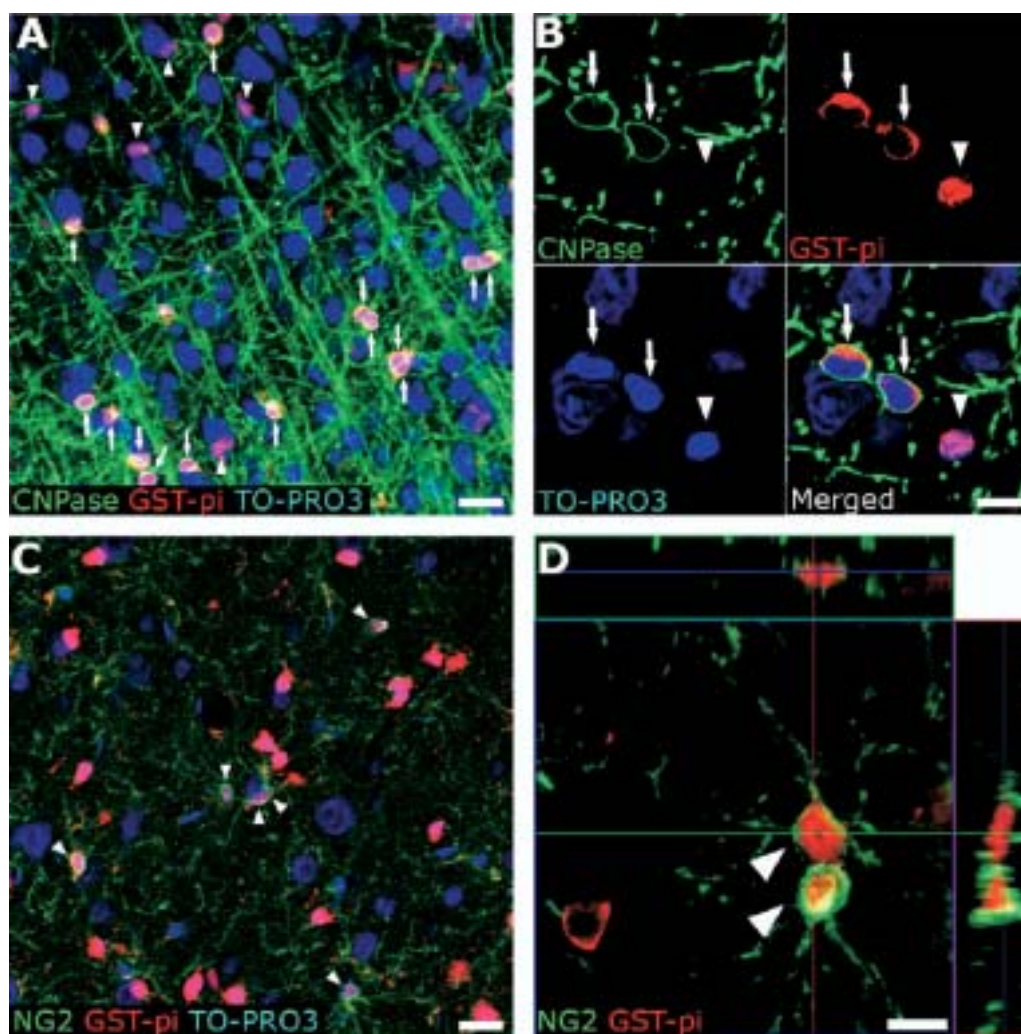


Fig. 2. Phenotypes of GST-pi (+) cells in cerebral cortex. (A, B) Triple staining for CNPase (green), GST-pi (red), and TO-PRO3 (blue) on images of single z-slices. Arrows, GST-pi (+)/CNPase (+) cells; arrowheads, GST-pi (+)/CNPase (-) cells. (C) Triple staining for NG2 (green), GST-pi (red), and TO-PRO3 (blue) on an image of a single z-slice. Arrowheads, GST-pi (+)/NG2 (+) cells. (D) A single-z-slice image with ortho-image of confocal z-stacks (upper and right panels in D) of cells double-labeled (arrowheads) with NG2 (green) and GST-pi (red). Scale bars=20 μm (A, C); 10 μm (B, D).

tified as CNPase (Watanabe et al., 2006). These findings suggested that approximately 70% of GST-pi (+) cells are CNPase (+) and RIP (+) mature oligodendrocytes, while the remaining (approximate 30%) of GST-pi (+) cells were not mature oligodendrocytes. Analysis of the intracellular distribution of GST-pi showed that all GST-pi (+)/CNPase (+) cells and GST-pi (+)/RIP (+) cells were GST-pi (+) C-type cells (arrows in Fig. 2B), whereas a majority of GST-pi (+)/CNPase (-) cells were GST-pi (+) N-type cells (arrowhead in Fig. 2B).

In the adult brain, oligodendrocyte progenitor cells (OPCs) have been identified as NG2-containing cells (Nishiyama et al., 1997; Dawson et al., 2000, 2003). We therefore next performed immunofluorescence staining for GST-pi and NG2 to examine the phenotype of residual GST-pi (+) cells containing neither CNPase nor RIP. In the cortex, all NG2 (+) cells observed in this study were

GST-pi (+) cells, and $28.5 \pm 2.3\%$ (mean \pm S.D., $n=1384$ cells from three animals) of GST-pi (+) cells were immunoreactive for NG2 (arrowheads in Fig. 2C); in addition, $77.2 \pm 3.1\%$ (mean \pm S.D., $n=498$ cells from three animals) of GST-pi (+)/NG2 (+) cells were GST-pi (+) N-type cells (arrowheads in Fig. 2D) and $22.8 \pm 3.1\%$ of them were GST-pi (+) C-type cells. Almost all ($99.2 \pm 0.1\%$) GST-pi (+) N-type cells ($n=376$ cells from three animals) were immunopositive for NG2, while some NG2 (+)/GST-pi (+) N-type cells exhibited very weak immunoreactivity for GST-pi. No clear differences in morphology including cell size and number of processes were noted between NG2 (+)/GST-pi (+) N-type cells and NG2 (+)/GST-pi (+) C-type cells. It was confirmed that neither immunoreactivity for CNPase nor that for RIP was observed in NG2 (+) cells, as previously reported (Keirstead et al., 1998; Dawson et al., 2003).

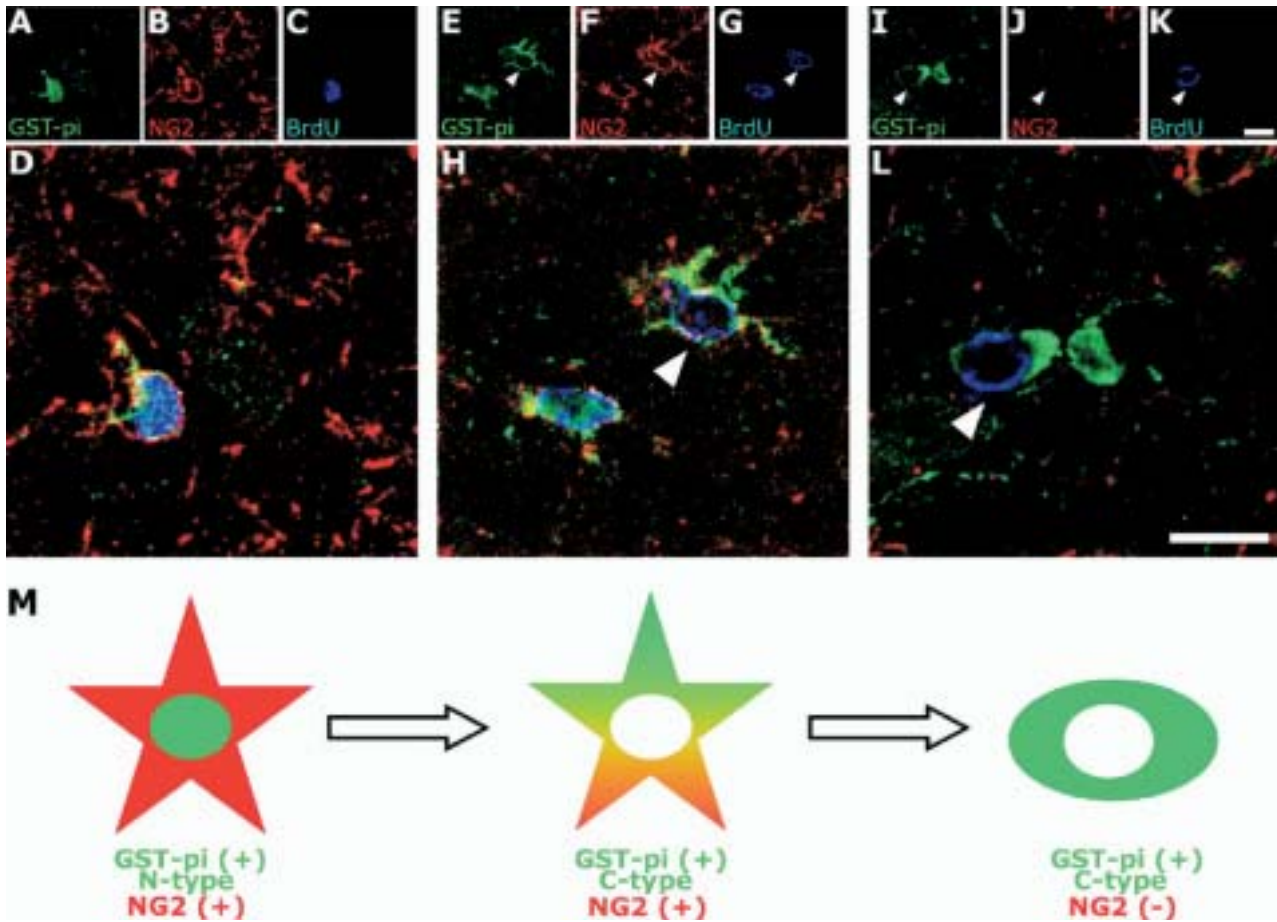


Fig. 3. GST-pi (+) N-type oligodendrocyte progenitor cells differentiated into GST-pi (+) C-type mature oligodendrocytes. (A–L) Triple immunolabeling for GST-pi (green), NG2 (red), and BrdU (blue) on images of single z-slices. An NG2 (+)/GST-pi (+) N-type BrdU-labeled cell at 2 h after BrdU injection (A–D). An NG2 (+)/GST-pi (+) N-type BrdU-labeled cell and an NG2 (+)/GST-pi (+) C-type BrdU-labeled cell (arrowheads) at 14 days after BrdU injection (E–H). An NG2 (–)/GST-pi (+) C-type BrdU-labeled cell at 28 days after BrdU injection (arrowheads in I–L). A–C, E–G, and I–K are at the same magnification; scale bar=10 μm (K). D, H, and L are at the same magnification; scale bar=10 μm (L). (M) Schema of pattern of immunoreactivity for GST-pi (green) and NG2 (red) in oligodendrocyte-lineage cells.

Nuclear GST-pi (+) (N-type) cells differentiate into cytoplasmic GST-pi (+) (C-type) cells

To determine whether GST-pi (+) N-type cells differentiate into GST-pi (+) C-type mature oligodendrocytes *in vivo*, triple-immunofluorescence staining for BrdU, GST-pi, and NG2 was performed using brain sections taken at several time points after a single injection of BrdU. At 2 h after BrdU injection, 94.7 \pm 1.9% of BrdU-labeled cells (mean \pm S.D., n =134 cells from three animals) were NG2 (+)/GST-pi (+) N-type cells (Fig. 3A–D). Almost all Ki67 (+) cells corresponded to GST-pi (+) N-type cells (data not shown), indicating that these cells were the major proliferating cell population. At 14 days after injection, in addition to BrdU-labeled NG2 (+)/GST-pi (+) N-type cells (82.8 \pm 4.6%; mean \pm S.D., n =201 cells from three animals), 9.7 \pm 2.0% (mean \pm S.D., n =201 cells from three animals) of BrdU-labeled cells were NG2 (+)/GST-pi (+) C-type cells (arrowheads in Fig. 3E–H). However, no NG2 (–)/GST-pi (+) C-type cells were observed among BrdU-labeled cells. These findings suggest that NG2 (+)/GST-pi (+) C-type cells are at the intermediate-differentiation

stage in the oligodendrocyte lineage. At 28 days after injection, in addition to BrdU-labeled NG2 (+)/GST-pi (+) N-type cells (74.0 \pm 4.0% of BrdU-labeled cells, mean \pm S.D., n =227 cells from three animals) and NG2 (+)/GST-pi (+) C-type cells (11.8 \pm 2.0% of BrdU-labeled cells, mean \pm S.D., n =227 cells from three animals), 8.5 \pm 1.2% of BrdU-labeled cells (mean \pm S.D., n =227 cells from three animals) were NG2 (–)/GST-pi (+) C-type cells (arrowheads in Fig. 3I–L). These findings indicate that GST-pi (+) N-type cells differentiate into GST-pi (+) C-type mature oligodendrocytes.

DISCUSSION

It has been reported that GST-pi is expressed in carbonic anhydrase- or CNPase-positive mature oligodendrocytes in the adult rodent brain (Cammer et al., 1989; Tansey and Cammer, 1991). In the present study, we found, in the cerebral cortex of adult rats, that approximately 70% of GST-pi (+) cells were CNPase (+) and RIP (+) mature oligodendrocytes (Fig. 2A and B), while the residual 30% were NG2 (+) oligodendrocyte progenitor cells expressing

neither CNPase nor RIP (Fig. 2B and C). Although GST-pi has been used as a specific marker protein for identification of mature oligodendrocytes (Tanaka et al., 2003; Mason et al., 2004; Gotts and Chesselet, 2005), our findings indicate that careful usage of it will be necessary.

We demonstrated that two types of GST-pi (+) cells exhibited different subcellular localizations of GST-pi protein; mature oligodendrocytes contained GST-pi protein mainly in the cytoplasm (C-type cells) (Fig. 1B and arrow in Fig. 1C), while progenitor cells contained the protein mainly within the nucleus (N-type cells) (arrowhead in Fig. 1C). Even on confocal laser microscopy, it was occasionally difficult to distinguish between the N-type and C-type cells at low magnification (Fig. 2C). However, use of the profile mode of confocal laser microscope software at high magnification permitted identification of such cell types on the basis of fluorescence intensity.

These findings were demonstrated by immunohistochemical studies with both monoclonal and polyclonal anti-GST-pi antibodies. Furthermore, we confirmed by Western blotting that both monoclonal and polyclonal antibodies recognized only 23 kDa GST-pi protein in tissue homogenates from cerebral cortex of adult rats (data not shown).

In the BrdU-labeling study, almost all BrdU-labeled cells were NG2 (+)/GST-pi (+) N-type cells at 2 h after BrdU injection (Fig. 3A–D). At 14 days after injection, NG2 (+)/GST-pi (+) C-type cells began to appear besides NG2 (+)/GST-pi (+) N-type cells among BrdU-labeled cells (arrowheads in Fig. 3E–H). At 28 days after injection, NG2 (–)/GST-pi (+) C-type cells could be observed among BrdU-labeled cells in addition to the types of cells observed at 14 days (arrowheads in Fig. 3I–L). These findings indicate that NG2 (+)/GST-pi (+) N-type cells differentiate into mature oligodendrocytes, which are NG2 (–)/GST-pi (+) C-type cells, through intermediate cells, which are NG2 (+)/GST-pi (+) C-type cells (Fig. 3M).

Nuclear expression of GST-pi has been reported in human uterine cancer (Shiratori et al., 1987), human metastatic neuroblastoma (Hall et al., 1994), and human glioma (Ali-Osman et al., 1997). These observations suggest that nuclear GST-pi expression is related to cellular proliferation. Indeed, in the present study, only NG2 (+)/GST-pi (+) N-type cells exhibited proliferative activity among GST-pi (+) cells in adult cortex (Fig. 3A–D). Although the functional significance of translocation of GST-pi protein from the cell nucleus to the cytoplasm remains to be determined, observation of the intracellular location of these markers permits identification of the stages of differentiation of oligodendrocyte lineage cells.

Acknowledgments—This work was supported in part by Special Coordination Funds for Promoting Science and Technology from the Ministry of Education, Culture, Sports, Science, and Technology, Japan, to Y.K., by consignment expenses from the Molecular Imaging Program on “Research Base for Exploring New Drugs” from the Ministry of Education, Culture, Sports, Science, and Technology to Y.W., and by a Grant-in-Aid for Scientific Research (No. 16590157) from the Japan Society for Promotion of Science to H.Y.

REFERENCES

- Abramovitz M, Homma H, Ishigaki S, Tansey F, Cammer W, Listowsky I (1988) Characterization and localization of glutathione-S-transferases in rat brain and binding of hormones, neurotransmitters, and drugs. *J Neurochem* 50:50–57.
- Abramovitz M, Listowsky I (1987) Selective expression of a unique glutathione S-transferase Yb3 gene in rat brain. *J Biol Chem* 262:7770–7773.
- Ali-Osman F, Brunner JM, Kutluk TM, Hess K (1997) Prognostic significance of glutathione S-transferase pi expression and subcellular localization in human gliomas. *Clin Cancer Res* 3:2253–2261.
- Board PG, Baker RT, Chelvanayagam G, Jermini LS (1997) Zeta, a novel class of glutathione transferases in a range of species from plants to humans. *Biochem J* 328(Pt 3):929–935.
- Board PG, Coggan M, Chelvanayagam G, Eastal S, Jermini LS, Schulte GK, Danley DE, Hoth LR, Griffor MC, Kamath AV, Rosner MH, Chrunyk BA, Perregaux DE, Gabel CA, Geoghegan KF, Pandit J (2000) Identification, characterization, and crystal structure of the omega class glutathione transferases. *J Biol Chem* 275:24798–24806.
- Cammer W, Tansey F, Abramovitz M, Ishigaki S, Listowsky I (1989) Differential localization of glutathione-S-transferase Yp and Yb subunits in oligodendrocytes and astrocytes of rat brain. *J Neurochem* 52:876–883.
- Cammer W, Zhang H (1992) Localization of Pi class glutathione-S-transferase in the forebrains of neonatal and young rats: evidence for separation of astrocytic and oligodendrocytic lineages. *J Comp Neurol* 321:40–45.
- Dawson MR, Levine JM, Reynolds R (2000) NG2-expressing cells in the central nervous system: are they oligodendroglial progenitors? *J Neurosci Res* 61:471–479.
- Dawson MR, Polito A, Levine JM, Reynolds R (2003) NG2-expressing glial progenitor cells: an abundant and widespread population of cycling cells in the adult rat CNS. *Mol Cell Neurosci* 24:476–488.
- Gotts JE, Chesselet MF (2005) Migration and fate of newly born cells after focal cortical ischemia in adult rats. *J Neurosci Res* 80:160–171.
- Hall AG, McGuckin AG, Pearson AD, Cattar AR, Malcolm AJ, Reid MM (1994) Glutathione S-transferase in bone marrow metastases of disseminated neuroblastoma. *J Clin Pathol* 47:468–469.
- Johnson JA, El Barbary A, Kornguth SE, Brugge JF, Siegel FL (1993) Glutathione S-transferase isoenzymes in rat brain neurons and glia. *J Neurosci* 13:2013–2023.
- Kataoka Y, Tamura Y, Takamori Y, Cui Y, Yamada H (2006) Perineuronal germinal cells in the rat cerebral cortex. *Med Mol Morphol* 39:28–32.
- Keirstead HS, Levine JM, Blakemore WF (1998) Response of the oligodendrocyte progenitor cell population (defined by NG2 labeling) to demyelination of the adult spinal cord. *Glia* 22:161–170.
- Li NQ, Reddanna P, Thyagaraju K, Reddy CC, Tu CP (1986) Expression of glutathione S-transferases in rat brains. *J Biol Chem* 261:7596–7599.
- Mannervik B, Alin P, Guthenberg C, Jansson H, Tahir MK, Warholm M, Jornvall H (1985) Identification of three classes of cytosolic glutathione transferase common to several mammalian species: correlation between structural data and enzymatic properties. *Proc Natl Acad Sci U S A* 82:7202–7206.
- Mason JL, Toews A, Hostettler JD, Morell P, Suzuki K, Goldman JE, Matsushima GK (2004) Oligodendrocytes and progenitors become progressively depleted within chronically demyelinated lesions. *Am J Pathol* 164:1673–1682.
- Meyer DJ, Coles B, Pemble SE, Gilmore KS, Fraser GM, Ketterer B (1991) Theta, a new class of glutathione transferases purified from rat and man. *Biochem J* 274(Pt 2):409–414.
- Meyer DJ, Thomas M (1995) Characterization of rat spleen prostaglandin H D-isomerase as a sigma-class GSH transferase. *Biochem J* 311(Pt 3):739–742.

- Nishiyama A, Yu M, Drazba JA, Tuohy VK (1997) Normal and reactive NG2+ glial cells are distinct from resting and activated microglia. *J Neurosci Res* 48:299–312.
- Paxinos G, Watson C (1998) *The rat brain in stereotaxic coordinates*, 4th ed. San Diego: Academic Press.
- Pemble SE, Wardle AF, Taylor JB (1996) Glutathione S-transferase class kappa: characterization by the cloning of rat mitochondrial GST and identification of a human homologue. *Biochem J* 319(Pt 3):749–754.
- Shiratori Y, Soma Y, Maruyama H, Sato S, Takano A, Sato K (1987) Immunohistochemical detection of the placental form of glutathione S-transferase in dysplastic and neoplastic human uterine cervix lesions. *Cancer Res* 47:6806–6809.
- Takamori Y, Tamura Y, Kataoka Y, Cui Y, Seo S, Kanazawa T, Kurokawa K, Yamada H (2007) Differential expression of nuclear lamin, the major component of nuclear lamina, during neurogenesis in two germinal regions of adult rat brain. *Eur J Neurosci* 25:1653–1662.
- Tamura Y, Kataoka Y, Cui Y, Yamada H (2004) Cellular proliferation in the cerebral cortex following neural excitation in rats. *Neurosci Res* 50:129–133.
- Tanaka K, Nogawa S, Suzuki S, Dembo T, Kosakai A (2003) Upregulation of oligodendrocyte progenitor cells associated with restoration of mature oligodendrocytes and myelination in peri-infarct area in the rat brain. *Brain Res* 989:172–179.
- Tansey FA, Cammer W (1991) A pi form of glutathione-S-transferase is a myelin- and oligodendrocyte-associated enzyme in mouse brain. *J Neurochem* 57:95–102.
- Terrier P, Townsend AJ, Coindre JM, Triche TJ, Cowan KH (1990) An immunohistochemical study of pi class glutathione S-transferase expression in normal human tissue. *Am J Pathol* 137:845–853.
- Theodore C, Singh SV, Hong TD, Awasthi YC (1985) Glutathione S-transferases of human brain. Evidence for two immunologically distinct types of 26500-Mr subunits. *Biochem J* 225:375–382.
- Watanabe M, Sakurai Y, Ichinose T, Aikawa Y, Kotani M, Itoh K (2006) Monoclonal antibody Rip specifically recognizes 2',3'-cyclic nucleotide 3'-phosphodiesterase in oligodendrocytes. *J Neurosci Res* 84:525–533.

(Accepted 13 June 2007)
(Available online 2 August 2007)

研究成果報告書

研究課題名	機能性分子の探索—免疫染色とレーザー・マイクロダイセクションを併用し高品質 mRNA を単離する手法の開発		
(英文)	Laser microdissection of immunopositive neurons on serial thin tissue sections: a simplified method for mRNA analysis		
事業推進者	杉本 哲夫	E-mail	sugimoto@takii.kmu.ac.jp
所属・職名	医学研究科・脳構築学（解剖学第2）講座・教授		
研究分担者名	宝谷 剛志、加瀬 政彦、丸山 正人		
キーワード	Laser microdissection、遺伝子発現プロファイリング、免疫組織化学		

1. 概要

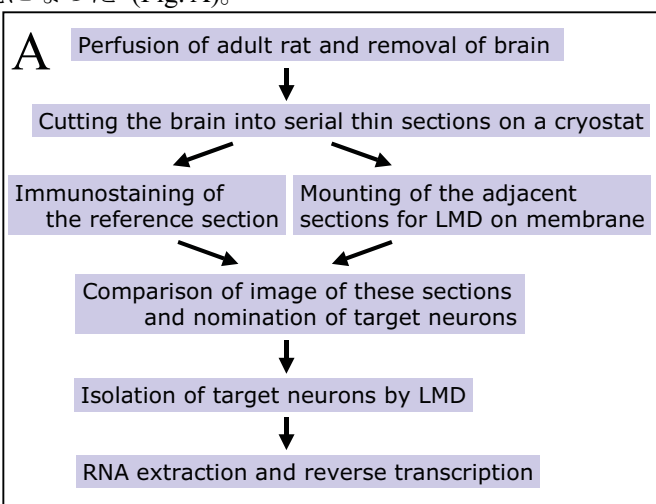
免疫組織化学とレーザー・マイクロダイセクションを併用した機能性分子の探索法には、多かれ少なかれ RNA 品質の劣化をきたすという弱点が指摘されている。本研究では細胞の遺伝子発現プロファイリングを進めるにあたり、この問題点を回避する手法を開発した。その骨子は、隣接する薄切切片を用いることで、免疫組織化学的に特徴付けられた細胞の RNA を効率よく分析することが可能になった (Fig. A)。

2. 研究の背景と目的

免疫組織化学で分類されたニューロン群の性質を調べるため、各細胞の遺伝子発現プロファイリングをする場合、免疫陽性の細胞を選択的に採取する必要がある。レーザー・マイクロダイセクション Laser Micro-Dissection (LMD) は特定の細胞のみを正確に採取するのにきわめて有用な手段である。LMDによって免疫陽性の細胞を採取する試みは今までにいくつか報告されているが、この手法に内在する最大の問題は、用いる切片を抗体とインキュベートする過程での RNA 分解酵素の混入である。このため RNA の品質低下を招来することになり、クローニングの効率を低下させる一番の原因になる。これを避ける工夫がいくつか提案されているが、決定的な解決策はない。今回私たちは、取得した RNA の品質低下という問題を回避するために隣接切片を用いる手法を開発した。すなわち、免疫染色した切片から免疫陽性を示した細胞を直接採取せず、隣接する切片に含まれる同じ細胞（部分）を同定し、その細胞（部分）に LMD を適用することによって RNA を採取した。この方法により免疫染色中の RNA 分解酵素による品質低下のない細胞を選択的に採取することが可能になった。

3. 研究方法

雄性成熟ラットを経心灌流法により固定し脳を摘出。凍結薄切切片（4ミクロン厚）を作製した (Fig. B)。



B Tissue preparation

Animal

Male Sprague-Dawley rats (7-week-old) weighing 200 g.

Perfusion

The animals were deeply anesthetized with intraperitoneal sodium pentobarbital (50 mg/kg) and perfused transcardially with 300 ml of fixative containing 2% paraformaldehyde in 0.1 M phosphate buffer, pH 7.4. The brain was immediately removed and stored overnight in the phosphate buffer containing 25% sucrose at 4°C.

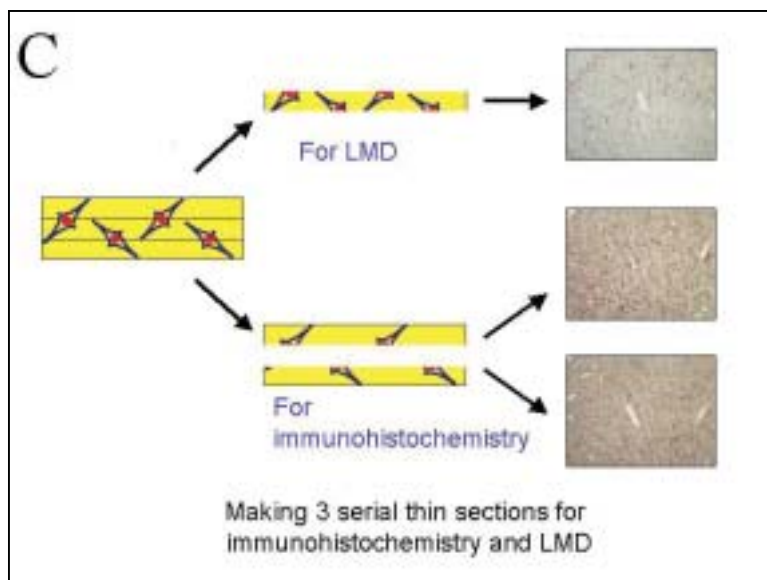
Tissue sectioning

The occipital cortex was removed from the fixed brain, embedded in OCT compound (Sakura, Torrance, CA) and stored at -80°C. Cryosectioning was performed on a cryostat into serial coronal sections of 4-μm thickness. The tissue section for immunohistochemistry was mounted on gelatin-coated slides and those for LMD were mounted on support membranes.

4. これまでの成果

隣接する組織切片を用いて、真ん中の一枚を LMD に供するため Clonis の supporting membrane に貼付した (Fig. C)。

この membrane は透明性が高いため、のちに組織切片を neutral red で染色して細胞を同定する際に透過光による観察が可能になる。前後に隣接する切片は免疫組織化学に供するため、スライドガラスに貼り付けた。これら二枚の組織切片は同一または別の種類の免疫染色に付することができる (Fig. D)。ここではラット後頭感覚皮質のパルブアルブミン免疫陽性細胞と免疫陰性細胞を例示している。免疫陽性の細胞を真ん中の切片上で確認したうえで、その細胞を LMD に付するために Clonis の試料台に移す (Fig. E)。Clonis によって target cell をほぼ正確に特定できた。しかも細胞周囲の組織と target cell を容易に離断することができた。単離した target cell から RNA 抽出、Reverse transcription-PCR を実施した (Fig. F)。感覚皮質に内在するニューロンに特徴的なパルブアルブミン mRNA 発現を確認した。なお target cell の PCR により 500-1000 bp 程度の PCR 産物が増幅できた。



D

Immunohistochemistry

The section was incubated overnight with mouse monoclonal anti-carp parvalbumin antibody (1/5000; Swant, Bellinzona, Switzerland) at room temperature in a moist chamber and then with goat anti-mouse IgG secondary antibody conjugated to HRP for 2 hours. Parvalbumin immunoreactivity was visualized through color reaction using DAB. Finally, the section was counterstained with neutral red and embedded with Bioleit (Koken, Tokyo, Japan).

Determination of target neurons

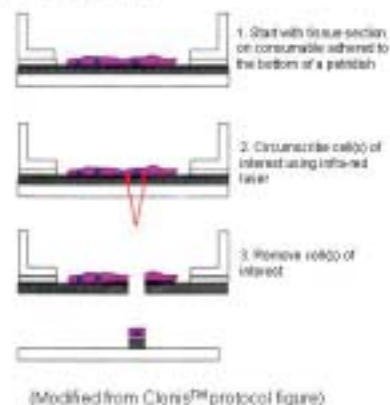
Both the immunostained section for reference and the adjacent ones for LMD were photographed. These images were compared in detail and the neurons identical to immunopositive ones were determined in the sections for LMD.

E

Laser Micro Dissection (LMD)

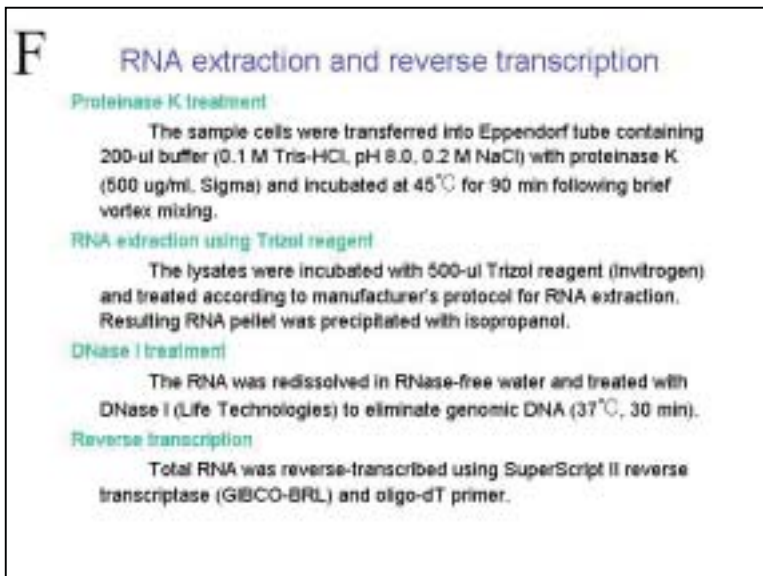
The section mounted on membrane for LMD was stained with neutral red. Target 120 neurons were carved out with laser power using Clonis™ (Carl-Zeiss Cell Science) at room temperature.

Methods of cell isolation



5. これまでの進捗状況と今後の計画

上記の成果は、本法が品質の劣化を免れた mRNA を取得する上で有用な方法であることを直接的に示すものである。LMD 単離細胞の PCR 産物は cDNA クローニングと遺伝子発現プロファイリングに使用可能であり、この成果は今後の機能性分子の探索に駆使できると見込まれる。



6. これまでの発表論文

(1) 発表論文

1) 原著論文

1. Trifonov, S., Houtani, T., Hamada, S., Kase, M., Maruyama, M. & Sugimoto, T.

In situ hybridization study of the distribution of choline acetyltransferase mRNA and its splice variants in the mouse brain and spinal cord. in press (2008).

2. Tsutsumi, T., Houtani, T., Toida, K., Kase, M., Yamashita, T., Ishimura, K. & Sugimoto, T.

Vesicular acetylcholine transporter-immunoreactive axon terminals enriched in the pontine nuclei of the mouse.

Neuroscience **146**, 1869-1878 (2007).

3. Kase, M., Houtani, T., Sakuma, S., Tsutsumi, T. & Sugimoto, T.

Laser microdissection combined with immunohistochemistry on serial thin tissue sections: a method allowing efficient mRNA analysis.

Histochem. Cell Biol. **127**, 215-219 (2007).

(2) 学会発表

国際学会

3) 一般発表

Houtani, T., Toida, K., Tsutsumi, T., Kase, M., Yamashita, T., Ishimura, K. & Sugimoto, T.
Characterization of cholinergic terminal-like structures in the mouse pontine nuclei.

7th International Brain Research Organization IBRO World Congress of Neuroscience, Melbourne, Australia, 2007. Proceedings of 7th International Brain Research Organization IBRO World Congress of Neuroscience and the Australian Neuroscience Society (ANS). p. 249, 2007.

7. これまでの成果の情報公開

ホームページ：解剖学第二講座＝<http://www3.kmu.ac.jp/anat2/>

VESICULAR ACETYLCHOLINE TRANSPORTER–IMMUNOREACTIVE AXON TERMINALS ENRICHED IN THE PONTINE NUCLEI OF THE MOUSE

T. TSUTSUMI,^{a,b} T. HOUTANI,^a K. TOIDA,^c M. KASE,^a
T. YAMASHITA,^b K. ISHIMURA^c AND T. SUGIMOTO^{a*}

^aDepartment of Anatomy and Brain Science, Kansai Medical University, Moriguchi, Osaka 570-8506, Japan

^bDepartment of Otolaryngology, Kansai Medical University, Moriguchi, Osaka 570-8507, Japan

^cDepartment of Anatomy and Cell Biology, Institute of Health Biosciences, The University of Tokushima Graduate School, Kuramoto, Tokushima, 770-8503, Japan

Abstract—Information to the cerebellum enters via many afferent sources collectively known as precerebellar nuclei. We investigated the distribution of cholinergic terminal-like structures in the mouse precerebellar nuclei by immunohistochemistry for vesicular acetylcholine transporter (VACHT). VACHT is involved in acetylcholine transport into synaptic vesicles and is regarded as a reliable marker for cholinergic terminals and preterminal axons. In adult male mice, brains were perfusion-fixed. Polyclonal antibodies for VACHT, immunoglobulin G-peroxidase and diaminobenzidine were used for immunostaining. In the mouse brain, immunoreactivity was seen in almost all major cholinergic cell groups including brainstem motoneurons. In precerebellar nuclei, the signal could be detected as diffusely beaded terminal-like structures. It was seen heaviest in the pontine nuclei and moderate in the pontine reticulotegmental nucleus; however, it was seen less in the medial solitary nucleus, red nucleus, lateral reticular nucleus, inferior olivary nucleus, external cuneate nucleus and vestibular nuclear complex. In particular, VACHT-immunoreactive varicose fibers were so dense in the pontine nuclei that detailed distribution was studied using three-dimensional reconstruction of the pontine nuclei. VACHT-like immunoreactivity clustered predominantly in the medial and ventral regions suggesting a unique regional difference of the cholinergic input. Electron microscopic observation in the pontine nuclei disclosed ultrastructural features of VACHT-immunoreactive varicosities. The labeled bouton makes a symmetrical synapse with unlabeled dendrites and contains pleomorphic synaptic vesicles. To clarify the neurons of origin of VACHT-immunoreactive terminals, VACHT immunostaining combined with wheat germ agglutinin–conjugated horseradish peroxidase retrograde labeling was conducted by injecting a retrograde tracer into the right pontine nuclei. Double-labeled neurons were seen bilaterally in the laterodorsal tegmental nucleus and pedunculo-pontine tegmental nucleus. It is assumed that mesopontine cholinergic neurons negatively regulate neocortico-ponto-cerebellar projections at the level of pontine nuclei. © 2007 IBRO. Published by Elsevier Ltd. All rights reserved.

*Corresponding author. Tel: +81-6-6993-9420; fax: +81-6-6995-2708. E-mail address: sugimoto@takii.kmu.ac.jp (T. Sugimoto).
Abbreviations: HRP, horseradish peroxidase; VACHT, vesicular acetylcholine transporter; WGA-HRP, wheat germ agglutinin–conjugated horseradish peroxidase.

0306-4522/07\$30.00+0.00 © 2007 IBRO. Published by Elsevier Ltd. All rights reserved.
doi:10.1016/j.neuroscience.2007.03.019

Key words: precerebellar nuclei, cholinergic modulation, pontocerebellar fibers, pedunculo-pontine tegmental nucleus, laterodorsal tegmental nucleus, cholinergic synapse.

The pontine nuclei convey neocortical input to the cerebellum and represent major precerebellar nuclei that send mossy fibers toward widespread areas of the cerebellar cortex (Ruigrok, 2004). Besides neocortical afferents, the pontine nuclei receive afferents from the tectum and cerebellar nuclei (Ruigrok, 2004). The pontine nuclei also receive cholinergic afferents that originate in the mesopontine tegmentum comprising the pedunculo-pontine tegmental nucleus (Ch5) and the laterodorsal tegmental nucleus (Ch6) (Woolf and Butcher, 1989; Aas et al., 1990; Butcher and Woolf, 2004; Winn, 2006). According to Aas et al. (1990), these cholinergic pontine afferents may modulate major cerebellar afferent information in accordance with the behavioral state of the subject. At present, however, little is known about the principal organization and functional aspects of these cholinergic pontine afferents.

Vesicular acetylcholine transporter (VACHT) is synthesized in major cholinergic neurons (Schafer et al., 1994; Erickson et al., 1994; Roghani et al., 1994, 1996; Usdin et al., 1995). It is involved in acetylcholine transport into synaptic vesicles and is regarded as a reliable marker for cholinergic terminals and preterminal axons. As a recently developed immunostaining method for VACHT successfully visualized cholinergic terminal fields more clearly than those employing antibodies for choline acetyltransferase (Schafer et al., 1995, 1998; Gilmore et al., 1996; Weihe et al., 1996; Arvidsson et al., 1997; Ichikawa et al., 1997; Roghani et al., 1998), we tried to delineate VACHT-immunoreactive terminal fields in the mouse pontine nuclei and numerically compared with the VACHT-immunoreactive terminal fields found in major precerebellar nuclei. The extent of pontine VACHT-immunoreactive terminal fields was mapped and analyzed using three-dimensional reconstruction. Further, VACHT-immunoreactive axon terminals were characterized by immunoelectron microscopy. These results suggest that mesopontine cholinergic neurons send massive afferents to widespread areas of the pontine nuclei and that they exert inhibitory control on pontine neurons. It is assumed that mesopontine cholinergic neurons negatively regulate neocortico-ponto-cerebellar projections at the level of pontine nuclei.

EXPERIMENTAL PROCEDURES

Animals and preparation of tissue section

All experiments were performed in compliance with the National Institutes of Health Guide for the Care and Use of Laboratory Animals (NIH Publication No. 80-23, revised 1996) and the Kansai Medical University local guidelines for animal experimentation; every effort was made to minimize the number of animals used and their suffering. The ddY mice (male, ranging from 8 to 10 weeks old) were used in this study. The animals were deeply anesthetized with 5% ketamine and 2% xylazine (2:1 vol., 0.1 ml/animal, i.m.) and were perfused transcardially with 50 ml of a fixative containing 4% paraformaldehyde in 0.1 M sodium phosphate buffer, pH 7.4. The brain was dissected out and stored overnight in sodium phosphate buffer containing 25% sucrose. The brain was frozen and sliced into coronal sections of 40- μ m thickness on a freezing microtome.

Immunohistochemistry

Sections were incubated with goat anti-VACHT polyclonal antibody (sc-7717; Santa Cruz Biotechnology, Inc., Santa Cruz, CA, USA; 1:500 dilution). According to the manufacturer's datasheet, this antibody was raised against a peptide corresponding to the amino-terminal region of VACHT of human origin, and it was shown by Western blot analysis to recognize VACHT in mouse brain. After being rinsed in phosphate-buffered 0.9% saline, the tissue sections were incubated with horse anti-goat immunoglobulin G (H+L)–horseradish peroxidase (HRP) conjugate (Bio-Rad Japan, Tokyo, Japan; 1:200 dilution) in 0.1% Triton X-100/0.1 M phosphate-buffered 0.9% saline for 60 min. The peroxidase reaction was developed in 50 mM Tris, pH 7.3, containing 0.02% diaminobenzidine and 0.003% H₂O₂ until a dark brown reaction product was evident. The sections were mounted onto gelatin-coated glass slides. They were defatted with ethanol and xylene,

embedded with balsam Canada and examined with an Eclipse E800M light microscope (Nikon, Tokyo, Japan) under bright-field illumination. To illustrate the detailed distribution of VACHT-immunoreactive varicose fibers in the basilar pons, low-power photomicrographs were prepared from serial sections. The nuclear boundaries were traced on the photomicrographs. VACHT-immunoreactive fibers were traced using a drawing tube. The resulting line drawings were retraced and edited with Adobe Illustrator CS2. The nomenclature of the precerebellar nuclei and related fiber systems was referred to according to Paxinos and Franklin (2001).

As controls, the sections were reacted with preabsorbed anti-VACHT antibody (1:500 dilution). For these purposes, the antibody was reacted with an excess amount of its antigenic peptide sc-7717p (Santa Cruz; derived from the amino-terminal region of human VACHT).

Analysis of images

The density of VACHT-immunoreactive terminal-like varicosities and beaded fibers was measured in pre-cerebellar nuclei by capturing photomicrographic images on Photoshop 6.0. The image files were then analyzed on NIH Image 1.62. The signal density (percent signal pixel/area pixel) was converted to gray-scale values by adjusting the white balance on the non-tissue area. Black sample spots served as the maximal limit of signal intensity for the calibration of gray-scale values. Signal density was measured at five sites of each precerebellar nucleus and displayed in a graph (Fig. 3) by averaging the gray-scale values obtained.

Image files of 10 line drawings (Fig. 4) that represent every other section through the pontine nuclei and pontine reticulotegmental nucleus were converted to stacks of images with NIH Image 1.62. By rotating the stacks, the regional distribution of VACHT-immunoreactive fibers was studied in the three-dimensional reconstruction of all sections through the pontine nuclei (Fig. 5).

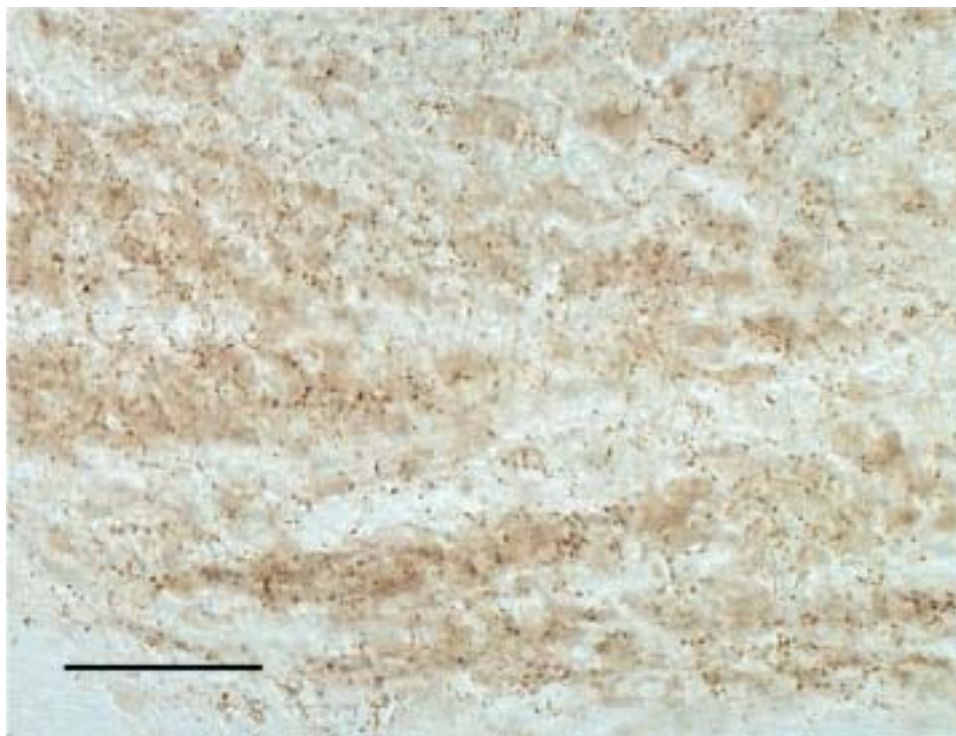


Fig. 1. Photomicrograph showing a wide distribution of VACHT-immunoreactive varicose fibers in the ventromedial region of the pontine nuclei. Scale bar=50 μ m.

Electron microscopic immunohistochemistry

The present immuno-electron microscopy was performed as in Toida et al. (2000). For ultrastructural studies, mice were perfused with 50 ml of 0.1 M phosphate buffer, pH 7.4, containing 4% paraformaldehyde. Transverse sections through the pontine nuclei were prepared and rinsed in 0.1 M phosphate buffer. For pre-embedding immunohistochemistry, they were then incubated with goat anti-VACHT antibody and HRP-conjugated anti-goat immunoglobulin G essentially as described above. Following HRP reaction with diaminobenzidine, sections were refixed in 3% glutaraldehyde for two more hours. The sections were postfixed with 1% OsO₄, stained en bloc in 1% uranyl acetate, dehydrated, and flat-embedded in Epon between a glass slide and coverslip, both of which were precoated with liquid releasing agent (EMS Inc., Hatfield, PA, USA; #70880). After identification of VACHT-immu-

noreactive elements by light microscopy, Epon-embedded sections were removed and remounted on epoxy cylinder. Serial ultrathin sections were prepared from several parts of the pontine nuclei. These sections were stained with lead citrate and were examined with an electron microscope (JEOL 1200EXII; JEOL, Akishima, Tokyo, Japan).

VACHT immunostaining combined with WGA-HRP retrograde labeling of neurons sending axons to the pontine nuclei

Mice ($n=3$) were anesthetized with i.p. sodium pentobarbital (40 mg/kg), and wheat germ agglutinin-conjugated horseradish peroxidase (WGA-HRP; Toyobo, Osaka, Japan; 3 μ g in 0.3 μ l distilled water) was injected stereotaxically into the pontine nuclei in accordance with the stereotaxic atlas (Paxinos and Franklin,

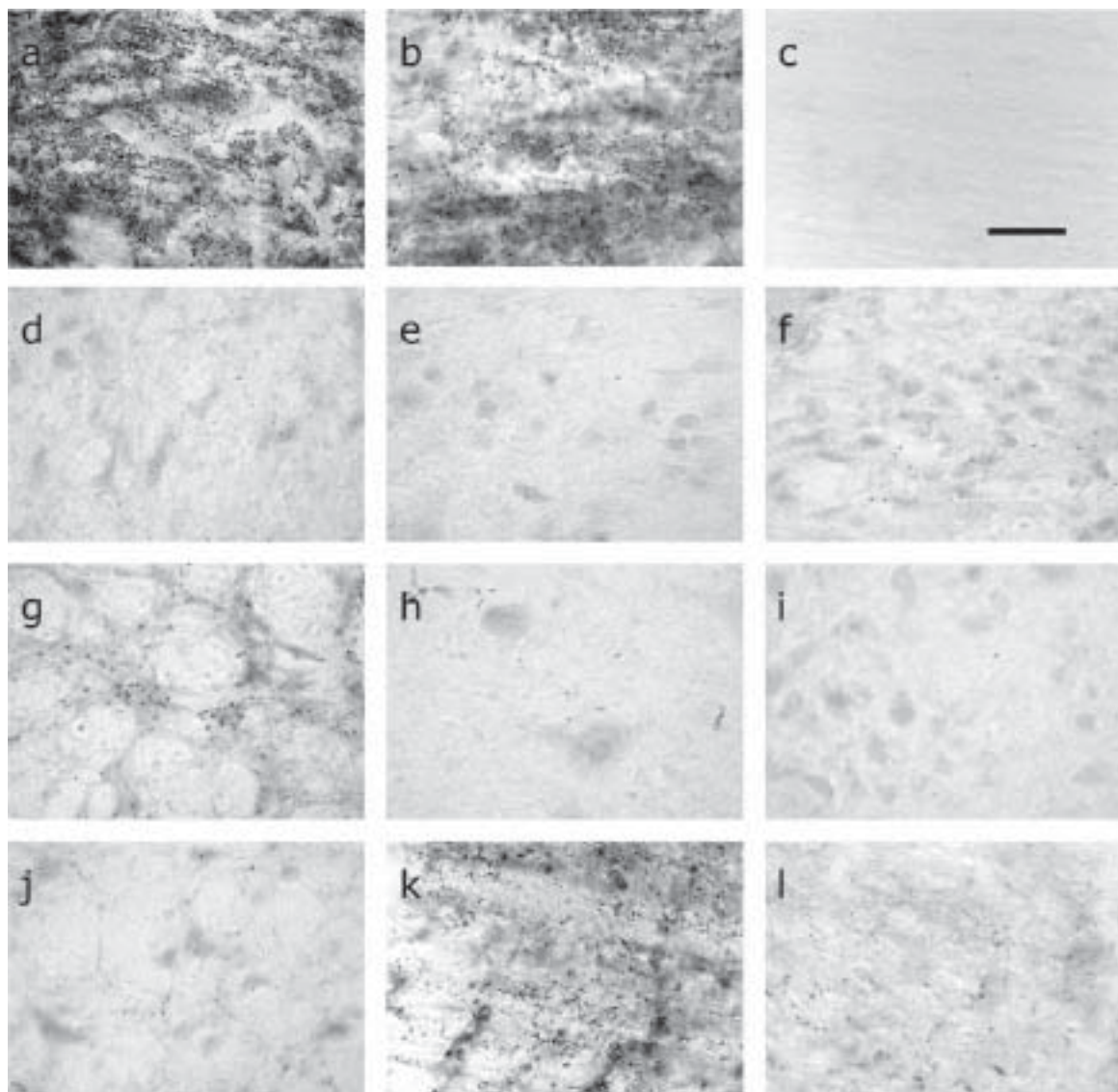


Fig. 2. Photomicrographs showing VACHT-immunoreactive varicose fibers in the precerebellar nuclei and interpeduncular nucleus. (a) Interpeduncular nucleus. (b) Pontine nuclei. (c) Pontine nuclei (absorption control). Absorption of antibody with the antigen peptide led to the absence of immunoreactivity. (d) Anterior interpositus nucleus. (e) External cuneate nucleus. (f) Inferior olivary nucleus principal lamella. (g) Lateral reticular nucleus. (h) Lateral vestibular nucleus. (i) Medial vestibular nucleus. (j) Red nucleus parvocellular part. (k) Pontine reticulotegmental nucleus. (l) Medial solitary nucleus. Scale bar=30 μ m.

2001). The injection was made manually by pressure through a glass micropipette attached to 1 μ l Hamilton microsyringe. After 3-day survival, animals were reanesthetized deeply with pentobarbital, and perfused intracardially with 50 ml of 4% paraformaldehyde in 0.1 M sodium phosphate buffer (pH 7.4). The brain was removed and immersed overnight in 25% sucrose dissolved in 0.1 M sodium phosphate buffer (pH 7.4). The brain was then frozen on a sliding microtome and cut into frontal sections of 40- μ m thickness. For WGA-HRP histochemistry, the sections were processed with 0.05% diaminobenzidine tetrahydrochloride and 0.01% hydrogen peroxide in 0.1 M sodium phosphate buffer–0.9% saline (pH 7.4). The color of the reaction product was intensified with cobalt chloride and nickel ammonium sulfate until a blue–black reaction product was evident (Adams, 1981). Next, the sections were rinsed intensely in phosphate-buffered 0.9% saline and immunostained for VAcHT. The secondary immunoglobulin-conjugated HRP was reacted for brown color with 0.02% diaminobenzidine tetrahydrochloride and 0.003% hydrogen peroxide in 50 mM Tris hydrochloride (pH 7.4).

RESULTS

Preferential distribution of VAcHT-immunoreactive varicose fibers in some precerebellar nuclei

The precerebellar nuclei examined in this study were the pontine nuclei, anterior interpositus nucleus, external cuneate nucleus, inferior olivary nucleus principal lamella, lateral reticular nucleus, lateral vestibular nucleus, medial vestibular nucleus, red nucleus parvocellular part, pontine reticulotegmental nucleus and medial solitary nucleus. In all precerebellar nuclei, immunoreactive material for VAcHT was localized to varicose fibers, but not to cell bodies. The varicose fibers were particularly dense in the pontine nuclei (Figs. 1, 2b). They were moderately accumulated in the pontine reticulotegmental nucleus (Fig. 2k) and were far less numerous in the remaining nuclei (Fig. 2d–j, l). In the brain sites known to receive massive cholinergic fibers such as the interpeduncular nucleus, VAcHT-like immunoreactivity was highly expressed in varicosities (Fig. 2a). The absorption of anti-VAcHT antibody with excess antigen resulted in the abolishment of VAcHT-like immunoreactivity in the terminal fields (Fig. 2b, c).

Measurement of the signal density of VAcHT-immunoreactive varicose fibers in the precerebellar nuclei

The density of VAcHT-immunoreactive varicose fibers was compared in these precerebellar nuclei by calculating the percent areas of immunoreactive elements (Fig. 3). Signal density was measured in five subregions and averaged. The values for the pontine nuclei and pontine reticulotegmental nucleus were 3.6 and 2.1, respectively. The other components of the precerebellar nuclei showed values less than 1.0. On the other hand, the value for the interpeduncular nucleus was 7.9, which is 2.2-fold higher than the pontine nuclei.

VAcHT-immunoreactive varicose fibers in the pontine nuclei and pontine reticulotegmental nucleus

The regional distribution of VAcHT-immunoreactive varicose fibers was examined in the pontine nuclei and pontine

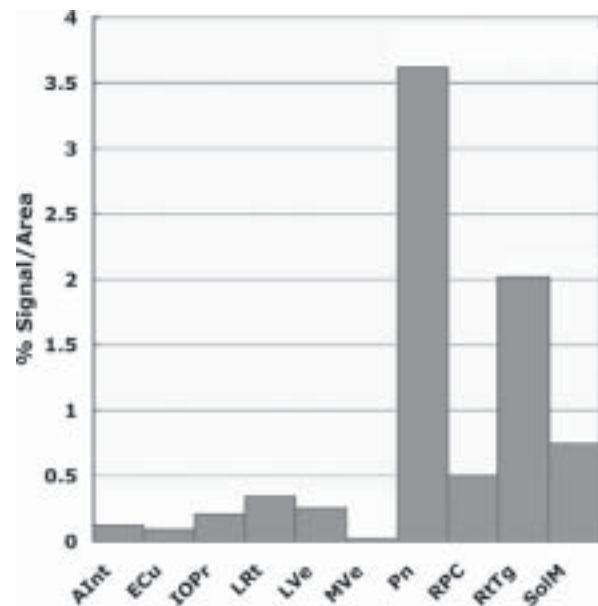


Fig. 3. Density of VAcHT-immunoreactive varicose fibers in precerebellar nuclei. In each precerebellar nucleus, signal density was measured at five subregions and averaged. The highest value (3.6) was obtained from pontine nuclei. The value for the interpeduncular nucleus (Fig. 2a), a site harboring the densest cholinergic fibers in the brain, was 7.9. This value is 2.2-fold higher than for pontine nuclei and it represents the upper limit of signal density in this measurement.

reticulotegmental nucleus, both of which harbor high to moderate densities of VAcHT-immunoreactive varicose fibers (Fig. 4). Line drawings of the pontine nuclei and pontine reticulotegmental nucleus showed that VAcHT-immunoreactive fibers are distributed throughout the rostrocaudal extent. In the pontine nuclei, these varicose fibers accumulated in the medial, ventral and lateral regions, and tend to spare the peripeduncular region. In the pontine reticulotegmental nucleus, these fibers were abundant in the medial and dorsomedial regions.

Three-dimensional reconstruction of cross-sections through the pontine nuclei

Three-dimensional reconstruction further showed the regional distribution of VAcHT-immunoreactive varicose fibers in the pontine nuclei and pontine reticulotegmental nucleus (Fig. 5). The clusters of VAcHT-immunoreactive varicose fibers were by far greatest in the pontine nuclei compared with the pontine reticulotegmental nucleus. In the pontine nuclei, these clusters were predominant in the medial and ventral regions; however, they were less numerous in the peripeduncular regions. In the pontine reticulotegmental nucleus, these clusters were prominent in the medial region.

VAcHT-immunoreactive axon terminals

Electron micrographs obtained by pre-embedding immunostaining showed the robust immunolocalization of VAcHT in presynaptic elements in the pontine nuclei (Fig. 6). Small

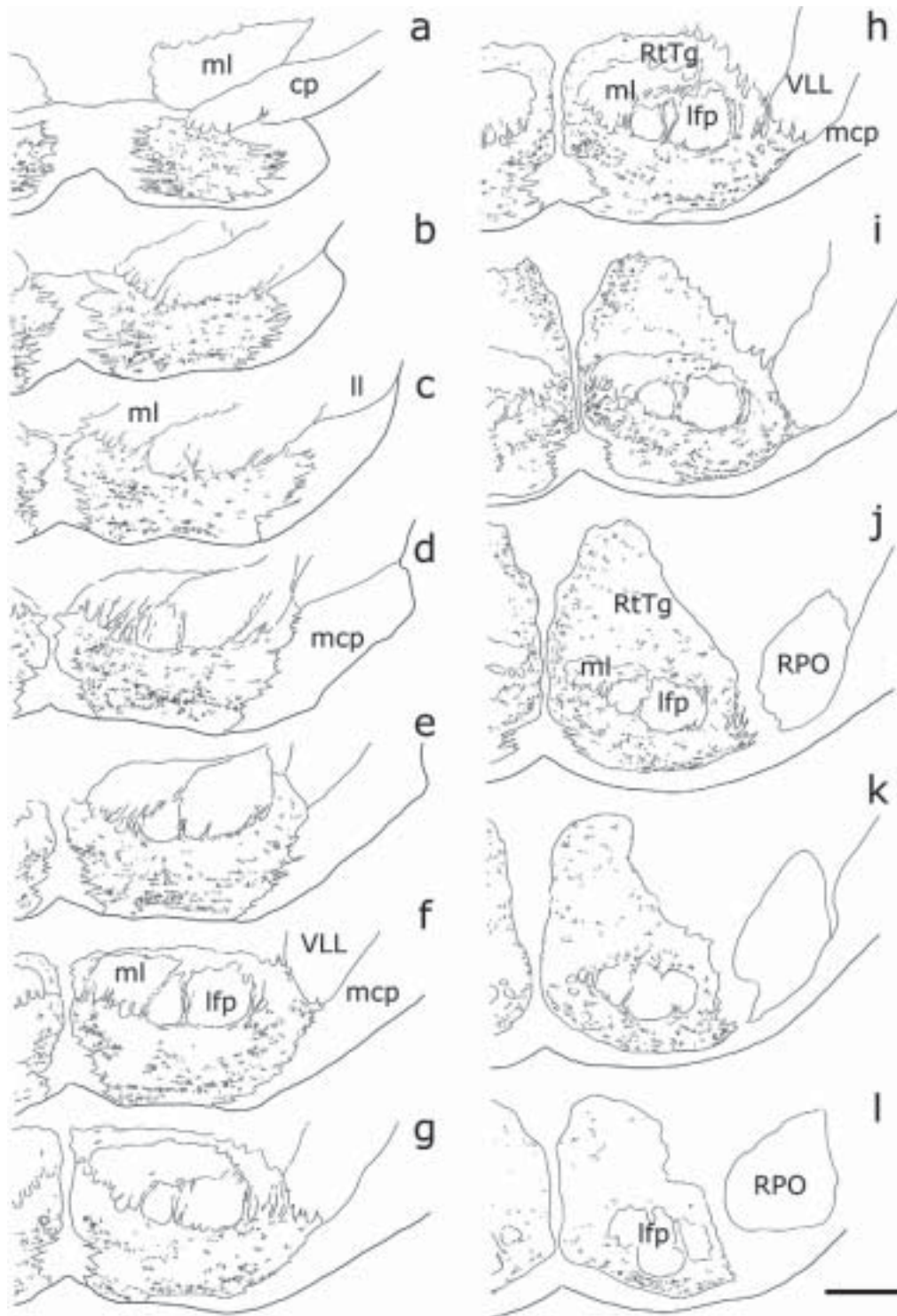


Fig. 4. Line drawings of VAcHT-immunoreactive varicose fibers in the pontine nuclei and pontine reticulotegmental nucleus. These drawings, arranged from rostral (a) to caudal (l), represent every other section. VAcHT-immunoreactive varicose fibers are distributed throughout the rostrocaudal extent of the pontine nuclei. They are accumulated in the medial, ventral and lateral regions, and tend to spare the peripeduncular region of the pontine nuclei. In the pontine reticulotegmental nucleus, they are abundant in medial and dorsomedial regions. In all illustrations, VAcHT-immunoreactive varicose fibers are plotted only in pontine nuclei and the pontine reticulotegmental nucleus. cp, cerebral peduncle; lfp, longitudinal fasciculus of the pons; ll, lateral lemniscus; mcp, middle cerebellar peduncle; ml, medial lemniscus; RPO, rostral periolivary region; RtTg, pontine reticulotegmental nucleus; VLL, ventral nucleus of the lateral lemniscus. Scale bar=500 μ m.

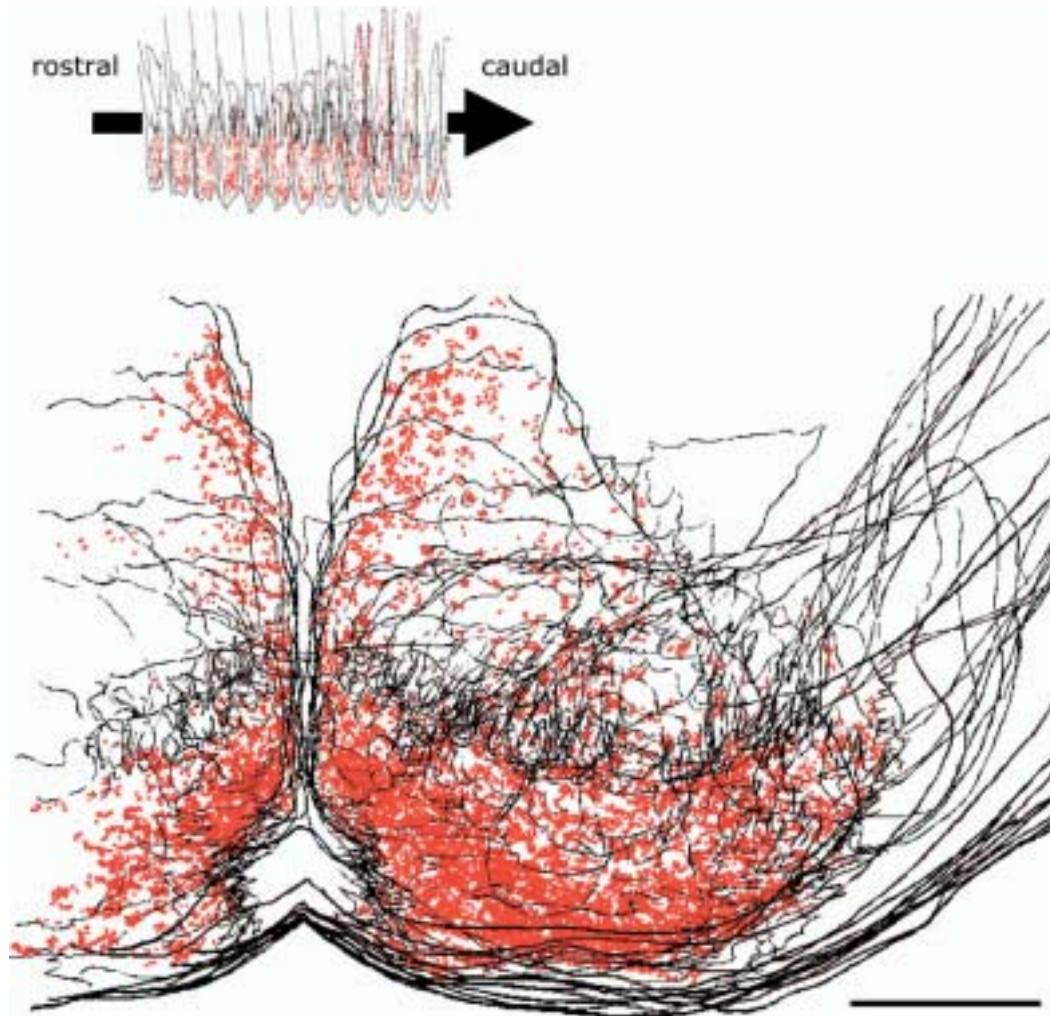


Fig. 5. Three-dimensional reconstruction of VAcHT-immunoreactive varicose fibers. Stacks of images display the regional accumulation of VAcHT-immunoreactive varicose fibers in the pontine nuclei and pontine reticulotegmental nucleus (dots in color). The image is based on line drawings of the basilar pons (Fig. 4) and viewed aslant from rostral to caudal as indicated in the inset (arrow). Scale bar=500 μm .

varicosities containing a collection of VAcHT-immunoreactive vesicular products were observed near the dendritic shafts of pontine nuclei neurons. Boutons of VAcHT-immunoreactive axons formed symmetrical contacts preferentially with the dendrites. These boutons frequently showed the local accumulation of pleomorphic synaptic vesicles close to the presynaptic membrane.

VAcHT immunostaining combined with WGA-HRP retrograde labeling of neurons sending axons to the pontine nuclei

In three mice, in which WGA-HRP was injected unilaterally into the right pontine nuclei, the deposits of the tracer were more or less centered on the pontine nuclei covering areas including the longitudinal fasciculus of the pons, middle cerebellar peduncle and small portions of the overlying reticular formation (Fig. 7a). In all animals, double-labeled neurons were seen bilaterally in the laterodorsal tegmental nucleus (Fig. 7b, e, f) and pedunculopontine tegmental nucleus (Fig. 7c, d, g, h); those distributed on the left side

are no less numerous than on the right side. Double-labeled neurons occurring bilaterally in the laterodorsal tegmental nucleus appeared similar in frequency to those in the pedunculopontine tegmental nucleus. In other brain and spinal cord areas harboring typical cholinergic cell groups, however, no double-labeled neurons could be detected. Single WGA-HRP-labeled neurons were found in several sites including the cerebral cortex and midbrain tegmentum. These neurons were seen preferentially on the side ipsilateral to the injection.

DISCUSSION

Symmetrical synapse

Previous immunolocalization studies revealed the presence of many cell bodies and terminal fields immunopositive for VAcHT in the brainstem (Gilmore et al., 1996; Weihe et al., 1996; Arvidsson et al., 1997; Ichikawa et al., 1997; Schafer et al., 1998; Roghani et al., 1998). Preferential accumulation of VAcHT-immunoreactive fibers was

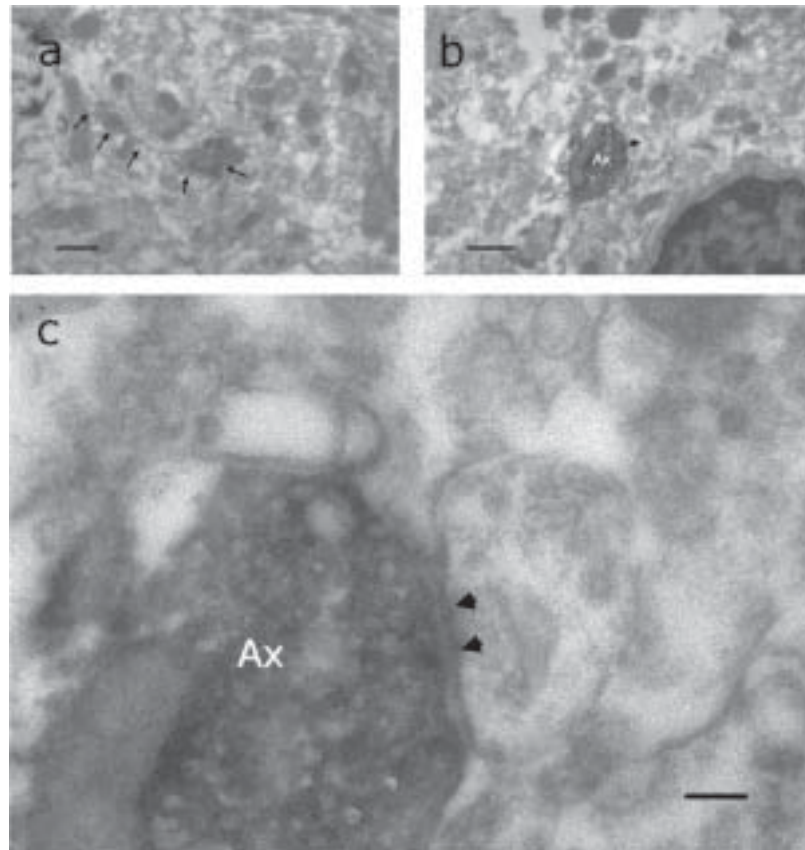


Fig. 6. Electron micrographs showing VAcHT-immunoreactive elements in pontine nuclei by pre-embedding immunohistochemistry. (a) VAcHT-immunoreactive varicosities are connected (arrow). Scale bar=0.5 μm . (b) VAcHT-immunoreactive axon terminal (Ax) makes axo-dendritic synapse. Scale bar=0.5 μm . (c) Enlargement of panel b showing detailed features of the synapse. VAcHT-immunoreactive Ax contains pleomorphic synaptic vesicles, and forms symmetrical synapse (arrowheads). Scale bar=0.1 μm .

noted in the pontine nuclei (Gilmore et al., 1996; Arvidsson et al., 1997; Schafer et al., 1998).

The present results suggest that mesopontine cholinergic neurons send massive afferents to widespread areas of the pontine nuclei and that they exert inhibitory control on pontine neurons. In an electron microscopic study that revealed the morphological correlation of the autoregulation of mesopontine cholinergic neurons, Garzon and Pickel (2000) pointed out symmetrical synapse as a dominant type of VAcHT-immunoreactive axon terminals in the pedunculopontine tegmental nucleus and laterodorsal tegmental nucleus. Gilmore et al. (1996) reported that VAcHT-immunoreactive axon terminals in the caudate putamen, dentate gyrus and facial nucleus form symmetrical synapses with dendrites or somata or both. Koch et al. (1993) reported the inhibitory nature of cholinergic projections originating from the pedunculopontine tegmental nucleus to the caudal pontine reticular nucleus in a pharmacophysiological study on the acoustic startle response in rats. Prado et al. (2006) developed VAcHT knockdown mice that show a notable decrease in VAcHT protein expression. The authors observed severe impairment of performance in cognitive tasks involving object and social recognition in these mutant mice. Lai and Siegel (1990) showed in decerebrate cats that electrical stimulation of

the pedunculopontine tegmental nucleus leads to the inhibition of muscle tone that takes place bilaterally with short latency. If this suppression originates selectively in the pedunculopontine tegmental nucleus neurons projecting to the pontine nuclei, it can be hypothesized that activation of the pedunculopontine tegmental nucleus neurons specifically suppressed the activity of the pontocerebellar mossy fiber system involved in the regulation of muscle tone and posture.

Diversity of corticopontine projections

In this study, the extent of pontine VAcHT-immunoreactive terminal fields was mapped and analyzed using three-dimensional reconstruction. VAcHT-like immunoreactivity was unevenly distributed in subnuclear divisions suggesting a unique regional difference of the cholinergic input. Brodal and Bjaalie (1997) stated that corticopontine projections are patchy and diverse. In a recent study, Perales et al. (2006) showed that auditory corticopontine projections diverge strongly throughout the pontine nuclei. Both the terminal fields of corticopontine projections and the neuron pools of pontocerebellar projections toward each cerebellar folium are arranged in a lamellar pattern (Brodal and Bjaalie, 1997). Further studies of pontine cholinergic

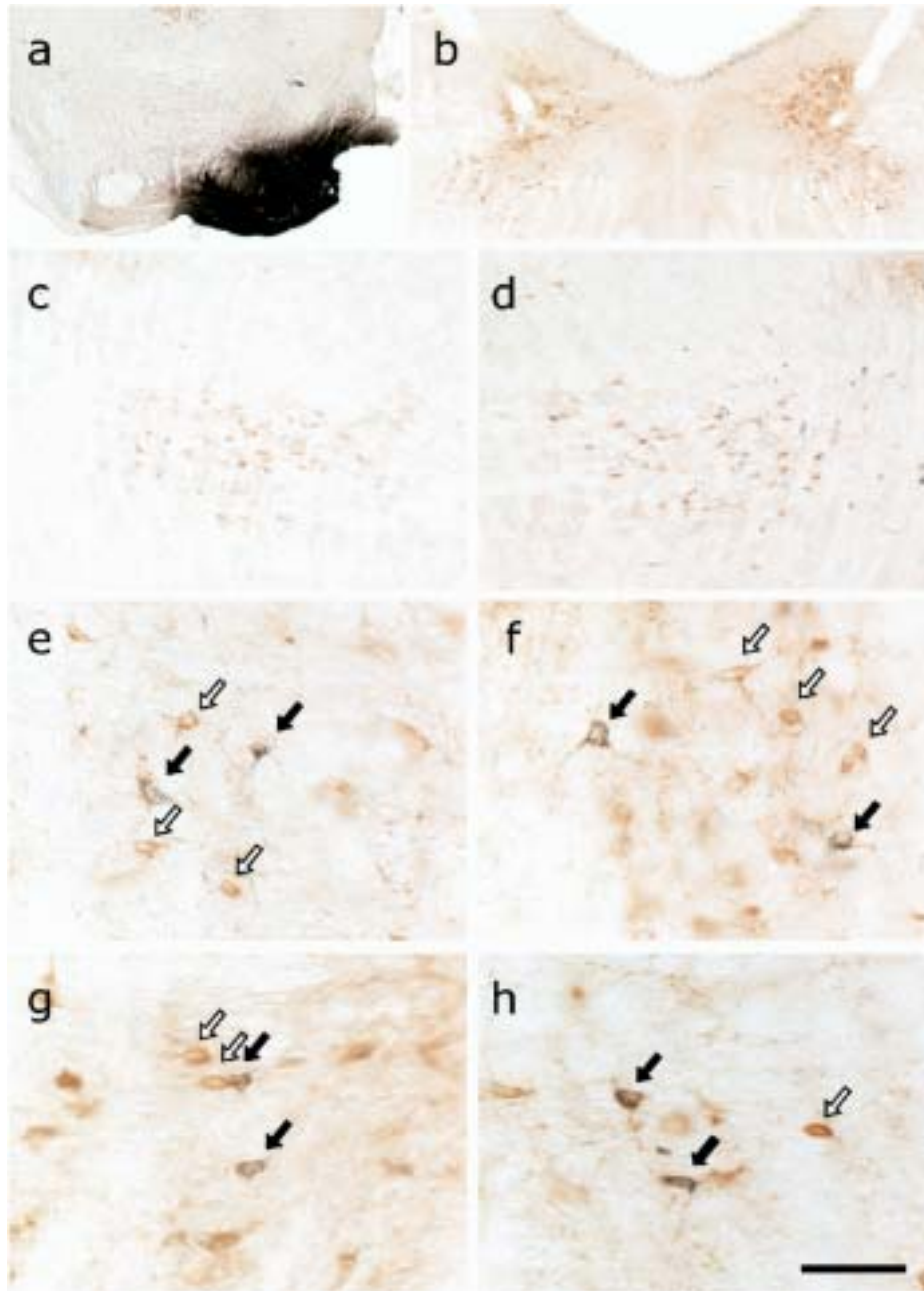


Fig. 7. VAcHT immunostaining combined with WGA-HRP retrograde labeling of neurons sending axons to pontine nuclei. WGA-HRP reaction product is displayed as blue–black and VAcHT-immunoreactive material appears brown. (a) WGA-HRP injections centered on the right pontine nuclei. (b) Laterodorsal tegmental nucleus. Many VAcHT-immunoreactive neurons are seen bilaterally. (c, d) Pedunculopontine tegmental nucleus. Many VAcHT-immunoreactive neurons are seen on the left (c) and right (d). (e, f) Enlarged view of the left (e) and right (f) laterodorsal tegmental nucleus, both of which are shown in panel b, displaying double-labeled neurons (solid arrow) among single VAcHT-immunoreactive neurons (open arrow). (g, h) Enlarged views of the left (g) and right (h) pedunculopontine tegmental nucleus, which correspond to panels c and d, respectively. Double-labeled neurons (solid arrow) are seen among single VAcHT-immunoreactive neurons (open arrow). Scale bar=1.2 mm (a), 500 μm (b), 200 μm (c, d) and 50 μm (e–h).

afferents combined with cortical topography will reveal the functional significance of diverse projections.

Muscarinic receptor

The pontine nuclei are shown to represent a site with high levels of muscarinic cholinergic receptors by studies using

in vivo receptor binding (Frey et al., 1985) and *in vitro* receptor binding in rats (Rotter et al., 1979; Wamsley et al., 1981; Rotter, 1984) and humans (Cortes et al., 1984). By contrast, the levels of muscarinic receptors in the inferior olive and several other precerebellar nuclei remain low or negligible (Rotter, 1984). Rotter et al. (1979) examined the

reaction of muscarinic receptors in the pontine nuclei to axotomy and deafferentation. In particular, destruction of the neocortical afferents caused no long-lasting changes in the density or distribution of the pontine muscarinic receptors. This indicates that muscarinic receptors are not located on the presynaptic terminals of the corticopontine axons.

According to Levey et al. (1991, 1994), m2 and m3 muscarinic receptors are enriched in the pontine nuclei as well as the mesopontine tegmentum including the pedunculo-pontine tegmental nucleus and laterodorsal tegmental nucleus. *In situ* hybridization study showed the distinct localization of mRNAs for m2 and m3 receptor proteins in the pontine nuclei (Buckley et al., 1988). Binding autoradiography revealed that M2 and M3 receptors are present at high levels in the pontine nuclei (Spencer et al., 1986; Levey et al., 1994). From our results, it is assumed that mesopontine cholinergic neurons negatively regulate neocortico-ponto-cerebellar projections via the activation of these muscarinic receptors at the level of pontine nuclei. Interestingly, M2 muscarinic receptor subtype has been shown to play a key role in the pathogenesis of tremor as revealed by the observation of pharmacologic deficits of M2 muscarinic cholinergic receptor knockout mice (Gomez et al., 1999; Wess, 2004).

CONCLUSION

We showed: 1) that, of mouse precerebellar nuclei, VACHT-immunoreactive terminal-like structures were seen heaviest in the pontine nuclei, clustering predominantly in the medial and ventral regions, 2) that VACHT-immunoreactive axon terminals observed in the pontine nuclei made symmetrical synapses with unlabeled dendrites and contained pleomorphic synaptic vesicles, and 3) that these axon-terminal components were sent bilaterally by VACHT-immunoreactive neurons found in the laterodorsal tegmental nucleus and pedunculo-pontine tegmental nucleus. This study pointed out the presence of cholinergic neurons that exert inhibitory control over the pontine nuclei.

Acknowledgments—The authors thank Fumio Yamashita and Tetsumi Yamamoto for technical assistance, and Yuki Okada for expert secretarial work. Supported in part by grants from the Ministry of Education, Culture, Sports, Science and Technology of Japan, and the Science Research Promotion Fund of the Japan Private School Promotion Foundation.

REFERENCES

- Aas JE, Brodal P, Baughman RW, Storm-Mathisen J (1990) Projections to the pontine nuclei from choline acetyltransferase-like immunoreactive neurons in the brainstem of the cat. *J Comp Neurol* 300:183–195.
- Adams JC (1981) Heavy metal intensification of DAB-based HRP reaction product. *J Histochem Cytochem* 29:775.
- Arvidsson U, Riedl M, Elde R, Meister B (1997) Vesicular acetylcholine transporter (VACHT) protein: a novel and unique marker for cholinergic neurons in the central and peripheral nervous systems. *J Comp Neurol* 378:454–467.
- Brodal P, Bjaalie JG (1997) Salient anatomic features of the cortico-ponto-cerebellar pathway. *Prog Brain Res* 114:227–249.
- Buckley NJ, Bonner TI, Brann MR (1988) Localization of a family of muscarinic receptor mRNAs in rat brain. *J Neurosci* 8:4646–4652.
- Butcher LL, Woolf NJ (2004) Cholinergic neurons and networks revisited. In: *The rat nervous system*, 3rd edition (Paxinos G, ed), pp 1257–1268. San Diego: Academic Press.
- Cortes R, Probst A, Palacios JM (1984) Quantitative light microscopic autoradiographic localization of cholinergic muscarinic receptors in the human brain: brainstem. *Neuroscience* 12:1003–1026.
- Erickson JD, Varoqui H, Schafer MK, Modi W, Diebler MF, Weihe E, Rand J, Eiden LE, Bonner TI, Usdin TB (1994) Functional identification of a vesicular acetylcholine transporter and its expression from a “cholinergic” gene locus. *J Biol Chem* 269:21929–21932.
- Frey KA, Ehrenkauf RL, Agranoff BW (1985) Quantitative *in vivo* receptor binding. II. Autoradiographic imaging of muscarinic cholinergic receptors. *J Neurosci* 5:2407–2414.
- Garzon M, Pickel VM (2000) Dendritic and axonal targeting of the vesicular acetylcholine transporter to membranous cytoplasmic organelles in laterodorsal and pedunculo-pontine tegmental nuclei. *J Comp Neurol* 419:32–48.
- Gilmor ML, Nash NR, Roghani A, Edwards RH, Yi H, Hersch SM, Levey AI (1996) Expression of the putative vesicular acetylcholine transporter in rat brain and localization in cholinergic synaptic vesicles. *J Neurosci* 16:2179–2190.
- Gomez J, Shannon H, Kostenis E, Felder C, Zhang L, Brodtkin J, Grinberg A, Sheng H, Wess J (1999) Pronounced pharmacologic deficits in M2 muscarinic acetylcholine receptor knockout mice. *Proc Natl Acad Sci U S A* 96:1692–1697.
- Ichikawa T, Ajiki K, Matsuura J, Misawa H (1997) Localization of two cholinergic markers, choline acetyltransferase and vesicular acetylcholine transporter in the central nervous system of the rat: *in situ* hybridization histochemistry and immunohistochemistry. *J Chem Neuroanat* 13:23–39.
- Koch M, Kungel M, Herbert H (1993) Cholinergic neurons in the pedunculo-pontine tegmental nucleus are involved in the mediation of prepulse inhibition of the acoustic startle response in the rat. *Exp Brain Res* 97:71–82.
- Lai YY, Siegel JM (1990) Muscle tone suppression and stepping produced by stimulation of midbrain and rostral pontine reticular formation. *J Neurosci* 10:2727–2734.
- Levey AI, Edmunds SM, Heilman CJ, Desmond TJ, Frey KA (1994) Localization of muscarinic m3 receptor protein and M3 receptor binding in rat brain. *Neuroscience* 63:207–221.
- Levey AI, Kitt CA, Simonds WF, Price DL, Brann MR (1991) Identification and localization of muscarinic acetylcholine receptor proteins in brain with subtype-specific antibodies. *J Neurosci* 11:3218–3226.
- Paxinos G, Franklin KBJ (2001) *The mouse brain in stereotaxic coordinates*, 2nd edition. San Diego: Academic Press.
- Perales M, Winer JA, Prieto JJ (2006) Focal projections of cat auditory cortex to the pontine nuclei. *J Comp Neurol* 497:959–980.
- Prado VF, Martins-Silva C, de Castro BM, Lima RF, Barros DM, Amaral E, Ramsey AJ, Sotnikova TD, Ramirez MR, Kim HG, Rossato JI, Koenen J, Quan H, Cota VR, Moraes MF, Gomez MV, Guatimosim C, Wetsel WC, Kushmerick C, Pereira GS, Gainetdinov RR, Izquierdo I, Caron MG, Prado MA (2006) Mice deficient for the vesicular acetylcholine transporter are myasthenic and have deficits in object and social recognition. *Neuron* 51:601–612.
- Roghani A, Feldman J, Kohan SA, Shirzadi A, Gundersen CB, Brecha N, Edwards RH (1994) Molecular cloning of a putative vesicular transporter for acetylcholine. *Proc Natl Acad Sci U S A* 91:10620–10624.
- Roghani A, Shirzadi A, Butcher LL, Edwards RH (1998) Distribution of the vesicular transporter for acetylcholine in the rat central nervous system. *Neuroscience* 82:1195–1212.
- Roghani A, Shirzadi A, Kohan SA, Edwards RH, Butcher LL (1996) Differential distribution of the putative vesicular transporter for acetylcholine in the rat central nervous system. *Brain Res Mol Brain Res* 43:65–76.

- Rotter A (1984) Cholinergic receptors. In: Handbook of chemical neuroanatomy, Vol. 3: Classical transmitters and transmitter receptors in the CNS, part II (Bjoerklund A, Hoekfelt T, Kuhar MJ, eds), pp 273–303. Amsterdam: Elsevier.
- Rotter A, Birdsall NJ, Burgen AS, Field PM, Smolen A, Raisman G (1979) Muscarinic receptors in the central nervous system of the rat. IV. A comparison of the effects of axotomy and deafferentation on the binding of [³H]propylbenzilylcholine mustard and associated synaptic changes in the hypoglossal and pontine nuclei. *Brain Res* 180:207–224.
- Ruigrok TJH (2004) Precerebellar nuclei and red nucleus. In: The rat nervous system, 3rd edition (Paxinos G, ed), pp 167–204. San Diego: Academic Press.
- Schafer MK, Eiden LE, Weihe E (1998) Cholinergic neurons and terminal fields revealed by immunohistochemistry for the vesicular acetylcholine transporter. I. Central nervous system. *Neuroscience* 84:331–359.
- Schafer MK, Weihe E, Erickson JD, Eiden LE (1995) Human and monkey cholinergic neurons visualized in paraffin-embedded tissues by immunoreactivity for VACHT, the vesicular acetylcholine transporter. *J Mol Neurosci* 6:225–235.
- Schafer MK, Weihe E, Varoqui H, Eiden LE, Erickson JD (1994) Distribution of the vesicular acetylcholine transporter (VACHT) in the central and peripheral nervous systems of the rat. *J Mol Neurosci* 5:1–26.
- Spencer DG Jr, Horvath E, Traber J (1986) Direct autoradiographic determination of M1 and M2 muscarinic acetylcholine receptor distribution in the rat brain: relation to cholinergic nuclei and projections. *Brain Res* 380:59–68.
- Toida K, Kosaka K, Aika Y, Kosaka T (2000) Chemically defined neuron groups and their subpopulations in the glomerular layer of the rat main olfactory bulb: IV. Intraglomerular synapses of tyrosine hydroxylase-immunoreactive neurons. *Neuroscience* 101:11–17.
- Usdin TB, Eiden LE, Bonner TI, Erickson JD (1995) Molecular biology of the vesicular ACh transporter. *Trends Neurosci* 18:218–224.
- Wamsley JK, Lewis MS, Young WS III, Kuhar MJ (1981) Autoradiographic localization of muscarinic cholinergic receptors in rat brainstem. *J Neurosci* 1:176–191.
- Weihe E, Tao-Cheng JH, Schafer MK, Erickson JD, Eiden LE (1996) Visualization of the vesicular acetylcholine transporter in cholinergic nerve terminals and its targeting to a specific population of small synaptic vesicles. *Proc Natl Acad Sci U S A* 93:3547–3552.
- Wess J (2004) Muscarinic acetylcholine receptor knockout mice: novel phenotypes and clinical implications. *Annu Rev Pharmacol Toxicol* 44:423–450.
- Winn P (2006) How best to consider the structure and function of the pedunculopontine tegmental nucleus: Evidence from animal studies. *J Neurol Sci* 248:234–250.
- Woolf NJ, Butcher LL (1989) Cholinergic systems in the rat brain: IV. Descending projections of the pontomesencephalic tegmentum. *Brain Res Bull* 23:519–540.

(Accepted 10 March 2007)
(Available online 26 April 2007)

Laser microdissection combined with immunohistochemistry on serial thin tissue sections: a method allowing efficient mRNA analysis

Masahiko Kase · Takeshi Houtani · Satoru Sakuma · Toshiyuki Tsutsumi · Tetsuo Sugimoto

Accepted: 25 September 2006 / Published online: 9 November 2006
© Springer-Verlag 2006

Abstract Laser microdissection (LMD) with subsequent reverse transcription-PCR analysis is a powerful histochemical technique subserving the molecular characterization of specific cell types. We developed an efficient method for selective sampling of specific cell populations using immunohistochemistry coupled with LMD. The cerebral cortex of adult rats was cut into serial thin sections. Some sections were immunostained for parvalbumin. The adjacent sections were mounted on Cell Support Film for LMD and stained with neutral red. By comparison of the two adjacent sections, neuronal profiles representing parts of parvalbumin-immunopositive somata were identified in the neutral red-stained sections. These neuronal profiles were safely captured with LMD and analyzed on reverse transcription-PCR using extracted RNA. The method presented here can be applied to cell-type-specific characterizations using fixed cells under RNase-free conditions.

Keywords Laser microdissection · Immunohistochemistry · Parvalbumin · Serial thin section

Introduction

Laser microdissection (LMD) is a reliable technique by which single cells can be carved out using laser power

(Emmert-Buck et al. 1996; Luo et al. 1999). The method using immunohistochemistry coupled with LMD (immuno-LMD) enables selective sampling of immunopositive cells for RNA extraction (Fend et al. 1999; Fend and Raffeld 2000; Fink et al. 2000; Murakami et al. 2000; Jin et al. 2001; Walch et al. 2001; Bi et al. 2002; Vincent et al. 2002; Burbach et al. 2004; Lu et al. 2005). Immunohistochemistry has gained popularity for the exact localization and analysis of the morphology of cells in the brain. An important recent application is the possibility of carrying out gene analyses on immunohistochemically identified cells. For this purpose, an efficient technique for collecting immunostained cells is required. However, RNA degradation is inevitable through the procedures of blocking, antibody incubation and color reaction largely due to RNase activity in the solutions for immunostaining (Kohda et al. 2000). Although some protocols have been proposed to counteract RNA degradation (Newton et al. 2002; Mojsilovic-Petrovic et al. 2004), complete exclusion of RNase activity is difficult. The avoidance of RNA degradation during immunostaining procedures is one of the major problems in immuno-LMD (Fend and Raffeld 2000).

In this study, we propose a novel strategy to extract RNA from immunohistochemically identified neurons. In a first step, serial thin sections of rat brain were prepared with a cryostat. One section was immunostained according to any conventional protocol and the adjacent section was simply stained with neutral red. Such pairs of serially adjacent thin sections were carefully compared. In neutral red-stained sections, neuronal profiles representing parts of immunopositive neuronal cell bodies were identified and subjected to LMD. Thus, we successfully localized parvalbumin

M. Kase · T. Houtani · S. Sakuma · T. Tsutsumi · T. Sugimoto (✉)
Department of Anatomy and Brain Science,
Kansai Medical University, Moriguchi,
Osaka 570-8506, Japan
e-mail: sugimoto@takii.kmu.ac.jp

neurons without immunohistochemical processing. Neuronal RNA could subsequently be extracted without appreciable contamination of exogenous RNase.

Materials and methods

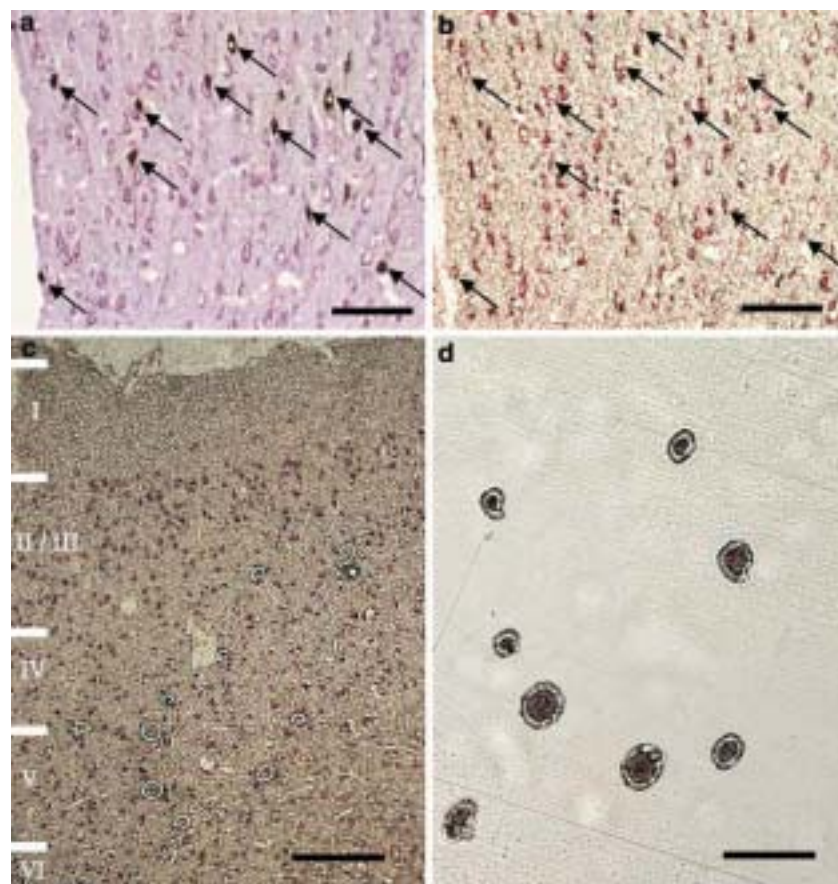
All experiments were performed in compliance with the NIH guidelines for the care and use of laboratory animals. Five male Sprague-Dawley rats (8 weeks old) weighing 200 g were used in this study. The animals were deeply anesthetized with intraperitoneal sodium pentobarbital (50 mg/kg) and perfused transcardially with 300 ml of fixative containing 2% paraformaldehyde in phosphate buffer, pH 7.4. The brain was immediately removed and stored overnight in phosphate buffer containing 25% sucrose at 4°C. The occipital cortex was removed from the fixed brain, embedded in OCT compound (Sakura, Torrance, CA, USA) and stored at -80°C. With close attention to avoid tissue distortion, the cortex was cut on a cryostat into serial coronal sections of 4 µm thickness. The tissue sections for immunohistochemistry were mounted on gelatin-coated slides and those for LMD were mounted on Cell Support Film (Clonis Cell Support Kit, Carl-Zeiss Cell Science, Tokyo, Japan).

For immunodetection, the sections were incubated overnight with mouse monoclonal anti-parvalbumin antibody (1/5,000: Swant McAB235, Bellinzona, Switzerland) at room temperature in a moist chamber after blocking with 2% normal goat serum for 30 min (Celio and Heizmann 1981; Celio 1986; Celio et al. 1988), and then with goat anti-mouse immunoglobulin G (H + L)-HRP conjugate (1:200 dilution: Bio-Rad, Hercules, CA, USA) for 2 h. Parvalbumin immunoreactivity was visualized through color reaction using diaminobenzidine. Finally, the sections were lightly counterstained with cresyl violet, embedded in Bioleit (Koken, Tokyo, Japan) and coverslipped (Fig. 1a).

Adjacent sections on Cell Support Film for LMD were stained with neutral red for 1 min at room temperature. After brief rinsing in water, they were soaked in 70% ethanol for 5–10 s and air-dried (Fig. 1b). All processes were performed in RNase-free solution. When not used immediately, these sections were conserved in a deep freezer at -80°C.

We captured images from both immunostained and adjacent LMD sections by a digital camera mounted on a Nikon Eclipse microscope. These images were compared in detail and profiles that represented neuronal cell bodies shown to be immunopositive on immunostained sections were identified in adjacent LMD

Fig. 1 Determination and carving of target neurons for LMD. **a** Parvalbumin immunostaining and cresyl violet counterstaining. Tissue is taken from rat occipital cortex. **b** Neutral red staining of the adjacent section. *Arrows*, parvalbumin-immunopositive neurons (**a**) and their corresponding neurons (**b**). Scale bar = 100 µm (**a**, **b**). The section in **b** was not coverslipped. **c** Target neurons carved out by laser power. I–VI, cortical layers. **d** Captured target neurons on Cell Support Film. Scale bar = 250 µm (**c**), 100 µm (**d**)



sections (Fig. 1a, b). Approximately two-thirds of the immunopositive neurons could be subjected to LMD.

In advance, we performed a preliminary experiment to confirm the accurate correspondence of the localization of the two parts of parvalbumin-immunoreactive neurons contained in serially adjacent sections. Two sequential sections were simultaneously immunostained and counterstained as described above, and it was confirmed that individual immunopositive neurons could be correctly identified in both sections (Fig. 2).

In LMD sections, 120 neuronal somata identified as parvalbumin immunopositive by comparison with the immunoreacted adjacent section were chosen. They were carved out with laser power using Clonis (Carl-Zeiss Cell Science, Tokyo, Japan) and collected at room temperature (Fig. 1c, d). For control purposes, neuronal somata identified as parvalbumin immunonegative ($n = 120$) were captured with Clonis. These two samples of captured cells were then analyzed by reverse transcription-PCR as described below. The number of neuronal somata chosen per sample was estimated as sufficient for PCR analysis of the sample according to quantitative gene expression analysis (Specht et al. 2001).

We also tested if PCR could work properly for cortical neurons immunostained for parvalbumin. For these purposes, parvalbumin immunostaining was carried out as described above using thin sections mounted on Cell Support Film for LMD. Parvalbumin-immunopositive neuronal somata ($n = 120$) were captured with Clonis and subjected to reverse transcription-PCR.

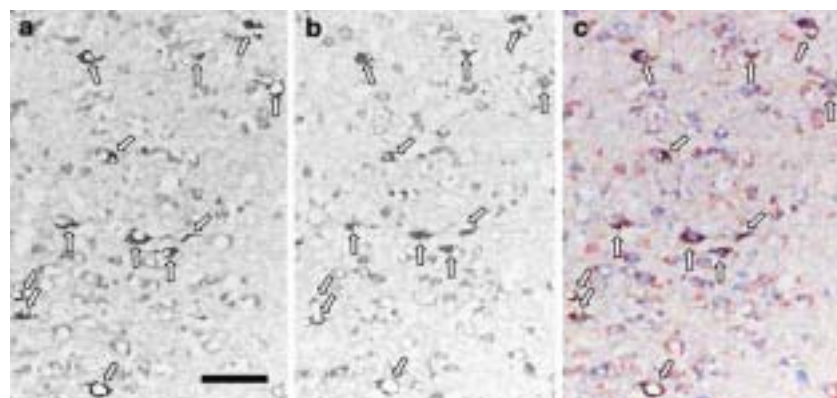
All sample cells were transferred into Eppendorf tubes containing 200 μ l buffer (0.1 M Tris-HCl, pH 8.0, 0.2 M NaCl) with proteinase K (500 μ g/ml; Sigma, Tokyo, Japan) and incubated at 45°C for 90 min following brief vortex mixing (Masuda et al. 1999). The lysates were incubated with 500 μ l Trizol reagent (Invitrogen, Carlsbad, CA, USA) and treated according to the manufacturer's protocol for RNA extraction. The

resulting RNA pellet was precipitated with 2-propanol, redissolved in RNase-free water and treated with DNase I (Invitrogen) to eliminate genomic DNA (37°C, 30 min). Total RNA was reverse-transcribed using SuperScript II reverse transcriptase (Invitrogen) and oligo-dT primer (42°C, 60 min).

Parvalbumin cDNA and glyceraldehyde 3-phosphate dehydrogenase (GAPDH) cDNA were amplified by PCR as described previously (Houtani et al. 2005). Briefly, PCR was performed using a 20 μ l volume with Eppendorf Mastercycler Gradient (parvalbumin: 95°C 10 s, 68°C 20 s, 72°C 30 s, 40 cycles; GAPDH: 95°C 10 s, 60°C 20 s, 72°C 30 s, 45 cycles) using Extaq HS (Takara, Ohtsu, Japan) and primers (parvalbumin: 5'-AAA CAA AGA CGC TGA TGG CTG CTG G-3' and 5'-GGT GTC ATT CGA GGG CCA TAA AGG A-3'; GAPDH: 5'-CCC TCA AGA TTG TCA GCA ATG C-3' and 5'-GTC CTC AGT GTA GCC CAG GAT-3'). The primer pairs for parvalbumin were set on different exons. The amplification products were visualized by agarose gel electrophoresis with ethidium bromide.

The LMD and reverse transcription-PCR studies described above were carried out in one rat and repeated four times using other rats. For sampling neuronal somata, 10–20 pairs of serially adjacent thin sections were prepared from a rat brain. To detect parvalbumin-immunopositive or -immunonegative neurons, three pairs of adjacent sections were respectively examined to finally collect 120 neuronal somata from the LMD sections. To harvest immunostained neuronal somata for PCR, three additional LMD sections were immunostained and viewed to collect 120 immunopositive neuronal somata. Accordingly, 120 neuronal somata were pooled in a tube and subjected to reverse transcription. Subsequently, aliquots of the sample were analyzed on PCR, and it was calculated that three neuronal somata on average were examined per lane of the PCR gel.

Fig. 2 Correspondence of neurons between serial thin sections. **a, b** The same parvalbumin-immunopositive neurons (white arrows) identified on adjacent sections. Digital photo images of these sections are color-displayed in red and sky blue and then merged. **c** Correspondence of neurons in serially adjacent sections. Scale bar = 50 μ m



Results and discussion

Many immunopositive neurons were seen in serially adjacent sections (Fig. 1). In the preliminary experiment, it was shown that serially adjacent thin sections could be used for identifying the same neurons by careful comparison of the sections. Fortunately, our tissue sections were free from serious tissue distortion (Fig. 2). The target neurons could be easily carved out and selectively collected by LMD (Fig. 1c, d).

The PCR studies yielded similar results with the material from five rats, showing that PCR products with a length of 228 bp (Fig. 3a, lane S1) and 410 bp (Fig. 3b, lanes S1 and S2) were amplified. This demonstrates that parvalbumin-immunopositive neurons provided cDNA pools manifesting parvalbumin phenotype (228 bp; Fig. 3a, lane S1). On the other hand, analysis of the PCR gel showed the absence of PCR-amplified product (228 bp) from parvalbumin-immunonegative neurons (Fig. 3a, lane S2) and parvalbumin-immunopositive neurons directly taken from immunostained sections (Fig. 3a, lane S3). PCR-amplified product for GAPDH (410 bp) was evident in cells taken from neutral red-stained adjacent sections (Fig. 3b, lanes S1 and S2) and absent from cells derived from immunostained sections (Fig. 3b, lane S3) suggesting that neutral red-stained sections, but not immunostained sections, escape RNA degradation.

Combined with immunolocalization of axoterminal transmitters, such cDNA pools can be further applied to single cell analysis of transmitter–receptor mismatch problems. Previous studies on the immuno-LMD method

devised several modifications of the immunostaining procedures to minimize the influence of RNase, including the use of fluorescent antibody, skipping the blocking process, increasing the concentration of primary and secondary antibodies, shortening the incubation time in the antibody solution, incubating under low temperature, and adding RNase inhibitor and solutions using DEPC-treated water (Fink et al. 2000; Kohda et al. 2000; Murakami et al. 2000; Vincent et al. 2002; Burbach et al. 2004; Mojsilovic-Petrovic et al. 2004; Ghosh et al. 2005). In this study, we developed an alternative immuno-LMD technique in which LMD can be combined with a variety of immunostaining procedures. Our technique enabled ordinary blocking and long antibody incubation under room temperature; moreover, the color reaction using any chromogen could be performed routinely.

Some fixatives significantly affect the integrity of extracted RNA as well as RNase activity (Goldsworthy et al. 1999; Walch et al. 2001; Srinivasan et al. 2002; Kihara et al. 2005); therefore, it is important to optimize fixation procedures in immuno-LMD. Our technique is applicable to several fixation procedures provided that serial thin sections can be made without serious tissue distortion.

Acknowledgments The authors thank Fumio Yamashita and Tetsuji Yamamoto for technical assistance, and Yuki Okada for expert secretarial work. Supported in part by grants from the Ministry of Education, Culture, Sports, Science and Technology of Japan, and the Science Research Promotion Fund of the Japan Private School Promotion Foundation.

References

- Bi WL, Keller-McGandy C, Standaert DG, Augood SJ (2002) Identification of nitric oxide synthase neurons for laser capture microdissection and mRNA quantification. *Bio-techniques* 33:1274–1283
- Burbach GJ, Dehn D, Nagel B, Del Turco D, Deller T (2004) Laser microdissection of immunolabeled astrocytes allows quantification of astrocytic gene expression. *J Neurosci Methods* 138:141–148
- Celio MR (1986) Parvalbumin in most γ -aminobutyric acid-containing neurons of the rat cerebral cortex. *Science* 231:995–997
- Celio MR, Heizmann CW (1981) Calcium-binding protein parvalbumin as a neuronal marker. *Nature* 293:300–302
- Celio MR, Baier W, Scharer L, de Viragh PA, Gerday C (1988) Monoclonal antibodies directed against the calcium binding protein parvalbumin. *Cell Calcium* 9:81–86
- Emmert-Buck MR, Bonner RF, Smith PD, Chuaqui RF, Zhuang Z, Goldstein SR, Weiss RA, Liotta LA (1996) Laser capture microdissection. *Science* 274:998–1001
- Fend F, Raffeld M (2000) Laser capture microdissection in pathology. *J Clin Pathol* 53:666–672
- Fend F, Emmert-Buck MR, Chuaqui R, Cole K, Lee J, Liotta LA, Raffeld M (1999) Immuno-LCM: laser capture microdissection of immunostained frozen sections for mRNA analysis. *Am J Pathol* 154:61–66

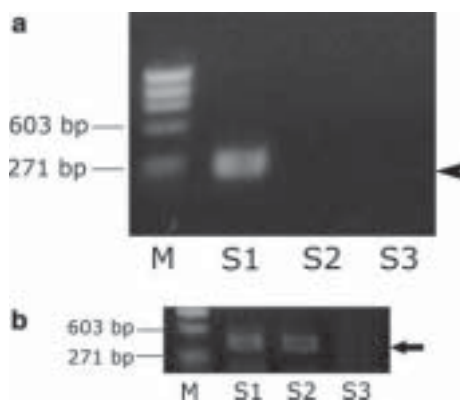


Fig. 3 Evaluation by PCR. **a** PCR-amplified product for parvalbumin (228 bp, *arrowhead*) and **b** PCR-amplified product for GAPDH (410 bp, *arrow*). *M* Φ X174/Hae III digest. *S1* Parvalbumin-immunopositive neurons taken from adjacent neutral red-stained sections. *S2* Parvalbumin-immunonegative neurons taken from adjacent neutral red-stained sections. *S3* Parvalbumin-immunopositive neurons directly taken from immunostained sections. 1% agarose gel

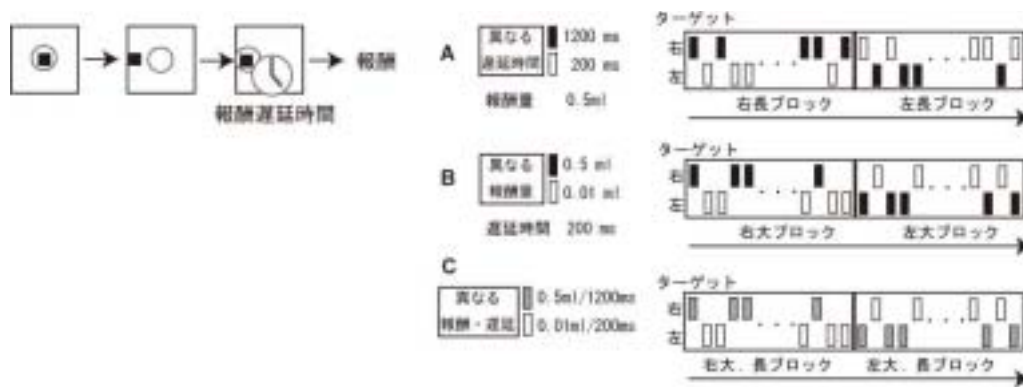
- Fink L, Kinfe T, Stein MM, Ermert L, Hanze J, Kummer W, Seeger W, Bohle RM (2000) Immunostaining and laser-assisted cell picking for mRNA analysis. *Lab Invest* 80:327–333
- Ghosh S, Steere AC, Stollar BD, Huber BT (2005) In situ diversification of the antibody repertoire in chronic Lyme arthritis synovium. *J Immunol* 174:2860–2869
- Goldsworthy SM, Stockton PS, Trempus CS, Foley JF, Maronpot RR (1999) Effects of fixation on RNA extraction and amplification from laser capture microdissected tissue. *Mol Carcinog* 25:86–91
- Houtani T, Munemoto Y, Kase M, Sakuma S, Tsutsumi T, Su1nsgimoto T (2005) Cloning and expression of ligand-gated ion-channel receptor L2 in central nervous system. *Biochem Biophys Res Commun* 335:277–285
- Jin L, Tsumanuma I, Ruebel KH, Bayliss JM, Lloyd RV (2001) Analysis of homogeneous populations of anterior pituitary folliculostellate cells by laser capture microdissection and reverse transcription-polymerase chain reaction. *Endocrinology* 142:1703–1709
- Kihara AH, Moriscot AS, Ferreira PJ, Hamassaki DE (2005) Protecting RNA in fixed tissue: an alternative method for LCM users. *J Neurosci Methods* 148:103–107
- Kohda Y, Murakami H, Moe OW, Star RA (2000) Analysis of segmental renal gene expression by laser capture microdissection. *Kidney Int* 57:321–331
- Lu L, Neff F, Alvarez-Fischer D, Henze C, Xie Y, Oertel WH, Schlegel J, Hartmann A (2005) Gene expression profiling of Lewy body-bearing neurons in Parkinson's disease. *Exp Neurol* 195:27–39
- Luo L, Salunga RC, Guo H, Bittner A, Joy KC, Galindo JE, Xiao H, Rogers KE, Wan JS, Jackson MR, Erlander MG (1999) Gene expression profiles of laser-captured adjacent neuronal subtypes. *Nat Med* 5:117–122
- Masuda N, Ohnishi T, Kawamoto S, Monden M, Okubo K (1999) Analysis of chemical modification of RNA from formalin-fixed samples and optimization of molecular biology applications for such samples. *Nucleic Acids Res* 27:4436–4443
- Mojsilovic-Petrovic J, Nestic M, Pen A, Zhang W, Stanimirovic D (2004) Development of rapid staining protocols for laser-capture microdissection of brain vessels from human and rat coupled to gene expression analyses. *J Neurosci Methods* 133:39–48
- Murakami H, Liotta L, Star RA (2000) IF-LCM: laser capture microdissection of immunofluorescently defined cells for mRNA analysis. *Kidney Int* 58:1346–1353
- Newton SS, Dow A, Terwilliger R, Duman R (2002) A simplified method for combined immunohistochemistry and in-situ hybridization in fresh-frozen, cryocut mouse brain sections. *Brain Res Brain Res Protoc* 9:214–219
- Specht K, Richter T, Mueller U, Walch A, Werner M, Hoefler H (2001) Quantitative gene expression analysis in microdissected archival formalin-fixed and paraffin-embedded tumor tissue. *Am J Pathol* 158:419–429
- Srinivasan M, Sedmak D, Jewell S (2002) Effect of fixatives and tissue processing on the content and integrity of nucleic acids. *Am J Pathol* 161:1961–1971
- Vincent VA, DeVoss JJ, Ryan HS, Murphy GM Jr (2002) Analysis of neuronal gene expression with laser capture microdissection. *J Neurosci Res* 69:578–586
- Walch A, Specht K, Smida J, Aubele M, Zitzelsberger H, Hoefler H, Werner M (2001) Tissue microdissection techniques in quantitative genome and gene expression analyses. *Histochem Cell Biol* 115:269–276

研究成果報告書

研究課題名	セロトニン・ドパミン相互作用による認知機能の基礎的研究		
(英文)	The role of serotonin-dopamine interaction in cognitive functions.		
事業推進者	中村 加枝	E-mail	nakamkae@takii.kmu.ac.jp
所属・職名	医学研究科・高次認知脳科学（生理学第2）講座・教授		
研究分担者名	久宝 真一、松崎 竜一、中尾 和子、市川 純		
キーワード	セロトニン、ドパミン、意志決定、霊長類、眼球運動		
<p>1. 概要</p> <p>報酬と、それを得るためのコスト・嫌悪刺激の両方の情報を計算して行動を選択する過程において、神経伝達物質であるドパミン・セロトニン系の相互抑制作用が報酬・コストバランスを調節する神経メカニズムであるという仮説が示唆されている。しかし、その神経メカニズムは不明である。本研究では神経伝達物質ドパミン・セロトニン含有細胞、および、これら両方の投射が強い腹側線条体における報酬とコスト・嫌悪情報の処理機構を明らかにするため、報酬量とコストの両方を考慮したサッケード(急速眼球運動) 課題を訓練したサルを用いて、単一神経細胞記録を行った。その結果、報酬をコードするドパミン系とは異なり、セロトニン系は、嫌悪またはコスト情報に関与していることがわかった。</p> <p>2. 研究の背景と目的</p> <p>報酬とそれを得るためのコスト・嫌悪刺激の情報を計算して行動を選択することは、生物の生存のみならず、経済活動・集団生活における利害関係に至るまで多様な行動様式に決定的な影響を与える。<u>意思決定における報酬と、コスト・嫌悪刺激の情報処理機構の研究の流れはふたつあり、一つは異なる領域、もう一つは異なる神経伝達物質によるものである。</u>領域については、主にヒトを対象とした機能的画像診断により、報酬情報は前頭諸領野・線条体・側坐核など、嫌悪刺激・コスト情報は前部島皮質・扁桃核・手綱核・中心灰白質の関与が指摘された。<u>神経伝達物質</u>については主に動物実験により、中脳ドパミン細胞の発火が報酬予測誤差(実際の報酬量と予測報酬量の差)を表現し、この信号が行動の学習を引き起こすことが示された。その過程は強化学習理論と関連付けられた。</p> <p>これまで、我々は、報酬量を操作した課題を遂行しているサルの眼球運動が期待報酬量によって変化し、そのメカニズムはドパミンの線条体への作用であることを示した(Nakamura & Hikosaka, 2006)。このように報酬に関しては研究が進んでいるが、嫌悪刺激・コスト情報に関しては不明な点が多い。</p> <p>一方、嫌悪刺激・コストの情報を調節する神経伝達物質としては、セロトニンが指摘されている(Cools <i>et al.</i>, 2008)。セロトニンが欠乏するとコスト・嫌悪刺激に過剰に敏感な行動決定をしやすい(Tanaka <i>et al.</i>, 2004)。我々は、報酬量を操作したサッケード課題を遂行中のサルの、セロトニン細胞を含む縫線核の単一細胞外神経活動記録を行い、縫線核細胞は tonic な発火パターンにより、報酬の大小をコードすることを示した(Nakamura & Hikosaka, 2008)。</p> <p>本研究は、さらにこれを発展させ、ドパミン・セロトニン含有細胞と、これら両者の強い投射先である側坐核における報酬かつコスト・嫌悪刺激の統合情報処理のメカニズムを明らかにすることを目的とする。特に、(1) 嫌悪情報刺激の情報処理について (2) 報酬の大小とコストの大小が相反する場合(たとえばコストも多いが報酬も多い)の計算機構について注目した。</p>			

3. 研究方法

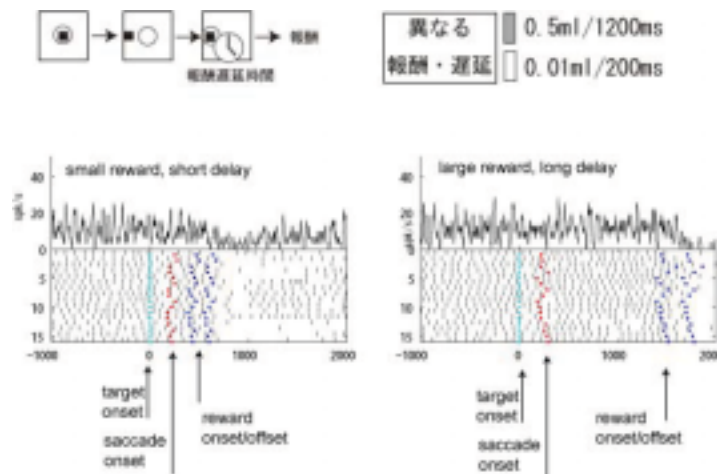
行動課題として「異なる遅延サックード課題」を行った。この課題では、左右へのサックード課題において動物にとっては嫌悪刺激である「遅延時間」の操作をする。サルが注視点を見つめていると、右か左にターゲットが現れ、それに向かってサックードをする。ここで、遅延時間の操作をする。異なる遅延時間(1200 ms と 200 ms)と一定の方向のターゲットを関連付け、ブロック内では一定化する。ターゲットの位置と遅延時間の関係は一定の試行数例えば 24 試行毎に (ブロック毎に) スイッチする。比較として報酬量の操作もする (0.01 ml と 0.5 ml のジュース)。これまで2頭のカニクイザルについて行動解析を行い、反応時間および error rate から、動物が確かにジュースを報酬、遅延時間を嫌悪刺激として認識していることを確認した。さらに、報酬と遅延時間を同時に変化させる場合も行った。



この課題を用いて、1頭のサルでは腹側線条体の一部である側坐核、もう一頭ではセロトニン細胞の分布する背側縫線核から単一神経細胞記録を開始した。

4. これまでの成果

側坐核細胞には、報酬そのものに反応し、報酬量に依存してその活動を変えるものや、報酬獲得前より、漸増性に神経活動を増加させ、報酬に対する期待を表すと考えられるものなど、報酬に関連した神経活動が認められた。側坐核における報酬の情報処理については主にラットにおいて指摘されているが、今回サルで、より詳細な行動パラメータと関連付けて調べることができた。



この背側縫線核ニューロンは、多い報酬を長く待った後に得られる、という場合に強く発火し続け、報酬を得ると抑制された。

背側縫線核では、報酬量の大小によって活動が tonic に変化するものが認められた。また、試行の間に特に発火する inter-trial-interval type の細胞も認められた。さらに、多い報酬を期待して遅延期間を待つ場合（すなわちベネフィットのためにコストを払う）に強く発火または抑制される細胞が認められた。これは背側縫線核細胞がコストの情報処理、さらにそれを報酬情報との統合に関与するメカニズムに関与している可能性を示唆している。

5. これまでの進捗状況と今後の計画

これまでの神経活動記録をさらに発展させ、さらに以下のことについて検討したい。

(1) 報酬や遅延の操作のみならず、古典的な嫌悪刺激に対する活動の検討。

Air-puff 刺激を用いて、conditioning 課題を用いて、側坐核・背側縫線核から記録する

(2) 動物に2者択一課題をさせ、個体の判断と神経活動の関連を調べる。

(3) 同様の課題におけるドパミン細胞の発火パターンと、その側坐核・背側縫線核との関連を調べるために、他部位同時記録を行う。

(4) ドパミン・セロトニン およびにおいて、それぞれの含有核が寄与するメカニズムを調べるため、局所的に dopamine および serotonin 作用薬を注入し、その投射先の神経活動の変化および行動パターンの変化を検討する。

6. これまでの発表論文

(1) 発表論文

1) 原著論文

Nakamura, K., Matsumoto, M., & Hikosaka, O.

Reward-dependent modulation of neuronal activity in the primate dorsal raphe nucleus.

J. Neurosci. **28**, 5331-5343 (2008).

(2) 学会発表

国際学会

2) シンポジウム講演

1. Nakamura, K.

Neuronal Activity of the Primate Dorsal Raphe Nucleus in the Biased Reward Saccade Tasks
Annual Meeting, Society for Neuroscience, mini symposium, San Diego, USA, 2007.

2. Nakamura, K.

Differential reward coding by dorsal raphe neurons and dopamine neurons

Champalimaud Neuroscience Workshops at the Instituto Gulbenkian de Ciência, “Theoretical and Experimental Perspectives on Serotonin Function”, Ericeira, Sintra, Portugal, 2007.

7. これまでの成果の情報公開

ホームページ：生理学第二講座＝<http://www3.kmu.ac.jp/psl2/>

Reward-Dependent Modulation of Neuronal Activity in the Primate Dorsal Raphe Nucleus

Kae Nakamura, Masayuki Matsumoto, and Okihide Hikosaka

Laboratory of Sensorimotor Research, National Eye Institute–National Institutes of Health, Bethesda, Maryland 20892-4435

The dopamine system has been thought to play a central role in guiding behavior based on rewards. Recent pharmacological studies suggest that another monoamine neurotransmitter, serotonin, is also involved in reward processing. To elucidate the functional relationship between serotonin neurons and dopamine neurons, we performed single-unit recording in the dorsal raphe nucleus (DRN), a major source of serotonin, and the substantia nigra pars compacta, a major source of dopamine, while monkeys performed saccade tasks in which the position of the target indicated the size of an upcoming reward. After target onset, but before reward delivery, the activity of many DRN neurons was modulated tonically by the expected reward size with either large- or small-reward preference, whereas putative dopamine neurons had phasic responses and only preferred large rewards. After reward delivery, the activity of DRN neurons was modulated tonically by the received reward size with either large- or small-reward preference, whereas the activity of dopamine neurons was not modulated except after the unexpected reversal of the position–reward contingency. Thus, DRN neurons encode the expected and received rewards, whereas dopamine neurons encode the difference between the expected and received rewards. These results suggest that the DRN, probably including serotonin neurons, signals the reward value associated with the current behavior.

Key words: serotonin; dopamine; raphe; saccade; primate; reinforcement; reward

Introduction

Many functions of the brain are modified by various kinds of monoamine neurons. In particular, dopamine and serotonin appear to be the two major modulators of motivational and emotional behaviors (for review, see Daw et al., 2002). The role of dopamine is particularly clear because dopamine neurons in the midbrain and around the substantia nigra pars compacta (SNc) are excited by a reward or a sensory event that predict the reward, either of which can change motivational or emotional states. More specifically, the activity of the dopamine neurons encodes the difference between the expected reward and the actual reward, which is often called reward prediction error. This signal is suggested to induce learning and modulate actions (Mirenowicz and Schultz, 1994; Montague et al., 1996; Schultz et al., 1997; Hollerman and Schultz, 1998; Schultz, 1998; Suri and Schultz, 1998).

Several lines of evidence suggest that serotonin is also related to reward-related behaviors (Rogers et al., 1999; Daw et al., 2002; Doya, 2002; Schweighofer et al., 2007), in addition to other functions such as the sleep–wake cycle (McGinty and Harper, 1976; Lydic et al., 1983; Guzman-Marín et al., 2000; Dugovic, 2001), appetite (Curzon, 1990), locomotion (Jacobs and Fornal, 1993),

emotion and social behavior (Davidson et al., 2000; Graeff, 2004), stress-coping behavior (Deakin, 1991; Graeff et al., 1996), and learning and memory (Meneses, 1999). Notably, it has been proposed that there are opponent interactions between dopamine and serotonin (for review, see Kapur and Remington, 1996). However, the physiological basis of the function of the serotonin system in the cognitive and motivational behavior has not been well understood. Electrophysiological studies of the raphe nuclei have been focused mainly on sleep–wake cycle and motor behavior (for review, see Jacobs and Fornal, 1993). Specifically, it is unknown whether and how serotonin neurons in the raphe nuclei encode reward-related information.

In a series of studies using saccade tasks with a biased reward schedule, we have shown that the activity of neurons in the caudate (Kawagoe et al., 1998; Lauwereyns et al., 2002) and the substantia nigra pars reticulata (SNr) (Sato and Hikosaka, 2002), as well as putative dopamine neurons in SNc (Nakahara et al., 2004; Takikawa et al., 2004), was modulated depending on the expected reward. We also showed that the reward-dependent changes in saccade behavior depended on the physiological dopamine release in the caudate (Nakamura and Hikosaka, 2006). Having found that these tasks engage the basal ganglia and the dopamine system, we hypothesized that they would also recruit the serotonin system. We therefore recorded from the dorsal raphe nucleus (DRN), the principal source of serotonergic innervations in the basal ganglia (van der Kooy and Hattori, 1980; Imai et al., 1986; Corvaja et al., 1993). As a comparison, we also recorded from dopamine neurons using the same tasks in the same animals. We found that neurons in the DRN relay signals related to cognitive and motivational processes, but in a different manner from the dopamine system.

Received Jan. 3, 2008; revised April 7, 2008; accepted April 8, 2008.

This work was supported by the intramural research program of the National Eye Institute. We thank Dr. Long Ding and Ethan Bromberg-Martin for helpful comments. We thank GC America, Inc., for providing us with dental acrylic.

Correspondence should be addressed to Kae Nakamura at her present address: Department of Physiology, Kansai Medical University, School of Medicine, 10-15, Fumizono-cho, Moriguchi-city, Osaka 570-8506, Japan. E-mail: nakamkae@takii.kmu.ac.jp.

DOI:10.1523/JNEUROSCI.0021-08.2008

Copyright © 2008 Society for Neuroscience 0270-6474/08/285331-13\$15.00/0

Materials and Methods

General. We used four hemispheres of two rhesus monkeys (*Macaca mulatta*; laboratory designations: E, male; L, female). Both animals had been implanted with scleral search coils for measuring eye position and a post for holding the head. The recording chambers were placed over the posterior cortices. All aspects of the behavioral experiment, including presentation of stimuli, monitoring of eye movements, monitoring of neuronal activity, and delivery of reward and electrical stimulation were under the control of a QNX-based real-time experimentation data acquisition system (REX; Laboratory of Sensorimotor Research, National Eye Institute–National Institutes of Health, Bethesda, MD). Eye position was monitored by means of a scleral search coil system with 1 ms resolution. Stimuli generated by an active matrix liquid crystal display projector (PJ550; ViewSonic, Walnut, CA) were rear-projected on a frontoparallel screen 25 cm from the monkey's eyes. On successful completion of each trial, drops of water or juice were delivered as reward through a spigot under control of a solenoid valve. Magnetic resonance images were obtained to determine the position of the electrode. The activity of single neurons was recorded using tungsten electrodes (Frederick Haer, Bowdoinham, ME; diameter, 0.25 mm; 1–3 M Ω). The signal was amplified with a bandpass filter (200 Hz to 5 kHz) (BAK, Mount Airy, MD) and collected at 1 kHz via custom-made window discriminator (MEX). We also collected spike wave form for each recorded neuron. All procedures were approved by the Institutional Animal Care and Use Committee and complied with Public Health Service Policy on the humane care and use of laboratory animals.

Behavioral task. The animal performed a memory-guided saccade task with a biased reward schedule [one-direction rewarded memory-guided saccade task (1DR-MGS)] (see Fig. 1A). The appearance of a central fixation point (FP) (diameter, 0.6°) signaled the trial initiation. The monkeys were required to fixate on the FP and maintain fixation within a window of $\sim 3^\circ$. After fixation on the FP for 1000–1500 ms ("fixation period"), a cue indicating the future target position (diameter, 1.2°) was presented for 100 ms either to the right or left 20° from the FP. The position of the target was chosen pseudorandomly such that within every "subblock" of four trials each of the two positions was chosen twice. The monkey had to keep fixating on the FP for another 800 ms until the FP went off. The disappearance of the FP was the cue for the monkey to make a saccade toward the memorized cue position. A correct saccade was signaled by the appearance of the target with a 100 ms delay. A liquid reward was delivered with an additional 100 ms delay. If the monkey broke fixation at any time during the fixation period or failed to make a saccade to the cued position, the trial was determined to be an error, and the same trial was repeated until a correct saccade occurred. The intertrial interval, which started at the time of reward offset and lasted until FP onset in the next trial, was 3 s.

The biased reward schedule was introduced in blocks (Kawagoe et al., 1998). In one block of 20–28 trials (10–14 trials for each direction), the amount of reward was always large (0.4 ml) for one direction of the target and small (0 or 0.01 ml) for the other direction (for example, left, large reward; right, small reward). In the next block, the position–reward contingency was reversed (i.e., left, small; right, large). These two kinds of blocks with opposite position–reward contingencies are called the left-large and right-large blocks, and they were alternated two or three times for each recording session (see Fig. 1C).

In a separate experiment, we also used a visually guided saccade task [one-direction rewarded visually guided saccade task (1DR-VGS)] (see Fig. 1B). After fixation on the FP for 1200 ms (fixation period), the FP disappeared and at the same time, the target (1.2°) appeared either to the right or left 20° from the FP. The monkey then had to make a saccade to the target immediately. The trial sequence and the reward schedule were the same as those in 1DR-MGS.

We used both 1DR-MGS and 1DR-VGS tasks for 64 DRN neurons, 1DR-MGS only for 20 neurons, and 1DR-VGS only for 103 neurons in two monkeys. For dopamine neuron recordings, we used only 1DR-VGS.

Mapping and recording of the DRN. The location of DRN was estimated using magnetic resonance imaging and was later verified histologically (see below). A recording chamber, which was angled 38° (monkey E) or

35° (monkey L) posteriorly, was implanted over the midline of the parietal cortex to access the brainstem between the superior colliculi and the inferior colliculi. For electrophysiological recordings, we used a grid system (Crist et al., 1988). A stainless-steel guide tube (outer diameter, 0.6 mm; inner diameter, 0.35 mm) was inserted through a grid hole, and, after penetrating the dura, it was lowered until its tip reached ~ 7 mm above the surface of the superior colliculi, which was estimated by magnetic resonance images. Through the guide tube, we inserted an electrode to reach the DRN. The distance of the recording sites from the midline was 1 or 1.5 mm. The anteroposterior extent of the recording sites was 2 mm, which corresponded to 6–8 mm anteriorly to the level of the ear canals (Horsley–Clarke coordinates) in both monkeys.

The DRN is known to be a major source of serotonin neurons (Dahlstrom and Fuxe, 1964; Leger et al., 2001). It has traditionally been accepted that DRN serotonin neurons spontaneously fire slowly and regularly with broad spikes, whereas nonserotonin neurons generally fire more rapidly and irregularly with narrow spikes (Aghajanian et al., 1978; Sawyer et al., 1985; Jacobs and Fornal, 1991; Hajos et al., 1998). Recent studies, however, report that serotonin neurons do not always differ significantly from nonserotonin neurons in terms of these electrophysiological features (Allers and Sharp, 2003; Kocsis et al., 2006). In this report, therefore, rather than choosing neurons with specific electrophysiological properties, we studied all well isolated neurons in the DRN whose activity changed during saccade tasks.

To record from putative dopamine neurons, we searched in and around the SNc. Dopamine neurons were identified by their irregular and tonic firing around 5 spikes/s with broad spike potentials. In this experiment, we focused on dopamine neurons that responded to reward-predicting stimuli with a phasic excitation.

Histology. At the conclusion of the experiments, we made electrolytic microlesions at selected recording sites in monkey L. The animal was then deeply anesthetized with pentobarbital and perfused with 10% formaldehyde. The brain was cut into 50 μ m coronal sections and stained with cresyl violet (see Fig. 1D).

Data analysis. A neuron was judged to be task-related if there was a statistical difference in its firing rate across the following seven task periods (Kruskal–Wallis, $p < 0.007 \approx 0.05/7$): fixation point onset to cue (target) onset, 0–200 ms after target onset, 700–0 ms before fixation point offset (only for 1DR-MGS), 200 ms before to 200 ms after saccade, and three postreward periods, which were 0–400, 400–1200, and 1200–2000 ms after reward onset.

Because reward-related modulation of neuronal activity was found mainly during a period after target onset (which indicated the size of an upcoming reward) and during a period after reward delivery, we focused our analysis on neuronal activity during the two task periods: (1) a 400 ms period after target onset, which we will call "prereward period," and (2) a 400 ms period starting 400 ms after reward onset, which we will call "postreward period." We analyzed the neuronal activity in each task period using a two-way ANOVA [reward (large or small) by direction (contralateral or ipsilateral target to the recording site)].

To examine changes in neuronal activity throughout the trial as a whole, we computed a receiver operating characteristic (ROC) value comparing the firing rate in a test window of 100 ms aligned with respect to a task-related event (e.g., target onset) to the firing rate in a control window of 400 ms before fixation onset. We repeated the ROC analysis on consecutive overlapping test windows (advanced in 20 ms steps), separately for the large-reward, small-reward, contraversive-saccade, and ipsiversive-saccade trials (see Fig. 3A–D). Similarly, to examine the changes in the reward and direction effects, we computed an ROC value comparing the firing rates in the same test window of 100 ms between the large- and small-reward trials (reward effects) (see Fig. 3E) and between the contraversive- and ipsiversive-saccade trials (direction effects) (see Fig. 3F).

To examine the changes in the neuronal activity in the prereward and postreward periods after the reversal of position–reward contingency, we normalized the firing rate in each trial by the following: (the firing rate in the trial – the mean firing rates across all trials)/(SD of the firing rate across all trials). We performed this calculation for each direction of saccades. Then we compared the firing rates for the i th (e.g., the first and

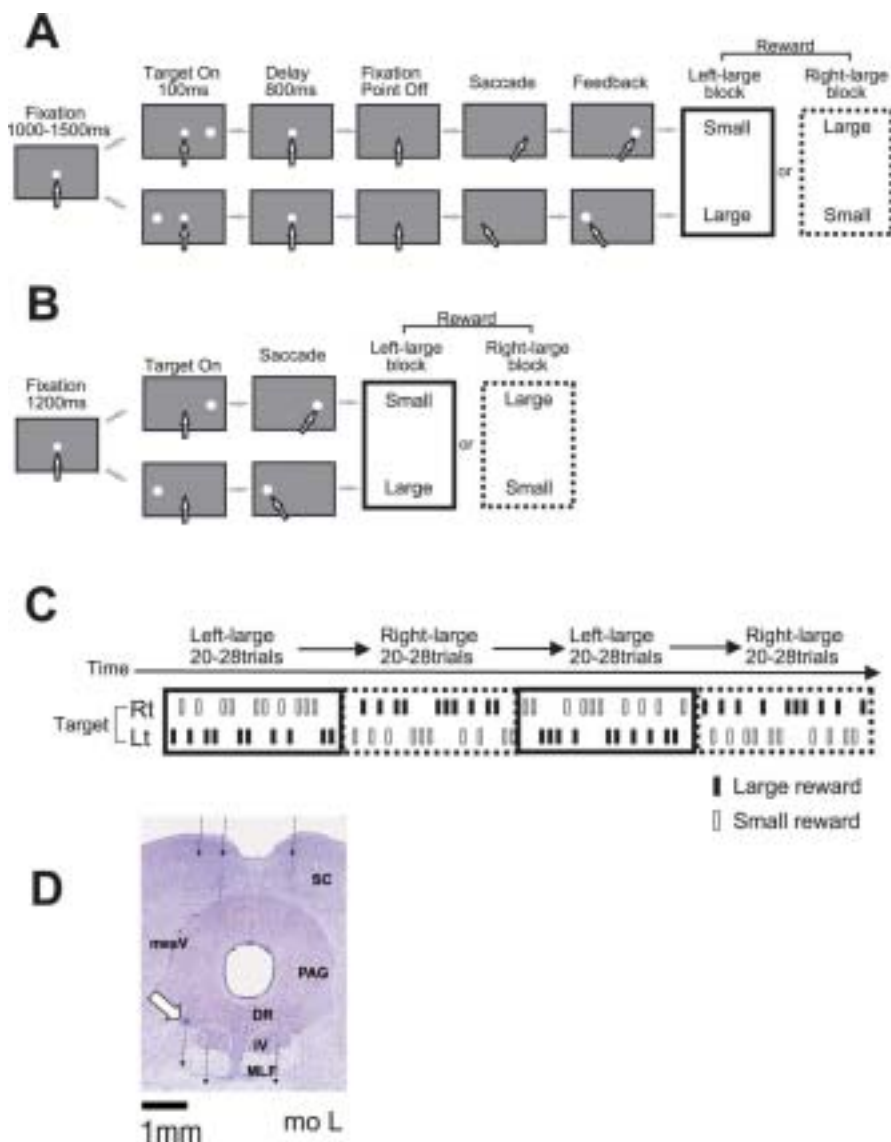


Figure 1. Experimental procedure. **A**, Memory-guided saccade task with biased reward schedule (1DR-MGS). After the monkey fixated on the central fixation point for 1000–1500 ms, one of the two target positions was flashed for 100 ms. After the fixation point disappeared, the monkey made a saccade to the cued position to receive a liquid reward. The white arrows indicate the direction of gaze. In a block of 20–28 trials (e.g., left-large block), one target position (e.g., left) was associated with a large reward and the other position (e.g., right) was associated with a small reward. The position–reward contingency was then reversed (e.g., right-large block). **B**, Visually guided saccade task with asymmetric reward schedule (1DR-VGS). After a 1200 ms fixation period, the fixation point disappeared and at the same time the target appeared, and the monkey immediately made a saccade to the target to receive a reward. **C**, Left-large and right-large conditions were alternated between blocks with no external cue. The location of the target was determined pseudorandomly. **D**, Histological reconstruction of recording sites in monkey L. The three broken lines, from right to left, indicate electrode penetrations at 1.0 mm to the right, 1.0 mm left, and 1.5 mm left. The white arrow indicates a microlesion made after recording of a DR neuron. DR, Dorsal raphe nucleus; MLF, medial longitudinal fasciculus; PAG, periaqueductal gray; SC, superior colliculus; IV, trochlear nucleus; mesV, mesencephalic trigeminal nucleus.

second) trials before and after the contingency reversal with the firing rates for the last five trials during the new block (Mann–Whitney *U* test, $p < 0.01$) (see Fig. 8).

We characterized the physiological properties of recorded neurons by (1) spike wave form, (2) baseline firing rate, and (3) irregularity of firing pattern. The typical spike shape consisted of the following waves in order: first, sharp negative; second, sharp positive; third, long-duration negative; fourth, long-duration positive. Thus, we measured the spike duration from the first sharp negative to the peak of the fourth, long-duration positive deflection (Kocsis et al., 2006). It ranged from 1.0 to 3.7 ms (mean, 2.2 ms; SD, 0.58 ms). Baseline firing rate is the mean firing rate during 1000 ms before the onset of the fixation point on the first trial of

each experiment, because the activity during the intertrial interval was often modulated tonically after the delivery of reward in the preceding trial. Finally, to quantify irregularity of spike trains, we used an irregularity metric introduced by Davies et al. (2006) which they called “IR.” First, interspike interval (ISIs) was computed for each “between-spikes.” If spike($i - 1$), spike(i), and spike($i + 1$) occurred in this order, the duration between spike($i - 1$) and spike(i) corresponds to ISI_i ; the duration between spike(i) and spike($i + 1$) corresponds to ISI_{i+1} . Second, the difference between adjacent ISIs was computed as $|\log(ISI_i/ISI_{i+1})|$. The value was then assigned to the timing when the spike(i) occurred. Thus, small IR values indicate regular firing and large IR values indicate irregular firing. We then computed a median of all IR values during the whole task period for all correct trials. This measure has an advantage over traditional measures of irregularity, such as the coefficient of variation of the interspike intervals, which require a constant firing rate during the measurement period. This requirement was not met in our experiments because neural responses often changed during the task periods. We analyzed IR values of DRN neurons, putative dopamine neurons, and putative projection neurons in the caudate (supplemental Fig. 1, available at www.jneurosci.org as supplemental material). The caudate data were obtained in the separate experiments (Davies et al., 2006).

Results

We analyzed the activity of DRN neurons using two tasks with biased reward schedules: a memory-guided saccade task (1DR-MGS) (Fig. 1A) (17 neurons from monkey E; 67 from monkey L) and a visually guided saccade task (1DR-VGS) (Fig. 1B) (96 neurons from monkey E; 71 from monkey L). Because the biased reward schedule was introduced in blocks, on each trial the animal could predict the reward value based on the location of the target cue (Fig. 1C). Indeed, saccadic reaction times were significantly shorter for large-reward than small-reward trials in both monkeys in both tasks (supplemental Table 1, available at www.jneurosci.org as supplemental material; see also Fig. 8G).

The electrode was directed to the DRN through a recording chamber that was implanted over the midline of the parietal cortex. During the initial survey of DRN, the following brain structures were identified and used as landmarks: superior colliculus with receptive fields in the upper visual field with large eccentricities, inferior colliculus with auditory responses, mesencephalic trigeminal nucleus with responses to mouth movements, the locus ceruleus with phasic responses to salient sensory stimuli, and trochlear nucleus with increased firing during downward eye movements. We analyzed neurons located 0–2 mm anterior to the trochlear nucleus.

Traditionally, it has been accepted that serotonin neurons fire broad spikes spontaneously in a slow and regular “clock-like” firing pattern (Aghajanian et al., 1978; Sawyer et al., 1985; Jacobs

and Fornal, 1991; Hajos et al., 1998). Therefore, we computed the baseline firing rate, spike duration, and regularity of sampled neurons (see Materials and Methods). The baseline firing rate across neurons ranged from 0 to 22 spikes/s with a mean of 4.9 spikes/s (SD, 4.3; median, 4.0). The spike duration ranged from 1.0 to 3.7 ms (mean, 2.2 ms; SD, 0.58 ms). Different methods have been used to quantify the regularity of neuronal firing (Shinomoto et al., 2003). In this study, we used the irregularity metric IR, which was the median value of the differences between adjacent interspike intervals during the whole task period (Davies et al., 2006) (see Materials and Methods). Smaller IR values indicate more regular firing. There was no significant difference in IR value between 1DR-MGS and 1DR-VGS (Wilcoxon signed rank test, $p = 0.79$) (supplemental Fig. 1A, available at www.jneurosci.org as supplemental material). The IR values for the DRN neurons we sampled were significantly smaller (i.e., more regular) than those for putative projection neurons in the caudate nucleus ($p < 0.0001$) and putative dopamine neurons in the substantia nigra pars compacta ($p = 0.02$) (supplemental Fig. 1B, available at www.jneurosci.org as supplemental material). Among DRN neurons, there was no significant correlation between IR values and spike duration ($p = 0.4$, Spearman rank correlation) or baseline firing rate ($p = 0.05$).

Reward-dependent modulations in DRN neuronal activity

DRN neurons exhibited task-related modulations with distinctive features during the performance of the 1DR-MGS. Most notably, DRN neurons often showed reward-dependent modulations in activity after reward onset. Figure 2A shows a representative example. This neuron was characterized by long spike duration (2.76 ms), low baseline activity (2 Hz), and regular firing (median IR, 0.31). The neuron exhibited an increase in activity after the onset of the fixation point (FPon) followed by regular and tonic firing until reward onset. The activity further increased after the onset of a large reward but ceased after the onset of a small reward. This modulation occurred regardless of the direction of the saccade, and lasted for 860 ms after reward onset (permutation test, $p < 0.05$) (see Materials and Methods). Such reward-dependent modulations during the postreward period lasted longer for other DRN neurons. For example, the neuron in Figure 2B was also characterized by long spike duration (2.6 ms), low baseline activity (6 Hz), and regular firing pattern (median IR, 0.50). For both saccade directions, there was a long-lasting decrease in activity starting 400 ms after the onset of large reward (permutation test, $p < 0.05$). The activity of the neuron in Figure 2C (baseline firing rate, 3 Hz; spike duration, 1.9 ms; IR = 0.47) was significantly stronger for large- than small-reward trials starting 800 to 1500 ms after reward onset. The neuron in Figure 2D (baseline firing rate, 10 Hz; spike duration, 1.4 ms; IR = 0.48) also exhibited a long-lasting reward effect starting around the time of reward offset. Note that, in all of these examples, the postreward modulations of activity disappeared before the next trial started (supplemental Fig. 2, available at www.jneurosci.org as supplemental material).

In some neurons, reward-dependent modulations were also observed before reward onset during the delay period. The neuron in Figure 2C exhibited stronger activity on small-reward than large-reward trials ($p = 0.8 \times 10^{-6}$). The neuron in Figure 2D also exhibited stronger activity on small- than large-reward trials, but only when leftward saccades were required (two-way ANOVA, reward effect, $p = 0.005$; interaction, $p = 0.02$). Such direction selectivity, however, was relatively rare among DRN neurons.

Reward-dependent modulations in activity during the delay and the postreward periods, as shown in the example neurons in Figure 2, were commonly observed in the population of DRN neurons. Figure 3, A–D, illustrate the time course of these modulations using ROC analysis, by comparing the firing rate of each neuron for each task condition to the baseline activity during 400 ms before fixation onset. During the delay and postreward periods of the task, many DRN neurons had tonic increases in activity (shown in warm colors) or decreases in activity (cool colors).

Figure 3E shows the time course of reward selectivity, using ROC analysis to compare the activity of each neuron between large- and small-reward trials. Figure 3F shows a similar analysis for direction selectivity, comparing contraversive- and ipsiversive-saccade trials. The reward effect was present in many neurons during both task periods before (mainly the delay period) and after reward, whereas direction effects were uncommon.

The data in Figure 3, A and B, reveal a notable difference in the reward-dependent modulations between the prereward period and the postreward period. For each neuron, the changes in activity during the prereward period, compared with the baseline activity, tended to be in the same direction on both large- and small-reward trials (Fig. 3A,B). On the contrary, the changes in activity during the postreward period, compared with the baseline activity, tended to be in opposite directions (Fig. 3A,B). For example, for the neuron shown in Figure 2A, the prereward activity increased compared with the baseline on both large- and small-reward trials. However, the postreward activity increased on large-reward trials, but it was inhibited on small-reward trials.

The main cause of the reward effect during the prereward period was that the changes in activity tended to be stronger on large-reward trials than on small-reward trials, which is illustrated by the greater intensity of colors in Figure 3A than in Figure 3B. To quantify the trend, we computed the prereward activity as the firing rate during 400 ms after target onset minus the baseline firing rate, and the results are shown in Figure 4A. Among 22 neurons (22 of 84; 26%) that showed significant reward effects during the prereward period, 20 neurons exhibited significant activity changes on large-reward trials, whereas only 10 neurons did on small-reward trials. This tendency is illustrated by a wider distribution of the prereward activity on large-reward trials than that on the small-reward trials (Fig. 4A, marginal histograms). When the firing rate in the prereward period was compared between the reward conditions, 16 neurons showed higher firing rates on the large-reward trials than on the small-reward trials; the other 6 neurons showed the opposite pattern (two-way ANOVA, $p < 0.01$).

Reward-dependent modulations were clearer and more prevalent in postreward activity. Among 42 neurons (42 of 84; 50%) that showed significant reward effects during the postreward period, 24 neurons showed changes in activity in opposite directions between large- and small-reward trials (Fig. 4B, data points in the top left and bottom right quadrants). When postreward activity was compared between the reward conditions, 18 neurons showed a large-reward preference (i.e., higher firing rates on large-reward trials than on small-reward trials); the other 24 neurons showed a small-reward preference (two-way ANOVA, $p < 0.01$).

As discerned from Figure 3, A–D, some DRN neurons also exhibited changes in activity (1) after fixation onset: increases for 23 of 84 (27.4%) or decreases for 12 of 84 (14.3%) neurons (comparison between activity during 400 ms before and 200 ms after fixation onset; Mann–Whitney U test, $p < 0.01$), and (2) during

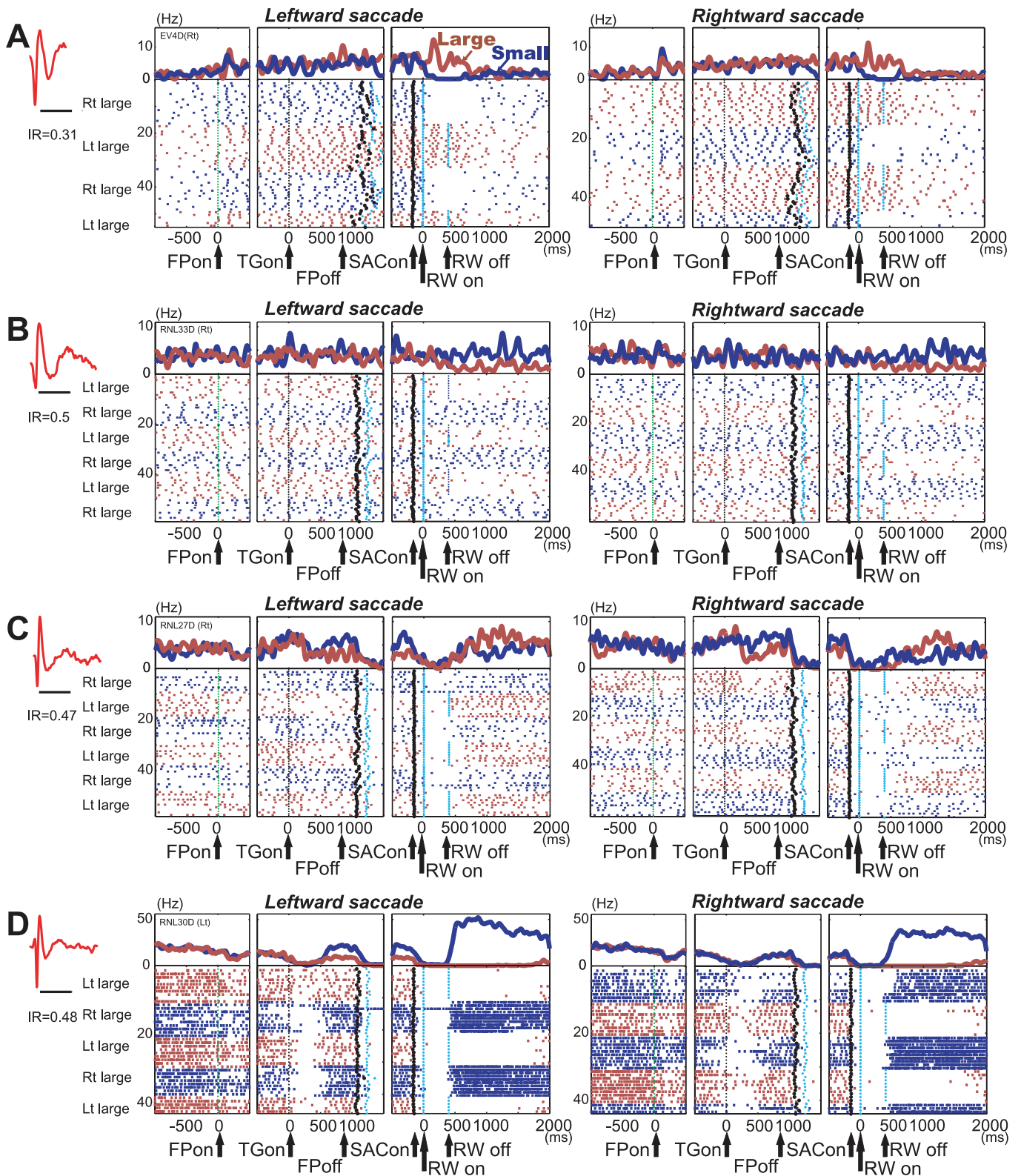


Figure 2. *A–D*, Activity of four neurons in the DRN in 1DR-MGS task. For each neuron, action potentials are shown by raster plots in chronological order of trials, separately for leftward and rightward saccades. The changes in firing rate are shown by perievent histograms at top [smoothed with a Gaussian kernel ($\sigma = 5$ ms; width, 5σ)]. The activity in large- and small-reward trials is shown in red and blue, respectively. The histograms and raster plots are shown in three sections, left section aligned at the time of fixation point onset (FPon), middle aligned on target onset (TGon) and fixation point offset (FPoff), and right aligned on reward onset (RWon). Note that the reward offset (RWoff) applies only to large-reward trials. Spike shape and irregularity metric (IR) for each neuron are shown on the left (timescale, 2 ms). The black dots indicate saccade onset (SACon), and the light blue dots indicate reward onset and offset.

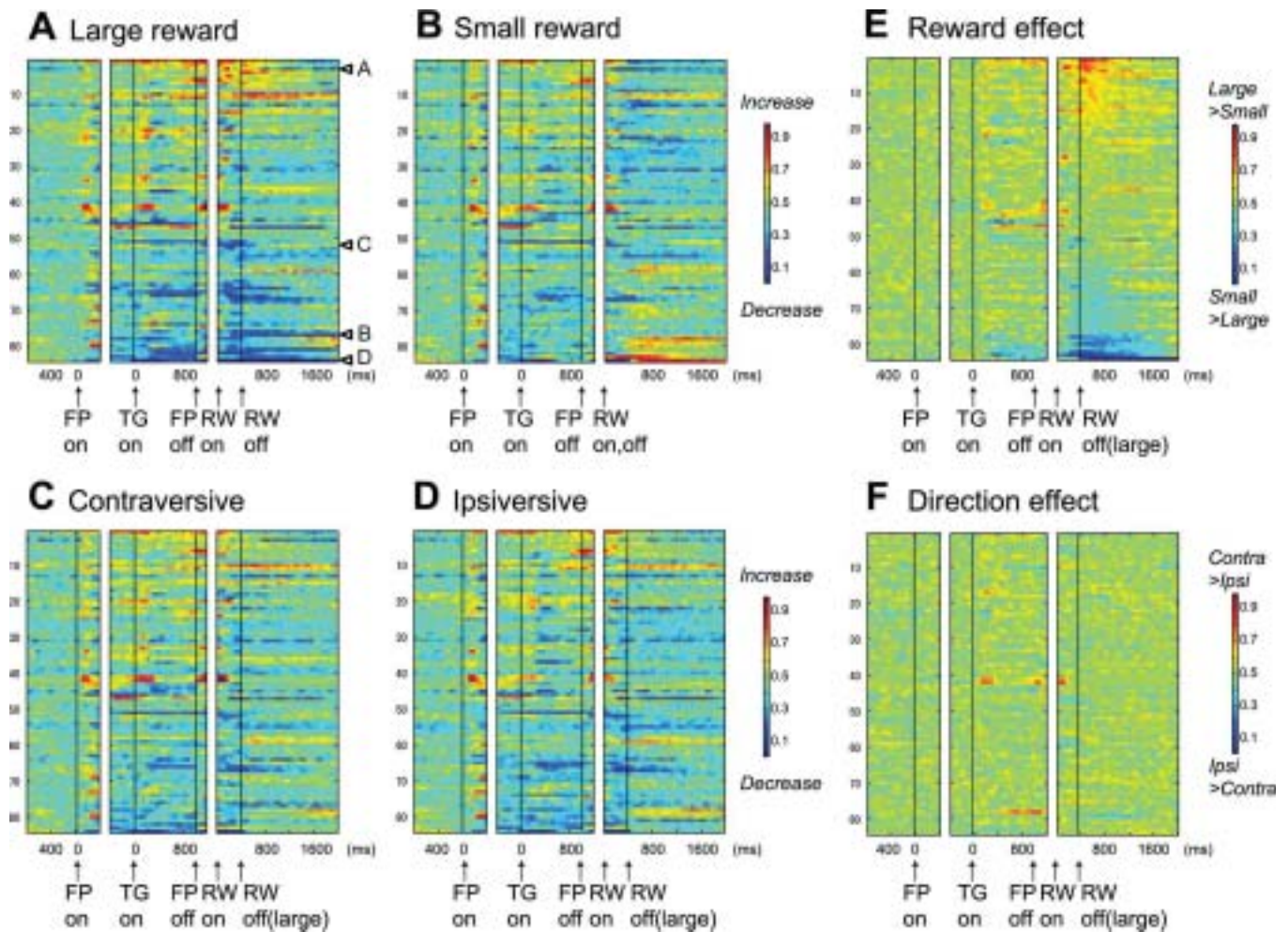


Figure 3. Population activity of DR neurons in 1DR-MGS task ($n = 84$). The activity of each neuron is presented as a row of pixels. **A–D**, Changes in neuronal firing rate from baseline are compared in large- and small-reward trials (**A, B**) and in contralateral and ipsilateral trials (**C, D**). The color in each pixel indicates ROC value based on the comparison of the firing rate between a control period just before fixation onset (400 ms duration) and a test window centered on the pixel (100 ms duration). This analysis was repeated by moving the test window in 20 ms steps. Warm colors (ROC > 0.5) indicate increases in firing rate relative to the control period, whereas cool colors (ROC < 0.5) indicate decreases in firing rate. **E, F**, Changes in reward-dependent (**E**) and direction-dependent (**F**) modulation. The ROC value in each pixel was based on the comparison of firing rate in the same test window centered on the pixel between large- and small-reward trials (**E**) and between contraversive- and ipsiversive-saccade trials (**F**). Warm colors (ROC > 0.5) indicate higher firing rates on large- than on small-reward trials (**E**) and on contraversive than on ipsiversive trials (**F**). In all panels (**A–F**), neurons have been sorted in order of ROC values for the reward effect during the postreward (400–800 ms) period (**E**). Arrows A–D in **A** indicate the data for neurons shown in Figure 2. FP, Fixation point; TG, target; RW, reward.

the later fixation period: increases for 17 of 84 (20.2%) or decreases for 20 of 84 (23.8%) neurons (comparison between activity during 400 ms before fixation onset and 800–400 ms before target onset, $p < 0.01$).

Comparison of reward-dependent modulations between DRN and dopamine neurons

To understand the functional significance of the reward-related activity of DRN neurons, we compared it to the activity of dopamine neurons in the same two monkeys. For this purpose, we used a visually guided version of the biased-reward saccade task (Fig. 1*B*, 1DR-VGS). We recorded from 167 DRN neurons (96 from monkey E; 71 from monkey L) and 64 dopamine neurons (20 from monkey E; 44 from monkey L).

The characteristics of the reward-dependent modulations in the activity of DRN neurons in 1DR-VGS were similar to those found in 1DR-MGS. Thus, many DRN neurons exhibited increases or decreases in tonic activity (usually increases) after the onset of the fixation point. These changes became more evident during the prereward period, after the onset of the saccade target

that indicated the size of the upcoming reward. As in 1DR-MGS, changes in prereward activity occurred in the same direction on both large- and small-reward trials (Fig. 5*A, B*), but tended to be greater on large-reward trials (Fig. 6*A*), thus leading to differences in activity between the two reward conditions (Fig. 5*E*). Among 44 neurons (44 of 167; 26%) that showed significant reward effects during the prereward period, 34 exhibited significant activity changes on large-reward trials (29 increase and 5 decrease), whereas only 15 did on small-reward trials (13 increase and 2 decrease).

In the postreward period, the same DRN neurons tended to exhibit opposite changes in activity (Fig. 5*A, B*). Among 74 neurons (74 of 167; 44%) that showed significant reward effects, 40 neurons changed their activity in opposite directions on large- and small-reward trials (Fig. 6*B*). About one-half ($n = 36$) showed a large-reward preference, whereas the other 38 neurons showed a small-reward preference (two-way ANOVA, $p < 0.01$). The direction of the reward preference was not always the same between the prereward and postreward periods (Fig. 6*E*).

The activity pattern of dopamine neurons was distinctively

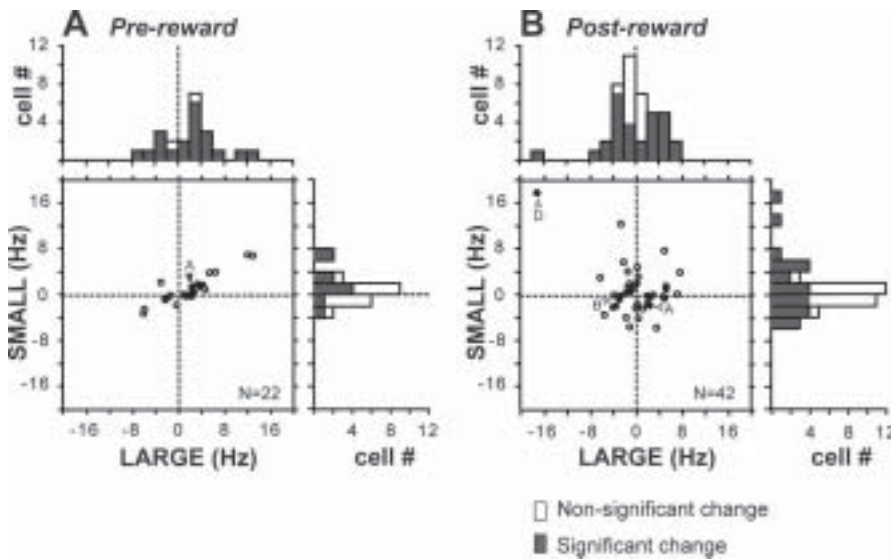


Figure 4. Comparison of DRN neuronal activity between large-reward trials and small-reward trials. **A, B.** In the scatter plot, the activity of each neuron in the two reward conditions is expressed as the change in firing rate from the pre-fixation period (duration, 400 ms) to the pre-reward period (**A**) and to the postreward period (**B**). For each period, data are presented for neurons that showed a significant reward effect during each period (two-way ANOVA, $p < 0.01$). The filled bars in the marginal histograms indicate neurons whose activity was significantly different from the pre-fixation period (Mann–Whitney U test, $p < 0.01$). The filled circles indicated by arrows **A**, **B**, and **D** show the data for neurons shown in Figure 2.

different from DRN neurons (Fig. 5C,D). Dopamine neurons exhibited a phasic increase in activity after fixation onset, as reported by Takikawa et al. (2004) for 1DR-MGS. They also exhibited a phasic increase in activity after the onset of the target indicating an upcoming large reward (Fig. 5C) and a phasic decrease in activity after the onset of the target indicating an upcoming small reward (Fig. 5D), leading to a strong and transient large-reward preference in the pre-reward period (Fig. 5F).

In contrast to the pre-reward period, changes in the postreward period were less clear in dopamine neurons. Small increases in activity were observed in some neurons after a large reward (Fig. 5C), leading to weak reward effects (Fig. 5F). Whereas 53 of 167 DRN neurons (31.7%) exhibited significant activation modulation long after reward (600–1000 ms after reward onset; sign test, $p < 0.01$), only 5 of 64 dopamine neurons (7.8%) did so. Thus, the duration of the postreward activity in dopamine neurons was shorter than that in DRN neurons (χ^2 test, $p < 0.0001$). Overall, most of dopamine neurons showed large-reward preference in the pre-reward period and some did so in the postreward period (Fig. 6F).

Figure 7 shows the proportions of neurons that exhibited significant reward and direction effects for both DRN and dopamine neurons. Statistical significance was determined using a two-way ANOVA for each task period ($p < 0.01$). In both DRN and dopamine neurons, reward effects were more prevalent than direction effects. For DRN neurons, the large-reward preference was more common than the small-reward preference in the pre-reward period, whereas these kinds of preferences were equally common in the postreward period. The reward effect was more robust among dopamine neurons. They predominantly showed the large-reward preference in the pre-reward period and less commonly in the postreward period. The ratio of large- versus small-reward preference was significantly different between DRN neurons and DA neurons (χ^2 , $p < 0.0001$ for both pre-reward and postreward periods).

Changes of pre-reward and postreward activity after the reversal of position–reward contingency

In both of our tasks, the contingency between target position and reward value was fixed during one block of trials, but was then reversed with no external cue. This allowed us to examine how the monkey's performance and neuronal activity changed adaptively to the new position–reward contingency. As in previous studies from our laboratory, the saccadic reaction time changed quickly after the reversal of the position–reward contingency (Fig. 8G) (Laureweyns et al., 2002; Watanabe and Hikosaka, 2005).

We therefore examined the time course of the changes in the activity of DRN and dopamine neurons (Fig. 8). We computed the mean normalized firing rates for the pre-reward period (0–400 ms after target onset) and the postreward period (400–800 ms after reward onset for DRN neurons; 0–400 ms after reward onset for dopamine neurons) as a function of the trial number after the reversal. To assess the speed of activity change after the reversal, we tested whether the neuronal activity on

each trial number was significantly different from the mean activity on the last five trials of the new block (Mann–Whitney U test, $p < 0.01$). This analysis was restricted to neurons whose firing rates were significantly modulated by reward value (two-way ANOVA, $p < 0.01$) and was performed separately for the pre-reward and postreward periods.

The changes in pre-reward activity after the contingency reversal were qualitatively similar for DRN neurons and dopamine neurons (Fig. 8A,C,E). In both DRN neurons and dopamine neurons, the activity on the first trial after the contingency reversal was not different from the last trial of the block before the reversal. This is not surprising because the changed reward had not yet been delivered when the activity occurred. Interestingly, however, the change in activity of DRN neurons was delayed by one trial after the reversal from large rewards to small rewards (Fig. 8A,C), unlike dopamine neurons (Fig. 8E).

The difference between DRN neurons and dopamine neurons was clearer in the postreward period (Fig. 8B,D,F). Unlike in the pre-reward period, the changed reward had already been delivered on the first trial after the contingency reversal. The activity of DRN neurons followed the size of the reward faithfully (Fig. 8B,D). In contrast, the activity of dopamine neurons only changed transiently on the first trial, and thereafter returned to a level close to baseline activity (Fig. 8F). Specifically, dopamine neurons decreased their activity on large-to-small reward reversals and increased their activity on small-to-large reversals. These transient changes in activity represent the “reward prediction error,” which is the difference between the expected reward value (e.g., small reward) and the actual reward value (e.g., large reward). This pattern of dopamine neuron activity has been shown previously using other tasks (Hollerman and Schultz, 1998; Takikawa et al., 2004). The results thus indicate that DRN neurons encode the actual reward value, not the reward prediction error.

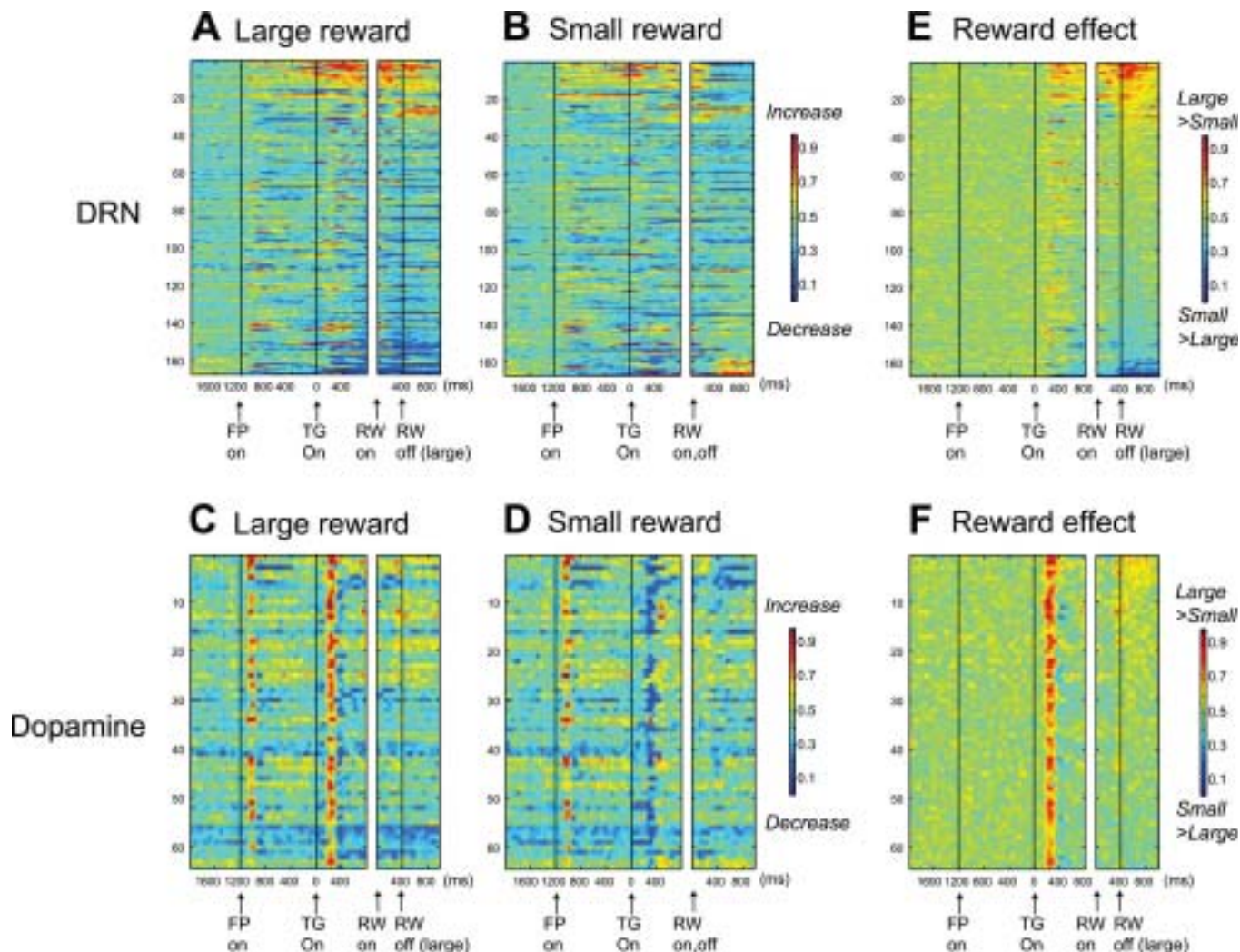


Figure 5. Comparison of reward-dependent activity between DRN neurons and dopamine neurons. Data were obtained from 167 DRN neurons and 64 dopamine neurons using 1DR-VGS. The format is the same as in Figure 3, A, B, and E.

Relationship between the firing pattern and the reward-effect of DRN neurons

In the present experiment, we studied all well isolated neurons in the DRN whose activity changed during saccade tasks. It has traditionally been accepted that serotonin neurons in the DRN show slow and regular firing with broad spikes (Aghajanian et al., 1978; Sawyer et al., 1985; Jacobs and Fornal, 1991; Hajos et al., 1998), although recent studies may not agree with this characterization (Allers and Sharp, 2003; Kocsis et al., 2006). To examine whether such electrophysiological properties were correlated with reward-related modulation, we first grouped 71 DRN neurons (whose spike shapes were successfully recorded) based on their spike durations (shorter or longer than 2 ms) and baseline firing rates (higher or lower than 3 Hz) (Tables 1 and 2). These criteria were chosen based on a previous study reporting that the mean spike duration of immunohistochemically identified serotonin neurons was 2.17 ms (range, 1.67–3.5) and the mean baseline firing rate was 1.67 Hz (range, 0.37–3.0), respectively (Allers and Sharp, 2003). During both prereward and postreward periods, there was no tendency that neurons in specific categories show specific types of reward modulation (χ^2 test, $p > 0.5$).

We further examined whether the reward-related features of DRN neurons were correlated with any combination of the electrophysiological properties (Fig. 9). There was no significant dif-

ference between large- and small-reward preferring neurons in baseline firing rate, spike duration, or irregularity (Kruskal–Wallis, $p > 0.05$). Furthermore, multiple regression analysis indicated that reward effects in ROC values could not be significantly predicted by any linear combination of these three variables (prereward, $p = 0.17$; postreward, $p = 0.68$).

Discussion

Neurochemical identity of recorded DRN neurons

Pharmacological and behavioral studies have suggested that the dorsal and median raphe nuclei (DRN and MRN) are important elements of the brain reward circuitry (Higgins and Fletcher, 2003; Liu and Ikemoto, 2007). However, it was unknown whether and how reward information is represented in the DRN. Our experiments now demonstrate that single neurons in the monkey DRN encode reward information before and after the delivery of reward.

Many serotonergic neurons in the brain (~40% in cats; 60% in rats) are located in the DRN (Wiklund et al., 1981). The lateral component (the wings) of DRN, best developed around the trochlear nucleus, is most prominent in primates (Jacobs and Azmitia, 1992) and that was where we sampled most of the neurons. Among heterogeneous DRN neurons containing different neurotransmitters (for review, see Michelsen et al., 2007), previ-

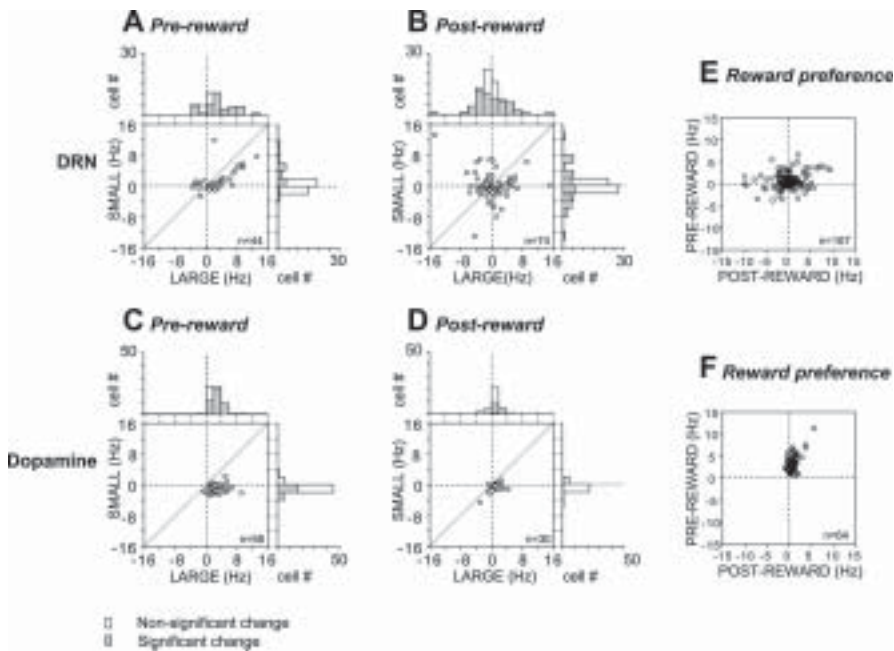


Figure 6. Contrasting effects of expected and received rewards on DRN neurons and dopamine neurons. **A–D**, The same format as in Figure 4. **E, F**, Relationship of reward preference between the prereward and the postreward periods. For each neuron, the following was computed for each task period: (mean firing rate for large-reward trials) – (mean firing rate for small-reward trials).

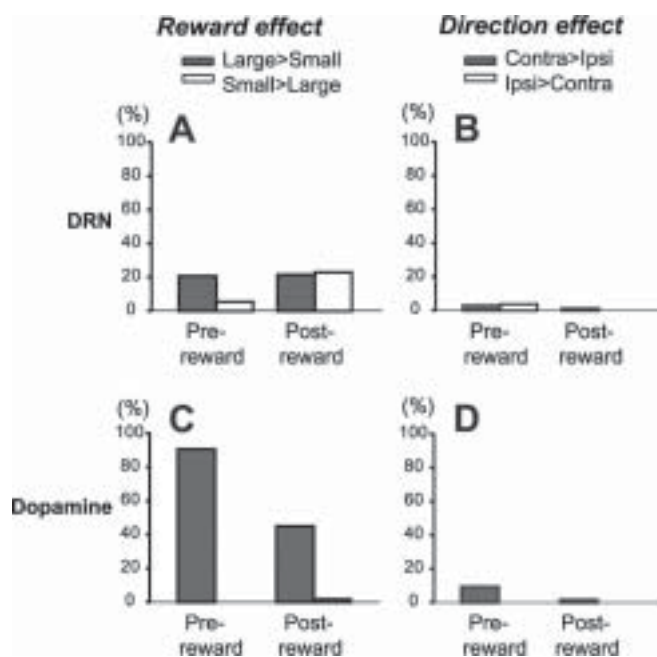


Figure 7. Similarities and differences between DRN neurons and dopamine neurons. **A**, Proportions of DRN neurons that showed significant reward-dependent modulations in activity during the prereward and postreward periods in 1DR-VGS (two-way ANOVA, $p < 0.01$). The filled bars indicate neurons that showed stronger activity on large-reward than on small-reward trials; the open bars indicate neurons that showed stronger activity on small-reward than on large-reward trials. **B**, Proportions of DRN neurons that showed significant direction-dependent modulations. The filled bars indicate neurons that showed stronger activity on contraversive-saccade than on ipsiversive-saccade trials; the open bars indicate stronger activity on ipsiversive-saccade than on contraversive-saccade trials. **C, D**, Data for dopamine neurons shown in the same format as in **A** and **B**.

ous studies report that a substantial proportion of DRN neurons are serotonergic: ~30% in rats (Descarries et al., 1982), 70% of medium-sized DRN neurons in cats (Wiklund et al., 1981), and 70% in human (Baker et al., 1991). Recent combined electro-

physiological and immunochemical studies revealed that DRN neurons with “traditional” electrophysiological characteristics, such as long spike duration and low and regular baseline firing, are not always serotonergic (Allers and Sharp, 2003; Kocsis et al., 2006). Nevertheless, as shown in Tables 1 and 2, 52% of our sample neurons exhibited long spike duration (>3 ms) and 50% exhibited low firing rate (<3 Hz), consistent with the proportion of “classical” serotonergic neurons in DRN. We also found that these neurons did show reward-dependent modulation in activity, indicating that a group of classical serotonergic DRN neurons modulate their activity depending on reward information. We also observed 12% of neurons exhibited baseline firing rate >10 Hz and they also exhibited reward-dependent modulation. Such DRN neurons with high firing rates may be GABA neurons [Allers and Sharp (2003), their Table 1].

Reward information is differently coded by dopamine and DRN neurons

Reward-dependent modulations in the activity of DRN neurons were different from those observed in putative dopamine neurons. First, whereas the dopamine neurons predominantly responded to a reward-predicting sensory stimulus, DRN neurons responded to both the reward-predicting stimulus and the reward itself. Second, whereas dopamine neurons respond to a reward only when it was larger or smaller than expected, DRN neurons reliably coded the value of the received reward whether or not it was expected. Unlike DRN neurons, dopamine neurons responded to reward delivery only when the cue position–reward contingency was switched so that the reward was unexpectedly small or large (Fig. 8). In other words, dopamine neurons encoded reward prediction error, as suggested previously (Schultz, 1998; Satoh et al., 2003; Kawagoe et al., 2004), but DRN neurons did not. Third, whereas dopamine neurons invariably preferred larger rewards (i.e., are excited by larger rewards), the DRN contains neurons preferring larger rewards and neurons preferring smaller rewards. Finally, whereas dopamine neurons exhibit phasic responses, DRN neurons typically exhibited tonic responses. Thus, whereas dopamine neurons provide phasic signals related to reward prediction error, DRN neurons provide tonic signals related to expected and received reward values.

The responses of DRN neurons were diverse, compared with relatively stereotyped responses of dopamine neurons. This may be because DRN neurons are heterogeneous, containing different neurotransmitters such as GABA, dopamine, noradrenaline, substance P, nicotine, and acetylcholine (for review, see Michelsen et al., 2007), in addition to serotonin neurons, which constitute 30–70% of DRN neurons (Descarries et al., 1982; Leger and Wiklund, 1982). However, in the current experiment, putative dopamine neurons were selected based on their firing rates, spike shapes, and responsiveness to 1DR-saccade tasks, which might be a reason why their task-related activity was quite homogeneous.

Reward processing in the DRN: inputs

The reward-related signals in DRN neurons may originate from the brain areas that project to the DRN (Aghajanian and Wang,

1977; Sakai et al., 1977; Behzadi et al., 1990; Peyron et al., 1998). Notable among them are (1) dopamine neurons in the substantia nigra pars compacta and the ventral tegmental area and (2) the lateral habenula. The dopamine neurons, which project to both the DRN and MRN (Kishikawa et al., 2000), may exert facilitatory effects on putative serotonin neurons in the DRN (Haj-Dahmane, 2001). Because the dopamine neurons are excited by the stimulus that predicts a large reward, DRN neurons would also be excited by the large-reward-predicting stimulus. Indeed, during the prereward period, large-reward preference was more common than small-reward preference. In contrast, DRN neurons are inhibited by electrical stimulation of the lateral habenula (Wang and Aghajanian, 1977; Stern et al., 1979; Varga et al., 2003). Using the same reward-biased saccade tasks, a recent study from our laboratory showed that lateral habenula neurons exhibit strong small-reward preference (i.e., inhibited by stimuli that predict large rewards and excited by stimuli that predict small rewards) (Matsumoto and Hikosaka, 2007). These changes in habenula activity would then be translated into the large-reward preference in DRN neurons.

In contrast, the postreward responses of DRN neurons are unlikely to be derived from dopamine or habenula neurons because neither of them exhibit reliable postreward responses. Possible origins of the postreward information include the hypothalamus (Celada et al., 2002) and the medial prefrontal cortex (Hajos et al., 1998; Varga et al., 2003). Hypothalamic orexin neurons are activated by arousal, feeding, and rewarding stimuli (Mieda and Yanagisawa, 2002; Harris and Aston-Jones, 2006). They project to the DRN in addition to many other areas (Peyron et al., 1998) and facilitate serotonin release (Tao et al., 2006). Medial prefrontal cortex inputs to the DRN and MRN attenuate the increase in serotonin release in response to aversive stimuli (Amat et al., 1998).

In the postreward period, about one-half of DRN neurons showed large-reward preference and the other one-half showed small-reward preference. One possible interpretation would be that the two kinds of reward-related signals are represented in other brain areas such as the anterior cingulate cortex (Niki and Watanabe, 1979; Amiez et al., 2006) and these signals are transmitted to DRN (Arnsten and Goldman-Rakic, 1984). Another possibility is that reward information is transferred from one group of neurons to the other via inhibitory connections within the DRN. It has been suggested that the ventral medial prefrontal cortex inhibits serotonin neurons in the DRN by targeting local GABAergic interneurons (Varga et al., 2001). Thus, the modulation in activity of some DRN neurons may be in opposite direction to the others depending on the direct or indirect projection from the cortex.

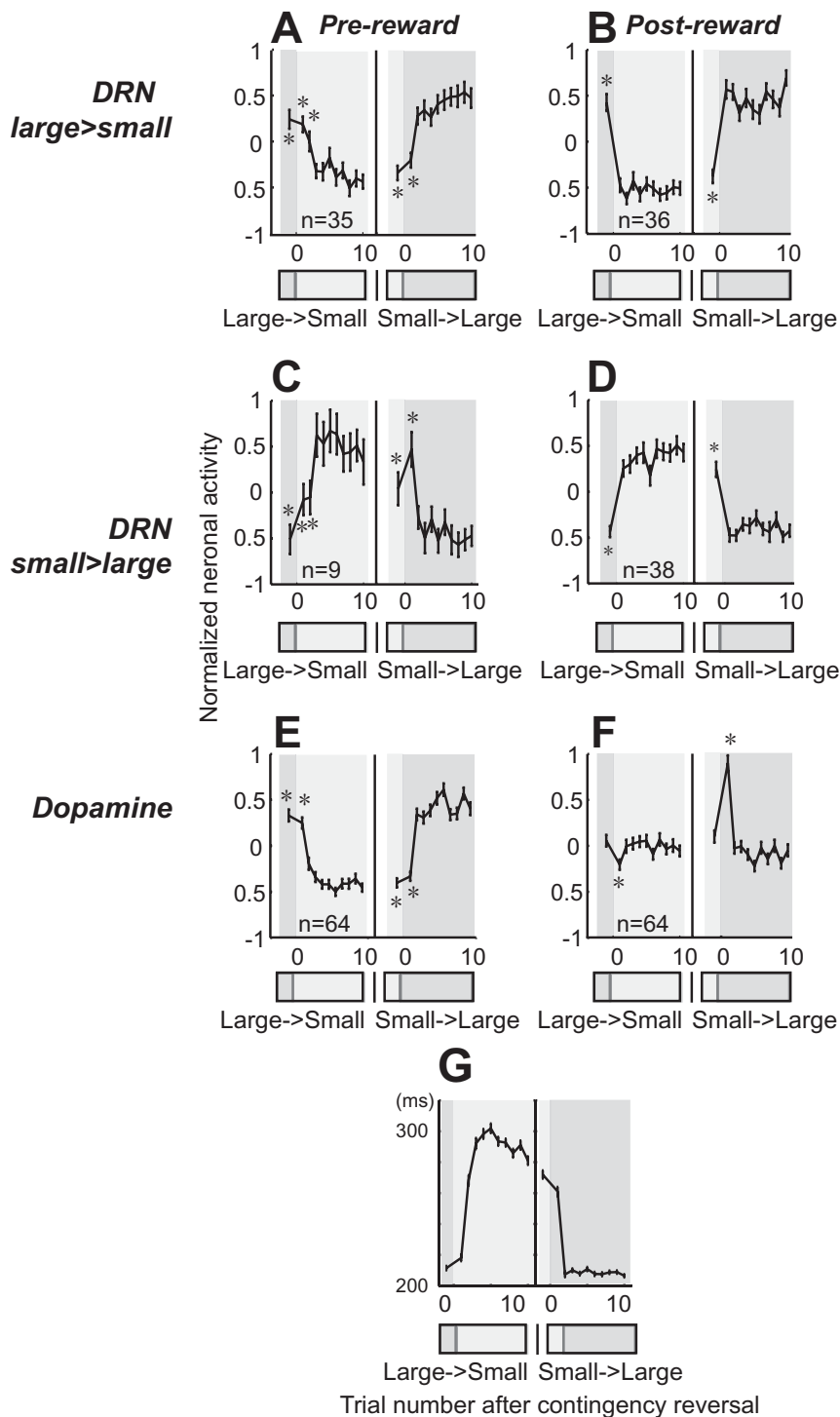


Figure 8. Changes in neuronal activity with the reversal of position–reward contingency. **A, B**, DRN neurons with large-reward preference. **C, D**, DRN neurons with small-reward preference. **E, F**, Dopamine neurons. For each group, the activity during the prereward period (400 ms after target onset) is shown on the left (**A, C, E**), and the activity during the postreward period (400–800 ms after reward onset for DRN neurons; 0–400 ms after reward onset for dopamine neurons) is shown on the right (**B, D, F**). Data were obtained using 1DR-VGS. For each graph, the left panel shows the large-to-small reward reversal; the right panel shows small-to-large reward reversal. Large-reward trials are indicated by dark gray bars; small-reward trials are indicated by clear areas. Shown are the mean and SE of the normalized neuronal activity for the n th trial after the contingency reversal. The asterisks (*) indicate activity that was significantly different from the activity on the last five trials of the block with the reversed contingency ($p < 0.01$, Mann–Whitney U test). **G**, Changes in the mean saccadic reaction times after the contingency reversal in 1DR-VGS.

Reward processing in the DRN: outputs

Among the widespread efferent projections of the DRN (Lavoie and Parent, 1990; Vertes, 1991), those to the basal ganglia structures, especially, the striatum and the substantia nigra (van der

Table 1. Number of neurons with reward-dependent modulation: spike duration

	Prereward		Postreward	
	Long	Short	Long	Short
Large > small	9	6	9	9
Small > large	1	4	9	8
Not significant	24	27	16	20

Long, ≥ 2 ms; short, < 2 ms.**Table 2. Number of neurons with reward-dependent modulation: baseline firing rate**

	Prereward		Postreward	
	Low	High	Low	High
Large > small	7	8	10	8
Small > large	5	0	7	10
Not significant	24	27	19	17

Low, < 3 Hz; high, ≥ 3 Hz.

Kooy and Hattori, 1980; Imai et al., 1986), may be particularly important because they are thought to control reward-dependent saccadic eye movements (Hikosaka et al., 2006).

Many lines of evidence suggest that an inhibition of raphe neurons causes a rewarding effect and that this is mediated, at least partly, by the disinhibition of dopamine neurons. Electrical stimulation of the DRN and MRN causes inhibitions of dopamine neurons, which are mediated by serotonin released in the substantia nigra (Dray et al., 1976; Tsai, 1989; Trent and Tepper, 1991). Self-administration of muscimol into the raphe nuclei causes rewarding effects in behavior, and this effect is dependent on normal dopamine function (Liu and Ikemoto, 2007). It has been suggested that dopamine actions in the basal ganglia are antagonized by serotonin that derives from the DRN or MRN (Kapur and Remington, 1996). Thus, the inhibition of the DRN/MRN followed by the enhancement of dopaminergic transmission in the basal ganglia appears to be rewarding (Fletcher et al., 1993).

The DRN may have a more direct route to influence saccadic eye movements, which is its projection to the substantia nigra pars reticulata (SNr) (Corvaja et al., 1993). The SNr is known to exert tonic GABAergic inhibition on the superior colliculus and to remove this inhibition in response to sensory, memory, and motivational demands (Hikosaka et al., 2006).

Possible functions of the DRN in reward processing

Characteristic features of the activity of DRN neurons were that (1) their reward-related response pattern was tonic, and (2) the changes were of either large- or small-reward preference. Such activation patterns may be useful in integrating appetitive or aversive reward information for a substantial time, as suggested by Solomon and Corbit (1974). This may also explain the experimental results indicating that serotonin-depleted animals show impulsive tendencies. That is, systemic or local depletion of serotonin renders the animal likely to choose a small but immediate reward rather than a large but delayed reward (Wogar et al., 1993; Brunner and Hen, 1997; Harrison et al., 1997; Mobini et al., 2000a,b; Winstanley et al., 2004, 2006; Denk et al., 2005). The human DRN was activated when subjects learned to obtain large future rewards (Tanaka et al., 2004). Long-lasting DRN activity may have other functions as well, because impulsivity has been associated with other serotonin-related behavioral tendencies such as aggression (Mehlman et al., 1994; van Erp and Miczek, 2000) and obsession (Insel et al., 1990).

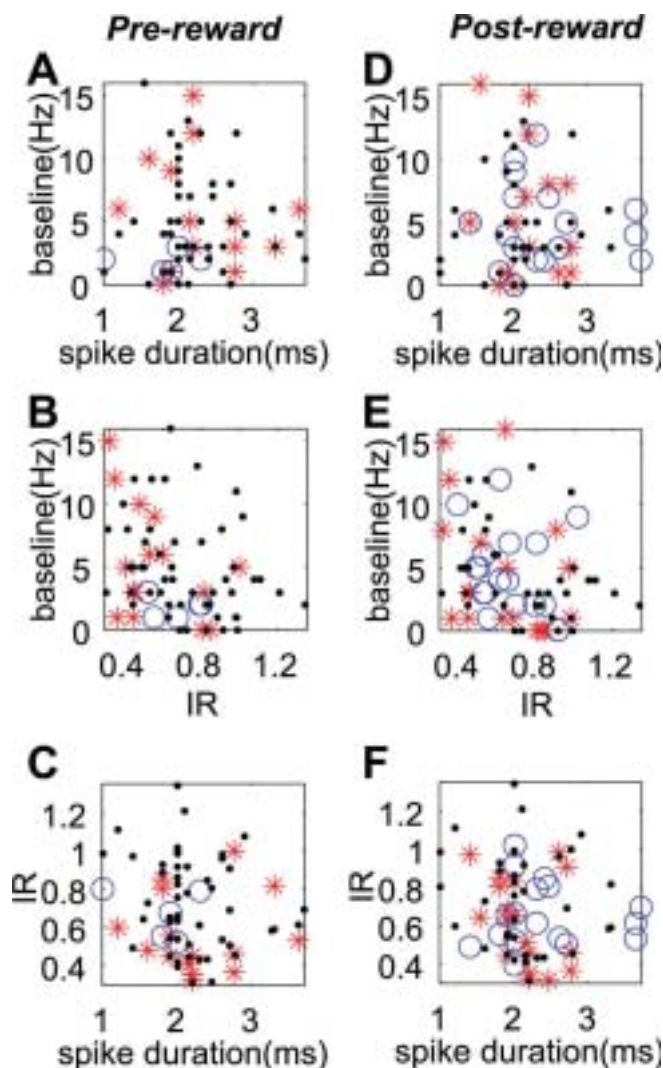


Figure 9. Electrophysiological properties of different groups of DRN neurons. *A–F*, Neurons with different reward-dependent modulation (large > small, red stars; small > large, blue circles; no significant change, black dots) during prereward (*A–C*) and postreward (*D–F*) periods are plotted in two-dimensional graphs. Each graph shows the correlation between two of three electrophysiological properties (spike width, IR, and baseline activity). Data were obtained using 1DR-VGS.

The coding of delayed rewards has been a long-standing issue in reinforcement learning theories (Cardinal et al., 2001). Recent studies have suggested that multiple neural systems may participate in the representation of rewards at different timescales (McClure et al., 2004; Tanaka et al., 2004). One hypothesis is that serotonin regulates the balance between immediate and delayed rewards (Doya, 2002). Daw et al. (2002) suggested that the current reward value is represented by the phasic activation of dopamine neurons, whereas the average value is represented by the tonic activation of serotonin neurons. We found indeed that one-half of DRN neurons exhibited such reward-related tonic activation. However, our results do not completely support the theory because the tonic activation of DRN neurons did not seem to accumulate across trials. Additional experiments using tasks involving long-term reward prediction will be necessary to test this hypothesis.

In conclusion, our experiments demonstrate that many neurons in the monkey DRN encode expected and received rewards. They do so in a manner distinctly different from dopamine neurons. It remains to be solved whether and how the DRN signals

are used for the reward-based modulation of motor behavior or learning.

References

- Aghajanian GK, Wang RY (1977) Habenular and other midbrain raphe afferents demonstrated by a modified retrograde tracing technique. *Brain Res* 122:229–242.
- Aghajanian GK, Wang RY, Baraban J (1978) Serotonergic and non-serotonergic neurons of the dorsal raphe: reciprocal changes in firing induced by peripheral nerve stimulation. *Brain Res* 153:169–175.
- Allers KA, Sharp T (2003) Neurochemical and anatomical identification of fast- and slow-firing neurons in the rat dorsal raphe nucleus using juxtacellular labelling methods in vivo. *Neuroscience* 122:193–204.
- Amat J, Matus-Amat P, Watkins LR, Maier SF (1998) Escapable and inescapable stress differentially and selectively alter extracellular levels of 5-HT in the ventral hippocampus and dorsal periaqueductal gray of the rat. *Brain Res* 797:12–22.
- Amiez C, Joseph JP, Procyk E (2006) Reward encoding in the monkey anterior cingulate cortex. *Cereb Cortex* 16:1040–1055.
- Arnsten AF, Goldman-Rakic PS (1984) Selective prefrontal cortical projections to the region of the locus coeruleus and raphe nuclei in the rhesus monkey. *Brain Res* 306:9–18.
- Baker KG, Halliday GM, Hornung JP, Geffen LB, Cotton RG, Tork I (1991) Distribution, morphology and number of monoamine-synthesizing and substance P-containing neurons in the human dorsal raphe nucleus. *Neuroscience* 42:757–775.
- Behzadi G, Kalen P, Parvopassu F, Wiklund L (1990) Afferents to the median raphe nucleus of the rat: retrograde cholera toxin and wheat germ conjugated horseradish peroxidase tracing, and selective D-[³H]aspartate labelling of possible excitatory amino acid inputs. *Neuroscience* 37:77–100.
- Brunner D, Hen R (1997) Insights into the neurobiology of impulsive behavior from serotonin receptor knockout mice. *Ann NY Acad Sci* 836:81–105.
- Cardinal RN, Pennicott DR, Sugathapala CL, Robbins TW, Everitt BJ (2001) Impulsive choice induced in rats by lesions of the nucleus accumbens core. *Science* 292:2499–2501.
- Celada P, Casanovas JM, Paez X, Artigas F (2002) Control of serotonergic neurons in the dorsal raphe nucleus by the lateral hypothalamus. *Brain Res* 932:79–90.
- Corvaja N, Doucet G, Bolam JP (1993) Ultrastructure and synaptic targets of the raphe-nigral projection in the rat. *Neuroscience* 55:417–427.
- Crist CF, Yamasaki DS, Komatsu H, Wurtz RH (1988) A grid system and a microsyringe for single cell recording. *J Neurosci Methods* 26:117–122.
- Curzon G (1990) Serotonin and appetite. *Ann NY Acad Sci* 600:521–531.
- Dahlstrom A, Fuxe K (1964) Localization of monoamines in the lower brain stem. *Experientia* 20:398–399.
- Davidson RJ, Putnam KM, Larson CL (2000) Dysfunction in the neural circuitry of emotion regulation—a possible prelude to violence. *Science* 289:591–594.
- Davies RM, Gerstein GL, Baker SN (2006) Measurement of time-dependent changes in the irregularity of neural spiking. *J Neurophysiol* 96:906–918.
- Daw ND, Kakade S, Dayan P (2002) Opponent interactions between serotonin and dopamine. *Neural Netw* 15:603–616.
- Deakin JF (1991) Depression and 5HT. *Int Clin Psychopharmacol* 6 [Suppl 3]:23–31.
- Denk F, Walton ME, Jennings KA, Sharp T, Rushworth MF, Bannerman DM (2005) Differential involvement of serotonin and dopamine systems in cost-benefit decisions about delay or effort. *Psychopharmacology (Berl)* 179:587–596.
- Descarries L, Watkins KC, Garcia S, Beaudet A (1982) The serotonin neurons in nucleus raphe dorsalis of adult rat: a light and electron microscope radioautographic study. *J Comp Neurol* 207:239–254.
- Doya K (2002) Metalearning and neuromodulation. *Neural Netw* 15:495–506.
- Dray A, Gonye TJ, Oakley NR, Tanner T (1976) Evidence for the existence of a raphe projection to the substantia nigra in rat. *Brain Res* 113:45–57.
- Dugovic C (2001) Role of serotonin in sleep mechanisms. *Rev Neurol (Paris)* 157:S16–S19.
- Fletcher PJ, Ming ZH, Higgins GA (1993) Conditioned place preference induced by microinjection of 8-OH-DPAT into the dorsal or median raphe nucleus. *Psychopharmacology (Berl)* 113:31–36.
- Graeff FG (2004) Serotonin, the periaqueductal gray and panic. *Neurosci Biobehav Rev* 28:239–259.
- Graeff FG, Guimaraes FS, De Andrade TG, Deakin JF (1996) Role of 5-HT in stress, anxiety, and depression. *Pharmacol Biochem Behav* 54:129–141.
- Guzman-Marin R, Alam MN, Szymusiak R, Drucker-Colin R, Gong H, McGinty D (2000) Discharge modulation of rat dorsal raphe neurons during sleep and waking: effects of preoptic/basal forebrain warming. *Brain Res* 875:23–34.
- Haj-Dahmane S (2001) D2-like dopamine receptor activation excites rat dorsal raphe 5-HT neurons in vitro. *Eur J Neurosci* 14:125–134.
- Hajos M, Richards CD, Szekeley AD, Sharp T (1998) An electrophysiological and neuroanatomical study of the medial prefrontal cortical projection to the midbrain raphe nuclei in the rat. *Neuroscience* 87:95–108.
- Harris GC, Aston-Jones G (2006) Arousal and reward: a dichotomy in orexin function. *Trends Neurosci* 29:571–577.
- Harrison AA, Everitt BJ, Robbins TW (1997) Central 5-HT depletion enhances impulsive responding without affecting the accuracy of attentional performance: interactions with dopaminergic mechanisms. *Psychopharmacology (Berl)* 133:329–342.
- Higgins GA, Fletcher PJ (2003) Serotonin and drug reward: focus on 5-HT2C receptors. *Eur J Pharmacol* 480:151–162.
- Hikosaka O, Nakamura K, Nakahara H (2006) Basal ganglia orient eyes to reward. *J Neurophysiol* 95:567–584.
- Hollerman JR, Schultz W (1998) Dopamine neurons report an error in the temporal prediction of reward during learning. *Nat Neurosci* 1:304–309.
- Imai H, Steindler DA, Kitai ST (1986) The organization of divergent axonal projections from the midbrain raphe nuclei in the rat. *J Comp Neurol* 243:363–380.
- Insel TR, Zohar J, Benkelfat C, Murphy DL (1990) Serotonin in obsessions, compulsions, and the control of aggressive impulses. *Ann NY Acad Sci* 600:574–586.
- Jacobs BL, Azmitia EC (1992) Structure and function of the brain serotonin system. *Physiol Rev* 72:165–229.
- Jacobs BL, Fornal CA (1991) Activity of brain serotonergic neurons in the behaving animal. *Pharmacol Rev* 43:563–578.
- Jacobs BL, Fornal CA (1993) 5-HT and motor control: a hypothesis. *Trends Neurosci* 16:346–352.
- Kapur S, Remington G (1996) Serotonin-dopamine interaction and its relevance to schizophrenia. *Am J Psychiatry* 153:466–476.
- Kawagoe R, Takikawa Y, Hikosaka O (1998) Expectation of reward modulates cognitive signals in the basal ganglia. *Nat Neurosci* 1:411–416.
- Kawagoe R, Takikawa Y, Hikosaka O (2004) Reward-predicting activity of dopamine and caudate neurons—a possible mechanism of motivational control of saccadic eye movement. *J Neurophysiol* 91:1013–1024.
- Kitahama K, Nagatsu I, Geffard M, Maeda T (2000) Distribution of dopamine-immunoreactive fibers in the rat brainstem. *J Chem Neuroanat* 18:1–9.
- Kocsis B, Varga V, Dahan L, Sik A (2006) Serotonergic neuron diversity: identification of raphe neurons with discharges time-locked to the hippocampal theta rhythm. *Proc Natl Acad Sci USA* 103:1059–1064.
- Lauwereyns J, Watanabe K, Coe B, Hikosaka O (2002) A neural correlate of response bias in monkey caudate nucleus. *Nature* 418:413–417.
- Lavoie B, Parent A (1990) Immunohistochemical study of the serotonergic innervation of the basal ganglia in the squirrel monkey. *J Comp Neurol* 299:1–16.
- Leger L, Wiklund L (1982) Distribution and numbers of indoleamine cell bodies in the cat brainstem determined with Falck-Hillarp fluorescence histochemistry. *Brain Res Bull* 9:245–251.
- Leger L, Charnay Y, Hof PR, Bouras C, Cespeglio R (2001) Anatomical distribution of serotonin-containing neurons and axons in the central nervous system of the cat. *J Comp Neurol* 433:157–182.
- Liu ZH, Ikemoto S (2007) The midbrain raphe nuclei mediate primary reinforcement via GABA(A) receptors. *Eur J Neurosci* 25:735–743.
- Lydic R, McCarley RW, Hobson JA (1983) The time-course of dorsal raphe discharge, PGO waves, and muscle tone averaged across multiple sleep cycles. *Brain Res* 274:365–370.
- Matsumoto M, Hikosaka O (2007) Lateral habenula as a source of negative reward signals in dopamine neurons. *Nature* 447:1111–1115.
- McClure SM, York MK, Montague PR (2004) The neural substrates of reward processing in humans: the modern role of fMRI. *Neuroscientist* 10:260–268.

- McGinty DJ, Harper RM (1976) Dorsal raphe neurons: depression of firing during sleep in cats. *Brain Res* 101:569–575.
- Mehlman PT, Higley JD, Faucher I, Lilly AA, Taub DM, Vickers J, Suomi SJ, Linnoila M (1994) Low CSF 5-HIAA concentrations and severe aggression and impaired impulse control in nonhuman primates. *Am J Psychiatry* 151:1485–1491.
- Meneses A (1999) 5-HT system and cognition. *Neurosci Biobehav Rev* 23:1111–1125.
- Michelsen KA, Schmitz C, Steinbusch HW (2007) The dorsal raphe nucleus—from silver stainings to a role in depression. *Brain Res Rev* 55:329–342.
- Mieda M, Yanagisawa M (2002) Sleep, feeding, and neuropeptides: roles of orexins and orexin receptors. *Curr Opin Neurobiol* 12:339–345.
- Mirenowicz J, Schultz W (1994) Importance of unpredictability for reward responses in primate dopamine neurons. *J Neurophysiol* 72:1024–1027.
- Mobini S, Chiang TJ, Al-Ruwaitea AS, Ho MY, Bradshaw CM, Szabadi E (2000a) Effect of central 5-hydroxytryptamine depletion on intertemporal choice: a quantitative analysis. *Psychopharmacology (Berl)* 149:313–318.
- Mobini S, Chiang TJ, Ho MY, Bradshaw CM, Szabadi E (2000b) Effects of central 5-hydroxytryptamine depletion on sensitivity to delayed and probabilistic reinforcement. *Psychopharmacology (Berl)* 152:390–397.
- Montague PR, Dayan P, Sejnowski TJ (1996) A framework for mesencephalic dopamine systems based on predictive Hebbian learning. *J Neurosci* 16:1936–1947.
- Nakahara H, Itoh H, Kawagoe R, Takikawa Y, Hikosaka O (2004) Dopamine neurons can represent context-dependent prediction error. *Neuron* 41:269–280.
- Nakamura K, Hikosaka O (2006) Role of dopamine in the primate caudate nucleus in reward modulation of saccades. *J Neurosci* 26:5360–5369.
- Niki H, Watanabe M (1979) Prefrontal and cingulate unit activity during timing behavior in the monkey. *Brain Res* 171:213–224.
- Peyron C, Petit JM, Rampon C, Jouvett M, Luppi PH (1998) Forebrain afferents to the rat dorsal raphe nucleus demonstrated by retrograde and anterograde tracing methods. *Neuroscience* 82:443–468.
- Rogers RD, Blackshaw AJ, Middleton HC, Matthews K, Hawtin K, Crowley C, Hopwood A, Wallace C, Deakin JF, Sahakian BJ, Robbins TW (1999) Tryptophan depletion impairs stimulus-reward learning while methylphenidate disrupts attentional control in healthy young adults: implications for the monoaminergic basis of impulsive behaviour. *Psychopharmacology (Berl)* 146:482–491.
- Sakai K, Salvat D, Touret M, Jouvett M (1977) Afferent connections of the nucleus raphe dorsalis in the cat as visualized by the horseradish peroxidase technique. *Brain Res* 137:11–35.
- Sato M, Hikosaka O (2002) Role of primate substantia nigra pars reticulata in reward-oriented saccadic eye movement. *J Neurosci* 22:2363–2373.
- Satoh T, Nakai S, Sato T, Kimura M (2003) Correlated coding of motivation and outcome of decision by dopamine neurons. *J Neurosci* 23:9913–9923.
- Sawyer SF, Tepper JM, Young SJ, Groves PM (1985) Antidromic activation of dorsal raphe neurons from neostriatum: physiological characterization and effects of terminal autoreceptor activation. *Brain Res* 332:15–28.
- Schultz W (1998) Predictive reward signal of dopamine neurons. *J Neurophysiol* 80:1–27.
- Schultz W, Dayan P, Montague PR (1997) A neural substrate of prediction and reward. *Science* 275:1593–1599.
- Schweighofer N, Tanaka SC, Doya K (2007) Serotonin and the evaluation of future rewards: theory, experiments, and possible neural mechanisms. *Ann NY Acad Sci* 1104:289–300.
- Shinomoto S, Shima K, Tanji J (2003) Differences in spiking patterns among cortical neurons. *Neural Comput* 15:2823–2842.
- Solomon RL, Corbit JD (1974) An opponent-process theory of motivation. I. Temporal dynamics of affect. *Psychol Rev* 81:119–145.
- Stern WC, Johnson A, Bronzino JD, Morgane PJ (1979) Effects of electrical stimulation of the lateral habenula on single-unit activity of raphe neurons. *Exp Neurol* 65:326–342.
- Suri RE, Schultz W (1998) Learning of sequential movements by neural network model with dopamine-like reinforcement signal. *Exp Brain Res* 121:350–354.
- Takikawa Y, Kawagoe R, Hikosaka O (2004) A possible role of midbrain dopamine neurons in short- and long-term adaptation of saccades to position-reward mapping. *J Neurophysiol* 92:2520–2529.
- Tanaka SC, Doya K, Okada G, Ueda K, Okamoto Y, Yamawaki S (2004) Prediction of immediate and future rewards differentially recruits cortico-basal ganglia loops. *Nat Neurosci* 7:887–893.
- Tao R, Ma Z, McKenna JT, Thakkar MM, Winston S, Strecker RE, McCarley RW (2006) Differential effect of orexins (hypocretins) on serotonin release in the dorsal and median raphe nuclei of freely behaving rats. *Neuroscience* 141:1101–1105.
- Trent F, Tepper JM (1991) Dorsal raphe stimulation modifies striatal-evoked antidromic invasion of nigral dopaminergic neurons in vivo. *Exp Brain Res* 84:620–630.
- Tsai CT (1989) Involvement of serotonin in mediation of inhibition of substantia nigra neurons by noxious stimuli. *Brain Res Bull* 23:121–127.
- van der Kooy D, Hattori T (1980) Dorsal raphe cells with collateral projections to the caudate-putamen and substantia nigra: a fluorescent retrograde double labeling study in the rat. *Brain Res* 186:1–7.
- van Erp AM, Miczek KA (2000) Aggressive behavior, increased accumbal dopamine, and decreased cortical serotonin in rats. *J Neurosci* 20:9320–9325.
- Varga V, Szekeley AD, Csillag A, Sharp T, Hajos M (2001) Evidence for a role of GABA interneurons in the cortical modulation of midbrain 5-hydroxytryptamine neurones. *Neuroscience* 106:783–792.
- Varga V, Kocsis B, Sharp T (2003) Electrophysiological evidence for convergence of inputs from the medial prefrontal cortex and lateral habenula on single neurons in the dorsal raphe nucleus. *Eur J Neurosci* 17:280–286.
- Vertes RP (1991) A PHA-L analysis of ascending projections of the dorsal raphe nucleus in the rat. *J Comp Neurol* 313:643–668.
- Wang RY, Aghajanian GK (1977) Physiological evidence for habenula as a major link between forebrain and midbrain raphe. *Science* 197:89–91.
- Watanabe K, Hikosaka O (2005) Immediate changes in anticipatory activity of caudate neurons associated with reversal of position-reward contingency. *J Neurophysiol* 94:1879–1887.
- Wiklund L, Leger L, Persson M (1981) Monoamine cell distribution in the cat brain stem. A fluorescence histochemical study with quantification of indolaminergic and locus coeruleus cell groups. *J Comp Neurol* 203:613–647.
- Winstanley CA, Dalley JW, Theobald DE, Robbins TW (2004) Fractionating impulsivity: contrasting effects of central 5-HT depletion on different measures of impulsive behavior. *Neuropsychopharmacology* 29:1331–1343.
- Winstanley CA, Theobald DE, Dalley JW, Cardinal RN, Robbins TW (2006) Double dissociation between serotonergic and dopaminergic modulation of medial prefrontal and orbitofrontal cortex during a test of impulsive choice. *Cereb Cortex* 16:106–114.
- Wogar MA, Bradshaw CM, Szabadi E (1993) Effect of lesions of the ascending 5-hydroxytryptaminergic pathways on choice between delayed reinforcers. *Psychopharmacology (Berl)* 111:239–243.

研究成果報告書

研究課題名	神経因性疼痛の発生・維持機構の解明とその修復・再生の基礎研究		
(英文)	Elucidation of mechanisms for generation and maintenance of neuropathic pain and translational research for the treatment by regeneration of injured nerves		
事業推進者	伊藤 誠二	E-mail	ito@takii.kmu.ac.jp
所属・職名	医学研究科・疼痛医科学（医化学）講座・教授		
研究分担者名	芦高 恵美子、松村 伸治、畝崎 佐和子、片野 泰代、好井 覚		
キーワード	神経因性疼痛、NMDA 受容体、一酸化窒素、神経再生、神経幹細胞		

1. 概要

神経因性疼痛は痛覚伝達系の形質転換や神経回路網の再構築といった非可逆的な器質的変化のため難治性と信じられてきた。本研究は神経損傷部位からの持続的入力によりグルタミン酸受容体のリン酸化やトラフフィングなど痛覚伝達経路の機能的変化で病態が発症・維持されることを体系的に解明し、研究成果を診断・治療に反映させることを目指す。

2. 研究の背景と目的

神経因性疼痛に焦点を当て、nNOS の活性化を指標にタンパクのリン酸化や遺伝子発現変化によるシナプス可塑性の分子機構から、脊髓組織レベルの神経回路網 *in situ* での NOS 活性化機構、さらに PET による *in vivo* での分子イメージングまで体系的に解析を行い、神経因性疼痛の発症・維持・認識機構を解明し、診断・治療につながる臨床応用研究をすることを目的とする。

3. 研究方法

- (1) 遺伝子改変マウスを用いた疼痛行動解析と神経再生
- (2) 蛋白化学とプロテオミクス解析
- (3) 新規生体分子の探索と機能解析

4. これまでの成果

(1) 神経因性疼痛の維持機構の解明

神経因性疼痛は脊髄後角での神経回路網の再構築や痛覚伝達系の形質転換といった非可逆的な器質的変化のため難治性と考えられてきた。神経損傷1週間後でも、Src キナーゼファミリーの Fyn によるグルタミン酸 NMDA 受容体 NR2B サブユニットの 1472 番目 Tyr 残基 (Y1472) のリン酸化と神経型一酸化窒素合成酵素 (nNOS) の活性化による機能的変化で維持されていることを本研究で明らかにした (図1)。プロスタグランジン E₂ (PGE₂) は EP 受容体サブタイプ EP1-EP4 を介して NMDA-nNOS 系を活性化し、PGE₂ と NO は順行性・逆行性メディエーターとしてクロストークし神経因性疼痛の維持に関与すると考えられる。

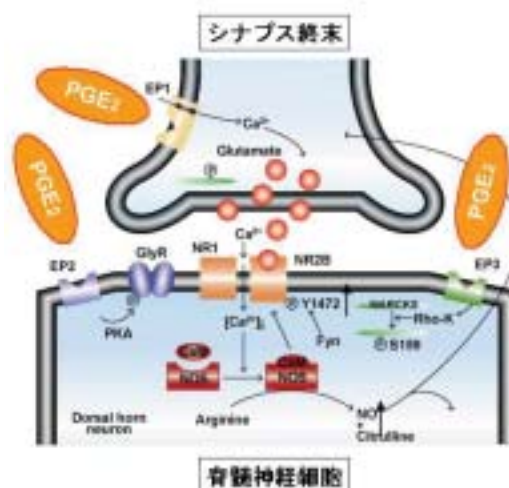


図1. 脊髄での神経因性疼痛の維持機構

我々は、1) 神経損傷1週間後でも、グルタミン酸 NMDA 受容体 NR2B サブユニットの 1472 番目の Tyr 残基 (Y1472) のリン酸化、Src キナーゼファミリーの Fyn の関与、神経型一酸化窒素合成酵素(nNOS)の活性化による機能的変化により維持されていること、2) DRG での PACAP (pituitary adenylate cyclase-activating polypeptide) の発現誘導が nNOS の活性化に関与すること、3) プロスタグランジン E₂ (PGE₂) と一酸化窒素 (NO) の順行性・逆行性メディエーターが脊髄における神経可塑性に重要な役割をすることを疼痛行動とさまざまな生化学的、細胞生化学的解析で示した。

(2) nNOS のトランスクレーションと nNOS 活性化機構の解明

PACAP と NMDA の共刺激によりトランスクレーションが生じ、nNOS の N 末側部分 (1-299) が NO 産生にドミナントネガティブに作用すること、さらに、トランクレーション変異

体を作製して nNOS の N 末側の β -finger が PSD-95 の会合とトランスロケーションに関与することを明らかにした。

(3) 炎症性疼痛モデルにおける AMPA 受容体のサブタイプスイッチの解明

炎症モデルラットの遷延期の腰部脊髄から PSD 画分を精製し、プロテオミクス解析をして AMPA 受容体のトラフフィッキングに関与する NSF(N-ethylmaleimide-sensitive fusion protein)が低下すること、*in vivo* patch-clamp (九州大学・医・吉村恵教授と共同研究) で電気生理的に Ca^{2+} 透過型 AMPA 受容体が痛覚伝達に関与する脊髄膠様質細胞で増加していることを明らかにした。

(4) Thy1-YFP マウスを用いた神経再生

神経損傷に伴う神経変性・神経再生過程を *in vivo* で可視化するために、神経選択的に蛍光タンパク YFP が発現する Thy1-YFP マウスで神経再生モデルを確立し、種々の薬剤の神経再生における効果、神経再生に関与する因子を検討している(図2)。神経因性疼痛による疼痛閾値を測定することにより、神経因性疼痛と神経再生の関係を *in vivo* で解明できると期待できる。

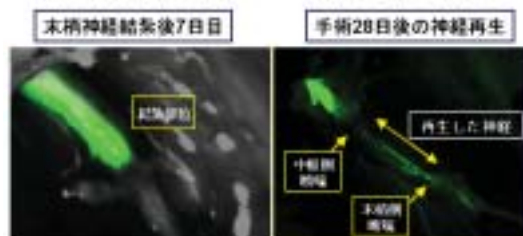


図2 Thy1-YFP マウスでの神経再生の *in vivo* 評価

5. これまでの進捗状況と今後の計画

研究は研究計画に沿って概ね順調に進捗しているだけでなく、予期しない結果から新たな学術的展開を期待している。さらに、臨床応用をめざした病態モデルや神経再生による治療の基礎研究を推進している。

6. これまでの発表論文

(1) 発表論文

1) 原著論文

- Ohnishi, T., Okuda-Ashitaka, E., Matsumura, S., Katano, T., Nishizawa, M. & Ito, S.
Characterization of signaling pathway for the translocation of neuronal nitric oxide synthase to the plasma membrane by PACAP. *J. Neurochem.* **105**, 2271-2285 (2008).
- Katano, T., Furue, H., Okuda-Ashitaka, E., Tagaya, M., Watanabe, M., Yoshimura, M. & Ito, S.
N-Ethylmaleimide-sensitive fusion protein (NSF) is involved in central sensitization in the spinal cord through GluR2 subunit composition switch after inflammation. *Eur. J. Neurosci.* **27**, 3161-3170 (2008).
- Takagi, K., Okuda-Ashitaka, E., Mabuchi, T., Katano, T., Ohnishi, T., Matsumura, S., Ohnaka, M., Kaneko, S., Abe, T., Hirata, T., Fujiwara, S., Minami, T. & Ito, S.
Involvement of stem cell factor and its receptor tyrosine kinase c-kit in pain regulation
Neuroscience **153**, 1278-1288 (2008).
- Moriuchi, H., Koda, N., Okuda-Ashitaka, E., Daiyasu, H., Ogasawara, K., Toh, H., Ito, S., David F. Woodward & Watanabe, K. Molecular Characterization of a Novel Type of Prostamide/Prostaglandin F Synthase, Belonging to the Thioredoxin-like Superfamily. *J. Biol. Chem.* **283**, 792-801 (2008).
- Xu, L., Okuda-Ashitaka, E., Matsumura, S., Mabuchi, T., Okamoto, S., Sakimura, K., Mishina, M. & Ito, S. Signal pathways coupled to activation of neuronal nitric oxide synthase in the spinal cord by nociceptin/orphanin FQ. *Neuropharmacology* **52**, 1318-1325 (2007).
- Unezaki, S., Horai, R., Sudo, K., Iwakura, Y. & Ito, S.
Ovol2/Movo, a homologue of *Drosophila ovo*, is required for angiogenesis, heart formation and placental development in mice. *Genes Cells* **12**, 773-785 (2007).
- Xu, L., Mabuchi, T., Katano, T., Matsumura, S., Okuda-Ashitaka, E., Sakimura, K., Mishina, M. & Ito, S. Nitric oxide (NO) serves as a retrograde messenger to activate neuronal NO synthase in the spinal cord via NMDA receptors. *Nitric oxide* **17**, 18-24 (2007).
- Soen, M., Minami, T., Tatsumi, S., Mabuchi, T., Fruta, K., Maeda, M., Suzuki, M. & Ito, S.
A synthetic kainoid, (2S,3R,4R)-3-carboxymethyl-4-(phenylthio) pyrrolidine-2-carboxylic acid (PSPA-1) serves as a novel analgesic for neuropathic pain. *Eur. J. Pharmacol.* **575**, 75-81 (2007).
- Sasaki, A., Mabuchi, T., Serizawa, K., Takasaki, I., Andoh, T., Shiraki, K., Ito, S. & Kuraishi, Y.
Different roles of nitric oxide synthase-1 and -2 between herpetic and postherpetic allodynia in mice. *Neuroscience* **150**, 459-466 (2007).
- Xu, L., Matsumura, S., Mabuchi, T., Takagi, K., Abe, T. & Ito, S.
In situ measurement of neuronal nitric oxide synthase activity in the spinal cord by NADPH-disphorase

histochemistry. *J. Neurosci. Methods* **150**, 174-184 (2006).

11. Okuda-Ashitaka, E., Minami, T., Matsumura, S., Takeshima, H., Reinscheid R.K., Civelli, O. & Ito, S. The opioid peptide nociceptin/orphanin FQ mediates prostaglandin E₂-induced allodynia, tactile pain associated with nerve injury. *Eur. J. Neurosci.* **23**, 995-1004 (2006).
12. Katano, T., Mabuchi, T., Okuda-Ashitaka, E., Inagaki, N., Kinumi, T. & Ito, S. Proteomic identification of a novel isoform of collapsin response mediator protein-2 (CRMP-2) in spinal nerves peripheral to dorsal root ganglia. *Proteomics* **6**, 6085-6094 (2006).

2) 総説

1. 荘園雅子, 南敏明, 伊藤誠二: アクロメリン酸と痛み
ペインクリニック **29**, 351-364 (2008).
2. 片野泰代, 伊藤誠二: シナプス後肥厚部の NMDA 受容体のリン酸化と神経因性疼痛
生体の科学 **58**, 139-143 (2007).
3. 伊藤誠二: 慢性疼痛研究の最近の進歩～機能的変化による慢性疼痛の維持機構～
ペインクリニック **28**, 199-207 (2007).
4. 芦高恵美子, 阿部哲也, 松村伸治, 伊藤誠二:
脊髄後角における NMDA 受容体リン酸化と神経因性疼痛
慢性疼痛 **26**, 41-47 (2007).

3) 著書

1. 片野泰代, 伊藤誠二: (分担執筆) 理学療法 MOOK3 「疼痛の理学療法 第2版 慢性痛の理解とエビデンス」 第2版 編集: 黒川幸雄、高橋正明、鶴見隆正
第1章 慢性痛のメカニズム 3.慢性痛における生化学的変化、31-40, 三輪書店、東京 (2008).
2. 伊藤誠二, 大西隆之: (分担執筆) 「慢性疼痛の理解と医療提携」 編集: 宮崎東洋、北出利勝
第2章 慢性疼痛研究 2.慢性疼痛の発生・維持の機序、57-69, 真興交易、東京 (2008).

(2) 学会発表

国際学会

2) シンポジウム講演

1. Ito, S. Characterization of signaling pathways for the translocation of neuronal nitric oxide synthase to the plasma membrane by pituitary adenylate cyclase-activating polypeptide (PACAP).
The 3rd Asian Pain Symposium, Fukuoka, 2008.
2. Ito, S. Maintenance of neuropathic pain by interaction of nitric oxide synthase and cyclooxygenase pathways. The 14th Takeda Science Foundation Symposium on Bioscience “The 50th Anniversary of Oxygenases-Advances and Reflections- Kyoto, 2006.
3. Ito, S. An approach to search and development of new analgesics in traditional Chinese medicines.
漢方薬新薬開発理論と技術新機軸研究討論会, 北京, 2006.

国内学会

2) シンポジウム講演

1. 伊藤誠二: 慢性痛の発生維持機構—治療のための疼痛の分子メカニズム
第9回近畿緩和医療研究会、大阪、2008.
2. 伊藤誠二: 慢性疼痛機序解明に向けた基礎的アプローチ
教育講演福岡ペイン 2008、福岡、2008.
3. 伊藤誠二, 陸景珊, 片野泰代, 南敏明, 裏出良博: 神経因性疼痛治療の評価への生化学的アプローチ 第80回日本薬理学会年会、名古屋、2007.
4. 伊藤誠二: 慢性疼痛研究の最近の進歩
日本慢性疼痛学会、京都、2007.
5. 伊藤誠二: 慢性痛の発生維持機構-治療のための疼痛の分子メカニズム-
日本ペインクリニック学会第40回大会、神戸、2006.
6. 伊藤誠二: 神経因性疼痛はなぜ治るのか
日本ペインクリニック学会第40回大会、神戸、2006.
7. 伊藤誠二: 神経因性疼痛の発症維持機構の分子メカニズムと治療戦略
第7回長井長義記念シンポジウム、徳島、2006.

7. これまでの成果の情報公開

ホームページ: 医化学講座 = <http://www3.kmu.ac.jp/medchem/>

Characterization of signaling pathway for the translocation of neuronal nitric oxide synthase to the plasma membrane by PACAP

Takayuki Ohnishi, Emiko Okuda-Ashitaka, Shinji Matsumura, Tayo Katano, Mikio Nishizawa¹ and Seiji Ito

Department of Medical Chemistry, Kansai Medical University, Moriguchi, Japan

Abstract

In the central nervous system, the activation of neuronal nitric oxide synthase (nNOS) is closely associated with activation of NMDA receptor, and trafficking of nNOS may be a prerequisite for efficient NO production at synapses. We recently demonstrated that pituitary adenylate cyclase activating polypeptide (PACAP) and NMDA synergistically caused the translocation of nNOS to the membrane and stimulated NO production in PC12 (pheochromocytoma) cells. However, the mechanisms responsible for trafficking and activation of nNOS are largely unknown. To address these issues, here we constructed a yellow fluorescent protein (YFP)-tagged nNOS N-terminal (1–299 a.a.) mutant, nNOSNT-YFP, and visualized its translocation in PC12 cells stably expressing it. PACAP enhanced the translocation synergistically with NMDA in a time- and concentration-dependent manner. The translocation

was blocked by inhibitors of protein kinase A (PKA), protein kinase C (PKC), and Src kinase; and the effect of PACAP could be replaced with PKA and PKC activators. The β -finger region in the PSD-95/disc large/zonula occludens-1 domain of nNOS was required for the translocation of nNOS and its interaction with post-synaptic density-95 (PSD-95), and NO formation was attenuated by dominant negative nNOSNT-YFP. These results demonstrate that PACAP stimulated nNOS translocation mediated by PKA and PKC via PAC₁-receptor (a PACAP receptor) and suggest cross-talk between PACAP and NMDA for nNOS activation by Src-dependent phosphorylation of NMDA receptors.

Keywords: neuronal nitric oxide synthase, NMDA receptor, pituitary adenylate cyclase activating polypeptide, PSD-95/disc large/zonula occludens-1, translocation.

J. Neurochem. (2008) **105**, 2271–2285.

In the central nervous system, nitric oxide (NO) is produced by neuronal NO synthase (nNOS), a Ca²⁺/calmodulin (CaM)-dependent enzyme (Bredt and Snyder 1990; Alderton *et al.* 2001; Oess *et al.* 2006), and has been implicated in synaptic plasticity including long-term potentiation in the hippocampus and in pain transmission (Meller and Gebhart 1993; Ji *et al.* 2003). Although NO production by nNOS is well accepted to be regulated by the influx of Ca²⁺ through NMDA receptor (NMDA-R; Garthwaite *et al.* 1988; Sattler *et al.* 1999), nNOS is not efficiently stimulated by non-NMDARs that also induce a calcium influx (Kiedrowski *et al.* 1992). During fractionation, nNOS is distributed largely to membrane-associated and cytoskeletal fractions (Hecker *et al.* 1994), and co-localization of nNOS with NMDA-R at the post-synaptic density (PSD) suggests that NMDA-R activity may be coupled to nNOS activation by a close spatial interaction (Valtschanoff and Weinberg 2001). nNOS might be efficiently activated only in the vicinity of NMDA-R, because of the high local Ca²⁺ concentration upon Ca²⁺ influx by the activation of NMDA-R; and the synaptic actions of NO

Received January 11, 2008; revised manuscript received February 16, 2008; accepted February 17, 2008.

Address correspondence and reprint requests to Seiji Ito, MD, PhD, Department of Medical Chemistry, Kansai Medical University, 10-15 Fumizono, Moriguchi 570-8506, Japan. E-mail: ito@takii.kmu.ac.jp

¹The present address of Mikio Nishizawa is the College of Science and Engineering, Ritsumeikan University, 1-1-1 Nojihigashi, Kusatsu, 525-8577, Japan.

Abbreviations used: [Ca²⁺]_i, intracellular free Ca²⁺ concentration; AM, acetoxymethyl ester; APV, 2-amino-5-phosphonovaleric acid; CaM, calmodulin; CaMKII, calcium/CaM-dependent protein kinase II; cAMP, cyclic AMP; DAR-4M, diaminorhodamine-4M; DMEM, Dulbecco's modified Eagle medium; HBS, HEPES-buffered saline solution; IBMX, 3-iso-butyl-1-methylxanthine; NGF, nerve growth factor; nNOS, neuronal NO synthase; nNOSNT-YFP, YFP-tagged nNOS N-terminal mutant encompassing amino acid residues 1–299; NO, nitric oxide; PACAP, pituitary adenylate cyclase activating polypeptide; PAC₁-R, PACAP-specific receptor; PBS, phosphate-buffered saline; PDZ, PSD-95/disc large/zonula occludens-1; PKA, protein kinase A; PKC, protein kinase C; PMA, phorbol 12-myristate-13-acetate; PP2, 4-amino-5-(4-chlorophenyl)-7-(*t*-butyl)pyrazolo[3,4-*d*]pyrimidine; PSD, post-synaptic density; RACK-1, receptor for activated C kinase-1; VIP, vasoactive intestinal peptide; VPAC, VIP/PACAP receptor; YFP, yellow fluorescent protein.

are facilitated by subcellular targeting of nNOS to membrane structures (Kornau *et al.* 1995). nNOS has been shown to associate with NMDA-R via a scaffold protein, PSD-95 (Husi *et al.* 2000; Kim and Sheng 2004), which contains PSD-95/disc large/zonula occludens-1 (PDZ) domains and is expressed abundantly in the PSD (Brenman *et al.* 1996). These PDZ domains of PSD-95 enable it to regulate the colocalization of nNOS and NMDA-R (Sattler *et al.* 1999; Brenman *et al.* 1996; Niethammer *et al.* 1996). Suppression of PSD-95 expression blocked NMDA-R and Ca²⁺-dependent nNOS activation, and dissociation of NMDA-R and PSD-95 interaction blocked NMDA-R signaling without affecting synaptic activity (Sattler *et al.* 1999; Aarts *et al.* 2002).

The neuropeptide pituitary adenylate cyclase activating polypeptide (PACAP) is widely distributed in the nervous system and has been implicated in neurotransmission, neural plasticity, and neurotrophic actions (Vaudry *et al.* 2000; McCulloch *et al.* 2002). PACAP potentiated NMDA-R responses in the hippocampus (Yaka *et al.* 2002, 2003; Macdonald *et al.* 2005; MacDonald *et al.* 2007) and impaired long-term potentiation in the hippocampus of PACAP-mutant mice (Matsuyama *et al.* 2003). We recently demonstrated that PACAP knockout mice did not exhibit neuropathic pain induced by peripheral nerve injury and concomitant with the increase in PACAP immunoreactivity after nerve injury, nNOS activity visualized by NADPH-diaphorase histochemistry markedly increased in the superficial layer of the spinal cord of wild-type mice, but not in that of PACAP knockout mice (Mabuchi *et al.* 2004). NO production in spinal slices was synergistically stimulated by 100 μ M NMDA and 1–50 nM PACAP, but not by NMDA alone. Furthermore, we and others demonstrated that nNOS activation might be reversibly regulated by the translocation of nNOS from the cytosol to the plasma membrane with 750 μ M NMDA alone or a lower concentration (100 μ M) of NMDA and 1 nM PACAP in pheochromocytoma (PC12) cells, a rat pheochromocytoma line (Arundine *et al.* 2003; Mabuchi *et al.* 2004). These results suggest that PACAP signaling plays an important role in the translocation of nNOS, which is followed by NO production. However, the mechanism by which PACAP stimulated the translocation of nNOS with NMDA in PC12 cells has remained unclear.

Unlike endothelial and inducible NOSs that anchor to the membrane by lipid modification, nNOS which is unique in having approximately 250 a.a. N-terminal extension containing a PDZ domain is recruited to membranes via protein-protein interactions (Alderton *et al.* 2001; Oess *et al.* 2006). This PDZ domain contains two non-overlapping binding sites that can bind PSD-95 PDZ2 and a COOH-terminal peptide simultaneously (Christopherson *et al.* 1999). In the present study to reveal the mechanism by which PACAP promotes the translocation of nNOS to the plasma membrane in the presence of NMDA, we constructed a yellow fluorescence protein (YFP)-tagged nNOS N-terminal mutant

encompassing amino acid residues 1–299 (nNOSNT-YFP) and biochemically examined the translocation of nNOS from the cytosol to the plasma membrane in PC12 cells stably expressing nNOSNT-YFP. We showed that nNOSNT-YFP was translocated to the plasma membrane by co-stimulation with NMDA and PACAP and that the latter was involved in nNOS translocation through the activation of both protein kinase C (PKC) following calcium mobilization and the cyclic AMP (cAMP)/protein kinase A (PKA) pathway mediated by the PACAP-specific receptor (PAC₁-R).

Materials and methods

Materials

Pheochromocytoma cells were maintained in Dulbecco's modified Eagle medium (DMEM) supplemented with 5% fetal calf serum, 10% horse serum, 50 U/mL penicillin, and 50 μ g/mL streptomycin at 37°C in a 5% CO₂ atmosphere. Nerve growth factor (NGF) was obtained from Wako Pure Chemical (Osaka, Japan). PACAP and vasoactive intestinal peptide (VIP) were supplied by Peptide Institute (Osaka, Japan). NMDA, MK-801, 2-amino-5-phosphonovaleic acid (APV), calphostin C, forskolin, phorbol 12-myristate-13-acetate (PMA), 4 α -PMA, KN-62, PP2, and 3-iso-butyl-1-methylxanthine (IBMX) were purchased from Sigma (St. Louis, MO, USA). Acetoxymethyl esters (AM) of fura-2 and diaminorhodamine-4M (DAR-4M) were obtained from Dojindo (Kumamoto, Japan) and Daiichi Pure Chemicals (Tokyo, Japan), respectively. Other chemicals were of reagent grade.

Construction of YFP-tagged N-terminal truncation mutants of nNOS

The PDZ domain of nNOSNT was amplified from the full-length nNOS gene by use of the following two primers: P1; 5'-GAATTCCACA GATAC CATGG AAGAG CACAC-3' (coding strand) and 5'-CTCTA GATTA GCGAG GGCAC CTGGA AGGAC-3' (non-coding strand). The amplified nNOSNT cDNA fragment was inserted into pEYFP-N1 (Clontech, Palo Alto, CA, USA). Five truncated mutants of nNOSNT were amplified from the nNOSNT cDNA fragment by use of P1 for the coding strand of nNOSNT as common coding strand and 5'-GTGGA TCCCG TGTGT TTTC ATCTC TGCTT TG-3', 5'-GTGGA TCCCG TCCGC TGTC TGGAG GTTGG C-3', 5'-GTGGA TCCCG AGGTC CGTTA CTGGG ACCTG G-3', 5'-GTGGA TCCCG GGTGG GTGTC CCCAG GGGCT G-3', and 5'-GTGGA TCCCG AGGGC CTCTC AGAAT GAGGA C-3' as non-coding strands for nNOSNT (1–231), (1–195), (1–159), (1–130), and (1–100), respectively. These amplified nNOSNT mutant cDNA fragments were inserted into pEYFP-N1. The resulting plasmids, nNOSNT-YFP, nNOSNT (1–231)-YFP, nNOSNT (1–195)-YFP, nNOSNT (1–159)-YFP, nNOSNT (1–130)-YFP, and nNOSNT (1–100)-YFP were sequenced to ensure correct reading frame, orientation, and sequence.

Stable expression of nNOSNT-YFP mutants in PC12 cells

For expression of the six nNOSNT-YFP mutants in PC12 cells, we transfected PC12 cells with the respective plasmids. Transfection was achieved by using the lipofection method with Lipofectamine

(Invitrogen Life Technologies, Carlsbad, CA, USA) according to the manufacturer's protocol. Cells stably expressing nNOSNT-YFP mutant proteins were selected in medium containing 700 µg/mL of geneticin (Invitrogen). Resistant colonies were trypsinized and sampled carefully by using cloning rings. The expression of these nNOSNT-YFP mutant proteins in PC12 cells was confirmed by western blotting with anti-nNOS rabbit polyclonal antibody (1 : 6000; Santa Cruz Biotech., Santa Cruz, CA, USA) and western blotting detection reagent (GE Healthcare, Piscataway, NJ, USA). PC12 cells stably expressing nNOSNT-YFP was designated as PC12N cells.

nNOSNT-YFP translocation assay

Pheochromocytoma (PC12N) cells were caused to differentiate by 5-day treatment with 50 ng/mL NGF, and translocation of nNOSNT-YFP was examined in the cells essentially as reported previously (Mabuchi *et al.* 2004). Briefly, after a 30-min incubation with test agents, the cells were rinsed with phosphate-buffered saline (PBS), fixed with 4% paraformaldehyde in 0.12 M sodium phosphate buffer, pH 7.4 for 20 min at 20–24°C, and then rinsed with PBS. Digital images were captured on a Zeiss LSM510 laser-scanning confocal microscope (Oberkochen, Germany). The intensity of nNOSNT-YFP was quantified by using IMAGEJ. To evaluate the translocation of nNOSNT-YFP to the plasma membrane in PC12N cells, we counted the number of cells possessing foci of yellow fluorescence of nNOSNT-YFP on their plasma membrane and expressed this number as a percentage of the total cells examined. More than 40 cells were observed for each datum point, and at least four experiments were carried out in each analysis. Translocation of the other nNOSNT-YFP truncation mutants was examined similarly.

RT-PCR analysis

Total RNAs were isolated from NGF-treated or untreated PC12 cells and PC12N cells with Trizol reagent (Invitrogen Life Technologies),

and the first-strand cDNA was synthesized from 1 µg of total RNA by using a ReverTra Ace-α kit (Toyobo, Osaka, Japan). PCR reactions were carried out in a total 25 µL of PCR buffer containing 1.25 units GeneTaq DNA polymerase (Nippon Gene, Tokyo, Japan), 1.5 mM MgCl₂, 200 µM concentration of each deoxynucleoside triphosphate, and 0.4 mM specific oligonucleotide primers defined in Table 1. The PCR conditions consisted of an initial denaturation at 94°C for 3 min followed by 25 cycles (PAC₁-R, NR1, and β-actin), 35 cycles (PSD-95) or 40 cycles (VIP/PACAP receptor, subtype 1-R, VIP/PACAP receptor, subtype 2-R, NR2A, NR2B, and nNOS) of amplification [94°C for 1 min, 50°C (nNOS) or 63°C (the other genes) for 1 min, and 72°C for 1 min] ending with a final 5-min extension at 72°C. PCR products were separated on 2% agarose gels in Tris-acetate EDTA buffer, stained with ethidium bromide, visualized under UV light and photographed.

Measurement of cAMP content

Intracellular cAMP levels were determined by use of a cAMP radioimmunoassay kit (GE Healthcare) as described previously (Xu *et al.* 2007). NGF-differentiated PC12 or PC12N cells were pre-incubated for 15 min with HEPES-buffered saline solution (HBS) containing in mM: 125 NaCl, 4.7 KCl, 1.2 CaCl₂, 1 MgCl₂, 1.2 KH₂PO₄, 15 NaHCO₃, 11 glucose, and 15 HEPES (pH 7.4) in the presence of 0.5 µM IBMX. Reactions were started by the addition of test agents. After a 15-min incubation at 37°C, reactions were terminated by removal of media and the addition of ice-cold 5% (w/v) trichloroacetic acid solution.

Measurement of intracellular free Ca²⁺ concentration ([Ca²⁺]_i)

Pheochromocytoma (PC12) cells were plated on poly-L-lysine-coated glass-bottomed dishes (35 mm) at a density of 1 × 10⁴ cells/cm², and changes in [Ca²⁺]_i in NGF-differentiated PC12 cells were measured as described previously (Muratani *et al.* 2003). After the cells had been incubated for 30 min with DMEM containing 5%

Table 1 Primer sequences employed for RT-PCR analysis

Gene	Primer sequences (5' to 3')	Product length (bp)	Reference
PAC ₁ -R (forward)	TTTCA TCGGC ATCAT CATCA TCATC CTT	374	Onoue <i>et al.</i> 2002
PAC ₁ -R (reverse)	CCTTC CAGCT CCTCC ATTTC CTCTT		
VPAC ₁ -R (forward)	GCCCC CATCC TCCTC TCCAT	299	Onoue <i>et al.</i> 2002
VPAC ₁ -R (reverse)	TCCGC CTGCA CCTCA CCATT G		
VPAC ₂ -R (forward)	ATGGA TAGCA ACTCG CCTTT CTTTA G	326	Onoue <i>et al.</i> 2002
VPAC ₂ -R (reverse)	GGAAG GAACC AACAC ATAAC TCAAA CAG		
NR1 (forward)	TCAGC GACGA CCACG AGGGA CG	604	Allgaier <i>et al.</i> 1999
NR1 (reverse)	TTGTA GATGC CCACT TGCAC CA		
NR2A (forward)	AGCCC CCTTC GTCAT CGTAG A	339	Allgaier <i>et al.</i> 1999
NR2A (reverse)	CAGAA GGGGA GACAG TGCCA TTA		
NR2B (forward)	GGAGG AGGCG CCATT TGTC A TTG	377	Karlsson <i>et al.</i> 2002
NR2B (reverse)	AGTCC CATTG CTGCG AGATA CCAT		
nNOS (forward)	GGCAC TGGCA TCGCA CCCTT	551	Onoue <i>et al.</i> 2002
nNOS (reverse)	CTTTG GCCTG TCCGG TTCCC		
PSD-95 (forward)	GTGGG CGGCG AGGAT GGTGA A	497	Arundine <i>et al.</i> 2003
PSD-95 (reverse)	CCGCC GTTTG CTGGG AATGA A		
β-actin (forward)	TTCTA CAATG AGCTG CGTGT GGC	456	Onoue <i>et al.</i> 2002
β-actin (reverse)	CTC(A/G)T AGCTC TTCTC CAGGG AGGA		

nNOS, neuronal NO synthase; PSD, post-synaptic density; PAC₁-R, pituitary adenylate cyclase receptor; VPAC, VIP/PACAP receptor.

fetal calf serum, 10% horse serum, and 5 μM fura-2AM, the fura-2-loaded PC12 cells were stimulated by PACAP with or without 100 μM NMDA in HBS or in Mg^{2+} -free HBS supplemented with 1 mM CaCl_2 (final concentration to 2.2 mM) in place of MgCl_2 and 50 μM glycine at 2–3 mL/min on an inverted fluorescence microscope (Olympus IX-70, Tokyo, Japan) equipped with a dichroic mirror (505 nm) and an emission filter (515–550 nm). The cells were excited at 340 and 380 nm by using a high-speed wavelength switcher, and the fluorescence emission signal was monitored by using an Aquacosmos-ratio imaging system (Hamamatsu Photonics, Hamamatsu, Japan) with a cooled charge-coupled device camera. $[\text{Ca}^{2+}]_i$ was expressed as a ratio of fluorescence emission intensity at 340 and 380 nm.

Immunoprecipitation

COS7 cells expressing Myc-PSD-95 or a nNOSNT-YFP truncation mutant were incubated at 4°C for 30 min in a lysis buffer (25 mM Tris-HCl, pH 7.4, containing 1 mM EDTA, 150 mM NaCl, 1% Triton X-100, and 1 mM phenylmethylsulfonyl fluoride). The lysates of COS7 cells expressing PSD-95 and one of the six truncation mutant proteins were mixed together and centrifuged at 17 000 g for 15 min, after which the supernatant was incubated overnight at 4°C with anti-c-Myc agarose affinity gel (Sigma). After the resin had been washed three times with the lysis buffer and boiled in the sample buffer, the proteins were resolved by sodium dodecyl sulfate polyacrylamide gel electrophoresis and processed for western blotting with anti-PSD-95 antiserum and monoclonal anti-green fluorescent protein antibody (Clontech). Antisera against PSD-95 were raised in rabbits by using the N-terminal region (1–64 a.a.) of rat PSD-95 as the immunogen. We confirmed that the antisera specifically immunoreacted with PSD-95.

NO formation

To detect YFP and NO formation in PC12N cells, we used DAR-4M as a fluorescent NO indicator. Briefly, NGF-differentiated PC12 cells or PC12N cells were loaded with 10 μM DAR-4M for 20 min at 37°C in HBS and washed three times with HBS. Then digital images were captured on a Zeiss LSM510 laser-scanning confocal microscope prior to the treatment with NMDA and PACAP. After the 30-min treatment with 100 μM NMDA and 1 nM PACAP, 2 mM arginine was added to the PC12 and PC12N cells, digital images for DAR-4M were captured by a confocal microscope by excitation with a HeNe1 laser at 543 nm and emission with a 560–615 nm band pass filter. Digital images for YFP were obtained by excitation with an argon laser at 514 nm and emission with a long-pass filter above 530 nm. The fluorescence intensities of DAR-4M and nNOSNT-YFP from the acquired images were measured by using a Zeiss LSM Image Browser and IMAGEJ. We confirmed that the fluorescence of YFP (blue) and DAR-4M (red) did not overlap each other by use of PC12N (Supplementary material, Fig. S1A) and DAR-4M-loaded PC12 (Supplementary material, Fig. S1B) cells. Increase in NO formation by PACAP and NMDA was expressed as the ratio of fluorescence intensity of DAR-4M to that prior to treatment.

Statistics

All data were presented as the mean \pm SEM. Statistical analyses of the results were made by Student's *t*-test or the Mann–Whitney *U*-test.

Results

Translocation of nNOSNT-YFP from the cytosol to the membrane by PACAP and NMDA

The interaction between the NMDA-R and nNOS may occur through the C-terminal tails of NMDA-R NR2 subunits and the PDZ domain of nNOS directly or indirectly via PDZ-PDZ interaction with PSD-95 and its associates (Alderton *et al.* 2001; Oess *et al.* 2006). nNOS could also be anchored to anionic phospholipids of the membrane by the CaM-binding domain of the enzyme (Watanabe *et al.* 1998), and the activity of nNOS was shown to be regulated in a complex fashion by phosphorylation of Ser847 by calcium/CaM-dependent protein kinase II (CaMKII) or of Ser1412 by Akt kinase (Watanabe *et al.* 2003; Rameau *et al.* 2007). The N-terminal extension unique to nNOS does not contain phosphorylation sites or CaM-binding domain. Therefore, to quantitatively examine the translocation of nNOS from the cytosol to the membrane through protein-protein interactions mediated by the PDZ domain in PC12 cells, we designed nNOSNT-YFP containing the whole PDZ domain (1–299 a.a.) of nNOS (Fig. 1a), and established PC12 cells stably expressing it, PC12N cells. In NGF-differentiated PC12N cells, the expression of nNOSNT-YFP was confirmed by western blot analysis (Fig. 1b). Although nNOSNT-YFP in most cells was exclusively observed in the cytosol in NGF-differentiated PC12N cells treated with vehicle, when NGF-differentiated PC12N cells were simultaneously treated for 30 min with 100 μM NMDA and 1 nM PACAP, the foci formation of nNOSNT-YFP was observed on the plasma membrane of some cells in the microscopic field. Figure 1c presents such cells before [Fig. 1c (i)] and after [Fig. 1c (ii)] the treatment. When the fluorescence intensity was quantified along the lines a'-b' and c'-d' [in Fig. 1c (i, ii)] using IMAGEJ, the difference in the distribution of nNOSNT-YFP in PC12N cells was evident, suggesting that nNOSNT-YFP was translocated from the cytosol to the plasma membrane by NMDA and PACAP and that the N-terminal region was sufficient for the translocation of nNOS. To quantitatively measure the translocation of nNOSNT-YFP to the plasma membrane, we considered the cells showing the foci of yellow fluorescence of nNOSNT-YFP on the membrane as being positive for nNOS translocation in subsequent experiments.

After 100 μM NMDA and 1 nM PACAP had been simultaneously added, we examined the time course of the translocation of nNOSNT-YFP to the plasma membrane in NGF-differentiated PC12N cells (Fig. 2a). To evaluate the translocation of nNOSNT-YFP to the plasma membrane in PC12N cells, we counted the number of cells possessing foci of yellow fluorescence of nNOSNT-YFP on their plasma membrane and expressed this number as a percentage of the

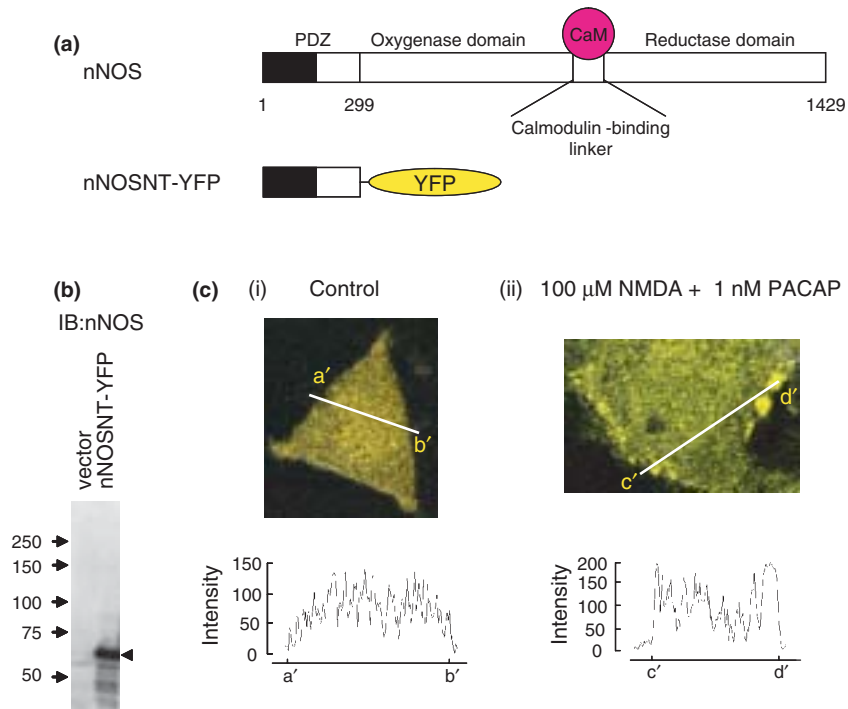


Fig. 1 Expression and translocation of yellow fluorescent protein-tagged neuronal nitric oxide synthase (nNOS) N-terminal mutant encompassing amino acid residues 1–299 (nNOSNT-YFP) in pheochromocytoma (PC12N) cells. a) Schematic diagram of nNOS and nNOSNT-YFP. The closed region represents N-terminal region containing the PSD-95/disc large/zonula occludens-1 (PDZ) domain. nNOSNT-YFP shows that YFP fused the C-terminus of the PDZ domain of nNOS (1–299 a.a.). b) Expression of nNOSNT-YFP in PC12N cells. Stable expression of nNOSNT-YFP was confirmed by

western blot analysis. Samples were separated by sodium dodecyl sulfate–polyacrylamide gel electrophoresis on 15% gel and probed with anti-nNOS antibody. c) Translocation of nNOSNT-YFP. After a 30-min incubation of nerve growth factor-differentiated PC12N cells without (i) or with (ii) 1 nM pituitary adenylate cyclase activating polypeptide and 100 μ M NMDA, the cells were fixed and fluorescence images were acquired by a confocal microscope. The fluorescence intensity of nNOSNT-YFP was quantified along the indicated lines by using IMAGEJ. In these digital images, points a–d' represent the edge of the cells.

total cells examined. The translocation of nNOSNT-YFP to the plasma membrane was observed in $12.0 \pm 2.5\%$ of the cells before stimulation, and it increased in a time-dependent manner and reached the plateau of $23.3 \pm 0.73\%$ of the PC12N cells at 30 min. Next, we examined the concentration dependency of PACAP for the translocation of nNOSNT-YFP in the presence of higher concentrations of NMDA [Fig. 2b (i)]. Consistent with a previous report (Arundine *et al.* 2003), whereas the translocation of nNOSNT-YFP was not significant at concentrations less than 500 μ M NMDA in the absence of PACAP ($10.8 \pm 0.99\%$ at 0 μ M NMDA vs. $13.9 \pm 1.3\%$ at 250 μ M NMDA, $p > 0.05$), a significant increase was observed above 500 μ M ($22.5 \pm 1.1\%$ at 500 μ M NMDA, $p < 0.01$). We previously demonstrated translocation of nNOS protein from the cytosol to the membrane by simultaneous stimulation with 100 μ M NMDA and 1 nM PACAP (Mabuchi *et al.* 2004). The translocation of nNOSNT-YFP was maximally increased by 100 μ M NMDA in the presence of PACAP at 1–10 nM [Fig. 2b (i)]. As the concentration-response curves for the translocation by

PACAP were apparently saturated at 1 nM with 100 μ M NMDA, the effect of PACAP was examined at concentrations lower than 100 μ M NMDA. While PACAP at 5 and 10 nM produced nNOSNT-YFP translocation maximally with 10 μ M NMDA, NMDA increased the nNOSNT-YFP translocation in a concentration-dependent manner from 0 to 50 μ M with PACAP at 1 nM [Fig. 2b (ii)].

Pituitary adenylate cyclase activating polypeptide and VIP are neuropeptides belonging to the VIP-glucagon-growth hormone releasing factor secretin superfamily and share 68% homology at their N-terminal domain (Vaudry *et al.* 2000; McCulloch *et al.* 2002). However, VIP failed to enhance the translocation of nNOSNT-YFP to the plasma membrane in the presence of 100 μ M NMDA ($11.4 \pm 0.6\%$ with vehicle vs. $12.7 \pm 0.47\%$ with 100 μ M NMDA + 50 nM VIP, $n = 4$, $p > 0.05$) (Fig. 2c). These results demonstrate that PACAP and NMDA synergistically caused translocation of nNOSNT-YFP to the membrane in PC12N cells.

To examine whether the activation of NMDA-R was involved in the translocation of nNOSNT-YFP, PC12N cells were treated with NMDA and PACAP in the presence of the

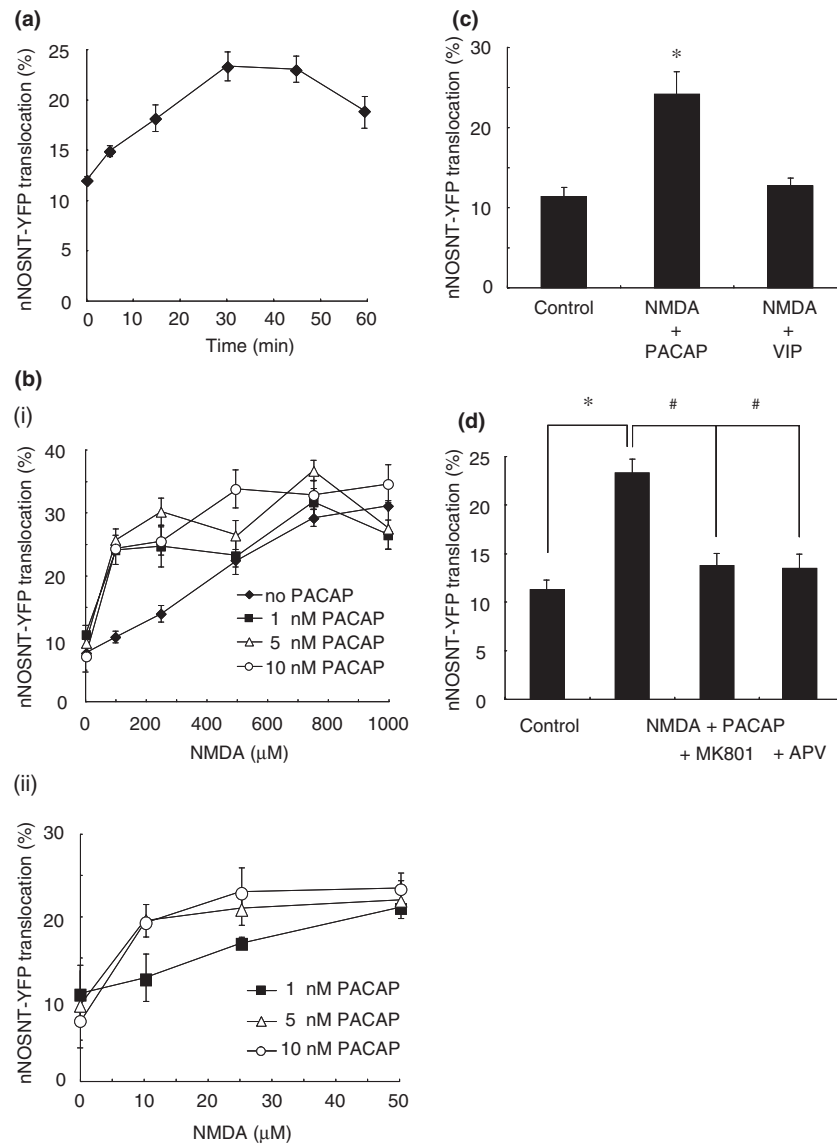


Fig. 2 Translocation of neuronal nitric oxide synthase (nNOS) in pheochromocytoma (PC12N) cells. a) Time course of translocation of yellow fluorescent protein-tagged neuronal nitric oxide synthase (nNOS) N-terminal mutant encompassing amino acid residues 1–299 (nNOSNT-YFP) elicited by NMDA and pituitary adenylate cyclase activating polypeptide (PACAP). After nerve growth factor (NGF)-differentiated PC12N cells had been incubated for the indicated times with 100 μM NMDA and 1 nM PACAP, they were washed three times with ice-cold phosphate-buffered saline and fixed with 4% paraformaldehyde. In each experiment, about 40 cells were examined at each time point using a confocal microscope; and the cells showing foci of yellow fluorescence of nNOSNT-YFP on their membrane were considered to be positive for nNOS translocation. Data (mean ± SEM, $n = 4$) show cells displaying nNOSNT-YFP translocation as a percentage of total number of cells examined. b) Concentration dependency of PACAP for the translocation of nNOSNT-YFP. After a 30-min incubation of NGF-differentiated PC12N cells with higher (i) and lower (ii) concentrations of NMDA with 0 nM (◆), 1 nM (■), 5 nM (△) or

10 nM (○) PACAP, the translocation of nNOSNT-YFP was observed by confocal microscopy. Data are presented as the mean ± SEM ($n = 4$). c) Stimulation of the translocation of nNOSNT-YFP by PACAP, but not by vasoactive intestinal peptide (VIP). After a 30-min incubation of NGF-differentiated PC12N cells with vehicle, 100 μM NMDA and 1 nM PACAP or 100 μM NMDA and 50 nM VIP, the translocation of nNOSNT-YFP was observed under a confocal microscope. Data are presented as the mean ± SEM ($n = 4$). * $p < 0.05$ compared with the vehicle. d) Effect of NMDA-R antagonists on the translocation of nNOSNT-YFP by NMDA and PACAP. After a 30-min incubation of NGF-differentiated PC12N cells with vehicle or with 100 μM NMDA and 1 nM PACAP in the absence and presence of 100 μM MK-801 or 100 μM 2-amino-5-phosphonovaleric acid, the translocation of nNOSNT was observed by confocal microscopy and quantified. Data are presented as the mean ± SEM ($n = 4$). * $p < 0.05$ compared with the vehicle. # $p < 0.05$ compared with PACAP and NMDA.

NMDA-R antagonist MK-801 or APV. The translocation of nNOSNT-YFP was increased by stimulation of NMDA and PACAP ($23.3 \pm 1.4\%$ with NMDA and PACAP, $p < 0.05$) (Fig. 2d). The increase in the translocation was completely blocked by NMDA-R antagonists ($13.7 \pm 1.2\%$ by MK-801 and $13.5 \pm 1.4\%$ by APV). These results suggest that the activation of NMDA-R was required for the translocation of nNOSNT-YFP.

Expression of PACAP/VIP receptor, NMDA-R, and nNOS mRNAs

To assign receptor subtypes for PACAP and NMDA involved in the translocation of nNOSNT-YFP, we examined the expression of PACAP/VIP family receptors, NMDA-R subunits, and nNOS in PC12 and PC12N cells by RT-PCR. Among the PACAP/VIP receptors, PAC₁-R and VPAC₂-R mRNAs, but not VPAC₁-R mRNA were expressed in PC12 cells and PC12N cells with the expected sizes regardless of NGF treatment as detected by RT-PCR (Fig. 3). As the PCR product corresponding to VPAC₂-R was detected with 40 amplification cycles, many more than in the case of PAC₁-R (25 cycles), the expression level of PAC₁-R was much higher than that of VPAC₂-R. Among the mRNAs of NMDA-R subunits examined, NR1 and NR2B mRNAs, but not NR2A mRNA were also constitutively expressed in PC12 cells and PC12N cells. PSD-95, the scaffold protein interacting with NMDA-R and nNOS was also constitutively expressed in PC12 cells and PC12N cells. In contrast, nNOS mRNA was expressed in PC12 cells and PC12N cells after NGF treatment, consistent with the results of earlier experiments (Schonhoff *et al.* 2001). These results demonstrate that receptors necessary for the translocation of nNOS by NMDA and PACAP were expressed in PC12 and PC12N cells and suggest that PAC₁-R was the predominant receptor of the PACAP/VIP family in PC12N cells.

PACAP signaling pathway in translocation of nNOSNT-YFP in PC12N cells

Pituitary adenylate cyclase activating polypeptide is coupled to stimulation of both adenylate cyclase and phosphoinositide metabolism via PAC₁-R, and NMDA increases the $[Ca^{2+}]_i$ via its receptor. To clarify the signal transduction involved in nNOS translocation by PACAP and NMDA, we first tested the effect of protein kinase inhibitors on the translocation of nNOSNT-YFP to the plasma membrane of PC12N cells (Fig. 4a). The translocation of nNOSNT-YFP was increased from $11.4 \pm 0.26\%$ to $27.4 \pm 3.9\%$ by 100 μ M NMDA and 1 nM PACAP. This increase was blocked by 50 nM H-89, a PKA inhibitor; 0.1 μ M calphostin C, a PKC inhibitor; and by 1 μ M PP2, an inhibitor of Src-family tyrosine kinase by 89.8%, 72.3%, and 93.1%, respectively; whereas 1 μ M KN-62, a CaMKII inhibitor, failed to inhibit the translocation of nNOSNT-YFP significantly. These results suggest that the activation of PKA and PKC as well as that of a member of the

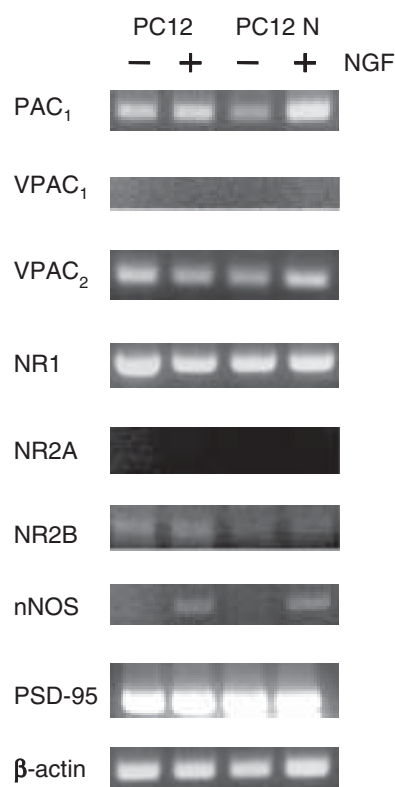
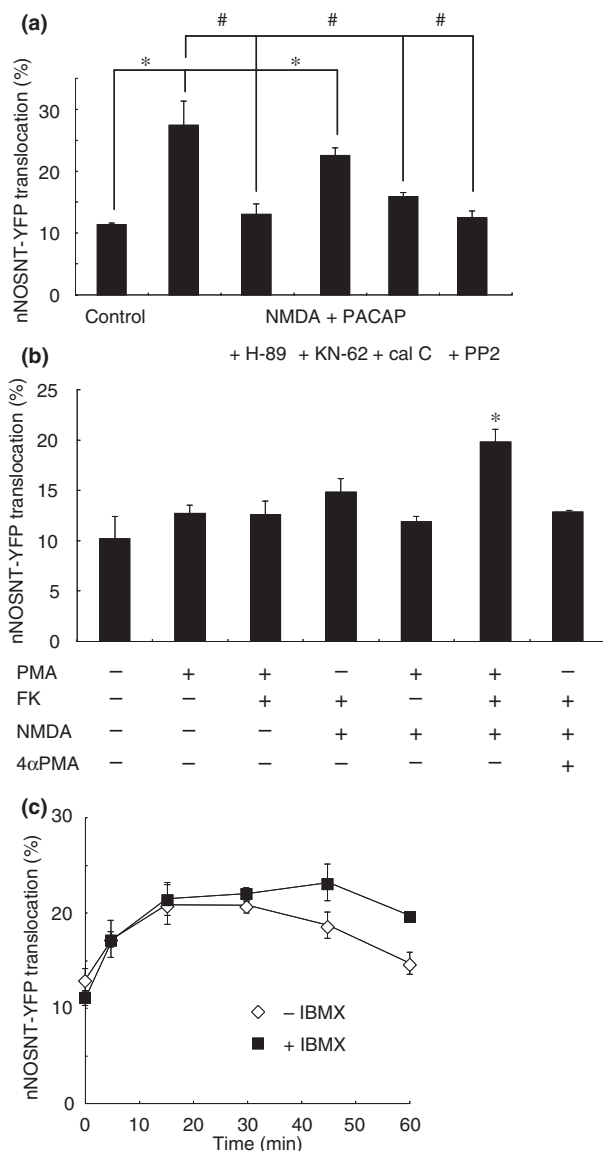


Fig. 3 mRNA expression of pituitary adenylate cyclase activating polypeptide/vasoactive intestinal peptide receptors, NMDA-R subunits, and neuronal nitric oxide synthase (nNOS) in pheochromocytoma (PC12) and PC12N cells. Cells were incubated without (-) or with (+) 50 ng/mL nerve growth factor for 5 days and total RNAs were extracted from the cells and subjected to RT-PCR using the primers shown in Table 1. PCR products were analyzed by 2% agarose gel electrophoresis and stained with ethidium bromide. β -actin was used as the control.

Src kinase family was required for the translocation of nNOSNT-YFP to the plasma membrane in PC12N cells. Therefore we next tested whether forskolin, an activator of adenylate cyclase, or PMA, a PKC activator would cause the translocation in the place of PACAP (Fig. 4b). Treatment with neither 10 μ M forskolin nor 1 μ M PMA alone resulted in translocation in the presence of 100 μ M NMDA. However, simultaneous application of forskolin and PMA with NMDA stimulated the translocation of nNOSNT-YFP to the plasma membrane two-fold, comparable to that obtained with PACAP and NMDA (Fig. 2); but the addition to 4 α -PMA, an inactive form of PMA did not enhance the translocation of nNOSNT-YFP with forskolin and NMDA.

When forskolin, PMA, and NMDA were simultaneously applied to NGF-differentiated PC12N cells, the translocation of nNOSNT-YFP reached a plateau at 15–30 min and then gradually decreased to a level closer to that before stimulation at 60 min (Fig. 4c). The decrease in the nNOS translocation was attenuated by the addition of IBMX, a



phosphodiesterase inhibitor, suggesting that the activation of PKA following the increase in intracellular cAMP and that of PKC were required for the translocation of nNOSNT-YFP.

Signal transduction coupled to PACAP and NMDA in PC12 cells

As the activation of PKA and PKC was involved in the translocation of nNOS by PACAP and NMDA, we next examined whether PACAP and NMDA stimulated the intracellular cAMP production and increased the $[Ca^{2+}]_i$ in PC12 cells. Whereas NMDA did not produce cAMP in PC12 cells even at 750 μ M, PACAP at 1 nM increased the intracellular cAMP level to 326 ± 48.6 pmol/well, comparable to that by 10 μ M forskolin, an activator of adenylate cyclase (Fig. 5a). Whereas 1 μ M PMA did not affect cAMP formation by 10 μ M forskolin, NMDA at 100 μ M rather

Fig. 4 Signal pathways coupled to the translocation of neuronal nitric oxide synthase (nNOS) by pituitary adenylate cyclase activating polypeptide (PACAP) and NMDA. a) Effect of kinase inhibitors on the translocation of yellow fluorescent protein-tagged nNOS N-terminal mutant encompassing amino acid residues 1–299 (nNOSNT-YFP) by PACAP and NMDA. After a 30-min incubation of nerve growth factor (NGF)-differentiated PC12N cells with vehicle or with 100 μ M NMDA and 1 nM PACAP in the presence of 50 nM H-89, 1 μ M KN-62, 0.1 μ M calphostin C (cal C) or 1 μ M PP2, the translocation of nNOSNT was observed by confocal microscopy and quantified. Data are presented as the mean \pm SEM ($n = 4$). * $p < 0.05$ compared with the control; # $p < 0.05$ compared with NMDA and PACAP. b) Effect of protein kinase A and protein kinase C activators on nNOS translocation. After a 30-min incubation of NGF-differentiated PC12N cells with the indicated combinations of 1 μ M phorbol 12-myristate-13-acetate (PMA), 10 μ M forskolin (FK), 1 μ M 4 α -PMA, and/or 100 μ M NMDA, the translocation was determined. Data are presented as the mean \pm SEM ($n = 4$). * $p < 0.05$ compared with the control. c) Effect of the phosphodiesterase inhibitor, 3-isobutyl-1-methylxanthine (IBMX) on nNOS translocation. NGF-differentiated pheochromocytoma (PC12N) cells were incubated for indicated times with 100 μ M NMDA, 10 μ M forskolin and 1 μ M PMA in the presence (■) or absence (◇) of 100 μ M IBMX and the translocation of nNOSNT-YFP was determined by confocal microscopy. Data are presented as the mean \pm SEM ($n = 4$).

reduced the cAMP formation with PACAP by 17.9% and with forskolin by 41.3%. PACAP stimulated cAMP formation in a concentration-dependent manner from 0.1 nM to 10 nM with an EC_{50} value of 0.24 nM, which was increased to 0.56 nM in the presence of 100 μ M NMDA (Fig. 5b).

Next we examined the effect of PACAP and NMDA on $[Ca^{2+}]_i$ in PC12 cells. While PACAP increased the $[Ca^{2+}]_i$ in PC12 cells at 10 nM, NMDA did not increase it at 100 μ M in the HBS solution or in the Mg^{2+} -free HBS solution supplemented with 50 μ M glycine (Fig. 6a). PACAP increased the peak level of $[Ca^{2+}]_i$ in a concentration-dependent manner with an EC_{50} value of 1.15 nM and NMDA did not affect the concentration-response curve for PACAP (EC_{50} value = 1.25 nM) at 100 μ M (Fig. 6b). Figure 6c shows a representative of $[Ca^{2+}]_i$ changes in 30–50 single cells stimulated by PACAP and NMDA in the absence or presence of NMDA-R antagonists. Whereas NMDA at 100 μ M did not increase the $[Ca^{2+}]_i$ level by itself (Fig. 6a), it prolonged the elevated level of $[Ca^{2+}]_i$ by 1 nM PACAP in PC12 cells (Fig. 6c). When a half time of the decay of the elevated $[Ca^{2+}]_i$ was calculated, NMDA significantly increased it from 1.46 ± 0.12 min to 2.96 ± 0.23 min (Fig. 6d). The prolongation of the decay time by NMDA was reduced to 0.86 ± 0.14 min and 0.89 ± 0.12 min by MK-801 and APV, respectively. These results suggest that PACAP increased both cAMP and $[Ca^{2+}]_i$ levels in PC12 cells via PAC₁-R and that the activation of NMDA-R affected the duration of $[Ca^{2+}]_i$ changes by PACAP in PC12 cells.

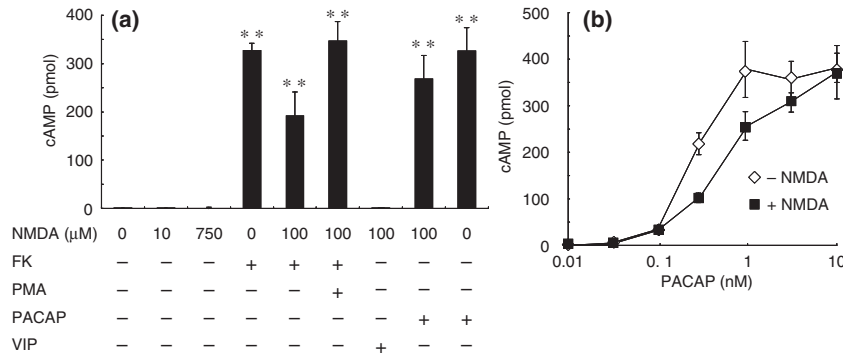


Fig. 5 Effect of pituitary adenylate cyclase activating polypeptide (PACAP) on cyclic AMP (cAMP) production in pheochromocytoma (PC12) cells. a) Effect of various agents on cAMP production in nerve growth factor (NGF)-differentiated PC12 cells. The cells (1×10^4 cells/well) in 24-well plates were incubated for 15 min at 37°C with the indicated combinations of 100 or 750 μM NMDA, 1 nM PACAP, 10 nM vasoactive intestinal peptide, 10 μM forskolin, and/or 1 μM phorbol

12-myristate-13-acetate. ** $p < 0.01$ compared with no addition. Data are presented as the mean \pm SEM ($n = 4-7$). b) Concentration dependency of PACAP for stimulating cAMP production in PC12 cells. NGF-differentiated PC12 cells were incubated at 37°C for 15 min with various concentrations of PACAP in the presence (■) or absence (◇) of 100 μM NMDA. The cAMP content in the cells was measured by using the cAMP assay kit, as described in Materials and methods.

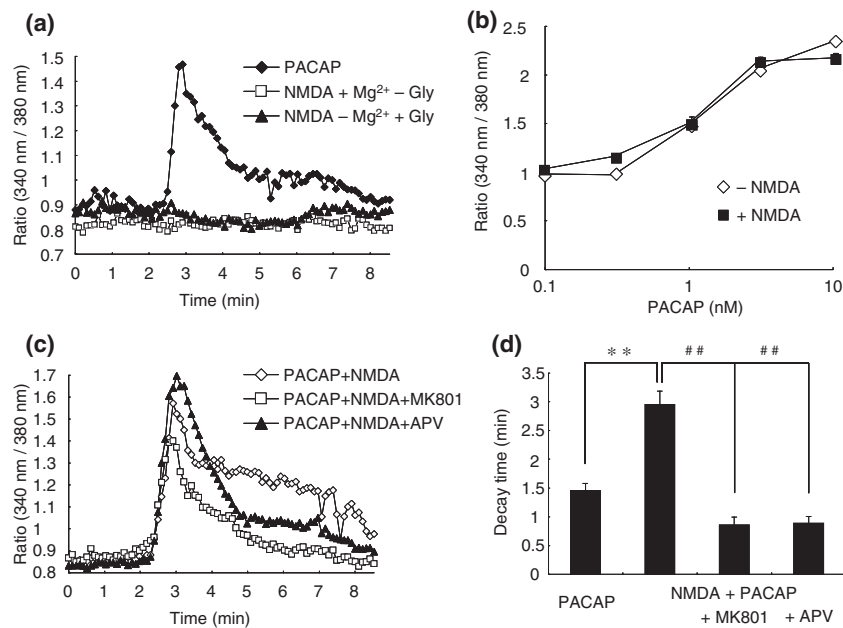


Fig. 6 Effect of pituitary adenylate cyclase activating polypeptide (PACAP) and NMDA on intracellular Ca^{2+} concentration ($[Ca^{2+}]_i$) in pheochromocytoma (PC12) cells. a) Representative changes of $[Ca^{2+}]_i$ by PACAP or NMDA in PC12 cells. The changes in $[Ca^{2+}]_i$ were measured by 100 μM NMDA alone in HEPES-buffered saline solution (HBS) (□) or Mg^{2+} -free HBS with 50 μM glycine (▲) or 1 nM PACAP in HBS (◆). The change in $[Ca^{2+}]_i$ in fura-2-loaded PC12 cells was measured as a fluorescence ratio obtained by excitation at 340 and 380 nm, as described in Materials and methods. b) Concentration dependency of PACAP for the peak level of $[Ca^{2+}]_i$ in the presence (■)

or absence (◇) of 100 μM NMDA. c) Representative traces of $[Ca^{2+}]_i$ change from single cells evoked by NMDA and PACAP in the absence (◇) or presence of the NMDA-R antagonist MK-801 (□) or 2-amino-5-phosphonovaleic acid (APV, ▲). d) Effect of NMDA-R antagonists on the duration of elevated $[Ca^{2+}]_i$ by PACAP and NMDA. The half-time of the decay of elevated $[Ca^{2+}]_i$ by 1 nM PACAP alone or 1 nM PACAP and 100 μM NMDA without and with 100 μM MK-801 or APV was calculated from individual traces of $[Ca^{2+}]_i$ changes and data are presented as the mean \pm SEM ($n = 30-60$). ** $p < 0.01$ compared with PACAP alone. ## $p < 0.01$ compared with PACAP and NMDA.

Determination of N-terminal region of nNOS translocation to the membrane

As shown in Fig. 7a, nNOSNT-YFP contains approximately a 30-residue fragment forming a two-stranded β-sheet

structure (the β-finger) C-terminal to its canonical PDZ domain (main body; Hillier *et al.* 1999; Tochio *et al.* 1999). To determine the important region of nNOSNT-YFP for the translocation of the enzyme and to examine whether the PDZ

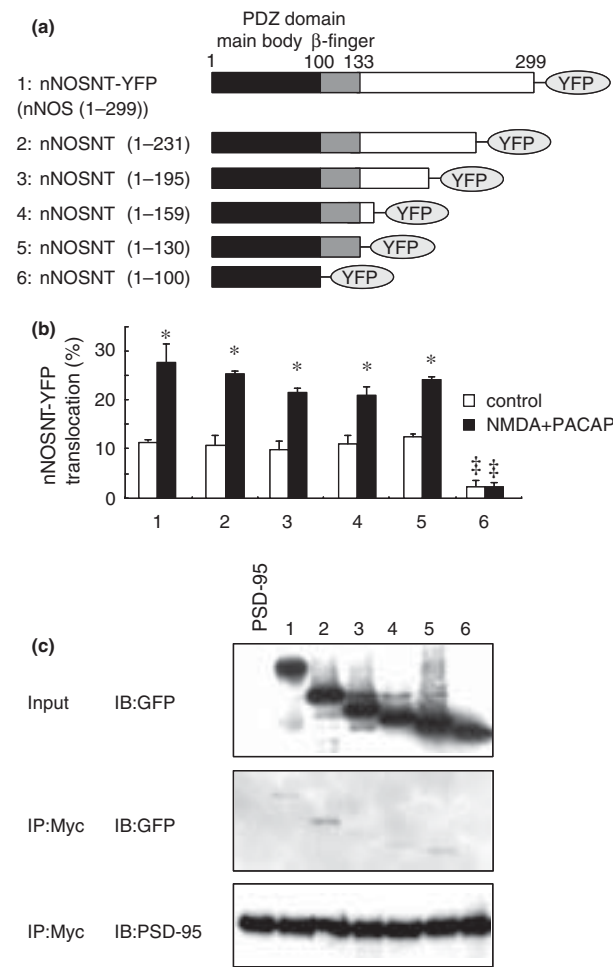


Fig. 7 Involvement of the β -finger region of the PSD-95/disc large/zonula occludens-1 (PDZ) domain in neuronal nitric oxide synthase (nNOS) translocation and interaction with PSD-95. a) Schematic diagram of yellow fluorescent protein-tagged neuronal nitric oxide synthase (nNOS) N-terminal mutant encompassing amino acid residues 1–299 (nNOSNT-YFP) and its truncation mutants. Residue numbers correspond to those in the amino acid sequence of nNOS. b) Translocation of N-terminal truncation mutants of nNOS. After nerve growth factor-differentiated pheochromocytoma (PC12) cells stably expressing a YFP-tagged mutant were incubated for 30 min without (open column) or with (closed column) 1 nM pituitary adenylate cyclase activating polypeptide (PACAP) and 100 μ M NMDA, the cells were fixed and the translocation of YFP-tagged nNOSNT mutants was determined using the confocal microscope. Numbers 1–6 correspond to those of the mutants shown in (a). Data are presented as the mean \pm SEM ($n = 4$). * $p < 0.05$ compared with the control of PC12N cells. ** $p < 0.01$ compared with PC12N cells treated with PACAP and NMDA. (c) Interaction of the β -finger region of the PDZ domain of nNOS with PSD-95. The lysate of COS7 cells expressing a nNOSNT-YFP mutant and Myc-PSD-95 were mixed together and incubated overnight with anti-c-Myc agarose for immunoprecipitation. Absorbed samples were analyzed by immunoblotting for PSD-95 (middle panel) and green fluorescent protein (upper and lower panels). Left lane shows Myc-PSD-95 alone.

domain of nNOSNT was responsible for coupling to NMDA-R via the versatile scaffolding protein PSD-95, we constructed five truncated mutants of nNOSNT-YFP (Fig. 7a). We stably transfected PC12 cells with the respective nNOS truncation mutants and then examined the translocation of these mutants to the plasma membrane (Fig. 7b). When the cells were stimulated for 30 min with 100 μ M NMDA and 1 nM PACAP, the nNOS mutants containing the β -finger of the PDZ domain were translocated to the plasma membrane to an extent similar to nNOSNT-YFP. On the other hand, the nNOSNT (1–100) mutant lacking the β -finger was scarcely localized at the plasma membrane prior to stimulation ($2.1 \pm 1.2\%$), and the translocation to the membrane was not increased by NMDA and PACAP ($2.2 \pm 0.98\%$). These results demonstrate that β -finger of the PDZ domain of nNOS was essential for nNOS to reach the plasma membrane.

As the β -finger is the major contact region of nNOS for binding to the PDZ2 domain of PSD-95 (Hillier *et al.* 1999; Tochio *et al.* 1999), we considered it likely that nNOSNT-YFP interacted with PSD-95 on the plasma membrane when PC12N cells were stimulated by PACAP and NMDA. To address this possibility, we expressed nNOSNT-YFP, its truncated mutants and Myc-PSD-95 in COS7 cells. A protein extract from the cells transfected with the PSD-95-Myc plasmid was mixed with one of cells transfected with the plasmid for nNOSNT-YFP or one of its truncated mutants, and immunoprecipitated with anti-c-Myc agarose (Fig. 7c). Among the nNOSNT-YFP truncation mutants, nNOSNT (1–100)-YFP was not precipitated with Myc-PSD-95. Being consistent with the results of the translocation experiment (Fig. 7b), these results also suggest that the β -finger was indeed critical for the physical interaction with PSD-95.

Inhibition of NO production by the translocation of nNOSNT-YFP

Previous studies demonstrated that NO formation was stimulated by the nNOS translocation to the plasma membrane by 100 μ M NMDA and 1 nM PACAP (Arundine *et al.* 2003; Mabuchi *et al.* 2004). To further study whether nNOSNT-YFP inhibited nNOS activation by NMDA and PACAP, we examined NO production in NGF-differentiated PC12 cells and PC12N cells loaded with the fluorescent NO indicator DAR-4M. When NO formation was assessed by fluorescence intensities of DAR-4M before and after 30-min treatment with 1 nM PACAP and 100 μ M NMDA, more than 1.4-fold increase in the intensity was observed in 8 out of 26 PC12 cells (30.7%), 11 out of 30 PC12 cells transfected with YFP (36.7%), and in 8 out of 70 PC12N cells (11.1%). Figure 8a and b respectively show a representative PC12 cell transfected by YFP and PC12N cell before and after 30-min incubation with 100 μ M NMDA and 1 nM PACAP. In the PC12 cell, NO formation (Fig. 8a, red line) was stimulated by NMDA and PACAP. On the other hand, the addition of

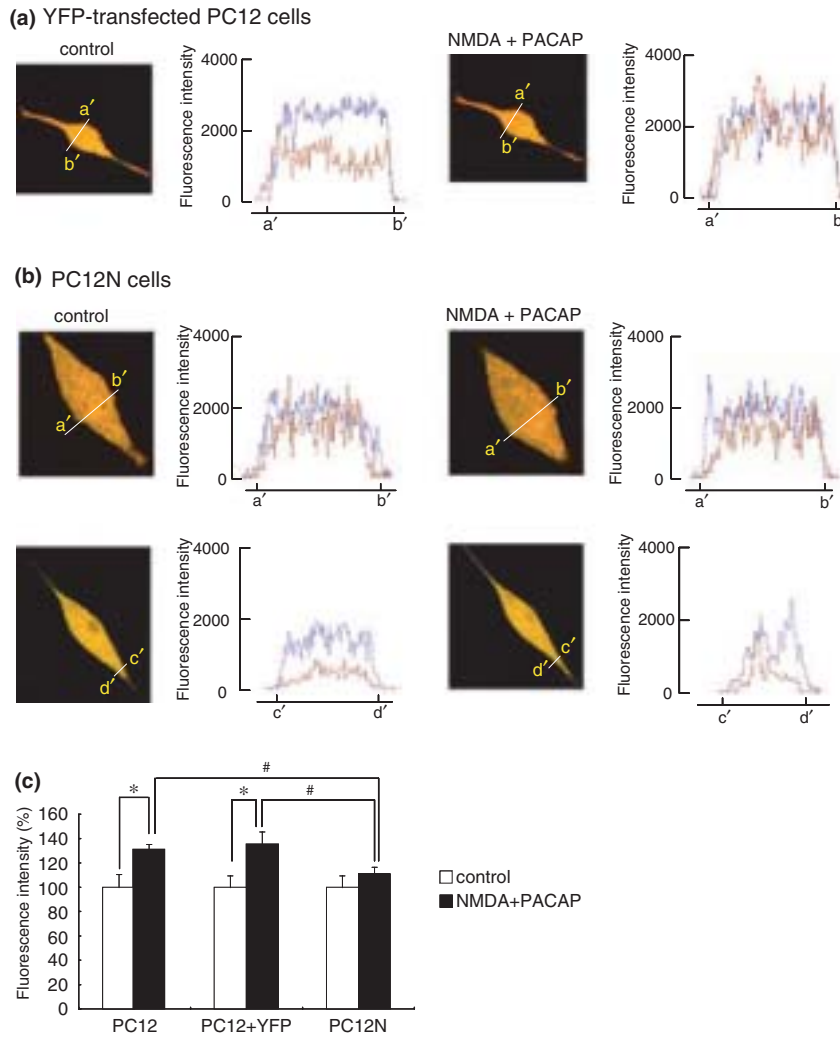


Fig. 8 Yellow fluorescent protein-tagged neuronal nitric oxide synthase (nNOS) N-terminal mutant encompassing amino acid residues 1–299 (nNOSNT-YFP)-mediated inhibition of NO formation by pituitary adenylate cyclase activating polypeptide (PACAP) and NMDA in pheochromocytoma (PC12N) cells. Representative images of nerve growth factor (NGF)-differentiated PC12 cells transfected by YFP (a) and by nNOSNT-YFP (equivalent to PC12N cells) (b) before (left) and after (right) 30-min treatment with 1 nM PACAP and 100 μ M NMDA. The fluorescence intensity of diaminorhodamine-4M (DAR-4M) and nNOSNT-YFP was quantified along the lines indicated as 'a'-b' and 'c'-d'. The red and blue traces show the fluorescence intensity of DAR-4M and YFP, respectively, on these lines. Before incubation with 100 μ M NMDA and 1 nM PACAP, cells were loaded with DAR-4M for

20 min and then washed with HEPES-buffered saline solution. After 30-min stimulation with 100 μ M NMDA and 1 nM PACAP, 2 mM L-arginine was added and NO production was fluorometrically measured. (c) Increase in NO production caused by NMDA and PACAP in PC12 cells, but not in PC12N cells. NGF-differentiated PC12 cells, PC12 cells transfected with YFP (a) and PC12N cells (b) were treated for 30 min with 100 μ M NMDA and 1 nM PACAP. Fluorescence intensity of DAR-4M before stimulation (open column) was taken as 100% and that after stimulation (closed column) was calculated as a percentage of that before stimulation. Data are presented as the mean \pm SEM ($n = 20-70$). * $p < 0.05$ compared with before stimulation. # $p < 0.05$ compared with PC12 or PC12 and YFP in the presence of NMDA and PACAP.

NMDA and PACAP caused the focus formation of nNOSNT-YFP in the PC12N cell and slightly increased NO formation (Fig. 8b). The foci were evident on the cell body and the neurites (Fig. 8b, a'-b', c'-d', blue line), where NO formation was blocked (Fig. 8b, a'-b', c'-d', red line). To quantitatively compare the NO formation by NMDA and PACAP in PC12 cells and PC12N cells, we used IMAGEJ to calculate the

fluorescence intensity of DAR-4M in the cell body along the lines indicated in Fig. 8. Whereas NMDA and PACAP significantly increased NO formation 1.31-fold in PC12 cells and 1.35-fold in PC12 cells transfected with YFP, they increased NO formation only 1.1-fold in PC12N cells (Fig. 8c). These results suggest that nNOSNT-YFP attenuated nNOS activation by NMDA and PACAP.

Discussion

We have recently demonstrated with Fyn and PACAP knockout mice that phosphorylation of NR2B subunit of NMDA-Rs at Tyr1472 by Fyn kinase may have dual roles in the retention of NMDA-Rs in the PSD and in activation of nNOS and that PACAP might promote the functional coupling of nNOS and NMDA-Rs (Mabuchi *et al.* 2004; Salter and Kalia 2004). All three isoforms of NOS are targeted to distinct subcellular locations, and targeting of NOS into the active compartments can be considered a prerequisite for efficient NO production (Oess *et al.* 2006). Although these NOS isoforms are all dimeric and bi-domain enzymes, nNOS is unique in terms of its N-terminal PDZ domain that targets it to synaptic sites in the brain and skeletal muscle (Fig. 1a). Membrane localization of nNOS in neuronal cells is mediated via the specific interaction of the extended PDZ domain of the enzyme with the second PDZ domain of PSD-95 (Brenman *et al.* 1996; Niethammer *et al.* 1996). Although we further showed that simultaneous addition of PACAP and NMDA caused the translocation of nNOS from the cytosol to the membrane and stimulated NO production in PC12 cells (Mabuchi *et al.* 2004), the mechanism by which PACAP stimulated the translocation of nNOS remained unknown. The structure and activity of nNOS are regulated by complex phosphorylation and dephosphorylation in catalytic domains (Watanabe *et al.* 2003; Rameau *et al.* 2007) and also by interaction of the CaM-binding domain of nNOS with anionic phospholipids in the membrane (Watanabe *et al.* 1998). To simplify the analysis of translocation of nNOS and to visualize the translocation in the cell, we designed a truncation mutant containing the PDZ domain of nNOS and nNOSNT-YFP, and established PC12N cells stably expressing it. The translocation of nNOSNT-YFP was visualized as the formation of foci of yellow fluorescence of nNOSNT-YFP on the membrane (Fig. 1c) and occurred in a time- and concentration-dependent manner after simultaneous stimulation with PACAP and NMDA (Fig. 2a and b). The concentration dependency of nNOSNT-YFP translocation elicited by NMDA and/or PACAP was consistent with that obtained by nNOS immunohistochemistry reported previously (Arundine *et al.* 2003; Mabuchi *et al.* 2004); nNOSNT-YFP was translocated to the membrane above 500 μM NMDA alone, the concentration of which could be markedly reduced to 10 μM in the presence of 5 nM PACAP and to 50 μM in the presence of 1 nM PACAP (Fig. 2b). nNOSNT-YFP was translocated to the membrane in 10–12% of the cells before stimulation and maximally in 25–30% of the cells after the stimulation with 100 μM NMDA and 1 nM PACAP. As nNOSNT-YFP translocation by NMDA alone was also approximately 30% even at 1000 μM (Fig. 2b), the reason that PACAP could not increase the maximum translocation might be ascribed to

the nature of NMDA-R as mentioned below, rather than that of PAC₁-R in PC12 cells.

Involvement of NMDA-R in the translocation of nNOSNT-YFP

We previously demonstrated that translocation of nNOS protein from the cytosol to the membrane and subsequent NO production occurred by simultaneous stimulation of 1 nM PACAP with 100 μM NMDA (Mabuchi *et al.* 2004). In the present study, PC12N cells stably expressing nNOSNT-YFP showed that co-stimulation of PACAP with NMDA enhanced nNOSNT-YFP translocation in a concentration-dependent manner (Figs 1 and 2) and that nNOSNT-YFP, but not YFP, inhibited NO production by nNOS (Fig. 8), suggesting that nNOS translocation was involved in NO production. NR1 and NR2 subunits of NMDA-Rs were functionally expressed in PC12 cells (Casado *et al.* 1996) and NO production by NMDA was observed by electron paramagnetic resonance spectroscopy (Schelman *et al.* 1997) and by a fluorescent NO indicator in PC12 cells in DMEM (Arundine *et al.* 2003). NMDA neither increased the $[\text{Ca}^{2+}]_i$ by itself in HBS and Mg^{2+} -free HBS solution with 50 μM glycine (Fig. 6a) nor affected the concentration-response curve of PACAP for the peak $[\text{Ca}^{2+}]_i$ level (Fig. 6b). However, the decay time of the elevated $[\text{Ca}^{2+}]_i$ by PACAP was prolonged by NMDA (Fig. 6c and d). This prolongation of the decay time (Fig. 6d) and the translocation of nNOSNT-YFP (Fig. 2d) by PACAP and NMDA were inhibited by NMDA-R antagonists, APV and MK-801. These results demonstrated that the activation of NMDA-R was crucial for nNOS translocation and subsequent NO formation.

Translocation of nNOSNT-YFP by PACAP via PAC₁-R

Pituitary adenylate cyclase activating polypeptide is a neuropeptide belonging to the VIP-glucagon-growth hormone releasing factor-secretin superfamily. PACAP binds with a high affinity to three G-protein-coupled receptors, PAC₁, VPAC₁, and VPAC₂. PAC₁-R is known to bind also VIP with a low affinity and is coupled to stimulation of both adenylate cyclase and phosphoinositide metabolism, whereas VPAC₁-R and VPAC₂-R bind VIP with an affinity similar to that for PACAP and are coupled to the former only (Vaudry *et al.* 2000; McCulloch *et al.* 2002). The present study demonstrated that PACAP synergistically stimulated nNOSNT-YFP translocation in PC12N cells in the presence of 100 μM NMDA via PAC₁-R for the following reasons: (i) PAC₁-R was expressed in PC12 and PC12N cells (Fig. 3), (ii) VIP failed to translocate nNOSNT-YFP in PC12N cells (Fig. 2c), (iii) PACAP increased the cAMP content and $[\text{Ca}^{2+}]_i$ in PC12 cells in a concentration-dependent manner with EC₅₀ values of 0.56 and 1.25 nM, respectively, in the presence of 100 μM NMDA, (iv) increase in translocation by PACAP and NMDA was almost completely inhibited by

H-89, a PKA inhibitor, and by calphostin C, a PKC inhibitor, but not by KN-62, a CaMKII inhibitor (Fig. 4a), and (v) conversely, forskolin and PMA could substitute for PACAP (Fig. 4b) and IBMX, a phosphodiesterase inhibitor, which prolonged the presence of nNOSNT-YFP on the membrane (Fig. 4c). These results demonstrate that PACAP stimulated nNOSNT-YFP translocation mediated by PKA and PKC in the presence of 100 μ M NMDA. Whereas VPAC₂-R mRNA was expressed in PC12 cells (Fig. 3), VIP (10 nM) failed to increase the cAMP content (Fig. 5a). As the effective concentration of VIP is 3–4 orders higher than that of PACAP (Deutsch and Sun 1992), the concentration of VIP employed here was not high enough to activate PAC₁-R. Although NMDA alone at 750 μ M did not increase the cAMP content in the cells at all, it could increase nNOSNT-YFP translocation in PC12N cells, suggesting that NMDA at higher concentrations may translocate nNOS through a signaling pathway different from that observed for PACAP with 100 μ M NMDA.

Role of PACAP signaling pathway for nNOS translocation

Src family kinases such as Src and Fyn are a crucial point of convergence for signaling pathways that enhance NMDA-R activity and act as a molecular hub for control of NMDA-Rs (Salter and Kalia 2004). We have recently shown that NMDA-Rs containing the NR2B subunit are involved in the maintenance of neuropathic pain and that Tyr1472 phosphorylation of this subunit by Fyn may have a dual role, being involved in the retention of NMDA-R in the PSD and in activation of nNOS (Abe *et al.* 2005). PACAP signaling potentiated NMDA-R via PAC₁-R [see MacDonald *et al.* (2007) for a review]. The cAMP/PKA pathway activated by PACAP releases the scaffold protein receptor for activated C kinase-1 (RACK-1) from NR2B and Fyn kinase. RACK-1 localizes Fyn in close proximity with its substrate, the NR2B subunit, but prevents the phosphorylation of the NR2B subunit until the appropriate signal occurs (Yaka *et al.* 2002). The activation of the cAMP/PKA pathway via PAC₁-R causes the dissociation of RACK-1 from the NMDA-R complex, allowing Fyn to phosphorylate the NR2B subunit, resulting in enhanced channel activity (Yaka *et al.* 2003). The PKC/Ca²⁺ pathway activated by PACAP is suggested to promote the phosphorylation of cell adhesion kinase β and its association with Src. In the present study, we showed that a Src-family kinase inhibitor, PP2, prevented nNOSNT-YFP from being translocated to the membrane. Recent studies suggest that RACK-1 serves as a hub for PKC, Fyn, and Src and facilitates the regulation of basal NMDA-R activity in CA1 hippocampal neurons (Macdonald *et al.* 2005) and that modulation of NMDA-R by Fyn, upstream of Src within the RACK-1 complex is required for Src activation (MacDonald *et al.* 2007). The present study showing that the nNOS activation by PACAP and NMDA in PC12 cells

was mediated by PKA, PKC, and Src kinases is in line with the regulation of NMDA-Rs by G protein-coupled receptors observed in the hippocampus, but the significance of activation of NMDA-Rs for nNOS translocation and the identity of the proteins targeted by PKA and PKC in PC12 cells remain to be clarified.

Role of PDZ domain of N-terminus of nNOS in the nNOS translocation and activation

Previous studies suggested that the binding of the β -finger of nNOS to PSD-95 left the nNOS PDZ domain peptide-binding pockets free to interact with other proteins such as C-terminal tail of NR2 subunits of NMDA-R via PDZ-peptide interactions (Christopherson *et al.* 1999; Oess *et al.* 2006). However, the truncation mutants of nNOSNT-YFP revealed that the β -finger (100–130 a.a.) of N-terminal PDZ domain was crucial for the translocation to the membrane and interaction with PSD-95 (Fig. 7). It should also be noted that the percentage of translocation of nNOSNT-YFP ((1–100) was markedly decreased before as well as after stimulation of PACAP and NMDA. These results suggest that PSD-95 bound both the nNOS and NMDA-R on the membrane and assembled them into a macromolecular signaling complex where nNOS was under NMDA-R control (Sattler *et al.* 1999; Husi *et al.* 2000). Nine C-terminal residues of NR2B-rendered cell-permeant by fusion to TaT protein (NR2B9c) was previously shown to function as dominant negative and protect cultured neurons from neurotoxicity and focal ischemic brain damage (Aarts *et al.* 2002). In the present study, we showed that nNOSNT-YFP also inhibited NO formation in PC12N cells and neuritis (Fig. 8), demonstrating that the translocation of nNOS to the membrane may be crucial for efficient NO formation at cell boundaries in PC12 cells, and possibly at synapses.

In summary, we established a fluorescence imaging system for examining nNOS translocation in PC12 cells. Unlike the other two isoforms of NOS that use lipid modification for membrane trafficking, we have demonstrated that the synergism of PACAP and NMDA was critical for the translocation and activation of nNOS through PKA, PKC, and Src kinase via PAC₁-R and NMDA-Rs and that the interaction of the β -finger of the nNOS PDZ domain with PSD-95 was essential for the translocation of nNOS.

Acknowledgments

We are grateful to Professor Takeshi Nishino of Nippon Medical School and Dr. Takanobu Nakazawa of Institute of Medical Science, The University of Tokyo for providing the plasmids of nNOS and PSD-95, respectively. This work was supported in part by grants from the programs Grants-in-Aid for COE Research, Scientific Research on Priority Areas from the Ministry of Education, Culture, Sports, Science and Technology of Japan, and Grants-in-Aid for

Scientific Research (S) and (C) from Japan Society for the Promotion of Science and Japan Foundation of Applied Enzymology.

Supplementary material

The following supplementary material is available for this article online:

Fig. S1 No overlap of fluorescence between YFP and DAR-4M, a NO fluorescent indicator.

This material is available as part of the online article from <http://www.blackwell-synergy.com>.

Please note: Blackwell Publishing are not responsible for the content or functionality of any supplementary materials supplied by the authors. Any queries (other than missing material) should be directed to the corresponding author for the article.

References

- Aarts M., Liu Y., Liu L., Besshoh S., Arundine M., Gurd J. W., Wang Y. T., Salter M. W. and Tymianski M. (2002) Treatment of ischemic brain damage by perturbing NMDA receptor PSD-95 protein interactions. *Science* **298**, 846–850.
- Abe T., Matsumura S., Katano T. *et al.* (2005) Fyn kinase-mediated phosphorylation of NMDA receptor NR2B subunit at Tyr1472 is essential for maintenance of neuropathic pain. *Eur. J. Neurosci.* **22**, 1445–1454.
- Alderton W. K., Cooper C. E. and Knowles R. G. (2001) Nitric oxide synthases: structure, function and inhibition. *Biochem. J.* **357**, 593–615.
- Allgaier C., Scheiber P., Müller D., Feuerstein T. J. and Illes P. (1999) NMDA receptor characterization and subunit expression in rat cultured mesencephalic neurons. *Br. J. Pharmacol.* **126**, 121–130.
- Arundine M., Sanelli T., He B. P. and Strong M. J. (2003) NMDA induces NOS 1 translocation to the cell membrane in NGF-differentiated PC 12 cells. *Brain Res.* **976**, 149–158.
- Bredt D. S. and Snyder S. H. (1990) Isolation of nitric oxide synthetase, a calmodulin-requiring enzyme. *Proc. Natl Acad. Sci. USA* **87**, 682–685.
- Brennan J. E., Chao D. S., Gee S. H. *et al.* (1996) Interaction of nitric oxide synthase with the postsynaptic density protein PSD-95 and alpha1-syntrophin mediated by PDZ domains. *Cell* **84**, 757–767.
- Casado M., López-Guajardo A., Mellström B., Naranjo J. R. and Lerma J. (1996) Functional N-methyl-D-aspartate receptors in clonal rat pheochromocytoma cells. *J. Physiol.* **490**, 391–404.
- Christopherson K. S., Hillier B. J., Lim W. A. and Bredt D. S. (1999) PSD-95 assembles a ternary complex with the N-methyl-D-aspartate receptor and a bivalent neuronal NO synthase PDZ domain. *J. Biol. Chem.* **274**, 27467–27473.
- Deutsch P. J. and Sun Y. (1992) The 38-amino acid form of pituitary adenylate cyclase-activating polypeptide stimulates dual signaling cascades in PC12 cells and promotes neurite outgrowth. *J. Biol. Chem.* **267**, 5108–5113.
- Garthwaite J., Charles S. L. and Chess-Williams R. (1988) Endothelium-derived relaxing factor release on activation of NMDA receptors suggests role as intercellular messenger in the brain. *Nature* **336**, 385–388.
- Hecker M., Mulsch A. and Busse R. (1994) Subcellular localization and characterization of neuronal nitric oxide synthase. *J. Neurochem.* **62**, 1524–1529.
- Hillier B. J., Christopherson K. S., Prehoda K. E., Bredt D. S. and Lim W. A. (1999) Unexpected modes of PDZ domain scaffolding revealed by structure of nNOS-syntrophin complex. *Science* **284**, 812–815.
- Husi H., Ward M. A., Choudhary J. S., Blackstock W. P. and Grant S. G. (2000) Proteomic analysis of NMDA receptor-adhesion protein signaling complexes. *Nat. Neurosci.* **3**, 661–669.
- Ji R. R., Kohno T., Moore K. A. and Woolf C. J. (2003) Central sensitization and LTP: do pain and memory share similar mechanisms? *Trends Neurosci.* **26**, 696–705.
- Karlsson U., Sjödin J., Möller K. A., Johansson S., Wikström L. and Näsström J. (2002) Glutamate-induced currents reveal three functionally distinct NMDA receptor populations in rat dorsal horn – effects of peripheral nerve lesion and inflammation. *Neuroscience* **112**, 861–868.
- Kiedrowski L., Costa E. and Wroblewski J. T. (1992) Glutamate receptor agonists stimulate nitric oxide synthase in primary cultures of cerebellar granule cells. *J. Neurochem.* **58**, 335–341.
- Kim E. and Sheng M. (2004) PDZ domain proteins of synapses. *Nat. Rev. Neurosci.* **5**, 771–781.
- Kornau H. C., Schenker L., Kennedy M. B. and Seeburg P. H. (1995) Domain interaction between NMDA receptor subunits and the postsynaptic density protein PSD-95. *Science* **269**, 1737–1740.
- Mabuchi T., Shintani N., Matsumura S., Okuda-Ashitaka E., Hashimoto H., Muratani T., Minami T., Baba A. and Ito S. (2004) Pituitary adenylate cyclase-activating polypeptide is required for the development of spinal sensitization and induction of neuropathic pain. *J. Neurosci.* **24**, 7283–7291.
- Macdonald D. S., Weerapura M., Beazely M. A., Martin L., Czerwinski W., Roder J. C., Orser B. A. and MacDonald J. F. (2005) Modulation of NMDA receptors by pituitary adenylate cyclase activating peptide in CA1 neurons requires G alpha q, protein kinase C, and activation of Src. *J. Neurosci.* **25**, 11374–11384.
- MacDonald J. F., Jackson M. F. and Beazely M. A. (2007) G protein-coupled receptors control NMDARs and metaplasticity in the hippocampus. *Biochim. Biophys. Acta* **1768**, 941–951.
- Matsuyama S., Matsumoto A., Hashimoto H., Shintani N. and Baba A. (2003) Impaired long-term potentiation in vivo in the dentate gyrus of pituitary adenylate cyclase-activating polypeptide (PACAP) or PACAP type 1 receptor-mutant mice. *Neuroreport* **14**, 2095–2098.
- McCulloch D. A., MacKenzie C. J., Johnson M. S., Robertson D. N., Holland P. J., Ronaldson E., Lutz E. M. and Mitchell R. (2002) Additional signals from VPAC/PAC family receptors. *Biochem. Soc. Trans.* **30**, 441–446.
- Meller S. T. and Gebhart G. F. (1993) Nitric oxide (NO) and nociceptive processing in the spinal cord. *Pain* **52**, 127–136.
- Muratani T., Nishizawa M., Matsumura S., Mabuchi T., Abe K., Shimamoto K., Minami T. and Ito S. (2003) Functional characterization of prostaglandin F2alpha receptor in the spinal cord for tactile pain (allodynia). *J. Neurochem.* **86**, 374–382.
- Niethammer M., Kim E. and Sheng M. (1996) Interaction between the C terminus of NMDA receptor subunits and multiple members of the PSD-95 family of membrane-associated guanylate kinases. *J. Neurosci.* **16**, 2157–2163.
- Oess S., Icking A., Fulton D., Govers R. and Müller-Esterl W. (2006) Subcellular targeting and trafficking of nitric oxide synthases. *Biochem. J.* **396**, 401–409.
- Onoue S., Endo K., Yajima T. and Kashimoto K. (2002) Pituitary adenylate cyclase activating polypeptide regulates the basal production of nitric oxide in PC12 cells. *Life Sci.* **71**, 205–214.
- Rameau G. A., Tukey D. S., Garcin-Hosfield E. D., Titcombe R. F., Misra C., Khatri L., Getzoff E. D. and Ziff E. B. (2007) Biphasic coupling of neuronal nitric oxide synthase phosphorylation to the

- NMDA receptor regulates AMPA receptor trafficking and neuronal cell death. *J. Neurosci.* **27**, 3445–3455.
- Salter M. W. and Kalia L. V. (2004) Src kinases: a hub for NMDA receptor regulation. *Nat. Rev. Neurosci.* **5**, 317–328.
- Sattler R., Xiong Z., Lu W. Y., Hafner M., MacDonald J. F. and Tymianski M. (1999) Specific coupling of NMDA receptor activation to nitric oxide neurotoxicity by PSD-95 protein. *Science* **284**, 1845–1848.
- Schelman W. R., Kurth J. L., Berdeaux R. L., Norby S. W. and Weyhenmeyer J. A. (1997) Angiotensin II type-2 (AT₂) receptor-mediated inhibition of NMDA receptor signalling in neuronal cells. *Mol. Brain Res.* **48**, 197–205.
- Schonhoff C. M., Bulseco D. A., Brancho D. M., Parada L. F. and Ross A. H. (2001) The Ras-ERK pathway is required for the induction of neuronal nitric oxide synthase in differentiating PC12 cells. *J. Neurochem.* **78**, 631–639.
- Tochio H., Zhang Q., Mandal P., Li M. and Zhang M. (1999) Solution structure of the extended neuronal nitric oxide synthase PDZ domain complexed with an associated peptide. *Nat. Struct. Biol.* **6**, 417–421.
- Valtschanoff J. G. and Weinberg R. (2001) Laminar organization of the NMDA receptor complex within the postsynaptic density. *J. Neurosci.* **21**, 1211–1217.
- Vaudry D., Gonzalez B. J., Basille M., Yon L., Fournier A. and Vaudry H. (2000) Pituitary adenylate cyclase-activating polypeptide and its receptors: from structure to functions. *Pharmacol. Rev.* **52**, 269–324.
- Watanabe Y., Nishio M., Hamaji S., Hayashi Y., Hu Y. and Hidaka H. (1998) Neuronal nitric oxide synthase-membrane phospholipid interactions. *Arch. Biochem. Biophys.* **358**, 68–73.
- Watanabe Y., Song T., Sugimoto K., Horii M., Araki N., Tokumitsu H., Tezuka T., Yamamoto T. and Tokuda M. (2003) Post-synaptic density-95 promotes calcium/calmodulin-dependent protein kinase II-mediated Ser847 phosphorylation of neuronal nitric oxide synthase. *Biochem. J.* **372**, 465–471.
- Xu L., Okuda-Ashitaka E., Matsumura S., Mabuchi T., Okamoto S., Sakimura K., Mishina M. and Ito S. (2007) Signal pathways coupled to activation of neuronal nitric oxide synthase in the spinal cord by nociceptin/orphanin FQ. *Neuropharmacology* **52**, 1318–1325.
- Yaka R., Thornton C., Vagts A. J., Phamluong K., Bonci A. and Ron D. (2002) NMDA receptor function is regulated by the inhibitory scaffolding protein, RACK1. *Proc. Natl Acad. Sci. USA* **99**, 5710–5715.
- Yaka R., He D. Y., Phamluong K. and Ron D. (2003) Pituitary adenylate cyclase-activating polypeptide PACAP(1-38) enhances N-methyl-D-aspartate receptor function and brain-derived neurotrophic factor expression via RACK1. *J. Biol. Chem.* **278**, 9630–9638.

N-ethylmaleimide-sensitive fusion protein (NSF) is involved in central sensitization in the spinal cord through GluR2 subunit composition switch after inflammation

Tayo Katano,^{1,*} Hidemasa Furue,^{2,*} Emiko Okuda-Ashitaka,¹ Mitsuo Tagaya,³ Masahiko Watanabe,⁴ Megumu Yoshimura² and Seiji Ito¹

¹Department of Medical Chemistry, Kansai Medical University, Moriguchi 570-8506, Japan

²Department of Integrative Physiology, Graduate School of Medical Sciences, Kyushu University, Fukuoka, Japan

³School of Life Science, Tokyo University of Pharmacy and Life Science, Hachioji, Japan

⁴Department of Anatomy, Hokkaido University School of Medicine, Sapporo, Japan

Keywords: Ca²⁺-permeable AMPA receptor, inflammatory pain, *in vivo* patch-clamp, postsynaptic density, proteomics

Abstract

Central sensitization, similar to long-term potentiation in the hippocampus, refers to the increased synaptic efficacy established in somatosensory neurons in the dorsal horn of the spinal cord following tissue injury or nerve damage. In the course of inflammation, many proteins including glutamate receptors are assumed to be dynamically reorganized in the postsynaptic density (PSD) and involved in persistent pain. Mechanical hyperalgesia induced by intraplantar injection of complete Freund's adjuvant (CFA) was inhibited at 4 h, but not at 24 h, by indomethacin, an inhibitor of prostanoid synthesis. To elucidate the nature of the molecule(s) involved in the late phase of inflammatory pain, we analysed the PSD fraction prepared from the lumbar spinal cord of rats before and 24 h after CFA injection by conducting two-dimensional differential gel electrophoresis. *N*-ethylmaleimide-sensitive fusion protein (NSF) was identified as a downregulated protein in the PSD by MALDI-TOF MS and immunoblotting. Concomitant with the decrease in NSF, GluR2 and GluR3 were decreased and GluR1 was conversely increased in the PSD fraction 24 h after CFA injection. *In vivo* patch-clamp recordings of rats 24 h after CFA injection showed that excitatory postsynaptic currents of dorsal horn neurons evoked by pinch stimuli to inflamed skin were inwardly rectified and inhibited by 60% by philanthotoxin-433, a selective inhibitor of the Ca²⁺-permeable α -amino-3-hydroxy-5-methyl-4-isoxazolepropionic acid (AMPA) receptor. These results suggest that peripheral inflammation gives rise to central sensitization in the spinal cord through subunit composition switch of AMPA receptors in the late phase.

Introduction

Non-steroidal anti-inflammatory drugs such as aspirin and indomethacin are widely used for the treatment of inflammation and pain, and they are thought to act via inhibition of prostanoid synthesis (Vane, 1971). The development of a variety of pain models in rodents has promoted our understanding of the mechanisms that contribute to enhanced nociceptive sensitivity in inflammatory pain and neuropathic pain (Ito *et al.*, 2001; Julius & Basbaum, 2001). It has been recently proposed that spinal central sensitization may share common characteristics of neural plasticity with other neural systems, such as in the case of hippocampal long-term potentiation (LTP; Ji *et al.*, 2003).

Glutamate is the main excitatory neurotransmitter at the vast majority of excitatory synapses, acting via ionotropic receptors for α -amino-3-hydroxy-5-methyl-4-isoxazole propionic acid (AMPA) and *N*-methyl-D-aspartate (NMDAR). Each of these receptors comprises a hetero- or homomeric assembly of receptor subunits, GluR1–4 for the former and NR1–3 for the latter (Bredt & Nicoll, 2003; Collingridge *et al.*, 2004). Because NMDARs are voltage- and ligand-gated and show high permeability to Ca²⁺, they have been considered

to play an essential role in activity-dependent synaptic plasticity. In contrast, because the great majority of AMPARs in principal neurons contain GluR2, this renders AMPARs impermeable to Ca²⁺; however, GluR2-lacking Ca²⁺-permeable (CP)-AMPA receptors are expressed in certain restricted neuronal populations and under certain pathological conditions. There is currently much interest as to how these receptors affect the regulation of synaptic transmission. Excitatory synapses in the mammalian CNS are present mostly on dendritic spines, where many proteins, including receptors, downstream signaling enzymes, adaptor molecules and cytoskeletal proteins, are clustered in the postsynaptic density (PSD) and become dynamically reorganized in response to neural activity. This elaborated postsynaptic structure provides a platform for regulation of glutamate receptor function and thus synaptic plasticity. Although many studies show that spinal neural plasticity contributes to persistent pain states, the exact mechanism of the maintenance of pain after longer periods of inflammation remains unknown. To address this problem, we analysed the PSD fraction before and 24 h after inflammation by a proteomic approach using two-dimensional differential gel electrophoresis (2D-DIGE), and identified *N*-ethylmaleimide-sensitive fusion protein (NSF) as a candidate molecule. Using *in vivo* patch-clamp recording in this present study, we demonstrate that CP-AMPA receptors were involved in the late-phase inflammatory pain by undergoing a switch in their subunit composition.

Correspondence: Dr S. Ito, as above.

E-mail: ito@takii.kmu.ac.jp

*T.K. and H.F. contributed equally to this work.

Received 31 January 2008, revised 14 April 2008, accepted 27 April 2008

Materials and methods

Materials

Polyclonal antibodies against mouse PSD-95 (amino acid residues 1–64), mouse GluR1 (841–907), mouse NR1 (22–69), mouse NR2A (1126–1408) and mouse NR2B (1–48) were raised in rabbits (Watanabe *et al.*, 1998; Fukaya & Watanabe, 2000; Shimuta *et al.*, 2001), and 2E5, a monoclonal antibody against recombinant NSF, was prepared in mice as described previously (Tagaya *et al.*, 1993). Commercially available antibodies against GluR2 (Zymed, South San Francisco, CA, USA), GluR3 (Chemicon, Temecula, CA, USA), synaptophysin (BD Bioscience, San Jose, CA, USA) and actin (BD Bioscience) were also used. Complete Freund's adjuvant (CFA) and philanthotoxin-433 (PhTx) were obtained from Sigma (St Louis, MO, USA). All other chemicals were of reagent grade.

Animals

About 250 male 8-week-old Wistar rats were obtained from Shimizu Laboratory Center (Hamamatsu, Japan) and Kyudo (Fukuoka, Japan). Rats were housed under conditions of a 12 h light : dark cycle, a constant temperature of 22 ± 2 °C and $60 \pm 10\%$ humidity. They received food and water *ad libitum*. This study was conducted with the approval of the animal care committees of Kansai Medical University and Kyushu University, and carried out in accordance with the ethical guidelines of the Ethics Committee of the International Association for the Study of Pain and with the guidelines for the Care and Use of Animals in the Field of Physiological Science of the Physiological Society of Japan.

Behavioral study

The inflammatory pain model was made by injecting CFA (0.1 mL, 1 mg/mL mycobacterium in oil) into the dorsal surface of one or both hind paws of male 8-week-old Wistar rats. Inflammatory pain induced by CFA was evaluated by paw withdrawal thresholds to mechanical stimulation by calibrated von Frey filaments (Stoelting, Wood Dale, IL, USA) in an ascending order five times at an interval of a few seconds to the plantar surface of the hind paw from the mesh floor, as described previously (Abe *et al.*, 2005).

Preparation of P2 and PSD fractions

After anesthesia with ether, male 8-week-old rats were killed and the PSD fractions were prepared from lumbar spinal cords at L4–L6 levels before and 24 h after CFA injection, essentially as described by Carlin *et al.* (1980). In the course of preparation of PSD fractions, the pellet obtained by centrifugation of the homogenate at 13 800 *g* for 20 min was used as the P2 fraction. The purity of the PSD fractions was confirmed by immunoblotting with anti-PSD-95 and anti-synaptophysin antibodies.

Immunoblotting

Aliquots (50 µg) of P2 and PSD fractions were subjected to 10% sodium dodecyl sulfate–polyacrylamide gel electrophoresis (SDS–PAGE; 9×7 cm, 1 mm), and proteins were transferred electrophoretically to polyvinylidene difluoride membranes. After blocking with 3% skim milk in a TBS-T buffer containing 0.1% Triton X-100, 150 mM NaCl and 10 mM Tris-HCl (pH 7.5) for 1 h at room temperature, the membrane was incubated overnight at 4 °C with first

antibodies. The membrane was washed with the TBS-T buffer and incubated for 1 h with anti-mouse IgG (1 : 10 000; GE Healthcare UK, Little Chalfont, Buckinghamshire, England, UK), anti-rabbit IgG (1 : 20 000; Biosource, Camarillo, CA, USA) or anti-rat IgG (1 : 20 000; Jackson Immuno Research, West Grove, PA, USA) horseradish peroxidase. The membrane was then washed four times with the TBS-T buffer. The immunoreactivity was detected using Enhanced Chemiluminescence (GE Healthcare). The intensity of immunostaining was quantified by use of ImageJ.

2D-DIGE

PSD fractions (50 µg of each) prepared from lumbar spinal cords at L4–L6 levels before and 24 h after CFA injection were dissolved in 10 mM Tris-HCl (pH 8.5) containing 7 M urea, 2 M thiourea and 4% CHAPS, and labeled with 400 pmol of Cy3 and Cy5, respectively, according to the manufacturer's protocol. The mixed CyDye-labeled samples were used to rehydrate 24-cm IPG strips (pH 3–10NL). The first-dimension isoelectric focusing was performed using the IPGphor system (GE Healthcare UK) for a total of 60 kVh. The strips were equilibrated for 15 min in 50 mM Tris-HCl (pH 8.8) containing 6 M urea, 30% glycerol, 2% SDS and 100 mM dithiothreitol, and then for another 15 min in the same buffer, except that dithiothreitol was replaced with 135 mM iodoacetamide. The equilibrated strips were applied to a 10% isocratic gel for SDS–PAGE overnight at constant current of 2 W/gel.

Cy3- and Cy5-labeled protein images were produced by excitation at 532 and 633 nm, respectively, and emission at 580 ± 15 and 670 ± 15 nm, respectively, using the Typhoon 9410 Imager, and the images were analysed using DeCyder (GE Healthcare UK). After normalization by sample multiplexing of six PSD preparations in three independent experiments by the DeCyder Differential In-gel Analysis software module, the spot volume was used as a measure of protein abundance, and its change in PSD fractions before and 24 h after CFA injection was analysed by using the DeCyder Biological Variation Analysis software module (Alban *et al.*, 2003). Experiments of 2D-DIGE were done in triplicate and reproducible results were obtained.

Mass spectrometry

Silver-stained proteins of interest were excised from the 2D-DIGE gels, destained and in-gel digested as described by Gharahdaghi *et al.* (1999). MALDI-TOF MS was carried out using a Voyager DE-PRO (Applied Biosystems, Foster City, MA, USA) as described previously (Katano *et al.*, 2006). All spectra were obtained in a positive reflector mode using an accelerating voltage of 20 kV. Database searches were carried out using the MASCOT search program (<http://www.matrixscience.com>) and NCBI protein databases. The specified taxonomy was rat or mammal, and the specified initial mass tolerance was 50–70 ppm.

Electrophysiology

In vivo patch-clamp recordings were carried out in inflamed rats 24 h after CFA injection into the hind paw essentially as described previously (Furue *et al.*, 1999). Briefly, under urethane anesthesia, a thoracolumbar laminectomy was performed, and then the animal was placed in a stereotaxic apparatus. The dura mater was removed, and the pia-arachnoid membrane was cut to make a window large enough to allow the patch electrode to enter the spinal cord. The

surface of the exposed area of the spinal cord was irrigated with Krebs solution (in mM: NaCl, 117; KCl, 3.6; CaCl₂, 2.5; MgCl₂, 1.2; NaH₂PO₄, 1.2; glucose, 11; NaHCO₃, 25) equilibrated with 95% O₂/5% CO₂. Drugs were added to the Krebs solution used for perfusion (Furue *et al.*, 2007). The patch pipettes were filled with K-gluconate solution for measurement of resting membrane potentials, and a Cs pipette solution containing 0.1 mM spermine was used for examination of the voltage dependence of synaptic currents. The electrode was advanced into the substantia gelatinosa (SG) of the dorsal horn, and then whole-cell voltage-clamp recording configurations were blindly performed from SG neurons. Membrane capacitance was extracted from the current response to 200-ms voltage steps from -70 to -60 mV, and the membrane capacitance value was calculated by fitting the decay phase of the current transient with a monoexponential function. Pinch stimulation was applied to inflamed or uninflamed skin of the hind limb by pinching the skin with a vice-like device fixed on a stand. The current charges of pinch-evoked excitatory postsynaptic currents (EPSCs) were obtained from the integration of the steady responses for 1–2 s. The transient responses observed at the beginning and end of the pinch stimulation were not included in the analysis. The rectification index (RI) was calculated from pinch-evoked charge responses recorded at +50 mV divided by the responses recorded at -50 mV, as described previously (Tong & MacDermott, 2006).

Statistics

Data were analysed by using the Mann–Whitney *U*-test for comparison between before and 24 h after CFA injection, and were presented as the mean \pm SD for immunoblots and the mean \pm SEM for behaviors. Data for electrophysiology were analysed by paired *t*-test between inflamed and uninflamed skin stimulation, and were presented as the mean \pm SEM. *P* < 0.05 was considered statistically significant.

Results

Difference in molecules involved in inflammatory pain between 4 and 24 h after CFA injection

To study functional molecules involved in inflammatory pain, we first examined the effect of indomethacin, an inhibitor of prostanoid

synthesis, on the paw withdrawal threshold 4 and 24 h after CFA. The paw withdrawal threshold to mechanical stimuli before the CFA injection (8.81 ± 1.0 g in Fig. 1A; 10.0 ± 0.54 g in Fig. 1B) started to decrease at 2 h, and the decrease continued for more than 24 h after the injection (1.53 ± 0.30 g; Fig. 1B). Oral administration of indomethacin (30 mg/kg) 4 h after the CFA injection (Fig. 1A) significantly attenuated the decrease in the mechanical threshold at 6 h (5.48 ± 1.1 g with indomethacin; 2.26 ± 0.79 g with vehicle). The attenuation by indomethacin was 49.6% at 6 h and continued by 8 h (Fig. 1A). The analgesic effect was not observed when indomethacin was administered 24 h after the CFA injection (Fig. 1B). These results suggest that molecules different from prostanoids may be involved in CFA-induced inflammatory pain in the late phase.

Identification of NSF as a protein related to CFA-induced inflammatory pain in the late phase

To elucidate a molecule(s) involved in the late phase of inflammatory pain, we used 2D-DIGE to analyse the PSD fraction before and at 4 h and 24 h after the CFA injection. The purity of the PSD fractions was checked by immunoblotting with antibodies against PSD-95 and synaptophysin, markers of PSD and presynaptic vesicles, respectively. While synaptophysin was detected in P2 fractions, PSD-95 was not detected in P2 fractions but enriched in PSD fractions (Fig. 2A). Thus, the purity of PSD fractions was confirmed and used for the following experiments.

CyDye-labeled protein images were reproducibly produced in three independent PSD fractions prepared from spinal cords before and 24 h after CFA injection (Fig. 2B). After normalization by sample multiplexing in 2D-DIGE, when analysis of variance (ANOVA) was applied to matched spots and the data were filtered to retain spots with ANOVA *P*-values of 0.05 or less, 37 spots were significant. Among them, two spots (arrows a and b in Fig. 2B and C) with high volume and good separation from other spots were significantly decreased to 0.78–0.79 at 24 h after the injection (Fig. 2C), but not at 4 h (data not shown), suggesting that they were unique to late-phase inflammatory pain. Because a protein amount in the PSD fraction prepared from L4–L6 spinal cords of 20 rats was just enough to run an analytical gel, to identify the spots 'a' and 'b', in-gel-digested peptides of the spots in the analytical gel were subjected to MALDI-TOF MS after silver staining. The mass spectrum of the spot 'b' is shown in Fig. 3A. The

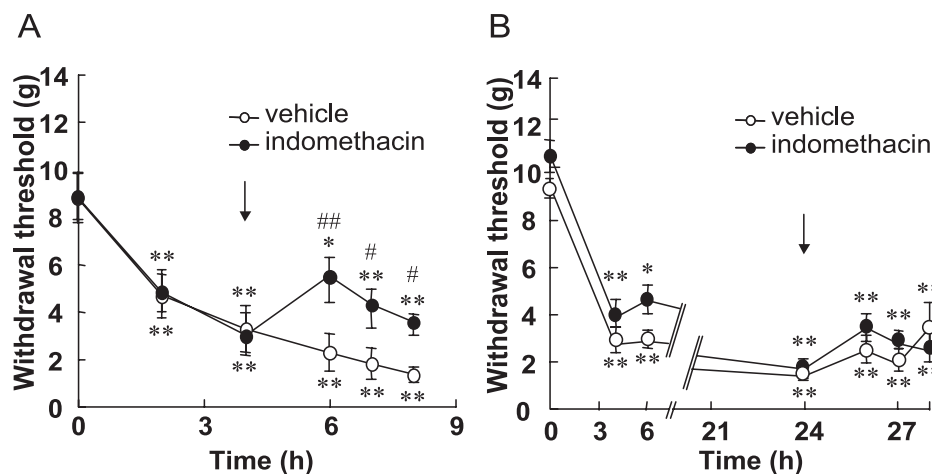


FIG. 1. Different effect of indomethacin on inflammatory pain 4 and 24 h after CFA injection. At 4 h (A) or 24 h (B) after CFA injection (time 0), the effect of indomethacin on inflammatory pain was assessed from 2 to 4 h after a single p.o. administration (arrows) of 30 mg/kg indomethacin in 0.5% methylcellulose (●) or vehicle (○). Data are expressed as the mean \pm SEM (*n* = 6–12). **P* < 0.05, ***P* < 0.01 vs. before CFA injection; #*P* < 0.05, ##*P* < 0.01 vs. vehicle.

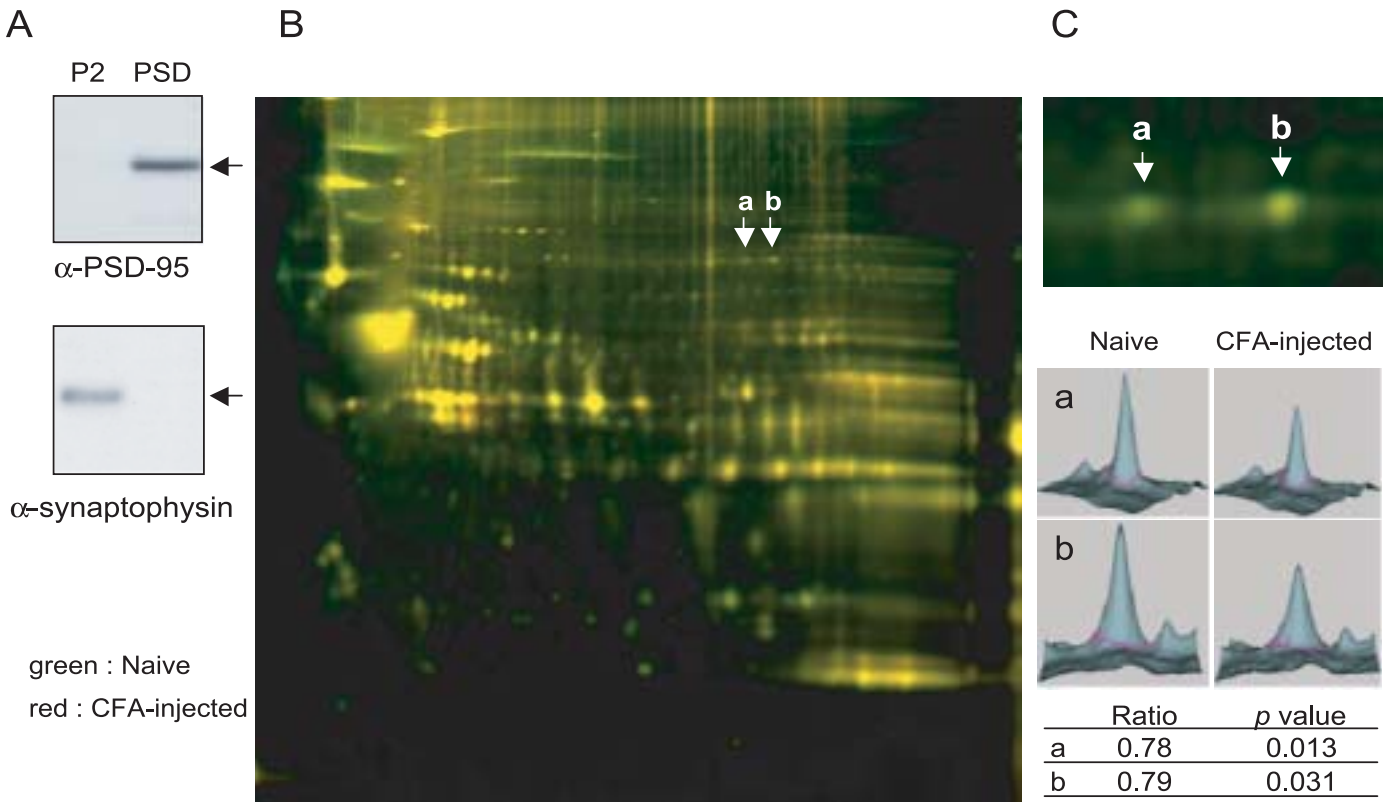


FIG. 2.

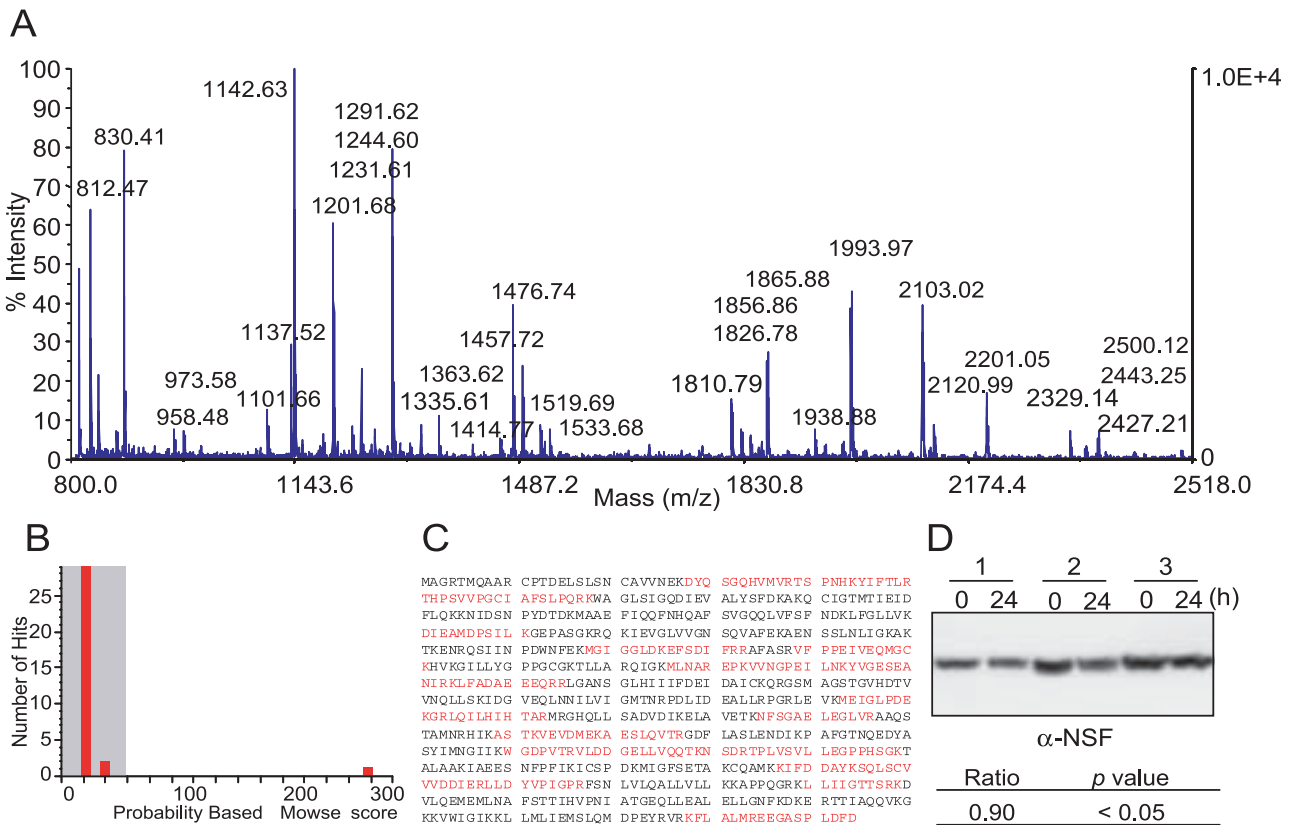


FIG. 3.

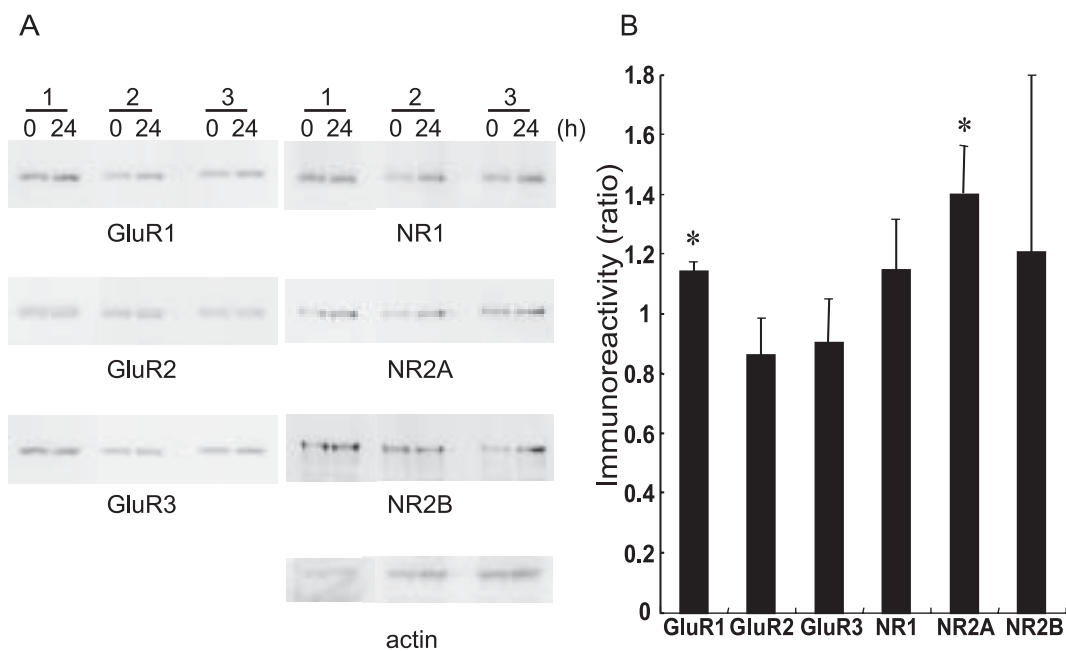


FIG. 4. Decrease in the levels of GluR2 and GluR3, but not GluR1 and NMDAR subunits, in the PSD 24 h after CFA injection. (A) The PSD fractions (50 μ g) prepared from the spinal cord before and 24 h after the CFA injection were applied onto 10% SDS-PAGE gels and immunoblotted with antibodies against GluR1, GluR2, GluR3, NR1, NR2A and NR2B. (B) Alteration of protein levels 24 h after CFA injection. Intensity of the protein bands was quantitatively measured by using ImageJ. Data (mean \pm SD, $n = 3$) are expressed as the ratio of the density after the CFA injection to that before it after normalization by actin. * $P < 0.05$ by the Mann-Whitney U -test.

probability-based MOWSE score was 278 with 33 peptides for NSF (Fig. 3B), and the spot 'b' was thus identified as NSF (Fig. 3C). The spot 'a' in Fig. 2B and C was also identified as NSF (data not shown). The decrease was confirmed by immunoblotting with 2E5, an anti-NSF antibody (Fig. 3D). These results show that NSF is a protein related to inflammatory pain in the late phase.

Decrease in GluR2 or GluR3 subunits of AMPAR 24 h after CFA injection

NSF, an ATPase that is involved in membrane fusion events, is known to bind directly to GluR2 subunits (Bredt & Nicoll, 2003; Collingridge *et al.*, 2004). In order to clarify the nature of the molecule associated with the reduction in the level of NSF, we compared the expression level of AMPAR and NMDAR subunits in the PSD fraction by immunoblotting (Fig. 4). The intensity of immunoreactive bands of GluR2 and GluR3 subunits tended to decrease in the PSD fraction 24 h after the CFA injection, but did not change significantly. Conversely, other AMPAR and NMDAR

subunits examined here increased 24 h after CFA injection, and the intensity of the GluR1 and NR2A subunits significantly increased to 1.14- and 1.40-fold of that before the injection. These results suggest that continued nociceptor inputs induced reorganization of subunits of AMPAR on synaptic membranes in the late phase of inflammation.

Differences in inward rectification of pinch-evoked EPSCs and polyamine toxin-sensitivity between SG neurons that had receptive fields in inflamed and uninfamed skin

We hypothesized that the decreased expression of GluR2 subunits altered the expression level of functional CP-AMPA receptors in the spinal nociceptive pathways in inflamed rats. To test this hypothesis, we recorded EPSCs *in vivo* evoked by cutaneous mechanical noxious stimulation of SG neurons where nociceptive information was monosynaptically transmitted through mostly A δ and C fibers, and examined the sensitivity to a polyamine toxin and the inward rectification as previously used for identification of CP-AMPA receptors in

FIG. 2. Detection of spots downregulated during late-phase inflammation in the postsynaptic density (PSD) fraction. (A) PSD fractions were purified from rat lumbar spinal cords by sucrose density gradient centrifugation. The purity of the fractions was checked by immunoblotting with anti-PSD-95 and synaptophysin antibodies. (B) The PSD fractions (50 μ g of each) before and 24 h after the complete Freund's adjuvant (CFA) injection were labeled with Cy3 and Cy5, respectively, and subjected to 2D-DIGE (24 \times 20 cm). (C) All spots were quantitatively analysed using DeCyder, and significant spots 'a' and 'b' (arrows) in (B) were shown at a higher magnification. The volume of spots 'a' and 'b' in (B) was also shown as 3D-view images. Data ($n = 3$) are expressed as the ratio of the density after the CFA injection to that before it with ANOVA.

FIG. 3. Identification of a protein downregulated during late-phase inflammation as *N*-ethylmaleimide-sensitive fusion protein (NSF). (A) In-gel-digested tryptic fragments of the spot 'b' in Fig. 2B and C were analysed by MALDI-TOF MS. (B) The probability plot in MASCOT search programs for MS in (A) and identified as NSF. (C) Amino acid sequence of rat NSF. The parts of the sequence in red correspond to the peptide fragments obtained by tryptic digestion of the spot 'b' in Fig. 2B and C. (D) The PSD fractions (50 μ g) prepared from the spinal cord before and 24 h after the CFA injection were applied onto 10% SDS-PAGE gels and immunoblotted with anti-NSF monoclonal antibody 2E5. Data (mean, $n = 3$) are expressed as the ratio of the density after the CFA injection to that before it, and statistical significance was examined by the Mann-Whitney U -test.

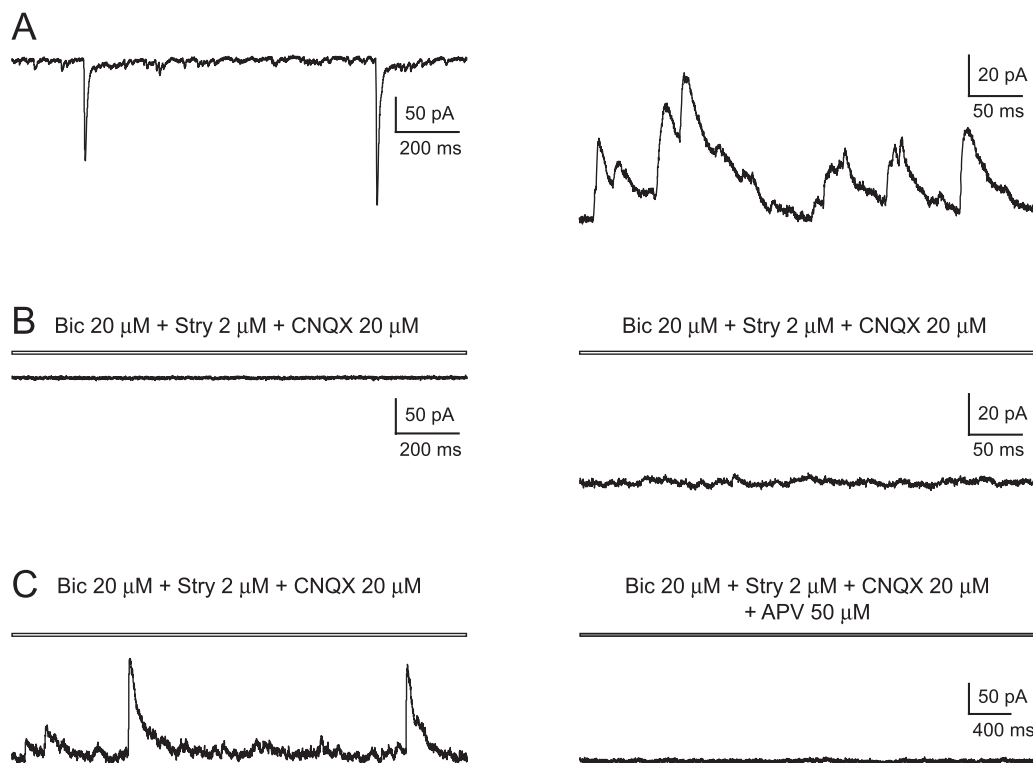


FIG. 5. EPSCs and IPSCs evoked in SG neurons in inflamed rats, and the sensitivity of receptor antagonists. (A) Spontaneous EPSCs (left trace) and IPSCs (right trace) elicited at holding potentials of -70 and 0 mV, respectively. (B and C) Application of 20 μ M bicuculline (Bic), a GABA_A receptor antagonist, 2 μ M strychnine (Stry), a glycine receptor antagonist, and 20 μ M 6-cyano-2,3-dihydroxy-7-nitro-quinoline acid (CNQX), a non-NMDA receptor antagonist, to the surface of the spinal cord completely inhibited spontaneous EPSCs at -70 mV (B, left trace) and IPSCs at 0 mV (B, right trace). In the presence of these antagonists, SG neurons exhibited spontaneous EPSCs with slow kinetics at $+40$ mV (C, left trace). Supplemental addition of 50 μ M D-APV completely suppressed the slow EPSCs. Records in (A), (B) and (C) were obtained from the same neuron.

dorsal horn neurons of slice preparations (Tong & MacDermott, 2006).

In inflamed rats 24 h after the CFA injection, whole-cell recordings were obtained from 38 SG neurons with resting membrane potentials of -59.6 ± 2.1 mV ($n = 11$) and input membrane resistances of 466 ± 51 M Ω ($n = 7$); these values were comparable to those for normal rats (Furue *et al.*, 1999). First, we examined sensitivities of receptor antagonists applied to the surface of the spinal cord to EPSCs and inhibitory postsynaptic currents (IPSCs) evoked in SG neurons. All SG neurons tested exhibited spontaneous EPSCs and IPSCs at holding potentials of -70 and 0 mV, respectively (Fig. 5A). Application of a γ -aminobutyric acid (GABA)_A receptor antagonist, bicuculline (20 μ M), a glycine receptor antagonist, strychnine (2 μ M) and a non-NMDAR antagonist, 6-cyano-2,3-dihydroxy-7-nitro-quinoline acid (CNQX; 20 μ M), completely inhibited spontaneous EPSCs at a holding potential of -70 mV and spontaneous IPSCs at a holding potential of 0 mV (Fig. 5B). At a holding potential of $+40$ mV under the actions of these antagonists, SG neurons exhibited spontaneous EPSCs having slower kinetics than those recorded at -70 mV in the absence of receptor antagonists. The supplemental addition of an NMDA receptor antagonist, D-APV (50 μ M), completely diminished the spontaneous EPSCs with slow kinetics (Fig. 5C), suggesting that the slow EPSCs recorded at positive holding potentials are mediated through NMDAR, and that EPSCs evoked in the presence of bicuculline, strychnine and D-APV are mediated predominantly through non-NMDAR.

Then, we tested whether the pinch-evoked EPSCs in SG neurons that had receptive fields located in the inflamed skin (Fig. 6A)

exhibited inward rectification in the presence of bicuculline (20 μ M), strychnine (2 μ M) and D-APV (50 μ M). In the presence of these receptor antagonists, all SG neurons tested exhibited spontaneous EPSCs at a holding potential of -70 mV. Large amplitudes of EPSCs (> 40 pA) were frequently observed in SG neurons that had receptive fields located in the inflamed skin of the hind paw or lower leg ($n = 12$) compared with the amplitudes of SG neurons that had receptive fields located in the uninflamed skin of the upper leg or thigh ($n = 8$; see spontaneous events in Figs 6B and C, and 7A and B). The spontaneous events were completely inhibited by CNQX (20 μ M, $n = 4$), as previously shown in normal rats (Furue *et al.*, 1999) and GYKI52466 (100 μ M, $n = 3$). Pinch stimulation applied to the skin elicited a barrage of EPSCs with large amplitudes. Whereas the I - V relationship of the pinch-evoked current charges for 1 s in the SG neurons that had receptive fields located in the uninflamed skin ('b' in Fig. 6A) was linear (Fig. 6C and D), that in the SG neurons having receptive fields located in the inflamed skin ('a' in Fig. 6A) was inwardly rectified (Fig. 6B and D). The average RI (0.36 ± 0.09 , $n = 3$) of pinch-evoked EPSCs in the SG neurons received from inflamed skin was lower than that (1.16 ± 0.33 , $n = 3$) from the uninflamed skin (Fig. 6E).

Next, we examined the sensitivity of the pinch-evoked EPSCs to a polyamine toxin in SG neurons. As shown in Fig. 7A, the application of PhTx (20 μ M), a CP-AMPA antagonist, markedly inhibited the pinch-evoked responses in SG neurons that had receptive fields located in the inflamed skin, though EPSCs with large amplitudes were still elicited at lower frequencies than those in the control in the absence of PhTx, thus suggesting that the

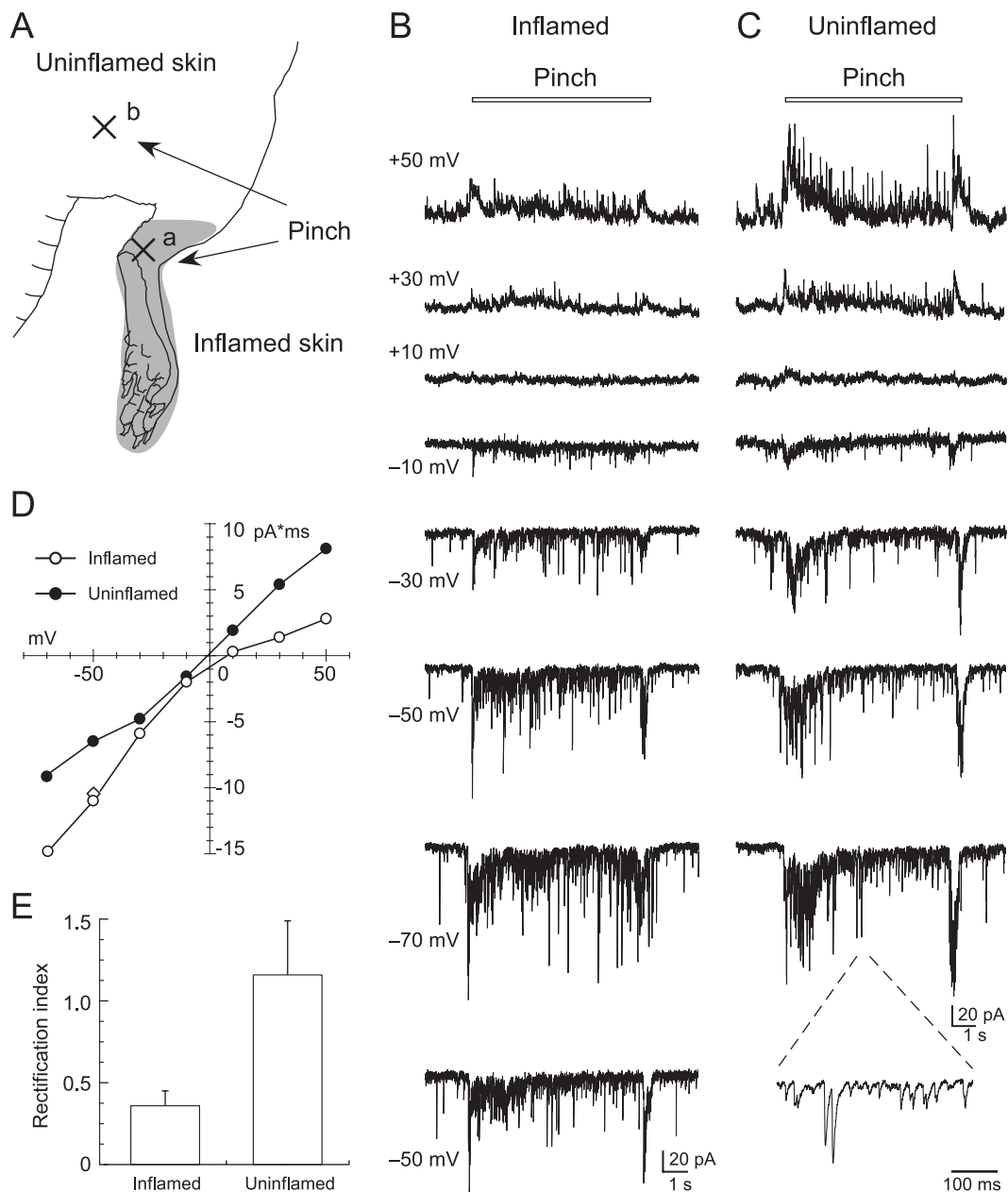


FIG. 6. Inward rectification and I - V relationship of pinch-evoked EPSCs in SG neurons having their receptive field located in the inflamed but not uninflamed skin. (A) Schematic diagram of the inflamed hind limb showing the locations where pinch stimulation was applied. (B and C) The EPSCs recorded at different holding potentials from neurons whose receptive fields were located in inflamed (B) or uninflamed (C) skin are shown. (D) I - V relationships for current charges shown in (B) and (C). Pinch-evoked responses were recorded in stages starting from -70 to $+50$ mV. The response shown at the bottom of (B) was recorded at -50 mV again (shown as the square in the I - V relationships), demonstrating that recording conditions remained unchanged during the examination and that the amplitude of the responses was reproducible. (E) Rectification indexes (RI) calculated from pinch-evoked charge responses at $+50$ and -50 mV (see Materials and methods). Data are expressed as mean \pm SEM ($n = 3$).

excitatory synaptic inputs in single SG neurons were mostly mediated by CP-AMPA. The amplitude of current charges of the pinch-evoked EPSCs for 2 s was significantly decreased in the presence of PhTx (control, 26.4 ± 6.5 pA*ms; in the presence of PhTx, 10.7 ± 3.7 pA*ms; $P < 0.01$, $n = 7$; Fig. 7C). Even at the same spinal level of the same rats, however, SG neurons with receptive fields located in the uninflamed skin were insensitive to PhTx ($n = 5$; Fig. 7B). The current charges of the pinch-evoked EPSCs for 2 s did not change in the presence of PhTx (control, 15.2 ± 2.7 pA*ms; in the presence of PhTx, 16.0 ± 1.7 pA*ms;

$P > 0.05$, $n = 5$; Fig. 7D). No significant difference in the membrane capacitance was found between the PhTx-sensitive and -insensitive SG neurons (PhTx-sensitive, 44.5 ± 7.7 pF, $n = 7$; PhTx-insensitive, 47.5 ± 7.9 pF, $n = 5$; $P > 0.05$).

Discussion

The activity-dependent central sensitization is only initiated by nociceptor sensory input, and is characterized by increases in the

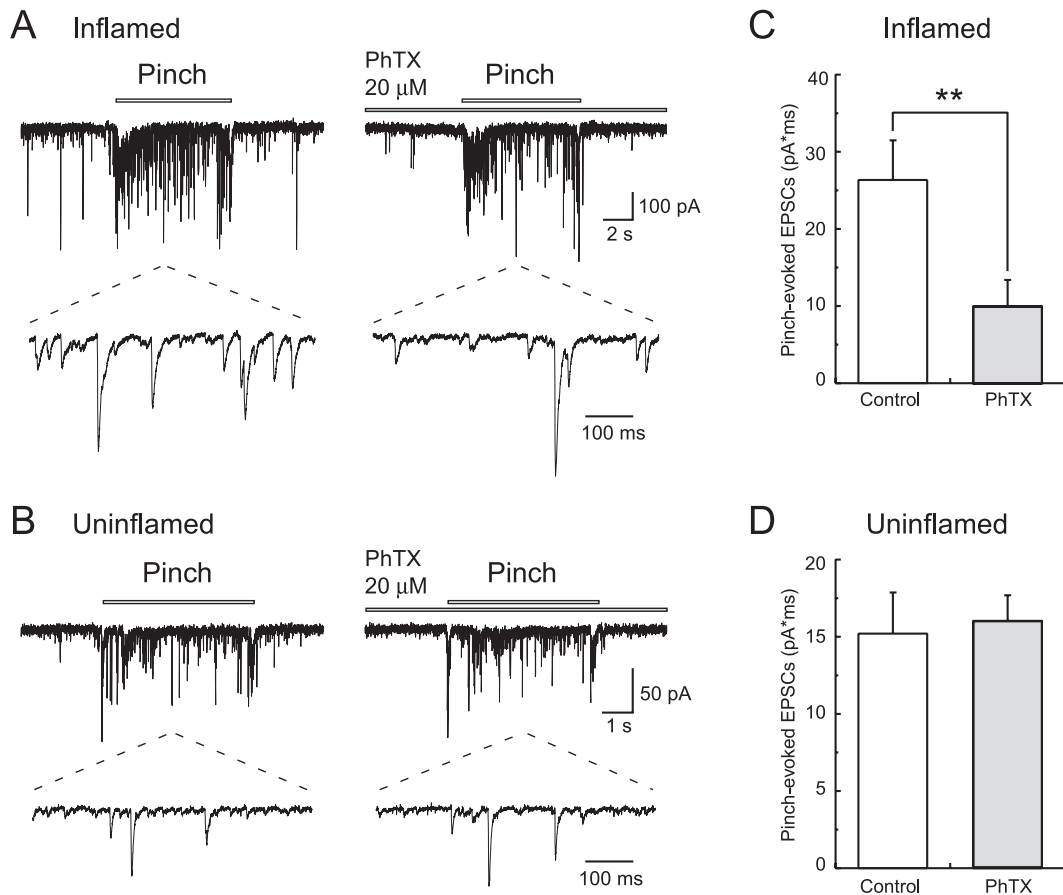


FIG. 7. Philanthotoxin-433 (PhTx) sensitivity of pinch-evoked EPSCs in SG neurons whose receptive fields were located in inflamed or uninfamed skin. (A) Inhibition of EPSCs elicited by pinch stimulation applied to the inflamed skin ('a' in Fig. 6A) by PhTx (20 μ M) applied to the surface of the spinal cord. (B) PhTx-insensitive pinch-evoked EPSCs in the neurons whose receptive field was in the uninfamed skin ('b' in Fig. 6A). (C and D) Effect of PhTx on pinch-evoked EPSCs. Data are expressed as mean \pm SEM ($n = 7$ for inflamed skin; $n = 5$ for uninfamed skin). $**P < 0.01$ vs. control.

responsiveness of dorsal horn neurons leading to the reduction in thresholds and the subsequent pain responses. Similar to hippocampal LTP, post-translational regulation of AMPARs and NMDARs and trafficking of AMPARs following phosphorylation have been suggested to be two major mechanisms underlying synaptic plasticity (Ji *et al.*, 2003). While many groups including ours showed that AMPAR and NMDAR subunits were phosphorylated in inflammatory and neuropathic pain, trafficking of GluR1-containing AMPAR was not shown to contribute to central sensitization in the spinal cord (Ji *et al.*, 2003). This was probably ascribed to the methods employed, i.e. immunohistochemistry or immunoblot and electrophysiology, because both phosphorylation and trafficking of AMPARs are rather rapid and reversible phenomena (Liu & Cull-Candy, 2000; Brecht & Nicoll, 2003). Furthermore, inflammation induced the expression of late-response genes such as prodynorphin, the substance P receptor, NK1 and synaptic scaffold protein Homer 1a, as well as immediate-early genes such as *c-fos* and cyclooxygenase-2 in the spinal cord (Ji *et al.*, 2002; Tappe *et al.*, 2006). Although more than 100 molecules have been implicated as mediators and modulators of synaptic plasticity in spinal sensitization, little is known about the global *in vivo* protein interactions within synapses in pain states. In light of high complexity and cross-talk between AMPARs and NMDARs in the same synapses, we first analysed the PSD fraction by use of proteomic technology and identified NSF as protein related to inflammatory pain in the late phase (Fig. 3). NSF is an ATPase important for general membrane fusion

events and functions to retain the expression of AMPARs containing GluR2 on synaptic membranes by disassembling protein interacting with C-kinase (PICK)–GluR2 complexes (Nishimune *et al.*, 1998; Hanley *et al.*, 2002). Disruption of NSF–GluR2 interaction leads to the functional elimination of AMPAR-containing GluR2 at synapses (Luthi *et al.*, 1999; Noel *et al.*, 1999), and the subsequent GluR2 subunit composition switch induces some forms of LTP and long-term depression (LTD) in the hippocampus and cerebellum. Consistent with this notion, GluR1 was significantly increased in the PSD fraction 24 h after CFA injection, whereas GluR2 and GluR3 were decreased (Fig. 4), suggesting that a composition switch of AMPARs may occur in the process of central sensitization in the spinal cord during inflammation.

GluR1 and GluR2 knockout mice showed alterations in CP-AMPA components in the spinal cord and subsequent nociceptive plasticity in inflammatory pain models (Hartmann *et al.*, 2004). In addition to behavioral studies, CP-AMPA receptors are supposed to be expressed on NK1-positive projection neurons and GABAergic neurons of laminae I–IV of the spinal cord, where primary afferents carrying nociceptive inputs terminate and make synapses with spinal projection neurons in the nociceptive pathway (Engelman *et al.*, 1999; Tong & MacDermott, 2006). Although the distribution of CP-AMPA receptors in the superficial dorsal horn suggests their involvement in the processing of pain transmission, how these receptors are dynamically reorganized in the course of pain states

remains unclear. Different from LTP and LTD in hippocampal and cerebellar slices observed by repetitive electrical stimulation, central sensitization based on pain can be only evaluated by behaviors evoked by cutaneous stimuli. Because trafficking of AMPARs is a reversible process, spinal slices prepared from animal pain models are not always suitable to analyse it by cobalt uptake and electrophysiology. *In vivo* whole-cell recordings from SG in the present study enabled us to analyse functional synaptic responses by cutaneous mechanical stimuli. The mechanical input conveyed to SG neurons by AMPAR through the glutamatergic A δ and C primary afferent fibers and SG neurons receives excitatory inputs from larger receptive fields throughout the hind limb than was previously thought (Furue *et al.*, 1999). So we took advantage of this finding and recorded EPSCs in SG neurons *in vivo* in response to noxious mechanical stimulation of inflamed and uninflamed skin of the same animal. AMPAR channels containing edited GluR2 have a linear *I-V* relationship, and those that lack GluR2 are inwardly rectifying due to a voltage-dependent block by endogenous intracellular polyamines. Whereas the *I-V* relationship of the pinch-evoked responses in the neurons with receptive fields in the uninflamed skin was linear, that from inflamed skin was inwardly rectified, and the RI values of pinch-evoked EPSCs were lower from inflamed skin, 0.36 ± 0.09 , than uninflamed skin, 1.16 ± 0.33 (Fig. 6E). Moreover, in the presence of PhTx, pinch-evoked EPSCs were significantly decreased only for inflamed skin (Fig. 7). Considering the previous observation that a mixture of Ca²⁺-impermeable AMPARs and CP-AMPARs at synapses in laminae I and III/IV showed RI indices between 0.4 and 1.0 in spinal slices (Tong & MacDermott, 2006), synapses in SG neurons (lamina II) receiving afferent inputs from uninflamed skin mostly contained Ca²⁺-impermeable AMPARs, whereas those from inflamed skin of the same animal mainly contained CP-AMPARs. Because enhancement of synaptic activation of GABAergic interneurons is expected to suppress nociceptive processing, it is likely that the switch to CP-AMPARs from Ca²⁺-impermeable AMPARs occurred on excitatory neurons in the SG during inflammation, but the cell types were not identified.

At mature synapses NMDARs are predominantly composed of NR1/NR2A or NR1/NR2A/NR2B assemblies, which associate with scaffolding proteins such as PSD-95, and activity-dependent regulation of NMDAR trafficking and internalization at synaptic sites is thought to be an important way for modulating the efficacy of synaptic transmission (Lau & Zukin, 2007). Coordinated phosphorylation of C1 domain of NR1 by protein kinase C and protein kinase A was shown to mediate the release of NR1/NR2 from the endoplasmic reticulum for subsequent traffic to synapse (Scott *et al.*, 2003). PSD-95 binds to the C-terminal binding motif of NR2 and inhibited NR2B-mediated internalization (Roche *et al.*, 2001). Conversely, targeted disruption of PSD-93 reduced surface expression of NR2A and NR2B and NMDAR-mediated EPSCs in spinal dorsal horns without affecting synaptic AMPAR expression and its synaptic function (Tao *et al.*, 2003). Interestingly, whereas PSD-93 knockout mice displayed intact nociceptive responses, they attenuated the development of inflammatory pain after CFA injection. Consistent with this, NR1, NR2A and NR2B tended to increase in the PSD fraction 24 h after CFA injection (Fig. 4), suggesting that the change of NMDAR expression on synaptic membranes influences NMDAR-mediated synaptic function and associated pain signaling. Although synaptic expression of AMPAR and NMDAR is independently regulated by distinct mechanisms (Lau & Zukin, 2007), the switch from GluR2-containing AMPARs to CP-AMPARs and the increase in NMDAR in the PSD might

additively or synergistically direct to central sensitization mediated by Ca²⁺-signaling in the spinal cord, leading to the maintenance of inflammatory pain in the late phase.

It was previously suggested that one of the differences between spinal central sensitization and LTP in the hippocampus is the involvement, in the former, of cyclooxygenase-2, a rate-limiting enzyme of prostanoid synthesis (Ji *et al.*, 2003). However, the present study did not show the involvement of cyclooxygenase (Fig. 1) but instead showed the switch of AMPAR subunit composition in the SG during the late phase of inflammatory pain (Figs 6 and 7). It is known that animals become more refractory to analgesics after longer periods of inflammation. The present study may explain this phenomenon.

Acknowledgements

This work was supported in part by grants from the programs Grants-in-Aids for COE Research and Scientific Research on Priority Areas from the Ministry of Education, Culture, Sports, Science and Technology of Japan, and Grants-in-Aid for Scientific Research (S) and (C) from Japan Society for the Promotion of Science and Japan Foundation of Applied Enzymology.

Abbreviations

2D-DIGE, two-dimensional differential gel electrophoresis; AMPAR, α -amino-3-hydroxy-5-methyl-4-isoxazolepropionic acid receptor; CFA, complete Freund's adjuvant; CNQX, 6-cyano-2,3-dihydroxy-7-nitroquinoxaline acid; CP, Ca²⁺-permeable; EPSC, excitatory postsynaptic current; GABA, γ -aminobutyric acid; IPSC, inhibitory postsynaptic current; LTD, long-term depression; LTP, long-term potentiation; NMDAR, *N*-methyl-D-aspartate receptor; NSF, *N*-ethylmaleimide-sensitive fusion protein; PhTx, philanthotoxin-433; PSD, postsynaptic density; RI, rectification index; SG, substantia gelatinosa; SDS-PAGE, sodium dodecyl sulfate-polyacrylamide gel electrophoresis.

References

- Abe, T., Matsumura, S., Katano, T., Mabuchi, T., Takagi, K., Xu, L., Yamamoto, A., Hattori, K., Yagi, T., Watanabe, M., Nakazawa, T., Yamamoto, T., Mishina, M., Nakai, Y. & Ito, S. (2005) Fyn kinase-mediated phosphorylation of NMDA receptor NR2B subunit at Tyr1472 is essential for maintenance of neuropathic pain. *Eur. J. Neurosci.*, **22**, 1445–1454.
- Alban, A., David, S.O., Bjorksten, L., Andersson, C., Sloge, E., Lewis, S. & Currie, I. (2003) A novel experimental design for comparative two-dimensional gel analysis: two-dimensional difference gel electrophoresis incorporating a pooled internal standard. *Proteomics*, **3**, 36–44.
- Bredt, D.S. & Nicoll, R.A. (2003) AMPA receptor trafficking at excitatory synapses. *Neuron*, **40**, 361–379.
- Carlin, R.K., Grab, D.J., Cohen, R.S. & Siekevitz, P. (1980) Isolation and characterization of postsynaptic densities from various brain regions: enrichment of different types of postsynaptic densities. *J. Cell Biol.*, **86**, 831–843.
- Collingridge, G.L., Isaac, J.T.R. & Wang, Y.T. (2004) Receptor trafficking and synaptic plasticity. *Nat. Rev. Neurosci.*, **5**, 952–962.
- Engelman, H.S., Allen, T.B. & MacDermott, A.B. (1999) The distribution of neurons expressing calcium-permeable AMPA receptors in the superficial laminae of the spinal cord dorsal horn. *J. Neurosci.*, **19**, 2081–2089.
- Fukaya, M. & Watanabe, M. (2000) Improved immunohistochemical detection of postsynaptically located PSD-95/SAP90 protein family by protease section pretreatment: a study in the adult mouse brain. *J. Comp. Neurol.*, **426**, 572–586.
- Furue, H., Narikawa, K., Kumamoto, E. & Yoshimura, M. (1999) Responsiveness of rat substantia gelatinosa neurones to mechanical but not thermal stimuli revealed by *in vivo* patch-clamp recording. *J. Physiol.*, **521**, 529–535.
- Furue, H., Katafuchi, T. & Yoshimura, M. (2007) *In vivo* patch-clamp technique. In Walz, W. (Ed), *Patch-Clamp Analysis: Advanced Techniques*, 2nd Edn. Humana Press Inc., Totowa, pp. 229–251.
- Gharahdaghi, F., Weinberg, C.R., Meagher, D.A., Imai, B.S. & Mische, S.M. (1999) Mass spectrometric identification of proteins from silver-stained

- polyacrylamide gel: a method for the removal of silver ions to enhance sensitivity. *Electrophoresis*, **20**, 601–605.
- Hanley, J.G., Khatri, L., Hanson, P.I. & Ziff, E.B. (2002) NSF ATPase and α -/ β -SNAPs disassemble the AMPA receptor-PICK1 complex. *Neuron*, **34**, 53–67.
- Hartmann, B., Ahmadi, S., Heppenstall, P.A., Lewin, G.R., Schott, C., Borchardt, T., Seeburg, P.H., Zeilhofer, H.U., Sprengel, R. & Kuner, R. (2004) The AMPA receptor subunits GluR-A and GluR-B reciprocally modulate spinal synaptic plasticity and inflammatory pain. *Neuron*, **44**, 637–650.
- Ito, S., Okuda-Ashitaka, E. & Minami, T. (2001) Central and peripheral roles of prostaglandins in pain and their interactions with novel neuropeptides nociceptin and nocistatin. *Neurosci. Res.*, **41**, 299–332.
- Ji, R.R., Befort, K., Brenner, G.J. & Woolf, C.J. (2002) ERK MAP kinase activation in superficial spinal cord neurons induces prodynorphin and NK-1 upregulation and contributes to persistent inflammatory pain hypersensitivity. *J. Neurosci.*, **22**, 478–485.
- Ji, R.R., Kohn, T., Moore, K.A. & Woolf, C.J. (2003) Central sensitization and LTP: do pain and memory share similar mechanisms? *Trends Neurosci.*, **26**, 696–705.
- Julius, D. & Basbaum, A.I. (2001) Molecular mechanisms of nociception. *Nature*, **413**, 203–210.
- Katano, T., Mabuchi, T., Okuda-Ashitaka, E., Inagaki, N., Kinumi, T. & Ito, S. (2006) Proteomic identification of a novel isoform of collapsin response mediator protein-2 in spinal nerves peripheral to dorsal root ganglia. *Proteomics*, **6**, 6085–6094.
- Lau, C.G. & Zukin, R.S. (2007) NMDA receptor trafficking in synaptic plasticity and neuropsychiatric disorders. *Nat. Rev. Neurosci.*, **8**, 413–426.
- Liu, S.Q. & Cull-Candy, S.G. (2000) Synaptic activity at calcium-permeable AMPA receptors induces a switch in receptor subtype. *Nature*, **405**, 454–458.
- Luthi, A., Chittajallu, R., Duprat, F., Palmer, M.J., Benke, T.A., Kidd, F.L., Henley, J.M., Isaac, J.T.R. & Collingridge, G.L. (1999) Hippocampal LTD expression involves a pool of AMPARs regulated by the NSF-GluR2 interaction. *Neuron*, **24**, 389–399.
- Nishimune, A., Isaac, J.T.R., Molnar, E., Noel, J., Nash, S.R., II, Tagaya, M., Collingridge, G.L., Nakanishi, S. & Henley, J.M. (1998) NSF binding to GluR2 regulates synaptic transmission. *Neuron*, **21**, 87–97.
- Noel, J., Ralph, G.S., Pickard, L., Williams, J., Molnar, E., Uney, J.B., Collingridge, G.L. & Henley, J.M. (1999) Surface expression of AMPA receptors in hippocampal neuron is regulated by an NSF-dependent mechanism. *Neuron*, **23**, 365–376.
- Roche, K.W., Standley, S., McCallum, J., Dune, Ly. C., Ehlers, M.D. & Wenthold, R.J. (2001) Molecular determinants of NMDA receptor internalization. *Nat. Neurosci.*, **4**, 794–802.
- Scott, D.B., Blanpied, T.A. & Ehlers, M.D. (2003) Coordinated PKA and PKC phosphorylation suppresses RXR-mediated ER retention and regulates the surface delivery of NMDA receptors. *Neuropharmacology*, **45**, 755–767.
- Shimuta, M., Yoshikawa, M., Fukaya, M., Watanabe, M., Takeshima, H. & Manabe, T. (2001) Postsynaptic modulation of AMPA receptor-mediated synaptic responses and LTP by the type 3 ryanodine receptor. *Mol. Cell. Neurosci.*, **17**, 921–930.
- Tagaya, M., Wilson, D.W., Brunner, M., Arango, N. & Rothman, J.E. (1993) Domain structure of an *N*-ethylmaleimide-sensitive fusion protein involved in vesicular transport. *J. Biol. Chem.*, **266**, 2662–2666.
- Tao, Y.X., Rumbaugh, G., Wang, G.D., Petralia, R.S., Zhao, C., Kauer, F.W., Tao, F., Zhuo, M., Wenthold, R.J., Raja, S.N., Hagan, R.L., Brecht, D.S. & Johns, R.A. (2003) Impaired NMDA receptor-mediated postsynaptic function and blunted NMDA receptor-dependent persistent pain in mice lacking postsynaptic density-93 protein. *J. Neurosci.*, **23**, 6703–6712.
- Tappe, A., Klugmann, M., Luo, C., Hirlinger, D., Agarwal, N., Benrath, J., Ehrenguber, M.U., Doring, M.J. & Kuner, R. (2006) Synaptic scaffolding protein Homer1a protects against chronic inflammatory pain. *Nat. Med.*, **12**, 677–681.
- Tong, C.K. & MacDermott, A.B. (2006) Both Ca^{2+} -permeable and -impermeable AMPA receptors contribute to primary synaptic drive onto rat dorsal horn neurons. *J. Physiol.*, **575**, 133–144.
- Vane, J.R. (1971) Inhibition of prostaglandin synthesis as a mechanism of action for aspirin-like drugs. *Nat. New Biol.*, **231**, 232–235.
- Watanabe, M., Fukayama, M., Sakimuram, K., Manabem, T., Mishinam, M. & Inoue, Y. (1998) Selective scarcity of NMDA receptor channel subunits in the stratum lucidum (mossy fibre-recipient layer) of the mouse hippocampal CA3 subfield. *Eur. J. Neurosci.*, **10**, 478–487.

DIFFERENT ROLES OF NITRIC OXIDE SYNTHASE-1 AND -2 BETWEEN HERPETIC AND POSTHERPETIC ALLODYNIA IN MICE

A. SASAKI,^a T. MABUCHI,^b K. SERIZAWA,^a
I. TAKASAKI,^c T. ANDOH,^a K. SHIRAKI,^d S. ITO^b
AND Y. KURAIISHI^{a,*}

^aDepartment of Applied Pharmacology, Graduate School of Medicine and Pharmaceutical Sciences, University of Toyama, 2630 Sugitani, Toyama 930-0194, Japan

^bDepartment of Medical Chemistry, Kansai Medical University, 10-15 Fumizono, Moriguchi 570-8506, Japan

^cDivision of Molecular Genetics Research, Life Science Research Center, University of Toyama, 2630 Sugitani, Toyama 930-0194, Japan

^dDepartment of Virology, Graduate School of Medicine and Pharmaceutical Sciences, University of Toyama, 2630 Sugitani, Toyama 930-0194, Japan

^e21st Century COE Program, University of Toyama, 2630 Sugitani, Toyama 930-0194, Japan

Abstract—We investigated using the mice role of nitric oxide synthase (NOS) in the spinal dorsal horn in herpetic and postherpetic pain, especially allodynia, which was induced by transdermal inoculation of the hind paw with herpes simplex virus type-1 (HSV-1). The virus inoculation induced NOS2 expression in the lumbar dorsal horn of mice with herpetic allodynia, but not postherpetic allodynia. There were no substantial alternations in the expression level of NOS1 at the herpetic and postherpetic stages. Herpetic allodynia was significantly inhibited by i.p. administration of the selective NOS2 inhibitor S-methylisothiourea, but not the selective NOS1 inhibitor 7-nitroindazole. NOS2 expression was observed around HSV-1 antigen-immunoreactive cells. On the other hand, postherpetic allodynia was significantly inhibited by i.p. administration of 7-nitroindazole, but not S-methylisothiourea. The activity of reduced nicotinamide adenine dinucleotide phosphate diaphorase, an index of NOS1 activity, significantly increased in the laminae I and II of the lumbar dorsal horn of mice with postherpetic allodynia, but not mice without postherpetic allodynia. The expression level of NOS1 mRNA in the dorsal root ganglia was similar between mice with and without postherpetic allodynia. The results suggest that herpetic and postherpetic allodynia is mediated by nitric oxide in the dorsal horn and that NOS2 and NOS1 are responsible for herpetic and postherpetic allodynia, respectively. It may be worth testing the effects of NOS2 and NOS1 inhibitors on herpetic pain and postherpetic neuralgia in human subjects, respectively.
© 2007 IBRO. Published by Elsevier Ltd. All rights reserved.

*Correspondence to: Y. Kuraishi, Department of Applied Pharmacology, Graduate School of Medicine and Pharmaceutical Sciences, University of Toyama, 2630 Sugitani, Toyama 930-0194, Japan. Tel: +81-76-434-7510; fax: +81-76-434-5045.

E-mail address: kuraisiy@pha.u-toyama.ac.jp (Y. Kuraishi).

Abbreviations: GAPDH, glyceraldehyde-3-phosphate dehydrogenase; HSV-1, herpes simplex virus type-1; L, lumbar; NADPH, nicotinamide adenine dinucleotide phosphate; NO, nitric oxide; NOS, nitric oxide synthase; PBS, phosphate-buffered saline; qRT-PCR, quantitative reverse transcription-polymerase chain reaction; S, sacral; SMT, S-methylisothiourea sulfate; TBS-T, Tris-buffered saline containing Tween; 7-NI, 7-nitroindazole.

0306-4522/07/\$30.00+0.00 © 2007 IBRO. Published by Elsevier Ltd. All rights reserved.

doi:10.1016/j.neuroscience.2007.09.067

Key words: herpes zoster, postherpetic neuralgia, nitric oxide synthase isoenzymes, dorsal horn, primary sensory nerve.

Herpes zoster characterized by clustered vesicles and severe pain is caused by the reactivation of human herpesvirus 3, varicella-zoster virus, in the sensory ganglion in human subjects (Loeser, 1986). Patients with herpes zoster complain of severe spontaneous pain and allodynia, pain due to a non-noxious stimulus. Early treatment with antiherpetic agents, such as acyclovir and vidarabine, shortens the duration of skin lesions and complications related to herpes zoster (Gnann, 1994). However, these medicines do not promptly relieve acute herpetic pain (Lancaster et al., 1995). In addition, although nonsteroidal anti-inflammatory drugs such as diclofenac, antidepressants such as amitriptyline and sympathetic nerve block are used for the management of herpetic pain, these treatments do not always relieve severe pain (Loeser, 1986; Dworkin and Portenoy, 1996). In some herpes zoster patients, pain persists long after healing of the skin lesions, which is postherpetic neuralgia (Loeser, 1986). Patients with postherpetic neuralgia report various types of pain, including a continuous burning or aching pain, a periodic piecing pain, and tactile allodynia (Loeser, 1986). Once established, postherpetic neuralgia is particularly difficult to treat and is often resistant to conventional analgesics (Argoff et al., 2004). The mechanisms of the induction and maintenance of herpetic pain and postherpetic neuralgia are still unclear.

We previously established mouse models of herpetic pain and postherpetic pain using human herpesvirus 1 (herpes simplex virus type-1, HSV-1) (Takasaki et al., 2000, 2002). When mice are given transdermal HSV-1 inoculation on the hind paw, they show herpes zoster-like skin lesions throughout the inoculated dermatome and pain-related behaviors (Takasaki et al., 2000). Pain-associated behaviors (herpetic pain) and vesicles become apparent 5 days after inoculation and skin lesions heal by day 15 after inoculation (Takasaki et al., 2000, 2002). In some mice, pain-associated behaviors subside by day 20 after inoculation and in the rest pain-associated behaviors (postherpetic pain) last long after the skin lesions completely heal (Takasaki et al., 2002).

Nitric oxide (NO) is produced mainly by nitric oxide synthase-1 (NOS1, neuronal NOS) in normal nervous system (Downen et al., 1999; Millan, 1999), but viral invasion induces NOS2 (inducible NOS) expression (Fujii et al., 1999; Christian et al., 1996; Dugas et al., 2001). Induction of NOS2 expression produces beneficial antiviral effects (Reiss and Komatsu, 1998). In addition, NO plays impor-

tant and complex roles in nociceptive modulation. There is considerable evidence that NO is involved in the generating of spinal cord hyperexcitability and hyperalgesia in some animal models of pain (Salter et al., 1996; Yoon et al., 1998; Osborne andCoderre, 1999). However, the involvement and role of NO in herpetic and postherpetic pain is not clear. In the present study, we examined the roles of NO and NOS isoenzymes in the spinal dorsal horn in herpetic and postherpetic pain, especially allodynia in mice.

EXPERIMENTAL PROCEDURES

Animals

Female C57BL/6j mice (Japan SLC, Shizuoka, Japan) were used; they were 6 weeks old at the start of experiments. Housing (six per cage) and behavioral experiments were done under controlled temperature (22 ± 1 °C), humidity ($55 \pm 10\%$) and lighting (lighted from 7:00 AM to 7:00 PM and during the behavioral test). Food and water were freely available. Experiments were conducted with the approval of the Animal Care Committee at University of Toyama. Behavioral pain test was done according to the guidelines for investigations of experimental pain in animals published by the International Association for the Study of Pain (Zimmermann, 1983). All efforts were made to minimize the number of animals used and their suffering.

HSV-1 inoculation

Mice were inoculated with HSV-1 as described previously (Takasaki et al., 2000). Briefly, HSV-1 (7401H strain; 1×10^6 plaque-forming units in $10 \mu\text{l}$) was inoculated on the shin skin of the right hind paw after scarification with 27-gauge needles. The contralateral hind paw was without inoculation. At the development stage of skin lesions (until day 8 after inoculation), they were scored as follows: 0=no lesions; 2=one or two vesicles on the back; 4=many vesicles on the back, the surrounding inoculated area, or both; 6=mild herpes zoster-like lesions; 8=apparent zoster-like lesions, paw inflammation, or both; 10=severe zoster-like lesions. At the recovery stage of skin lesions (from day 10 after inoculation), they were scored as follows: 10=severe herpes zoster-like lesions; 5=the presence of scabs flaking off from cutaneous lesions; 0=complete recovery of the lesions (Takasaki et al., 2002).

Assessment of allodynia

Tactile allodynia of the hind paw was assessed as described (Takasaki et al., 2000). After at least 30-min acclimation period, von Frey filament with a bending force of 1.6 Nm (0.16 g) was pressed perpendicularly against the plantar skin and held for 1–3 s with it slightly buckled. The responses to the stimulus were ranked as follows: 0, no response; 1, lifting of the hind paw; 2, flinching or licking of the hind paw. The stimulation of the same intensity was applied six times to each hind paw at intervals of several seconds and the average served as pain-related score. Since most of normal mice tested do not respond to von Frey filament of 1.6 Nm strength, mice that show 0.5 or higher pain-related scores were considered to have allodynia (Kuraishi et al., 2004).

Agents

The selective NOS2 inhibitor S-methylisothiourea sulfate (SMT) (Szabo et al., 1994) and the selective NOS1 inhibitor 7-nitroindazole (7-NI) (Moore et al., 1993; Murakami et al., 2002) were purchased from Sigma Chemical Co. (St. Louis, MO, USA). SMT

was dissolved in physiological saline. 7-NI was dissolved in a mixture of 10% dimethyl sulfoxide and 30% propylene glycol in distilled water. Both drugs were administered intraperitoneally in a volume of 0.1 ml/10 g body weight. The effects of the drugs on herpetic and postherpetic allodynia were tested on day 6 and days 35–40, respectively, after HSV-1 inoculation.

Immunohistochemistry

Under deep anesthesia with sodium pentobarbital (70 mg/kg, i.p.), the mice were perfused transcardially with phosphate-buffered saline (PBS, pH 7.4) and subsequently with 4% paraformaldehyde in PBS. The lumbar enlargement was removed and post-fixed in the same fixative at 4 °C for 4 h. The tissues were then transferred to 30% sucrose in PBS at 4 °C overnight for cryoprotection. They were cut on a freezing microtome (Leica CM 3050S IV, Nussloch, Germany) at a 40- μm thickness. After being preincubated in blocking solution (1.5% fetal bovine serum and 0.2% Triton X-100 in PBS) for 30 min at room temperature, sections were incubated with a rabbit anti-NOS2 antibody (1:200; Santa Cruz Biotechnology, Inc., Santa Cruz, CA, USA) at 4 °C for 3 days. Subsequently the sections were incubated for 2 h at room temperature with either of the following reagents: 1) biotinylated anti-rabbit IgG antibody (1:200; DAKO Japan Co. Ltd., Kyoto, Japan) and avidin-Cy3 or FITC (1:500; Vector Laboratories, Inc., Burlingame, CA); or 2) Cy3-conjugated anti-rabbit IgG antibody (1:200; DAKO Japan Co. Ltd.).

For double immunostaining, sections were reacted with the anti-NOS2 antibody as mentioned above. Sections were then further reacted with FITC-conjugated polyclonal rabbit anti-HSV-1 antibody (1:100; DAKO Japan Co. Ltd.) at 4 °C overnight. Fluorescence signals were observed using Bio-Rad Radiance 2000 confocal system (Bio-Rad Microscopy Division, Cambridge, MA, USA); sequential confocal images were collected at 2- μm steps and were used to construct the fluorescence image of the whole specimens.

Western blot analysis

The expression of NOS1 and NOS2 protein in the dorsal horn of lumbar enlargement was analyzed by Western blot. Tissues were homogenized with 100 μl of lysis buffer (137 mM NaCl, 20 mM Tris-HCl (pH 7.5), 1% Nonidet P40, 1 mM phenylmethyl sulfonyl fluoride, 10 $\mu\text{g}/\text{ml}$ aprotinin, 1 $\mu\text{g}/\text{ml}$ leupeptin, 10% glycerol) and centrifuged at 5000 r.p.m. for 15 min at 4 °C. The protein extracts (50 μg) were separated by 7.5% sodium dodecylsulfate–polyacrylamide gel electrophoresis and then transferred to a polyvinylidene difluoride membrane. After blocking with 5% skim milk solution for 1 h, the membrane was reacted with a rabbit anti-NOS1 antibody (1:1000; Santa Cruz Biotechnology, Inc.), a rabbit anti-NOS2 antibody (1:500; Santa Cruz Biotechnology, Inc.) or a mouse anti- β -actin monoclonal antibody (1:5000; Sigma Chemical Co.) at 4 °C overnight. After washing with Tris-buffered saline containing Tween (TBS-T; 100 mM NaCl, 10 mM Tris-HCl (pH 7.5), and 0.1% Tween 20), the membrane was reacted with horseradish peroxidase–conjugated anti-rabbit IgG antibody for NOS2 or anti-mouse IgG antibody for β -actin at a dilution of 1:5000 for 2 h at room temperature. After washing with TBS-T, the membrane was reacted with chemiluminescence reagents (Amersham Bioscience, Piscataway, NJ, USA) and signals were detected using X-ray film. The density of the band was analyzed using NIH Image program and values were normalized to β -actin.

Zymohistochemistry

The activity of reduced nicotinamide adenine dinucleotide phosphate (NADPH) diaphorase is a reliable index of NOS1 activity (Laing et al., 1994) and the distribution of NADPH diaphorase serves as an index of the distribution of NOS1 activity (Mabuchi et

al., 2003). The animals were anesthetized with sodium pentobarbital (50 mg/kg, i.p.) and transcardially perfused with 50 ml of physiological saline followed by a fixative containing 4% paraformaldehyde in 0.12 M sodium phosphate (pH 7.4). Following dissection, spinal cords were postfixed overnight in the same fixative at 4 °C and then kept in 0.1 M sodium phosphate buffer (pH 7.4) containing 30% (w/v) sucrose for 1 day. Transverse L5 spinal cord sections (40 μ m thickness) were cut on a cryostat. The incubation was carried out on free-floating sections for 2 h at 37 °C in a reaction mixture containing 0.5 mg/ml β -NADPH, 0.2 mg/ml nitroblue tetrazolium and 0.25% Triton X-100 in 0.1 M PBS.

Sections of a set of naive mice and mice with and without postherpetic allodynia 40 days after inoculation were simultaneously processed for zymohistochemistry and digital images were captured under same conditions by using a charge-coupled device camera mounted on an optic microscope (E-1000, Nikon, Tokyo, Japan). The intensity of NADPH diaphorase staining in the superficial dorsal horn (laminae I and II) was quantified with NIH Image; an area of laminae I and II was specified and staining intensity in the area was determined with the software. The number of NADPH diaphorase-positive neurons in the laminae I and II was counted under a microscope.

Quantitative reverse transcription–polymerase chain reaction analysis (qRT-PCR)

qRT-PCR was employed to measure the level of NOS1 mRNA in the dorsal root ganglia. After decapitation under diethyl ether anesthesia, the lumbar (L) and sacral (S) dorsal root ganglia at the L2–S1 levels were rapidly removed. L2–L4 and L5–S1 dorsal root ganglia were separately pooled in each animal to get mRNA adequate for reliable qRT-PCR. Total RNA was isolated from the tissues with GenElute™ mammalian total RNA kit (Sigma Chemical Co.) according to the manufacturer's protocol. The first strand cDNA was synthesized from total RNA using oligo (dT)16 primer and ReverScript® III (Wako Pure Chemical Industries, Ltd., Osaka, Japan). qRT-PCR analysis was performed using Mx3000P™ real-time PCR system (Stratagene Japan K.K., Tokyo, Japan) using SYBR® Premix Ex Taq™ reagent (TaKaRa, Kyoto, Japan). The cDNA was amplified with the following primers: 5'-GAATACCAGCCTGATCCATGGAA-3' (sense) and 5'-TCCTCCAGGAGGGTGTCCACCGCATG-3' (antisense) for NOS1, 5'-CAAAGGTCATCCATGACAAC-3' (sense) and 5'-TTACTCCTTGGAGGCCATGT-3' (antisense) for glyceraldehyde-3-phosphate dehydrogenase (GAPDH). PCR was performed with 40 cycles (denaturation at 95 °C for 30 s, primer annealing at 52 °C for 30 s and elongation at 72 °C for 50 s). NOS1 mRNA expression levels were normalized to GAPDH mRNA expression in each sample.

Data analysis

The means of data are presented together with S.E.M. Data on the time course of anti-allodynic effects were analyzed with the Friedman repeated-measures analysis of variance on ranks followed by post hoc Dunnett's test. Statistical differences between two groups were analyzed with Student's *t*-test or Mann-Whitney rank sum test, and among three groups were with Kruskal-Wallis one-way analysis of variance on ranks or one-way analysis of variance with post hoc Dunnett's test. A value of $P < 0.05$ was considered significant.

RESULTS

Development of herpetic and postherpetic allodynia

HSV-1 inoculation on the hind paw produced herpes zoster-like skin lesions and induced allodynia in all mice examined. Vesicular lesion erupted on day 5 after inoculation,

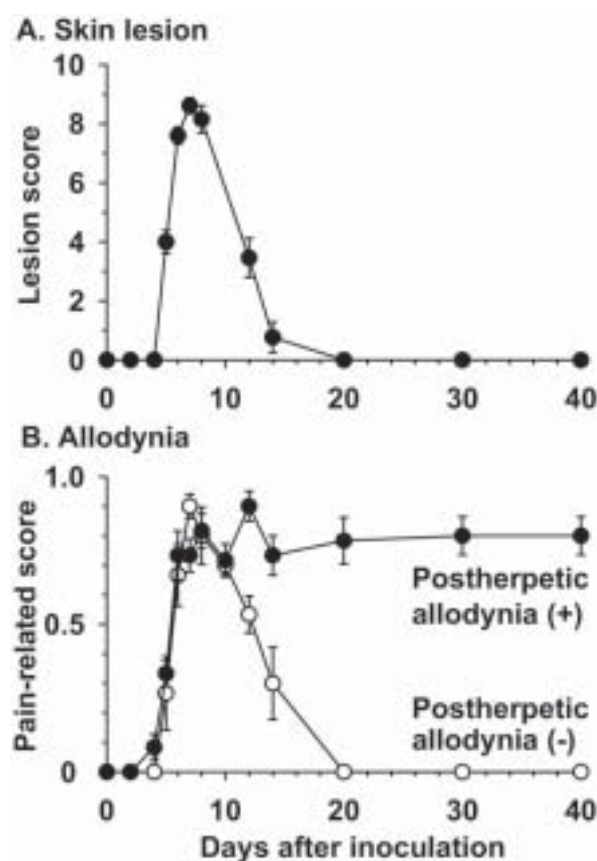


Fig. 1. Time course of the development of skin lesions and allodynia after HSV-1 inoculation. (A) Skin lesions. (B) Pain-related response to von Frey filament with bending force of 1.6 Nm. Fifteen mice were inoculated with HSV-1 unilaterally on the hind paw. All mice inoculated had skin lesions and allodynia from day 5 to about day 20 after inoculation. When mice showed allodynia on day 20, they were considered to have postherpetic allodynia. Of the mice inoculated, 10 had postherpetic allodynia and 5 were free of allodynia. The data presented are means \pm S.E.M.

tion, peaked around day 7 and subsided by day 20 (Fig. 1A). Allodynia also became apparent on day 5 and then gradually increased over a few days (Fig. 1B). In 5 of 15 mice, allodynia gradually subsided from day 8 and completely resolved by day 20 after inoculation (Fig. 1B). However, the rest (10 of 15) showed allodynia long after the complete cure of the skin lesions (from day 20 to at least day 40 after inoculation) (Fig. 1B). The mouse that showed allodynia on day 20 was considered to have postherpetic allodynia.

Effects of NOS inhibitors on herpetic and postherpetic allodynia

I.p. injections of 7-NI at doses of 3 and 10 mg/kg did not affect herpetic allodynia (Fig. 2A), but the same doses produced the dose-dependent inhibition of postherpetic allodynia; the effects peaked 1–2 h after injection and were slightly reduced after 4 h (Fig. 2B). On the other hand, i.p. injections of SMT at doses of 3 and 10 mg/kg produced the dose-dependent inhibition of herpetic allodynia; the effects

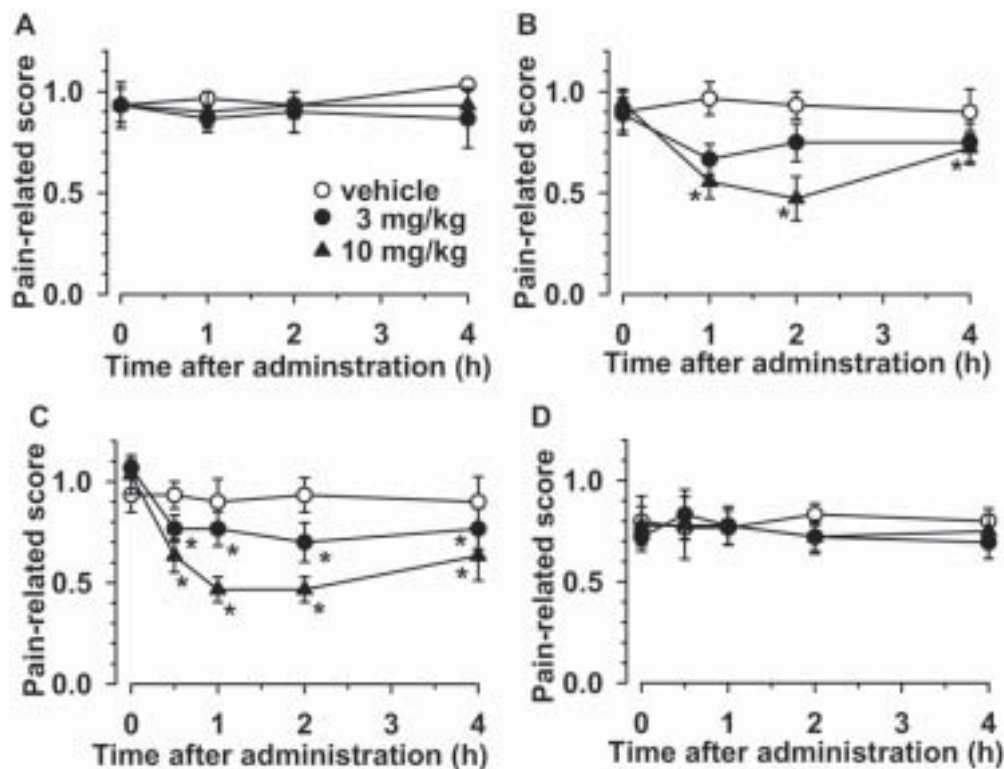


Fig. 2. Effects of NOS inhibitors on herpetic and postherpetic allodynia. Mice were given an i.p. administration of the selective NOS1 inhibitor 7-NI (A and B) and the selective NOS2 inhibitor SMT (C and D) on day 7 (A and C) or day 35–40 after inoculation (B and D). * $P < 0.05$ as compared with pre-administration (Dunnett's test). The data presented are means \pm S.E.M. ($n=5$ or 6).

peaked 1–2 h after injection and were slightly reduced after 4 h (Fig. 2C). Postherpetic allodynia was not affected by SMT at the same doses (Fig. 2D).

Expression of NOS1 and NOS2 protein in the lumbar dorsal horn

NOS1 was substantially present in the lumbar dorsal horn of naive mice, and the expression level was not altered in mice with herpetic allodynia and ones with or without postherpetic allodynia (Fig. 3A, B). NOS2 was not detected in the lumbar dorsal horn of naive mice, but it was markedly induced on day 6 after inoculation (Fig. 3C). NOS2 induction subsided on day 40 in mice with or without postherpetic allodynia (Fig. 3C). Fig. 3D shows the time course of NOS2 induction during the acute phase. NOS2 was not detected even on day 4, markedly induced on day 6, and then gradually decreased on days 8 and 10.

NOS2- and HSV-1 antigen-immunoreactive cells in the lumbar dorsal horn

In the lumbar dorsal horn ipsilateral to inoculation, HSV-1 antigen-immunoreactive cells were observed by days 5, 6 and 8 after inoculation, but not before days 3 and 10 after inoculation (Fig. 4A). The number of the immunoreactive cells peaked at day 6 after inoculation and markedly decreased on days 8 (Fig. 4A). The size of most NOS2-immunoreactive cells was less than 20 μm . In the spinal cord section prepared from the mouse at day 6 after inoculation,

a few clusters of HSV-1 antigen-immunoreactive cells were observed in the dorsal horn and NOS2-immunoreactive cells were localized in the same area (Fig. 4B–D). NOS2-immunoreactive cells were distributed around the HSV-1 antigen-immunoreactive cells, but there were no cells in which HSV-1 antigen and NOS2 immunoreactivities were co-localized (Fig. 4B–D). There were no HSV-1- and NOS2-immunoreactive cells on the contralateral dorsal horn (Fig. 4E–G).

NADPH diaphorase in the lumbar dorsal horn

The content of NOS1 in the lumbar dorsal horn was similar between naive mice and mice with postherpetic allodynia and NOS2 was not observed in the lumbar dorsal horn of mice with postherpetic allodynia. Therefore, to determine whether NOS activity would be altered in the mice with postherpetic allodynia, we investigated NOS activity by NADPH diaphorase histochemistry. NADPH diaphorase activities were distributed mainly in the superficial dorsal horn, especially laminae I and II (Fig. 5A–C). The intensity of NADPH diaphorase staining and the number of cells with NADPH diaphorase activity were similar between naive mice and mice without postherpetic allodynia (Fig. 5A, B, D and E). The intensity of NADPH diaphorase staining was significantly increased in mice with postherpetic allodynia (Fig. 5A, C and D). There was an increased tendency of the number of cells with NADPH diaphorase activity in mice with postherpetic allodynia (Fig. 5A, C and E).

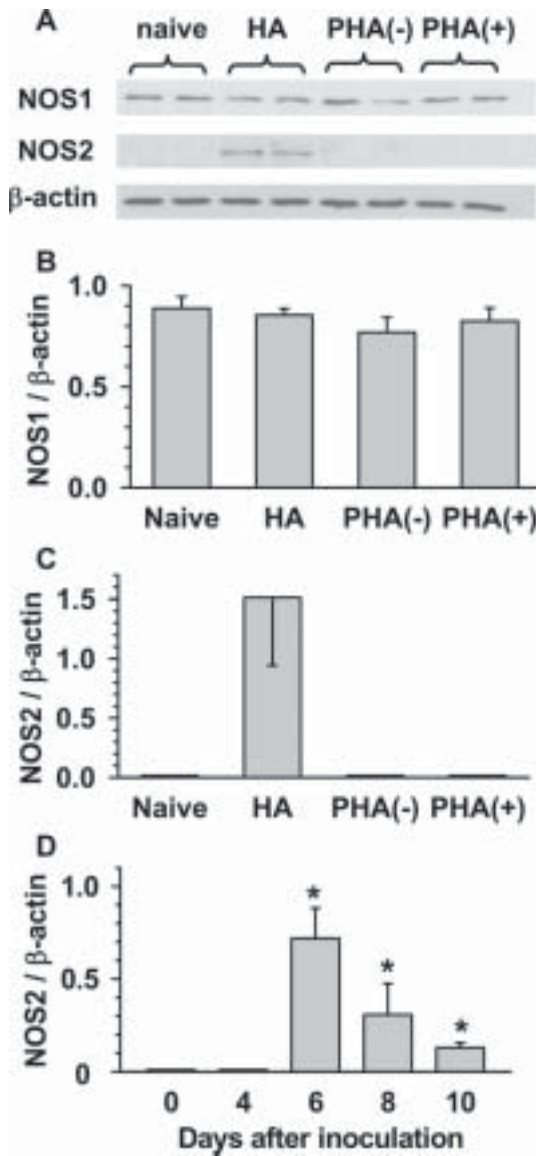


Fig. 3. Effects of HSV-1 inoculation on the expression of NOS1 and NOS2 in the lumbar dorsal horn. (A) Typical examples of Western blot analysis of NOS1, NOS2 and β -actin. (B) Expression level of NOS1 in mice with herpetic allodynia (HA, day 6 after inoculation) and mice with or without postherpetic allodynia (PHA, day 40 after inoculation). (C) Expression level of NOS2 in mice with HA and mice with or without PHA. (D) Time-dependent alteration in the expression level of NOS2 during the HA stage. Naive mice and mice with HA were the same age. The expression levels of NOS1 and NOS2 were normalized to that of β -actin. The data presented are means \pm S.E.M. ($n=4$). * $P<0.05$ as compared with naive (Dunnnett's test).

Expression of NOS1 mRNA in the dorsal root ganglia

Increased activity of NADPH diaphorase in the laminae I and II of the dorsal horn of mice with postherpetic allodynia suggested that NOS activity was increased mainly in the primary sensory fibers. The result that the level of NOS1 protein in the dorsal horn was not increased in the state of postherpetic allodynia raised two possibilities; one is that the turnover of NOS1 was increased and another is that NOS1 activity was increased without alteration in the

NOS1 turnover. To address these questions, the levels of NOS1 mRNA in the dorsal root ganglia, in which there are the cell bodies of primary sensory fibers, were determined by qRT-PCR. In this study, mechanical stimuli were applied to the hind paw, which are mainly innervated by primary sensory neurons in the L5 and L6 dorsal root ganglia. In our preliminary experiments, L3 dorsal root ganglion was found to be most extensively infected with HSV-1. Therefore, we determined NOS1 mRNA separately at L2–L4 and L5–S1 levels. The expression of NOS1 mRNA in the dorsal root ganglia at the both levels was not

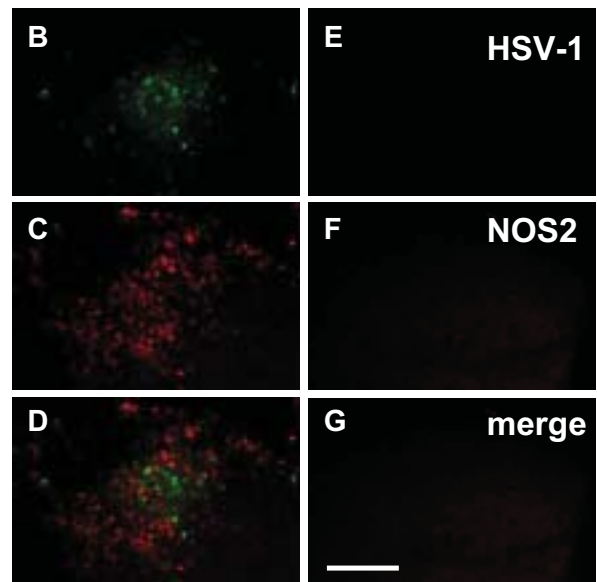
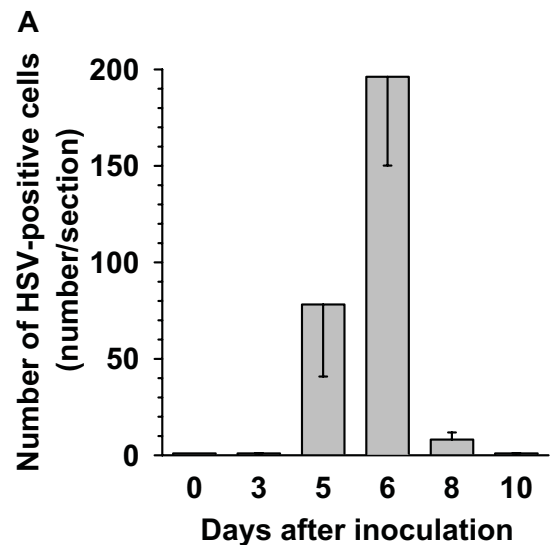


Fig. 4. Expression of NOS2 in the dorsal horn cells negative for HSV-1 antigen. (A) Time-dependent changes in the number of HSV-1 antigen-positive cells in the lumbar dorsal horn on the inoculated side. (B–G) Double immunostaining of HSV-1 and NOS2. The spinal cord was removed from mice on day 6 after inoculation and the lumbar dorsal horns on the inoculated (B–D) and contralateral sides (E–G) were immunostained for HSV-1 antigen (B and E) and NOS2 (C and F). (D, G) Merged images of immunoreactive signals of HSV-1 and NOS2. The data presented are means \pm S.E.M. ($n=6$).

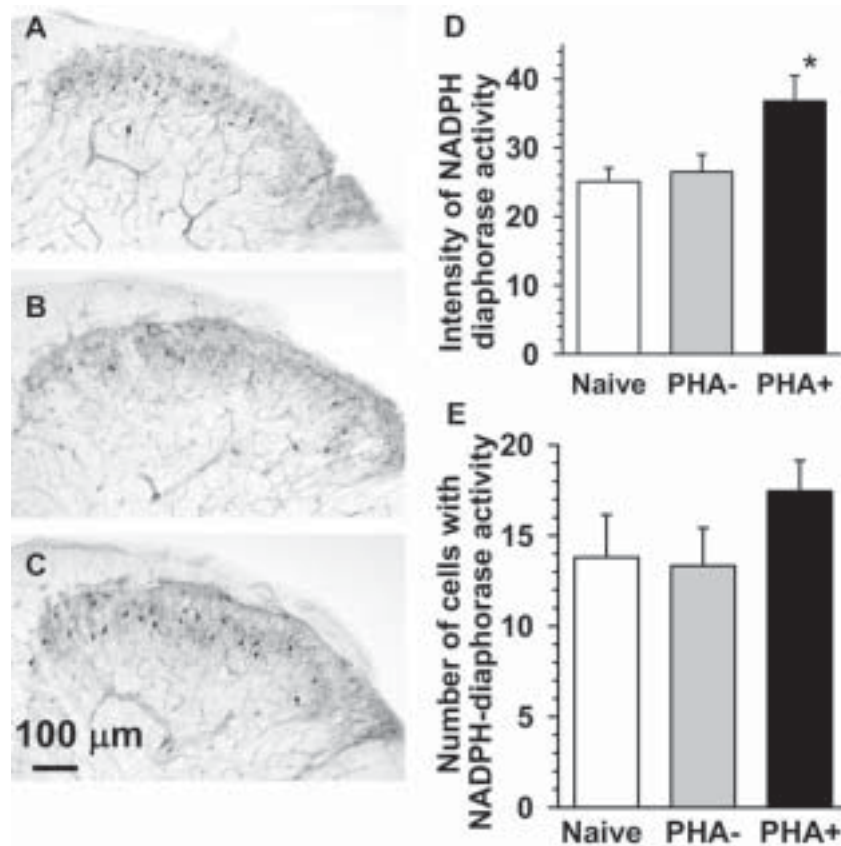


Fig. 5. The activity of reduced NADPH diaphorase in the lumbar dorsal horn of mice with or without postherpetic allodynia (PHA). (A–C) Typical examples of NADPH diaphorase staining of the lumbar dorsal horn. (D) The intensity of NADPH diaphorase staining in the laminae I and II. (E) The number of neurons with NADPH diaphorase activity in the laminae I and II. The spinal cord was dissected from age-matched naive mice and mice with or without PHA day 40 after inoculation. The data presented are means \pm S.E.M. ($n=6$). * $P<0.05$ as compared with naive (Dunnett's test).

altered in mice with or without postherpetic allodynia and also mice with herpetic allodynia (Fig. 6).

DISCUSSION

NO is produced from L-arginine by NOS and acts as inter- and intracellular messenger in a variety of cells and tissues (Moncada and Higgs, 1993). NO mediates pathological pain processing in the spinal cord (Meller and Gebhart, 1993). Behavioral evidence of NO involvement in pain mainly comes from studies using intrathecal injection of agents, in which the suppression of NO production with NOS inhibitors blocked hyperalgesia and allodynia (Salter et al., 1996; Dolan and Nolan, 1999; Osborne and Coderre, 1999). In the present study herpetic allodynia was significantly inhibited by the selective NOS2 inhibitor SMT, but not the selective NOS1 inhibitor 7-NI. On the other hand, postherpetic allodynia was significantly inhibited by 7-NI, but not SMT. These results suggest that NO is responsible for herpetic and postherpetic allodynia and that NOS2 and NOS1 are involved in herpetic and postherpetic allodynia, respectively. NOS2 was markedly induced in the dorsal horn at the herpetic stage, supporting the idea that NOS2-derived NO is responsible for herpetic allodynia. On the other hand, NOS2 almost disappeared at

the postherpetic stage and NADPH-dependent NOS activity markedly increased in the lumbar dorsal horn of mice with postherpetic allodynia, but not those without postherpetic allodynia. These results support the idea that NOS1-derived NO is responsible for postherpetic allodynia.

In the CNS, NO is thought to be primarily produced by NOS1, which is Ca^{2+} /calmodulin-dependent (Downen et al., 1999; Millan, 1999). Ca^{2+} -independent NOS2 is present in macrophages and inflammatory cells while not normally expressed in the brain and spinal cord (Guhning et al., 2000; Van Dam et al., 1995). However, central virus infections induce NOS2 expression in the CNS (Fujii et al., 1999; Christian et al., 1996; Dugas et al., 2001). The production of NO by this isoenzyme is 10–100 times more than that of the other constitutive isoenzymes, NOS1 and NOS3 (Akaie and Maeda, 2000). Therefore, although NOS1 is constitutively present at the herpetic stage, NO produced by NOS2 rather than NOS1 may play an important role in the herpetic allodynia. The degree of allodynia was similar between day 6 and day 8–10 after inoculation, but NOS2 expression was much less on day 8–10 than on day 6. Therefore, the role of NOS2 in the allodynia may be more important at the early phase than at the late phase of herpetic pain.

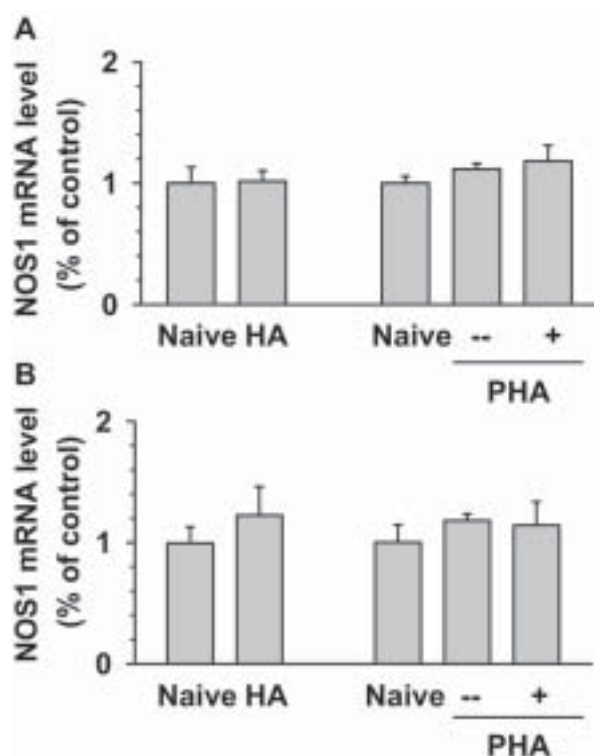


Fig. 6. Effects of HSV-1 inoculation on the expression of NOS1 mRNA in the dorsal root ganglia. Mice were inoculated with HSV-1 and the dorsal root ganglia at the L2–S1 levels on the inoculated side were isolated from mice with herpetic allodynia (HA) on day 6 after inoculation and mice with or without postherpetic allodynia (PHA) on day 40 after inoculation. Age-matched naive mice were used for control. The dorsal root ganglia at the L2–L4 (A) and L5–S1 levels (B) were separately pooled and NOS1 mRNA was determined by qRT-PCR analysis. The expression level of NOS1 mRNA was normalized to GAPDH mRNA in each sample. The data presented are means \pm S.E.M. ($n=4$).

Pathological studies on patients with herpes zoster pain demonstrated inflammatory changes in the spinal cord (Schmidbauer et al., 1992) and segmental atrophy of the spinal dorsal horn (Watson et al., 1991; Haanpaa et al., 1998), which might be induced by the virus centripetally traveling along the dorsal root to the spinal cord (Devinsky et al., 1991). These findings raise the possibility that the invasion of varicella zoster virus into the spinal cord is a cause of zoster pain. In the present study, HSV-1 antigen-immunoreactive cells were observed in the lumbar dorsal horn on days 5 and 6 after inoculation and the number of the immunoreactive cells peaked on day 6 after inoculation. The temporal pattern of HSV-1 proliferation was similar to that of NOS2 expression. Similar results were reported in an experimental model of HSV-1 encephalitis in rats after intranasal inoculation (Fujii et al., 1999). The temporal and spatial patterns of NOS2 expression coincide with those of viral proliferation, suggesting that NOS2 expression is triggered by HSV-1 invasion and proliferation in the spinal dorsal horn.

The size of most immunoreactive cells was less than 20 μ m and in our preliminary experiments, NOS2 immunoreactivity was not observed in cells immunoreactive for

neuron-specific nuclear protein, a neuronal marker (Sasaki et al., unpublished observations). Therefore, NOS2-immunoreactive cells may not be neurons. Viral infections of the CNS induce the activation of glial cells and the infiltration of macrophages and neutrophils which have the ability of NOS2 expression (Fujii et al., 1999; Christian et al., 1996; Andrews et al., 1999; Dugas et al., 2001). At present, the type of NOS2-immunoreactive cells is unclear, but we are trying to identify the type of dorsal horn cells expressing NOS2 at the herpetic stage.

As mentioned above, NOS1, but not NOS2, may be involved in postherpetic allodynia. NOS1 is abundant in the normal dorsal horn and is localized mainly in neurons (Downen et al., 1999; Millan, 1999). The activity of NOS1 generally depends on increase in intracellular calcium rather than on the expression level of the enzyme (Downen et al., 1999; Millan, 1999). In the present study, NADPH-dependent NOS activity markedly increased in the laminae I and II of the lumbar dorsal horn, suggesting the increase of NOS activity in the primary sensory fibers. There were no substantial alternations in the expression level of NOS1 protein in the area of nerve fiber distribution (dorsal horn) and NOS1 mRNA in the area of nerve cell body distribution (dorsal root ganglion). The results were similar to the report that spinal nerve ligation increased NOS1 activity in spinal dorsal horn with NOS1 immunoreactivity unchanged (Mabuchi et al., 2004). Taken together, it is suggested that neuronal NOS1-derived NO is responsible for postherpetic allodynia and that the increase of NOS activity is due to an increase in intracellular calcium but not an increase in synthesis or turnover of the enzyme.

Spinal sensitization contributes to pathological pain, consisting of tissue injury-induced inflammatory pain and nerve injury-induced neuropathic pain (Ji and Woolf, 2001). NO has been hypothesized to facilitate glutamate release (Moncada and Higgs, 1993) leading to an ongoing activity in primary afferents, increased sensitivity of dorsal horn neurons and finally spinal sensitization (Ji and Woolf, 2001). NOS1 is normally a constitutive enzyme whose activity is thought to depend on increase in intracellular calcium after the activation of NMDA receptor, an ionotropic glutamate receptor that is voltage- and ligand-gated and shows high permeability to Ca^{2+} (Meller and Gebhart, 1993). NMDA receptor is important in the synaptic events that lead to spinal sensitization (Besson, 1999). Clinically, the NMDA receptor antagonist ketamine was reported to be effective in some patients with postherpetic neuralgia (Eide et al., 1994). However, the relatively common adverse effects such as fatigue, dizziness and disturbances of somatosensory perception limit its usefulness in treating pain (Klepstad et al., 1990; Eide et al., 1994). NOS1 inhibitor may be an alternative analgesic for postherpetic neuralgia.

CONCLUSION

In summary, HSV-1 invasion of the spinal dorsal horn induced the expression of NOS2 in the dorsal horn and the NOS2-mediated overproduction of NO is responsible for

herpetic allodynia. On the other hand, postherpetic allodynia was modulated by spinal NOS1, but not NOS2. It may be worth testing the effects of NOS2 and NOS1 inhibitors on herpetic pain and postherpetic neuralgia in human subjects, respectively.

REFERENCES

- Akaike T, Maeda H (2000) Nitric oxide and virus infection. *Immunology* 101:300–308.
- Andrews DM, Matthews VB, Sammels LM, Carrello AC, McMinn PC (1999) The severity of Murray Valley encephalitis in mice is linked to neutrophil infiltration and inducible nitric oxide synthase activity in the central nervous system. *J Virol* 73:8781–8790.
- Argoff CE, Katz N, Backonja M (2004) Treatment of postherpetic neuralgia: a review of therapeutic options. *J Pain Symptom Manage* 28:396–411.
- Besson JM (1999) The neurobiology of pain. *Lancet* 353:1610–1615.
- Christian AY, Barna M, Bi Z, Reiss CS (1996) Host immune response to vesicular stomatitis virus infection of the central nervous system in C57BL/6 mice. *Viral Immunol* 9:195–205.
- Devinsky O, Cho ES, Petito CK, Price RW (1991) Herpes zoster myelitis. *Brain* 114:1181–1196.
- Dolan S, Nolan AM (1999) N-methyl D-aspartate induced mechanical allodynia is blocked by nitric oxide synthase and cyclooxygenase-2 inhibitors. *Neuroreport* 10:449–452.
- Downen M, Zhao ML, Lee P, Weidenheim KM, Dickson DW, Lee SC (1999) Neuronal nitric oxide synthase expression in developing and adult human CNS. *J Neuropathol Exp Neurol* 58:12–21.
- Dugas N, Lacroix C, Kilchherr E, Delfraissy JF, Tardieu M (2001) Role of CD23 in astrocytes inflammatory reaction during HIV-1 related encephalitis. *Cytokine* 15:96–107.
- Dworkin RH, Portenoy RK (1996) Pain and its persistence in herpes zoster. *Pain* 67:241–251.
- Eide PK, Jorum E, Stubhaug A, Bremnes J, Breivik H (1994) Relief of post-herpetic neuralgia with the N-methyl-D-aspartic acid receptor antagonist ketamine: a double-blind, cross-over comparison with morphine and placebo. *Pain* 58:347–354.
- Fujii S, Akaike T, Maeda H (1999) Role of nitric oxide in pathogenesis of herpes simplex virus encephalitis in rats. *Virology* 256:203–212.
- Gnann JW Jr (1994) New antivirals with activity against varicella-zoster virus. *Ann Neurol* 35:S69–S72.
- Guhring H, Gorig M, Ates M, Coste O, Zeilhofer HU, Pahl A, Rehse K, Brune K (2000) Suppressed injury-induced rise in spinal prostaglandin E2 production and reduced early thermal hyperalgesia in iNOS-deficient mice. *J Neurosci* 20:6714–6720.
- Haanpaa M, Dastidar P, Weinberg A, Levin M, Miettinen A, Lapinlampi A, Laippala P, Nurmikko T (1998) CSF and MRI findings in patients with acute herpes zoster. *Neurology* 51:1405–1411.
- Ji RR, Woolf CJ (2001) Neuronal plasticity and signal transduction in nociceptive neurons: implications for the initiation and maintenance of pathological pain. *Neurobiol Dis* 8:1–10.
- Klepstad P, Maurset A, Moberg ER, Oye I (1990) Evidence of a role for NMDA receptors in pain perception. *Eur J Pharmacol* 187: 513–518.
- Kuraishi Y, Takasaki I, Nojima H, Shiraki K, Takahata H (2004) Effects of the suppression of acute herpetic pain by gabapentin and amitriptyline on the incidence of delayed postherpetic pain in mice. *Life Sci* 74:2619–2626.
- Laing I, Todd AJ, Heizmann CW, Schmidt HH (1994) Subpopulations of GABAergic neurons in laminae I–III of rat spinal dorsal horn defined by coexistence with classical transmitters, peptides, nitric oxide synthase or parvalbumin. *Neuroscience* 61:123–132.
- Lancaster T, Silagy C, Gray S (1995) Primary care management of acute herpes zoster: systematic review of evidence from randomized controlled trials. *Br J Gen Pract* 45:39–45.
- Loeser JD (1986) Herpes zoster and postherpetic neuralgia. *Pain* 25: 149–164.
- Mabuchi T, Matsumura S, Okuda-Ashitaka E, Kitano T, Kojima H, Nagano T, Minami T, Ito S (2003) Attenuation of neuropathic pain by the nociceptin/orphanin FQ antagonist JTC-801 is mediated by inhibition of nitric oxide production. *Eur J Neurosci* 17:1384–1392.
- Mabuchi T, Shintani N, Matsumura S, Okuda-Ashitaka E, Hashimoto H, Muratani T, Minami T, Baba A, Ito S (2004) Pituitary adenylate cyclase-activating polypeptide is required for the development of spinal sensitization and induction of neuropathic pain. *J Neurosci* 24:7283–7291.
- Meller ST, Gebhart GF (1993) Nitric oxide (NO) and nociceptive processing in the spinal cord. *Pain* 52:127–136.
- Millan MJ (1999) The induction of pain: an integrative review. *Prog Neurobiol* 57:1–164.
- Moncada S, Higgs A (1993) The L-arginine-nitric oxide pathway. *N Engl J Med* 329:2002–2012.
- Moore PK, Wallace P, Gaffen Z, Hart SL, Babbedge RC (1993) Characterization of the novel nitric oxide synthase inhibitor 7-nitroindazole and related indazoles: antinociceptive and cardiovascular effects. *Br J Pharmacol* 110:219–224.
- Murakami Y, Okada S, Yokotani K (2002) Brain inducible nitric oxide synthase is involved in interleukin-1 β -induced activation of the central sympathetic outflow in rats. *Eur J Pharmacol* 455:73–78.
- Osborne MG, Coderre TJ (1999) Effects of intrathecal administration of nitric oxide synthase inhibitors on carrageenan-induced thermal hyperalgesia. *Br J Pharmacol* 126:1840–1846.
- Reiss CS, Komatsu T (1998) Does nitric oxide play a critical role in viral infections? *J Virol* 72:4547–4551.
- Salter M, Strijbos PJ, Neale S, Duffy C, Follenfant RL, Garthwaite J (1996) The nitric oxide-cyclic GMP pathway is required for nociceptive signalling at specific loci within the somatosensory pathway. *Neuroscience* 73:649–655.
- Schmidbauer M, Budka H, Pilz P, Kurata T, Hondo R (1992) Presence, distribution and spread of productive varicella zoster virus infection in nervous tissues. *Brain* 115:383–398.
- Szabo C, Southan GJ, Thiemeermann C (1994) Beneficial effects and improved survival in rodent models of septic shock with S-methylisothiourea sulfate, a potent and selective inhibitor of inducible nitric oxide synthase. *Proc Natl Acad Sci U S A* 91:12472–12476.
- Takasaki I, Andoh T, Shiraki K, Kuraishi Y (2000) Allodynia and hyperalgesia induced by herpes simplex virus type-1 infection in mice. *Pain* 86:95–101.
- Takasaki I, Sasaki A, Andoh T, Nojima H, Shiraki K, Kuraishi Y (2002) Effects of analgesics on delayed postherpetic pain in mice. *Anesthesiology* 96:1168–1174.
- Van Dam AM, Bauer J, Man-A-Hing WK, Marquette C, Tilders FJ, Berkenbosch F (1995) Appearance of inducible nitric oxide synthase in the rat central nervous system after rabies virus infection and during experimental allergic encephalomyelitis but not after peripheral administration of endotoxin. *J Neurosci Res* 40:251–260.
- Watson CP, Deck JH, Morshead C, Van der Kooy D, Evans RJ (1991) Post-herpetic neuralgia: further post-mortem studies of cases with and without pain. *Pain* 44:105–117.
- Yoon YW, Sung B, Chung JM (1998) Nitric oxide mediates behavioral signs of neuropathic pain in an experimental rat model. *Neuroreport* 9:367–372.
- Zimmermann M (1983) Ethical guidelines for investigations of experimental pain in conscious animals. *Pain* 16:109–110.

Fyn kinase-mediated phosphorylation of NMDA receptor NR2B subunit at Tyr1472 is essential for maintenance of neuropathic pain

Tetsuya Abe,^{1,2} Shinji Matsumura,¹ Tayo Katano,¹ Tamaki Mabuchi,¹ Kunio Takagi,¹ Li Xu,¹ Akitsugu Yamamoto,³ Kotaro Hattori,⁴ Takeshi Yagi,⁴ Masahiko Watanabe,⁵ Takanobu Nakazawa,⁶ Tadashi Yamamoto,⁶ Masayoshi Mishina,⁷ Yoshihide Nakai² and Seiji Ito¹

Departments of ¹Medical Chemistry and ²Psychosomatic Medicine, Kansai Medical University, Moriguchi 570-8506, Japan

³Nagahama Institute of Bio-Science and Technology, Nagahama 526-0829, Japan

⁴KOKORO Biology Group and CREST, Laboratories for Integrated Biology, Graduate School of Frontier Biosciences, Osaka University, Suita 565-0871, Japan

⁵Department of Anatomy, Hokkaido University School of Medicine, Sapporo 060-8638, Japan

⁶Division of Oncology, Institute of Medical Science, The University of Tokyo, Tokyo 108-8639, Japan

⁷Department of Molecular Neurobiology and Pharmacology, Graduate School of Medicine, The University of Tokyo, Tokyo 113-0033, Japan

Keywords: CP-101,606, knock-out mice, NADPH diaphorase, nitric oxide, prostaglandin E₂

Abstract

Despite abundant evidence implicating the importance of *N*-methyl-D-aspartate (NMDA) receptors in the spinal cord for pain transmission, the signal transduction coupled to NMDA receptor activation is largely unknown for the neuropathic pain state that lasts over periods of weeks. To address this, we prepared mice with neuropathic pain by transection of spinal nerve L5. Wild-type, NR2A-deficient, and NR2D-deficient mice developed neuropathic pain; in addition, phosphorylation of NR2B subunits of NMDA receptors at Tyr1472 was observed in the superficial dorsal horn of the spinal cord 1 week after nerve injury. Neuropathic pain and NR2B phosphorylation at Tyr1472 were attenuated by the NR2B-selective antagonist CP-101,606 and disappeared in mice lacking Fyn kinase, a Src-family tyrosine kinase. Concomitant with the NR2B phosphorylation, an increase in neuronal nitric oxide synthase activity was visualized in the superficial dorsal horn of neuropathic pain mice by NADPH diaphorase histochemistry. Electron microscopy showed that the phosphorylated NR2B was localized at the postsynaptic density in the spinal cord of mice with neuropathic pain. Indomethacin, an inhibitor of prostaglandin (PG) synthesis, and PGE receptor subtype EP1-selective antagonist reduced the NR2B phosphorylation in these mice. Conversely, EP1-selective agonist stimulated Fyn kinase-dependent nitric oxide formation in the spinal cord. The present study demonstrates that Tyr1472 phosphorylation of NR2B subunits by Fyn kinase may have dual roles in the retention of NMDA receptors in the postsynaptic density and in activation of nitric oxide synthase, and suggests that PGE₂ is involved in the maintenance of neuropathic pain via the EP1 subtype.

Introduction

Glutamate is the main excitatory neurotransmitter at the vast majority of excitatory synapses and is an essential component of experience-dependent synaptic plasticity that may underlie the mechanism of persistent pain, as well as that of learning and memory (Bliss & Collingridge, 1993; Ji *et al.*, 2003). The *N*-methyl-D-aspartate (NMDA) receptor is an ionotropic glutamate receptor that is voltage- and ligand-gated and shows high permeability to Ca²⁺ (Mayer *et al.*, 1984; MacDermott *et al.*, 1986). These properties enable it to detect coincident synaptic input and postsynaptic depolarization and to mediate the effect of glutamate through activation of intracellular signaling cascades, many of which are initiated by an increase in the postsynaptic Ca²⁺ concentration. Functional NMDA receptor channels

are formed by the assembly of two classes of subunits, an essential subunit NR1 (GluR ζ in mice) and modulatory subunits NR2A–NR2D (GluR ϵ 1–GluR ϵ 4) (Nakanishi, 1992; Mori & Mishina, 1995). As there are four NR2 subunits, which are distinct in their functional properties, regulation, and temporal and spatial expression, they confer functional variability to the receptor. The gene targeting strategy has revealed their different physiological roles in synaptic transmission, plasticity and development (Forrest *et al.*, 1994; Ikeda *et al.*, 1995; Sakimura *et al.*, 1995; Kadotani *et al.*, 1996; Kutsuwada *et al.*, 1996).

Chronic neuropathic pain is an important and largely unresolved medical problem. Although there is extensive evidence to implicate spinal NMDA receptors in nociceptive processing and pathological pain (Meller & Gebhart, 1993; Scholz & Woolf, 2002), little is known about the mechanism for the involvement of glutamate in the maintenance of neuropathic pain that lasts over periods of weeks. Central sensitization refers to the increased synaptic efficacy established in somatosensory neurons in the dorsal horn of the spinal cord following inflammation or

Correspondence: Dr S. Ito, as above.

E-mail: ito@takii.kmu.ac.jp

Received 20 April 2005, revised 25 June 2005, accepted 19 July 2005

nerve injury. It has been proposed recently that there are striking similarities rather than differences in the molecular mechanisms of synaptic plasticity between spinal central sensitization and hippocampal long-term potentiation (Ji *et al.*, 2003). NMDA receptors are concentrated in the postsynaptic density (PSD), a specialized structure localized in the inner part of the postsynaptic membrane, where they are dynamically clustered with receptors, cytoskeletal proteins and signal transducers including neuronal nitric oxide synthase (nNOS) (Husi & Grant, 2001). We recently showed that the increase in nNOS activity in the superficial dorsal horn of the spinal cord reflects a neuropathic pain state even 1 week after nerve injury (Mabuchi *et al.*, 2003) and that this nNOS activation may be reversibly regulated by the translocation of nNOS from the cytosol to the membrane in the presence of NMDA (Mabuchi *et al.*, 2004b). Because NMDA receptor channel activity is modulated by protein kinases and phosphatases (Wang & Salter, 1994; Yu *et al.*, 1997), these findings together suggest that neuropathic pain is maintained by phosphorylation and dephosphorylation of NMDA receptors, which contributes to the regulation of postsynaptic responses in the spinal cord.

The development of selective antagonists for the NR2B subunit has provided a tool to examine the role of this subunit in pain transmission under pathophysiological conditions (Chizh *et al.*, 2001a). The NR2B-selective antagonist CP-101,606 ((1*S*,2*S*)-1-(4-hydroxyphenyl)-2-(4-hydroxy-4-phenylpiperidino)-1-propanol) showed anti-nociceptive activity in both inflammatory and neuropathic pain without motor dysfunction (Boyce *et al.*, 1999). However, the involvement of spinal NR2B receptors in nociceptive transmission is controversial (Momiya, 2000; Chizh *et al.*, 2001b). Here we show that phosphorylation of NR2B-containing NMDA receptors is crucial for the maintenance of neuropathic pain and provide data that elucidate the signal transduction pathways coupled to NR2B activation.

Materials and methods

Materials

Polyclonal antibodies against amino acid residues 1–48 of NR2B (ϵ 2N) and phospho-Tyr1472 of NR2B (pY1472-NR2B) were raised in rabbits as described previously (Watanabe *et al.*, 1998; Nakazawa *et al.*, 2001). Commercially available antibodies against NR2B (Upstate Biotech, Lake Placid, NY, USA), pY1472-NR2B (Calbiochem, La Jolla, CA, USA) and nNOS (Santa Cruz Biotech, Santa Cruz, CA, USA) were also used. CP-101,606 was a gift from Pfizer Inc. (New London, CT, USA). EP1-selective agonist (ONO-DI-004) and antagonist (ONO-8713) were kindly donated by Ono Pharmaceutical Co. (Osaka, Japan).

Behavioral studies

All animal experiments were carried out in accordance with the National Institutes of Health guide for the care and use of laboratory animals and were approved by the Animal Experimentation Committee of Kansai Medical University. Mice lacking either the NR2A (NR2A^{-/-}; Sakimura *et al.*, 1995) or the NR2D (NR2D^{-/-}; Ikeda *et al.*, 1995) subunit of NMDA receptor channels or the Src-family tyrosine kinase Fyn (Fyn^{-/-}; Yagi *et al.*, 1993) were obtained by the gene targeting technique. Briefly, these knockout mice were generated using TT2 embryonic stem cells derived from C57BL/6 \times CBA F1 hybrid mice. The resultant chimeric mice were crossed with C57BL/6 mice to yield heteromeric F2 mice with a 75% C57BL/6 genetic background. These F2 heteromeric mice were further crossed with each other to generate knockout and control lines and used here as NR2 knockout mice and wild-type mice, respectively. The genetic

background of Fyn^{-/-} mice employed here was purified ten times by backcrossing to the C57BL/6 strain and the calculated homogeneity of the C57BL/6 genetic background was >99.99%. C57BL/6 mice were used as control wild-type mice. A model of inflammatory pain was made by subcutaneous injection of complete Freund's adjuvant into the left dorsal hindpaw of mice (Guo *et al.*, 2002). The neuropathic pain model of selective transection of the L5 spinal nerve (L5-SNT) was made as reported previously (Mabuchi *et al.*, 2003), prepared under sodium pentobarbital (50 mg/kg) anaesthesia.

To assess paw withdrawal thresholds, we applied calibrated von Frey filaments (Stoelting, Wood Dale, IL, USA) in an ascending order five times at an interval of a few seconds to the plantar surface of the hindpaw from the mesh floor. The threshold was taken as the lowest force required to elicit a withdrawal reflex of the paw.

Histochemistry

Mice were anesthetized by intraperitoneal administration of sodium pentobarbital (50 mg/kg) and intracardially perfused with 50 mL of physiological saline followed by a fixative containing 4% paraformaldehyde in 0.12 M sodium phosphate (pH 7.4). Spinal cords were removed and immersed in the fixative for 4 h and then cryoprotected overnight in 20% (w/v) sucrose in 0.1 M phosphate-buffered saline (pH 7.4). Transverse L5 spinal cord sections (20 μ m thick) were cut on a cryostat and processed for immunohistochemistry with anti-NR2B antibody (1 μ g/mL), pY1472-NR2B antibody (1 : 2000) or anti-nNOS antibody (1 : 2000), and then with Cy3-conjugated goat anti-rabbit IgG (1 : 300; Jackson ImmunoResearch, West Grove, PA, USA) as primary and secondary antibodies, respectively. The slides were mounted with Vectashield medium (Vector Laboratories, Burlingame, CA, USA) and fluorescent images were captured with a cooled charge-coupled device camera mounted on a fluorescence microscope (BX-50, Olympus, Tokyo, Japan). nNOS activity and its distribution in the spinal cord were determined by NADPH diaphorase histochemistry, as described by Mabuchi *et al.* (2003). Incubation was carried out for 3 h at 37 °C. Images were captured with a color cooled charge-coupled device camera mounted on a microscope (E1000, Nikon, Tokyo, Japan).

Sections of a set of control and experimental tissues were concurrently immunostained or simultaneously processed as for the NADPH diaphorase reactions and images were captured under the same conditions. The experiments were carried out 3–5 times and similar results were obtained. The intensity of immunostaining and NADPH diaphorase staining was quantified with Scion Image (arbitrary units), and the number of NADPH diaphorase-positive neurons was counted under a microscope.

Immunoelectron microscopy

The pre-embedding silver enhancement immunogold method was used (Murata *et al.*, 2002). Cryosections (6 μ m) of the spinal cord were reacted overnight with pY1472-NR2B antibody, and then incubated with colloidal gold (1.4 nm in diameter)-conjugated secondary antibody. The gold labeling was intensified by a silver enhancement kit (Aurion R-Gent SE-EM, Wageningen, The Netherlands). Ultrathin sections were observed under an H7600 electron microscope (Hitachi, Tokyo, Japan) at 80 kV.

Western blotting

Tissues were homogenized in a solubilization buffer containing 2% SDS, 10 mM EDTA, 1 mM NaF, 1 mM Na₃VO₄, 1 mM PMSF,

1 $\mu\text{g}/\text{mL}$ aprotinin, 1 $\mu\text{g}/\text{mL}$ leupeptin and 10 mM Tris-HCl (pH 7.5), and the homogenates (50 μg for the spinal cord; 2.5 μg for the hippocampus) were subjected to 6% SDS-PAGE, and proteins were transferred electrophoretically to PVDF membranes. The membrane was incubated overnight at 4 °C with rabbit polyclonal pY1472-NR2B antibody at 1 $\mu\text{g}/\text{mL}$ and then incubated for 1 h with anti-rabbit IgG horseradish peroxidase (1 : 20 000; Biosource, Camarillo, CA, USA). The immunoreactivity was detected by using Enhanced Chemiluminescence (Amersham Biosciences, Piscataway, NJ, USA). After the pY1472-NR2B antibody had been stripped from the membrane, the membrane was reprobed with rabbit polyclonal anti-NR2B (ϵ2N) antibody (1 $\mu\text{g}/\text{mL}$). Western blotting was carried out three times and similar results were obtained.

Measurement of nitric oxide (NO)

Slices (350 μm thick) obtained from lumbar segments L4–L6 of 2–3-week-old mice were used for NO measurement. NO formation was measured by use of the fluorescent NO indicator diaminofluorescein-FM (DAF-FM) as the fluorescence intensity obtained by excitation at 480 nm, as reported previously (Mabuchi *et al.*, 2004b). Optical signals were recorded with the AQUACOSMOS imaging system (Hamamatsu Photonics, Hamamatsu, Japan) with a cooled charge-coupled device camera.

Statistics

Data were analysed by non-repeated measures ANOVA or the Kruskal–Wallis *H*-test. Statistical significance was further examined by paired and unpaired *t*-tests, Wilcoxon *t*-test, Mann–Whitney *U*-test alone or with Bonferroni correction, or Dunnett's test. Data were expressed as the mean \pm SEM. $P < 0.05$ was considered to be statistically significant.

Results

NR2B subunits are crucial for neuropathic pain

To clarify which NR2 subunit(s) is involved in neuropathic pain, we assessed paw withdrawal thresholds before and after L5-SNT in wild-type, NR2A^{-/-} and NR2D^{-/-} mice. Before the operation, wild-type, NR2A^{-/-} and NR2D^{-/-} mice showed no difference in their withdrawal threshold of the left paw to mechanical stimuli. On days 5–14 after L5-SNT when the inflammatory pain had subsided, the paw withdrawal threshold to mechanical stimuli markedly decreased in the paw on the side ipsilateral to the nerve injury, from 1.49–1.85 g to 0.06–0.17 g in wild-type, NR2A^{-/-} and NR2D^{-/-} mice, suggesting that neither the NR2A nor the NR2D subunit was involved in the initiation and maintenance of neuropathic pain (Fig. 1A).

As NR2B^{-/-} mice could not be used for studies on pain behavior because of neonatal death (Kutsuwada *et al.*, 1996), we next examined the analgesic effect of the NR2B-selective antagonist CP-101,606 in wild-type mice on day 7 after L5-SNT, when neuropathic pain had been established, as indicated by the reduced threshold on the ipsilateral side on day 7 (Fig. 1B). Consistent with a previous report (Boyce *et al.*, 1999), CP-101,606 (30 mg/kg) significantly increased the paw withdrawal threshold to 0.90 \pm 0.25 g ($n = 6$) on the ipsilateral side of the nerve injury 1 h after oral administration without motor dysfunction; the animal then returned to a neuropathic pain state (0.31 \pm 0.16 g) at 2 h (Fig. 1B). CP-101,606 did not affect the

threshold on the contralateral side (Fig. 1B). When assessed 1 h after oral administration, CP-101,606 dose-dependently increased the threshold of the injured paw to the mechanical stimulus (Fig. 1C). These results thus suggest that the NMDA receptor containing NR2B subunits is essential for the maintenance of neuropathic pain.

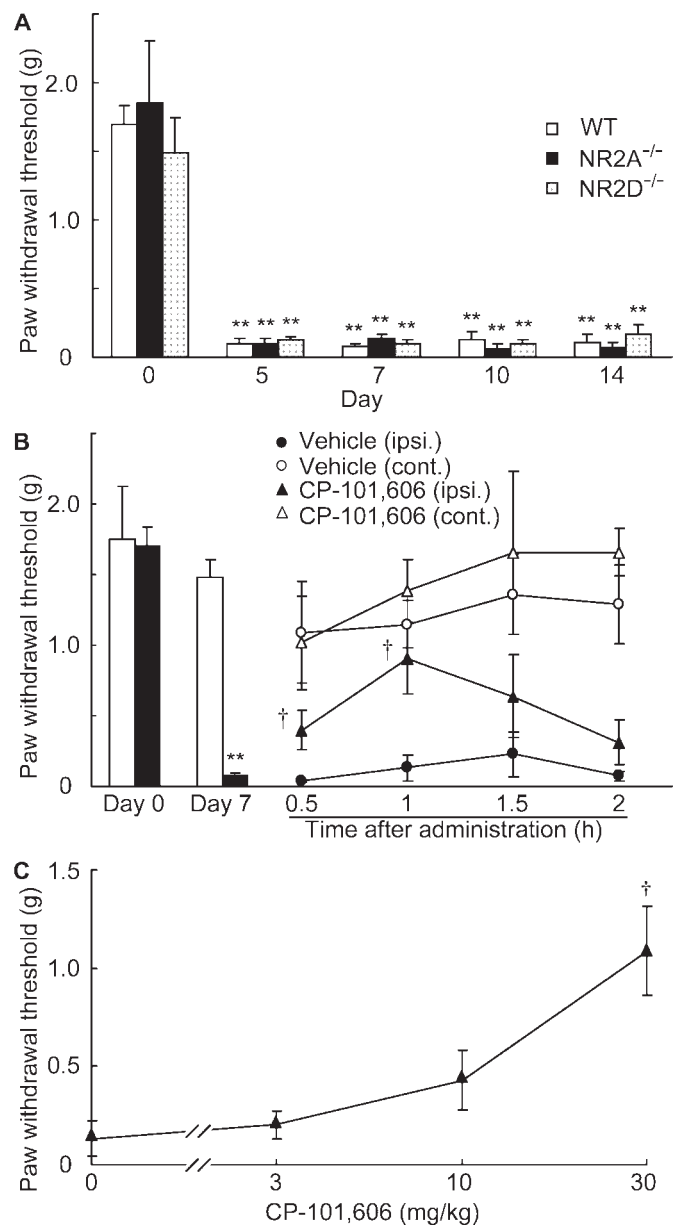
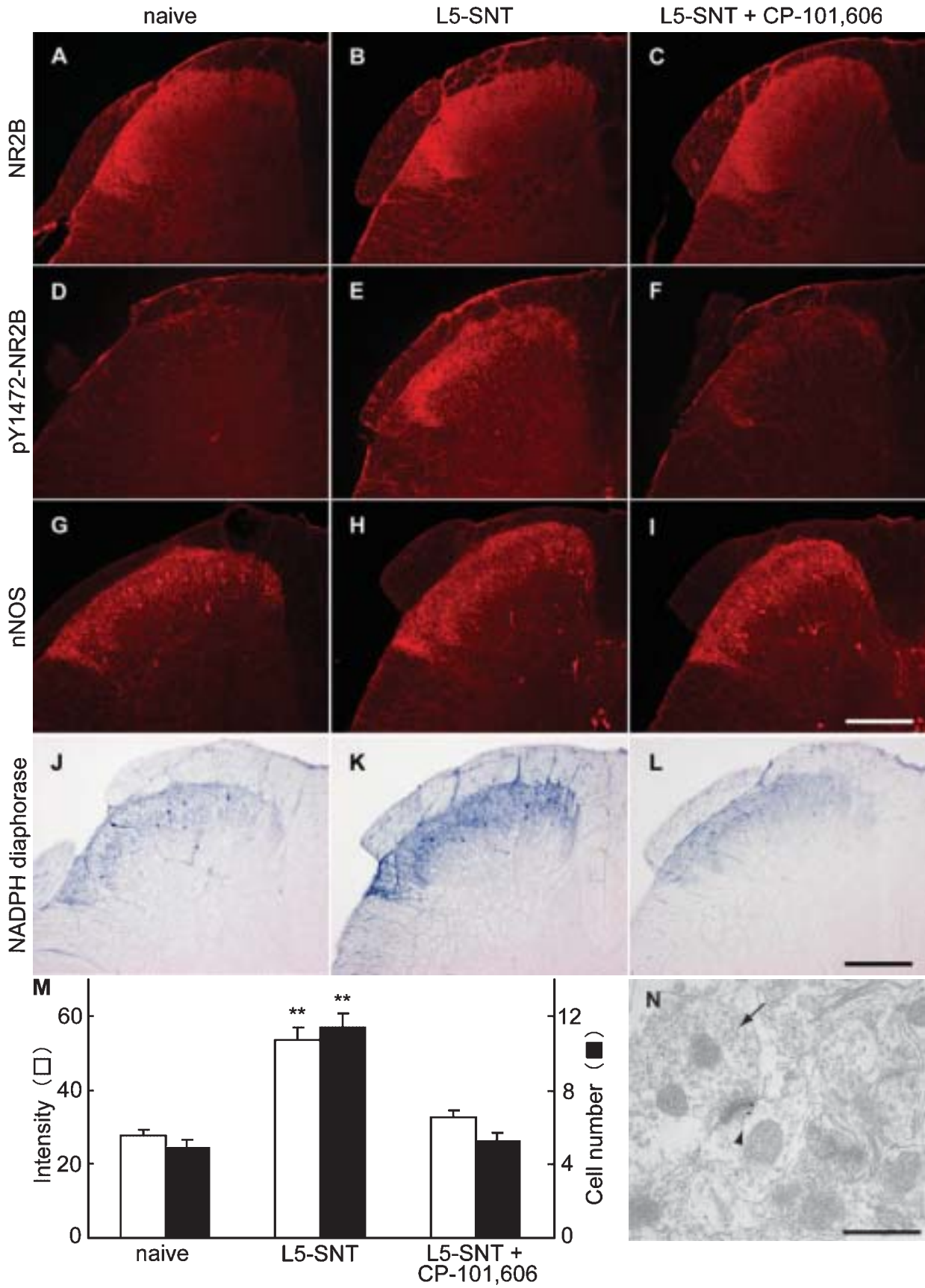


FIG. 1. Involvement of NR2B in the maintenance of neuropathic pain. (A) Time course of paw withdrawal threshold on the ipsilateral side to L5-SNT in wild-type (WT), NR2A^{-/-} and NR2D^{-/-} mice. (B) Effect of the NR2B antagonist CP-101,606 on neuropathic pain in nerve-injured mice. Left: paw withdrawal threshold in the ipsilateral (closed) and contralateral (open) sides before and on day 7 after L5-SNT in wild-type mice. Right: time courses of paw withdrawal threshold following oral administration of CP-101,606 (30 mg/kg) or saline on day 7 after L5-SNT. (C) Dose dependency of CP-101,606 for the analgesic effect on paw withdrawal threshold in neuropathic-pain mice 1 h after oral administration of CP-101,606. Values are the mean \pm SEM ($n = 6$). ** $P < 0.01$ as compared with day 0; † $P < 0.05$ as compared with the saline-administered group.



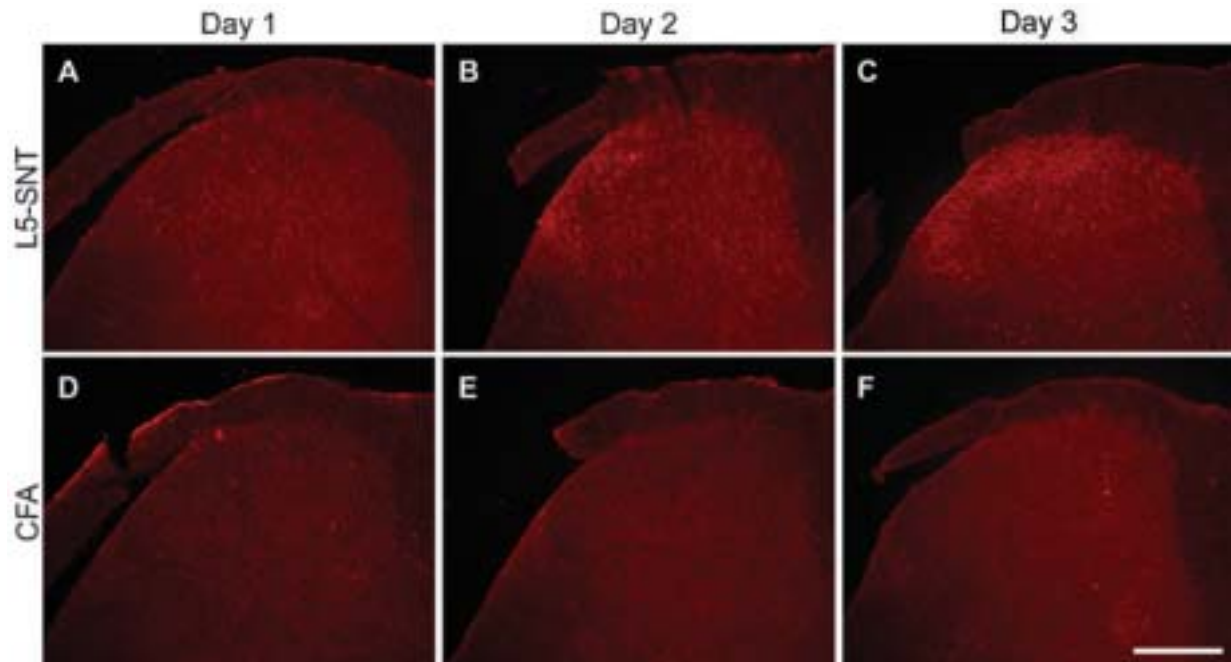


FIG. 3. No phosphorylation of NR2B subunit at Tyr1472 in the spinal cord of inflammatory-pain mice. Transverse sections of lumbar spinal dorsal horn prepared from mice on day 1 (A and D), day 2 (B and E) and day 3 (C and F) after L5-SNT (A–C) or intraplantar injection of complete Freund's adjuvant (D–F) were immunostained with pY1472-NR2B antibody. Scale bar, 200 μ m.

Tyr1472 phosphorylation of NR2B subunit with neuropathic pain

To clarify the mechanism for the involvement of NR2B subunits in the maintenance of neuropathic pain, we examined the protein level and tyrosine phosphorylation of NR2B subunits in the spinal cord prepared from naive mice and neuropathic-pain mice on day 7 after L5-SNT. Immunostaining with anti-NR2B antibody was restricted to the superficial dorsal horn of the spinal cord, and NR2B expression did not change between naive mice and neuropathic-pain mice or by oral administration of CP-101,606 to the latter (Fig. 2A–C). By contrast, whereas the spinal cord of naive mice was only negligibly stained with the antibody against pY1472-NR2B, there was a marked increase in the intensity of immunostaining in laminae I and II inner (Ili) of the spinal cord of the pain-model mice, which was reduced close to the basal level 1 h after oral administration of CP-101,606 (Fig. 2D–F). To confirm this, the intensity of immunostaining with anti-NR2B and pY1472-NR2B antibodies was quantified by Scion Image. Whereas the intensities (mean \pm SEM, $n = 5$) of NR2B immunoreactivity for naive mice, L5-SNT mice and L5-SNT mice pretreated with CP-101,606 were 39.1 ± 8.1 , 48.4 ± 12.7 and 42.1 ± 12.1 , respectively, those ($n = 4$) of pY1472-NR2B immunoreactivity were 11.4 ± 1.3 , 41.8 ± 0.4 ($P < 0.01$ as compared with naive mice) and 19.7 ± 4.2 ($P < 0.05$ as compared with L5-SNT mice), respectively.

The increase in pY1472-NR2B immunostaining was observed in neuropathic-pain mice on day 3 (25.1 ± 1.1 , $n = 3$, $P < 0.01$ as compared with naive mice) after L5-SNT (Fig. 3A–C), but not in inflammatory-pain mice at all (Fig. 3D–F). These results suggest that phosphorylation of NR2B subunits at Tyr1472 was involved in the initiation and maintenance of neuropathic pain.

Coupling of nNOS to NR2B phosphorylation

We have recently demonstrated that NO production by nNOS is involved in the maintenance of neuropathic pain and that inhibition of NO production alleviates neuropathic pain (Mabuchi *et al.*, 2003). Similar to the distribution of Tyr1472-phosphorylated NR2B subunits, nNOS immunoreactivity was localized in laminae I and Ili of the dorsal horn in naive mice; and the expression and distribution of nNOS protein did not change statistically significantly ($n = 4$) in the spinal cord of the model mice regardless of oral administration of CP-101,606 (Fig. 2G–I). To examine further the involvement of nNOS in neuropathic pain, we measured NADPH diaphorase reactivity, a reliable marker of spinal nNOS activity (Laing *et al.*, 1994), in the dorsal horn of the lumbar spinal cord. Consistent with pY1472-NR2B immunostaining (Fig. 2D–F), although NADPH diaphorase-reactive neurons were sparsely distri-

FIG. 2. Increases in Tyr1472 phosphorylation of NR2B and nNOS activity in the spinal cord of neuropathic-pain mice. (A–L) Transverse sections of lumbar spinal dorsal horn prepared from naive mice (A, D, G and J), mice on day 7 after L5-SNT (B, E, H and K), and mice pretreated for 1 h with CP-101,606 on day 7 after L5-SNT (C, F, I and L) were immunostained with NR2B (A–C), pY1472-NR2B (D–F) and nNOS (G–I) antibodies or subjected to NADPH diaphorase staining (J–L). Scale bar, 200 μ m. (M) Intensity of NADPH diaphorase staining and number of NADPH diaphorase-positive neurons. The intensity of NADPH diaphorase staining (open bars) was quantitated with Scion Image, and the number of NADPH diaphorase-positive neurons (closed bars) was counted in 16 sections from four mice for each group. Values are the mean \pm SEM. $**P < 0.01$ as compared with naive mice. (N) Immunogold electron microscopic localization of phosphorylated NR2B in the spinal cord. Immunogold particles attached to secondary antibody complexed with the pY1472-NR2B antibody (arrowhead) were mainly found in the PSD. Arrow indicates the synaptic terminal. Scale bar, 500 nm.

buted and neuropiles were weakly stained in the superficial dorsal horn of naive mice, the intensity of NADPH diaphorase staining was obviously increased in the neuropathic-pain mice; this increase was reversibly reduced to the basal level of naive mice 1 h after oral administration of CP-101,606 (Fig. 2J–L). These changes in NADPH diaphorase staining after treatment were confirmed by measuring the intensity with Scion Image and counting the number of NADPH diaphorase-positive neurons using 16 slices from four mice (Fig. 2M). These results suggest a link between phosphorylation of NR2B at Tyr1472 and nNOS activation.

We also analysed the subcellular localization of Tyr1472-phosphorylated NR2B by electron microscopy. Whereas the labeling was rather sparse in the spinal cord of neuropathic-pain mice, immunogold particles showing the presence of Tyr1472-phosphorylated NR2B were mainly detected in the PSD (1.4 ± 0.22 per synapse, $n = 10$; $P < 0.01$ vs. naive mice and $P < 0.01$ vs. presynapse), but not in presynaptic terminals (0.1 ± 0.1 , $n = 10$), of neuronal synapses (Fig. 2N). Significant labeling was not detected by pY1472-NR2B antibody in the PSD (0.3 ± 0.15 , $n = 10$) of the spinal cord of naive

mouse, and only a small number of gold particles were observed with control rabbit or mouse IgG.

Tyr1472 phosphorylation of NR2B subunits by Fyn kinase

It was previously reported that Fyn kinase mainly phosphorylated NR2B at Tyr1472 among seven tyrosine residues *in vitro* (Nakazawa *et al.*, 2001) and that the level of Tyr1472 phosphorylation of NR2B was significantly reduced in $Fyn^{-/-}$ mice, which showed impaired hippocampal long-term potentiation and spatial learning (Nakazawa *et al.*, 2001). To clarify the involvement of Tyr1472 phosphorylation of NR2B in neuropathic pain and to specify the enzyme responsible for it, we subjected $Fyn^{-/-}$ mice to L5-SNT. As shown in Fig. 4A, in contrast to that for wild-type mice, the paw withdrawal threshold did not change on the side ipsilateral to nerve injury of $Fyn^{-/-}$ mice between before (1.63 ± 0.22 g, $n = 6$) and on day 7 after L5-SNT (1.57 ± 0.19 g), suggesting that Fyn kinase may play a crucial role in the development of neuropathic pain. As compared with that

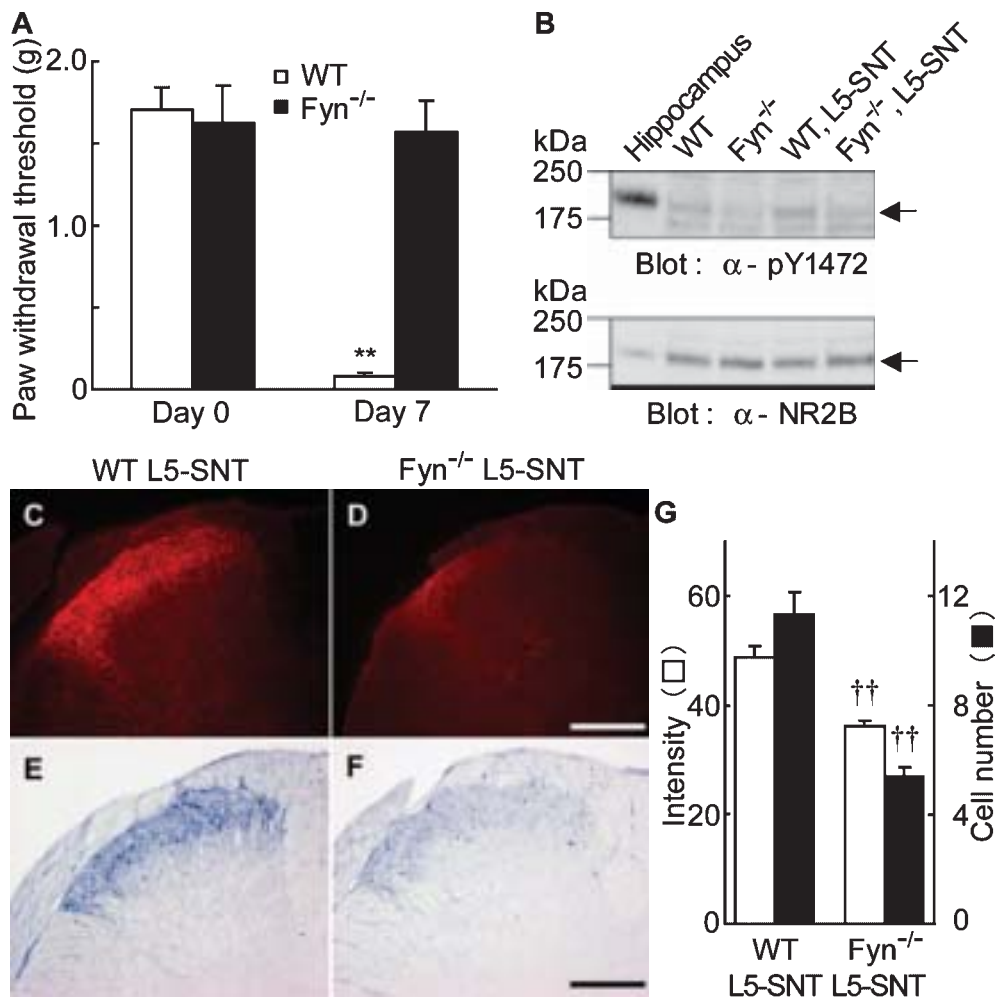


FIG. 4. Lack of neuropathic pain and Tyr1472 phosphorylation of NR2B in $Fyn^{-/-}$ mice after nerve injury. (A) Paw withdrawal threshold on the ipsilateral side before and on day 7 after L5-SNT in wild-type (open bars) and $Fyn^{-/-}$ (close bars) mice. Values are the mean \pm SEM ($n = 6$). $**P < 0.01$ as compared with naive mice. (B) Immunoblot detection of NR2B and Tyr1472-phosphorylated NR2B in a lysate from the dorsal half of the spinal cord at the L4–L6 level from wild-type and $Fyn^{-/-}$ mice. Hippocampal lysate of wild-type naive mice was used as a positive control. (C and D) Immunostaining of spinal dorsal horn by pY1472-NR2B antibody from wild-type (C) and $Fyn^{-/-}$ (D) mice on day 7 after L5-SNT. (E and F) NADPH diaphorase staining in spinal dorsal horn from wild-type (E) and $Fyn^{-/-}$ (F) mice on day 7 after L5-SNT. Scale bars in D and F, 200 μ m. (G) Intensity of NADPH diaphorase staining (open bars) and number of NADPH diaphorase-positive neurons (closed bars) in 16 sections from four mice for each group. Values are the mean \pm SEM. $\dagger\dagger P < 0.01$ as compared with wild-type mice.

(41.8 ± 0.4 , $n = 4$) of wild-type mice in the neuropathic pain state (Fig. 4C), the intensity (9.9 ± 0.4 , $P < 0.01$ vs. wild-type mice) of Tyr1472-phosphorylated NR2B immunostaining was negligible in the dorsal horn of $Fyn^{-/-}$ mice (Fig. 4D). Immunoblot analysis showed that an immunoreactive band with an apparent molecular mass of 180 kDa was similarly detected by anti-NR2B antibody in the left dorsal half of the spinal cord prepared from naive mice and neuropathic-pain mice of wild-type and $Fyn^{-/-}$ origin (Fig. 4B). Tyrosine phosphorylation associated with a 180-kDa protein band was faintly detected with pY1472-NR2B antibody in naive spinal cord, and the level in the spinal cord was approximately 100-fold less than that in the hippocampus of naive mice. The tyrosine phosphorylation increased 1.1-fold in wild-type mice ($n = 3$, $P < 0.01$ vs. $Fyn^{-/-}$ mice) on day 7 after L5-SNT, but was very weakly detected in $Fyn^{-/-}$ mice regardless of L5-SNT. As compared with those for wild-type mice, the intensity of NADPH diaphorase staining and the number of NADPH diaphorase-positive neurons in the superficial dorsal horn of the spinal cord were significantly lower in $Fyn^{-/-}$ mice after L5-SNT (Fig. 4E–G). These results demonstrate that *Fyn* kinase-mediated phosphorylation of NR2B at Tyr1472 is well correlated with nNOS activation, which may lead to the development of neuropathic pain.

Involvement of prostaglandin E_2 in Tyr1472 phosphorylation of NR2B via EP1 subtype

It is well known that non-steroidal anti-inflammatory drugs such as aspirin and indomethacin produce analgesia by blocking the synthesis of prostanoids. Among them, prostaglandin E_2 (PGE_2) is the principal pro-inflammatory prostanoid; it exerts its actions through four PGE_2 receptor subtypes, EP1–EP4 (Narumiya *et al.*, 1999; Ito *et al.*, 2001). We previously showed that CP-101,606 blocked allodynia, a tactile pain often associated with neuropathic pain, induced via EP1 by intrathecal administration of PGE_2 (Minami *et al.*, 2001a,b) and that neuropathic pain did not appear in mice lacking membrane-associated PGE_2 synthase-1 (Mabuchi *et al.*, 2004a). Tyr1472 phosphorylation of NR2B in the superficial dorsal horn was markedly reduced in neuropathic-pain mice pretreated for 3 h with oral administration of indomethacin or for 30 min with intrathecal administration of ONO-8713, an EP1-selective antagonist (Fig. 5A–C). When immunostaining with pY1472-NR2B antibody was quantified by Scion Image, the intensity (mean \pm SEM, $n = 4$) was decreased to 16.3 ± 1.8 ($P < 0.01$ vs. L5-SNT mice) and 13.3 ± 1.6 ($P < 0.01$ vs. L5-SNT mice) by pretreatment with indomethacin and the EP1-selective antagonist, respectively.

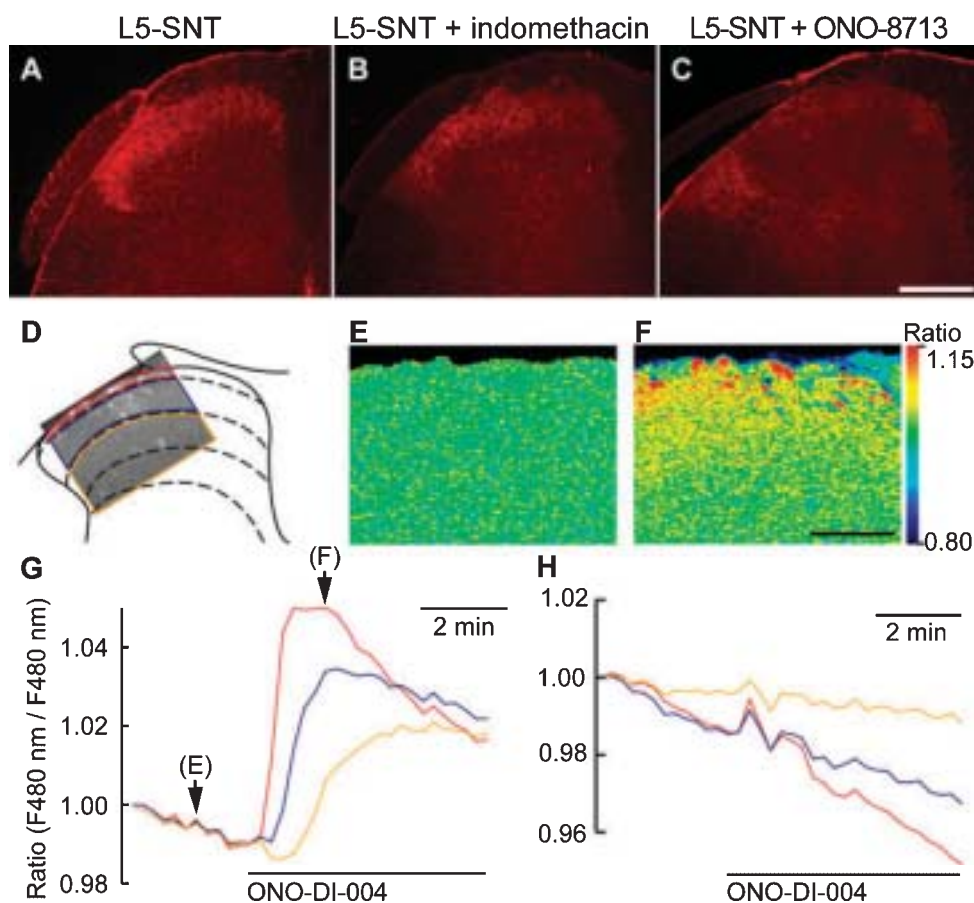


FIG. 5. Role of prostaglandin E_2 in NR2B phosphorylation and NO formation. (A–C) Effect of indomethacin and EP1-selective antagonist on Tyr1472 phosphorylation of NR2B in the spinal cord of mice with neuropathic pain. Transverse sections of lumbar spinal dorsal horn were prepared from the pain-model mice and immunostained by pY1472-NR2B antibody. The sources of the spinal cord were from mice without (A) or with pretreatment by oral indomethacin for 3 h (B) or intrathecal EP1-selective antagonist for 30 min (C). Scale bar, 200 μ m. (D–H) NO production by EP1-selective agonist in spinal slices *in vitro*. Fluorescent image of DAF-FM-loaded transverse spinal section at L5 level prepared from wild-type mice (D) and NO formation in pseudocolor as ratio images before (E) and 1 min after (F) the addition of 10 μ M EP1-selective agonist are shown. Scale bar, 100 μ m. Time courses of NO formation by EP1-selective agonist in the spinal cord of wild-type (G) and $Fyn^{-/-}$ (H) mice. NO formation in DAF-FM-loaded spinal slices was measured at 15-s intervals. The rectangle in D indicates the region in which fluorescent images obtained with excitation at 480 nm were monitored and broken lines indicate laminae in DAF-FM-loaded dorsal horn.

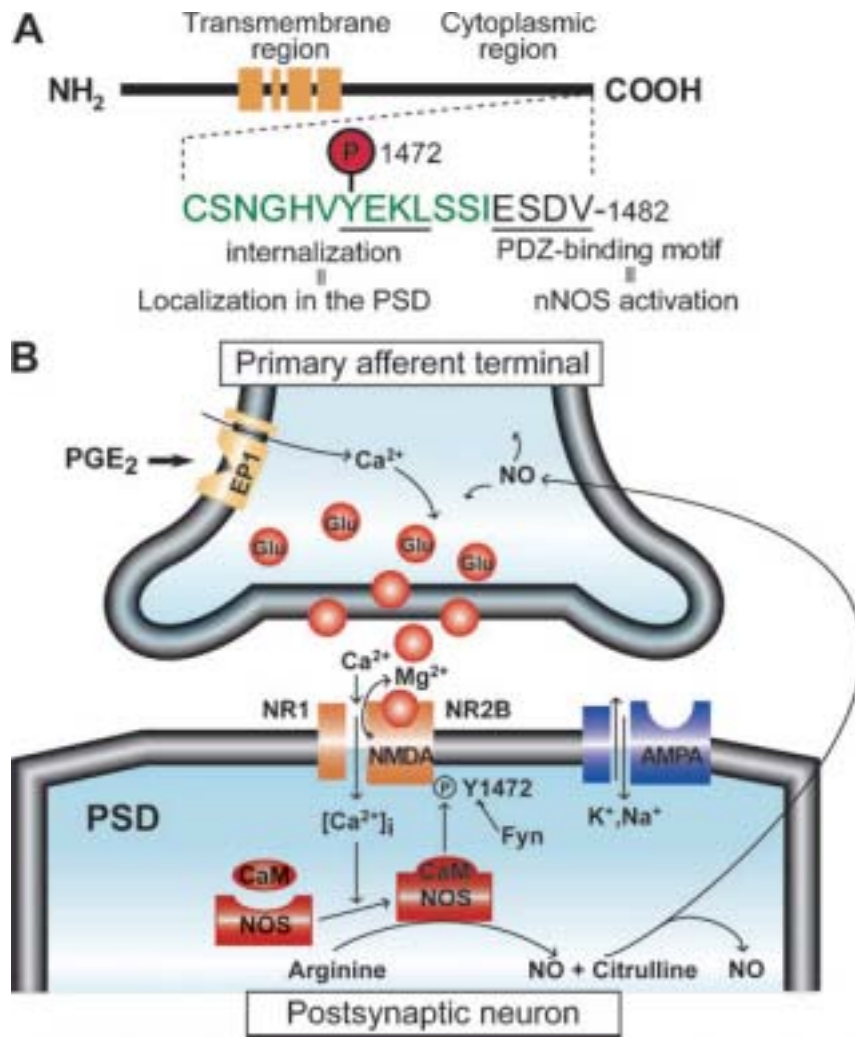


FIG. 6. Proposed mechanism for the maintenance of neuropathic pain. (A) Dual roles of Tyr1472 phosphorylation of NR2B at the synapse. (B) Functional coupling of NMDA receptors and nNOS in the spinal cord leading to central sensitization in the spinal cord. In the state of neuropathic pain, PGE₂ induces Ca²⁺ influx through the EP1 subtype and releases glutamate (Glu) from synaptic terminals of primary afferent fibers. The released glutamate activates NMDA receptors in the PSD and increases the intracellular Ca²⁺ concentration in the postsynaptic neuron, which leads to activation of nNOS and subsequent NO production. NO then serves as intra- and intercellular messengers at synapses in the dorsal horn. Continuous production of PGE₂ by persistent inputs from the periphery and nNOS activation associated with NR2B phosphorylation at Tyr1472 by Fyn kinase sustain central sensitization in the spinal cord.

We also examined whether the EP1-selective agonist ONO-DI-004 would enhance NO formation in spinal slices loaded with the fluorescent NO indicator DAF-FM. Figure 5D–G shows representative fluorescence and ratio images of NO formation, before and after the addition of 10 μ M ONO-DI-004, in the dorsal horn of spinal slices prepared from wild-type mice. The EP1-selective agonist increased NO formation in the superficial layer (1.03 ± 0.004 , $P < 0.05$ vs. Fyn^{-/-} mice), but only weakly in the deeper layer (1.02 ± 0.005 , $P < 0.05$ vs. Fyn^{-/-} mice), of all spinal slices examined (26 slices from 17 mice). By contrast, NO formation (1.00 ± 0.004 in the superficial layer, and 0.99 ± 0.004 in the deeper layer) was not observed at all in the presence of ONO-DI-004 in nine slices from four Fyn^{-/-} mice (Fig. 5H).

Discussion

NMDA receptor-mediated currents are potentiated by Src-family tyrosine kinases and suppressed by tyrosine phosphatases (Wang & Salter, 1994; Yu *et al.*, 1997). In the NMDA receptor complex, the

NR2A, NR2B and NR2D subunits are tyrosine phosphorylated in the brain; the NR2B subunit is the major tyrosine-phosphorylated protein in forebrain synapses (Moon *et al.*, 1994). The present study demonstrates that NR2B-containing NMDA receptors in the spinal cord are responsible for the maintenance of neuropathic pain (Fig. 1) and that NR2B phosphorylation at Tyr1472 by Fyn kinase is essential for the maintenance of neuropathic pain (Fig. 4). As NR2B^{-/-} mice die perinatally (Kutsuwada *et al.*, 1996), the NR2B-selective antagonist CP-101,606 was employed in the present study. NR2C^{-/-} was not examined due to predominant expression of this subunit in the cerebellum (Mori & Mishina, 1995). Recent studies have shown that NR2B subunits were phosphorylated at Tyr residue(s) by protein kinase C and Src-family kinase in a rat model of acute inflammation (Guo *et al.*, 2002) and that the phosphorylation of NR2B subunits occurred by coupling to a group I metabotropic glutamate receptor (Guo *et al.*, 2004). However, NR2B phosphorylation at Tyr1472 was not observed in the superficial layer of the spinal cord in inflammatory-pain mice (Fig. 3). NR2 subunits have unusually long C-terminal tails that extend into the cytoplasm (Mori *et al.*, 1995), and their

importance was demonstrated by gene targeting (Mori *et al.*, 1998; Sprengel *et al.*, 1998). Phenotypic defects in mice expressing C-terminally truncated NR2B are similar to those in mice lacking entire NR2B. The mutant mice die neonatally, and the mutation greatly decreases the NMDA receptor-mediated component of hippocampal excitatory postsynaptic potentials, as this component is not localized in synapses. Phosphorylation at Tyr1472 on the distal C-terminus of NR2B, the major phosphorylation site *in vitro*, enhances long-term potentiation in hippocampal region CA1, and is greatly reduced in *Fyn*^{-/-} mice (Nakazawa *et al.*, 2001). The present study demonstrates the similarity in the molecular mechanism of synaptic plasticity between spinal central sensitization and hippocampal long-term potentiation.

NMDA receptors are organized into multiprotein signaling complexes within the PSD (Husi & Grant, 2001). Efficacy and specificity in cellular signaling cascades are often mediated by the assembly of multiprotein transduction networks. Signaling by Ca²⁺/calmodulin regulates nNOS activity in cerebellar neurons by calcium influx through NMDA receptors, but not by non-NMDA receptors, demonstrating that a mechanism exists to specifically couple NMDA receptor-mediated calcium influx to nNOS (Garthwaite *et al.*, 1988; Kiedrowski *et al.*, 1992). PSD-95, a member of the family of PSD proteins containing PDZ domains, is known to bind the C-terminus ESDV motif of NR2B subunits as well as nNOS through its second PDZ domain (Fig. 6A). This binding couples the NMDA receptor activity to NO production, which mediates NMDA-dependent excitotoxicity (Sattler *et al.*, 1999). In cultured cells, PSD-95 mediates the interaction of tyrosine kinase *Fyn* with NR2A and NR2B receptor subunits, this resulting in promotion of *Fyn* kinase-mediated tyrosine phosphorylation of these subunits (Tezuka *et al.*, 1999). We showed here that NR2B phosphorylation at Tyr1472 and subsequent activation of nNOS, as was visualized by NADPH diaphorase histochemistry in the superficial dorsal horn of the spinal cord, were essential for the maintenance of neuropathic pain (Figs 2 and 4). In this regard, PSD-95 knockdown delayed the onset of mechanical and thermal hyperalgesia in a model of neuropathic pain (Tao *et al.*, 2001). Interestingly, NR2B possesses the internalization motif YEKL (Fig. 6A), which includes the phosphorylation site of Tyr1472, and PSD-95 inhibits NR2B-mediated internalization (Roche *et al.*, 2001). Phosphorylated NR2B was detected in the PSD of the dorsal horn of neuropathic-pain mice (Fig. 2N), but not in that of naive mice. Therefore, the C-terminal tail of NR2B subunits has a dual function in NMDA receptor-mediated signal transduction and in their synaptic localization, which are both likely to be regulated by Tyr1472 phosphorylation. The present study demonstrates that these mechanisms observed with long-term potentiation in the hippocampus are fundamental to the maintenance of neuropathic pain in the spinal cord that lasts over 1 week.

How is the central sensitization leading to neuropathic pain maintained? Because the antinociceptive effect of CP-101,606 was transient and reversible (Fig. 1B), clearance of CP-101,606 from the cerebrospinal fluid might have allowed resumption of central sensitization in the spinal cord by inputs from the peripheral nerve-injured region. As PGE₂ is known to stimulate the release of glutamate from spinal slices via the EP1 subtype, which is linked to Ca²⁺ mobilization (Nishihara *et al.*, 1995), it has been proposed that one of the actions of PGE₂ on primary sensory neurons is the facilitation of neurotransmitter release (Ji *et al.*, 2003). Pretreatment with indomethacin or an EP1-selective antagonist reduced Tyr1472 phosphorylation of NR2B in the neuropathic-pain mice *in vivo* (Fig. 5B and C). By contrast, an EP1-selective agonist stimulated NO formation in the superficial dorsal horn of the spinal cord, which did not occur in *Fyn*^{-/-} mice

(Fig. 5H). The disappearance of neuropathic pain in membrane-associated PGE synthase-1 knockout mice supports the involvement of PGE₂ in the induction and maintenance of neuropathic pain that lasts for one week (Mabuchi *et al.*, 2004a). At present, more than 100 molecules have been proposed to be mediators and modulators in spinal central sensitization and subsequent generation of pain hypersensitivity (Ji *et al.*, 2003), and long-term neural plasticity such as transcriptional phenotype change in nociceptors (Neumann *et al.*, 1996) and sprouting of Aβ fibers into the superficial layer of the spinal cord (Woolf *et al.*, 1992) has been considered to be involved in neuropathic pain. However, we propose a model in which the functional coupling of NMDA receptor activation by Tyr1472 phosphorylation of NR2B subunits and nNOS is fundamental to central sensitization in a state of neuropathic pain (Fig. 6B).

Acknowledgements

This work was supported in part by grants from the programs Grants-in-Aid for 21st-Century Center of Excellence, Scientific Research on Priority Areas, Creative Scientific Research and Exploratory Research from the Ministry of Education, Culture, Sports, Science and Technology of Japan, Grants-in-Aid for Scientific Research (S) and (C) from the Japan Society for the Promotion of Science, and by grants from the Science Research Promotion Fund of the Japan Private School Promotion Foundation.

Abbreviations

CP-101,606, (1S,2S)-1-(4-hydroxyphenyl)-2-(4-hydroxy-4-phenyl-piperidino)-1-propanol; DAF-FM, diaminofluorescein-FM; L5-SNT, selective transection of L5 spinal nerve; NMDA, *N*-methyl-D-aspartate; nNOS, neuronal nitric oxide synthase; NO, nitric oxide; PGE₂, prostaglandin E₂; PSD, postsynaptic density; pY1472-NR2B, phospho-Tyr1472 of NR2B.

References

- Bliss, T.V. & Collingridge, G.L. (1993) A synaptic model of memory: long-term potentiation in the hippocampus. *Nature*, **361**, 31–39.
- Boyce, S., Wyatt, A., Webb, J.K., O'Donnell, R., Mason, G., Rigby, M., Sirinathsinghji, D., Hill, R.G. & Rupniak, N.M.J. (1999) Selective NMDA NR2B antagonists induce antinociception without motor dysfunction: correlation with restricted localisation of NR2B subunit in dorsal horn. *Neuropharmacology*, **38**, 611–623.
- Chizh, B.A., Headley, P.M. & Tzschentke, T.M. (2001a) NMDA receptor antagonists as analgesics: focus on the NR2B subtype. *Trends Pharmacol. Sci.*, **22**, 636–642.
- Chizh, B.A., Reißmüller, E., Schlütz, H., Scheede, M., Haase, G. & Englberger, W. (2001b) Supraspinal vs spinal sites of the antinociceptive action of the subtype-selective NMDA antagonist ifenprodil. *Neuropharmacology*, **40**, 212–220.
- Forrest, D., Yuzaki, M., Soares, H.D., Ng, L., Luk, D.C., Sheng, M., Stewart, C.L., Morgan, J.I., Connor, J.A. & Curran, T. (1994) Targeted disruption of NMDA receptor 1 gene abolishes NMDA response and results in neonatal death. *Neuron*, **13**, 325–338.
- Garthwaite, J., Charles, S.L. & Chess-Williams, R. (1988) Endothelium-derived relaxing factor release on activation of NMDA receptors suggests role as intercellular messenger in the brain. *Nature*, **336**, 385–388.
- Guo, W., Wei, F., Zou, S., Robbins, M.T., Sugiyama, S., Ikeda, T., Tu, J.C., Worley, P.F., Dubner, R. & Ren, K. (2004) Group I metabotropic glutamate receptor NMDA receptor coupling and signaling cascade mediate spinal dorsal horn NMDA receptor 2B tyrosine phosphorylation associated with inflammatory hyperalgesia. *J. Neurosci.*, **24**, 9161–9173.
- Guo, W., Zou, S., Guan, Y., Ikeda, T., Tal, M., Dubner, R. & Ren, K. (2002) Tyrosine phosphorylation of the NR2B subunit of the NMDA receptor in the spinal cord during the development and maintenance of inflammatory hyperalgesia. *J. Neurosci.*, **22**, 6208–6217.
- Husi, H. & Grant, S.G.N. (2001) Proteomics of the nervous system. *Trends Neurosci.*, **24**, 259–266.
- Ikeda, K., Araki, K., Takayama, C., Inoue, Y., Yagi, T., Aizawa, S. & Mishina, M. (1995) Reduced spontaneous activity of mice defective in the $\epsilon 4$ subunit of the NMDA receptor channel. *Mol. Brain Res.*, **33**, 61–71.

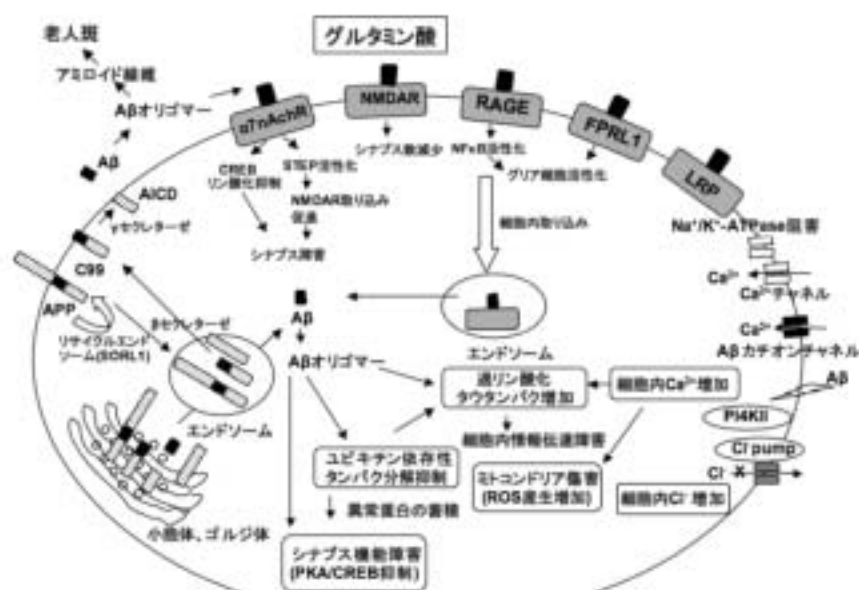
- Ito, S., Okuda-Ashitaka, E. & Minami, T. (2001) Central and peripheral roles of prostaglandins in pain and their interactions with novel neuropeptides nociceptin and nocistatin. *Neurosci. Res.*, **41**, 299–322.
- Ji, R.R., Kohno, T., Moore, K.A. & Woolf, C.J. (2003) Central sensitization and LTP: Do pain and memory share similar mechanisms? *Trends Neurosci.*, **26**, 696–705.
- Kadotani, H., Hirano, T., Masugi, M., Nakamura, K., Nakao, K., Katsuki, M. & Nakanishi, S. (1996) Motor discoordination results from combined gene disruption of the NMDA receptor NR2A and NR2C subunits, but not from single disruption of the NR2A or NR2C subunit. *J. Neurosci.*, **16**, 7859–7867.
- Kiedrowski, L., Costa, E. & Wroblewski, J.T. (1992) Glutamate receptor agonists stimulate nitric oxide synthase in primary cultures of cerebellar granule cells. *J. Neurochem.*, **58**, 335–341.
- Kutsuwada, T., Sakimura, K., Manabe, T., Takayama, C., Katakura, N., Kushiya, E., Natsume, R., Watanabe, M., Inoue, Y., Yagi, T., Aizawa, S., Arakawa, M., Uematsu, S., Nakamura, Y., Mori, H. & Mishina, M. (1996) Impairment of suckling response, trigeminal neuronal pattern formation, and hippocampal LTD in NMDA receptor $\epsilon 2$ subunit mutant mice. *Neuron*, **16**, 333–344.
- Laing, I., Todd, A.J., Heizmann, C.W. & Schmidt, H.H.H.W. (1994) Subpopulations of GABAergic neurons in laminae I–III of rat spinal dorsal horn defined by coexistence with classical transmitters, peptides, nitric oxide synthase or parvalbumin. *Neuroscience*, **61**, 123–132.
- Mabuchi, T., Kojima, H., Abe, T., Takagi, K., Sakurai, M., Ohmiya, Y., Uematani, S., Akira, S., Watanabe, K. & Ito, S. (2004a) Membrane-associated prostaglandin E synthase-1 is required for neuropathic pain. *Neuroreport*, **15**, 1395–1398.
- Mabuchi, T., Matsumura, S., Okuda-Ashitaka, E., Kitano, T., Kojima, H., Nagano, T., Minami, T. & Ito, S. (2003) Attenuation of neuropathic pain by nociceptin/orphanin FQ antagonist JTC-801 is mediated by inhibition of nitric oxide production. *Eur. J. Neurosci.*, **17**, 1384–1392.
- Mabuchi, T., Shintani, N., Matsumura, S., Okuda-Ashitaka, E., Hashimoto, H., Muratani, T., Minami, T., Baba, A. & Ito, S. (2004b) Pituitary adenylate cyclase-activating polypeptide is required for the development of spinal sensitization and induction of neuropathic pain. *J. Neurosci.*, **24**, 7283–7291.
- MacDermott, A.B., Mayer, M.L., Westbrook, G.L., Smith, S.J. & Barker, J.L. (1986) NMDA-receptor activation increases cytoplasmic calcium concentration in cultured spinal cord neurones. *Nature*, **321**, 519–522.
- Mayer, M.L., Westbrook, G.L. & Guthrie, P.B. (1984) Voltage-dependent block by Mg^{2+} of NMDA responses in spinal cord neurones. *Nature*, **309**, 261–263.
- Meller, S.T. & Gebhart, G.F. (1993) Nitric oxide (NO) and nociceptive processing in the spinal cord. *Pain*, **52**, 127–136.
- Minami, T., Matsumura, S., Okuda-Ashitaka, E., Shimamoto, K., Sakimura, K., Mishina, M., Mori, H. & Ito, S. (2001a) Characterization of the glutamatergic system for induction and maintenance of allodynia. *Brain Res.*, **895**, 178–185.
- Minami, T., Nakano, H., Kobayashi, T., Sugimoto, Y., Ushikubi, F., Ichikawa, A., Narumiya, S. & Ito, S. (2001b) Characterization of EP receptor subtypes responsible for prostaglandin E_2 -induced pain responses by use of EP₁ and EP₃ receptor knockout mice. *Br. J. Pharmacol.*, **133**, 438–444.
- Momiyama, A. (2000) Distinct synaptic and extrasynaptic NMDA receptors identified in dorsal horn neurones of the adult rat spinal cord. *J. Physiol.*, **523**, 621–628.
- Moon, I.S., Apperson, M.L. & Kennedy, M.B. (1994) The major tyrosine-phosphorylated protein in the postsynaptic density fraction is N-methyl-D-aspartate receptor subunit 2B. *Proc. Natl Acad. Sci. USA*, **91**, 3954–3958.
- Mori, H., Manabe, T., Watanabe, M., Satoh, Y., Suzuki, N., Toki, S., Nakamura, K., Yagi, T., Kushiya, E., Takahashi, T., Inoue, Y., Sakimura, K. & Mishina, M. (1998) Role of the carboxy-terminal region of the GluR $\epsilon 2$ subunit in synaptic localization of the NMDA receptor channel. *Neuron*, **21**, 571–580.
- Mori, H. & Mishina, M. (1995) Structure and function of the NMDA receptor channel. *Neuropharmacology*, **34**, 1219–1237.
- Murata, Y., Sun-Wada, G.H., Yoshimizu, T., Yamamoto, A., Wada, Y. & Futai, M. (2002) Differential localization of the vacuolar H^+ pump with G subunit isoforms (G1 and G2) in mouse neurons. *J. Biol. Chem.*, **277**, 36296–36303.
- Nakanishi, S. (1992) Molecular diversity of glutamate receptors and implications for brain function. *Science*, **258**, 597–603.
- Nakazawa, T., Komai, S., Tezuka, T., Hisatsune, C., Umemori, H., Semba, K., Mishina, M., Manabe, T. & Yamamoto, T. (2001) Characterization of Fyn-mediated tyrosine phosphorylation sites on GluR $\epsilon 2$ (NR2B) subunit of the N-methyl-D-aspartate receptor. *J. Biol. Chem.*, **276**, 693–699.
- Narumiya, S., Sugimoto, Y. & Ushikubi, F. (1999) Prostanoid receptors: structures, properties, and functions. *Physiol. Rev.*, **79**, 1193–1226.
- Neumann, S., Doubell, T.P., Leslie, T. & Woolf, C.J. (1996) Inflammatory pain hypersensitivity mediated by phenotypic switch in myelinated primary sensory neurons. *Nature*, **384**, 360–364.
- Nishihara, I., Minami, T., Watanabe, Y., Ito, S. & Hayaishi, O. (1995) Prostaglandin E_2 stimulates glutamate release from synaptosomes of rat spinal cord. *Neurosci. Lett.*, **196**, 57–60.
- Roche, K.W., Standley, S., McCallum, J., Ly, C.D., Ehlers, M.D. & Wenthold, R.J. (2001) Molecular determinants of NMDA receptor internalization. *Nat. Neurosci.*, **4**, 794–802.
- Sakimura, K., Kutsuwada, T., Ito, I., Manabe, T., Takayama, C., Kushiya, E., Yagi, T., Aizawa, S., Inoue, Y., Sugiyama, H. & Mishina, M. (1995) Reduced hippocampal LTP and spatial learning in mice lacking NMDA receptor $\epsilon 1$ subunit. *Nature*, **373**, 151–155.
- Sattler, R., Xiong, Z., Lu, W.Y., Hafner, M., MacDonald, J.F. & Tymianski, M. (1999) Specific coupling of NMDA receptor activation to nitric oxide neurotoxicity by PSD-95 protein. *Science*, **284**, 1845–1848.
- Scholz, J. & Woolf, C.J. (2002) Can we conquer pain? *Nat. Neurosci.*, **5**, 1062–1067.
- Sprengel, R., Suchanek, B., Amico, C., Brusa, R., Burnashev, N., Rozov, A., Hvalby, Ø., Jensen, V., Paulsen, O., Andersen, P., Kim, J.J., Thompson, R.F., Sun, W., Webster, L.C., Grant, S.G.N., Eilers, J., Konnerth, A., Li, J., McNamara, J.O. & Seeburg, P.H. (1998) Importance of the intracellular domain of NR2 subunits for NMDA receptor function in vivo. *Cell*, **92**, 279–289.
- Tao, F., Tao, Y.X., Gonzalez, J.A., Fang, M., Mao, P. & Johns, R.A. (2001) Knockdown of PSD-95/SAP90 delays the development of neuropathic pain in rats. *Neuroreport*, **12**, 3251–3255.
- Tezuka, T., Umemori, H., Akiyama, T., Nakanishi, S. & Yamamoto, T. (1999) PSD-95 promotes Fyn-mediated tyrosine phosphorylation of the N-methyl-D-aspartate receptor subunit NR2A. *Proc. Natl Acad. Sci. USA*, **96**, 435–440.
- Wang, Y.T. & Salter, M.W. (1994) Regulation of NMDA receptors by tyrosine kinases and phosphatases. *Nature*, **369**, 233–235.
- Watanabe, M., Fukaya, M., Sakimura, K., Manabe, T., Mishina, M. & Inoue, Y. (1998) Selective scarcity of NMDA receptor channel subunits in the stratum lucidum (mossy fibre-recipient layer) of the mouse hippocampal CA3 subfield. *Eur. J. Neurosci.*, **10**, 478–487.
- Woolf, C.J., Shortland, P. & Coggeshall, R.E. (1992) Peripheral nerve injury triggers central sprouting of myelinated afferents. *Nature*, **355**, 75–78.
- Yagi, T., Aizawa, S., Tokunaga, T., Shigetani, Y., Takeda, N. & Ikawa, Y. (1993) A role for Fyn tyrosine kinase in the suckling behaviour of neonatal mice. *Nature*, **366**, 742–745.
- Yu, X.M., Askalan, R., Keil, G.J.I.I. & Salter, M.W. (1997) NMDA channel regulation by channel-associated protein tyrosine kinase Src. *Science*, **275**, 674–678.

研究成果報告書

研究課題名	グルタミン酸受容体刺激による神経変性の分子機構と薬理的防御		
(英文)	The molecular mechanism of neurodegeneration by glutamic acid and pharmacological approaches to prevent it		
事業推進者	中邨 智之	E-mail	nakamtom@takii.kmu.ac.jp
所属・職名	医学研究科・神経病態薬理学（薬理学講座）・教授		
研究分担者名	服部 尚樹、大谷 ひとみ、北川 香織		
キーワード	アミロイドβ、グルタミン酸、神経細胞死、クロライドポンプ		

1. 概要

アミロイドβ蛋白(Aβ)はアミロイド前駆蛋白(APP)からβ-およびγ-セクレターゼによってペプチド分解されて生成され、Aβオリゴマーとなって神経細胞毒性を生じる。細胞外のAβ沈着に先立って細胞内に主にAβ1-42が蓄積し、神経細胞傷害をきたす。細胞内Aβの起源として、細胞内産生よりも細胞外に分泌されたAβが細胞内に取り込まれる経路が優位であると考えられている。細胞外Aβによる神経細胞毒性機構としてNMDA受容体の細胞内取り込み増加によるシナプス機能障害やグリア細胞の活性化が報告されている。一方、細胞内Aβによる神経細胞毒性機構としてこれまでに、1) ユビキチン依存性蛋白分解の抑制、2) シナプス機能障害、3) 過リン酸化タウ蛋白の増加、4) カルシウム仮説、5) ミトコンドリア傷害とフリーラジカルの増加等が示されてきた。我々は、Aβによる神経細胞傷害の新たな原因としてホスファチジルイノシトール-4-キナーゼ (PI4K) 阻害作用を見出した。アルツハイマー病脳ではPI4K活性が約50%に低下しており、ホスファチジルイノシトール (PI) やホスファチジルイノシトールリン酸 (PIP) のレベルも低下している。塩素イオンポンプ (Cl⁻ポンプ) はその活性発現にPI4Pを必要とする事から、AβによるPI4K活性抑制に伴うPI4Pレベルの低下がCl⁻ポンプ活性を抑制し、神経細胞傷害をきたすかを検討した。病態生理濃度のAβ(1-10 nM)は、ラット脳細胞膜分画中のII型PI4K活性を阻害し、細胞膜のPIPレベルを低下させた。初代培養ラット海馬神経細胞にAβ1-40、Aβ1-42、Aβ25-35を投与すると、神経毒性の強さに平行して細胞内塩素イオン濃度[Cl⁻]_iが上昇し、グルタミン酸興奮毒性が増強された。この機構に、神経細胞[Cl⁻]_iの増加によるII型ホスファチジルイノシチド依存性キナーゼ (PDK2) 活性低下とそれに伴うリン酸化Aktレベルの低下が考えられた。今後、Aβの新たな標的であるPI4Kを作用点とするAβ標的拮抗薬の開発が期待される。



2. 研究の背景と目的

アルツハイマー病は、進行性の記名・記憶障害、見当識障害、大脳巣症状、精神症状を臨床的特徴とする神経変性疾患である。病理組織上、アミロイド β ($A\beta$)が重合してできたアミロイド線維、変性した神経突起、反応性グリア細胞から成る老人斑が大脳皮質や海馬の細胞外実質に見られ、過リン酸化タウ蛋白が重合した神経原線維変化が大脳皮質や海馬の神経細胞内に出現する。アルツハイマー病における神経傷害の原因として、 $A\beta$ の脳内での異常重合・蓄積が重要であるという考え方（アミロイドカスケード仮説）が広く受け入れられているが、老人斑形成部位と神経細胞脱落部位とが時間的・空間的に一致しないことから、老人斑形成が神経変性に必須ではないとする反論もある。

本研究では、病態生理濃度 $A\beta$ によるグルタミン酸神経細胞毒性増強機構について検討し、 $A\beta$ /グルタミン酸神経細胞毒性を軽減する薬理的アプローチを試みた。

3. 研究方法

- (1) 培養海馬神経細胞を用いたグルタミン酸/クロライドポンプ 55kDa サブユニットに対する antisense 処置の神経細胞アポトーシスに対する効果の検討。
- (2) 培養海馬神経細胞を用いた $A\beta$ フラグメントの PI4K 活性に及ぼす効果の検討。
- (3) 培養海馬神経細胞を用いたグルタミン酸/ $A\beta$ による神経細胞障害の Cl 依存性の検討。
- (4) 培養海馬神経細胞を用いた $A\beta$ フラグメントの、グルタミン酸/ $A\beta$ による神経細胞障害に対する神経保護効果の検討。
- (5) アルツハイマー病発症モデルマウス (V337M human tau expressing mice) を用いた $A\beta$ 誘発海馬神経細胞死に対する大豆由来ホスファチジルイノシトールの効果の検討。

4. これまでの成果

- (1) 培養海馬神経細胞を用いたグルタミン酸/クロライドポンプ 55kDa サブユニットに対する antisense 処置の神経細胞アポトーシスに対する効果の検討
神経細胞内の Cl 濃度上昇がグルタミン酸神経毒性作用を増強するか否かを、クロライドポンプ 55kDa サブユニットに対するアンチセンス実験で検討した。55kDa サブユニットアンチセンス処理により、ラット海馬神経細胞内 Cl 濃度は上昇し、グルタミン酸負荷による神経細胞死が増加した。細胞内 Cl 濃度の上昇が、グルタミン酸神経毒性を増強する事が示唆された。
- (2) 培養海馬神経細胞を用いた $A\beta$ フラグメントの PI4K 活性に及ぼす効果の検討
 $A\beta$ フラグメント ($A\beta$ 20-29, $A\beta$ 31-35) の、グルタミン酸/神経毒性 $A\beta$ フラグメント ($A\beta$ 25-35)による神経毒性に対する効果を検討した。 $A\beta$ 20-29, $A\beta$ 31-35 は、PI4 kinase II 活性を回復させ、神経保護効果を示した。
- (3) 培養海馬神経細胞を用いたグルタミン酸/ $A\beta$ による神経細胞障害の Cl 依存性の検討
細胞外液中のクロライドをイセチオン酸で置換し、低クロライドイオン濃度で検討すると、培養海馬神経細胞に対する、グルタミン酸/ $A\beta$ 誘発神経細胞障害が軽減されたことから、 $A\beta$ によるグルタミン酸神経毒性は Cl 依存性であり、Cl 感受性 Akt 経路が関与する事が推測された。
- (4) 培養海馬神経細胞を用いた $A\beta$ フラグメントの、グルタミン酸/ $A\beta$ による神経細胞障害に対する神経保護効果の検討
 $A\beta$ フラグメントの、グルタミン酸/神経毒性 $A\beta$ フラグメント ($A\beta$ 1-42)による神経毒性に対する効果を更に検討した。 $A\beta$ 21-34, $A\beta$ 32-35, $A\beta$ 32-34 は、PI4 kinase II 活性を回復させ、神経保護効果を示した。
- (5) アルツハイマー病発症モデルマウス (V337M human tau expressing mice)を用いた $A\beta$ 誘発海馬神経細胞死に対する大豆由来ホスファチジルイノシトールの効果の検討
V337M human tau expressing mice に大豆由来ホスファチジルイノシトールを脳内投与すると、 $A\beta$ 25-35 脳内投与による神経細胞死が抑制された。

5. これまでの進捗状況と今後の計画

事業は研究計画に沿って概ね順調に進捗しているだけでなく、予期しない結果から新たな学術的展開を期待している。さらに、臨床応用をめざした病態モデルや新たなA β 拮抗薬を探索する。

6. これまでの発表論文

(1) 発表論文

1) 原著論文

1. Li, T., Nakayama, Y., Kitagawa, K., Hattori, N., Xiong, Z.M. & Inagaki, C.
Down-regulation of Cl⁻ pump CIP55 subunit induced enhancement of glutamate neurotoxicity in cultured rat hippocampal neurons.
Brain Res. **1130**, 235-238 (2007).
2. Xiong, Z.M., Kitagawa, K., Nishiuchi, Y., Kimura, T. & Inagaki, C.
Protective effects of A β -derived tripeptide, A β (32-34), on A β (1-42)-induced phosphatidylinositol 4-kinase inhibition and neurotoxicity.
Neurosci. Lett. **419**, 247-252 (2007).
3. Zhang, N.Y., Kitagawa, K., Hattori, N., Nakayama, Y., Xiong, Z.M., Wu, B., Liu, B. & Inagaki, C.
Soybean-derived phosphatidylinositol inhibits in vivo low concentrations of amyloid beta protein-induced degeneration of hippocampal neurons in V337M human tau-expressing mice.
Life Sci. **80**, 1971-1976 (2007).
4. Wu, B., Kitagawa, K., Liu, B., Zhang, N.Y., Xiong, Z.M. & Inagaki, C.
Attenuation of amyloid β (A β)-induced inhibition of phosphatidylinositol 4-kinase activity by A β fragments, A β 20-29 and A β 31-35.
Neurosci. Lett. **396**, 148-152 (2006).
5. Zhang, N.Y., Kitagawa, K., Wu, B., Xiong, Z.M., Otani, H. & Inagaki, C.
Chloride-dependency of amyloid beta protein-induced enhancement of glutamate neurotoxicity in cultured rat hippocampal neurons.
Neurosci. Lett. **399**, 175-180 (2006).

2) 総説

服部尚樹、北川香織、中山靖久、稲垣千代子
アミロイド β 蛋白の神経毒性機構
日薬理誌 **131**, 326-332 (2008).

(2) 学会発表

国内学会

2) シンポジウム講演

服部尚樹、北川香織、中山靖久、稲垣千代子
「アルツハイマー病の診断・治療の基礎理論と臨床の現状—解決すべき問題は何か」
アミロイド β 蛋白の神経毒性機構
第80回日本薬理学会、名古屋、2007.

7. これまでの成果の情報公開

ホームページ：薬理学講座=<http://www3.kmu.ac.jp/pharmac/>

available at www.sciencedirect.comwww.elsevier.com/locate/brainres

**BRAIN
RESEARCH**

Short Communication

Down-regulation of Cl⁻ pump ClP55 subunit induced enhancement of glutamate neurotoxicity in cultured rat hippocampal neurons

Tiesong Li, Yasuhisa Nakayama, Kaori Kitagawa, Naoki Hattori,
Zheng-Mei Xiong, Chiyoko Inagaki*

Department of Pharmacology, Kansai Medical University, Fumizono-cho 10-15, Moriguchi, Osaka 570-8506, Japan

ARTICLE INFO

Article history:

Accepted 14 October 2006

Available online 13 December 2006

Keywords:

Intracellular Cl⁻ concentration

Glutamate

Akt

ClP55

Apoptosis

ABSTRACT

To test whether the increased intracellular Cl⁻ concentration ([Cl⁻]_i) is responsible for the enhanced glutamate toxicity, antisense oligonucleotide of ClP55, a Cl⁻-ATPase/pump associated protein, was transfected in cultured rat hippocampal neurons. Neuronal [Cl⁻]_i in the antisense oligonucleotide-transfected culture increased to a level 3- to 4-fold higher than that in control. Glutamate exposure (10 μM, 10 min) increased neuronal apoptosis and decreased Akt-pS⁴⁷³ level in the antisense oligonucleotide-transfected neurons, but not in control or sense oligonucleotide-transfected ones, suggesting the responsibility of elevated [Cl⁻]_i in the enhancement of glutamate neurotoxicity.

© 2006 Published by Elsevier B.V.

We previously reported that pathophysiological concentrations of amyloid β (Aβ) proteins (1–10 nM) reduced neuronal Cl⁻-ATPase activity with an increase in the intracellular Cl⁻ concentration ([Cl⁻]_i) and enhancement of glutamate neurotoxicity in cultured rat hippocampal neurons (Yagyu et al., 2001). Since such Aβ-induced enhancement of glutamate neurotoxicity was not observed when the neurons were cultured in a low Cl⁻ medium (Zhang et al., 2006), an increase in neuronal [Cl⁻]_i was supposed to be responsible for the enhancement. To test this possibility, effects of increased [Cl⁻]_i by a method other than Aβ-treatment on glutamate neurotoxicity were examined. Cl⁻-ATPase is a candidate for an outwardly directed active Cl⁻ transport system (ATP-dependent Cl⁻ pump) in neurons (Shiroya et al., 1989), and a cDNA encoding one of its subunits, 55 kDa protein (ClP55), has already been cloned (GenBank Accession No.: AF332142) (Kitagawa et al., 2001). In the present study, we used ClP55

antisense oligonucleotides to increase neuronal [Cl⁻]_i and examined whether such an increase in [Cl⁻]_i enhances glutamate neurotoxicity in primary cultured rat hippocampal neurons.

ClP55 antisense or sense oligodeoxynucleotides were labeled with Cy3, phosphothioated and purified by high-performance liquid chromatography: antisense, 5'-ACCAGCG-TAGCGGCGAA-3' (+12 relative to the ATG starting signal); sense, 5'-TTCGCCGCTAGCTGGT-3' (+12).

Hippocampal tissues of 19-day-old Wistar rat embryos were triturated in Ca²⁺- and Mg²⁺-free Hank's solution as described previously (Yagyu et al., 2001). The cells were suspended in Dulbecco's modified Eagle's medium (DMEM) supplemented with 2 mM L-glutamine, 100 IU/ml penicillin G sulfate, 10% fetal calf serum (FCS) and 10% horse serum. The cells were seeded in poly-L-lysine-coated plastic dishes at a density of 2.5 × 10⁵ cells/cm². After incubation for 2 days, the

* Corresponding author. Fax: +81 6 6992 2940.

E-mail address: inagaki@takii.kmu.ac.jp (C. Inagaki).

cells were exposed to 5 μM adenine-9 β -arabinofuranoside (Ara-A) in modified Eagle's medium (MEM) supplemented with 2 mM L-glutamine and 5% horse serum for 4 days. On the 8th day of culture, the culture medium was replaced with MEM-5% horse serum. Sense or antisense oligodeoxynucleotide (0.5 $\mu\text{g}/\text{ml}$) and LipofectAMINE 2000 (1.2 $\mu\text{l}/\text{ml}$; Life Technologies, Rockville, MD, USA) were separately diluted in DMEM-10% FCS, and incubated at 37 $^{\circ}\text{C}$ for 30 min. Cells were washed with DMEM-10% FCS, overlaid with DMEM-10% FCS to which the DNA-lipid complexes were added, and then incubated at 37 $^{\circ}\text{C}$ for 1 h. The medium was replaced with DMEM-10% FCS, and 3 days later the cells were used to measure $[\text{Cl}^-]_i$.

$[\text{Cl}^-]_i$ was measured as described previously (Hara et al., 1992). Dissociated hippocampal cells were cultured on poly-L-lysine-coated coverslips in plastic dishes, and treated as described above. The cells were washed with modified Krebs-HEPES buffer solution containing 128 mM NaCl, 2.5 mM KCl, 2.7 mM CaCl_2 , 1 mM MgSO_4 , 20 mM HEPES and 16 mM glucose, exposed to 5 mM N-(6-methoxyquinolyl)-acetoethyl ester (MQAE), a Cl^- -sensitive fluorescent dye, in the same buffer solution at 37 $^{\circ}\text{C}$ for 1 h, and then washed with a dye-free buffer solution. Fluorescence intensity of each single cell was measured using a fluorescence reflected upright microscope BX50 (Olympus, Tokyo, Japan) with a Quantix1400 camera and IPLab software with UV excitation and emission at 360 and 510 nm, respectively. The $[\text{Cl}^-]_i$ was estimated to be a value corresponding to the initial fluorescence intensity on a calibration line for MQAE fluorescence and Cl^- concentration.

For monitoring glutamate excitotoxicity, cells cultured on poly-L-lysine-coated coverslips in plastic dishes were treated with sense or antisense oligodeoxynucleotides as described above. The cells were exposed to glutamate (10 μM , 10 min) on the 11th day of culture, and examined for apoptotic neuronal death after another 2 days (Kitagawa et al., 2001). Cells were fixed in 4% paraformaldehyde in phosphate-buffered saline (PBS) for 1 h, stained with dibenzimidazole dye, Hoechst 33258 (10 $\mu\text{g}/\text{ml}$) (Araki et al., 1987) in PBS for 1 h, and then analyzed in fluorescence microscopy using an excitation and emission wavelength at 346 and 460 nm, respectively. More than 100 pyramidal cell-like neurons for each coverslip were counted.

For Western blots, the cells were rinsed with cold PBS and lysed in a lysis buffer containing 50 mM Tris/HCl at pH 7.5, 150 mM NaCl, 1% NP40, 0.1% sodium dodecyl sulfate (SDS), 0.5% deoxycholate, 50 mM NaF, 0.2 mM Na_3VO_4 , 1 mM ethylenediamine tetraacetic acid (EDTA) and complete protease inhibitor cocktail (Roche Applied Science, Mannheim, Germany) on ice for 1 h. The lysates were clarified by centrifugation at 10,000 $\times g$ for 5 min. Aliquots (20 μg of protein) of lysates were mixed with the same volume of Laemmli loading buffer, and boiled for 5 min. Samples were separated by electrophoresis on a 7.5% SDS polyacrylamide gel, transferred to polyvinylidene difluoride membrane, and blotted with Akt-pS⁴⁷³ antibody (Sigma, St. Louis, MO, USA; 1:1000). Membrane was reprobed by anti-Akt antibody (Sigma, St. Louis, MO, USA; 1:1000) to show the total Akt level.

Data were expressed as mean \pm SE. Differences between groups were evaluated by one-way analysis of variance (ANOVA) followed by Fisher PLSD test. When only two groups were compared, Student's t-test was used. The differences between means with $P < 0.05$ were considered to be significant.

As shown in Fig. 1, $[\text{Cl}^-]_i$ of the cultured rat hippocampal neurons treated with antisense oligonucleotides of CIP55 increased to 26.5 \pm 5.5 mM, i.e., a level 3- to 4-fold higher than that in control (7.3 \pm 1.3 mM). Treatment of the neurons with sense oligonucleotides did not affect the $[\text{Cl}^-]_i$.

Glutamate-induced neurotoxicity in these neurons was examined using Hoechst 33258 staining. As shown in Fig. 2a, in the antisense oligonucleotide-treated neurons, glutamate-induced changes such as chromatin condensation and nuclear fragmentation were frequently observed as compared to those in control or sense oligonucleotide-treated cells. Percentages of the apoptotic cells in total neurons counted were calculated (Fig. 2b). Glutamate (10 μM , 10 min)-induced neuronal apoptosis was thus obvious only in antisense oligonucleotides-transfected neurons.

Since we recently suggested that a decrease in the activated (phosphorylated) form of anti-apoptotic molecule Akt is at least partly responsible for the $\text{A}\beta$ -induced Cl^- -dependent enhancement of glutamate toxicity (Zhang et al., 2006), levels of Akt-pS⁴⁷³ were examined by Western blotting using anti-Akt-pS⁴⁷³ antibody. As shown in Fig. 3, in the neurons treated with antisense oligonucleotides of CIP55, glutamate treatment (10 μM , 10 min) decreased the level of Akt-pS⁴⁷³ to 68% that in non-glutamate-treated cells, without changes in Akt level. In contrast, such glutamate-induced changes were not observed in either control or the sense oligonucleotide-treated cells.

In this study, enhancement of glutamate neurotoxicity was demonstrated in neurons with high $[\text{Cl}^-]_i$ caused by CIP55 antisense oligonucleotide treatment. Since such enhancement as estimated by cell damage and Akt-pS⁴⁷³ level was also observed in parallel with the changes in $[\text{Cl}^-]_i$ of $\text{A}\beta$ -treated cells (Zhang et al., 2006), the present findings support an idea that $\text{A}\beta$ -induced enhancement of glutamate neurotoxicity is

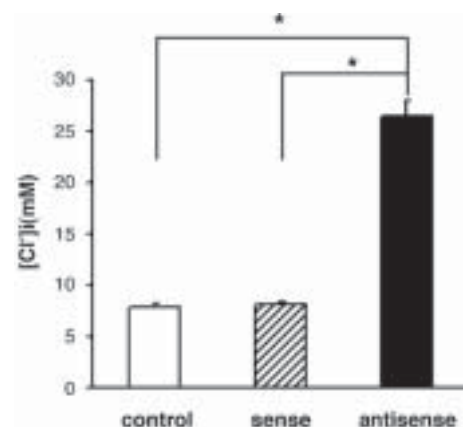


Fig. 1 – Effects of antisense oligonucleotides of CIP55 on intracellular chloride concentration ($[\text{Cl}^-]_i$) in cultured rat hippocampal neurons. Neurons on the 8th day of culture were treated with sense or antisense oligonucleotides (0.5 $\mu\text{g}/\text{ml}$) and Lipofectamine 2000 (1.5 $\mu\text{l}/\text{ml}$) for 1 h. After 3 days of incubation, $[\text{Cl}^-]_i$ of pyramidal cell-like neurons was assayed fluorometrically using a Cl^- -sensitive fluorescent dye (MQAE) ($*P < 0.01$ vs. control (with LipofectAMINE 2000 only) and sense, $n = 11$ –15). Sense or antisense means CIP55 sense or antisense oligonucleotide-treated cells.

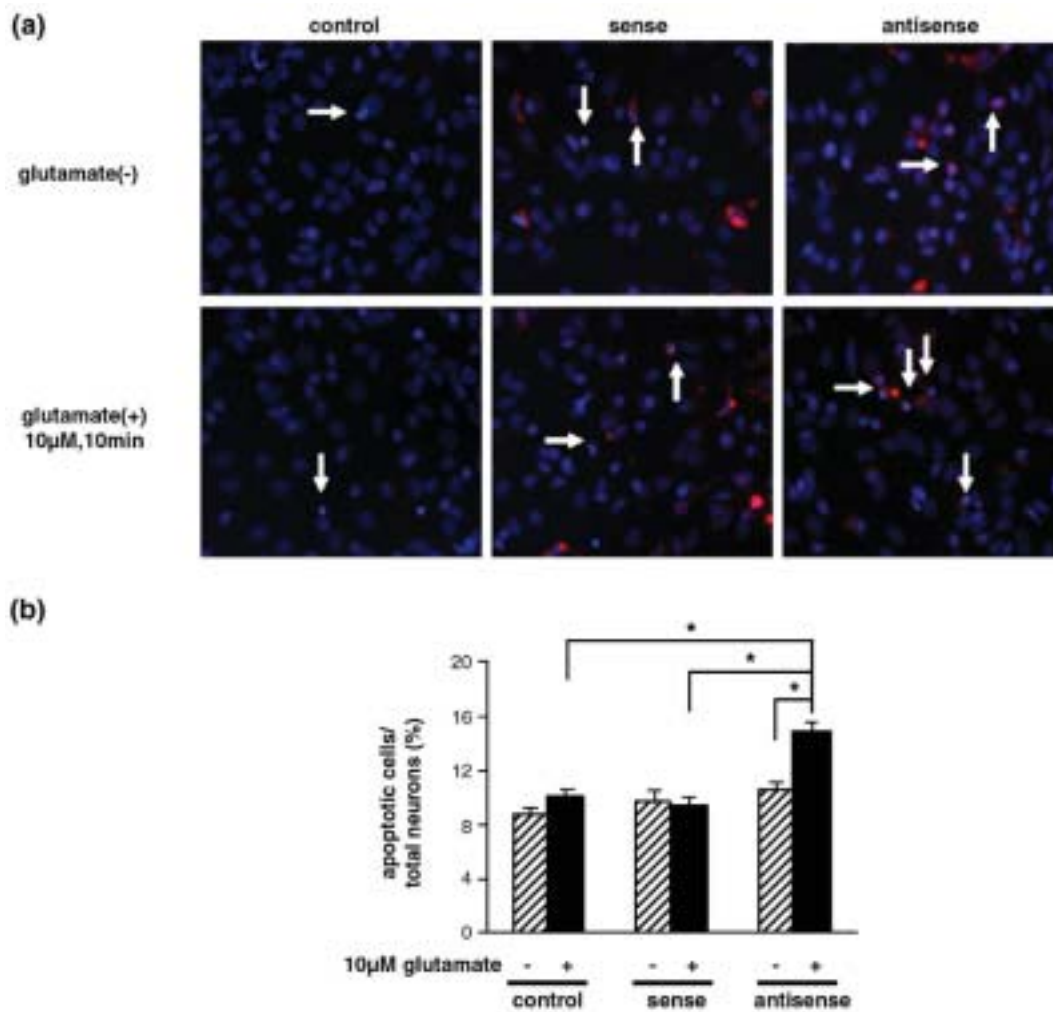


Fig. 2 – Effects of Clp55 antisense oligonucleotide treatment with or without glutamate exposure on the apoptosis of cultured rat hippocampal neurons. Neurons on the 8th day of culture were treated with sense or antisense oligonucleotides (0.5 µg/ml) and Lipofectamine 2000 (1.5 µl/ml). After 3 days, the neurons were exposed to 10 µM glutamate for 10 min. Apoptotic cells were measured by Hoechst 33258 staining 48 h after the glutamate exposure. (a) Representative photomicrographs of cultured neurons with apoptotic cells indicated by arrows. Red fluorescence is from remaining Cy3-label used to confirm usual oligonucleotide-transfection. (b) Results are summarized as percentage of apoptotic cells to total number of neurons (**P* < 0.05, *n* = 8–9).

mediated by A β -induced increase in [Cl⁻]_i. This increase seems to be caused by inhibition by A β of type II phosphatidylinositol 4-kinase (Wu et al., 2004) resulting in decreases in plasma membrane level of phosphatidylinositol 4-monophosphate (PI4P) and Cl⁻-ATPase/pump activity (Yagyu et al., 2001) which requires PI4P for its maximal activity (Zeng et al., 1994).

Elevated [Cl⁻]_i (26.5 mM) itself did not decrease the Akt-pS⁴⁷³ level (Fig. 3). As we previously reported using amyloid β protein (Zhang et al., 2006), the elevation of [Cl⁻]_i alone, even though it reached a higher level (36 mM), was not enough to lower the Akt-pS⁴⁷³ level, but decreased the level when the cells were exposed to glutamate. Although the elevation of [Cl⁻]_i decreases the activity of phosphatidylinositol-dependent protein kinase 2 (PDK2) (Hresko et al., 2003) which phosphorylates Akt at Ser473, a decrease in the Akt-pS⁴⁷³

level becomes obvious only when its turnover is increased. Glutamate is known to activate protein phosphatase 1 or 2A (Glaum and Miller 1994; Huang et al., 2001), which dephosphorylates phospho-Akt (Nakazawa et al., 2005). However, glutamate exposure alone did not change the phospho-Akt level (Fig. 3), suggesting that a normal PDK2 activity maintained the level. It is assumed that, under the conditions of elevated [Cl⁻]_i, glutamate exposure resulted in down-regulation of the Akt-pS⁴⁷³ level via enhanced dephosphorylation and attenuated phosphorylation. Such changes in the Akt-pS⁴⁷³ level paralleled with the changes in neuronal apoptotic parameter (Fig. 2), suggesting the responsibility of decreased Akt-pS⁴⁷³ levels in the enhancement of glutamate neurotoxicity in neurons with high [Cl⁻]_i.

All these findings suggest that regulation of neuronal [Cl⁻]_i is important for neuronal cell signaling and survival.

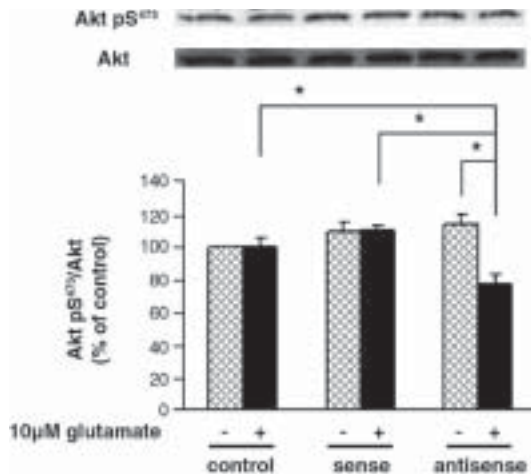


Fig. 3 – Effects of antisense oligonucleotides of ClP55 with or without glutamate exposure on the level of phosphorylated Akt at serine 473 (Akt-pS⁴⁷³) in cultured rat hippocampal neurons. Neurons on the 8th day of culture were treated with sense or antisense oligonucleotides (0.5 μg/ml) and Lipofectamine 2000 (1.5 μl/ml). After 3 days, the neurons were exposed to 10 μM glutamate for 10 min. Another 2 days later, whole cell lysates were prepared. Akt-pS⁴⁷³ were assessed by Western blot and membranes were reprobed by anti-Akt antibody. Optical density of immuno-stained Akt-pS⁴⁷³ and Akt bands were measured. Akt-pS⁴⁷³ level was expressed as the relative Akt-pS⁴⁷³ protein to total Akt protein ratio (**P* < 0.05, *n* = 7).

ClP55 antisense oligonucleotide-transfected neurons may be a good model system to test the effects of elevated [Cl⁻]_i on various neuronal functions.

Acknowledgments

This work was supported by grants from the Japanese Ministry of Education, Science, Sports, and Culture; Japanese Private School Promotion Foundation; and Salt Science Research Foundation, Japan.

REFERENCES

- Araki, T., Yamamoto, A., Yamada, M., 1987. Accurate determination of DNA content in single cell nuclei stained with Hoechst 33258 fluorochrome at high salt concentration. *Histochemistry* 87, 331–338.
- Glaum, S.R., Miller, R.J., 1994. Inhibition of phosphoprotein phosphatases blocks metabotropic glutamate receptor effects in the rat nucleus tractus solitarius. *Mol. Pharmacol.* 45, 1221–1226.
- Hara, M., Inoue, M., Yasukura, T., Ohnishi, S., Mikami, Y., Inagaki, C., 1992. Uneven distribution of intracellular Cl⁻ in rat hippocampal neurons. *Neurosci. Lett.* 143, 135–138.
- Hresko, R.C., Murata, H., Mueckler, M., 2003. Phosphoinositide dependent kinase-2 is a distinct protein kinase enriched in a novel cytoskeletal fraction associated with adipocyte plasma membranes. *J. Biol. Chem.* 278, 21615–21622.
- Huang, C.C., Liang, Y.C., Hsu, K.S., 2001. Characterization of the mechanism underlying the reversal of long term potentiation by low frequency stimulation at hippocampal CA1 synapses. *J. Biol. Chem.* 276, 48108–48117.
- Kitagawa, K., Yagyu, K., Yamamoto, A., Hattori, N., Omori, K., Zeng, X.T., Inagaki, C., 2001. Molecular cloning and characterization of the Cl⁻ pump-associated 55-kDa protein in rat brain. *Biochem. Biophys. Res. Commun.* 289, 363–371.
- Nakazawa, T., Shimura, M., Endo, S., Takahashi, H., Mori, N., Tamai, M., 2005. N-methyl-D-aspartic acid suppresses Akt activity through protein phosphatase in retinal ganglion cells. *Mol. Vis.* 11, 1173–1182.
- Shiroya, T., Fukunaga, R., Akashi, K., Shimada, N., Takagi, Y., Nishino, T., Hara, M., Inagaki, C., 1989. An ATP-driven Cl⁻ pump in the brain. *J. Biol. Chem.* 264, 17416–17421.
- Wu, B., Kitagawa, K., Zhang, N.Y., Liu, B., Inagaki, C., 2004. Pathophysiological concentrations of amyloid beta proteins directly inhibit rat brain and recombinant human type II phosphatidylinositol 4-kinase activity. *J. Neurochem.* 91, 1164–1170.
- Yagyu, K., Kitagawa, K., Irie, T., Wu, B., Zeng, X.T., Hattori, N., Inagaki, C., 2001. Amyloid beta proteins inhibit Cl⁻-ATPase activity in cultured rat hippocampal neurons. *J. Neurochem.* 78, 569–576.
- Zeng, X.T., Hara, M., Inagaki, C., 1994. Electrogenic and phosphatidylinositol-4-monophosphate-stimulated Cl⁻ transport by Cl⁻ pump in the rat brain. *Brain Res.* 641, 167–170.
- Zhang, N.Y., Kitagawa, K., Wu, B., Xiong, Z.M., Otani, H., Inagaki, C., 2006. Chloride-dependency of amyloid beta protein-induced enhancement of glutamate neurotoxicity in cultured rat hippocampal neurons. *Neurosci. Lett.* 399, 175–180.

Protective effects of A β -derived tripeptide, A β _{32–34}, on A β _{1–42}-induced phosphatidylinositol 4-kinase inhibition and neurotoxicity

Zheng-Mei Xiong^{a,c}, Kaori Kitagawa^{a,*}, Yuji Nishiuchi^b,
Terutoshi Kimura^b, Chiyoko Inagaki^a

^a Department of Pharmacology, Kansai Medical University, Fumizono-cho 10-15, Moriguchi, Osaka 570-8506, Japan

^b Peptide Institute, Inc., Saito-asagi 7-2-9, Ibaraki, Osaka 567-0085, Japan

^c Department of Pharmacology, Guiyang Medical College, Guiyang 550004, China

Received 16 January 2007; received in revised form 10 April 2007; accepted 10 April 2007

Abstract

We previously reported that the neurotoxicity of pathophysiological concentrations of amyloid β proteins (A β s, 0.1–10 nM) as assessed by the inhibition of type II phosphatidylinositol 4-kinase (PI4KII) activity and the enhancement of glutamate toxicity was blocked by a short fragment of A β , A β _{31–35}. Such protective effects of shorter fragments derived from A β _{31–35} were examined in this study to reach the shortest effective peptide, using recombinant human PI4KII and primary cultured rat hippocampal neurons. Among the peptides tested (A β _{31–34}, A β _{31–33}, A β _{31–32}, A β _{32–35}, A β _{33–35}, A β _{34–35}, A β _{32–34}, A β _{33–34} and A β _{32–33}), A β _{31–34}, A β _{32–35} and A β _{32–34} blocked both the A β _{1–42}-induced inhibition of PI4KII activity and enhancement of glutamate toxicity on cell viability. The shortest peptide among them, A β _{32–34}, showed a dose-dependent protective effect with 50% effective concentration near 1 nM, while A β _{34–32}, with a reverse amino acid sequence for A β _{32–34}, showed no protective effects. Thus, a tripeptide, A β _{32–34} i.e. Ile–Gly–Leu, may be available as a lead compound for designing effective A β antagonists.
© 2007 Elsevier Ireland Ltd. All rights reserved.

Keywords: Type II phosphatidylinositol 4-kinase; Amyloid β protein; Tripeptide (Ile–Gly–Leu); Glutamate toxicity; Alzheimer's disease

Amyloid β proteins (A β s) are pathogenic peptides of Alzheimer's disease (AD), strategies for blocking their toxicity being long searched based on their toxic mechanisms without successful efficacy in human trials [7]. Although relatively high concentrations (>10 μ M) of A β s have been used to analyse their toxicity in previous reports [11,18], pathophysiological concentrations (\leq 10 nM) of A β s were demonstrated in our laboratory to induce the enhancement of glutamate toxicity [21–23], resulting in neuronal cell death via the inhibition of type II phosphatidylinositol 4-kinase (PI4KII) activity [20,21], raising a possibility that reagents blocking such effects of A β s yield candidates for new therapeutics for AD. Most recently, we found that A β _{31–35} and A β _{20–29} peptides with partial amino acid sequences of toxic A β _{1–42} or A β _{25–35} peptides recovered such A β -induced inhibition of PI4KII activity and enhancement of glutamate toxicity, showing that a peptide as short as A β _{31–35} is effective to protect the toxic effects of pathophysiological concentrations of A β s

[21]. In the present study, we tried to determine the A β _{31–35}-derived shortest peptide fragment interfering with A β s' effects. Nine shorter peptides with 2–4 amino acid residues derived from A β _{31–35} were synthesized and applied to examine their effects on A β _{1–42}-induced inhibition of recombinant human type II α phosphatidylinositol 4-kinase (α PI4KII) activity and enhancement of glutamate toxicity in primary cultured rat hippocampal neurons.

A β _{1–42}, A β _{31–35} and nine A β _{31–35}-derived short peptides (A β _{31–34}, A β _{31–33}, A β _{31–32}, A β _{32–35}, A β _{33–35}, A β _{34–35}, A β _{32–34}, A β _{33–34} and A β _{32–33}), as well as A β _{34–32} with a reverse sequence of A β _{32–34}, were synthesized in Peptide Institute, Inc., Osaka, Japan. A β _{1–42} was synthesized by the solution procedure as reported previously [10]. A β short peptides were synthesized with an automatic peptide synthesizer, ABI 433A (Foster City, CA, USA), employing 9-fluoremethoxycarbonyl (Fmoc) chemistry on Wang resin. Stock solutions of A β _{1–42} and A β short peptides were prepared by dissolving in 10% dimethylsulfoxide at 20 μ M and aliquoted before freezing at -80° C. These peptides were applied to PI4KII assay or culture medium immediately after dilution of the stock

* Corresponding author. Tel.: +81 66993 9428; fax: +81 66992 2940.
E-mail address: kitagawa@takii.kmu.ac.jp (K. Kitagawa).

solution with distilled water without incubation for peptide aggregation.

Recombinant human type II phosphatidylinositol 4-kinase α was prepared by transfection of the plasmid (pGEX-KG) containing the open reading frame of human type II PI4K α (PI4KII α) in *Escherichia coli* DH5 α competent cells (Toyobo, Osaka, Japan) as described previously [20]. Type II phosphatidylinositol 4-kinase activity was measured by phosphorylation of exogenous L- α -phosphatidylinositol (PI, Nacalai Tesque, Kyoto, Japan) using 10 mCi/mmol [γ - 32 P] ATP (Amersham Biosciences, Piscataway, NJ, USA) as a phosphate donor [3]. Briefly, recombinant PI4KII α bound to glutathione–sepharose 4B (Amersham Pharmacia Biotech, Uppsala, Sweden) was pre-incubated with or without A β _{1–42} in the presence or absence of different short peptides for 30 min at room temperature, and then with 150 μ M PI for 5 min at room temperature in 50 μ L reaction buffer containing 20 mM Tris, pH 7.5, 100 g/L glycerol, 0.1 M NaCl, 10 g/L Triton X-100, 1 mM dithiothreitol and protease inhibitors set (Roche Diagnostics GmbH, Mannheim, Germany). Reactions were initiated by the addition of [γ - 32 P] ATP and MgCl₂ at final concentrations of 0.1 mM and 15 mM, respectively, carried out at 37 °C for 10 min and then terminated by the addition of four volumes of chloroform/methanol/HCl (20:40:1, v/v) followed by the addition of one volume each of chloroform and 0.2 M KCl to extract phospholipids. Extraction and development of phospholipids were performed as described by Andrews and Conn [1]. Labeled PIP was detected by autoradiography at –80 °C using Kodak X-Omat AR film followed by densitometry using a color scanner and a public domain image processing and analysis program

(NIH IMAGE; National Institute of Mental Health, Bethesda, MD, USA). Labeled PIP was regarded as a product of kinase activity.

Primary culture of rat hippocampal neurons was prepared as described previously [22]. The animal treatment and experimental procedures were all based on the Guidelines for Animal Care and Use Committee at Kansai Medical University. Hippocampal tissues removed from the brains of 19-day-old Wistar rat embryos were triturated in Ca²⁺- and Mg²⁺-free Hank's solution. The cells were suspended in Dulbecco's modified Eagle's medium supplemented with 4 mM L-glutamine, 100 IU/mL penicillin G sulfate, 10% fetal calf serum and 10% horse serum, and then seeded in poly-L-lysine-coated plastic dishes at a density of 2.55 \times 10⁵ cells/cm². After incubation for 2 days, the cells were exposed to 5 μ M adenine-9 β -arabinofuranoside (Ara-A) in modified Eagle's medium (MEM) supplemented with 2 mM L-glutamine and 5% horse serum for 4 days. A β _{1–42} and/or short peptides were applied for 2 days from the 8th day of culture. For monitoring glutamate excitotoxicity, the cells were exposed to glutamate (10 μ M, 10 min, in serum-free MEM) on the 10th day of culture and assayed for cell viability after another 2-day culture in the same media as used during the 8–10 days of culture. Cell viability was assayed by measuring 2-(2-methoxy-4-nitrophenyl)-3-(4-nitro-phenyl)-5-(2,4-disulfophenyl)-2H-tetrazolium monosodium salt (WST-8) reduction reflecting mitochondrial activity using a Cell Counting Kit-8 (Dojindo, Tokyo, Japan) and lactate dehydrogenase (LDH) release from damaged plasma membranes using an LDH-Cytotoxic Test (Wako, Osaka, Japan). Cl[–]-ATPase activity was measured

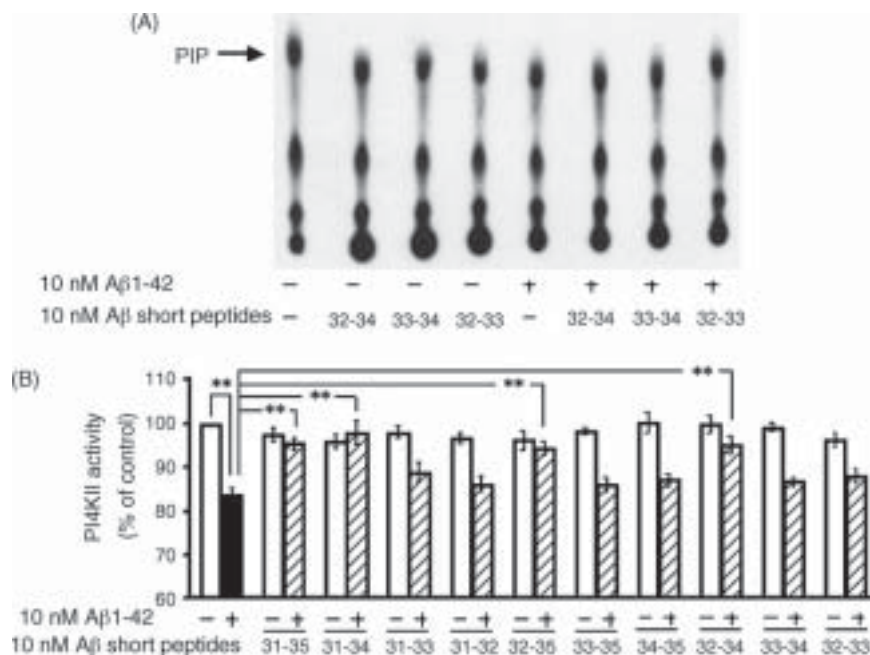


Fig. 1. Effects of A β short peptide derived from A β _{31–35} on the A β _{1–42}-induced inhibition of recombinant human PI4KII α activity. PI4KII α was prepared freshly and was pre-incubated with or without A β _{1–42} in the presence or absence of different short peptides for 30 min at room temperature. The kinase activity assay was initiated by the addition of [γ - 32 P] ATP and MgCl₂ at 37 °C for 10 min, then terminated by the addition of four volumes of chloroform/methanol/HCl (20:40:1, v/v). (A) Typical spots of phosphatidylinositol monophosphate (PIP) as products of PI4KII activities. (B) Summary of the effects of nine A β short peptides as well as A β _{31–35}. (**) p \leq 0.01, n = 4–5. Each bar represents the mean \pm S.E.M.

as described previously [22] immediately before glutamate application.

Values are expressed as the mean \pm standard error of the mean (S.E.M.). Differences between groups were evaluated by one-way analysis of variance (ANOVA) followed by Scheffe's *F*-test. When only two groups were compared, Student's paired or unpaired *t*-test was used. Differences between mean values with $p < 0.05$ were considered to be significant.

As shown in Fig. 1, 10 nM A β_{1-42} reduced recombinant PI4KII activity to $83.6 \pm 1.7\%$ of the control, while

none of the nine A β short peptides as well as A β_{31-35} at 10 nM alone affected kinase activity. When recombinant PI4KII proteins were incubated with 10 nM A β_{1-42} in the presence of 10 nM A β short peptides, inhibition by A β_{1-42} was significantly attenuated by A β_{31-35} and three A β_{31-35} -derived shorter peptides, A β_{31-34} , A β_{32-35} and A β_{32-34} , kinase activity being recovered to $95.2 \pm 1.8\%$, $98.0 \pm 2.7\%$ and $94.4 \pm 1.4\%$ of the control. The other six short peptides at the same concentration did not show any protective effects.

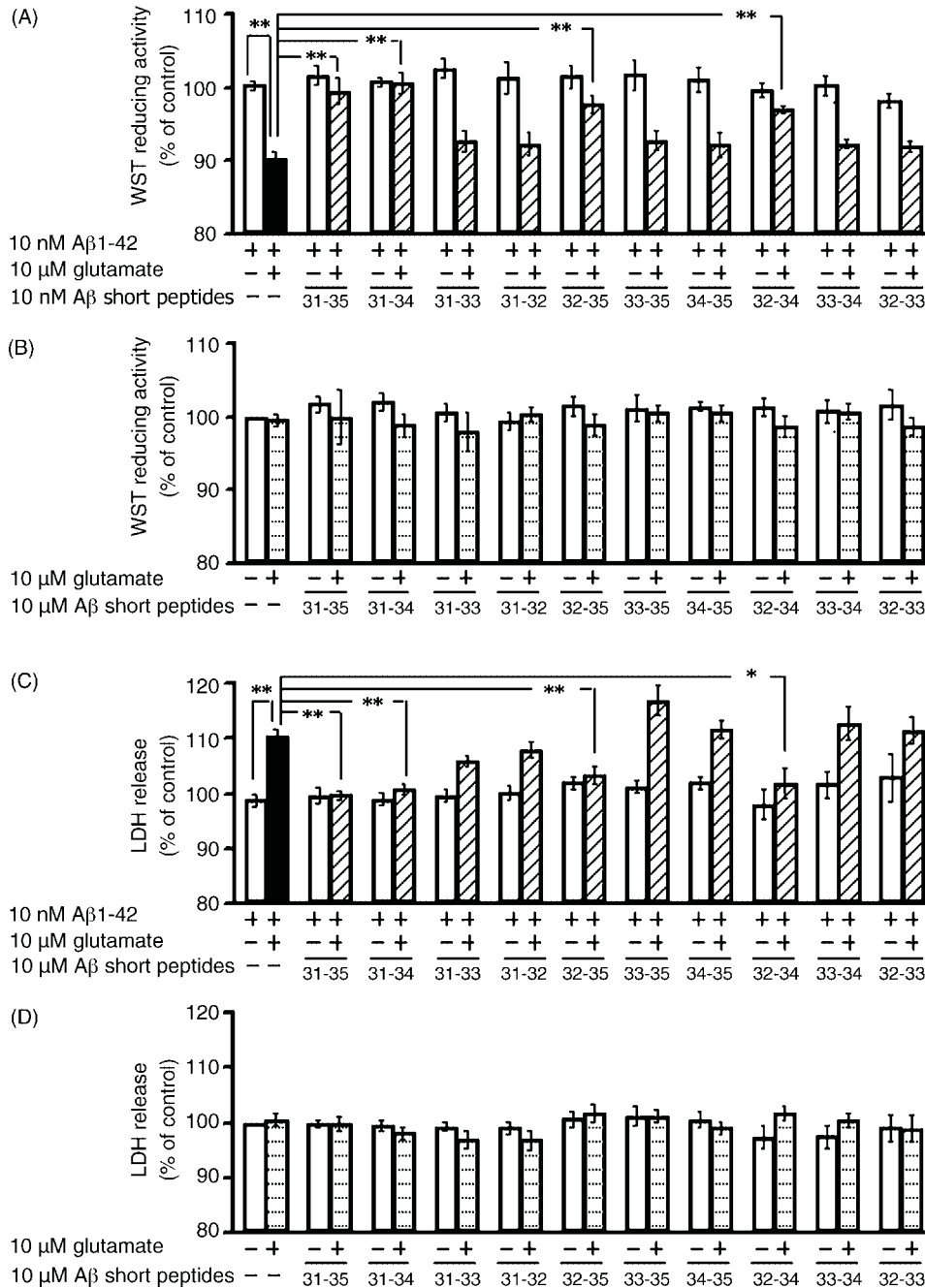


Fig. 2. Effects of A β short peptide derived from A β_{31-35} on A β_{1-42} -induced enhancement of glutamate toxicity in primary cultured hippocampal neurons. Neurons on the 8th day of culture were treated with 10 nM A β_{1-42} with or without 10 nM each of nine A β short peptides, or as well as A β_{31-35} for 2 days, and then exposed to 10 μ M glutamate for 10 min (A and C) or not (B and D). After further incubation for 2 days in the absence of glutamate, neurons were assayed for mitochondrial WST-8 reducing activity (A and B) and release of lactate dehydrogenase (C and D), (*) $p \leq 0.05$; (**) $p \leq 0.01$, $n = 6-8$. Each bar represents the mean \pm S.E.M.

To test whether these short peptides protect neurons from $A\beta_{1-42}$ -enhanced glutamate toxicity, cultured rat hippocampal neurons were treated with 10 nM $A\beta_{1-42}$ in the presence or absence of $A\beta$ short peptides. In 10 nM $A\beta_{1-42}$ -treated cells (Fig. 2A), but not in $A\beta_{1-42}$ -untreated cells (Fig. 2B), glutamate exposure (10 μ M, 10 min) significantly reduced mitochondrial activity assayed by WST-8 reduction, showing $A\beta_{1-42}$ -induced enhancement of glutamate toxicity. When neurons were treated with $A\beta_{1-42}$ in the presence of short peptides, three shorter peptides, $A\beta_{31-34}$, $A\beta_{32-35}$ and $A\beta_{32-34}$, as well as $A\beta_{31-35}$, significantly attenuated such $A\beta_{1-42}$ -induced enhancement of glutamate toxicity. The other six short peptides did not show any protective effects. None of the $A\beta$ short peptides alone or with glutamate exposure affected mitochondrial activity (Fig. 2B). Plasma membrane leakiness assayed by LDH release was significantly increased by glutamate exposure (10 μ M, 10 min) in 10 nM $A\beta_{1-42}$ -treated cells (Fig. 2C), but not in $A\beta_{1-42}$ -untreated cells (Fig. 2D), confirming the $A\beta_{1-42}$ -induced enhancement of glutamate toxicity. When neurons were treated with $A\beta_{1-42}$ in the presence of short peptides, the three shorter peptides, $A\beta_{31-34}$, $A\beta_{32-35}$ and $A\beta_{32-34}$, as well as $A\beta_{31-35}$, again significantly attenuated $A\beta_{1-42}$ plus glutamate-induced increase in LDH release (Fig. 2C). The other six short peptides did not show such protective effects. None of the

short peptides with or without glutamate exposure significantly affected LDH release (Fig. 2D). Thus, similarly to $A\beta_{31-35}$, the three short peptides, $A\beta_{31-34}$, $A\beta_{32-35}$ and $A\beta_{32-34}$, protected neurons from $A\beta_{1-42}$ -induced enhancement of glutamate neurotoxicity, the shortest effective peptide being $A\beta_{32-34}$. Since such $A\beta_{1-42}$ -induced neurotoxicity appeared to be mediated by a decrease in Cl^- -ATPase activity [22], the effects of $A\beta_{32-34}$ on the $A\beta_{1-42}$ -induced decrease in this ATPase activity was examined. As previously reported, 10 nM $A\beta_{1-42}$ reduced Cl^- -ATPase activity to $68.5 \pm 4.4\%$ ($n = 3$) of the control (without $A\beta$ treatment). Such reduction was significantly recovered in the presence of 10 nM $A\beta_{32-34}$ to $93.2 \pm 5.9\%$ ($n = 3$) of the control ($p < 0.05$), suggesting that this short peptide protected against the $A\beta_{1-42}$ -induced enhancement of glutamate toxicity by interfering with the Cl^- -dependent toxic signalling of $A\beta_{1-42}$ [25].

To test the dose dependency of the protective effects of $A\beta_{32-34}$ on $A\beta_{1-42}$ -induced inhibition of PI4KII activity, recombinant PI4KII activity was assayed in the presence of 10 nM $A\beta_{1-42}$ and/or $A\beta_{32-34}$ at concentrations ranging 0.1–50 nM. As shown in Fig. 3A and B, PI4KII activity was significantly recovered from $A\beta_{1-42}$ -induced inhibition by $A\beta_{32-34}$ over 1–50 nM, a half-maximal effect being observed at about 1 nM. $A\beta_{32-34}$ peptide alone at any concentrations did not affect kinase activity. To further test the dose dependency of $A\beta_{32-34}$ in the protec-

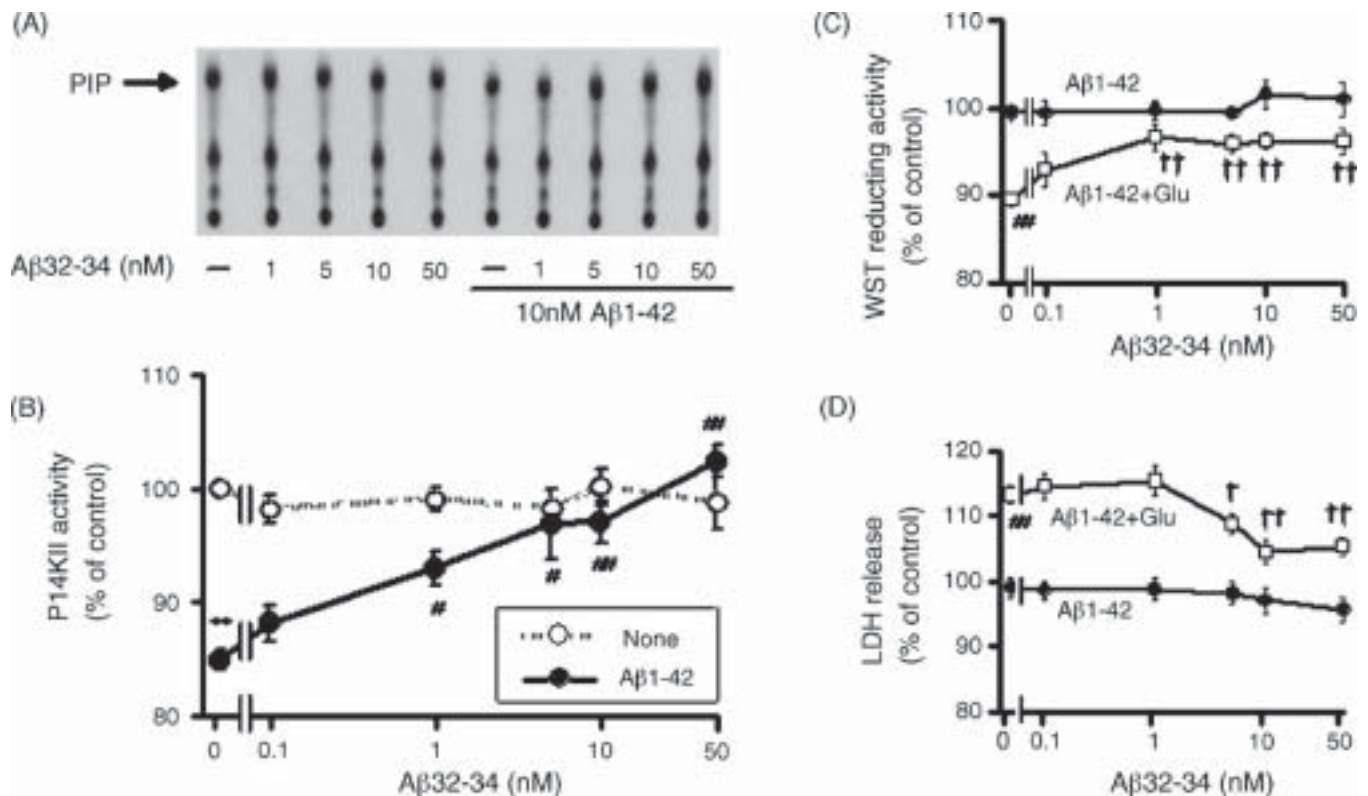


Fig. 3. Dose-dependent protective effects of tripeptide $A\beta_{32-34}$ on the $A\beta_{1-42}$ -induced inhibition of recombinant human PI4KII α activity and enhancement of glutamate toxicity in primary cultured hippocampal neurons. (A) Typical spots of phosphatidylinositol monophosphate (PIP) as products of PI4KII α activities. (B) Summary of the effects of 0.1–50 nM $A\beta_{32-34}$ on $A\beta_{1-42}$ -induced inhibition of PI4KII α activities. Neurons on the 8th day of culture were treated with 10 nM $A\beta_{1-42}$ in the presence or absence of 0.1–50 nM of $A\beta_{32-34}$ for 2 days, and then exposed to 10 μ M glutamate for 10 min. After further incubation for 2 days in the absence of glutamate, neurons were assayed for mitochondrial WST-8 reducing activity (C) and release of lactate dehydrogenase (D), (***) $p \leq 0.01$ vs. control; (#) $p \leq 0.05$; (##) $p \leq 0.01$ vs. $A\beta_{1-42}$; (†) $p \leq 0.05$; (††) $p \leq 0.01$ vs. $A\beta_{1-42}$ plus glutamate treatment. Values are shown as the mean \pm S.E.M., $n = 3$ –10 for PI4KII activity assay, $n = 11$ –15 for cell viability assay.

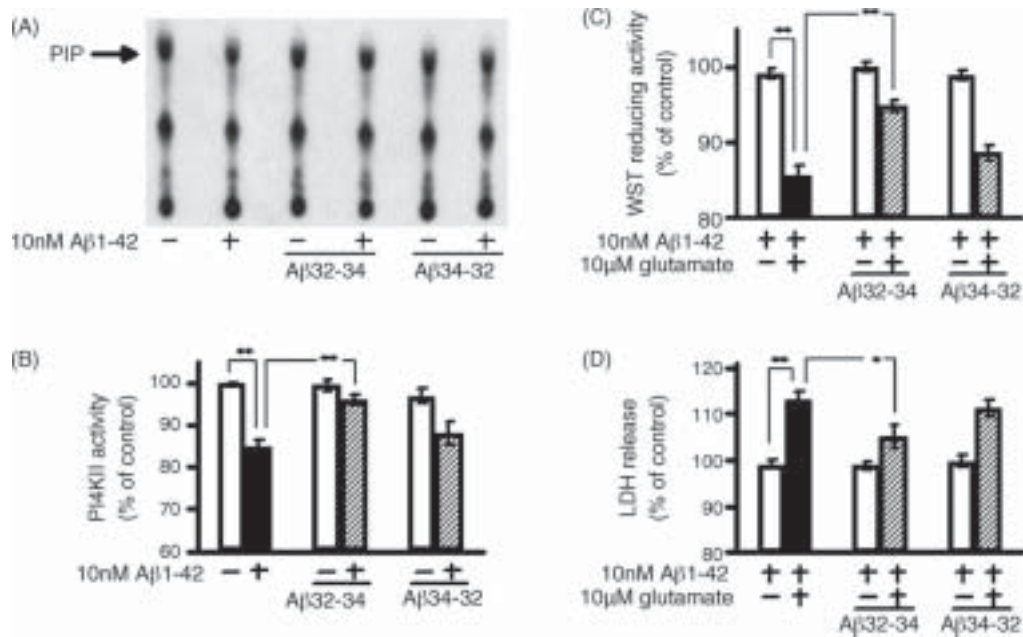


Fig. 4. Effects of a peptide Aβ₃₄₋₃₂ with reverse sequence for Aβ₃₂₋₃₄ on Aβ₁₋₄₂-induced inhibition of PI4KIIα activity and enhancement of glutamate toxicity in primary cultured hippocampal neurons. (A) Typical spots of phosphatidylinositol monophosphate (PIP) as products of PI4KIIα activities. (B) Summary of the effects of Aβ₃₂₋₃₄ and Aβ₃₄₋₃₂ on the Aβ₁₋₄₂-induced inhibition of PI4KII activities. Effects of Aβ₃₄₋₃₂ on Aβ₁₋₄₂-induced glutamate toxicity were assayed by measuring mitochondrial WST-8 reducing activity (C) and release of lactate dehydrogenase (D) following the same treatment protocol described previously, (*) $p \leq 0.05$; (**) $p \leq 0.01$, $n = 4-8$ for PI4KII activity assay; $n = 8-13$ for cell viability assay.

tion of neurons from Aβ₁₋₄₂ plus glutamate-induced cell death, WST-8 reduction and LDH release were assayed after incubation of primary cultured rat hippocampal neurons with 10 nM Aβ₁₋₄₂ and/or 0.1–50 nM Aβ₃₂₋₃₄, followed by glutamate exposure. As shown in Fig. 3C and D, 10 nM Aβ₁₋₄₂ plus glutamate (10 μM, 10 min)-induced reduction in cell viability (decrease in WST-8 reducing activity and increase in LDH release) was dose-dependently attenuated by Aβ₃₂₋₃₄, half-maximal effects being observed at about 1 nM for mitochondrial activity and at about 5 nM for LDH release, in profiles similar to that in PI4KII activity. Aβ₃₂₋₃₄ over 0.1–50 nM alone did not affect cell viability.

To test the specificity of the amino acid sequence in the protective effect of Aβ₃₂₋₃₄ (Ile–Gly–Leu), effects of a tripeptide with a reverse sequence Aβ₃₄₋₃₂ (Leu–Gly–Ile) were examined. As shown in Fig. 4A and B, incubation of recombinant PI4KIIα with 10 nM Aβ₃₄₋₃₂ did not show any protective effect on the Aβ₁₋₄₂-induced inhibition of kinase activity in contrast to the protective effect of 10 nM Aβ₃₂₋₃₄. Aβ₃₄₋₃₂ at 10 nM alone did not affect kinase activity. The effects of Aβ₃₄₋₃₂ on Aβ₁₋₄₂ plus glutamate-induced cell death were also examined. As shown in Fig. 4C and D, 10 nM Aβ₃₄₋₃₂ did not attenuate Aβ₁₋₄₂-enhanced glutamate neurotoxicity in contrast to the protective effects of 10 nM Aβ₃₂₋₃₄. Aβ₃₄₋₃₂ at 10 nM alone, or co-incubation with Aβ₁₋₄₂ or glutamate did not affect the cell viability (data not shown).

PI4KIIα is the major one of PI 4-kinases (PI4KIIα, PI4KIIβ and PI4KIIs) in brain, and catalyzes the production of phosphatidylinositol 4-phosphate (PI4P) from phosphatidylinositol which is further phosphorylated to form PI (4,5)P₂ and PI (3,4,5)P₃ as important regulatory molecules in many intra-

cellular signal pathways [2]. In the brains of AD patients, phosphatidylinositol kinase activities [4,19] and membrane phosphoinositides [16,17] are significantly lower than those in age-matched non-AD brains. In our previous reports, PIP and PIP₂ levels in the neuronal plasma membrane of cultured rat hippocampal neurons were reduced by a low concentration of Aβ₂₅₋₃₅ (10 nM), along with a decrease in the activity of PI4P-requiring Cl⁻-pump/ATPase and a resulting increase in intracellular Cl⁻ concentration ([Cl⁻]_i) in neurons [22,23]. Such an increase in [Cl⁻]_i appeared to lower the level of phosphorylated Akt, a cell survival signal molecule, on glutamate exposure, resulting in the enhancement of glutamate neurotoxicity [25]. Thus, direct inhibition of PI4KII by Aβ [20] is probably one of the major pathogenic mechanisms of Aβ.

In the present study, 10 nM each of tetrapeptides Aβ₃₁₋₃₄ and Aβ₃₂₋₃₅, and a tripeptide, Aβ₃₂₋₃₄, as well as Aβ₃₁₋₃₅ [21] were demonstrated to effectively protect against the Aβ₁₋₄₂-induced inhibition of PI4KII activity and enhancement of glutamate toxicity without toxic effects of the peptides themselves. In previous reports from other groups, Aβ₃₁₋₃₅ at 0.1 μM suppressed the induction of long-term potentiation in rat hippocampus [24], at 20 μM inhibited fast axonal transport in cultured rat hippocampal neurons [9], and at 40 μM induced apoptosis in PC 12 cells [15]. Modified Aβ₃₁₋₃₅ peptides with oxidized Met-35 or with norleucine substituted for Met-35 reportedly attenuated and even eliminated such Aβ₃₁₋₃₅-induced neurotoxicity, suggesting a crucial role of the redox state of the single Met-35 residue in Aβ₃₁₋₃₅ toxicity [5,14]. Despite these reports, Aβ₃₁₋₃₅ at 10 nM used in our studies ([21] and the present report) showed a neuroprotective effect against Aβ₁₋₄₂-induced neurotoxicity without any toxic effects in itself. The mechanisms that differentiate

these responses may be differences in A β _{31–35} concentrations used and/or experimental parameters. A β _{31–35}-derived peptides without Met-35 such as A β _{32–34} may be beneficial to their low toxicities even at rather higher concentrations.

On the other hand, propionyl-Ile-Ile-Gly-Leu (Pr-IIGL), a derivative of the tetrapeptide A β _{31–34}, has been reported to antagonize A β _{1–42} (1 μ M and 200 μ M)-mediated toxicity both in vitro at 1 μ M in glial cells [13] and in vivo at 200 μ M in rat nucleus basalis [8]; while it induced massive hyperphosphorylation of τ -protein and swelling of cell bodies at 0.125 μ M in primary cultured hippocampal neurons [12]. RIIGL_a, a pentapeptide synthesized based on tetrapeptide IIGL, was reportedly non-toxic to neurons at 50 μ M and reduced the cytotoxic effect of 10 μ M A β _{1–42} by inhibiting A β _{1–42} aggregation [6]. In this study, A β _{31–34} was found to be neuroprotective against A β _{1–42}-induced neurotoxicity at about a 1000 times lower concentration as compared with these studies.

In conclusion, a tripeptide, A β _{32–34}, is the shortest peptide ever reported showing protective effects against A β -enhanced glutamate neurotoxicity by attenuating the A β _{1–42}-induced inhibition of PI4KII activity, a new target in the pathogenic mechanism of Alzheimer's disease. The amino acid sequence Ile-Gly-Leu in A β _{32–34} may serve as a lead molecule for designing a novel putative drug for the treatment of Alzheimer's disease.

Acknowledgements

We thank Dr. Shane Minogue (Centre for Molecular Cell Biology, Department of Medicine, Royal Free and University College Medical School, London, UK) for the generous gift of plasmid containing the open reading frame of human type II PI4K α . This work was supported by grants from the Japanese Private School Promotion Foundation, High-Tech Research Center, the Science Frontier program and the 21st Century Center of Excellence (COE) program of the Ministry of Education, Culture, Sports, Science and Technology, Japan.

References

- [1] W.V. Andrews, P.M. Conn, Measurement of inositol phospholipids metabolites by one-dimensional thin-layer chromatography, *Methods Enzymol.* 141 (1987) 156–168.
- [2] A. Balla, T. Balla, Phosphatidylinositol 4-kinases: old enzymes with emerging functions, *Trends Cell Biol.* 16 (2006) 351–361.
- [3] B. Barylko, S.H. Gerber, D.D. Binns, N. Grichine, M. Khvotchev, T.C. Südhof, J.P. Albanesi, A novel family of phosphatidylinositol 4-kinases conserved from yeast to humans, *J. Biol. Chem.* 276 (2001) 7705–7708.
- [4] J. Bothmer, M. Markerink, J. Jolles, Phosphoinositide kinase activities in synaptosomes prepared from brains of patients with Alzheimer's disease and controls, *Neurosci. Lett.* 176 (1994) 169–172.
- [5] M.E. Clementi, S. Marini, M. Coletta, F. Orsini, B. Giardina, F. Misiti, A β (31–35) and A β (25–35) fragments of amyloid beta-protein induce cellular death through apoptotic signals: role of the redox state of methionine-35, *FEBS Lett.* 579 (2005) 2913–2918.
- [6] L. Fülöp, M. Zarándi, Z. Datki, K. Soós, B. Penke, β -Amyloid-derived pentapeptide RIIGL_a inhibits A β _{1–42} aggregation and toxicity, *Biochem. Biophys. Res. Commun.* 324 (2004) 64–69.
- [7] T.E. Golde, Disease modifying therapy for AD? *J. Neurochem.* 99 (2006) 689–707.
- [8] T. Harkany, I. Ábrahám, G. Laskay, W. Timmerman, K. Jost, M. Zarándi, B. Penke, C. Nyakas, P.G. Luiten, Propionyl-IIGL tetrapeptide antagonizes β -amyloid excitotoxicity in rat nucleus basalis, *Neuroreport* 10 (1999) 1693–1698.
- [9] H. Hiruma, T. Katakura, S. Takahashi, T. Ichikawa, T. Kawakami, Glutamate and amyloid β -protein rapidly inhibit fast axonal transport in cultured rat hippocampal neurons by different mechanisms, *J. Neurosci.* 23 (2003) 8967–8977.
- [10] T. Inui, J. Bódi, H. Nishio, Y. Nishiuchi, T. Kimura, Synthesis of amyloid β -peptides in solution employing chloroform-phenol mixed solvent for facile segment condensation of sparingly soluble protected peptides, *Lett. Pept. Sci.* 8 (2001) 319–330.
- [11] K.J. Ivins, J.K. Ivins, J.P. Sharp, C.W. Cotman, Multiple pathways of apoptosis in PC12 cells, *J. Biol. Chem.* 274 (1999) 2107–2112.
- [12] E. Lain, B. Penke, A. Delacourte, D. Gündisch, H. Schröder, B. Witter, Effects of A β _{1–42} fibrils and of the tetrapeptide Pr-IIGL on the phosphorylation state of the τ -protein and on the α 7 nicotinic acetylcholine receptor in vitro, *Eur. J. Neurosci.* 21 (2005) 879–888.
- [13] G. Laskay, M. Zarándi, J. Varga, K. Jost, A. Fónagy, C. Torday, L. Latzkovits, B. Penke, A putative tetrapeptide antagonist prevents β -amyloid-induced long-term elevation of [Ca²⁺]_i in rat astrocytes, *Biochem. Biophys. Res. Commun.* 235 (1997) 479–481.
- [14] F. Misiti, M.E. Clementi, G. Tringali, M. Vairano, F. Orsini, M. Pezzotti, P. Navarra, B. Giardina, G. Pozzoli, Fragment 31–35 of β -amyloid peptide induces neurodegeneration in rat cerebellar granule cells via bax gene expression and caspase-3 activation. A crucial role for the redox state of methionine-35 residue, *Neurochem. Int.* 49 (2006) 525–532.
- [15] F. Misiti, B. Sampaiolese, M. Pezzotti, S. Marini, M. Coletta, L. Ceccarelli, B. Giardina, M.E. Clementi, A β (31–35) peptide induce apoptosis in PC 12 cells: contrast with A β (25–35) peptide and examination of underlying mechanisms, *Neurochem. Int.* 46 (2005) 575–583.
- [16] J.W. Pettegrew, K. Panchalingam, R.L. Hamilton, R.J. McClure, Brain membrane phospholipid alterations in Alzheimer's disease, *Neurochem. Res.* 26 (2001) 771–782.
- [17] M.R. Prasad, M.A. Lovell, M. Yatin, H. Dhillon, H. Dhillon, W.R. Markesbery, Regional membrane phospholipid alterations in Alzheimer's disease, *Neurochem. Res.* 23 (1998) 81–88.
- [18] C.M. Troy, S.A. Rabacchi, Z.H. Xu, A.C. Maroney, T.J. Connors, M.L. Shelanski, L.A. Greene, β -Amyloid-induced neuronal apoptosis requires c-Jun N-terminal kinase activation, *J. Neurochem.* 77 (2001) 157–164.
- [19] M.A. Wallace, Effects of Alzheimer's disease-related beta amyloid protein fragments on enzymes metabolizing phosphoinositides in brain, *Biochim. Biophys. Acta* 1227 (1994) 183–187.
- [20] B. Wu, K. Kitagawa, N.Y. Zhang, B. Liu, C. Inagaki, Pathophysiological concentrations of amyloid β proteins directly inhibit rat brain and recombinant human type II phosphatidylinositol 4-kinase activity, *J. Neurochem.* 91 (2004) 1164–1170.
- [21] B. Wu, K. Kitagawa, B. Liu, N.Y. Zhang, Z.M. Xiong, C. Inagaki, Attenuation of amyloid β (A β)-induced inhibition of phosphatidylinositol 4-kinase activity by A β fragments, A β 20–29 and A β 31–35, *Neurosci. Lett.* 396 (2006) 148–152.
- [22] K. Yagyu, K. Kitagawa, T. Irie, B. Wu, X.T. Zeng, N. Hattori, C. Inagaki, Amyloid β proteins inhibit Cl[−]-ATPase activity in cultured rat hippocampal neurons, *J. Neurochem.* 78 (2001) 569–576.
- [23] K. Yagyu, K. Kitagawa, B. Wu, N.Y. Zhang, T. Irie, N. Hattori, C. Inagaki, Protective effects of estradiol against amyloid β protein-induced inhibition of neuronal Cl[−]-ATPase activity, *Neuropharmacology* 43 (2002) 1297–1304.
- [24] L. Ye, J.T. Qiao, Suppressive action produced by β -amyloid peptide fragment 31–35 on long-term potentiation in rat hippocampus is N-methyl-D-aspartate receptor-independent: it's offset by (−)huperzine A, *Neurosci. Lett.* 275 (1999) 187–190.
- [25] N.Y. Zhang, K. Kitagawa, B. Wu, Z.M. Xiong, C. Inagaki, Chloride-dependency of amyloid β protein-induced enhancement of glutamate neurotoxicity in cultured rat hippocampal neurons, *Neurosci. Lett.* 399 (2006) 175–180.



Soybean-derived phosphatidylinositol inhibits *in vivo* low concentrations of amyloid β protein-induced degeneration of hippocampal neurons in V337M human tau-expressing mice

Nan-Yan Zhang, Kaori Kitagawa, Naoki Hattori, Yasuhisa Nakayama, Zheng-Mei Xiong, Bo Wu, Bing Liu, Chiyoko Inagaki *

Department of Pharmacology, Kansai Medical University, Fumizono-cho 10-15, Moriguchi, Osaka 570-8506, Japan

Received 14 September 2006; accepted 20 February 2007

Abstract

In our previous reports using primary cultured rat hippocampal neurons, pathophysiological concentrations (≤ 10 nM) of amyloid β proteins (A β s) showed neurotoxicity via a phosphatidylinositol metabolism disorder, and soybean-derived phosphatidylinositol protected the neurons against the A β 's neurotoxicity. In the present study, such a neurotoxic effect of A β and a neuroprotective effect of phosphatidylinositol were examined *in vivo* using transgenic mice expressing V337 M human tau. Intrahippocampal CA1 injection of 1.5 μ l of 100 nM or 1 μ M A β 25–35 increased the number of degenerating neurons with an apoptotic feature in bilateral hippocampal CA1, CA2, CA3 and dentate gyrus regions in 1 month, demonstrating an *in vivo* neurotoxic effect of A β at lower concentrations after diffusion. Intrahippocampal co-injection or intracerebroventricular administration of 1.5 μ l of 500 nM phosphatidylinositol prevented the A β 25–35-induced neuronal degeneration in all the hippocampal regions, while co-injection of another acidic phospholipid, phosphatidylserine (1.5 μ l, 500 nM) with A β 25–35 showed no protective effects. Thus, exogenously applied phosphatidylinositol appeared to minimize the toxic effects of A β *in vivo*. These results suggest that soybean-derived phosphatidylinositol may be effective in the treatment of Alzheimer's disease.

© 2007 Elsevier Inc. All rights reserved.

Keywords: Amyloid β ; peptide (25–35); Phosphatidylinositol; Neurodegeneration; Phosphatidylserine; Alzheimer's disease

Introduction

Alzheimer's disease (AD) is one of the most common progressive neurodegenerative diseases, afflicting over one percent of individuals over age 65 years, with characteristic pathological features such as neuronal loss, intraneuronal neurofibrillary tangles composed of hyperphosphorylated tau, and extracellular senile plaques primarily composed of amyloid β proteins (A β s) (Selkoe, 2001). We previously reported that pathophysiological concentrations (≤ 10 nM) of A β enhanced neurotoxicity of a physiological concentration (10 μ M) of

glutamate resulting in neuronal degeneration in association with decreases in the plasma membrane levels of phosphatidylinositol (PI) and phosphorylated PI (PIP and PIP₂) in primary cultured rat hippocampal neurons (Yagyu et al., 2001). Since such neurotoxicity of A β was prevented by exogenously applied soybean-derived PI (Zhang et al., 2003), it seems to be worthwhile to test *in vivo* effects of the phospholipid on A β -induced degeneration of neurons. To our knowledge, however, *in vivo* degenerating effects of pathophysiological concentrations of exogenous A β can hardly be observed in natural animals. We recently found that intrahippocampal administration of such concentrations of A β degenerated hippocampal neurons of mice expressing mutant human tau (V337M) in 1 month. We therefore examined the *in vivo* effects of soybean-derived PI against neuronal damage induced by intrahippocampal injection of A β in the transgenic mice.

* Corresponding author. Tel.: +81 66993 9427; fax: +81 66992 2940.

E-mail address: inagaki@takii.kmu.ac.jp (C. Inagaki).

Materials and methods

Materials

Transgenic mice expressing V337 M human tau were kindly donated by Dr. Akihiko Takashima, Laboratory for Alzheimer's disease, The Institute of Physical and Chemical Research (RIKEN), Saitama, Japan. Soybean-derived phosphatidylinositol (PI) was purchased from Nacalai Tesque, Kyoto, Japan; A β 25–35, soybean-derived phosphatidylserine (PS) and pyronin Y were from Sigma, St. Louis, MO, USA; Tissue-Tek O.C.T. compound was from Sakura Finetek USA, Torrance, CA, USA; 3,3'-diaminobenzidine tetrahydrochloride (DAB) and methyl green solution and Mayer's hematoxylin solution were from Wako, Osaka, Japan; Histofine simple stain DAB solution was from Nichirei Bioscience, Tokyo, Japan; entellan was from Merck KGaA, Darmstadt, Germany; and anti-cleaved caspase-3 antiserum was from Cell Signaling Technology, Inc., Danvers, MA, USA. Other reagents were of the highest quality commercially available.

Intrahippocampal and intracerebroventricular injection

Four-month-old V337 M human tau transgenic mice were anesthetized with trichloroacetaldehyde monohydrate (0.5 g/kg). An aliquot (1.5 μ l) of solution containing A β 25–35 (100 nM or 1 μ M) and/or PI (500 nM) or PS (500 nM), all dissolved in artificial cerebrospinal fluid (aCSF: 124 mM NaCl, 2.5 mM KCl, 25 mM NaHCO₃, 1.25 mM NaH₂PO₄, 10 mM glucose, 1.3 mM MgSO₄, 2.0 mM CaCl₂, pH 7.4), were injected into the CA1 region of the hippocampal formation of the right hemisphere (coordinates: AP –2.0 mm from the bregma, LAT –1.0 mm, DV +1.5 mm) over 7 min (about 0.22 μ l/min). The needle was kept in the injection site for another 10 min and then slowly withdrawn. Since, in our previous *in vitro* study, 50 nM of soybean-derived PI prevented 10 nM A β 's neurotoxicity (Zhang et al., 2003), the concentrations of A β and PI used in this *in vivo* study were determined considering possible diffusion of the solutes. In a series of experiments, PI (1.5 μ l, 500 nM) was administered into the lateral ventricle contralateral to the A β -injection site (AP –0.2 mm from the bregma, LAT +1.0 mm, DV +2.5 mm). None of the mice developed infections or died during the experiments.

Preparation of brain sections

One month after the injection, mice were deeply anesthetized with ether and perfused transcardially with saline for 10 min and then with 4% paraformaldehyde in 0.1 M sodium phosphate buffer (pH 7.4) for 10 min. The brains were removed, post-fixed in the same fixation buffer for 3 days, and then immersed sequentially in a 20% and 30% sucrose solution for 24 h each. The tissues were mounted in Tissue-Tek O.C.T. compound and frontal sections near the injection sites were cut with a cryostat at 6 μ m in thickness and mounted directly on amino silane coated slides.

Histology

To evaluate neurodegeneration, methyl green pyronin Y (MGPY) staining, terminal deoxynucleotidyl transferase dUTP nick-end labeling (TUNEL) staining and cleaved caspase-3 staining were used. For MGPY staining, staining solution was freshly prepared by adding 100 mg of pyronin Y to 50 ml of 0.5% methyl green stock solution. Brain sections were placed in the staining solution for 3 h at room temperature, rinsed with distilled water, and twice dehydrated with t-butyl alcohol for 3 s. The slides were immersed in xylene and then coverslipped with entellan mounting media. In MGPY staining sections, DNA is stained blue and RNA is stained pink. Viable cells exhibited a light blue nucleus, confirming nuclear integrity, and a pink cytoplasm, indicative of RNA transcription. Damaged cells exhibited hyperchromatic nuclei and cytoplasm, or lack of cytoplasmic (RNA) staining (Cheung et al., 2005). TUNEL staining using an *in situ* apoptosis detection kit (Takara, Shiga, Japan) was performed according to manufacturer's instruction to detect DNA fragmentation. For cleaved caspase-3 staining, frozen sections were cut on a cryostat and stained using an avidin-biotin complex method (Vector Labs, Burlingame, CA, USA). After incubation with anti-cleaved caspase-3 antiserum (1:70), the sections were further incubated with biotinylated goat anti-rabbit IgG (5 μ g/ml: Vector Labs) and the bound antibodies were visualized using DAB. The nuclei were counterstained with hematoxylin.

Image analysis

Sections were examined under the light microscope. To quantify degenerating neurons, 40x magnifications were used. The number of living or degenerating neurons in each hippocampus was counted in 6–8, 2, 4 and 4 separate optical fields (210 μ m \times 170 μ m) in CA1, CA2, CA3 and dentate gyrus regions, respectively, twice separately by two persons without knowledge of treatments. Population of degenerating neurons was expressed as a percentage to the total counted neurons in each region (215–352, 67–109, 119–192 and 251–440 neurons in CA1, CA2, CA3 and dentate gyrus from a hemisphere, respectively).

Statistical analysis

Summarized data were expressed as mean \pm SE. Differences between mean values were evaluated by analysis of variance (ANOVA) followed by Fisher's PLSD (protected least significant difference) test, and those with $p < 0.05$ were considered to be significant.

Results

As shown in Fig. 1A, injection of the materials into hippocampal CA1 region was affirmed by the needle track in each animal. Intrahippocampal injection of 1.5 μ l of 100 nM amyloid β peptide (A β ; A β 25–35) resulted in an increase in the number of degenerating neurons scattering throughout the hippocampal

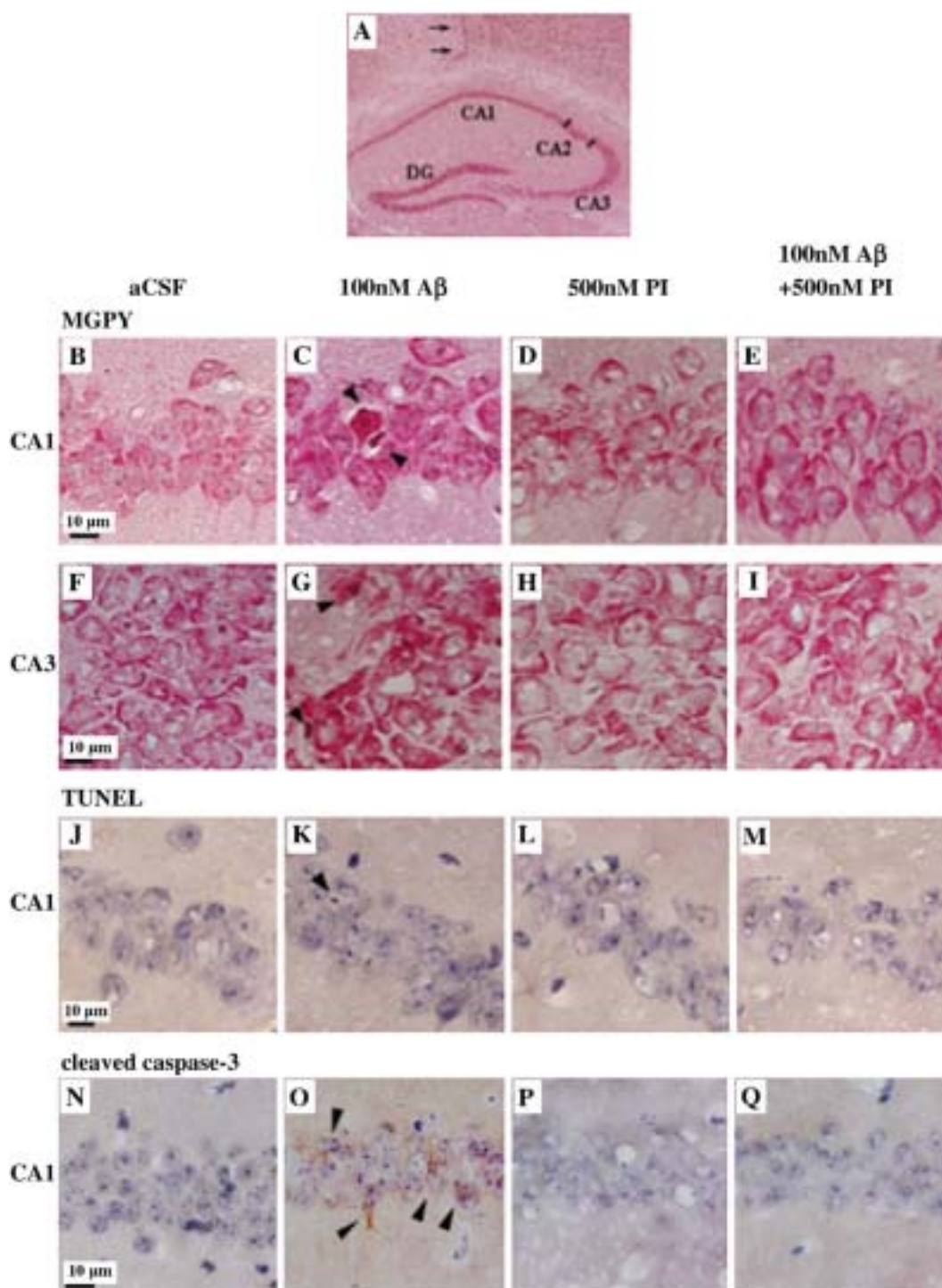


Fig. 1. Neurodegeneration after intrahippocampal injection of amyloid β protein ($A\beta$) and/or phosphatidylinositol (PI) in mice expressing V337M human tau. (A) Hippocampal section showing the injection site. Arrows point out the needle track. Brain sections were stained with methyl green pyronin Y (MGPY, A–I), TUNEL (J–M) or anti-cleaved caspase-3 antibody (N–Q) 1 month after the intrahippocampal injection of 1.5 μ l of the following solutions: artificial cerebrospinal fluid (aCSF) (B, F, J and N); 100 nM $A\beta$ 25–35 (C, G, K and O); 500 nM PI (D, H, L and P); 100 nM $A\beta$ 25–35 + 500 nM PI (E, I, M and Q). B–E, J–M and N–Q: Examples of the CA1 pyramidal cell layer. F–I: Examples of the CA3 pyramidal cell layer. Arrowheads point out the degenerating neurons (C, G) or apoptotic neuron (K, O). Scale bar = 10 μ m.

formation; CA1, CA2, CA3 and dentate gyrus (DG). In MGPY stained sections, two types of abnormally stained cells were observed; one, mainly observed in CA1 and CA2 regions, was characterized by intensely stained cytoplasm by pyronin Y as

well as dispersed chromatin clumps or lack of nuclear structure (Fig. 1C), and the other type mainly existing in CA3 and DG regions showed hyperchromatic nucleus and lack of cytoplasmic (RNA) staining (Fig. 1G). The injection of artificial

cerebrospinal fluid (aCSF) or phosphatidylinositol (PI) alone did not cause such neuronal degeneration (Fig. 1B, D, F and H). Co-injection of 500 nM PI with A β 25–35 (1.5 μ l) prevented the A β -induced neuronal degeneration (Fig. 1E and I).

To test the involvement of apoptotic mechanism in the neuronal degeneration, TUNEL staining was carried out. Injection of A β 25–35 induced the occurrence of TUNEL-positive cells, i.e. neurons with apoptotic nuclei (Fig. 1K) in 2 of 6 mice examined, no such apoptotic cells being detected in aCSF-injected control mice (Fig. 1J). In mice co-injected with PI and A β , or those injected with PI alone, TUNEL-positive cells were not observed at all (Fig. 1L and M). Another apoptotic effector, activated (i.e. cleaved) caspase-3, was also stained. Injection of A β 25–35 markedly increased the number of neurons with activated caspase-3 (Fig. 1O) as compared with those in aCSF-injected control mice (Fig. 1N). In the mice co-injected with PI and A β (Fig. 1Q) or those injected with PI alone (Fig. 1P), such activation of caspase-3 was not observed. Though the number of TUNEL-positive neurons in A β -injected mice was not as much as that of degenerating neurons in MGPY-stained sections, the number of active caspase-3 positive neurons appeared to change in a parallel and comparable manner to that in the degenerating neurons in MGPY-staining (Table 1), suggesting that an apoptotic mechanism may be involved in the A β -induced neuronal degeneration.

Changes in the number of degenerating neurons, as expressed by percentage of damaged neurons to total counted neurons, in each region of the ipsilateral (A β -injected) side of hippocampi were summarized in Fig. 2A. Injection of 1.5 μ l of 100 nM A β 25–35 significantly increased the number of degenerating neurons in all ipsilateral hippocampal regions; CA1, CA2, CA3 and DG as compared with those in aCSF-injected control mice. DG appeared to be less vulnerable to A β 25–35 compared with the other regions. After the injection of 10 times higher concentration of A β (1.5 μ l, 1 μ M), no further increases in the number of degenerating neurons were observed, except a slight increase in DG. When PI was co-injected, the A β -induced neuronal damage was prevented in all regions (Fig. 2A, +PI). To rule out the possibility that PI inactivated A β 25–35 in the mixture within injection pipette, PI was then injected separately into the lateral ventricle of contralateral hemisphere (+PI i.c.v.). The protective effect of

PI was again observed in all hippocampal regions, suggesting that exogenously applied PI blocked A β 's neuronal toxicity *in vivo*. In contrast, another acidic phospholipid, phosphatidylserine (PS), did not show any protective effects against the A β -induced neuronal degeneration (Fig. 2A, +PS), suggesting that the protective effect of PI is not due to a non-specific feature of acidic phospholipid.

Fig. 2B shows the changes in the number of degenerating neurons in the contralateral (left, non-injected side) hippocampi of the A β -injected mice with or without PI or PS administration. The changes were quite similar to those observed in the ipsilateral hippocampi (Fig. 2A), suggesting massive diffusion of injected A β as well as phospholipids at least into the space of the bilateral whole hippocampus.

Discussion

The transgenic mice used in this study reportedly develop AD-like histological changes after 11-month-old (Tanemura et al., 2002). In this study, exogenously administered A β 25–35 (100 nM, 1.5 μ l) into their hippocampi at an earlier stage (4-month-old) induced mild but significant degeneration in hippocampal neurons after 1 month, suggesting some acceleration of neuronal degeneration by the A β . When wild type rats were used, much higher concentrations of A β (0.5–1.5 mM, 1–2 μ l) were administered into hippocampus to detect A β -induced neuronal cell death (Frautschy et al., 1991; Kowall et al., 1991; Miguel-Hidalgo and Cacabelos, 1998; Ryu et al., 2004; Stepanichev et al., 2003). In these studies, neuronal loss or degeneration occurred massively over wide areas of hippocampus in about 1 week after A β injection. Compared with such rather acute and severe neuronal degenerations induced by approximately 1000 times higher concentrations of A β , neuronal degeneration observed under the present conditions may represent the neuronal degeneration similar to that observed in chronic process of human AD.

Since the injected A β also affected the contralateral hippocampus, A β at concentrations after diffusion appears to be cytotoxic. When 1.5 μ l of 100 nM A β 25–35 was injected, simple calculation for A β concentration after diffusion in ipsilateral or bilateral hippocampus based on their weight (27 mg each) yields 5.6 or 2.8 nM, respectively. Considering the

Table 1
Percentage of degenerating or apoptotic neurons in mouse hippocampi injected with A β 25–35 and/or phosphatidylinositol (PI)

Treatment	Degenerating neurons		Apoptotic neurons	
	Total neurons counted	Degenerating neurons (%)	Total neurons counted	Apoptotic neurons (%)
aCSF	947 \pm 36	15 \pm 2.0 (1.6 \pm 0.18)	1523 \pm 28	4 \pm 1.2 (0.2 \pm 0.08)
100 nM A β	992 \pm 71	42 \pm 5.6 (4.4 \pm 0.65*)	1523 \pm 437	35 \pm 8.2 (2.4 \pm 0.17*)
1 μ M A β	846 \pm 54	48 \pm 4.8 (5.8 \pm 0.70*)	1342 \pm 136	30 \pm 8.8 (2.2 \pm 0.54*)
500 nM PI	1008 \pm 54	12 \pm 1.6 (1.1 \pm 0.14)	1358 \pm 47	7 \pm 3.7 (0.5 \pm 0.26)
PI+100 nM A β	993 \pm 70	11 \pm 2.8 (1.2 \pm 0.30)	1717 \pm 71	4 \pm 0.3 (0.3 \pm 0.02)
PI+1 μ M A β	927 \pm 76	11 \pm 1.8 (1.3 \pm 0.27)	1423 \pm 288	10 \pm 0.9 (0.7 \pm 0.10)

An aliquot (1.5 μ l) of solution containing A β 25–35 (100 nM or 1 μ M) and/or PI (500 nM) dissolved in artificial cerebrospinal fluid (aCSF) was injected into the CA1 region of the right hippocampus of four-month-old V337M human tau expressing mouse. Total and MGPY-positive degenerating or cleaved caspase-3 positive apoptotic neurons of whole hippocampi on the injected side were counted. Values are mean \pm SEM (n =3–17).

* p <0.01 vs. each control (aCSF injected).

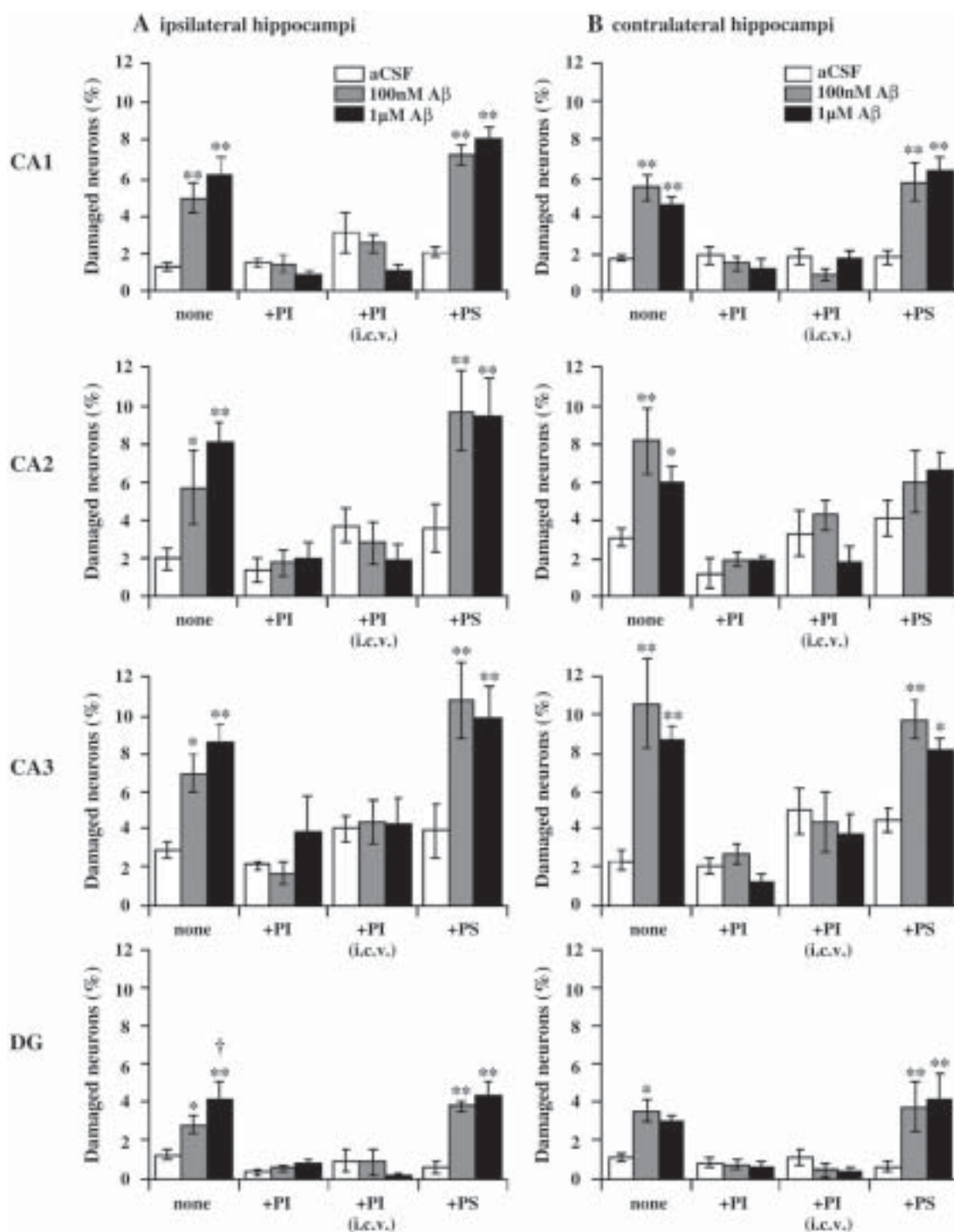


Fig. 2. Effects of phosphatidylinositol (PI) and phosphatidylserine (PS) on the A β -induced neurodegeneration in CA1–CA3 pyramidal cells and dentate gyrus (DG) granule cells from ipsilateral (injected side; A) and contralateral (B) hippocampi. Brain sections were prepared and stained with methyl green pyronin Y (MGPY) 1 month after the intrahippocampal injection of 1.5 μ l aCSF (white bar) or A β 25–35 (100 nM, gray bar or 1 μ M, black bar). PI (500 nM) was co-injected into the CA1 region of hippocampus with A β , or intracerebroventricularly (i.c.v.) injected separately. PS (500 nM) was co-injected into the CA1 region with A β . The damaged neurons in each hippocampal region were expressed as a percentage of the total counted neuronal cell population in each region. Data are presented as the mean \pm S.E. from 4 to 15 animals. * p < 0.05 ** p < 0.01 versus each control (aCSF-injected). † p < 0.05 versus 100 nM A β .

low concentration range of toxic A β and the relatively short period (1 month) to obtain the results, this protocol may be a suitable model to evaluate neurotoxicity of A β and *in vivo* anti-A β activity of test drugs.

Phosphatidylinositol (PI) is an essential phospholipid not only in maintaining membrane structure, but also required in the production of other phosphoinositides (PIP, PIP₂ and PIP₃) with important roles in cellular signal transduction. Since the

phosphoinositides levels are reportedly decreased in the brains of AD patients and A β -treated neurons (Pettegrew et al., 2001; Prasad et al., 1998; Stokes and Hawthorne, 1987; Yagyu et al., 2001), supplement of PI rescued A β 's toxicity probably through PI-related amelioration of cell signaling. As we previously reported (Zeng et al., 1994), phosphatidylinositol-4-monophosphate (PI4P) is required for the maximal activity of Cl⁻-ATPase/pump, a candidate for outwardly directed active Cl⁻ transport system. Pathophysiological concentrations of A β reduced the Cl⁻-ATPase activity via inhibition of PI4P production in plasma membranes, resulting in an increase in [Cl⁻]_i and enhanced glutamate neurotoxicity in primary cultured rat hippocampal neurons (Wu et al., 2004; Yagyu et al., 2001). An increase in neuronal [Cl⁻]_i appeared to result in enhancement of glutamate neurotoxicity through a decreased level of phosphorylated Akt, an important signaling molecule for cell survival (Zhang et al., 2006), probably due to inhibition of an Akt phosphorylating enzyme PDK2 by an increase in [Cl⁻]_i (Hresko et al., 2003). Exogenously applied PI protected the neurons against such A β 's neurotoxicity in neuronal cultures *in vitro* (Wu et al., 2002; Zhang et al., 2003), and *in vivo* in this study, supporting an idea that A β -induced neuronal degeneration is related to the disorder of PI metabolism.

Although oral administrations of phosphatidylserine (PS, 300 mg/day, 2–6 months) reportedly attenuated memory impairment associated with aging (McDaniel et al., 2003), this phospholipid did not show any protective effects against neurotoxicity induced by pathophysiological concentrations of A β both *in vitro* (Wu et al., 2002) and *in vivo* (Fig. 2). PS is normally localized in the inner layer of plasma membranes, and its translocation to the outer leaflet is recognized by phagocytes to remove the cell (Farooqui et al., 2000). Further, exogenous PS dose-dependently results in apoptosis (Uchida et al., 1998). Taking these findings in consideration, use of PI rather than PS appears to be effective especially for AD treatment.

In summary, neurodegeneration induced by intrahippocampal injection of low pathophysiological concentrations of A β was successfully observed in early stage V337M human tau expressing mice, and co-administration of PI, an *in vitro* anti-A β reagent, blocked the A β 's neurotoxicity. This system may be a useful animal model to evaluate the neurotoxicity of pathophysiological concentrations of A β proteins and the potency of anti-A β drugs *in vivo*.

Acknowledgements

This work was supported by grants from Japanese Private School Promotion Foundation, High-Tech Research Center, the Science Frontier Project and The 21st Century Center of Excellence (COE) Project of the Ministry of Education, Culture, Sports, Science and Technology, Japan.

References

- Cheung, E.C., Melanson-Drapeau, L., Cregan, S.P., Vanderluit, J.L., Ferguson, K.L., McIntosh, W.C., Park, D.S., Bennett, S.A., Slack, R.S., 2005. Apoptosis-inducing factor is a key factor in neuronal cell death propagated by BAX-dependent and BAX-independent mechanisms. *Journal of Neuroscience* 25 (6), 1324–1334.
- Farooqui, A.A., Horrocks, L.A., Farooqui, T., 2000. Glycerophospholipids in brain: their metabolism, incorporation into membranes, functions, and involvement in neurological disorders. *Chemistry and Physics of Lipids* 106 (1), 1–29.
- Frautschy, S.A., Baird, A., Cole, G.M., 1991. Effects of injected Alzheimer β -amyloid cores in rat brain. *Proceedings of the National Academy of Sciences of the United States of America* 88 (19), 8362–8366.
- Hresko, R.C., Murata, H., Mueckler, M., 2003. Phosphoinositide-dependent kinase-2 is a distinct protein kinase enriched in a novel cytoskeletal fraction associated with adipocyte plasma membranes. *Journal of Biological Chemistry* 278 (24), 21615–21622.
- Kowall, N.W., Beal, M.F., Busciglio, J., Duffy, L.K., Yankner, B.A., 1991. An *in vivo* model for the neurodegenerative effects of β amyloid and protection by substance P. *Proceedings of the National Academy of Sciences of the United States of America* 88 (16), 7247–7251.
- McDaniel, M.A., Maier, S.F., Einstein, G.O., 2003. “Brain-specific” nutrients: a memory cure? *Nutrition* 19, 957–975.
- Miguel-Hidalgo, J.J., Cacabelos, R., 1998. β -Amyloid(1–40)-induced neurodegeneration in the rat hippocampal neurons of the CA1 subfield. *Acta Neuropathologica (Berlin)* 95 (5), 455–465.
- Pettegrew, J.W., Panchalingam, K., Hamilton, R.L., McClure, R.J., 2001. Brain membrane phospholipid alterations in Alzheimer's disease. *Neurochemical Research* 26 (7), 771–782.
- Prasad, M.R., Lovell, M.A., Yatin, M., Dhillon, H., Markesbery, W.R., 1998. Regional membrane phospholipid alterations in Alzheimer's disease. *Neurochemical Research* 23 (1), 81–88.
- Ryu, J.K., Franciosi, S., Sattayaprasert, P., Kim, S.U., McLamorn, J.G., 2004. Minocycline inhibits neuronal death and glial activation induced by β -amyloid peptide in rat hippocampus. *Glia* 48 (1), 85–90.
- Selkoe, D.J., 2001. Alzheimer's disease: genes, proteins and therapy. *Physiological Reviews* 81 (2), 741–766.
- Stepanichev, M.Y., Zdobnova, I.M., Yakovlev, A.A., Onufriev, M.V., Lazareva, N.A., Zarubenko, I.I., Gulyaeva, N.V., 2003. Effects of tumor necrosis factor-alpha central administration on hippocampal damage in rat induced by amyloid β -peptide (25–35). *Journal of Neuroscience Research* 71 (1), 110–120.
- Stokes, C.E., Hawthorne, J.N., 1987. Reduced phosphoinositide concentrations in anterior temporal cortex of Alzheimer-diseased brains. *Journal of Neurochemistry* 48 (4), 1018–1021.
- Tanemura, K., Murayama, M., Akagi, T., Hashikawa, T., Tominaga, T., Ichikawa, M., Yamaguchi, H., Takashima, A., 2002. Neurodegeneration with tau accumulation in a transgenic mouse expressing V337M human tau. *Journal of Neuroscience* 22 (1), 133–141.
- Uchida, K., Emoto, K., Daleke, D.L., Inoue, K., Umeda, M., 1998. Induction of apoptosis by phosphatidylserine. *Journal of Biochemistry (Tokyo)* 123 (6), 1073–1078.
- Wu, B., Kitagawa, K., Yagyu, K., Zhang, N.-Y., Hattori, N., Inagaki, C., 2002. Phosphatidylinositol and PI-4-monophosphate recover amyloid β protein-induced inhibition of Cl⁻-ATPase activity. *Life Sciences* 72 (4–5), 455–463.
- Wu, B., Kitagawa, K., Zhang, N.-Y., Liu, B., Inagaki, C., 2004. Pathophysiological concentrations of amyloid β proteins directly inhibit rat brain and recombinant human type II phosphatidylinositol 4-kinase activity. *Journal of Neurochemistry* 91 (5), 1164–1170.
- Yagyu, K., Kitagawa, K., Irie, T., Wu, B., Zeng, X.-T., Hattori, N., Inagaki, C., 2001. Amyloid β proteins inhibit Cl⁻-ATPase activity in cultured rat hippocampal neurons. *Journal of Neurochemistry* 78 (3), 569–576.
- Zeng, X.-T., Hara, M., Inagaki, C., 1994. Electrogenic and phosphatidylinositol-4-monophosphate-stimulated Cl⁻ transport by Cl⁻ pump in the rat brain. *Brain Research* 641 (1), 167–170.
- Zhang, N.-Y., Kitagawa, K., Wu, B., Inagaki, C., 2003. Soybean-derived phosphatidylinositol recovers amyloid β protein-induced neurotoxicity in cultured rat hippocampal neurons. *Neuroscience Letters* 350 (2), 105–108.
- Zhang, N.-Y., Kitagawa, K., Wu, B., Xiong, Z.-M., Otani, H., Inagaki, C., 2006. Chloride-dependency of amyloid β protein-induced enhancement of glutamate neurotoxicity in cultured rat hippocampal neurons. *Neuroscience Letters* 399 (1–2), 175–180.

研究成果報告書

研究課題名	修復・再生過程における組織幹細胞の in vivo で追跡可能な解析系の開発		
(英文)	Establishment of in vivo imaging system to trace the tissue stem cells in the process of repair and regeneration		
事業推進者	藤澤 順一	E-mail	fujisawa@takii.kmu.ac.jp
所属・職名	医学研究科・ウイルス腫瘍学（微生物学）講座・教授		
研究分担者名	西川 正雄		
キーワード	レトロウイルスベクター、in vivo イメージング、造血幹細胞		
<p>1. 概要</p> <p>修復・再生過程における造血幹細胞および組織幹細胞の関与を解明するために、分子イメージングの指標となる遺伝子を簡便かつ高率に幹細胞に導入できるウイルスベクターを開発し、幹細胞の個体内での動態を in vivo イメージング装置で解析する。</p> <p>2. 研究の背景と目的</p> <p>脊髄損傷等の修復・再生治療として骨髄移植の有効性が示唆されているが、その細胞生物学的な検証は未だ不完全である。また、移植骨髄細胞による神経再生過程は長期にわたり、かつ、移植細胞の形態変化と細胞分化を伴うことから、移植細胞の標識と生体の状態での経時的な追跡が必要となる。そこで、移植骨髄細胞にあらかじめルシフェラーゼ遺伝子や蛍光蛋白遺伝子を導入することにより、発光あるいは蛍光を指標に生体内における細胞の経時的な追跡が可能な in vivo イメージング装置 (IVIS100) を用いた、移植細胞の動態解析を試みる。そのために必要な、骨髄細胞に簡便かつ高率に遺伝子導入することが出来るウイルスベクターの開発をおこなう。</p> <p>3. 研究方法</p> <p>(1) ルシフェラーゼ/蛍光蛋白発現レトロウイルスベクターの作成 (2) 織特異的レトロウイルスベクターの開発 (3) in vivo イメージング装置を用いたルシフェラーゼ/蛍光蛋白標識細胞の個体内動態の解析</p> <p>4. これまでの成果</p> <p>(1) ルシフェラーゼ発現レトロウイルスベクターの作成 マウス白血病ウイルス(MLV)ゲノムを基本骨格とするレトロウイルスベクターを、ルシフェラーゼ遺伝子とプューロマイシンあるいはブラストサイジンに対する薬剤耐性遺伝子をポリシストロニックに発現するように改変した。これらを、Ecotropic virus packaging 細胞 (BOSC) にトランスフェクションすることで、その 2 日間培養上清中に 10⁵ 感染価/ml 前後の組換えウイルスの産生が得られた。</p> <p>(2) 組織特異的レトロウイルスベクターの開発 組換えウイルスの感染宿主域を拡大する目的で、上記レトロウイルスベクターを VSV G 蛋白発現ベクターと共に 293 細胞にトランスフェクションし、VSV-G pseudotype virus を作成したところ、ラット由来細胞株(Rat-1)に対しては MLV 型組換えウイルスと同等の感染価が得られたが、ヒト由来細胞株(Hela)に対しては感染性を示さなかった。</p> <p>そこで、組換えウイルスベクターの転写調節領域をヒトサイトメガロウイルスのものに置き換えたところ、VSV-G pseudotype virus としたときのみ Hela 細胞に対しても同等の感染性を示すようになった。この結果より、VSV-G pseudotype virus とすることで齧歯類以外の細胞に対して感染性を示し、かつ、転写調節領域を任意の組織特異的転写調節領域に置き換えることにより、それぞれの特異的発現を誘導できることが示された。</p> <p>(3) in vivo イメージング装置を用いた標識細胞の個体内動態の解析 ルシフェラーゼ遺伝子導入マウスリンパ腫細胞株 EL-4 を同系 C57BL6 マウス個体内に、</p>			

様々な経路で移植し、*in vivo* イメージング装置を用いて、個体内における移植細胞の動態を経時的に観察した。その結果、皮下、腹腔内、眼窩静脈、骨髄内いずれの経路において導入された EL-4 細胞も、経時的に高感度で観察することが可能であることが確認された。

また、赤色蛍光蛋白 Ds-Red を融合した蛋白を発現した EL-4 細胞も、個体内における動態を追跡可能であったが、緑色蛍光蛋白 EGFP を用いた場合は、十分な感度が得られなかった。

さらに、ルシフェラーゼによる発光を指標とした場合、黒色のマウスでも個体内の細胞を検出できるが、白色(アルビノ)変異体マウスを用いると、約 10 倍感度が上昇した。

5. これまでの進捗状況と今後の計画

これまでに得られたレトロウイルスベクターを用いて、複数の腫瘍細胞株にルシフェラーゼ遺伝子を導入し、動物個体内における位置および増殖を経時的に追跡することに成功している。今後、同ウイルスを用いて骨髄由来造血幹細胞にルシフェラーゼ遺伝子を導入し、動物個体内に移植することで、修復・再生の場における移植細胞の動態を観察する予定である。

6. これまでの発表論文

(1) 発表論文

1) 原著論文

1. Iwanaga, R. Ozono, E. Fujisawa, J. Ikeda, M. A. Okamura, N. Huang, Y. & Ohtani, K. Activation of the cyclin D2 and cdk6 genes through NF-kappaB is critical for cell-cycle progression induced by HTLV-I Tax. *Oncogene in press*
2. Nitta, T. Tanaka, M. Sun, B. Sugihara, E. Kimura, M. Kamada, Y. Takahashi, H. Hanai, S. Jiang, S. W. Fujisawa, J. & Miwa, M. Reduction of human T-cell leukemia virus type-1 infection in mice lacking nuclear factor-kappaB-inducing kinase. *Cancer Sci.* **99**, 872-878 (2008).
3. Gohda, J., Irisawa, M., Tanaka, Y., Sato, S., Ohtani, K., Fujisawa, J. & Inoue, J. HTLV-1 Tax-induced NFkappaB activation is independent of Lys-63-linked-type polyubiquitination. *Biochem. Biophys. Res. Commun.* **357**, 225-230 (2007).
4. Yasui, K., Miyazaki, T., Matsuyama, N., Kojima, Y., Furuta, R. A., Fujisawa, J., Tani, Y., Shibata, H., Sato, S., Kato, T., Ikeda, H. & Hirayama, F. Establishment of cell lines stably expressing HNA-1a, -1b, and -2a antigen with low background reactivity in flow cytometric analysis. *Transfusion* **47**, 478-485 (2007).
5. Matsuzaki, K. Murata, M. Yoshida, K. Sekimoto, G. Uemura, Y. Sakaida, N. Kaibori, M. Kamiyama, Y. Nishizawa, M. Fujisawa, J. Okazaki K. & Seki, T. Chronic inflammation associated with hepatitis C virus infection perturbs hepatic transforming growth factor beta signaling, promoting cirrhosis and hepatocellular carcinoma. *Hepatology* **46**, 48-57 (2007).
6. Sekimoto, G. Matsuzaki, K. Yoshida, K. Mori, S. Murata, M. Seki, T. Matsui, H. Fujisawa, J. & Okazaki, K. Reversible Smad-dependent signaling between tumor suppression and oncogenesis. *Cancer Res.* **67**, 5090-5096 (2007).
7. Sugiura, K. Taketani, S. Yoshimura, T. Nishino, T. Nishino, N, Fujisawa, J. Hisha, H. Inaba, T. & Ikehara, S. Effect of hepatocyte growth factor on long term hematopoiesis of human progenitor cells in transgenic-severe combined immunodeficiency mice. *Cytokine* **37**, 218-226 (2007).
8. Furuta, R.A., Nishikawa, M. & Fujisawa, J.-i. Real-time analysis of human immunodeficiency virus type 1 Env-mediated membrane fusion by fluorescence resonance energy transfer. *Microbes and Infection* **8**, 520-532 (2006).
9. Okamoto, K. Fujisawa, J.-i. Reth, M. & Yonehara, S. Human T-cell leukemia virus type-I oncoprotein Tax inhibits Fas-mediated apoptosis by inducing cellular FLIP through activation of NF-kB. *Genes Cells* **11**, 177-91 (2006).
10. Sun, P., Watanabe, H., Takano, K., Yokoyama, T., Fujisawa, J.-i. & Endo, T. Sustained activation of M-Ras induced by nerve growth factor is essential for neuronal differentiation of PC12 cells. *Genes Cells* **11**, 1097-1113 (2006).
11. 保井一太、松山宣樹、小島芳隆、古田里佳、谷慶彦、柴田弘俊、平山文也、宮崎孔、佐藤進一郎、加藤俊明、池田久實、藤澤順一：顆粒球抗体検出用の HNA-1a, -1b, および -2a 遺伝子発現パネル細胞株の作成. *日本輸血・細胞治療学会誌* **53**, 558-565 (2007).

3) 著書

藤澤順一 : 分担執筆「HTLV-1 と疾患」編集：渡邊俊樹、上平 憲、山口一成
第 IV 章 ウイルス学・分子生物学 4 HTLV-1 とウイルス学 第 1 版 152-165、文光堂、東京 (2007).

(2) 学会発表

国際学会

1. Jiang SW, Inada T, Furuta RA, Fujisawa JI: Possible involvement of TORC2 in the transcriptional suppression of HTLV-1 *in vivo*. 第13回国際ヒトレトロウイルス HTLV 会議、箱根、2007.
2. Miwa M, Kawazu Y, Konishi T, Shiokawa K, Nitta T, Yagami K-I, Sugimura H, Fujisawa J-I, Tanaka M : HTLV-1 infection greatly modified the characteristics of radiation-induced lymphoma in mice. 第13回国際ヒトレトロウイルス HTLV 会議、箱根(2007)
3. Tanaka M, Shiokawa K, Konishi T, Kawazu Y, Tsuda H, Fujisawa J-i, Miwa M: Effect of Lactoferrin on HTLV-1 infection. 第13回国際ヒトレトロウイルス HTLV 会議、箱根、2007.

国内学会

1. 藤澤順一、蔣 時文、稲田武文：HTLV-1 の個体内発現制御における転写補助因子 TORC2 の関与 第66回日本癌学会学術総会、横浜、2007.
2. 田中正和、塩川くみ、鄭 真美、小西智子、河津祐介、津田洋幸、藤澤順一、三輪正直：HTLV-1 感染におけるラクトフェリンの効果について 第66回日本癌学会学術総会、横浜、2007.
3. 蔣 時文、藤澤順一：HTLV-1 の個体内発現制御における転写補助因子 TORC の関与 第55回日本ウイルス学会学術集会、札幌、2007.
4. 河津祐介、田中正和、小西智子、長谷川翔、鄭 真美、梶村春彦、藤澤順一、三輪正直：HTLV-1 感染マウスで放射線照射における腫瘍発生のメカニズムについて 第55回日本ウイルス学会学術集会、札幌、2007.
5. 長谷川翔、田中正和、河津祐介、三輪正直、藤澤順一：In vivo イメージングを用いた Tax 発現細胞の個体内動態解析 第55回日本ウイルス学会学術集会、札幌、2007.
6. 小西智子、田中正和、河津祐介、鄭 真美、長谷川翔、藤澤順一、三輪正直：HTLV-1 感染マウスにおける感染細胞のクローン増殖生について 第55回日本ウイルス学会学術集会、札幌、2007.
7. 田中浩司、田中正和、酒井博幸、藤澤順一、三輪正直：Friend-MLV における組み込み過程での宿主 DNA 修復系(PARP-1 及び PARP-2)の関与について 第55回日本ウイルス学会学術集会、札幌、2007.
8. 手塚健太、田中正和、孫 鬢蓮、植月太一、藤澤順一、三輪正直：HTLV-1 感染系におけるノイラミン酸の役割について 第55回日本ウイルス学会学術集会、札幌、2007.
9. 鄭 真美、田中正和、小西智子、河津祐介、長谷川翔、津田洋幸、藤澤順一、三輪正直：HTLV-1 感染におけるラクトフェリンの効果について 第55回日本ウイルス学会学術集会、札幌、2007.
10. 蔣時文、稲田武文、藤澤順一：HTLV-1 の個体内発現制御における低酸素シグナルの関与 第30回日本分子生物学会年会、第80回日本生化学会大会合同大会、横浜、2007.
11. 山田真生、河津祐介、田中正和、藤澤順一、三輪正直：DNA damage における中心体増幅を起こす経路の特定 第30回日本分子生物学会年会、第80回日本生化学会大会合同大会、横浜、2007.
12. 伊藤道恭、芳賀 泉、藤澤順一：Sam68 による細胞内 mRNA 分子の発現調節 第8回 RNA ミーティング、淡路、2006.
13. 関本剛、松崎恒一、吉田勝紀、森茂生、山縣英生、松井裕史、藤澤順一、岡崎和一：H-RAS v12 導入癌細胞の Smad 依存性癌化シグナルはリンカー部リン酸化を阻害すると細胞増殖抑制シグナルに回帰する 第65回日本癌学会学術総会、横浜、2006.
14. 田中正和、小西智子、川津祐介、藤澤順一、三輪正直：HTLV-1 感染マウスにおける腫瘍発生 第65回日本癌学会学術総会、横浜、2006.
15. 巽 理恵、齊藤峰輝、大原義朗、藤澤順一：高い HAM 発症率を示すイラン型 HTLV-1 Tax/Rex の機能 第54回日本ウイルス学会学術集会、名古屋、2006.
16. 木村富紀、橋本岩雄、藤澤順一：HIV-1 Revによるインターフェロン- α mRNA核外輸送阻害に関与するRNA結合因子のクローニング 第54回日本ウイルス学会学術集会、名古屋、2006.
17. 川津祐介、田中正和、小西智子、塩川くみ、八神健一、梶村春彦、巽 理恵、藤澤順一、三輪正直：HTLV-1 感染マウスでの放射線照射における腫瘍発生のメカニズムについて 第54回日本ウイルス学会学術集会、名古屋、2006.
18. 小西智子、田中正和、川津祐介、塩川くみ、巽 理恵、藤澤順一、三輪正直：HTLV-1 感染マウスにおける感染細胞のクローン増殖性について 第54回日本ウイルス学会学術集会、名古屋、2006.

7. これまでの成果の情報公開

ホームページ：微生物学講座=<http://www3.kmu.ac.jp/microbiol/>

Establishment of cell lines stably expressing HNA-1a, -1b, and -2a antigen with low background reactivity in flow cytometric analysis

Kazuta Yasui, Toru Miyazaki, Nobuki Matsuyama, Yoshitaka Kojima, Rika A. Furuta, Jun-ichi Fujisawa, Yoshihiko Tani, Hirotohi Shibata, Shin-ichirou Sato, Toshiaki Kato, Hisami Ikeda, and Fumiya Hirayama

BACKGROUND: Antibodies to neutrophil antigens have been implicated in neonatal alloimmune neutropenia, autoimmune neutropenia, and transfusion-related acute lung injury. Most often, neutrophil-specific antibodies are directed toward human neutrophil antigen (HNA)-1 (Fcγ receptor 3b) and HNA-2a (CD177) in these disorders.

STUDY DESIGN AND METHODS: To detect the alloantibodies in the serum samples, a panel of cell lines was established in which the HNA-1a, HNA-1b (polymorphisms of HNA-1), or HNA-2a gene was transduced with a retrovirus vector to confer stable transgene expression in K562 cells that exhibited low background reactivity to human serum samples obtained from healthy donors in flow cytometric analysis.

RESULTS: It was shown that several well-characterized human serum samples containing antibodies against HNA-1a, -1b, and -2a were unambiguously identified by the established panel cell lines and observed a lower background reactivity and longer shelf life of the K562 panel cell lines compared with isolated neutrophils, which have been used for the cell panel to identify antibodies against HNA in human serum samples.

CONCLUSION: These results indicate that the K562 panel cell lines provide a good panel for detecting HNA-reactive neutrophil antibodies in human serum samples.

The Fcγ receptor 3b (FcγRIIIb, CD16b)¹⁻⁵ and NB1 glycoprotein (CD177)^{1-3,6-8} are considered the most important neutrophil-specific antigens for clinical purposes. Immunologic studies have shown that FcγRIIIb is polymorphic, bearing the high-frequency human neutrophil antigens (HNA)-1a and -1b and the low-frequency antigen HNA-1c.^{4,5} The NB1 glycoprotein, recently designated HNA-2a, is heterogeneously expressed on the neutrophils of 88 to 97 percent of healthy individuals.^{6,7} Antibodies to these four antigens, especially HNA-1a, -1b, and -2a, can cause a number of disorders, including alloimmune neonatal neutropenia,^{9,10} autoimmune neutropenia,^{11,12} immune neutropenia after marrow transplantation,^{13,14} and transfusion-related acute lung injury.¹⁵ In addition, neutrophil alloimmunization can result in refractoriness to granulocyte transfusions.^{16,17} Therefore, it is necessary to identify antibodies to neutrophil antigens in test serum samples to evaluate these disorders.

Although flow cytometric (FCM) analysis with a typed panel of neutrophils has been widely used to screen for the presence of neutrophil antibodies and to determine their specificity, this procedure has a few limitations. First, it is often inconvenient to prepare such a panel because

ABBREVIATIONS: ATCC = American Type Culture Collection; FcγRIIIb = Fcγ receptor 3b; FCM = flow cytometric; GIFT = granulocyte immunofluorescence test.

From the Japanese Red Cross Osaka Blood Center, and the Kansai Medical University, Osaka, Japan; and the Japanese Red Cross Hokkaido Blood Center, Sapporo, Japan.

Address reprint requests to: Kazuta Yasui, PhD, Japanese Red Cross Osaka Blood Center, 2-4-43, Morinomiya, Joto-ku, Osaka 536-8505, Japan; e-mail: yasui-kazuta@osaka.bc.jrc.or.jp.

Received for publication June 7, 2006; revision received July 31, 2006, and accepted August 1, 2006.

doi: 10.1111/j.1537-2995.2006.01139.x

TRANSFUSION 2007;47:478-485.

only freshly prepared neutrophils can be used in FCM analysis.¹⁸ Second, the assay cannot identify an HNA antibody in the presence of anti-HLA Class I antibodies that react to panel neutrophils. There are two ways to avoid the latter problem: use neutrophils that do not express the relevant HLA Class I¹⁸ or absorb these antibodies before the test.¹⁹ These solutions, however, can only be applied at a limited number of institutions that maintain blood samples for screening. To overcome these limitations, several groups of investigators have attempted to establish panel cell lines that express neutrophil antigens, but the only cell lines described in the literature express HNA-1a, -1b, and -1c, not HNA-2a.²⁰ Although the cell lines could be stored for 4 weeks after fixation for use with the monoclonal antibody (MoAb)-specific isolation of granulocyte antigens assay, they were difficult to use in high-sensitivity FCM analysis because normal human sera showed high background reactivity to the panel cell lines.

In this study, we applied a retrovirus vector for the transduction of HNA genes into a target cell line, the human erythroleukemic cell line K562, which does not express HLA or HNA or exhibit background reactivity to normal human serum samples. We established cell lines that stably express HNA-1a, -1b, and -2a antigens and were able to directly use these panel cell lines for FCM analysis. Our panel cell lines should be useful for detecting neutrophil antibodies in human serum samples that react with HNA-1a, -1b, and -2a.

MATERIALS AND METHODS

Preparation of peripheral blood and serum samples

For blood cell samples, whole blood anticoagulated with ethylenediaminetetraacetate was collected from healthy personnel at our blood center who had been typed previously for HLA Class I, HLA Class II, HNA-1, and HNA-2a. Normal serum samples were also obtained from healthy personnel at the blood center. Serum samples containing white blood cell (WBC) antibodies were obtained from recipients of nonhemolytic transfusion reactions, patients who were refractory to platelet (PLT) transfusion, and patients with autoimmune neutropenia or alloimmune neutropenia. Some of the serum samples were provided by M. Kobayashi (Hiroshima University, Hiroshima, Japan). The specificity of each serum had been determined with a modified granulocyte immunofluorescence test (GIFT) assay.¹⁸

Cell lines

Jurkat cells (a human T-cell line obtained from the American Type Culture Collection [ATCC], Manassas, VA), THP-1 cells (a human monocyte cell line from ATCC), Namalwa

cells (a human B-cell line from ATCC), L-cells (a mouse B-cell line from ATCC), K562 cells (a human erythroleukemia cell line provided by Y. Kanakura, Osaka University, Osaka, Japan), and CMK cells (a human megakaryocytic cell line provided by Y. Kanakura) were cultured in RPMI 1640 supplemented with 10 percent fetal bovine serum (FBS), 50 U per mL penicillin, and 50 µg per mL streptomycin (Gibco BRL, Grand Island, NY). HeLa cells (a human epithelial-like cell line from ATCC), 293T cells (a human kidney cell line from ATCC), Cos7 cells (African green monkey kidney cell line from ATCC), and 3T3 cells (a mouse fibroblast cell line from ATCC) were cultured in Dulbecco's modified Eagle's medium supplemented with 10 percent FBS, 50 U per mL penicillin, and 50 µg per mL streptomycin. The Chinese hamster ovary cell line from ATCC was cultured in Ham's F12 medium supplemented with 10 percent FBS, 50 U per mL penicillin, and 50 µg per mL streptomycin.

Establishment of cell lines expressing HNA-1a, -1b, and -2a

Full-length HNA-1a, -1b, and -2a cDNAs were synthesized by nested reverse transcription-polymerase chain reaction^{4,20,21} with total RNA extracted from the peripheral blood mononuclear cells of two subjects typed as HNA-1a/a and b/b or one HNA-2a-positive subject. The cDNAs were cloned into pCR2.1-TOPO (Invitrogen, Carlsbad, CA), and the sequences were confirmed. Each cDNA fragment was subcloned into a retroviral vector, pQCXIP (Becton Dickinson, San Jose, CA), at the *Bam*HI and *Not*I recognition sites. The resultant plasmids, pQCXIP-1a, pQCXIP-1b, and pQCXIP-2a, were packaged into viral particles as previously described.²² Briefly, 2×10^6 gp-293T packaging cells (Becton Dickinson) were transfected with 2.1 µg of pVSV-G (Becton Dickinson) and 2.1 µg of vector plasmid with reagent (LipofectAMINE Plus, Invitrogen) according to the manufacturer's instructions. Culture supernatants collected 48 hours after transfection were subjected to titration with Rat-1 cells. We obtained titers in the range of 10^5 transduction units per milliliter.

For infection, 1×10^6 K562 cells were incubated with 0.1 mL of the viral supernatant, 0.9 mL of RPMI 1640 containing 10 percent FBS, and 8 µg per mL polybrene for 2 hours; washed twice with the same medium; and then cultured for 2 days in the medium. The cells were cloned by a limiting dilution method in the presence of 0.5 µg per mL puromycin. Clones KY-1a, KY-1b, and KY-2a were selected as panel cell lines for HNA-1a, -1b, and -2a, respectively, owing to their high level of HNA expression with a low background in the FCM analysis.

FCM analysis

For direct immunofluorescence, aliquots of cells that had been maintained in culture with RPMI 1640 containing

TABLE 1. Profile of cell lines summarized on the basis of background reactivity and expression of WBC antigens

Normal serum*	Nonadherent cell lines						Adherent cell lines				
	K562 0/3	Jurkat 0/3	THP-1 0/3	Namalwa 0/3	CMK 0/3	L cell 3/3	HeLa 1/3	293T 2/3	Cos7 0/3	3T3 2/3	CHO 2/3 weak
HLA†											
ABC	-	+	+	+	+	-	+	+	+	-	-
DR	-	-	-	+	-	+	-	-	+	-	-
DR,DQ,DP	-	NT	NT	NT	NT	NT	NT	NT	NT	NT	NT
HNA											
1‡	-	-	-	-	-	-	-	-	-	-	Weak
2a§	-	-	-	-	-	-	-	-	-	-	-
3	-	NT	NT	NT	NT	NT	NT	NT	NT	NT	NT
4¶	-	-	-	-	+	-	-	-	+	-	-
5¶	-	+	+	+	+	-	-	-	-	-	-

* Determined by indirect IFT using FITC-anti-human IgG after incubating with three kinds of normal human sera.
† Determined by direct IFT with FITC-anti-HLA ABC, PE-anti-HLA DR, and PE-anti-HLA DR, DQ, DP antibodies.
‡ Determined by direct IFT with FITC-TAG-1, FITC-TAG-2, and TAG-3.
§ Determined by direct IFT with FITC-TAG-4.
|| Determined by indirect IFT using FITC-anti-human IgG after incubating with HNA-3a-reactive serum sample.
¶ Determined by direct IFT using PE-anti-HNA4 (anti-Mac-1) and FITC-anti-HNA5 (anti-LFA-1).
NT = not tested.

10 percent FBS and 0.5 µg per mL puromycin were collected by centrifugation at 1000 × g for 2 minutes, washed at 1000 × g for 1 minute with the washing buffer (PBS-0.1% bovine serum albumin-5 mmol/L EDTA) two times, and stained for 15 minutes at 4°C with fluorescein isothiocyanate (FITC)- or phycoerythrin (PE)-conjugated MoAbs. The MoAbs used were FITC-TAG-1 (against HNA-1a);²³ FITC-TAG-2 (against HNA-1b);²³ FITC-TAG-3 (against HNA-1);²³ FITC-TAG-4 (against HNA-2a);²⁴ FITC-anti-HLA ABC (Becton Dickinson); PE-anti-HLA-DR (Becton Dickinson); PE-anti-HLA-DR, -DQ, and -DP (Beckman Coulter, Fullerton, CA); PE-anti-Mac-1 (Becton Dickinson); and FITC-anti-LFA-1 (Becton Dickinson). FITC-immunoglobulin G1 (IgG1) and PE-IgG1 (Becton Dickinson) were used as isotype controls. TAG-1, -2, -3, and -4 were gifts from K. Taniguchi (Hiroshima College of Medical Technology, Hiroshima, Japan). The labeled cells were analyzed with a flow cytometer (FACSCalibur, Becton Dickinson).

For indirect immunofluorescence, blood cells or cell lines were first incubated with human serum for 15 minutes at 4°C and subsequently stained with FITC-labeled mouse anti-human IgG F(ab')₂ (Jackson ImmunoResearch, West Grove, PA) for 15 minutes at 4°C. To stain blood cells, red cells were subsequently lysed by adding lysing solution (FACS, Becton Dickinson).¹⁸ Autologous serum samples were used as negative controls when blood cells were stained, and serum samples obtained from healthy laboratory personnel were used when cell lines were stained. In some experiments, K562 cells were treated with a MoAb, 3G8 (anti-CD16, Becton Dickinson), at 10 µg per mL for 15 minutes at 4°C before the incubation with human serum samples to be tested.

RESULTS

Establishment of panel cell lines

To select a parental cell line for the establishment of HNA-expressing panel cell lines, we examined six nonadherent and five adherent cell lines, focusing on the background reactivity against healthy personnel-derived serum (normal serum) and on the cell surface expression of several WBC antigens. The reactivity of HeLa, 293T, and Chinese hamster ovary cells and L cells with at least one of three human serum samples obtained from healthy personnel was slightly higher than with the PBS control (Table 1). No background reactivity was observed for five nonadherent cell lines (K562, Jurkat, THP-1, Namalwa, and CMK) and one adherent cell line, Cos7 (Table 1). When the expression of HLA and HNA antigens was tested, only K562 cells did not show expression of all the antigens (Table 1). Therefore, we selected K562 as a target parental cell line and transduced the HNA-1a, -1b, and -2a cDNAs into K562 cells with a retrovirus vector, pQCXIP. We have observed that HNA expression in the transduced K562 cells, called K562 panel cells hereafter, has been maintained for more than 1 year in the presence of puromycin (Fig. 1), probably because of an IRES-mediated cotranscription.^{25,26}

To confirm the specificity of HNA expression in the K562 panel cells expressing HNA-1a (designated KY-1a), HNA-1b (KY-1b), and HNA-2a (KY-2a), we used the MoAbs TAG-1, -2, -3, and -4, which react against HNA-1a, -1b, -1, and -2a, respectively. KY-1a expressed only HNA-1a, KY-1b expressed only HNA-1b, and KY-2a expressed only HNA-2a (data not shown). KY-mock showed no reactivity to any of the MoAbs (data not shown). Titration with TAG-1, -2, -3, and -4 showed that as little as 1 µg per mL of the antibodies could reveal antigen signals on the cells

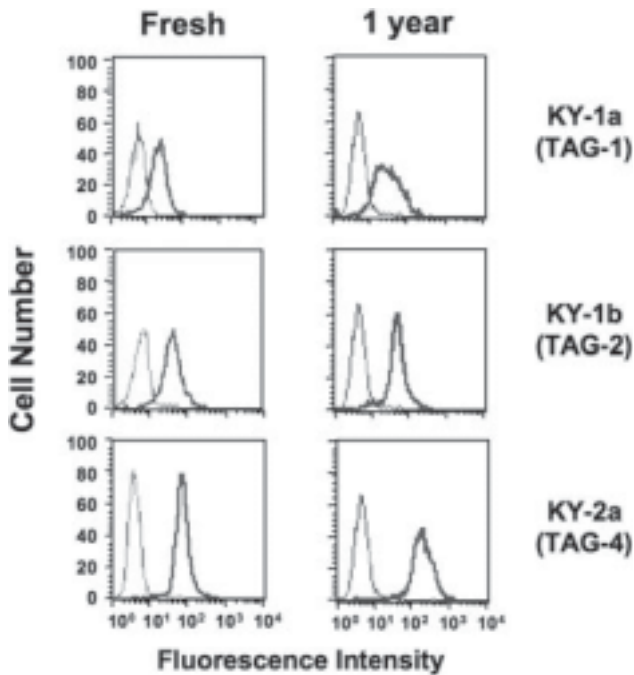


Fig. 1. Stability of HNA-1a, HNA-1b, and HNA-2a expression in the K562 panel cells. KY cells were maintained in culture for 1 year and tested in the FCM assay for their reactivity with HNA MoAbs compared to freshly established KY cells. These cells were stained with 10 μg per mL FITC-TAG-1, -2, or -4 or isotype-matched mouse IgG as a control. Thin lines represent the results with the isotype control antibody.

(Fig. 2). These data indicate that the K562 panel cells can be clearly identified by MoAbs against HNA-1a, -1b, and -2a without background reactivity.

Reactivity of K562 panel cells to normal human serum samples

Although we had shown that the parental K562 cells had a low reactivity to normal human serum (Table 1), we nevertheless tested the reactivity of the four K562 panel cell lines to 15 normal serum samples. Unexpectedly, more than half of the serum samples showed greater reactivity to KY-1b and especially to KY-1a than to KY-mock (Fig. 3A). Both KY-1a and KY-1b express Fc γ RIIIb, and Fc γ RIIIb binds to monomeric IgG with low affinity ($K_a = 5 \times 10^5$ L/mol) and to polymeric IgG with high affinity ($K_a > 5 \times 10^7$ L/mol).²⁷ Therefore, we speculated that sera with higher reactivity would contain more IgG aggregates (polymeric IgG) than serum samples with lower reactivity and that the IgG aggregates would bind to the transduced Fc γ RIIIb molecules as their ligand. To test this possibility, we incubated the K562 panel cells with an anti-Fc γ RIIIb MoAb, 3G8, known to specifically block ligand binding to Fc γ RIIIb.^{2,28-30} The MoAb 3G8 did not affect the binding of the HNA-1 allotype-specific antibodies TAG-1 and -2 (data not shown) because

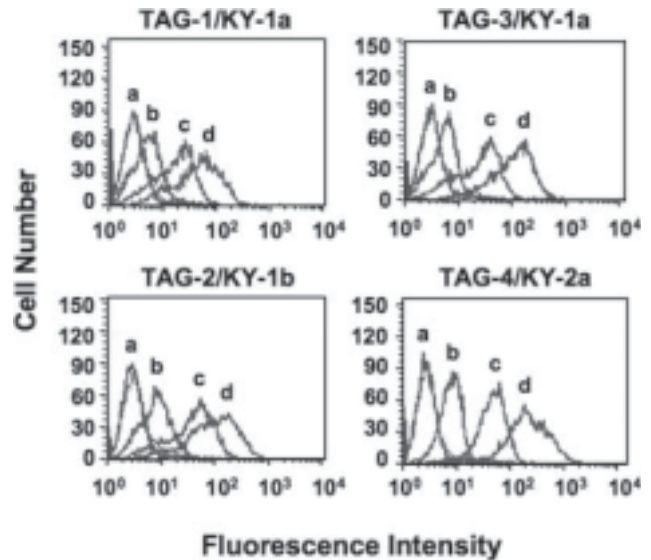


Fig. 2. HNA-1a, HNA-1b, and HNA-2a expression in the K562 panel cells. Various concentrations of TAG-1, -2, -3, and -4 bound to the corresponding K562 panel cells. Thin lines represent the results with the isotype control antibody. a = 0.1 μg per mL; b = 1 μg per mL; c = 10 μg per mL; d = 100 μg per mL.

3G8 and TAG-1 (or -2) bind at different domains, a membrane proximal domain containing receptor-binding sites for IgG and a distal domain, respectively.²⁸⁻³⁰ As shown in Fig. 3B, treatment of each panel cell line with MoAb 3G8 successfully lowered the reactivity of the 15 normal serum samples to KY-1a and KY-1b, with the most reactive serum samples showing levels as low as those to KY-mock. Therefore, it is likely that the reactivity of normal sera to KY-1a and KY-1b was attributable to the receptor function of the introduced Fc γ RIIIb. Similar experiments were conducted with and without 3G8 treatment with 15 serum samples identified as positive to HLA Class I and Class II to examine the effects of HLA antibodies on the reactivity to the panel cells. The results indicated that HLA antibodies in the test serum samples bound to the Fc-binding domain of Fc γ RIIIb through their Fc region but not their antigen-combining region, because the binding capacity of the test serum samples was almost completely inhibited by 3G8 (data not shown). We also revealed that 3G8 did not interfere with the binding of HNA allotype-specific antibodies to the panel cells (data not shown). These results demonstrate that each of the panel cell lines pretreated with 3G8 was able to detect allotype-specific antibodies in the test serum samples without background reactivity.

Application of K562 panel cells for the detection of human HNA-reactive antibodies

To examine whether our K562 panel cell lines would be practical for use, we performed an FCM assay of the panel

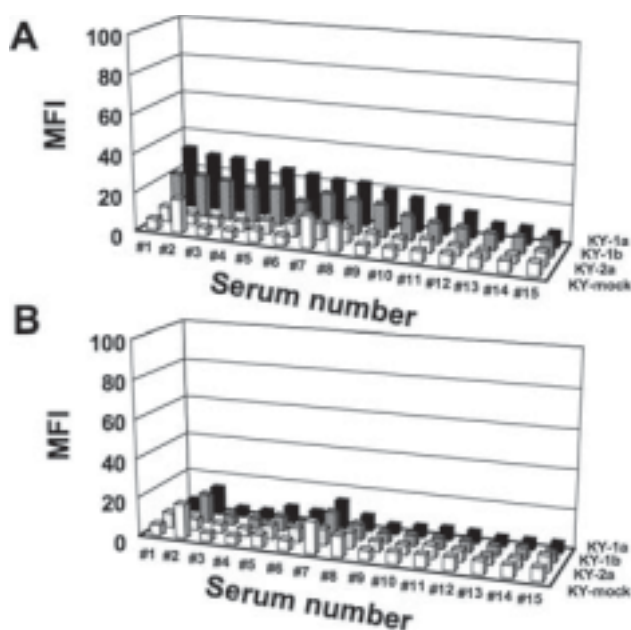


Fig. 3. Reactivity of normal human sera to K562 panel cells in the absence and presence of anti-Fc γ RIIIb MoAb 3G8. K562 panel cells were stained with several normal human serum samples, washed, and labeled with FITC-conjugated goat anti-human IgG. (A) The mean fluorescence intensities (MFIs) of the K562 panel cells incubated with human sera obtained from 15 healthy donors (Samples 1-15) are shown. (B) The MFIs of K562 panel cells incubated with MoAb 3G8 are shown.

cells with serum samples from seven individuals diagnosed with certain blood disorders. All serum samples contained HNA antibodies, and their specificities had been typed in a GIFT assay (data not shown).^{10,31} We further determined that five of them were IgG and the remainder were IgM, in a modified GIFT assay (data not shown).¹⁸

Among the five IgG serum samples, Serum Samples 1 and 2, which had been typed as anti-HNA-1a, definitely bound to KY-1a, but a slight peak shift was observed in the reactivity to both KY-1b and KY-2a (Fig. 4A, columns 1 and 2). Among the HNA-1b-specific sera, Sample 3 exclusively reacted with KY-1b, but Sample 4 reacted with both KY-1a and -1b (Fig. 4A, columns 3 and 4). In contrast, the anti-HNA-2a serum sample, Sample 5, was clearly identified by our panel cells. The ambiguous results shown in Fig. 4A might be attributable to nonspecific binding of serum antibodies to Fc γ R through the Fc-binding domain. Thus, to improve the reliability of our assay system, we performed the same experiment but pretreated each panel cell line with an anti Fc γ RIIIb MoAb, 3G8. As shown in Fig. 4B, pretreatment with 3G8 completely abrogated the slight peak shift seen in Fig. 4A (columns 1, 3, and 4), but it did not produce an appreciable peak shift (Fig. 4B, columns 1, 3, and 4). These results indicate that our panel

cells were able to identify HNA antibodies classified as IgG in test serum samples. We examined the quantifiability of the K562 panel cells with dilutions of two IgG serum samples, Samples 2 and 4. The binding of serum HNA antibodies to the panel cells depended on the concentration of the serum (Fig. 4C). Finally, we examined the remaining two IgM serum samples by replacing the second antibody with anti-human IgM. The anti-HNA-1a-specific and the anti-HNA-1b-specific serum samples reacted exclusively with KY-1a and KY-1b, respectively (data not shown). Taken together, these results clearly demonstrate that our K562 panel cell lines were able to detect the clinically important HNA-1 and HNA-2 antibodies in test serum samples, suggesting their usefulness in diagnosing certain disorders caused by HNA-reactive antibodies.

DISCUSSION

Before performing the experiments presented in this study, we attempted to transduce HNA gene into K562 cell by several conventional transfection systems and yet found that the transduction efficiency in K562 cells was very low (data not shown). In this study, therefore, we used a retrovirus vector to transduce HNA genes into the target cell line K562 and successfully established panel cell lines stably expressing HNA-1a, -1b, and -2a antigen over a long period of time. Because we used a retrovirus vector to transduce the HNA genes, we expect that the genes were integrated into the host DNA and that we will see long-lasting expression of these genes.^{22,32} In addition, puromycin selection is expected to rescue the cells from transgene silencing because of the cotranscription of both puromycin and each HNA gene as a bicistronic mRNA mediated via the internal ribosome entry site in the vector.^{25,26}

To examine the possibility of the KY cells for a long term, we tested how long KY cells can be stored at 4°C and found that KY cells could be stored at 4°C without loss of reactivity no longer than 2 weeks. In addition, 1 percent paraformaldehyde treatment failed to improve the stability at 4°C (data not shown).

Although the K562 panel cells were clearly identified by MoAbs against HNA-1a, -1b, and -2a without background reactivity, several human serum samples obtained from healthy donors showed slight background reactivity with the KY-1a and KY-1b cells (Fig. 3A). To determine whether the background reactivity was caused by the binding of IgG aggregates, we incubated the K562 panel cells with an anti-Fc γ RIIIb MoAb, 3G8,²⁹ and succeeded in lowering the background reactivity (Fig. 3B). To discriminate specific signals from nonspecific signals, the 3G8 treatment of KY cells would be able to specifically detect HNA antibodies in human serum when both of KY-1a and KY-1b cells exhibit positive signals. In addition to this kind of nonspecific reactivity, another kind of nonspecific

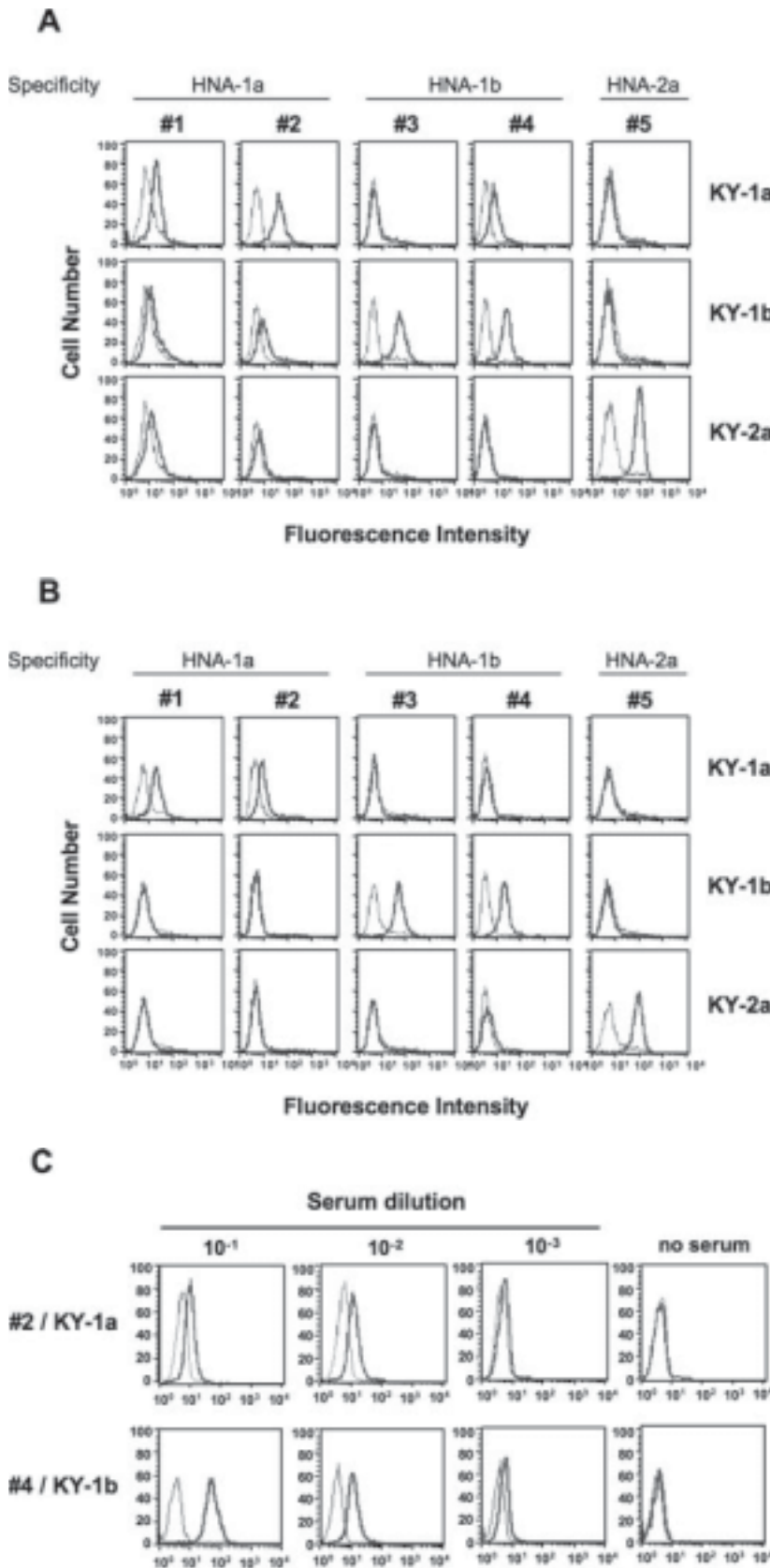


Fig. 4. Histogram profiles of the K562 panel cells stained with various anti-HNA antiserum. The test serum samples were derived from patients with autoimmune neutropenia (first and second panels), a patient with alloimmune neutropenia (third panel), a case of nonhemolytic transfusion reaction (fourth panel), and a case of TRALI (fifth panel). The K562 panel cells were incubated in the absence (A) or presence (B) of anti-Fc γ RIIIb MoAb 3G8, stained with various test serum samples, washed, and labeled with FITC-conjugated goat anti-human IgG. Representative FCM profiles are shown. (C) Various concentrations of Serum Samples 2 and 4 bound to the K562 panel cells. Thin lines indicate the results with K562 mock-transduced cells.

reactivity was found in some normal serum samples like the named Serum Samples 2, 7, and 8. Although fluorescence signals were observed on KY-mock, KY-1a, and KY-1b cells, when stained with these serum samples, Samples 2, 7, and 8, there were no differences in the strength of the signals among those three types of the KY cells (Figs. 3A,B). Therefore, the signals do not impair our test in detecting anti-HNA-1a or -1b. At this time, we are not able to explain what exactly caused these signals, but, at least, it is likely that HLA antibody and HNA antibody were not involved, because these serum samples contained no HLA or HNA antibody.

Several systems exist for screening neutrophil antibodies, including the GIFT,^{10,31} granulocyte agglutination test,³³ MoAb-specific immobilization of granulocyte antigens,³⁴ and micro-mixed passive hemagglutination methods.³⁵ In these methods, however, purified neutrophils from a healthy donor are applied as the only test cells for antibodies in human serum. Purified neutrophils exhibit higher background reactivity against human serum than the neutrophils in whole blood, and thus several serum samples analyzed by these methods showed complicated results owing to the background.

We have also reported a modified GIFT assay (named five-cell-lineage IFT) with whole blood as the target cells and FCM to analyze anti-HNA in the test serum samples; this modified method has lower background reactivity than previous methods.¹⁸ Information about cells of other lineages, including T cells, B cells, monocytes, and PLTs, can be helpful in identifying HNA antibodies. The five-cell-lineage IFT, however, was not able to identify anti-HNA in several serum samples when anti-HLA Class I had been produced in test serum samples and bound to the HLA Class I molecule on the panel neutrophils prepared for the assay (data not shown). In contrast, the detection system with our K562 panel cells was not affected by HLA antibodies in the test serum samples because the expression of HLA Class I antigens on the K562 panel cells was not observed (data not shown). In addition, previous methods, including the five-cell-lineage IFT, were not able to exactly identify HNA antibodies in test serum samples that included immune complexes or IgG aggregates.¹⁸ As we have shown, the K562 panel cells were able to overcome this limitation after treatment with the MoAb 3G8 (Figs. 3, 4). Recently, Hart and coworkers³⁶ reported that immune complex and aggregated IgG bound preferentially to FcγRIIa on neutrophils, and Benoist and coworkers³⁷ reported that K562 cells expressed small quantities of FcγRIIa. Therefore, we examined whether FcγRIIa affects the results of HNA antibody detection by pretreating with an anti-FcγRIIa MoAb and found that the FcγRIIa on K562 panel cells did not interfere with the results (data not shown).

In our blood center, to screen for WBC antibodies, we now screen for HLA antibodies by microbead test first (LABScreen, One Lambda, Inc., Canoga Park, CA). When HLA antibodies are present, we determine their specificity. We then screen for antibodies other than HLA antibodies by five-cell-lineage IFT with panel cells previously typed for HNA-1 and HNA-2.¹⁸ Finally, we perform IFT with KY cells to confirm the results of five-cell-lineage IFT. In addition to KY-1a, KY-1b, and KY-2a cells, we are now planning to establish K562 panel cells expressing HNA-4a or HNA-5a, to detect HNA-4a and HNA-5a antibodies with KY cells. The only HNA antibody we were not able to detect with our K562 panel cells is against HNA-3a. It is not so difficult, however, to identify HNA-3a antibody with five-cell-lineage IFT because the frequency of HNA-3a-negative person is approximately 1 of 20, and we have already found two HNA-3a-negative personnel in our blood center.

As reported by several groups, the duration of neutropenia was significantly dependent on the strength of HNA in patient serum samples.^{23,38} Our K562 panel cells were able to identify the antibodies in the serum sample (Sample 2) from a patient diagnosed with chronic neutropenia after dilution of up to 1000 times (Fig. 4C). Therefore, the K562 panel cells will be useful in evaluating the clinical course of chronic neutropenia. Further serum

samples should be analyzed to standardize the panel cells as a precise diagnostic tool for HNA antibody-related diseases.

ACKNOWLEDGMENT

We thank M. Kobayashi, MD, PhD (Hiroshima University) for providing some of the serum samples containing neutrophil antibodies; K. Taniguchi, PhD (Hiroshima College of Medical Technology) for providing the TAG-1, -2, -3, and -4 monoclonal; and Y. Kanakura, MD, PhD (Osaka University) for providing the K562 and CMK cells.

REFERENCES

1. Bux J. Molecular nature of granulocyte antigens. *Transfus Clin Biol* 2001;8:242-7.
2. Bux J. Molecular genetics of granulocyte polymorphisms. *Vox Sang* 2000;78:125-30.
3. Stroncek D. Neutrophil alloantigens. *Transfus Med Rev* 2002;16:67-75.
4. Koene HR, Kleijer M, Roos D, de Hass M, dem Borne AE. Fc gamma RIIIB gene duplication: evidence for presence and expression of three distinct Fc gamma RIIIB genes in NA(1+,2+) SH(+) individuals. *Blood* 1998;91:673-9.
5. Bux J, Stein EL, Bierling P, et al. Characterization of new alloantigen (SH) on the human neutrophil Fcγ receptor 3b. *Blood* 1997;89:1027-34.
6. Kissel K, Scheffler S, Kerowgan M, Bux J. Molecular basis of NB1 (HNA-2a, CD177) deficiency. *Blood* 2002;99:4231-3.
7. Taniguchi K, Nagata H, Katsuki T, et al. Significance of human neutrophil antigen-2a (NB1) expression and neutrophil number in pregnancy. *Transfusion* 2004;44:581-5.
8. Kissel K, Santoso S, Hofmann C, Stroncek D, Bux J. Molecular basis of the neutrophil glycoprotein NB1 (CD177) involved in the pathogenesis of immune neutropenias and transfusion reactions. *Eur J Immunol* 2001;31:1301-9.
9. Marin L, Torio A, Muro M, et al. Alloimmune neonatal neutropenia and thrombocytopenia associated with maternal anti HNA-1a, HPA-3b and HLA antibodies. *Pediatr Allergy Immunol* 2005;16:279-82.
10. Bux J, Jung KD, Kauth T, Mueller-Eckhardt C. Serological and clinical aspects of granulocyte antibodies leading to alloimmune neonatal neutropenia. *Transfus Med* 1992;2:143-9.
11. Kwon SW, Procter J, Dale JK, Straus SE, Stroncek DF. Neutrophil and platelet antibodies in autoimmune lymphoproliferative syndrome. *Vox Sang* 2003;85:307-12.
12. Bruin M, Dassen A, Pajkrt D, et al. Primary autoimmune neutropenia in children: a study of neutrophil antibodies and clinical course. *Vox Sang* 2005;88:52-9.
13. Herzog P, Korinkova P, Stambergova M, Lukasova M. Auto anti-A1 and auto anti-NA1 after bone marrow

- transplantation. *Folia Haematol (Leipz)* 1987;114:874-80.
14. Klumpp TR, Herman JH, Schnell MK, Goldberg SL, Mangan KF. Association between antibodies reactive with neutrophils, rate of neutrophil engraftment, and incidence of post-engraftment neutropenia following BMT. *Bone Marrow Transplant* 1996;18:559-64.
 15. Webert KE, Blajchman MA. Transfusion-related acute lung injury. *Transfusion Med Rev* 2003;17:252-62.
 16. McCullough J, Weiblen BJ, Clay ME, Forstrom L. Effect of leukocyte antibodies on the fate in vivo of indium-111-labeled granulocytes. *Blood* 1981;58:164-70.
 17. Stroncek DF, Leonard K, Eiber G, et al. Alloimmunization after granulocyte transfusions. *Transfusion* 1996;36:1009-15.
 18. Matsuyama N, Kojima Y, Hirayama F, et al. Simultaneous 5 cell-lineage flow cytometric analysis system for detection of leukocyte antibodies. *Transfus Med* 2006;16:111-8.
 19. Prou O, Kaplan C, Muller JY. Freeze dried platelets for HLA alloantibodies absorption. *Tissue Antigens* 1980;16:105-7.
 20. Bux J, Kissel K, Hofmann C, Santoso S. The use of allele-specific recombinant Fcγ receptor 3b antigens for the detection of granulocyte antibodies. *Blood* 1999;93:357-62.
 21. Wolff J, Brendel C, Fink L, Bohle RM, Kissel K, Bux J. Lack of NB1 (CD177/HNA-2a) gene transcription in NB1 GP-neutrophils from NB1 GP-expressing individuals and association of low expression with NB1 gene polymorphisms. *Blood* 2003;102:731-3.
 22. Yasui K, Furuta RA, Matsumoto K, Tani Y, Fujisawa J. HIV-1-derived self-inactivating lentivirus vector induces megakaryocyte lineage-specific gene expression. *Microbes Infect* 2005;7:240-7.
 23. Kobayashi M, Nakamura K, Kawaguchi H, et al. Significance of the detection of antineutrophil antibodies in children with chronic neutropenia. *Blood* 2002;99:3468-71.
 24. Taniguchi K, Kobayashi M, Harada H, et al. Human neutrophil antigen-2a expression on neutrophils from healthy adults in western Japan. *Transfusion* 2002;42:651-7.
 25. Adam MA, Ramesh N, Miller AD, Osborne WR. Internal initiation of translation in retroviral carrying picornavirus 5' nontranslated regions. *J Virol* 1991;65:4985-90.
 26. Ghattas IR, Sanes JR, Majors JE. The encephalomyocarditis virus internal ribosome entry site allows efficient coexpression of two genes from a recombinant provirus in cultured cells and in embryos. *Mol Cell Biol* 1991;11:5848-59.
 27. Tamm A, Kister A, Nolte UK, Gessner EJ, Schmidt RE. The IgG binding site of human Fcγ3B receptor involves CC' and FG loops of the membrane-proximal domain. *J Biol Chem* 1996;271:3659-66.
 28. Takai T. Roles of Fc receptors in autoimmunity. *Nat Rev Immunol* 2002;2:580-92.
 29. Tamm A, Schmidt RE. The binding epitopes of human CD16 (FcγR3) monoclonal antibodies: implication for ligand binding. *J Immunol* 1996;157:1576-81.
 30. Watanabe Y, Shimada E, Fujiwara K, et al. Nucleotide sequence of a new Fc gamma receptor 3B allele that codes for a neutrophil antigen. *Tissue Antigens* 2000;56:272-5.
 31. Verheugt FW, dem Borne AE, Decary F, Engelfriet CP. The detection of granulocyte alloantibodies with an indirect immunofluorescence test. *Br J Haematol* 1977;36:533-44.
 32. Sabatino DE, Seidel NE, Cline AP, et al. Development of a stable retrovirus vector capable of long-term expression of gamma-globin mRNA in mouse erythrocytes. *Ann N Y Acad Sci* 2001;938:246-61.
 33. Jiang AF, Lalezari P. A micro-technique for detection of leukocyte agglutinins. *J Immunol Methods* 1975;7:103-8.
 34. Bux J, Kober B, Kiefel V, Mueller-Eckhardt C. Analysis of granulocyte-reactive antibodies using an immunoassay based upon monoclonal-antibody-specific immobilization of granulocyte antigens. *Transfus Med* 1993;3:157-62.
 35. Araki N, Nose Y, Kohsaki M, Mito H, Ito K. Anti-granulocyte antibody screening with extracted granulocyte antigens by a micro-mixed passive hemagglutination method. *Vox Sang* 1999;77:44-51.
 36. Hart SP, Alexander KM, Dransfield I. Immune complexes bind preferentially to Fc gamma RIIA (CD32) on apoptotic neutrophils, leading to augmented phagocytosis by macrophages and release of proinflammatory cytokines. *J Immunol* 2004;172:1882-7.
 37. Benoist H, Joly P, Broglio C, et al. Studies on the susceptibility to NK-mediated lysis and the simultaneous expression of various surface molecules in anthracyclin-treated K562 cells and in four K562 cell clones. *Immunol Lett* 1992;34:45-55.
 38. Bux J, Behrens G, Jaeger G, Welte K. Diagnosis and clinical course of autoimmune neutropenia in infancy: analysis of 240 cases. *Blood* 1998;91:181-6. ■

Reversible Smad-Dependent Signaling between Tumor Suppression and Oncogenesis

Go Sekimoto,¹ Koichi Matsuzaki,¹ Katsunori Yoshida,¹ Shigeo Mori,¹ Miki Murata,¹ Toshihito Seki,¹ Hirofumi Matsui,^{3,4} Jun-ichi Fujisawa,² and Kazuichi Okazaki¹

Departments of ¹Gastroenterology and Hepatology and ²Microbiology, Kansai Medical University, Osaka, Japan; ³Division of Gastroenterology, Institute of Clinical Medicine, University of Tsukuba; and ⁴RIKEN Cell Bank, The Institute of Chemistry and Physics, Tsukuba, Japan

Abstract

Cancer cells often gain advantage by reducing the tumor-suppressive activity of transforming growth factor- β (TGF- β) together with stimulation of its oncogenic activity as in Ras-transformed cells; however, molecular mechanisms remain largely unknown. TGF- β activates both its type I receptor (T β RI) and c-Jun NH₂-terminal kinase (JNK), which phosphorylate Smad2 and Smad3 at the COOH-terminal (pSmad2/3C) and linker regions (pSmad2/3L). Here, we report that Ras transformation suppresses T β RI-mediated pSmad3C signaling, which involves growth inhibition by down-regulating c-Myc. Instead, hyperactive Ras constitutively stimulates JNK-mediated pSmad2/3L signaling, which fosters tumor invasion by up-regulating plasminogen activator inhibitor-1 and matrix metalloproteinase-1 (MMP-1), MMP-2, and MMP-9. Conversely, selective blockade of linker phosphorylation by a mutant Smad3 lacking JNK-dependent phosphorylation sites results in preserved tumor-suppressive function via pSmad3C in Ras-transformed cells while eliminating pSmad2/3L-mediated invasive capacity. Thus, specific inhibition of the JNK/pSmad2/3L pathway should suppress cancer progression by shifting Smad-dependent signaling from oncogenesis to tumor suppression. [Cancer Res 2007;67(11):5090–6]

Introduction

Smads are central mediators of signals from the receptors for transforming growth factor- β (TGF- β) superfamily members to the nucleus (1). Smads are modular proteins with conserved Mad-homology 1 (MH1), intermediate linker, and MH2 domains (2). The catalytically active T β RI phosphorylates the COOH-terminal serine residues of receptor-activated Smads (3), which are Smad2 and the highly related protein Smad3. The linker domain can undergo regulatory phosphorylation by other kinases, including mitogen-activated protein kinases such as extracellular signal-regulated kinase (Erk), c-Jun NH₂-terminal kinase (JNK) and p38, or cyclin-dependent kinases (4–7). Phosphorylated Smad2 and Smad3 rapidly oligomerize with Smad4, forming functional trimeric protein complexes (2). Although monomeric Smad proteins constantly shuttle in and out of the nucleus, formation of the activated Smad complex favors their nuclear accumulation (2). In

the nucleus, the Smad complex binds directly to DNA and associates with a plethora of transcription factors, coactivators, or corepressors, leading to transcriptional induction or repression of the target genes (3).

TGF- β can inhibit epithelial cell growth (8), acting as a tumor suppressor. As currently understood, loss of sensitivity to growth inhibition by TGF- β in most cancer cells is not synonymous with complete shutdown of all TGF- β signaling. Instead, cancer cells gain advantage by selective reduction of the tumor-suppressive activity of TGF- β together with augmentation of its oncogenic activity (9, 10). Such a state of altered TGF- β responsiveness is observed in Ras-transformed cells, which typically exhibit a limited growth-inhibitory response to TGF- β , while acquiring ability to invade tissues and form metastases (11). One, therefore, needs to distinguish between the tumor-suppressive function of TGF- β in epithelial cells and its tumor-promoting role in Ras-transformed cells. In the present study, we sought to better understand molecular mechanisms regulating responses to TGF- β in these cells.

Materials and Methods

Domain-specific antibodies against phosphorylated Smad2 and Smad3. Nine polyclonal anti-phospho-Smad3 and anti-phospho-Smad2 sera were raised against the phosphorylated linker and COOH-terminal regions of Smad2 and Smad3 by immunization of rabbits with synthetic peptides (Supplementary Fig. S1). Relevant antisera were affinity purified using the phosphorylated peptides as previously described (6).

Constructs. H-Ras^{V12} was inserted into a pRX retroviral vector together with *blasticidin deaminase* gene. Smad3WT, Smad3EPSM, and Smad3(3SA) were inserted into another retroviral vector, pQCXIN (Clontech), containing a puromycin resistance marker. Integrity of the constructs was confirmed by sequencing.

Retroviral infection, expression of Ras^{V12}, and mutant Smad3. An ecotropic virus packaging cell line, BOSC23, was seeded at 1×10^6 cells per 100-mm dish. Twenty-four hours later, the cells were subjected to transfection with LipofectAMINE (Invitrogen) and 3 μ g of the indicated constructs for 4 h. After culture of the cells for 48 h, the filtrated culture supernatants were used for infection.

Parental RGM1 cells (1×10^5 per a six-well plate) were infected with a retroviral solution carrying H-Ras^{V12} in the presence of 8 μ g/mL polybrene (Sigma) for 6 h, and then were incubated in 10% FCS/DMEM. After trypsinizing and replating the cells at a 1:10 dilution on the 3rd day, selection was initiated with 1 μ g/mL blasticidin (Funacoshi), continuing for several weeks until blasticidin-resistant Ras-transformed cells (RGM Ras) emerged.

RGM Ras cells were infected additively with other retroviral solutions carrying Smad3WT, Smad3EPSM, or Smad3(3SA). Selection was initiated with 3 μ g/mL puromycin (Nacalai Tesque), continuing for several weeks until puromycin-resistant RGM Ras cells expressing Smad3 derivatives emerged. Five colonies per each infection were cloned and were subjected to assay or passage.

Note: Supplementary data for this article are available at Cancer Research Online (<http://cancerres.aacrjournals.org/>).

Requests for reprints: Koichi Matsuzaki, Department of Gastroenterology and Hepatology, Kansai Medical University, 10-15 Fumizono-cho, Moriguchi, Osaka, Japan. Phone: 81-6-6992-1001; Fax: 81-6-6996-4874; E-mail: matsuzak@takii.kmu.ac.jp.

©2007 American Association for Cancer Research.
doi:10.1158/0008-5472.CAN-06-4629

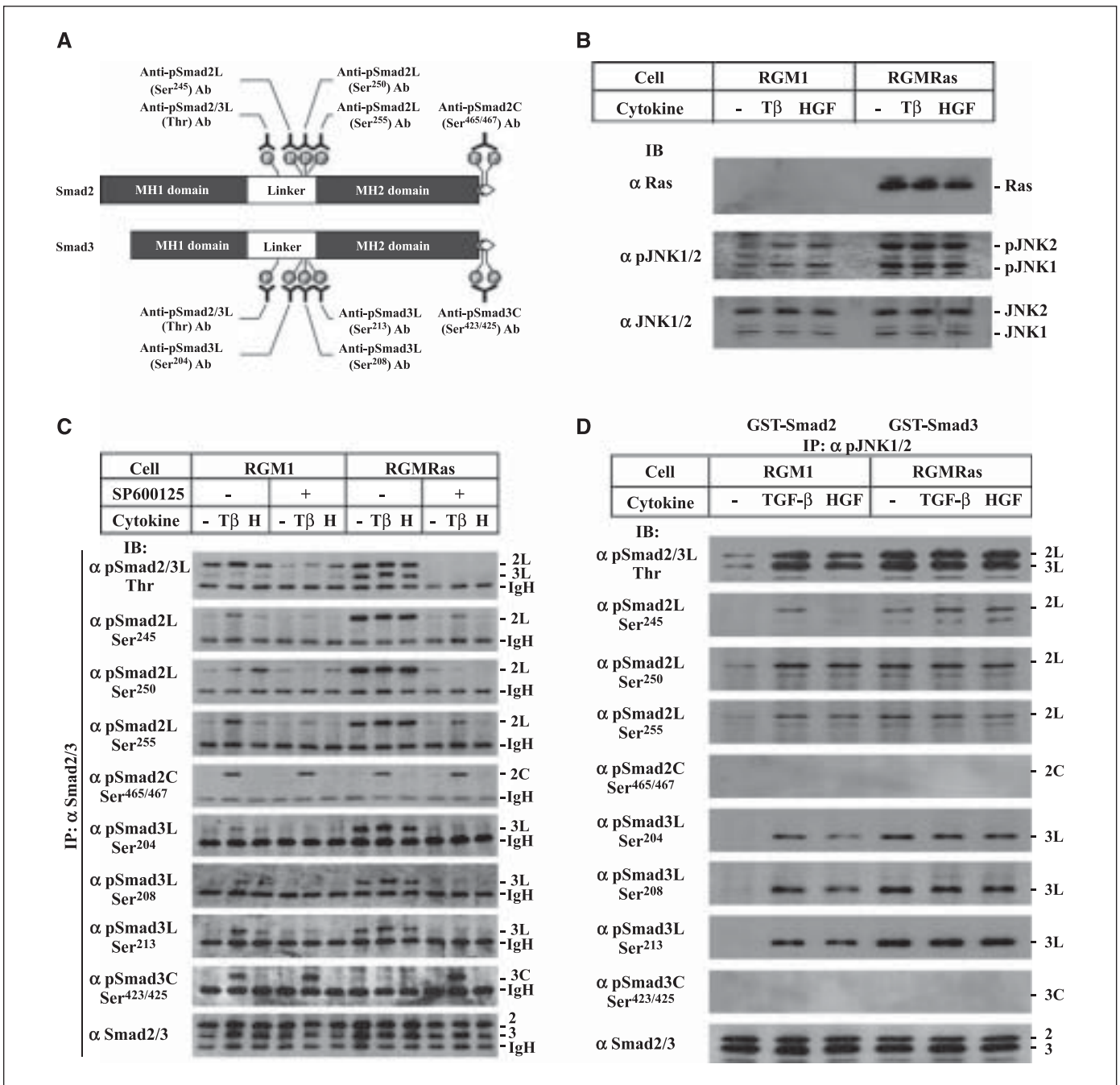


Figure 1. Hyperactive Ras alters Smad2 and Smad3 signaling via the JNK pathway, with increased basal pSmad2/3L and shutdown of TGF- β -dependent pSmad3C. **A**, schematic diagram of phosphorylation sites in Smad2 and Smad3 recognized by antibodies (Ab). Anti-pSmad2/3L (Thr) antibody, anti-pSmad2L (Ser²⁴⁵, Ser²⁵⁰, and Ser²⁵⁵) antibodies, anti-pSmad3L (Ser²⁰⁴, Ser²⁰⁸, and Ser²¹³) antibodies recognized JNK phosphorylation sites in the middle linker regions of Smad2 and Smad3, whereas anti-pSmad2C (Ser^{465/467}) antibody and anti-pSmad3C (Ser^{423/425}) antibody recognized phosphorylated COOH-terminal SXS sites activated by T β RI. Antisera were affinity-purified with the phosphorylated peptides followed by absorption with nonphosphorylated peptides. **B**, either TGF- β or HGF treatment caused inducible JNK phosphorylation in parental RGM1 cells, whereas Ras-transformed cells showed constitutively elevated phosphorylation of JNK1/2. Serum-depleted RGM-1 and Ras-transformed (RGM Ras) cells were incubated for 30 min with 20 pmol/L TGF- β 1 or 400 pmol/L HGF. Ras was analyzed by immunoblotting (IB) using anti-Ras antibody (α Ras). Phosphorylation of JNK was monitored by immunoblotting using anti-phospho-JNK1/2 antibody (α pJNK1/2). The total amount of JNK did not change during stimulation (α JNK1/2). **C**, Ras-transformed cells showed restoration of TGF- β -dependent pSmad3C upon treatment with a JNK inhibitor, SP600125. Serum-depleted RGM-1 and RGM Ras cells were incubated for 30 min with 20 pmol/L TGF- β 1 or 400 pmol/L HGF in the absence or presence of 15 μ mol/L SP600125. Following immunoprecipitation (IP) of cell lysates with anti-Smad2/3 antibody, phosphorylation of Smad2 and Smad3 was analyzed by immunoblotting using each anti-phospho-Smad2/3 antibody (top). The total amount of endogenous Smad2 and Smad3 did not change during stimulation (bottom). Either TGF- β or HGF treatment caused inducible Smad2 and Smad3 phosphorylation at the linker regions in parental RGM1 cells, whereas RGM Ras cells showed constitutively elevated phosphorylation. Although TGF- β treatment caused Smad2 phosphorylation at the COOH-terminal region in RGM Ras cells, COOH-terminal phosphorylation of Smad3 was not induced by TGF- β treatment. SP600125 inhibited TGF- β or HGF-dependent phosphorylation of Smad2L and Smad3L in parental RGM1 cells, as well as constitutive phosphorylation in RGM Ras cells. RGM Ras cells showed restoration of TGF- β -dependent pSmad3C upon treatment with SP600125. **D**, JNK activated by either TGF- β or HGF signal, as well as JNK constitutively activated by Ras signal directly phosphorylated Smad2L and Smad3L. Serum-depleted RGM1 and RGM Ras cells were incubated for 30 min with 20 pmol/L TGF- β 1 or 400 pmol/L HGF. Cell extracts were immunoprecipitated with anti-phospho-JNK1/2 antibody. *In vitro* kinase assays were done using GST-tagged Smad2 and Smad3 as substrates. Phosphorylation of Smad2/3 was analyzed by immunoblotting using each anti-phospho-Smad2/3 antibody (top). Total Smad2 and Smad3 were monitored by immunoblotting using anti-Smad2/3 antibody (bottom).

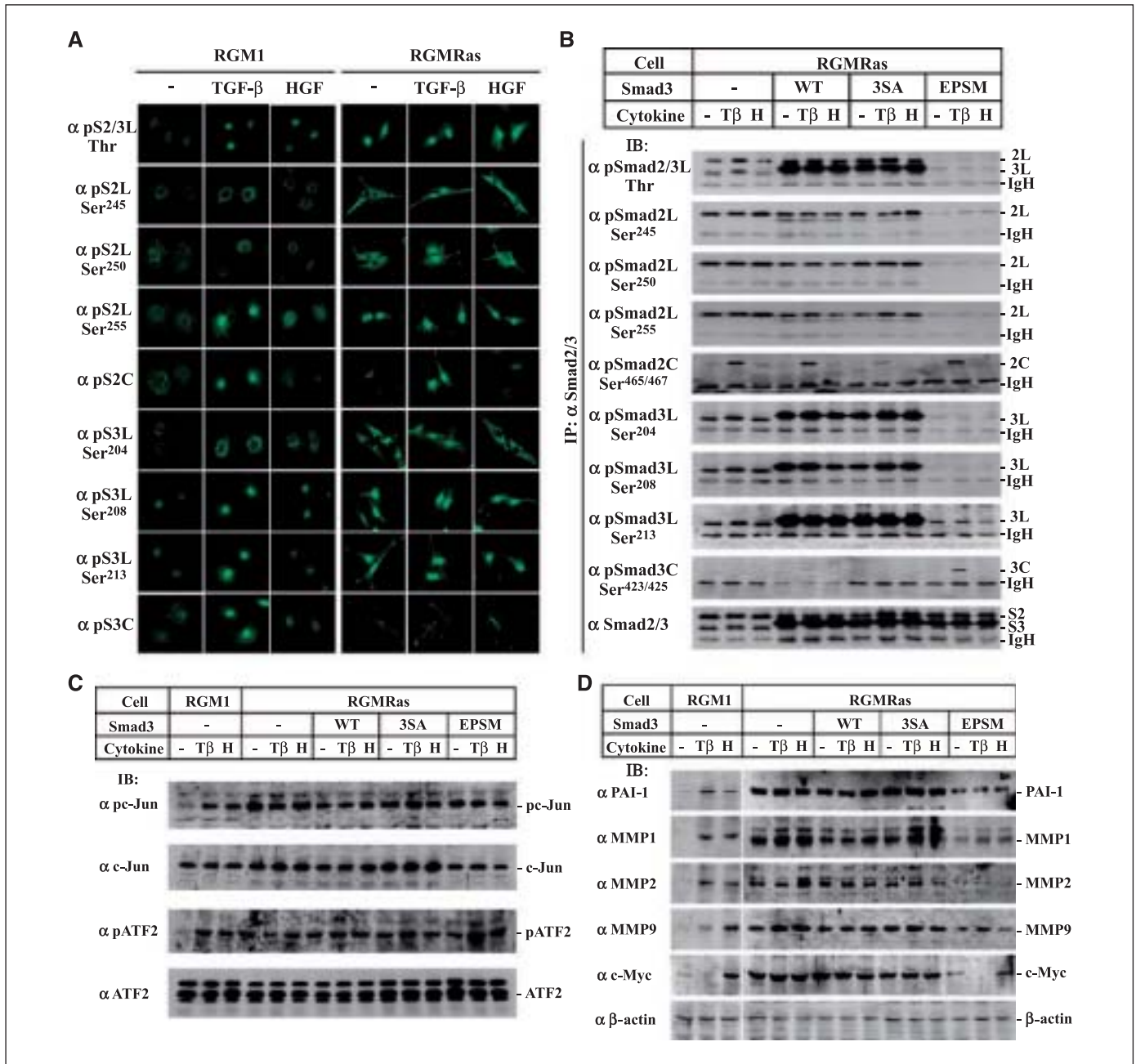


Figure 2. Ras-transformed cells show restoration of pSmad3C-mediated down-regulation of c-Myc together with minimized expression of PAI-1, MMP-1, MMP-2, and MMP-9 upon selective blockade of Smad2 and Smad3 linker phosphorylation. **A**, hyperactive Ras-mediated signal translocates Smad2 and Smad3 into nuclei. Serum-deprived RGM1 and RGM-Ras cells were incubated on slide for 1 h with 20 pmol/L TGF- β_1 or 400 pmol/L HGF. After fixation with 4% paraformaldehyde, slides were incubated with primary antibody for 16 h. Intracellular localization of phosphoisoforms was carried out in each anti-phospho-Smad2/3 immunofluorescence sample. Either TGF- β or HGF treatment of parental RGM1 cells resulted in nuclear translocation of pSmad2L (Thr²²⁰ and Ser²⁵⁵) and pSmad3L (Thr¹⁷⁹, Ser²⁰⁸, and Ser²¹³). The phosphoisoforms were already located in RGM-Ras cell nuclei before any exogenous TGF- β or HGF treatment. Although pSmad2C was detected in the nuclei of RGM-Ras cells after TGF- β treatment, neither basal nor TGF- β -dependent pSmad3C was demonstrable in the nuclei. **B**, selective blockade of Smad3 linker phosphorylation by a mutant Smad3 lacking JNK-dependent phosphorylation sites resulted in restored TGF- β -dependent Smad3 phosphorylation at the COOH-terminal region of Ras-transformed cells. RGM-Ras cells expressing Smad3WT, Smad3(3SA), or Smad3EPSM were incubated for 30 min with 20 pmol/L TGF- β_1 or 400 pmol/L HGF. Cell lysates were subjected to anti-Smad2/3 immunoprecipitation and then were immunoblotted with each anti-phospho-Smad2/3 antibody (*top*). Total Smad2 and Smad3 were monitored by immunoblotting using anti-Smad2/3 antibody (*bottom*). High expression of Smad3EPSM, but not those of Smad3WT or Smad3(3SA), blocked linker phosphorylation of Smad2 as well as Smad3 in RGM-Ras cells, resulting in TGF- β -dependent Smad3 phosphorylation at the COOH-terminal region as in parental RGM1 cells. **C**, blockade of Smad3 linker phosphorylation did not affect c-Jun or ATF2 phosphorylation of Ras-transformed cells. Serum-deprived RGM1 and RGM-Ras cells expressing Smad3WT, Smad3(3SA), or Smad3EPSM were incubated for 30 min with 20 pmol/L TGF- β_1 or 400 pmol/L HGF. Phosphorylation of c-Jun and ATF2 was monitored by immunoblotting using anti-phospho-c-Jun antibody (α pc-Jun) or anti-phospho-ATF2 antibody (α pATF2). The total amount of c-Jun and ATF2 did not change during stimulation (α c-Jun and α ATF2). RGM-Ras cells retained a high degree of c-Jun and ATF2 phosphorylation, despite highly expressed Smad3EPSM. **D**, blockade of Smad3 linker phosphorylation resulted in restoration of TGF- β -dependent down-regulation of c-Myc in Ras-transformed cells. Serum-deprived RGM1 and RGM-Ras cells expressing Smad3WT, Smad3(3SA), or Smad3EPSM were incubated for 4 h with 20 pmol/L TGF- β_1 or 400 pmol/L HGF. Expression of PAI-1, MMP-1, MMP-2, MMP-9, and c-Myc was monitored by immunoblotting using specific primary antibodies. Either TGF- β or HGF treatment caused inducible expression of PAI-1 and the MMPs in parental RGM1 cells. HGF treatment of RGM1 cells resulted in up-regulation of c-Myc, whereas TGF- β signaling rather repressed c-Myc expression. Hyperactive Ras caused constitutively high expression of PAI-1, the MMPs, and c-Myc. RGM-Ras cells expressing Smad3EPSM, but not those expressing Smad3WT or 3SA, showed decreased basal expression of PAI-1 and the MMPs, and restored TGF- β -dependent repression of c-Myc.

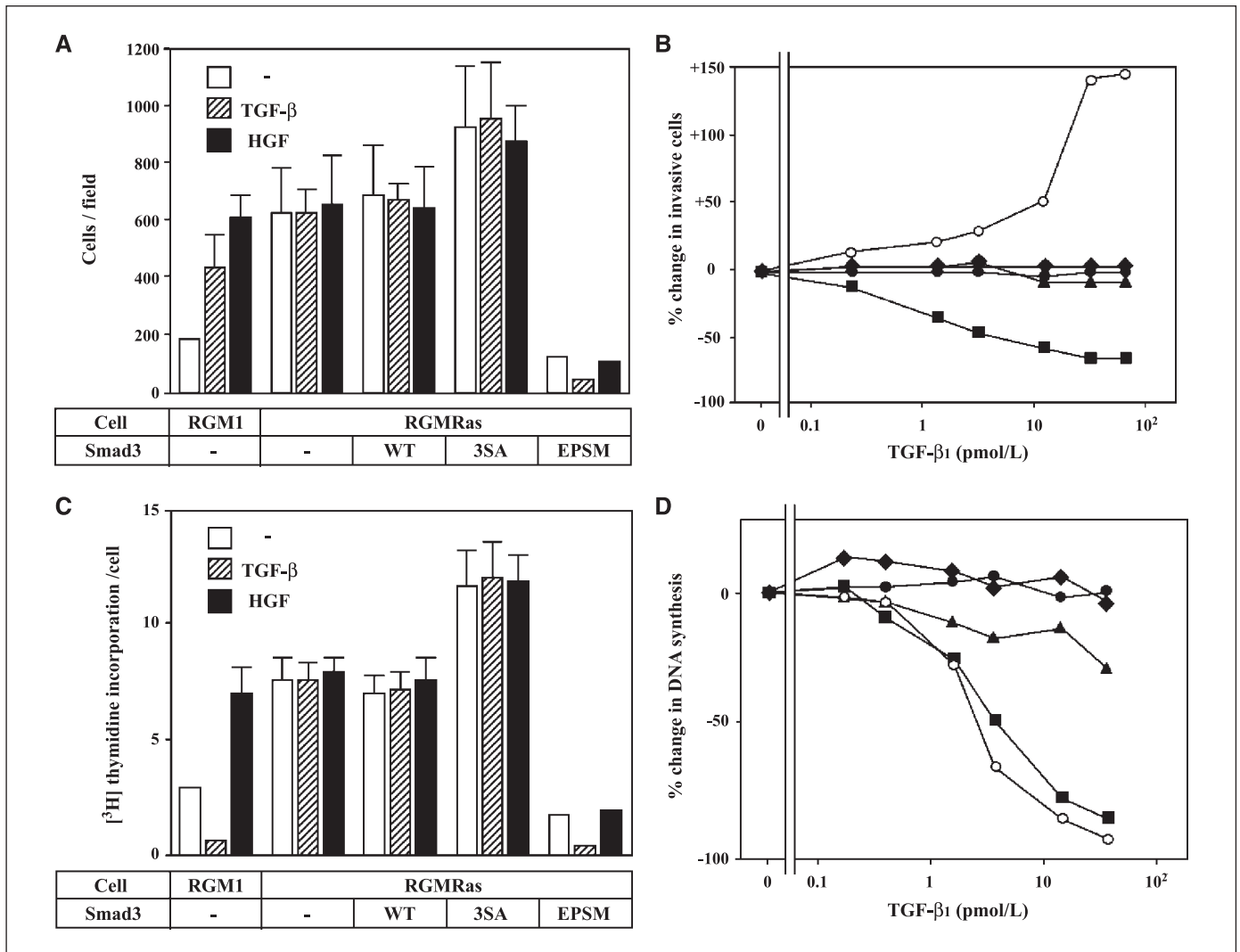


Figure 3. Ras-transformed cells show restoration of TGF- β -dependent tumor-suppressive function together with lack of invasive capacity upon selective blockade of Smad2 and Smad3 linker phosphorylation. **A** and **B**, blockade of Smad3 linker phosphorylation minimized invasive capacity of Ras-transformed cells in Matrigel. RGM-1 and RGM1 cells expressing Smad3WT, Smad3(3SA), or Smad3EPSM were cultured on Matrigel for 48 h with 20 pmol/L TGF- β and/or 400 pmol/L HGF (**A**). Infiltrating cells were counted in five regions selected at random, and the extent of invading cells was determined by the mean count. *Columns and points*, mean ($n = 4$) from a representative experiment; *bars*, SD. Percentage of invasion in response to various concentrations of TGF- β was calculated relative to the invading cell count obtained without exogenous TGF- β (**B**). Parental RGM1 cells invaded in response to TGF- β (\circ) or HGF stimulation. RGM1 cells expressing Smad3WT (\blacktriangle) or 3SA (\blacklozenge) retained constitutively high basal invasive capacity, like RGM1 cells (\bullet); RGM1 cells expressing Smad3EPSM (\blacksquare) did not show invasiveness. **C** and **D**, blockade of Smad3 linker phosphorylation resulted in restoration of growth-inhibitory response to TGF- β in Ras-transformed cells. RGM-1 and RGM1 cells expressing Smad3WT, Smad3(3SA), or Smad3EPSM were cultured in a six-well plate for 20 h with 20 pmol/L TGF- β and/or 400 pmol/L HGF (**C**). DNA synthesis was measured by incorporation of [³H]thymidine (1 μ Ci/well) after a 4-h pulse exposure. Extent of DNA synthesis was determined as a mean value for cpm. *Points and columns*, mean ($n = 4$) from a representative experiment; *bars*, SD. Percentage of DNA synthesis in response to various concentrations of TGF- β was calculated relative to [³H]thymidine incorporation obtained without exogenous TGF- β (**D**). HGF signal increased [³H]thymidine incorporation, whereas TGF- β signal rather reduced DNA synthesis in parental RGM1 cells (\circ). RGM1 cells expressing Smad3WT (\blacktriangle) or 3SA (\blacklozenge) maintained constitutively high levels of basal DNA synthesis, like RGM1 cells (\bullet). RGM1 cells expressing Smad3EPSM (\blacksquare) showed a growth-inhibitory response to TGF- β similar to that of parental RGM1 cells.

Immunoprecipitation and immunoblotting. Immunoprecipitation and immunoblotting of endogenous Smad2 and Smad3 were done as previously described (6).

Immunoblots of total cell lysates also were analyzed using 0.5 μ g/mL anti-Ras antibody (BD Biosciences), 5 μ g/mL anti- β -actin (Sigma), 3 μ g/mL anti-phosphorylated JNK1/2 antibody (Promega), 0.1 μ g/mL anti-JNK1/2 antibody (Cell Signaling), 1 μ g/mL anti-c-Myc antibody (Santa Cruz Biotechnology), 0.1 μ g/mL anti-plasminogen activator inhibitor-1 (PAI-1) antibody (BD Bioscience), 1 μ g/mL anti-matrix metalloproteinase 1 (MMP1) antibody (Chemicon International), 1 μ g/mL anti-MMP2 antibody (Chemicon International), and 0.5 μ g/mL anti-MMP9 antibody (Daiichi Fine Chemicals).

In vitro kinase assay. Bacterial expression and purification of glutathione *S*-transferase (GST)-Smad2 and GST-Smad3 were carried out according to the manufacturer's instructions (GE Healthcare). Endogenous kinases were isolated from the protein extracts using anti-pJNK1/2 antibody (Promega). Immunocomplexes, collected with protein G-Sepharose, were suspended in kinase assay buffer supplemented with 100 μ mol/L ATP and bacterially expressed GST-Smad2 or GST-Smad3. Assays were carried out as described previously (5). Degrees of phosphorylation of Smad2/3 were monitored by immunoblotting using each domain-specific phospho-Smad2/3 antibody.

Immunofluorescence. The subcellular localization of Smads was determined as previously described (5). To block binding of anti-pSmad3C

antibody to phosphorylated domains in Smad2, anti-pSmad3C antibody was adsorbed with 1 $\mu\text{g}/\text{mL}$ COOH-terminally phosphorylated Smad2 peptide.

[^3H]thymidine incorporation. DNA synthesis was measured by incorporation of 1 $\mu\text{Ci}/\text{mL}$ [^3H]thymidine (GE Healthcare) into 5% trichloroacetic acid-precipitable material after 4-h pulse as described previously (5).

Matrigel invasion assay. Membranes with 8- μm pores covered with Matrigel (BD Biosciences) on the upper surface were coated with type I collagen on the lower side. Infiltrating cells were counted in five regions selected at random as described previously (5).

Results

As lack of antibodies able to selectively distinguish phosphorylation sites in Smad2 and Smad3 has impeded investigation of the role of each phosphorylation domain in TGF- β signaling, we generated nine antibodies directed at various phosphorylation sites (Fig. 1A), and then verified that anti-phospho-Smad2/3L antibody would react only with specific phosphorylated domains in the linker regions (Supplementary Fig. S1).

Initially, we investigated TGF- β signaling in well-characterized cells (RGM1), which were isolated from normal rat gastric epithelial cells and were sensitive to growth inhibition by TGF- β (5). Previous work showed that both TGF- β and hepatocyte growth factor (HGF) were physiologic activators of the JNK pathway, which was shown to have important implications for Smad2 and Smad3 signaling (12, 13). In support of this notion, TGF- β or HGF treatment caused inducible JNK phosphorylation in RGM1 cells (Fig. 1B). Subsequently, the signal stimulated linker phosphorylation of Smad2 and Smad3 (Fig. 1C). The JNK inhibitor SP600125 inhibited TGF- β - or HGF-dependent linker phosphorylation *in vivo*. In addition, JNK activated by TGF- β or HGF signals could directly phosphorylate Smad2 and Smad3 at linker regions *in vitro* (Fig. 1D). We conclude from these findings that the JNK/pSmad2/3L pathway can be activated in response to TGF- β or HGF signal in the immortalized epithelial cells.

We previously reported that TGF- β signaling converted Smad2 and Smad3 into distinct phosphoisoforms: COOH-terminally phosphorylated Smad2/3 (pSmad2/3C) and linker phosphorylated Smad2/3 (pSmad2/3L; ref. 14). Translocation of Smad2 and Smad3 into the nucleus upon COOH-terminal phosphorylation by T β RI is a central event in TGF- β signal transduction (3). To gain additional insight into the significance of linker phosphorylation, we examined intracellular localization of each Smad2/3 phosphoisoform in RGM1 cells in response to TGF- β or HGF (Fig. 2A). As expected, most pSmad2C and pSmad3C were located in RGM1 cell nuclei after TGF- β treatment. In contrast, exposure to excess HGF did not lead to nuclear accumulation of pSmad2C or pSmad3C. Although weak pSmad2L (Ser²⁴⁵ and Ser²⁵⁰) and pSmad3L (Ser²⁰⁴) staining remained in the cytoplasm of RGM1 cells after TGF- β or HGF treatment, these treatments led to nuclear translocation of pSmad2/3L (Thr, pSmad2L (Ser²⁵⁵), and pSmad3L (Ser²⁰⁸ and Ser²¹³). Likewise, Smad2/3 phosphorylation by activated JNK has been shown to facilitate nuclear accumulation of Smad2 and Smad3 (12, 13). Taken together, the various results show that the linker phosphorylation can allow the Smad2/3 phosphoisoforms to translocate into nuclei via the activated JNK pathway, irrespective of COOH-terminal phosphorylation.

Ras participates importantly in human carcinogenesis; mutational activation of Ras is frequent in human cancer, and facilitates

tumor invasion and metastasis. To investigate whether excessively active Ras altered TGF- β signaling in immortalized epithelial cells, hyperactive Ras was expressed in RGM1 cells by retroviral infection using a vector carrying H-Ras^{V12}, which had a simple amino acid replacement of a glycine residue by valine. This substitution represents the critical change in conversion of the proto-oncogene to an active oncogene (15). Ras-transformed cells (RGM1Ras) selected by exposure to blasticidin (Fig. 1B) had a fibroblast phenotype, resisted growth inhibition by TGF- β , and showed increased invasiveness.

Hyperactive Ras resulted in sustained JNK activation (16). Similarly to the JNK phosphorylation profile (Fig. 1B), the linker regions of Smad2 and Smad3 were constitutively phosphorylated in RGM1Ras cells (Fig. 1C). SP600125 inhibited the linker phosphorylation *in vivo*. In addition, JNK activated by Ras-mediated signal could directly phosphorylate Smad2 and Smad3 at linker regions *in vitro* (Fig. 1D). These results indicate that the linker regions are constitutively phosphorylated via the Ras/JNK pathway. Although nuclear translocation of pSmad2L (Ser²⁴⁵ and Ser²⁵⁰) and pSmad3L (Ser²⁰⁴) required TGF- β addition in RGM1Ras cells, pSmad2/3L (Thr), pSmad2L (Ser²⁵⁵), and pSmad3L (Ser²⁰⁸ and Ser²¹³) were located in nuclei without exposure to exogenous TGF- β and HGF (Fig. 2A). In contrast, neither basal nor TGF- β -dependent Smad3 phosphorylation at the COOH-terminal region was demonstrable (Fig. 1C). Impaired Smad3 phosphorylation at the COOH-terminal region was not a result of T β RI inactivation because Ras-transformation did not interfere with T β RI-mediated Smad2 phosphorylation at the COOH-terminal region. On the other hand, RGM1Ras cells showed restoration of TGF- β -dependent Smad3 phosphorylation at the COOH-terminal region upon treatment with SP600125. Taken together, the results indicate that a high degree of JNK-dependent Smad3 phosphorylation at the linker region in Ras-transformed cells indirectly suppresses Smad3 phosphorylation at the COOH-terminal region.

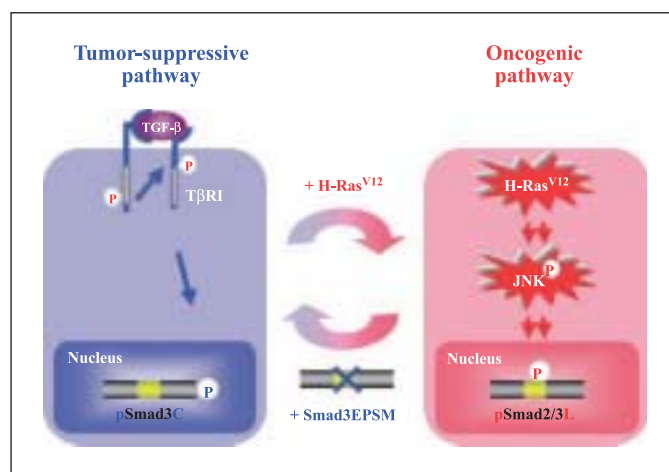


Figure 4. Smad-dependent signaling shows reversible switching between tumor suppression and oncogenesis. Normal epithelial cells exhibit TGF- β -dependent Smad3 phosphorylation at the COOH-terminal region, which involves growth inhibition by repression of c-Myc. Hyperactive H-Ras^{V12} transforms epithelial cells to shutdown pSmad3C-mediated signaling, while acquiring constitutively active JNK-mediated pSmad2/3L signaling that fosters tumor growth and invasion by up-regulating c-Myc, PAI-1, and MMP-1, MMP-2, and MMP-9. Selective blockade of linker phosphorylation by a mutant Smad3 lacking the JNK-dependent linker phosphorylation sites abolishes pSmad2/3L-mediated invasive properties and restores the TGF- β -dependent tumor-suppressive function involving pSmad3C that is shown by parental epithelial cells.

A JNK inhibitor can block alternative Smad-independent signaling pathway in the nucleus (17). To inactivate Smad2/3L selectively, a Smad3 mutant lacking four phosphorylation sites in the linker region (Erk/prodirected kinase site mutant; Smad3EPSM) was expressed in an additive manner in RGM1 cells by retroviral infection using another vector, carrying a puromycin resistance gene. RGM1 cells additively expressing wild-type Smad3 (Smad3WT) or Smad3(3SA), in which three COOH-terminal serine residues phosphorylated by T β RI were changed to alanine, were used as controls. Although endogenous Smad2 and Smad3 were phosphorylated constitutively at linker regions in RGM1 cells expressing Smad3WT and Smad3(3SA), their linker phosphorylation dramatically reduced in RGM1 cells expressing Smad3EPSM (Fig. 2B). Blockade of the linker phosphorylation by highly expressed Smad3EPSM did not affect Smad-independent signaling pathway because RGM1 cells retained a high degree of c-Jun and ATF2 phosphorylation, despite highly expressed Smad3EPSM (Fig. 2C). These results suggest that high Smad3EPSM expression specifically blocks linker phosphorylation of endogenous Smad2 as well as Smad3 in a dominant-negative manner.

We further investigated oncogenic Smad signaling in RGM1 cells. Tumor cell invasion, the first step toward metastasis, requires complex interactions including recognition and attachment of tumor cells to extracellular matrix (ECM)-binding sites, proteolytic dissociation of the ECM, and tumor cell migration within the surrounding tissue. In particular, because degradation of the ECM is conspicuous, enzymes with a proteolytic effect on the ECM such as MMP-1, MMP-2, and MMP-9 have been investigated (18). In addition, PAI-1 facilitates cell migration and invasion by enhancing cell adhesion. Reflecting the pSmad2/3L profile in RGM1 cells (Fig. 1C), PAI-1, and the MMPs involved in cell invasion were constitutively up-regulated (Fig. 2D). Although expression of Smad3WT and Smad3(3SA) in RGM1 cells did not affect amounts of PAI-1 or the MMPs, expression of Smad3EPSM notably reduced these invasion-related proteins in RGM1 cells. Moreover, RGM1 cells expressing Smad3EPSM showed less capacity to invade in a chamber assay than the cells expressing Smad3WT or Smad3(3SA) (Fig. 3A and B). The results suggest that pSmad2/3L-mediated signaling maintains overexpression of PAI-1 and the MMPs that promotes malignant behavior in Ras-transformed cells.

Consistent with restoration of Smad3 phosphorylation at the COOH-terminal region upon treatment to RGM1 cells with SP600125 (Fig. 1C), RGM1 cells expressing Smad3EPSM showed TGF- β -dependent Smad3 phosphorylation at the COOH-terminal region (Fig. 2B). This restoration could be explained in terms of remobilization of the Smad3 molecule from the nucleus to the cytoplasm where it would have access to membrane-anchored T β RI. In sum, hyperactive Ras drastically alters TGF- β signaling through the JNK pathway, increasing basal nuclear pSmad2/3L activity while shutting down TGF- β -dependent pSmad3C available for action in the nuclei. This could account for a lack of TGF- β -dependent Smad3C phosphorylation in cell nuclei of sporadic human colorectal cancer (19) and hepatocellular carcinoma (20).

TGF- β inhibits cell growth via Smad-mediated transcriptional regulation of critical regulators of the cell cycle (1). The first direct transcriptional target of the TGF- β pathway that explains how this cytokine inhibits proliferation of epithelial cells is c-Myc (8), the expression of which in parental RGM1 cells was repressed

by TGF- β (Fig. 2D). Aberrant expression of c-Myc in RGM1 cells (Fig. 2D) might contribute to resistance to the growth suppression in response to TGF- β (Fig. 3C and D), because c-Myc actively represses expression of critical cell cycle regulatory genes like *p15^{Ink4B}* and *p21^{Cip1}* (2). Similarly to restoration of TGF- β -dependent Smad3 phosphorylation at the COOH-terminal region in RGM1 cells expressing Smad3EPSM (Fig. 2B), the cells exhibited TGF- β -dependent inhibition of c-Myc expression (Fig. 2D) and [³H]thymidine incorporation (Fig. 3C and D) comparable with findings in parental RGM1 cells.

Discussion

In this study, we showed that TGF- β transmitted a signal through T β RI-dependent pSmad3C, participating in the cytosolic response by repressing transcriptional activity of *c-Myc* gene. On the other hand, Ras-activated JNK/pSmad2/3L signaling alone was able to provide oncogenic potential to the epithelial cells via up-regulation of c-Myc, PAI-1, MMP-1, MMP-2, and MMP-9, resulting in strongly enhanced tumor growth and invasion. Taken together, domain-specific phosphorylation of Smad2 and Smad3 is a key determinant regulating transcriptional activation of several target genes, ultimately selecting either tumor suppression or oncogenesis (Fig. 4).

Oncogenic Ras has been reported to activate Erk1/2, which directly phosphorylate the linker regions of Smad2 and Smad3 (4), with consequent blockage of all Smad signaling including Smad-dependent transcriptional activities of several target genes. However, our current results showed that hyperactive Ras constitutively activated the JNK pathway (Fig. 1B), leading to sustained linker phosphorylation of Smad2 and Smad3 (Fig. 1C and D), their nuclear translocation (Fig. 2A), and expression of PAI-1 and MMPs (Fig. 2D). Accordingly, exogenous TGF- β and HGF were unable to additionally enhance the JNK/pSmad2/3L-mediated invasive capacity of the Ras-transformed cells (Fig. 3A and B). In support of this notion, selective blockade of the linker phosphorylation in the Ras-transformed cells by a mutant Smad3 lacking JNK-dependent phosphorylation sites (Fig. 2B) resulted in minimal expression of PAI-1 and MMPs (Fig. 2D), and consequent disappearance of invasion by the cells (Fig. 3A and B). Taking the findings together, we conclude that oncogenic TGF- β signaling results from the functional collaboration of Ras and Smad rather than from Ras-mediated inhibition of the Smad pathway.

Deepening molecular understanding of signaling pathways closely associated with changes in human tissues during carcinogenesis has spurred and guided efforts to develop new molecularly targeted therapeutics for human cancer. The intrinsic value of target evaluation in model systems ultimately lies in the extent to which these systems accurately represent characteristics of human disease. In this respect, we have reported that TGF- β signaling conferred a selective advantage upon tumor cells by shifting from a tumor-suppressive T β RI/pSmad3C pathway to an oncogenic JNK/pSmad3L pathway during sporadic human colorectal carcinogenesis (19), an observation extended to hepatic carcinogenesis (20).

Our current results showed reversibility of Smad-dependent signaling between tumor suppression and oncogenesis (Fig. 4). By using genetic as well as pharmacologic approaches, we showed that blockade of linker phosphorylation abolished oncogenic properties in Ras-transformed cells and restored the pSmad3C-mediated tumor-suppressive function present in parental epithelial cells. A key therapeutic aim in cancer would be restoration of

the lost tumor-suppressive function observed in normal epithelial cells, together with disruption of fundamental signaling pathways that enable tumors to grow and invade. Accordingly, we have reason to hope that specific inhibition of the JNK/pSmad3L pathway can suppress progression of human cancer by a shift from oncogenesis to tumor suppression. In evaluating effectiveness of targeted therapies for human cancer, pSmad2/3L and pSmad3C should serve as useful biological markers that measure patient responses.

References

- Heldin CH, Miyazono K, ten Dijke P. TGF- β signaling from cell membrane to nucleus through SMAD proteins. *Nature* 1997;390:465-71.
- Massague J, Seoane J, Wotton D. Smad transcription factors. *Genes Dev* 2005;19:2783-810.
- Wrana JL. Crossing Smads. *Sci STKE* 2000;23:RE1.
- Kretzschmar M, Doody J, Timokhina I, Massague J. A mechanism of repression of TGF- β /Smad signaling by oncogenic Ras. *Genes Dev* 1999;13:804-16.
- Mori S, Matsuzaki K, Yoshida K, et al. TGF- β and HGF transmit the signals through JNK-dependent Smad2/3 phosphorylation at the linker regions. *Oncogene* 2004; 23:7416-29.
- Furukawa F, Matsuzaki K, Mori S, et al. p38 MAPK mediates fibrogenic signal through Smad3 phosphorylation in rat myofibroblasts. *Hepatology* 2003;38:879-89.
- Matsuura I, Denissova NG, Wang G, He D, Long J, Liu F. Cyclin-dependent kinases regulate the anti-proliferative function of Smads. *Nature* 2004;430: 226-31.
- Moses HL, Yang EY, Pietenpol JA. A TGF- β stimulation and inhibition of cell proliferation: new mechanistic insights. *Cell* 1990;63:245-7.
- de Caestecker MP, Piek E, Roberts AB. Role of transforming growth factor- β signaling in cancer. *J Natl Cancer Inst* 2000;92:1388-402.
- Pardali K, Moustakas A. Actions of TGF- β as tumor suppressor and pro-metastatic factor in human cancer. *Biochim Biophys Acta* 2007;1775:21-62.
- Oft M, Peli J, Rudaz C, Schwarz H, Beug H, Reichmann E. TGF- β 1 and Ha-Ras collaborate in modulating the phenotypic plasticity and invasiveness of epithelial tumor cells. *Genes Dev* 1996;10: 2462-77.
- Brown JD, DiChiara MR, Anderson KR, Gimbrone MA, Jr., Topper JN. MEKK-1, a component of the stress (stress-activated protein kinase/c-Jun N-terminal kinase) pathway, can selectively activate Smad2-mediated transcriptional activation in endothelial cells. *J Biol Chem* 1999;274:8797-805.
- Engel ME, McDonnell MA, Law BK, Moses HL. Interdependent SMAD and JNK signaling in transforming growth factor- β -mediated transcription. *J Biol Chem* 1999;274:37413-20.
- Matsuzaki K. Smad3 phosphoisoform-mediated signaling during sporadic human colorectal carcinogenesis. *Histol Histopathol* 2006;21:645-62.
- Tabin CJ, Bradley SM, Bargmann CI, Weinberg RA. Mechanism of activation of a human oncogene. *Nature* 1982;300:143-9.
- Derijard B, Hibi M, Wu IH, et al. JNK1: a protein kinase stimulated by UV light and Ha-Ras that binds and phosphorylates the c-Jun activation domain. *Cell* 1994;76: 1025-37.
- Derynck R, Zhang YE. Smad-dependent and Smad-independent pathways in TGF- β family signalling. *Nature* 2003;425:577-84.
- McCawley LJ, Matrisian LM. Matrix metalloproteinases: they're not just for matrix anymore! *Curr Opin Cell Biol* 2001;13:534-40.
- Yamagata H, Matsuzaki K, Mori S, et al. Acceleration of Smad2 and Smad3 phosphorylation via c-Jun NH(2)-terminal kinase during human colorectal carcinogenesis. *Cancer Res* 2005;65:157-65.
- Matsuzaki K, Murata M, Yoshida K, et al. Chronic inflammation associated with hepatitis C viral infection perturbs hepatic TGF- β signaling, promoting cirrhosis and hepatocellular carcinoma. *Hepatology*. In press 2007.

Acknowledgments

Received 12/21/2006; revised 2/17/2007; accepted 3/23/2007.

Grant support: the Ministry of Education, Science, and Culture of Japan (K. Matsuzaki and K. Okazaki).

The costs of publication of this article were defrayed in part by the payment of page charges. This article must therefore be hereby marked *advertisement* in accordance with 18 U.S.C. Section 1734 solely to indicate this fact.

We thank Dr. R. Derynck (University of California at San Francisco, San Francisco, CA) for providing us with cDNAs encoding human Smad2 and Smad3; C. Kitano for assistance in constructing ecotropic retrovirus; and N. Ohira for assistance with immunoblotting.



Original article

Real-time analysis of human immunodeficiency virus type 1 Env-mediated membrane fusion by fluorescence resonance energy transfer

Rika A. Furuta, Masao Nishikawa, Jun-ichi Fujisawa *

Department of Microbiology, Kansai Medical University, 15-10 Fumizono-cho, Moriguchi, Osaka 570-8506, Japan

Received 21 June 2005; accepted 16 August 2005

Available online 18 October 2005

Abstract

Human immunodeficiency virus type 1 (HIV-1) envelope glycoprotein (Env)-mediated membrane fusion occurs as a sequence of events that is triggered by CD4 binding to the Env gp120 subunit. In this study, we analyzed the dynamics of Env-mediated membrane fusion at the single-cell level using fluorescent fusion proteins and confocal laser fluorescent microscopy. Either enhanced cyan or yellow fluorescent protein (CFP and YFP, respectively) was fused to the end of the cytoplasmic regions of the HIV-1 receptors (CD4 and CCR5) and Env proteins. Real-time imaging of membrane fusion mediated by these recombinant proteins revealed that the kinetics of fusion in our system was faster than that previously reported. Analysis of the receptor interaction by fluorescence resonance energy transfer (FRET) at the single-cell level demonstrated a tendency for oligomerization of CD4–CD4, but not of CD4–CCR5, in the absence of Env-expressing cells. However, when Env-expressing cells attached to the receptor cells, FRET produced by CD4–CCR5 interaction was increased; the FRET intensity began to decline before the formation of the fusion pore. These changes in FRET may represent the temporal association of these receptors, triggered by gp120 binding, and their dissociation during the formation of the fusion pore. In addition, the FRET analysis of receptor interactions in the presence of fusion inhibitors showed that not only inhibitors acting on CCR5 but also the gp41-derived peptide T-20 interfered with CD4–CCR5 interaction during fusion. These data suggest that T-20 could affect the formation of Env-receptors complexes during the membrane fusion.

© 2005 Elsevier SAS. All rights reserved.

Keywords: HIV-1; Membrane fusion; FRET; Real-time imaging

1. Introduction

The human immunodeficiency virus type 1 (HIV-1) envelope glycoprotein (Env) forms trimers on the virion surface, with each monomer consisting of a surface subunit, gp120, and a transmembrane subunit, gp41 [1]. During virus entry, the gp120 glycoprotein binds to the CD4 molecules on the target cell and undergoes conformational changes that allow a high affinity interaction with certain chemokine receptors on the same target membranes [2–6]. Receptor binding is thought to trigger conformational changes in the gp41 glycoproteins

that eventually catalyze the fusion of the viral and target cell membranes, in which the heptad hydrophobic repeat regions of the gp41 trimer, N-HR and C-HR, form a 6-helix bundle (6HB) core structure [7–9]. It is hypothesized that multiple receptor-activated gp41 trimers assemble to form fusion pores [10–12], but the precise molecular mechanism of fusion pore formation is unknown.

Crystallographic studies have revealed some of the Env structures involved in the sequential events of membrane fusion [8,13,14], providing important information for understanding the contributions of each molecule to membrane fusion. In addition, biochemical studies have elucidated some of the conformational changes of Env and its molecular interactions with HIV-1 receptors during membrane fusion [15–20]. These studies, in combination with insights derived from the analogous hemagglutinin-mediated membrane fusion process of influenza virus (reviewed in [21]), have led to a model of an Env-

Abbreviations: CFP, cyan fluorescence protein; Env, envelope glycoprotein; FRET, fluorescence resonance energy transfer; HIV-1, human immunodeficiency virus type 1; PMT, photomultiplier tube; ROI, region of interest; YFP, yellow fluorescence protein.

* Corresponding author. Tel: +81 6 6993 9433; fax: +81 6 6993 1668.

E-mail address: fujisawa@naki.kmu.ac.jp (J.-I. Fujisawa).

mediated HIV-1 fusion process involving conformational changes of Env and receptors (reviewed in [22]). To fill the remaining gaps in our understanding of this process, we exploited a new real-time technology to monitor fusion as it occurs.

Fluorescence resonance energy transfer (FRET) microscopy has attracted widespread interest owing to its ability to detect protein–protein interactions in cells. FRET is a non-destructive spectroscopic method that can monitor the proximity and relative angular orientation of fluorophores and has been used to quantify the distance between two different fluorophores [23, 24]. In this system, excitation of the donor (cyan) molecule by a light beam leads to emission from the acceptor (yellow) molecule, provided that the proteins are close enough for energy transfer to occur. FRET between cyan and yellow fluorescent proteins (CFP and YFP, respectively) has been successfully applied to monitor intra- and inter-molecular associations of proteins [25–29]. Recently, FRET techniques have also been used to analyze membrane proteins in living cells and have demonstrated the formation of protein homo- and hetero-oligomers on the cell surface [30–34]. In this study, we applied the FRET technique to the analysis of the spatiotemporal changes in HIV-1 receptors during Env-mediated membrane fusion. We constructed CFP- or YFP-fused CD4 and CCR5 recombinant receptors that showed co-localization of two receptors on the introduced cell surface during the cell fusion. Real-time analysis of FRET between these recombinant proteins successfully demonstrated the temporal association of CD4 and CCR5 induced by Env binding in the living cell.

2. Materials and methods

2.1. Plasmids

All CFP- and YFP-fusion constructs were based on the pECFP-N1 and pEYFP-N1 plasmids (Clontech, Palo Alto, CA). To produce the CFP–YFP fusion construct (pCFPYFP), a CFP fragment was amplified by the polymerase chain reaction (PCR) with a reverse primer containing a new *HindIII* cleavage site that disrupts the termination codon of CFP and cloned at *BglII*–*HindIII* sites of pEYFP-N1.

To construct the CD4-containing plasmids, a human CD4 cDNA was amplified by RT-PCR using mRNAs extracted from peripheral blood mononuclear cells of a healthy volunteer, sub-cloned into pCDNA3.1(–) (Invitrogen, Carlsbad, CA), and designated pCD4. A CD4 cDNA fragment was then amplified by PCR using a primer pair that creates an *XhoI* site at the 5' end and a *BamHI* site at the 3' end, disrupting the termination codon of CD4. The amplified fragment was cloned into *XhoI*- and *BamHI*-digested pECFP-N1 and pEYFP-N1 plasmids to generate pCD4CFP and pCD4YFP, respectively. To elongate the spacer region between CD4 and CFP in pCD4CFP, a *BamHI* site was changed to a *HindIII* site using a 12-mer *HindIII* linker (5'-GATCCACCGGTCGCC-3') and an *XhoI*–*HindIII* CD4 fragment was cloned into *XhoI*- and *HindIII*-digested pECFP-N1. The resultant plasmid was subjected to blunting

and self-ligation at the *HindIII* and *SalI* sites to adjust the coding frames of CD4 and CFP. The spacer region between the CD4 and CFP coding sequences in the new plasmid, pCD4CFP25, was 18 amino acids (aa) longer than that in pCD4CFP.

A human CCR5 expression vector, pCCR5, was a gift from Takeda Pharmaceutical Company Ltd. (Osaka, Japan). A PCR-amplified CCR5 fragment with a *BamHI* site at the 5' end and an *AgeI* site at the 3' end that disrupted the termination codon of CCR5 was cloned into the *BamHI* and *AgeI* sites of pECFP-N1 and pEYFP-N1 to yield pCCR5CFP and pCCR5YFP, respectively. To generate pCCR5CC, which contains a tandem repeat of the CFP sequence, we first constructed pCFPCFP by insertion of a 741 bp *BamHI*/blunted-*NotI* fragment of pECFP-N1 into the blunted *BspI*1470I and *NotI* sites of pECFP-N1. Then a PCR, amplified 1059 bp fragment of CCR5 was cloned into the *BamHI* and *AgeI* sites of pCFPCFP, resulting in pCCR5CC. The pCCR5YY plasmid, which contains a tandem repeat of the YFP sequence, was constructed using a similar strategy.

To produce the Env expression constructs, the pSM-wt plasmid (a gift from C.D. Weiss), which expresses the Env protein of the HXB2 strain of HIV-1, was used as a PCR template. To replace 111 bp of 3' env gene by either CFP or YFP coding sequences, a new *AgeI* recognition site was introduced at the nucleotide position 2687 of env gene in pSM-wt by using the PCR technique and a 2687 bp *EcoRI*–*AgeI* env gene fragment from pSM-wt was ligated into *EcoRI*- and *AgeI*-digested pECFP-N1 and pEYFP-N1 plasmids to generate pHXBCFP and pHXBYFP, respectively. To construct Env expressers that utilize an alternative co-receptor [35–38], the 580 bp *BglII* fragments containing the V3 regions of pHXBCFP and pHXBYFP were swapped with a corresponding region of the Env coding sequence from the JRFL strain of HIV-1 (a gift from D.R. Littman), resulting in pH/JCFP and pH/JYFP, respectively. The Rev expression vector, pRev, a gift from S. Kubota, was used to induce Rev-mediated Env expression.

The primer pairs used in the PCR reactions described above were: 5'-CCGACTCAGATCTCGAGCTC-3' and 5'-AAGC TTGTACAGCTCGTCCATGCC-3' for pCFPYFP; 5'-CTCGA GCGGCCGCGGGAATTCGATTCCAACCATGGACCGG-3' and 5'-GCCAAAGTCTTCTGTACTTCGGGCCTAGG-3' for pCD4CFP, pCD4YFP, and pCD4CFP25; 5'-GAGCTCG GATCCGATGGATTATC-3' and 5'-ACCGGTGACAAGCC CACAGATATTTCTG-3' for pCCR5CFP, pCCR5YFP, pCCR5CC, and pCCR5YY; and 5'-CGGATCCTTGGCACT TATCTGGGAC-3' and 5'-ACCGGTGTGGCATTGAG CAAGCTAACAGC-3' for pHXB2CFP, pHXB2YFP, pH/JCFP, and pH/JYFP.

2.2. Cell culture and transfection

The human embryonic kidney 293T cells were purchased from American Type Culture Collection and maintained in Dulbecco's modified Eagle's medium (DMEM) containing 10% fetal bovine serum (FBS), 100 U/ml of penicillin, and

100 µg/ml of streptomycin. The U87.CD4.CXCR4 and U87.CD4.CCR5 target cell lines (gifts from D.R. Littman) were maintained in DMEM supplemented with 15% FBS and antibiotics. The cells were transfected using 7 µl of LipofectAmine (Invitrogen) and 2–3 µg of plasmid DNAs in six well dishes. By this method, 20–30% of cells were consistently transformed by plasmid DNAs.

2.3. Protein expression

For analysis of the expression of the CFP- or YFP-fused CD4 and Env proteins, the transfected 293T cells were lysed with NP-40 lysis buffer (0.5% NP-40, 0.1% TritonX-100, 0.1% deoxycholate, 10 mM Tris-Cl, 150 mM NaCl, 1 mM EDTA) containing a proteinase inhibitor mixture (Complete™; Roche, Mannheim, Germany) for 30 min on ice. After centrifugation at $10,000 \times g$ for 10 min at 4 °C, the supernatant was analyzed by 7.5–15% gradient sodium dodecylsulfate-polyacrylamide gel electrophoresis (SDS-PAGE), immunoblotted using an anti-GFP antibody mixture (clones 7.1 and 13.1; Roche) and detected using enhanced chemiluminescence (Amersham, Arlington Heights, IL).

To detect the expression of CCR5 fusion proteins, 1×10^6 transfected 293T cells were suspended in 0.5 ml of DMEM containing 5% FBS and 5 µg/ml anti-CCR5 monoclonal antibody (2D7; BD Biosciences, CA) for 1 h at room temperature. After being washed three times with PBS, the cells were lysed with 0.4 ml of IP lysis buffer (10 mM Tris-Cl [pH 6.8], 50 mM NaCl, 1% n-dodecyl maltoside, 1 mM CaCl₂, 10 mM EDTA, and $1 \times$ Complete™) on ice for 30 min. After clarification by centrifugation, the supernatants were incubated with 20 µl of protein G-sepharose beads for 1 h at 4 °C. The immunocomplexes were washed four times with IP lysis buffer and eluted with $1 \times$ Laemmli gel loading buffer containing 8 M urea. The complexes were analyzed by 8% SDS-PAGE, immunoblotted with the anti-GFP antibody mixture, and detected using chemiluminescence.

2.4. Single-round infection assay

To produce pseudotyped luciferase-expressing reporter virus, 293T cells growing in six-well plates were co-transfected with 0.2 µg of pNL43-Luc-E⁻R⁻ [39,40], 0.4 µg of a JRFL Env expression vector (both plasmids were gifts from D.R. Littman), 0.6 µg of Gag/Pol expression vector (pCMVΔ8.2; a gift from I.M. Verma), and 0.8 µg pRev using LipofectAmine. The culture supernatants containing the viruses were collected 48 h after transfection and centrifuged at $2350 \times g$ at 4 °C for 10 min; the supernatants were frozen at –80 °C until use. The amount of virus in the supernatants was quantified by measuring p24^{gag} using a commercial ELISA kit (RETRO-TEK, Zep-toMatrix Corp., Buffalo, NY).

For a single-round infection assay, 5×10^4 293T cells were transfected with 0.5 µg of both the CD4 and CCR5 expression vectors; 24 h after transfection, the cells were infected with 500 µl of the pseudotyped luciferase reporter virus (equivalent

to 20 ng of p24^{gag}) in the presence of 8 µg/ml polybrene. Forty-eight hours post-infection, the cells were harvested and the luciferase activities were measured using a commercially available dual-luciferase assay system (Promega, Madison, WI) according to manufacturer's instructions.

2.5. Cell–cell fusion assay

To evaluate the membrane fusion activity of the CFP- or YFP-fused Env proteins, cell–cell fusion assays were performed [41]. Briefly, 293T cells co-transfected with vectors expressing an Env fusion protein and Rev were labeled with calcein AM fluorescent dye (Molecular Probes Inc., Eugene, OR). Then, 2×10^5 of the labeled cells were co-cultivated with 1×10^5 of U87 cells expressing CD4 and either CXCR4 or CCR5 for 30 min at 37 °C. Cell fusion was determined by observation of dye transfer.

2.6. FRET analysis

All FRET analysis was performed using a Zeiss LSM510META confocal microscope (Carl Zeiss Inc., Thornwood, NY) equipped with an argon laser. For excitation of CFP and YFP, a 458/514 dual dichroic beam splitter was used as a primary dichroic mirror in the excitation path. A secondary 515 dichroic mirror was inserted in the emission path to separate CFP- and YFP-derived fluorescence. To improve the specific detection of CFP emissions at photomultiplier tube (PMT) 2, a 470–500 nm band pass filter was inserted. For specific detection of the YFP emissions, a 530–600 nm band pass filter was placed before PMT3. The FRET channel was designated as the YFP emissions detected at PMT3 using an excitation wavelength of 458 nm. To detect receptor FRET in the absence of Env-expressing effector cells, the acceptor bleaching method was used [42], whereby we bleached the cells by scanning a region of interest (ROI) 300 times using the 514 nm argon laser line at 100% intensity. The time required for bleaching ranged from 60 to 120 s, depending on the area of the ROI. Before and after bleaching, CFP images were collected to assess changes in donor fluorescence. To calculate the FRET efficiencies as a percentage (EF), we used the formula, $EF = 100 \times (I_{\text{after}} - I_{\text{before}})/I_{\text{after}}$, where I_{after} and I_{before} are the CFP intensities before and after bleaching, respectively [43]. We also calculated the I_{after} and I_{before} for an area outside of the ROI as a control. The background CFP intensity changed by less than 2% when determined at 60–120 s intervals in the same specimen, so we did not subtract background intensities. All the ROIs analyzed in the receptor FRET assays were on the plasma membrane.

2.7. Real-time imaging of cell fusion

For real-time imaging, 2×10^5 of 293T cells transfected with plasmids expressing either the HIV-1 receptors or the Env protein were suspended in 1 ml of DMEM supplemented with 10% FBS and passed through a nylon mesh filter

(Falcon® 352235; Becton Dickinson Discovery Labware, San Jose, CA) to disperse cell aggregations. The receptor- and Env-expressing cells (1 ml of each) were mixed in a 35 mm glass-bottomed dish (Matsunami Glass Ind., Ltd., Japan) and were monitored using 10 s time-lapse imaging on a confocal laser fluorescence microscope at 37 °C in a 5% CO₂ atmosphere.

2.8. Fusion inhibitors

The synthetic fusion inhibitors TAK-779 (*N,N*-dimethyl-*N*-(4-[[[2-(4-methylphenyl)-6,7-dihydro-5*H*-benzocyclohepten-8-yl]carbon-*y*]amino]benzyl)-tetrahydro-2*H*-pyran-4-ammonium chloride; Mr = 531.13) and T-20 were provided by Takeda Pharmaceutical Company Ltd. (Osaka, Japan). The 2D7 anti-CCR5 monoclonal antibodies were purchased from Clontech.

2.9. Statistics

A non-parametric analysis was performed with the Mann-Whitney *U*-test to determine statistically significant differences between two groups.

3. Results

3.1. Expression of fluorescent fusion proteins of HIV-1 Env and cellular receptors

To analyze the spatiotemporal dynamics of CD4 and CCR5 interaction during membrane fusion induced by the HIV-1 Env protein, we constructed a series of plasmids that express fluorescent fusion proteins of the HIV-1 receptors and Env proteins (Fig. 1A). The pCFPYFP plasmid, which expresses a fusion protein of YFP and CFP, was used as a positive control for FRET analysis. In all the receptor and Env constructs, either CFP or YFP was fused in frame at the C-terminal end of a cytoplasmic region of each protein. The pCD4CFP25, pCCR5CFP or YFP, pCCR5CC, and pCCR5YY plasmids were constructed in order to improve the efficiency of FRET. In the Env expression vectors, a 111 bp fragment of the 3' HXB2 env gene sequence was replaced by the coding sequence of CFP or YFP because the expression of full length Env protein fused with CFP- or YFP somehow resulted in severe cell death and the C-terminal truncation improved the cell viability (data not shown). To examine the involvement of an alternative co-receptor, a 580 bp fragment of HXB2 env that encompassed the V3 region was replaced with that of the JRFL env gene, resulting in vectors that express HXB2/JRFL chimeric Env proteins fused with a fluorescent protein (pH/JCFP and pH/JYFP).

The expression of protein by all constructs was confirmed using Western blot analysis (Fig. 1B). Bands corresponding to the expected molecular weights of the receptor fusion proteins CFPYFP, CD4CFP, CD4YFP, and CD4CFP25 (54 kDa for CFPYFP and 85 kDa for the CD4 derivatives) were detected (Fig. 1B, left panel). Co-transfection of a Rev expression vector was required to induce expression of the Env proteins because HIV-1 Env is expressed in a Rev-dependent manner (re-

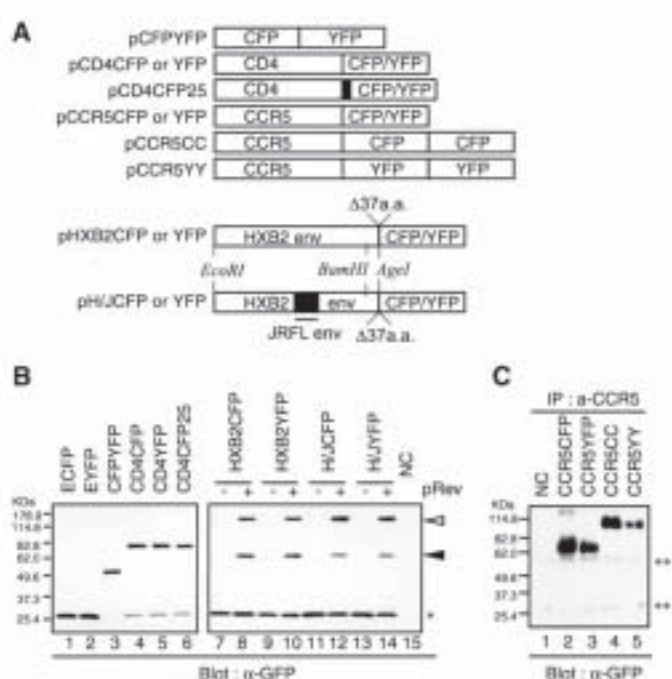


Fig. 1. (A) Schematic presentations of the structures of the fluorescent proteins fused with HIV-1 Env or cellular receptor proteins. pCFPYFP was used as a positive control in the FRET assay. Either CFP or YFP was fused in frame at the end of the cytoplasmic regions of CD4, CCR5, HXB2 Env, and chimeric HXB2/JRFL Env (H/J). In pCD4CFP25, the length of the gap between CD4 and CFP was increased by insertion of a linker sequence (solid box). In pCCR5CC and pCCR5YY, two tandem fragments of CFP or YFP, respectively, were fused with CCR5. The chimeric HXB2/JRFL Env expression vectors (pH/JCFP and pH/JYFP) were constructed by swapping a 580 bp fragment of HXB2 env containing the V3 region with that of the JRFL env, which results in the use of CCR5 as the co-receptor, instead of CXCR4. (B) Western blot analysis of the expression of CFP and YFP fusion constructs using anti-GFP monoclonal antibodies. Human 293T cells were transfected with the plasmids indicated above each lane. A Rev expression vector was co-transfected to induce Env expression (lanes 8, 10, 12, and 14). A 7.5–15% SDS-polyacrylamide gel was loaded with 3 (in lanes 1–3) or 10 (lanes 4–15) μ g of cell lysate and electrophoresed. Non-transfected 293T cell lysates were used as a negative control (lane 15, NC). (C) Surface IP and Western blot analysis of the expression of CCR5 derivatives. The IP complexes formed with an anti-CCR5 antibody were analyzed using 8% SDS-PAGE and blotted with anti-GFP monoclonal antibodies. Open arrowhead, uncleaved Env precursor; closed arrowhead, cleaved Env transmembrane subunit; * CFP or YFP; ** IgG.

viewed in [44,45]). In the lysates of Env-transfected 293T cells, both the uncleaved precursor (180 kDa) and cleaved Env (67 kDa) were observed in the presence of Rev (Fig. 1B, right panel). Regardless of whether Rev was expressed, we detected unfused CFP or YFP in cells transfected with any of the fusion constructs except in pCFPYFP (Fig. 1B, lanes 3–14), especially in those transfected with the Env constructs (Fig. 1B, lanes 7–14). The origin of these free proteins was unclear; in the cells transfected with the Env constructs, it is possible that substantial amounts of the mRNAs encoding the fusion proteins were spliced in such a way as to permit translation of the unfused CFP or YFP.

Overall integrity of the 3-D structure of the fusion proteins used for the assay was also confirmed to be maintained, since an immunoprecipitation (IP) assay of these Envs using a conformation sensitive anti-gp120 mAb (#13-8-100, ABI, MD)

and anti-gp41 mAb (2F5, NIH AIDS Research and Reference Reagent Program) resulted in the same pattern of precipitation between wild type and the recombinant Envs (data not shown).

To detect the CCR5 derivatives, we performed cell-surface IP with an anti-CCR5 antibody; the IP complexes were analyzed using SDS-PAGE in the presence of 8 M urea because the CCR5 protein was not well denatured under the usual SDS-PAGE conditions (Fig. 1C). In the Western blot analysis of the IP complexes, bands corresponding to the cell surface CCR5 derivatives were detected at the expected relative molecular weights of 68 kDa (CCR5CFP and CCR5YFP, Fig. 1C, lanes 2 and 3) or 95 kDa (CCR5CC and CCR5YY, lanes 4 and 5). In all of the Western blots, the recombinant proteins were detected using a mixture of anti-GFP monoclonal antibodies that efficiently recognized both CFP and YFP. We also confirmed the surface expression of the CD4 and CCR5 derivatives by FACS analysis with either anti-CD4 or anti-CCR5 antibody (data not shown).

3.2. Membrane fusion activities of CFP- or YFP-fusion proteins with Env and cellular receptors

We then examined the functionality of the recombinant receptors for mediation of HIV-1 infection using a single-round infection assay [40]. As shown in Fig. 2A, 293T cells co-transfected with a wild type CCR5 expression vector and either pCD4CFP or pCD4YFP were infected to the same extent as

the control cells co-transfected with wild type CCR5 and CD4 expression vectors, indicating that the modification of CD4 by fusion with CFP or YFP at the end of the cytoplasmic region did not impair its ability to function as an HIV-1 receptor. In contrast, cells co-transfected with CCR5YFP and either CD4CFP or CD4YFP were less susceptible to infection with the reporter virus than the control cells ($P > 0.1$), although a substantial level of infection was still observed. These data indicate that the HIV-1 co-receptor function of CCR5 is more sensitive to modification than is the receptor function of CD4.

We also evaluated the fusion activities of the Env-CFP and Env-YFP fusion proteins in a cell–cell fusion assay [41] using U87 cells stably expressing the HIV-1 receptors (Fig. 2B). After transfection with plasmids expressing Rev and one of the fluorescent HXB2 Env fusion proteins, 293T cells fused only with U87 cells expressing CD4 and CXCR4. As expected, 293T cells transfected with plasmids expressing the chimeric HXB2/JRFL Env fusion protein (H/J Env) and Rev were able to fuse with U87 cells expressing CD4 and CCR5, but did not fuse with those expressing CD4 and CXCR4. We also examined the ability of the chimeric H/J Env to infect with U87. CD4.CCR5 cells using a single-round infection assay with a pseudotyped reporter virus; pseudotyped viruses with chimeric H/J Env exhibited a similar level of infectivity to that exhibited by pseudotyped viruses with wild-type JRFL Env (data not shown). Moreover, the fusion activity of the H/J Env protein in this assay was not impaired by either the 111 bp C-terminal deletion or the fusion with the fluorescent proteins. Therefore, we concluded that the modifications of the receptors and Env proteins used in this study only minimally perturbed their fusion activities.

3.3. Real-time analysis of Env-mediated membrane fusion

To examine the kinetics of cell–cell fusion at the single-cell level, two types of 293T transfectants, one expressing a fusion protein of CFP or YFP with an HIV-1 receptor (“receptor cells”) and another expressing an CFP- or YFP-fused Env protein (“Env cells”), were mixed and placed on the stage of a confocal laser microscope at 37 °C. The fluorescence signals were monitored using time-lapse imaging over 10 s recording intervals (Fig. 3). In many cases, the cells had already begun to fuse when observation was initiated. Fig. 3A shows the images of two 293T cells expressing CD4CFP25 and CCR5YY and one expressing H/JYFP Env protein. The substantial amount of YFP signals in the Env cell were observed not only on the cell surface but also in the cytoplasm (arrowhead) because unfused YFP proteins were also expressed from the pH/JYFP vector even in the presence of Rev, as discussed above. The localization pattern of the YFP–Env fusion protein allowed us to distinguish the Env cells from the receptor cells. At 3' 20" after mixing, some CCR5YY protein had accumulated in the membrane of one of the receptor cells where it was in contact with the Env cell. The cyan blue signals from the CD4CFP25 protein were observed not only on the surface of the receptor cells but also on the Env cell membrane adjacent to the contact

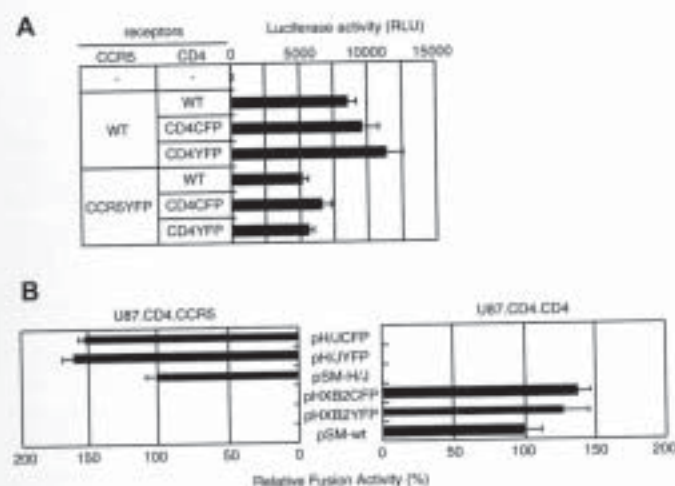


Fig. 2. Membrane fusion activity of CFP or YFP-fusion proteins with Env and cellular receptors. (A) The susceptibilities of cells expressing recombinant receptors to HIV-1 infection were determined using a single-round infection assay. Human 293T cells transfected with the receptor expression vectors were infected with a luciferase reporter virus pseudotyped by JRFL Env (equivalent to 20 ng of p24). The infectivity was scored as the luciferase activity in the cells after the infection period ($N = 4$). (B) The fusion activities mediated by the CFP- or YFP–Env fusion proteins as determined using the cell–cell fusion and dye transfer assay. Human 293T cells co-transfected with vectors expressing an Env fusion protein and Rev were labeled with calcein AM fluorescent dye and co-cultivated with U87 cells expressing CD4 and either CCR5 or CXCR4. The relative fusion activity of the Env fusion proteins was calculated as a percentage of the fusion activity observed in cells transfected with plasmids expressing the wild-type HXB2 (pSM-wt) or chimeric HXB2/JRFL (pSM-H/J) Env proteins, as measured by the number of fused cells ($N = 4$).

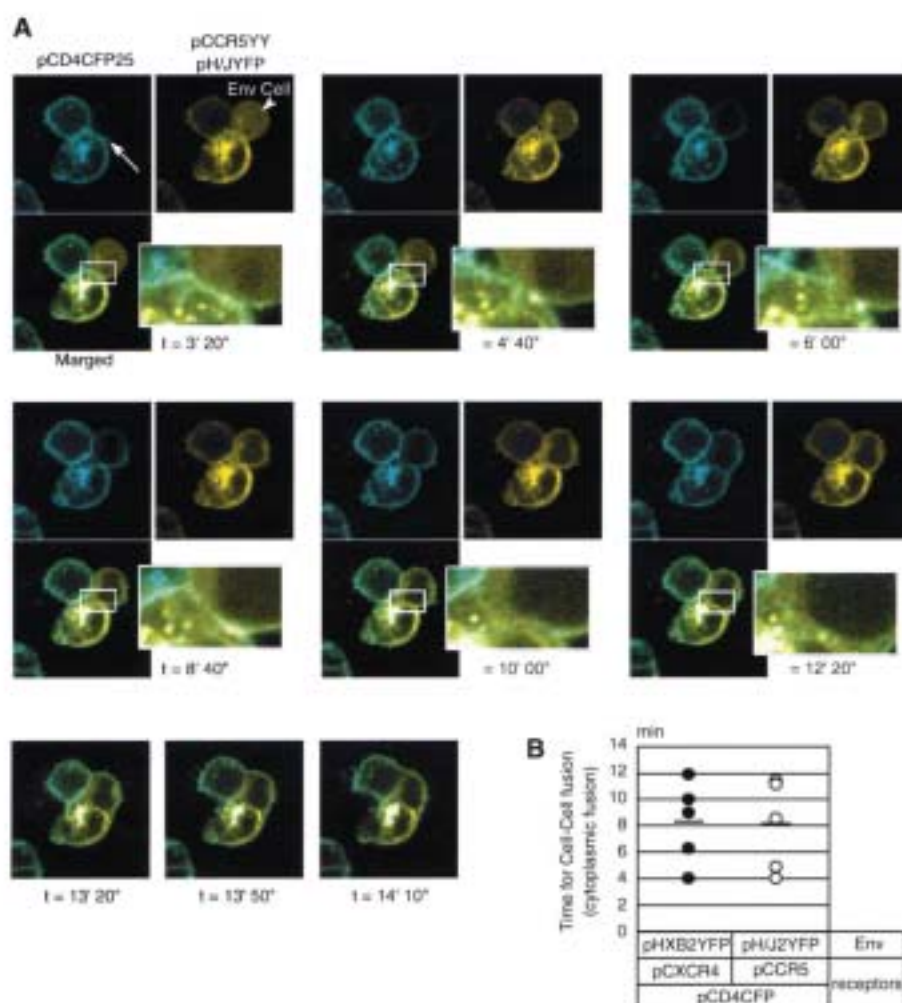


Fig. 3. Real-time analysis of HIV-1 Env-mediated cell fusion. (A) Human 293T cells were transfected with pCD4CFP25 and pCCR5YY to yield receptor-expressing cells or pH/JYFP and a Rev expression vector to yield Env-expressing cells. The transfected cells were detached from the dish by pipetting and co-cultivated at 37 °C. Time-lapse imaging was performed with 458/514 nm dual excitation over 10 s recording intervals. The insets are enlarged images of the regions indicated with open white squares. (B) The elapsed times from cell mixing to cytoplasmic fusion (pore formation) was measured for five independent cell fusion events using cells expressing different co-receptors and Env proteins. Human 293T cells were transfected with pCD4CFP and a vector expressing either wild type CXCR4 or CCR5 to generate the receptor cells. To generate the Env cells, 293T cells were transfected with either pHXB2YFP or pH/JYFP Env, which interact with CXCR4 and CCR5, respectively. The receptor and Env cells were co-cultivated at 37 °C and time-lapse images were obtained over 10 s recording intervals using 458/514 nm dual excitation.

region (arrow), indicating that membrane fusion had already begun.

We detected an apparent opening in the membrane between the receptor and Env cells and noted the accumulation of CD4CFP25 and CCR5YY around this area. The opening gradually increased in size and the cytoplasmic YFP signal in the Env cell was translocated into the receptor cell. Therefore, we concluded that the open area was a fusion pore. The fusion pore reached its maximum size at 13' 20"; fusion with a second receptor cell was observed thereafter ($t = 13' 50''$ and 14' 10"). Clear internalization of CD4 or CCR5 during the course of cell fusion was not detected with the magnification and time-lapse interval that we used. We also measured the elapsed time from cell mixing to cytoplasmic fusion (pore formation) for five independent cell fusion events using cells expressing either HXB2 or H/J Env proteins and receptor cells expressing the appropriate co-receptor (Fig. 3B). With both types of Env cells,

the fastest fusion was observed 4 min after mixing and no significant differences in the fusion kinetics were detected between the two types of Env proteins. We concluded that co-receptor usage does not affect fusion kinetics when the receptors and Env proteins are expressed at similar levels; therefore, we examined membrane fusion mediated by CCR5, rather than CXCR4, in all subsequent studies, because 293T cells do not express endogenous CCR5.

3.4. FRET analysis of HIV-1 receptors

To examine the interactions among HIV-1 receptors in a living cell, FRET analysis was performed using cells transfected with plasmids expressing fusion proteins of the HIV-1 receptors with CFP or YFP. By following a method described by Karpova et al. [43], we established PMT gain settings that consistently yielded no cross-talk when imaging cells expressing

either CFP or YFP. We used excitation with 458 nm and detection of emissions at PMT3 using a 530–600 nm band path filter to produce the FRET images (FRET channel), that is, the FRET signal is defined as YFP emission produced by CFP excitation. As controls, we performed FRET analysis on cells transfected with pECFP-N1, pEYFP-N1, or pCFPYFP (Fig. 4A, upper left). The 293T cells expressing either CFP or YFP alone did not show any cross-talk when the PMT gain settings were adjusted so that the intensity of the CFP signal was 90–180 and that of the YFP signal was 60–120 for a ROI. Under these conditions, we observed no FRET signals in cells expressing both CFP and YFP from separate constructs, whereas a distinct FRET signal was detected in cells expressing the CFPYFP fusion proteins. Based on the observations from this control assay, we determined the PMT gain settings for all subsequent experiments using cells transfected with only a

CFP- or YFP-fusion construct to avoid signal cross-talk. In addition, we selected cells that expressed CFP and YFP at an intensity ratio of approximately 1.5:1 (CFP/YFP) in the same PMT gain setting to avoid the confounding effects of the molar ratios of CFP and YFP molecules on FRET analysis.

We examined the subcellular localization and oligomeric status of CD4 and CCR5 in transfected 293T cells before membrane fusion. CD4 was expressed predominantly on the cell surface (Fig. 4A, upper right), whereas CCR5 was localized on the cell surface and in the cytoplasm (Fig. 4A, lower left). FRET signals derived from CD4–CD4 and CCR5–CCR5 were consistently observed but CD4–CCR5 interaction was hardly detected on the images even though it could be measured digitally (Fig. 4A, upper right, lower right, and lower left, respectively). Although the PMT gain settings that had been determined using the controls yielded no cross-talk signals in most ROIs, some regions

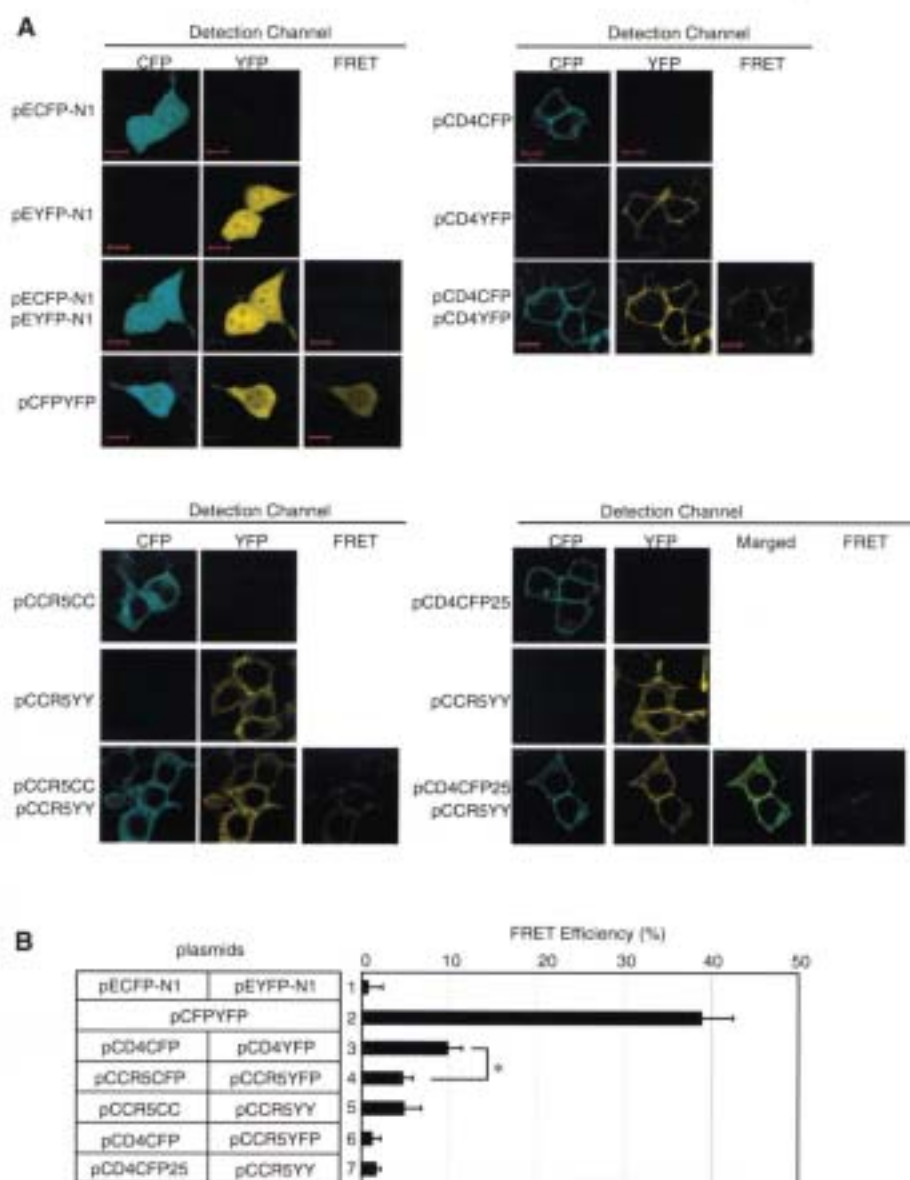


Fig. 4. FRET analysis of HIV-1 receptors in the absence of Env-expressing cells. (A) Human 293T cells were transfected with the plasmid(s) indicated to the left of each image. The signals were detected in the channels indicated at the top of the images. (B) FRET efficiencies in cells transfected with the plasmid(s) indicated to the left of the graph were calculated using the acceptor bleaching method ($N = 40$). * $P < 0.05$.

with particularly large accumulations of fluorescent molecules produced signal cross-talk and/or bleeding. Therefore, we measured FRET efficiencies by an acceptor bleaching method, in which FRET was assessed as the increase in CFP fluorescence intensity (donor dequenching) following YFP (acceptor) photobleaching. Using this method, the calculated FRET efficiencies were less than 1% in the negative control (Fig. 4B, lane 1) and almost 40% in the positive control (lane 2), indicating that our assay system had a good dynamic range. In cells expressing CD4CFP and CD4YFP or CCR5CFP and CCR5YFP in combination, the calculated FRET efficiencies were 9.8% and 4.6%, respectively (Fig. 4B, lanes 3 and 4). The formation of homo-oligomers of CD4 or CCR5 in these cells would produce three different fluorophore combinations, that is, CFP–CFP, YFP–YFP, and CFP–YFP. As only the last combination would yield FRET, the actual tendencies of HIV-1 receptors to form homo-oligomers are presumed to be much higher than those estimated by the FRET efficiencies. Therefore, we concluded that both CD4 and, to a lesser extent, CCR5 molecules preferentially form homo-oligomers on the surface of transfected 293T cells.

Several modifications of the C-terminal region of each receptor fusion protein were made in attempts to improve the intensity of the fluorescence and/or the FRET signals. First, we duplicated portions of CFP and YFP in the CCR5 constructs to produce CCR5CC and CCR5YY, respectively, which resulted in the expected enhancement of the fluorescence signals (data not shown). However, the intensity of the FRET signals in cells expressing both CCR5CC and CCR5YY was not increased as compared to those in cells expressing the original fusion constructs, CCR5CFP and CCR5YFP (Fig. 4B, lanes 4 and 5), suggesting that CCR5–CCR5 interactions indeed occur at a lower frequency than do CD4–CD4 interactions. Next, we modified the length of the spacer region between the receptor protein sequence and that of the fluorescent protein to permit the proteins to adopt more appropriate orientations for the production of FRET. The lengths of the cytoplasmic regions of CD4 and CCR5 were estimated to be 37 aa [46] and 56 aa [47]. We constructed a series of CD4CFP expression vectors with different lengths of spacer sequence between CD4 and CFP: the pCD4CFP11, pCD4CFP21, and pCD4CFP25 plasmids have 11, 21 and 25 aa spacer regions, respectively, whereas the original plasmid, pCD4CFP, has a seven aa spacer. In combination with either CCR5YFP or CCR5YY, CD4CFP produced the lowest (1.1%) FRET efficiency and CD4CFP25 produced the highest (1.7%; Fig. 4B, lanes 6 and 7). Other combinations resulted in intermediate FRET efficiencies (data not shown). We next examined the FRET efficiency for the combination of CD4CFP25 and CCR5YY, and found that it was consistently less than that of the homomeric interactions of both CD4 and CCR5. These data suggest that CD4 and CCR5 do not form stable heteromers on the cell surface in the absence of Env proteins, as has been previously reported based on biochemical analysis [15].

3.5. Real-time analysis of FRET during membrane fusion

To analyze the FRET efficiencies produced by interactions between CD4 and CCR5 during Env-mediated membrane fusion,

we monitored transfected cells using time-lapse imaging over 10 s recording intervals. In this assay, the cells were scanned over 50 times on average, resulting in fading of the fluorescence output. Consequently, the PMT gain settings that were determined before fusion became inappropriate after multiple scans. As an alternative method of measuring the signal intensities in the FRET channel, we excited the fluorescent proteins with a 458 nm laser line and measured both the YFP (= FRET) and CFP signal intensities from two ROIs on the receptor-expressing cell: the area of contact with the Env expressing cell (fusing area, F) and a region distant from the area of contact (non-fusing area, NF). Then, we normalized the intensity of the FRET signals to the intensity of the CFP signal in the same ROI by calculating the YFP/CFP ratios at 458 nm excitation (=FRET/CFP), and compared these ratios for the F and NF areas (Fig. 5A). Although the FRET/CFP ratio is not identical to the FRET efficiency, it can serve as a useful approximation of FRET efficiency in real-time studies in which multiple scans of the same ROI are required.

We examined the receptor interactions in receptor-expressing cells that were in contact with Env-expressing cells. We found that CD4–CD4 interactions, as measured by the FRET/CFP ratios, did not differ significantly between the F and NF regions, indicating that the status of CD4 oligomerization/association does not change dramatically during membrane fusion (Fig. 5A, upper row). In contrast, the FRET/CFP ratios in the F regions were significantly enhanced as compared to the NF regions in both CCR5CC–CCR5YY- and CD4CFP25–CCR5YY-expressing cells (Fig. 5A, middle and lower rows). These data indicate that Env-mediated membrane fusion induces increased interaction between CD4 and CCR5 as well as enhanced CCR5 homomeric interaction. To rule out the possibility that the measurement of the FRET produced by the receptor interaction in the F region was affected by the YFP signals from the Env-expressing cell that was attached to the receptor cell, we performed the same experiments using H/JCFP in place of H/JYFP as the Env protein and obtained the same results (data not shown). Therefore, we concluded that the enhancement of the FRET signals in the F regions indicated increased interactions among the receptors during fusion.

To examine the association between CD4 and CCR5 during membrane fusion, we monitored the FRET/CFP ratios in the F and NF regions of a cell expressing CD4CFP25 and CCR5YY during fusion with an-Env-expressing cell, and calculated the FRET/CFP ratios in the F and NF regions, (FRET/CFP)_F/(FRET/CFP)_{NF} or F/NF, every 10 s (Fig. 5B). At time = 0, defined as the time that a receptor cell was first observed attaching to an Env cell, the FRET/CFP ratio in F was almost twice that in NF (Fig. 5A, bottom). Between time = 0 and time = 50 s, the F/NF ratio increased to 2.8 and then gradually decreased. We identified a visible fusion pore at time = 150 s, at which point the F/NF ratio was less than 2. The F/NF ratio finally stabilized at approximately 1.5 when cell fusion was complete. These data suggest that the Env-receptor complexes undergo two distinct conformational changes before the fusion pore becomes visible: in the first step CD4 and CCR5 are closely associated, and in the subsequent step the complexes become dissociated, probably in tandem with the formation of the fusion-active form(s) of gp41.

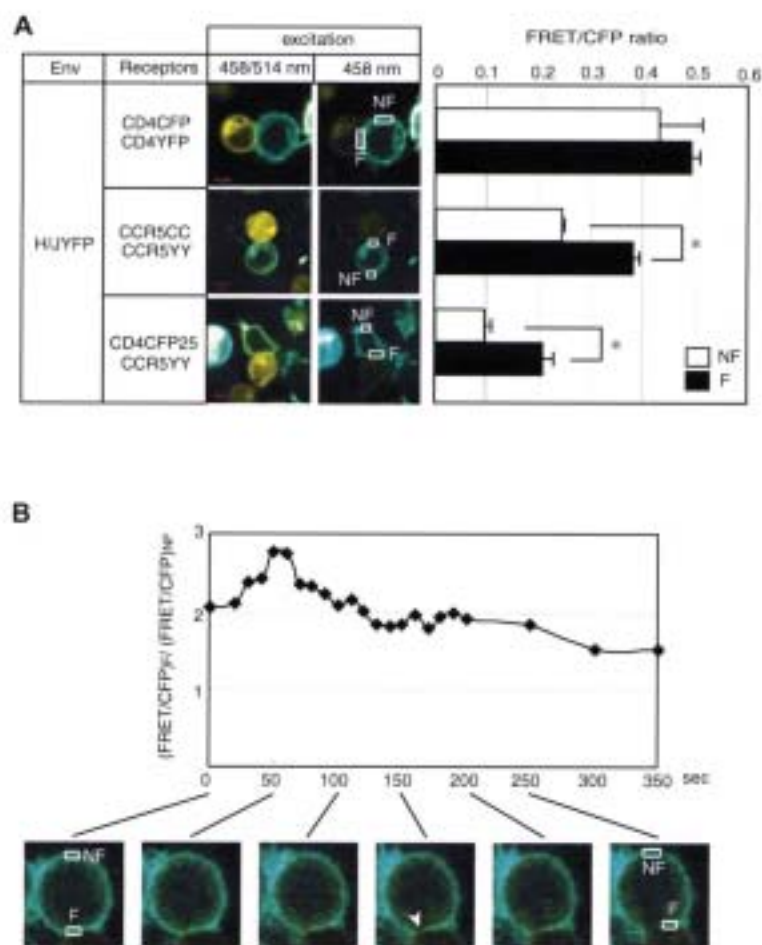


Fig. 5. FRET produced by receptor interactions during membrane fusion. (A) The receptor cells were generated by transfecting 293T cells with the following combinations of plasmids: pCD4CFP, pCD4YFP and pCCR5 for CD4–CD4 interactions (top); pCD4, pCCR5CC and pCCR5YY for CCR5–CCR5 interactions (middle); and pCD4CFP25, pCCR5YY for CD4–CCR5 interactions (bottom). The receptor cells were co-cultivated at 37 °C with 293T cells transfected with pH/JYFP and a Rev expression plasmid. Images were obtained using 458/514-nm dual excitation (left panels) or 458 nm excitation (right panels). Both the CFP and FRET signal intensity were measured in ROIs in the area of contact with the Env-expressing cell (fusing area, F) and in a region distant from the area of contact (non-fusing area, NF) using 458 nm excitation. The FRET/CFP ratio in each ROI was calculated (left graph). * $P < 0.05$. (B) The FRET for CD4–CCR5 interactions was monitored during cell fusion. The ratios of the FRET/CFP in the F and NF areas were calculated every 10 s. Human 293T cells were transfected with pH/JCFP and pRev to generate the Env cells or with pCD4CFP25 and pCCR5YY to generate the receptor cells. The Env and receptor cells were co-cultivated at 37 °C. We began monitoring when a pair of fusing cells was identified (time = 0). Images obtained on the FRET channel at 50 s intervals are indicated below the graph. Arrowhead, fusion pore.

3.6. Effects of fusion inhibitors on the FRET produced by receptor interactions

Several fusion inhibitors are available that block HIV-1-mediated membrane fusion (reviewed in [22,48]). To examine the details of the fusion steps in terms of CCR5–CD4 association, we examined CD4–CCR5 FRET during membrane fusion in the presence of either an anti-CCR5 neutralizing antibody (2D7) [49], a CCR5 antagonist (TAK-779) [50], or a gp41-derived peptide (T-20, formally DP-178) [51]. For this assay, 293T cells expressing CD4CFP25 and CCR5YY were mixed with cells expressing H/JCFP Env in the presence of a single inhibitor at a concentration sufficient for complete block of fusion and incubated at 37 °C. Relatively high concentrations of the inhibitors were required to block fusion (IC_{50} of T-20 was 3 μ M, for example) probably because of the accelerated ki-

netics of membrane fusion in our system [52]. In the presence of the inhibitor, the receptor and Env cells attached to each other, but neither membrane fusion nor fusion pore formation was observed (data not shown). We measured the FRET signals in the attaching cells as was done for the experiments in Fig. 5, because the movements of the suspended 293T cells during laser scanning were prohibitive for the application of acceptor bleaching. In the absence of inhibitors, the FRET/CFP ratio in F was over twice that in NF (Fig. 6, lanes 1 and 2), which was similar to the results shown in Fig. 5A. However, when 2D7, TAK-779, or T-20 was added at concentrations sufficient to completely block fusion, the FRET/CFP ratio in F was not significantly greater than that in NF. These data suggested that the CD4–CCR5 association was fairly inhibited in the membrane in contact with the Env-expressing cell in the presence of 2D7, TAK-779, or T-20.

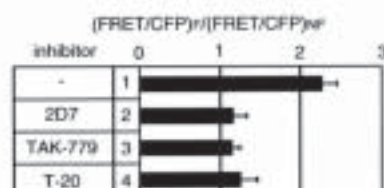


Fig. 6. The FRET for CD4–CCR5 interactions in the presence of fusion inhibitors. Human 293T cells were transfected with pCD4CFP25 and pCCR5YY to generate receptor cells or with pH/ICFP and pRev to generate Env cells. The receptor and Env cells were co-cultivated at 37 °C in the presence of 10 µg/ml 2D7, 0.5 µM TAK-779, or 10 µM T-20 ($N = 7$). The FRET and CFP signals were measured in fusing (F) and non-fusing areas (NF), as described for Fig. 5, and the ratios of FRET/CFP in F and NF were calculated.

4. Discussion

We performed real-time analysis of HIV-1 Env-mediated membrane fusion to detect the interactions among the HIV-1 receptors during the course of fusion at the single-cell level. We used fusion proteins consisting of CFP or YFP connected to the C-terminal cytoplasmic regions of CD4 or CCR5 to reveal the dynamics of the receptor interactions during membrane fusion (Fig. 5). Several assays for HIV-1 fusion or entry have been reported, in which Env-mediated fusion occurs after a lag phase that is usually longer than 10 min and completed in about 1 h [52–55]. In our assay, however, Env-mediated fusion exhibited very fast kinetics; fusion was complete within 12 min of starting co-cultivation and no distinctive lag phase was observed. The faster kinetics of cell fusion in our assay are mainly attributable to the higher densities of receptors, particularly CD4, expressed on the cell surface, because the kinetics that we observed were similar to those reported for CD4-independent Env-mediated membrane fusion [55–57]. In addition, the Env protein expression plasmids that we used here have a 37 aa truncation in the cytoplasmic region that connects with CFP or YFP, which also probably contributed to the more rapid fusion kinetics [58]. Whereas the transient expression of a full-length Env fusion protein with either CFP or YFP resulted in severe cell death (data not shown), the truncated Env fusion proteins exhibited both improved cell viability after transfection and increased fusion activity. Although the reasons for these differences are not yet clear, it is noteworthy that the truncated gp41 expressed in our assay preserved the internalization motifs (YXXL) [59]; therefore, the mechanism underlying the accelerated fusion kinetics did not involve blocking the internalization of Env proteins via the YXXL motifs.

In this study, FRET analysis demonstrated the formation of some homo-oligomeric CD4 and CCR5 in the absence of Env-expressing cells (Fig. 4). It has been reported that the CD4 molecules on the plasma membranes of lymphocytes and monocytes were expressed predominantly as monomers, but that oligomeric forms CD4 were also observed [60]. Furthermore, a recent report demonstrated the predominant expression of CD4 dimers on Langerhans' cells [61]. Therefore, it is probable that the recombinant CD4 molecules transiently expressed in 293T cells formed oligomers to some extent. Monomeric expression of CCR5 has been previously demonstrated by co-IP analysis in a transient expression system [62]. It is possible that limited homo-oligomerization of CCR5 on the cell surface

was not previously detected because, whereas our FRET data were obtained from the cell surface only, substantial amounts of CCR5 protein are expressed in the cytoplasm of transfected cells as well (Fig. 4A), and this could mask oligomerization that occurs only on the surface.

Though FRET analysis has been used to reveal the molecular dynamics of various proteins, including cell membrane proteins, the evaluation of FRET data has been difficult and varies among assay systems [63]. For example, if the expression level of the fluorescent proteins differs from cell to cell in a single specimen, selecting the appropriate PMT gain settings for all cells is problematic; this is the case in transient expression assays. Therefore, the acceptor bleaching method has been widely used to quantify FRET [43]. In this study, we obtained highly reproducible values for FRET efficiency using this method (Fig. 4B), and we consequently concluded that detection of the interactions of HIV-1 receptors was feasible using the FRET assay. To monitor the spatiotemporal changes of FRET emissions, however, the acceptor bleaching method cannot be used because it quenches the YFP signal. In addition, the fluorescence signals gradually decline with increasing numbers of scans for time-lapse imaging. Thus, we measured the FRET signal using a fixed PMT gain setting (that would have become inappropriate over a series of scans), and normalized the intensity of the FRET signal by dividing it by that of the CFP signal in the same ROI to compensate for signal fading. While this procedure cannot be used to calculate accurate FRET values, comparisons of the normalized FRET signals from membrane areas undergoing fusion with those from non-fusing membrane areas on the same cell provide an approximation of the changes in FRET that occur during fusion.

Using 458 nm excitation, the FRET/CFP ratios determined for the CD4–CD4, CCR5–CCR5, and CD4–CCR5 interactions in the non-fusion areas of transfected cells correlated well with the FRET efficiencies calculated using the acceptor bleaching method, although the absolute values differed (Figs. 4B and 5A). It is possible that the accumulation of receptors in the membrane fusion area contributed to the FRET produced by receptor interactions; however, there were no significant differences in the FRET/CFP ratios calculated for the CD4–CD4 interactions in the fusion and non-fusion areas, indicating that CD4 accumulation resulting in increased FRET did not occur. In contrast, the FRET/CFP signal from the CCR5–CCR5 and CD4–CCR5 interactions was enhanced in the fusion area. These results indicate that specific interactions between these receptors are involved in the fusion process, rather than simply their accumulation. The FRET/CFP ratio for the CD4–CCR5 interaction was very low in cell membranes not involved in cell fusion and was clearly enhanced in fusing membranes before the fusion pore became visible, and declined thereafter (Fig. 5B). We, therefore, concluded that the method used in this study captured the real-time changes in the CD4–CCR5 interactions during the course of cell fusion.

We obtained both expected and unexpected results from the experiments using fusion inhibitors (Fig. 6). In the FRET assay using an anti-CCR5 antibody (2D7) that can neutralize HIV-1 infection [49], it was not surprising that the CD4–CCR5 association was inhibited, as the antibody blocks CCR5 binding to gp120 after CD4 engagement. Similarly, the observation of no

significant enhancement of FRET in the fusion area in the presence of the CCR5 antagonist TAK-779 appeared to be consistent with a proposed inhibitory mechanism in which TAK-779 binds a pocket area composed of transmembrane regions of CCR5 and interferes with gp120 binding [64]. In both cases, CCR5 is thought to be inaccessible to gp120 and would, thus, be unlikely to make stable associations with CD4. However, the gp41-derived peptide T-20 (also called DP-178, enfuvirtide and fuzeon) has been thought to bind to an activated structure of gp41 that is triggered by CD4 and co-receptor binding and to interfere with the formation of the 6HB core structure of gp41 [16,65]. Based on this proposed inhibitory mechanism, T-20 would be expected to function after co-receptor binding to gp120, when the CD4–CCR5 association would already be engaged. Nevertheless, we observed substantial inhibition of the CD4–CCR5 interaction by T-20 in the FRET assay although there remained a possibility that the high concentration of T-20 used could somewhat affect the result. However, two recent reports may provide a new perspective for understanding the inhibitory mechanism of T-20. First, Yuan et al. [66] reported that T-20 binds gp120 glycoproteins that utilize CXCR4 as a co-receptor and blocks the interaction of the gp120–CD4 complexes with CXCR4. They demonstrated the apparent ability of T-20 to bind to gp120 in combination with CXCR4, but also showed very weak binding of T-20 to gp120 glycoproteins in IP assays in the presence of CCR5. It is possible that the high concentration of T-20 that we used results in binding not only to gp41 but also to gp120, and that such binding plays a role in the inhibition of gp120–CCR5 interaction. More recently, Liu et al. [67] used a biochemical approach to demonstrate that T-20 has a different mechanism of action from that of C34, which is another peptide derived from gp41 that overlaps with the T-20 sequence [68]. The authors showed that T-20 cannot form a stable 6HB with N-terminal heptad repeat peptides of gp41, nor can it inhibit the formation of the 6HB core structure of gp41, which the C34 peptide is able to do [14]. Instead, they demonstrated that inhibition of virus entry by T-20 was significantly abrogated by peptides derived from the membrane-spanning domain of gp41 and the V3 region of gp120, suggesting the possibility that T-20 inhibits HIV-1 entry by targeting multiple sites in gp41 and gp120. These findings are consistent with our data from the FRET assay, indicating that T-20 interfered with the Env-induced interaction of CD4–CCR5; however, more research is needed to elucidate the entire mechanisms of inhibition of virus entry by T-20. The high density of recombinant receptor and Env molecules on the cell surface would account for the low sensitivity to inhibitors in the current assay system. If this is the case, a cell–cell fusion assay with cells stably expressing a low amount of Env protein will improve the sensitivity and provide a useful system for drug screening.

Although further investigation is necessary to improve the real-time detection of FRET signals during membrane fusion, the FRET technology is expected to become a very powerful tool for understanding membrane fusion where a dynamic process involving Env-engaged receptor and co-receptor organization that trigger the further Env activation would take place. The direction of our study, particularly in combination with new methods such as a single-molecule FRET technique [69],

can provide insights will assist in the development of new strategies to block virus entry.

Acknowledgements

We thank Dr. D.R. Littman for the gift of HIV-1 receptor expressing cells and an HIV luciferase reporter plasmid, Dr. I.M. Verma for a gag-pol expression plasmid, Dr. C.D. Weiss for Env expression plasmids and for giving critical comments. We thank Takeda Pharmaceutical Company Ltd. for giving TAK-779 and T-20, and Mr. I.M. Kobayashi for help in manipulating the Zeiss confocal fluorescence laser microscopy. This study was supported by a grant from the Japanese Private School Foundation.

References

- [1] M. Kowalski, J. Potz, L. Basiripour, T. Dorfman, W.C. Goh, E. Terwilliger, A. Dayton, C. Rosen, W. Haseltine, J. Sodroski, Functional regions of the envelope glycoprotein of human immunodeficiency virus type 1, *Science* 237 (1987) 1351–1355.
- [2] G. Alkhatib, C. Combadiere, C.C. Broder, Y. Feng, P.E. Kennedy, P.M. Murphy, E.A. Berger, CC CKR5: a RANTES, MIP-1alpha, MIP-1beta receptor as a fusion cofactor for macrophage-tropic HIV-1, *Science* 272 (1996) 1955–1958.
- [3] H. Choe, M. Farzan, Y. Sun, N. Sullivan, B. Rollins, P.D. Poth, L. Wu, C.R. Mackay, G. LaRosa, W. Newman, N. Gerard, C. Gerard, J. Sodroski, The beta-chemokine receptors CCR3 and CCR5 facilitate infection by primary HIV-1 isolates, *Cell* 85 (1996) 1135–1148.
- [4] H. Deng, R. Liu, W. Ellmeier, S. Choe, D. Umatmaz, M. Burkhart, P. Di Marzio, S. Mamon, R.E. Sutton, C.M. Hill, C.B. Davis, S.C. Peiper, T.J. Schall, D.R. Littman, N.R. Landau, Identification of a major co-receptor for primary isolates of HIV-1, *Nature* 381 (1996) 661–666.
- [5] T. Dragic, V. Litwin, G.P. Allaway, S.R. Martin, Y. Huang, K.A. Nagashima, C. Cayanan, P.J. Maddon, R.A. Koup, J.P. Moore, W.A. Paxton, HIV-1 entry into CD4+ cells is mediated by the chemokine receptor CC-CKR-5, *Nature* 381 (1996) 667–673.
- [6] Y. Feng, C.C. Broder, P.E. Kennedy, E.A. Berger, HIV-1 entry cofactor: functional cDNA cloning of a seven-transmembrane, G protein-coupled receptor, *Science* 272 (1996) 872–877.
- [7] D.C. Chan, P.S. Kim, HIV entry and its inhibition, *Cell* 93 (1998) 681–684.
- [8] W. Weissenhorn, A. Dessen, S.C. Harrison, J.J. Skehel, D.C. Wiley, Atomic structure of the ectodomain from HIV-1 gp41, *Nature* 387 (1997) 426–430.
- [9] K. Yan, J. Liu, J. Wang, S. Shen, M. Lu, Atomic structure of a thermostable subdomain of HIV-1 gp41, *Proc. Natl. Acad. Sci. USA* 94 (1997) 12303–12308.
- [10] S. Frey, M. Marsh, S. Gunther, A. Pelchen-Matthews, P. Stephens, S. Ortlepp, T. Stegmann, Temperature dependence of cell–cell fusion induced by the envelope glycoprotein of human immunodeficiency virus type 1, *J. Virol.* 69 (1995) 1462–1472.
- [11] S. Genoud, F. Kajumo, Y. Guo, D. Thompson, T. Dragic, CCR5-Mediated human immunodeficiency virus entry depends on an amino-terminal gp120-binding site and on the conformational integrity of all four extracellular domains, *J. Virol.* 73 (1999) 1645–1648.
- [12] S.P. Layne, M.J. Merges, M. Dembo, J.L. Spouge, P.L. Nara, HIV requires multiple gp120 molecules for CD4-mediated infection, *Nature* 346 (1990) 277–279.
- [13] P.D. Kwong, R. Wyatt, J. Robinson, R.W. Sweet, J. Sodroski, W.A. Hendrickson, Structure of an HIV gp120 envelope glycoprotein in complex with the CD4 receptor and a neutralizing human antibody, *Nature* 393 (1998) 648–659.
- [14] D.C. Chan, D. Fass, J.M. Berger, P.S. Kim, Core structure of gp41 from the HIV envelope glycoprotein, *Cell* 89 (1997) 263–273.
- [15] C.K. Lapham, J. Ouyang, B. Chandrasekhar, N.Y. Nguyen, D.S. Dimitrov, H. Golding, Evidence for cell–surface association between fusin

- and the CD4-gp120 complex in human cell lines, *Science* 274 (1996) 602–605.
- [16] R.A. Furuta, C.T. Wild, Y. Weng, C.D. Weiss, Capture of an early fusion-active conformation of HIV-1 gp41, *Nat. Struct. Biol.* 5 (1998) 276–279.
- [17] Q.J. Sattentau, J.P. Moore, Conformational changes induced in the human immunodeficiency virus envelope glycoprotein by soluble CD4 binding, *J. Exp. Med.* 174 (1991) 407–415.
- [18] Q.J. Sattentau, J.P. Moore, F. Vignaux, F. Traincard, P. Pognard, Conformational changes induced in the envelope glycoproteins of the human and simian immunodeficiency viruses by soluble receptor binding, *J. Virol.* 67 (1993) 7383–7393.
- [19] L. Wu, N.P. Gerard, R. Wyatt, H. Choe, C. Parolin, N. Ruffing, A. Borsetti, A.A. Cardoso, E. Desjardins, W. Newman, C. Gerard, J. Sodroski, CD4-induced interaction of primary HIV-1 gp120 glycoproteins with the chemokine receptor CCR-5, *Nature* 384 (1996) 179–183.
- [20] Y. He, R. Vassell, M. Zaitseva, N. Nguyen, Z. Yang, Y. Weng, C.D. Weiss, Peptides trap the human immunodeficiency virus type 1 envelope glycoprotein fusion intermediate at two sites, *J. Virol.* 77 (2003) 1666–1671.
- [21] J. Bentz, A. Mittal, Architecture of the influenza hemagglutinin membrane fusion site, *Biochim. Biophys. Acta* 1614 (2003) 24–35.
- [22] M. Greenberg, N. Cammack, M. Salgo, L. Smiley, HIV fusion and its inhibition in antiretroviral therapy, *Rev. Med. Virol.* 14 (2004) 321–337.
- [23] R.M. Clegg, A.I. Murchie, A. Zechel, C. Carlberg, S. Diekmann, D.M. Lilley, Fluorescence resonance energy transfer analysis of the structure of the four-way DNA junction, *Biochemistry* 31 (1992) 4846–4856.
- [24] R.M. Clegg, Fluorescence resonance energy transfer, in: X. Wana, B. Herman (Eds.), *Fluorescence Imaging Spectroscopy and Microscopy*, Chemical Analysis series V, Wiley, New York, 1996, pp. 179–252 (B).
- [25] A. Miyawaki, J. Llopis, R. Heim, J.M. McCaffery, J.A. Adams, M. Ikura, R.Y. Tsien, Fluorescent indicators for Ca^{2+} based on green fluorescent proteins and calmodulin, *Nature* 388 (1997) 882–887.
- [26] R. Omaki, A. Nagasaki, H. Kawasaki, T. Baba, T.Q. Uyeda, K. Taira, Confirmation by FRET in individual living cells of the absence of significant amyloid beta-mediated caspase 8 activation, *Proc. Natl. Acad. Sci. USA* 99 (2002) 14716–14721.
- [27] X. Jiang, A. Sorkin, Coordinated traffic of Grb2 and Ras during epidermal growth factor receptor endocytosis visualized in living cells, *Mol. Biol. Cell* 13 (2002) 1522–1535.
- [28] M.C. Overton, K.J. Blumer, G-protein-coupled receptors function as oligomers in vivo, *Curr. Biol.* 10 (2000) 341–344.
- [29] K.Q. Luo, V.C. Yu, Y. Pu, D.C. Chang, Application of the fluorescence resonance energy transfer method for studying the dynamics of caspase-3 activation during UV-induced apoptosis in living HeLa cells, *Biochem. Biophys. Res. Commun.* 283 (2001) 1054–1060.
- [30] K. Herrick-Davis, E. Grinde, J.E. Mazurkiewicz, Biochemical and biophysical characterization of serotonin 5-HT_{2C} receptor homodimers on the plasma membrane of living cells, *Biochemistry* 43 (2004) 13963–13971.
- [31] S. Damjanovich, L. Bene, J. Matko, A. Alileche, C.K. Goldman, S. Sharrow, T.A. Waldmann, Preassembly of interleukin 2 (IL-2) receptor subunits on resting Kit 225 K6 T cells and their modulation by IL-2, IL-7, and IL-15: a fluorescence resonance energy transfer study, *Proc. Natl. Acad. Sci. USA* 94 (1997) 13134–13139.
- [32] A.K. Kenworthy, N. Petranova, M. Edidin High-resolution, FRET microscopy of cholera toxin B-subunit and GPI-anchored proteins in cell plasma membranes, *Mol. Biol. Cell* 11 (2000) 1645–1655.
- [33] L.G. Tertoolen, C. Blanchetot, G. Jiang, J. Overvoorde, T.W. Gadella Jr., T. Hunter, J. den Hertog, Dimerization of receptor protein-tyrosine phosphatase alpha in living cells, *BMC Cell Biol.* 2 (2001) 8.
- [34] J.F. Mercier, A. Salahpour, S. Angers, A. Breit, M. Bouvier, Quantitative assessment of beta 1- and beta 2-adrenergic receptor homo- and heterodimerization by bioluminescence resonance energy transfer, *J. Biol. Chem.* 277 (2002) 44925–44931.
- [35] F. Verrier, A.M. Borman, D. Brand, M. Girard, Role of the HIV type 1 glycoprotein 120 V3 loop in determining coreceptor usage, *AIDS Res. Hum. Retroviruses* 15 (1999) 731–743.
- [36] M.W. Cho, M.K. Lee, M.C. Carney, J.F. Berson, R.W. Doms, M.A. Martin, Identification of determinants on a dualtropic human immunodeficiency virus type 1 envelope glycoprotein that confer usage of CXCR4, *J. Virol.* 72 (1998) 2509–2515.
- [37] F. Cocchi, A.L. DeVico, A. Garzino-Demo, A. Cara, R.C. Gallo, P. Lusso, The V3 domain of the HIV-1 gp120 envelope glycoprotein is critical for chemokine-mediated blockade of infection, *Nat. Med.* 2 (1996) 1244–1247.
- [38] J.R. Trujillo, W.K. Wang, T.H. Lee, M. Essex, Identification of the envelope V3 loop as a determinant of a CD4-negative neuronal cell tropism for HIV-1, *Virology* 217 (1996) 613–617.
- [39] B.K. Chen, K. Saksela, R. Andino, D. Baltimore, Distinct modes of human immunodeficiency virus type 1 proviral latency revealed by superinfection of nonproductively infected cell lines with recombinant luciferase-encoding viruses, *J. Virol.* 68 (1994) 654–660.
- [40] R.I. Connor, B.K. Chen, S. Choe, N.R. Landau, Vpr is required for efficient replication of human immunodeficiency virus type-1 in mononuclear phagocytes, *Virology* 206 (1995) 935–944.
- [41] C.D. Weiss, S.W. Barnett, N. Cacalano, N. Killeen, D.R. Littman, J.M. White, Studies of HIV-1 envelope glycoprotein-mediated fusion using a simple fluorescence assay, *AIDS* 10 (1996) 241–246.
- [42] A.K. Kenworthy, Imaging protein-protein interactions using fluorescence resonance energy transfer microscopy, *Methods* 24 (2001) 289–296.
- [43] T.S. Karpova, C.T. Baumann, L. He, X. Wu, A. Grammer, P. Lipsky, G.L. Hager, J.G. McNally, Fluorescence resonance energy transfer from cyan to yellow fluorescent protein detected by acceptor photobleaching using confocal microscopy and a single laser, *J. Microsc.* 209 (2003) 56–70.
- [44] C.A. Rosen, Regulation of HIV gene expression by RNA-protein interactions, *Trends Genet.* 7 (1991) 9–14.
- [45] B.R. Cullen, RNA-sequence-mediated gene regulation in HIV-1, *Infect. Agents Dis.* 3 (1994) 68–76.
- [46] P.D. Kwong, S.E. Ryu, W.A. Hendrickson, R. Axel, R.M. Sweet, G. Follen-Wasserman, P. Hensley, R.W. Sweet, Molecular characteristics of recombinant human CD4 as deduced from polymorphic crystals, *Proc. Natl. Acad. Sci. USA* 87 (1990) 6423–6427.
- [47] M.G. Paterlini, Structure modeling of the chemokine receptor CCR5: implications for ligand binding and selectivity, *Biophys. J.* 83 (2002) 3012–3031.
- [48] S.E. Kuhmann, J.P. Moore, HIV-1 entry inhibitor entrances, *Trends Pharmacol. Sci.* 25 (2004) 117–120.
- [49] L. Wu, G. LaRosa, N. Kassam, C.J. Gordon, H. Heath, N. Ruffing, H. Chen, J. Humblies, M. Samson, M. Parmentier, J.P. Moore, C.R. Mackay, Interaction of chemokine receptor CCR5 with its ligands: multiple domains for HIV-1 gp120 binding and a single domain for chemokine binding, *J. Exp. Med.* 186 (1997) 1373–1381.
- [50] M. Baba, O. Nishimura, N. Kanzaki, M. Okamoto, H. Sawada, Y. Iizawa, M. Shiraishi, Y. Aramaki, K. Okonogi, Y. Ogawa, K. Meguro, M. Fujino, A small-molecule, nonpeptide CCR5 antagonist with highly potent and selective anti-HIV-1 activity, *Proc. Natl. Acad. Sci. USA* 96 (1999) 5698–5703.
- [51] C.T. Wild, D.C. Shugars, T.K. Greenwell, C.B. McDanal, T.J. Matthews, Peptides corresponding to a predictive alpha-helical domain of human immunodeficiency virus type 1 gp41 are potent inhibitors of virus infection, *Proc. Natl. Acad. Sci. USA* 91 (1994) 9770–9774.
- [52] J.D. Reeves, S.A. Gallo, N. Ahmad, J.L. Miamidian, P.E. Harvey, M. Sharron, S. Pohlmann, J.N. Sfakianos, C.A. Derdeyn, R. Blumenthal, E. Hunter, R.W. Doms, Sensitivity of HIV-1 to entry inhibitors correlates with envelope/coreceptor affinity, receptor density, and fusion kinetics, *Proc. Natl. Acad. Sci. USA* 99 (2002) 16249–16254.
- [53] H. Golding, M. Zaitseva, E. de Rosny, L.R. King, J. Manischewitz, I. Sidorov, M.K. Guenly, S. Zolla-Pazner, D.S. Dimitrov, C.D. Weiss, Dissection of human immunodeficiency virus type 1 entry with neutralizing antibodies to gp41 fusion intermediates, *J. Virol.* 76 (2002) 6780–6790.
- [54] G.B. Melikyan, R.M. Markosyan, H. Hemmati, M.K. Delmedico, D.M. Lambert, F.S. Cohen, Evidence that the transition of HIV-1 gp41 into a six-helix bundle, not the bundle configuration, induces membrane fusion, *J. Cell Biol.* 151 (2000) 413–423.
- [55] S.A. Gallo, A. Puri, R. Blumenthal, HIV-1 gp41 six-helix bundle formation occurs rapidly after the engagement of gp120 by CXCR4 in the HIV-1 Env-mediated fusion process, *Biochemistry* 40 (2001) 12231–12236.
- [56] T.L. Hoffman, C.C. LaBranche, W. Zhang, G. Canziani, J. Robinson, I. Chalken, J.A. Hoxie, R.W. Doms, Stable exposure of the coreceptor-

- binding site in a CD4-independent HIV-1 envelope protein, *Proc. Natl. Acad. Sci. USA* 96 (1999) 6359–6364.
- [57] C.C. LaBranche, T.L. Hoffman, J. Romano, B.S. Haggarty, T.G. Edwards, T.J. Matthews, R.W. Doms, J.A. Hoxie, Determinants of CD4 independence for a human immunodeficiency virus type 1 variant map outside regions required for coreceptor specificity, *J. Virol.* 73 (1999) 10310–10319.
- [58] T.G. Edwards, S. Wyss, J.D. Reeves, S. Zolla-Pazner, J.A. Hoxie, R.W. Doms, F. Baribaud, Truncation of the cytoplasmic domain induces exposure of conserved regions in the ectodomain of human immunodeficiency virus type 1 envelope protein, *J. Virol.* 76 (2002) 2683–2691.
- [59] M. Boge, S. Wyss, J.S. Bonifacino, M. Thali, A membrane-proximal tyrosine-based signal mediates internalization of the HIV-1 envelope glycoprotein via interaction with the AP-2 clathrin adaptor, *J. Biol. Chem.* 273 (1998) 15773–15778.
- [60] G.W. Lynch, A.J. Sloane, V. Raso, A. Lai, A.L. Cunningham, Direct evidence for native CD4 oligomers in lymphoid and monocytoid cells, *Eur. J. Immunol.* 29 (1999) 2590–2602.
- [61] G.W. Lynch, E.K. Slaytor, F.D. Elliott, A. Saurjen, S.G. Turville, A.J. Sloane, P.U. Cameron, A.L. Cunningham, G.M. Halliday, CD4 is expressed by epidermal Langerhans' cells predominantly as covalent dimers, *Exp. Dermatol.* 12 (2003) 700–711.
- [62] G.J. Babcock, M. Farzan, J. Sodroski, Ligand-independent dimerization of CXCR4, a principal HIV-1 coreceptor, *J. Biol. Chem.* 278 (2003) 3378–3385.
- [63] G.W. Gordon, G. Berry, X.H. Liang, B. Levine, B. Herman, Quantitative fluorescence resonance energy transfer measurements using fluorescence microscopy, *Biophys. J.* 74 (1998) 2702–2713.
- [64] T. Dragic, A. Trkola, D.A. Thompson, E.G. Cormier, F.A. Kajumo, E. Maxwell, S.W. Lin, W. Ying, S.O. Smith, T.P. Sakmar, J.P. Moore, A binding pocket for a small molecule inhibitor of HIV-1 entry within the transmembrane helices of CCR5, *Proc. Natl. Acad. Sci. USA* 97 (2000) 5639–5644.
- [65] Y. Kliger, Y. Shai, Inhibition of HIV-1 entry before gp41 folds into its fusion-active conformation, *J. Mol. Biol.* 295 (2000) 163–168.
- [66] W. Yuan, S. Craig, Z. Si, M. Farzan, J. Sodroski, CD4-induced T-20 binding to human immunodeficiency virus type 1 gp120 blocks interaction with the CXCR4 coreceptor, *J. Virol.* 78 (2004) 5448–5457.
- [67] S. Liu, H. Lu, J. Niu, Y. Xu, S. Wu, S. Jiang, Different from the HIV fusion inhibitor C34, the anti-HIV drug fuzeon (T-20) inhibits HIV-1 entry by targeting multiple sites in gp41 and gp120, *J. Biol. Chem.* (2005).
- [68] M. Lu, S.C. Blacklow, P.S. Kim, A trimeric structural domain of the HIV-1 transmembrane glycoprotein, *Nat. Struct. Biol.* 2 (1995) 1075–1082.
- [69] H. Murakoshi, R. Iino, T. Kobayashi, T. Fujiwara, C. Ohshima, A. Yoshimura, A. Kusumi, Single-molecule imaging analysis of Ras activation in living cells, *Proc. Natl. Acad. Sci. USA* 101 (2004) 7317–7322.

研究成果報告書

研究課題名	ヒト骨髄及び臍帯血由来未分化組織幹細胞の同定と 細胞移植・再生医療への応用		
(英文)	Identification of human bone marrow- and cord blood-derived tissue committed stem cells and their application for cell transplantation and regenerative medicine		
事業推進者	藺田 精昭	E-mail	sonoda@takii.kmu.ac.jp
所属・職名	医学研究科・幹細胞生物学(衛生学)講座・教授		
研究分担者名	佐々木 豊、植村靖史、河野比良夫、長谷 真、中塚隆介、松岡由和		
キーワード	組織幹細胞、可塑性、骨髄、臍帯血、細胞移植、再生医療		
<p>1. 概要</p> <p>本研究では、ヒト骨髄及び臍帯血中に存在する組織幹細胞 (TCSC) を同定し、<i>in vitro</i> 培養系、及び重症免疫不全マウスを用いる <i>in vivo</i> 異種間移植系を用いてその多分化能・可塑性を明らかにして、近い将来に細胞移植・再生医療に応用するためのトランスレーショナル研究を推進することを目指している。</p> <p>2. 研究の背景と目的</p> <p>白血病、癌などの悪性腫瘍の治療には、造血幹細胞移植 (HSCT) が唯一治療を期待できる治療法といえる。また、高度な心不全、肝不全、腎不全などの臓器障害に対しては、臓器・細胞移植が不可欠である。しかしながら、少子高齢化社会を迎えて臓器提供者不足は深刻な問題であり、その解決は社会的にも強く要請されている。現在、最も確立した再生医療が造血幹細胞 (HSC) の移植医療であるが、その根幹をなすヒト HSC の本体は国内外でいまだ十分に明らかにされていない。さらに近年、間葉系幹細胞 (MSC,PNAS 2003)、多能性成体幹細胞 (MAPC, Nature 2002)、さらに神経、肝臓、膵臓、心筋、血管系など各種臓器における幹 (前駆) 細胞の存在が明らかにされたことにより、これらの臓器・組織幹細胞を用いる再生医療が注目されている (Nature 2000, Nature Immunol 2002, N Engl J Med 2003)。各種 TCSC の本体はいまだ不明であり、この課題の解明には各々の TCSC の同定と特性の解明が不可欠である。加えて、ヒトの骨髄や臍帯血中に多分化能を示す新規幹細胞 (USSC, hBMSC, TCSC, CB-SC) の存在が次々と報告されている (J Exp Med 2004, J Clin Invest 2005, Leukemia 2005, Exp Cell Res 2006)。今後の重要な課題は、これらの幹細胞の本体を解明して、その異同や相互関係を解明して再生医療に応用することである。</p> <p>本研究の目的は、自家移植が可能で最も安全性が高く、かつ倫理的な問題もない体性幹細胞、中でも骨髄・臍帯血中に存在する組織幹細胞 (TCSC) に焦点を絞り、臨床応用に直結する臓器・組織幹細胞の同定とその幹細胞特性の解明を目指している。</p> <p>3. 研究方法</p> <p>(1) ヒト骨髄及び臍帯血に由来する有核細胞より、FACS を用いて既知、未知の CD45 抗原陰性 TCSC を効率的に分取する方法を開発する。</p> <p>(2) (1) で得られた TCSC を用いて、<i>in vitro</i> 分化誘導系、及び重症免疫不全マウスを用いる <i>in vivo</i> 異種間移植系を用いてその多分化能・可塑性を明らかにする。</p> <p>(3) ヒト骨髄及び臍帯血に由来する有核細胞より、<i>in vitro</i> 培養系で MSC を分離して、脂肪細胞、骨細胞、軟骨細胞への分化誘導に加えて神経系細胞への分化誘導を試みる。さらに、CD271, CD90 に対する抗体を用いて prospective に MSC を分取し、同様に多分化能について <i>in vitro</i> 分化誘導系で検討する。</p> <p>(4) われわれがヒト臍帯血中に初めて同定した未分化 CD34 抗原陰性 HSC の可塑性について <i>in vitro</i> 分化誘導系、及び <i>in vivo</i> 異種間移植系で検討する。特に、CD45 抗原陰性 TCSC (hemangioblast, late EPC などを含む) との hierarchy 上の位置付けについても詳細な検討を行う。</p>			

4. これまでの成果

1) ヒト臍帯血由来 CD34⁺HSC の特性解明

われわれは、骨髄内直接移植 (Intra-bone marrow injection, IBMI) 法を用いる非常に効率的な SCID-repopulating cell (SRC)測定系を開発することにより、マウス CD34⁺KSL 細胞の counterpart であるヒト臍帯血由来 CD34⁺HSC を初めて確実に同定することに成功した (Blood 101:2924,2003)。重要な発見は、この CD34⁺HSC における CXCR4 などのホーミング関連分子の発現レベルが低いことである。その後の研究で、ヒト CD34⁺HSC の免疫特性が Lin⁻CD34⁺c-kit⁺flt3⁻であることを明らかにした (Stem Cells 25:1348,2007)。

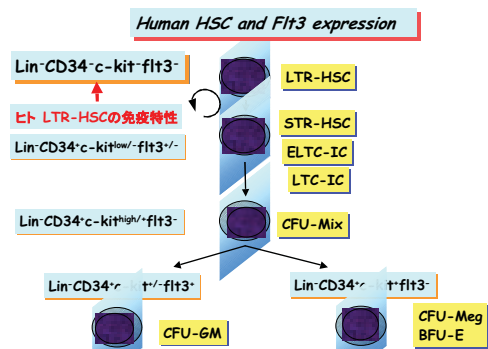


(図 1)

さらに、従来未分化とされていた CD34⁺CD38⁻HSC に比べて、CD34⁺HSC がより未分化な HSC であることを明らかにしている (投稿準備中)。

2) ヒト臍帯血由来 late EPC の同定とその機能解析

ヒト臍帯血由来単核細胞を type I コラーゲン処理した培養皿中で EGM2 培地を加えて 1~2 週間培養し、cobblestone 様の late EPC (OEC)のコロニーを同定した (図 2-A)。本細胞は、CD31, KDR, CD34 抗原陽性で LDL-uptake, lectin 結合能を示したことから OEC と確認された。本細胞は、matrigel 中で培養すると tube formation を認めた (図 2-B)。現在、OEC 細胞の機能解析を行っている (投稿準備中)。



(図 2-A) OEC

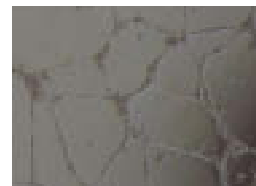


(図 2-B) OEC の tube formation

3) ヒト骨髄由来間葉系幹細胞 (MSC) を用いた神経系細胞への分化誘導

図 3

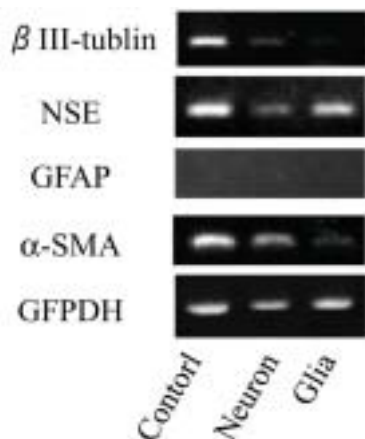
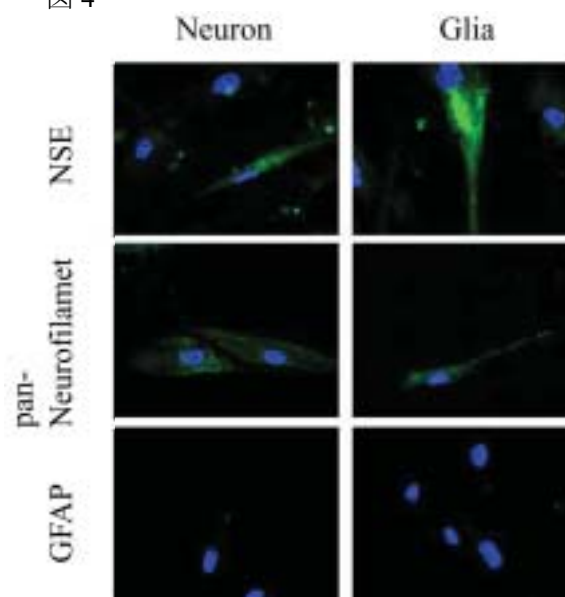


図 4



ヒト骨髄由来CD45⁺細胞から誘導した継代2回目のNeurosphere様細胞塊をTrypsin-EDTA処理後、Harmannらの報告による分化条件で培養した。培養16日目に細胞を回収し、RT-PCR及び免疫染色により神経及びグリア細胞のマーカーの発現を調べた。RT-PCRにより神経マーカーであるβIII-tubelin、NSE、グリア細胞のマーカーであるGFAP、平滑筋マーカーであるα-smooth muscle actinの発現を認めた。内在性コントロールとしてGAPDHを用いた。対照群には同期間αMEM+10%FCSで培養したCD45⁺細胞を用いた。その結果、条件によらず、対照群、神経分化誘導群(Neuron)、およびグリア細胞分化誘導群(Glia)の全ての群で、βIII-tubelinとNSEの発現がみられたが、GFAPの発現は見られなかった(図3)。加えて、α-smooth muscle actinの発現が全ての群で見られた。免疫染色(図4)においても神経分化誘導群、およびグリア細胞分化誘導群においてNSE陽性の細胞が見られた。また、神経マーカーであるNeurofilament陽性細胞も見られたが、RT-PCRの結果と同様にGFAP陽性の細胞は見られなかった。現在、さらに解析を進めている。

4) ヒト骨髄、臍帯血中の多能性組織幹細胞(TCSC)の同定に関する研究

われわれはヒトの骨髄や臍帯血由来のLin⁻CD45⁺CD133⁺細胞分画中にOct4, nanogを発現する非常に未分化なTCSCを同定した。現在、本細胞の効率的な分離方法の確立と多分化能についてin vitro分化誘導系、及びin vivo異種間移植系を用いて解析を進めている。

5. これまでの進捗状況と今後の計画

事業は研究計画に沿って概ね順調に進んでいる。これまでの研究により、ヒトの骨髄、臍帯血中にはHSCに加えてMSC, OEC, TCSCなど多くの幹細胞が存在することが明らかになってきた。今後は、HSCと各種CD45⁺抗原陰性幹細胞のhierarchy上の位置付けを明らかにすることと、各々の幹細胞の多分化能や可塑性を明らかにすることを通じて、これらの細胞を用いる細胞治療・再生医療(特に、神経系細胞)の開発に繋げたい。

6. これまでの発表論文

(1) 発表論文

1) 原著論文

1. Kimura, T., Asada, R., Wang, J., Kimura, T., Morioka, M., Matsui, K., Kobayashi, K., Henmi, K., Imai, S., Kita, M., Tsuji, T., Sasaki, Y., Ikehara, S. & Sonoda, Y. Identification of long-term repopulating potential of human cord blood-derived CD34⁺flt3⁻ severe combined immunodeficiency-repopulating cells by intra-bone marrow injection. *Stem Cells* **25**, 1348-1355 (2007).
2. Harada, S., Kimura, T., Fujiki, H., Nakagawa, H., Ueda, Y., Itoh, T., Yamagishi, H. & Sonoda, Y. Flt3 ligand promotes myeloid dendritic cell differentiation of human hematopoietic progenitor cells: Possible application for cancer immunotherapy. *Int. J. Oncol.* **30**, 1461-1468 (2007).
3. Ueda, Y., Itoh, T., Fujii, N., Harada, S., Fujiki, H., Shimizu, K., Shiozaki, A., Iwamoto, A., Shimizu, T., Mazda, O., Kimura, T., Sonoda, Y. & Tniwaki, M., Yamagishi, H. Successful induction of clinically competent dendritic cells from granulocyte colony-stimulating factor-mobilized monocytes for cancer vaccine therapy. *Cancer Immunol. Immunother* **56**, 381-389 (2007).

2) 総説

1. Sonoda, Y. Immunophenotype and functional characteristics of human primitive CD34⁻ hematopoietic stem cells: The significance of the intra-bone marrow injection. *J. Autoimmunity* **30**, 136-144 (2008).

3) 著書

1. 藪田精昭、池原 進：骨髄内移植法「臍帯血移植の基礎と臨床」医学書院(2008)。印刷中
2. 藪田精昭：造血幹細胞の本体はどこまで解明されたのか「造血器腫瘍アトラス」日本医事新報社(2008)。印刷中
3. 藪田精昭：幹細胞の可塑性と分化—再生医療への応用の可能性—「造血器腫瘍アトラス」日本医事新報社(2008)。印刷中
4. 藪田精昭：骨髄内造血幹細胞移植「造血器腫瘍アトラス」日本医事新報社(2008)。印刷中
5. 藪田精昭：「幹細胞と再生医学」造血幹細胞移植のすべて血液・腫瘍科特別増刊号 **55**、52-62、科学評論社、東京(2007)。

(2) 学会発表

国際学会

2) シンポジウム講演

1. Sonoda, Y. Immunophenotype and functional characteristics of human primitive CD34-negative hematopoietic stem cells: The significance of the intra-bone marrow injection. The 21st Century Center of Excellence (COE) Program “Novel BMT Methods for Intractable Diseases: From Benching to Bedside”, Osaka, 2007.

3) 一般発表

1. Sonoda, Y., Kimura, T., Asada, R., Kimura, T., Morioka, M., Sasaki, Y., Ikehara, S. Different proliferative potential and redistribution kinetics of human cord blood-derived CD34⁺SCID-repopulating cells (SRCs) in comparison with CD34⁺CD38⁺ SRCs using intra-bone marrow injection. The 48th Annual Meeting of American Society of Hematology, Orland, USA, 2006.

国内学会

1) 学会特別講演

1. 藪田精昭：
ヒト造血幹細胞の本体はどこまで解明されたのか—骨髄内骨髄移植の臨床的意義—
第15回奈良県造血細胞移植研究会特別講演、奈良、2007.
2. 藪田精昭：
再生医療における幹細胞。
第68回日本血液学会総会教育講演、福岡、2006.

2) シンポジウム講演

1. 木村貴文、浅田留美子、木村 卓、二宗みのり、長谷 真、佐々木 豊、藪田精昭：
ヒト CD34 抗原陰性未分化造血幹細胞の幹細胞特性の解明
第17回日本サイトメトリー学会総会シンポジウム、浦安、2007.
2. 木村貴文、浅田留美子、木村 卓、長谷 真、佐々木 豊、藪田精昭：
ヒト CD34 抗原陰性造血幹細胞の未分化性について
第5回幹細胞シンポジウム、淡路、2007.

3) 一般発表

1. 木村貴文、浅田留美子、木村 卓、松岡由和、長谷 真、佐々木 豊、藪田精昭：
ヒト CD34 陰性造血幹細胞の *in vivo* 増殖分化動態とその未分化性の解明
第69回日本血液学会総会、横浜、2007.
2. 原田佐智夫、木村貴文、伊藤 剛、上田祐二、藪田精昭：
Flt3 リガンドによるヒト PBSC 由来 DC 前駆細胞の増幅とその機能解析
第17回日本サイトメトリー学会総会、浦安、2007.
3. 木村貴文、浅田留美子、木村 卓、森岡美帆、佐々木 豊、藪田精昭：
ヒト CD34 陰性造血幹細胞の *in vivo* 増殖分化動態の解析
第68回日本血液学会総会ワークショップ、福岡、2006.
4. 藪田精昭：
再生医学 バイオ・ソサエティ平成18年度医学入門講座、京都、2006.
5. 藪田精昭、浅田留美子、木村 卓、佐々木 豊、木村貴文：
ヒト未分化造血幹細胞の免疫特性：FLT3 発現とその幹細胞特性
第16回日本サイトメトリー学会総会、長崎、2006.
6. 藪田精昭：
骨髄内造血幹細胞移植について
第6回さい帯血移植セミナー、大阪、平成18年6月9日
7. 兼子裕人、木村貴文、野村憲一、堀池重夫、谷脇雅史、藪田精昭、大川原康夫：
高齢（70歳以上）多発性骨髄腫患者に対する自己末梢血幹細胞移植
第28回日本造血細胞移植学会総会、東京、2006.

7. これまでの成果の情報公開

ホームページ：幹細胞生物学講座 = <http://www3.kmu.ac.jp/hygiene/>

Identification of Long-Term Repopulating Potential of Human Cord Blood-Derived CD34⁻flt3⁻ Severe Combined Immunodeficiency-Repopulating Cells by Intra-Bone Marrow Injection

TAKAFUMI KIMURA,^a RUMIKO ASADA,^a JIANFENG WANG,^a TAKASHI KIMURA,^{a,g} MIHO MORIOKA,^a KAZUO MATSUI,^b KATSUYA KOBAYASHI,^c KAE HENMI,^c SHIRO IMAI,^c MASAKAZU KITA,^d TAKASHI TSUJI,^e YUTAKA SASAKI,^a SUSUMU IKEHARA,^f YOSHIAKI SONODA^a

^aDepartment of Stem Cell Biology and Regenerative Medicine, Graduate School of Medical Science, Kansai Medical University, Moriguchi, Osaka, Japan; ^bDepartment of Gynecology and Obstetrics, Fukuda Hospital, Kumamoto, Japan; ^cDepartment of Obstetrics and Gynecology, Aizenbashi Hospital, Osaka, Japan; ^dDepartment of Microbiology, Kyoto Prefectural University of Medicine, Kawaramachi-Hirokoji, Kamikyo-ku, Kyoto, Japan; ^eDepartment of Industrial Science and Technology, Tokyo University of Science, Noda, Chiba, Japan; ^fFirst Department of Pathology, Transplantation Center, ^gFirst Department of Internal Medicine, Kansai Medical University, Moriguchi, Osaka, Japan

Key Words. Flt3 • Severe combined immunodeficiency-repopulating cell • Intra-bone marrow injection • Cord blood • Hematopoiesis

ABSTRACT

Recently, we have identified human cord blood (CB)-derived CD34-negative (CD34⁻) severe combined immunodeficiency (SCID)-repopulating cells (SRCs) using the intra-bone marrow injection (IBMI) method (Blood 2003; 101:2924). In contrast to murine CD34⁻ Kit⁺Sca-1⁺Lin⁻ (KSL) cells, human CB-derived Lin⁻CD34⁻ cells did not express detectable levels of c-kit by flow cytometry. In this study, we have investigated the function of flt3 in our identified human CB-derived CD34⁻ SRCs. Both CD34⁺flt3^{+/-} cells showed SRC activity. In the CD34⁻ cell fraction, only CD34⁻flt3⁻ cells showed distinct SRC activity by IBMI. Although CD34⁺flt3⁺ cells showed a rather weak secondary repopulating activity, CD34⁺flt3⁻ cells repopulated many more secondary re-

cipient mice. However, CD34⁻flt3⁻ cells repopulated all of the secondary recipients, and the repopulating rate was much higher. Next, we cocultured CD34⁻flt3⁻ cells with the murine stromal cell line HESS-5. After 1 week, significant numbers of CD34⁺flt3^{+/-} cells were generated, and they showed distinct SRC activity. These results indicated that CB-derived CD34⁻flt3⁻ cells produced CD34⁺flt3⁻ as well as CD34⁺flt3⁺ SRCs in vitro. The present study has demonstrated for the first time that CB-derived CD34⁻ SRCs, like murine CD34⁻ KSL cells, do not express flt3. On the basis of these data, we propose that the immunophenotype of very primitive long-term repopulating human hematopoietic stem cells is Lin⁻CD34⁻c-kit⁻flt3⁻. STEM CELLS 2007;25:1348-1355

Disclosure of potential conflicts of interest is found at the end of this article.

INTRODUCTION

It is well documented that the tyrosine kinase receptors c-kit and flt3 are expressed and function in early mouse [1-10] and human hematopoiesis [1, 11-21]. Moreover, their respective ligands, stem cell factor (SCF) and flt3 ligand (FL), synergistically act with each other and play an important role in the regulation (generation, maintenance, proliferation, differentiation, and expansion) of early stages of murine and human candidate hematopoietic stem cells (HSCs) [1-21]. The most primitive HSCs in mammals, including mice and humans, have long been believed to be CD34 antigen-positive (CD34⁺) [22]. However, Osawa et al. [23] revealed that murine long-term lymphohematopoietic reconstituting HSCs are lineage marker-negative (Lin⁻) c-kit⁺Sca-1⁺CD34-low/negative (CD34^{lo/-} KSL). In a murine model, it was recently reported that flt3⁻

KSL cells supported long-term multilineage hematopoietic reconstitution [24]. In contrast, flt3⁺ KSL cells are progenitors for the common lymphoid stage [24]. These flt3⁺ KSL cells have also been shown to lack erythro-megakaryocytic potential [25]. This notion was supported by the other reports that mice deficient in the expression of flt3 or FL showed deficient lymphopoiesis [26-28].

Recently, using the intra-bone marrow injection (IBMI) method, we have successfully identified human cord blood (CB)-derived CD34-negative (CD34⁻) severe combined immunodeficiency (SCID)-repopulating cells (SRCs) with extensive lymphoid and myeloid repopulating ability [29]. These CD34⁻ SRCs seemed to be more primitive HSCs than CD34⁺ SRCs [29, 30]. They could home into the BM niche only by IBMI, because they expressed lower levels of homing receptors, including CXCR4, and had poor SDF-1/CXCR4-mediated migration ability [29]. In contrast to the murine candidate HSCs

Correspondence: Yoshiaki Sonoda, M.D., Department of Stem Cell Biology and Regenerative Medicine, Graduate School of Medical Science, Kansai Medical University, Moriguchi, Osaka 570-8506, Japan. Telephone: +81-6-6993-9435; Fax: +81-6-6992-3522; e-mail: sonoda@takii.kmu.ac.jp Received November 8, 2006; accepted for publication February 6, 2007; first published online in STEM CELLS EXPRESS February 15, 2007. ©AlphaMed Press 1066-5099/2007/\$30.00/0 doi: 10.1634/stemcells.2006-0727

STEM CELLS 2007;25:1348-1355 www.StemCells.com

(CD34⁻ KSL cells) [23], our identified CD34⁻ SRCs did not express detectable levels of c-kit tyrosine kinase receptor by flow cytometry. However, the degree to which flt3 is expressed on human HSCs, including CD34⁺ and CD34⁻ SRCs, which are capable of *in vivo* lymphomyeloid reconstitution, has not been fully elucidated.

Until now, a number of studies have reported that flt3 is expressed and functioned in the human CD34⁺ hematopoietic progenitor cells [11–17, 19, 20], including long-term culture-initiating cells (LTC-ICs) [15, 20, 31]. However, only two reports have demonstrated, using the conventional intravenous injection method, that human CB- and bone marrow (BM)-derived CD34⁺ HSCs capable of multilineage reconstitution in nonobese diabetic (NOD)/SCID mice express flt3 tyrosine kinase receptor [31, 32].

In this study, we have investigated, using the IBMI method, the function of flt3, which is expressed in early mouse [1–10] and human [11–21] hematopoiesis like c-kit, in our identified very primitive human CB-derived CD34⁻ SRCs [29, 30], as well as more committed CD34⁺ SRCs. Our data clearly demonstrate that part of human CB-derived CD34⁺ SRCs express flt3, as reported previously [31, 32]. However, only CD34⁺flt3⁻ cells showed significant secondary repopulating ability, even when a comparable number of CD34⁺flt3⁻ cells as CD34⁺flt3⁺ cells was transplanted. Moreover, CD34⁻flt3⁻ cells showed distinct and potent SRC activity by IBMI, and they showed high and efficient secondary repopulating ability compared with CD34⁺flt3⁻ cells. The CD34⁻flt3⁻ cells also produced CD34⁺flt3⁻ and CD34⁺flt3⁺ SRCs after the coculture with the murine stromal cell line HESS-5 *in vitro*, suggesting that these CD34⁻flt3⁻ cells contained very primitive human CB-derived HSCs. The results of the present study are consistent with recent studies of the significance of flt3 expression in murine primitive hematopoiesis [24–28] and provide a new concept of hierarchy in the human primitive HSC compartment.

MATERIALS AND METHODS

Collection of CB Samples and Processing

CB samples were obtained from normal full-term deliveries with signed informed consent and approved by the institutional review boards of Kansai Medical University and Kyoto Prefectural University of Medicine. CB-derived mononuclear cells (MNCs) were isolated using Ficoll-Paque (Amersham Biosciences AB, Uppsala, Sweden; <http://www.amersham.com>) density gradient centrifugation. The MNCs were further enriched by negative depletion of eight lineage-positive cells, including CD3, CD14, CD16, CD19, CD24, CD56, CD66b, and Glycophorin A using a StemSep device (StemCell Technologies, Vancouver, BC, Canada; <http://www.stemcell.com>), as reported previously [29, 30].

Purification of Lin⁻CD34⁺flt3^{+/-} and Lin⁻CD34⁻flt3^{+/-} Cells

The above-mentioned lineage-negative (Lin⁻) cells were stained with fluorescein isothiocyanate (FITC)-conjugated anti-CD45 monoclonal antibody (mAb) (Beckman Coulter, Fullerton, CA, <http://www.beckmancoulter.com>), PC5-conjugated anti-CD34 mAb (Beckman Coulter), and biotinylated anti-flt3 mAb (M22, Immunex, Seattle, <http://immunex.com>) followed by incubation with streptavidin-phycoerythrin (SA-PE; Becton Dickinson, Franklin Lakes, NJ, <http://www.bd.com>), as reported previously [20, 29, 30]. These stained cells were then sorted into four fractions, including CD34⁺flt3^{+/-} and CD34⁻flt3^{+/-} cells, as shown in Figure 1C using a FACSVantage (Becton Dickinson) as reported [29, 30]. The viability of these sorted cells was consistently more than 99%. Approximately 80% of the CD34⁺ cell fraction in these Lin⁻

www.StemCells.com

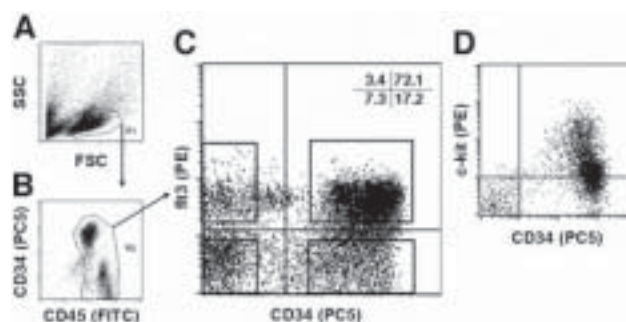


Figure 1. Expression of flt3 or c-kit receptor on cord blood-derived Lin⁻ cells. **(A):** The forward scatter/SSC profile of immunomagnetically separated Lin⁻ cells. The R1 gate was set on the lymphocyte window. **(B):** Lin⁻CD45⁺CD34^{+/-} cells present in R1 gate were gated as R2. **(C):** The expression pattern of CD34 and flt3 on R2 gated cells is shown. Cells residing in the four cell fractions were classified as Lin⁻CD34⁺flt3⁺, Lin⁻CD34⁺flt3⁻, Lin⁻CD34⁻flt3⁺, and Lin⁻CD34⁻flt3⁻ cells, respectively. Each sorting window is shown as a solid square. Figures in upper right corner show percentages of cells in each quadrant. **(D):** The expression pattern of c-kit on Lin⁻CD34^{+/-} cells in a separate experiment. Abbreviations: FITC, fluorescein isothiocyanate; FSC, forward scatter; PE, phycoerythrin; SSC, side scatter.

cells expressed flt3 receptor. On the other hand, only 30% of the CD34⁻ cell fraction in the same Lin⁻ cells expressed this receptor. In separate experiments, we stained these immunomagnetically separated Lin⁻ cells with 13 FITC-conjugated lineage-specific mAbs as reported previously [29], PC5-conjugated anti-CD34 mAb (Beckman Coulter), and PE-conjugated anti-c-kit mAb (Beckman Coulter) and examined the expression pattern of c-kit receptor (Fig. 1D).

Clonal Cell Culture

Human colony-forming cells (CFCs) were assayed using our standard methylcellulose cultures as reported previously [18–21, 29, 30, 33, 34]. Briefly, 200 or 500 sorted Lin⁻CD34^{+/-}flt3^{+/-} cells were plated in 1 ml of culture containing 1.2% methylcellulose (Shinetsu Chemical, Tokyo, <http://www.shinetsu.co.jp/e>), 30% fetal calf serum (FCS; Hyclone, Laboratories, Logan, UT, <http://www.hyclone.com>), 1% bovine serum albumin (Sigma-Aldrich, St Louis, <http://www.sigmaaldrich.com>), 5×10^{-5} mol/L 2-mercaptoethanol (Sigma-Aldrich), and various recombinant human (rh) cytokines, including SCF, interleukin (IL)-3, granulocyte macrophage colony-stimulating factor (GM-CSF), granulocyte colony-stimulating factor (G-CSF), and erythropoietin (Epo) in 35-mm Lux suspension culture dishes (Nunc, Rochester, NY, <http://www.nuncbrand.com>). For culture of megakaryocyte colony-forming cell (CFU-Meg), 10% platelet-poor plasma (PPP) [33] instead of 30% FCS, and rh thrombopoietin (TPO) were used. Cytokines, including G-CSF, Epo, and TPO were provided by Kirin Brewery Company (Takasaki, Japan, <http://www.kirin.com>). SCF, IL-3, and GM-CSF were purchased from R&D Systems Inc. (Minneapolis, <http://www.rndsystems.com>). Dishes were incubated at 37°C in a fully-humidified atmosphere flushed with a combination of 5% CO₂, 5% O₂, and 90% N₂. On days 12–14 of incubation, all colonies were scored under an inverted microscope according to their typical morphologic features, as reported elsewhere [18–21, 29, 30, 33]. CFU-Meg-derived pure megakaryocyte colonies were identified *in situ* as clusters of large cells, which were highly refractile and showed irregular contour and hyaline nongranulated cytoplasm. The types of colonies identified *in situ* were granulocyte (CFU-G), macrophage (CFU-M), granulocyte/macrophage (CFU-GM), erythroid burst (BFU-E), erythrocyte-containing mixed (CFU-Mix), and the above-mentioned CFU-Meg. The numbers of all types of hematopoietic colonies were determined as the mean of three independent experiments.

IBMI of Purified Cells

IBMI was carried out as reported previously [29, 30, 35]. Briefly, after sterilization of the skin around the left knee joint, the knee was flexed to 90 degrees and the proximal side of the tibia was drawn to the anterior. A 27-gauge needle was inserted into the joint surface of the tibia through the patellar tendon and then inserted into the BM cavity. Using a Hamilton's microsyringe, the number-specified donor cells per under 10 μ l of α -medium were carefully and slowly injected from the bone hole into the BM cavity.

SCID-Repopulating Cell Assay

An SRC assay was performed using the methods reported previously [36, 37] with modifications [29, 30, 38]. Five-week-old NOD/Shi-*scid/scid* (NOD/SCID) mice were purchased from Clea Japan (Tokyo, Japan, <http://www.clea-japan.com>). The animal experiments were approved by the Animal Care Committees of Kansai Medical University and Kyoto Prefectural University of Medicine. All mice were handled in sterile conditions and maintained in germ-free isolators located in the Central Laboratory Animal Facilities of Kansai Medical University and Kyoto Prefectural University of Medicine. In this study, purified 3×10^4 to 5×10^4 CB-derived Lin⁻CD34⁺flt3^{+/-}, or 2×10^4 to 7×10^4 CB-derived Lin⁻CD34⁻flt3^{+/-} cells were transplanted by IBMI into sublethally irradiated (250 cGy using a ¹³⁷Cs- γ irradiator) 8–12-week-old mice. As we reported previously [29, 30], CB-derived CD34⁻SRCs were detected only by the IBMI technique. Moreover, the repopulation rate of CD34⁺ SRCs by IBMI was significantly higher than that by the conventional tail-vein injection method [29]. Therefore, we used the IBMI technique to analyze SRC activities of Lin⁻CD34^{+/-}Flt3^{+/-} cells in this study. The mice were killed 8–12 weeks after transplantation, and the BMs from the pairs of femurs, tibiae, and humeri of each mouse were flushed into α -medium. The rates of human CD45⁺ cells in the murine BMs were analyzed by flow cytometry (FACS Calibur; Becton Dickinson) as described in the next section. Mice were scored as positive if over 0.1% of total murine BM cells were human CD45⁺.

Analysis of Human Cell Engraftment in NOD/SCID Mice by Flow Cytometry

The repopulation of human hematopoietic cells in murine BMs was determined by detecting the number of cells positively stained with PC5-conjugated anti-human CD45 mAb (Beckman Coulter) by flow cytometry. The cells were also stained with PE-conjugated anti-human CD34 mAb (Becton Dickinson), and FITC-conjugated mAbs for human lineage-specific Ags, including CD19 (eBioscience, San Diego, <http://www.ebioscience.com>), and CD33 (Beckman Coulter) for the detection of human lymphoid and myeloid hematopoietic cells, respectively.

Secondary Transplantation

For secondary transplantations, murine BM cells were obtained from the pairs of femurs, tibiae, and humeri of moderately engrafted primary recipient mice 8–12 weeks after transplantation with 3×10^3 to 5×10^3 Lin⁻CD34⁺flt3⁺, 4×10^3 to 5×10^3 Lin⁻CD34⁺flt3⁻, or 2×10^4 to 3×10^4 Lin⁻CD34⁻flt3⁻ cells, respectively. The human cell repopulation rates in the primary recipients' BMs were comparable and approximately 4%–8%. Whole BM cells were transplanted by IBMI into sublethally (250 cGy) irradiated secondary recipient mice. Eight to 10 weeks after transplantation, the presence of human CD45⁺ cells in the secondary recipients' BMs was analyzed by flow cytometry, as described for primary transplantation.

Coculture with HESS-5 Cells and SRC Activity of Culture-Generated CD34⁺flt3^{+/-} Cells

A total of 5×10^4 purified Lin⁻CD34⁻flt3⁻ cells per 12.5-cm² culture flask (BD Falcon; Becton Dickinson) onto preestablished irradiated HESS-5 [39] layers in StemPro-34 medium (Gibco Laboratories, Grand Island, NY, <http://www.invitrogen.com>) and a cocktail of cytokines, including 300 ng/ml SCF (R&D), 300 ng/ml TPO (Kirin), 10 ng/ml IL-3 (R&D), 10 units/ml IL-6 (provided by

Dr. Akira Okano, Ajinomoto Co. Inc., Yokohama, Japan, <http://www.ajinomoto.com>), 10 ng/ml G-CSF (Kirin), and 5% FCS (HyClone). After 1 week, all cells were collected by vigorous pipetting, and stained with PC5-conjugated anti-CD34 mAb (Beckman Coulter) and biotinylated anti-flt3 mAb (Immunex) as mentioned herein. Cells were then stained with SA-PE (Becton Dickinson). The rates of CD34⁺flt3^{+/-} cells were analyzed by flow cytometry. Simultaneously, these CD34⁺flt3^{+/-} cells were separately obtained by cell sorting (FACSVantage) for the detection of SRC activity. One to 2×10^4 CD34⁺flt3⁺ or 2×10^4 to 4×10^4 CD34⁺flt3⁻ cells were transplanted by IBMI into sublethally (250 cGy) irradiated recipient mice. Eight weeks after transplantation, the presence of human CD45⁺ cells in the recipients' BMs was analyzed by flow cytometry, as described for primary transplantation.

Statistical Analysis

The significance of differences in the SRC assays and the numbers of hematopoietic colonies was determined using the Mann-Whitney *U* test and the two-tailed Student's *t* test, respectively.

RESULTS

Expression of flt3 and c-kit Receptors on Lin⁻CD45⁺CD34^{+/-} Cells

First, we depleted the eight lineage-positive cells from CB-derived MNCs using the immunomagnetic beads system [29, 30]. Then, Lin⁻CD45⁺CD34^{+/-} cells were gated as R2 as shown in Figure 1B. These Lin⁻CD45⁺ cells were subdivided into four distinct populations on the basis of their surface CD34 and flt3 expression (Fig. 1C). We sorted these four fractions for further stem cell characterization. The phenotypic purity of the sorted cells consistently exceeded 98% when checked using postsorting flow cytometric analysis (data not shown). Importantly, these Lin⁻CD34⁻ cells did not express detectable levels of c-kit receptors by flow cytometry, as shown in Figure 1D.

Characteristics of Colony-Forming Capacity by CB-Derived Lin⁻CD34^{+/-}flt3^{+/-} Cells

The colony-forming capacities of these four fractions were quite different. The plating efficiency of each Lin⁻CD34⁺flt3⁺ or Lin⁻CD34⁺flt3⁻ cell fraction was approximately 50% and comparable (Fig. 2A). Lin⁻CD34⁺flt3⁺ cells contained approximately 81% CFU-GM, 17% BFU-E, and 2% CFU-Mix. In contrast, Lin⁻CD34⁺flt3⁻ cell fraction contained 21% CFU-GM, 66% BFU-E, and 12% CFU-Mix. The Lin⁻CD34⁻flt3^{+/-} cell fractions showed almost no colony formation (data not shown). On the other hand, the vast majority of CFU-Megs (more than 90%) were detected in the Lin⁻CD34⁺flt3⁻ cell fraction (Fig. 2B).

These results clearly demonstrate that CB-derived Lin⁻CD34⁺flt3⁺ cells display weak erythroid and megakaryocytic potentials. These findings were consistent with a recent study in which murine flt3⁺ KSL cells failed to produce significant erythroid and megakaryocytic progeny [25].

SRC Activity and Lymphomyeloid-Reconstituting Capacity of CB-Derived Lin⁻CD34^{+/-}flt3^{+/-} Cells by IBMI

In this study, we have investigated the function of flt3 in our identified human CB-derived CD34⁻ SRCs. First, we studied the SRC activity of CB-derived Lin⁻CD34⁺flt3^{+/-} or CD34⁻flt3^{+/-} cells using IBMI, as shown in Figure 3. Both CD34⁺flt3^{+/-} cells repopulated all 20 recipient mice (10 mice each). The level of human CD45⁺ cells in the murine BMs that

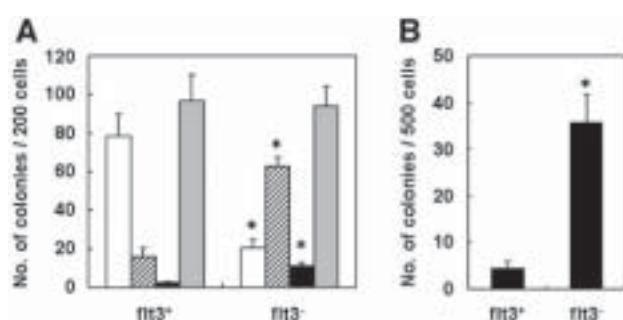


Figure 2. Colony-forming capacities of $\text{Lin}^- \text{CD34}^+ \text{flt3}^{+/-}$ cells. **(A):** The colony-forming capacities of 200 $\text{Lin}^- \text{CD34}^+ \text{flt3}^{+/-}$ cells in the presence of stem cell factor, interleukin-3, granulocyte macrophage (GM) colony-stimulating factor (CSF), granulocyte (G) CSF, and erythropoietin. Open, shaded, closed, and gray bars represent the number of granulocyte/macrophage colony-forming units (CFUs; including CFU-G, CFU-macrophage, and CFU-GM), erythroid burst, CFU-Mix, and total colony, respectively. **(B):** The colony-forming capacities of 500 $\text{Lin}^- \text{CD34}^+ \text{flt3}^{+/-}$ cells in the presence of thrombopoietin. Closed bars represent the number of megakaryocyte CFUs. The numbers of all types of colonies were determined as the mean of three independent experiments. Vertical bars represent standard deviation, and asterisks show statistical significance ($p < .01$) between the numbers of designated colonies formed by flt3^+ and flt3^- cells, respectively.

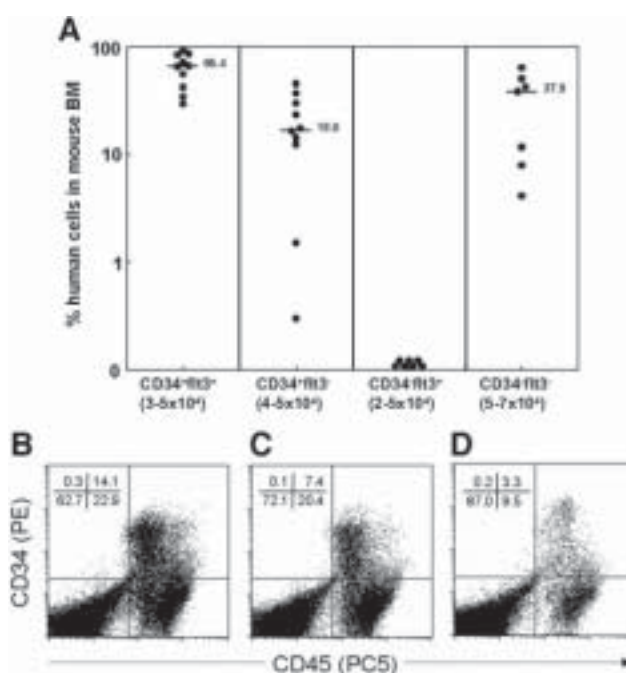


Figure 3. Severe combined immunodeficiency-repopulating cell activities of $\text{Lin}^- \text{CD34}^{+/-} \text{flt3}^{+/-}$ cells by intra-BM injection (IBMI). **(A):** Each mouse transplanted with designated numbers of cord blood-derived $\text{Lin}^- \text{CD34}^+ \text{flt3}^+$, $\text{Lin}^- \text{CD34}^+ \text{flt3}^-$, $\text{Lin}^- \text{CD34}^- \text{flt3}^+$, and $\text{Lin}^- \text{CD34}^- \text{flt3}^-$ cells was sacrificed 8–12 weeks after transplantation. Closed circles represent the repopulation rates in total murine BMs by the IBMI, respectively. Horizontal bars represent each median of the repopulation rates. **(B–D):** The human CD45^+ cell reconstitution in the representative mouse presented in **(A)** received transplants of $\text{CD34}^+ \text{flt3}^+$ **(B)**, $\text{CD34}^+ \text{flt3}^-$ **(C)**, and $\text{CD34}^- \text{flt3}^-$ **(D)** cells, respectively. Percentages of cells in each quadrant are presented in the upper left corner. Abbreviations: BM, bone marrow; PE, phycoerythrin.

received transplants of $\text{CD34}^+ \text{flt3}^+$ cells ($n = 10$; 29.3% to 90.8%; median, 65.4%) was higher than those that received transplants of $\text{CD34}^+ \text{flt3}^-$ cells ($n = 10$; 0.3% to 45.1%; median, 16.9%).

www.StemCells.com

Table 1. Lymphomyeloid reconstitution abilities of $\text{CD34}^+ \text{flt3}^{+/-}$ and $\text{CD34}^- \text{flt3}^-$ severe combined immunodeficiency repopulating cells by intra-bone marrow (BM) injection

Cells	%	
	CD33	CD19
$\text{CD34}^+ \text{flt3}^+$	5.9	44.4
	4.5	41.5
	2.8	29.5
$\text{CD34}^+ \text{flt3}^-$	1.3	16.9
	1.1	6.1
	0.5	2.1
$\text{CD34}^- \text{flt3}^-$	7.4	19.3
	3.3	21.1
	1.9	13.4

Each mouse transplanted with designated numbers of cord blood-derived $\text{Lin}^- \text{CD34}^+ \text{flt3}^+$, $\text{Lin}^- \text{CD34}^+ \text{flt3}^-$, and $\text{Lin}^- \text{CD34}^- \text{flt3}^-$ cells was sacrificed 8 to 12 weeks after transplantation. First, the R1 gate was set on the total murine BM cells obtained from these representative mice, and then human CD45^+ cells were gated as R2. Expression of lineage markers, including CD19 (lymphoid) and CD33 (myeloid) on the R2 gated cells, was analyzed by three color flow cytometry. Boldfacing represents each median of the repopulation rates.

On the other hand, the seven mice that received transplants of $\text{CD34}^- \text{flt3}^+$ cells did not show human cell repopulation. Only $\text{CD34}^- \text{flt3}^-$ cells repopulated all seven recipient mice, and the level of human CD45^+ cells in the murine BMs was 4.1% to 63.3% (median, 37.9%). These results indicated for the first time that the CB-derived $\text{Lin}^- \text{CD34}^- \text{flt3}^-$ cell population contained SRCs, as detected by IBMI.

To further evaluate the function of flt3 expression in CD34^+ and CD34^- SRCs, we studied their lymphomyeloid reconstitution abilities using IBMI. In our SRC assay system, all NOD/SCID mice transplanted either with 3×10^4 to 5×10^4 $\text{Lin}^- \text{CD34}^+ \text{flt3}^{+/-}$ cells or 5×10^4 to 7×10^4 $\text{Lin}^- \text{CD34}^- \text{flt3}^-$ cells by IBMI showed signs of human cell engraftment. The analyses of the three representative mice transplanted either with $\text{Lin}^- \text{CD34}^+ \text{flt3}^{+/-}$ cells or $\text{Lin}^- \text{CD34}^- \text{flt3}^-$ cells clearly indicate that these three classes of SRCs have an extensive differentiation capacity to B-lymphoid (CD19) and myeloid (CD33) lineages in vivo (Table 1).

Next, the percentages of lineage-positive cells expressing CD19 and CD33 were compared (Table 1). These results demonstrated that all three classes of SRCs could supply lymphoid as well as myeloid cells at 8–12 weeks after the transplantation. Interestingly, $\text{CD34}^+ \text{flt3}^+$ SRCs showed a lymphoid-dominant repopulation pattern compared with the other two classes of SRCs. These results are consistent with the notion that cells in the $\text{Lin}^- \text{Sca-1}^+ \text{c-kit}^+$ murine HSC compartment coexpressing flt3 tyrosine kinase receptor sustain lymphoid potential [24, 25], and also that mice deficient in the expression of flk2/flt3 or FL show deficient lymphopoiesis [26–28].

Secondary Repopulating Ability of $\text{Lin}^- \text{CD34}^+ \text{flt3}^{+/-}$ or $\text{Lin}^- \text{CD34}^- \text{flt3}^-$ Cells by IBMI

To further evaluate the long-term repopulating potential of these three populations ($\text{CD34}^+ \text{flt3}^+$, $\text{CD34}^+ \text{flt3}^-$, and $\text{CD34}^- \text{flt3}^-$ cells), BM cells obtained from each engrafted primary recipient mouse were assessed for their SRC activity by secondary transplantation by IBMI. Only one of six mice that received whole BM cells obtained from primary recipient mice that received transplants of $\text{CD34}^+ \text{flt3}^+$ cells showed secondary repopulating activity (Fig. 4). On the other hand, 83% (five of six) of the

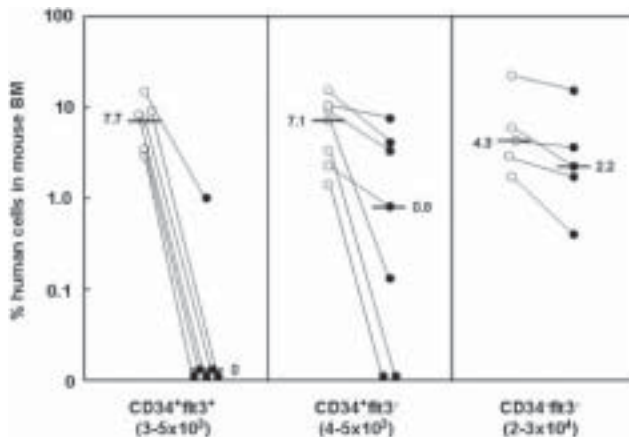


Figure 4. Secondary repopulating capacities of Lin⁻CD34⁺flt3^{+/-} or Lin⁻CD34⁻flt3⁻ cells. Cells transplanted to primary recipients (PRs) by intra-BM injection (IBMI) numbered 3×10^3 to 5×10^3 CD34⁺flt3⁺ cells, 4×10^3 to 5×10^3 CD34⁺flt3⁻ cells, or 2×10^4 to 3×10^4 CD34⁻flt3⁻ cells. Human cell repopulations of BMs in PRs (open circles) analyzed 8–12 weeks after transplantation were comparable and 4%–8%. Whole BM cells obtained from PRs were transplanted to secondary recipients (SRs) by IBMI. Human cell repopulation in SRs (closed circles) was analyzed 8–10 weeks after secondary transplantation. Horizontal bars represent each median of the repopulation rates in PRs and SRs, respectively. Abbreviation: BM, bone marrow.

secondary recipients that received whole BM cells from primary recipients that received CD34⁺flt3⁻ cells could be repopulated. Moreover, all five secondary recipient mice that received whole BM cells from primary recipients that received CD34⁻flt3⁻ cells could be repopulated with a higher secondary repopulating rate (Fig. 4). These results demonstrated that CD34⁻flt3⁻ SRCs have more potent secondary reconstituting abilities in comparison with the other two types of SRCs, and could sustain long-term human hematopoiesis in NOD/SCID mice.

SRC Activity of Culture-Generated CD34⁺flt3^{+/-} Cells by IBMI

Recently, we reported that our identified CD34⁻ SRCs could produce CD34⁺ SRCs after being cocultured with the murine stromal cell line HESS-5 [29]. Therefore, we cocultured CD34⁻flt3⁻ cells with HESS-5 in the presence of SCF, TPO, IL-3, IL-6, and G-CSF, as reported previously [29]. After 1 week, significant numbers of CD34⁺flt3⁻ and CD34⁺flt3⁺ cells were generated, as shown in Figure 5C. We then sorted these two populations (CD34⁺flt3^{+/-} cells) and tested their SRC activities by IBMI. Seven of 10 and 5 of 10 mice that received either CD34⁺flt3⁺ or CD34⁺flt3⁻ cells were repopulated with human cells. (Table 2). Human cell repopulation rates in mice that received transplants of either CD34⁺flt3⁺ or CD34⁺flt3⁻ cells were 1.2%–8.8% (median, 4.5%) and 1.4%–7.8% (median, 3.7%), respectively.

DISCUSSION

A number of studies have demonstrated that flt3 tyrosine kinase receptor plays a pivotal role in the regulation of primitive murine [1–10] and human [11–17, 19, 20] hematopoietic stem/progenitor cells such as c-kit. In the murine model, the expression and functional significance of flt3 and c-kit receptors in early hematopoiesis has been investigated extensively [1–10, 23–28, 40–42]. Many studies have suggested that murine plu-

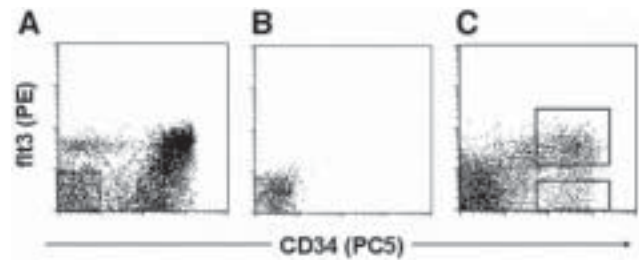


Figure 5. Expression pattern of CD34 and flt3 on sorted Lin⁻CD34⁻flt3⁻ cells after the 7-day coculture with HESS-5 cells. (A): Flow cytometry pattern of immunomagnetically separated cord blood-derived Lin⁻ cells stained with anti-flt3 (PE) and anti-CD34 (PC5) monoclonal antibodies. Lin⁻CD34⁻flt3⁻ cells were sorted for the coculture with HESS-5 cells. The sorting gate is indicated by the solid square. (B): Postsorting analysis of the sorted Lin⁻CD34⁻flt3⁻ cells. (C): The expression pattern of flt3 on CD34⁺ cells derived from the 7-day cocultures of sorted Lin⁻CD34⁻flt3⁻ cells with the murine stromal cell line, HESS-5, in the presence of a cocktail of cytokines. The sorting gates for culture-generated CD34⁺flt3^{+/-} cells are indicated by two solid squares. Abbreviation: PE, phycoerythrin.

Table 2. Severe combined immunodeficiency (SCID) repopulating cell activity of culture-generated CD34⁺flt3^{+/-} cells

Sorted cell fraction	No. of cells transplanted	Engraftment	Human CD45 ⁺ cells (%)	
			Range	Median
CD34 ⁻ flt3 ⁺ cells	1×10^4 to 2×10^4	7/10	1.2–8.8	4.5
CD34 ⁺ flt3 ⁻ cells	2×10^4 to 4×10^4	5/10	1.4–7.8	3.7

Designated numbers of culture-generated CD34⁺flt3⁺ and CD34⁺flt3⁻ cells obtained by cell sorting were transplanted to nonobese diabetic/SCID mice by intra-bone marrow (BM) injection. After 8 weeks, repopulation of human CD45⁺ cells in murine BMs was analyzed.

ripotent long-term repopulating hematopoietic stem cells (LTR-HSCs) express c-kit [40–42]. Particularly, Osawa et al. [23] clearly indicated that a single CD34⁻ KSL cell efficiently reconstituted as many as one of five recipient mice. However, they did not rule out the possibility of coexistence of a less frequent c-kit⁻ LTR-HSC, which might fail to home into the BM niche by intravenous injection. In support of the potential existence of c-kit⁻ murine HSCs, several studies have reported the existence of LTR-HSCs with little or no c-kit expression [43–45]. Among them, Doi et al. [43] clearly demonstrated that candidate HSC could be subdivided into c-kit^{low} and c-kit^{<low} (no detectable cell surface expression but positive for mRNA expression) populations. Both populations could support donor-type long-term multilineage reconstitution in primary recipients. However, only c-kit^{<low} HSCs showed secondary and tertiary reconstituting capacity. In addition, Ortiz et al. [44] reported that c-kit⁻ pluripotent stem cells can give rise to c-kit⁺ cells with colony-forming unit in spleen (CFU-S) activity, suggesting that c-kit⁺ HSCs are recruited from a more primitive quiescent c-kit⁻ HSC population. Collectively, these reported studies suggest that most of the murine LTR-HSCs express a low to high level of c-kit on their surfaces, but also that there is a less frequent subpopulation expressing less than a low level of c-kit coexisting in murine BMs.

On the other hand, the flt3 receptor has also been shown to be expressed and to function in murine candidate HSCs [1–10, 24–28], including Lin⁻Sca-1⁺AA4⁺ fetal liver cells [5], CD34^{+/-} KSL BM cells [10, 24–26], and Thy-1.1^oKLS cells [9]. In particular, Jacobsen et al. have extensively studied the expression and functional significance of flt3 receptor on mu-

rine LTR-HSCs [7, 8, 10, 24–26]. Adolfsson et al. [24] first reported that the upregulation of *flt3* on BM-derived KSL cells is accompanied by loss of self-renewal capacity. In other words, *flt3*⁺ KSL cells rapidly and efficiently reconstituted B and T lymphopoiesis, and only *flt3*⁻ KSL cells supported sustained multilineage reconstitution [24–26]. On the basis of these data, they proposed that *flt3*⁺ KSL cells are progenitors for the common lymphoid progenitor (CLP) [24–26]. Earlier, Kondo et al. [46] identified other CLPs that have the *Lin*⁻*Thy-1*⁻*Sca-1*^{low}*c-kit*^{low}*IL-7Rα*⁺ immunophenotype. In Adolfsson's study [25], it was shown that the *flt3*⁺ KSL cells produced this *IL-7Rα*⁺ CLP in vitro as well as in vivo. These results suggested that the *flt3*⁺ KSL population is distinct and most likely an intermediate between *flt3*⁻ KSL (LTR-HSC) and this *IL-7Rα*⁺ CLP. Interestingly, *flt3*⁺ KSL cells were found to be almost exclusively *CD34*⁺, whereas *flt3*⁻ KSL cells contained a small but significant (5%) fraction of *CD34*⁻ cells [24]. This notion was further supported by the recent study reported by Sitnicka et al. [26]. In this study, FL-deficient mice had severely (10-fold) reduced levels of CLP, although the numbers of common myeloid progenitors (CMPs) and *CD34*⁻ KSL were unaffected [26]. Very recently, Adolfsson et al. [25] have clearly demonstrated that the herein-mentioned *flt3*⁺ KSL cells sustain granulocyte, monocyte, and B- and T-cell potential, but fail to produce significant erythroid and megakaryocytic progeny. On the basis of these observations, they proposed an alternative road map for adult mouse blood lineage commitment [25].

In contrast to murine LTR-HSC, the expression and functional significance of *flt3* and *c-kit* on human LTR-HSC has yet to be fully elucidated. Earlier studies have shown that most, if not all, long-term culture-initiating cell (LTC-IC) are *c-kit*⁺ [47, 48]. However, we observed that extended LTC-IC (ELTC-IC; assayed after 7–9 weeks of coculture with allogeneic BM stromal layer) are apparently enriched in a CB-derived *CD34*⁺*c-kit*^{low/-} cell population [21]. Of note was that ELTC-ICs assayed after 9 weeks of coculture were detected only in the *CD34*⁺*c-kit*⁻ cell population [21]. Our data are consistent with several other in vitro studies [49–51]. Sogo et al. [49] have clearly demonstrated that CB-derived *CD34*⁺*c-kit*^{<low} cells mature into *CD34*⁺*c-kit*^{low} and *CD34*⁺*c-kit*⁺ cells in vitro, suggesting that the upregulation of *c-kit* protein on *c-kit*^{<low} cells is the first maturational step of human HSCs [49]. Enrichment of human BM-derived primitive HSCs in the *CD34*⁺*c-kit*^{low} fraction was also confirmed using long-term engraftment studies in preimmune fetal sheep [51]. The findings showed that BM-derived *CD34*⁺*c-kit*^{low} cells transplanted to fetal sheep sustained long-term donor-derived hematopoiesis (up to 16 months) [52]. There is, however, no direct evidence yet for a distinct population of *c-kit*⁻ or *c-kit*^{<low} human primitive HSCs with long-term repopulating potential. Such a stem cell population is likely to be present at very low frequency in human BM- or CB-derived hematopoietic cells. Recently, we identified very primitive *CD34*⁻ SRCs in human CB detected only by the IBMI method [29, 30]. As shown in Figure 1D, the CB-derived *Lin*⁻*CD34*⁻ cell population did not express detectable levels of *c-kit* protein by flow cytometry. Therefore, our identified *CD34*⁻ SRCs may correspond to such *c-kit*⁻ or *c-kit*^{<low} LTR-HSCs [29, 30].

In contrast to *c-kit*, the information regarding *flt3* expression on human LTR-HSCs is much more limited. Recently, Sitnicka et al. [31], using the conventional intravenous injection method, clearly demonstrated that human BM- or CB-derived *CD34*⁺ HSC capable of multilineage engrafting NOD/SCID mice do express *flt3* receptors. Moreover, they also showed that CB-derived *CD34*⁺*flt3*⁻ cells could repopulate recipient mouse BMs. On the basis of these data, they proposed that most BM- and CB-derived *CD34*⁺ SRCs ex-

press *flt3*, and that the expression pattern of *flt3* and *c-kit* receptors on primitive mouse and human HSCs is different and contrasting. However, they did not investigate the secondary repopulating capacity of *CD34*⁺*flt3*^{+/-} cells as well as the repopulation capacity of the *CD34*⁻ counterpart.

In this study, we have investigated the SRC activity of CB-derived *Lin*⁻*CD34*⁺*flt3*^{+/-} cells as well as *Lin*⁻*CD34*⁻*flt3*^{+/-} cells using the IBMI method. First, we confirmed that CB-derived *Lin*⁻*CD34*⁺*flt3*^{+/-} cells showed distinct SRC activity by IBMI (Fig. 3; Table 1). Interestingly, we demonstrated for the first time that *Lin*⁻*CD34*⁻*flt3*⁻ cells showed significant and potent SRC activity by IBMI. Moreover, our secondary transplantation study clearly indicated that the secondary repopulating capacity is most potently observed in *CD34*⁻*flt3*⁻ cells in comparison with *CD34*⁺*flt3*^{+/-} cells (Fig. 4). Finally, we observed that these *Lin*⁻*CD34*⁻*flt3*⁻ cells could produce *CD34*⁺*flt3*^{+/-} SRCs after being cocultured with HESS-5 cells in the presence of a cocktail of cytokines (Fig. 5). These results suggest that *CD34*⁻*flt3*⁻ SRCs are the precursor for *CD34*⁺*flt3*^{+/-} SRCs. On the basis of the results of our present study, we propose that the immunophenotype of very primitive human LTR-HSCs is *Lin*⁻*CD34*⁻*c-kit*⁻*flt3*⁻. Primitive human LTR-HSCs may express lower levels of *c-kit* and *flt3* receptors on their surfaces when they commit to more mature short-term repopulating HSCs (STR-HSCs). It is still unclear whether such a distinct pattern of *c-kit* and *flt3* expression might identify distinct subpopulations of LTR-HSC or STR-HSC within the human HSC hierarchy.

From another point of view, we and many other investigators have planned to expand candidate human HSCs ex vivo using several cytokines, including SCF, FL, TPO, and IL-6/soluble IL-6 receptor (or fusion protein) [53–56]. However, the present study and other reported studies [24–26, 41–43, 49–52] have demonstrated/suggested that very primitive LTR-HSCs do not express their receptors, such as *c-kit* and *flt3*. Furthermore, *Lin*⁻*CD34*⁻*c-kit*⁻*flt3*⁻ cells are still heterogeneous, and putative human LTR-HSC may express other potentially important stem cell molecules. Therefore, for clinical application in the near future, further studies will be required to elucidate the proposed model of the human HSC hierarchy as well as to identify hitherto unidentified molecules that are important (indispensable) for stem cell expansion.

In conclusion, the present study provides evidence that human CB-derived *CD34*⁻ SRCs do not express *flt3* tyrosine kinase receptors, like murine candidate HSCs *CD34*⁻ KSL cells. According to our data, the immunophenotype of human LTR-HSC is *Lin*⁻*CD34*⁻*c-kit*⁻*flt3*⁻. Therefore, further studies will be required to identify positive markers, such as *Sca-1* for murine *CD34*⁻ KSL cells, for these primitive human LTR-HSCs in the near future.

ACKNOWLEDGMENTS

We thank Dr. Takeshi Todo of Department of Mutagenesis, Radiation Biology Center, Kyoto University, for his advice on the irradiation of NOD/SCID mice; Kirin Brewery Co. Ltd. (Tokyo) and Ajinomoto Co. Inc. (Yokohama, Japan) for providing the various growth factors used in this study; and Yuko Masai for assistance in preparation of the manuscript. This work was supported by Grants-in-Aid for Scientific Research on Priority Areas (Grant number 15039227) and for Scientific Research C (Grant number 15591015) from the Ministry of Education, Science and Culture of Japan, a grant from Haiteku Research Center of the Ministry of Education, a grant from the Science Frontier Program of the Ministry of Education, a grant

from the 21st Century Center of Excellence (COE) program of the Ministry of Education, a grant from the Promotion and Mutual Aid Corporation for Private Schools of Japan, a grant from Kansai Medical University (Research Grant B), a grant from the Japan Leukemia Research Foundation, and a grant from the Mitsubishi Pharma Research Foundation.

DISCLOSURE OF POTENTIAL CONFLICTS OF INTEREST

The authors indicate no potential conflicts of interest.

REFERENCES

- Lyman SD, Jacobsen SEW. c-kit ligand and flt3 ligand: Stem/progenitor cell factors with overlapping yet distinct activities. *Blood* 1998;91:1101–1134.
- Matthews W, Jordan CT, Wiegand GW et al. A receptor tyrosine kinase specific to hematopoietic stem and progenitor cell-enriched populations. *Cell* 1991;65:1143–1152.
- Lyman SD, James L, Bos TV et al. Molecular cloning of a ligand for the flt3/flk2 tyrosine kinase receptor: A proliferative factor for primitive hematopoietic cells. *Cell* 1993;75:1157–1167.
- Hannum C, Culpepper J, Cambell D et al. Ligand for flt3/flk2 receptor tyrosine kinase regulates growth of haematopoietic stem cells and is encoded by variant RNAs. *Nature* 1994;368:643–648.
- Zeigler FC, Bennett B, Jordan CT et al. Cellular and molecular characterization of the role of the flk-2/flt-3 receptor tyrosine kinase in hematopoietic stem cells. *Blood* 1994;84:2422–2430.
- Hirayama F, Lyman SD, Clark SC et al. The flt3 ligand supports proliferation of lymphohematopoietic progenitors and early B-lymphoid progenitors. *Blood* 1995;85:1762–1768.
- Jacobsen SEW, Okkenhaug C, Myklebust J et al. The flt3 ligand potently and directly stimulates the growth and expansion of primitive murine bone marrow progenitor cells in vitro: Synergistic interactions with interleukin (IL) 11, IL-12, and other hematopoietic growth factor. *J Exp Med* 1995;181:1357–1363.
- Veiby OP, Jacobsen FW, Cui L et al. The flt3 ligand promotes the survival of primitive hematopoietic progenitor cells with myeloid as well as B lymphoid potential. *J Immunol* 1996;157:2953–2960.
- Christensen JL, Weissman IL. Flk-2 is a marker in hematopoietic stem cell differentiation: A simple method to isolate long-term stem cells. *Proc Natl Acad Sci U S A* 2001;98:14541–14546.
- Yang L, Bryder D, Adolfsson J et al. Identification of Lin⁻Scal⁺kit⁺CD34⁺Flt3⁻ short-term hematopoietic stem cells capable of rapidly reconstituting and rescuing myeloablated transplant recipients. *Blood* 2005;105:2717–2723.
- Lyman SD, James L, Johnson L et al. Cloning of the human homologue of the murine flt3 ligand: A growth factor for early hematopoietic progenitor cells. *Blood* 1994;83:2795–2801.
- Muench MO, Roncarolo MG, Menon S et al. Flk-2/flt-3 ligand regulates the growth of early myeloid progenitors isolated from human fetal liver. *Blood* 1995;85:963–972.
- Shah AJ, Smogorzewska EM, Hannum C et al. Flt3 ligand induces proliferation of quiescent human bone marrow CD34⁺CD38⁻ cells and maintains progenitor cells in vitro. *Blood* 1996;87:3563–3570.
- Rusten LS, Lyman SD, Veiby OP et al. The flt3 ligand is a direct and potent stimulator of the growth of primitive and committed human CD34⁺ bone marrow progenitor cells in vitro. *Blood* 1996;87:1317–1325.
- Rappold I, Ziegler BL, Kohler I et al. Functional and phenotypic characterization of cord blood and bone marrow subsets expressing flt3 (CD135) receptor tyrosine kinase. *Blood* 1997;90:111–125.
- Gotze KS, Ramirez M, Tabor K et al. Flt3^{high} and flt3^{low} CD34⁺ progenitor cells isolated from human bone marrow are functionally distinct. *Blood* 1998;91:1947–1958.
- Xiao M, Oppenlander BK, Plunkett JM et al. Expression of flt3 and c-kit during growth and maturation of human CD34⁺CD38⁻ cells. *Exp Hematol* 1999;27:916–927.
- Sonoda Y, Sakabe H, Ohmizono Y et al. Synergistic actions of stem cell factor and other burst-promoting activities on proliferation of CD34⁺ highly purified blood progenitors expressing HLA-DR or different levels of c-kit protein. *Blood* 1994;84:4099–4106.
- Sonoda Y, Kimura T, Sakabe H et al. Human flt3 ligand acts on myeloid as well as multipotential progenitors derived from purified CD34⁺ blood progenitors expressing different levels of c-kit protein. *Eur J Haematol* 1997;58:257–264.
- Sakabe H, Kimura T, Zeng ZZ et al. Haematopoietic action of flt3 ligand on cord blood-derived CD34⁺ positive cells expressing different levels of flt3 or c-kit tyrosine kinase receptor: Comparison with stem cell factor. *Eur J Haematol* 1998;60:297–306.
- Sakabe H, Yahata N, Kimura T et al. Human cord blood-derived primitive progenitors are enriched in CD34⁺c-kit⁻ cells: Correlation between long-term culture-initiating cells and telomerase expression. *Leukemia* 1998;12:728–734.
- Krause DS, Fackler MJ, Civin CI et al. CD34: Structure, biology, and clinical utility. *Blood* 1996;87:1–13.
- Osawa M, Hanada K, Hamada H et al. Long-term lymphohematopoietic reconstitution by a single CD34-low/negative hematopoietic cell. *Science* 1996;273:242–245.
- Adolfsson J, Borge OJ, Bryder D et al. Upregulation of flt3 expression within the bone marrow Lin⁻Scal⁺c-kit⁺ stem cell compartment is accompanied by loss of self-renewal capacity. *Immunity* 2001;15:659–669.
- Adolfsson J, Mansson R, Buza-Vidas N et al. Identification of flt3⁺ lympho-myeloid stem cells lacking erythro-megakaryocytic potential: A revised road map for adult blood lineage commitment. *Cell* 2005;121:295–306.
- Sitnicka E, Bryder D, Theilgaard-Monch K et al. Key role of flt3 ligand in regulation of the common lymphoid progenitor but not in maintenance of the hematopoietic stem cell pool. *Immunity* 2002;17:463–472.
- Mackarehtschian K, Hardin JD, Moore KA et al. Targeted disruption of the flk2/flt3 gene leads to deficiencies in primitive hematopoietic progenitors. *Immunity* 1995;3:147–161.
- McKenna HJ, Socking KL, Miller RE et al. Mice lacking flt3 ligand have deficient hematopoiesis affecting hematopoietic progenitor cells, dendritic cells, and natural killer cells. *Blood* 2000;95:3489–3497.
- Wang J, Kimura T, Asada R et al. SCID-repopulating cell activity of human cord blood-derived CD34⁻ cells assured by intra-bone marrow injection. *Blood* 2003;101:2924–2931.
- Kimura T, Wang J, Matsui K et al. Proliferative and migratory potentials of human cord blood-derived CD34⁻ severe combined immunodeficiency repopulating cells that retain secondary reconstituting capacity. *Int J Hematol* 2004;79:328–333.
- Sitnicka E, Buza-Vidas N, Larsson S et al. Human CD34⁺ hematopoietic stem cells capable of multilineage engrafting NOD/SCID mice express flt3: Distinct flt3 and c-kit expression and response patterns on mouse and candidate human hematopoietic stem cell. *Blood* 2003;102:881–886.
- Ebihara Y, Wada M, Ueda T et al. Reconstitution of human haematopoiesis in non-obese diabetic/severe combined immunodeficient mice by clonal cells expanded from single CD34⁺CD38⁻ cells expressing flk2/flt3. *Br J Haematol* 2002;119:525–534.
- Kimura T, Sakabe H, Tanimukai S et al. Simultaneous activation of signals through gp130, c-kit, and interleukin-3 receptor promotes a trilineage blood cell production in the absence of terminally acting lineage-specific factors. *Blood* 1997;90:4767–4778.
- Kimura T, Wang J, Minamiguchi H et al. Signal through gp130 activated by soluble interleukin (IL)-6 receptor(R) and IL-6 or IL-6R/IL-6 fusion protein enhances ex vivo expansion of human peripheral blood-derived hematopoietic progenitors. *STEM CELLS* 2000;18:444–452.
- Kushida T, Inaba M, Hisha H et al. Intra-bone marrow injection of allogeneic bone marrow cells: A powerful new strategy for treatment of intractable autoimmune diseases in MRL/lpr mice. *Blood* 2001;97:3292–3299.
- Larochelle A, Vormoor J, Hanenberg H et al. Identification of primitive human hematopoietic cells capable of repopulating NOD/SCID mouse bone marrow: Implications for gene therapy. *Nat Med* 1996;2:1329–1337.
- Bhatia M, Bonnet D, Murdoch B et al. A newly discovered class of human hematopoietic cells with SCID-repopulating activity. *Nat Med* 1998;4:1038–1045.
- Ogata K, Satoh C, Tachibana M et al. Identification and hematopoietic potential of CD45⁻ clonal cells with very immature phenotype (CD45⁻CD34⁻CD38⁻Lin⁻) in patients with myelodysplastic syndromes. *STEM CELLS* 2005;23:619–630.
- Tsuji T, Ogasawara H, Aoki Y et al. Characterization of murine stromal cell clones established from bone marrow and spleen. *Leukemia* 1996;10:803–812.
- Osawa M, Nakamura K, Nishi N et al. In vivo self-renewal of c-kit⁺Scal⁺Lin^{low} hematopoietic stem cells. *J Immunol* 1996;156:3207–3214.
- Ogawa M, Matsuzaki Y, Nishikawa S et al. Expression and function of c-kit in hemopoietic progenitor cells. *J Exp Med* 1991;174:63–71.
- Orlic D, Fischer R, Nishikawa S et al. Purification and characterization of heterogeneous pluripotent hematopoietic stem cell populations expressing high levels of c-kit receptor. *Blood* 1993;82:762–770.
- Doi H, Inaba M, Yamamoto Y et al. Pluripotent hemopoietic stem cells are c-kit^{low}. *Proc Natl Acad Sci U S A* 1997;94:2513–2517.
- Ortiz M, Wine JW, Lohrey N et al. Functional characterization of a novel

- hematopoietic stem cell and its place in the c-kit maturation pathway in bone marrow cell development. *Immunity* 1999;10:173–182.
- 45 Randall TD, Weissman IL. Characterization of a population of cells in the bone marrow that phenotypically mimics hematopoietic stem cells: Resting stem cells or mystery population? *STEM CELLS* 1998;16:38–48.
- 46 Kondo M, Weissman IL, Akashi K. Identification of clonogenic common lymphoid progenitors in mouse bone marrow. *Cell* 1997;91:661–672.
- 47 Simmons PJ, Aylett GW, Niutta S et al. C-kit is expressed by primitive human hematopoietic cells that give rise to colony-forming cells on stroma-dependent or cytokine-supplemented culture. *Exp Hematol* 1994;22:157–165.
- 48 Briddell RA, Broudy VC, Bruno E et al. Further phenotypic characterization and isolation of human hematopoietic progenitor cells using a monoclonal antibody to the c-kit receptor. *Blood* 1992;79:3159–3167.
- 49 Sogo S, Inaba M, Ogata H et al. Induction of c-kit molecules on human CD34⁺/c-kit^{low} cells: Evidence for CD34⁺/c-kit^{low} cells as primitive hematopoietic stem cells. *STEM CELLS* 1997;15:420–429.
- 50 Gunji Y, Nakamura M, Osawa H et al. Human primitive hematopoietic progenitor cells are more enriched in KIT^{low} cells than in KIT^{high} cells. *Blood* 1993;82:3283–3289.
- 51 Laver JH, Abboud MR, Kawashima I et al. Characterization of c-kit expression by primitive hematopoietic progenitors in umbilical cord blood. *Exp Hematol* 1995;23:1515–1519.
- 52 Kawashima I, Zanjani ED, Almada-Porada G et al. CD34⁺ human marrow cells that express low levels of kit protein are enriched for long-term marrow-engrafting cells. *Blood* 1996;87:4136–4142.
- 53 Ohmizono Y, Sakabe H, Kimura T et al. Thrombopoietin augments ex vivo expansion of human cord blood-derived hematopoietic progenitors in combination with stem cell factor and flt3 ligand. *Leukemia* 1997;11:524–530.
- 54 Bhatia M, Bonnet D, Kapp U et al. Quantitative analysis reveals expansion of human hematopoietic repopulating cells after short-term ex vivo culture. *J Exp Med* 1997;186:619–624.
- 55 Conneally E, Cashman J, Petzer A et al. Expansion in vitro of transplantable human cord blood stem cells demonstrated using a quantitative assay of their lympho-myeloid repopulating activity in nonobese diabetic-scid/scid mice. *Proc Natl Acad Sci U S A* 1997;94:9836–9841.
- 56 Ueda T, Tsuji K, Yoshino H et al. Expansion of human NOD/SCID-repopulating cells by stem cell factor, flk2/flt3 ligand, thrombopoietin, IL-6, and soluble IL-6 receptor. *J Clin Invest* 2000;105:1013–1021.

**Identification of Long-Term Repopulating Potential of Human Cord
Blood-Derived CD34 –flt3– Severe Combined Immunodeficiency-Repopulating
Cells by Intra-Bone Marrow Injection**

Takafumi Kimura, Rumiko Asada, Jianfeng Wang, Takashi Kimura, Miho Morioka,
Kazuo Matsui, Katsuya Kobayashi, Kae Henmi, Shiro Imai, Masakazu Kita, Takashi
Tsuji, Yutaka Sasaki, Susumu Ikehara and Yoshiaki Sonoda
Stem Cells 2007;25;1348-1355; originally published online Feb 15, 2007;
DOI: 10.1634/stemcells.2006-0727

This information is current as of September 11, 2008

**Updated Information
& Services**

including high-resolution figures, can be found at:
<http://www.StemCells.com/cgi/content/full/25/6/1348>

 **AlphaMed Press**

Flt3 ligand promotes myeloid dendritic cell differentiation of human hematopoietic progenitor cells: Possible application for cancer immunotherapy

SACHIO HARADA^{1,2}, TAKAFUMI KIMURA¹, HIROSHI FUJIKI², HITOSHI NAKAGAWA³, YUJI UEDA², TSUYOSHI ITOH², HISAKAZU YAMAGISHI² and YOSHIAKI SONODA¹

¹Department of Stem Cell Biology and Regenerative Medicine, Graduate School of Medical Science, Kansai Medical University, Osaka; ²Department of Surgery and Oncology of Digestive System, Graduate School of Medical Science, Kyoto Prefectural University of Medicine; ³Department of Hematology, Kyoto First Red Cross Hospital, Kyoto, Japan

Received January 15, 2007; Accepted February 23, 2007

Abstract. Current *in vitro* culture systems allow the generation of human dendritic progenitor cells (CFU-DCs). The aim of this study was to assess the effect of Flt3 ligand (FL) on the proliferation of human peripheral blood-derived myeloid CFU-DCs and their differentiation into more committed precursor cells (pDCs) using *in vitro* culture systems. Immunomagnetically separated CD34⁺ cells were cultured in serum-free, as well as in serum-containing, liquid suspension cultures to investigate the expansion and/or proliferation/differentiation of CFU-DCs, pDCs, and more mature dendritic cells (DCs). FACS-sorted CD34⁺Flt3^{+/-} cells were cultured in methylcellulose to assay hematopoietic progenitors, including CFU-DCs. In the clonal cell culture supplemented with granulocyte/macrophage (GM) colony-stimulating factor (CSF), interleukin-4, and tumor necrosis factor α , the frequency of CFU-DCs was significantly higher in the CD34⁺Flt3⁺ fraction than in the CD34⁺Flt3⁻ population, thus suggesting functional Flt3 expression on CFU-DCs. Serum-free suspension culture of CD34⁺ cells revealed the potent effect of FL on the expansion of CFU-DCs in synergy with GM-CSF and thrombopoietin (TPO). In addition, FL strongly induced the maturation of CFU-DCs into functional CD1a⁺ pDCs in serum-containing liquid suspension culture. Moreover, these FL-generated pDCs showed remarkable potential to differentiate into mature DCs with surface CD83/CD86 expression, which induced a distinct allogeneic T-cell response. These

results clearly demonstrate that FL supports not only the proliferation of early hematopoietic progenitor cells, but also the maturation process of committed precursor cells along with the DC-lineage differentiation. Therefore, it is possible to develop a more efficient DC-based cancer immunotherapy using this specific cytokine combination, GM-CSF+TPO+FL *in vitro* in the near future.

Introduction

Hematopoietic stem cells (HSCs) are known to have a robust capacity of multilineage differentiation, which is mainly regulated by the extrinsic environment, including cytokines or adhesion molecules expressed on neighboring cells (1,2). However, targeted deletion or overexpression of lineage-specific transcription factors leads to recovery of the differentiation potential into alternative lineages. For instance, pre-B cells in Pax-5-null mice can differentiate into mature T lymphoid and myeloid cells despite their defective potential for B lymphoid maturation (3). In addition, with the enforced expression of a myeloid-restricted cytokine receptor (R), granulocyte/macrophage colony-stimulating factor-R (GM-CSF-R) on hematopoietic progenitors (HPCs) results in a biased generation of myeloid cells (4). Lineage restriction in HSC/HPC differentiation may thus be controlled not only stochastically by intrinsic factors, but also instructively by expression levels of transcription factors or cytokine receptors.

Dendritic cells (DCs) are known as one of the most important players in the regulation of innate and adaptive immunity (5-8). They are recruited from the HSC pool like cells in other hematopoietic lineages (9-13). In mice, several DC compartments have been identified according to their immunophenotypes. It has also been reported that DCs are produced only from HPCs which express Flt3 on their surfaces (14,15).

While Flt3 is a receptor tyrosine kinase showing some structural homology to c-kit and c-fms (16), Flt3 ligand (FL) has the most potent activity for DC differentiation in mouse

Correspondence to: Dr Yoshiaki Sonoda, Department of Stem Cell Biology and Regenerative Medicine, Graduate School of Medical Science, Kansai Medical University, Moriguchi, Osaka 570-8506, Japan
E-mail: sonoda@takii.kmu.ac.jp

Key words: Flt3 ligand, hematopoietic progenitor cell, dendritic cell, CD34⁺ cell, cancer immunotherapy

bone marrow cells *in vitro* when used as a single cytokine (17,18). In human hematopoiesis, FL acts on the proliferation and differentiation of myeloid as well as erythroid stem/progenitor cells *in vitro* in synergy with other early-acting cytokines, such as stem cell factor (SCF, c-kit ligand) and thrombopoietin (TPO) (19-23). A combination of these three factors is also well known to support the *in vitro* expansion of DC progenitors (24,25), although the mechanisms of the factor-specific functions, as well as their synergistic actions, still remain unclear. We herein show the precise role of FL on the proliferation and differentiation of human CD34⁺ HPCs into functional DC precursors (pDCs) using *in vitro* culture systems. Our results indicate that FL is more reliable than SCF in instructing human DC progenitors expressing Flt3 to generate functional progenies.

Materials and methods

Recombinant factors. Purified bacterially-derived recombinant human (rh) granulocyte (G) colony-stimulating factor (CSF), and thrombopoietin (TPO), as well as purified Chinese hamster ovary cell-derived rh erythropoietin (Epo), were kindly supplied by Kirin Brewery Co., Ltd. (Tokyo, Japan). Purified rh IL-4 was a generous gift from Ono Pharmaceutical Co., Ltd. (Osaka, Japan). Yeast-derived rh Flt3 ligand (FL) was provided by Immunex Research and Development Corp. (Seattle, WA, USA). Purified rh interleukin (IL)-3, granulocyte/macrophage (GM)-CSF, stem cell factor (SCF), and tumor necrosis factor α (TNF α) were all purchased from R&D systems (Minneapolis, MN, USA).

Cell preparation. After informed consent was obtained, peripheral blood mononuclear cells (PBMNCs) were collected from patients with non-Hodgkin's lymphoma in first complete remission by leukapheresis using Fenwall CS-3000 Plus (Fenwall Laboratories, Inc., Deerfield, IL, USA), and were stored in liquid nitrogen until use in the present study, according to a method previously reported (26-28). After rapid thawing, cells were incubated on plastic dishes containing α MEM (Invitrogen Corp., Carlsbad, CA, USA) supplemented with 10% fetal calf serum (FCS, Hyclone Laboratories, Logan, UT, USA) overnight at 37°C in a fully humidified atmosphere flushed with 5% CO₂. The mononuclear non-adherent cell (MNNAC) fraction was then recovered for subsequent immunomagnetic isolation or flow cytometric cell sorting.

Immunomagnetic isolation and flow cytometric cell sorting. The above-mentioned MNNACs were further enriched for CD34⁺ cells using a MACS immunomagnetic microbeads system (Miltenyi Biotec, Bergisch Gladbach, Germany) or for lineage-depleted (Lin⁻) cells using a StemSep device (Stem Cell Technologies, Vancouver, BC, Canada), according to the manufacturer's instructions, and as described previously (29,30). The purity of CD34⁺ cells in these isolated cell fractions was confirmed by flow cytometry to be constantly more than 95%. The isolated cells were subsequently processed for liquid suspension culture or cell sorting as described below.

For flow cytometric cell sorting, Lin⁻ cells were incubated for 30 min at room temperature with purified anti-human Flt3 mAb (clone M22, kindly provided by Immunex Corp.), which

had been biotinylated as described previously (23,26,28), and followed by staining with fluorescein isothiocyanate (FITC)-conjugated HPCA-2 [CD34 mAb, Becton Dickinson Immunocytometry Systems (BD), San Jose, CA, USA] and streptavidin (SA)-phycoerythrin (PE) (BD) for 30 min on ice. Negative controls included unstained cells and cells stained only with FITC-conjugated isotype IgG₁ (BD) and SA-PE. Cell sorting was performed using a FACSVantage (BD), as previously reported (28-30). Sorting windows were established for CD34⁺Flt3⁺ or CD34⁺Flt3⁻ cells as shown in Fig. 1a and b. Data acquisition was performed using CELLQuest software (BD). The phenotypic purity of the sorted cells consistently exceeded 98%.

Clonal cell culture. CD34⁺Flt3⁺ or CD34⁺Flt3⁻ cells were cultured in 35-mm Lux suspension culture dishes (no. 171099, Nunc Inc., Naperville, IL, USA), as reported previously (26-30). Briefly, 1 ml of culture contained 200 sorted cells, 1.2% methylcellulose (Shinetsu Chemicals, Tokyo, Japan), 30% FCS, 1% bovine serum albumin (fraction V, Sigma Chemical Co., St. Louis, MO, USA), 5x10⁻⁵ mol/l 2-mercaptoethanol (Sigma), and 5 CSFs (20 ng/ml SCF, 10 ng/ml IL-3, 10 ng/ml GM-CSF, 20 ng/ml G-CSF, and 2 U/ml Epo). Dishes were incubated at 37°C in a fully humidified atmosphere flushed with a combination of 5% CO₂, 5% O₂, and 90% N₂. On days 12-14 of incubation, colonies were scored according to their typical morphological features using an inverted microscope, as reported (26-30). Colony types identified *in situ* were granulocyte/macrophage (CFU-GM), erythroid (BFU-E), and erythrocyte-containing mixed (CFU-Mix) colonies.

To examine dendritic colony (CFU-DC) formation, 500 sorted CD34⁺Flt3⁺ or ⁻ cells or cells recovered from serum-containing liquid cultures described below were cultured in the presence of 20 ng/ml GM-CSF, 100 U/ml IL-4, and 100 U/ml TNF α . On days 12-14 of incubation, DC colonies were scored, as described previously (31).

Liquid suspension culture. A total of 5x10³ immunomagnetically isolated CD34⁺ or Lin⁻ cells were cultured in 35-mm Lux suspension dishes containing 1 ml of StemPro-34 medium (Invitrogen) supplemented with the designated combination of CSFs, which included 20 ng/ml GM-CSF, 100 ng/ml TPO, 20 ng/ml SCF, and 20 ng/ml FL. Dishes were incubated at 37°C in a fully humidified chamber flushed with a combination of 5% CO₂, 5% O₂, and 90% N₂. On day 7, half of the culture medium was exchanged with freshly prepared medium. After 14 days of incubation, the number of viable cells in each dish was counted and replaced into clonal cell cultures.

In addition, CD34⁺ or Lin⁻ cells were incubated in RPMI 1640 (Invitrogen) supplemented with 10% FCS and the designated factors. After 14 days of incubation, these cells were transferred into DC maturation culture medium containing 10% FCS/RPMI supplemented with GM-CSF, IL-4, and TNF α . On day 7, 14, and 21 of incubation, a portion of cultured cells was processed for flow cytometry, as described below.

Flow cytometry. Immunomagnetically isolated cells or cells harvested from suspension cultures were stained with FITC-conjugated mAbs against human CD11c (eBioscience, San

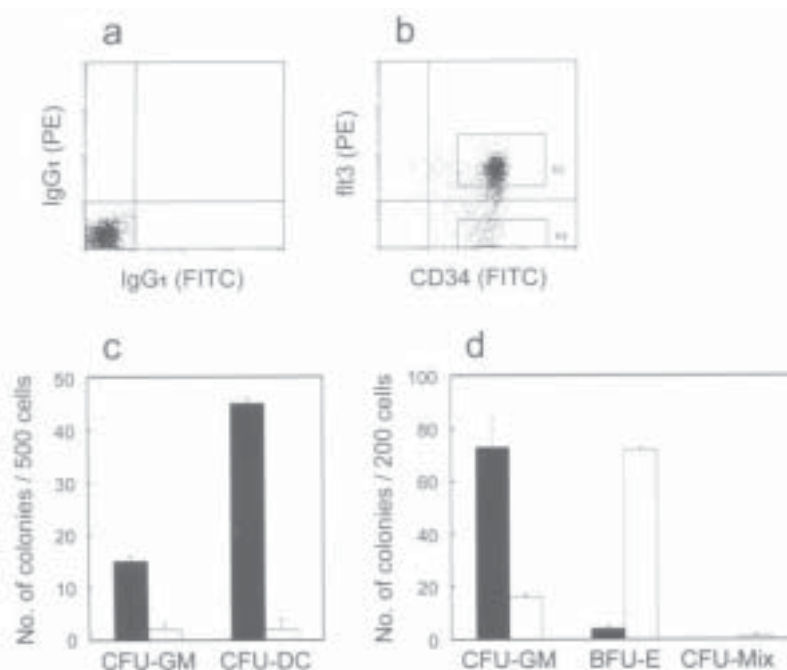


Figure 1. Characterization of PB-derived Lin-CD34⁺Flt3^{+/-} cells and their colony-forming capacity. The R1 gate was set on the lymphocyte window on the FSC/SSC profile of immunomagnetically isolated Lin⁻ cells (not shown). (a) Isotype control. (b) Cells in the R1 gate were further enriched by cell sorting as CD34⁺Flt3⁺ (R2) and CD34⁺Flt3⁻ (R3) cells, respectively. The sorted cells were incubated in methylcellulose culture. (c) A total of 500 sorted cells were incubated with GM-CSF, IL-4 and TNF α . (d) Two hundred sorted cells were cultured in the presence of SCF, IL-3, GM-CSF, G-CSF and Epo. The number of GM, erythroid, mixed, and DC colonies were directly counted *in situ* on days 12-14 of incubation. The data represent the mean \pm SEM from three independent experiments. Closed and open bars show the number of colonies generated from CD34⁺Flt3⁺ and CD34⁺Flt3⁻ cells, respectively.

Diego, CA, USA), CD14 (BD), CD54 (Beckman Coulter, Fullerton, CA, USA), CD80 and CD86 (both from Caltag Laboratories, Burlingame, CA, USA), PE-conjugated anti-human CD1a (Coulter), CD83 (Caltag), and HLA-DR (BD) mAbs. Dead cells were gated out by simultaneous staining with 7-AAD (Coulter). Data acquisition and analysis were performed using CELLQuest software on a FACSCalibur (BD).

Mixed lymphocyte reaction (MLR). The antigen-presenting capacities of DCs were assessed by MLR, as previously described (25), with some modifications. In brief, allogeneic T-cells were isolated as responders using nylon fiber columns (Wako, Osaka, Japan). A total of 1×10^5 cells were incubated in 96-well microtiter plates (Nunc) with the designated numbers of γ -irradiated (250 cGy) DCs generated from CD34⁺ cells in the above-mentioned serial liquid suspension culture for 21 days. After 5 days of incubation, cultures were pulsed with $1.0 \mu\text{Ci/well}$ [^3H]-thymidine for 8-12 h to measure the T-cell proliferation, expressed as [^3H]-thymidine incorporation by scintillation counting.

Statistical analysis. The significance of differences was determined by the paired t-test.

Results

Functional expression of Flt3 on human DC progenitors. We first investigated the Flt3 receptor expression on PB-derived CD34⁺ cells. As shown in Fig. 1a and b, $82.4 \pm 3.0\%$ ($n=6$)

of CD34⁺ cells expressed Flt3 on their surfaces. We then assessed the colony-forming capacity of sorted CD34⁺Flt3⁺ and CD34⁺Flt3⁻ cells. Data obtained from the three independent clonal cell culture experiments are presented in Fig. 1c and d. Of note was that the number of myeloid DC colonies supported by GM-CSF+IL-4+TNF α (G4TN) was strikingly higher in the culture of CD34⁺Flt3⁺ cells compared to the CD34⁺Flt3⁻ cell fraction ($P < 0.01$). In addition, CD34⁺Flt3⁺ cells generated a significantly ($P < 0.01$) higher number of CFU-GM-derived colonies, while most colonies in cultures of CD34⁺Flt3⁻ cells were derived from BFU-E or CFU-Mix ($P < 0.01$). These results indicated the possibility that Flt3 is expressed as a functional molecule on CFU-DC as well as CFU-GM.

Ex vivo expansion of DC progenitors by FL. It has been well documented that GM-CSF has the most potent effect on the DC-lineage differentiation of hematopoietic progenitors (HPCs) (11), while TPO, SCF, and FL have been shown to synergistically support the efficient expansion of early hematopoietic stem/progenitor cells *in vitro* (21,24,25). A combination of these early-acting CSFs also strongly enhances the proliferation of CD1a⁺ precursor DCs (pDCs) (24,25). On the other hand, c-kit and Flt3, which are activated with their respective ligands, SCF and FL, have been shown to have similar but specific tyrosine kinase activities (32). We therefore aimed to evaluate and compare the effect of FL and SCF on the proliferation of DC progenitors.

Representative data from three independent serum-free suspension cultures of CD34⁺ cells are shown in Fig. 2. Although the total cell number at day 14 significantly ($P < 0.05$)

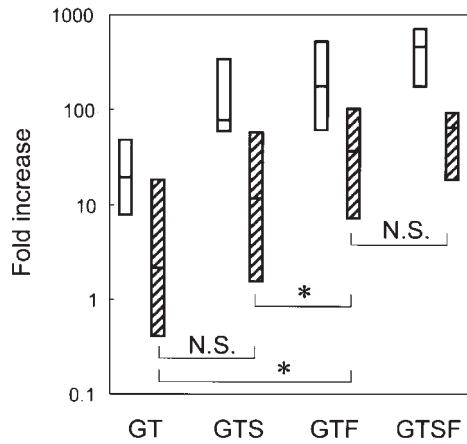


Figure 2. Effects of various cytokine combinations on *ex vivo* expansion of DC progenitors. The data represent the fold increase of cultured cells at day 14 of incubation. Open and striped columns show the values from total cell numbers and CFU-DCs, respectively. Horizontal bars represent the respective medians. NS, not significant. *P<0.05.

increased in the cultures containing GM-CSF+TPO+SCF (GTS) or GM-CSF+TPO+FL (GTF), in comparison to GM-CSF+TPO (GT), no significant difference was observed between GTS and GTF. The proliferation of DC progenitors (CFU-DCs) was more strongly supported by GTF than by GTS (P<0.05), while a combination of four cytokines (GTSF) did not enhance CFU-DC proliferation more profoundly. These results suggest that, in comparison to SCF, FL acts more specifically and potently on the proliferation of myeloid DC progenitors expressing its receptor Flt3, as well as on other lineage-committed progenitors.

Differentiation of CD34⁺ cells to DC precursors (pDCs) by FL. We assessed the serial effects of FL on the DC-lineage differentiation of CD34⁺ HPCs. Purified CD34⁺ cells were cultured in serum-containing media supplemented with GTS, GTF or GTSF. After 14 days of culture with GTS, ~10% of cells weakly expressed both CD11c and CD1a antigens (Fig. 3b), which are specific for pDCs. Interestingly, >50% of cells expressed these antigens after the same period of culture with GTF, whose fluorescence intensities were significantly higher than those with GTS (Fig. 3e). On the other hand, a combination of GTSF did not increase these DC-markers' expression as compared to GTF (Fig. 3h). Cells harvested from cultures supplemented with GTS, GTF and GTSF were further incubated with G4TN for another 7 days. As shown in Fig. 3c, f and i, the expression levels of CD11c and CD1a in these cells on day 21 were comparable despite the initial cytokine combination. These results indicate that FL can accelerate the differentiation of CD34⁺ HPCs to pDCs.

As with CD11c expression, a combination of GTF induced the differentiation of CD34⁺ cells to CD14⁺CD1a⁺ pDCs more rapidly than GTS or GTSF (Fig. 4b, e and h). As clearly seen in Fig. 4-c, f and i, CD14⁺CD1a⁺ pDCs turned to CD14⁻ fully mature DCs after stimulation with G4TN for another 7 days.

These findings provide evidence that FL acts on CD34⁺Flt3⁺ DC progenitor cells and accelerates their differentiation to mature DCs in the presence of GM-CSF and TPO. The combination of four factors (GTSF), however, did not show any additive effects as compared to GTF.

Induction of functional DCs by FL. As shown in Figs. 3 and 4, the cytokine combination of G4TN induced DC-lineage differentiation of cultured CD34⁺ cells to CD11c⁺CD14⁺CD1a⁺

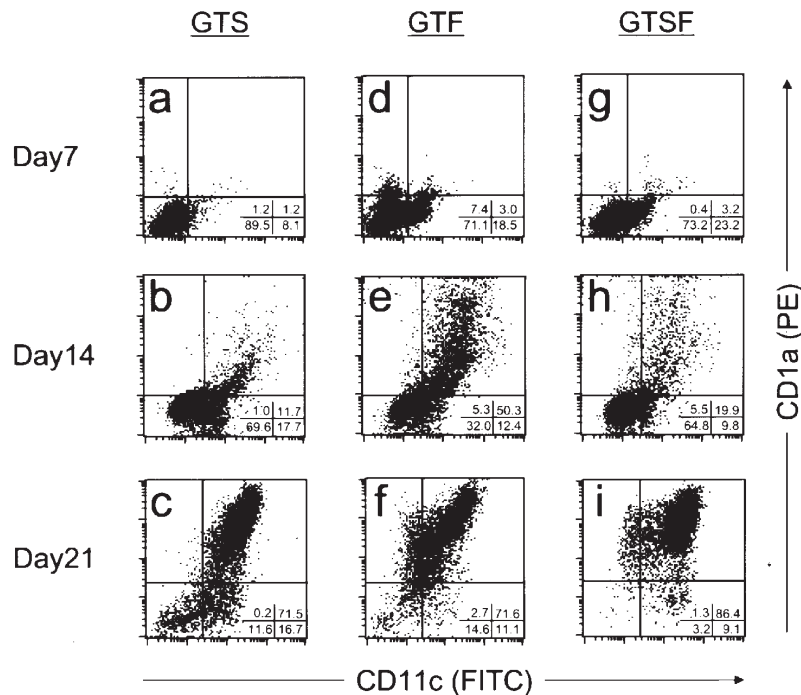


Figure 3. Differentiation of CD34⁺ cells to CD11c⁺CD1a⁺ pDCs. The expression profile of CD11c and CD1a of cultured CD34⁺ cells was assessed by flow cytometry (FCM) on days 7, 14 and 21 of incubation. The R1 gate was set on viable cells (negative for 7AAD). FCM data show the R1-gated events. (a-c) FCM data of cells initially cultured with GTS. (d-f) FCM data of cells initially cultured with GTF. (g-i) FCM data of cells initially cultured with GTSF. The percentages of cells in each quadrant are presented in the lower right corner.

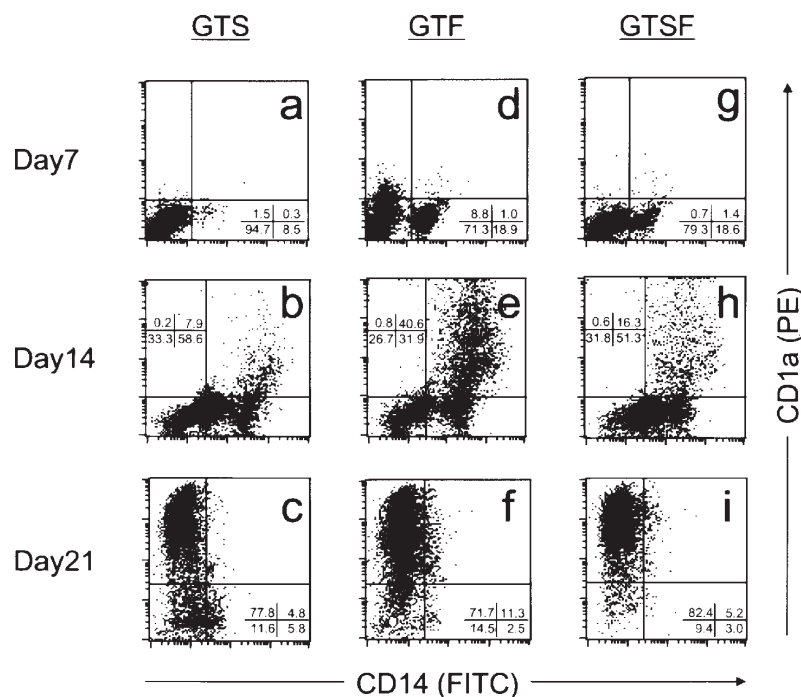


Figure 4. Differentiation of CD34⁺ cells to CD14⁺CD1a⁺ pDCs. The expression profile of CD14 and CD1a of cultured CD34⁺ cells was assessed on days 7, 14 and 21 of incubation. (a-c) FCM data of cells initially cultured with GTS. (d-f) FCM data of cells initially cultured with GTF. (g-i) FCM data of cells initially cultured with GTSF. The percentages of cells in each quadrant are presented in the lower right or upper left corner.

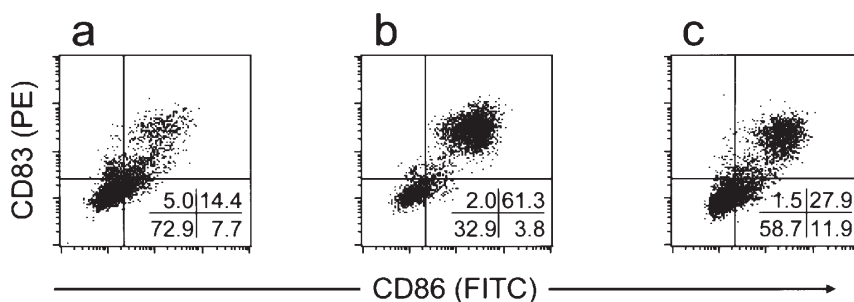


Figure 5. Expression of CD83 and CD86 on pDCs. Day-14 cells, which originated from CD34⁺ cells cultured with GTS (a), GTF (b) and GTSF (c), were further transferred to a terminal differentiation culture medium with G4TN and incubated for another 7 days. The R1 gate was set on viable cells. The data represent the R2-gated events, which were defined as high FSC/SSC fraction (DC gate). The percentages of cells in each quadrant are presented in the lower right corner.

pDCs, regardless of the initial cytokine combination used in the first step serum-containing culture. As well-documented in previous literature, neither CD11c, CD14 or CD1a, however, directly show the immunological function of DCs or pDCs. Therefore, it seems most important to clarify whether FL could contribute to the effective generation of functional and beneficial pDCs or not.

We compared the expression profiles of active antigen-presenting cell (APC) markers, CD83 and CD86, on culture-generated DCs induced in the maturation cultures containing G4TN after the initial cultures with the designated combinations of cytokines, GTS, GTF, and GTSF. As shown in Fig. 5, the percentage of CD83⁺CD86⁺ functional DCs, induced by G4TN after the initial cultures with GTF (Fig. 5b), was significantly higher than those induced after the other two initial combinations (Fig. 5a and c). These results suggest that FL can accelerate the differentiation of HPCs to pDCs, which are

potentially ready to become APCs expressing surface co-stimulatory molecules.

We also estimated the functional properties of culture-generated DCs by assessing their stimulating activity against proliferation of allogeneic T-lymphocytes. Representative data from three independent experiments are shown in Fig. 6. As clearly shown, DCs generated by GTF+G4TN more potently induced allogeneic T-cell responses than those generated by GTS+G4TN or GTSF+G4TN. These results again illustrate that FL did advantageously induce the differentiation of HPCs to pDCs, which are ready to fully function as APCs in T-cell-mediated immune responses.

Discussion

DCs are known as the professional APCs (6-8). Namely, they play an important role of capturing and processing antigen

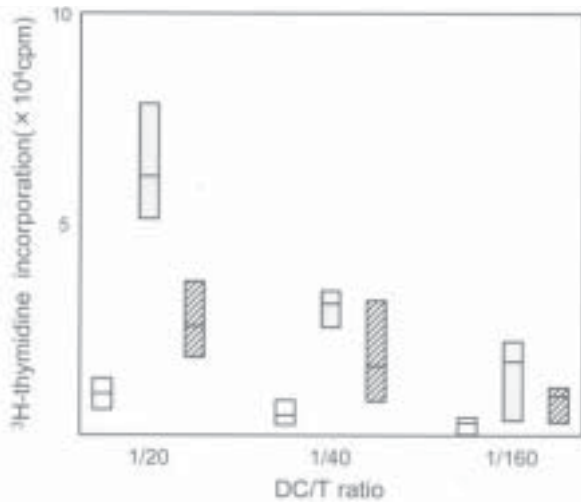


Figure 6. Proliferative response of allogeneic T-lymphocytes stimulated by culture-generated DCs. Day-21 cells, which were incubated with G4TN from day 14, were irradiated at 250 cGy. Various numbers of these cells (stimulator-to-responder ratios are 1:20, 1:40, and 1:160) were incubated with HLA-mismatched responder T-cells at 1×10^5 /well. The cells were harvested on day 5 after 8-12 h of exposure to [3 H]-thymidine. Open, gray and shaded columns respectively show data of DCs generated in initial 14-day cultures with GTS, GTF and GTSF. Horizontal bars represent the respective median values.

and presenting it to naïve helper T-cells to initiate the immune responses, including cytotoxic T lymphocyte (CTL) induction (5-7). Based on these findings, many doctors try to develop DC-based cancer immunotherapy (31).

Since G-CSF mobilizes monocytes as well as HPCs/HSCs in PB (34), many investigators used leukapheresis products to generate DCs for cancer immunotherapy (33,35). However, recent studies have suggested that monocytes mobilized by G-CSF have a T helper (Th)-2 type cytokine production profile (36). In fact, G-CSF was reported to suppress the production of IL-12 and TNF α (37,38). Furthermore, another study suggested that G-CSF mobilizes DC2, not DC1, which stimulate T cell response into Th-2 type (36,39). Collectively, apheresis products obtained by G-CSF may not be useful as a cell source for DC-based cancer immunotherapy, because Th-1 type immune response is required for elimination of tumor cells. In this context, we have investigated if apheresis products mobilized by G-CSF could be used for cancer immunotherapy considering their cytokine production profiles and the immune responses elicited by DCs generated from monocytes obtained after G-CSF mobilization (40). As a result, consistent with a previous report (41), these generated DCs were phenotypically and functionally equivalent to DCs generated from control monocytes. In fact, we have demonstrated that peptide-pulsed DCs generated in this manner could elicit optimal cytotoxic T-cell responses in some patients in a clinical study for cancer immunotherapy on patients bearing CEA-expressing solid cancer (42). On the other hand, we also previously demonstrated that a substantial number of CD34 $^+$ cells were mobilized in the peripheral blood and thus proposed the potential use of these G-CSF-mobilized CD34 $^+$ cells as a cell source for the expansion of pDCs *in vitro* (40). In the present study, we tried to address this possibility and also assessed their further use in the more efficient production of mature DCs for future cancer immunotherapy.

The *ex vivo* expansion and differentiation of myeloid DCs from PB-derived CD34 $^+$ HPCs require a combination of various cytokines, as previously reported (24,25,43). It is well documented that there are three types of cytokine-generated DCs, including two types of myeloid DCs, such as CD14 $^+$ blood monocyte-derived DCs and CD34 $^+$ HPC-derived DCs, and CD11c-negative lymphoid DCs (44). Interestingly, CD34 $^+$ HPCs can give rise to any or all types of these DCs under the influence of particular cytokines *in vitro*. Among them, GM-CSF and IL-3 are the key cytokines to generate myeloid and lymphoid DCs, respectively (44). TNF α , IL-4, transforming growth factor β , IL-10, and vascular endothelial growth factor support or suppress the maturation/differentiation of these DCs (44). On the other hand, it was reported that SCF and FL, which are known to be early-acting cytokines (32), could support pDC expansion (24,25). SCF stimulates DC formation from human BM- and CB-derived CD34 $^+$ cells in combination with GM-CSF and TNF α without affecting DC differentiation (31,45). FL also increases the production of DCs from BM-derived CD34 $^+$ cells in combination with GM-CSF+IL-4+TNF α (46,47). This enhanced DC production is similar to the observed effects of SCF. However, as with SCF, FL does not affect the differentiation of DCs, but rather enhances the proliferation (46,47). From another point of view, FL differs somewhat from SCF when used singly *in vivo*; however, it can increase both myeloid and lymphoid DCs (48). Preclinical human trials indicate a similar increase in circulating DCs, however, the precise mechanisms of action of these two cytokines remains unclear. In addition, FL has been reported to induce DC differentiation *in vivo* (46). However, precisely how the FL acts on CD34 $^+$ HPCs and/or pDCs thus inducing them to generate mature DCs remains to be elucidated. It was therefore considered to be necessary to truly understand the basic mechanisms of actions of FL on these DC precursor cells, in order to clarify the role of FL *in vivo* and to develop more effective anti-cancer immunotherapy in the near future.

In this context, we herein focused on the precise effects of FL on the process of DC maturation of human PB-derived CD34 $^+$ HPCs. Our data clearly demonstrated that FL has more potent and specific actions on human DC development, compared to SCF, another early-acting cytokine. Of note was that FL, in combination with GM-CSF plus TPO, induced a dramatic effect on the *ex vivo* expansion of CFU-DCs (Fig. 2). The addition of SCF did not show any additive effects. Moreover, this GTF combination accelerated the maturation of CD34 $^+$ HPCs to CD14 $^+$ CD11c $^+$ CD1a $^+$ pDCs, as shown in Figs. 3 and 4. Because the expression of CD14 on CD34 $^+$ cells was first seen on day 7 in cultures containing GTF (but not GTS), a substantial proportion of DCs developing from CD34 $^+$ HPCs do so via CD14 $^+$ bipotential intermediates (41,45) (Figs. 3 and 4). These pDCs could then mature into CD14 $^-$ CD11c $^+$ CD1a $^+$ DCs in the presence of GM-CSF, IL-4, and TNF α . These mature DCs express co-stimulatory molecules, such as CD83 and CD86 (Fig. 5). Importantly, these GTF-generated mature DCs induce the most potent allogeneic T-cell responses in MLR in comparison to those of GTS and GTSF (Fig. 6). Both FL and SCF can expand pDCs as previously reported (24,25). However, our results indicate for the first time that in comparison to SCF, FL acts differently on CD34 $^+$ HPCs, where it induced the proliferation/differentiation

of G-CSF-mobilized PB-derived CD34⁺ cells to pDCs in the presence of GM-CSF and TPO.

In conclusion, our present study clearly demonstrated that a combination of GTF could efficiently expand CFU-DCs and generate functional mature DCs *in vitro*. Therefore, it is possible to develop a more efficient DC-based cancer immunotherapy using this specific cytokine combination, GM-CSF+TPO+FL *in vitro* in the near future.

Acknowledgements

The authors are grateful to Dr Kaori Okugawa for her kind support. The authors also thank Kirin Brewery Co. Ltd. (Tokyo, Japan) and Ono Pharmaceutical Co. Ltd. (Osaka, Japan) for providing the various growth factors used in this study. This study was supported by Grants-in-Aid for Scientific Research on Priority Areas (grant no. 15039227) and for Scientific Research C (grant no. 15591015) from the Ministry of Education, Science and Culture of Japan, and grants from Haiteku Research Center of the Ministry of Education, the Science Frontier Program of the Ministry of Education, the Japan Leukemia Research Foundation, and the Mitsubishi Pharma Research Foundation.

References

- Miyani H, Dragowska W and Lansdorp PM: Lineage commitment of human hemopoiesis involves asymmetric cell division of multipotent progenitors and does not appear to be influenced by cytokines. *J Cell Physiol* 157: 579-586, 1993.
- Zipori D: The renewal and differentiation of hemopoietic stem cells. *FASEB J* 6: 2691-2697, 1992.
- Nutt SL, Thevenin C and Busslinger M: Essential functions of Pax-5 (BSAP) in pro-B cell development. *Immunobiology* 198: 227-235, 1997.
- Metcalf D, Elliot MJ and Nicola NA: The excess numbers of peritoneal macrophages in granulocyte-macrophage colony-stimulating factor transgenic mice are generated by local proliferation. *J Exp Med* 175: 877-884, 1992.
- Steinmann RM: The dendritic cell system and its role in immunogenicity. *Ann Rev Immunol* 9: 271-296, 1991.
- Cella M, Sallusto F and Lanzavecchia A: Origin, maturation and antigen presenting function of dendritic cells. *Curr Opin Immunol* 9: 10-16, 1997.
- Banchereau J and Steinmann RM: Dendritic cells and the control of immunity. *Nature* 392: 245-252, 1998.
- Sallusto F and Lanzavecchia A: Mobilizing dendritic cells for tolerance, priming, and chronic inflammation. *J Exp Med* 189: 611-614, 1999.
- Ardavin C, Wu L, Li CL and Shortman K: Thymic dendritic cells and T cells develop simultaneously in the thymus from a common precursor population. *Nature* 362: 761-763, 1993.
- Shortman K, Vremec D, Corcoran LM, Georgopoulos K, Lucas K and Wu L: The linkage between T-cell and dendritic cell development in the mouse thymus. *Immunol Rev* 165: 39-46, 1998.
- Inaba K, Inaba M, Romani N, *et al*: Generation of large numbers of dendritic cells from mouse bone marrow cultures supplemented with granulocyte/macrophage colony-stimulating factor. *J Exp Med* 176: 1693-1702, 1992.
- Inaba K, Inaba M, Deguchi M, *et al*: Granulocytes, macrophages, and dendritic cells arise from a common major histocompatibility complex class II-negative progenitor in mouse bone marrow. *Proc Natl Acad Sci USA* 90: 3038-3042, 1993.
- Young JW and Steinman RM: The hematopoietic development of dendritic cells: a distinct pathway for myeloid differentiation. *Stem Cells* 14: 3376-3387, 1996.
- Small D, Levenstein M, Kim E, *et al*: STK-1, the human homolog of Flk-2/Flt-3, is selectively expressed in CD34⁺ human bone marrow cells and is involved in the proliferation of early progenitor/stem cells. *Proc Natl Acad Sci USA* 91: 459-463, 1994.
- Mackarehtschian K, Hardin JD, Moore KA, Boast S, Goff SP and Lemischka IR: Targeted disruption of the flk2/flt3 gene leads to deficiencies in primitive hematopoietic progenitors. *Immunity* 3: 147-161, 1995.
- Matthews W, Jordan CT, Wiegand GW, Pardoll D and Lemischka IR: A receptor tyrosine kinase specific to hematopoietic stem and progenitor cell-enriched populations. *Cell* 65: 1143-1152, 1991.
- Brasel K, De Smedt T, Smith JL and Maliszewski CR: Generation of murine dendritic cells from flt3-ligand-supplemented bone marrow cultures. *Blood* 96: 3029-3039, 2000.
- Gilliet M, Boonstra A, Paturel C, *et al*: The development of murine plasmacytoid dendritic cell precursors is differentially regulated by FLT3 ligand and granulocyte/macrophage colony-stimulating factor. *J Exp Med* 195: 953-958, 2002.
- Gabbianelli M, Pelosi E, Motesoro E, *et al*: Multi-level effects of flt3 ligand on human hematopoiesis: expansion of putative stem cells and proliferation of granulomonocytic progenitors/monocytic precursors. *Blood* 86: 1661-1670, 1995.
- Rusten LS, Lyman SD, Veiby OP and Jacobsen SEW: The FLT3 ligand is a direct and potent stimulator of the growth of primitive and committed human CD34⁺ bone marrow progenitor cells *in vitro*. *Blood* 87: 5016-5026, 1996.
- Ohmizono Y, Sakabe H, Kimura T, *et al*: Thrombopoietin augments *ex vivo* expansion of human cord blood-derived hematopoietic progenitors in combination with stem cell factor and flt3 ligand. *Leukemia* 11: 524-530, 1997.
- Sonoda Y, Kimura T, Sakabe H, *et al*: Human flt3 ligand acts on myeloid as well as multipotential progenitors derived from purified CD34⁺ blood progenitors expressing different levels of c-kit protein. *Eur J Haematol* 58: 257-264, 1997.
- Sakabe H, Kimura T, Zeng ZZ, *et al*: Haematopoietic action of flt3 ligand on cord blood-derived CD34-positive cells expressing different levels of flt3 or c-kit tyrosine kinase receptor: comparison with stem cell factor. *Eur J Haematol* 60: 297-306, 1998.
- Bontkes HJ, De Gruijl TD, Schuurhuis GJ, Scheper RJ, Meijer CLM and Hooijberg E: Expansion of dendritic cell precursors from human CD34⁺ progenitor cells isolated from healthy donor blood; growth factor combination determines proliferation rate and functional outcome. *J Leukoc Biol* 72: 321-329, 2002.
- Arrighi JF, Hauser C, Chapuis B, Zubler RH and Kindler V: Long-term culture of human CD34⁺ progenitors with FLT3-ligand, thrombopoietin, and stem cell factor induces extensive amplification of a CD34⁺CD14⁻ and a CD34⁺CD14⁺ dendritic cell precursor. *Blood* 93: 2244-2252, 1999.
- Kimura T, Sakabe H, Tanimukai S, *et al*: Simultaneous activation of signals through gp130, c-kit, and interleukin-3 receptor promotes a trilineage blood cell production in the absence of terminally acting lineage-specific factors. *Blood* 90: 4767-4778, 1997.
- Kimura T, Wang J, Minamiguchi H, *et al*: Signal through gp130 activated by soluble interleukin (IL)-6 receptor (R) and IL-6 or IL-6R/IL-6 fusion protein enhances *ex vivo* expansion of human peripheral blood-derived hematopoietic progenitors. *Stem Cells* 18: 444-452, 2000.
- Fujiki H, Kimura T, Minamiguchi H, *et al*: Role of human interleukin-9 as a megakaryocyte potentiator in culture. *Exp Hematol* 30: 1373-1380, 2002.
- Kimura T, Minamiguchi H, Wang J, *et al*: Impaired stem cell function of CD34⁺ cells selected by two different immunomagnetic beads systems. *Leukemia* 18: 566-574, 2004.
- Wang J, Kimura T, Asada R, *et al*: SCID-repopulating cell activity of human cord blood-derived CD34⁺ cells assured by intra-bone marrow injection. *Blood* 101: 2924-2931, 2003.
- Young JW, Szabolcs P and Moore MA: Identification of dendritic cell colony-forming units among normal human CD34⁺ bone marrow progenitors that are expanded by c-kit-ligand and yield pure dendritic cell colonies in the presence of granulocyte/macrophage colony-stimulating factor and tumor necrosis factor α . *J Exp Med* 182: 1111-1119, 1995.
- Lyman SD and Jacobsen SEW: c-kit ligand and Flt3 ligand: stem/progenitor cell factors with overlapping yet distinct activities. *Blood* 91: 1101-1134, 1998.
- Banchereau J and Palucka AK: Dendritic cells as therapeutic vaccines against cancer. *Nat Rev Immunol* 5: 296-306, 2005.
- Herrmann F, Brugger W, Kanz L and Mertelsmann R: *In vivo* biology and therapeutic potential of hematopoietic growth factors and circulating progenitor cells. *Semin Oncol* 19: 422-431, 1992.

35. Reinhard G, Marten A, Kiske SM, Feil F, Bieber T and Schmidt-Wolf IG: Generation of dendritic cell-based vaccines for cancer therapy. *Br J Cancer* 86: 1529-1533, 2002.
36. Sloan EM, Kim S, Maciejewski JP, *et al*: Pharmacologic doses of granulocyte colony-stimulating factor affect cytokine production by lymphocytes *in vitro* and *in vivo*. *Blood* 95: 2269-2274, 2000.
37. Sivakumaran M, Vasconcelos ZF, Diamond HR, *et al*: Modulation of Th1/Th2 subsets by granulocyte-colony stimulating factor. *Blood* 97: 333-335, 2001.
38. Vasconcelos ZF, Diamond HR, Tabak DG, Barcinski MA and Bonomo A: Th1/Th2 lymphokine profile of T cells present in the blood of granulocyte-colony stimulating factor-treated stem-cell donors: up or down modulation. *Blood* 95: 333-335, 2001.
39. Arpinati M, Green CL, Heimfeld S, Heuser JE and Anasetti C: Granulocyte-colony stimulating factor mobilizes T helper 2-inducing dendritic cells. *Blood* 95: 2484-2490, 2000.
40. Ueda Y, Itoh T, Fuji N, *et al*: Successful induction of clinically competent dendritic cells from granulocyte colony-stimulating factor-mobilized monocytes for cancer vaccine therapy. *Cancer Immunol Immunother* 8 (e-pub ahead of print), 2006.
41. Szabolcs P, Avigan D, Gezelter S, *et al*: Dendritic cells and macrophages can mature independently from a human bone marrow-derived, post-CFU intermediate. *Blood* 87: 4520-4530, 1996.
42. Ueda Y, Itoh T, Nukaya I, *et al*: Dendritic cell-based immunotherapy of cancer with carcinoembryonic antigen-derived, HLA-A24-restricted CTL epitope: clinical outcomes of 18 cases with metastatic gastrointestinal or lung adenocarcinomas. *Int J Oncol* 24: 909-918, 2004.
43. Young JW: Dendritic cells: expansion and differentiation with hematopoietic growth factors. *Curr Opin Hematol* 6: 135-144, 1999.
44. Romani N, Gruner S, Brang D, *et al*: Proliferating dendritic cell progenitors in human blood. *J Exp Med* 180: 83-93, 1994.
45. Caux C, Vanbervliet B, Massacrier C, *et al*: CD34⁺ hematopoietic progenitors from human cord blood differentiate along two independent dendritic cell pathways in response to GM-CSF+TNF α . *J Exp Med* 184: 695-706, 1996.
46. Lyman SD: Biologic effects and potential clinical application of FLT-3 ligand. *Curr Opin Hematol* 5: 192-196, 1998.
47. Szabolcs P, Moore MAS and Young JW: Expansion of immunostimulatory dendritic cells among the myeloid progeny of human CD34⁺ bone marrow precursors cultured with c-kit ligand, granulocyte-macrophage colony-stimulating factor, and tumor necrosis factor- α . *J Immunol* 154: 5851-5861, 1995.
48. Morse MA, Nair S, Fernandez-Casal M, *et al*: Preoperative mobilization of circulating dendritic cells by Flt3 ligand administration to patients with metastatic colon cancer. *J Clin Oncol* 18: 3383-3393, 2000.

Review

Immunophenotype and functional characteristics of human primitive CD34-negative hematopoietic stem cells: The significance of the intra-bone marrow injection

Yoshiaki Sonoda*

Department of Stem Cell Biology and Regenerative Medicine, Graduate School of Medical Science,
Kansai Medical University, Fumizoncho, Moriguchi, Osaka 570-8506, Japan

Abstract

The biology of hematopoietic stem cell (HSC) is a current topic of interest which has important implications for clinical HSC transplantation as well as for the basic research of HSC. The most primitive HSCs in mammals, including mice and humans, have long been believed to be CD34 antigen (Ag)-positive (CD34⁺) cells. In fact, bone marrow (BM), peripheral blood (PB), and cord blood (CB) stem cell transplantation studies indicate that a CD34⁺ subpopulation in the BM, PB, or CB can provide durable long-term donor-derived lymphohematopoietic reconstitution. Therefore, CD34 Ag was used to identify/purify immature HSCs. However, Osawa et al. reported that murine long-term lymphohematopoietic reconstituting HSCs are lineage marker-negative (Lin⁻) c-kit⁺Sca-1⁺CD34-low/negative (CD34^{low/-}), which are called CD34^{low/-} KSL cells. Recently, human CB-derived CD34⁻ HSCs, a counterpart of murine CD34^{low/-} KSL cells, were successfully identified using an intra-bone marrow injection (IBMI) method. This review will update the concept of the immunophenotype and the functional characteristics of human primitive CD34⁻ HSCs. In addition, the significance of the application of the IBMI technique in clinical HSC transplantation is also discussed. Recent rapid advances in understanding the biological nature of HSCs may make it possible to fully characterize the most primitive class of human HSCs in the near future.

© 2007 Elsevier Ltd. All rights reserved.

Keywords: Hematopoietic stem cell (HSC); CD34-negative; SCID-repopulating cell (SRC); Intra-bone marrow injection (IBMI); SDF-1/CXCR4 axis

1. Introduction

Hematopoietic stem cells (HSCs) are well-characterized populations, which reside in bone marrow (BM), peripheral blood (PB), and cord blood (CB) cells. The definition of primitive long-term repopulating (LTR) HSCs is as follows: (1) a self-renewing ability, which can maintain the total pool of HSC at a constant level throughout life, and (2) a multiple differentiating capability, which can produce hematopoietic progenitor cells (HPCs) that differentiate into every type of mature blood cell in a well-defined hierarchy [1–3].

Fig. 1 shows that the most primitive human HSCs are detected as severe combined immunodeficiency (SCID)-repopulating cells

(SRCs) using nonobese diabetic (NOD)/Shi-scid/scid (NOD/SCID) mice or NOD/Shi-scid, IL-2 receptor common γ chain null (NOG) mice [4]. These SRCs have been assumed to represent the most primitive human HSCs responsible for the long-term maintenance of hematopoiesis [5–7]. On the other hand, committed HPCs, including colony-forming unit-granulocyte/erythroid/macrophage/megakaryocyte (CFU-GEMM), colony-forming unit-granulocyte/macrophages (CFU-GM), erythroid burst-forming units (BFU-E), and colony-forming unit-megakaryocytes (CFU-Meg), are assayed using clonal methylcellulose cultures [1–3]. HPCs located on the intermediate stage of human HSC development, such as long-term culture-initiating cells (LTC-ICs), are assayed using co-cultures with murine stromal cell (HESS-5) [1,8,9].

These HSCs/HPCs are characterized by their surface expression of various kinds of antigens, including CD34, adhesion

* Tel.: +81 6 6993 9435; fax: +81 6 6992 3522.

E-mail address: sonoda@takii.kmu.ac.jp

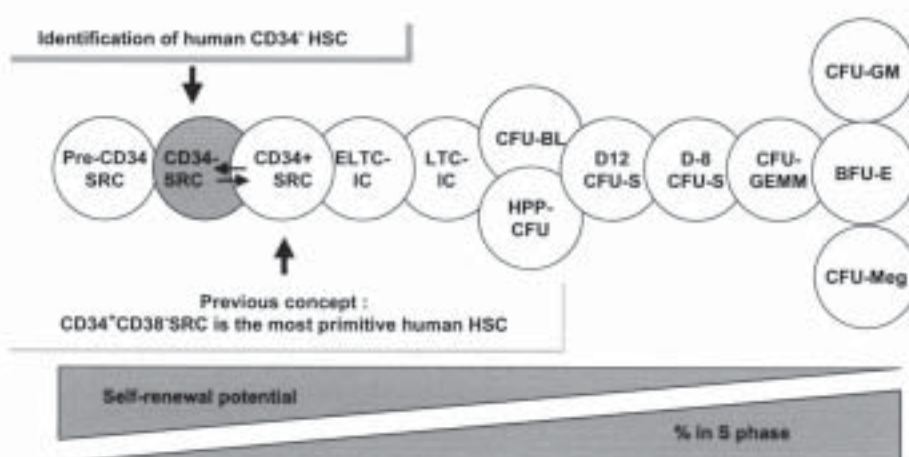


Fig. 1. Hierarchical organization of human/mouse HSCs/HPCs compartment as identified by currently available bioassays. The compartments are shown in relationship to self-renewal potential and cell-cycle status in steady-state hematopoiesis.

molecules/chemokine receptors, CXCR4, cytokine receptors, and receptor type tyrosine kinases, c-kit and flt3 [1–3] (Fig. 2). Among these markers, the cell surface glycoprotein CD34 antigen has been believed to be a particularly reliable marker for murine as well as human HSCs/HPCs [10].

Until now, a number of studies have revealed the SRC activity to be detected in CD34-positive (CD34⁺) cell fractions derived from BM, CB, and PB [5–7,10,11]. Hogan et al. clearly demonstrated that CB-derived SRCs present in the CD34⁺ cell fraction could be segregated into subpopulations with distinct repopulation characteristics [7]. The CD34⁺CD38⁺ SRCs could repopulate recipient NOD/SCID mice rapidly, but they could only maintain a human cell repopulation for 12 weeks, while demonstrating no secondary repopulating potential. In contrast, the more primitive CD34⁺CD38⁻ SRCs could repopulate recipients more gradually, and maintain human hematopoiesis for at least 20 weeks. Importantly, they had a secondary repopulating potential throughout the engraftment period [7]. The long-term repopulating potential (up to 24 weeks after transplantation) of these

CD34⁺CD38⁻ SRCs was confirmed [52]. These findings clearly demonstrated that human CD34⁺ SRCs are a heterogeneous population, which contain short-term repopulating (STR) and LTR-HSCs/HPCs. In other words, these STR- and LTR-HSCs/HPCs can be evaluated in the SRC assay system. According to these reported data, the immunophenotype of the most primitive human HSC seems to be lineage-negative (Lin⁻) CD34⁺CD38⁻ (Fig. 1). A limiting dilution analysis clearly demonstrated that the frequency of SRCs in CB-derived CD34^{high} cells was 1/1010 cells using the intra-bone marrow injection (IBMI) technique (precisely described later), as previously reported [13,14]. Moreover, the frequencies of SRCs in CB-derived Lin⁻CD34⁺CD38⁺ and Lin⁻CD34⁺CD38⁻ cells were 1/6000 and 1/40 cells using the IBMI, respectively (Kimura and Sonoda, unpublished data).

Based on these data, the usefulness/significance of CD34 antigen as a reliable positive marker for human HSCs has thus been established. However, the functional significance of CD34 antigen in early human hematopoiesis has not yet been fully elucidated.

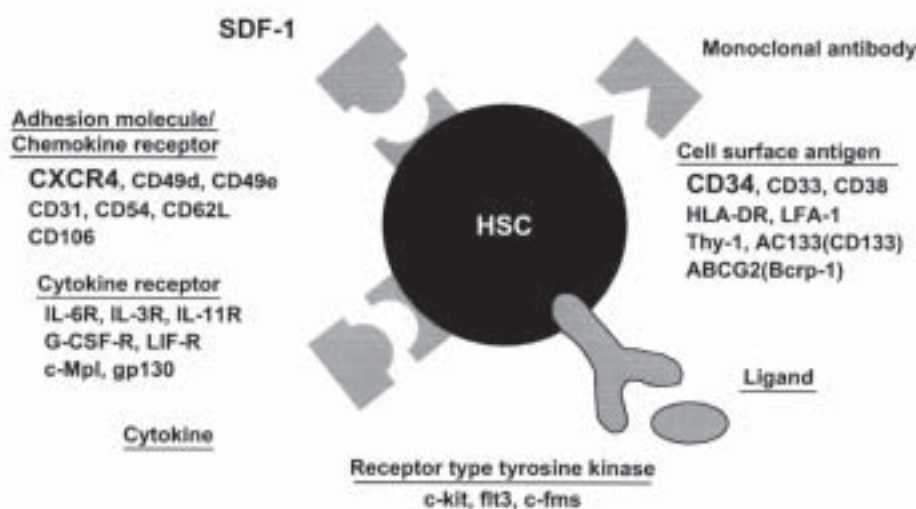


Fig. 2. Illustration of cell surface expressions of various markers on human HSCs/HPCs, including antigens, adhesion molecules/chemokines, cytokine receptors, and receptor type tyrosine kinases.

2. Identification of murine CD34-negative hematopoietic stem cells

The CD34 antigen is a positive marker of human HSCs, and all colony-forming cell (CFC) activity of human BM, PB, and CB cells is detected in the CD34⁺ cell fraction [1–3,10]. Indeed, positively selected CD34⁺ cells have been used for clinical hematopoietic stem cell transplantation (HSCT) in an autologous as well as allogeneic setting [15]. In these cases, the engraftment of BM by donor-derived cells has been successfully achieved, thus demonstrating the presence of HSCs with a long-term repopulating ability within the CD34⁺ cells [5–7,11–14].

Unlike human HSCs, Nakauchi and his colleagues reported that primitive adult mouse BM-derived HSCs are detected in the mouse CD34 low to negative cell fraction [16]. First, they developed a monoclonal antibody (Ab) to the mouse homologue of CD34. Using this monoclonal Ab, they purified BM-derived c-kit⁺ Sca-1⁺Lin⁻ (KSL) cells into CD34⁺, CD34^{low}, and CD34⁻ cell fractions. An *in vivo* analysis of the HSC activity in these three subpopulations clearly demonstrated that the CD34^{low/-} populations support long-term lymphomyeloid reconstitution. In contrast, CD34⁺ cells support only short-term reconstitution. Surprisingly, the injection of a single CD34^{low/-} KSL cell results in long-term lymphomyeloid reconstitution in 21% (9/41) of the recipient mice. Because the marrow seeding efficiency of murine repopulating stem cells was reported to be approximately 20% [17], these CD34^{low/-} KSL cells seem to be an almost purified HSC population. Until now, the self-renewal and multilineage differentiation potential of individual HSCs was extensively investigated using this purified HSC population [18].

From another point of view, Goodell et al. demonstrated that a unique class of HSCs (side population (SP) cells) expressing either low or undetectable levels of CD34 Ag exists in multiple species, including mice, rhesus monkeys, and humans, using the fluorescent DNA-binding dye, Hoechst 33342 [19]. They speculated that human SP cells have a long-term repopulating ability just as murine SP cells do. Collectively, these studies imply the existence of a hitherto unidentified population of primitive human HSCs that lack the expression of CD34 Ag.

3. Development of highly sensitive SRC assay system using the intra-bone marrow injection (IBMI) technique

The measurement of the repopulation and differentiation capabilities of primitive human HSCs has been greatly facilitated by the development of the xenotransplantation assay (SRC assay) system developed by Dick and his colleagues [5,6,11,12]. Originally, they injected cells through the tail vein. When candidate human HSCs are transplanted by tail vein injection (TVI), the cells circulate in the blood vessel into the right atrium, ventricle, and lungs in which most of the cells (over 95%) are trapped, then a small part of the cells can circulate into the systemic circulation. Finally, a small fraction of the injected cells can lodge in the BM niche. In fact, van Hennik et al. demonstrated that the seeding efficiencies of

human CB CD34⁺ cells in NOD/SCID mice are 4.4% by week 6 cobblestone area-forming cell (CAFC) assay [20]. Therefore, this SRC assay using TVI possibly underestimates the frequencies of SRCs in target cell populations.

Previously, a novel technique for obtaining BM cells by aspiration from the femur of living mice was reported [21]. Thereafter, Ikehara and his colleagues developed an intra-bone marrow injection technique for the treatment of intractable autoimmune diseases in MRL/lpr mice [22]. This intra-bone marrow injection technique was applied for the development of a highly sensitive SRC assay system [13,14]. Using the IBMI technique, the frequency of SRCs in CB-derived Lin⁻CD34⁺CD38⁻ cells was 1/40 cells (Sonoda and Kimura, unpublished data). When these cells were injected by TVI, the SRC frequency decreased to approximately 1/600 cells. These results demonstrated that the IBMI technique is associated with a seeding efficiency 15 times greater than the TVI. Therefore, this SRC assay system using the IBMI technique is very useful for investigating the HSC activity of certain target populations.

4. Identification of human CD34-negative hematopoietic stem cells using IBMI

A number of studies concerning human CD34⁻ primitive HSCs have suggested that the CD34^{low/-} cell population contains long-term lymphohematopoietic repopulating HSCs [19,23–25].

One of the assay systems that can measure the repopulation and differentiation capacities of human HSCs is the SRC assay [5–7,11,12]. Using this system, Bhatia et al. first reported that SRCs are present in human BM- and CB-derived Lin⁻CD34⁻ cells [23]. Their multilineage reconstituting analyses of CD34⁻ SRCs demonstrated that the vast majority of CD45⁺ human cells in murine BMs are CD19⁺ B cells. Also, limiting dilution analysis indicated that there is one SRC in 125,000 Lin⁻CD34⁻ cells. On the other hand, the frequency of CD34⁻ SRCs increases to 1 in 38,000 cells after 4 days of short-term culture of these Lin⁻CD34⁻ cells in the presence of a cocktail of cytokines or human umbilical vein endothelial cell-conditioned medium. These findings suggested that unidentified cells, termed 'pre-SRCs' present in the CD34⁻ cell population, might acquire some homing molecules necessary for redistribution to NOD/SCID mouse BM after TVI [23].

The existence of long-term repopulating CD34⁻ HSCs in human BM-derived Lin⁻ cells is also supported by the other reported data, in which the CD34⁻ fraction of normal human BM contains cells capable of engraftment and differentiation into CD34⁺ progenitors as well as multiple lymphohematopoietic lineages using the human/sheep competitive engraft model [24]. However, precise analysis of human CD34⁻ HSCs has been hindered by the lack of (1) a positive marker, comparable to the Sca-1 in mice, and (2) a simple and reliable assay system of these rare cells. Further attempts to characterize the CD34⁻ SRCs present in the human CB revealed the unidentified 'pre-SRCs' using the highly sensitive SRC assay system developed by us [13,14].

First, the lineage-negative (Lin^-) cells were separated from CB-derived mononuclear cells using an immunomagnetic beads system. These cells were further labeled with a mixture of 13 monoclonal antibodies (mAbs) and then were subdivided into three distinct populations based on their surface CD34 Ag expression (Fig. 3A). These three fractions were sorted and transplanted to NOD/SCID mice using TVI as reported [13]. All 13 mice transplanted with $\text{Lin}^- \text{CD34}^{\text{high}}$ cells were engrafted with human cells. The level of human CD45⁺ cells in murine BMs was 3.0–70.8% (median, 26.2%) (Fig. 3B (a), left column). In contrast, neither nine mice transplanted with $\text{Lin}^- \text{CD34}^{\text{low}}$ cells nor the 10 mice transplanted with $\text{Lin}^- \text{CD34}^-$ cells were engrafted with human cells (Fig. 3B (b, c), left columns).

Phenotypic and functional characterization of these three fractions were further determined by the co-culture of these cells with the HESS-5 [9], and in the presence of stem cell factor (SCF), flt3 ligand (FL), thrombopoietin (TPO), interleukin (IL)-3, IL-6, and granulocyte colony-stimulating factor (G-CSF). After the 7-day-co-culture of $\text{Lin}^- \text{CD34}^{\text{high}}$ cells with HESS-5, 30% of them were still CD34⁺ cells. In the case of the $\text{Lin}^- \text{CD34}^-$ cells, 18% of them turned out to be CD34⁺. On the other hand, the flow cytometric pattern for $\text{Lin}^- \text{CD34}^{\text{low}}$ cells was very different from the other two patterns. Only 1.6% of this population was CD34⁺ after the co-culture. These three fractions of cells recovered from the co-cultures were then transplanted into five NOD/SCID mice each using TVI. Very interestingly, cultured $\text{Lin}^- \text{CD34}^-$ cells repopulated all five recipient mice. These results clearly indicate that the cultured $\text{Lin}^- \text{CD34}^-$ cell fraction contains the SRCs, which could not home into the BM niche by TVI before the co-culture. However, none of the five mice transplanted with cultured $\text{Lin}^- \text{CD34}^{\text{low}}$ cells were repopulated [13].

Lapidot and his colleagues clearly demonstrated that chemokine stromal cell-derived factor (SDF)-1 and its receptor CXCR4 play a pivotal role in the homing and repopulation

of CD34⁺ SRC in NOD/SCID mice [26,27]. It was recently reported that CXCR4, VLA-4, and VLA-5 play important roles in the homing of CD34⁺ SRCs by TVI as well as IBMI [28]. Moreover, the homing of HSCs to the BM can be considered as a multistep process, in which various adhesion molecules present both on HSCs and BM endothelial cells are involved [28–30]. Accordingly, the expression patterns of CXCR4 and other adhesion molecules on the surfaces of CB-derived $\text{Lin}^- \text{CD34}^{\text{high}}$, $\text{Lin}^- \text{CD34}^{\text{low}}$, or $\text{Lin}^- \text{CD34}^-$ cells were analyzed by flow cytometry. Significant numbers of CB-derived $\text{Lin}^- \text{CD34}^{\text{high}}$ cells express CXCR4, CD31, CD49d, CD54, CD62L, and CD106. However, $\text{Lin}^- \text{CD34}^-$ cells express lower levels of CXCR4, CD62L, and CD106 [13]. This suggests that very primitive repopulating HSCs which lack the CD34 Ag expression may not home into the BM niche by TVI, since $\text{Lin}^- \text{CD34}^-$ cells express low levels of these homing receptors. Therefore, the IBMI technique [13,14] was used to determine the SRC activity of these three fractions of cells (Fig. 3).

When $\text{Lin}^- \text{CD34}^{\text{high}}$ cells were transplanted using IBMI, all mice were repopulated and the level of human cell engraftment was 12.8–80.0% (median, 64.8%) (Fig. 3B (a), right column). Very interestingly, this repopulating rate was significantly higher than that by conventional TVI ($P < 0.02$). Next, $\text{Lin}^- \text{CD34}^-$ cells were transplanted using IBMI. Surprisingly, all seven mice were repopulated and the level of human cell engraftment was 10.0–52.6% (median, 19.3%) (Fig. 3B (c), right column). On the other hand, none of the seven mice transplanted with $\text{Lin}^- \text{CD34}^{\text{low}}$ cells using IBMI were repopulated with human cells (Fig. 3B (b), right column). These results clearly indicate that the CB-derived $\text{Lin}^- \text{CD34}^-$ cell population contains SRCs detected only by IBMI. A limiting dilution analysis demonstrated the frequencies of SRCs in CB-derived $\text{Lin}^- \text{CD34}^{\text{high}}$ and $\text{Lin}^- \text{CD34}^-$ cells to be 1/1010 and 1/24,100, respectively [13,14].

CD34⁺ SRCs cannot home into the BM niche when transplanted by TVI. This is partly explained by their lower

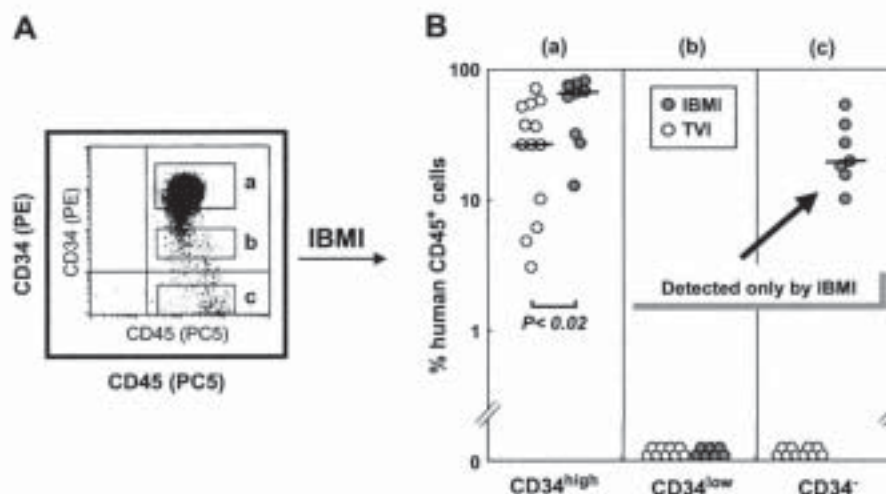


Fig. 3. Characterization of purified CB-derived $\text{Lin}^- \text{CD34}^{\text{high/low/-}}$ cells and their SRC activities. (A) The FACS profile of immunomagnetically separated lineage-negative cells, demonstrating $\text{CD34}^{\text{high}}$ (a), CD34^{low} (b), and CD34^- (c) cells. (B) Human CD45⁺ cell engraftment of NOD/SCID mice, receiving a transplant of 5×10^4 $\text{Lin}^- \text{CD34}^{\text{high}}$ (a), $\text{Lin}^- \text{CD34}^{\text{low}}$ (b), and $\text{Lin}^- \text{CD34}^-$ (c) cells. Open and closed circles represent the repopulation rates in total murine BMs by conventional TVI (left column) and by IBMI (right column), respectively.

expression levels of homing receptors, including CXCR4. A transwell migration assay toward a gradient of SDF-1 clearly indicated that CD34⁻ SRCs have poor SDF-1/CXCR4-mediated migration and homing abilities [13]. An analysis of the *in vivo* migration ability of HSCs demonstrated that a significant proportion of CD34⁻ SRCs as well as CD34⁺ SRCs are redistributed from the injected left tibia to the other bones, and proliferate at the migrated sites, where both SRCs generate significant numbers of CD34⁺ progenies [13,14]. However, it remains unknown whether the CD34⁻ SRCs migrate to the other bones with either the CD34⁻ immunophenotype or after their conversion to the CD34⁺ state. Furthermore, the molecular mechanisms involved in this migratory (redistribution and homing) process are yet to be clarified.

Secondary transplantation studies of sorted CD45⁺CD34⁺ and CD45⁺CD34⁻ cells obtained from primary recipient mice transplanted either with CD34⁻ SRCs or CD34⁺ SRCs demonstrated that only CD34⁺ cells can repopulate secondary recipient mice. These results indicate that CD34⁻ SRCs generate CD34⁺ SRCs *in vivo*, and these findings are consistent with reported data that human CB-derived Lin⁻CD34⁻ cells generate a large number of CD34⁺ stem cells in an *ex vivo* culture system using HESS-5 and various human cytokines [13,25]. More importantly, the secondary transplantation studies demonstrate for the first time that CB-derived CD34⁻ SRCs have a long-term (for up to 28 weeks) human cell repopulating capacity in NOD/SCID mice [13].

In contrast to murine BM-derived HSCs [31], human CB-derived CD34⁺ SRCs do not convert to CD34⁻ SRCs for at least 16 weeks after transplantation [13]. However, a longer period of observation (over 1 year) will be required to elucidate the possibility of reversion of CD34 antigen expressed on human CB-derived CD34⁺ HSCs, as demonstrated by Zanjani et al. using human BM-derived HSCs [32]. In addition, it remains unclear whether the CD34⁻ cell population obtained from primary mice transplanted with Lin⁻CD34⁻ cells still contains CD34⁻ HSCs, which indicates the self-renewal of CD34⁻ HSCs in NOD/SCID mice. There is a possibility that the self-renewing CD34⁻ HSCs cannot home into the BM niche in secondary recipients, even by IBMI. Further studies will be required to clarify this important issue.

5. Identification of non-migrating CD34-positive and CD34-negative HSCs toward SDF-1/CXCR4 axis and their clinical implications

To assess the migration ability toward a gradient of SDF-1 of CD34⁻ SRCs as well as CD34⁺ SRCs *in vitro*, a transwell migration assay was used [13]. As expected, migrating Lin⁻CD34^{high} cells repopulated all five NOD/SCID mice both by TVI and by IBMI. Interestingly, non-migrating Lin⁻CD34^{high} cells also showed a distinct SRC activity only by IBMI [13]. These results suggest that the CB-derived Lin⁻CD34^{high} cell population contains at least two types of SRCs. The identified non-migrating CD34⁺ SRCs may represent the CD34⁺CXCR4⁻ SRCs, recently reported by Kollet et al. [27]. These unique SRCs express intracellular CXCR4,

which can be functionally expressed on the cell membrane to mediate SDF-1-induced homing and repopulation. In the case of Lin⁻CD34⁻ cells, the migrating cells did not show any SRC activity by IBMI. Surprisingly, non-migrating Lin⁻CD34⁻ cells did repopulate all three mice by IBMI. These results demonstrate that IBMI is much more sensitive than TVI for detecting both CD34⁻ and CD34⁺ SRCs, which have a poor SDF-1/CXCR4-mediated migration ability [13].

The identification of these non-migrating CD34⁺ SRCs has an important clinical significance, because these non-migrating CD34⁺ SRCs can efficiently home into the BM niche only by IBMI, as did CD34⁻ SRCs. It therefore seems to be imperative that these CD34⁻ SRCs should be transplanted with migrating and non-migrating CD34⁺ SRCs in clinical HSCT using the IBMI technique.

6. Reversible expression of CD34 by murine and human long-term repopulating hematopoietic stem cells: Are they CD34-positive or CD34-negative?

Primitive long-term lymphomyeloid reconstituting HSCs in mice lack CD34 expression [16]. However, Ogawa and his colleagues performed a series of experiments and demonstrated that the expression of surface CD34 antigen on murine primitive HSCs is under the influence of developmental stages and the kinetic state of the HSCs [31,33,34]. Sato et al. reported that the majority of long-term reconstituting BM cells in adult mice are CD34⁻ [31]. Interestingly, after *in vivo* 5-fluorouracil (FU) treatment, high-level engraftment is obtained from both CD34⁺ and CD34⁻ HSCs 5 months post-transplantation, thus suggesting a phenotypic change due to the activation of HSCs by 5-FU. In addition, *in vitro* cultures of CD34⁻ HSCs in the presence of early-acting cytokines [53], such as IL-11 and SCF, have been observed to produce CD34⁺ cells. These CD34⁺ cells generate long-term and multilineage engraftment in lethally irradiated mice after the transplantation. This phenotypic change may indicate that CD34⁻ HSCs can develop into CD34⁺ HSCs after *in vitro* culture. They also showed that mobilized adult mice PB-derived HSCs using G-CSF express CD34 [34]. These results suggest that the CD34 expression on murine primitive HSCs reflects their activation state caused by 5-FU or *in vitro* cytokine exposure. Moreover, the CD34 expression on murine HSCs has been reported to change developmentally [33]. Namely, BM-derived long-term repopulating HSCs in fetal, newborn, and young mice are CD34⁺, whereas CD34⁻ HSCs emerge in 7- to 10-week old mice and increase thereafter. All these findings give rise to the concept that the expression of CD34 by murine HSCs is reversible, and also provide the possibility that the surface phenotype of murine HSCs may be reversible.

On the other hand, human BM-derived CD34⁺ HSCs have been reported to convert to CD34⁻ HSCs *in vivo* [32,35]. Both of these studies demonstrated that the conversion of CD34 expression occurs at least 8–15 months after the transplantation of purified Lin⁻CD34⁺ or CD34⁺CD38⁻ cells in preimmune fetal sheep or homozygous bg.bg/nu.nu/xid.xid (bnx) mice. These studies indicate the possibility that the

human BM-derived CD34⁺ cell population can act as a reservoir for the generation of CD34⁻ cells. Conversely, the human BM-derived CD34⁻ cell population generates CD34⁺ repopulating cells *in vivo*, thus indicating that the expression of CD34 antigen can be reversible on human BM-derived HSCs [32,35]. As we reported previously [13], human CB-derived CD34⁻ SRCs generated CD34⁺ SRCs *in vitro* as well as *in vivo*. In contrast to BM-derived HSCs [32,35], human CB-derived CD34⁺ SRCs do not convert to CD34⁻ SRCs for at least 16 weeks after transplantation. However, it remains to be determined whether human CB-derived CD34⁺ SRCs can convert to CD34⁻ SRCs. Therefore, much longer observation periods (more than 1 year) will thus be needed, as suggested in previous reports [32,35].

7. Immunophenotype and functional characteristics of human primitive hematopoietic stem cells: A heterogeneous population

Recently, Guenechea et al. clearly demonstrated that the human cell repopulation in NOD/SCID mice transplanted with Lin⁻ CB cells is generally oligoclonal with extensive variability in the life span and proliferative capacity of individual SRCs [6]. An analysis of unique retroviral integration sites of the SRCs revealed the existence of different clones of SRCs with variable self-renewal potential and short- and long-term repopulating capacity [6]. Therefore, it is important to clarify the functional heterogeneity of CD34⁺ and CD34⁻ SRCs in order to elucidate the hierarchy of human HSCs.

As described in the introduction, the immunophenotype of the most primitive human HSCs has been believed to be Lin⁻ CD34⁺CD38⁻ (Fig. 1). However, functional studies, including analyses of multilineage reconstituting ability, the kinetics of engraftment, the productivity of CD34⁺ progenies, proliferative and migratory potentials, and secondary repopulating ability revealed that CB-derived CD34⁻ SRCs have different HSC characteristics from CD34⁺ SRCs [13,14]. Based on these data, the identified CB-derived CD34⁻ SRCs may therefore be a novel class of primitive repopulating HSCs that can be detected only by the sensitive IBMI technique [13,14].

It is well-documented that the tyrosine kinase receptors, c-kit and flt3, are expressed and function in early mouse and human hematopoiesis [36,37]. Moreover, their respective ligands, SCF and FL, synergistically act with each other, while also playing an important role in the regulation (generation, maintenance, proliferation, differentiation, and expansion) of early stages of murine and human candidate HSCs [1–3,36,37]. In a murine model, flt3⁻ KSL cells were recently reported to support long-term multilineage hematopoietic reconstitution [38]. In contrast, flt3⁺ KSL cells are progenitors for the common lymphoid stage [38]. These flt3⁺ KSL cells have also been shown to lack erythro-megakaryocytic potential [39]. This notion was supported by other reports which demonstrated that mice deficient in the expression of flt3 or FL show deficient lymphopoiesis.

In contrast to the murine candidate HSCs (CD34⁻ KSL cells) [16], the identified CD34⁻ SRCs do not express detectable levels of c-kit tyrosine kinase receptor by flow cytometry

[40]. However, to what degree flt3 is expressed on human HSCs, including CD34⁺ and CD34⁻ SRCs, which are capable of *in vivo* lymphomyeloid reconstitution, has not yet been fully elucidated.

A number of studies have reported that flt3 is expressed and functions in the human CD34⁺ hematopoietic progenitor cells, including LTC-ICs [37]. However, only two reports have demonstrated, using the conventional intra-venous injection method, that human CB- and BM-derived CD34⁺ HSCs capable of multilineage reconstitution in NOD/SCID mice express flt3 tyrosine kinase receptor [54,55].

Very recently, we reported the function of flt3 in the identified very primitive human CB-derived CD34⁻ SRCs [12,13,40] as well as more committed CD34⁺ SRCs using the sensitive IBMI method. These data clearly demonstrate that a portion of human CB-derived CD34⁺ SRCs express flt3, as reported previously [40]. However, only CD34⁺flt3⁻ cells showed a significant secondary repopulating ability, even when a comparable number of CD34⁺flt3⁻ cells as CD34⁺flt3⁺ cells were transplanted. Moreover, CD34⁻flt3⁻ cells showed a distinct and potent SRC activity by IBMI, while also showing a high and efficient secondary repopulating ability in comparison to CD34⁺flt3⁻ cells. The CD34⁻flt3⁻ cells also produce CD34⁺flt3⁻ and CD34⁺flt3⁺ SRCs after the co-culture with the HESS-5 [9], *in vitro*, thus suggesting that these CD34⁻flt3⁻ cells contain very primitive human CB-derived HSCs. These observations suggest that the immunophenotype of very primitive human LTR-HSCs is Lin⁻CD34⁻c-kit⁻flt3⁻ [40]. As illustrated in Fig. 4, primitive LTR-HSCs may express lower levels of c-kit and flt3 receptors on their surfaces when they commit to more mature STR-HSCs. It is still unclear, however, whether such a distinct pattern of c-kit and flt3 expression might identify distinct subpopulations of either LTR-HSC or STR-HSC within the human HSC hierarchy (Fig. 1). These results are consistent with recent studies regarding the significance of flt3 expression in murine primitive hematopoiesis [38,39], while also providing a new concept of hierarchy in the human primitive HSC compartment.

8. Concluding remarks and future directions

A sensitive SRC assay system using the IBMI technique was developed which was able to identify a new class of CB-derived CD34⁻ HSCs [12,13,40]. Based on our data, we proposed that the immunophenotype of the most primitive human LTR-HSCs is Lin⁻CD34⁻c-kit⁻flt3⁻. However, the frequency of CB-derived CD34⁻ SRCs is 1/24,100 [13,14], which is still very low in comparison to that of CD34⁺CD38⁻ SRCs (1/40 cells, Sonoda and Kimura, unpublished data). In order to more effectively enrich/purify human CD34⁻ LTR-HSCs, it is very important to identify reliable positive markers for human LTR-HSCs, such as Sca-1 for murine CD34⁻ KSL cells (Fig. 2).

The application of this sensitive SRC assay system using the IBMI technique may make it possible to discover other hitherto unidentified HSCs in various organs, including pre-CD34⁻ SRCs (Fig. 1), or to identify new markers for LTR-HSCs. It is also important to clarify whether the BM or mobilized PB

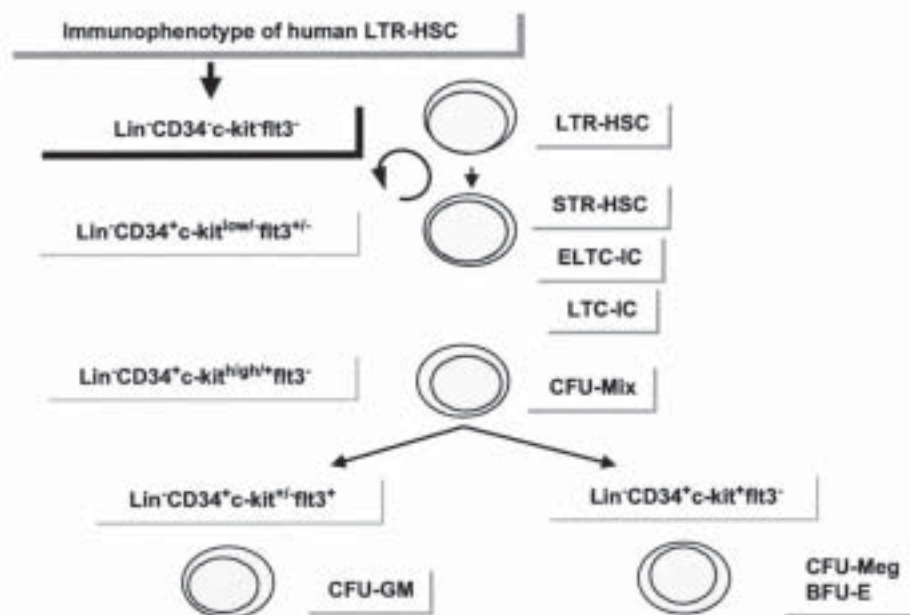


Fig. 4. Summarization of the immunophenotypes of human HSCs/HPCs. The figure illustrates expression patterns of solely CD34, c-kit, and flt3 on various classes of HSCs/HPCs detected by flow cytometry as described in the text. Because most HSCs/HPCs populations are still heterogeneous and hard to purify, it is not possible to exclude CD34, c-kit, and flt3 expression on a minority of cells in the different cell populations. Therefore, this figure indicates the c-kit and flt3 receptor expression status on the majority of cells within the CD34⁺ HSCs/HPCs populations based on our studies and other reported studies, concerning the expression of these receptors and/or the findings of functional studies.

contains an equivalent class of CD34⁻ SRCs. Moreover, IBMI provides a more efficient engraftment of CD34⁺ SRCs (Fig. 3B), which can thus contribute to the early phase of BM reconstitution. In addition, the identified non-migrating CD34⁺ SRCs can efficiently home into the BM niche only when transplanted by IBMI. It therefore seems to be imperative that these CD34⁻ SRCs should be transplanted with migrating and non-migrating CD34⁺ SRCs in clinical HSC transplantation using the IBMI technique. As described in this review, CD34⁻ HSCs are still heterogeneous populations; therefore, there is a possibility that these populations contain several subpopulations and their plasticity (trans-differentiation potential) also needs to be further investigated.

In clinical HSCT, the number of CBSCT has recently been rapidly increasing. However, they are difficult to transplant for an adult patient, due to the limited numbers of HSCs in a single CB sample. Therefore, successfully engrafting adults on a routine basis using the IBMI technique would greatly expand the clinical applicability of CBSCT. In the near future, the utilization of the IBMI technique is therefore expected to have a great impact on clinical HSCT. For additional reading on the use of bone marrow transplantation for autoimmunity, we refer the reader to the companion papers published in this special issue [41–51].

Acknowledgements

The author is grateful to Drs. Y. Sasaki, T. Kimura, J. Wang, S. Yokota, M. Hase, Y. Matsuoka, T. Kimura, and M. Murakami for their contributions. The author also thanks Kirin

Brewery Co. Ltd. (Tokyo, Japan) for providing the various growth factors. Ms. Sayoko Torigoe's valuable assistance in the preparation of the manuscript is also acknowledged.

This work was supported by Grants-in-Aid for Scientific Research on Priority Areas (Grant No. 15039227) and for Scientific Research C (Grant Nos. 15591015 and 19591144) from the Ministry of Education, Science and Culture of Japan, a grant from Haiteku Research Center of the Ministry of Education, a grant from the Science Frontier Program of the Ministry of Education, a grant from the 21st Century Center of Excellence (COE) Program of the Ministry of Education, a grant from the Promotion and Mutual Aid Corporation for Private Schools of Japan, a grant from Kansai Medical University (Research grant B), a grant from the Japan Leukemia Research Foundation, a grant from the Takeda Science Foundation, and a grant from the Mitsubishi Pharma Research Foundation.

References

- [1] Kondo M, Wagers AJ, Manz MG, Prohaska SS, Scherer DC, Beilhack GF, et al. Biology of hematopoietic stem cells and progenitors: implications for clinical application. *Annu Rev Immunol* 2003;21: 759–806.
- [2] Ogawa M. Differentiation and proliferation of hematopoietic stem cells. *Blood* 1993;81:2844–53.
- [3] Moore MAS. Clinical implications of positive and negative hematopoietic cell regulators. *Blood* 1991;78:1–19.
- [4] Ito M, Hiramatsu H, Kobayashi K, Suzue K, Kawabata M, Hiki K, et al. NOD/SCID^{γc} mouse: an excellent recipient mouse model for engraftment of human cells. *Blood* 2002;100:3175–82.
- [5] Larochelle A, Vormoor J, Hamenberg H, Wang JCY, Bhatia M, Lapidot T, et al. Identification of primitive human hematopoietic cells capable of

- repopulating NOD/SCID mouse bone marrow: implications for gene therapy. *Nat Med* 1996;2:1329–37.
- [6] Guenechea G, Gan OI, Dorrell C, Dick JE. Distinct classes of human stem cells that differ in proliferative and self-renewal potential. *Nat Immunol* 2001;2:75–82.
- [7] Hogan CJ, Stipall EJ, Keller G. Differential long-term and multilineage engraftment potential from subfractions of human CD34⁺ cord blood cells transplanted into NOD/SCID mice. *Proc Natl Acad Sci U S A* 2002;99:413–8.
- [8] Sakabe H, Yahata N, Kimura T, Zeng ZZ, Minamiguchi H, Kaneko H, et al. Human cord blood-derived primitive progenitors are enriched in CD34⁺c-kit⁺ cells: correlation between long-term culture-initiating cells and telomerase expression. *Leukemia* 1998;12:728–34.
- [9] Tsuji T, Ogasawara H, Aoki Y, Tsurumaki Y, Kodama H. Characterization of murine stromal cell clones established from bone marrow and spleen. *Leukemia* 1996;10:803–12.
- [10] Krause DS, Fackler MJ, Civin CI, May WS. CD34: structure, biology, and clinical utility. *Blood* 1996;87:1–13.
- [11] Bhatia M, Wang JCY, Kapp U, Bonnet D, Dick JE. Purification of primitive human hematopoietic cells capable of repopulating immune-deficient mice. *Proc Natl Acad Sci U S A* 1997;94:5320–5.
- [12] Wang JCY, Doedens M, Dick JE. Primitive human hematopoietic cells are enriched in cord blood compared with adult bone marrow or mobilized peripheral blood as measured by the quantitative in vivo SCID-repopulating cell assay. *Blood* 1997;89:3919–24.
- [13] Wang J, Kimura T, Asada R, Harada S, Yokota S, Kawamoto Y, et al. SCID-repopulating cell activity of human cord blood-derived CD34⁺ cells assured by intra-bone marrow injection. *Blood* 2003;101:2924–31.
- [14] Kimura T, Wang J, Matsui K, Inai S, Yokoyama S, Nishikawa S, et al. Proliferative and migratory potentials of human cord blood-derived CD34⁺ severe combined immunodeficiency repopulating cells that retain secondary reconstituting capacity. *Int J Hematol* 2004;79:328–33.
- [15] Civin C, Trischmann T, Kadan NS, Davis J, Noga S, Cohen K, et al. Highly purified CD34-positive cells reconstitute hematopoiesis. *J Clin Oncol* 1996;14:2224–33.
- [16] Osawa M, Hanada K, Hamada H, Nakauchi H. Long-term lymphohematopoietic reconstitution by a single CD34-low/negative hematopoietic cell. *Science* 1996;273:242–5.
- [17] van der Loo JC, Ploemacher RE. Marrow- and spleen-seeding efficiencies of all murine hematopoietic stem cell subsets are decreased by preincubation with hematopoietic growth factors. *Blood* 1995;85:2598–606.
- [18] Seita J, Ema H, Ooehara J, Yamazaki S, Tadokoro Y, Yamasaki A, et al. Lnk negatively regulates self-renewal of hematopoietic stem cells by modifying thrombopoietin-mediated signal transduction. *Proc Natl Acad Sci U S A* 2007;104:2349–54.
- [19] Goodell MA, Rosenzweig M, Kim H, Marks DF, Demaria M, Paradis G, et al. Dye efflux studies suggest that hematopoietic stem cells expressing low or undetectable levels of CD34 antigen exist in multiple species. *Nat Med* 1997;3:1337–45.
- [20] van Hennik PB, Koning AE, Ploemacher RE. Seeding efficiency of primitive human hematopoietic cells in nonobese diabetic/severe combined immunodeficiency mice: implications for stem cell frequency assessment. *Blood* 1999;94:3055–61.
- [21] Verlinden SEF, van Es HHG, van Bekkum DW. Serial bone marrow sampling for long-term follow up of human hematopoiesis in NOD/SCID mice. *Exp Hematol* 1998;26:627–30.
- [22] Kushida T, Inaba M, Hisha H, Ichioka N, Esumi T, Ogawa R, et al. Intra-bone marrow injection of allogeneic bone marrow cells: a powerful new strategy for treatment of intractable autoimmune diseases in MRL/lpr mice. *Blood* 2001;97:3292–9.
- [23] Bhatia M, Bonnet D, Murdoch B, Gan OI, Dick JE. A newly discovered class of human hematopoietic cells with SCID-repopulating activity. *Nat Med* 1998;4:1038–45.
- [24] Zanjani ED, Almeida-Porada G, Livingston AG, Flake AW, Ogawa M. Human bone marrow CD34⁺ cells engraft in vivo and undergo multilineage expression that includes giving rise to CD34⁺ cells. *Exp Hematol* 1998;26:353–60.
- [25] Nakamura Y, Ando K, Chargui J, Kawada H, Sato T, Tsuji T, et al. Ex vivo generation of CD34⁺ cells from CD34⁺ hematopoietic cells. *Blood* 1999;94:4053–9.
- [26] Peled A, Petit I, Kollet O, Magid M, Ponomarev T, Byk T, et al. Dependence of human stem cell engraftment and repopulation of NOD/SCID mice on CXCR4. *Science* 1999;283:845–8.
- [27] Kollet O, Petit I, Kahn J, Samira S, Dar A, Peled A, et al. Human CD34⁺CXCR4⁺ sorted cells harbor intracellular CXCR4, which can be functionally expressed and provide NOD/SCID repopulation. *Blood* 2002;100:2778–86.
- [28] Yahata T, Ando K, Sato T, Miyatake H, Nakamura Y, Muguruma Y, et al. A highly sensitive strategy for SCID-repopulating cell assay by direct injection of primitive human hematopoietic cells into NOD/SCID mice bone marrow. *Blood* 2003;101:2905–13.
- [29] Papayannopoulou T, Priestley GV, Nakamoto B. Anti-VLA4/VCAM-1-induced mobilization requires cooperative signaling through the kit/kit ligand pathway. *Blood* 1998;91:2231–9.
- [30] Peled A, Kollet O, Ponomarev T, Petit I, Franitza S, Grabovsky V, et al. The chemokine SDF-1 activates the integrins LFA-1, VLA-4, and VLA-5 on immature human CD34⁺ cells: role in transendothelial/stromal migration and engraftment of NOD/SCID mice. *Blood* 2000;95:3289–96.
- [31] Sato T, Laver JH, Ogawa M. Reversible expression of CD34 by murine hematopoietic stem cells. *Blood* 1999;94:2548–54.
- [32] Zanjani ED, Almeida-Porada G, Livingston AG, Zeng H, Ogawa M. Reversible expression of CD34 by adult human bone marrow long-term engrafting hematopoietic stem cells. *Exp Hematol* 2003;31:406–12.
- [33] Ito T, Tajima F, Ogawa M. Developmental changes of CD34 expression by murine hematopoietic stem cells. *Exp Hematol* 2000;28:1269–73.
- [34] Tajima F, Sato T, Laver JH, Ogawa M. CD34 expression by murine hematopoietic stem cells mobilized by granulocyte colony-stimulating factor. *Blood* 2000;96:1989–93.
- [35] Dao MA, Arevalo J, Nolte JA. Reversibility of CD34 expression on human hematopoietic stem cells that retain the capacity for secondary reconstitution. *Blood* 2003;101:112–8.
- [36] Sonoda Y, Sakabe H, Ohmisono Y, Tanimukai S, Yokota S, Nakagawa S, et al. Synergistic actions of stem cell factor and other burst-promoting activities on proliferation of CD34⁺ highly purified blood progenitors expressing HLA-DR or different levels of c-kit protein. *Blood* 1994;84:4099–106.
- [37] Lyman SD, Jacobsen SEW. c-kit ligand and flt3 ligand: stem/progenitor cell factors with overlapping yet distinct activities. *Blood* 1998;91:1101–34.
- [38] Adolfsson J, Borge OJ, Bryder D, Theilgaard-Monch K, Astrand-Grundstrom I, Sitnicka E, et al. Upregulation of flt3 expression within the bone marrow Lin[−]Sea-1⁺c-kit⁺ stem cell compartment is accompanied by loss of self-renewal capacity. *Immunity* 2001;15:659–69.
- [39] Adolfsson J, Mansson R, Buza-Vidas N, Hultquist A, Liuba K, Jensen CT, et al. Identification of flt3⁺ lympho-myeloid stem cells lacking erythro-megakaryocytic potential: a revised road map for adult blood lineage commitment. *Cell* 2005;121:295–306.
- [40] Kimura T, Asada R, Wang J, Kimura T, Morioka M, Matsui K, et al. Identification of long-term repopulating potential of human cord blood-derived CD34⁺ flt3[−] severe combined immunodeficiency-repopulating cells by intra-bone marrow injection. *Stem Cells* 2007;25:1348–55.
- [41] Abraham N, Li M, Vanella L, Peterson S, Ikehara S, Asprinio D. Bone marrow stem cell transplant into intra-bone cavity prevent type 2 diabetes: role of heme oxygenase-adiponectin. *J Autoimmun* 2008;30:128–35.
- [42] Boren EJ, Cheema GS, Naguwa SM, Ansari AA, Gershwin ME. The emergence of progressive multifocal leukoencephalopathy (PML) in rheumatic diseases. *J Autoimmun* 2007;30(1–2):90–8.
- [43] Burt R, Craig R, Cohen B, Suffit R, Barr W. Hematopoietic stem cell transplantation for autoimmune diseases: what have we learned? *J Autoimmun* 2008;30:116–20.
- [44] Deane S, Meyers F, Gershwin M. On reversing the persistence of memory: hematopoietic stem cell transplant for autoimmune disease in the first ten years. *J Autoimmun* 2008;30:180–96.

- [45] Gershwin ME. Bone marrow transplantation, refractory autoimmunity and the contributions of Susumu Ikehara. *J Autoimmun* 2008;30: 105–7.
- [46] Hara M, Murakami T, Kobayashi E. In vivo bioimaging using photogenic rats: fate of injected bone marrow-derived mesenchymal stromal cells. *J Autoimmun* 2008;30:163–71.
- [47] Ikehara S. Innovative BMT method for intractable diseases. *Immunol Res* 2007;38(1–3):251–60.
- [48] Marmont A. Will hematopoietic stem cell transplantation cure human autoimmune diseases? *J Autoimmun* 2008;30:145–50.
- [49] Ozawa K, Sato K, Oh I, Ozaki K, Uchibori R, Obara Y, et al. Cell and gene therapy using mesenchymal stem cells (MSCs). *J Autoimmun* 2008;30:121–7.
- [50] Ratajczak MZ, Zuba-Surma EK, Wysoczynski M, Wan W, Ratajczak J, Wojakowski W, et al. Hunt for pluripotent stem cell – regenerative medicine search for almighty cell. *J Autoimmun* 2008; 30:151–62.
- [51] Rezvani A, Storb R. Separation of graft-vs.-tumor effects from graft-vs.-host disease in allogeneic hematopoietic cell transplantation. *J Autoimmun* 2008;30:172–9.
- [52] Sonoda Y, Kimura T, Asada R, Kimura T, Morioka M, Sasaki Y, et al. Different proliferative potential and redistribution kinetics of human cord blood-derived CD34- SCID-repopulating cells (SRCs) in comparison with CD34+CD38+/- SRCs using intra-bone marrow injection. *Blood* 2006;108(11):470a.
- [53] Sonoda Y, Yang Y-C, Wong CG, Clark SC, Ogawa M. Analysis in serum-free culture of the targets of recombinant human hematopoietic growth factors: Interleukin 3 and granulocyte/macrophage-colony-stimulating factor are specific for early developmental stages. *Proc Natl Acad Sci USA* 1988;85:4360–4.
- [54] Sitnicka E, Buza-Vidas N, Larsson S, Nygren JM, Liuba K, Jacobsen SEW. Human CD34+ hematopoietic stem cells capable of multilineage engrafting NOD/SCID mice express flt3: distinct flt3 and c-kit expression and response patterns on mouse and candidate human hematopoietic stem cells. *Blood* 2003;102:881–6.
- [55] Ebihara Y, Wada M, Ueda T, X-u M-J, Manabe A, Tanaka R, et al. Reconstitution of human haematopoiesis in non-obese diabetic/severe combined immunodeficient mice by clonal cells expanded from single CD34+CD38- cells expressing flk2/flt3. *Br J Haematol* 2002;119: 525–34.

2 基礎編

幹細胞と再生医学*

藪田 精昭**

Key Words : regenerative medicine, stem cell, plasticity

はじめに

最近、臨床の広い分野において再生医学・再生医療が注目されている。その背景には、従来知られていた造血幹細胞だけでなく、表皮細胞、消化管粘膜上皮細胞、精巣生殖細胞、肝細胞、脾細胞、神経細胞、骨格筋細胞、心筋細胞、脂肪細胞など多くの細胞群が組織固有の幹細胞システムにより産生されることが明らかにされたことがあげられる。そして、これらの組織特異的な幹細胞(体性幹細胞)を利用した臓器組織の再生が近未来の医療として脚光を浴びている。加えて、これらの組織幹細胞は、固有な組織への分化能以外に、幹細胞が本来所属する組織・臓器の枠組みを越えて分化する現象(可塑性、分化転換能)をもつことが示されたことにより、一層、これらの組織幹細胞の再生医療への応用が期待されている^{1,2)}。

本稿では、移植・再生医療の中心となる組織幹細胞の中でも造血幹細胞(hematopoietic stem cell; HSC)に焦点をあてながら、間葉系幹細胞(mesenchymal stem cell; MSC)³⁾や、多能性成体幹細胞(multipotent adult progenitor cell; MAPC)⁴⁾、さらに、新たに同定されつつある新

規の体性幹細胞についても、最近の研究成果に基づいて再生医療への応用の可能性について紹介する。

再生医療に用いられる
体性幹細胞の種類と特徴

本稿では倫理的な問題がなく、自家移植も可能な体性幹細胞に焦点を絞って、再生医療への応用の可能性について述べる。

体性幹細胞としては、造血組織、脳、肝臓など多くの臓器組織に存在する組織幹細胞、あるいは骨髄、臍帯血、羊膜などに由来するMSC³⁾、さらに骨髄細胞の長期培養により同定されるMAPC⁴⁾などが知られている(図1)。最近では、ヒトの骨髄や臍帯血に由来する新規の多能性幹細胞(一部はES細胞様の多能性を示す)の存在も報告されている⁵⁻⁷⁾。

幹細胞の特徴は、自己複製能をもつことで一生にわたり枯渇することがなく、また、複数の細胞系列に分化する多分化能をもつことである。そして、最近では、造血幹細胞や神経幹細胞に代表される組織幹細胞が、所属する臓器組織の枠組みを越えて分化する現象(可塑性、分化転換能)が注目されている^{1,2)}。なかでも、MAPCの多能性は、ES細胞に匹敵すると報告⁴⁾されていることから、これが事実であれば、骨髄細胞を用いればほとんどの臓器組織を再生することが

* Stem cells and regenerative medicine.

** Yoshiaki SONODA, M.D., Ph.D.: 関西医科大学大学院医学研究科先端医療学専攻修復医療応用幹細胞生物学 [〒570-8506 守口市文圃町10-15]; Department of Stem Cell Biology & Regenerative Medicine, Graduate School of Medical Science, Kansai Medical University, Moriguchi 570-8506, JAPAN

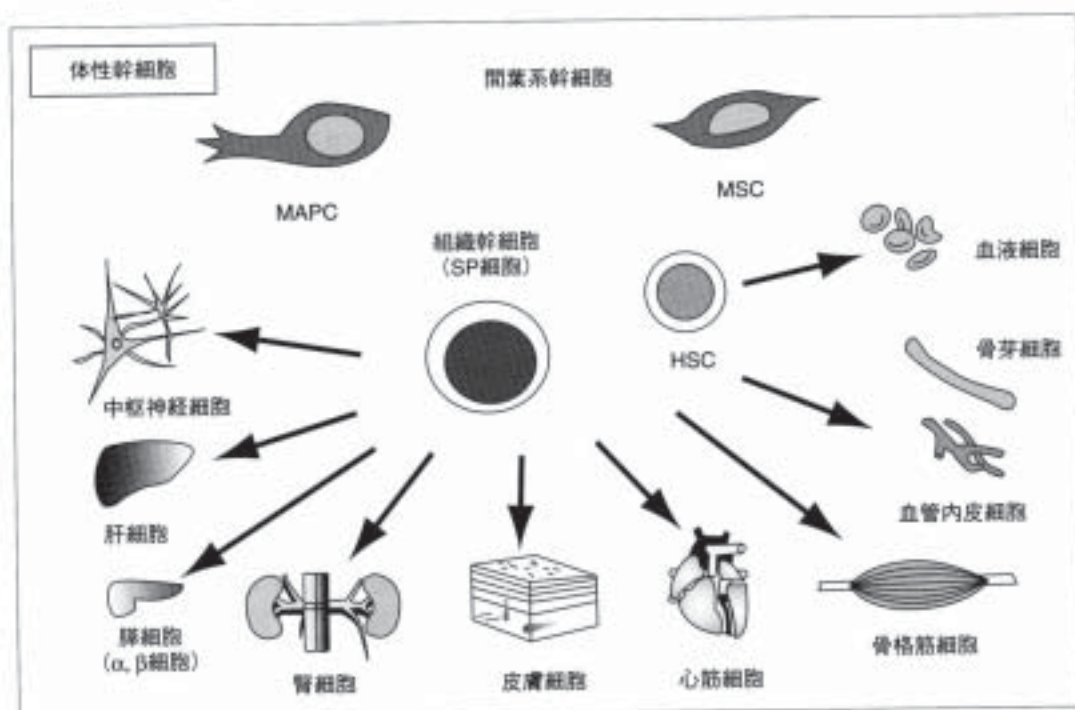


図1 体性幹細胞の可塑性と再生医療

MAPC : multi-potent adult progenitor cell, MSC : mesenchymal stem cell, HSC : hematopoietic stem cell

できると考えられる。

組織幹細胞 (SP細胞) の同定法について

幹細胞の可塑性を明らかにして再生医療へ応用するためには、それぞれの臓器における組織幹細胞を同定することが必須不可欠といえる。骨髄に代表される造血組織に存在するHSCはもっとも早くから研究され、FACS (fluorescent activated cell sorter) 法を駆使することにより、マウスにおいてはすでに純化が可能な段階⁹⁾にまできている。これについては、ヒトHSCの純化の現状を含めて次項で詳しく述べることにする。

Hoechst33342というDNA結合色素で細胞を染色して紫外線で励起すると405nmと600nmの2種類の蛍光を発生し、通常の細胞周期測定で見られるG0/G1よりもさらに暗い分画に非常に特異な形をしたHoechst陰性の細胞集団を観察することができる¹⁰⁾。この細胞群は、linearな細胞集団から横に突き出た形で存在することからSide population (SP) 細胞と名づけられた。このSP細胞分画は、VerapamilなどのMDR (multi-drug resis-

tance gene) 分子阻害剤を添加すると完全に消失することから、MDR様の分子により細胞内から色素を汲み出しているものと考えられていた。最近になり、この機能の責任分子としてABCトランスポーターの一つであるBcrp-1 (breast cancer resistant protein-1) が同定されている。

マウス骨髄細胞に由来するSP細胞の大半が、長い間造血幹細胞のマーカーと信じられてきたCD34抗原陰性 (CD34⁻) であることはすでに報告されていた⁹⁾。最近、このSP細胞の中でも先端にあたるTip SP細胞を1個ずつレシビエントマウスに移植することによりほとんどすべてのマウスにおいて骨髄が再構築されることが報告された¹⁰⁾。すなわち、このTip-SP CD34⁻ KSL (c-kit⁺ Sca-1⁺ Lineage⁻) 細胞がマウスの造血幹細胞と考えられるわけである。一般的に自己複製能の大きな未分化幹細胞ほど深いcell cycle dormancyにあると考えられていることから、このTip-SP CD34⁻ KSL細胞は非常に未分化な幹細胞と考えることができる。

さらに重要なことは、このSP細胞がマウス骨

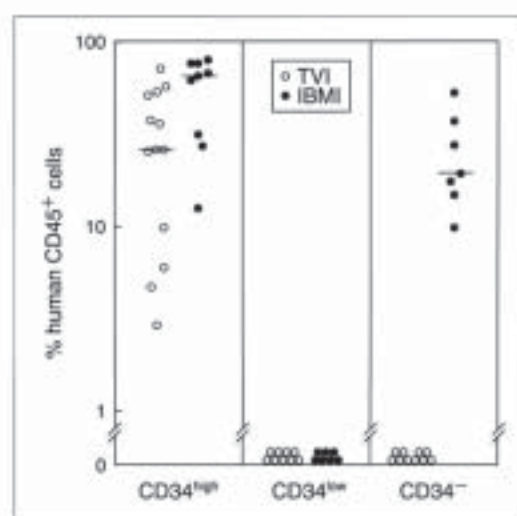


図2 ヒト臍帯血由来CD34^{high/bm-1}細胞のSRC活性
ヒト臍帯血より純化した5万個のLin⁻CD34^{high/bm-1}細胞を従来の尾静脈注入法(TVI)あるいは骨髄腔内直接移植(IBMI)法で移植した場合のNOD/SCIDマウス骨髄中のヒトCD45⁺細胞の割合。CD34⁺細胞は、IBMI法でのみ生着することがはじめて示された。また、CD34⁺SRCの生着率もIBMIではTVI法に比べて有意($p < 0.02$)に高いことが明らかになった。以上より、IBMI法は、TVI法に比較して非常に高い感度をもっていることが示された。(文献¹³⁾より引用改変)

髄だけでなく脳、肝臓、脾臓、腎臓、小腸など多くの臓器にも認められることである。また、SP細胞は、マウスだけでなくヒト、サル、ブタ、イスあるいはゼブラフィッシュなどさまざまな動物種の造血組織にも存在することが報告されている⁹。このことから、Hoechst33342を用いるSP細胞の同定方法は、動物種を越えて組織幹細胞の純化に汎用できる方法であると考えられる。

CD34抗原陰性幹細胞の同定 —ヒト造血幹細胞の本体は どこまで解明されたのか—

次に、ヒトHSCの純化がどこまで進んでいるかについて述べてみたい。マウスに関しては、骨髄細胞に由来するCD34⁺KSL細胞が、1個の細胞の移植により致死量の放射線照射を受けたマウスの造血を再構築することから幹細胞に近い細胞と考えられている¹⁰。一方、ヒトHSCの場合には、マウスのSca-1に相当する陽性マーカーが利用できないことから、いまだに完全に純化

したという報告はない。

CD34抗原は、長い間HSCの重要なマーカーと信じられてきた。しかし、すでに述べたように、マウスにおいて長期の造血再構築能を示す幹細胞がCD34抗原を発現していないか、弱く発現している(CD34^{low/-})ことが示されている^{11,12}。臨床でCD34⁺細胞移植に用いられている免疫磁気ビーズ法では、CD34^{low/-}分画の細胞は失われてしまうため、ここに含まれているCD34⁻HSCが長期(life-long)の造血再構築能をもつHSCと仮定すると、移植後数十年で造血不全となる可能性も考えられる。しかし、マウスにおいては骨髄再構築能を示す幹細胞レベルでCD34抗原のreversionが認められるなど、CD34⁺-HSCの階級樹は必ずしも明らかではない。

われわれは最近になり、骨髄腔内直接移植(IBMI)法を開発することにより、これまで概念的に報告されてきたヒト臍帯血由来CD34⁻HSCの確実な同定にはじめて成功し(図2)¹³、その幹細胞特性について詳細な解析を行った^{14,15}。実験データの解析から、CD34⁻SRCがCD34⁺SRCに比べてより深いdormancyにある未分化な細胞であることが示唆された。さらに、CD34⁻SRCにおけるc-kit, flt3の発現とその幹細胞特性について詳細な解析を行い、現時点で同定されるもっとも未分化なヒトHSCの免疫特性は、Lin⁻CD34⁻c-kit⁻flt3⁻であることを明らかにしている(図3)¹⁶。しかしながら、IBMI法を用いる限界希釈法によるCD34⁻SRCの頻度は1/24,100個であり¹³、その頻度が約1/40個であるCD34⁺CD38⁻SRCに比べるとその純化度は高くない。したがって、今後、ヒトHSC本体のさらなる解明のためには、その陽性マーカーの同定が必須不可欠といえる。

動物モデルにおける幹細胞の可塑性 (分化転換能)と再生医療への応用

最近、種々の臓器において同定される組織幹細胞の可塑性が注目されている¹⁷。1999年にカナダのBjornsonらは、マウス神経幹細胞から血液細胞が産生されることを示し、世界中に衝撃を与えた¹⁸。この実験結果が正しいとすると(追試は成功していない)、従来の発生の基本概念と異なり、胚葉を越えた分化転換(これを可塑性と

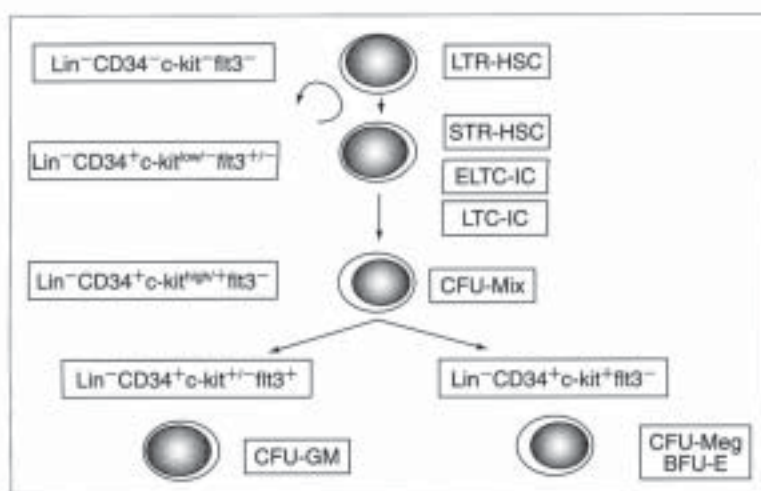


図3 階級制(hierarchy)よりみたヒト未分化造血幹細胞におけるCD34, c-kit, flt3の発現パターンと幹細胞特性

LTR-HSC : long-term repopulating hematopoietic stem cell, STR-HSC : short-term repopulating hematopoietic stem cell, ELTC-IC : extended LTC-IC, LTC-IC : long-term culture-initiating cell, CFU-Mix : mixed colony-forming unit, CFU-GM : colony-forming unit-granulocyte/macrophage, BFU-E : burst-forming unit-erythrocyte, CFU-Meg : colony-forming unit-megakaryocyte

呼ぶ)が起こることになる(図4)。

その後、HSCが肝細胞になる、骨格筋サテライト細胞が血液細胞になる、造血幹細胞移植が心筋梗塞における心筋の再生や血管の新生、あるいは閉塞性動脈硬化症における血管新生にも有用であるなど、動物モデルにおけるHSCを含めた組織幹細胞の可塑性に関する報告が相次いでなされた。最近の幹細胞の可塑性に関する主な報告を表1にまとめて示す。この表から明らかかなように、HSCに関しては3胚葉への可塑性が報告されている。

しかしながら、2002年になって2つの重要な報告がなされた^{10,11)}。これらの報告は、マウスの骨髄あるいは脳に由来する成体幹細胞をES細胞と一緒に *in vitro* で培養すると、これらの2種類の幹細胞がES細胞と自発的に融合してハイブリッド細胞を形成するというものである。このハイブリッド細胞はES細胞の性質を獲得しており、筋肉(心筋)、神経、肝臓、腎臓、腸管などいろいろな種類の細胞を作り出した。これらの細胞の染色体数を調べてみると、多くは4倍体細胞であることが示された。細胞融合の起こる

頻度は1~10万個の細胞あたり1個と低いものであるが、彼らはこれまでに幹細胞の可塑性として報告された結果のいくつかはこの細胞融合で説明できるとしている。しかし、彼らの細胞融合の実験条件はきわめて特殊なものであり、これまでの可塑性に関する報告をすべて否定するものでもない。しかし、幹細胞の可塑性を証明するためには、その細胞の2倍体性を示すことが求められていることも事実である。最近の研究により、細胞融合の頻度は臓器により異なっており、肝臓、心臓においては高率に認められるが、一方、腎臓、脾臓においては真の分化転換が認められると報告されている。

このように、幹細胞の可塑性の本態はまだ混沌としており、画期的な成果が他の研究者によって追試できないことも多い(表1)。最近、Wagersらは、1個のHSCの移植によって骨髄が再構築されたマウスでは、血液細胞以外にはほとんどドナー由来の細胞が存在しないことから、HSCが各種組織の生理的な再生にほとんど寄与しないことを報告している¹²⁾。

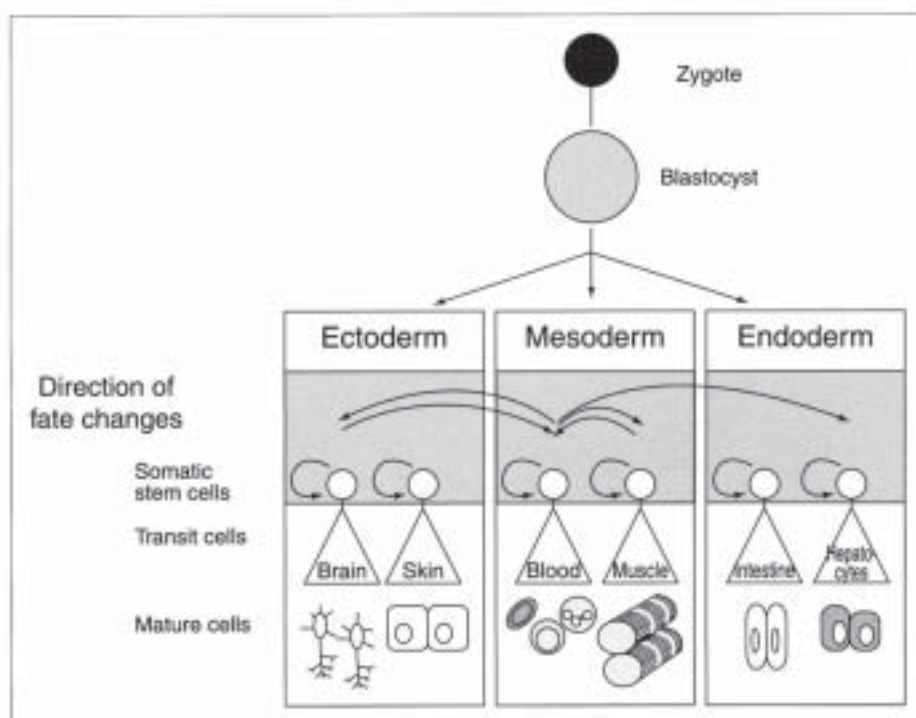


図4 哺乳動物の体性幹細胞の可塑性(分化転換能)
胚葉を越える可塑性を矢印で示す。(Wei G, et al. Stem Cells 2000; 18: 409-14より引用改変)

ヒト(造血)幹細胞の再生医療への 応用とその課題

次に、ヒトHSCの可塑性に関する主な報告を表2にまとめて示す。同種移植で観察された可塑性は、主に異種間骨髄移植を受けた患者の臓器組織を免疫組織化学的方法やY染色体FISH (fluorescent *in situ* hybridization)法で解析したものである。これらの報告では、ドナー由来の肝細胞、血管平滑筋細胞、神経細胞、消化管上皮細胞¹⁹⁾などが同定されている。このことは移植された骨髄中に含まれていた幹細胞(HSC, MSC, MAPC, その他の未知の幹細胞)が、宿主の臓器組織細胞を再生したことを示唆している。しかしながら、その起源を特定することは難しい。

一方、実験的には、NOD/SCIDマウスを用いる異種間移植系などにおいて可塑性が検討されている。多くの実験で、部分純化したヒトHSCを移植した後に、四塩化炭素で肝障害を惹起し、マウス肝臓内でヒトアルブミン産生細胞(肝細胞)が認められたとしている¹⁸⁾。このほか、神経細胞、

心筋細胞など複数の胚葉への分化転換も報告されている。ヒト造血幹細胞の可塑性を明らかにするためには、マウスと同様に純化した幹細胞を用いて*in vitro*の分化誘導系あるいは*in vivo*異種間移植系を用いて検討する必要がある。

このほか、表には示していないが、心筋虚血や心筋梗塞患者、あるいは下肢の虚血などに対して自己の骨髄細胞や末梢血幹細胞分画を直接患部に注射することにより、主に新たな血管新成を通じて虚血状態が改善するという臨床報告が多くみられる²⁰⁾。血管新成に寄与した幹細胞の起源は必ずしも明らかではないが、新たな細胞療法として注目されている。

間葉系幹細胞(MSC)を用いる再生医療

MSCは、骨髄、臍帯血、羊膜などに由来する細胞を*ex vivo*で培養することによって培養皿に附着する細胞として同定される²¹⁾。形態学的には、多角あるいは紡錘型を示す。HSCは、CD45抗原陽性であるが、MSCはCD45抗原陰性であり、これ以外の表面抗原の特徴としてはCD29⁺CD44⁺

表 1 動物モデルにおける幹細胞の可塑性(分化転換能)に関する報告

報告者	実験動物	幹細胞の起源・種類	観察された可塑性	文献
(1) 造血幹細胞の可塑性 (肯定的報告)				
A) 外胚葉への分化転換				
Eglitis & Mezey	マウス	全骨髓細胞	大脳中のmicroglia, astrogliaの再生	PNAS, 1997
Mezey	マウス	PL1 KOマウス骨髓細胞	大脳皮質の神経細胞の再生	Science, 2000
Krause	マウス	骨髓由来の1個のPKH26 ⁺ 細胞	肝臓, 腸, 消化管, 皮膚の上皮細胞再生	Cell, 2001
Lang	マウス	GFP ⁺ 骨髓細胞	マウス新生仔でのGFP ⁺ 内耳細胞の再生	J Comp Neurol, 2006
B) 中胚葉への分化転換				
Ferrari	マウス	骨髓細胞	筋細胞の再構築	Science, 1998
Gussoni	マウス	全骨髓細胞あるいは少数の骨髓由来SP細胞	mdxマウスの骨格筋でのdystrophin発現	Nature, 1999
Orlic	マウス	末梢血由来lin ⁻ c-kit ⁺ 細胞	心筋細胞の再生	PNAS, 2001
Orlic	マウス	骨髓由来のlin ⁻ c-kit ⁺ 細胞	心筋細胞, 血管の新生	Nature, 2001
Otani	マウス	骨髓幹細胞	網膜の血管再生	Nat Med, 2002
Grant	マウス	骨髓造血幹細胞	成体マウス網膜の血管新生	Nat Med, 2002
Masaya	マウス	1個の骨髓由来CD34 ⁺ KSL ⁺ 細胞	腎糸球体メサネンゴウム細胞の再生	Blood, 2003
Kale	マウス	末梢血由来のLin ⁻ Sca1 ⁺ 細胞	虚血障害腎尿管上皮細胞の再生	JCI, 2003
Camargo	マウス	骨髓由来の1個のCD45 ⁺ 細胞	骨格筋細胞の再生	Nat Med, 2003
Corbel	マウス	骨髓由来の1個のSP KLS細胞	骨格筋細胞の再生	Nat Med, 2003
C) 内胚葉への分化転換				
Petersen	ラット	骨髓細胞	肝細胞の再生	Science, 1999
Theise	マウス	全骨髓細胞あるいはlin ⁻ CD34 ⁺ 細胞	肝細胞の再生	Hepatology, 2000
Lagasse	マウス	全骨髓細胞あるいは少数のKTLS細胞	FAH ^{-/-} レシビエントマウスでの肝細胞の再生	Nature Med, 2000
Hess	マウス	骨髓由来c-kit ⁺ 細胞	実験的肝障害マウスで高血糖の改善	Nat Biotech, 2003
Ianus	マウス	骨髓細胞	脾島β細胞の再生	JCI, 2003
Jang	マウス	骨髓由来Fr25 lin ⁻ PKH26 ⁺ 細胞	肝細胞の再生	Nat Cell Biol, 2004
Wagers	マウス	骨髓由来の1個のGFP ⁺ KTLS細胞	血液以外の組織への分化転換はほとんどなし	Science, 2002
Castro	マウス	Rosa26マウス骨髓細胞あるいはSP細胞	神経細胞に分化転換せず	Science, 2002
Balsam	マウス	骨髓由来KTLS細胞	心筋再生に寄与せず	Nature, 2004
Murry	マウス	骨髓由来Lin ⁻ c-kit ⁺ 細胞	まったく心筋再生に寄与せず	Nature, 2004
Nygren	マウス	骨髓由来のHSC	ほとんど心筋細胞に分化転換せず(細胞融合あり)	Nat Med, 2004
(2) 神経幹細胞の可塑性				
Bjornson	マウス	胎仔あるいは成体由来神経幹細胞	骨髄系およびリンパ系造血再構築能	Science, 1999
Clarke	マウス	成体由来神経幹細胞	3胚葉の臓器形成に関与(造血への関与なし)	Science, 2000
Rieze	マウス	成体由来神経幹細胞	筋細胞由来神経細胞との共培養系で筋細胞に分化	Nature, 2001
Santambrogio	マウス	新生仔由来microglia	樹状細胞, マクロファージに分化	PNAS, 2001
Morshead	マウス	神経幹細胞	造血再構築に寄与することは稀な現象	Nat Med, 2002
(3) 筋内由来の幹細胞の可塑性				
Jackson	マウス	骨格筋由来Ho33342 ⁺ Sca1 ⁺ kit ⁻ CD45 ⁻ 細胞	造血再構築能	PNAS, 1999
Gussoni	マウス	骨格筋由来SP細胞	mdxマウスにおける造血再構築とdystrophinの発現	Nature, 1999
Kawada	マウス	骨格筋中造血幹細胞	骨髄幹細胞由来(可塑性を否定)	Blood, 2001
M-Freeman	マウス	骨格筋中造血幹細胞	造血幹細胞由来(可塑性を否定)	PNAS, 2002
Issarachai	マウス	骨格筋中造血幹細胞	骨髄幹細胞由来(可塑性を否定)	Exp Hematol, 2002

表2 ヒト造血幹細胞の可塑性(肯定的な報告)

報告者	移植の概要	検査方法*	観察された可塑性(ドナー由来細胞の分化転換)	文献
Theise	2例のCMML患者におけるallo BMT	IHC + FISH	肝細胞, 胆管細胞	Hepatology, 2000
Alison	9例の異位間allo BMT(M→F)	Y染色体FISH	肝細胞	Nature, 2000
Okamoto	4例の男性間allo BMT(M→F)	Y染色体FISH	消化管上皮細胞(食道, 胃, 小腸, 大腸)	Nat Med, 2002
Korbling	allo PBSCT/BMTの12例のがん患者	IHC	肝細胞, 消化管上皮細胞, 皮膚上皮細胞	N Engl J Med, 2002
Gussoni	allo BMT for SCID(1歳時)	IHC + FISH	12歳時にEhlers-Danlos症候群の一部の骨格筋でドナー由来myotrophin系型(細胞融合)	JCI, 2002
Caplice	13例の造血器腫瘍患者へのallo BMT	IHC + FISH	冠動脈の血管平滑筋	PNAS, 2003
Mezey	4例ALL患者等におけるallo BMT	前検時IHC + FISH	海馬および大脳皮質の神経細胞	PNAS, 2003
Weinmann	10例の造血器腫瘍患者へのallo BMT	前検時IHC + FISH	Parkinson神経細胞	PNAS, 2003
Cogle	3例のAML/CMMLへのallo BMT	前検時IHC + FISH	神経細胞およびグリア細胞(astrocyte, microglia)	Lancet, 2004

* IHC: immunohistochemistry, FISH: fluorescent *in situ* hybridization

B) NOD/SCIDマウスなどの異種間移植系あるいは*in vitro*培養系で観察された可塑性

報告者	幹細胞の起源・種類	実験系	観察された可塑性(ドナー由来細胞の分化転換)	文献
1) 外胚葉への分化転換				
Habich	CB由来CD34 ⁺ 単核細胞	<i>In vitro</i> 培養系	神経細胞, グリア細胞(astrocyte, oligodendrocyte)	Exp Hematol, 2006
2) 中胚葉への分化転換				
Ishikawa	CB由来Lin ⁻ CD34 ⁺ CD38 ⁻ 細胞	NOG新生仔マウス	心筋細胞(細胞融合)	FASEB J, 2006
3) 内胚葉への分化転換				
Danet	BM/CB由来Lin ⁻ CD45 ⁺ CD34 ⁺ CD117 ⁺ 細胞	NOD/SCIDマウス	血液細胞, 肝細胞	PNAS, 2002
Wang	CB/BM由来CD34 ⁺ CD38 ⁻ CD7 ⁻ 細胞	NOD/SCIDマウス	ヒトアルブミン産生細胞(肝細胞)とサイトケラチン19 ⁺ 細胞(胆管細胞)	Blood, 2003
Kollet	PB/CB由来のCD34 ⁺ 細胞	NOD/SCIDマウス	HGF, SDF-1, MMP9がCCl ₄ 障害マウス肝臓において, 肝臓再生に関与	JCI, 2003
Almeida-Porada	BM, CB, PB由来CD34 ⁺ 細胞	半胎仔移植系	肝細胞	Blood, 2004
Yoshida	CB由来T ⁺ 単核細胞	NOD/SCID新生仔マウス	インスリン産生細胞	Stem Cells, 2005
Campil	CB由来CD34 ⁺ AC133 ⁺ c-kit ⁺ 細胞	NOD/SCIDマウス	肝細胞	Transplant Proc, 2005
Kashofer	CB由来CD34 ⁺ 細胞	NOD/SCIDマウス	肝細胞(細胞融合)	Stem Cells, 2006
4) 複数の胚葉への分化転換				
Zeng	CB由来CD34 ⁺ GFP ⁺ 細胞	山形胎仔移植系	血液(PB, BM)以外に, 肝, 脾, 腎, 骨髄, 筋, 心にGFP ⁺ 細胞を認め, 臓器障害は与えず, 細胞融合は否定している。	PNAS, 2006

表3 間葉系幹細胞の多分化能(可塑性)に関する報告

報告者	MSCの起源	実験系(移植の概要)	観察された多分化能(可塑性)	文献
(1) ヒト由来MSC				
Pittenger	骨髓由来MSC	In vitro培養系	脂肪, 軟骨, 骨への分化	Science, 1999
Horwitz	骨髓細胞	Osteogenesis imperfectaに対するallo BMT	骨形成の促進, ドナー由来の骨芽細胞の生着(1.2~2%)	Nat Med, 1999
Liechty	骨髓由来MSC	羊胎仔移植系	軟骨, 脂肪, 筋, 心筋, 骨髄および胸腺ストロマ細胞への分化	Nat Med, 2000
Zhao	骨髓由来MSC	脳梗塞ラットへの移植系	Astrocyte, oligodendroglia, neuronへの分化	Exp Neurol, 2002
Hou	臍帯血由来MSC	In vitro培養系	NF, NSE陽性neuron様細胞への分化	Int J Hematol, 2003
Lee	臍帯血由来MSC	In vitro培養系	骨, 軟骨, 脂肪, neuroglial cell, 肝細胞への分化	Blood, 2004
(2) マウス由来MSC				
Kopen	骨髓由来MSC	新生仔マウス脳腫瘍への移入	Astrocyte, neuronへの分化	PNAS, 1999
Makino	骨髓由来ストロマ細胞	CMG株細胞のin vitro培養系	心筋細胞への分化	J Clin Invest, 1999
Kawada	骨髓由来MSC, CMG細胞	心筋梗塞マウスへのG-CSF投与	心筋細胞への分化	Blood, 2004

CD73⁺CD105⁺CD166⁺CD14⁻CD34⁻であるとされている。なかでもlow-affinity nerve growth factor receptor (LNGFR)として知られるCD271は、ヒト骨髓細胞から直接MSCを分離する陽性マーカーとして報告されている。CD271で分離されたMSCは、従来の培養皿への接着で単離されたMSCに比べてより高い増殖能をもつと報告されている。

MSCの機能は大きく2つに分けられる。1つは、HSCの維持, 増殖, 分化を支持する機能であり, 今ひとつは, 骨芽細胞, 軟骨細胞, 脂肪細胞, 内皮細胞などに分化する機能である。最近では, 心筋細胞, 血管細胞, 骨格筋細胞, 神経細胞, 肝細胞に分化することが報告されている(表3)。MSCを用いる再生医療は, 自家軟骨細胞移植, 歯槽骨の再生, 血管新生, 心筋再生など, すでに臨床で用いられている。

多能性成体幹細胞(MAPC)を用いる再生医療

Verfaillieらは, マウス, ラット, ヒトの骨髓に由来するCD45⁻GPA⁻細胞を低い細胞密度で長期間培養することにより, それまで知られていなかった多能性成体幹細胞(MAPC)を同定することに成功している⁴³⁾。MAPCは, CD45⁻CD34⁻である点ではMSCに似ている。しかしながら, MHC-class I 陰性で, Oct4, Rex1などのES細胞マーカーを発現しており, 高いテロメラーゼ活性をもっていることから, 非常に未分化な幹細胞と考えられる。実際, このMAPCの分化能をin vitroおよびin vivoで調べてみると, 骨, 軟骨, 骨格筋, 脂肪細胞といった間葉系細胞にとどまらず, 血管内皮様細胞などの中胚葉, 神経細胞, グリア細胞などの外胚葉, さらに肝細胞などの内胚葉系細胞にも分化することが示されている。さらに, GFP遺伝子を導入したMAPCを単一細胞レベルで分化誘導しても, 血管内皮細胞, 神経外胚葉系細胞, 肝細胞様細胞に分化することが示されている⁴⁴⁾。

注目すべきことは, 1個のMAPCを胚盤胞に注入してキメラマウスを作製すると, 生まれてきた固体の約半数でほとんどすべて(脳, 網膜, 肺, 心筋, 骨格筋, 肝, 小腸, 腎, 脾, 骨髄, 末梢

血、および皮膚)の臓器組織中にMAPC由来の細胞が認められたことである(最大45%の含有率)⁴⁾。しかしながら、ES細胞と異なり生殖細胞への分化能については明らかにされていない。

ヒト骨髓中に存在するMAPCは、*ex vivo*ではほぼ無限に増殖可能で、3つの胚葉系細胞に分化する能力をもっている。自己の細胞を用いることが可能であることから、倫理的問題もなく、将来的にあらゆる臓器組織の再生医療に応用できるかもしれない。しかしながら、問題点として骨髓細胞からFACSなどで直接純化することができず、唯一、長期間の培養によって同定される細胞であることがあげられる。可能性としては、既知のMSCなどが培養中のepigeneticな変化によりMAPCに変換する可能性も否定できない。

新規なヒト由来幹細胞の 再生医療への応用の可能性

最近になり、ヒト骨髓や臍帯血中にこれまで知られていなかった多能性幹細胞が存在することが相次いで報告されている^{5)~7)}。Yoonらは、ヒト骨髓細胞より限界希釈法を用いて、生体外で140分裂回数以上未分化な状態で増殖し続ける多能性幹細胞(human BM-derived multipotent stem cell; hBMSC)を同定している⁵⁾。この細胞は直径15 μ mで、円形ないし紡錘形を示す。*In vitro*で単一細胞培養を行うと、血管内皮、平滑筋、神経、肝細胞など3胚葉系の細胞に分化する。さらに、心筋梗塞を惹起したラット心臓に移植すると、心筋、血管内皮、平滑筋細胞に分化して心機能の改善に寄与したという。hBMSCは、MSCのマーカーであるCD29, CD44, CD73, CD105, CD90を発現しておらず、また、MAPCに認められるOct3/4も発現していないなど、これらの幹細胞とは異なるものと考えられる。

Koglerらは、ヒト臍帯血細胞より、45分裂回数以上増殖($\sim 10^{13}$ 個)する多能性体性幹細胞(unrestricted somatic stem cell; USSC)を分離した⁶⁾。このUSSCは、培養開始後平均15日程度で培養皿に接着する紡錘形の細胞(大きさ20~25 μ m)として同定される。USSCを*In vitro*で培養すると、骨、軟骨、脂肪、血液、神経系細胞に分化する。また、羊胎仔に*in utero*で移植すると、

血液細胞($\sim 5\%$)、アルブミン産生肝細胞($>20\%$)、および心筋細胞に分化したと報告されている。USSCの表面マーカー解析では、CD45陰性で、CD13, CD29, CD44, CD49e, CD90, CD105, HLA-class I陽性であり、MSCの免疫特性に似ている。ただし、将来的に再生医療への応用を考える場合に、培養した臍帯血の約40%(94/233)でしか分離されなかったことが問題となろう。

2006年になり、Zhaoらはヒトの臍帯血よりES細胞様の未分化な幹細胞(cord blood-stem cell; CB-SC)を分離したと報告している⁷⁾。この細胞は培養皿の底に付着して増殖し、2か月間以上(継代7代以上)維持される。表面マーカー解析では、CD9, CD45, SSEA-3, SSEA-4を発現しており、ES細胞に特徴的なOct4, Nanogという転写因子を発現していることから、非常に未分化な幹細胞と考えられる。CB-SCは、MHCの発現レベルが低く、MLRを惹起しないことから将来の再生医療への応用が期待される。*In vitro*において、血管内皮あるいは神経系細胞へ分化するとともに、*in vivo*でインスリン産生細胞にも分化するなどの多能性を示すと報告されている。hBMSCやUSSCとの大きな違いは、このCB-SCがCD45抗原を発現している点である。

幹細胞の可塑性

一異なる角度からの可能性について一

HSCの可塑性に関する多くの報告では、heterogeneousな幹細胞の集団が移植されている。しかしながら、1個の幹細胞を移植するというクローナルな解析では、可塑性がほとんど認められないとする報告がみられる⁸⁾。これらの報告のdiscrepancyに関して、いくつかの説明が可能である。もし、クローナルな解析が正しいとすれば幹細胞は可塑性をもたないことになる。すると、従来、動物実験やヒトの骨髓移植などで観察された可塑性は、すべて細胞融合や、移植に用いられた骨髓細胞などに含まれていた別の組織幹細胞によるものと解釈できる。最近、Ratajczakらはユニークな仮説を提唱し、マウスにおいてその仮説を証明している⁹⁾。彼らは、マウスの骨髓中のCD45⁻CXCR4⁺Sca-1⁺Lin⁻細胞中にtissue-

committed stem cell (TCSC) と呼ぶ幹細胞が存在すると主張している。定常状態では、このTCSCが末梢血中を循環しており、脳、心臓、肝臓などの組織障害発生時にSDF-1の濃度勾配によって組織にホーミングし、臓器に本来存在する臓器幹細胞とともに、その再生に寄与するという。彼らは、SDF-1の濃度勾配下でのトランスウェル遊走細胞よりFACSを用いてCD45⁻細胞を分離し、実際に、TCSCが*in vitro*で心筋や神経細胞に分化することを示している。また、ヒトにおいても、CXCR4⁺CD34⁺AC133⁺CD45⁻の免疫特性をもつTCSCの存在を示唆している。

TCSCと従来報告されているMSC/MAPCとの異同や、前項で述べたhBMSC、USSCとの関連は明らかにされていないが、CD45抗原を発現していない点で似かよっている。換言すると、マウスやヒトの骨髄中にCD45抗原陰性の組織幹細胞が存在することはほぼ確実と思われる。

おわりに

近未来の医療として注目されている移植・再生医療において、組織幹細胞、とくに、HSCの応用という観点から述べてみた。基礎的臨床的にもっとも重要なヒトHSCの本体はいまだに明らかにされていないが、その新たな能力である可塑性の再生医療への応用が、臨床的な観察からも期待されている。今後は、基礎的な研究の積み重ねによるHSCの本体の解明(純化および特異的なマーカーの同定)はもちろんのこと、そのheterogeneityのさらなる究明、各種細胞系列への増殖分化系の開発など、HSCの効率的な移植・再生医療への応用を目指した開発研究が必要不可欠と考えられる。この目的のためには、HSCの可塑性(分化転換能)の発現に関する分子機構の解明も併せて行う必要がある。また、別の観点からは、CD45抗原陰性の組織幹細胞の本体の解明と再生医療への応用に関する研究の進歩が期待されている。

文 献

- 1) Orkin S, Zon LI. Hematopoiesis and stem cells: plasticity versus developmental heterogeneity. *Nat Immunol* 2002; 3: 323.
- 2) Herzog E, Chai L, Krause DS. Plasticity of marrow-derived cells. *Blood* 2003; 102: 3483.
- 3) Pittenger MF, Mackay AM, Beck SC, et al. Multilineage potential of adult human mesenchymal stem cells. *Science* 1999; 284: 143.
- 4) Jiang Y, Jahagirdar BN, Reinhardt RL, et al. Pluripotency of mesenchymal stem cells derived from adult marrow. *Nature* 2002; 418: 41.
- 5) Kogler G, Sensken S, Airey JA, et al. A new human somatic stem cell from placental cord blood with intrinsic pluripotent differentiation potential. *J Exp Med* 2004; 200: 123.
- 6) Yoon Y, Wecker A, Heyd L, et al. Clonally expanded novel multipotent stem cells from human bone marrow regenerate myocardium after myocardial infarction. *J Clin Invest* 2005; 115: 326.
- 7) Zhao Y, Wang H, Mazzone T. Identification of stem cells from human umbilical cord blood with embryonic and hematopoietic characteristics. *Exp Cell Res* 2006; 312: 2454.
- 8) Osawa M, Hanada K, Hamada H, et al. Long-term lymphohematopoietic reconstitution by a single CD34-low/negative hematopoietic stem cell. *Science* 1996; 273: 242.
- 9) Goodell MA, Rosenzweig M, Kim H, et al. Dye efflux studies suggest that hematopoietic stem cells expressing low or undetectable levels of CD34 antigen exist in multiple species. *Nat Med* 1997; 3: 1337.
- 10) Matsuzaki Y, Kinjo K, Mulligan RC, et al. Unexpectedly efficient homing capacity of purified murine hematopoietic stem cells. *Immunity* 2004; 20: 87.
- 11) Wang J, Kimura T, Asada R, et al. SCID-repopulating cell activity of human cord blood-derived CD34⁻ cells assured by intra-bone marrow injection. *Blood* 2003; 101: 2924.
- 12) Kimura T, Wang J, Matsui K, et al. Proliferative and migratory potentials of human cord blood-derived CD34⁻ severe combined immunodeficiency repopulating cells that retain secondary reconstituting capacity. *Int J Hematol* 2004; 79: 328.
- 13) Sonoda Y, Kimura T, Asada R, et al. Identification and long-term repopulating potential of human cord

- blood-derived CD34⁺Flt3⁻ cells with very immature phenotype using intra-bone marrow injection. *Blood* 2005 ; 106 : 235a.
- 14) Bjornson CR, Rietze RL, Reynolds BA, et al. Turning brain into blood : a hematopoietic fate adopted by adult neural stem cells in vivo. *Science* 1999 ; 283 : 534.
- 15) Terada N, Hamazaki T, Oka M, et al. Bone marrow cells adopt the phenotype of other cells by spontaneous cell fusion. *Nature* 2002 ; 416 : 542.
- 16) Ying Q-L, Nicols J, Evans EP, et al. Changing potency by spontaneous fusion. *Nature* 2002 ; 416 : 545.
- 17) Wagers AJ, Sherwood RI, Christensen JL, et al. Little evidence for developmental plasticity of adult hematopoietic stem cells. *Science* 2002 ; 297 : 2256.
- 18) Okamoto R, Yajima T, Yamazaki M, et al. Damaged epithelia regenerated by bone marrow-derived cells in the human gastrointestinal tract. *Nature Med* 2002 ; 8 : 1011.
- 19) Wang X, Ge S, McNamara G, et al. Albumin-expressing hepatocyte-like cells develop in the livers of immune-deficient mice that received transplants of highly purified human hematopoietic stem cells. *Blood* 2003 ; 101 : 4201.
- 20) Tateishi-Yuyama E, Matsubara H, Murohara T, et al. Therapeutic angiogenesis for patients with limb ischaemia by autologous transplantation of bone-marrow cells : a pilot study and a randomized controlled trial. *Lancet* 2002 ; 360 : 427.
- 21) Prockop DJ, Gregory CA, Spees JL. One strategy for cell and gene therapy : harnessing the power of adult stem cells to repair tissues. *Proc Natl Acad Sci USA* 2003 ; 100 : 11917.
- 22) Reyes M, Lund T, Lenvik T, et al. Purification and ex vivo expansion of postnatal human marrow mesodermal progenitor cells. *Blood* 2001 ; 98 : 2615.
- 23) Kucia M, Reca R, Jala VR, et al. Bone marrow as a home of heterogeneous populations of nonhematopoietic stem cells. *Leukemia* 2005 ; 19 : 1118.

* * *

研究成果報告書

研究課題名	神経系の再構築・機能修復における細胞接着分子の役割		
(英文)	Roles of adhesion molecules in neural regeneratioon		
事業推進者	木梨 達雄	E-mail	kinashi@takii.kmu.ac.jp
所属・職名	附属生命医学研究所 分子遺伝学部門・教授		
研究分担者名	片桐 晃子、片貝 智哉		
キーワード	Integrin、Rap1、RAPL、Mst1、live imaging、cell migration		
<p>1. 概要</p> <p>低分子量Gタンパク質 Rap1 は、免疫系ではリンパ球、樹状細胞のインテグリン接着や細胞極性を調節し、活発な生体内移動を制御している。RAPL (Rassf5b) は活性化型 Rap1 に結合し、Rap1 による細胞接着制御のエフェクター分子として機能している。Rap1 は免疫系だけでなく、神経系に多く発現していることから、免疫系の細胞移動や細胞極性のシグナル伝達との共通性を有することが予想される。免疫系で得られた細胞接着制御シグナルである、Rap1-RAPL シグナルを解明し、その機能を神経系の発生、再生、神経と免疫が関与する疾患モデル等で検討する。</p> <p>2. 研究の背景と目的</p> <p>免疫系は全身性の動態制御を基盤とするシステムであり、生体内移動には様々な接着分子、遊走因子が関与する。特にリンパ球は生体内で最も活発に移動する細胞であり、その制御機構について接着分子、遊走因子、組織間葉系・細胞外マトリックスの関与など、多くの知見が蓄積している。神経系でもの発生過程でおこる神経幹細胞の活発な移動や神経樹状突起の可塑性に細胞移動や接着の制御が重要と考えられている。細胞接着や移動制御は多細胞生物の根幹をなしており、神経系と免疫系に共通な接着分子や遊走因子がみつまっていることから、その制御様式に関しても共通点があると予想される。そこで、免疫系で細胞接着・移動の重要なシグナルである Rap1 シグナルを解明し、神経系での機能を探り、神経系の修復と再生に応用できるか検討する。</p> <p>3. 研究方法</p> <p>(1) Rap1-RAPL シグナル下流分子の同定と機能改変マウスの作成 RAPL 会合分子を単離し、その機能解析から接着・移動への関与を調べる。同定された分子について遺伝子欠損マウスを作成し、生体内機能を探る。</p> <p>(2) In vivo イメージング等による神経系と免疫系の相互作用解析 生体内細胞移動を可視化し、直接生体内の細胞接着・移動を解析する。そのため、多光子顕微鏡を用いた生体内顕微鏡技術を樹立し、神経発生過程や神経免疫病の病態での神経・グリア細胞の変化を解析する。</p> <p>4. これまでの成果</p> <p>(1) 低分子量Gタンパク質 Rap1 は、免疫系ではリンパ球、樹状細胞のインテグリン接着や細胞極性を調節し、活発な生体内移動を制御している。RAPL (Rassf5b) は活性化型 Rap1 に結合し、Rap1 による細胞接着制御のエフェクター分子として機能している。RAPL のC末端側の coiled-coil 領域がその機能制御に重要である。我々は今年度、この領域に結合する分子として Ste20 ファミリーに属する Mst1 (STK4) を同定した。Rap1/RAPL シグナルは Mst1 のキ</p>			

ナーゼ活性と細胞内局在を調節することによってインテグリンの細胞内輸送を制御し、細胞先端側にインテグリンを集積させ、移動方向に新たな接着点を形成する。

(2) RAPL に結合する下流エフェクター分子 Mst1 キナーゼの conditional knockout マウスを樹立した。現在、細胞系列特異的プロモーター (Lck, CD19) やユビキタス発現プロモーターによる Cre recombinase 発現マウスと交配しており、その効果を調べる予定である。

(3) 高感度カメラを用いて生体内で血管内皮細胞とリンパ球の接着様子を解析し、in vitro で灌流リンパ球と血管内皮細胞の接着過程の再構築と解析を行った結果、血管内皮接着過程に Rap、RAPL によるインテグリン接着の安定化が必要であることを明らかにした。

(4) 多光子レーザー顕微鏡を用いた生体内観察系を樹立した。麻酔下のマウスのリンパ節を顕微鏡下に露出し、移入した蛍光ラベルラベルされたリンパ球が皮膜下 100–200 ミクロンの組織深部での移動する過程を追跡し、RAPL 欠損による移動障害を明らかにした。

5. これまでの進捗状況と今後の計画

Rap1 シグナル解析から Mst1 の同定まで細胞接着・移動の細胞内制御過程の解析が前進した。また生体内機能解析に必要な遺伝子改変マウスや生体内顕微鏡技術の確立が順調に進んでいる。今後、発生過程や神経免疫病 (EAE) 等を進める。神経系の細胞移動と再生・修復への応用を進める。

6. これまでの発表論文

(1) 発表論文

英文

1. Yoshikawa, Y., Satoh, T., Tamura, T., Wei, P., Bilasy, SE., Edamatsu, H., Aiba, A., Katagiri, K., Kinashi, T., Nakao, K. & Kataoka, T.
The M-Ras-RA-GEF-2Rap1 pathway mediates tumor-necrosis factor-alpha-dependent regulation of integrin activation in splenocytes.
Mol. Biol. Cell, **18**, 2949-2959 (2007).
2. Kinashi, T.
Integrin regulation of lymphocyte trafficking: Lessons from structural and signaling studies.
Adv. Immunol. **93**, 185-227 (2007).
3. Kinashi, T.
Adhere upright: A switchblade-like extension of $\beta 2$ integrins.
Immunity **25**, 521-522 (2006).
4. Katagiri, K., Imamura, M. & Kinashi, T.
Spatiotemporal regulation of the Kinase Mst1 by binding protein RAPL is critical for lymphocyte polarity and adhesion.
Nat. Immunol. **7**, 919-927 (2006).

和文

1. 戎野幸彦、片桐晃子、木梨達雄：
接着分子による免疫細胞動態調節と免疫応答
炎症と免疫 **16**, 436-441 (2008).
2. 片桐晃子、大西典子、椛島健治、伊豫田知典、竹田直樹、真貝洋一、稲葉カヨ、木梨達雄
リンパ球及び樹状細胞の生体内動態における Rap1 エフェクター分子 RAPL の重要な機能
細胞工学 **16**, 54-61 (2005).
3. 片桐晃子、木梨達雄

Rap1/RAPL 相互作用による血液系細胞の生体内動態制御
免疫 2006 42, 92-98 (2005).

(2) 学会発表

国際学会

1. Kinashi, T.
Lymphocyte adhesion cascade regulated by Rap1 signaling.
The 2008 ASIP Annual Meeting at Experimental Biology 2008, San Diego, USA, 2008.
2. Kinashi, T., Katagiri, K. & Ebisuno, Y.
The Rap1-RAPL-Mst1 signaling .
Gordon Research Conference: Mechanisms of Cell Signaling, Oxford, United Kingdom, 2007.
3. Kinashi, T., Katagiri, K. & Ebisuno, Y.
Roles of Rap1-RAPL signaling in lymphocyte adhesion.
Bonner Forum Biomedizin Symposium Cell Adhesion in the Immune System, Bonn, Germany, 2007.
4. Kinashi, T., Katagiri, K. & Ebisuno, Y.
Regulation of integrin-mediated adhesion.
The second international symposium on immune surveillance, Tokyo, Japan, 2007.
5. Kinashi, T.
Roles of Rap1-RAPL signaling in immune cell trafficking
20th IUBMB International Congress of Biochemistry and Molecular Biology and 11th FAOBMB, Kyoto, Japan, 2006.

国内学会

1. 木梨達雄、片桐晃子、戎野幸彦、片貝智哉
Regulation of integrin-dependent lymphocyte adhesion by Rap1-RAPL signaling.
第 37 回日本免疫学会シンポジウム、東京、2007.
2. 木梨達雄、片桐晃子、戎野幸彦
Regulation of integrin-dependent immune cell trafficking by RAPL signaling.
日本分子生物学会シンポジウム「免疫系・血液系細胞の生体内での移動・定着とその時間空間的制御」、名古屋、2006.

7. これまでの成果の情報公開

ホームページ：附属生命医学研究所 分子遺伝学部門

<http://www3.kmu.ac.jp/molgent/>

Integrin Regulation of Lymphocyte Trafficking: Lessons from Structural and Signaling Studies

Tatsuo Kinashi

*Department of Molecular Genetics, Institute of Biomedical Science,
Kansai Medical University, Kyoto 606, Japan*

Abstract.....	185
1. Introduction.....	185
2. Leukocyte Integrins.....	186
3. Affinity and Valency Regulation.....	189
4. Integrin Conformational Changes.....	189
5. Integrin-Mediated Adhesion Steps in Lymphocyte Trafficking.....	195
6. Talin as Intracellular Regulator for Lymphocyte Adhesion and Migration.....	201
7. Intracellular Signals in Chemokine-Induced Adhesion and Migration.....	203
8. Inside-Out Signaling Events in TCR-Stimulated Lymphocytes.....	211
9. Concluding Remarks.....	215
References.....	216

Abstract

High trafficking capability of lymphocytes is crucial in immune surveillance and antigen responses. Central to this regulatory process is a dynamic control of lymphocyte adhesion behavior regulated by chemokines and adhesion receptors such as integrins. Modulation of lymphocyte adhesive responses occurs in a wide range of time window from less than a second to hours, enabling rolling lymphocyte to attach to and migrate through endothelium and interact with antigen-presenting cells. While there has been a rapid progress in the understanding of integrin structure, elucidation of signaling events to relay extracellular signaling to integrins in physiological contexts has recently emerged from studies using gene-targeting and gene-silencing technique. Regulatory molecules critical for integrin activity control distribution of integrins, polarized cell morphology and motility, suggesting a signaling network that coordinates integrin function with lymphocyte migration. Here, I review recent studies of integrin structural changes and intracellular signal molecules that trigger integrin activation (inside-out signals), and discuss molecular mechanisms that control lymphocyte integrins and how inside-out signals coordinately modulate adhesive reactions and cell shape and migration.

1. Introduction

Immune cells are the most motile cells in the body. Multiphoton microscopy has been used to reveal a vivid picture of the robust motility that occurs during lymphocyte interactions with dendritic cells (DCs) in peripheral lymphoid

tissues (Mempel *et al.*, 2004; Miller *et al.*, 2002). The dynamic regulation of immune cell adhesive interactions is fundamentally integrated into immunological responses, and the integrin adhesion receptors play critical roles in this process (Butcher and Picker, 1996; Butcher *et al.*, 1999; Springer, 1990, 1995). Integrins constitute a large family of surface glycoproteins, and they are composed of α and β subunits (Hemler, 1990). In particular, leukocyte integrins, such as lymphocyte function-associated antigen (LFA-1; α L/ β 2) and the α 4 integrins are important in lymphocyte trafficking to peripheral lymphoid tissues through binding to the endothelial ligands ICAM (intercellular adhesion molecule)-1 and ICAM-2 for LFA-1 and VCAM (vascular cell adhesion molecule)-1 and MAdCAM (mucosal addressin cell adhesion molecule)-1 for α 4 integrins. LFA-1 and α 4 integrins mediate firm attachment of lymphocytes to high endothelial venules (HEV) and facilitate subsequent migration into tissues (Butcher *et al.*, 1999). LFA-1 is also the critical adhesion molecule in the immunological synapse, a specialized adhesion complex between T cells and antigen-presenting cells (APC), and these interactions promote the activation of naive T cells (Sims and Dustin, 2002).

The ability of cells to modulate the strength of integrin adhesion in response to extracellular stimuli such as antigen or chemokines is essential to proper immune function. This activation process, referred to as “inside-out signaling” (Dustin and Springer, 1989), ultimately modulates integrin adhesiveness through affinity modulation (Carman and Springer, 2003), in which ligand-binding affinity is altered, and avidity modulation, in which integrin cell surface diffusion and clustering are modified (van Kooyk and Figdor, 2000), which is referred to as valency modulation here. Recently, our understanding of these phenomena has been facilitated by three-dimensional structures of integrins. Distinct conformational changes in the integrin extracellular domains are clearly associated with affinity changes on ligand binding or cell activation (Shimaoka *et al.*, 2002; Takagi and Springer, 2002). Although integrin activation following physiological adhesion has been documented, the molecules that relay the inside-out signal and the mechanism(s) by which affinity and valency modulation are regulated have been elusive. In this article, I review the recent studies of lymphocyte integrin regulations from viewpoints of structure and valency, intracellular signaling, and their physiological relevancies in lymphocyte trafficking.

2. Leukocyte Integrins

Integrin adhesion molecules are a large family of 24 members of heterodimeric cell-surface receptors composed of 18 α and 8 β subunits (Fig. 1). Cell-matrix and cell-cell interactions mediated by integrins are central to

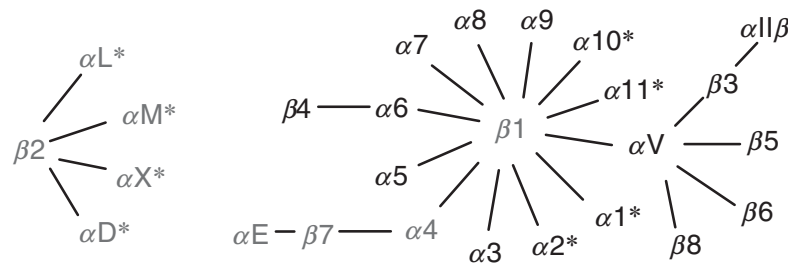


Figure 1 Integrin family. The associations between the 18 α chains and 8 β chains form at least 24 integrins. Leukocyte integrins are in gray. The integrins that contain the αI domain are indicated with asterisks (*).

many fundamental biological processes such as embryogenesis, angiogenesis, organ formation, and immune functions (Hynes, 2002). The leukocyte integrin, LFA-1 ($\alpha L\beta 2$) is a member of the $\beta 2$ integrins exclusively expressed on leukocytes, and shares a common $\beta 2$ subunit with Mac-1 ($\alpha M\beta 2$), p150/95 ($\alpha X\beta 2$), and αD ($\alpha D\beta 2$). LFA-1 plays important roles in binding to endothelium during leukocyte extravasation, lymphocyte homing, and in immunological synapse formation between T cells and APC (Sims and Dustin, 2002). Lymphocytes also express $\alpha 4$ integrins ($\alpha 4\beta 1$, $\alpha 4\beta 7$) that contribute to lymphocyte trafficking to inflamed or peripheral lymphoid tissues. Ligands for LFA-1 include ICAM-1, -2, -3, and junctional adhesion molecule-1 (JAM-1) that are expressed on endothelium or APC. $\alpha M\beta 2$ and $\alpha X\beta 2$, also known as complement receptor (CR)-3 and -4, bind to iC3b-coated particles in addition to ICAM-1, and mediate phagocytosis of microbes. A hereditary defect in the $\beta 2$ subunit that impairs expressions of leukocyte integrins causes a life-threatening immunodeficiency, leukocyte-adhesion deficiency (LAD; Etzioni, 1996). $\beta 2$ and $\alpha 4$ integrins have been attractive drug targets for inhibition of inflammatory or autoimmune diseases (Staunton *et al.*, 2006).

In the absence of activation, $\alpha L\beta 2$ has low affinity for ligand. In inside-out signaling, signals received by other receptors activate intracellular signaling pathways that impinge on integrin cytoplasmic domains and make the extracellular domain competent for ligand binding on a timescale of less than 1s. This property enables leukocytes to rapidly respond to signals in the environment, such as cognate antigen or chemoattractant, to activate adhesion, and direct cell migration. Rapid progress in the integrin extracellular structure has recently made, which provides important clues how the integrin conformational changes are propagated through the cytoplasmic domain to the leg domains to the ligand-binding headpiece (Carman and Springer, 2003; Dustin *et al.*, 2004).

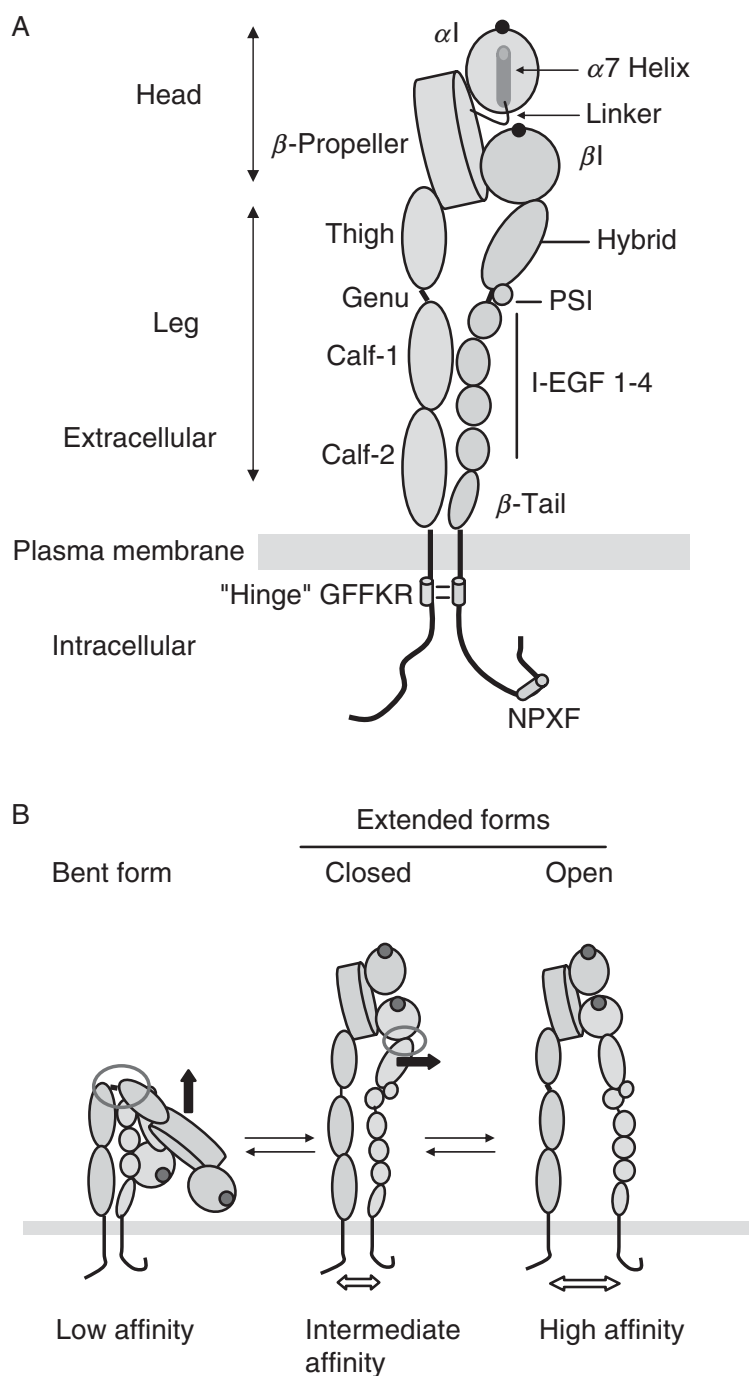


Figure 2 Structure of β_2 integrin. (A) Schematic representation of the β_2 integrin. The head region comprises the αI domain and β -propeller domain of the α subunit (light shade) and βI domain of the β subunit (dark shade). The leg region comprises the thigh, calf-1, calf-2 of the α subunit and the hybrid domain, N-terminal PSI (plexin, semaphorin, and integrin) domain, four I-EGF (epidermal growth factor) repeats, and β -tail domain. Both subunits have a transmembrane domain and short cytoplasmic domain. A MIDAS is indicated by black spheres. The glycine-phenylalanine-phenylalanine-lysine-arginine (GFFKR) motif in the α subunit cytoplasmic domain and corresponding amino acids in the β subunit cytoplasmic domain constitute a "hinge" region.

3. Affinity and Valency Regulation

Before going into details of integrin structural changes and regulatory signaling pathways, how integrin controls total cell adhesiveness (avidity) is briefly considered. Theoretically, avidity is related to affinity and surface density (valency) of integrins. Inside-out signals are thought to modulate either or both of these parameters and act in a time window ranging from less than a second to minutes. Initial attachments are often transient and weak, and stabilization subsequently occurs by ligand-induced conformational changes, linkage to the cytoskeleton, or cell spreading. It is difficult to distinguish avidity changes by inside-out signals from those induced by ligand occupancy even in a short time window. To distinguish inside-out signals from postadhesion events, integrin affinity or valency changes should be examined before cell adhesion. Since conventional affinity measurements are not sensitive enough to detect affinity changes in micromolar ranges, affinity modulation has been underestimated. Thus, valency regulation has been often inferred when activators induce adhesion without detectable affinity changes. Availability of monoclonal antibodies to detect distinct conformations of integrins eases this difficulty, and more sensitive methods to detect affinity (Chan *et al.*, 2003; Lollo *et al.*, 1993), conformation (Chigaev *et al.*, 2003; Larson *et al.*, 2005), and mobility (Cairo *et al.*, 2006) are reported and shown to be instrumental to dissect effects of inside-out signals on integrins (Sections 4 and 5). These materials and methods are expected to be exploited widely to study roles of inside-out signals.

4. Integrin Conformational Changes

4.1. Global Changes of Extracellular Domains in Integrins That Lack the α I Domains

The overall integrin structure resembles a “head” connected to “two legs” (Fig. 2A). The α subunit comprises an N-terminal β -propeller at the top, followed by three β -sandwich modules (thigh, calf-1, and calf-2). The β subunit comprises an N-terminal PSI (plexin, semaphorin, and integrin) domain, followed by a β -sandwich hybrid domain, a β I domain (von Willebrand factor

The β cytoplasmic domain contains a talin-binding asparagine-proline-(any amino acid)-phenylalanine (NPXF) motif. (B) Equilibrium of the bent (low affinity) and extended conformations with the “closed” (intermediate affinity) and the “open” (high affinity) states triggered by separation of the cytoplasmic tails. The extended-open, high-affinity conformation is induced/stabilized by separation of the α and β cytoplasmic and leg regions. The flexible joints at the genu and between I-EGF-1 and I-EGF-2, and the β I/hybrid domain interface are indicated by circles. The upright and outward motions of the extracellular domains and the hybrid domain in transition from the bent to the extended and from the closed to the open states are indicated by thick arrows.

A domain), four epidermal growth factor (EGF) repeats, and a β -tail domain. Half of the 18 integrin α subunits ($\alpha 1$, $\alpha 2$, $\alpha 10$, $\alpha 11$, αL , αM , αX , αD , and αE) also include an I domain in their α subunits (α I-domain) inserted through short linkers into the upper face of the β -propeller. Where present, this domain is the major site of ligand binding. The major sites of ligand recognition of integrins that lack the α I domain are the top face of the β I domain and the loops on the upper surface of the β -propeller. Both the α I and β I domains contain a metal ion-dependent adhesion site (MIDAS), where a divalent metal is coordinated by a ligand's acidic residue (Hynes, 2002).

Recent structural studies of integrins that lack the I domain have led to a general model of integrin conformational changes; in the low-affinity conformation, the leg region is acutely bent at the “genu” (knee) between the thigh and calf-1 domains and between the I-EGF-1 and I-EGF-2, with the ligand-binding headpiece in proximity to the membrane proximal leg region, topologically pointing toward the plasma membrane (Xiong *et al.*, 2001, 2002; Fig. 2B). The electron microscopic analysis of negatively stained soluble recombinant integrins together with mutational studies and physicochemical measurement elegantly demonstrate that the switch blade-like extension of the leg regions shifts the molecule to the intermediate or high-affinity conformations in a manner dependent on the orientation of the β I domain and hybrid domain. In a “closed” conformation, the β I makes an acute angle with the hybrid domain, and in an “open” high-affinity conformation, the outward motion of the hybrid domain occurs, making an obtuse angle with the β I domain (Takagi *et al.*, 2002). Therefore, the extension of the legpiece and the orientation between the hybrid and β I domains of the headpiece are the key translator for converting global conformational changes into regulation of affinity (Takagi and Springer, 2002). Although a bent conformation may not be equated with low-affinity binding in all situations (Adair *et al.*, 2005; Xiong *et al.*, 2002), the extension is thought to be particularly relevant in cell–cell adhesion mediated by leukocyte integrins. Indeed, it has been suggested from many studies using monoclonal antibodies that integrins undergo dynamic conformational changes in the legpiece (Lu *et al.*, 2001a) as well as the headpiece (Humphries, 2004; Lu *et al.*, 2001b, 2004), depending on divalent metals, ligand binding, or inside-out signals.

4.2. Extensions of Extracellular Domains of $\beta 2$ Integrins

It has been recently demonstrated by using soluble recombinant $\alpha X\beta 2$ and $\alpha L\beta 2$ that $\beta 2$ integrins also show three distinct conformations: a bent conformation, extended conformations with closed or open states of the headpiece (Nishida *et al.*, 2006; Fig. 2B), as seen in integrins that lack I domains (Takagi

et al., 2002). When the entire extracellular domains of α and β subunits are linked via a disulfide bond and coiled-coil sequences fused at the C-terminal ends (clasped form), $\alpha X\beta 2$ predominantly showed V-shaped bent forms in physiological Mg^{2+} and Ca^{2+} concentrations. Compared with clasped $\alpha X\beta 2$, clasped $\alpha L\beta 2$ appears to be more relaxed in conformation, showing both the bent (55%) and extended-closed (45%). This is in line with the characteristics of $\alpha X\beta 2$, which requires stronger cellular activation for adhesion than other members of $\beta 2$ integrins. Removal of C-terminal clasp (unclasped) of $\alpha X\beta 2$ increased extends forms with the closed (50%) and open (25%) headpiece with the rest remained bent. Unclasping of $\alpha L\beta 2$ also increased the extended-open conformation. These results are in an excellent agreement with those of integrins without the αI -domain, and support a coherent model of integrin conformational changes through the bent to the extended-closed to the extended-open states. Since these distinct states can coexist under the defined conditions, the conformational changes are not all-or-none responses, but should be regarded as equilibria among multiple states (Carman and Springer, 2003). Thus, in basal states integrin molecules are continually flexing (breathing) to some degree, and stabilization of the legpiece prefers the bent form, and its separation shifts an equilibrium toward the extended forms. The equilibrium points likely differ in integrin family members. A $\beta 2$ monoclonal antibody (CBR-LFA1/2; Petruzzelli *et al.*, 1995), which induces high-affinity states and stimulates adhesion by binding an epitope in the I-EGF3 domain, separates α and β leg regions and induced or stabilized extended conformations. Thus, disruption of the interaction of the α and β cytoplasmic tails by inside-out signals probably leads to a loss of the interactions between the leg regions, resulting in repositioning of the ligand-binding headpiece pointing away from the plasma membrane (Fig. 2B). This model is consistent with studies on epitopes of stimulatory mAb that have now been shown to lie in the knee or leg regions (Lu *et al.*, 2001a; Xie *et al.*, 2004). Exposure of these epitopes is low in the bent state of the integrin (where they are masked) but high in the extended state (Lu *et al.*, 2001a; Xie *et al.*, 2004). The βI domain appears to play a regulatory role in this conformational change relay. The treatment of the clasped and unclasped $\alpha X\beta 2$ with a small molecule antagonist, XVA143, greatly increased extended conformations predominantly with the open state (Nishida *et al.*, 2006). This is consistent with the proposed mechanism of XVA143, acting on the MIDAS of the βI domain, leading to the βI activation with the hybrid domain swing-out, while inhibiting activation of the αI domain (Shimaoka *et al.*, 2003a). The βI and hybrid domains may serve as a switch in transmitting the conformational signals from the ligand-binding αI domain to the C-terminal regions on ligand binding and from the cytoplasmic tails to the αI domain by inside-out signals.

4.3. Multiple Affinity States of the α I Domain

The I domain was crystallized in three major forms: closed (low affinity, ~ 2 mM), intermediate (3–9 μ M), and open (high affinity, ~ 0.2 μ M; [Shimaoka *et al.*, 2002, 2003b](#)). The major conformational changes during the transition from the closed to open states include a rearrangement of the cation-coordinating residues in the MIDAS site, accompanied by a small inward movement of the $\alpha 1$ helix and a large downward shift of the mobile C-terminal ($\alpha 7$) helix. Crystal structures of α L I domain reveal that the $\alpha 7$ helix can adopt three different positions. An intermediate state between the fully closed and fully open forms of the domain involves a downward shift halfway to that observed for the fully open state. Thus, rearrangement of the MIDAS into the ligand-binding configuration is tightly coupled to a downward movement of the C-terminal helix.

4.4. Regulation of the α I Domain Conformations by the β I Domain

The open and closed conformations of the α I domain are regulated by interaction of the C-terminal linker with the β I domain. A conserved glutamic acid in the C-terminal linker appears to act as an internal ligand to the β I domain and plays important role in conformational changes of the α I domain ([Huth *et al.*, 2000](#); [Yang *et al.*, 2004b](#)). Mutations of the glutamic acid in the linker or amino acids constituting the MIDAS of the β I domain result in the low-affinity state of the α I domain. Furthermore, double mutation of these residues to cysteine, allowing formation of the disulfide bond between the linker and β I, results in a constitutive high-affinity state of α I ([Yang *et al.*, 2004b](#)). These results support the hypothesis that the β I domain regulates the activity of α I by pulling down on the linker region leading to a downward movement of the C-terminal α helix by exertion of a bell-rope-like pull on a segment within the C-terminal linker region ([Carman and Springer, 2003](#)). Because this site is equivalent to the ligand-binding site in integrins that lack I domains, the interaction of the linker with the MIDAS of the β I domain may occur that are analogous to those that regulated interactions with ligands in integrins that lack I domains. Thus, the three headpiece units, the α I, β -propeller, and β I domains, make a ternary interaction interface where structural rearrangements of the latter two domains affect the conformation of the α I domain.

4.5. Regulation of the β I Domain by Extensions and Divalent Metals

Affinity regulation of the β I domain is thought to occur by the same mechanism as that regulating the α I domain. Both $\alpha 1$ and $\alpha 7$ helix movements are critical for β I domain regulation generating low- and high-affinity states ([Luo](#)

et al., 2004; Mould *et al.*, 2002, 2003b; Yang *et al.*, 2004a). The outward motion of the hybrid domain is linked to $\alpha 7$ helix movements presumably because the hybrid domain exerts a downward pull on this structural element. The orientation between the hybrid and βI domains is therefore thought to be a key translator for converting global conformational changes into regulation of affinity. However, the high-affinity state of the $\beta 3$ integrin locked by a disulfide bond between the $\beta 6$ and $\alpha 7$ loop remains in the bent conformer. This suggests that $\alpha 7$ helix downward movement of the βI domain leading to the high-affinity states does not necessarily lead to extended conformers (Luo *et al.*, 2004).

It has been well known that divalent metal ions affect integrin activities, depending on concentrations and metal species. For examples, Mn^{2+} has a potent stimulatory effect on integrin activity, and Mg^{2+} and Ca^{2+} are stimulatory and inhibitory on lymphocyte integrins, depending on concentrations, respectively (Dransfield *et al.*, 1992; Shimizu and Mobley, 1993). The major sites of the modulatory effects of the divalent metals are in the βI domain. The βI domain contains a MIDAS (β MIDAS) centered between two other metal-binding sites, the adjacent MIDAS, ADMIDAS, and the ligand-induced metal-binding site, LIMBS (Xiong *et al.*, 2001). Ligand-binding activity of the βI domain is regulated by variable divalent cation occupancy. Occupation of the ADMIDAS in high Ca^{2+} decreases ligand binding, whereas replacement by competing Mn^{2+} activates ligand binding. Low Ca^{2+} , with Ca^{2+} occupancy at the LIMBS, may synergize with Mg^{2+} to support ligand binding (Chen *et al.*, 2003; Mould *et al.*, 2003a). A mutation of the LIMBS site in $\alpha 4\beta 7$ results in a low-affinity state, capable of supporting lymphocyte rolling, whereas mutation of the ADMIDAS results in a high-affinity state, supporting firm adhesion of lymphocytes (Chen *et al.*, 2003), suggesting that the ADMIDAS and LIMBS also have global effects on integrin bent/extension conformations.

4.6. Cytoplasmic Domain

Both α and β subunits have short cytoplasmic domains (Sastry and Horwitz, 1993). The cytoplasmic domains have categorically three functions: α/β heterodimer formation, signaling interface from the inside and outside, and integrin endocytosis/recycling. It is becoming clear that these functions may cross-talk in lymphocyte trafficking.

From the studies using soluble extracellular regions of integrins, a physical association of C-terminal regions induces or stabilizes bent conformations and its separation trigger the extension and affinity upregulation. The membrane proximal glycine-phenylalanine-phenylalanine-lysine-arginine (GFFKR) motif of the α subunit, referred to as the “hinge” domain, is conserved throughout all integrin families. This motif acts as a negative regulatory sequence suppressing

integrin adhesion (Hughes *et al.*, 1996); deletion of the motif converts inactive LFA-1 into constitutively active LFA-1 (Lu and Springer, 1997). The arginine in this GFFKR motif and an aspartic acid at the corresponding position in the β chain form a salt bridge, placing the α and β cytoplasmic regions in close juxtaposition. This may stabilize bent conformations of integrins, making adhesive activities low. Consistently, lymphocytes generated from “knock-in” mice expressing the α L subunit that lacks the GFFKR motif show higher basal adhesion levels than wild-type lymphocytes (Semmrich *et al.*, 2005). Deletion of the GFFKR motif also lowers surface amounts of LFA-1, but not other integrins members, supporting an important role of the GFFKR motif in heterodimer formation with the β 2 subunit (Lu and Springer, 1997). Thus, the GFFKR motif facilitates a heterodimer formation, which is a requisite process to transport an α/β heterodimer to cell surface as an inactive, perhaps bent conformer. On the other hand, regulatory functions through the GFFKR motif in inside-out signaling, or outside-in signaling are less clear, compared to its structural requirement for inactive integrin on cell surface. The LFA-1 that lacks the GFFKR motif still responds to inside-out signals including the TCR complex for attachment to ICAM-1, and activation of JNK or Erk is not altered on binding to ICAM-1 (Semmrich *et al.*, 2005). Interestingly, lymphocyte expressing LFA-1 that lacks the GFFKR motif is impaired in detachment on ICAM-1. This defect may underlie hypoplastic peripheral lymph nodes, and impaired humoral responses to T cell-dependent antigen and leukocyte recruitment into inflamed peritoneum (Semmrich *et al.*, 2005).

The integrin cytoplasmic domains play crucial roles in transmitting the inside-out signals to the extracellular domains as well as outside-in signals from ligand-bound I domains, through binding to cytoskeletal linker proteins and intracellular proteins to the distinct sites of the cytoplasmic domains (Calderwood, 2004; Liu *et al.*, 2000). The NPxY/F is well conserved in all β integrins and is shown to interact with an actin cytoskeleton linker protein, talin (Calderwood, 2004). In addition, phosphorylation of amino acids in the cytoplasmic domains is increased by inside-out signals or after ligand binding (Fagerholm *et al.*, 2004). Both α L and β 2 cytoplasmic phosphorylations are triggered by inside-out signals or modulates integrin functions (Fagerholm *et al.*, 2005; Hibbs *et al.*, 1991), perhaps through recruitment of binding proteins that recognize phosphorylated amino acids.

The integrin surface distribution is thought to be regulated by lateral diffusion through linkage of cytoplasmic domains to the cytoskeleton. Distinct conformations of LFA-1 are shown to have different surface mobility measured by single-particle tracking (Cairo *et al.*, 2006; Kucik *et al.*, 1996). Intracellular transport also plays an important role of integrin distribution. Integrins are endocytosed and recycled back between the plasma membrane

and intracellular pools. The critical role of the cytoplasmic domain is demonstrated for polarized endocytic recycle of $\alpha v \beta 3$ to the migrating front in neutrophils and fibroblasts (Jones *et al.*, 2006; Lawson and Maxfield, 1995). The mutation of the membrane proximal endocytosis motif Y735xx Φ (Φ , a bulky hydrophobic amino acid) of the human $\beta 2$ subunit inhibits internalization of LFA-1, and impairs detachment (Tohyama *et al.*, 2003) and transporting of LFA-1 to the ruffling membrane (Fabbri *et al.*, 1999), resulting in defective migration. Endocytic recycling pathways of LFA-1 are different from conventional clathrin-mediated pathways and depend on lipid raft (Fabbri *et al.*, 2005). The polarized redistribution of LFA-1 to the leading edge after chemokine stimulation is also inhibited by mutations of the αL cytoplasmic region after the GFFKR motif (Katagiri *et al.*, 2003). These mutations make LFA-1 in low-affinity bent conformations with a low exposure of a NKI-L16 epitope (Tohyama *et al.*, 2003), a legpiece extension reporter antibody that recognizes the interface the αL genu and thigh domains (Xie *et al.*, 2004). Thus, the cytoplasmic regions also have key roles in endocytosis and recycling of leukocyte integrins and link affinity/conformational changes with spatial regulation.

In summary, the extension and the hybrid domain- βI interface can act as flexible joints and may adopt distinct positions, each of which is likely to have a global effect on the overall ligand-binding affinity of the integrin. Integrin extension may affect cell adhesion through two distinct modes: accessibility to ligands by extending the head region into a position appropriate for recognition of extracellular ligands, and affinity to ligands by freeing the hybrid domain from the structural restraint. Association and separation of α/β cytoplasmic domains play regulatory roles in transmitting signals from inside-out and outside-in signals and also control integrin distribution coupled with cytoskeleton and endocytic recycling.

5. Integrin-Mediated Adhesion Steps in Lymphocyte Trafficking

It has been becoming apparent that chemokines and antigens play decisive roles in adhesive interactions with endothelial cells and APC. In this section, I focus the critical steps of lymphocyte trafficking from attachment and migration through endothelial venules to interactions with APC (Fig. 3), and discuss how lymphocyte adhesiveness is modulated by chemokines and antigens in terms of integrin affinity/conformation and spatial regulation.

5.1. Conversion of Rolling to Firm Adhesion by Chemokines

During entry into peripheral lymph nodes, naive T cells interact with HEV in a process involving sequential adhesion steps: (1) tether (capture) or roll on HEV through selectin-mediated interactions, (2) arrest (stop) mediated by

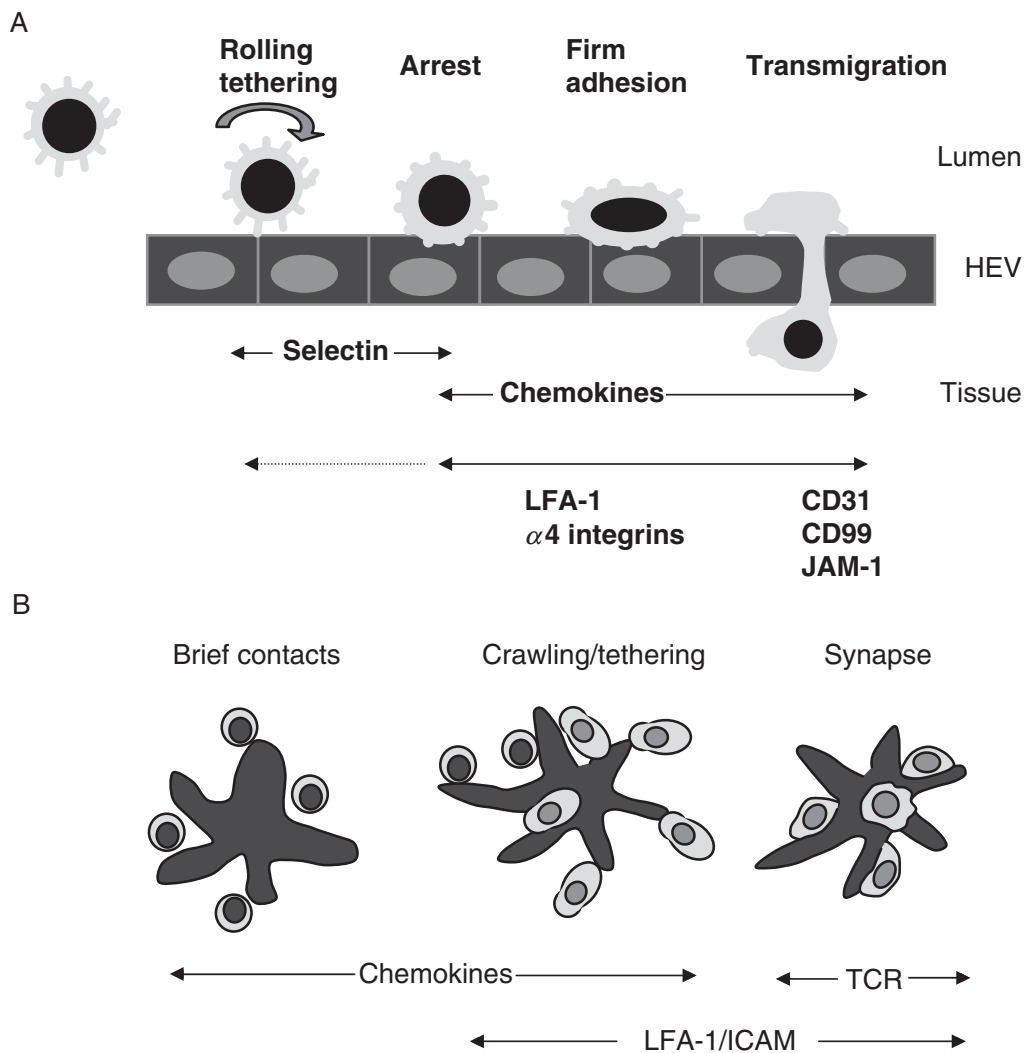


Figure 3 Integrin-mediated adhesive interactions of lymphocytes. (A) Adhesion cascades from rolling to transmigration. The weak interaction of selectins on lymphocytes with cognate sialyl glycoproteins on the vascular endothelium induces lymphocyte rolling/tethering. Chemokines associated with the apical surface of the endothelium activate the LFA-1/ α 4 integrins of rolling lymphocytes, augmenting their adhesiveness to ICAMs, MAdCAM-1, or VCAM-1 to mediate arrest (stop), followed by firm attachment. Attached lymphocytes migrate over the endothelium and transmigration through these layers, usually at intercellular junctions where junctional adhesion molecules such as CD31, CD99, or JAM-1 accumulate to mediate diapedesis. (B) Sequential steps of T-APC interactions. Migrating T lymphocytes transiently contacts with APC under guidance with chemokines, which may be associated with cell surface of APC. Chemokine-activated lymphocytes crawl over APC to scan cognate antigens. During this step, tethering of lymphocytes may be occurred through the uropod, depending on LFA-1 and ICAMs. Antigen recognition through TCR converts unstable adhesion to firm adhesion, leading to immunological synapse formations through LFA-1 and ICAM-1.

LFA-1 and $\alpha 4$ integrins on lymphocytes activated by chemokines through binding to ICAM-1 and MAdCAM-1 on the endothelium, and (3) diapedesis (transendothelial migration; Fig. 3A). Although rolling is facilitated by lymphocyte expression of L-selectin, with a minor contribution from LFA-1 and $\alpha 4$ integrins, LFA-1 and $\alpha 4\beta 7$ have major roles in the firm attachment of lymphocytes to HEVs of peripheral lymph nodes and Peyer's patches (Butcher *et al.*, 1999). Chemokines, including C-C-chemokine ligand 21 (CCL21), CXC-chemokine ligand 12 (CXCL12), and CXCL13 (Ebisuno *et al.*, 2003; Okada *et al.*, 2002; Stein *et al.*, 2000; Warnock *et al.*, 2000), localized on the apical endothelial surface rapidly increase integrin avidity, resulting in lymphocyte arrest. Since upregulation of lymphocyte adhesion by chemokines are transient and affinity changes likely occur in micromolar ranges, it is technically difficult to detect affinity modulation using conventional assays. Thus, it has been often controversial whether affinity modulation occurs in physiological contexts. Nonetheless, the modality of integrin avidity regulation in this step has been reported to involve both affinity and valency regulation. Stimulation of primary T cells with chemokines induces the patch-like clustering of LFA-1 and the microclustering of $\alpha 4\beta 1$, which correlate respectively with increased cellular adhesion to low-density ICAM-1 (Constantin *et al.*, 2000) and transient tethering and firm adhesion under shear flow (Grabovsky *et al.*, 2000). LFA-1 and $\alpha 4$ integrin affinity is also augmented by chemokine signaling (Chan *et al.*, 2003; Grabovsky *et al.*, 2000; Shimaoka *et al.*, 2006) and is important for lymphocyte homing to peripheral lymph nodes (Constantin *et al.*, 2000).

In terms of currently understood integrin conformations, the conformation mediating rolling appears to most closely correspond to lymphocyte integrins in an extended conformation with a low-affinity I domain, whereas the conformation that mediates arrest adhesion appears to most closely correspond to an extended conformation with an intermediate or high-affinity I domain. The experiments using K562 cells reconstituted LFA-1 carrying a locked αL I domain with either low, intermediate, or high-affinity state demonstrate that rolling adhesion occurs when extension of low-affinity LFA-1 is induced by the treatment with XVA143 and that the shift from low to intermediate affinity transforms rolling adhesion to firm adhesion in shear flow (Salas *et al.*, 2002, 2004, 2006). In neutrophil LFA-1, a shift from low to intermediate affinity stabilized by IC487475, an αL I domain allosteric antagonist, supports rolling, whereas high affinity is associated with shear-resistant leukocyte arrest (Green *et al.*, 2006). Thus, extension with affinity changes is thought to be a key step in transition of lymphocyte rolling to arrest triggered by chemokines.

Does chemokines actually induce extension of integrins and affinity changes during a shift from rolling? It has been shown that immobilized chemokines induce extended conformations under physiological shear flow, whereas

soluble chemokines do not (Shamri *et al.*, 2005). Immobilized chemokines induce lymphocyte $\beta 2$ legpiece extension recognized by a reporter antibody KIM127 (Robinson *et al.*, 1992; Xie *et al.*, 2004) with intermediate affinity changes under shear flow (Shamri *et al.*, 2005). The extension depends on Gi-coupled signaling, suggesting endothelial chemokines induce extension of LFA-1 with affinity changes in less than a second (Shamri *et al.*, 2005). This study proposes a model, in which extension of bent LFA-1 is the critical first step of lymphocyte arrest, making LFA-1 accessible to surface ICAM-1, leading to ICAM-1-induced high-affinity LFA-1 conformations and stabilization of cell adhesion under flow (Shamri *et al.*, 2005). The whole process occurs within a second at restricted sites on the lymphocyte surface and requires cooperation of inside-out and outside-in signaling.

To examine unbending more directly, conformational changes in cell surface $\alpha 4 \beta 1$ are probed using fluorescent resonance energy transfer (FRET) between an FITC-labelled ligand peptide donor and rhodamine B acceptors in the plasma membrane. Stimulation with Mn^{2+} induced a high affinity to ligand and placing the headpiece of the resting integrin near the membrane surface allows for an extension of the Mn^{2+} activated headpiece ~ 50 Å from the surface. This distance is approximately one-half that expected if the integrin molecule undergoes the conformational change from the fully folded to the fully extended conformation. The activation of the integrin by inside-out signaling through a G-protein-coupled receptor, resulting in the intermediate affinity, leads to the head region moving away from the surface by ~ 25 Å after stimulation by a chemoattractant. The distance change is correlated with ligand-binding affinity. The half-time corresponding the diminution of FRET due to activation of the integrin is less than 30 s. The results indicate that there is a coordination between extension of the ligand-binding headpiece away from the cell surface and affinity to ligand, and the fully extended conformation were not observed with this method. Although it could be possible that the extended-open conformations are not induced by inside-out signals alone, the fully extended conformation may exist at the moment of the engagement of the integrin by the natural endothelial ligand under shear flow. The transient bond formation in rolling would allow the forces to induce a molecular extension, and a ligand-bound I domain induces or stabilizes fully extended conformations with the open headpiece, resulting in arrest and firm adhesion (Shamri *et al.*, 2005).

Interestingly, a study using FRET technology demonstrates that separation of the αL and $\beta 2$ cytoplasmic regions occurs following chemokine stimulation and ligand binding (Kim *et al.*, 2003). This study indicates that separation of cytoplasmic regions occurs by inside-out and outside-in signaling and support the notion that chemokine-stimulated inside-out signals inhibit close associations of

α and β cytoplasmic regions, which likely releases a restraint on bent conformations and induce unbending of the extracellular domains to mediate lymphocyte arrest.

5.2. Transmigration

Given the presence of chemokines on the apical side of the endothelium, it is unlikely that a chemokine gradient across the endothelium stimulate transmigration of T cells *in vivo*. Thus, apical chemokines arrest rolling lymphocytes and subsequently stimulate cell motility over the endothelium. When migrating lymphocytes reach intercellular junctions, they begin diapedesis between apposed endothelial cells (Johnson-Leger *et al.*, 2000). β 1 and β 2 integrins are involved in transmigration step, in addition to adhesion molecules such as CD31, CD99, or JAM-1 (Muller, 2003). In addition, shear flow is required for efficient lymphocyte transmigration (Cinamon *et al.*, 2001). Lymphocyte transmigration needs apical chemokines and Gi-dependent signaling under shear flow conditions (Cinamon *et al.*, 2001). Requirement of shear stress in lymphocyte transmigration suggest a mechanosensitive regulatory process (Vogel and Sheetz, 2006) acting on migrating lymphocytes and endothelial barriers through activation of intracellular signaling such as focal adhesion kinases (Li *et al.*, 1997) and small GTPases (de Bruyn *et al.*, 2003; Tamada *et al.*, 2004). This may cause enhancement lymphocyte adhesion and motility in vertical directions, or modulation of junctional permeability.

In addition to paracellular pathways of transmigration, lymphocyte may migrate in a transcellular fashion (Carman and Springer, 2004), as reported in leukocytes *in vivo* (Feng *et al.*, 1998). During transcellular migration, cuplike-endothelial projections enriched for ICAM-1 and VCAM-1 surround leukocytes. β 2 and α 4 integrins are distributed in linear clustering patterns oriented parallel to the direction of diapedesis (Carman and Springer, 2004). Vimentin is also involved in transcellular machineries (Nieminen *et al.*, 2006). Apparently, transcellular migration does not require chemokine gradients, and arrested lymphocytes may go through endothelial barrier directly, perhaps skipping firm attachment and migration steps. Further studies are necessary using recent advances in imaging technology to address the site of lymphocyte transmigration *in vivo*.

5.3. Interstitial Migration in Lymphoid Tissues

In situ imaging techniques using multiphoton microscopy have revealed robust interstitial migration of naive lymphocytes into peripheral lymph nodes (Miller *et al.*, 2002), probably under the control of chemokines and

integrins. Lymphocyte migration behavior appears to be a random walk, but with spatial restrictions; the movement of T cells is confined to subcortical T cell areas and they are excluded from B cell follicles. The high motility of naive T cells enables them to encounter the rare population of antigen-presenting DCs that have migrated into draining lymph nodes from peripheral tissues. Specific targeting of lymphocyte migration to T cell areas depends on chemokines such as CCL21 and CXCL12, and migration to B cell follicles depends on CXCL13 (Moser *et al.*, 2004), and lymphocyte homing to splenic white pulp has been shown to depend on LFA-1 and $\alpha 4$ integrins (Lo *et al.*, 2003). Soluble chemokine gradients might direct lymphocyte migration to specific compartments through chemotaxis in lymphoid tissues. But there are little convincing data to indicate gradient distributions of chemokines *in vivo*. Chemokines are highly charged molecules and readily associated with extracellular matrix (ECM) proteins and cell surface via heparan sulfates or glycosaminoglycans, as seen in HEV (Miyasaka and Tanaka, 2004). Chemokines bound to ECM or cell surface of reticular stromal cells could guide lymphocyte interstitial migration in chemokinetic (migration dependent on nongradient chemoattractants) and haptokinetic (migration dependent on substrates) fashions, independently of chemokine gradients.

5.4. Interactions with APC

The transient activation of integrins by chemokines enables lymphocytes to scan for cognate antigen during brief contacts with APCs (Fig. 3B). LFA-1 activation by inside-out signaling is demonstrated for binding of T cells to ICAM-1 on stimulation with TCR ligation (Dustin and Springer, 1989). Once T cells recognize cognate antigen through peptide–MHC ligation of the TCR, a dynamic redistribution of TCR and LFA-1 to the contact site occurs within minutes (Grakoui *et al.*, 1999); LFA-1 then translocates from the center of the contact site to the periphery, accompanied by the reciprocal movement of the TCR complex. These events lead to the formation of a stable adhesion termed immunological synapses (IS), or supramolecular activating clusters (SMACs), a characteristic structure in which an external LFA-1 ring surrounds central TCR clusters (cSMAC; Monks *et al.*, 1998). In the peripheral SMAC (pSMAC), ICAM-1-engaged LFA-1 is colocalized with talin, and likely takes extended conformations. Thus, segregation of LFA-1 to the peripheral is structurally relevant distribution so that large extracellular domains of LFA-1 and ICAM-1 do not sterically hinder relatively small TCR and antigen–peptide–MHC complex, allowing stable antigen recognition (Sims and Dustin, 2002). However, the mechanisms underlying the SMAC, especially how LFA-1 molecules are redistributed as a ring remains elusive.

It is becoming clear that T cells, particularly naive cells are activated during short contacts with antigen peptide-MHC bearing APC. For example, T cells in a collagen matrix stop very infrequently but still get activated and proliferate (Gunzer *et al.*, 2000). Multiphoton scanning laser microscopy have shown that after encountering APC-presented cognate antigen *in vivo*, T cells undergo distinct changes in their adhesion patterns (Bousso and Robey, 2003; Mempel *et al.*, 2004; Miller *et al.*, 2004): initial short-lived contacts with antigen-presenting DCs followed by the formation of stable T cell-APC conjugates, which eventually lead to autonomous T cells migration and cell division. Integrins and intracellular signaling from receptors for chemokines and antigens likely regulate these changes in T cell behavior after activation (Friedman *et al.*, 2005). It has been recently demonstrated that CCL21 is bound to cell surface of CD11c⁺ dendritic APC (Friedman *et al.*, 2006). Interestingly, chemokines bound to APC stimulate the initial short-lived interactions of lymphocytes via LFA-1 and ICAMs, and enhances the subsequent formations of an antigen-dependent stable adhesion. During initial contacts, a T cell moves over a chemokine-bound APC, which often results in tethering at uropod, while the leading edge is active and the cell often appears to crawl away from the APC. The uropod tethering occurs depending on LFA-1 and ICAMs. When the leading edge subsequently engages with antigen-bearing cell surface of the same (*in cis*) or a neighboring cell (*in trans*), the uropod tether rapidly released, concomitant with initiation of Ca²⁺ influx and IS formation, indicating antigen recognition and activation (Friedman *et al.*, 2006). The initial transient interaction and tethering may help keep lymphocytes in proximity to APC until LFA-1 is sufficiently activated. Antigen engagement triggers TCR-mediated inside-out signals and further stabilizes attachments and initiates IS formation (Fig. 3B). Thus, this two-step “tether-to-synapse” dynamic is mediated by sequential activation of LFA-1 by surface-bound chemokines and cognate antigens and may correspond to a transition from a “swarming” pattern of lymphocyte interactions with antigen-bearing APC to stopping and IS formation *in vivo* (Miller *et al.*, 2004).

6. Talin as Intracellular Regulator for Lymphocyte Adhesion and Migration

Talin is a 250-kDa cytoskeletal protein that links integrins and the actin cytoskeleton (Horwitz *et al.*, 1986). It is a component of focal adhesion complexes in fibroblasts (BurrIDGE and Connell, 1983). Talin has an additional function in regulating cadherin gene expression, which is independent of integrins (Becam *et al.*, 2005). Talin is localized in the leading edge of chemokine-stimulated lymphocytes (Foger *et al.*, 2006; Gomez-Mouton *et al.*, 2001) and in immunological synapse (Monks *et al.*, 1998). In addition to linking integrins

with actin cytoskeleton, it has been proposed that talin serves as inside-out signals (Calderwood, 2004). Talin has an N-terminal integrin-binding FERM (4.1 ezrin, radixin, moesin) domain and a C-terminal actin-binding tail domain and serves as a linker between integrins and actin cytoskeleton. The FERM domain contains a region that directly associates with the NPXY/F motif, which is conserved in the β chains of most integrins (Calderwood, 2004). Overexpression of this domain activates β_1 , β_2 , and β_3 integrins (Calderwood *et al.*, 1999; Kim *et al.*, 2003). Knockdown of talin by small interference RNA inhibits β_3 integrin activation (Tadokoro *et al.*, 2003). Proteolytic cleavage of talin by calpain produces talin head fragments (Yan *et al.*, 2001). Separation of the cytoplasmic domains of $\alpha_L\beta_2$ is detected by FRET by overexpression of the talin head (Kim *et al.*, 2003). Thus, generation of this talin fragment potentially serves as an inside-out signal to modulate LFA-1 affinity by separation of LFA-1 cytoplasmic domains. However, it was reported that calpain inhibitors reduce TCR-stimulated LFA-1-mediated adhesion of lymphocytes to ICAM-1 (Stewart *et al.*, 1998). But this study did not focus on either talin cleavage or affinity regulation of LFA-1. Rather it was proposed that calpain induced release of LFA-1 from a cytoskeletal restraint that prevents lateral diffusion and clustering. Thus, the result was interpreted in terms of valency regulation. In support of a negative function for talin, LFA-1 is constitutively associated with talin in resting neutrophils, but after activation LFA-1 dissociates from talin and associates with α -actinin (Sampath *et al.*, 1998). Furthermore, treatment with a low dose of cytochalasin D, which inhibits actin polymerization, upregulates integrin surface diffusion and adhesion (Kucik *et al.*, 1996). Latrunculin A, which also prevents actin polymerization by binding to actin monomers, increases rolling and firm adhesion by LFA-1 (Salas *et al.*, 2002). Although talin and actin cytoskeletons are important in postadhesion events by strengthening of adhesion complex or cell migration (Smith *et al.*, 2005), cleavage of talin is not involved in transition from rolling adhesion to firm adhesion (Constantin *et al.*, 2000; Shamri *et al.*, 2005). Knockdown of talin lowers chemokine-triggered lymphocyte interactions to low-density, but not high-density ICAM-1 in shear flow, indicating an important role of talin in adhesion strengthening (Shamri *et al.*, 2005).

Interestingly, in migrating lymphocytes ICAM-1-engaged, high-affinity conformations of LFA-1 recognized by mAb24 is localized in the midbody area termed focal zone and colocalized with talin (Smith *et al.*, 2005). Internal reflection microscopy shows that a cell attaches strongly in the focal zone and to a lesser extent at the leading edge, but not in the uropod. Thus, this suggests that LFA-1 affinity/conformation changes are spatially regulated: high in the focal zone, low in the uropod, perhaps intermediate in the leading edge. ICAM-1-engaged, high-affinity LFA-1 is low mobility on the cell surface,

suggesting a linkage of this subpopulation of LFA-1 to cytoskeleton via talin. This study shows that the LFA-1–talin complex formation is required for efficient migration on ICAM-1 (Smithi, 2005).

7. Intracellular Signals in Chemokine-Induced Adhesion and Migration

Chemokines activate multiple signaling pathways, including the phosphatidylinositol 3-kinase (PI3K), phospholipase C (PLC), Ras/Rho family of small GTPases, and mitogen activated protein (MAP) kinase cascades, each of which has been implicated in the inside-out signaling cascades that control integrin affinity and valency regulation and the associated changes in cytoskeleton, cell polarity, and morphology, which regulate lymphocyte migration (Fig. 4).

7.1. PI3K Pathways

PI3K plays a crucial role in chemotaxis or directed migration along a chemokine gradient (Ward, 2004). Experiments using PI3K inhibitors have shown that inhibition of PI3K activity blocks chemokine-triggered LFA-1 clustering and adhesion to low density ICAM-1. However, treatment with PI3K inhibitors did not block adhesion to high density ICAM-1 or *in vivo* lymphocyte homing

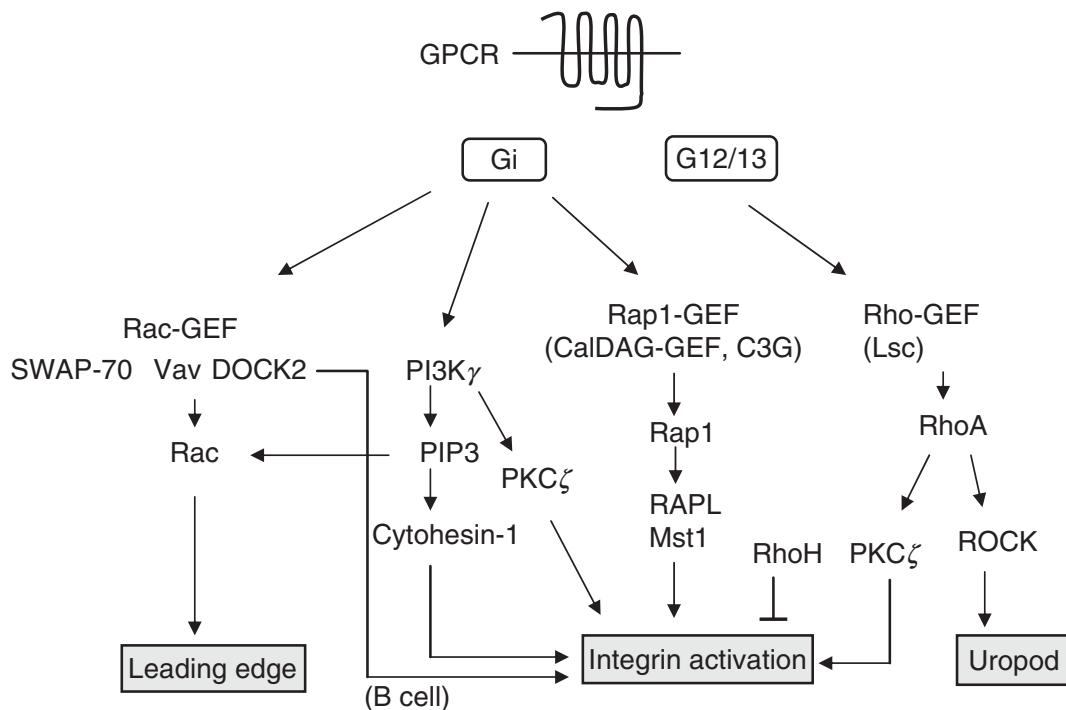


Figure 4 GPCR-triggered signals lead to integrin activation and development of the leading edge and uropod structures.

(Constantin *et al.*, 2000). Therefore, whereas it is clear that activation of PI3K can function in inside-out signaling following ligation of costimulatory molecules (Shimizu *et al.*, 1995; Zell *et al.*, 1996) or activation of c-kit (Kinashi *et al.*, 1995), and that a constitutively active form of the PI3K α catalytic subunit increases ligand-binding affinity and the observed conformational changes in LFA-1 (Katagiri *et al.*, 2000), the contribution of PI3K signaling pathways to integrin activation by chemokines remain ill-defined. Indeed, although PI3K is required for efficient chemotaxis of myeloid cells (Hirsch *et al.*, 2000; Li *et al.*, 2000) and lymphocytes (Reif *et al.*, 2004), studies using gene targeting of the catalytic subunits of PI3K γ , PI3K δ , or other isoforms did not show any defects indicative of reduced integrin function (Nombela-Arrieta *et al.*, 2004; Okkenhaug and Vanhaesebroeck, 2003). These results suggest that PI3K is critical in directional sensing but does not play a major role in integrin activation in lymphocytes.

Cytohesin-1, isolated in a yeast two-hybrid screen using the β 2 integrin cytoplasmic region as bait (Kolanus *et al.*, 1996), has a plekstrin homology (PH) domain that binds to phosphatidylinositol (3,4,5) triphosphate (PIP3). This protein also functions as a guanine exchange factor (GEF) for members of the ADP ribosylation factor (ARF) family of GTPases (Meacci *et al.*, 1997). Overexpression and mutational analyses showed that cytohesin-1 upregulates LFA-1 adhesion through valency modulation in a manner dependent on the PH domain and its association with LFA-1. These experiments indicate a role for cytohesin-1 in leukocyte arrest and transmigration, which also requires the actin regulator ARF6 (Weber *et al.*, 2001). Cytohesin-1 is reportedly involved in outside-in signaling pathways leading to MAP kinase activation (Perez *et al.*, 2003); however, its physiological function as an inside-out signaling molecule has yet to be demonstrated *in vivo*.

7.2. Rho Pathways

RhoA is involved in lymphoid polarization and chemotaxis (Sanchez-Madrid and del Pozo, 1999). Rho signaling is thought to be critical in both chemokine-triggered LFA-1 activation and LFA-1 mediated lymphocyte homing *in vivo* (Constantin *et al.*, 2000; Laudanna *et al.*, 1996). In a transgenic mouse model, a constitutively active mutant of RhoA increase basal adhesion of thymocytes and peripheral lymphocytes to VCAM-1, ICAM-1, and fibronectin (Vielkind *et al.*, 2005). The distinct RhoA effector regions differentially modulate LFA-1 affinity and valency regulation by chemokines (Giagulli *et al.*, 2004). For example, the high-affinity form of LFA-1 induced by chemokines is inhibited by the peptide containing RhoA amino acids 24–40, which also impairs lymphocyte adhesion to high-density ICAM-1 and *in vivo* homing to Peyer's

patches HEVs. Chemokine-stimulated PKC- ζ kinase activity and its translocation to the plasma membrane depends on PI3K partially and the RhoA 24–40 effector region, respectively. ROCK, a serine/threonine kinase effector molecule of RhoA, is ruled out in these processes using specific inhibitors. The effector molecule interacting with the RhoA 24–40 region responsible for the generation of high affinity LFA-1 or PKC- ζ translocation has not yet been identified.

Rho signaling also has a negative role in integrin-mediated adhesion. RhoA is required to retract the tail of the migrating lymphocytes and monocytes through ROCK (Smith *et al.*, 2003; Worthyake *et al.*, 2001). Inhibition of RhoA or ROCK increases LFA-1-mediated adhesion through valency modulation in human T cells (Rodriguez-Fernandez *et al.*, 2001). Lsc, a murine homologue of human p115 Rho GEF, is specifically expressed in hematopoietic-lineage cells and is shown to be critical in lymphocyte motility and antigen responses (Girkontaite *et al.*, 2001; Rubtsov *et al.*, 2005). Lsc-deficient B cells, especially a marginal zone B (MZB) cells display enhanced chemotactic responses to serum and sphingosine 1-phosphate (S1P), but not chemokines. Furthermore, S1P-induced attachment to ICAM-1 and VCAM-1 is increased in Lsc-deficient MZB cells, which display defective detachment at the trailing edge (Rubtsov *et al.*, 2005). The chemotactic response of MZB cells to S1P is largely mediated by S1P₃ (Cinamon *et al.*, 2004), a seven transmembrane receptor coupled with Gi as well as G13 and Gq (Windh *et al.*, 1999); the latter two activate RhoA (Sah *et al.*, 2000). Lsc contains a regulator of G-protein signaling (RGS) domain that downmodulates heterotrimeric G-proteins, especially G α 13 (Hart *et al.*, 1998; Kozasa *et al.*, 1998). Lsc deficiency may result in sustained activation of G α 13 and impaired Rho activation at the trailing edge. Thus, “wiring” of Rho signaling to upstream and downstream elements may vary in distinct subcellular regions, generating positive and negative influences on integrin-mediated adhesion and migration.

7.3. Rap1 Pathways

The small GTPase Rap proteins have emerged as an important regulator of integrin adhesiveness (Bos *et al.*, 2001). The Rap1 family consists of two highly homologous *rap1a* and *rap1b*, and two related *rap2* genes. Constitutively active mutants of Rap1A and Rap1B potently increase β 1, β 2, and β 3 integrin (Bertoni *et al.*, 2002; Caron *et al.*, 2000; Katagiri *et al.*, 2000; Reedquist *et al.*, 2000; Sebzda *et al.*, 2002). Rap2 is also stimulatory in B cell migration (McLeod *et al.*, 2002). Rap1 is activated by the chemokines CCL21, CXCL12, CXCL13 (Durand *et al.*, 2006; McLeod *et al.*, 2002; Shimonaka *et al.*, 2003). Inhibition of Rap1 abrogates chemokine-stimulated adhesion mediated by LFA-1 and VLA-4

(Shimonaka *et al.*, 2003), indicating an important role for Rap1 in inside-out signaling triggered by chemokines. Rap1 activation is also required for a chemoattractant S1P (Rosen and Goetzl, 2005) to induce B cell migration and adhesion to ICAM-1 and VCAM-1 (Durand *et al.*, 2006).

Rap1 upregulates ligand-binding affinity to soluble dimeric ICAM-1-Fc and induces extended conformations of LFA-1 detected with NKI L-16 mAb (Katagiri *et al.*, 2000; Reedquist *et al.*, 2000; Tohyama *et al.*, 2003) and also stimulates LFA-1 clustering (Katagiri *et al.*, 2003; Sebzda *et al.*, 2002). Activated Rap1 also robustly stimulates lymphocyte migration on ICAM-1 and transendothelial migration under shear flow (Shimonaka *et al.*, 2003). The adhesion-stimulatory effect of Rap1 requires the α L cytoplasmic domain, especially, the lysine residues at positions 1097 and 1099 after the GFFKR motif; replacement of these lysines with alanines suppressed the increases in LFA-1 affinity and the accompanying conformational changes impairs LFA-1 activation on stimulation with chemokines or TCR cross-linking (Tohyama *et al.*, 2003), emphasizing the physiological importance of this region in transmitting inside-out signals to the extracellular region.

In agreement with the proposed importance of Rap1 in chemokine-mediated integrin activation, defective regulation of Rap1 occurs in Epstein-Barr virus (EBV)-transformed lymphocytes derived from some patients with LAD (Kinashi *et al.*, 2004). Although Rap1 activation by chemokines is a pertussis toxin-sensitive Gi/o-dependent process (Shimonaka *et al.*, 2003), regulatory processes to trigger Rap1 activation including GDP/GTP exchange factors are not clear. A Rap1 exchange factor CalDAG-GEFI and Rap1b are critically important for platelet aggregation and thrombus formation via α IIB β 3 (Chrzanowska-Wodnicka *et al.*, 2005; Crittenden *et al.*, 2004), but their importance on leukocyte trafficking are not reported.

Chat-H, a hematopoietic-specific isoform of a Cas family protein (Sakakibara *et al.*, 2003), is shown to be involved in Rap1 activation by chemokines in lymphocytes (Regelmann *et al.*, 2006). Knockdown of Chat-H by lentivirus-mediated RNA interference impairs chemokine-stimulated Rap1 activation and adhesion mediated by LFA-1. Chat-H deficient lymphocytes are also defective in lymphocyte trafficking to peripheral lymph nodes. Chat-H localization with the plasma membrane and association with an adaptor protein CasL are required for T cell migration. Chat-H knockdown neither affects Rac activation by chemokines nor impairs Rap1 activation by TCR ligation (Regelmann *et al.*, 2006). Chat-H may act as a critical signaling molecule upstream of Rap1 to regulate chemokine-induced adhesion and migration.

A Rap1-binding protein, RAPL (regulator of adhesion and cell polarization enriched in lymphoid tissues) is isolated in a yeast two-hybrid screen using Rap1V12 as bait (Katagiri *et al.*, 2003). RAPL possesses a central Ras/Rap

association (RA) domain, which has a protein-interacting coiled-coil region at the C-terminus. RAPL is an alternatively spliced form of *Rassf5* (also known as *Nore1*), which belongs to the *Rassf* tumor suppressor family (Tommasi *et al.*, 2002). RAPL, which is highly expressed in lymphocytes, binds to active Rap1-GTP, but not inactive Rap1-GDP, and associates with Rap1 on lymphocyte stimulation with CXCL12 or following TCR ligation, and overexpression of RAPL was shown to increase LFA-1 avidity by both affinity and valency modulation (Katagiri *et al.*, 2003). Activated Rap1 or RAPL overexpression also induces cell polarization similar to that seen in chemokine-stimulated lymphocytes, showing membrane ruffling at one end (the leading edge) and formation of a uropod at the rear. Furthermore, RAPL forms a complex with LFA-1, the formation of which is dependent on Rap1 activation as well as the presence of lysines 1097 and 1099 in the α L chain. The association of RAPL and LFA-1 is spatially regulated; on stimulation with chemokines or the introduction of activated Rap1, RAPL associates with LFA-1 and relocates to the leading edge, forming large patch-like clusters (Katagiri *et al.*, 2003). Thus, affinity and valency modulations by Rap1 and RAPL are concurrent and coordinated with cell polarization. This result is further supported by studies of lymphocytes derived from RAPL-deficient mice (Katagiri, 2004a); RAPL-deficient T and B cells were defective in chemokine-stimulated adhesion, a process dependent on LFA-1 and VLA-4. These cells exhibited poorly polarized morphology and minimal LFA-1 clustering. Studies of RAPL-deficient mice have also shown a crucial role for RAPL in other integrin-dependent processes controlled by chemokine stimulation, such as the trafficking of lymphocytes and DCs to peripheral lymph nodes and the spleen (Katagiri, 2004). Recently, mammalian Ste20-like kinase MST1/STK4 is identified as a critical effector of RAPL. RAPL regulates the localization and kinase activity of Mst1 (Katagiri *et al.*, 2006). Knockdown of Mst1 demonstrates its requirement for the induction of both a polarized morphology and integrin LFA-1 clustering and adhesion triggered by chemokines and TCR ligation. RAPL and Mst1 localize to vesicular compartments and dynamically translocate with LFA-1 to the leading edge on Rap1 activation, suggesting the regulatory role of RAPL-Mst1 complex in intracellular transport of LFA-1 (Katagiri *et al.*, 2006).

Rap1-interacting adaptor molecule (RIAM also known as RARPI; Inagaki *et al.*, 2003) is isolated by yeast two-hybrid screening with an active Rap1 mutant as bait (Lafuente *et al.*, 2004). RIAM is a proline-rich 100-kDa protein bearing RA and PH domains. RIAM interacts with the active Rap1 mutant but not H-Ras mutant in two-hybrid assays. RIAM interacts with actin-regulating enabled (Ena)/vasodilator-stimulated phosphoprotein (VASP) proteins and profilin, and belongs to the MRL (Mig10/RIAM/Lamillipodin) family of proteins (Legg and Machesky, 2004). Overexpression of RIAM-induced conformational

changes of $\beta 1$ and $\beta 2$ integrins and augmented cell spreading and adhesion of Jurkat T cells to fibronectin and ICAM-1. Knockdown of RIAM expression by RNA interference reduces levels of polymerized actin and impairs Rap1-induced adhesion. Interestingly, RIAM knockdown displaces active Rap1 from the plasma membrane. Actin polymerization by RIAM required Ena–VASP interactions, but the pro-adhesive effect does not require these interactions, suggesting that actin polymerization is not involved in integrin activation. RIAM is also shown to enhance talin-dependent $\alpha \text{IIb}\beta 3$ activation (Han *et al.*, 2006). It is not known whether RIAM regulates integrin-mediated lymphocyte adhesion by chemokines or TCR.

A murine orthologue of human RIAM is independently identified by cross-reactivity of an antibody that binds a proline-rich sequence of zyxin, and termed proline-rich EVH1 ligand 1 (PREL1; Jenzora *et al.*, 2005). PREL1 modestly associates with an active H-Ras mutant, but not other Ras/Rho family members, including Rap1 by pulldown assays using the RA domain of PREL1, or coimmunoprecipitation with the full-length PREL1. PREL1 is shown to relocate to the tips of circular lamellipodia and focal adhesion, and colocalized with VASP transiently in a time course similar to that of H-Ras activation (Jenzora *et al.*, 2005). Although the discrepancy regarding the specificities of small GTPases to which RIAM and PREL1 interact is not clear, the conserved function of RIAM and PREIL appears to translocate and activate actin-remodeling machineries. Further studies are required to clarify the relationship of RIAM/PREL1 and Rap1-regulated adhesion.

7.4. Rac Pathways

The deletion of both Rac1 and Rac2 genes leads to a massive egress of hematopoietic stem/progenitor cells (HSC/Ps) into the blood. HSC/Ps deficient for Rac1 and Rac2 displays decreased adhesion to fibronectin, defective chemotaxis to CXCL12, and a failure of bone marrow engraftment (Gu *et al.*, 2003), suggesting a critical role of Rac1 and Rac2 in integrin-mediated stem cell adhesion. Rac2-deficient leukocytes are defective in shear-dependent L-selectin-mediated capture on Glycam-1 as well as F-actin generation, and chemoattractant-stimulated MAP kinase activation (Roberts *et al.*, 1999). Neutrophils deficient for both Rac1 and Rac2 show normal integrin-mediated adhesion but markedly reduced migration and defective cell spreading (Gu *et al.*, 2003). The effects of Rac deficiency on lymphocytes trafficking has not been described yet.

DOCK2, a hematopoietic-specific member of the CDM (Ced-5, DOCK180, Myoblast city) family of proteins, regulates Rac activation in lymphocytes (Fukui *et al.*, 2001). Deficiency in DOCK2 severely impairs Rac1 and Rac2 activation and

defective development of the actin cytoskeleton in lymphocytes and neutrophils stimulated by chemokines (Fukui *et al.*, 2001; Kunisaki *et al.*, 2006; Sanui *et al.*, 2003). As a consequence, both *in vitro* lymphocyte chemotactic responses and *in vivo* trafficking to peripheral lymphoid organs are severely diminished in these mice (Nombela-Arrieta *et al.*, 2004). DOCK2 deficiency differentially affects integrin activity in T and B cells; adhesive responses to chemokines and phorbol esters through LFA-1 and $\alpha 4$ integrins are diminished in B cells, but not in T cells (Nombela-Arrieta *et al.*, 2004). This effect was also observed *in vivo* using intravital microscopy to show that firm attachment to peripheral lymph node venules was only impaired for B cells. Changes in affinity for ligand, however, is not observed in DOCK2-deficient B cells. Furthermore, as LFA-1 clustering occurs normally in CXCL13-stimulated B cells, it remains unclear if DOCK2 deficiency affects integrin function directly. In *in vitro* experiments, DOCK2-deficient T cells are normal in arrest and firm attachment but defective in lateral lymphocyte motility before and after transendothelial migration under flow (Shulman *et al.*, 2006). Since actin polymerization triggered by chemokines is defective in both T and B cells from DOCK2-deficient mice (Fukui *et al.*, 2001; Shulman *et al.*, 2006), but the integrin defect was seen only in DOCK2-deficient B, it is possible that actin polymerization is not an effector executing lymphocyte integrin activation. Instead, DOCK2 may serve a regulatory role controlling Rac activation or a cytoskeleton-independent function, which could affect other inside-out signaling molecules in a B cell-specific manner. Further investigation to clarify the defect in B cell integrins activation will provide insight into lineage-specific integrin modulation.

Vav1, a hematopoietic exchange factor for Rac is activated by CXCL12 (Vicente-Manzanares *et al.*, 2005) in human peripheral blood lymphocytes, and overexpression of a dominant-negative form of Vav1 abolish lymphocyte polarization, actin polymerization, and migration. In one study (Garcia-Bernal *et al.*, 2005), Vav1 and Rac are shown to be a critical role in CXCL12-triggered $\alpha 4\beta 1$ integrin activation to mediate VCAM-1-dependent attachment of Molt4 and primary T cells under static and shear flow conditions. Vav1 is also shown to be involved in LFA-1 activation by TCR (Krawczyk *et al.*, 2002) (see below). In contrast, neutrophils deficient for both Vav1 and Vav3, major isoforms expressed in neutrophils, are shown to be normal in chemotaxis and attachment on ICAM-1 under shear flow or on inflamed venule *in vivo* but are defective in stable attachment and spreading (Gakidis *et al.*, 2004). Activation of Rac1 and Rac2 by a chemoattractant f-MLP are normal in Vav1/Vav3-deficient neutrophils, but signaling through $\alpha M\beta 2$ to activate protein kinases including PAK are severely diminished, indicating a prominent role of Vav proteins in outside-in signaling (Gakidis *et al.*, 2004).

SWAP-70 is a B-cell specific Rac exchange factor that binds to PIP3 and F-actin through a PH domain and C-terminal region, respectively (Ihara *et al.*, 2006; Shinohara *et al.*, 2002). SWAP-70-deficient mice does not show any abnormalities in homeostatic lymphocyte trafficking. However, lymphocyte migration to inflamed lymph nodes is reduced (Pearce *et al.*, 2006). SWAP-70-deficient B blasts show impairment in cell polarization displaying defective uropod formation and enhanced cell spreading on anti-CD44 antibody cross-linking. Although chemokine-stimulated adhesive responses to ICAM-1 and MAdCAM-1 are normal, lymphocyte polarization of SWAP-70-deficient B cells by chemokines is also impaired with enhanced cell spreading. SWAP-70-deficient B cells normally adhere to HEV but do not enter into lymph node tissues efficiently (Pearce *et al.*, 2006). Since SWAP-70 is shown to modulate a transitional subset of actin filaments in fibroblastic motile cells (Hilpela *et al.*, 2003), SWAP-70 may have a similar role in B cells and control lymphocyte polarization and migration that is necessary during diapedesis.

Coronin1, an inhibitory protein opposing actin-polymerizing Arp2/3, has important roles in T cell morphology and migration (Foger *et al.*, 2006). Coronin1-deficient mice display reduced T cell numbers in peripheral blood and lymph nodes and spleens. Coronin1-deficient T cells do not develop chemokine-stimulated polarized cell shapes with talin segregation to the leading edge. Moreover, steady-state F-actin is reduced and Rac1 activation by chemokine stimulation is diminished. Consequently, coronin1-deficient T cells are defective in chemotaxis and reduced trafficking to peripheral lymph nodes (Foger *et al.*, 2006), but it is not reported whether coronin1 modulate integrin functions.

7.5. RhoH

The small GTPase RhoH is identified as a negative regulator of LFA-1 avidity (Cherry *et al.*, 2004). Gene inactivation of *RHOH* by insertional mutagenesis or knockdown of mRNA expression with *RHOH*-specific siRNA induces constitutive activation of LFA-1 and the structural changes associated with high-affinity or extended LFA-1 conformations (Cherry *et al.*, 2004). Inactivation of *RHOH* also activates $\alpha 4\beta 1$. These findings strongly suggest that the low adhesive state of lymphocyte integrins is actively controlled and maintained by RhoH. RhoH is a leukocyte-specific inhibitory Rho family member known to suppress the effects of Rac, Cdc42, and RhoA on nuclear factor- κ B, or p38 MAP kinase activation. This protein does not appear to have an effect on assembly of the actin cytoskeleton induced by activated RhoA or platelet-derived growth factor (PDGF; Li *et al.*, 2002), but reduced CXCL12-stimulated F-actin and chemotaxis, and also impairs proliferation of HSC and Rac

activation by stem cell factor (Gu *et al.*, 2005). Although RhoH is a member of the Ras superfamily of small GTPases, it is GTPase-deficient and constitutively in the active GTP-bound form. It is therefore tempting to speculate that RhoH protein levels could set a default basal level of integrin activity in resting lymphocytes.

8. Inside-Out Signaling Events in TCR-Stimulated Lymphocytes

Once T cells recognize cognate antigen through peptide–MHC ligation of the TCR, transient, unstable adhesion to APC transforms sustained, firm adhesion, concomitant with dynamic redistribution of TCR and LFA-1 to the contact site; LFA-1 then translocates from the center of the contact site to the periphery, accompanied by the reciprocal movement of the TCR complex, forming a mature IS. The molecular basis of inside-out signaling by TCR has been intensively examined, implicating Tec tyrosine kinases, Vav1, ADAP (Fyb/SLAP130), and Rap1-RAPL, PDK1 as inside-out signaling molecules triggered by TCR engagement (Fig. 5).

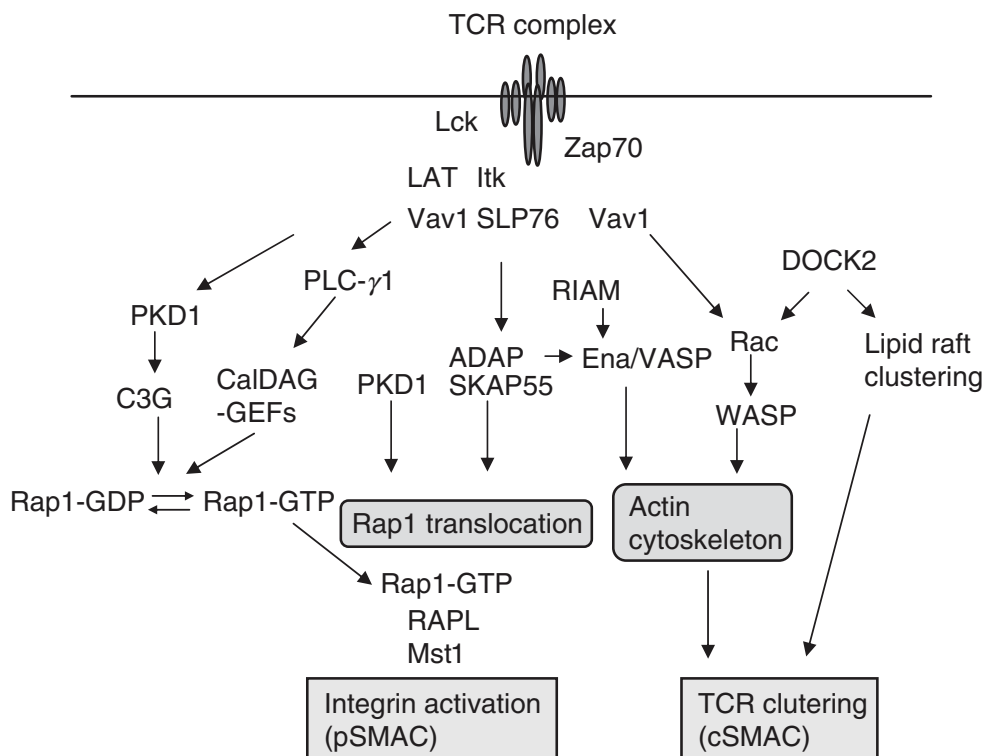


Figure 5 TCR-triggered signals, leading to integrin activation, actin cytoskeleton, and TCR clustering, also lead to the development of the peripheral (pSMAC) and central (cSMAC) SMACs.

8.1. Tec Family Kinases

The Tec family kinases Itk, Rlk, and Tec are important mediators of TCR signaling pathways that regulate T cell activation and differentiation (Lucas *et al.*, 2003). For example, TCR-triggered Itk activation stimulates β 1 integrin-dependent T cell adhesion, which requires PI3K-dependent Itk membrane localization and kinase activity (Woods *et al.*, 2001). Itk activation also induces actin polymerization triggered by TCR ligation (Woods *et al.*, 2001) or chemokine stimulation (Takesono *et al.*, 2004). Consistent with this, T cells from Itk^{-/-} mice are defective in IS formation, adhesion through β 1 and β 2 integrins, calcium flux, and actin polymerization (Labno *et al.*, 2003). Itk has also been shown to be required for chemokine-stimulated lymphocyte migration (Fischer *et al.*, 2004), and adhesion of chemokine-stimulated Itk^{-/-} thymocytes to fibronectin was impaired, indicating that Itk is also involved in integrin regulation by chemokines (Fischer *et al.*, 2004). Mechanistically, Itk is shown to be required for activation of WASP and Cdc42 at the IS, likely explaining the defect in actin polymerization and IS formation in Itk-deficient T cells (Labno *et al.*, 2003). However, since WASP deficiency does not affect integrin activation (Krawczyk *et al.*, 2002), defective actin polymerization is not likely a cause of impaired integrin activity in Itk^{-/-} T cells. In contrast, Itk is important in formation of the LAT, Vav1, and SLP-76 signaling complex and activation of PLC γ -1 (Lucas *et al.*, 2003), indicating that inside-out signaling triggered by Itk is mediated by these downstream elements.

8.2. Rac Signaling Pathways

The importance of Vav1 in LFA-1 activation is demonstrated by gene targeting (Krawczyk *et al.*, 2002). Vav1-deficient thymocytes and peripheral T cells show impaired TCR-dependent LFA-1 activation and IS formation, concurrent with both defective actin cytoskeleton assembly and TCR clustering. In addition, Vav1-deficient thymocytes and T cells exhibit deficiencies in TCR-triggered calcium flux and PLC γ -1 and PI3K activation, leading to inhibition of T cell and thymocyte growth and differentiation (Tybulewicz *et al.*, 2003). These pleiotropic defects in Vav1-deficient mice make it difficult to identify the signaling molecule downstream of Vav1 crucial for LFA-1 activation. As Vav1 is a GEF for Rho family GTPases, especially Rac, it was thought that defects in the actin cytoskeleton in Vav1-deficient T cells impaired LFA-1 function. However, deficiency in the Rac effector WASP affects only TCR clustering, and not LFA-1 activation, indicating distinct pathways control LFA-1 and TCR surface distribution (Krawczyk *et al.*, 2002). This conclusion is further supported by studies with DOCK2-deficient lymphocytes, which demonstrate

impaired clustering of TCR molecules. In contrast, DOCK2 deficiency had little effect on the formation of the LFA-1 ring, suggesting that the actin cytoskeleton is dispensable for LFA-1 ring formation (Sanui *et al.*, 2003).

8.3. Rap1 Signaling Pathways

Although previous studies have indicated that enhanced Rap1 activity is associated with T cell anergy (Boussiotis *et al.*, 1997), Rap1 has been shown to positively regulate LFA-1 avidity and T cell–APC conjugate formation (Katagiri *et al.*, 2002). Consistently, disruption of the *rap1a* gene reduced Rap1 activation by TCR ligation concomitant with modestly impaired LFA-1 clustering and adhesion (Duchniewicz *et al.*, 2006). Considerable Rap1 activation remained in Rap1A-deficient lymphocytes is likely contributed by Rap1B. On TCR engagement, Rap1 is activated, altering its localization at the T-cell–APC interface (Katagiri *et al.*, 2002) and plasma membrane (Bivona *et al.*, 2004). Rap1 associates with RAPL and quickly initiates translocation from the perinuclear region to the peripheral boundaries of the immunological synapse (Katagiri *et al.*, 2003). Dominant-negative RAPL inhibits TCR-induced upregulation of LFA-1 avidity and T cell–APC conjugate formation. MST1/STK4 isolated as a RAPL-binding partner is also colocalized at the T cell–APC interface and is required by TCR-stimulated adhesion to ICAM-1 (Katagiri *et al.*, 2006).

In Jurkat T cells, PLC γ -1 is required for Rap1 activation, suggesting that the calcium and diacylglycerol (DAG)-responsive CalDAG-GEF family of proteins, which include the Rap1 GEFs, are perhaps involved in signaling downstream of PLC γ -1 (Katagiri *et al.*, 2004b). The requirement for PLC γ -1 for Rap1 activation in T cells is in line with studies demonstrating a requirement for PLC γ -2 in Rap1 activation following B cell receptor ligation (McLeod and Gold, 2001). Another Rap1 GEF, C3G, may also contribute to TCR-stimulated Rap1 activation, particularly in thymocytes (Amsen *et al.*, 2000), anergic T cells (Boussiotis *et al.*, 1997), and Cbl-b-deficient T cells (Zhang *et al.*, 2003). PLC γ -1 activation is regulated by a complex containing linker for activated T cells (LAT), the adaptor proteins Gads and SLP-76, and Itk (Samelson, 2002). Consistent with this, signaling molecules required for TCR-stimulated PLC- γ 1 activation, such as ZAP-70, SLP-76, and Itk, are critical for the activation of β 1 integrins (Kellermann *et al.*, 2002). Vav1 is also involved in PLC- γ 1 activation following TCR stimulation through its association with SLP-76 and also activation by Itk (Reynolds *et al.*, 2002), placing Rap1 and RAPL downstream of Vav1, SLP-76, and Itk activation. This organization raises the possibility that defective LFA-1 activation in Vav1-deficient cells may result from insufficient Rap1 activation.

8.4. PKD1

A serine/threonine kinase PKD1 (PKC μ) is shown to form a complex with Rap1 and plays an important role in β 1 integrin activation (Medeiros *et al.*, 2005). PDK1 is a DAG-responsive PKC, which is activated by PKC ϵ and a variety of external stimuli, including TCR (Rozenfurt *et al.*, 2005). PDK1 associates with active Rap1, but not inactive Rap1, through a PH domain of PKD1 (Medeiros *et al.*, 2005). PKD1 further forms a complex with the β 1 integrin subunit, depending on the C-terminal five amino acids of the β 1 subunit that are required in activation-dependent adhesion (Romzek *et al.*, 1998). This tertiary complex is formed in Jurkat and primary T cells and translocated to the plasma membrane on stimulation with phorbol ester PMA and TCR ligation (Medeiros *et al.*, 2005). Furthermore, PKD1 associates with C3G, suggesting that PKD1 acts upstream of Rap1. Surprisingly, Rap1 activation also depends on the β 1 integrin expression, as Rap1 activation is diminished in β 1-deficient Jurkat cells, which is restored by the β 1 expression. Knockdown of PKD1 expression reduces β 1 integrin clustering and adhesion to fibronectin. A mutant PKD1 lacking the PH domain (PKD1 Δ PH) also decreases adhesion to fibronectin as well as Rap1 activation and membrane translocation, presumably through an abortive complex formation with the β 1 integrin and C3G. The kinase activity of PKD1 Δ PH is not required for the inhibitory effects. Collectively, these results support the notion that PKD1 acts as an adaptor to localize Rap1 activation to β 1 integrin (Medeiros *et al.*, 2005). It is also reported that PKD1 associates with α v β 3 integrin by binding to the β 3 integrin C-terminus, and thereby promotes recycling of α v β 3 to newly forming focal adhesion, suggesting a regulatory role of PDK1 in vesicle transport of integrins (Woods *et al.*, 2004). This is in agreement with a proposed function of the Rap1/RAPL/Mst1 signaling in polarized LFA-1 transport to the leading edge (Katagiri *et al.*, 2006) and could be also involved in PDK1 regulation of β 1 integrins.

8.5. Adhesion and Degranulation Adaptor Protein

Unexpected effects of adhesion and degranulation adaptor protein (ADAP; Fyb/SLAP-130) gene targeting on LFA-1 activation indicate that it is an important inside-out signaling molecule. ADAP-deficient lymphocytes exhibit impaired TCR-triggered β 1 and β 2 integrin-dependent adhesion, defective interleukin-2 production, and decreased proliferation, despite normal calcium flux and MAP kinase activation (Griffiths *et al.*, 2001; Peterson, 2003). ADAP does not appear to be involved in chemokine-stimulated integrin activation. ADAP is a hematopoietic adaptor protein, which associates with SLP-76 on

TCR engagement, although it can also associate with the Fyn, the Ena/VASP family of actin regulators and SKAP-55 (Peterson, 2003). ADAP deficiency impairs TCR-stimulated LFA-1 clustering, but does not affect TCR clustering itself or assembly of the actin cytoskeleton (Griffiths *et al.*, 2001; Peterson *et al.*, 2001). ADAP colocalizes with LFA-1 in IS (Wang *et al.*, 2004). Its association with SLP-76 appears to be crucial for its function in LFA-1 activation. SKAP-55 is involved in LFA-1 activation downstream of ADAP (Wang *et al.*, 2003). Disruption of ADAP and SKAP-55 complex results in displacement of Rap1 from the plasma membrane without influencing its GTPase activity. Thus, ADAP/SKAP-55 complex may control targeting of activated Rap1 to the membrane (Kliche *et al.*, 2006). This result is consistent with the study reporting that the localization of active Rap1-GTP at the plasma membrane is critical for Rap1-dependent integrin regulation in T cells (Bivona *et al.*, 2004).

9. Concluding Remarks

Recent progress prompts us to think dynamic lymphocyte trafficking in terms of a spectrum of conformational states of integrins. Structural studies support a unifying model of global conformational changes from the bent to the extended-closed to the extended-open on activation of integrins, and further suggest that extended conformations by separation of the leg and cytoplasmic domains triggered by inside-out signals transmit allostery to activate the ligand-binding I domain. Lymphocyte integrins are also regulated spatially, which is often coupled with affinity modulation, during the processes of cell polarization, migration, and IS formations. A wide variety of intracellular molecules involved in integrin-mediated adhesion are now identified by genetic approaches and characterized at cellular and organismic levels but needs further studies to clarify their regulatory mechanisms at molecular levels. The better appreciation of physiological relevance of each state of conformation and valency regulation should be required to dissect integrin regulation that occurs in from rolling through firm adhesion to transendothelial and interstitial migration and interactions with APC. It is important to elucidate what and how intracellular signaling processes coordinately regulate conformation and spatial regulation of integrins to translate external stimulation into dynamic adhesive responses. The answers to these questions will shed light on crucial roles of integrin regulation in immunological surveillance and antigen response.

Acknowledgments

I would like to thank Koko Katagiri for helpful comments.

References

- Adair, B. D., Xiong, J. P., Maddock, C., Goodman, S. L., Arnaout, M. A., and Yeager, M. (2005). Three-dimensional EM structure of the ectodomain of integrin $\alpha V\beta 3$ in a complex with fibronectin. *J. Cell Biol.* **168**, 1109–1118.
- Amsen, D., Kruisbeek, A., Bos, J. L., and Reedquist, K. (2000). Activation of the Ras-related GTPase Rap1 by thymocyte TCR engagement and during selection. *Eur. J. Immunol.* **30**, 2832–2841.
- Becam, I. E., Tanentzapf, G., Lepesant, J. A., Brown, N. H., and Huynh, J. R. (2005). Integrin-independent repression of cadherin transcription by talin during axis formation in *Drosophila*. *Nat. Cell Biol.* **7**, 510–516.
- Bertoni, A., Tadokoro, S., Eto, K., Pampori, N., Parise, L. V., White, G. C., and Shattil, S. J. (2002). Relationships between Rap1b, affinity modulation of integrin alpha IIb beta 3, and the actin cytoskeleton. *J. Biol. Chem.* **277**, 25715–25721.
- Bivona, T. G., Wiener, H. H., Ahearn, I. M., Silletti, J., Chiu, V. K., and Philips, M. R. (2004). Rap1 up-regulation and activation on plasma membrane regulates T cell adhesion. *J. Cell Biol.* **164**, 461–470.
- Bos, J. L., de Rooij, J., and Reedquist, K. A. (2001). Rap1 signaling: Adhering to new models. *Nat. Rev. Mol. Cell. Biol.* **2**, 369–377.
- Boussiotis, V. A., Freeman, G. J., Berezovskaya, A., Barber, D. L., and Nadler, L. M. (1997). Maintenance of human T cell anergy: Blocking of IL-2 gene transcription by activated Rap1. *Science* **278**, 124–128.
- Bouso, P., and Robey, E. (2003). Dynamics of CD8+ T cell priming by dendritic cells in intact lymph nodes. *Nat. Immunol.* **4**, 579–585.
- Burridge, K., and Connell, L. (1983). Talin: A cytoskeletal component concentrated in adhesion plaques and other sites of actin-membrane interaction. *Cell Motil.* **3**, 405–417.
- Butcher, E. C., and Picker, L. J. (1996). Lymphocyte homing and homeostasis. *Science* **272**, 60–66.
- Butcher, E. C., Williams, M., Youngman, K., Rott, L., and Briskin, M. (1999). Lymphocyte trafficking and regional immunity. *Adv. Immunol.* **72**, 209–253.
- Cairo, C. W., Mirchev, R., and Golan, D. E. (2006). Cytoskeletal regulation couples LFA-1 conformational changes to receptor lateral mobility and clustering. *Immunity* **25**, 297–308.
- Calderwood, D. A. (2004). Integrin activation. *J. Cell Sci.* **117**, 657–666.
- Calderwood, D. A., Zent, R., Grant, R., Rees, D. J., Hynes, R. O., and Ginsberg, M. H. (1999). The Talin head domain binds to integrin beta subunit cytoplasmic tails and regulates integrin activation. *J. Biol. Chem.* **274**, 28071–28074.
- Carman, C. V., and Springer, T. A. (2003). Integrin avidity regulation: Are changes in affinity and conformation underemphasized? *Curr. Opin. Cell Biol.* **15**, 547–556.
- Carman, C. V., and Springer, T. A. (2004). A transmigratory cup in leukocyte diapedesis both through individual vascular endothelial cells and between them. *J. Cell Biol.* **167**, 377–388.
- Caron, E., Self, A. J., and Hall, A. (2000). The GTPase Rap1 controls functional activation of macrophage integrin alpha M beta 2 by LPS and other inflammatory mediators. *Curr. Biol.* **10**, 974–978.
- Chan, J. R., Hyduk, S. J., and Cybulsky, M. I. (2003). Detecting rapid and transient upregulation of leukocyte integrin affinity induced by chemokines and chemoattractants. *J. Immunol. Methods* **273**, 43–52.
- Chen, J., Salas, A., and Springer, T. A. (2003). Bistable regulation of integrin adhesiveness by a bipolar metal ion cluster. *Nat. Struct. Biol.* **10**, 995–1001.
- Cherry, L. K., Li, X., Schwab, P., Lim, B., and Klickstein, L. B. (2004). RhoH is required to maintain the integrin LFA-1 in a nonadhesive state on lymphocytes. *Nat. Immunol.* **5**, 961–967.

- Chigaev, A., Buranda, T., Dwyer, D. C., Prossnitz, E. R., and Sklar, L. A. (2003). FRET detection of cellular $\alpha 4$ -integrin conformational activation. *Biophys. J.* **85**, 3951–3962.
- Chrzanowska-Wodnicka, M., Smyth, S. S., Schoenwaelder, S. M., Fischer, T. H., and White, G. C., 2nd (2005). Rap1b is required for normal platelet function and hemostasis in mice. *J. Clin. Invest.* **115**, 680–687.
- Cinamon, G., Shinder, V., and Alon, R. (2001). Shear forces promote lymphocyte migration across vascular endothelium bearing apical chemokines. *Nat. Immunol.* **2**, 515–522.
- Cinamon, G., Matloubian, M., Lesneski, M. J., Xu, Y., Low, C., Lu, T., Proia, R. L., and Cyster, J. G. (2004). Sphingosine 1-phosphate receptor 1 promotes B cell localization in the splenic marginal zone. *Nat. Immunol.* **5**, 713–720.
- Constantin, G., Majeed, M., Giagulli, C., Piccio, L., Kim, J. Y., Butcher, E. C., and Laudanna, C. (2000). Chemokines trigger immediate $\beta 2$ integrin affinity and mobility changes: Differential regulation and roles in lymphocyte arrest under flow. *Immunity* **13**, 759–769.
- Crittenden, J. R., Bergmeier, W., Zhang, Y., Piffath, C. L., Liang, Y., Wagner, D. D., Housman, D. E., and Graybiel, A. M. (2004). CalDAG-GEFI integrates signaling for platelet aggregation and thrombus formation. *Nat. Med.* **10**, 982–986.
- de Bruyn, K. M., Zwartkruis, F. J., de Rooij, J., Akkerman, J. W., and Bos, J. L. (2003). The small GTPase Rap1 is activated by turbulence and is involved in integrin $\alpha \text{IIb}\beta 3$ -mediated cell adhesion in human megakaryocytes. *J. Biol. Chem.* **278**, 22412–22417.
- Dransfield, I., Cabanas, C., Craig, A., and Hogg, N. (1992). Divalent cation regulation of the function of the leukocyte integrin LFA-1. *J. Cell Biol.* **116**, 219–226.
- Duchniewicz, M., Zemojtel, T., Kolanczyk, M., Grossmann, S., Scheele, J. S., and Zwartkruis, F. J. (2006). Rap1A-deficient T and B cells show impaired integrin-mediated cell adhesion. *Mol. Cell. Biol.* **26**, 643–653.
- Durand, C. A., Westendorf, J., Tse, K. W., and Gold, M. R. (2006). The Rap GTPases mediate CXCL13- and sphingosine1-phosphate-induced chemotaxis, adhesion, and Pyk2 tyrosine phosphorylation in B lymphocytes. *Eur. J. Immunol.* **36**, 2235–2249.
- Dustin, M. L., and Springer, T. A. (1989). T-cell receptor cross-linking transiently stimulates adhesiveness through LFA-1. *Nature* **341**, 619–624.
- Dustin, M. L., Bivona, T. G., and Philips, M. R. (2004). Membranes as messengers in T cell adhesion signaling. *Nat. Immunol.* **5**, 363–372.
- Ebisuno, Y., Tanaka, T., Kanemitsu, N., Kanda, H., Yamaguchi, K., Kaisho, T., Akira, S., and Miyasaka, M. (2003). Cutting edge: The B cell chemokine CXC chemokine ligand 13/B lymphocyte chemoattractant is expressed in the high endothelial venules of lymph nodes and Peyer's patches and affects B cell trafficking across high endothelial venules. *J. Immunol.* **171**, 1642–1646.
- Etzioni, A. (1996). Adhesion molecules: Their role in health and disease. *Pediatr. Res.* **39**, 191–198.
- Fabbri, M., Fumagalli, L., Bossi, G., Bianchi, E., Bender, J. R., and Pardi, R. (1999). A tyrosine-based sorting signal in the $\beta 2$ integrin cytoplasmic domain mediates its recycling to the plasma membrane and is required for ligand-supported migration. *EMBO J.* **18**, 4915–4925.
- Fabbri, M., Di Meglio, S., Gagliani, M. C., Consonni, E., Molteni, R., Bender, J. R., Tacchetti, C., and Pardi, R. (2005). Dynamic partitioning into lipid rafts controls the endo-exocytic cycle of the $\alpha \text{L}/\beta 2$ integrin, LFA-1, during leukocyte chemotaxis. *Mol. Biol. Cell* **16**, 5793–5803.
- Fagerholm, S. C., Hilden, T. J., and Gahmberg, C. G. (2004). P marks the spot: Site-specific integrin phosphorylation regulates molecular interactions. *Trends Biochem. Sci.* **29**, 504–512.
- Fagerholm, S. C., Hilden, T. J., Nurmi, S. M., and Gahmberg, C. G. (2005). Specific integrin α and β chain phosphorylations regulate LFA-1 activation through affinity-dependent and -independent mechanisms. *J. Cell Biol.* **171**, 705–715.

- Feng, D., Nagy, J. A., Pyne, K., Dvorak, H. F., and Dvorak, A. M. (1998). Neutrophils emigrate from venules by a transendothelial cell pathway in response to FMLP. *J. Exp. Med.* **187**, 903–915.
- Fischer, A. M., Mercer, J. C., Iyer, A., Ragin, M. J., and August, A. (2004). Regulation of CXC chemokine receptor 4-mediated migration by the Tec family tyrosine kinase ITK. *J. Biol. Chem.* **279**, 29816–29820.
- Foger, N., Rangell, L., Danilenko, D. M., and Chan, A. C. (2006). Requirement for coronin 1 in T lymphocyte trafficking and cellular homeostasis. *Science* **313**, 839–842.
- Friedman, R. S., Jacobelli, J., and Krummel, M. F. (2005). Mechanisms of T cell motility and arrest: Deciphering the relationship between intra- and extracellular determinants. *Semin. Immunol.* **17**, 387–399.
- Friedman, R. S., Jacobelli, J., and Krummel, M. F. (2006). Surface-bound chemokines capture and prime T cells for synapse formation. *Nat. Immunol.* **7**, 1101–1108.
- Fukui, Y., Hashimoto, O., Sanui, T., Oono, T., Koga, H., Abe, M., Inayoshi, A., Noda, M., Oike, M., Shirai, T., and Sasazuki, T. (2001). Haematopoietic cell-specific CDM family protein DOCK2 is essential for lymphocyte migration. *Nature* **412**, 826–831.
- Gakidis, M. A., Cullere, X., Olson, T., Wilsbacher, J. L., Zhang, B., Moores, S. L., Ley, K., Swat, W., Mayadas, T., and Brugge, J. S. (2004). Vav GEFs are required for $\beta 2$ integrin-dependent functions of neutrophils. *J. Cell Biol.* **166**, 273–282.
- Garcia-Bernal, D., Wright, N., Sotillo-Mallo, E., Nombela-Arrieta, C., Stein, J. V., Bustelo, X. R., and Teixido, J. (2005). Vav1 and Rac control chemokine-promoted T lymphocyte adhesion mediated by the integrin $\alpha 4 \beta 1$. *Mol. Biol. Cell.* **16**, 3223–3235.
- Giagulli, C., Scarpini, E., Ottoboni, L., Narumiya, S., Butcher, E. C., Constantin, G., and Laudanna, C. (2004). RhoA and zeta PKC control distinct modalities of LFA-1 activation by chemokines: Critical role of LFA-1 affinity triggering in lymphocyte *in vivo* homing. *Immunity* **20**, 25–35.
- Girkontaite, I., Missy, K., Sakk, V., Harenberg, A., Tedford, K., Potzel, T., Pfeffer, K., and Fischer, K. D. (2001). Lsc is required for marginal zone B cells, regulation of lymphocyte motility and immune responses. *Nat. Immunol.* **2**, 855–862.
- Gomez-Mouton, C., Abad, J. L., Mira, E., Lacalle, R. A., Gallardo, E., Jimenez-Baranda, S., Illa, I., Bernad, A., Manes, S., and Martinez, A. C. (2001). Segregation of leading-edge and uropod components into specific lipid rafts during T cell polarization. *Proc. Natl. Acad. Sci. USA* **98**, 9642–9647.
- Grabovsky, V., Feigelson, S., Chen, C., Bleijs, D. A., Peled, A., Cinamon, G., Baleux, F., Arenzana, S. F., Lapidot, T., van Kooyk, Y., Lobb, R. R., and Alon, R. (2000). Subsecond induction of $\alpha 4$ integrin clustering by immobilized chemokines stimulates leukocyte tethering and rolling on endothelial vascular cell adhesion molecule 1 under flow conditions. *J. Exp. Med.* **192**, 495–506.
- Grakoui, A., Bromley, S. K., Sumen, C., Davis, M. M., Shaw, A. S., Allen, P. M., and Dustin, M. L. (1999). The immunological synapse: A molecular Machine controlling T cell activation. *Science* **285**, 221–226.
- Green, C. E., Schaff, U. Y., Sarantos, M. R., Lum, A. F., Staunton, D. E., and Simon, S. I. (2006). Dynamic shifts in LFA-1 affinity regulate neutrophil rolling, arrest, and transmigration on inflamed endothelium. *Blood* **107**, 2101–2111.
- Griffiths, E. K., Krawczyk, C., Kong, Y. Y., Raab, M., Hyduk, S. J., Bouchard, D., Chan, V. S., Kozieradzki, I., Oliveira-Dos-Santos, A. J., Wakeham, A., Ohashi, P. S., Cybulsky, M. I., *et al.* (2001). Positive regulation of T cell activation and integrin adhesion by the adapter Fyb/Slap. *Science* **293**, 2260–2263.
- Gu, Y., Filippi, M. D., Cancelas, J. A., Siefring, J. E., Williams, E. P., Jasti, A. C., Harris, C. E., Lee, A. W., Prabhakar, R., Atkinson, S. J., Kwiatkowski, D. J., and Williams, D. A. (2003). Hematopoietic cell regulation by Rac1 and Rac2 guanosine triphosphatases. *Science* **302**, 445–449.

- Gu, Y., Jasti, A. C., Jansen, M., and Siefring, J. E. (2005). RhoH, a hematopoietic-specific Rho GTPase, regulates proliferation, survival, migration, and engraftment of hematopoietic progenitor cells. *Blood* **105**, 1467–1475.
- Gunzer, M., Schafer, A., Borgmann, S., Grabbe, S., Zanker, K. S., Broker, E.-B. E. K., and Friedl, P. (2000). Antigen presentation in extracellular matrix: Interactions of T cells with dendritic cells are dynamic, short lived, and sequential. *Immunity* **13**, 323–332.
- Han, J., Lim, C. J., Watanabe, N., Soriani, A., Ratnikov, B., Calderwood, D. A., Puzon-McLaughlin, W., Lafuente, E. M., Boussiotis, V. A., Shattil, S. J., and Ginsberg, M. H. (2006). Reconstructing and deconstructing agonist-induced activation of integrin α IIb β 3. *Curr. Biol.* **16**, 1796–1806.
- Hart, M. J., Jiang, X., Kozasa, T., Roscoe, W., Singer, W. D., Gilman, A. G., Sternweis, P. C., and Bollag, G. (1998). Direct stimulation of the guanine nucleotide exchange activity of p115 RhoGEF by G α 13. *Science* **280**, 2112–2114.
- Hemler, M. E. (1990). VLA proteins in the integrin family: Structures, functions, and their role on leukocytes. *Annu. Rev. Immunol.* **8**, 365–400.
- Hibbs, M. L., Jakes, S., Stacker, S. A., Wallace, R. W., and Springer, T. A. (1991). The cytoplasmic domain of the integrin lymphocyte-function-associated antigen 1 b subunit: Sites required for binding to intercellular adhesion molecules 1 and the phorbol ester-stimulated phosphorylation site. *J. Exp. Med.* **174**, 1227–1238.
- Hilpela, P., Oberbanscheidt, P., Hahne, P., Hund, M., Kalhammer, G., Small, J. V., and Bahler, M. (2003). SWAP-70 identifies a transitional subset of actin filaments in motile cells. *Mol. Biol. Cell* **14**, 3242–3253.
- Hirsch, E., Katanaev, V. L., Garlanda, C., Azzolino, O., Pirola, L., Silengo, L., Sozzani, S., Mantovani, A., Altruda, F., and Wymann, M. P. (2000). Central role for G protein-coupled phosphoinositide 3-kinase gamma in inflammation. *Science* **287**, 1049–1053.
- Horwitz, A., Duggan, K., Buck, C., Beckerle, M. C., and Burridge, K. (1986). Interaction of plasma membrane fibronectin receptor with talin: A transmembrane linkage. *Nature* **320**, 531–533.
- Hughes, P. E., Diaz-Gonzalez, F., Leong, L., Wu, C., McDonald, J. A., Shattil, S. J., and Ginsberg, M. H. (1996). Breaking the integrin hinge. *J. Biol. Chem.* **271**, 6571–6574.
- Humphries, M. J. (2004). Monoclonal antibodies as probes of integrin priming and activation. *Biochem. Soc. Trans.* **32**, 407–411.
- Huth, J. R., Olejniczak, E. T., Mendoza, R., Liang, H., Harris, E. A., Lupher, M. L., Jr., Wilson, A. E., Fesik, S. W., and Staunton, D. E. (2000). NMR and mutagenesis evidence for an I domain allosteric site that regulates lymphocyte function-associated antigen 1 ligand binding. *Proc. Natl. Acad. Sci. USA* **97**, 5231–5236.
- Hynes, R. O. (2002). Integrins: Bidirectional, allosteric signalling machines. *Cell* **110**, 673–687.
- Ihara, S., Oka, T., and Fukui, Y. (2006). Direct binding of SWAP-70 to non-muscle actin is required for membrane ruffling. *J. Cell Sci.* **119**, 500–507.
- Inagaki, T., Suzuki, S., Miyamoto, T., Takeda, T., Yamashita, K., Komatsu, A., Yamauchi, K., and Hashizume, K. (2003). The retinoic acid-responsive proline-rich protein is identified in promyeloleukemic HL-60 cells. *J. Biol. Chem.* **278**, 51685–51692.
- Jenzora, A., Behrendt, B., Small, J. V., Wehland, J., and Stradal, T. E. (2005). PREL1 provides a link from Ras signalling to the actin cytoskeleton via Ena/VASP proteins. *FEBS Lett.* **579**, 455–463.
- Johnson-Leger, C., Aurrand-Lions, M., and Imhof, B. A. (2000). The parting of the endothelium: Miracle, or simply a junctional affair? *J. Cell Sci.* **113**(Pt. 6), 921–933.
- Jones, M. C., Caswell, P. T., and Norman, J. C. (2006). Endocytic recycling pathways: Emerging regulators of cell migration. *Curr. Opin. Cell Biol.* **18**, 549–557.
- Katagiri, K., Hattori, M., Minato, N., Irie, S., Takatsu, K., and Kinashi, T. (2000). Rap1 is a potent activation signal for leukocyte function-associated antigen 1 distinct from protein kinase C and phosphatidylinositol-3-OH kinase. *Mol. Cell. Biol.* **20**, 1956–1969.

- Katagiri, K., Hattori, M., Minato, N., and Kinashi, T. (2002). Rap1 functions as a key regulator of T-cell and antigen-presenting cell interactions and modulates T-cell responses. *Mol. Cell. Biol.* **22**, 1001–1015.
- Katagiri, K., Maeda, A., Shimonaka, M., and Kinashi, T. (2003). RAPL, a Rap1-binding molecule that mediates Rap1-induced adhesion through spatial regulation of LFA-1. *Nat. Immunol.* **4**, 741–748.
- Katagiri, K., Ohnishi, N., Kabashima, K., Iyoda, T., Takeda, N., Shinkai, Y., Inaba, K., and Kinashi, T. (2004a). Crucial roles of Rap1 effector molecule RAPL in lymphocyte and dendritic cell trafficking. *Nat. Immunol.* **5**, 1045–1051.
- Katagiri, K., Shimonaka, M., and Kinashi, T. (2004b). Rap1-mediated LFA-1 activation by the T cell antigen receptor is dependent on PLC- γ 1. *J. Biol. Chem.* **279**, 11875–11881.
- Katagiri, K., Imamura, M., and Kinashi, T. (2006). Spatiotemporal regulation of the kinase Mst1 by binding protein RAPL is critical for lymphocyte polarity and adhesion. *Nat. Immunol.* **7**, 919–928.
- Kellermann, S. A., Dell, C. L., Hunt, S. W., 3rd, and Shimizu, Y. (2002). Genetic analysis of integrin activation in T lymphocytes. *Immunol. Rev.* **186**, 172–188.
- Kim, M., Carman, C. V., and Springer, T. A. (2003). Bidirectional transmembrane signaling by cytoplasmic domain separation in integrins. *Science* **301**, 1720–1725.
- Kinashi, T., Escobedo, J. A., Williams, L. T., Takatsu, K., and Springer, T. A. (1995). Receptor tyrosine kinase stimulates cell-matrix adhesion by phosphatidylinositol 3 kinase and phospholipase C- γ 1 pathways. *Blood* **86**, 2086–2090.
- Kinashi, T., Aker, M., Sokolovsky-Eisenberg, M., Grabovsky, V., Tanaka, C., Shamri, R., Feigelson, S., Etzioni, A., and Alon, R. (2004). LAD-III, a leukocyte adhesion deficiency syndrome associated with defective Rap1 activation and impaired stabilization of integrin bonds. *Blood* **103**, 1033–1036.
- Kliche, S., Breitling, D., Togni, M., Pusch, R., Heuer, K., Wang, X., Freund, C., Kasirer-Friede, A., Menasche, G., Koretzky, G. A., and Schraven, B. (2006). The ADAP/SKAP55 signaling module regulates T-cell receptor-mediated integrin activation through plasma membrane targeting of Rap1. *Mol. Cell. Biol.* **26**, 7130–7144.
- Kolanus, W., Nagel, W., Schiller, B., Zeitlmann, L., Godar, S., Stockinger, H., and Seed, B. (1996). α L β 2 integrin/LFA-1 binding to ICAM-1 induced by cytohesin-1, a cytoplasmic regulatory molecule. *Cell* **86**, 233–242.
- Kozasa, T., Jiang, X., Hart, M. J., Sternweis, P. M., Singer, W. D., Gilman, A. G., Bollag, G., and Sternweis, P. C. (1998). p115 RhoGEF, a GTPase activating protein for G α 12 and G α 13. *Science* **280**, 2109–2111.
- Krawczyk, C., Oliveira-dos-Santos, A., Sasaki, T., Griffiths, E., Ohashi, P. S., Snapper, S., Alt, F., and Penninger, J. M. (2002). Vav1 controls integrin clustering and MHC/peptide-specific cell adhesion to antigen-presenting cells. *Immunity* **16**, 331–343.
- Kucik, D. F., Dustin, M. L., Miller, J. M., and Brown, E. J. (1996). Adhesion-activating phorbol ester increases the mobility of leukocyte integrin LFA-1 in cultured lymphocytes. *J. Clin. Invest.* **97**, 2139–2144.
- Kunisaki, Y., Nishikimi, A., Tanaka, Y., Takii, R., Noda, M., Inayoshi, A., Watanabe, K., Sanematsu, F., Sasazuki, T., Sasaki, T., and Fukui, Y. (2006). DOCK2 is a Rac activator that regulates motility and polarity during neutrophil chemotaxis. *J. Cell Biol.* **174**, 647–652.
- Labno, C. M., Lewis, C. M., You, D., Leung, D. W., Takesono, A., Kamberos, N., Seth, A., Finkelstein, L. D., Rosen, M. K., Schwartzberg, P. L., and Burkhardt, J. K. (2003). Itk functions to control actin polymerization at the immune synapse through localized activation of Cdc42 and WASP. *Curr. Biol.* **13**, 1619–1624.

- Lafuente, E. M., van Puijenbroek, A. A., Krause, M., Carman, C. V., Freeman, G. J., Berezovskaya, A., Constantine, E., Springer, T. A., Gertler, F. B., and Boussiotis, V. A. (2004). RIAM, an Ena/VASP and Profilin ligand, interacts with Rap1-GTP and mediates Rap1-induced adhesion. *Dev. Cell* **7**, 585–595.
- Larson, R. S., Davis, T., Bologna, C., Semenuk, G., Vijayan, S., Li, Y., Oprea, T., Chigaev, A., Buranda, T., Wagner, C. R., and Sklar, L. A. (2005). Dissociation of I domain and global conformational changes in LFA-1: Refinement of small molecule-I domain structure-activity relationships. *Biochemistry* **44**, 4322–4331.
- Laudanna, C., Campbell, J. J., and Butcher, E. C. (1996). Role of Rho in chemoattractant-activated leukocyte adhesion through integrins. *Science* **271**, 981–983.
- Lawson, M. A., and Maxfield, R. R. (1995). Ca²⁺- and calcineurin-dependent recycling of an integrin to the front of migrating neutrophils. *Nature* **377**, 75–79.
- Legg, J. A., and Machesky, L. M. (2004). MRL proteins: Leading Ena/VASP to Ras GTPases. *Nat. Cell Biol.* **6**, 1015–1017.
- Li, S., Kim, M., Hu, Y. L., Jalali, S., Schlaepfer, D. D., Hunter, T., Chien, S., and Shyy, J. Y. (1997). Fluid shear stress activation of focal adhesion kinase: Linking to mitogen-activated protein kinases. *J. Biol. Chem.* **272**, 30455–30462.
- Li, X., Bu, X., Lu, B., Avraham, H., Flavell, R. A., and Lim, B. (2002). The hematopoiesis-specific GTP-binding protein RhoH is GTPase deficient and modulates activities of other Rho GTPases by an inhibitory function. *Mol. Cell. Biol.* **22**, 1158–1171.
- Li, Z., Jiang, H., Xie, W., Zhang, Z., Smrcka, A. V., and Wu, D. (2000). Roles of PLC- β 2 and - β 3 and PI3K γ in chemoattractant-mediated signal transduction. *Science* **287**, 1046–1049.
- Liu, S., Calderwood, D. A., and Ginsberg, M. H. (2000). Integrin cytoplasmic domain-binding proteins. *J. Cell Sci.* **113**(Pt. 20), 3563–3571.
- Lo, C. G., Lu, T. T., and Cyster, J. G. (2003). Integrin-dependence of lymphocyte entry into the splenic white pulp. *J. Exp. Med.* **197**, 353–361.
- Lollo, B. A., Chan, K. W., Hanson, E. M., Moy, V. T., and Brian, A. A. (1993). Direct evidence for two affinity states for lymphocyte function-associated antigen 1 on activated T cells. *J. Biol. Chem.* **268**, 21693–21700.
- Lu, C., Ferzly, M., Takagi, J., and Springer, T. A. (2001a). Epitope mapping of antibodies to the C-terminal region of the integrin beta 2 subunit reveals regions that become exposed upon receptor activation. *J. Immunol.* **166**, 5629–5637.
- Lu, C., Shimaoka, M., Zang, Q., Takagi, J., and Springer, T. A. (2001b). Locking in alternate conformations of the integrin alphaLbeta2 I domain with disulfide bonds reveals functional relationships among integrin domains. *Proc. Natl. Acad. Sci. USA* **98**, 2393–2398.
- Lu, C., Shimaoka, M., Salas, A., and Springer, T. A. (2004). The binding sites for competitive antagonistic, allosteric antagonistic, and agonistic antibodies to the I domain of integrin LFA-1. *J. Immunol.* **173**, 3972–3978.
- Lu, C.-H., and Springer, T. A. (1997). The α subunit cytoplasmic domain regulates the assembly and adhesiveness of integrin lymphocyte-function-associated antigen-1. *J. Immunol.* **159**, 268–278.
- Lucas, J. A., Miller, A. T., Atherly, L. O., and Berg, L. J. (2003). The role of Tec family kinases in T cell development and function. *Immunol. Rev.* **191**, 119–138.
- Luo, B. H., Takagi, J., and Springer, T. A. (2004). Locking the beta3 integrin I-like domain into high and low affinity conformations with disulfides. *J. Biol. Chem.* **279**, 10215–10221.
- McLeod, S. J., and Gold, M. R. (2001). Activation and function of the Rap1 GTPase in B lymphocytes. *Int. Rev. Immunol.* **20**, 763–789.
- McLeod, S. J., Li, A. H., Lee, R. L., Burgess, A. E., and Gold, M. R. (2002). The Rap GTPases regulate B cell migration toward the chemokine stromal cell-derived factor-1 (CXCL12): Potential role for Rap2 in promoting B cell migration. *J. Immunol.* **169**, 1365–1371.

- Meacci, E., Tsai, S. C., Adamik, R., Moss, J., and Vaughan, M. (1997). Cytohesin-1, a cytosolic guanine nucleotide-exchange protein for ADP-ribosylation factor. *Proc. Natl. Acad. Sci. USA* **94**, 1745–1748.
- Medeiros, R. B., Dickey, D. M., Chung, H., Quale, A. C., Nagarajan, L. R., Billadeau, D. D., and Shimizu, Y. (2005). Protein kinase D1 and the beta 1 integrin cytoplasmic domain control beta 1 integrin function via regulation of Rap1 activation. *Immunity* **23**, 213–226.
- Mempel, T. R., Henrickson, S. E., and Von Andrian, U. H. (2004). T-cell priming by dendritic cells in lymph nodes occurs in three distinct phases. *Nature* **427**, 154–159.
- Miller, M. J., Wei, S. H., Parker, I., and Cahalan, M. D. (2002). Two-photon imaging of lymphocyte motility and antigen response in intact lymph node. *Science* **296**, 1869–1873.
- Miller, M. J., Safrina, O., Parker, I., and Cahalan, M. D. (2004). Imaging the single cell dynamics of CD4+ T cell activation by dendritic cells in lymph nodes. *J. Exp. Med.* **200**, 847–856.
- Miyasaka, M., and Tanaka, T. (2004). Lymphocyte trafficking across high endothelial venules: Dogmas and enigmas. *Nat. Rev. Immunol.* **4**, 360–370.
- Monks, C. R., Freiberg, B. A., Kupfer, H., Sciaky, N., and Kupfer, A. (1998). Three-dimensional segregation of supramolecular activation clusters in T cells. *Nature* **395**, 82–86.
- Moser, B., Wolf, M., Walz, A., and Loetscher, P. (2004). Chemokines: Multiple levels of leukocyte migration control. *Trends Immunol.* **25**, 75–84.
- Mould, A. P., Askari, J. A., Barton, S., Kline, A. D., McEwan, P. A., Craig, S. E., and Humphries, M. J. (2002). Integrin activation involves a conformational change in the alpha 1 helix of the beta subunit A-domain. *J. Biol. Chem.* **277**, 19800–19805.
- Mould, A. P., Barton, S. J., Askari, J. A., Craig, S. E., and Humphries, M. J. (2003a). Role of ADMIDAS cation-binding site in ligand recognition by integrin $\alpha 5\beta 1$. *J. Biol. Chem.* **278**, 51622–51629.
- Mould, A. P., Barton, S. J., Askari, J. A., McEwan, P. A., Buckley, P. A., Craig, S. E., and Humphries, M. J. (2003b). Conformational changes in the integrin beta A domain provide a mechanism for signal transduction via hybrid domain movement. *J. Biol. Chem.* **278**, 17028–17035.
- Muller, W. A. (2003). Leukocyte-endothelial-cell interactions in leukocyte transmigration and the inflammatory response. *Trends Immunol.* **24**, 327–334.
- Nieminen, M., Henttinen, T., Merinen, M., Marttila-Ichihara, F., Eriksson, J. E., and Jalkanen, S. (2006). Vimentin function in lymphocyte adhesion and transcellular migration. *Nat. Cell Biol.* **8**, 156–162.
- Nishida, N., Xie, C., Shimaoka, M., Cheng, Y., Walz, T., and Springer, T. A. (2006). Three distinctive ectodomain conformations and their interconversion in leukocyte $\beta 2$ integrins. *Immunity* **25**, 583–594.
- Nombela-Arrieta, C., Lacalle, R. A., Montoya, M. C., Kunisaki, Y., Megias, D., Marques, M., Carrera, A. C., Manes, S., Fukui, Y., Martinez, A. C., and Stein, J. V. (2004). Differential requirements for DOCK2 and phosphoinositide-3-kinase gamma during T and B lymphocyte homing. *Immunity* **21**, 429–441.
- Okada, T., Ngo, V. N., Ekland, E. H., Forster, R., Lipp, M., Littman, D. R., and Cyster, J. G. (2002). Chemokine requirements for B cell entry to lymph nodes and Peyer's patches. *J. Exp. Med.* **196**, 65–75.
- Okkenhaug, K., and Vanhaesebroeck, B. (2003). PI3K in lymphocyte development, differentiation and activation. *Nat. Rev. Immunol.* **3**, 317–330.
- Pearce, G., Angeli, V., Randolph, G. J., Junt, T., von Andrian, U., Schnittler, H. J., and Jessberger, R. (2006). Signaling protein SWAP-70 is required for efficient B cell homing to lymphoid organs. *Nat. Immunol.* **7**, 827–834.

- Perez, O. D., Mitchell, D., Jager, G. C., South, S., Murriel, C., McBride, J., Herzenberg, L. A., Kinoshita, S., and Nolan, G. P. (2003). Leukocyte functional antigen 1 lowers T cell activation thresholds and signaling through cytohesin-1 and Jun-activating binding protein 1. *Nat. Immunol.* **4**, 1083–1092.
- Peterson, E. J. (2003). The TCR ADAPts to integrin-mediated cell adhesion. *Immunol. Rev.* **192**, 113–121.
- Peterson, E. J., Woods, M. L., Dmowski, S. A., Derimanov, G., Jordan, M. S., Wu, J. N., Myung, P. S., Liu, Q. H., Pribila, J. T., Freedman, B. D., Shimizu, Y., and Koretzky, G. A. (2001). Coupling of the TCR to integrin activation by Slap-130/Fyb. *Science* **293**, 2263–2265.
- Petruzzelli, L., Maduzia, L., and Springer, T. A. (1995). Activation of lymphocyte function-associated molecule-1 (CD11a/CD18) and Mac-1 (CD11b/CD18) mimicked by an antibody directed against CD18. *J. Immunol.* **155**, 854–866.
- Reedquist, K. A., Ross, E., Koop, E. A., Wolthuis, R. M., Zwartkruis, F. J., van Kooyk, Y., Salmon, M., Buckley, C. D., and Bos, J. L. (2000). The small GTPase, Rap1, mediates CD31-induced integrin adhesion. *J. Cell Biol.* **148**, 1151–1158.
- Regelmann, G. A., Danzi, N. M., Wanjalla, C., and Alexandropoulos, K. (2006). Chat-H regulates T lymphocyte trafficking by acting upstream of Rap1 in chemokine-induced inside-out signaling. *Immunity*. **25**, 907–918.
- Reif, K., Okkenhaug, K., Sasaki, T., Penninger, J. M., Vanhaesebroeck, B., and Cyster, J. G. (2004). Cutting edge: Differential roles for phosphoinositide 3-kinases, p110gamma and p110delta, in lymphocyte chemotaxis and homing. *J. Immunol.* **173**, 2236–2240.
- Reynolds, L. F., Smyth, L. A., Norton, T., Freshney, N., Downward, J., Kioussis, D., and Tybulewicz, V. L. (2002). Vav1 transduces T cell receptor signals to the activation of phospholipase C- γ 1 via phosphoinositide 3-kinase-dependent and -independent pathways. *J. Exp. Med.* **195**, 1103–1114.
- Roberts, A. W., Kim, C., Zhen, L., Lowe, J. B., Kapur, R., Petryniak, B., Spaetti, A., Pollock, J. D., Borneo, J. B., Bradford, G. B., Atkinson, S. J., Dinauer, M. C., *et al.* (1999). Deficiency of the hematopoietic cell-specific Rho family GTPase Rac2 is characterized by abnormalities in neutrophil function and host defense. *Immunity* **10**, 183–196.
- Robinson, M. K., Andrew, D., Rosen, H., Brown, D., Orllepp, S., Stephens, P., and Butcher, E. C. (1992). Antibody against the Leu-CAM beta-chain (CD18) promotes both LFA-1- and CR3-dependent adhesion events. *J. Immunol.* **148**, 1080–1085.
- Rodriguez-Fernandez, J. L., Sanchez-Martin, L., Rey, M., Vicente-Manzanares, M., Narumiya, S., Teixido, J., Sanchez-Madrid, F., and Cabanas, C. (2001). Rho and Rho-associated kinase modulate the tyrosine kinase PYK2 in T-cells through regulation of the activity of the integrin LFA-1. *J. Biol. Chem.* **276**, 40518–40527.
- Romzek, N. C., Harris, E. S., Dell, C. L., Skronek, J., Hasse, E., Reynolds, P. J., Hunt, S. W., 3rd, and Shimizu, Y. (1998). Use of a beta1 integrin-deficient human T cell to identify beta1 integrin cytoplasmic domain sequences critical for integrin function. *Mol. Biol. Cell* **9**, 2715–2727.
- Rosen, H., and Goetzl, E. J. (2005). Sphingosine 1-phosphate and its receptors: An autocrine and paracrine network. *Nat. Rev. Immunol.* **5**, 560–570.
- Rozengurt, E., Rey, O., and Waldron, R. T. (2005). Protein kinase D signaling. *J. Biol. Chem.* **280**, 13205–13208.
- Rubtsov, A., Strauch, P., Digiacoimo, A., Hu, J., Pelanda, R., and Torres, R. M. (2005). Lsc regulates marginal-zone B cell migration and adhesion and is required for the IgM T-dependent antibody response. *Immunity* **23**, 527–538.
- Sah, V. P., Seasholtz, T. M., Sagi, S. A., and Brown, J. H. (2000). The role of Rho in G protein-coupled receptor signal transduction. *Annu. Rev. Pharmacol. Toxicol.* **40**, 459–489.

- Sakakibara, A., Hattori, S., Nakamura, S., and Katagiri, T. (2003). A novel hematopoietic adaptor protein, Chat-H, positively regulates T cell receptor-mediated interleukin-2 production by Jurkat cells. *J. Biol. Chem.* **278**, 6012–6017.
- Salas, A., Shimaoka, M., Chen, S., Carman, C. V., and Springer, T. (2002). Transition from rolling to firm adhesion is regulated by the conformation of the I domain of the integrin lymphocyte function-associated antigen-1. *J. Biol. Chem.* **277**, 50255–50262.
- Salas, A., Shimaoka, M., Kogan, A. N., Harwood, C., von Andrian, U. H., and Springer, T. A. (2004). Rolling adhesion through an extended conformation of integrin α L β 2 and relation to alpha I and beta I-like domain interaction. *Immunity* **20**, 393–406.
- Salas, A., Shimaoka, M., Phan, U., Kim, M., and Springer, T. A. (2006). Transition from rolling to firm adhesion can be mimicked by extension of integrin α L β 2 in an intermediate affinity state. *J. Biol. Chem.* **281**, 10876–10882.
- Samelson, L. E. (2002). Signal transduction mediated by the T cell antigen receptor: The role of adapter proteins. *Annu. Rev. Immunol.* **20**, 371–394.
- Sampath, R., Gallagher, P. J., and Pavalko, F. M. (1998). Cytoskeletal interactions with the leukocyte integrin beta2 cytoplasmic tail: Activation-dependent regulation of associations with talin and α -actinin. *J. Biol. Chem.* **273**, 33588–33594.
- Sanchez-Madrid, F., and del Pozo, M. A. (1999). Leukocyte polarization in cell migration and immune interactions. *EMBO J.* **18**, 501–511.
- Sanui, T., Inayoshi, A., Noda, M., Iwata, E., Oike, M., Sasazuki, T., and Fukui, Y. (2003). DOCK2 is essential for antigen-induced translocation of TCR and lipid rafts, but not PKC- θ and LFA-1, in T cells. *Immunity* **19**, 119–129.
- Sastry, S. K., and Horwitz, A. F. (1993). Integrin cytoplasmic domains: Mediators of cytoskeletal linkages and extra- and intracellular initiated transmembrane signaling. *Curr. Biol.* **5**, 819–831.
- Sebzda, E., Bracke, M., Tugal, T., Hogg, N., and Cantrell, D. A. (2002). Rap1A positively regulates T cells via integrin activation rather than inhibiting lymphocyte signaling. *Nat. Immunol.* **3**, 251–258.
- Semrich, M., Smith, A., Feterowski, C., Beer, S., Engelhardt, B., Busch, D. H., Bartsch, B., Laschinger, M., Hogg, N., Pfeffer, K., and Holzmann, B. (2005). Importance of integrin LFA-1 deactivation for the generation of immune responses. *J. Exp. Med.* **201**, 1987–1998.
- Shamri, R., Grabovsky, V., Gauguier, J. M., Feigelson, S., Manevich, E., Kolanus, W., Robinson, M. K., Staunton, D. E., von Andrian, U. H., and Alon, R. (2005). Lymphocyte arrest requires instantaneous induction of an extended LFA-1 conformation mediated by endothelium-bound chemokines. *Nat. Immunol.* **6**, 497–506.
- Shimaoka, M., Takagi, J., and Springer, T. A. (2002). Conformational regulation of integrin structure and function. *Annu. Rev. Biophys. Biomol. Struct.* **485**, 485–516.
- Shimonaka, M., Katagiri, K., Nakayama, T., Fujita, N., Tsuruo, T., Yoshie, O., and Kinashi, T. (2003). Rap1 translates chemokine signals to integrin activation, cell polarization, and motility across vascular endothelium under flow. *J. Cell Biol.* **161**, 417–427.
- Shimaoka, M., Salas, A., Yang, W., Weitz-Schmidt, G., and Springer, T. A. (2003a). Small molecule integrin antagonists that bind to the β 2 subunit I-like domain and activate signals in one direction and block them in the other. *Immunity* **19**, 391–402.
- Shimaoka, M., Xiao, T., Liu, J. H., Yang, Y., Dong, Y., Jun, C. D., McCormack, A., Zhang, R., Joachimiak, A., Takagi, J., Wang, J. H., and Springer, T. A. (2003b). Structures of the alpha L I domain and its complex with ICAM-1 reveal a shape-shifting pathway for integrin regulation. *Cell* **112**, 99–111.
- Shimaoka, M., Kim, M., Cohen, E. H., Yang, W., Astrof, N., Peer, D., Salas, A., Ferrand, A., and Springer, T. A. (2006). AL-57, a ligand-mimetic antibody to integrin LFA-1, reveals chemokine-induced affinity up-regulation in lymphocytes. *Proc. Natl. Acad. Sci. USA* **103**, 13991–13996.

- Shimizu, Y., and Mobley, J. L. (1993). Distinct divalent cation requirements for integrin-mediated CD4+ T lymphocyte adhesion to ICAM-1, fibronectin, VCAM-1, and invasins. *J. Immunol.* **151**, 4106–4115.
- Shimizu, Y., Mobley, J. L., Finkelstein, L. D., and Chan, A. S. (1995). A role for phosphatidylinositol 3-kinase in the regulation of beta 1 integrin activity by the CD2 antigen. *J. Cell Biol.* **131**, 1867–1880.
- Shinohara, M., Terada, Y., Iwamatsu, A., Shinohara, A., Mochizuki, N., Higuchi, M., Gotoh, Y., Ihara, S., Nagata, S., Itoh, H., Fukui, Y., and Jessberger, R. (2002). SWAP-70 is a guanine-nucleotide-exchange factor that mediates signalling of membrane ruffling. *Nature* **416**, 759–763.
- Shulman, Z., Pasvolsky, R., Woolf, E., Grabovsky, V., Feigelson, S. W., Erez, N., Fukui, Y., and Alon, R. (2006). DOCK2 regulates chemokine-triggered lateral lymphocyte motility but not transendothelial migration. *Blood* **108**, 2150–2158.
- Sims, T. N., and Dustin, M. L. (2002). The immunological synapse: Integrins take the stage. *Immunol. Rev.* **186**, 100–117.
- Smith, A., Bracke, M., Leitinger, B., Porter, J. C., and Hogg, N. (2003). LFA-1-induced T cell migration on ICAM-1 involves regulation of MLCK-mediated attachment and ROCK-dependent detachment. *J. Cell Sci.* **116**, 3123–3133.
- Smith, A., Carrasco, Y. R., Stanley, P., Kieffer, N., Batista, F. D., and Hogg, N. (2005). A talin-dependent LFA-1 focal zone is formed by rapidly migrating T lymphocytes. *J. Cell Biol.* **170**, 141–151.
- Springer, T. A. (1990). Adhesion receptors of the immune system. *Nature* **346**, 425–434.
- Springer, T. A. (1995). Traffic signals on endothelium for lymphocyte recirculation and leukocyte emigration. *Annu. Rev. Physiol.* **57**, 827–872.
- Staunton, D. E., Lupper, M. L., Liddington, R., and Gallatin, W. M. (2006). Targeting integrin structure and function in disease. *Adv. Immunol.* **91**, 111–157.
- Stein, J. V., Rot, A., Luo, Y., Narasimhaswamy, M., Nakano, H., Gunn, M. D., Matsuzawa, A., Quackenbush, E. J., Dorf, M. E., and von Andrian, U. H. (2000). The CC chemokine thymus-derived chemotactic agent 4 (TCA-4, secondary lymphoid tissue chemokine, 6CKine, exodus-2) triggers lymphocyte function-associated antigen 1-mediated arrest of rolling T lymphocytes in peripheral lymph node high endothelial venules. *J. Exp. Med.* **191**, 61–76.
- Stewart, M. P., McDowall, A., and Hogg, N. (1998). LFA-1-mediated adhesion is regulated by cytoskeletal restraint and by a Ca²⁺-dependent protease, calpain. *J. Cell Biol.* **140**, 699–707.
- Tadokoro, S., Shattil, S. J., Eto, K., Tai, V., Liddington, R. C., de Pereda, J. M., Ginsberg, M. H., and Calderwood, D. A. (2003). Talin binding to integrin beta tails: A final common step in integrin activation. *Science* **302**, 103–106.
- Takagi, J., and Springer, T. A. (2002). Integrin activation and structural rearrangement. *Immunol. Rev.* **186**, 141–163.
- Takagi, J., Petre, B. M., Walz, T., and Springer, T. A. (2002). Global conformational rearrangements in integrin extracellular domains in outside-in and inside-out signaling. *Cell* **110**, 599–611.
- Takesono, A., Horai, R., Mandai, M., Dombroski, D., and Schwartzberg, P. L. (2004). Requirement for Tec kinases in chemokine-induced migration and activation of Cdc42 and Rac. *Curr. Biol.* **14**, 917–922.
- Tamada, M., Sheetz, M. P., and Sawada, Y. (2004). Activation of a signaling cascade by cytoskeleton stretch. *Dev. Cell* **7**, 709–718.
- Tohyama, Y., Katagiri, K., Pardi, R., Lu, C., Springer, T. A., and Kinashi, T. (2003). The critical cytoplasmic regions of the α L/ β 2 integrin in Rap1-induced adhesion and migration. *Mol. Biol. Cell* **14**, 2570–2582.

- Tommasi, S., Dammann, R., Jin, S. G., Zhang, X. F., Avruch, J., and Pfeifer, G. P. (2002). RASSF3 and NORE1: Identification and cloning of two human homologues of the putative tumor suppressor gene RASSF1. *Oncogene* **21**, 2713–2720.
- Tybulewicz, V. L., Ardouin, L., Prisco, A., and Reynolds, L. F. (2003). Vav1: A key signal transducer downstream of the TCR. *Immunol. Rev.* **192**, 42–52.
- van Kooyk, Y., and Figdor, C. G. (2000). Avidity regulation of integrins: The driving force in leukocyte adhesion. *Curr. Opin. Cell Biol.* **12**, 542–547.
- Vicente-Manzanares, M., Cruz-Adalia, A., Martin-Cofreces, N. B., Cabrero, J. R., Dosil, M., Alvarado-Sanchez, B., Bustelo, X. R., and Sanchez-Madrid, F. (2005). Control of lymphocyte shape and the chemotactic response by the GTP exchange factor Vav. *Blood* **105**, 3026–3034.
- Vielkind, S., Gallagher-Gambarelli, M., Gomez, M., Hinton, H. J., and Cantrell, D. A. (2005). Integrin regulation by RhoA in thymocytes. *J. Immunol.* **175**, 350–357.
- Vogel, V., and Sheetz, M. (2006). Local force and geometry sensing regulate cell functions. *Nat. Rev. Mol. Cell Biol.* **7**, 265–275.
- Wang, H., Moon, E. Y., Azouz, A., Wu, X., Smith, A., Schneider, H., Hogg, N., and Rudd, C. E. (2003). SKAP-55 regulates integrin adhesion and formation of T cell-APC conjugates. *Nat. Immunol.* **4**, 366–374.
- Wang, H., McCann, F. E., Gordan, J. D., Wu, X., Raab, M., Malik, T. H., Davis, D. M., and Rudd, C. E. (2004). ADAP-SLP-76 binding differentially regulates supramolecular activation cluster (SMAC) formation relative to T cell-APC conjugation. *J. Exp. Med.* **200**, 1063–1074.
- Ward, S. G. (2004). Do phosphoinositide 3-kinases direct lymphocyte navigation? *Trends Immunol.* **25**, 67–74.
- Warnock, R. A., Campbell, J. J., Dorf, M. E., Matsuzawa, A., McEvoy, L. M., and Butcher, E. C. (2000). The role of chemokines in the microenvironmental control of T versus B cell arrest in Peyer's patch high endothelial venules. *J. Exp. Med.* **191**, 77–88.
- Weber, K. S., Weber, C., Ostermann, G., Dierks, H., Nagel, W., and Kolanus, W. (2001). Cytohesin-1 is a dynamic regulator of distinct LFA-1 functions in leukocyte arrest and transmigration triggered by chemokines. *Curr. Biol.* **11**, 1969–1974.
- Windh, R. T., Lee, M. J., Hla, T., An, S., Barr, A. J., and Manning, D. R. (1999). Differential coupling of the sphingosine 1-phosphate receptors Edg-1, Edg-3, and H218/Edg-5 to the G(i), G(q), and G(12) families of heterotrimeric G proteins. *J. Biol. Chem.* **274**, 27351–27358.
- Woods, A. J., White, D. P., Caswell, P. T., and Norman, J. C. (2004). PKD1/PKCmu promotes $\alpha\text{V}\beta\text{3}$ integrin recycling and delivery to nascent focal adhesions. *EMBO J.* **23**, 2531–2543.
- Woods, M. L., Kivens, W. J., Adelman, M. A., Qiu, Y., August, A., and Shimizu, Y. (2001). A novel function for the Tec family tyrosine kinase Itk in activation of beta 1 integrins by the T-cell receptor. *EMBO J.* **20**, 1232–1244.
- Worthylake, R. A., Lemoine, S., Watson, J. M., and Burridge, K. (2001). RhoA is required for monocyte tail retraction during transendothelial migration. *J. Cell Biol.* **154**, 147–160.
- Xie, C., Shimaoka, M., Xiao, T., Schwab, P., Klickstein, L. B., and Springer, T. A. (2004). The integrin α -subunit leg extends at a Ca^{2+} -dependent epitope in the thigh/genu interface upon activation. *Proc. Natl. Acad. Sci. USA* **101**, 15422–15427.
- Xiong, J. P., Stehle, T., Diefenbach, B., Zhang, R., Dunker, R., Scott, D. L., Joachimiak, A., Goodman, S. L., and Arnaout, M. A. (2001). Crystal structure of the extracellular segment of integrin $\alpha\text{V}\beta\text{3}$. *Science* **294**, 339–345.
- Xiong, J. P., Stehle, T., Zhang, R., Joachimiak, A., Frech, M., Goodman, S. L., and Arnaout, M. A. (2002). Crystal structure of the extracellular segment of integrin alpha Vbeta3 in complex with an Arg-Gly-Asp ligand. *Science* **296**, 151–155.
- Yan, B., Calderwood, D. A., Yaspan, B., and Ginsberg, M. H. (2001). Calpain cleavage promotes talin binding to the beta 3 integrin cytoplasmic domain. *J. Biol. Chem.* **276**, 28164–28170.

- Yang, W., Shimaoka, M., Chen, J., and Springer, T. A. (2004a). Activation of integrin beta-subunit I-like domains by one-turn C-terminal alpha-helix deletions. *Proc. Natl. Acad. Sci. USA* **101**, 2333–2338.
- Yang, W., Shimaoka, M., Salas, A., Takagi, J., and Springer, T. A. (2004b). Intersubunit signal transmission in integrins by a receptor-like interaction with a pull spring. *Proc. Natl. Acad. Sci. USA* **101**, 2906–2911.
- Zell, T., Hunt, S. W. R., Mobley, J. L., Finkelstein, L. D., and Shimizu, Y. (1996). CD28-mediated up-regulation of beta 1-integrin adhesion involves phosphatidylinositol 3-kinase. *J. Immunol.* **156**, 883–886.
- Zhang, W., Shao, Y., Fang, D., Huang, J., Jeon, M. S., and Liu, Y. C. (2003). Negative regulation of T cell antigen receptor-mediated Crk-L-C3G signaling and cell adhesion by Cbl-b. *J. Biol. Chem.* **278**, 23978–23983.

Spatiotemporal regulation of the kinase Mst1 by binding protein RAPL is critical for lymphocyte polarity and adhesion

Koko Katagiri¹, Masashi Imamura² & Tatsuo Kinashi¹

RAPL, a protein that binds the small GTPase Rap1, is required for efficient immune cell trafficking. Here we have identified the kinase Mst1 as a critical effector of RAPL. RAPL regulated the localization and kinase activity of Mst1. 'Knockdown' of the gene encoding Mst1 demonstrated its requirement for the induction of both a polarized morphology and integrin LFA-1 clustering and adhesion triggered by chemokines and T cell receptor ligation. RAPL and Mst1 localized to vesicular compartments and dynamically translocated with LFA-1 to the leading edge upon Rap1 activation, suggesting a regulatory function for the RAPL-Mst1 complex in intracellular transport of LFA-1. Our study demonstrates a previously unknown function for Mst1 of relaying the Rap1-RAPL signal to induce cell polarity and adhesion of lymphocytes.

The immune system requires considerable trafficking ability of immune cells; lymphocytes recirculate in the blood and peripheral lymphoid tissues, searching for foreign antigens carried by migrating antigen-presenting dendritic cells. Dynamic modulation of integrin adhesive function is critical during such trafficking^{1,2}. After stimulation with chemokines or antigens, lymphocyte integrin adhesion is transiently upregulated with little change in surface expression. The intracellular signaling triggered after stimulation that mediates this change, called 'inside-out signaling', is ultimately thought to control integrin conformation³ and surface distribution^{4,5}. Cellular and genetic studies have shown that immune cell adhesion mediated by β_1 and β_2 integrins is modulated by protein and lipid kinases, small GTPases of the Ras and Rho families, and their regulators and adaptor proteins^{6,7}.

Integrin-mediated attachment facilitates lymphocyte transendothelial and interstitial migration. Cell migration is a coordinated process: asymmetrical cell morphology develops, forming a protrusion and uropod, and new adhesion sites form at the leading edge and detach at the rear, pulling the cell body in the direction of cell migration^{8,9}. Cell polarization and regulated adhesion are induced by extrinsic and intrinsic cues, which prompt cytoskeletal reorganization and vesicle transport, including endocytosis and recycling of integrins¹⁰⁻¹⁴. Understanding of the molecular network that orchestrates activation of integrin and cell migration, however, remains incomplete.

The small GTPase Rap1 is an important inside-out signal in controlling cell adhesion through modulating the affinity and/or spatial organization of integrins¹⁵. Stimulation with chemokines or antigen stimulation through the T cell antigen receptor (TCR) activates Rap1, which is required for transmigration of lymphocytes through endo-

thelial cells under flow and immunological synapse formation with antigen-presenting cells^{16,17}. Rap1 activation has been found to be defective in human leukocyte adhesion deficiency¹⁸. Rap1A-deficient T cells and B cells show impaired β_1 and β_2 integrin clustering and adhesion¹⁹. Those studies support the idea that Rap1 is a crucial inside-out signaling molecule *in vivo*. RAPL is a Rap1-binding effector protein that mediates Rap1-dependent affinity and spatial distribution of the integrin LFA-1 (ref. 20). Lymphoid tissues are enriched for RAPL²⁰ and Nore1, an alternatively spliced product of the gene encoding RAPL (*Rassf5*). Targeted deletion of the locus encoding RAPL has demonstrated defective adhesion and migration of lymphocytes and dendritic cells²². After Rap1 activation, RAPL forms a complex with LFA-1 and relocates to the leading edge and also accumulates at immunological synapses. A patch-like distribution of LFA-1 at the leading edge is critical for triggering adhesion and motility²⁰. Rap1- and RAPL-triggered changes in integrin spatial distribution in concert with the induction of cell polarity result in robust cell motility.

To explore further the molecular mechanisms by which Rap1 and RAPL regulate integrin functions and cell polarity, we have used yeast two-hybrid screening for RAPL-associated molecules with an activated RAPL mutant protein as the 'bait'. This analysis identified the kinase Mst1 as a 'downstream' effector molecule of RAPL. In drosophila, the Mst ortholog Hipo has many crucial functions in the regulation of cell growth and apoptosis²³. In mammals, Mst1 is also associated with apoptosis, although its physiological function remains unclear²⁴. Here we demonstrate a previously unknown function for Mst1 in the regulation of lymphocyte polarization and adhesion 'downstream' of Rap1 and RAPL.

¹Department of Molecular Genetics, Institute of Biomedical Science, Kansai Medical University, Osaka 570-8506, Japan. ²Center Research Institute, Ishihara Sangyo Kaisha, Kusatsu, Shiga 525-0025, Japan. Correspondence should be addressed to T.K. (kinashi@takii.kmu.ac.jp).

Received 30 March; accepted 12 July; published online 6 August 2006; doi:10.1038/ni1374

RESULTS

Association of RAPL with MST1

Using an activated RAPL mutant as the bait, we isolated cDNA encoding human MST1 or MST2 by yeast two-hybrid screening and did RT-PCR of a human leukocyte cDNA library using activated RAPL mutant as the bait. We determined that MST2 protein was barely detectable in lymphocytes, so we focused on MST1 in subsequent analyses. To confirm the association of RAPL with MST1, we transfected COS cells with Myc-tagged RAPL and V5-tagged MST1 and examined their association by immunoprecipitation (Fig. 1a). MST1 and RAPL could be immunoprecipitated together using antibody to V5 (anti-V5) or anti-Myc. Deletion of the C-terminal region of RAPL abolished its association with MST1 but deletion of the N-terminal region of RAPL did not (Fig. 1a). MST1 has an N-terminal kinase domain followed by a C-terminal regulatory region. A truncated MST1 mutant lacking the C-terminal regulatory region lost the ability to associate with RAPL. A fusion protein of glutathione S-transferase (GST) and the RAPL coiled-coil domain precipitated wild-type MST1 but not the MST1 mutant lacking the C-terminal regulatory region (Fig. 1b). These results indicate that the coiled-coil region of RAPL associates with the MST1 regulatory domain.

We then examined if endogenous RAPL and mouse Mst1 could be immunoprecipitated together using anti-Mst1 (Fig. 1c, left) or anti-RAPL (Fig. 1c, right) in the mouse pro-B cell line BAF stably expressing a constitutively active mutant form of Rap1 (Rap1V12) or vector alone (as a control).

RAPL and Mst1 were associated each other in the absence of exogenous stimuli. That association increased in the presence of Rap1V12. As the amount of RAPL and Mst1 protein in Rap1V12-expressing cells was similar to that in the control cells, these results indicate that active Rap1 promotes the association of RAPL and Mst1.

Activation and subcellular localization of Mst1 by RAPL

We next examined the activation of Mst1 by Rap1 and RAPL. Using an 'anti-phosphopeptide' antibody to p20-activated kinase (PAK) that cross-reacts with phosphorylated active Mst1 (refs. 25,26), we examined the effect of Rap1 and RAPL on Mst1 phosphorylation in BAF cells (Fig. 2a). Although Mst1 was basally phosphorylated in BAF cells, phosphorylation was augmented after overexpression of Rap1V12 and RAPL; the phosphorylation of PAK was not substantially changed (Fig. 2a). Consistent with those results, *in vitro* immune complex kinase assays using anti-Mst1 showed that the kinase activity against myelin basic protein (MBP) as a substrate was increased by Rap1V12 and RAPL; this increase was accompanied by autophosphorylation of a protein corresponding to the size of Mst1 (Fig. 2b, left). To confirm that the increased kinase activity was derived from Mst1 but not associated kinases, we stably introduced V5-tagged wild-type MST1 and kinase-inactive (K59R) MST1 into Rap1V12-expressing BAF cells and did an immune complex kinase assay. Wild-type MST1 precipi-

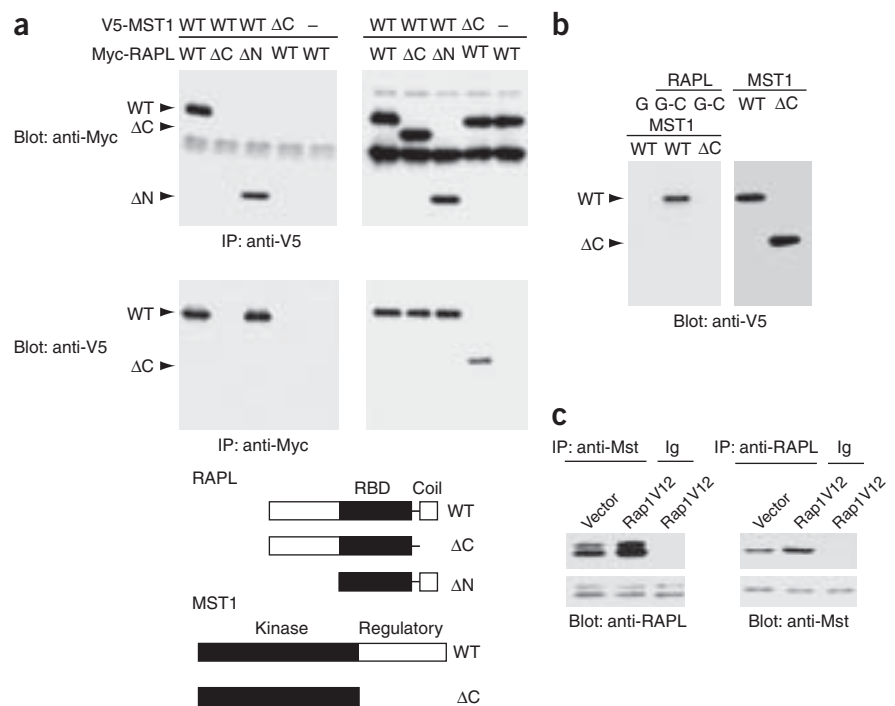


Figure 1 Association of RAPL and MST1. (a) Immunoprecipitation (IP) of RAPL and MST1. COS cells were transfected with Myc-tagged RAPL constructs (Myc-RAPL: wild-type (WT) or deletion mutants lacking the coiled-coil region (ΔC) or the N-terminal region (ΔN)), together with V5-tagged MST1 constructs (V5-MST1: wild-type (WT), a deletion mutant lacking the regulatory region (ΔC) or empty vector (-)). Cell lysates were immunoprecipitated with anti-V5 or anti-Myc followed by immunoblot with anti-Myc (top left blot) or anti-V5 (bottom left blot). Input amounts, top right blot (RAPL) and bottom right blot (MST1). RBD (top diagram), Ras binding domain. (b) Association of the coiled-coil domain of RAPL with MST1. A fusion protein of GST and the coiled-coil domain of RAPL (G-C) was used to precipitate V5-tagged MST1 (WT and ΔC). Bound proteins were eluted with glutathione and were analyzed by immunoblot with anti-V5. G, GST alone. (c) Augmentation of the Mst1-RAPL association by active Rap1 (Rap1V12). Endogenous RAPL and Mst1 were immunoprecipitated with anti-Mst1 (left) or anti-RAPL (right) from BAF cells transfected with vector alone or with Rap1V12; proteins isolated were analyzed by sequential immunoblot with anti-RAPL or anti-Mst1, respectively. Ig, rabbit serum (right) and rat IgG (left; controls). Data are representative of two (b) or three (a,c) independent experiments.

tated with anti-V5 increased the phosphorylation of MBP, accompanied by autophosphorylation of V5-MST1, whereas immunoprecipitated kinase-inactive mutant poorly phosphorylated MBP (Fig. 2b, right). These results indicated that MST1 itself was mostly responsible for the increased kinase activity. Because MST1 can form dimers, the residual kinase activity could have been due to endogenous Mst1 associated with the kinase-inactive mutant²⁷. These results collectively indicate that Rap1 and RAPL can activate Mst1.

As Rap1 is activated by treatment with chemokines or by TCR crosslinking, we investigated if Mst1 activation occurred in those conditions. We also determined whether Mst1 activation required RAPL using T cells derived from RAPL-deficient mice. In wild-type T cells, we detected phosphorylated Mst1 in unstimulated cells, but phosphorylated Mst1 was transiently upregulated in the 5–10 min after stimulation by TCR crosslinking or treatment with the chemokine CCL21 (Fig. 2c). There was also an increase in PAK phosphorylation along a similar time course. In contrast, Mst1 phosphorylation was undetectable or was substantially reduced in RAPL-deficient T cells, even after stimulation with CCL21 or TCR crosslinking (Fig. 2c). Mst1 expression was similar in wild-type and RAPL-deficient T cells. The increase in PAK phosphorylation was unaffected by RAPL deficiency. These results indicate that RAPL is required for Mst1 activation in lymphocytes.

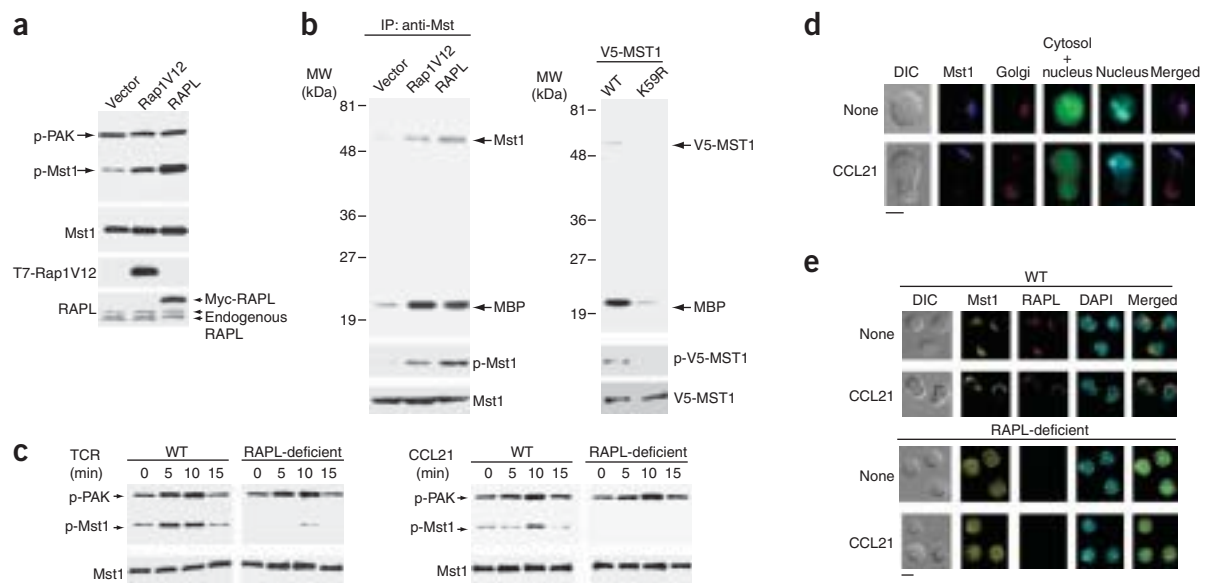


Figure 2 Mst1 activation by RAPL and Rap1. **(a)** Phosphorylation (p-) of endogenous Mst1 and PAK in BAF cells transfected with RAPL, Rap1V12 or a vector control, examined with anti-phosphorylated PAK that cross-reacts with phosphorylated Mst1 and Mst2. Below, expression of Mst1, Rap1V12 and RAPL. **(b)** *In vitro* kinase assay. Endogenous Mst1 was immunoprecipitated from BAF cells transfected with vector alone, Rap1V12 or RAPL. V5-tagged wild-type (WT) or kinase-inactive (K59R) MST1 was introduced into BAF cells expressing Rap1V12, followed by immunoprecipitation with anti-V5. Immune complex kinase assays with [γ - 32 P]ATP and myelin basic protein (MBP) detect Mst1 autophosphorylation and MBP phosphorylation. Bottom blots, endogenous Mst1. **(c)** Activation of Mst1 in T lymphocytes from wild-type and RAPL-deficient mice. T cells were stimulated with anti-CD3 (TCR) or CCL21 (times, above lanes) and phosphorylation of Mst1 was assessed by immunoblot of cell lysates as described in **a**. Bottom blots, total Mst1. **(d)** Localization of Mst1 in mouse T cells in the presence (CCL21) or absence (None) of CCL21 stimulation, detected by immunostaining for Mst1 (blue). Bodipy-ceramide, BCECF and Hoechst 33342 dyes stain the Golgi complex (red), cytosol and nucleus (green), and nucleus (light blue), respectively. **(e)** Localization of Mst1 and RAPL in wild-type and RAPL-deficient T cells in the presence (CCL21) or absence (None) of CCL21 stimulation, detected by immunostaining for Mst1 (yellow) and RAPL (red); DAPI counterstaining (4,6-diamidino-2-phenylindole; blue) indicates nuclei. DIC, differential interference contrast. Scale bars (**d,e**), 5 μ m. All data are representative of three or four independent experiments.

Those results prompted us to investigate the subcellular localization of Mst1. Mst1 was localized in perinuclear regions in close proximity to the Golgi complex in primary T cells (**Fig. 2d** and **Supplementary Fig. 1** online). When stimulated with CCL21, T cells were transformed into polarized cells with a leading edge and uropod, and Mst1 was redistributed to the leading edge, dissociated from the Golgi complex (**Fig. 2d** and **Supplementary Fig. 1**). RAPL and Mst1 localized together in unstimulated T cells and also at the leading edge in CCL21-stimulated T cells (**Fig. 2e**). In contrast, Mst1 was distributed diffusely throughout both the cytoplasm and the nucleus in RAPL-deficient T cells. Chemokine-stimulated RAPL-deficient T cells showed defective cell polarization, maintaining a round, nonpolarized morphology, as reported before²²; Mst1 remained diffusely distributed (**Fig. 2e**). These results demonstrate that RAPL is indispensable for Mst1 activation and maintenance of subcellular localization in T cells in both basal and stimulated states.

Upregulation of LFA-1-dependent adhesion by Mst1

To test the stimulation of adhesion by Mst1, we stably transfected BAF cells expressing human LFA-1 (BAF-LFA-1 cells)²⁸ with the gene encoding MST1 (*STK4*) and assessed their adhesion to intercellular adhesion molecule 1 (ICAM-1). Initially, BAF-LFA-1 cells were not adherent, but they adhered to ICAM-1 after stimulation with phorbol-12-myristate-13-acetate (PMA), a potent activator of integrins (**Fig. 3a**). When MST1 was overexpressed in BAF-LFA-1 cells, adhesion to ICAM-1 in unstimulated BAF-LFA-1 transfectants was augmented in a way that correlated with MST1 expression (**Fig. 3a**). Cells overexpressing MST1 showed cell spreading on ICAM-1

(**Fig. 3b**). Both a truncated MST1 mutant lacking the C-terminal regulatory region (MST1 amino acids 1–326) and a kinase-inactive (K59R) MST1 mutant failed to stimulate adhesion, although they responded to PMA in the same way as wild-type cells (**Fig. 3a**). MST1 also stimulated adhesion to ICAM-1 and augmented TCR-induced adhesion after being introduced into the mouse T cell hybridoma 3A9 (**Fig. 3c**). Whereas the MST1 mutant with C-terminal truncation did not affect the basal or TCR-stimulated adhesion, the kinase-inactive (K59R) MST1 mutant inhibited TCR-stimulated adhesion, indicating that the kinase-inactive mutant acted as a dominant negative protein. These results collectively indicate that MST1 can activate LFA-1 in a way requiring the kinase activity and C-terminal regulatory region of MST1.

We next examined whether MST1 could affect LFA-1 clustering and affinity. In control BAF-LFA-1 cells, LFA-1 was uniformly distributed over the plasma membrane (**Fig. 3d**). In contrast, overexpression of MST1 induced patch-like LFA-1 clustering, accompanied by morphological changes similar to those seen in lymphocyte polarization. To quantify LFA-1 clustering, we measured the relative intensity of surface LFA-1 along the front-to-back and side-to-side lines in z-stack images obtained by confocal microscopy. There were increases of up to tenfold in LFA-1 intensity on the front membrane compared with the peak value of intensity on the side and rear (**Fig. 3e** and **Supplementary Fig. 2** online). Although Rap1 and RAPL increase the ligand-binding affinity of LFA-1 (refs. 20,28), we did not detect affinity changes in MST1-overexpressing BAF cells using a soluble ICAM-1-Fc chimera for the measurements (**Supplementary Fig. 3** online). We also did not detect Mst1 immunoprecipitated together with LFA-1

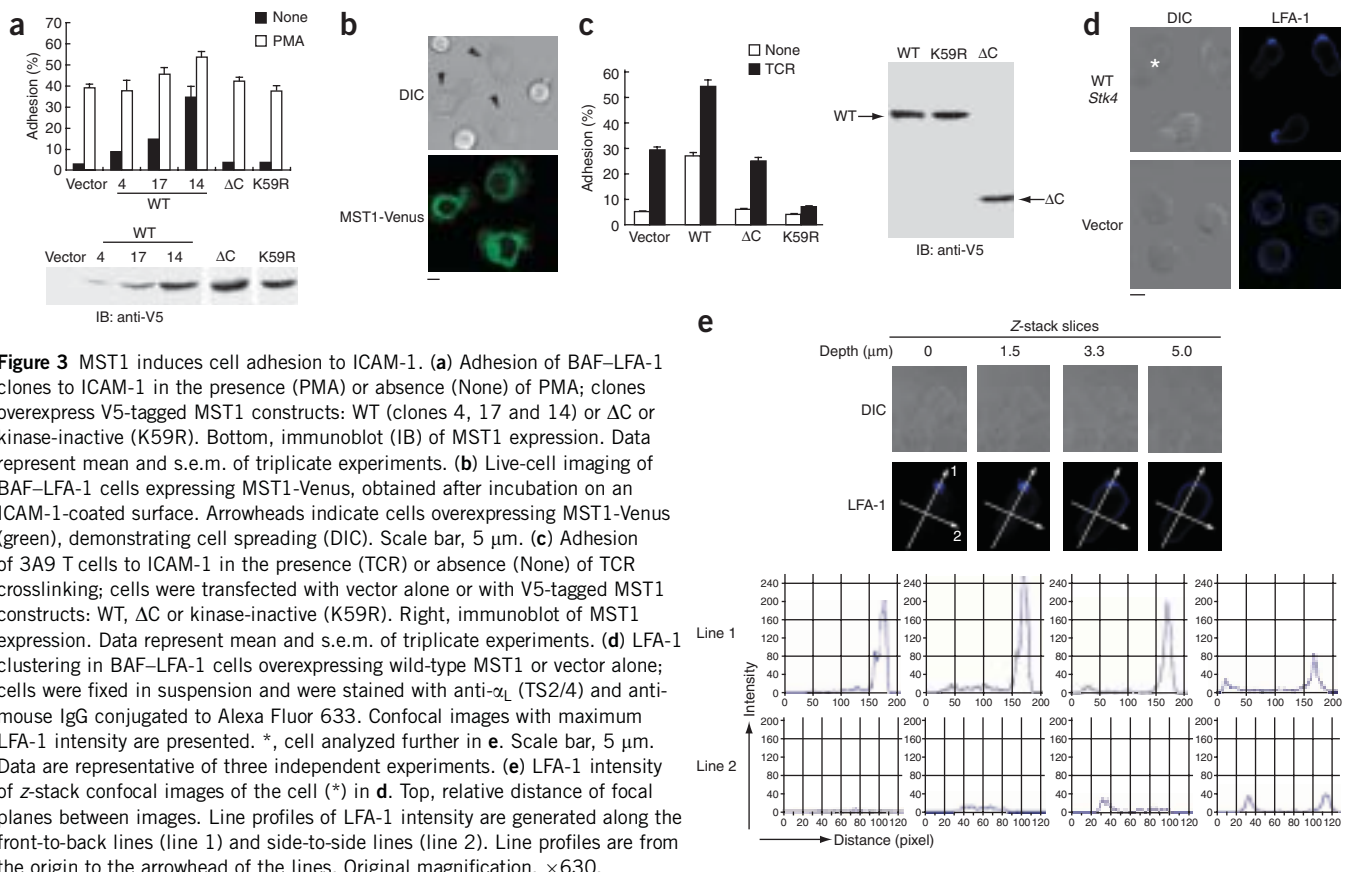


Figure 3 MST1 induces cell adhesion to ICAM-1. **(a)** Adhesion of BAF-LFA-1 clones to ICAM-1 in the presence (PMA) or absence (None) of PMA; clones overexpress V5-tagged MST1 constructs: WT (clones 4, 17 and 14) or Δ C or kinase-inactive (K59R). Bottom, immunoblot (IB) of MST1 expression. Data represent mean and s.e.m. of triplicate experiments. **(b)** Live-cell imaging of BAF-LFA-1 cells expressing MST1-Venus, obtained after incubation on an ICAM-1-coated surface. Arrowheads indicate cells overexpressing MST1-Venus (green), demonstrating cell spreading (DIC). Scale bar, 5 μ m. **(c)** Adhesion of 3A9 T cells to ICAM-1 in the presence (TCR) or absence (None) of TCR crosslinking; cells were transfected with vector alone or with V5-tagged MST1 constructs: WT, Δ C or kinase-inactive (K59R). Right, immunoblot of MST1 expression. Data represent mean and s.e.m. of triplicate experiments. **(d)** LFA-1 clustering in BAF-LFA-1 cells overexpressing wild-type MST1 or vector alone; cells were fixed in suspension and were stained with anti- α _L (TS2/4) and anti-mouse IgG conjugated to Alexa Fluor 633. Confocal images with maximum LFA-1 intensity are presented. *, cell analyzed further in **e**. Scale bar, 5 μ m. Data are representative of three independent experiments. **(e)** LFA-1 intensity of z-stack confocal images of the cell (*) in **d**. Top, relative distance of focal planes between images. Line profiles of LFA-1 intensity are generated along the front-to-back lines (line 1) and side-to-side lines (line 2). Line profiles are from the origin to the arrowhead of the lines. Original magnification, \times 630.

(Supplementary Fig. 3), suggesting that Mst1 does not directly associate with LFA-1.

Mst1 'knockdown' inhibits cell polarization and adhesion

Next we examined the requirement for Mst1 in cell polarization and adhesion by a gene 'knockdown' approach using small RNA-mediated interference technology. We tested several 21-nucleotide oligonucleotides specific for *Stk4* for gene-silencing efficiency after transient introduction into NIH 3T3 cells (data not shown). We then expressed the most efficient sequence in BAF-LFA-1 cells as short hairpin RNA (*Stk4* iRNA). We expressed a scrambled sequence in a similar way as a control (scrambled iRNA). We established stable 'knockdown' transfectants (BAF-LFA-1-*Stk4* iRNA cells) and control transfectants (BAF-LFA-1-scrambled iRNA cells) and assessed their Mst1 expression. Mst1 protein in BAF-LFA-1-*Stk4* iRNA cells was reduced to approximately 20% that in the parental BAF-LFA-1 cells and control BAF-LFA-1-scrambled iRNA cells (Fig. 4a, left). We investigated if depletion of Mst1 by iRNA could inhibit the cell polarization and adhesion induced by chemokines, a process that requires Rap1 and RAPL²². Mst1 depletion did not affect expression of LFA-1 or the chemokine receptor CXCR4 or CXCL12-stimulated Rap1 activation (data not shown). After stimulation with CXCL12, approximately 40% of both the parental BAF-LFA-1 cells and control BAF-LFA-1-scrambled iRNA cells had distinctive morphologies, with a leading edge, to which CXCR4 and LFA-1 localized, and a uropod, to which the uropod marker CD44 localized (Fig. 4b,c). In contrast, BAF-LFA-1-*Stk4* iRNA cells developed a polarized cell shapes only poorly when stimulated with CXCL12. Most cells remained round, retaining diffuse distribution of LFA-1, CXCR4 and CD44 (Fig. 4b,c). Rap1V12 expression in

parental BAF-LFA-1 cells induced cell polarization at higher frequencies (60–70%) than in BAF cells expressing vector only, whereas Mst1 'knockdown' also substantially reduced the number of polarized cells after Rap1V12 introduction (Fig. 4a, right, and c). Furthermore, the ability of BAF-LFA-1 cells to adhere to ICAM-1 in response to CXCL12 treatment or Rap1V12 exogenous expression was greatly diminished by Mst1 depletion, whereas that of control scrambled iRNA cells was similar to that of parental cells (Fig. 4d). This result indicates that Mst1 is critical for cell polarization, LFA-1 redistribution, and adhesion induced by Rap1V12 and CXCL12, at least in BAF cells.

As Mst1 seemed to accumulate at the leading edge in lymphocytes stimulated with CCL21 (Fig. 2), we examined the spatial relationship of MST1 and LFA-1. For this, we introduced a limited amount of MST1 fused with monomeric red fluorescent protein 1 (MST1-mRFP) into BAF-LFA-1 cells. MST1-mRFP was distributed as patch-like clusters in close proximity to LFA-1 patches in CXCL12-stimulated BAF-LFA-1 cells (Fig. 4e). Confocal microscopy of z-stack images showed that the MST1-mRFP intensity was approximately fourfold higher at the front area than at the rear (Fig. 4f), which was in parallel with the LFA-1 intensity with a high colocalization value ($r = 0.91$) at the front (Fig. 4f and Supplementary Fig. 4 online).

To determine the requirement for Mst1 in TCR-triggered adhesion, we depleted hen egg lysozyme (HEL)-specific 3A9 T cells of Mst1 by stably introducing *Stk4*-specific iRNA. We transfected control cells with a scrambled iRNA sequence. Mst1 protein abundance was reduced to approximately 15% that of parental or control cells (Fig. 5a). Depletion of Mst1 had little effect on the interleukin 2 (IL-2) production induced by TCR crosslinking, suggesting that Mst1 is not involved in the control of IL-2 production (Fig. 5b). When we

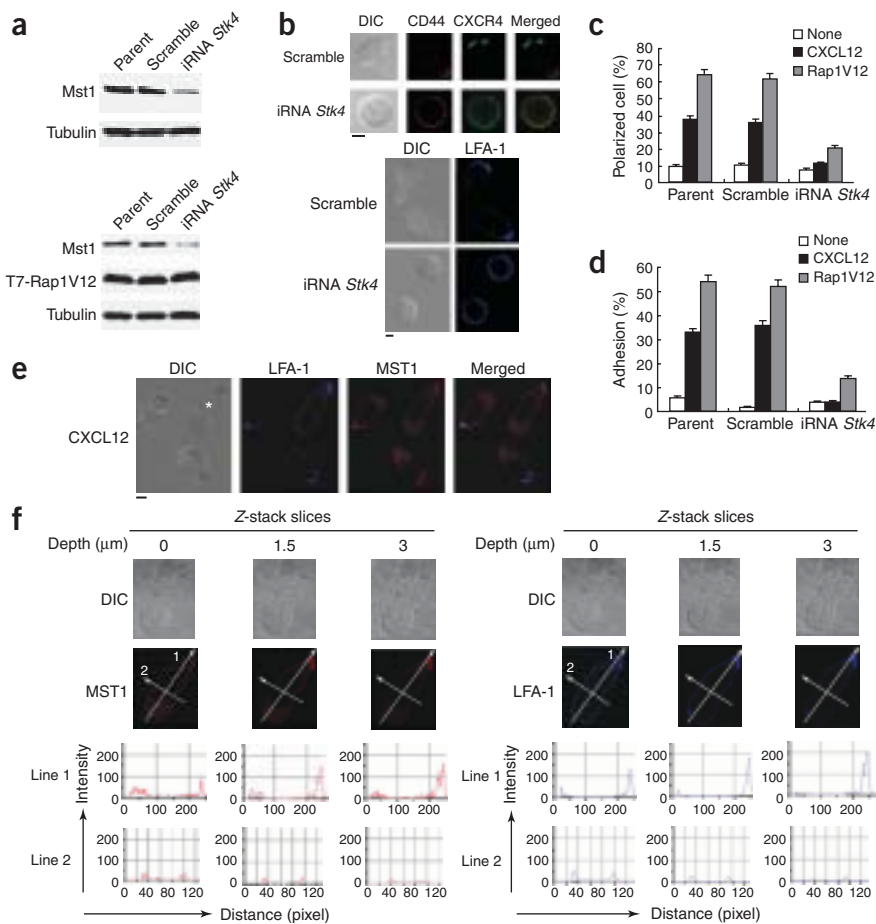


Figure 4 Mst1 'knockdown' abrogates cell polarization and adhesion. **(a)** Immunoblot of Mst1 expression by parental cells (Parent) or by BAF-LFA-1 cells (left) or BAF-LFA-1 cells transfected with T7-tagged Rap1V12 (right) after the introduction of *Stk4*-specific iRNA (iRNA *Stk4*) or control, scrambled iRNA sequence (Scramble). Tubulin, loading control. **(b)** Cell polarization of BAF-LFA-1 cells containing *Stk4*-specific or control, scrambled iRNA, after stimulation with 100 nM CXCL12. Left, DIC and fluorescence images of the distribution of CD44 (red) and CXCR4 (green). Bottom, surface distribution of LFA-1. Scale bars, 5 μ m. **(c,d)** Frequency of cell polarization **(c)** and adhesion to ICAM-1 **(d)** of BAF-LFA-1 cells containing *Stk4*-specific or control, scrambled iRNA or of parental cells, in the absence (None) or presence of CXCL12 stimulation or Rap1V12 expression. Data represent mean and s.e.m. of three independent experiments. **(e)** Distribution of LFA-1 and MST1 in BAF-LFA-1 cells expressing MST1-mRFP, incubated in the presence of CXCL12, fixed in suspension and stained with anti- α_L (TS2/4) and Alexa Fluor 633-conjugated anti-mouse IgG. *, cell analyzed further in **f**. Scale bar, 5 μ m. **(f)** MST1-mRFP intensity (left) and LFA-1 intensity (right) of z-stack confocal images of the cell (*) in **e**. Top, relative distance of focal planes between images. Line profiles drawn along lines 1 and 2 are presented as described in **Figure 3**. All data are representative of three or four independent experiments.

stimulated 3A9 T cells by TCR crosslinking, both the parental and control cells showed a 2.5- to threefold increase in adhesion to ICAM-1. In contrast, Mst1-depleted 3A9 cells adhered poorly to ICAM-1, even after stimulation by TCR crosslinking (**Fig. 5c**). Expression of LFA-1 and TCR was similar in Mst1-depleted 3A9 T cells and in parental and control cells (data not shown). Thus, Mst1 is also crucial in TCR-stimulated adhesion mediated by LFA-1.

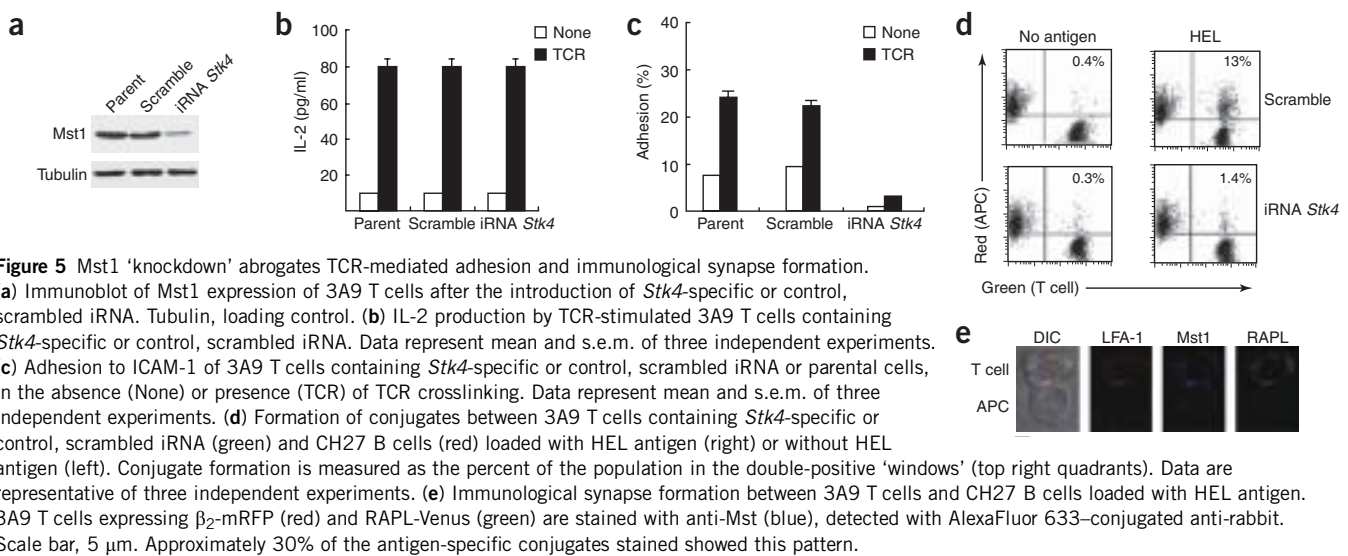
Upregulation of LFA-1 adhesive activity is a prerequisite for the formation of an immunological synapse between a T cell and an antigen-presenting cell (APC). To examine the function of Mst1 in this process, we did conjugation assays using 3A9 T cells with *Stk4* expression 'knocked down'. Wild-type 3A9 T cells conjugated with CH27, a mouse B cell lymphoma used as APCs, in the presence of HEL antigen in an LFA-1-ICAM-1-dependent way¹⁷ (**Fig. 5d**). In contrast, Mst1-depleted 3A9 T cells interacted poorly with HEL antigen-loaded APCs (**Fig. 5d**), indicating that Mst1 expression is required for conjugation with APCs. In agreement with its proposed function in immunological synapse formation, endogenous Mst1 accumulated in the contact zone, and overlapped with fusion proteins of β_2 integrin and mRFP (β_2 -mRFP) and RAPL with the variant yellow fluorescent protein Venus (RAPL-Venus; **Fig. 5e** and **Supplementary Fig. 5** online).

We also attempted to examine the importance of Mst1 in primary lymphocytes. We used a lentivirus vector containing iRNA constructs under control of the promoter of the gene encoding H1 RNA polymerase III and green fluorescent protein (GFP) as a reporter. We cultured primary T cells for 2 d with anti-CD3 and anti-CD28 in the presence of vesicular stomatitis virus glycoprotein-pseudotyped

viral particles, then cultured the cells for an additional 24 h without stimulation before 'sorting out' the GFP^{hi} infected cells. In GFP^{hi} T cells, Mst1 was reduced to 15% that of control cells on a 'per-cell' basis (**Fig. 6a,b**). We next examined cellular adhesion to ICAM-1 in response to chemokine stimulation or TCR crosslinking. Control T cells showed a threefold increased in adhesion to ICAM-1, whereas Mst1-depleted T cells did not show a substantial increase in adhesion in response to CCL21 (**Fig. 6c**). Mst1-depleted T cells adhered poorly to ICAM-1 after TCR crosslinking, whereas control T cells strongly attached to ICAM-1 (**Fig. 6d**). As there were no changes in the surface abundance of LFA-1, CCR7 or CD3 in wild-type or Mst1-depleted T cells (data not shown), these results indicate that Mst1 is indispensable in the adhesive responses of normal T cells to chemokines and TCR crosslinking.

Rapid intracellular trafficking of Mst1 and RAPL

The redistribution of RAPL and Mst1 to the leading edge and contact zone with APCs, where LFA-1 also accumulated, suggested their involvement in the intracellular trafficking of LFA-1. Mst1 was present mainly in particulate fractions, with a small quantity in the cytosol (**Fig. 7a**). Rap1, RAPL and β_2 integrin were present only in particulate fractions (**Fig. 7a**). Subcellular fractionation by continuous sucrose density gradient centrifugation showed that RAPL and Mst1 fractionated together exclusively in light fractions (fractions 2 and 3), which contained early (EEA1 and Rab5) and late (Rab11) endosomal marker proteins, but lacked β -COP and transferrin receptor, indicative of the Golgi-derived vesicles and recycling endosomes, respectively (**Fig. 7b**). We also detected both Rap1 and LFA-1 in those fractions, as well as in

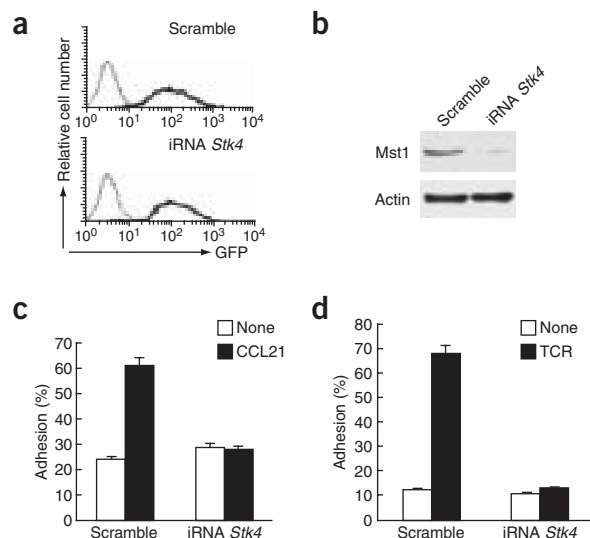


heavier fractions such as the plasma membrane and the Golgi complex. Immunoelectron microscopic studies demonstrated the presence of RAPL in vesicular structures (Fig. 7c and Supplementary Fig. 6 online). Although we did not successfully detect Mst1 by microscopy using antibodies now available, this result suggests that Mst1 and RAPL exist in the same vesicular compartment that also contains Rap1 and LFA-1.

To monitor translocation of Mst1 and RAPL to the membrane, we introduced MST1-mRFP and RAPL-Venus, respectively, into BAF-LFA-1 cells. We then used confocal microscopy to examine the redistribution of these proteins in live cells after stimulation with CXCL12. Cells adopted a polarized phenotype after stimulation (Fig. 8a). In a series of time-lapse images in the same focal plane, the intensity of MST1-mRFP at the ruffling leading edge area was increased within 30 s, with a reciprocal decrease of that in the cell body and uropod, while the nucleus was maintained at the same position (Fig. 8a and Supplementary Fig. 7 online). MST1-mRFP and RAPL-Venus localized together, quickly translocating to the membrane protrusion with a similar time course (Fig. 8b and Supplementary Fig. 7). The movement of MST1-mRFP and RAPL-Venus coincided with development of the leading edge. Control mRFP and Venus alone had diffuse distribution in both nonpolarized and polarized cells (Supplementary Fig. 7). Notably, a portion of the MST1-mRFP and RAPL-Venus proteins often showed a tubular distribution stretching toward the leading edge, especially at the early time points during the development of the leading edge (Fig. 8c and Supplementary Fig. 8 online). Colocalization analysis of immunostaining of fixed cells showed that those tubules tended to be lined along microtubules targeted to the leading edge region (Fig. 8d and Table 1). These data suggest that RAPL and Mst1 translocate along microtubules.

Figure 6 Mst1 'knockdown' in mouse T lymphocytes abrogates the cell adhesion triggered by CCL21 stimulation and TCR ligation. (a) Flow cytometry of sorted GFP⁺ populations of T cells transduced with lentiviruses encoding *Stk4*-specific or control, scrambled iRNA. (b) Immunoblot analysis of Mst1 expression by T cells transduced with *Stk4*-specific or control, scrambled iRNA. Actin, loading control. (c,d) Adhesion to ICAM-1 of T cells expressing *Stk4*-specific or control, scrambled iRNA, in the presence (CCL21) or absence (None) of CCL21 (c) or in the presence (TCR) or absence (None) of TCR crosslinking (d). Data represent mean and s.e.m. of three independent experiments.

To examine redistribution of LFA-1, we introduced both subunits of α_L and β_2 -mRFP in BAF cells. Exogenous β_2 -mRFP was located perinuclearly in the cytoplasm as well as on the cell surface, as detected by confocal microscopy using anti- β_2 (Supplementary Fig. 9 online) and by flow cytometry (data not shown). These proteins were functionally active in mediating adhesion to ICAM-1 after CXCL12 stimulation and clustered at the leading edge membrane, as is the case with wild-type LFA-1 (Supplementary Fig. 9). After stimulation with CXCL12, β_2 -mRFP molecules in the mid-body and uropod moved quickly toward the cellular protrusion, producing a patch-like distribution at the leading edge (Fig. 8e). To determine the spatial relationship between MST1 and LFA-1, we introduced limited amounts of MST1-Venus into BAF cells expressing α_L and β_2 -mRFP. MST1-Venus translocated to the leading edge after CXCL12 stimulation with a time course and distribution similar to that of β_2 -mRFP (Fig. 8f). These results indicate that Mst1 exists in close proximity to LFA-1; this protein may be directly involved in the intracellular transport of LFA-1 to the leading edge, causing clustering at the front membrane.



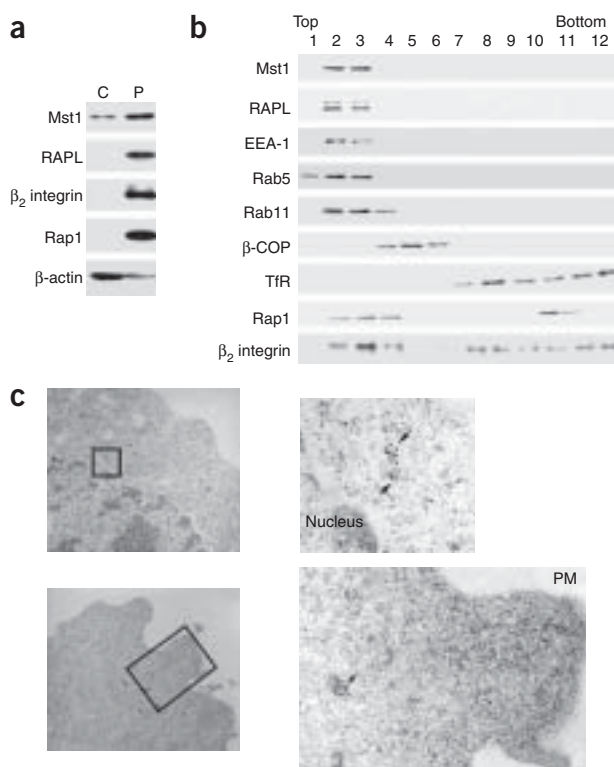


Figure 7 Subcellular distribution of Mst1 and RAPL. **(a)** Immunoblot analysis Mst1, RAPL, β_2 integrin, Rap1 and β -actin expression in cytosolic (C) and particulate (P) fractions from primary lymphocytes. **(b)** Immunoblot analysis of fractions from primary lymphocytes obtained by subcellular fractionation using continuous sucrose density gradient centrifugation (10–40%). Antibodies, left margin. **(c)** Immunoelectron microscopy of 3A9 T cells stained with anti-RAPL (E11.2). Control antibody did not produce staining above background. PM, plasma membrane. Original magnification, $\times 30,000$ (left) and $\times 60,000$ (right; enlargement of boxed areas at left). Data are representative of three independent experiments.

regulation of lymphocyte integrin function may be a unique feature acquired during the diversification of Ste20 kinases. Our results suggest that Cdc42-PAK1 and Rap1-RAPL-Mst1 pathways orchestrate the control of cell polarity, morphology and adhesion triggered by chemokine stimulation and TCR ligation.

Activated Rap1 promoted association of the coiled-coil region of RAPL with Mst1, suggesting that binding of Rap1-GTP to RAPL induces conformational changes in the coiled-coil region that favor association with Mst1. Rap1-GTP binding stabilizes a conformation of RAPL exposing the coiled-coil region, which we detected by surface plasmon resonance using antibodies to a RAPL epitope (unpublished data). Thus, Rap1 activation by chemokines or TCR triggering probably stabilizes a RAPL conformer that exposes the coiled-coil region.

Our results indicated that Rap1 and RAPL activated Mst1 through direct interactions. In contrast, it has been reported that Nore1 inhibits Mst1 kinase activity⁴⁰, suggesting differential effects of two forms of *Rassf5* products on Mst1. Thus, the predominant expression of RAPL in lymphocytes favors Mst1 activation, which is required for cell adhesion and polarization after Rap1 activation. Mst1 exists as an autoinhibitory homodimer²⁷. By analogy to Cdc42-induced PAK1 activation⁴¹, we hypothesize that stable interactions with RAPL destabilize the Mst1 homodimer, increasing autophosphorylation and augmenting Mst1 kinase activity.

Nuclear localization of truncated Mst1 after caspase cleavage has been reported^{37,42}, but the localization of endogenous Mst1 has not been studied in detail. We have demonstrated here that RAPL and Mst1 were located mainly in the perinuclear region in close proximity to the Golgi complex in resting lymphocytes and lymphoid cell lines. RAPL deficiency led to the diffuse distribution of Mst1 throughout the cytoplasm and nucleus and impaired translocation of Mst1 to the leading edge after activation by chemokines. Those results indicate that RAPL is critical in the maintenance of the proper cytoplasmic location of Mst1. Forced overexpression of Mst1, resulting in diffuse distribution of Mst1 throughout the cytoplasm, could induce cell adhesion with nonpolarized morphology. Thus, regulated localization of Mst1 by RAPL is critical for cell polarization and attachment at the leading edge.

RAPL signaling may regulate lymphocyte adhesion and cell polarization²⁰. RAPL formed a complex with LFA-1 through the α_L subunit cytoplasmic region and modulated both the affinity and distribution of LFA-1 in concert with cell polarization. We initially proposed intracellular trafficking of LFA-1 via RAPL as the mechanism underlying adhesion. Overexpression or 'knockdown' of Mst1 did not change the affinity of LFA-1 for soluble ICAM-1-Fc, in contrast to the apparent effect on LFA-1 clustering. Mst1 'knockdown' decreased the adhesion almost completely, indicating that LFA-1 clustering is indispensable for Rap1-RAPL-dependent adhesion. We have also demonstrated the localization of RAPL to small vesicles and its association with Mst1, supporting the idea that RAPL-Mst1 signaling is involved in vesicle transport to the leading edge. That mechanism is

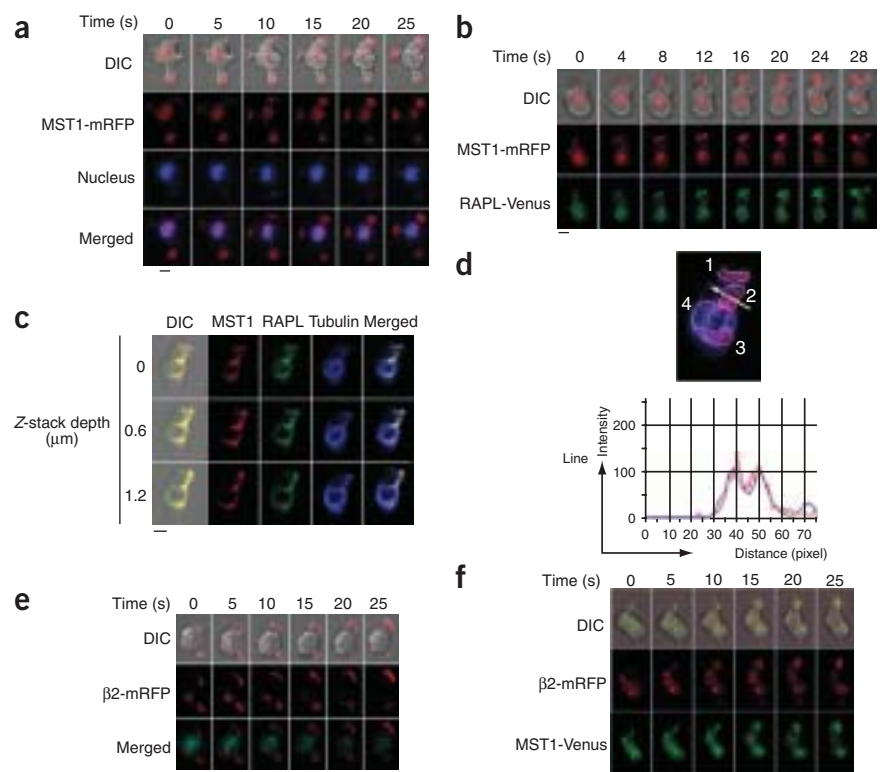
DISCUSSION

Here we have identified Mst1 as an important effector of RAPL functions in cell adhesion and polarization. RAPL bound directly to Mst1 via its coiled-coil region, modulating Mst1 kinase activity and subcellular localization. Using lymphocytes derived from RAPL-deficient mice and 'knockdown' of Mst1 expression in wild-type cells, we have shown that this mechanism was crucial for both LFA-1 clustering and cell polarization. Thus, Mst1 is a key enzyme 'translating' Rap1 and RAPL signaling into the generation of attachment that facilitates immune cell trafficking.

Mst1 is a serine-threonine kinase belonging to a family of kinases homologous to yeast Ste20 (sterile 20)^{29,30}. In budding yeast, Ste20 serves to link G protein-coupled pheromone receptors to the mitogen-activated protein kinase pathway controlling cell proliferation, cell morphology and polarity³¹. Mammalian Ste20-like kinases are divided mainly into two subfamilies, PAKs and germinal center kinases; Mst1 belongs to the latter³². Although PAKs are involved in many cellular processes, including the control of cell morphology and motility³³, published studies have suggested that Mst1 is involved mainly in apoptosis. After stimulation of apoptosis, Mst1 is cleaved by caspase 3, generating a catalytically active kinase fragment^{34–36}. That fragment in turn phosphorylates histone H2B at serine 14, a hallmark of apoptotic chromatin³⁷. Nore1, an isoform of RAPL, is reported to bind Mst1 and promote Kirsten-RasV12-induced apoptosis³⁸. Although the involvement of Mst1 in apoptosis is well documented, the physiological necessity of Mst1 for apoptosis, the 'upstream' regulatory elements and the functions of intact Mst1 remain to be clarified. Our results demonstrating the integration of intact Mst1, but not truncated Mst1, into Rap1-RAPL signaling represent a previously unknown pathway leading to Mst1 activation that regulates integrin function. PAK1 regulates cell polarity and the actin cytoskeleton during chemotaxis via Cdc42 (ref. 39). Involvement of Mst1 in the

Figure 8 Rapid intracellular translocation of MST1, RAPL and LFA-1. **(a)** Translocation of MST1-mRFP in BAF-LFA-1 cells on ICAM-1-coated surfaces after stimulation with 100 nM CXCL12. Loading of cells with Hoechst 33342 indicates nuclei. Time zero (0) represents the first time-lapse image; subsequent images were obtained on the same focal plane (time points, above images). DIC images are overlaid with MST1-mRFP images; merged images are of MST1-mRFP and Hoechst 33342.

(b) Translocation of MST1-mRFP and RAPL-Venus in BAF-LFA-1 cells incubated on ICAM-1-coated surfaces in the presence of CXCL12, assessed as described in **a**. **(c)** Immunostaining for tubulin in CXCL12-stimulated BAF-LFA-1 cells expressing MST1-mRFP and RAPL-Venus. Images were obtained in different focal planes. DIC images are overlaid with MST1-mRFP and RAPL-Venus images. **(d)** Colocalization analysis. Pearson's correlation coefficient (r) of the colocalization of signals between tubulin and MST1-mRFP in areas 1–4 of the first z-stack image in **c** is in **Table 1**. The highest coefficient is in area 2, in which microtubule 'cables' emanate toward the leading edge. Pearson's coefficient between MST1-mRFP and a randomized pixel image of tubulin is 0.002. Bottom, line profiles of MST1-mRFP (red) and tubulin (blue) along the arrow. **(e)** Translocation of β_2 -mRFP on ICAM-1-coated surfaces after stimulation with CXCL12, assessed as described in **a**. Loading of BAF cells expressing both α_L and β_2 -mRFP with Hoechst 33342 indicates nuclei. DIC images are overlaid with β_2 -mRFP images; merged images are of Hoechst 33342 and β_2 -mRFP. **(f)** Intracellular translocation of β_2 -mRFP and MST1-Venus in BAF cells expressing both α_L and β_2 -mRFP and MST1-Venus, incubated on ICAM-1-coated surface in the presence of CXCL12, assessed as described in **a**. DIC images are overlaid with β_2 -mRFP and Mst1-Venus images. Scale bars (**a–c,e,f**), 5 μ m. Original magnification, $\times 630$ (**d**). All data are representative of four or five independent experiments.



not unexpected, as Rap1 is located in endocytic and exocytic vesicles^{43–46}. LFA-1 was also present in vesicle fractions and moved from the perinuclear region to the front membrane. Intracellular localization of LFA-1 partially overlapped with that of RAPL and Mst1 in unstimulated cells. After Rap1 activation, translocation of Mst1, RAPL and LFA-1 to the leading edge was similar both kinetically and spatially, suggesting that these proteins are associated with the same vesicle compartment moving along microtubule tracks destined for the leading edge. We found biochemical evidence that RAPL associated with Mst1 and LFA-1, but we did not detect a complex of Mst1 and LFA-1 by coimmunoprecipitation, suggesting that Mst1 does not interact with LFA-1 directly. Although it is still possible that Mst1, RAPL and LFA-1 form a labile ternary complex, it is also conceivable that the Mst1-RAPL complex has a distinct function in the spatial regulation of vesicles carrying LFA-1.

The relationship of Rap1-dependent LFA-1-mediated adhesion with vesicle transport has been demonstrated in experiments using a

dominant negative mutant of Rab11 binding protein⁴⁷. Mst1 might modulate the activation and effector functions of Rab11 in targeting and docking vesicles. The ability of RAPL to associate with microtubules⁴⁸, as seen for other proteins of the family encoded by *Rassf5* (ref. 49), facilitates polarized vesicle transport or contributes to the microtubule reorganization. A likely hypothesis that has emerged is that Rap1-RAPL-Mst1 signaling may mobilize an intracellular membrane pool that can be recruited for the assembly of specialized plasma membrane domains, such as a migrating leading edge. Polarized transport of LFA-1 to the leading edge in this process generates new attachment points at the migratory front. Thus, signaling coordinates cell adhesion and migration through vesicle transport. Further characterization of RAPL-Mst1-containing vesicles should assess proteins and lipids contained in this membrane compartment. In addition to possible involvement in vesicle transport, Mst1 may also regulate LFA-1 adhesive activity directly, possibly through phosphorylation of the cytoplasmic regions⁵⁰. Additional studies are needed to identify Mst1 kinase substrates to clarify this issue.

Here we have identified Mst1 as a key participant in the control of cell polarization and adhesion 'downstream' of Rap1 and RAPL activation triggered by chemokine and antigen stimulation. We propose polarized vesicle transport as the critical point of this signaling pathway. Our experimental system has provided useful tools for delineating this process. The involvement of Mst1 in apoptosis and growth, and now also as a regulator of lymphocyte adhesion, indicates the possibility that adhesive events may be tightly linked to growth control. Elucidation of Rap1-RAPL-Mst1 functions will provide new insights into the control of cell adhesion and migration.

Table 1 Colocalization assay

Area	r
1	0.59
2	0.75
3	0.23
4	0.10

Data are Pearson's correlation coefficient (Rr) of the colocalization of tubulin and MST1-mRFP signals in areas 1–4 of the image in **Figure 8d**.

METHODS

Yeast two-hybrid screening and DNA constructs. An activated form of RAPL (M4) was generated by the introduction of substitution of alanine by lysine residues at positions 123, 135, 154 and 155, by arginine at position 124, by aspartic acid at position 160, and by asparagine at position 161. A human cDNA library (Clontech) was screened using the M4 mutant as bait, according to the manufacturer's instructions. The screen identified cDNA containing partial sequences of *STK4* and *STK3*. Full-length *STK4* cDNA was isolated by RT-PCR using primers designed from the published sequence. A cDNA construct encoding full-length MST1 plus the N-terminal V5 epitope tag was subcloned into pcDNA3 and pcDNA4 vectors (Invitrogen). RAPLAN (amino acids 101–265), RAPLAC (amino acids 1–222), MST1ΔC (amino acids 1–330) and kinase-inactive MST1 (K59R) mutants have been described^{20,27}. A cDNA sequence encoding the coiled-coil domain of RAPL (amino acids 223–265) was subcloned into pGEX vector (GE Healthcare Bio-Sciences) and was expressed in *Escherichia coli* BL21 as a GST fusion protein. Venus and mRFP1 (gifts from A. Miyawaki, RIKEN, Wako, Japan) were fused to the C termini of RAPL, MST1, α_1 or β_2 integrins by the linker (GGGG)₄. All constructs were verified by sequencing.

Mice. RAPL-deficient mice were generated from the mouse embryonic stem cell line TT2 with disruption of the gene encoding RAPL, as reported²², and were crossed with wild-type C57BL/6 mice for six generations. Mice were housed in specific pathogen-free conditions and all experiments were in accordance with protocols approved by the Animal Care and Use Committee of Kansai Medical University (Osaka, Japan).

Antibodies. Anti-RAPL has been described²⁰. Antibodies to the following were purchased: Myc (9E10), human α_1 subunit (TS2/4) and β_2 subunit (TS1/18; all from American Tissue Culture Collection); Mst1/2 (Upstate); V5 (Novagen); phosphorylated PAK1/2, (Cell Signaling Technology); tubulin, β -actin and β -COP (all from Sigma); Rab11, mouse β_2 subunit, EEA1, mouse α_1 subunit and Rap1 (all from BD Transduction Laboratories); Rab5 (Santa Cruz); and transferrin receptor (Zymed Laboratories). Alexa Fluor 488-conjugated anti-rabbit and Alexa Fluor 546-conjugated anti-rat were from Molecular Probes.

Immunoprecipitation and immunoblots. COS cells were transfected with Myc-RAPL and V5-MST1 by electroporation and were collected and lysed with buffer (1% (volume/volume) Nonidet P-40, 150 mM NaCl, 25 mM Tris-HCl, pH 7.4, 10% (volume/volume) glycerol, 2 mM MgCl₂, 1 mM phenylmethylsulfonyl fluoride and 0.1 mM aprotinin). Immunoprecipitation and immunoblots were done as described²⁰. For precipitation assays using GST proteins, lysates of COS cells transfected with V5-MST1 were incubated for 2 h with glutathione Sepharose coupled to GST or a fusion protein of GST and the RAPL coiled-coil domain, followed by washing with lysis buffer. Bound proteins were eluted with 10 mM glutathione and were analyzed by immunoblot. Lysates prepared from BAF-LFA-1 cells expressing either T7-tagged-Rap1V12 or Myc-RAPL were also analyzed by immunoblot. T cells from wild-type and RAPL-deficient mice were stimulated with 5 μ g/ml of anti-CD3 (2C11) or 100 nM CCL21 (R&D); cell lysates from stimulated cells prepared as described above were then analyzed by immunoblot.

Kinase assays. Proteins from lysates of BAF-LFA-1 cells transfected with vector alone, Rap1V12, RAPL, V5-MST1 or the kinase-inactive (K59R) MST1 mutant were immunoprecipitated with anti-MST or anti-V5. Equal amounts of precipitated MST1 were incubated for 15 min at 30 °C with 10 μ g myelin basic protein in 20 μ l kinase buffer (40 mM HEPES, pH 7.4, 10 mM MgCl₂, 25 μ M ATP and 10 μ Ci [γ -³²P]ATP). Reactions were terminated by the addition of 2 \times SDS sample buffer. Phosphorylated proteins were detected using a PhosphorImager (BAS1000; Fujifilm).

Cell adhesion, IL-2 production and conjugate assays. Cell adhesion assays and ligand-binding affinity measurement using recombinant ICAM-1-Fc have been described^{17,20}. Conjugation assays and measurement of IL-2 production by TCR crosslinking using anti-CD3 were done exactly as described¹⁷. Adhesion of lentivirus-transduced lymphocytes was measured in a parallel-plate flow chamber (Biotech) under shear stress (5 dynes/cm²) as described¹⁶.

RNA-mediated interference. The iRNA-mediated interference technique was used to suppress mouse Mst1 expression. A 19-nucleotide *Stk4*-specific sense iRNA sequence (5'-GTGTTTGATGTCTTAGAGA-3') or a scrambled control iRNA sequence (5'-GTTAGAGGTTCCGTGATTAT-3') was ligated into pSUPER.puro (OligoEngine). The iRNA plasmids were transfected into BAF and 3A9 cells by electroporation; positive clones were selected with puromycin.

The *Stk4*-specific iRNA was introduced into T cells using lentivirus with a lentivirus vector expressing GFP (CS-RfA-EG; a gift from H. Miyoshi, RIKEN, Wako, Japan) containing the iRNA construct under control of the H1 promoter cassette. Production and concentration of lentivirus particles were done as described^{51,52}. Purified mouse T lymphocytes from C57BL/6 mice were cultured for 2 d with 5 μ g/ml of anti-CD3 and 1 μ g/ml of anti-CD28 (BD Transduction Laboratories) in the presence of viral particles at a multiplicity of infection of 100. Cells were cultured for an additional 24 h without stimulation. Transduction efficiencies were greater than 90%. A GFP^{hi} population, collected by cell sorting, was subjected to adhesion assays and immunoblot analysis.

Confocal microscopy and time-lapse imaging. Immunostaining and live-cell imaging were done as described²⁰. Lymphocytes and other nonadherent cell lines were fixed in suspension and were immobilized on poly-L-lysine-coated slides before staining. Confocal images were obtained using a LSM510 META microscope (Carl Zeiss) with a 63 \times objective lens. Bodipy TR ceramide, Hoechst 33342 and BCECF dyes (Invitrogen) were used to visualize the Golgi complex and nuclei and/or cytosol. Time-lapse confocal images were obtained in multitrack mode using a LSM510 microscope with a 63 \times objective lens. There was no detectable 'bleeding' of Venus or mRFP fluorescence into alternate channels. Line profile and colocalization analysis of z-stacks of confocal images were done with the software ImagePro plus (MediaCybernetics) and ImageJ (W.S. Rasband, National Institutes of Health, Bethesda, Maryland; <http://rsb.info.nih.gov/ij/>).

Immunoelectron microscopy. The 3A9 T cells were fixed for 1 h in 4% paraformaldehyde with 0.5% glutaraldehyde in PBS. Cells were rinsed in PBS and were centrifuged into a pellet. Fixed cell pellets were infused with 1% agarose and were embedded with epoxy for ultrathin sectioning (70 nm). After incubation with primary antibody to RAPL (E11.2), sections were rinsed with 1% BSA and 0.1% Na₂S₂O₃ in PBS and were incubated with gold-conjugated goat anti-rat immunoglobulin G (IgG; EY Laboratories). Controls included the substitution of purified rat IgG for the primary antibody.

Cellular fractionation. Primary mouse lymphocytes suspended in a hypotonic buffer (20 mM HEPES and 1 mM EDTA, pH 7.45) were lysed with a Dounce homogenizer. Post-nuclear supernatants were centrifuged for 60 min at 100,000g. Pellets (particulate fractions) were rinsed twice with PBS and were made soluble in SDS sample buffer. The supernatant obtained comprised the cytosol fraction. Equal quantities of particulate and cytosolic proteins were analyzed by immunoblot.

For sucrose density gradient fractionation, lymphocytes were suspended and were lysed in cold (0 °C) buffer (250 mM sucrose, 10 mM triethanolamine, 10 mM acetic acid and 1 mM EDTA, pH 7.45) by Dounce homogenization. Post-nuclear supernatants were layered on a continuous sucrose gradients (10–40%) and were centrifuged at 4 °C for 16 h at 75,500g. After centrifugation, 0.3-ml fractions were collected from the top and were separated by SDS-PAGE and analyzed by immunoblot.

Statistical analysis. Student's two-tailed *t*-test was used to compare experimental group, with *P* values less than 0.05 considered significant.

Note: Supplementary information is available on the Nature Immunology website.

ACKNOWLEDGMENTS

We thank N. Shimomura, C. Tanaka and R. Hamaguchi for technical assistance. Supported by a grant-in-aid from the Ministry of Education, Science, Sports, and Culture of Japan; Uehara Memorial Foundation; and Toray Science Foundation.

AUTHOR CONTRIBUTIONS

K.K. and T.K. contributed to discussions of experimental design, data analysis and manuscript preparation and did all experimental studies unless otherwise indicated; M.I. did immunoelectron microscopy.

COMPETING INTERESTS STATEMENT

The authors declare that they have no competing financial interests.

Published online at <http://www.nature.com/natureimmunology/>

Reprints and permissions information is available online at <http://npg.nature.com/reprintsandpermissions/>

- Springer, T.A. Traffic signals on endothelium for lymphocyte recirculation and leukocyte emigration. *Annu. Rev. Physiol.* **57**, 827–872 (1995).
- Butcher, E.C. & Picker, L.J. Lymphocyte homing and homeostasis. *Science* **272**, 60–66 (1996).
- Carman, C.V. & Springer, T.A. Integrin avidity regulation: are changes in affinity and conformation underemphasized? *Curr. Opin. Cell Biol.* **15**, 547–556 (2003).
- van Kooyk, Y. & Figdor, C.G. Avidity regulation of integrins: the driving force in leukocyte adhesion. *Curr. Opin. Cell Biol.* **12**, 542–547 (2000).
- Dustin, M.L., Bivona, T.G. & Philips, M.R. Membranes as messengers in T cell adhesion signaling. *Nat. Immunol.* **5**, 363–372 (2004).
- Pribila, J.T., Quale, A.C., Mueller, K.L. & Shimizu, Y. Integrins and T cell-mediated immunity. *Annu. Rev. Immunol.* **22**, 157–180 (2004).
- Kinashi, T. Intracellular signalling controlling integrin activation in lymphocytes. *Nat. Rev. Immunol.* **5**, 546–559 (2005).
- Ridley, A.J. *et al.* Cell migration: integrating signals from front to back. *Science* **302**, 1704–1709 (2003).
- Sanchez-Madrid, F. & del Pozo, M.A. Leukocyte polarization in cell migration and immune interactions. *EMBO J.* **18**, 501–511 (1999).
- Horton, A.C. & Ehlers, M.D. Neuronal polarity and trafficking. *Neuron* **40**, 277–295 (2003).
- Rodriguez-Boulau, E., Kreitzer, G. & Musch, A. Organization of vesicular trafficking in epithelia. *Nat. Rev. Mol. Cell Biol.* **6**, 233–247 (2005).
- Lawson, M.A. & Maxfield, R.R. Ca²⁺- and calcineurin-dependent recycling of an integrin to the front of migrating neutrophils. *Nature* **377**, 75–79 (1995).
- Bretscher, M.S. Getting membrane flow and the cytoskeleton to cooperate in moving cells. *Cell* **87**, 601–606 (1996).
- Ng, T. *et al.* PKC α regulates β_1 integrin-dependent cell motility through association and control of integrin traffic. *EMBO J.* **18**, 3909–3923 (1999).
- Bos, J.L., de Rooij, J. & Reedquist, K.A. Rap1 signaling: Adhering to new models. *Nat. Rev. Mol. Cell Biol.* **2**, 369–377 (2001).
- Shimonaka, M. *et al.* Rap1 translates chemokine signals to integrin activation, cell polarization, and motility across vascular endothelium under flow. *J. Cell Biol.* **161**, 417–427 (2003).
- Katagiri, K., Hattori, M., Minato, N. & Kinashi, T. Rap1 functions as a key regulator of T-cell and antigen-presenting cell interactions and modulates T-cell responses. *Mol. Cell Biol.* **22**, 1001–1015 (2002).
- Kinashi, T. *et al.* LAD-III, a leukocyte adhesion deficiency syndrome associated with defective Rap1 activation and impaired stabilization of integrin bonds. *Blood* **103**, 1033–1036 (2004).
- Zemojtel, T., Penzkofer, T., Duchniewicz, M. & Zwartkruis, F.J. hRap1B-retro: a novel human processed Rap1B gene blurs the picture? *Leukemia* (2005).
- Katagiri, K., Maeda, A., Shimonaka, M. & Kinashi, T. RAPL, a Rap1-binding molecule that mediates Rap1-induced adhesion through spatial regulation of LFA-1. *Nat. Immunol.* **4**, 741–748 (2003).
- Tommasi, S. *et al.* RASSF3 and NORE1: identification and cloning of two human homologues of the putative tumor suppressor gene RASSF1. *Oncogene* **21**, 2713–2720 (2002).
- Katagiri, K. *et al.* Crucial functions of the Rap1 effector molecule RAPL in lymphocyte and dendritic cell trafficking. *Nat. Immunol.* **5**, 1045–1051 (2004).
- Edgar, B. From cell structure to transcription: Hippo forges a new path. *Cell* **124**, 267–273 (2006).
- de Souza, P.M. & Lindsay, M.A. Mammalian sterile20-like kinase 1 and the regulation of apoptosis. *Biochem. Soc. Trans.* **32**, 485–488 (2004).
- Sells, M.A., Pfaff, A. & Chernoff, J. Temporal and spatial distribution of activated Pak1 in fibroblasts. *J. Cell Biol.* **151**, 1449–1458 (2000).
- Glantschnig, H., Rodan, G.A. & Reszka, A.A. Mapping of MST1 kinase sites of phosphorylation. Activation and autophosphorylation. *J. Biol. Chem.* **277**, 42987–42996 (2002).
- Creasy, C.L., Ambrose, D.M. & Chernoff, J. The Ste20-like protein kinase, Mst1, dimerizes and contains an inhibitory domain. *J. Biol. Chem.* **271**, 21049–21053 (1996).
- Katagiri, K. *et al.* Rap1 is a potent activation signal for leukocyte function-associated antigen 1 distinct from protein kinase C and phosphatidylinositol-3-OH kinase. *Mol. Cell Biol.* **20**, 1956–1969 (2000).
- Creasy, C.L. & Chernoff, J. Cloning and characterization of a member of the MST subfamily of Ste20-like kinases. *Gene* **167**, 303–306 (1995).
- Taylor, L.K., Wang, H.C. & Erikson, R.L. Newly identified stress-responsive protein kinases, Krs-1 and Krs-2. *Proc. Natl. Acad. Sci. USA* **93**, 10099–10104 (1996).
- Gulli, M.P. & Peter, M. Temporal and spatial regulation of Rho-type guanine-nucleotide exchange factors: the yeast perspective. *Genes Dev.* **15**, 365–379 (2001).
- Dan, I., Watanabe, N.M. & Kusumi, A. The Ste20 group kinases as regulators of MAP kinase cascades. *Trends Cell Biol.* **11**, 220–230 (2001).
- Hofmann, C., Shepelev, M. & Chernoff, J. The genetics of Pak. *J. Cell Sci.* **117**, 4343–4354 (2004).
- Graves, J.D. *et al.* Caspase-mediated activation and induction of apoptosis by the mammalian Ste20-like kinase Mst1. *EMBO J.* **17**, 2224–2234 (1998).
- Lee, K.K. *et al.* Proteolytic activation of MST/Krs, STE20-related protein kinase, by caspase during apoptosis. *Oncogene* **16**, 3029–3037 (1998).
- Kekeya, H., Onose, R. & Osada, H. Caspase-mediated activation of a 36-kDa myelin basic protein kinase during anticancer drug-induced apoptosis. *Cancer Res.* **58**, 4888–4894 (1998).
- Cheung, W.L. *et al.* Apoptotic phosphorylation of histone H2B is mediated by mammalian sterile twenty kinase. *Cell* **113**, 507–517 (2003).
- Khokhlatchev, A. *et al.* Identification of a novel Ras-regulated proapoptotic pathway. *Curr. Biol.* **12**, 253–265 (2002).
- Li, Z. *et al.* Directional sensing requires G $\beta\gamma$ -mediated PAK1 and PIX α -dependent activation of Cdc42. *Cell* **114**, 215–227 (2003).
- Praskova, M., Khokhlatchev, A., Ortiz-Vega, S. & Avruch, J. Regulation of the MST1 kinase by autophosphorylation, by the growth inhibitory proteins, RASSF1 and NORE1, and by Ras. *Biochem. J.* **381**, 453–462 (2004).
- Parrini, M.C., Lei, M., Harrison, S.C. & Mayer, B.J. Pak1 kinase homodimers are autoinhibited in trans and dissociated upon activation by Cdc42 and Rac1. *Mol. Cell* **9**, 73–83 (2002).
- Lee, K.K., Ohyama, T., Yajima, N., Tsubuki, S. & Yonehara, S. MST, a physiological caspase substrate, highly sensitizes apoptosis both upstream and downstream of caspase activation. *J. Biol. Chem.* **276**, 19276–19285 (2001).
- Quinn, M.T., Mullen, M.L., Jesaitis, A.J. & Linner, J.G. Subcellular distribution of the Rap1A protein in human neutrophils: colocalization and cotranslocation with cytochrome b559. *Blood* **79**, 1563–1573 (1992).
- Maridonneau-Parrini, I. & de Gunzburg, J. Association of Rap1 and Rap2 proteins with the specific granules of human neutrophils. Translocation to the plasma membrane during cell activation. *J. Biol. Chem.* **267**, 6396–6402 (1992).
- Pizon, V., Desjardins, M., Bucci, C., Parton, R.G. & Zerial, M. Association of Rap1a and Rap1b proteins with late endocytic/phagocytic compartments and Rap2a with the Golgi complex. *J. Cell Sci.* **107**, 1661–1670 (1994).
- Berger, G. *et al.* Ultrastructural localization of the small GTP-binding protein Rap1 in human platelets and megakaryocytes. *Br. J. Haematol.* **88**, 372–382 (1994).
- Bivona, T.G. *et al.* Rap1 up-regulation and activation on plasma membrane regulates T cell adhesion. *J. Cell Biol.* **164**, 461–470 (2004).
- Fujita, H. *et al.* Local activation of Rap1 contributes to directional vascular endothelial cell migration accompanied by extension of microtubules on which RAPL, a Rap1-associating molecule, localizes. *J. Biol. Chem.* **280**, 5022–5031 (2005).
- Song, M.S. *et al.* The tumour suppressor RASSF1A regulates mitosis by inhibiting the APC-Cdc20 complex. *Nat. Cell Biol.* **6**, 129–137 (2004).
- Fagerholm, S.C., Hilden, T.J., Nurmi, S.M. & Gahmberg, C.G. Specific integrin alpha and beta chain phosphorylations regulate LFA-1 activation through affinity-dependent and -independent mechanisms. *J. Cell Biol.* **171**, 705–715 (2005).
- Miyoshi, H., Smith, K.A., Mosier, D.E., Verma, I.M. & Torbett, B.E. Transduction of human CD34⁺ cells that mediate long-term engraftment of NOD/SCID mice by HIV vectors. *Science* **283**, 682–686 (1999).
- Katayama, K. *et al.* RNA interfering approach for clarifying the PPAR γ pathway using lentiviral vector expressing short hairpin RNA. *FEBS Lett.* **560**, 178–182 (2004).

Adhere Upright: A Switchblade-like Extension of β_2 Integrins

In this issue of *Immunity*, Nishida et al., (2006) demonstrate a spectrum of dynamic conformation changes, from a bent form to extended forms, in extracellular domains in $\alpha_X\beta_2$ and $\alpha_L\beta_2$ upon separation of the α and β subunits, providing structural evidence for activation of leukocyte integrins.

Unstimulated leukocytes are nonadherent, yet become adhesive to other cells and extracellular-matrix proteins within a short time period in response to chemokine or antigen encounter. Fundamental to this process is the ability of integrins to alter their adhesiveness through an intracellular signaling process referred to as inside-out signaling. This pathway ultimately modulates integrin-ligand binding affinity (affinity modulation) and/or clustering on the cell surface (valency modulation). Inside-out signals impinge on integrin cytoplasmic domains and make the extracellular domain competent for ligand binding. This property enables lymphocytes to rapidly respond to foreign antigens or chemoattractants to activate adhesion, direct cell migration, and form immunological synapses (Carman and Springer, 2003) (Dustin et al., 2004). One of major unresolved issues in integrin-regulated adhesion is how integrin adhesiveness is modulated structurally and spatially in response to signals in the environment. In this issue, Nishida et al., (2006) demonstrate distinct conformational changes—which may underlie dynamic changes of leukocyte adhesion behavior—of extracellular domains in $\alpha_X\beta_2$ and $\alpha_L\beta_2$ from the bent form to the extended forms by separating the C-terminal ends.

The overall integrin structure resembles a “head” connected to two “legs” (Figure 1A). The α subunit comprises an N-terminal β -propeller at the top, followed by three β sandwich modules (thigh, calf-1, calf-2). The β subunit comprises an N-terminal plexin, semaphorin, and integrin (PSI) domain, followed by a β sandwich hybrid domain, a β I domain, four epidermal growth factor (EGF) repeats, and a β -tail domain. Half of the 18 integrin α subunits (α_1 , α_2 , α_{10} , α_{11} , α_L , α_M , α_X , α_D , α_E) also include in their α subunits an I domain (α I domain) inserted through short linkers into the upper face of the β -propeller. Where present, this domain is the major site of ligand binding. The major site of ligand recognition of integrins that lack the α I domain is the top face of the β I domain and the loops on the upper surface of the β -propeller. Both the α I and the β I domain contain a metal-ion-dependent adhesion site (MIDAS), where a divalent metal is coordinated by a ligand’s acidic residue (Hynes, 2002).

Recent structural studies of integrins that lack the I domain have led to a general model of integrin conformational changes (Takagi and Springer, 2002); in the low-affinity conformation, the leg region is acutely bent at the “genu” (knee) between the thigh and calf-1 domains

and between the I-EGF1 and I-EGF2, with the ligand-binding headpiece in close proximity to the membrane-proximal leg region, topologically pointing toward the plasma membrane. The switchblade-like extension of the leg regions shifts the molecule to the intermediate- or high-affinity conformations in a manner dependent on the orientation of the β I domain and hybrid domain. In a “closed” conformation, the β I makes an acute angle with the hybrid domain, and in an “open” high-affinity conformation, the outward motion of the hybrid domain occurs, making an obtuse angle with the β I domain. Therefore, the extension of the leg piece and the orientation between the hybrid and β I domains of the headpiece are the key translators for converting global conformational changes into regulation of affinity. Although a bent conformation may not be equated with low-affinity binding in all situations (Adair et al., 2005), the extension is thought to be particularly relevant in cell-cell adhesion mediated by leukocyte integrins.

Nishida et al. (2006) demonstrate with soluble recombinant $\alpha_X\beta_2$ and $\alpha_L\beta_2$ that both of them show three distinct conformations: a bent conformation and extended conformations with closed or open states of the headpiece (Figure 1B), as reported in integrins that lack I domains. When the entire extracellular domains of α and β subunits were linked via a disulfide bond and coiled-coil sequences fused at the C-terminal ends (“clasped” form) in order to make a soluble α/β heterodimer, $\alpha_X\beta_2$ predominantly showed V shaped bent forms. Compared with $\alpha_X\beta_2$, clasped $\alpha_L\beta_2$ appears to be more relaxed in conformation, showing both the bent (55%) and the extended, closed (45%) forms. This is in line with the characteristics of $\alpha_X\beta_2$, which requires stronger cellular activation for adhesion than other members of β_2 integrins. Removal of the C-terminal clasp (“unclasped”) of $\alpha_X\beta_2$ increased extended forms with the closed (50%) and open (25%) headpiece with the rest remaining bent. Unclasping of $\alpha_L\beta_2$ also increased the extended, open conformation. These results are in a good agreement with those of integrins without the α I domain, and they support a coherent model of integrin conformational changes through the bent and the extended, closed to the extended, open states (Takagi and Springer, 2002). Because these distinct states can coexist under defined conditions, the conformational changes are not all-or-nothing responses, but should be regarded as equilibria among multiple states (Figure 1B). Thus, in basal states, integrin molecules are continually flexing (“breathing”) to some degree; and close associations of the leg-piece regions prefer the bent form, and their separation shifts an equilibrium toward the extended forms. The equilibrium points may differ in integrin family members. A β_2 monoclonal antibody (CBR LFA-1/2), which stimulates adhesion by binding an epitope in the I-EGF3 domain, separated α and β leg regions and induced or stabilized extended conformations. Thus, disruption of the interaction of the α and β cytoplasmic tails by inside-out signals probably leads to a loss of the interactions between the leg regions, resulting in repositioning of the ligand-binding headpiece pointing

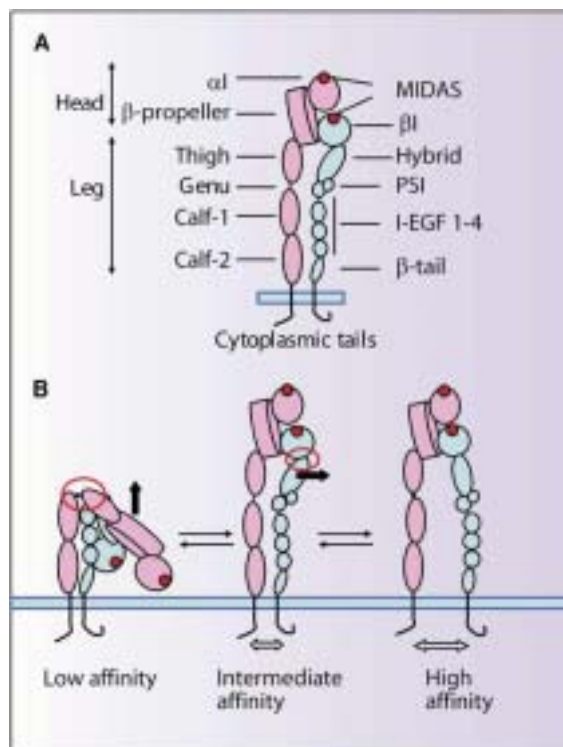


Figure 1. Structure of β_2 Integrin

(A) Schematic representation of the β_2 integrin. The head region comprises the α I domain and β -propeller domain of the α subunit (pink) and β I domain of the β subunit (blue). The leg region comprises the thigh, calf-1, and calf-2 of the α subunit and the hybrid domain, N-terminal PSI, four I-EGF repeats, and the β -tail domain. Both subunits have a transmembrane domain and short cytoplasmic tail. A MIDAS is indicated by red spheres.

(B) Equilibrium of the bent (low-affinity) and extended conformations with the "closed" (intermediate-affinity) and the "open" (high-affinity) states. Equilibrium is modulated by separation of the cytoplasmic tails. The extended, open, high-affinity conformation is induced and stabilized by separation of the α and β cytoplasmic and leg regions. The flexible joints at the genu and between I-EGF1 and I-EGF2, as well as at the β I/hybrid domain interface, are indicated by red circles. The upright and outward motions of the extracellular domains and the hybrid domain in transition from the bent to the extended and from the closed to the open states are indicated by thick arrows.

away from the plasma membrane. The β I domain also plays a regulatory role in this conformational-change relay. The treatment of $\alpha_x\beta_2$ with a small-molecule antagonist, XVA143, greatly increased extended conformations predominantly with the open state. This is consistent with the proposed mechanism of XVA143: acting on the MIDAS of the β I domain and leading to the β I activation with the hybrid domain swing-out while inhibiting activation of the α I domain (Shimaoka et al., 2003). The β I and hybrid domains may serve as a switch in transmitting the conformational signals from the cytoplasmic tails to the α I domain by inside-out signals.

The ligand-binding α_L I domain has three affinity states (low, intermediate, and high affinity) with distinct conformations depending on its C-terminal α helix (Shimaoka et al., 2002). The bent form represents low-

affinity states, and extended, closed and extended, open conformations likely represent the intermediate- and high-affinity states. It is not clear at present how leg-piece extension relays signals to induce the intermediate affinity, because β I and hybrid domain orientations were either "open" or "closed" without evidence for apparent intermediate conformations. In contrast, the genu appears to be much more flexible, suggesting that a possible fine-tuning of affinity and/or accessibility to ligands occurs through unbending.

The current study gives convincing evidence to support a unifying model of global conformational changes from the bent to the extended, closed to the extended, open upon activation among distantly related members of integrins, and it further suggests that extended conformations induced by separation—triggered by inside-out signals transmit allostery to activate the ligand-binding α I domain—of the leg and cytoplasmic domains. This modality of integrin activation may explain rolling and firm adhesion with endothelial venules, as well as interactions with antigen-presenting cells. In support of this notion, a recent study suggests rapid extensions of $\alpha_L\beta_2$ by chemokines (Shamri et al., 2005).

This study sets a framework of future studies to examine which conformations are induced by physiological stimuli to mediate responses to dynamic leukocyte adhesion and what intracellular signaling regulates these processes. Because distinct conformations of $\alpha_L\beta_2$ have different mobilities (Cairo et al., 2006), affinity and conformational regulation coordinated with spatial changes of integrins may play a pivotal role in cell migration and immunological-synapse formation. Addressing these issues will shed light on crucial roles of integrins in immunological surveillance and antigen response.

Tatsuo Kinashi¹

¹Department of Molecular Genetics
Institute of Biomedical Science
Kansai Medical University
Moriguchi, Osaka 570-8506
Japan

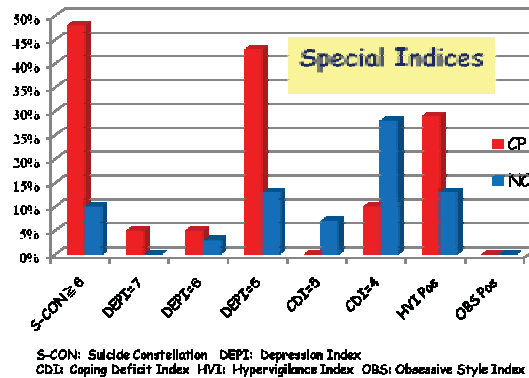
Selected Reading

- Adair, B.D., Xiong, J.P., Maddock, C., Goodman, S.L., Arnaout, M.A., and Yeager, M. (2005). *J. Cell Biol.* 168, 1109–1118.
- Cairo, C.W., Mirchev, R., and Golan, D.E. (2006). *Immunity* 25, 297–308.
- Carman, C.V., and Springer, T.A. (2003). *Curr. Opin. Cell Biol.* 15, 547–556.
- Dustin, M.L., Bivona, T.G., and Philips, M.R. (2004). *Nat. Immunol.* 5, 363–372.
- Hynes, R.O. (2002). *Cell* 110, 673–687.
- Shamri, R., Grabovsky, V., Gauguet, J.M., Feigelson, S., Manevich, E., Kolanus, W., Robinson, M.K., Staunton, D.E., von Andrian, U.H., and Alon, R. (2005). *Nat. Immunol.* 6, 497–506.
- Shimaoka, M., Salas, A., Yang, W., Weitz-Schmidt, G., and Springer, T.A. (2003). *Immunity* 19, 391–402.
- Shimaoka, M., Takagi, J., and Springer, T.A. (2002). *Annu. Rev. Biophys. Biomol. Struct.* 485, 485–516.
- Nishida, N., Xie, C., Shimaoka, M., Cheng, Y., Walz, T., and Springer, T.A. (2006). *Immunity* 25, this issue, 583–594.
- Takagi, J., and Springer, T.A. (2002). *Immunol. Rev.* 186, 141–163.

研究成果報告書

研究課題名	慢性疼痛発症の予測因子に関する研究		
(英文)	Psychosomatic Predictive factor of the chronic pain patients		
事業推進者	中井 吉英	E-mail	nakaiky@takii.kmu.ac.jp
所属・職名	医学研究科・ストレス科学・行動医学（心療内科学）講座・教授		
研究分担者名	福永 幹彦、阿部 哲也、水野 泰行、山本 和美、神原 憲治		
キーワード	疼痛行動、性格因子、Rorschach テスト、疼痛閾値		
<p>1. 概要</p> <p>疼痛の慢性化には、心理的、社会的、行動学的な因子が関与する。これらを包括的に検討することで慢性化の予測因子を推定し疼痛の慢性化予防をめざす。</p> <p>2. 研究の背景と目的</p> <p>「日本における慢性疼痛を保有する患者に関する大規模調査」(服部ら 2004)では、約 1,700 万人程度とされ多くの患者が存在する。また痛みは、「実質的または潜在的な組織損傷、あるいはそのような組織損傷に関連して表現される不快な感覚的、情動的な経験である」(IASP:国際疼痛学会 1986)と定義され、慢性的な痛みは身体のみならず心理的な苦痛を与え、思考や感情にまで悪影響を及ぼしている。患者の多くは複数の医療機関で様々な治療を試みたものの症状が治まらない上に、医療者や身近な人々への心身の苦痛の訴えも思うような理解が得られず、周囲との関係性も悪化し、心身共に疲弊し病態が複雑化している。患者の痛みが慢性化していく過程は、心理学的、行動学的にどのようなものであるかが解明できれば、早い時期に慢性化を予測することで予防が可能になる。</p> <p>3. 研究方法</p> <p>(1) Rorschach テストを用いた慢性疼痛患者の心理学的特性の検討 (2) 慢性疼痛患者の行動学的特性による分類 (3) 疼痛患者の包括的 database の作成</p> <p>4. これまでの成果</p> <p>(1) 慢性疼痛患者 26 名を対象に、ロールシャッハ・テスト (以下 ロ・テスト) を実施し標準値と比較した。情報処理・媒介・思考では、対象群の方が情報処理の効率が良く (Zd↑)、情報の統合過程の質も高い (DQ+↑)。しかし怒りなど否定的な感情による認知的媒介の機能低下が認められる (S-%↑)。積極性はあるものの (a, Ma↑)、思考の柔軟性に乏しく (a>p)、考えが悲観的に傾きがちで (MOR↑)、優柔不断 (DR↑) になり判断力が低下しやすい状態である (Sum6, Wsum6↑)。統制では、対象群の方が利用可能な資質は多い (EA↑) が、刺激に影響されやすく (L↓)、刺激要求も強く (es↑) 精神的苦痛が高まっている (SumShd↑)。感情抑制 (C↑)、自己の否定的な面へのとらわれ (V↑)、そして状況ストレスから心理的な不快感や複雑さが増し (Y↑)、対人関係に慎重になって</p>			

いる様子が示唆される (T↓)。感情では、対象群の方が情緒不安で衝動的に表出されやすく混乱がみられる (FC↓, CF↑, Col-Shad BI↑)。自己知覚では、対象群の方が身体的関心が高く (An↑)、また対人関係では、対象群の方がやや防衛的 (PER↑) で攻撃性を知覚しやすい (AG↑) ことが示唆される、といった特徴が抽出された。



(2) 疼痛患者(大学病院 52 名、市中病院 26 名)を対象に、痛みの強さと痛みによる苦痛を分けて VAS で数値化し、それらのギャップ (IS gap) を求め gap が大きい群 (G) とない群 (NG) を比較した。[IS gap] G 群 33 名、NG 群 45 名。大学病院は G 群 18 名、NG 群 34 名、市中病院は G 群 15 名、NG 群 11 名で、大学病院の方が NG 群の割合が多かった ($p < 0.05$)。NG 群の患者の特徴として、痛みの強さを主に訴え身体的要因に関心が強いことが挙げられ、心理的介入には拒否感を持つ可能性が強いと考えられ、心身医学的治療の際には特別の配慮が必要である。

5. これまでの進捗状況と今後の計画

- (1) 今後の課題は、統計手法の改善および慢性疼痛患者への適切な心理的援助につなげて行く。
- (2) 主観的認識にとどまらず、心理検査や生理学的検査など客観的指標との関係を検討することで、より詳細な患者理解が可能になる。また、治療に伴う変化を明らかにすることで、指標が治療効果の判定への応用を検討する。

6. これまでの発表論文

(1) 発表論文

2) 総説

1. 水野泰行、阿部哲也、中井吉英：慢性疼痛に対する集学的アプローチ—心療内科の立場から。 *ペインクリニック* **28**, 1589-1597 (2007).
2. 中井吉英、水野泰行、阿部哲也：
システム論的な見方による難治性疼痛の予防と治療。
医学のあゆみ **223**, 784-789 (2007).
3. 阿部哲也、中井吉英：痛みの臨床心理学。 *理学療法* **13**, 23-27 (2006).
4. 西山順滋、中井吉英：胸部の慢性疼痛。 *痛みと臨床* **6**, 264-271 (2006).

5. 水野泰行、中井吉英：抑肝散が有効であった慢性疼痛の1例。

日本東洋心身医学研究 **21**, 52-55 (2006).

3) 著書

1. 中井吉英、阿部哲也、水野泰行：

心身症としての慢性疼痛の病態 (分担執筆) 「慢性疼痛の理解と医療連携」宮崎東洋ほか編 35-45, 真興交易(株) 医書出版部、東京 (2008).

2. 町田英世、中井吉英：

「SSRI による身体症状・疾患へのアプローチ—慢性疼痛」(分担執筆) 「SSRI のすべて」 小山 司編、先端医学社、東京 (2007).

(2) 学会発表

国際学会

1) 一般発表

1. Mizuno, Y.

The difference between actual pain intensity and perceived degree of suffering scores which measure severity of chronic pain.

IASP (国際疼痛学会) Glasgow, 2008.

2. Yamamoto, K., Fukunaga, M., Kanbara, K., Mutsuura, H., Ban, I. & Nakai Y.

Psychological Gender Differences in Chronic Pain Patients Using the Rorschach Test. IASP (国際疼痛学会) Glasgow, 2008.

3. Yamamoto, K., Fukunaga, M. & Nakai, Y.

Chronic Pain Patients examined by Rorschach Test: ICPM (国際心身医学会) Quebec, 2007.

国内学会

1) 学会特別講演

中井吉英：

特別講演:慢性疼痛—痛みからくるストレス、ストレスからくる痛み。

第22回日本ストレス学会学術総会、弘前、2006.

2) シンポジウム講演

中井吉英：

「痛みと情動」—トータルストレスとしての慢性痛。

第29回日本生物学的精神医学会・第37回日本神経精神薬理学会合同年会、札幌、2007.

3) 一般発表

1. 水野泰行、小林貴美子、計屋典子、福永幹彦、中井吉英：

重症度の異なる疼痛患者の比較 —重症化予測因子の検討に向けて—

心療内科学会、大阪、2007.

2. 水野泰行、福永幹彦、中井吉英：

患者の主観的症状認識にもとづく疼痛患者の分類。慢性疼痛学会、埼玉、2008.

7. これまでの成果と情報公開

ホームページ：心療内科学講座=<http://www3.kmu.ac.jp/psm/>

中井吉英 読賣新聞 2008/06/26 「医療ルネッサンス No4377:高齢者の痛み④」

研究成果報告書

研究課題名	神経・筋難病疾患における変性機序の解明と神経・筋再生医療の検討		
(英文)	Elucidation of the mechanism of degeneration of neuromuscular disorders and translational study toward regeneration of injured neurons and muscles		
事業推進者	日下 博文	E-mail	kusaka@takii.kmu.ac.jp
所属・職名	医学研究科・神経・筋難病医学（神経内科学）講座・教授		
研究分担者名	伊東 秀文、中野 智		
キーワード	筋萎縮性側索硬化症、モデルマウス、免疫組織化学、蛋白解析		
<p>1. 概要</p> <p>神経・筋難病疾患の多くを占める神経変性疾患は、不明の原因により神経細胞が徐々に脱落して死に至る疾患であり、有効な治療法は確立されていない。本事業は、筋萎縮性側索硬化症(ALS)を中心とした神経変性疾患の病態解明と治療法確立のためのトランスレーショナル研究を推進することを目指す。</p> <p>2. 研究の背景と目的</p> <p>パーキンソン病や脊髄小脳変性症などに代表される神経変性疾患は、原因が不明で有効な治療法が確立していない神経難病である。その中でも筋萎縮性側索硬化症(ALS)は、発症後数年以内に呼吸筋麻痺によって死に至る難病中の難病である。ALS では脊髄前角の運動神経細胞が変性脱落するが、その病態や変性過程の詳細はほとんど明らかになっておらず、したがって変性を阻止しうる有効な治療法は全く見出されていない。</p> <p>神経変性疾患は高齢者に多く発症するため、高齢化がますます進行している我が国では今後患者数が激増することが予想される。しかも、患者は運動障害のために日常生活に支障をきたし、進行期には寝たきりとなるため、多大な医療費や介護費を要することとなる。したがって、神経変性疾患の進行を抑制し、さらに発症を予防することは、個人のQOLの向上だけでなく医療費の軽減など社会的にも貢献できると期待される。</p> <p>本研究ではALSに焦点を当て、運動神経変性の機序を解明し、治療につながる臨床応用研究をすることを目的とする。</p> <p>3. 研究方法</p> <ol style="list-style-type: none"> (1) 遺伝子改変 ALS モデルマウスを用いた神経病理学的研究 (2) ヒト ALS 剖検材料を用いた神経病理学的研究 (3) 遺伝子改変 ALS モデルマウスを用いた治療薬投与・幹細胞移植実験 (4) 培養細胞を用いた異常蛋白蓄積機序の解析 <p>4. これまでの成果</p> <p>(1) ALS モデルマウスにおける免疫組織化学的研究</p> <p>変異 SOD1 トランスジェニックマウスの脊髄に対してリン酸化 smad2/3(pSmad2/3)に対する免疫染色を行い、このモデルマウスの脊髄前角細胞(AHC)では核の染色性が正常コントロールマウスに比して増強していることを報告し、このモデルマウスでは TGF-β-Smad シグナル伝達系が増強している可能性を示唆した。</p> <p>また、このモデルマウスの脊髄に対して、importin β、importin α、Histone H1、β-catenin に対する抗体で免疫染色を行い、これらの蛋白が正常コントロールでは核内に存在するのに対して、ALS モデルマウスでは主として細胞質に見られ、またこれらが hyaline inclusion に陽性であることから、このモデルマウスでは核—細胞質間輸送が障害されている可能性を示唆した。さらにこのマウスに対して核膜孔複合体の構成蛋白 nucleoporin に対する抗体で染色したところ、免疫反応産物の分布異常が認められたことから、核—細胞質間輸送障害は核膜孔複合体そのものの異常による可能性を示唆した。</p> <p>さらに、小胞体シャペロンに対する抗体を用いて ALS モデルマウスを染色したところ、hyaline inclusion が陽性であり、SOD1 と共存していたことから、このマウスにおいては SOD の品質管理に小胞体が関与しており、過剰な SOD 産生により小胞体ストレスが誘導され、細</p>			

胞死に関与している可能性を示唆した。

(2) ヒト ALS 患者剖検脳における免疫組織化学的研究

孤発性 ALS(SALS)患者の AHC では、モデルマウスと同様に pSmad2/3 の染色性が核で増強していること、SALS 脊髄前角に出現する round inclusion, skein-like inclusion が pSmad2/3 陽性であること、封入体を有する AHC の核の染色性は増強していないことを明らかにし、SALS の病態に TGF- β -Smad シグナル伝達系の異常が関与している可能性を示唆した。一方、家族性 ALS(FALS)患者の AHC の核の染色性はやはり増強していたが、異常構造物である Lewy body-line hyaline inclusion は陽性反応を示さず、SALS と FALS の封入体形成機序は異なる可能性を指摘した。

また、SALS および FALS においてもモデルマウスと同様に核膜孔複合体蛋白の分布異常が認められ、またこの所見は過去にアルツハイマー病において報告されている所見と類似していた。以上から、核膜孔複合体の分布異常は ALS とアルツハイマー病に共通の神経変性機序である可能性を示唆した。

さらに、好塩基性封入体(BIs)を伴う特殊な運動ニューロン病(MND-BI)に出現する BIs が、RNA 関連蛋白 PABP1, TIA-1, rpS6 に対する抗体で陽性に染色され、一方、Dcp1, rpL28 に対する抗体では陰性であったことから、BIs の形成過程に RNA stress granule が関与している可能性を示唆した。

(3) ALS モデルマウスに対するエダラボン投与実験

変異 SOD1 トランスジェニックマウスに対して、症状発症後から free-radical scavenger であるエダラボンを投与し、運動機能、生存日数、病理学的解析、生化学的解析を行った。エダラボンは投与量依存性に運動障害の進行抑制効果を示し、高用量エダラボン投与群で、脊髄運動神経が有意に残存し、酸化ストレスの指標である 3-nitortyrosine(3-NT)/tyrosine 比が低下していた。また 3-NT に対する免疫染色では、高用量群で 3-NT の染色性が低下していた。また、SOD1 に対する免疫染色では、高用量群で脊髄への SOD1 の沈着が高用量群で有意に抑制されていた。以上の結果から、エダラボンは ALS の治療に有用である可能性を報告した。

(4) ALS モデルマウスに対する骨髄内骨髄移植実験

変異 SOD1 トランスジェニックマウスに対して、コントロールマウスの骨髄幹細胞を骨髄内に移植し、運動機能、生存日数、病理学的解析を行った。正常骨髄幹細胞移植群では、非移植群・変異マウス骨髄細胞移植群に比して運動障害の進行が有意に抑制され、生存日数も有意に延長した。病理学的には、モデルマウスの脊髄内に移植された GFP 陽性の正常マウス由来細胞が認められ、一部は microglia の表面マーカーである Iba-1 に対する免疫染色で陽性反応を示した。以上から、骨髄内骨髄移植は ALS の治療に有用である可能性が示唆され、その機序として移植された細胞が microglia に分化して神経細胞保護的に作用した可能性を指摘した。

(5) 培養細胞を用いた TDP-43, リン酸化 smad2/3, Smurf2 の interaction

Hela 細胞に野生型の TDP-43 を発現させたところ、TDP-43 のオリゴマー化を認めた。さらにユビキチンプロテアソームの阻害因子である MG132 を加えると TDP-43 のオリゴマーは蓄積した。以上より TDP-43 タンパク質の過剰及び分解抑制によりオリゴマー化が促進されることが示唆された。TDP-43 のオリゴマー化に関わる因子として、最近 CK1 の報告があるが、われわれは ALS の細胞質内封入体にリン酸化 Smad2/3 の染色性を報告したことから TDP-43 と TGF- β -Smad シグナルとの関係について現在検討中である。

5. これまでの進捗状況と今後の計画

事業は研究計画に沿って概ね順調に進捗している。さらに、臨床応用をめざした病態モデルや神経再生による治療の基礎研究を推進している。

6. これまでの発表論文

(1) 発表論文

1) 原著論文

1. Ito, H., Wate, R., Zhang, J., Ohnishi, S., Kaneko, S., Ito, H., Nakano, S. & Kusaka, H. Treatment with edaravone, initiated at symptom onset, slows motor decline and decreases SOD1 deposition in ALS mice. *Exp. Neurol.* in press.
2. Fujita, K., Ito, H., Nakano, S., Kinoshita, Y., Wate, R. & Kusaka, H. Immunohistochemical identification of messenger RNA-related proteins in basophilic inclusions of adult-onset atypical motor neuron disease. *Acta Neuropathol (Berl)*. Epub ahead of print (2008).
3. Nakamura, M., Ito, H., Wate, R., Nakano, S., Hirano, A. & Kusaka, H. Phosphorylated Smad2/3 immunoreactivity in sporadic and familial amyotrophic lateral sclerosis and its mouse model. *Acta Neuropathol (Berl)*. **115**, 327-334 (2008).
4. Shinde, A., Nakano, S., Sugawara, M., Toyoshima, I., Ito, H., Tanaka, K. & Kusaka, H. Expression of caveolar components in primary desminopathy. *Neuromuscul. Disord.* **18**, 215-219 (2008).
5. Nakano, S., Shinde, A., Fujita, K., Ito, H. & Kusaka, H. Histone H1 is released from myonuclei and present in rimmed vacuoles with DNA in inclusion body myositis. *Neuromuscul. Disord.* **18**, 27-33 (2008).
6. Zhang, J., Ito, H., Wate, R., Ohnishi, S., Nakano, S. & Kusaka, H. Altered distributions of nucleocytoplasmic transport-related proteins in the spinal cord of a mouse model of amyotrophic lateral sclerosis. *Acta Neuropathol (Berl)*. **112**, 673-680 (2006).
7. Ito, H., Kawakami, H., Wate, R., Matsumoto, S., Imai, T., Hirano, A. & Kusaka, H. Clinicopathologic investigation of a family with expanded SCA8 CTA/CTG repeats. *Neurology* **67**, 1479-1481 (2006).

(2) 学会発表

国際学会

2) シンポジウム講演

Ito, H.

Neuropathology of SCA8.

第3回東京医科歯科大学 21世紀 COE プログラム国際シンポジウム, Tokyo, 2007.

3) 一般発表

1. Kinoshita, Y., Ito, H., Zhang, J., Wate, R., Ohnishi, S., Fujita, K., Shinde, A., Nakano, S. & Kusaka, H. Nucleocytoplasmic Transport Involvement in the Spinal Cord of a Mouse Model of Amyotrophic Lateral Sclerosis. *17th International Symposium on ALS/MND*, Yokohama, 2006.
2. Ito, H., Kawakami, H., Wate, R., Shinde, A., Nakano, S., Matsumoto, S., Imai, T., Hirano, A. & Kusaka, H. Clinical and neuropathologic investigation of a family with the CTA/CTG expansions on SCA8 allele. *16th International Congress of Neuropathology*, San Francisco, USA, 2006.
3. Wate, R., Ito, H., Zhang, J., Ohnishi, S., Shinde, A., Nakano, S., Hirano, A. & Kusaka, H. Involvement of Endoplasmic Reticulum-Related Proteins, GRP78, CALNEXIN, and SREBPS in the Spinal Cord of ALS Model Mouse. *16th International Congress of Neuropathology*, San Francisco, USA, 2006.

国内学会

3) 一般発表

1. 藤田賢吾, 伊東秀文, 木下芳美, 中村正孝, 西井誠, 和手麗香, 新出明代, 中野智, 目下博文: 好塩基性封入体 (BI) を伴う成人発症運動ニューロン病の大脳皮質における BI の分布.
第49回日本神経学会総会、横浜、2008.
2. 新出明代, 中野智, 中村聖香, 朝山真哉, 朝山知子, 和手麗香, 伊東秀文, 目下博文: 高齢発症重症筋無力症 (MG) 例の治療と予後についての検討.

第 49 回日本神経学会総会、横浜、2008.

3. 中村正孝、伊東秀文、和手麗香、西井誠、木下芳美、藤田賢吾、新出明代、中野智、平野朝雄、日下博文：

筋萎縮性側索硬化症におけるリン酸化 Smad2/3 の免疫組織化学的検討.

第 49 回日本神経学会総会、横浜、2008.

4. 和手麗香、伊東秀文、平野朝雄、中村正孝、西井誠、木下芳美、藤田賢吾、新出明代、中野智、日下博文：Guam 島パーキンソン痴呆複合の封入体形成におけるリン酸化 Smad2/3 の関与.

第 49 回日本神経学会総会、横浜、2008.

5. 西井誠、中野智、藤田賢吾、新出明代、伊東秀文、日下博文：

筋炎における DNA 二本鎖切断修復酵素 DNA-PK の検討.

第 49 回日本神経学会総会、横浜、2008.

6. 中野智、新出明代、日下博文：

Nemaline 小体と核の apoptotic change を伴い、myofibrillar myopathy 様の免疫組織化学反応を示したミオパチー. 第 48 回日本神経病理学会総会学術研究会、東京、2007.

7. 藤田賢吾、伊東秀文、中野智、木下芳美、和手麗香、新出明代、日下博文：

成人期発症の好塩基性封入体を伴う運動ニューロン病における RNA 関連蛋白の免疫組織化学的検討. 第 48 回日本神経学会総会、名古屋、2007.

8. 木下芳美、伊東秀文、藤田賢吾、和手麗香、新出明代、中野智、日下博文：

筋萎縮性側索硬化症における核膜孔複合体構成蛋白 Nup62 の免疫組織化学的検討.

第 48 回日本神経学会総会、名古屋、2007.

9. 中野智、藤田賢吾、新出明代、伊東秀文、日下博文：

炎症性ミオパチーにおける DNA2 本鎖切断の証明： γ -H2AX の免疫組織化学による検討.

第 48 回日本神経病理学会総会学術研究会、東京、2007.

10. 藤田賢吾、伊東秀文、中野智、木下芳美、和手麗香、新出明代、日下博文：

好塩基性封入体を伴う成人発症の運動ニューロン病における RNA 関連蛋白の免疫組織化学的検討. 第 48 回日本神経病理学会総会学術研究会、東京、2007.

11. 木下芳美、伊東秀文、藤田賢吾、和手麗香、新出明代、中野智、日下博文：

成人発症核内封入体病の 1 剖検例.

第 48 回日本神経病理学会総会学術研究会、東京、2007.

12. 中野智、新出明代、日下博文：

Apoptotic nuclei とネマリン小体を認めたミオパチー.

第 38 回日本臨床分子形態学会総会、宇部、2006.

13. 新出明代、中野智、伊東秀文、日下博文：

Myofibrillar myopathy における caveolin-3 と lipid rafts の分布.

第 47 回日本神経学会総会、東京、2006.

14. 新出明代、中村聖香、齋藤朱実、大西静生、張建華、和手麗香、中野智、

伊東秀文、日下博文：

進行する自律神経障害を伴った硬膜移植後クロイツフェルトヤコブ病の 1 剖検例.

第 47 回日本神経病理学会総会、岡山、2006.

15. 中野智、新出明代、日下博文、川本未知、幸原伸夫：

Cytoplasmic body、rimmed vacuole を有するミオパチーと拡張型心筋症の合併を認めた同胞例. 第 47 回日本神経病理学会総会、岡山、2006.

16. 藤田賢吾、伊東秀文、木下芳美、新出明代、伊藤恒、中野智、日下博文：

第 47 回日本神経病理学会総会、岡山、2006.

7. これまでの成果の情報公開

ホームページ：神経内科学講座=<http://www3.kmu.ac.jp/neurolog/>

Phosphorylated Smad2/3 immunoreactivity in sporadic and familial amyotrophic lateral sclerosis and its mouse model

Masataka Nakamura · Hidefumi Ito · Reika Wate · Satoshi Nakano · Asao Hirano · Hirofumi Kusaka

Received: 30 November 2007 / Revised: 21 December 2007 / Accepted: 21 December 2007 / Published online: 22 January 2008
© Springer-Verlag 2008

Abstract Phosphorylated Smad2/3 (pSmad2/3), the central mediators of transforming growth factor (TGF)-beta signaling, were recently identified in tau-positive inclusions in certain neurodegenerative disorders. To clarify whether the localization of pSmad2/3 is altered in amyotrophic lateral sclerosis (ALS), we immunohistochemically examined spinal cords from sporadic ALS (SALS), from familial ALS (FALS) patients with the A4V mutation in their Cu/Zn superoxide dismutase (SOD1) gene, and from G93A mutant SOD1 transgenic (mSOD1 Tg) mice. In control spinal cords, pSmad2/3 immunoreactivity was observed exclusively in neuronal and glial nuclei. In SALS and FALS patients the nuclei showed increased immunoreactivity for pSmad2/3. Noticeably, round hyaline inclusions (RHIs) and skein-like inclusions of SALS patients were immunoreactive for pSmad2/3. Double immunofluorescence staining for pSmad2/3 and transactive response-DNA-binding protein (TDP)-43 revealed co-localization of these proteins within RHIs. In contrast, Bunina bodies in SALS and Lewy body-like hyaline inclusions (LBHIs) in FALS were devoid of labeling for pSmad2/3. Similarly, in the mSOD1 Tg mice pSmad2/3 immunoreactivity was increased in the nuclei, while LBHIs were not labeled. These findings suggest increased TGF-beta-Smad signaling in SALS, FALS, and mSOD1 Tg mice, as well as impaired TGF-beta signal transduction in RHI-bearing neurons of SALS patients,

presumably at the step of pSmad2/3 translocation into the nucleus. The pathomechanisms, including the process of inclusion development, appears to be different between SALS and mSOD1-related FALS or Tg mice.

Keywords Smad · Amyotrophic lateral sclerosis (ALS) · Transforming growth factor-beta (TGF-beta) · Transactive response-DNA-binding protein 43 (TDP-43) · Copper/zinc superoxide dismutase (SOD1)

Introduction

Amyotrophic lateral sclerosis (ALS) is a devastating lethal disease in which relentless motor neuron degeneration causes weakness and death within several years. The pathogenesis of ALS is unknown, and effective treatment has not been established. Although most cases are sporadic ALS (SALS), approximately 10% of cases are familial (FALS), and the disease in approximately 20% of FALS patients is caused by dominantly inherited mutations in the gene encoding the antioxidant enzyme copper- and zinc-dependent superoxide dismutase (SOD1) [18]. Neuropathologically, the motor neurons of SALS patients are characterized by having intracytoplasmic Bunina bodies and ubiquitinated skein-like inclusions (SLIs) or round hyaline inclusions (RHIs). SLIs and RHIs were recently shown to be immunopositive for transactive response-DNA-binding protein 43 (TDP-43) [2, 17], which is suggested to be a useful marker for ALS [8]. On the other hand, Lewy body-like hyaline inclusions (LBHIs) are present in the cytoplasm of spinal motor neurons of SOD1-related FALS patients, and, in the anterior horns of the mutant SOD1 transgenic (mSOD1 Tg) mice, these inclusions appear somewhat to resemble, morphologically, the RHIs. However, the LBHIs

M. Nakamura · H. Ito (✉) · R. Wate · S. Nakano · H. Kusaka
Department of Neurology, Kansai Medical University,
10-15, Fumizono-cho, Moriguchi, Osaka 570-8507, Japan
e-mail: itoh@takii.kmu.ac.jp

A. Hirano
Division of Neuropathology, Department of Pathology,
Montefiore Medical Center, New York, NY 10467-2490, USA

are reactive with anti-SOD1 antibodies as well as with anti-ubiquitin antibodies, but they are negative for TDP-43 [16, 21]. The mechanisms of the formation of these cytoplasmic inclusions remain unknown.

Among several proposed hypotheses concerning the pathogenesis of ALS, we recently suggested that dysfunctional nucleocytoplasmic transport might be involved in the process of neurodegeneration in ALS [28]. In that study we demonstrated aberrant intracytoplasmic accumulation of proteins related to nucleocytoplasmic transport, such as importin-beta, and thus speculated that beneficial regeneration signals would not be successfully transported into the nucleus in ALS patients. Similar findings have been reported in Alzheimer's disease [20].

Transforming growth factor (TGF)-beta is a multifunctional cytokine, and its signal transduction pathway plays an important role in regulating cellular responses such as proliferation, differentiation, migration, and apoptosis [22]. The TGF-beta family is composed of three TGF-beta isoforms, four activin beta-chains, the protein nodals, ten bone morphogenetic proteins, and 11 growth and differentiation factors [19]. When TGF-betas bind to their specific receptors, the intracellular mediators Smad2/3 are phosphorylated at their C-terminal serine residues (pSmad2/3) by the kinase activity of TGF-beta type I receptor [1]. The activated Smad2/3 are then translocated to the nucleus and there initiate the transcription of certain target genes. The phosphorylated Smad3 associates with importin-beta in the cytoplasm and is then imported into the nucleus, whereas the phosphorylated Smad2 is autonomously imported into the nucleus [14]. Therefore, we speculated that TGF-beta-Smad signaling might be impaired in ALS.

In the present study we investigated the distribution of the immunoreactivity for pSmad2/3, the central mediators of TGF-beta signal transduction. We found, for the first time, that they could be detected immunohistochemically in the RHIs and SLIs of the SALS, but not in the LBHIs of the SOD1-related FALS patients and Tg mice.

Materials and methods

Human material

Lumbar spinal cords from seven SALS patients after death (Table 1; cases 1–7, ages 62–81 years, mean \pm SD = 69.1 \pm 8.2 years) and three FALS patients with the A4V SOD1 gene mutation (Table 1; cases 8–10, ages 39–66 years, mean \pm SD = 50.3 \pm 14.0 years) [11] were investigated. Eight age-matched subjects without neurological disorder served as control (Table 1; cases 11–18, ages 56–79 years, mean \pm SD = 67.9 \pm 8.6 years). All of the ALS patients fulfilled the criteria of 'definite ALS' [4].

Table 1 Clinical findings of patients with sporadic and familial amyotrophic lateral sclerosis and of control subjects (ALS amyotrophic lateral sclerosis, SALS sporadic amyotrophic lateral sclerosis, FALS familial amyotrophic lateral sclerosis, M male, F female)

Case no.	Age (years)	Gender	Postmortem delay (h)	Diagnosis	Duration of the disease (months)
ALS					
1	62	M	17.0	SALS	22
2	63	F	16.5	SALS	16
3	63	M	5.5	SALS	14
4	64	M	5.0	SALS	29
5	72	F	3.5	SALS	18
6	79	F	1.5	SALS	29
7	81	F	6.5	SALS	19
8	39	M	Unknown	FALS (Ala4Val)	7
9	46	M	Unknown	FALS (Ala4Val)	8
10	66	M	Unknown	FALS (Ala4Val)	24
Control					
11	56	M	8.0	Malignant melanoma	–
12	57	M	10.5	Cerebral infarction	–
13	63	F	3.0	Gastric cancer	–
14	68	F	6.5	Pancreatic cancer	–
15	70	M	24.5	Cerebral infarction	–
16	74	F	3.5	Gastric cancer	–
17	76	M	3.0	Cerebral infarction	–
18	79	F	4.0	Malignant lymphoma	–

Briefly, they presented progressive spread of signs of lower motor neuron degeneration (weakness, wasting and fasciculation) as well as those of upper motor neuron involvement (increased tendon reflexes, spasticity, pseudobulbar features and extensor plantar response) in the bulbar region and at least two of the other spinal regions.

Mouse material

Founder male mice, heterozygous for the ALS-linked G93A mutation of the human gene for SOD1 (TgN[B6SJL-Tg (SOD1-G93A) 1Gur]), and female non-transgenic B6SJL/J mice were originally obtained from the Jackson Laboratory (Bar Harbor, ME, USA), and crossed in the Kansai Medical University animal facility. All animal breeding and experimental protocols were approved by the Institutional Committee for Animal Safety and Welfare of Kansai Medical University and were in agreement with the Guidelines from the National Institutes of Health for the use of live animals.

We previously reported that the LBHIs were first detected at 14 weeks of age in the G93A Tg mouse lumbar

spinal cord and that their number increased with disease progression [25]. Therefore, in this study, histological examinations were carried out on the 12 female Tg mice at 15–20 weeks of age. Twelve age-matched non-Tg littermates served as controls.

Immunohistochemistry

Paraffin-embedded blocks of human and mouse lumbar spinal cords were cut at a thickness of 7 μm . The sections were deparaffinized and stained with hematoxylin and eosin (H&E). After having been photographed, the same sections were decolorized with 70% ethanol and then immunostained with the rabbit polyclonal antibody against pSmad2/3 (sc-11769R; Santa Cruz Biotechnology, Inc., Santa Cruz, CA, USA) diluted 1:1000 with phosphate-buffered saline at pH 7.2 containing 3% bovine serum albumin (PBS–BSA) after having been microwaved in 0.1 M citrate buffer, pH 6, as a pretreatment. We also applied goat polyclonal antibody against pSmad2/3 (sc-11769; Santa Cruz; 1:2,000) in the same manner to confirm the findings. Incubation was carried out overnight at 4°C. The bound primary antibody was detected with the appropriate Vectastain Elite ABC kit (Vector Laboratories, Burlingame, CA, USA), and 3,3'-diaminobenzidine tetrahydrochloride was used as the chromogen.

In addition, we performed double immunofluorescence staining on lumbar sections from SALS patients. We applied the combination of rabbit polyclonal antibody against pSmad2/3 (sc-11769R; Santa Cruz; 1:100) and mouse monoclonal antibody against ubiquitin (sc-8017; Santa Cruz; 1:400) and that of goat polyclonal antibody against pSmad2/3 (sc-11769; Santa Cruz; 1:100) and rabbit polyclonal antibody against TDP-43 (10782-2-AP; ProteinTec Group Inc. Chicago, IL, USA; 1:4,000). These primary antibodies were detected with Alexa Fluor 546 goat anti-rabbit IgG (Molecular Probes, Eugene, OR, USA; 1:100) and Alexa Fluor 488 goat anti-mouse IgG (Molecular Probes; 1:100), for the former, and Cy3-labeled donkey anti-goat IgG (Chemicon International AP180C; 1:25) and Alexa Fluor 488 donkey anti-rabbit IgG (Molecular Probes; 1:100), for the latter. The slides were mounted with Vectashield (Vector), and viewed with an Olympus photomicroscope (Tokyo, Japan) equipped for epifluorescence. Images were acquired with a PXL1400 cooled charge-coupled device (CCD) camera (Photometrics, Huntington Beach, AZ, USA) controlled by software (Scanalytics, Fairfax, VA, USA).

In examining the immunostained sections, we determined motor neurons and glial cells morphologically with size, shape, cytologic features, and distribution.

Semiquantitative analysis of pSmad2/3-immunoreactive nuclei

The density of the pSmad2/3 immunoreactivity in each nuclei of the spinal motor neurons was assessed on a four-point scale (3 = more than 75% of each nuclear area is robustly immunolabeled; 2 = 50–75%; 1 = 25–50%; 0 = less than 25%). Mean nuclear pSmad2/3 score of each case was calculated, and the score of each group was expressed as mean \pm SD.

Results

H&E staining demonstrated the RHIs and Bunina bodies in all of the SALS cases, and the LBHIs in all of the FALS patients and mSOD1 Tg mice examined. SLIs were not certainly recognizable with H&E staining. In the control subjects no pathological structures were identified.

Immunohistochemically, there was no essential difference in immunostaining results between the goat and rabbit polyclonal antibodies against pSmad2/3.

In the control subjects, deposits of pSmad2/3 immunoreaction product were observed in the nucleus of neurons and glial cells, whereas the cytoplasm of these cells was thoroughly devoid of immunoreactivity (Fig. 1a). The nuclear labeling by these antibodies appeared reticular or vesicular, irrespective of their postmortem delay.

In the SALS patients, the staining density of the nuclei of the remaining spinal motor neurons and a subset of the glial cells reacted with anti-pSmad2/3 was evidently increased, and, in many instances, the stain was homogeneously distributed (Fig. 1b). The nuclear pSmad2/3 score was 2.12 ± 0.43 in the SALS patients, in contrast to that of 0.67 ± 0.68 in the control subjects. A further conspicuous finding was the obvious labeling of the RHIs by the antibodies (Fig. 1b–d). The immunoreactivity was observed to be homogeneous within the entire RHI, and was even seen in the eosinophilic core or pale halo. The pSmad2/3-staining density of the neuronal nuclei containing the RHIs appeared to be reduced or at least comparable to that of the control subjects (Fig. 1b, d). No immunoreactivity was observed in the cytoplasm of those cells. In addition, the SLIs were also immunopositive for pSmad2/3 (Fig. 1e). Bunina bodies were not labeled by the same antibodies (Fig. 1f, g).

The double immunofluorescence technique for pSmad2/3 (Fig. 2a, d) and for either ubiquitin (Fig. 2b) or TDP-43 (Fig. 2e) revealed the co-localization of pSmad2/3 immunoreactivity with that of ubiquitin or TDP-43 within the RHIs (Fig. 2c, f).

In the SOD1-related FALS patients, LBHIs were observed in the anterior horn cells (Fig. 3a). pSmad2/3

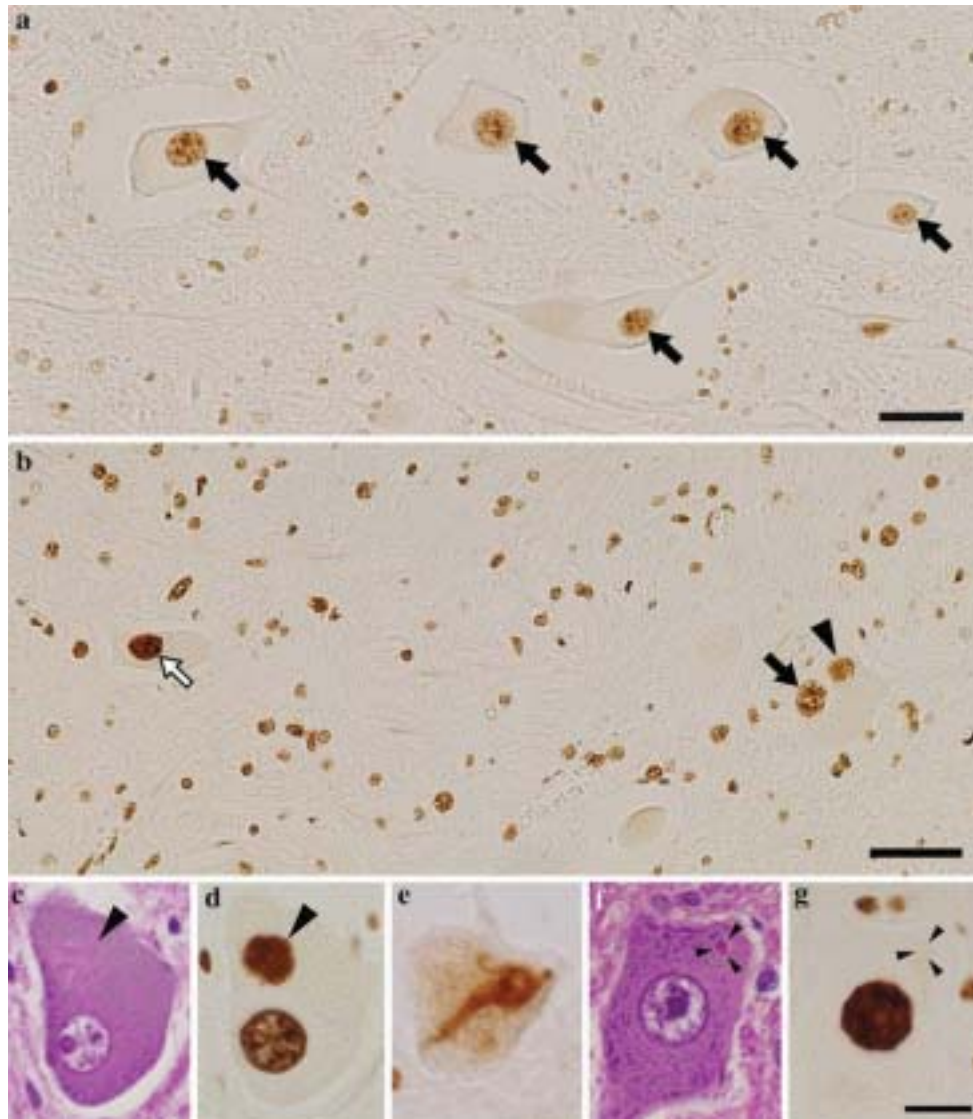


Fig. 1 Lumbar anterior horns from a control subject (**a**) and from patients with SALS (**b–g**). The nuclei of the anterior horn cells and the glial cells are immunopositive for pSmad2/3, with the stain showing a reticular appearance (**a**, *closed arrows*). In SALS specimens, the staining density of the neuronal (**b**, *open arrow*) and the glial nuclei is increased (**b**). The round hyaline inclusions (RHIs) are evidently immunopositive for pSmad2/3 (**b–d**, *arrowheads*). Note that the Smad2/3-staining density of the nucleus of the RHI-bearing neuron is

not increased (**b**, *closed arrow*). A skein-like inclusion is also detected with the anti-pSmad2/3 antibody (**e**). The Bunina bodies (**f**, *arrowheads*) identified by H&E staining are not immunoreactive for pSmad2/3 (**g**, *arrowheads*). The nucleus is robustly labeled homogeneously by the antibody (**g**). **a**, **b**, **d**, **e**, **g** Immunohistochemistry with the anti-rabbit polyclonal antibody against pSmad2/3; **c**, **f** H&E; Bars represent 50 μ m (**a**, **b**) and 20 μ m (**c–g**)

immunoreactivity was readily demonstrable in the neuronal (Fig. 3b) and glial nuclei, and their staining density was apparently increased in comparison with that in the control specimens (nuclear pSmad2/3 score was 2.42 ± 0.59 in the FALS patients). However, the LBHIs were not stained with the antibodies (Fig. 3b). Similarly, in the G93A Tg mice, pSmad2/3 deposits of the immunoreaction product were heavier in the neuronal and glial nuclei than in those of the control specimens (Fig. 3c, d). Nuclear pSmad2/3 score in the mSOD1 Tg mice was 3.00 ± 0.00 , whereas that in the control littermates was 1.53 ± 0.69 . The cytoplasm of the

anterior horn cells of the Tg mice showed faint immunoreactivity for pSmad (Fig. 3d), but the LBHIs were not labeled with the antibodies (Fig. 3e, f).

We assessed the staining specificity by replacing the primary antibodies with the appropriate amount of non-immune rabbit or goat serum or phosphate-buffered saline solution containing 3% bovine serum albumin or by pre-incubating the primary antibodies with an excess of the peptide immunogen (sc-11769P; Santa Cruz). No deposits of reaction products were seen in the sections thus treated.

Fig. 2 Double immunofluorescence labeling of lumbar spinal cord sections from a SALS patient for pSmad2/3 (red) and ubiquitin (green) (a–c) or for Smad2/3 (red) and TDP-43 (green) (d–f). pSmad2/3 is co-localized with ubiquitin and TDP-43 in the round hyaline inclusions of the anterior horn cells (a–f, arrows). The nucleus is also labeled by the anti-pSmad2/3 antibody (a, arrowhead). Auto-fluorescent lipofuscin granules (a, d, small arrows) are also visible. Bar 20 μ m

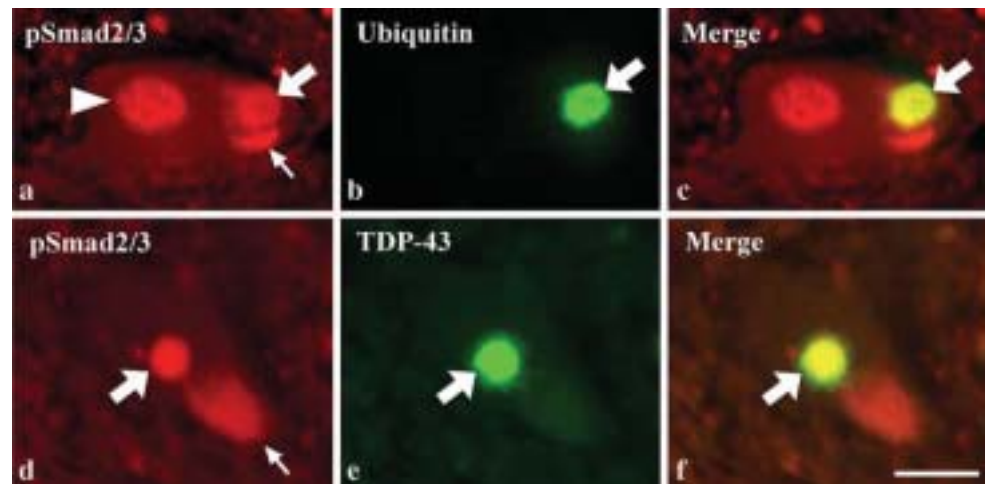
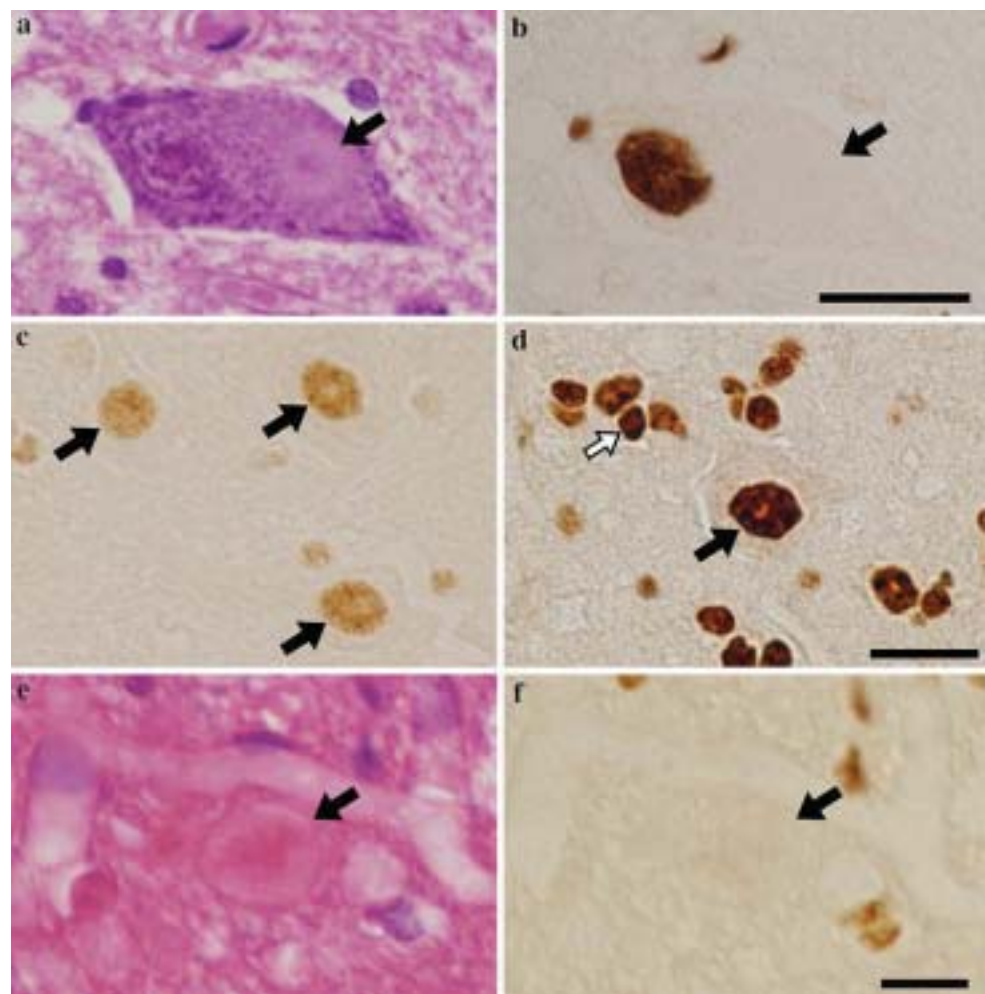


Fig. 3 Lumbar spinal cord sections from a FALS patient with the A4V SOD1 mutation (a, b) and a G93A mutant SOD1 Tg mouse (c–f). The Lewy body-like hyaline inclusion (LBHI) of the FALS specimen is not immunoreactive toward the anti-pSmad2/3 antibody (a, b, closed arrows). The nucleus of a neuron containing an LBHI in its cytoplasm shows increased immunoreactivity for pSmad2/3, with the stain having a homogeneous appearance (b). In comparison with those of a normal littermate (c, closed arrows indicate the neuronal nuclei), the neuronal (d, closed arrow) and the glial (d, open arrow) nuclei of the Tg mouse show increased pSmad2/3 immunoreactivity. Note the faint pSmad2/3 staining of the cytoplasm of the anterior horn neuron (d). The LBHI demonstrated by H&E shows no immunoreactivity for Smad2/3 (e, f, closed arrows). a, e H&E; b–d, f Immunohistochemistry with the anti-rabbit polyclonal antibody against pSmad2/3; bars 20 μ m (a, b) and 10 μ m (c–f)



Discussion

The principal findings of this study are the demonstration of pSmad2/3 immunoreactivity in the RHIs and SLIs from the SALS patients. Within these inclusions pSmad2/3 immunoreactivity was co-localized with that of ubiquitin and TDP-43.

Even though the physiological functions of Smad proteins have not been thoroughly elucidated to date, they are supposed to act as the central mediators of the TGF-beta signal transduction pathway [27]. Among several isoforms of Smad proteins, Smad2 and Smad3 belong to the receptor-regulated Smads, and they are predominantly localized

in the cytoplasm in the basal state. To initiate a TGF-beta response, the members of the TGF-beta superfamily bind to their specific receptors on the cell surface. The activated receptors move to early endosomal compartments, where they phosphorylate the Smad2/3 at their C-terminal serine residues. These pSmad2/3 form heteromeric complexes with Smad4, and are then translocated into the nucleus, where they control gene expression in a cell-type-specific and ligand dose-dependent manner through interactions with various transcription factors, co-activators, and co-repressors. Then, Smad signaling is terminated by dephosphorylation by as yet unidentified phosphatases as well as by ubiquitination and proteasome-mediated degradation of activated Smad2/3. Only the dephosphorylated forms of Smad2/3 are exported from the nucleus to the cytoplasm.

TGF-beta-Smad signaling is essential for maintaining the survival of neurons. Among several growth factors of the TGF-beta superfamily, TGF-beta1, TGF-beta2, and TGF-beta3 are expressed in the adult central nervous system (CNS) [9]. TGF-beta1 mRNA is reported to be normally present at low levels in healthy adult CNS cells, and its level increases with age [3]. Therefore, even in unaffected adult control subjects, the TGF-beta-Smad signal transduction pathway is constantly active, to a certain extent. It is thus not surprising that pSmad2/3 immunoreactivity could be identified in neuronal and glial nuclei of the unaffected controls in this study as well as in earlier studies [15, 24]. In response to various neuronal insults, such as ischemia or oxidative stress, TGF-beta1 mRNA is rapidly up-regulated, which induces the expression of multiple genes to oppose the injury and protect neurons, thus reducing neuronal damage [10]. Up-regulated TGF-beta1 would consequently increase the amount of pSmad2/3 accumulated in the nucleus. Our observations that increased pSmad2/3 immunoreactivity in the remaining neuronal and glial nuclei of the SALS, FALS, and Tg mouse specimens was common imply that these cells had been subjected to certain unknown insults that induced TGF-beta-Smad signaling.

The pathomechanism underlying the presence of pSmad2/3 immunoreactivity in the cytoplasmic inclusions of SALS is currently uncertain. If one considers the cascade of TGF-beta-Smad signaling, the C-terminally phosphorylated Smad2/3 that accumulated in these inclusions were unlikely to have been derived from Smad2/3 in the basal state before phosphorylation or from those exported from the nucleus after finishing their role, but from those having been phosphorylated by the TGF-beta receptors but kept from entering the nucleus.

One possible explanation for their accumulation in the inclusions is that the translocation of pSmad2/3 into the nucleus might have been blocked by dysfunctional nucleocytoplasmic transport, resulting in abnormal aggregation in

the cytoplasm. This speculation is supported by our recent study demonstrating that importin-beta and its related proteins accumulate in the perinuclear cytoplasm and in the LBHIs of mSOD1 Tg mice, presumably due to impaired nucleocytoplasmic transport and passive involvement of importin-beta in the process of LBHI formation [28]. In the present study, the cytoplasm of the anterior horn cells from the Tg mice was faintly labeled by anti-pSmad2/3 antibodies. This finding further supports our previous speculation on mSOD1 Tg mice. However, the LBHIs of these mice were immunonegative for pSmad2/3. In contrast, pSmad2/3 were not detected in the neuronal cytoplasm of patients with SALS and FALS. Moreover, the RHIs were immunoreactive for pSmad2/3 homogeneously within their entire structure. These notions imply that pSmad2/3 proteins may play a crucial role in the formation of RHIs rather than being secondarily involved by being sequestered within the inclusions during the process of inclusion formation. A similar mechanism has been very recently proposed to operate in Alzheimer's disease [5]. The pSmad2/3 accumulation in the neurofibrillary tangles in the brains of those with Alzheimer's disease has been reported previously [5, 15, 24], but Chalmers and Love [5] additionally revealed a reduction in nuclear pSmad2/3 immunoreactivity in tangle-bearing cells, and the binding of pSmad3 with the aggregates of hyperphosphorylated tau. Although the neuroprotective effect of TGF-beta signaling has been controversial [23, 26], the above researchers speculated that the neurofibrillary tangles sequester the pSmad2/3, thereby interfering with the nuclear translocation of these proteins and, therefore, with TGF-beta signal transduction in Alzheimer's disease. In our study, we observed in the SALS patients that the nuclear staining density for pSmad2/3 of RHI-possessing neurons was reduced, or not increased, when compared with those without RHIs. This finding suggests that a similar pathomechanism to that in Alzheimer's disease would underlie SALS. However, the interaction of Smad proteins with the known constituent proteins of RHIs and SLIs, especially with TDP-43, in SALS has not been elucidated, and so this situation warrants further investigation.

Taken together, our findings and those of others imply that, in SALS, TGF-beta signal transduction would be impaired. Previous reports have demonstrated that, in ALS patients with a terminal clinical status, TGF-beta1 concentration was significantly higher in the serum [12, 13] and in the cerebrospinal fluid [13] than those levels in controls. Moreover, intraperitoneal administration of TGF-beta2 has been reported to improve the motor performance of mSOD1 Tg ALS mice [7]. These data indicate that the dysfunctional TGF-beta-Smad signal transduction pathway would be involved in the pathogenesis of ALS. Our present results are consistent with those observations, but additionally provide novel information that the critical disruption

within the pathway resulting in neurodegeneration in SALS would be at the step of pSmad2/3 translocation into the nucleus. Our findings would be reinforced by, for instance, evidence that TGF-beta or TGF-beta mRNA levels are increased in ALS and in the mSOD1 Tg mice. On the other hand, the absence of pSmad2/3 immunoreactivity in the LBHIs in the mSOD1-associated FALS patients and in the mSOD1 Tg mice implies that the pathomechanisms of neurodegeneration in those conditions might be different from those in SALS.

We speculate that, in SALS, the disturbed translocation of pSmad2/3 into the nucleus might impair the neuroprotective TGF-beta signaling and lead to neurodegeneration. However, our finding that pSmad2/3 immunoreactivity in the neuronal nuclei possessing inclusions was comparable to that in those of the control subjects prompt an alternative explanation, i.e., that, on the contrary, pSmad2/3 themselves might function neuroprotectively to actively sequester harmful proteins, such as TDP-43, but might be ineffective for detoxifying mSOD1.

Very recently, Chalmers and Love [6] reported that, besides being found in neurofibrillary tangles in Alzheimer's disease, pSmad2/3 also co-localize with abnormally phosphorylated tau inclusions in Pick's disease, progressive supranuclear palsy, and corticobasal degeneration, but not with alpha-synuclein inclusions in dementia with Lewy bodies or in multiple system atrophy. Those authors concluded that pSmad2/3 would interact with tau inclusions. Our result is, to our knowledge, the first demonstration that tau-negative, TDP-43- and ubiquitin-positive intracytoplasmic inclusions in SALS are immunopositive for pSmad2/3. Further investigations into the involvement of TGF-beta-Smad signaling might offer a key to the clarification of the pathomechanism of ALS and other neurodegenerative diseases.

Acknowledgments We express our sincere appreciation to Drs. Kengo Fujita, Yoshimi Kinoshita, and Makoto Nishii, as well as to Miss Tomoko Takemi, for their assistance.

References

- Abdollah S, Macías-Silva M, Tsukazaki T, Hayashi H, Attisano L, Wrana JL (1997) TbetaRI phosphorylation of Smad2 on Ser465 and Ser467 is required for Smad2-Smad4 complex formation and signaling. *J Biol Chem* 272:27678–27685
- Arai T, Hasegawa M, Akiyama H, Ikeda K, Nonaka T, Mori H, Mann D, Tsuchiya K, Yoshida M, Hashizume Y, Oda T (2006) TDP-43 is a component of ubiquitin-positive tau-negative inclusions in frontotemporal lobar degeneration and amyotrophic lateral sclerosis. *Biochem Biophys Res Commun* 351:602–611
- Brionne TC, Tesseur I, Masliah E, Wyss-Coray T (2003) Loss of TGF-beta 1 leads to increased neuronal cell death and microgliosis in mouse brain. *Neuron* 40:1133–1145
- Brooks BR (1994) El Escorial world federation of neurology criteria for the diagnosis of amyotrophic lateral sclerosis. Subcommittee on Motor Neuron Diseases/Amyotrophic Lateral Sclerosis of the World Federation of Neurology Research Group on Neuromuscular Diseases and the El Escorial "Clinical limits of amyotrophic lateral sclerosis" workshop contributors. *J Neurol Sci* 124 [Suppl]:96–107
- Chalmers KA, Love S (2007) Neurofibrillary tangles may interfere with Smad 2/3 signaling in neurons. *J Neuropathol Exp Neurol* 66:158–167
- Chalmers KA, Love S (2007) Phosphorylated Smad 2/3 colocalizes with phospho-tau inclusions in Pick disease, progressive supranuclear palsy, and corticobasal degeneration but not with alpha-synuclein inclusions in multiple system atrophy or dementia with Lewy bodies. *J Neuropathol Exp Neurol* 66:1019–1026
- Day WA, Koishi K, Nukuda H, McLennan IS (2005) Transforming growth factor-beta 2 causes an acute improvement in the motor performance of transgenic ALS mice. *Neurobiol Dis* 19:323–330
- Dickson DW, Josephs KA, Amador-Ortiz C (2007) TDP-43 in differential diagnosis of motor neuron disorders. *Acta Neuropathol* 114:71–79
- Flanders KC, Ren RF, Lipka CF (1998) Transforming growth factor-betas in neurodegenerative disease. *Prog Neurobiol* 54:71–85
- Henrich-Noack P, Prehn JH, Kriegstein J (1994) Neuroprotective effects of TGF-beta 1. *J Neural Transm Suppl* 43:33–45
- Hirano A, Kurland LT, Sayre GP (1967) Familial amyotrophic lateral sclerosis: a subgroup characterized by posterior and spinocerebellar tract involvement and hyaline inclusions in the anterior horn cells. *Arch Neurol* 16:232–243
- Houji K, Kobayashi T, Kato S, Mochio S, Inoue K (2002) Increased plasma TGF-beta 1 in patients with amyotrophic lateral sclerosis. *Acta Neurol Scand* 106:299–301
- Izicka J, Stelmasiak Z, Dobosz B (2002) Transforming growth factor-beta 1 (TGF-beta 1) in patients with amyotrophic lateral sclerosis. *Cytokine* 20:239–243
- Kurisaki A, Kose S, Yoneda Y, Heldin CH, Moustakas A (2001) Transforming growth factor-beta induces nuclear import of Smad3 in an importin-beta1 and Ran-dependent manner. *Mol Biol Cell* 12:1079–1091
- Lee HG, Ueda M, Zhu X, Perry G, Smith MA (2006) Ectopic expression of phospho-Smad2 in Alzheimer's disease: uncoupling of the transforming growth factor-beta pathway? *J Neurosci Res* 84:1856–1861
- Mackenzie IR, Bigio EH, Ince PG, Geser F, Neumann M, Cairns NJ, Kwong LK, Forman MS, Ravits J, Stewart H, Eisen A, McClusky L, Kretzschmar HA, Monoranu CM, Highley JR, Kirby J, Siddique T, Shaw PJ, Lee VM, Trojanowski JQ (2007) Pathological TDP-43 distinguishes sporadic amyotrophic lateral sclerosis from amyotrophic lateral sclerosis with SOD1 mutations. *Ann Neurol* 61:427–434
- Neumann M, Sampathu DM, Kwong LK, Truax AC, Micsenyi MC, Chou TT, Bruce J, Schuck T, Grossman M, Clark CM, McCluskey LF, Miller BL, Masliah E, Mackenzie IR, Feldman H, Feiden W, Kretzschmar HA, Trojanowski JQ, Lee VM (2006) Ubiquitinated TDP-43 in frontotemporal lobar degeneration and amyotrophic lateral sclerosis. *Science* 314:130–133
- Rosen DR, Siddique T, Patterson D, Figlewicz DA, Sapp P, Hentati A, Donaldson D, Goto J, O'Regan JP, Deng H-X, Rahmani Z, Krizus A, McKenna-Yasek D, Cayabyab A, Gaston SM, Berger R, Tanzi RE, Halperin JJ, Herzfeldt B, Van den Bergh R, Hung W-Y, Bird T, Deng G, Mulder DW, Smyth C, Laing NG, Soriano E, Pericak-Vance MA, Haines J, Rouleau GA, Gusella JS, Horvitz HR, Brown RH Jr (1993) Mutations in Cu/Zn superoxide dismutase gene are associated with familial amyotrophic lateral sclerosis. *Nature* 362:59–62
- Schmierer B, Hill CS (2007) TGFbeta-SMAD signal transduction: molecular specificity and functional flexibility. *Nat Rev Mol Cell Biol* 8:970–982

20. Sheffield LG, Miskiewicz HB, Tannenbaum LB, Mirra SS (2006) Nuclear pore complex proteins in Alzheimer disease. *J Neuropathol Exp Neurol* 65:45–54
21. Tan CF, Eguchi H, Tagawa A, Onodera O, Iwasaki T, Tsujino A, Nishizawa M, Kakita A, Takahashi H (2007) TDP-43 immunoreactivity in neuronal inclusions in familial amyotrophic lateral sclerosis with or without SOD1 gene mutation. *Acta Neuropathol* 113:535–542
22. Ten Dijke P, Hill CS (2004) New insights into TGF-beta-Smad signalling. *Trends Biochem Sci* 29:265–273
23. Tesseur I, Zou K, Esposito L, Bard F, Berber E, Can JV, Lin AH, Crews L, Tremblay P, Mathews P, Mucke L, Masliah E, Wyss-Coray T (2006) Deficiency in neuronal TGF-beta signaling promotes neurodegeneration and Alzheimer's pathology. *J Clin Invest* 116:3060–3069
24. Ueberham U, Ueberham E, Gruschka H, Arendt T (2006) Altered subcellular location of phosphorylated Smads in Alzheimer's disease. *Eur J Neurosci* 24:2327–2334
25. Wate R, Ito H, Zhang JH, Ohnishi S, Nakano S, Kusaka H (2005) Expression of an endoplasmic reticulum-resident chaperone, glucose-regulated stress protein 78, in the spinal cord of a mouse model of amyotrophic lateral sclerosis. *Acta Neuropathol* 110:557–562
26. Wyss-Coray T, Masliah E, Mallory M, McConlogue L, Johnson-Wood K, Lin C, Mucke L (1997) Amyloidogenic role of cytokine TGF-beta1 in transgenic mice and in Alzheimer's disease. *Nature* 389:603–606
27. Xu L (2006) Regulation of Smad activities. *Biochim Biophys Acta* 1759:503–513
28. Zhang J, Ito H, Wate R, Ohnishi S, Nakano S, Kusaka H (2006) Altered distributions of nucleocytoplasmic transport-related proteins in the spinal cord of a mouse model of amyotrophic lateral sclerosis. *Acta Neuropathol* 112:673–680

Altered distributions of nucleocytoplasmic transport-related proteins in the spinal cord of a mouse model of amyotrophic lateral sclerosis

Jianhua Zhang · Hidefumi Ito · Reika Wate ·
Shizuo Ohnishi · Satoshi Nakano · Hirofumi Kusaka

Received: 14 April 2006 / Revised: 5 August 2006 / Accepted: 5 August 2006 / Published online: 7 September 2006
© Springer-Verlag 2006

Abstract Recent investigations have indicated that the nucleocytoplasmic transport system is essential for maintaining cell viability and cellular functions and that its dysfunction could lead to certain disorders. To investigate the involvement of this system in the pathomechanisms of amyotrophic lateral sclerosis (ALS), we examined the immunohistochemical localization of proteins associated with nucleocytoplasmic transport in the lumbar spinal cord in a mutant SOD1 (G93A) transgenic mouse model of ALS. This model is widely used for ALS research, and the mutant mice are known to exhibit neuronal loss and Lewy body-like hyaline inclusions (LBHIs) in the anterior horns, similar to the pathology seen in familial ALS patients associated with an SOD1 mutation and in several other transgenic rodent models. Using antibodies against the importin beta family of proteins, the major carrier proteins of nucleocytoplasmic transport, and those against their adapter protein, importin alpha, we found that the immunoreactivities were decreased within the nuclei and increased within the cytoplasm of a subset of the surviving anterior horn cells of the transgenic mice. In addition, LBHIs were invariably reactive toward these antibodies. Furthermore, the immunoreactivities for histone H1 and beta-catenin, representative cargo

proteins transported by importin beta-dependent and beta-independent nucleocytoplasmic transport pathways, respectively, showed distributions similar to those for importin beta family and importin alpha proteins. The altered distributions of these proteins were not associated with caspase-3 expression, suggesting that the findings are unlikely to be a manifestation of apoptotic processes. Chronological quantitative analysis of importin beta-immunostained sections from the transgenic mice revealed a statistically significant progressive decrease in the proportion of the anterior horn cells exhibiting a more intense reactivity for these proteins in the nucleus than in the cytoplasm. To the contrary, we found that the anterior horn cells with the immunoreactivity in their cytoplasm, being more pronounced than that in their nucleus, were significantly increased in number along with the disease progression. This is the first report investigating nucleocytoplasmic transport in the ALS model mouse, and our present results imply that its dysfunction could be involved in the pathomechanisms underlying ALS.

Keywords Amyotrophic lateral sclerosis · Transgenic mouse · Importin · Nucleocytoplasmic transport · Lewy body-like hyaline inclusion

J. Zhang · H. Ito (✉) · R. Wate · S. Ohnishi · S. Nakano ·
H. Kusaka
Department of Neurology, Kansai Medical University,
10-15, Fumizono-cho, Moriguchi, Osaka 570-8507, Japan
e-mail: itoh@takii.kmu.ac.jp

J. Zhang
Department of Neurology, Harbin Medical University,
No.23 Youzheng Street, Nangang District, Harbin,
Heilongjiang 150001, China

Introduction

Knowledge of the molecular mechanisms responsible for intercommunication between the cytoplasm and the nucleus has been recently growing remarkably [8, 10, 22]. The nucleocytoplasmic protein transport system would obviously be expected to play a crucial role in this intercommunication. Using this transport

system, various nuclear proteins, transcription factors, and large molecules functioning in the nucleus are imported into the nucleus across the nuclear envelope after having been synthesized in the cytoplasm; whereas transfer RNA, ribosomal RNA, and messenger RNA are synthesized in the nucleus and exported to the cytoplasm for translation and protein synthesis. Therefore, the nucleocytoplasmic transport is absolutely essential for maintaining cell viability and cellular functions.

Transport of proteins and nucleic acids between the nucleus and the cytoplasm occurs through nuclear pore complexes (NPCs) [26, 29]. Importin (karyopherin) beta1 and other members of this family of molecules are regarded as representative carrier proteins, and members of the importin (karyopherin) alpha family supposedly function as adapter proteins. To date, three distinct nucleocytoplasmic transport pathways have been identified, i.e., importin beta/alpha heterodimer-dependent, importin beta family-dependent only, and importin beta and alpha-independent ones. One or more of these pathways are thought to be employed by each cargo protein [10].

Nuclear pore complexes have been only recently investigated in patients with autoimmune, neoplastic, viral, or hereditary disorders [3]. Regarding neurodegenerative diseases, very recently Sheffield et al. [28] reported the first evidence for the involvement of NPCs in Alzheimer's disease. In Parkinson's disease, RanBP2, a component of cytoplasmic filaments in the NPCs, was shown to be a substrate of Parkin [30]. In contrast, in a rat sciatic nerve lesion model [11] importin beta1 was reported to be translated at the lesion site from preexisting axonal messenger RNA. The authors speculated that lesion-induced up-regulation of importin beta1 may enable retrograde transport of appropriate signals for regeneration toward the nucleus [11]. In neurodegenerative diseases, it is conceivable that similar regeneration mechanisms would be activated; however, the involvement of the importin beta family has not been explored in such disorders.

In the present immunohistochemical study, we investigated the distributions of importin (Imp) beta family, Imp alpha, and representative cargo proteins in the spinal cord of ALS model mice.

Materials and methods

Animals

Founder male mice, heterozygous for the ALS-linked G93A mutation of the human gene for SOD1 (TgN

[B6SJL-Tg (SOD1-G93A) 1Gur]), and female non-transgenic B6SJLF1/J mice were originally obtained from the Jackson Laboratory (Bar Harbor, ME, USA), and crossed in the Kansai Medical University animal facility.

The animals were housed in micro-isolater cages in an animal room on a 12 h light/12 h dark cycle, and given free access to food and water. Procedures involving animals and their care were conducted in conformity with our institutional guidelines, which are in compliance with international laws and policies (NIH Guide for the Care and Use of Laboratory Animals, U.S. National Research Council, 1996).

Genetic analysis

Animals were genotyped by using an ASTEC research thermal cycler for polymerase chain reaction amplification of mouse DNA extracted from tail snips [25]. The detailed protocol was described previously [32].

Immunohistochemistry

Under deep anesthesia with diethyl ether, two G93A SOD1 transgenic (Tg) female mice of each of various ages, i.e., 4, 8, 10 weeks (pre-symptomatic stage of the progression of the motor dysfunction), 12, 13, 14 weeks (early-symptomatic), 15, 16, 17 weeks (middle-symptomatic), and 18, 19, 20 weeks (late-symptomatic) were perfused and fixed with 4% paraformaldehyde in 0.1 M phosphate buffer through the left cardiac ventricle. After having been stored at 4°C for 2 weeks, the spinal cords were dissected; and their lumbar regions were embedded in paraffin and sectioned transversely at a thickness of 7 µm. Female wild-type littermates at 8–20 weeks of age (15 mice) served as controls.

The sections were deparaffinized and stained with hematoxylin and eosin. We confirmed the previously reported neuropathology [4, 5] in the G93A Tg mice of 10 weeks of age and older employed in this study. The anterior horn cells (AHCs) showed vacuolation changes and were progressively lost along as the disease advanced. Lewy body-like hyaline inclusions (LBHIs) were identifiable in the anterior horn neuropil of animals as early as 8 weeks of age, and increased in number along with the progression. LBHI structures similar to those in the G93A Tg mice have been reported in human familial ALS [12] and other Tg rodent models [1, 2, 31].

After we photographed the surviving AHCs and LBHIs, the same sections were decolorized in 70% alcohol, and then immunostained with antibodies specific for the importin beta family (karyopherin beta1

[Imp beta], karyopherin beta2 [transportin], and karyopherin beta3 [importin 5]; polyclonal 1:40, Santa Cruz [19, 27]); karyopherin alpha2/Rch-1 (Imp alpha; monoclonal 1:7,000, BD Biosciences [21]); histone H1 + core proteins (monoclonal 1:10,000, Chemicon [7]), beta-catenin (polyclonal 1:4,000, Chemicon), and caspase-3 (monoclonal 1:100, Chemicon). Incubation was carried out overnight at 4°C. Bound primary antibodies were detected with the appropriate Vectastain Elite ABC kit (Vector Laboratories, Burlingame, CA, USA), and 3,3'-diaminobenzidine was used as the chromogen. We also performed double immunofluorescence staining on lumbar sections from the Tg mice by using anti-Imp beta antibody (mouse monoclonal 1:50, BD Biosciences [21]) and anti-ubiquitin antibody (rabbit polyclonal 1:200, Chemicon). These primary antibodies were detected with Texas red-labeled anti-mouse IgG and anti-rabbit IgG conjugated with FITC. The stained sections were examined with a laser scanning confocal microscope (Olympus FluoView™ FV300 Version 4.3). In addition, the sections from the Tg mice stained with anti-caspase-3 antibody were photographed and then re-stained with the polyclonal anti-Imp beta antibody.

The staining specificity was assessed by replacing the primary antibodies with the appropriate amount of non-immune rabbit serum or phosphate-buffered saline solution containing 3% bovine serum albumin or by pre-incubating the primary antibodies with an excess of the peptide immunogen [32]. No deposits of reaction products were seen in the sections thus treated.

Quantitative analysis

Under 400× magnification, we counted the number of AHCs immunoreactive for Imp beta on three non-consecutive lumbar cord sections from each mouse of each age group. The examiners were properly blinded with respect to the genotype and age of the mice used for preparing the sections. The AHCs were classified into five categories according to the relative staining intensity of the nucleus or of the cytoplasm: (1) virtually only the nucleus was labeled (nucleus only), (2) the nucleus was more robustly stained than the cytoplasm ($n > c$), (3) the nucleus and the cytoplasm were comparably reactive ($n = c$), (4) the cytoplasm was more intensely stained than the nucleus ($n < c$), and (5) the reaction products were seen in the cytoplasm but not recognizable in the nucleus (cytoplasm only). After summing up the cell count for each of these five categories in three sections from each of the wild-type and early-, middle-, and late-symptomatic mice groups, we

calculated the percentage of cells in each category. Statistical analysis between the mean percentage of each category of the Tg mice and that of the controls was carried out by using Student's *t* test.

Results

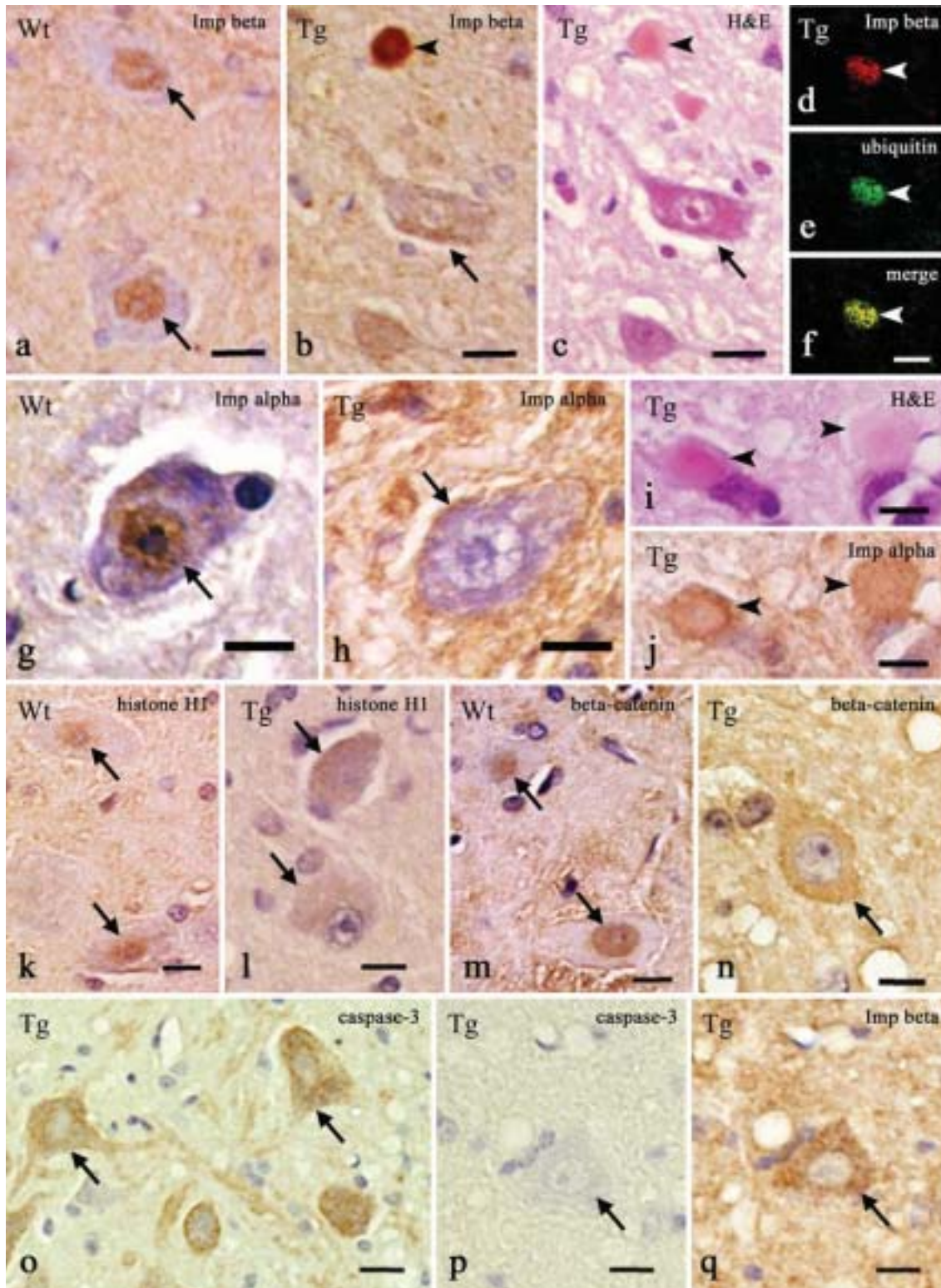
Each antibody employed in the present study gave similar immunohistochemical results in the controls, irrespective of their age, indicating that no age-related changes occurred in the immunohistochemical distributions in the mice between 8 and 20 weeks of age. In the Tg mice in the pre-symptomatic stage, the distributions of the reaction product deposits indicating positive immunoreactions were the same as in the controls. In contrast, in the symptomatic Tg mice the distributions appeared obviously distinct from those of the controls.

The three anti-importin beta family antibodies and the anti-Imp alpha antibody yielded immunostaining patterns essentially similar to each other. In the control mice, Imp beta and Imp alpha immunoreactivities showed a diffuse or granular pattern within the nuclei of the AHCs (Fig. 1a, g). On the other hand, the reactivity in the cytoplasm was variable, and the staining intensity of the cytoplasm was usually no greater than that of the nucleus. In some neurons, the reaction product deposits were recognizable only in the nucleus. In the symptomatic Tg mice, the immunoreactivities for Imp beta and Imp alpha were obviously decreased in the nucleus of a subset of the AHCs, whereas those in the cytoplasm were unchanged or increased (Fig. 1b, h). In addition, these antibodies reacted strongly with the LBHIs (Fig. 1b, c, i, j), and the staining intensity of the neuropil was apparently increased (Fig. 1b, h).

Using the double immunofluorescence technique, we ascertained the colocalization of Imp beta and ubiquitin in LBHIs (Fig. 1d–f).

The anti-histone H1 antibody invariably labeled, as expected, the nuclei of the AHCs of the control mice (Fig. 1k). In a small subset of AHCs the cytoplasm showed additional immunoreactivity for histone H1. In contrast, in the symptomatic Tg mice we encountered several AHCs with their cytoplasm stained more intensely with the antibody than their nucleus (Fig. 1l). LBHIs were also positively stained (data not shown).

Beta-catenin immunoreactivity in the control mice was detected in the AHCs either at comparable levels in both the cytoplasm and the nucleus or with the nuclei being obviously more intensely labeled than their cytoplasm (Fig. 1m). Moreover, immunopositive neurites were seen in the neuropil. In the symptomatic



Tg mice the reaction product deposits were diffusely distributed in the cytoplasm, but conspicuously decreased in the nucleus, of most of the surviving AHCs (Fig. 1n). This antibody faintly recognized certain LBHIs.

The anti-caspase-3 immunoreactive AHCs were most abundant in the lumbar cord from pre- and early-symptomatic (8–13 weeks of age) Tg mice (Fig. 1o). On the other hand, only a few AHCs of the late-symptomatic Tg mice exhibited caspase-3 immunoreactivity

◀ **Fig. 1** Lumbar spinal anterior horn cells of control (**a, g, k, m**) and G93A SOD1 transgenic (Tg) mice (**b–f, h–j, l, n–q**). **a** Immunohistochemistry for karyopherin beta1 (Imp beta) in the control anterior horn cells (AHCs) shows the nuclei having been labeled diffusely (*arrows*). In contrast, the cytoplasm shows less immunoreactivity than the nucleus. **b** In the Tg mice AHC, reduced nuclear immunoreactivity for Imp beta is evident (*arrow*). An accumulation of the protein is seen in the cytoplasm, and in the Lewy body-like hyaline inclusion (LBHI, *arrowhead*). **c** The same section as in “**b**,” stained with H&E shows that the Imp beta-immunoreactive round structure is a typical LBHI (*arrowhead*). **d–f** Double immunofluorescence staining with anti-Imp beta (**d**, red), anti-ubiquitin (**e**, green), and the merged image (**f**, yellow) demonstrates the colocalization of these proteins in the LBHI. (**g–l**) Immunostaining for karyopherin alpha2 (Imp alpha, **g**) and histone H1 (**k**) shows a similar distribution between these proteins and Imp beta in the control AHCs. Note that the nuclei have

been invariably labeled (**g, k, arrows**). In the Tg mouse AHCs, the immunoreactivities in the nuclei are reduced (**h, l, arrows**). Cytoplasmic accumulation of histone H1 is recognizable (**l, arrows**). The LBHIs are immunopositive for Imp alpha, as demonstrated by the re-staining technique (**i, j, arrowheads**). Additionally, the immunoreactivity of the neuropil appears to have increased (**h**). **m** Beta-catenin immunoreactivity is seen in the nucleus of the AHCs (*arrows*), as well as in the neuropil, of a control mouse. **n** In the Tg mouse AHCs the cytoplasm reacts diffusely with the anti-beta-catenin, whereas the immunoreactivity of the nucleus is obviously decreased (*arrow*). **o** Caspase-3 immunohistochemistry of a 12-week-old Tg mouse demonstrates that the cytoplasm of many of the AHCs is labeled by the anti-caspase-3 antibody. **p** An AHC of an 18-week-old Tg mouse, showing no reactivity for caspase-3. **q** The neuron depicted in “**p**” was re-stained with the anti-Imp beta antibody, which resulted in diffuse cytoplasmic labeling with the antibody. Bars = 10 μ m

(Fig. 1p). These findings are consistent with those of a previous report on this immunoreactivity in low G93A SOD1 expression-type Tg mice [33]. Re-staining of the anti-caspase-3-immunostained sections with the anti-Imp beta antibody demonstrated the cytoplasmic accumulation of Imp beta in the same AHCs lacking anti-caspase-3 immunoreactivity (Fig. 1q).

Quantitative analysis (Fig. 2) of the sections immunostained for Imp beta revealed a chronological change in its subcellular localization in AHCs of the Tg mice. Along with the disease progression the Imp beta immunoreactivity progressively shifted its localization from the nucleus to the cytoplasm within the AHCs. Statistic analysis indicated a significant progressive decrease in the number of Tg mouse AHCs with their nucleus more reactive than their cytoplasm. Likewise, the increase in the number of Tg mouse AHCs in which the cytoplasm was more intensely labeled than the nucleus with the anti-Imp beta antibody was also statistically significant (Fig. 2d).

Discussion

In the present study, we for the first time demonstrated the abnormal distributions of the proteins associated with nucleocytoplasmic transport in the surviving AHCs of symptomatic mutant SOD1 Tg mice.

Importin beta family proteins are the key carrier molecules in nucleocytoplasmic transport, conveying certain cargo proteins between the cytoplasm and the nucleus [10, 22, 24]. Investigators in an earlier study mentioned that importin beta did not enter the nucleus [21]. However, subsequent findings showing that importin beta family molecules do cross the nuclear envelope and function in the nucleus [8, 10, 22] are consistent with our present ones on the immunohistochemically detected distribution of importin beta family

molecules in the control mice. In the spinal cords of the Tg mice, we found a decrease in importin beta family immunoreactivity in the nucleus and an increase in it in the cytoplasm of a subset of the surviving AHCs. These findings imply that entry of importin beta-bearing cargo molecules into the nucleus would be impaired in these mice. The immunoreactivity of LBHI with these antibodies might be attributable to the consequent incidental trapping of the importin beta proteins during the process of LBHI formation. The quantitative analysis of the anti-Imp beta-reactive AHCs further suggests that the abnormal distribution of importin beta family molecules would be related to the ALS pathogenesis in the SOD1 Tg mice.

To confirm the findings obtained with the anti-importin beta family antibodies, we applied the anti-Imp alpha and the anti-histone H1 antibodies. Imp alpha is an adapter protein that binds to both Imp beta and certain cargo proteins, and contributes to the transport of the cargo proteins from the cytoplasm into the nucleus [16]. Immunohistochemically this protein was detected mainly in the nucleus of the control mouse AHCs, in accordance with an earlier observation [21]. Histone H1 is a major structural protein in eukaryotic chromosomes, and is imported into the nucleus through an Imp beta/importin 7 heterodimer-mediated energy-dependent process [14]. Our results demonstrating that the amounts of reaction product deposits derived from these antibodies were reduced in the nuclei of AHCs similarly as those for Imp beta indicate that, like Imp beta, neither Imp alpha nor histone H1 would be successfully transported into the nucleus in certain AHCs. These proteins would be expected to accumulate as an Imp beta/Imp alpha complex or an Imp beta/importin 7/histone H1 complex in the cytoplasm of the AHCs and in the LBHIs of the Tg mice. It is thus plausible that the altered distributions of the above-examined proteins could be

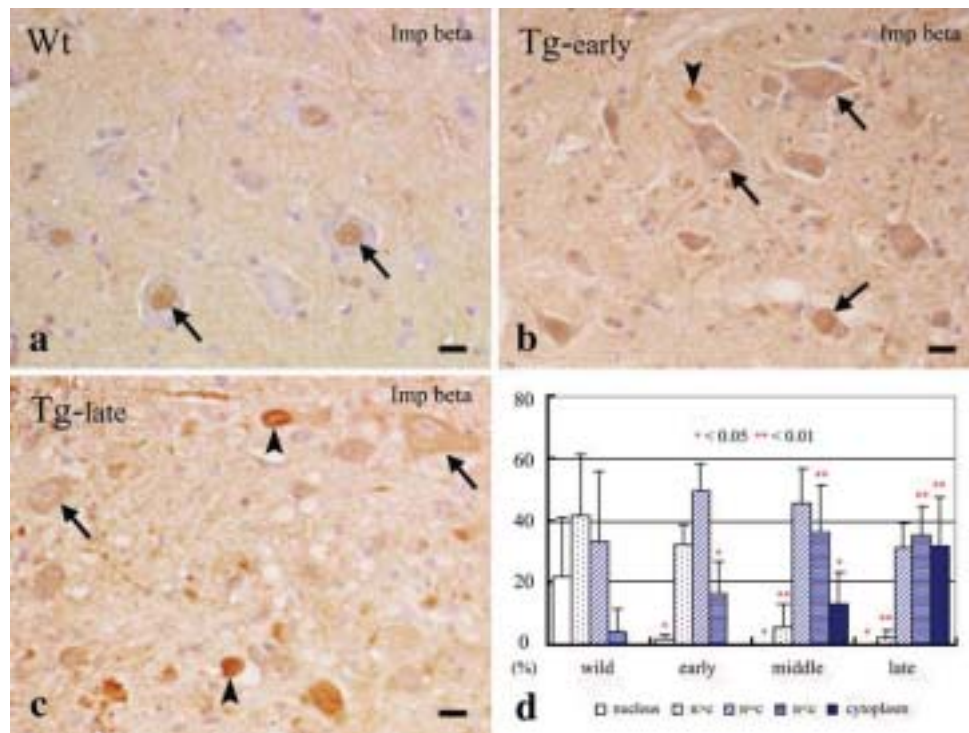


Fig. 2 Low-power magnifications of anti-Imp beta-immunostained lumbar spinal anterior horns from wild-type (**a**), early-symptomatic Tg (**b**), and late-symptomatic Tg (**c**) mice. **a** Arrows indicate AHCs belonging to the category “nucleus only.” **b** Arrows indicate AHCs in the categories “n=c”, “n < c”, and “n > c”, respectively, in order from the *top* to the *bottom* (for abbreviations, see text). The *arrowhead* points to an LBHI. **c** Arrows indicate AHCs reactive with anti-Imp beta in “cytoplasm only”. *Arrowheads* indicate LBHIs. **d** Graphic representation of

quantitative analysis of the sections immunostained for Imp beta. In the symptomatic Tg mice, AHCs with only their nucleus labeled are significantly few or not observed at all. Moreover, the percentage of the AHCs in which the nucleus was more intensely reactive than the cytoplasm progressively decreases and reaches a statistically significant difference. Likewise, the proportion of the AHCs with only their cytoplasm stained or with their cytoplasm more intensely stained than their nucleus increases significantly along with the progression of the disease

attributable to the dysfunction of Imp beta or to that of the NPCs themselves.

To address this issue, we examined the distribution of beta-catenin, an example of a typical molecule that can be translocated bidirectionally through NPCs on its own in a facilitated manner, but not requiring Imp beta or Imp alpha/beta heterodimers [17]. The present subcellular distribution of beta-catenin immunoreactivity in the control mice AHCs was in accordance with that of rat pyramidal neurons reported recently [9]. The present findings that the cytoplasm of most of the Tg mice AHCs showed diffuse immunopositivity for beta-catenin, along with conspicuously decreased immunoreactivity in the nucleus, suggest that beta-catenin would also fail to pass through NPCs into the nucleus in the Tg mice and indicate a dysfunctional NPC. Alternatively, since a decreased level of nuclear beta-catenin has been reported in GSK-3beta-overexpressing mice [20], our findings might reflect increased activity of this kinase in the Tg mice. However, previous expression analysis of various protein kinases including GSK-3beta did not reveal any significant

changes [13]. Another report [9] demonstrated that the proteasome inhibitor lactacystin induces beta-catenin-positive aggresomes in the cytoplasm of cultured cells. Indeed, decreased proteasomal activity has been observed in the spinal cord from G93A SOD1 Tg mice [15]. However, in our present study beta-catenin accumulation in the cytoplasm was diffuse, not sequestered in inclusions. Therefore, in consideration of all of our data taken together, it is conceivable that the dysfunction of the NPCs themselves would be responsible for the abnormal localization of the nucleocytoplasmic transport-related proteins examined in the present study. Furthermore, the fact that the number of the AHCs with an abnormal distribution of these proteins progressively increased in the ALS model mice suggests a positive correlation between this abnormality and ALS pathogenesis.

A very recently reported immunohistochemical investigation on NPCs in Alzheimer’s disease [28] detected nuclear membrane irregularity in the hippocampal and neocortical neurons. These investigators also indicated an abnormal accumulation of nuclear

transport factor 2 (NTF2), a protein carrying RanGDP from the cytoplasm into the nucleus [8, 18, 23], in the cytoplasm of hippocampal pyramidal cells of this disorder. Thus, they postulated that faulty NPCs and nucleocytoplasmic transport would be involved in the pathogenesis of Alzheimer's disease [28]. NTF2 is transported independently of Imp beta/alpha [8, 18, 23], similarly as in the case of beta-catenin; and, intriguingly, the altered immunohistochemical distribution of NTF2 in the pyramidal neurons of Alzheimer's disease [28] appear to resemble that of beta-catenin observed presently. Thus, these notions suggest that common pathogenetic processes of neurodegeneration would underlie both Alzheimer's and ALS diseases.

Nuclear pore complex abnormality has been observed in the case of apoptosis *in vitro* [6]. However, in Alzheimer's disease the changes in NPCs have not been reported to be associated with apoptosis [28]. In our study, the chronological distributions of the caspase-3 immunopositive neurons and those showing cytoplasmic accumulations of nucleocytoplasmic transport carrier and cargo proteins were different. Moreover, we identified instances of altered distribution of Imp beta in the absence of anti-caspase-3 immunoreactivity. Indeed all neurons immunopositive for caspase-3 would not be in the process of undergoing apoptosis, but we can at least state that the neurons devoid of anti-caspase-3 immunoreactivity would not be apoptotic. Thus, these findings imply that the suggested NPC abnormality in the G93A SOD1 Tg mice would not be associated with apoptosis. Further investigations are needed to elucidate the relationship between the present findings and apoptosis.

In summary, we demonstrated a progressive decrease in the nucleus and increase in the cytoplasm of proteins involved in nucleocytoplasmic transport in the surviving AHCs of G93A mSOD1 Tg ALS model mice. In addition, these proteins were found in the LBHIs of the mice. These findings imply that in ALS beneficial regeneration signals would not be successfully transported into the nucleus, resulting in facilitation of neurodegeneration. Thus, our findings indicate that dysfunctional nucleocytoplasmic transport might be involved in the pathomechanisms of ALS. Further investigations on other types of mSOD1 Tg animals and human ALS material are warranted.

Acknowledgments We express our sincere appreciation to Professor Asao Hirano (Division of Neuropathology, Department of Pathology, Montefiore Medical Center) for helpful comments, and to Miss Tomoko Takemi for her technical assistance. This work was supported in part by a grant-in-aid for scientific research from the Japan Society for the Promotion of Science (No. 15590917) and by a grant from Kansai Medical University (Research Grant B, 2005).

References

1. Buijij LI, Becher MW, Lee MK, Anderson KL, Jenkins NA, Copeland NG, Sisodia SS, Rothstein JD, Borchelt DR, Price DL, Cleveland DW (1997) ALS-linked SOD1 mutant G85R mediates damage to astrocytes and promotes rapidly progressive disease with SOD1-containing inclusions. *Neuron* 18:327–338
2. Buijij LI, Houseweart MK, Kato S, Anderson KL, Anderson SD, Ohama E, Reaume AG, Scott RW, Cleveland DW (1998) Aggregation and motor neuron toxicity of an ALS-linked SOD1 mutant independent from wild-type SOD1. *Science* 281:1851–1854
3. Cronshaw JM, Matunis MJ (2004) The nuclear pore complex: disease associations and functional correlations. *Trends Endocrinol Metab* 15:34–39
4. Dal Canto MC, Gurney ME (1994) Development of central nervous system pathology in a murine transgenic model of human amyotrophic lateral sclerosis. *Am J Pathol* 145:1271–1279
5. Dal Canto MC, Gurney ME (1995) Neuropathological changes in two lines of mice carrying a transgene for mutant human Cu,Zn SOD, and in mice overexpressing wild type human SOD: a model of familial amyotrophic lateral sclerosis (FALS). *Brain Res* 676:25–40
6. Faleiro L, Lazebnik Y (2000) Caspases disrupt the nuclear-cytoplasmic barrier. *J Cell Biol* 151:951–959
7. Feng H, Zhong W, Punkosdy G, Gu S, Zhou L, Seabolt EK, Kipreos ET (1999) CUL-2 is required for the G1-to-S-phase transition and mitotic chromosome condensation in *Caenorhabditis elegans*. *Nat Cell Biol* 1:486–492
8. Fried H, Kutay U (2003) Nucleocytoplasmic transport: taking an inventory. *Cell Mol Life Sci* 60:1659–1688
9. Ghanevati M, Miller CA (2005) Phospho- β -catenin accumulation in Alzheimer's disease and in aggresomes attributable to proteasome dysfunction. *J Mol Neurosci* 25:79–94
10. Görlich D, Kutay U (1999) Transport between the cell nucleus and the cytoplasm. *Annu Rev Cell Dev Biol* 15:607–660
11. Hanz S, Perlson E, Willis D, Zheng JQ, Massarwa R, Huerta JJ, Koltzenburg M, Kohler M, van-Minnen J, Twiss JL, Fainzilber M (2003) Axoplasmic importins enable retrograde injury signaling in lesioned nerve. *Neuron* 40:1095–1104
12. Hirano A, Kurland LT, Sayre GP (1967) Familial amyotrophic lateral sclerosis. A subgroup characterized by posterior and spinocerebellar tract involvement and hyaline inclusions in the anterior horn cells. *Arch Neurol* 16:232–243
13. Hu JH, Chernoff K, Pelech S, Krieger C (2003) Protein kinase and protein phosphatase expression in the central nervous system of G93A mSOD over-expressing mice. *J Neurochem* 85:422–431
14. Jäkel S, Albig W, Kutay U, Bischoff FR, Schwamborn K, Doenecke D, Görlich D (1999) The importin β /importin 7 heterodimer is a functional nuclear import receptor for histone H1. *EMBO J* 18:2411–2423
15. Kabashi E, Agar JN, Taylor DM, Minotti S, Durham HD (2004) Focal dysfunction of the proteasome: a pathogenic factor in a mouse model of amyotrophic lateral sclerosis. *J Neurochem* 89:1325–1335
16. Köhler M, Speck C, Christiansen M, Bischoff FR, Prehn S, Haller H, Görlich D, Hartmann E (1999) Evidence for distinct substrate specificities of importin α family members in nuclear protein import. *Mol Cell Biol* 19:7782–7791
17. Koike M, Kose S, Furuta M, Taniguchi N, Yokoya F, Yoneda Y, Imamoto N (2004) beta-Catenin shows an overlapping sequence requirement but distinct molecular interactions for its bidirectional passage through nuclear pores. *J Biol Chem* 279:34038–34047

18. Kuersten S, Ohno M, Mattaj IW (2001) Nucleocytoplasmic transport: Ran, beta and beyond. *Trends Cell Biol* 11:497–503
19. Loveland KL, Hogarth C, Szczepny A, Prabhu SM, Jans DA (2006) Expression of nuclear transport importins beta 1 and beta 3 is regulated during rodent spermatogenesis. *Biol Reprod* 74:67–74
20. Lucas JJ, Hernández F, Gómez-Ramos P, Morán MA, Hen R, Avila J (2001) Decreased nuclear β -catenin, tau hyperphosphorylation and neurodegeneration in GSK-3 β conditional transgenic mice. *EMBO J* 20:27–39
21. Moroianu J, Hijikata M, Blobel G, Radu A (1995) Mammalian karyopherin $\alpha_1\beta$ and $\alpha_2\beta$ heterodimers: α_1 or α_2 subunit binds nuclear localization signal and β subunit interacts with peptide repeat-containing nucleoporins. *Proc Natl Acad Sci USA* 92:6532–6536
22. Mosammaparast N, Pemberton LF (2004) Karyopherins: from nuclear-transport mediators to nuclear-function regulators. *Trends Cell Biol* 14:547–556
23. Ribbeck K, Lipowsky G, Kent HM, Stewart M, Görlich D (1998) NTF2 mediates nuclear import of Ran. *EMBO J* 17:6587–6598
24. Rollenhagen C, Muhlhauser P, Kutay U, Panté N (2003) Importin β -dependent nuclear import pathways: role of the adapter proteins in the docking and releasing steps. *Mol Biol Cell* 14:2104–2115
25. Rosen DR, Siddique T, Patterson D, Figlewicz DA, Sapp P, Hentati A, Donaldson D, Goto J, O'Regan JP, Deng HX, Rahmani Z, Krizus A, McKenna-Yasek D, Cayabyab A, Gaston SM, Berger R, Tanzi RE, Halperin JJ, Herzfeldt B, Van den Bergh R, Hung WY, Bird T, Deng G, Mulder DW, Smyth C, Laing NG, Soriano E, Pericak-Vance MA, Haines J, Rouleau GA, Gusella JS, Horvitz HR, Brown Jr RH (1993) Mutations in Cu/Zn superoxide dismutase gene are associated with familial amyotrophic lateral sclerosis. *Nature* 362:59–62
26. Rout MP, Aitchison JD (2001) The nuclear pore complex as a transport machine. *J Biol Chem* 276:16593–16596
27. Salman H, Abu-Arish A, Oliel S, Loyter A, Klafter J, Granek R, Elbaum M (2005) Nuclear localization signal peptides induce molecular delivery along microtubules. *Biophys J* 89:2134–2145
28. Sheffield LG, Miskiewicz HB, Tannenbaum LB, Mirra SS (2006) Nuclear pore complex proteins in Alzheimer disease. *J Neuropathol Exp Neurol* 65:45–54
29. Suntharalingam M, Wentz SR (2003) Peering through the pore: nuclear pore complex structure, assembly, and function. *Dev Cell* 4:775–789
30. Um JW, Min DS, Rhim H, Kim J, Paik SR, Chung KC (2006) Parkin ubiquitinates and promotes the degradation of Ran-BP2. *J Biol Chem* 281:3595–3603
31. Watanabe M, Dykes-Hoberg M, Culotta VC, Price DL, Wong PC, Rothstein JD (2001) Histological evidence of protein aggregation in mutant SOD1 transgenic mice and in amyotrophic lateral sclerosis neural tissues. *Neurobiol Dis* 8:933–941
32. Wate R, Ito H, Zhang JH, Ohnishi S, Nakano S, Kusaka H (2005) Expression of an endoplasmic reticulum-resident chaperone, glucose-regulated stress protein 78, in the spinal cord of a mouse model of amyotrophic lateral sclerosis. *Acta Neuropathol* 110:557–562
33. Wengenack TM, Holasek SS, Montano CM, Gregor D, Curran GL, Poduslo JF (2004) Activation of programmed cell death markers in ventral horn motor neurons during early presymptomatic stages of amyotrophic lateral sclerosis in a transgenic mouse model. *Brain Res* 1027:73–86

Clinicopathologic investigation of a family with expanded SCA8 CTA/CTG repeats

Abstract—We investigated a family manifesting progressive ataxia, with expanded SCA8 CTA/CTG repeats. Neuropathologically, degeneration of Purkinje, inferior olivary, and nigral neurons and periaqueductal gliosis were evident. The sites of Purkinje cell loss were occupied by fibrillary accumulations. The remaining Purkinje cells showed somatic sprouts, and intracytoplasmic 1C2-positive granular structures were recognizable. This characteristic distribution of neurodegeneration and Purkinje cell cytopathology were distinct from those of other hereditary spinocerebellar ataxias previously reported.

NEUROLOGY 2006;67:1479–1481

H. Ito, MD, PhD; H. Kawakami, MD, PhD; R. Wate, MD; S. Matsumoto, MD, PhD; T. Imai, MD, PhD; A. Hirano, MD, PhD; and H. Kusaka, MD, PhD

Spinocerebellar ataxia type 8 (SCA8) is a hereditary neurodegenerative disorder, manifesting itself as a slowly progressive cerebellar ataxia.^{1,2} It has been reported that SCA8 is caused by a CTA/CTG repeat expansion in the 3' untranslated region of a gene of unknown function.¹ However, the pathogenic role of this expansion remains an issue of debate, because this expanded repeat has also been observed in healthy control subjects and there is poor segregation of the expansion with ataxia in several families.^{3,4} To address the etiology of this controversial type of hereditary SCA (hSCA), neuropathologic findings of patients with an expanded SCA8 allele should be informative. However, no report besides a single abstract⁵ has appeared to date.

Herein we describe our clinicopathologic findings on a Japanese family expressing the SCA8 CTA/CTG repeat expansion.

Methods. *Clinical features.* A 41-year-old man developed progressive gait unsteadiness. Neurologic examination revealed moderate ataxic dysarthria and mild limb and truncal ataxia. His upward gaze was limited. Other systems including reflexes, sensation, and psychiatric function were not impaired. Wechsler Adult Intelligence Scale testing indicated his verbal IQ to be 90. Cranial MRI demonstrated cerebellar atrophy, but the brainstem was of normal size. During follow-up, slight bradykinesia and rigidity developed. His symptoms progressed very slowly and were followed by difficulty in swallowing. He died suddenly of accidental suffocation by sputum while hiking at age 45. Artificial ventilation was not performed.

One of his two sons, on whom we reported previously,⁶ pre-

sented dysarthria at age 14. Examination at age 17 demonstrated cerebellar ataxia, facial grimacing, and exaggerated deep tendon reflexes; his verbal IQ was 63 at age 23. He is now 28 years old and shows severe dysarthria, ataxia, and rigospasticity of all four limbs, dystonia of the left arm, and bradykinesia, but remains ambulatory. His range of eye movement is slightly limited. A cranial MRI disclosed marked cerebellar and mild frontal lobe atrophy with a normal brainstem.

We examined the patient's father, wife, and other son and confirmed them to be unaffected. The mother had died earlier.

Genotype analysis. After having obtained informed consent, we extracted genomic DNA from a fragment of frozen frontal lobe from the proband and leukocytes from his father, wife, and two sons by standard methods. PCR analysis for SCA8 CTA/CTG repeats and CAG repeats in the loci of SCA1, 2, 3, 6, 7, 17 and dentatorubropallidolusian atrophy (DRPLA) were performed as previously described.⁶

Neuropathologic examination. We performed hematoxylin-eosin and Luxol fast blue (LFB) staining and also used the Bielschowsky and Gallyas silver impregnation methods. For immunohistochemistry, mouse monoclonal antibodies against expanded polyglutamine (1C2; Chemicon; 1:8,000), phosphorylated neurofilament (SMI-31; Sternberger; 1:10,000), and rabbit polyclonal antibodies against ubiquitin (Sigma; 1:1,000), synaptophysin (Dako; 1:100), calbindin-D28k (SWANT; 1:10,000), glial fibrillary acidic protein (GFAP; Chemicon; 1:1,000), and α -synuclein (Chemicon; 1:1,000) were employed.

Results. The number of the SCA8 CTA/CTG repeats in genomic DNA from the proband was 240/14 and from his manifested son was 221/24; those from the other individuals were normal. The examined CAG repeat lengths of all the subjects were within the normal range.

The brain weighed 1,145 g. Macroscopically, the cerebellum was atrophic, whereas the cerebrum and brainstem appeared to be of normal size (figure 1A). The examination of sections, however, revealed that the substantia nigra (SN) was conspicuously depigmented (figure 1B). The basis pontis and the locus ceruleus appeared preserved (figure 1, B and D).

Histologically, very severe loss of Purkinje cells was the most prominent finding. The sites of Purkinje cell loss had been replaced by eosinophilic fibrillary accumulations (figure 2A). These structures gave positive staining by Bielschowsky method (figure 2B) and LFB and were immunohistochemically positive for phosphorylated neurofilament (figure 2C) and synaptophysin (figure 2D), but negative for GFAP.

The remaining Purkinje cells appeared atrophic (figure 2F). We occasionally identified characteristic Purkinje cells with somatic sprouts (figure 2, G and H). 1C2 immunohistochemistry demonstrated multiple clusters of granular

From the Department of Neurology (H.I., R.W., H.K.), Kansai Medical University, Department of Neurology (S.M.), Kitano Hospital and Neurological Center, Osaka 530-0025, and Department of Neurology (T.I.), Shiroyama Hospital, Osaka, and Department of Epidemiology (H.K.), Research Institute for Radiation Biology and Medicine, Hiroshima University, Japan; and Division of Neuropathology (A.H.), Department of Pathology, Montefiore Medical Center, Bronx, NY.

Supported in part by a grant-in-aid for scientific research from the Japan Society for the Promotion of Science (no. 15590917) and by a grant from Kansai Medical University (research grant B, 2005).

Disclosure: The authors report no conflicts of interest.

Received January 31, 2006. Accepted in final form June 22, 2006

Address correspondence and reprint requests to Dr. H. Ito, Department of Neurology, Kansai Medical University, 10-15, Fumizono-cho, Moriguchi, Osaka 570-8507, Japan; e-mail: itoh@takii.kmu.ac.jp

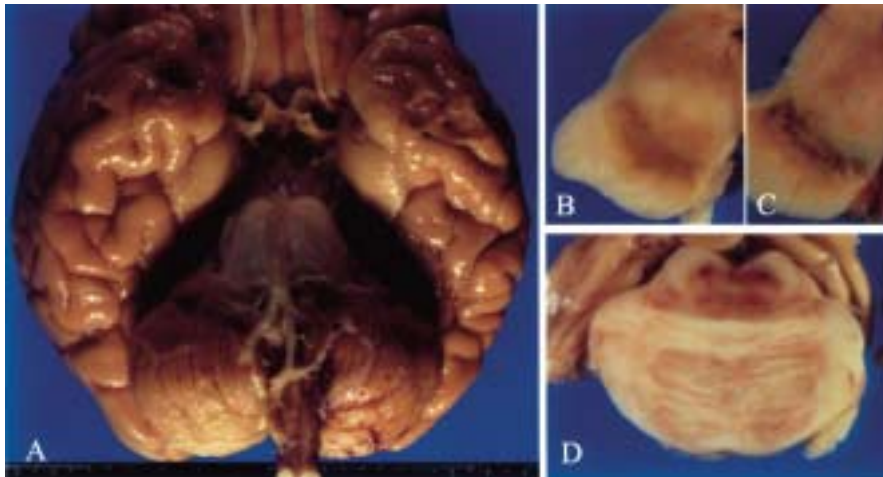


Figure 1. Representative photographs of the external cerebellar appearance (A) and transverse sections of the midbrain (B) and the pons (D) from the patient with spinocerebellar ataxia type 8 and the midbrain from a control subject (C). (A) Cerebellar atrophy is clearly recognizable. (B) Pronounced depigmentation and brownish discoloration of the substantia nigra are evident, when compared with that of a control (C). (D) The normal architecture of the basis pontis and the locus ceruleus is well preserved.

structures within the cytoplasm of the residual Purkinje cells (figure 2I). These granular structures were not recognizable by any of the staining procedures employed presently.

In the dentate nucleus, the neuronal population in general appeared to have been preserved (figure 3A). By contrast, neuronal loss in the pars compacta of the SN (figure 3B) and in the inferior olivary nucleus (figure 3C) was noticeable. 1C2 immunohistochemistry demonstrated no inclusions in the neurons of these structures. In the periaqueductal gray matter, extensive gliosis was noted.

In contrast, pontine neurons were well preserved (figure 3D); no glial inclusions were seen. Neurons in the frontal and temporal lobes, hippocampus, striatum, pallidum, thalamus, subthalamic and red nuclei, locus ceruleus, cranial nerve nuclei, and the spinal cord were preserved. Sudan III staining of the spinal cord showed no tract degeneration.

Discussion. Neuropathology of hSCAs has been reported to date in cases with SCA1, 2, 3, 4, 6, 7, 17, 23, DRPLA, and 16q-linked autosomal dominant cerebellar ataxia type III⁷ (16q-ADCA). Purkinje cells are usually preserved in SCA3 and DRPLA; and the dentate nucleus is more than moderately affected in SCA1, 4, 7, and 23. Also, the pontine neurons are degenerated definitely in SCA1 and 2 and variably in 7. Therefore, such reports indicate that our patient had a different condition from the above hSCAs neuropathologically. On the other hand, Purkinje cell degeneration with preserved dentate and pontine nuclei is a common finding in SCA6,⁸ 17,⁹ and 16q-ADCA.⁷ In these conditions, the inferior olivary changes are variable. However, nigral pathology, if any, is reported to be generally mild.⁷⁻⁹ Thus, the distribution pattern of neurodegeneration in our patient was dissimilar to that of any of the previously reported hSCAs.

Our immunohistochemical findings suggest that the fibrillary accumulations in the Purkinje cell layer probably consisted of afferent terminal axons. We noted similar structures in the figures depicting SCA6 pathology.⁸ Recently reported amorphous materials around Purkinje cells in a patient with

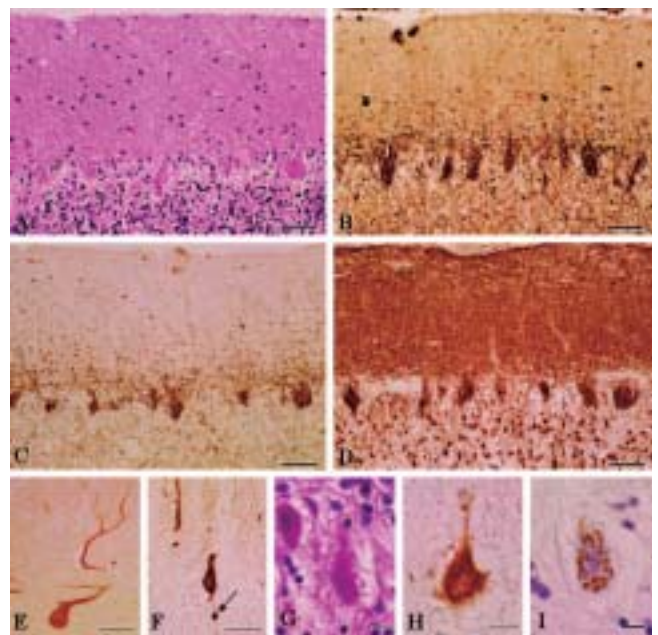


Figure 2. Representative photomicrographs of the cerebellum. (A) Hematoxylin-eosin-stained cerebellar cortex from the patient with spinocerebellar ataxia type 8 (SCA8) shows Purkinje cell loss, with the missing cells having been replaced by eosinophilic fibrillary accumulations. (B through D) Sections nearby the one shown in A stained by Bielschowsky silver impregnation method (B) and immunohistochemically for phosphorylated neurofilament (C) and synaptophysin (D). Fibrillary accumulations are invariably detectable by these staining procedures. The molecular layer is thinner than normal, and the granule cells are mildly decreased in number (A through D). (E and F) Calbindin-D28k immunostaining of a normal subject (E) and the SCA8 patient (F) demonstrates the atrophic nature of the remaining Purkinje cells and torpedo formation (arrow) of the latter. (G through I) The Purkinje cells of the SCA8 patient, stained with hematoxylin-eosin (G) and immunohistochemically for calbindin-D28k (H) and with the 1C2 antibody (I). Somatic sprouts are noticeable in some of the remaining Purkinje cells, readily seen with the anti-calbindin-D28k antibody (G and H). The 1C2 antibody reveals multiple positive granular cytoplasmic inclusions, but intranuclear inclusions are not evident (I). Bars = 50 μ m (A-F) and 10 μ m (G-I).

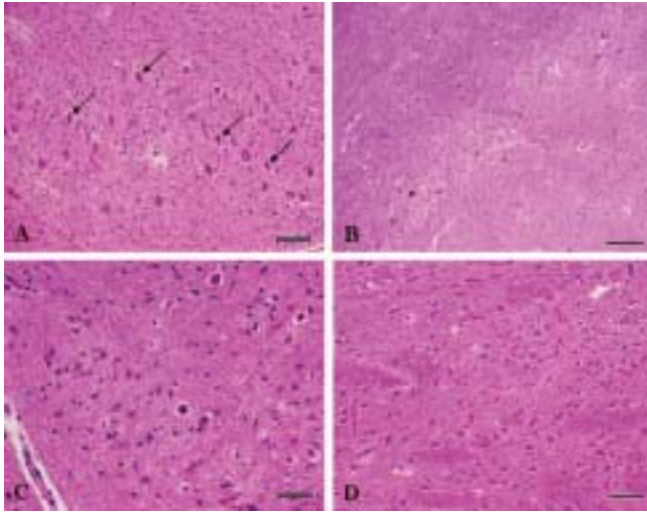


Figure 3. Photomicrographs of the cerebellar dentate nucleus and the brainstem structures from the patient with spinocerebellar ataxia type 8, stained with hematoxylin-eosin. (A) The dentate nucleus contains several neurons that are atrophic and darkly stained (arrows), but the neuronal populations in general are preserved. (B) The substantia nigra demonstrates remarkable depletion of pigmented neurons. (C) The inferior olivary nucleus reveals significant neuronal loss and astrocytosis. (D) The pontine neurons are preserved. Bars = 100 μ m (A, D), 200 μ m (B), and 50 μ m (C).

16q-ADCA⁷ also partly resembled the above accumulations, but they lacked SMI-31 immunoreactivity. Purkinje cells with somatic sprouts were identified in SCA6 and 16q-ADCA patients but have not been reported in other sporadic or hSCAs.

1C2-positive, ubiquitin-negative intracytoplasmic inclusions have been identified in patients with SCA2, SCA6, and SCA7, being caused by CAG repeat expansion in common. However, the 1C2 monoclonal antibody was recently shown to recognize not only polyglutamine but also polyleucine.¹⁰ As a CTG triplet codes leucine, the 1C2 immunoreactivity in the inclusions of our case might represent polyleucine translated abnormally from the expanded CTG repeat. This gene might encode a bicistronic transcript.

Even though the nigral findings were different, the neuropathology of our patient showed some resemblance to that of SCA6. This is consistent with our previous speculation based on the genetic data, sug-

gesting the possible etiologic relationship between SCA8 and SCA6.⁶ Finally, comparing the current findings with the formerly described neuropathology concerning SCA8 cases,⁵ we found that the Purkinje, granular, and olivary neuronal loss was a common feature. In contrast, the nigral degeneration or the periaqueductal gliosis was not mentioned in that earlier study,⁵ and intranuclear instead of intracytoplasmic, 1C2-positive inclusions in Purkinje cells were reported. It is known that there is a great clinical and pathologic variability in SCA patients within the same genotype or even belonging to the same family. Certain variant clinical features of our patients from the previously reported SCA8 subjects^{1,2} raise the possibility that the SCA8 repeat expansion in our patients could have been incidental and that they could have another as yet unknown disease. For determination of the neuropathologic features of SCA8 patients, further studies with additional cases are needed.

Acknowledgment

The authors thank Prof. Hidehiro Mizusawa and Dr. Kinuya Ishikawa (Department of Neurology and Neurologic Science, Graduate School, Tokyo Medical and Dental University) for their helpful comments.

References

1. Koob MD, Moseley ML, Schut LJ, et al. An untranslated CTG expansion causes a novel form of spinocerebellar ataxia (SCA8). *Nat Genet* 1999;21:379–384.
2. Day JW, Schut LJ, Moseley ML, Durand AC, Ranum LPW. Spinocerebellar ataxia type 8: clinical features in a large family. *Neurology* 2000;55:649–657.
3. Stevanin G, Herman A, Durr A, et al. Are (CTG)_n expansions at the SCA8 locus rare polymorphisms? *Nat Genet* 2000;24:213.
4. Worth PF, Houlden H, Giunti P, Davis MB, Wood NW. Large, expanded repeats in SCA8 are not confined to patients with cerebellar ataxia. *Nat Genet* 2000;24:214–215.
5. Ikeda Y, Moseley ML, Dalton JC et al. Purkinje cell degeneration and 1C2 positive neuronal intranuclear inclusions in SCA8 patients. American Society of Human Genetics Annual Meeting 2004. Abstract/session information for program no. 2438. Abstract.
6. Izumi Y, Maruyama H, Oda M, et al. SCA8 repeat expansion: large CTA/CTG repeat alleles are more common in ataxic patients, including those with SCA6. *Am J Hum Genet* 2003;72:704–709.
7. Owada K, Ishikawa K, Toru S, et al. A clinical, genetic, and neuropathologic study in a family with 16q-linked ADCA type III. *Neurology* 2005;65:629–632.
8. Gomez CM, Thompson RM, Gammack JT, et al. Spinocerebellar ataxia type 6: gaze-evoked and vertical nystagmus, Purkinje cell degeneration, and variable age of onset. *Ann Neurol* 1997;42:933–950.
9. Rolfs A, Koeppen AH, Bauer I, et al. Clinical features and neuropathology of autosomal dominant spinocerebellar ataxia (SCA17). *Ann Neurol* 2003;54:367–375.
10. Dorsman JC, Pepers B, Langenberg D, et al. Strong aggregation and increased toxicity of polyleucine over polyglutamine stretches in mammalian cells. *Hum Mol Genet* 2002;11:1487–1496.

研究成果報告書

研究課題名	脳血管障害後の運動機能修復・再生にむけた臨床応用研究		
(英文)	Repairment of motor function following by cerebral ischemia and spinal cord injury for clinical application		
事業推進者	河本圭司	E-mail	kawamoto@takii.kmu.ac.jp
所属・職名	医学研究科・脳神経再生医学（脳神経外科学）講座・教授		
研究分担者名	浅井 昭雄、藤岡 政行、龍 堯志		
キーワード	Spinal cord injury、ischemic brain、edaravone、serofendic acid		
<p>急性期脊髄損傷及び虚血脳に対する新しい神経保護薬による治療-ラットモデルを用いて-</p> <p>1. 概要</p> <p>(1) 我々は既存の神経保護物質を用いることで急性期脊髄損傷に対して症状の軽減を図れないかと考えた。神経保護物質には現在日本で使用されている edaravone、MCI-186、そしてまだ開発中ではあるが強い神経保護作用を持つことが <i>in vitro</i> で示された serofendic acid を用いた。これらの薬剤はフリーラジカルスカベンジャーとよばれ、様々な方面での効果が期待される薬剤である。</p> <p>(2) 再生医療の中で神経再生は不可能という時代から、最近になって神経移植・再生が注目されてきた。国内では岡野栄之らは ES 細胞を用いた神経細胞への分化・移植を行い、再生に向けて試みつつある。虚血脳の神経再生をフリーラジカルスカベンジャーを用いて試みる。</p> <p>2. 研究の背景と目的</p> <p>(1) Edaravone は脳虚血疾患急性期に対しすでに日本で臨床応用されており、虚血に対する報告例はあるが、脊髄疾患にたいする実験報告は少ない。Serofendic acid は <i>in vitro</i> の報告にとどめ、<i>in vivo</i> での初めての実験となる。薬剤を使用し、脊髄損傷の治療を行うことは臨床的に実現する可能性が高いと考えられる。われわれはこれらの薬剤を用いて急性期脊髄損傷に対しより臨床に近い形で投与し、その後の機能および組織標本の検討を行った。</p> <p>(2) 骨髄幹細胞を用いた虚血脳の神経再生については世界的には未知の分野である。我々は臨床応用に最も近いモデルとして、骨髄幹細胞に注目し、神経再生に有効な骨髄幹細胞を採取することである。このために、トランスジェニックラットの胎児から骨髄幹細胞を採取する方法を確立すること、フローサイトメトリー (FCM) で神経分化能を有する細胞を分取する方法を確立すること③GFP (Green Fluorescent Protein) 遺伝子によるトランスジェニックラットの胎児骨髄幹細胞の移植による虚血脳の神経再生の可能性を検討する。</p> <p>3. 研究方法</p> <p>(1) <u>脊髄損傷モデルの作成</u></p> <p>Rat はペントバルビタールナトリウムを蒸留水で希釈し、5 mg/kg となる量を腹腔内投与し、麻酔を行った。次に背中の中毛を剃り、Th9~12 のレベルで皮膚切開を行い、脊髄を損傷しないように Laminectomy を行った。Spine を露出した後、同脊髄の部位に New York University (NYU) impactor を用いて 25 mm の高さより重さ 10 g の棒を垂直方向より直接脊髄に落下させ、脊髄損傷モデルを作成した。止血を確認した後に、皮膚を縫合した。</p>			

薬剤の投与

治療群に対する薬剤投与方法は脊髄損傷作成し、皮膚縫合終了後約 5 分経過してから各々の薬剤を経静脈的に 5 mg/kg ずつ投与した。また対照群として薬剤を含まない純粋な蒸留水を 0.3 ml 投与した。

比較対象は三グループとし、①薬剤を投与しなかった群 (control、n=10) ②edaravone を投与した群 (n=10) ③serofendic acid (n=10) を投与した群とした。

効果の判定

後肢の運動機能評価は open field (125 × 75 cm) を用いて二人の観察者により、Basso-Beattie-Bresnahan (BBB) locomotor rating score を決定した。

組織の染色

脊髄損傷モデル作成後 14 日目に脊髄組織の作成を行った。染色は HE・GFAP・シナプトフィジン・ルクソールファストブルー・TUNEL・CD4・CD8・CD11b を行った。

(2) 虚血脳モデル作成

ラットを用いて一側の中大脳動脈閉塞の実験を行い、完全閉塞するモデルは完成した。

骨髄幹細胞の採取と培養

GFP 遺伝子トランスジェニックラットをすでに開発し、研究分担者の池原より提供を受けた。今までは成人ラットの長管骨の骨髄細胞を用いていたが、より未熟な幹細胞の採取のために、幼若なラットより骨組織を採取し、細切し、培養した。この幼若なラットの骨をどの時期に採取するかが重要であり、採取時期、採取量について検討した。次に、細切した全骨を培養し、非付着細胞は造血細胞なので除去し、付着した細胞が骨髄間葉系幹細胞としてこれを採取した。

骨髄幹細胞の分化能

骨髄幹細胞でも、造血系と間葉系の細胞が混合しており、さらに間葉系細胞が神経系へ分化する細胞として必要となる。PDGF-BB やβ-FGF を付加し、神経系に分化させることを試みる。どの時期にどのくらいの細胞が神経系に分化するかを検討した。種々に分化した細胞を免疫組織的、分子生物学的に同定した。

4. これまでの成果

(1) BBB score は Control 群では脊髄損傷直後はほとんど後肢運動は認められなかったが、日が経過するにつれて徐々に回復を示した。Day 1 で 4.0 ± 0.2 であり、day 14 には 10.0 ± 1.2 となっていた。薬物投与群は損傷後翌日より、改善を示し、day 1 で 8.0 ± 0.3 となり、day 14 には 15.0 ± 1.1 となっていた。また、トレッドミルを用いた運動機能測定は損傷前を 100% とし、損傷後の歩行速度を測定した。Control 群において day 1 で $27.2 \pm 0.2\%$ 、day 14 で $59.1 \pm 0.1\%$ となった。Edaravone においては day 1 で $61.9 \pm 7.8\%$ 、day 14 で $79.1 \pm 7.2\%$ となった。Serofendic acid においては day 1 で $86.2 \pm 2.9\%$ 、day 14 で $93.8 \pm 2.1\%$ となった。Day 1、4 では両方の薬剤投与群とも後肢運動機能に有意差をもって改善を示したが Day 7、14 では Serofendic acid のみが有意差をもって改善した。

HE 染色において control 群は脊髄損傷部の多数の空胞化および灰白質の断裂と共に白質の広範な変性壊死が見られた。神経細胞の脱落像も目立ち、損傷部位に多数のリンパ球を中心とした炎症細胞の浸潤を伴っていた。それに対し、治療群ではエダラボン、セロフェンド酸ともに 14 日目では脊髄損傷部の空胞化や神経細胞の脱落が減少しており、損傷部周辺の炎症細胞の浸潤もほとんど認めなかった。

TUNEL 染色において control 群では脊髄損傷部に TUNEL 陽性細胞が多く認められ、その多

くは損傷をうけた部位でなく損傷部の周辺で見られた。TUNEL 陽性細胞は day 14 で 29 ± 10.1 であった。治療群は TUNEL 陽性細胞をわずかに認める程度であった。エダラボン day 14 で 4.8 ± 1.8 、セロフェンド酸 day 14 で 4.3 ± 2.11 であった。

(2) ラットを用いて、一側中大脳動脈閉塞の実験を行い、完全閉塞モデルは完成した。骨髄幹細胞でも、造血系と間葉系の細胞が混合しており、さらに間葉系細胞が神経系へ分化する細胞として必要となる。PDGF-BB や β -FGF を付加し、神経系に分化させることに成功した。骨髄細胞の局所移植により、脳梗塞の volume の減少、梗塞巣の周囲に移植骨髄由来細胞が認められた。

【まとめ】

エダラボン、セロフェンド酸を投与することで急性期脊髄損傷に対し、機能的改善および組織学的改善を示した。組織学的検討からこれらの薬剤は二次損傷における apoptosis と炎症に対し抑制的に働いていると考えられた。今回の実験でセロフェンド酸が生体内においても有効であると世界で始めて示された。

虚血脳についても、エダラボン、セロフェンド酸が有効であった。

5. これまでの進捗状況と今後の計画

現在、急性脊髄損傷の症例及び脳梗塞の患者に対する臨床応用に向けて進行中である。

6. これまでの発表論文

(1) 発表論文

Li, Q., Hosaka, N., Cui, W., Wang, X., Cui, Y., Cui, Y., Song, C., Li, Q., Ryu, T., Fan, T., Kawamoto, K. & Ikehara, S.

Lin-CD34⁺ bone marrow cells from adult mice can differentiate into neural-like cells.
Neurosci. Lett. **408**, 51-56 (2006).

(2) 学会発表

国内学会

2) シンポジウム講演

李強、龍堯志、池原進、河本圭司:

成体骨髄由来造血幹細胞の神経系細胞へ分化誘導の研究.

第7回日本分子脳神経外科学会、東京、2006.

3) 一般発表

1. 李強、龍堯志、池原進、河本圭司:

成体骨髄由来造血幹細胞の神経系細胞へ分化誘導の研究.

第65回日本脳神経外科学会総会、京都、2006.

2. 龍堯志、吉村晋一、我妻敬一、李強、保坂直樹、久米利明、赤池昭紀、池原進、河本圭司:

急性期脊髄損傷に対する新しい神経保護薬の治療-ラットモデルを用いて-

第65回日本脳神経外科学会総会、京都、2006.

7. これまでの成果の情報公開

ホームページ：脳神経外科学講座 = <http://www3.kmu.ac.jp/nsurg/>

Lin⁻CD34⁻ bone marrow cells from adult mice can differentiate into neural-like cells

Qiang Li^{a,b}, Naoki Hosaka^{a,c,d}, Wenhao Cui^a, Xiaoli Wang^a, Yilong Cui^e, Yunze Cui^a,
Changye Song^a, Qing Li^a, Takashi Ryu^{a,b}, Tianxue Fan^a,
Keiji Kawamoto^b, Susumu Ikehara^{a,c,d,*}

^a First Department of Pathology, Kansai Medical University, 10-15 Fumizono-cho, Moriguchi City, Osaka 570-8506, Japan

^b Department of Neurosurgery, Kansai Medical University, Japan

^c Regeneration Research Center for Intractable Diseases, Kansai Medical University, Japan

^d Department of Transplantation for Regeneration Therapy, Kansai Medical University, Japan

^e Department of Anatomy and Cell Science, Kansai Medical University, Japan

Received 2 June 2006; received in revised form 20 July 2006; accepted 11 August 2006

Abstract

Numerous studies have shown that some populations of bone marrow cells (BMCs) have the capacity to differentiate into neural cells, which is useful for repairing brain lesions. In this paper, we analyze neural differentiation features of lineage-negative/CD34-negative (Lin⁻CD34⁻) cells in the bone marrow of adult mice. The population of Lin⁻CD34⁻ in BMCs was isolated by magnetic bead sorting and fluorescence-activated cell sorter (FACS) using specific lineage (CD4, CD8a, CD11b, CD45R, Gr-1 and TER-119) antibodies and CD34 antibody. First, we cultured Lin⁻CD34⁻ BMCs in the presence of RNIF: vitamin A derivative retinoic acid (RA) and neural-inducing factors (platelet-derived growth factor BB (PDGF-BB), epidermal growth factor (EGF) and fibroblast growth factor-basic (FGF-b)). Analyses of RT-PCR and immunocytochemistry indicated that RNIF-treated Lin⁻CD34⁻ BMCs expressed neural phenotypes as well as neurogenic transcription factors. When we implanted the Lin⁻CD34⁻ BMCs isolated from enhanced green fluorescent protein (eGFP) transgenic mice into the subventricular zone (SVZ) of postnatal mice, eGFP-positive cells survived 3 weeks after the injection in the various brain regions, some of which expressed the neural phenotypes. Our data suggest that certain subsets in the CD34⁻ populations of adult bone marrow could have the capacity to differentiate into neural cells in a suitable environment.

© 2006 Elsevier Ireland Ltd. All rights reserved.

Keywords: CD34-negative cells; Bone marrow cells; Neurogenesis; Mice

Stem cell therapies that could alleviate neurodegeneration or facilitate neural regeneration have become a high priority in neuromedical research. Considering the problems of ethics, immunorejection and isolation technique, bone marrow-derived cells as well as hematopoietic stem cells (HSCs) are of special interest [19]. HSCs are a rare population in bone marrow and give rise to all lymphoid, myeloid, megakaryocytic and erythroid cells. It has long been believed that HSCs express the cell surface glycoprotein CD34 [1]. However, it has been recently reported that CD34⁻ cells

can also reconstitute hematopoiesis [5], and that primitive HSCs lack the CD34 antigen in bone marrow [7]. In adult mice, Lin⁻ (myeloid/lymphoid/megakaryocytic/erythroid lineage-negative) CD34⁻ bone marrow cells (BMCs) are regarded as HSCs, since these cells can differentiate into multilineage colony-forming cells *in vitro* [15], and have long-term reconstituting ability after being transplanted into lethally irradiated mice [9]. In the present study, we examine the capacity of Lin⁻CD34⁻ BMCs obtained from adult mice to differentiate into neural phenotypes.

Retinoic acid (RA) has been used as a neurogenic stimulator of many type cells, including neural stem cells, embryonic stem cells and stem cells from the bone marrow [8,18,12]. Platelet-derived growth factor BB (PDGF-BB), epidermal growth factor (EGF) and fibroblast growth factor-basic (FGF-b) promote the

* Corresponding author at: First Department of Pathology, Kansai Medical University, 10-15 Fumizono-cho, Moriguchi City, Osaka 570-8506, Japan.

Tel.: +81 6 6993 9429/9430; fax: +81 6 6994 8283.

E-mail address: ikehara@takii.kmu.ac.jp (S. Ikehara).

expansion and neural differentiation of neural stem cells, and stimulate the neural differentiation of embryonic stem cells and multipotent adult progenitor cells [2,17,3,16,11]. Therefore, we cultured Lin⁻CD34⁻ BMCs in the medium with RNIF (including RA, PDGF-BB, EGF and FGF-b) and examined whether these cells can be induced into neural phenotypes *in vitro*.

It is believed that the subventricular zone (SVZ) of developing brains is a neurogenically active region, and the region is rich in neurotrophic factors, which supports neural differentiation of neural stem cells or non-neural stem cells [23,24]. To test the neural differentiation potential of Lin⁻CD34⁻ BMCs *in vivo*, we implanted Lin⁻CD34⁻ BMCs isolated from enhanced green fluorescent protein (eGFP)-transgenic mice into the SVZ of postnatal mice to determine whether these cells would be able to differentiate into neural phenotypes in the brains.

Whole BMCs were flushed from the femurs and tibias of 16-week-old C57BL/6-Ly5.2 (B6) mice (for *in vitro* culture) or 16-week-old eGFP-transgenic mice (C57BL/6-Ly5.2 background; for *in vivo* implantation), and suspended in phosphate-buffered saline (PBS) containing 2% heat-inactivated fetal bovine serum (FBS; GIBCO). Mononuclear BMCs were collected by Ficoll-paque plus (1.077 g/cm³; Amersham-Pharmacia) density gradient centrifugation. Lin⁻CD34⁻ BMCs were prepared by incubating the mononuclear cells with monoclonal antibodies, biotin-conjugated anti-CD4 (No. 553649), anti-CD8a (No. 553029), anti-CD11b (No. 553309), anti-CD45R (No. 553086), anti-Gr-1 (No. 553125), anti-TER-119 (No. 553672) and anti-CD34 (No. 553732) (BD Biosciences Pharmingen), and by removing positive cells with streptavidin-conjugated magnetic beads (Dynabeads M-280 Streptavidin; DYNAL A.S.). After the resulting cells were stained with streptavidin-conjugated PE-Cy5 (Dakocytomation), the cells were washed, and resuspended in PBS containing 0.5% bovine serum albumin (BSA; GIBCO) and kept on ice for cell sorting. Cell-type analysis and cell sorting were performed using a fluorescence-activated cell sorter (FACS) (EPICS ALTRA; Beckman Coulter, Inc., Fullerton, CA). After cell sorting, the cell purity of the Lin⁻CD34⁻ populations was examined using the FACS. In all experiments, only cell populations in which both the Lin⁻ purity and the CD34⁻ purity were >99.5% were used.

FACS-sorted Lin⁻CD34⁻ BMCs were planted at 1×10^5 cells/cm² in 24-well plates with coverslips pre-coated with poly-L-ornithine hydrobromide (Sigma) and fibronectin (Sigma). Cells were grown at 37 °C in humidified 10% CO₂/90% air. Base medium consisted of Dulbecco's Modified Eagle Medium: Nutrient Mixture F-12 (GIBCO) with 10% FBS, 1 × N2 supplement (GIBCO), 100 units of penicillin (GIBCO), 1000 units of streptomycin (GIBCO) and 1 mM 2-mercaptoethanol (Sigma). To induce neural differentiation, cells were treated with RNIF: base medium supplemented with 0.5 μM RA (Sigma), 5 ng/ml PDGF-BB (520-BB, R&D SYSTEMS), 10 ng/ml EGF (315-09, PEPROTECH EC LTD) and 100 ng/ml FGF-b (100-18B, PEPROTECH EC LTD). As control groups, cells were grown in base medium. Half the medium in the culture plates was replaced with the same volume of fresh medium with supplements twice per week. The Lin⁻CD34⁻ BMCs were grown on the coverslips for 16 days as described above. On Days 4, 8 and 16, culture cells

were fixed with 4% paraformaldehyde (in PBS). For immunocytochemistry, cells were incubated with primary antibodies: anti-nestin (1:200; No. 611658, BD Biosciences Pharmingen), anti-TuJ1 (1:200; GT431195, Genzyme-Techne), anti-MAP2 (1:100; MAB364, CHEMICON), anti-GFAP (1:400; G3893, Sigma), and anti-CNPase (1:400; MAB326, CHEMICON). To eliminate the background problems, a Vector M.O.MTM fluorescein kit (Vector) was used to block secondary antibody reaction using a modification of the manufacturer's instructions. After being incubated with a biotin-conjugated secondary antibody contained in the kit, cells were exposed to Texas red avidin D (1:50; Vector), and stained with 4',6-diamino-2-phenylindole (DAPI; 2 μg/ml; Sigma) to identify cellular nuclei. DAPI-staining cells and Texas red-immunofluorescent cells were examined and counted using a confocal fluorescence microscopy system (LSM510META, Ver 3.2; ZEISS, Carl Zeiss Co., Ltd). To assess the frequency of cell types in a given culture, we counted the number of cells staining positive with a given antibody in 10 visual fields (30–300 cells per field) per well.

Total RNA was extracted from the culture cells on Days 0 (fresh FACS-sorted Lin⁻CD34⁻ BMCs), 4 and 8 using a Rneasy mini kit (Qiagen) as described by the manufacturer, and then total RNA was reverse transcribed with MMLV reverse transcriptase (ReverTra Ace-aTM kit; TOYOBO) in the presence of random primer. The cDNA was amplified using Platinum Pfx DNA Polymerase (Invitrogen). Primer sequences (forward and reverse), and the lengths of the amplified products were as follows: nestin (5'-GGAGTGTGCTTAGAGGTGC-3', 5'-TC-CAGAAAGCCAAGAGAAGC-3', 327); neurofilament-H (NF-H) (5'-TGAACAGCTCCGAGAGTACCA-3', 5'-CTTGGCC-TCTTCTTTCACACG-3' 435); GABA (5'-AGGTTGACCGT-GAGAGCTGAAT-3', 5'-TGGGCAGGCATGGGC-3', 68); GFAP (5'-GAGGAGTGGTATCGGTCTAAGTTTG-3', 5'-GC-CGCTCTAGGGACTCGTT-3', 165); MBP (5'-GTGCAGCT-TGTTCCGACTCCG-3', 5'-ATGCTCTCTGGCTCCTTGGC-3' 153); Sox1 (5'-CCTCGGATCTCTGGTCAAGT-3', 5'-TACA-GAGCCGGCAGTCATAC-3', 593); Pax5 (5'-CAGATGTA-GTCCGCCAAAGGATAG-3', 5'-ATGCCACTGATGGAGTA-TGAGGAGCC-3', 451); Otx2 (5'-CCATGACCTATACTCA-GGCTTCAGG-3', 5'-GAAGCTCCATATCCCTGGGTGGA-AAG-3', 211); GAPDH (5'-ATCAAAGAAGGACTGGCGAG-3', 5'-CCACTCGGTTACTGTAGCCATA-3', 401).

As donor cells, the FACS-sorted Lin⁻CD34⁻ BMCs from eGFP-transgenic mice (purity of eGFP-positive cells >85%) were adjusted to 5×10^4 cells/μl in PBS with 2% FBS for implantation. As recipients, 2- to 3-day-old B6 mice were anesthetized by hypothermia on ice. Finely drawn glass micropipette needles were backfilled with 1 μl of the cell suspension, and the suspension was slowly delivered to the SVZ (1 mm left from the midline, 0 mm anterior to Bregma, and 1.5 mm deep to the dermal surface) using a dissection microscope.

At time points after implantation from 3 days up to 3 weeks, mice to be sacrificed were deeply anesthetized and perfused with PBS via a cardiac catheter, followed by 4% paraformaldehyde. The brains were removed, postfixed, and sliced into 2-mm thick coronal sections with a brain-slicer (MUROMACHI). The sections were embedded in cryo-embedding compound, frozen, and

sectioned at 20 μm thickness. For immunohistochemistry, the Vector M.O.M fluorescein kit was used as described above. After being incubated with primary antibodies: anti-MAC-1 (1:100; No.550282, BD Biosciences Pharmingen), anti-MAP2 (1:100), anti-GFAP (1:400) and anti-CNPase (1:400), sections were incubated with the secondary antibody contained in the kit, and exposed to Texas red avidin D. eGFP-positive cells and Texas red-immunofluorescent cells were examined using confocal microscopy. For quantitative estimation, we randomly selected

six sections of the forebrain from one animal ($n = 4$) for staining the every antibody to estimate the perimeters of the grafted cells.

After RNIF treatment, bipolar and multipolar cells appeared from Day 2 or Day 3, and spindle-shaped, flat cells and cells with two or more long processes were more frequently observed with longer culture periods (Fig. 1A and B). In the control groups, these changes were seldom observed, and a significant proportion of cells died when maintained in base medium for >4 days (Fig. 1C). More than 30% of the cells still survived over

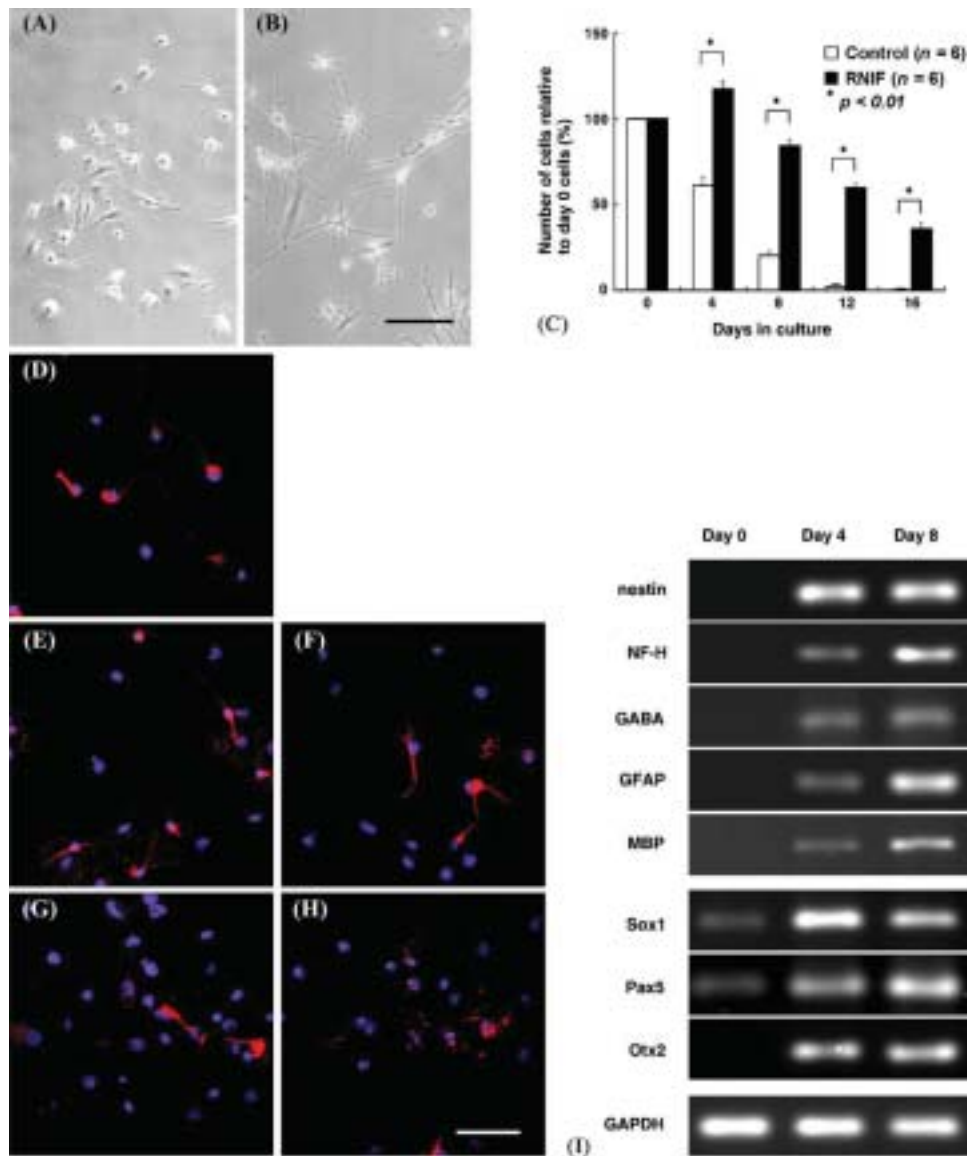


Fig. 1. (A and B) Culture of Lin⁻CD34⁻ BMCs. After RNIF treatment, floating FACS-sorted cells began to attach to the plates and develop into heterogeneous features. On Day 8 (A) and Day 16 (B), extensive outgrowth of cellular processes is noted. Scale bars = 100 μm . (C) Survival and proliferation of Lin⁻CD34⁻ BMCs in culture without (Control) and with RNIF treatment (RNIF). A growth change of cells revealed by enumerating the cells at each time point is shown. Statistical differences were analyzed by Student's two-tailed *t*-test. (D–H) Expression of neural antigens in Lin⁻CD34⁻ BMCs *in vitro*. After RNIF treatment, the cultured cells were incubated with primary antibodies against nestin, TuJ1, MAP2, GFAP and CNPase, followed by incubation with biotin-conjugated secondary antibody and Texas red avidin D (red), and counterstained with DAPI (blue). Nestin-positive cells are detected on Day 8 (D). Data show cells stained positive by anti-TuJ1 (E), MAP2 (F), GFAP (G) and CNPase (H) on Day 16, respectively. Scale bars = 100 μm . (I) RT-PCR analysis of neural markers and neurogenic transcription factors in Lin⁻CD34⁻ BMCs. Transcripts for Nestin, NF-H, GABA, GFAP and MBP are absent in non-stimulated initial Lin⁻CD34⁻ BMCs (Day 0), but the expression was induced by RNIF treatment (Days 4 and 8). Expression of the transcription factors, Sox1 and Pax5, was detected in Lin⁻CD34⁻ BMCs on Day 0, and increased after 4–8 days of RNIF treatment. There was no expression of Otx2 in non-stimulated initial Lin⁻CD34⁻ BMCs, but the expression was induced by RNIF treatment for 4–8 days.

Table 1
Percentage of cells expressing neuronal markers during differentiation in Lin⁻CD34⁻ BMCs

Markers	Day 4 (%)		Day 8 (%)		Day 16 (%)	
	RNIF	Control	RNIF	Control	RNIF	Control
Nestin	15.3 ± 6.2	0	23.2 ± 9.4	0	12.7 ± 6.1	0
TuJ1	1.6 ± 0.8	0	13.9 ± 6	0	17 ± 7.6	0
MAP2	0	0	2.4 ± 1.1	0	7.9 ± 3.6	0
GFAP	0	0	1.2 ± 0.6	0	3.3 ± 1.3	0
CNPase	0	0	1 ± 0.7	0	2.7 ± 1.7	0

Lin⁻CD34⁻ BMCs were grown in base medium with RNIF treatment (RNIF) or without RNIF treatment (Control), and processed for immunocytochemistry, after 4–16 days. Results shown are mean ± S.E.M. from six independent experiments ($n=6$).

16 days in the RNIF treatment groups (Fig. 1C). Although no expression of neural antigens was detected in the fresh FACS-sorted Lin⁻CD34⁻ BMCs (data not shown), the expression was induced by RNIF treatment. Data showed that cells expressed nestin (a specific marker for neural stem cells), as well as TuJ1 (neuron-specific classIII beta-tubulin; a specific marker for immature neurons), after 4 days of RNIF treatment (Table 1). On Day 8, 23.2 ± 9.4% of the cells expressed nestin (Fig. 1D), and 13.9 ± 6% for TuJ1. Furthermore, the cells could be labeled by MAP2 (a specific marker for mature neurons), as well as an astrocytic marker GFAP, and a specific marker for oligodendrocytes, CNPase. After 16 days of RNIF treatment, 12.7 ± 6.1% of the cells still stained positive for nestin, and 17 ± 7.6% for TuJ1 (Fig. 1E). In addition, on Day 16, 7.9 ± 3.6% of the cells tested positive for MAP2 (Fig. 1F), 3.3 ± 1.3% for GFAP (Fig. 1G), and 2.7 ± 1.7% for CNPase (Fig. 1H). On Day 4, day 8 and Day 16, we also evaluated the expression of these neural-specific markers in the control groups, but we could not find any positive expression at every time point (Table 1).

By RT-PCR, the expression of nestin, neurofilament-H (a specific marker for mature neurons), GABA (gamma-aminobutyric acid, a specific marker for GABA-ergic neurons), GFAP and MBP (myelin basic protein; a specific marker for oligodendrocytes) was detected on Day 4 and Day 8 after RNIF treatment (Fig. 1I). In addition, we found expression of transcription factors, Sox1 and Pax5, in the primary Lin⁻CD34⁻ BMCs (Day 0) by RT-PCR, and the expression increased on Day 4 and Day 8 after RNIF treatment (Fig. 1I). RNIF treatment also induced expression of transcription factor Otx2 (Fig. 1I). We isolated total mRNA from the cells in the control groups on Days 4 and 8, but no expression of these markers and transcription factors was detected at either time point (data not shown).

To evaluate the neural differentiation potential of Lin⁻CD34⁻ BMCs *in vivo*, implanted mice were followed up for 3 weeks. Three days after implantation, the majority of the eGFP-positive cells were located at the site of the injection, though some cells had begun to migrate to the corpus callosum (CC), cortex (CTx) and caudate putamen (CPu) (Fig. 2A). Three weeks after grafting, some eGFP-positive cells were observed at the site of the injection, and the cells were also localized in the caudate putamen, corpus callosum, subcortical white matter and cortex (Fig. 2B and C). The majority of the eGFP-positive cells were found in the section layers near the injection site, and few cells could be detected in

the opposite cerebral hemisphere. Morphologically, these cells were heterogeneous: some grafted cells were characterized by a small, nonprocess-bearing morphology, and the remainder were erose with short or longer processes (Fig. 2D). By immunohistochemistry, 34.2 ± 6.6% of the eGFP-positive cells expressed Mac-1 (a microglial marker; Fig. 2E and Table 2). Additionally, a small percentage (1.3 ± 0.5%) of the grafted cells were immunopositive for MAP2 (Fig. 2F), 3.8 ± 0.7% for GFAP (Fig. 2G), and 2.5 ± 0.7% for CNPase (Fig. 2H).

In the present study, we isolated Lin⁻CD34⁻ cells from adult mouse bone marrow, and evaluated the neural differentiation potential of these cells *in vitro* and *in vivo*.

After exposure to RNIF *in vitro*, markers specific for neural stem cells, neurons and glial cells were identified by immunocytochemistry and RT-PCR. We also cultured Lin⁻CD34⁻ BMCs in base medium without RNIF. In the no-RNIF treatment groups, no markers specific for neural cells were identified, and a significant proportion of cells could not survive in base medium. Therefore, it seems reasonable that RNIF played an important role not only in promoting the neural differentiation of Lin⁻CD34⁻ BMCs but also in maintaining the self-renewal or survival ability of these cells. Notably, after RNIF treatment, the expression of nestin was detected from Day 4, and remained strong even until Day 16. It seems that RNIF treatment could not induce all Lin⁻CD34⁻ cells toward the neurogenic differentiation pathway to become mature neurons or glial cells; mixed populations, such as neural stem cells, neuron-like cells, glia-like cells and other BMCs, coexist in the culture. We also demonstrated the

Table 2
Lin⁻CD34⁻ BMCs implanted in postnatal mouse brains express microglial and neural antigens

Markers	No. of eGFP-positive cells	No. of marker-positive cells	Percentage of positive cells (%)
Mac-1	278.8 ± 63.2	100.6 ± 30.5	34.2 ± 6.6
MAP2	265 ± 60.6	3.3 ± 1.7	1.3 ± 0.5
GFAP	331.5 ± 106.8	12.5 ± 4.3	3.8 ± 0.7
CNPase	296 ± 73.7	7.3 ± 2.5	2.5 ± 0.7

Three weeks after implanting eGFP-positive Lin⁻CD34⁻ BMCs into the postnatal mouse SVZ, every sixth section of the forebrain was analyzed per animal ($n=4$). A total of 24 sections were inspected for each marker. The average numbers of the eGFP-positive cells, cells positive for each marker, and the percentages of the number of marker-positive cells among the total eGFP-positive cells are shown (mean ± S.E.M.).

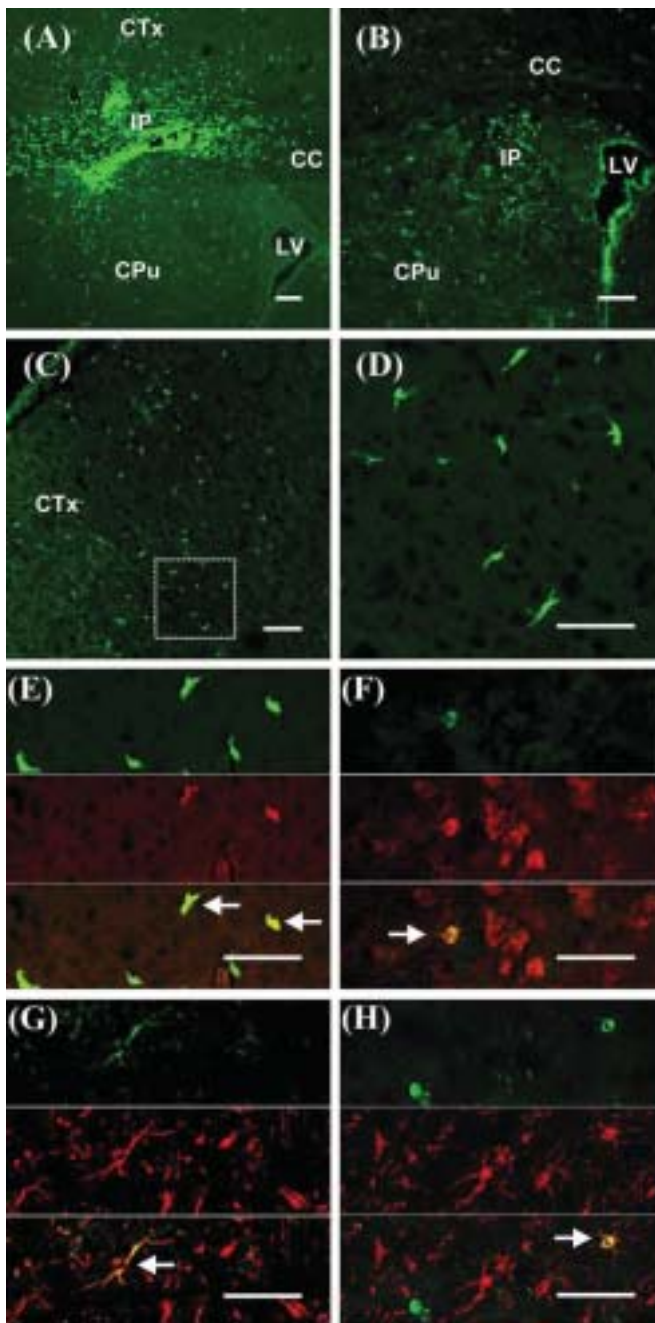


Fig. 2. $\text{Lin}^- \text{CD34}^-$ BMCs survive in the postnatal mouse brain. (A) The eGFP-positive grafted cells (green) reside at the injection point (IP), and begin to migrate into the corpus callosum (CC), the cortex (CTx) and the caudate putamen (CPU), 3 days after implantation. LV, the lateral ventricles. Scale bars = 200 μm . (B and C) The grafted cells (green) reside at the IP, CC, CPU and CTx, 3 weeks after implantation. Scale bars = 200 μm . (D) Higher magnification of box in (C), showing a variety of the grafted cells' morphologies. Scale bars = 100 μm . (E–H) eGFP expression of the grafted cells (green) colocalizes with immunostaining with primary antibodies against microglial and neural-specific proteins, followed by incubation with biotin-conjugated secondary antibody and Texas red avidin D (red). The grafted cells (green) are positive for MAC-1 (E), MAP2 (F), GFAP (G), CNPase (H). Scale bars = 100 μm .

expression of several neurogenic transcription factors, including Sox1 [22], Pax5 [14] and Otx2 [20]. These transcription factors are known to be expressed in the early stages of neuroectoderm development and regulate neural differentiation of stem cells. In the present study, these transcription factors seem to play central roles in the process of induction and differentiation.

By implanting cells into the SVZ of postnatal brains, we demonstrated that $\text{Lin}^- \text{CD34}^-$ BMCs were able to migrate from the site of injection into the various brain regions, and some grafted cells expressed marker-specific antigens for microglia and neural cells. The acquisition of microglial phenotypes by grafted $\text{Lin}^- \text{CD34}^-$ BMCs clearly occurred in our implantation experiments. This would underscore the close relationship between microglia and HSCs [6]. Several studies indicate that bone marrow-derived stem cells can differentiate into neural cells after injection into the brain [13,4]. In the present study, we also observed a small number of grafted cells expressing the neuron-, the astrocyte-, and the oligodendrocyte-specific markers. Although these grafted cells do have an antigenic profile consistent with neurons or glial cells, suggesting that $\text{Lin}^- \text{CD34}^-$ BMCs can differentiate into the neural lineage cells under certain environmental influences such as the SVZ of postnatal brains, their morphologies are ambiguous and they do not resemble typical *in vivo* neurons or glial cells. In addition, morphological, electrophysiological and functional data are required to definitively prove these neural differentiations.

Our results indicate that the CD34^- populations of adult bone marrow, which possibly contain pluripotent stem cells or the stem cells bearing plasticity, can adopt characteristics of neural cells. Fusion is a possible contributing factor of "trans-differentiation" [21]. However, our *in vitro* data indicate that neural phenotypes are acquired without coculture with brain-derived cells. Moreover, different research groups have shown that stem cells from bone marrow do not fuse with cells of host tissues [10], and that fusion is not a contributing factor to the neural differentiation of implanted donor cells [19,4]. We presume that the majority of the large number of donor-labeled neural cells is a product of trans-differentiation.

Experiments using bone marrow cells from both mice and humans suggest that the most primitive progenitors might lack CD34 and are capable of generating CD34^+ stem cells [7]. Moreover, it has been reported that the majority of HSCs are CD34^- in adult mice [9]. This work has focused on the neural differentiation aspects of these $\text{Lin}^- \text{CD34}^-$ BMCs in adult mice. If similar phenomena can be found in humans, CD34^- cells from a patient's own bone marrow would also be an ideal source for therapeutic cell replacement in diseases or injury of the brain and spinal cord, by obviating the problems of immunohistocompatibility and pathogen transfer from donor to host.

Acknowledgments

We thank Ms. Miura and Ms. Tokuyama for their expert technical assistance. We also thank Mr. Hilary Eastwick-Field and Ms. Ando for the preparation of this manuscript.

References

- [1] R.J. Berenson, R.G. Andrews, W.I. Bensinger, D. Kalamasz, G. Knitter, C.D. Buckner, I.D. Bernstein, Antigen CD34⁺ marrow cells engraft lethally irradiated baboons, *J. Clin. Invest.* 81 (1988) 951–955.
- [2] M.A. Caldwell, X. He, N. Wilkie, S. Pollack, G. Marshall, K.A. Waford, C.N. Svendsen, Growth factors regulate the survival and fate of cells derived from human neurospheres, *Nat. Biotechnol.* 19 (2001) 475–479.
- [3] F. Ciccolini, C.N. Svendsen, Fibroblast growth factor 2 (FGF-2) promotes acquisition of epidermal growth factor (EGF) responsiveness in mouse striatal precursor cells: identification of neural precursors responding to both EGF and FGF-2, *J. Neurosci.* 18 (1998) 7869–7880.
- [4] J. Deng, B.E. Petersen, D.A. Steindler, M.L. Jorgensen, E.D. Laywell, Mesenchymal stem cells spontaneously express neural proteins in culture and are neurogenic after transplantation, *Stem Cells* 24 (2006) 1054–1064.
- [5] D.S. Donnelly, D. Zelterman, S. Sharkis, D.S. Krause, Functional activity of murine CD34⁺ and CD34⁻ hematopoietic stem cell populations, *Exp. Hematol.* 27 (1999) 788–796.
- [6] M.A. Eglitis, E. Mezey, Hematopoietic cells differentiate into both microglia and macroglia in the brains of adult mice, *Proc. Natl. Acad. Sci. U.S.A.* 94 (1997) 4080–4085.
- [7] M.A. Goodell, M. Rosenzweig, H. Kim, D.F. Marks, M. DeMaria, G. Paradis, S.A. Grupp, C.A. Sieff, R.C. Mulligan, R.P. Johnson, Dye efflux studies suggest that hematopoietic stem cells expressing low or undetectable levels of CD34 antigen exist in multiple species, *Nat. Med.* 3 (1997) 1337–1345.
- [8] P.D. Henion, J.A. Weston, Retinoic acid selectively promotes the survival and proliferation of neurogenic precursors in cultured neural crest cell populations, *Dev. Biol.* 161 (1994) 243–250.
- [9] T. Ito, F. Tajima, M. Ogawa, Developmental changes of CD34 expression by murine hematopoietic stem cells, *Exp. Hematol.* 28 (2000) 1269–1273.
- [10] Y.Y. Jang, M.I. Collector, S.B. Baylin, A.M. Diehl, S.J. Sharkis, Hematopoietic stem cells convert into liver cells within days without fusion, *Nat. Cell Biol.* 6 (2004) 532–539.
- [11] Y. Jiang, D. Henderson, M. Blackstad, A. Chen, R.F. Miller, C.M. Verfaillie, Neuroectodermal differentiation from mouse multipotent adult progenitor cells, *Proc. Natl. Acad. Sci. U.S.A.* (2003) 11854–11860.
- [12] T. Kondo, S.A. Johnson, M.C. Yoder, R. Romand, E. Hashino, Sonic hedgehog and retinoic acid synergistically promote sensory fate specification from bone marrow-derived pluripotent stem cells, *Proc. Natl. Acad. Sci. U.S.A.* 102 (2005) 4789–4794.
- [13] G.C. Kopen, D.J. Prockop, D.G. Phinney, Marrow stromal cells migrate throughout forebrain and cerebellum, and they differentiate into astrocytes after injection into neonatal mouse brains, *Proc. Natl. Acad. Sci. U.S.A.* 96 (1999) 10711–10716.
- [14] S.H. Lee, N. Lumelsky, L. Studer, J.M. Auerbach, R.D. McKay, Efficient generation of midbrain and hindbrain neurons from mouse embryonic stem cells, *Nat. Biotechnol.* 18 (2000) 675–679.
- [15] H. Nakauchi, H. Takano, H. Ema, M. Osawa, Further characterization of CD34-low/negative mouse hematopoietic stem cells, *Ann. N.Y. Acad. Sci.* 872 (1999) 57–66.
- [16] T. Nakayama, T. Momoki-Soga, K. Yamaguchi, N. Inoue, Efficient production of neural stem cells and neurons from embryonic stem cells, *Neuroreport* 15 (2004) 487–491.
- [17] T.D. Palmer, E.A. Markakis, A.R. Willhoite, F. Safar, F.H. Gage, Fibroblast growth factor-2 activates a latent neurogenic program in neural stem cells from diverse regions of the adult CNS, *J. Neurosci.* 19 (1999) 8487–8497.
- [18] M. Schuldiner, R. Eiges, A. Eden, O. Yanuka, J. Itskovitz-Eldor, R.S. Goldstein, N. Benvenisty, Induced neuronal differentiation of human embryonic stem cells, *Brain Res.* 913 (2001) 201–205.
- [19] O.E. Sigurjonsson, M.C. Perreault, T. Egeland, J.C. Glover, Adult human hematopoietic stem cells produce neurons efficiently in the regenerating chicken embryo spinal cord, *Proc. Natl. Acad. Sci. U.S.A.* 102 (2005) 5227–5232.
- [20] A. Simeone, Otx1 and Otx2 in the development and evolution of the mammalian brain, *EMBO J.* 17 (1998) 6790–6798.
- [21] N. Terada, T. Hamazaki, M. Oka, M. Hoki, D.M. Mastalerz, Y. Nakano, E.M. Meyer, L. Morel, B.E. Petersen, E.W. Scott, Bone marrow cells adopt the phenotype of other cells by spontaneous cell fusion, *Nature* 416 (2002) 542–545.
- [22] H.B. Wood, V. Episkopou, Comparative expression of the mouse Sox1, Sox2 and Sox3 genes from pre-gastrulation to early somite stages, *Mech. Dev.* 86 (1999) 197–201.
- [23] H. Yang, T. Mujtaba, G. Venkatraman, Y.Y. Wu, M.S. Rao, M.B. Luskin, Region-specific differentiation of neural tube-derived neuronal restricted progenitor cells after heterotopic transplantation, *Proc. Natl. Acad. Sci. U.S.A.* 97 (2000) 13366–13371.
- [24] T. Zigova, S. Song, A.E. Willing, J.E. Hudson, M.B. Newman, S. Saporta, J. Sanchez-Ramos, P.R. Sanberg, Human umbilical cord blood cells express neural antigens after transplantation into the developing rat brain, *Cell Transplant.* 11 (2002) 265–274.

研究成果報告書

研究課題名	灌流式骨髄細胞採取法により採取した新鮮全骨髄細胞骨髄細胞を用いた椎間板再生の検討		
(英文)	Regeneration of degenerated intervertebral disc using whole bone marrow cells collected by the perfusion method		
事業推進者	飯田 寛和	E-mail	iida@takii.kmu.ac.jp
所属・職名	医学研究科・骨・軟骨再生治療学（整形外科）講座・教授		
研究分担者名	串田 剛俊、梅田 眞志、笹井 邦彦、浅田 卓、おおえ 賢一、岡本 尚史		
キーワード	椎間板、再生、骨髄細胞、腰痛		

1. 概要

灌流式骨髄細胞採取法により採取した新鮮全骨髄細胞骨髄細胞を用い、さまざまな臨床症状を引き起こす変性した椎間板の治療を目指す。

2. 研究の背景と目的

近年、変性椎間板に対する治療として、動物モデルで椎間板内への遺伝導入やサイトカイン治療が報告され、良好な結果を示している。しかし、長期的な安全性については不明な点が多い。また、自己細胞移植では、椎間板細胞や間葉系幹細胞が使われており、椎間板の機能や構造の改善において良好な結果を得ている。しかし、椎間板細胞や間葉系幹細胞は体外で培養するため、専用設備の整備が必要となり、実施施設に限られる。

従来方法である吸引法で採取した新鮮全骨髄細胞の使用は、末梢リンパ球や赤血球が混入するため、特に椎間板内への使用を考えると、末梢血が再生の阻害因子となる可能性があり、その使用は困難であった。今回、末梢血の混入を防ぐことが可能な灌流式骨髄細胞採取法により採取した新鮮全骨髄細胞用い、変性した椎間板の再生を目的とする。

3. 研究方法

< *in vitro* >

Fisher344/slc ラット雄の尾椎より採取した。骨髄細胞は、灌流法と吸引法の2種類で採取した。骨髄細胞による椎間板細胞の活性化を評価した。

- (i) 椎間板髓核細胞の単独培養；単培養群、
- (ii) 椎間板髓核細胞と間葉系幹細胞との共培養；間葉系幹細胞群、
- (iii) 椎間板髓核細胞と新鮮全骨髄細胞との共培養；全骨髄細胞群とした。

さらに、全骨髄細胞群を、2グループに細分化

- (i) 灌流法により採取した新鮮全骨髄細胞と椎間板髓核細胞との共培養；PF群、
- (ii) 吸引法により採取した新鮮全骨髄細胞と椎間板髓核細胞との共培養；AS群とした。

① 細胞増殖能は、培養2週後の椎間板髓核細胞の増殖数と $[^3\text{H}]$ -thymidine の uptake、cell cycle の G1 phase の測定で評価した。

② 細胞外器質の合成能は、RT-PCR のアグリカンの発現と3次元培養下における $[^{35}\text{S}]$ -sulfate

の uptake を評価した。

- ③ 増殖因子の評価として、TGF- β を培養 2 日後に測定した。

< *in vivo* >

日本白色家兎を使用した。変性椎間板は 22G 注射針を挿入し数回吸引を行うことにより作成した。変性椎間板作成後、灌流法により採取した新鮮骨髄細胞を椎間板に移植した。

- ① X線で椎体、椎間を計測し、disc height index を算出した。
② MRI の 2 強調像で、T2 signal intensity index を算出した。

4. これまでの成果

< *in vitro* >

- ① 培養後 14 日目の椎間板髄核細胞の増殖数、 $[^3\text{H}]$ -thymidine の uptake、cell cycle のいずれにおいても、全骨髄細胞群 (PF 群と AS 群) は、単培養群と間葉系幹細胞群に比べて有意に活性化していた。
② RT-PCR のアグリカンの発現と $[^{35}\text{S}]$ -sulfate の uptake はどちらも、全骨髄細胞群 (PF 群と AS 群) が、単培養群と間葉系幹細胞群に比べて有意に活性化していた。
③ 培養 2 日後の TGF- β 分泌量は、全骨髄細胞群 (PF 群と AS 群) が、単培養群と間葉系幹細胞群に比べて有意に活性化していた。
①から③の測定について、AS 群と PF 群には有意差を認めなかった。

< *in vivo* >

未治療群に比べ、治療群で有意に disc height index が保たれていた。

未治療群に比べ、治療群で有意に T2 signal intensity index が保たれていた。

5. これまでの進捗状況と今後の計画

in vitro の実験において、培養された間葉系幹細胞に比べ、新鮮全骨髄細胞を用いることにより椎間板髄核細胞の高い活性化が得られた。*in vivo* の実験において、灌流法を用いた新鮮全骨髄細胞の変性椎間板に対する移植で、治療効果が得られた。今後、培養された間葉系幹細胞の移植との比較や、安全性に対する基礎研究を推進する。

6. これまでの発表論文

(1) 発表論文

1) 原著論文

Umeda, M., Kushida, T., Sasai, K., Asada, T., Oe, K., Sakai, D., Mochida, J., Ikehara, S. & Iida, H.

Activation of rat nucleus pulposus cells by co-culture with whole bone marrow cells collected by the perfusion method.

J. Orthop. Res. in press (2008).

(2) 学会発表

国際学会

3) 一般発表

Umeda, M., Kushida., Sasai, K., Asada, T., & Iida, H.

Activation of nucleus pulposus cells by co-culturing with whole bone marrow cells collected by perfusion method in rats.

World Forum for Spine Research—The intervertebral Disc, Kyoto, 2007.

国内学会

3) 一般発表

1. 梅田 眞志、串田 剛俊、笹井 邦彦、飯田 寛和

ラット椎間板髄核細胞の新鮮全骨髄細胞との共培養下における活性化の検討

第 37 回日本脊椎脊髄病学会、東京、2008.

2. 梅田 眞志、串田 剛俊、浅田 卓、笹井 邦彦、飯田 寛和

Analyses of the viability of nucleus pulposus cells co-cultured by bone marrow cells using perfusion method

第 20 回日本軟骨代謝学会、岡山、2007.

3. 梅田 眞志、串田剛俊、笹井邦彦、上田祐輔、浅田卓、飯田寛和

全骨髄細胞を用いた、ラット椎間板髄核細胞の活性化の検討

第 109 回中部日本整形外科災害外科学会、奈良、2007.

7. これまでの成果の情報公開

ホームページ：整形外科科学講座=<http://www3.kmu.ac.jp/orth/>

Activation of Rat Nucleus Pulposus Cells by Coculture with Whole Bone Marrow Cells Collected by the Perfusion Method

Masayuki Umeda,¹ Taketoshi Kushida,¹ Kunihiro Sasai,¹ Taku Asada,¹ Kenichi Oe,¹ Daisuke Sakai,³ Joji Mochida,³ Susumu Ikehara,² Hirokazu Iida¹

¹Department of Orthopedic Surgery, Kansai Medical University, 10-15 Fumizono-cho, Moriguchi-City, Osaka 570-8506, Japan, ²First Department of Pathology, Kansai Medical University, Osaka, Japan, ³Department of Orthopaedic Surgery, Surgical Science and Center for Regenerative Medicine, Tokai University School of Medicine, Shimokasuya 143, Isehara, Kanagawa, 259-1143, Japan

Received 1 November 2007; accepted 9 June 2008

Published online in Wiley InterScience (www.interscience.wiley.com). DOI 10.1002/jor.20740

ABSTRACT: Cell proliferation and matrix synthesis were compared for rat nucleus pulposus cells cocultured with mesenchymal stem cells (MSCs) or fresh whole bone marrow cells (BMCs), harvested by the perfusion or aspiration methods. Nucleus pulposus cells were isolated from tail intervertebral discs of F344/slc rats, and BMCs were obtained from femora. Proteoglycan synthesis, DNA synthesis, and aggrecan mRNA expression were measured. The level of transforming growth factor- β in supernatants from the culture system was also measured. Cell number, aggrecan mRNA expression, and uptake of [³⁵S]-sulfate and [³H]-thymidine by nucleus pulposus cells cocultured with fresh whole BMCs all increased significantly compared with nucleus pulposus cells cocultured with MSCs. TGF- β secreted by nucleus pulposus cells cocultured with fresh whole BMCs also significantly increased when compared with cocultures with MSCs. The perfusion method was superior to the aspiration method for preventing contamination of BMCs with peripheral red blood cells and lymphocytes, which may cause an autoimmune response in the disc. In conclusion, we suggest that fresh whole BMCs harvested by the perfusion method are more effective for increasing the proliferative and matrix synthesis capacity of nucleus pulposus cells. © 2008 Orthopaedic Research Society. Published by Wiley Periodicals, Inc. *J Orthop Res* 0:1–7, 2008

Keywords: nucleus pulposus cells; mesenchymal stem cells; bone marrow cells; intervertebral disc degeneration; coculture

Progressive degeneration of the intervertebral disc (IVD) causes back pain, sciatica, and other distressing and disabling symptoms.^{1,2} The IVD has a ring of flexible fibrocartilage, the annulus fibrosus (AF), which surrounds the soft center, the nucleus pulposus (NP). Nucleus pulposus cells (NPCs) primarily produce aggrecan, together with other proteoglycans, and type II collagen and other collagens.^{3–5} Decreased production of aggrecan and type II collagen by NPCs compromises the disc's structure. Approaches for increasing the proliferative capacity and matrix synthesis of NPCs include gene therapy with transforming growth factor- β (TGF- β)⁶ or Sox9⁷ transferred into the IVD. Growth factor induction therapies include injection of TGF- β ,^{8,9} insulin-like growth factor (IGF),^{8,9} growth differentiation factor-5 (GDF-5),^{9,10} and osteogenic protein-1 (OP-1).¹¹

To apply these methods clinically, safety and ethical issues must be resolved. New techniques using autologous materials are required to increase the capacity of NPCs to proliferate and synthesize matrix. These capacities (in the notochordal disc cell phenotype) are better maintained by using a coculture system with AF cells; reinsertion of such stimulated NPCs into the degenerative disc in a rabbit model was beneficial.¹² Other investigators found that cell proliferation and matrix synthesis by rabbit NPCs were significantly increased when NPCs were grown in a novel coculture system allowing cell-to-cell contact with autologous bone marrow-derived stromal cells (mesenchymal cells).¹³ Richardson et al.¹⁴ reported that coculture of human

NPCs (mature nucleus cell phenotype) with mesenchymal stem cells (MSCs) caused MSC differentiation into a NP-like phenotype only if cells had cell-to-cell contact. Sakai et al.¹⁵ reported that the transplantation of cultured MSCs effectively led to regeneration in a rabbit model of disc degeneration. However, whether the proliferating NPCs were permanently maintained in vivo in the absence of such stimulators remains unclear.

TGF- β , an important cytokine affecting NPC proliferation, is secreted by NPCs themselves. TGF- β can also be secreted by hematopoietic stem cells (HSCs) and MSCs.^{16,17} Therefore, we suggest that MSCs and HSCs are necessary for continuous NPC proliferation. Peripheral lymphocytes mediate autoimmune responses in the disc.^{18–21} Therefore, injection of fresh whole bone marrow cells (BMCs) contaminated with peripheral lymphocytes presents a potential problem for treatment. Recently, a new method of obtaining BMCs, the perfusion (PF) method, was developed; briefly, bone marrow fluid from long bones or the ilium is flushed out using saline.^{22,23} This PF method proved to be better for prevention of peripheral blood contamination than the conventional aspiration (AS) method.

In this study, we compared the proliferative capacity and matrix synthesis in cultures of rat NPCs (notochordal disc cell phenotype) cocultured with MSCs or fresh whole BMCs. We also compared the proliferative and matrix synthesis capacities of the same type of NPCs cocultured with fresh whole BMCs harvested by the PF or AS method.

MATERIALS AND METHODS

The animal research protocol was approved in accordance with the Guidelines for Animal Experimentation, Kansai Medical University. Fischer 344 (F344/slc) rats at 12–13 weeks of age

Correspondence to: Taketoshi Kushida (T: +81-6-6992-1001, ext. 3292 or 3294; F: +81-6-6993-7773; E-mail: kushidat@takii.kmu.ac.jp)

© 2008 Orthopaedic Research Society. Published by Wiley Periodicals, Inc.

were purchased from SLC (Shizuoka, Japan) and maintained until use in our animal facilities under specific pathogen-free conditions.

Rat tails were removed under aseptic conditions. Each disc was cut transversely, and the gel-like NP was separated from the disc. To release NPCs, the NP was treated with 0.01% trypsin (Invitrogen Corp., Grand Island, NY) at 37°C for 12 min. These isolated cells were washed three times with DMEM (Invitrogen) before collection by centrifugation at 1500 rpm. Cells were maintained in DMEM with 10% fetal bovine serum (FBS) (Invitrogen) supplemented with antibiotics in a humidified atmosphere with 5% CO₂ at 37°C for 12 h. Nonadherent cells were discarded and adherent cells were released by treatment with trypsin for use in this study.

BMCs were obtained from femora by the PF method.^{22,23} Two 18-gauge needles were inserted into the femur (Fig. 1A). One needle was connected to a syringe containing 5 mL of DMEM, which was injected into the medullary cavity to flush out the bone marrow. The medium containing the bone marrow fluid was collected in the other syringe. The AS method was performed by inserting an 18-gauge needle into the distal femur and aspirating BMCs from the medullary cavity. MSCs were cultured as previously described.^{14,15} In brief, BMCs obtained

by the AS method were cultured in DMEM with 10% FBS and antibiotics in a humidified 5% CO₂ atmosphere at 37°C for 2 weeks. Nonadherent cells were discarded.

NPCs (5 × 10⁴) and BMCs (5 × 10⁴) were cocultured in six-well plates with cell culture inserts with 0.4 μm pores at the bottom (Becton-Dickinson, Franklin Lakes, NJ). Cultures were fed with DMEM with 10% FBS and antibiotics and were maintained in 5% CO₂ at 37°C for 2 weeks. The NPCs and BMCs were separated by a cell culture insert; no cell-to-cell contact could occur.

Four protocols were established (Fig. 1): (1) NPCs were monocultured for 2 weeks; (2) NPCs were cocultured for 2 weeks with fresh whole BMCs obtained by the PF method; (3) NPCs were cocultured for 2 weeks with fresh whole BMCs obtained by the AS method and (4) NPCs were cocultured with MSCs for 2 weeks (NPCs + MSCs).

Analyses of Red Blood Cell/White Blood Cell (RBC/WBC) Ratios

To quantify the number of RBCs in the peripheral blood and to assess contamination of fluid isolated by the PF and AS methods, we counted the numbers of RBCs and WBCs to calculate a RBC/WBC ratio.

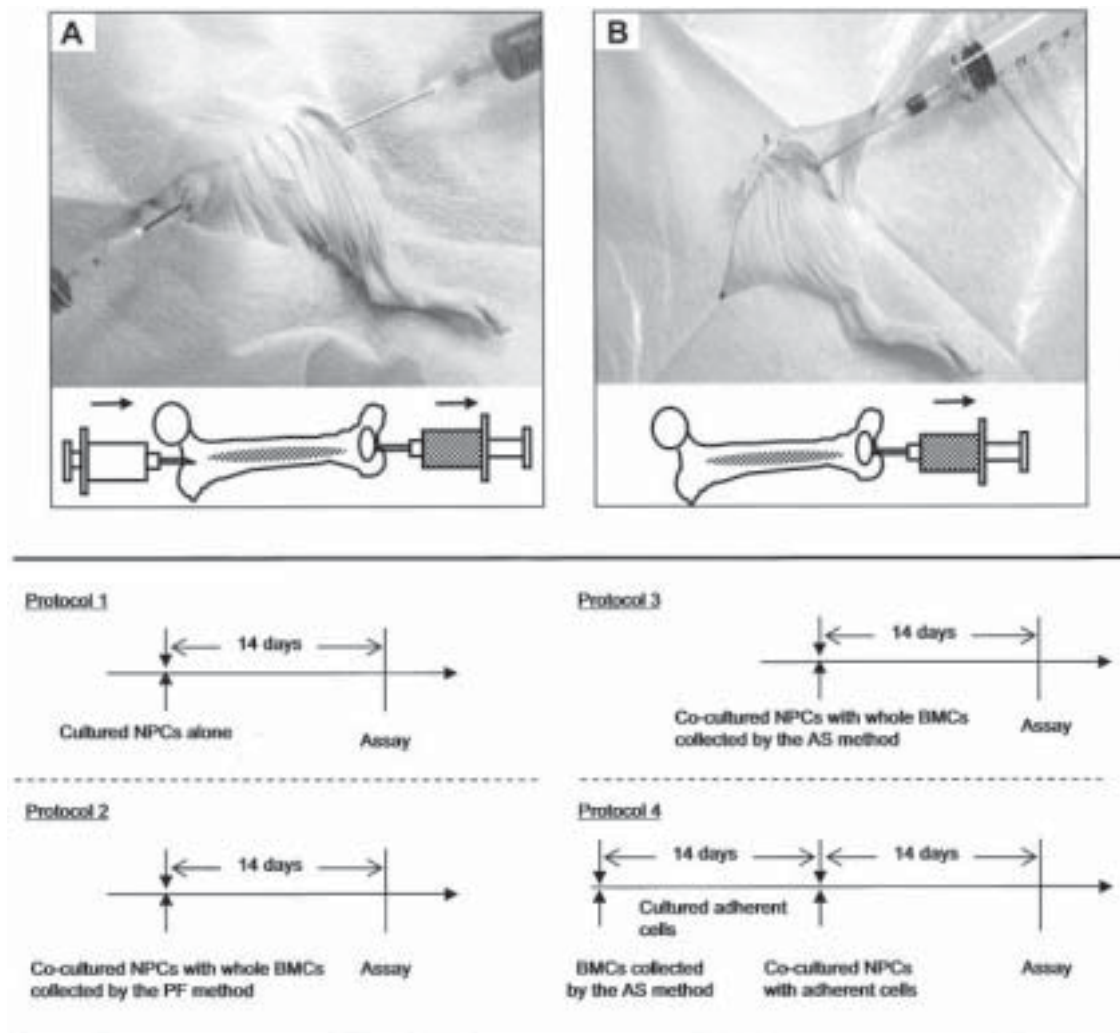


Figure 1. BMCs were obtained from femora by the PF (A) or AS method (B). The four experimental groups (bottom) were: (1) nucleus pulposus cells (NPCs) alone, (2) NPCs + BMCs by PF, (3) NPCs + BMCs by AS, and (4) NPCs + mesenchymal stem cells (MSCs).

Analyses of CD4⁺ and CD8⁺ T Cells

To measure percentages of CD4⁺ and CD8⁺ T cells in the peripheral blood mononuclear cells (PBMNCs) fraction and in BMCs isolated by the PF and AS methods, cells were stained with fluorescein isothiocyanate-conjugated anti-CD4 and phycoerythrin-conjugated anti-CD8 mAbs (PharMingen, San Diego, CA). The stained cells were analyzed by FACScan (Becton-Dickinson).

Measurement of Cell Number

The number of live NPCs was determined using a Cell Counting Kit-8 (CCK-8; Dojindo Molecular Technology, Kumamoto, Japan).¹⁴ This kit counts live cell numbers using 2-(2-methoxy-4-nitrophenyl)-3-(4-nitrophenyl)-5-(2,4-disulfo-phenyl)-2H-tetrazolium (WST-8). Adherent NPCs, regardless of the cell cycle stage, were harvested using 0.05% trypsin. The wells of a 96-well plate (Becton-Dickinson) containing NPCs from all four groups were inoculated with 10 μ L of prepackaged CCK-8 solution. The plate was incubated at 37°C in 5% CO₂ for 2 h. Absorbance was measured at OD 450 nm. Cell counts were determined using a calibration curve.

Quantification of Cytokines

The TGF- β ₁ amount in cell-free supernatants from the four groups was quantified using an enzyme-linked immunosorbent assay (ELISA) kit (BioSource Intl., Inc., Camarillo, CA) according to the manufacturer's protocol. Supernatants from wells cultured for 2 days were collected, and concentrations were measured by absorbance at OD 450 nm.

Cell Cycle Analyses

To evaluate activation of NPCs, we analyzed cell cycle stage using flow cytometry. Cells were treated with propidium iodide (PI; Sigma-Aldrich Co., St. Louis, MO) and ribonuclease A (RNase; Sigma-Aldrich). The stained cells were then analyzed using a FACScan.

Reverse Transcription–Polymerase Chain Reaction (RT-PCR)

Levels of mRNA for NP phenotypic markers were determined using the sequences of primers for GAPDH, type II collagen²⁴ and aggrecan²⁵ (Nisshinbo, Inc., Chiba, Japan). The sequences were: GAPDH, 5'-AGAATCATCCCTGCATCC-3' and 5'-TTACTCCTTGGAGGCCATGT-3'; type II collagen, 5'-CAAGTCGCTGAACAACCAGA-3' and 5'-GCCCTCATCTCCACATCATT-3'; aggrecan, 5'-CACAGGCAGCACAGACACTT-3' and 5'-CCC-ACCTTCTACAGGCAAGC-3'. GAPDH mRNA was amplified with a pair of primers at 94°C for 1 min, 57°C for 1 min, 72°C for 1 min \times 30 cycles, and a final extension at 72°C for 10 min. Aggrecan and type II collagen mRNA were amplified by pairs of primers at 94°C for 1 min, 57°C for 1 min, 72°C for 1 min \times 35 cycles, and a final extension at 72°C for 10 min. PCR products were electrophoresed on a 1% agarose gel (Invitrogen), stained with ethidium bromide (0.5 μ g/mL), and visualized on a UV transilluminator (ATTO, Tokyo).

Measurement of DNA Synthesis

DNA synthesis was assessed by measuring [³H]-thymidine uptake (Perkin Elmer, Inc., Waltham, MA). Cultured NPCs were released by 0.05% trypsin and transferred to 96-well culture plates at 5 \times 10⁴ per well. The NPCs were labeled with 18.5 kBq of [³H]-thymidine per well for 2 h, and nuclear incorporation of radioactivity was quantified. Count per minute (CPM) was divided by number of cells.

Measurement of Proteoglycan Synthesis

Incorporation of [³⁵S]-sulfate (American Radiolabeled Chemicals, Inc., Saint Louis, MO) was measured in a 3D culture system using alginate beads. NPCs were harvested with 0.05% trypsin. Collected cells were suspended in a solution of 1.2% low viscosity alginate (Lonza, Walkersville, MD) at 1 million cells/mL. Semisolid spherical beads were formed by expressing the cell suspension through a 23-gauge needle into a CaCl₂ solution (102 mM). Beads were washed three times with 0.9% NaCl and placed into a six-well plate (10 beads per well). The NPCs were labeled with 370 kBq of [³⁵S]-sulfate per well for 16 h. Beads were washed five times with 0.9% NaCl supplemented with 5 mM CaCl₂ and 5 mM Na₂SO₄. The cells were then dissolved in a sodium citrate solution (55 mM in 90 mM NaCl). Trichloroacetic acid (TCA, final concentration = 10%) was added to the cell associated matrix, and the TCA-insoluble product was filtered on glass microfibre filters (Whatman Intl., Maidstone, UK) and washed three times by 5% TCA, then dried by 70% ethanol. The dried material was measured with a liquid scintillation counter (Tri-Carb Liquid Scintillation Analyzer 2700TR; Packard Instruments, Meriden, CT). Disintegrations per minute (DPM) of these result was divided by number of cells.

Statistical Analyses

Analyses were accomplished with Student *t*-tests. Differences were considered significant at *p* < 0.05.

RESULTS

RBC/WBC Ratios and Percentages of T Cells Collected by the PF and AS Methods

The RBC/WBC ratios were >900 in the peripheral blood and >400 in the bone marrow fluid collected by the AS method, but <10 in the bone marrow fluid harvested by the PF method (Fig. 2A). T cells (CD4⁺ and CD8⁺ T cells) were >49% of the PBMNCs and >24% of BMCs harvested by the AS method, while they constituted <7% of BMCs harvested by the PF method (Fig. 2B).

Assessment of Cell Numbers

Cell yields in cultured NPCs from the four groups were: (1) NPCs alone: 0.83 \times 10⁵ cells; NPCs + MSCs: 1.52 \times 10⁵ cells; NPCs + BMCs by PF: 2.14 \times 10⁵; NPCs + BMCs by AS: 2.36 \times 10⁵ cells. The yield from NPCs + BMCs by PF and NPCs + BMCs by AS was significantly increased compared to NPCs + MSCs and NPCs alone.

Measurement of Growth Factors in Culture Supernatants

Significantly more TGF- β ₁ was found in cultures of NPCs + BMCs by PF and NPCs + BMCs by AS compared with NPCs alone or NPCs + MSCs (Fig. 3). Fresh whole BMCs, obtained by either method, stimulated the secretion of TGF- β ₁ to a greater degree than cultured MSCs alone.

Analyses of Cell Cycle Distribution

The percentages of cells in the G₁ phase in cultures of NPCs + BMCs by PF and NPCs + BMCs by AS were significantly decreased compared with NPCs alone and NPCs + MSCs (Fig. 4).

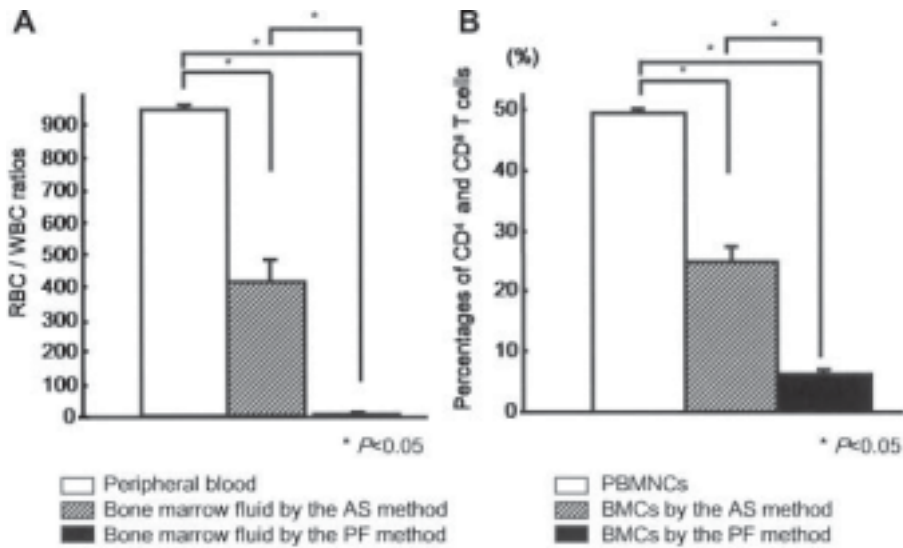


Figure 2. (A) RBC/WBC ratios in peripheral blood and in bone marrow fluid collected by the AS and PF methods. (B) Percentages of CD4⁺ and CD8⁺ T cells in the PBMNCs fraction, AS harvested BMCs, and PF harvested BMCs. Results are mean ± SD of six rats. **p* < 0.05.

Electrophoretic Analyses of RT-PCR Products

Expression of aggrecan mRNA in cultures of NPCs + BMCs by PF and NPCs + BMCs by AS was significantly increased compared with NPCs alone and NPCs + MSCs (Fig. 5). In contrast, no significant differences in levels of type II collagen mRNA were noted between the groups.

Proteoglycan Synthesis

NPCs + BMCs by PF and NPCs + BMCs by AS both showed significantly increased uptake compared with NPCs alone and NPCs + MSCs (Fig. 6A).

DNA Synthesis

Cultures of NPCs + BMCs by PF and NPCs + BMCs by AS showed significantly increased [³H]-thymidine

incorporation compared with NPCs alone and NPCs + MSCs (Fig. 6B).

DISCUSSION

Genetic and environmental factors cause degeneration of the intervertebral disc. A recent report identified genetic risk factors for lumbar disc disease.²⁶ In the pathogenesis of disc degeneration an important role is played by inflammatory cytokines produced by monocytes, macrophages, or disc cells.^{27,28} Notably, levels of tumor necrosis factor- α (TNF- α) and interleukin-1 (IL-1) are greatly increased in the degenerating compared to the normal disc.²⁷ Monocytes and macrophages also cause autoimmune responses in the disc.¹⁸⁻²¹ On the other hand, TGF- β and IGF-1, growth factors secreted by NPCs, maintain cell proliferation and matrix synthesis in the disc^{9,29} and are considered major regulatory cytokines.^{29,30}

Adult human disc cells are thus important in maintaining IVD structure. Cultured MSCs differentiate into NP-like cells under certain microenvironmental conditions similar to those in the intact IVD, for example, when cultured with TGF- β 1 under hypoxic conditions.³¹ Cultured MSCs or AF cells also stimulate increased proliferation of rabbit NPCs in vitro.^{12,13} Autologous cell transplantation therapy using cultured MSCs has been used with the aim of repairing the degenerative disc.^{15,32,33} Because MSCs must be harvested over a few weeks from fresh whole BMCs to accumulate sufficient purified cultured MSCs for transplantation, the need exists to develop an improved coculture system using new materials to stimulate cultured MSCs.

Rat models are widely used in biological investigations, but rat disc cells consist mainly of notochordal cells whose phenotype differs from adult human disc cells.³⁴ In humans, Le Visage et al.³⁵ reported that coculturing disc cells with MSCs enhanced extracellular matrix production. Because ours is a pilot study using whole BMCs harvested by the PF method for delaying or

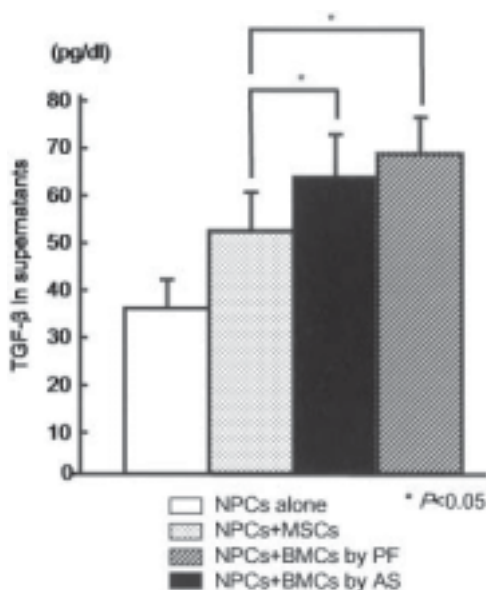


Figure 3. TGF- β 1 in the supernatants from the four experimental groups. Results are mean ± SD of six rats. **p* < 0.05.

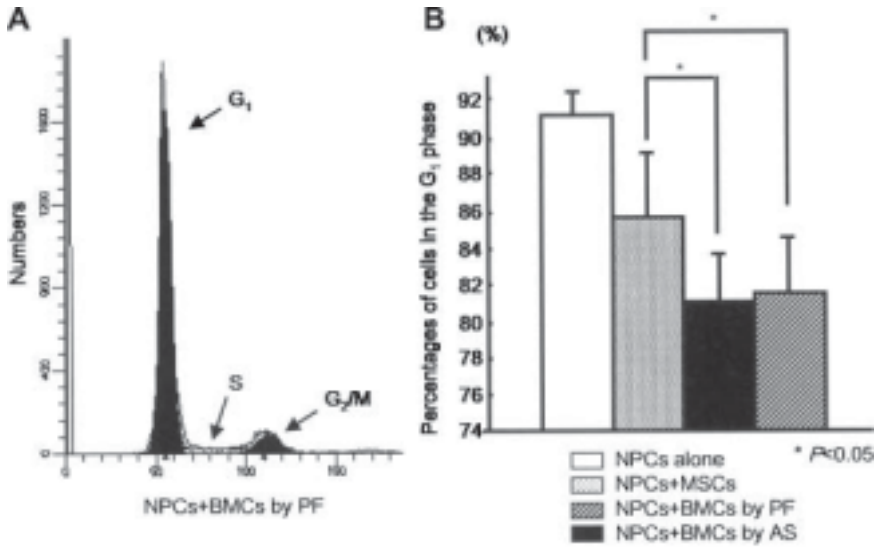


Figure 4. (A) Representative data of NPCs + BMCs by the PF method. (B) Percentages of NPCs in the G1 phase from the four experimental groups. Results are mean ± SD of eight rats. **p* < 0.05.

preventing degenerative disc disease, disc cells from rats were used for availability and cost reasons. We found that rat NPCs cocultured with fresh whole BMCs increased in cell number, progressed through the cell cycle, and had higher proliferation rates than NPCs cocultured with cultured MSCs. Proteoglycan synthesis in rat NPCs cocultured with fresh whole BMCs was significantly greater than that with cultured MSCs.

Because TGF-β plays an essential role in the proliferation and matrix synthesis of rat NPCs, we assessed its production by rat NPCs cocultured with fresh whole BMCs and found it to be significantly increased compared with cultures of these cells with cultured MSCs. Therefore, we suggest that whole BMCs consist of MSCs and HSCs and that MSCs may be more activated in combination with HSCs. Furthermore, when MSCs

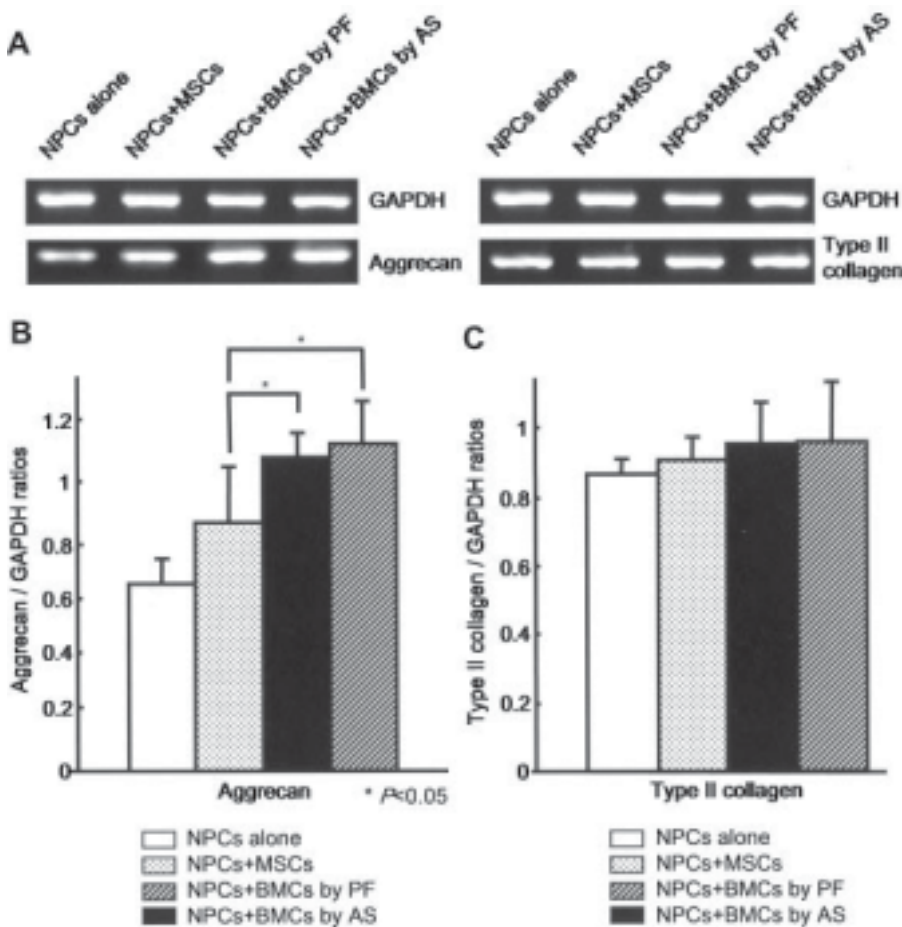


Figure 5. (A) Representative gel of RT-PCR products in NPCs from the four experimental groups. Aggrecan (B) and type II collagen (C) expression was analyzed by RT-PCR with GAPDH as the internal control for normalization. Results are mean ± SD of six rats. **p* < 0.05.

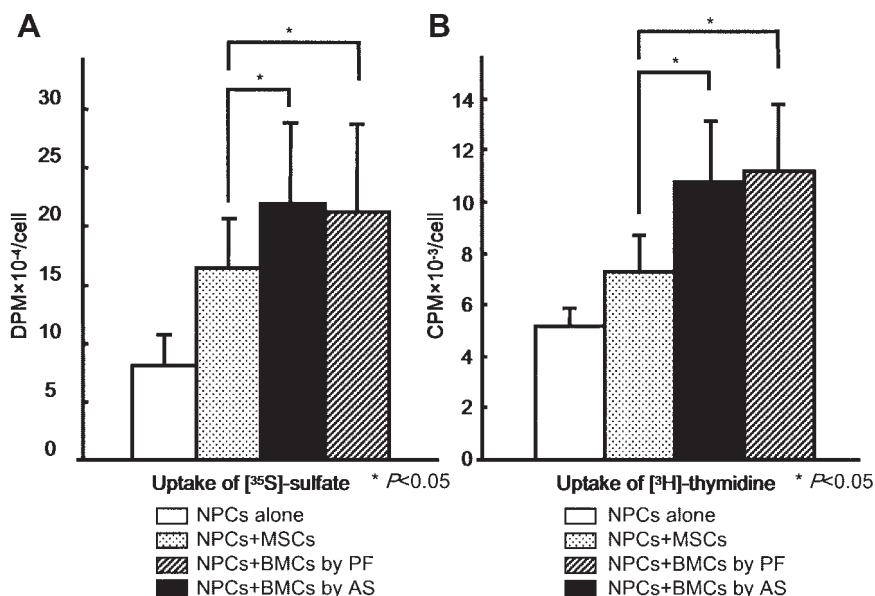


Figure 6. (A) Proteoglycan synthesis and (B) DNA synthesis by NPCs from the four experimental groups. Results are mean \pm SD of six rats. * $p < 0.05$.

are cultured in vitro, nonadherent cells, which could be important for activation of NPCs, may be discarded. We suggest that fresh whole BMCs are more effective at activating NPCs and stimulating their proliferation than cultured MSCs.

Although peripheral lymphocytes have been reported to cause autoimmune responses in the degenerated disc, it is difficult to obtain fresh whole BMCs without peripheral lymphocyte contamination. Haufe et al.³⁶ reported discouraging results from a trial implantation of autologous HSCs into human degenerated IVDs. Peripheral blood contamination may have created autoimmune reactions that reduced the ability of HSCs to regenerate the IVD. We developed a new harvesting method, the PF method,^{22,23} which results in a significant reduction of peripheral blood contamination compared with the conventional AS method in monkeys. In ours, we found that the PF method in rats was significantly better than the AS method for preventing contamination of BMCs with peripheral RBCs and lymphocytes.

The number of disc cells is decreased in advanced degeneration.³⁷ A primary cause of degeneration is failure of the nutrient supply to the disc, and that nutrient transport is affected in degeneration.^{38–40} Therefore, biological treatments are ineffective in advanced disc degeneration. Studies have shown that the biological approach is effective in early to moderate degeneration when the disc cells are viable and nutrition is preserved.^{41,42} We suggest that transplantation by injection of whole BMCs harvested by the PF method into early to moderately degenerative discs (Thompson grade II or III)⁴³ may be an effective therapy. If fresh whole bone marrow cells harvested by the PF method can be used, treatment for early degeneration may be simple and safe because the PF method prevents contamination with peripheral blood, which causes an autoimmune

response in the IVD and necessitates a decreased volume of transplantation.

In conclusion, we found that fresh whole BMCs collected by the PF method contain important cells in addition to adherent cells (the MSCs), which facilitate activation of rat NPCs (notochordal disc cell phenotype). But because human disc cells (mature nucleus cell phenotype) are different from rat disc cells, it is unclear whether this method can be effective in humans. However, we believe that fresh whole BMCs collected by the PF method will prove to be effective for therapeutic use in treatment of degenerated IVD.

ACKNOWLEDGMENTS

The authors thank Hiroko Omi, Futoshi Tamura, Toru Iwashina, Kenji Serigano, and Akihiko Hiyama of the Department of Orthopedic Surgery, Tokai University School of Medicine. This work was supported by a grant from the High-Tech Research Center Project of the Ministry of Education, a grant from the Academic Frontier Project, a grant from The 21st Century Center of Excellence program of the Ministry of Education, Culture, Sports, Science and Technology of Japan, and a grant from AO Spine International.

REFERENCES

1. Salminen JJ, Erkintalo MO, Pentti J, et al. 1994. Recurrent low back pain and early disc degeneration in the young. *Spine* 24:1316–1321.
2. Urban JP, Roberts S. 2003. Degeneration of the intervertebral disc. *Arthritis Res Ther* 5:120–130.
3. Sive JJ, Baird P, Jeziorski M, et al. 2002. Expression of chondrocyte markers by cells of normal and degenerate intervertebral discs. *Mol Pathol* 55:91–97.
4. Sztrolovics R, Grover J, Cs-Szabo G, et al. 2002. The characterization of versican and its message in human articular cartilage and intervertebral disc. *J Orthop Res* 20: 257–266.

5. Feng H, Danfelter M, Strömquist B, Heinegård D. 2006. Extracellular matrix in disc degeneration. *J Bone Joint Surg Am* 88:25–29.
6. Nishida K, Kang JD, Gilbertson LG, et al. 1999. Modulation of the biologic activity of the rabbit intervertebral disc by gene therapy: an in vivo study of adenovirus-mediated transfer of the human transforming growth factor beta 1 encoding gene. *Spine* 24:2419–2525.
7. Paul R, Haydon RC, Cheng H, et al. 2003. Potential use of Sox9 gene therapy for intervertebral degenerative disc disease. *Spine* 28:755–763.
8. Thompson JP, Oegema TR Jr, Bradford DS. 1991. Stimulation of mature canine intervertebral disc by growth factors. *Spine* 16:253–260.
9. Walsh AJ, Bradford DS, Lotz JC. 2004. In vivo growth factor treatment of degenerated intervertebral discs. *Spine* 29:156–163.
10. Chujo T, An HS, Akeda K, et al. 2006. Effects of growth differentiation factor-5 on the intervertebral disc—in vitro bovine study and in vivo rabbit disc degeneration model study. *Spine* 31:2909–2917.
11. Masuda K, Imai Y, Okuma M, et al. 2006. Osteogenic protein-1 injection into a degenerated disc induces the restoration of disc height and structural changes in the rabbit annular puncture model. *Spine* 31:742–754.
12. Okuma M, Mochida J, Nishimura K, et al. 2000. Reinsertion of stimulated nucleus pulposus cells retards intervertebral disc degeneration: an in vitro and in vivo experimental study. *J Orthop Res* 18:988–997.
13. Yamamoto Y, Mochida J, Sakai D, et al. 2004. Up regulation of the viability of nucleus pulposus cells by bone marrow-derived stromal cells: significance of direct cell-to-cell contact in coculture system. *Spine* 29:1508–1514.
14. Richardson SM, Walker RV, Parker S, et al. 2006. Intervertebral disc cell-mediated mesenchymal stem cell differentiation. *Stem Cells* 24:707–716.
15. Sakai D, Mochida J, Iwashina T, et al. 2006. Regenerative effects of transplanting mesenchymal stem cells embedded in atelocollagen to the degenerated intervertebral disc. *Biomaterials* 27:335–345.
16. Baylink DJ, Finkelman RD, Mohan S. 1993. Growth factors to stimulate bone formation. *J Bone Miner Res* 8:S565–S572.
17. Sporn MB, Roberts AB, Wakefield LM, Assoian RK. 1986. Transforming growth factor-beta: biological function and chemical structure. *Science* 233:532–534.
18. Bobechko WP, Hirsch C. 1965. Auto-immune response to nucleus pulposus in the rabbit. *J Bone Joint Surg Br* 47:574–580.
19. Doita M, Kanatani T, Harada T, Mizuno K. 1996. Immunohistologic study of the ruptured intervertebral disc of the lumbar spine. *Spine* 21:235–241.
20. Yoshida M, Nakamura T, Sei A, et al. 2005. Intervertebral disc cells produce tumor necrosis factor alpha, interleukin-1beta, and monocyte chemoattractant protein-1 immediately after herniation: an experimental study using a new hernia model. *Spine* 30:55–61.
21. Geiss A, Larsson K, Rydevik B, et al. 2007. Autoimmune properties of nucleus pulposus: an experimental study in pigs. *Spine* 32:168–173.
22. Kushida T, Inaba M, Ikebukuro K, et al. 2000. A new method for bone marrow cell harvesting. *Stem Cells* 18:453–456.
23. Kushida T, Inaba M, Ikebukuro K, et al. 2002. Comparison of bone marrow cells harvested from various bones of cynomolgus monkeys at various ages by perfusion or aspiration methods: a preclinical study for human BMT. *Stem Cells* 20:155–162.
24. Risbud MV, Fertala J, Vresilovic EJ, et al. 2005. Nucleus pulposus cells upregulate PI3K/Akt and MEK/ERK signaling pathways under hypoxic conditions and resist apoptosis induced by serum withdrawal. *Spine* 30:882–889.
25. Uei H, Matsuzaki H, Oda H, et al. 2006. Gene expression changes in an early stage of intervertebral disc degeneration induced by passive cigarette smoking. *Spine* 31:510–514.
26. Ala-Kokko L. 2002. Genetic risk factors for lumbar disc disease. *Ann Med* 34:42–47.
27. Le Maitre CL, Hoyland JA, Freemont AJ. 2007. Catabolic cytokine expression in degenerate and herniated human intervertebral discs: IL-1beta and TNFalpha expression profile. *Arthritis Res Ther* 9:R77.
28. Weiler C, Nerlich AG, Bachmeier BE, Boos N. 2005. Expression and distribution of tumor necrosis factor alpha in human lumbar intervertebral discs: a study in surgical specimen and autopsy controls. *Spine* 30:44–53.
29. Osada R, Ohshima H, Ishihara H, et al. 1996. Autocrine/paracrine mechanism of insulin-like growth factor-1 secretion, and the effect of insulin-like growth factor-1 on proteoglycan synthesis in bovine intervertebral discs. *J Orthop Res* 14:690–699.
30. Masuda K, Oegema TR Jr, An HS. 2004. Growth factors and treatment of intervertebral disc degeneration. *Spine* 29:2757–2769.
31. Risbud MV, Albert TJ, Guttapalli A, et al. 2004. Differentiation of mesenchymal stem cells towards a nucleus pulposus-like phenotype in vitro: implications for cell-based transplantation therapy. *Spine* 29:2627–2632.
32. Iwashina T, Mochida J, Sakai D, et al. 2006. Feasibility of using a human nucleus pulposus cell line as a cell source in cell transplantation therapy for intervertebral disc degeneration. *Spine* 31:1177–1186.
33. Crevensten G, Walsh AJ, Ananthakrishnan D, et al. 2004. Intervertebral disc cell therapy for regeneration: mesenchymal stem cell implantation in rat intervertebral discs. *Ann Biomed Eng* 32:430–434.
34. Hunter CJ, Matyas JR, Duncan NA. 2004. Cytomorphology of notochordal and chondrocytic cells from the nucleus pulposus: a species comparison. *J Anat* 205:357–362.
35. Le Visage C, Kim SW, Tateno K, et al. 2006. Interaction of human mesenchymal stem cells with disc cells: changes in extracellular matrix biosynthesis. *Spine* 31:2036–2042.
36. Haufe SM, Mork AR. 2006. Intradiscal injection of hematopoietic stem cells in an attempt to rejuvenate the intervertebral discs. *Stem Cells Dev* 15:136–137.
37. Gruber HE, Hanley EN Jr. 1998. Analysis of aging and degeneration of the human intervertebral disc. Comparison of surgical specimens with normal controls. *Spine* 23:751–757.
38. Urban JP, Roberts S. 2003. Degeneration of the intervertebral disc. *Arthritis Res Ther* 5:120–130.
39. Nachemson A, Lewin T, Maroudas A, Freeman MA. 1970. In vitro diffusion of dye through the end-plates and the annulus fibrosus of human lumbar inter-vertebral discs. *Acta Orthop Scand* 41:589–607.
40. Bartels EM, Fairbank JC, Winlove CP, et al. 1998. Oxygen and lactate concentrations measured in vivo in the intervertebral discs of patients with scoliosis and back pain. *Spine* 23:1–8.
41. Paesold G, Nerlich AG, Boos N. 2007. Biological treatment strategies for disc degeneration: potentials and shortcomings. *Eur Spine J* 16:447–468.
42. Masuda K, An HS. 2006. Prevention of disc degeneration with growth factors. *Eur Spine J* 15:S422–S432.
43. Thompson JP, Pearce RH, Schechter MT, et al. 1990. Preliminary evaluation of a scheme for grading the gross morphology of the human intervertebral disc. *Spine* 15:411–415.

研究成果報告書

研究課題名	網膜神経節細胞の細胞死抑制と神経細胞の再生		
(英文)	Inhibitoin of neuronal cell death of retinal ganglion cell and regeneration of optic nerve		
事業推進者	高橋 寛二	E-mail	takahask@hitakata.kmu.ac.jp
所属・職名	医学研究科・視覚修復医学（眼科学）講座・教授		
研究分担者名	安藤 彰、山田 晴彦、緒方 奈保子		
キーワード	網膜神経節細胞、アポトーシス、細胞死抑制、神経保護、神経再生		

1. 概要

緑内障は社会的失明を来たす頻度の高い疾患であり、網膜神経節細胞の細胞死が病態に深く関与している。本事業はトランスレーショナル研究を推進することを目指す。

2. 研究の背景と目的

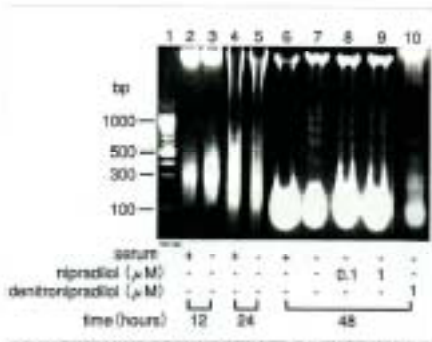
わが国における視覚障害の原因の第一位である緑内障は網膜神経節細胞の細胞死が発生することにより、視神経萎縮から視野障害、社会的失明へとつながる疾患であり、その治療と失明患者における視覚再生は非常に重要な課題となっている。特にわが国では正常眼圧緑内障と呼ばれる高眼圧の関与が少なく網膜神経節細胞死、すなわちアポトーシスがより病態に深くかかわっている病型の頻度が高く、神経節細胞保護を中心とした治療法の開発が待ち望まれている。本研究の目的は、網膜神経節細胞の細胞死を抑制する神経保護と神経再生についての基礎的研究を行うことにより、臨床における緑内障治療への応用を目指すことである。

3. 研究方法

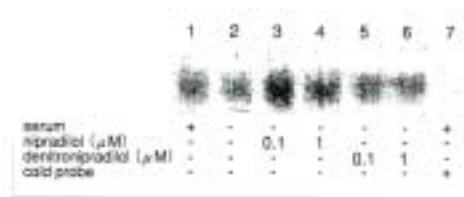
アポトーシス関連分子の遺伝子発現に対するニプラジロールの作用解明：
血清非添加培地でアポトーシスを誘導できる PC12 細胞を用いて、各種濃度のニプラジロールまたは脱ニトロ・ニプラジロールを添加し、12、24、48 時間培養して生存細胞数への影響を検討し、さらに染色体 DNA を抽出してアガロースゲ電気泳動にてラダー形成を確認してアポトーシスの程度を確認した。また、各種アポトーシス関連分子の遺伝子発現を定量的リアルタイム・ポリメラーゼ連鎖反応で検討し、転写因子 NF- κ B は EMSA を行って調べた。

4. これまでの成果

3. の結果、ニプラジロールが NO 供与を介して NF- κ B を活性化してアポトーシス関連分子の発現を抑制することが明らかになった。
- 1) 結果 1 : PC12 細胞を血清非添加培地で培養すると、血清添加培地と比べて 48 時間で細胞死がみられたが、1 μ M のニプラジロールによって細胞死は抑制された。一方、脱ニトロ・ニプラジロールでは抑制されなかった。
 - 2) 結果 2 : 図 1 のように、染色体 DNA のラダー形成は 12 時間、24 時間では不鮮明であるが、48 時間で明らかであり、0.1 または 1 μ M のニプラジロールによって抑制された。一方脱ニトロ・ニプラジロールでは抑制されなかった。
 - 3) 結果 3 : Bax、Caspase-9 と Smac/DIABLO の遺伝子発現は血清非添加培地で 12 時間後に上昇し、ニプラジロールによって有意に低下したが、脱ニトロ・ニプラジロールは影響を及ぼさなかった。
 - 4) 結果 4 : 図 2 のように、PC12 細胞の NF- κ B 活性は 2 時間後に血清非添加培地で低下し、ニプラジロールにより上昇したが、脱ニトロ・ニプラジロールは効果を示さなかった。



【図3】血清非添加培養におけるPC12細胞のDNAラダー形成とニブラジロールの効果
 レーン 1: DNA サイズマーカー, 2, 4, 6: 血清添加培養地で培養後 12, 24, 48 時間後, 染色体 DNA ラダー形成はみられる, 3, 5, 7: 血清非添加培養地で培養後 12, 24, 48 時間後, 48 時間後 PC12 細胞の染色体 DNA ラダー形成がみられる, 8, 9: 0.1 および 1 μM のニブラジロール添加, 10: 1 μM のニトロ・ニブラジロール添加 (文献より引用)



【図4】血清非添加培養におけるPC12細胞のNF-κB活性の阻害とニブラジロールの効果
 electrophoresis mobility shift assay (EMSA) の結果
 レーン 1: 血清添加培養地, 2: 血清添加培養地 + ニブラジロール, 3, 4: 血清非添加培養地 + ニブラジロール, 5, 6: 血清非添加培養地 + ニトロ・ニブラジロール, 7: 非標的プローブを大量に添加したコントロール (文献より引用)

5. これまでの進捗状況と今後の計画

事業は研究計画に沿って概ね順調に進捗している。さらに、臨床応用をめざした病態モデルや神経再生による治療の基礎研究を検討している。

6. これまでの発表論文

(1) 発表論文

1) 原著論文

1. Yamazaki, Y., Matsunaga, H., Nishikawa, M., Ando, A., Kaneko, S., Okuda, K., Wada, M., Ito, S. & Matsumura, M.

Senescence in cultured trabecular meshwork cells.

Br. J. Ophthalmol. **91**, 808-811 (2007).

2. Ando, A., Yamazaki, Y., Kaneko, S., Miyake, M., Nambu, R., Taomoto, M., Unezaki, S., Okuda-Ashitaka, E., Okumura, T., Ito, S. & Matsumura, M.

Cytoprotection by nipradilol, an anti-glaucomatous agent, via down-regulation of apoptosis related gene expression and activation of NF-κB.

Exp. Eye Res. **80**, 501-507 (2005).

3) 著書

1. Ando, A., Kaneko, S., Ohnaka, M., Tsuda, M., Unezaki, S., Okuda-Ashitaka, E., Okumura, T., Nishimura, T., Matsumura, M. & Ito, S.

Nipradilol, a nonselective β- and selective α1-adrenergic receptor antagonist, displays anti-apoptotic activity through regulation of apoptosis-related gene expression by nitric oxide donative action. In: Beta blocker new research, Nova Science Publishers, Inc., New York, in press.

2. Ando, A., Kaneko, S., Kiriya, N., Unezaki, S., Okuda-Ashitaka, E., Okumura, T., Nishimura, T., Matsumura, M. & Ito, S.

Prevention of Apoptosis by Down-Regulation of Apoptosis Related Gene Expression Obtained by Nipradilol Via Nitric Oxide Donative Action. In: Shultz LB (ed). Cell apoptosis: regulation and environmental factors. 55-69, Nova Science Publishers, Inc., New York (2007).

1) 原著論文

安藤彰、尾辻剛、福井智恵子、桑原敦子、嶋千絵子、松山加耶子、松原敬忠、城信雄、南部裕之、松村美代

ラタノプロスト点眼投与中の正常眼圧緑内障に追加したニプラジロール点眼の眼圧と視野への効果.

臨床眼科 **62**, 329-333 (2008).

3) 著書

安藤彰 :

「緑内障診療の進めかた」

神経保護の戦略. 根木昭 (編) 眼科プラクティス 11 巻、370-372, 文光堂 (2006).

(2) 学会発表

国際学会

2) シンポジウム講演

Tsuda, M., Ando, A., Fukui, C., Matsuyama, K., Kuwahara, A., Nishimura, T., Nambu, H. & Matsumura, M.

Intraocular Pressure Reduction by Latanoprost for Normal Tension Glaucoma: Results over Five Years Compared between High-tension and Low-tension Japanese Patients.

International Symposium on Ocular Pharmacology and Therapeutics, Budapest, Hungary, 2008.

3) 一般発表

1. Ando, A., Tsuda, M., Kaneko, S., Ohnaka, M., Okuda-Ashitaka, E., Ito, S., Nishimura, T., Taomoto, M. & Matsumura, M.

Controllable Urokinase Gene Expression into Cultured Porcine Trabecular Meshwork Cells.

ARVO, Florida, USA, 2008.

2. Ando, A., Kiriyama, N., Kaneko, S., Nishimura, T., & Matsumura, M.

Aquaporin Gene Expression in Trabecular Meshwork Cells.

ARVO, Florida, USA, 2006.

国内学会

3) 一般発表

1. 安藤彰、尾辻剛、福井智恵子、桑原敦子、嶋千絵子、松山加耶子、松原敬忠、城信雄、南部裕之、松村美代

ラタノプロスト投与中の正常眼圧緑内障に追加したニプラジロールの眼圧と視野への影響.

第 61 回日本臨床眼科学会、京都、2007.

2. 安藤彰、桐山直子、金子志帆、西村哲哉、松村美代

線維柱帯細胞におけるアクアポリンおよび Kir と Na⁺, K⁺ ATPase 遺伝子発現.

第 110 回日本眼科学会総会、大阪、2006.

7. これまでの成果の情報公開

ホームページ : 眼科学講座 = <http://www3.kmu.ac.jp/opthal/>



Senescence in cultured trabecular meshwork cells

Yukari Yamazaki, Hiroshi Matsunaga, Maki Nishikawa, Akira Ando, Shiho Kaneko, Koji Okuda, Mitsumasa Wada, Seiji Ito and Miyo Matsumura

Br. J. Ophthalmol. 2007;91:808-811; originally published online 10 Jan 2007;
doi:10.1136/bjo.2006.108423

Updated information and services can be found at:
<http://bjournal.bmj.com/cgi/content/full/91/6/808>

These include:

References

This article cites 20 articles, 6 of which can be accessed free at:
<http://bjournal.bmj.com/cgi/content/full/91/6/808#BIBL>

Rapid responses

You can respond to this article at:
<http://bjournal.bmj.com/cgi/eletter-submit/91/6/808>

Email alerting service

Receive free email alerts when new articles cite this article - sign up in the box at the top right corner of the article

Notes

To order reprints of this article go to:
<http://journals.bmj.com/cgi/reprintform>

To subscribe to *British Journal of Ophthalmology* go to:
<http://journals.bmj.com/subscriptions/>

SCIENTIFIC REPORT

Senescence in cultured trabecular meshwork cells

Yukari Yamazaki, Hiroshi Matsunaga, Maki Nishikawa, Akira Ando, Shiho Kaneko, Koji Okuda, Mitsumasa Wada, Seiji Ito, Miyo Matsumura

Br J Ophthalmol 2007;**91**:808–811. doi: 10.1136/bjo.2006.108423

Background: It has been suggested that replicative senescence might be involved in the pathophysiology of age-related diseases.

Aim: To study the process of senescence in trabecular meshwork (TM) cells.

Methods: Porcine TM tissues were obtained and placed in primary cultures with Dulbecco's modified Eagle's medium/Ham's F-12 medium. After 2–3 weeks, migrated and proliferated TM cells were trypsinised and cultured in serial passages, and identified with fluorescein-labelled low-density lipoprotein (Dil-Ac-LDL), a marker of TM cells. Staining for senescence-related β -galactosidase activity was performed at population doubling level (PDL) 2, 8 and 16 at pH 6. Terminal restriction fragment (TRF) length was examined by Southern blot analysis using a 32 P-labelled telomere-specific sequence (TTAGGG)₃ at each PDL.

Results: Dil-Ac-LDL staining revealed that most (nearly 100%) of the cells in the culture were TM cells, which were flattened in shape and positive for senescence-related β -galactosidase staining at PDL 16. Reduction of TRF length as a function of population doubling was also shown.

Conclusions: TM cells exhibited characteristics of senescence at PDL 16 in vitro. The results demonstrated that cellular senescence may be related to the pathophysiology of primary open-angle glaucoma.

Normal diploid cells have a finite proliferative life span and finally enter a non-dividing state termed senescence.¹ Senescent cells are unable to duplicate themselves and are accompanied with altered gene expression, at least when cultured in vitro.² It has been suggested that replicative senescence might be involved in the pathophysiology of age-related disorders, such as progeria and Werner's syndrome, as well as related atherothrombotic diseases.^{3–5} Primary open-angle glaucoma (POAG) is an optic neuropathy associated with abnormally increased intraocular pressure that can lead to blindness, especially in elderly patients, and age- and disease-related losses of trabecular meshwork (TM) cells have been reported in patients with POAG.^{6–7} It has also been suggested that a loss of TM cells, followed by substitution with extracellular matrix, might contribute to an increased resistance to aqueous outflow in those patients, resulting in an increase in intraocular pressure.^{8–9} Thus, ageing is thought to have a relationship with the pathophysiology of POAG. Our previous study results showed that aged retinal pigment epithelial (RPE) cells exhibited characteristics of cellular senescence and suggested that senescent RPE cells could be involved in the pathogenesis of age-related macular degeneration.¹⁰ TM cells are derived from the embryonic neural crest,¹¹ and are known to have phagocytic¹² and migratory¹³ abilities similar to RPE cells. Therefore, we speculated that TM cells also exhibit

Abbreviations: PDL, population doubling level; POAG, primary open-angle glaucoma; LDL, low-density lipoprotein; TM, trabecular meshwork; TRF, terminal restriction fragment; RPE cells, retinal pigment epithelial cells

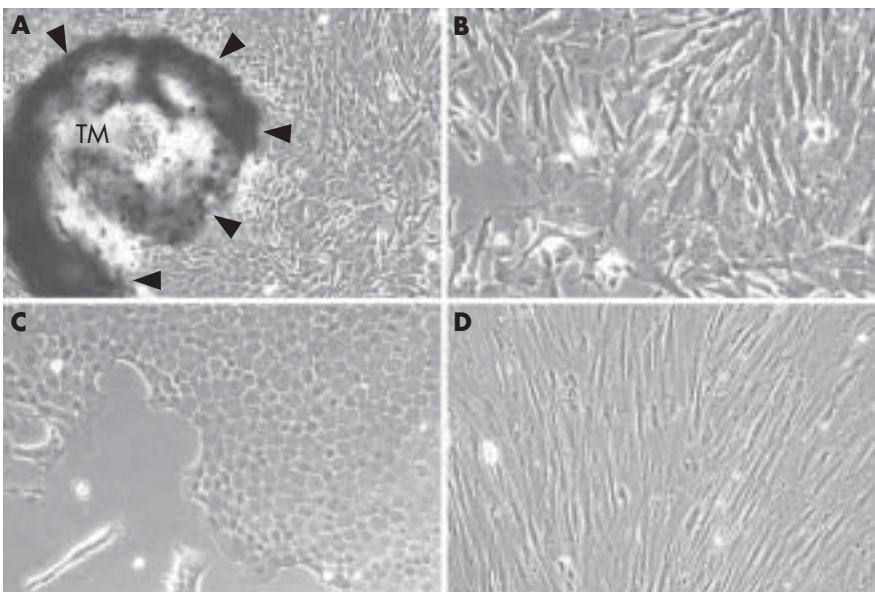


Figure 1 Trabecular meshwork (TM) tissue explant (A arrowheads) and phenotypical differences among trabecular meshwork cells (B), corneal endothelial cells (C) and fibroblasts from Tenon's connective tissue (D). Original magnification $\times 100$ (A), $\times 400$ (B–D).

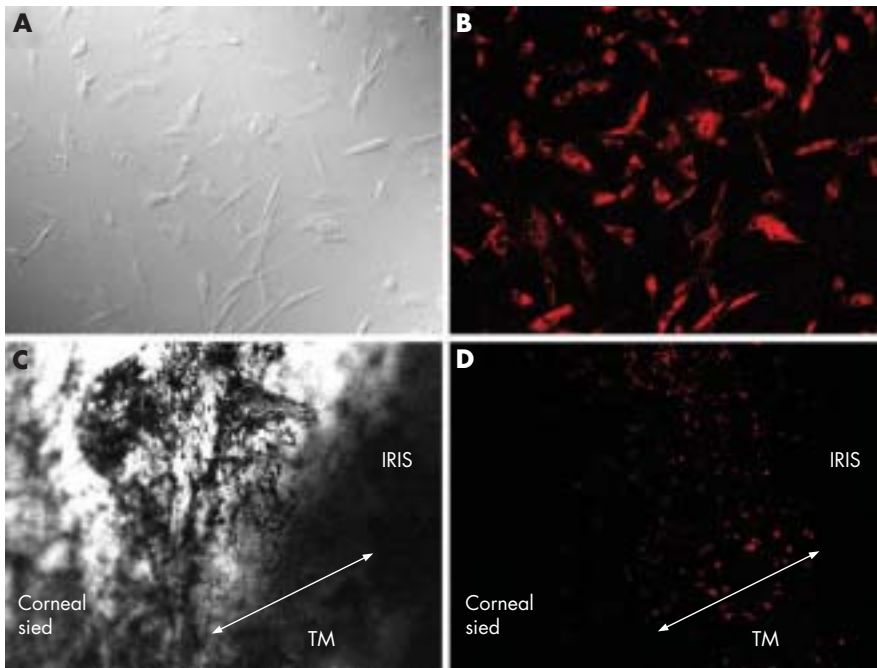


Figure 2 Nomarsky view (A,C) and low-density lipoprotein staining (B,D) of trabecular meshwork cells (A,B) and trabecular meshwork (TM) tissue (C,D). Original magnification $\times 400$ (A,B), $\times 100$ (C,D).

cellular senescence, which may be involved in the pathophysiology of POAG, as it was reported previously that levels of type VI collagen, thrombospondin and fibronectin were increased in aged TM cells.¹⁴ In this study, we investigated whether cellular senescence occurred in cultured TM cells.

MATERIALS AND METHODS

Tissue and cell culture

Porcine eyes were transported to our laboratory in ice-cold saline. The eyeballs were cut and opened at a point 3 mm

posterior from the limbus under a dissection microscope. TM tissue and Tenon's connective tissue samples were also obtained, and placed separately in six-well plates (Falcon, New York, New York, USA) with Dulbecco's modified Eagle's medium/Ham's F-12 culture medium (Sigma-Aldrich, St Louis, Missouri, USA) supplemented with 10% fetal bovine serum (HyClone Laboratories, South Logan, Utah, USA), 100 U/ml of penicillin and 100 mg/ml of streptomycin for 4 weeks, to allow the TM cells and fibroblasts to migrate and proliferate. Primary cultures of each sample were maintained in an atmosphere of

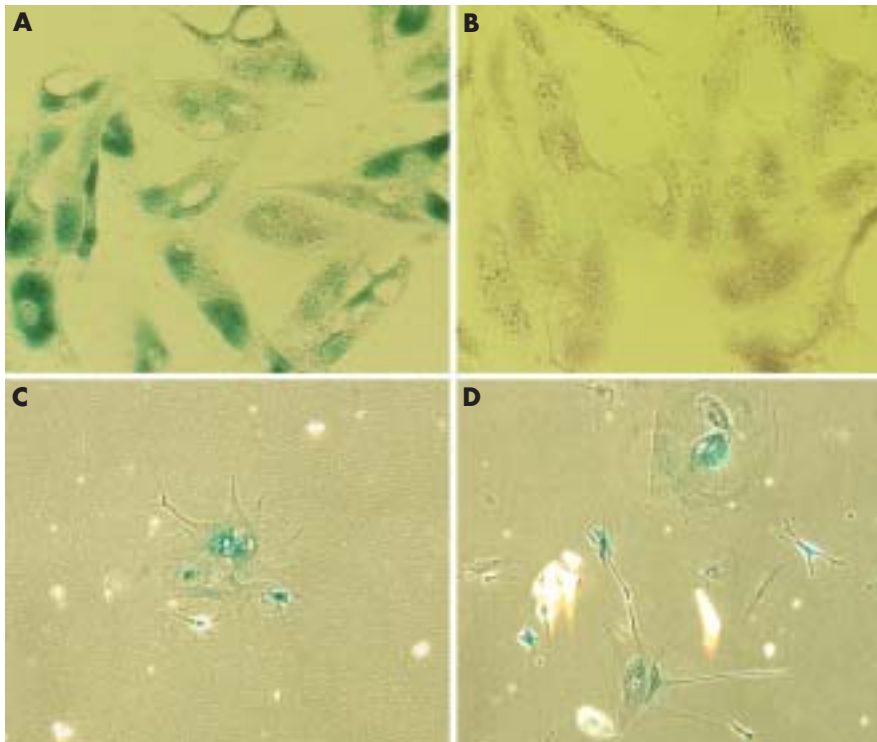


Figure 3 Lysosomal (pH 4; A,C) and senescence-related (pH 6; B,D) β -galactosidase staining of young (PDL 2; A,B) and senescent (PDL 16; C,D) trabecular meshwork cells. Original magnification $\times 400$.

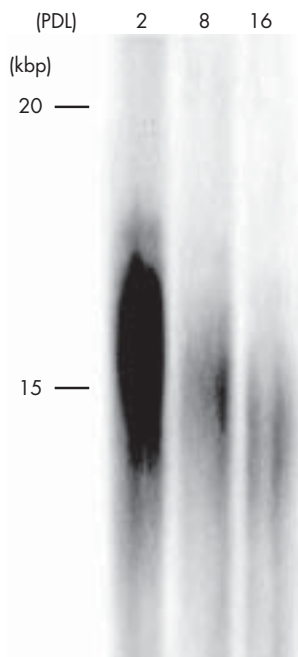


Figure 4 Results of terminal restriction fragment length analysis. Telomere shortening associated with multiple passages of trabecular meshwork cells was seen.

5% CO₂/95% air at 37°C and supplied with fresh medium once a week. Further, corneal samples were obtained and covered with Hanks's balanced salt solution containing 0.025% trypsin and 0.01% EDTA for 30 min at 37°C to obtain corneal endothelial cells. TM cells obtained from confluent primary cultures were arbitrarily designated as population doubling level (PDL) 0. When the cells became confluent, they were subcultured at a split ratio of 1:4 using Hanks's balanced salt solution (Gibco, Grand Island, New York, USA) containing 0.05% trypsin and 0.01% EDTA; thus, subcultured cells increased by two PDLs at each passage. Cells without tissue were seeded separately in six-well plates (Falcon), and then incubated under the same conditions and supplied with fresh medium every 3 days.

Low-density lipoprotein staining

Cells were examined for expression of the low-density lipoprotein (LDL) receptor, which has been shown to be a surface marker of TM cells.¹⁵ Cells were grown in 35 mm diameter glass-bottom dishes (Matsunami Glass, Ind., Osaka, Japan) and incubated for 6 h in 2 ml of medium containing 20 µg of DiI-labelled acetylated LDL (DiI-Ac-LDL, Molecular Probes, Eugene, Oregon, USA). After the dishes were washed three times with phosphate-buffered saline (pH 7.4), they were processed for fluorescence microscopy examinations. Corneal endothelial cells and fibroblasts obtained from porcine eyes were used as negative controls for DiI-Ac-LDL staining. The samples were observed and analysed using a fluorescence microscope (FluoView, Olympus, Tokyo, Japan).

β-Galactosidase staining

TM cells at PDL 2, 8 and 16 were trypsinised and seeded in 35 mm diameter glass-bottom dishes. Cells were incubated for 12 h under the same culture conditions as in the above experiment to allow them to adhere to the glass bottom of the dish, and then washed with phosphate-buffered saline and stained for senescence-related β-galactosidase (pH 6) or lysosomal β-galactosidase (pH 4) activities. Details of the staining procedures have been described previously.^{10,16} The cells were fixed in 3% formaldehyde for 4 min at room

temperature, washed three times with phosphate-buffered saline, then incubated in 1 ml of a solution containing 5 mM of X-gal in 40 mM of citric acid-sodium phosphate buffer (pH 6) at 37°C in air for 8 h to develop the blue colour in senescent cells. Control incubations were performed at pH 4 to show the presence of lysosomal β-galactosidase in all cells. Samples were examined with a bright field microscope (IMT-2, Olympus) equipped with a computer-controlled display camera (HC-1000, Fujix, Tokyo, Japan).

Measurements of mean terminal restriction fragment lengths

Mean terminal restriction fragment (TRF) length was analysed using a method previously described,^{10,17,18} with a slight modification. Genomic DNA was isolated from TM cells at PDL 2, 8 and 16. Cells were lysed in a lysis buffer (150 mM NaCl, 10 mM Tris-HCl, 10 mM EDTA and 0.1% sodium dodecyl sulphate) containing 0.1 µg/ml of proteinase K (Sigma-Aldrich). Samples were incubated at 55°C for 30 min and subsequent DNA extraction was performed as described previously.¹⁷ Each DNA sample was limit digested with the restriction enzymes *Rsa* I and *Hinf* I, to yield terminal restriction fragments containing the telomere and a small amount of sub-telomeric DNA sequence. Each sample (1 µg) was subjected to electrophoresis on a 0.7% agarose gel in 1× Tris-acetate-EDTA buffer for 200 V-h, then transferred onto a Hibond-N⁺ (Amersham Biosciences, Piscataway, New Jersey, USA) membrane and hybridised with a ³²P-labelled telomere-specific oligonucleotide of TTAGGG₃. After washing with saline sodium citrate containing 0.1% sodium dodecyl sulphate at 42°C for 5 min, the membranes were exposed to x ray films (Fujifilm, Tokyo, Japan).

RESULTS AND DISCUSSION

TM cell morphology

TM cells migrated from TM tissue and proliferated to form colonies around each TM tissue specimen (fig 1A), and showed a cell shape (fig 1B) that was different from fibroblasts and corneal endothelial cells. Corneal endothelial cells showed a round or hexagonal shape, with a cobblestone-like phenotype (fig 1C), whereas fibroblasts from Tenon's connective tissue showed a spindle-like shape with a longitudinal axis (fig 1D).

LDL staining

Nearly all the cultured TM cells at PDL 2 showed a cell shape identical (fig 2A) to that seen in the primary culture (fig 1B) and were strongly positive for DiI-Ac-LDL staining, a reported previously¹⁵ surface marker of TM cells (fig 2B). LDL staining was also performed with TM tissue (fig 2C) to confirm whether in situ TM cells expressed the LDL receptor, and those cells were also positive for DiI-Ac-LDL (fig 2D). By contrast, corneal endothelial cells and fibroblasts from Tenon's connective tissue were negative for LDL staining (data not shown).

Upregulation of senescence-related β-galactosidase in senescent TM cells

TM cells were flattened in shape at PDL 16 (fig 3C,D) as compared with those at PDL 2 (fig 3A,B). TM cells at PDL 2 were positive only for lysosomal β-galactosidase staining (pH 4; fig 3A) and not for senescence-related β-galactosidase staining (pH 6; fig 3B). On the other hand, senescent TM cells at PDL 16 stained positive for both senescence-related β-galactosidase (fig 3D) and lysosomal β-galactosidase (fig 3C).

Reduction of TRF length in senescent TM cells

A reduction in TRF length in relation to PDL was shown by genomic Southern blot analysis, as the chromosomal telomeres became shorter with increased numbers of passages (fig 4). TM

cells exhibited a mean TRF length of approximately 16, 15 and 14.5 kb at PDL 2, 8 and 16, respectively.

DISCUSSION

Cellular senescence is characterised by telomere loss and altered gene expression,^{1,2} and senescent cells are unable to duplicate and have altered functional characteristics. Takeda *et al*¹⁹ reported that human skin fibroblasts showed similar modulations in the expression of extracellular matrix components during ageing in in vitro and in vivo experiments, whereas we previously found that cultured human RPE cells exhibited characteristics of cellular senescence.¹⁰ Further, Tombran-Tink *et al*²⁰ showed that age-related down regulation of pigment epithelium-derived factor, a protein possessing neurotrophic and neuronal-survival activities, occurred in cultured fetal monkey RPE cells.

In this study, TM cells exhibited characteristics of senescence at PDL 16 in vitro, as well as a shorter replicative life span and longer TRF length with senescence, as compared with the RPE cells in our previous report. We consider that these differences might have been because the RPE cells were from an established cell line, whereas the TM cells were from primary cultures. However, the differences may also have been due to cellular differences between human and porcine specimens. Additional experiments are required to understand the pathophysiology of POAG. Nevertheless, if senescent cells are shown to accumulate with age, cellular senescence may play an important role.

ACKNOWLEDGEMENTS

This work was supported in part by a Grant-in-Aid for Young Scientists (B) (number 17791262) from the Japan Society for the Promotion of Science and the Ministry of Education, Culture, Sports, Science and Technology of Japan, and grants from the Science Research Promotion Fund of the Japan Private School Promotion Foundation.

Authors' affiliations

Yukari Yamazaki, Hiroshi Matsunaga, Maki Nishikawa, Akira Ando, Shiho Kaneko, Mitsumasa Wada, Miyo Matsumura, Department of Ophthalmology, Kansai Medical University, Moriguchi, Osaka, Japan
Koji Okuda, Department of Paediatrics, Kansai Medical University, Moriguchi, Osaka, Japan
Seiji Ito, Department of Medical Chemistry, Kansai Medical University, Moriguchi, Osaka, Japan

Competing interests: None.

Correspondence to: Dr H Matsunaga, Department of Ophthalmology, Kansai Medical University, 10-15 Fumizono-cho, Moriguchi, Osaka 570-8507, Japan; matsunag@takii.kmu.ac.jp

Accepted 1 January 2007

Published Online First 10 January 2007

REFERENCES

- Hayflick L. Limited in vitro lifetime of human diploid cell strains. *Exp Cell Res* 1965;**37**:614-36.
- Campisi J. Replicative senescence: an old lives' tale? *Cell* 1996;**84**:497-500.
- Goldstein S. Increased procoagulant activity in cultured fibroblasts from progeria and Werner's syndromes of premature ageing. *Nature* 1976;**260**:711-13.
- Goldstein S. Studies on age-related diseases in cultured skin fibroblasts. *J Invest Dermatol* 1979;**73**:19-23.
- Norwood TH, Hoehn H, Salk D, *et al*. Cellular aging in Werner's syndrome: a unique phenotype? *J Invest Dermatol* 1979;**73**:92-6.
- Alvarado J, Murphy C, Polansky J, *et al*. Age-related changes in trabecular meshwork cellularity. *Invest Ophthalmol Vis Sci* 1981;**21**:714-27.
- Alvarado J, Murphy C, Juster R. Trabecular meshwork cellularity in primary open-angle glaucoma and nonglaucomatous normals. *Ophthalmology* 1984;**91**:564-79.
- Tripathi RC. Pathologic anatomy of the outflow pathway of aqueous humor in chronic simple glaucoma. *Exp Eye Res* 1977;**25**(Suppl):403-7.
- Lütjen-Drecoll E, Rittig M, Rauterberg J, *et al*. Immunomicroscopical study of type VI collagen in the trabecular meshwork of normal and glaucomatous eyes. *Exp Eye Res* 1989;**48**:139-47.
- Matsunaga H, Handa JT, Aotaki-Keen A, *et al*. β -Galactosidase histochemistry and telomere loss in senescent retinal pigment epithelial cells. *Invest Ophthalmol Vis Sci* 1999;**40**:197-202.
- Tripathi BJ, Tripathi RC. Neural crest origin of human trabecular meshwork and its implications for the pathogenesis of glaucoma. *Am J Ophthalmol* 1989;**107**:583-90.
- Buller C, Johnson DH, Tschumper RC. Human trabecular meshwork phagocytosis. *Invest Ophthalmol Vis Sci* 1990;**31**:2156-63.
- Calthorpe CM, Grierson I. Fibronectin induces migration of bovine trabecular meshwork cells in vitro. *Exp Eye Res* 1990;**51**:39-48.
- Tripathi BJ, Li T, Li J, *et al*. Age-related changes in trabecular cells in vitro. *Exp Eye Res* 1997;**64**:57-66.
- Chang IL, Elnor G, Yue YJ, *et al*. Expression of modified low-density lipoprotein receptors by trabecular meshwork cells. *Curr Eye Res* 1991;**10**:1101-12.
- Dimri GP, Lee X, Basile G, *et al*. A biomarker that identifies senescent human cells in culture and in aging skin in vivo. *Proc Natl Acad Sci USA* 1995;**92**:9363-7.
- Allsopp RC, Vaziri H, Patterson C, *et al*. Telomere length predicts replicative capacity of human fibroblasts. *Proc Natl Acad Sci USA* 1992;**89**:10114-18.
- Okuda K, Bardeguet A, Gardner JP, *et al*. Telomere length in the newborn. *Pediatr Res* 2002;**52**:377-81.
- Takeda K, Gosiewska A, Peterkofsky B. Similar, but not identical, modulation of expression of extracellular matrix components during in vitro and in vivo aging of human skin fibroblasts. *J Cell Physiol* 1992;**153**:450-9.
- Tombran-Tink J, Shivaram SM, Chader GJ, *et al*. Expression, secretion, and age-related downregulation of pigment epithelium-derived factor, a serpin with neurotrophic activity. *J Neurosci* 1995;**15**:4992-5003.



神経保護の戦略

関西医科大学眼科 安藤 彰

■緑内障の視神経障害メカニズム

緑内障進行の因子として眼圧は大きなパラメータである。高眼圧は栄養因子の刺激、機械的または虚血性の細胞障害などを引き起こして神経節細胞と網膜神経線維を障害すると考えられている。エビデンスのある治療法は眼圧下降のみであり、また正常眼圧緑内障でも有効性が確認されたため緑内障治療薬は眼圧下降が狙いである。しかし網膜神経節細胞障害にプログラムされた細胞死であるアポトーシスが関与することが報告され、神経保護作用をもつ薬剤の緑内障治療への応用が期待されている。

■アポトーシスの経路

アポトーシスにはさまざまなシグナルや因子が関与し、FasL, Fas, Bax, Bcl-2 やカスパーゼと呼ばれる一連の分子群が複雑な経路を形成している。それらの活性化がアポトーシスを促進したり抑制したりしている(図1)。

■神経保護と一酸化窒素

一酸化窒素 nitric oxide (NO) がアポトーシスを抑制することや、一酸化窒素合成酵素 nitric oxide synthase (NOS) が緑内障患者の視神経乳頭に存在し、NO が細胞保護的な働きをもつことを示唆する報告がある。緑内障治療薬であるニブラジロール (3,4-dihydro-8-(2-hydroxy-3-isopropyl-amino)propoxy-3-nitroso-2H-1-benzopyran) が NO 供与作用を介した神経細胞保護効果をもつ可能性が報告された¹⁾。反対に緑内障のラットモデルで誘導型 NOS (iNOS) を抑制すると網膜神経節細胞の障害が阻止され、iNOS が産生する過剰な NO が網膜神経節細胞を障害する可能性が報告されている。NO は緑内障以外の網膜変性でも重要な役割を果たすことや、アポトーシス抑制と促進の両方向に関与することが明らかにされている²⁾。また NO はアポトーシス関連分子の遺伝子発現や転写因子 nuclear factor- κ B (NF- κ B) の活性を調節していることがわかっている。

■転写因子 NF- κ B

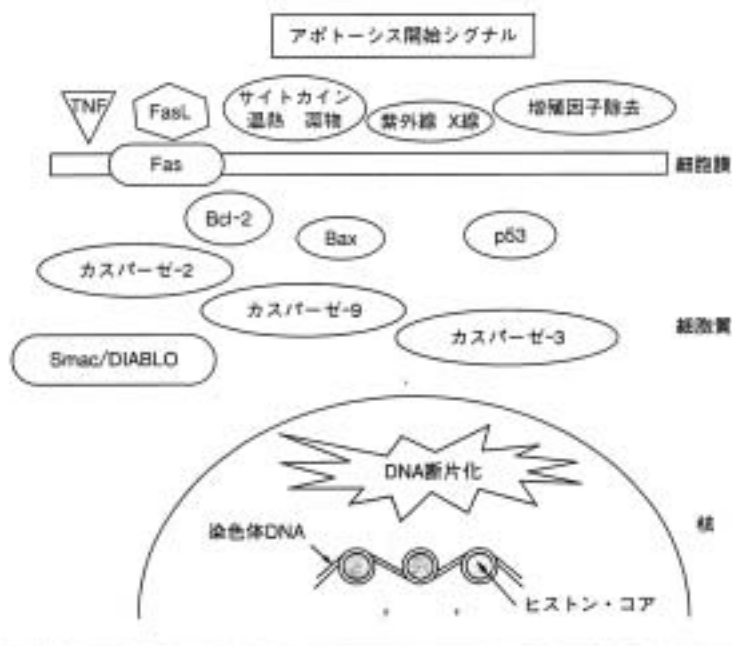
転写因子 NF- κ B は、さまざまな遺伝子発現を左右する因子の一つである。実験的に低酸素状態で誘導されるアポトーシスには NF- κ B 活性の低下を伴い、再酸素化することで NF- κ B が活性化され Bcl-2 と Bcl-x の発現を促進し、Bax の発現を抑制することから NF- κ B がアポトーシスの制御に関与していることがわかっている。

■実験的根拠

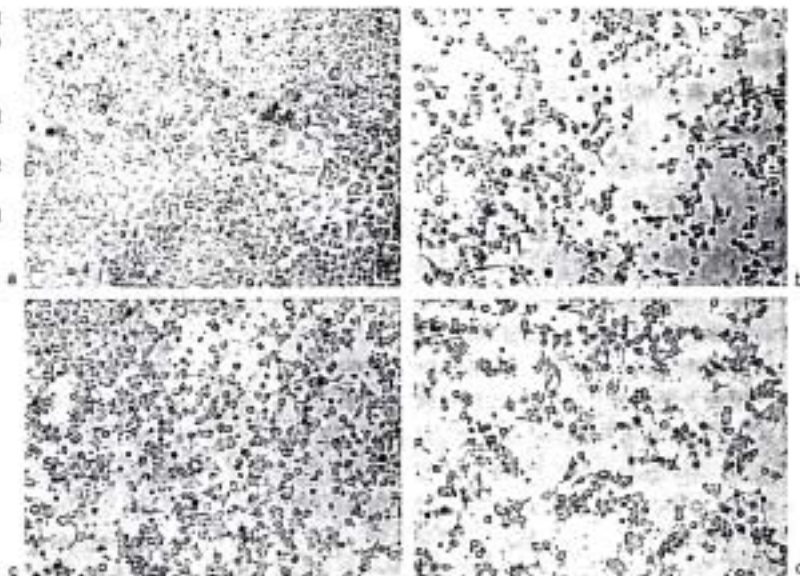
ニブラジロールと NO がカスパーゼ3の活性を低下させてアポトーシスを阻害することが報告された³⁾。われわれはアポトーシス関連分子の遺伝子発現に対するニブラジロールの作用を検討し、ニブラジロールが NO 供与を介して NF- κ B を活性化してアポトーシス関連分子の遺伝子発現を抑制することを明らかにした⁴⁾。われわれの実験で用いた PC 12 細胞は血清非添加培地でアポトーシスを誘導できるが、そこへ 0.01, 0.1, 1 または 10 μ M のニブラジロールまたは NO 供与能力をもたない脱ニトロ・ニブラジロールを添加して 12, 24, 48 時間培養して生存細胞数への影響を検討し、さらに染色体 DNA を抽出してアガロースゲル電気泳動にてラダー形成を確認してアポトーシスの程度を検討した。また Bax, Bcl-2, Fas, FasL, Caspase-1 から 9, p53 と Smac/DIABLO のアポトーシス関連分子の遺伝子発現を定量的リアルタイム・ポリメラーゼ連鎖反応法(リアルタイム PCR)で検討し、転写因子 NF- κ B 活性は electrophoresis mobility shift assay (EMSA) を行って調べた。PC 12 細胞を血清非添加培地で培養すると、血清添加培地(図2a)と比較して 48 時間で細胞死がみられたが(図2b)、1 μ M のニブラジロールによって抑制された(図2c)。脱ニトロ・ニブラジロールではみられなかった(図2d)。アガロースゲル電気泳動による染色体 DNA のラダー形成は 12 または 24 時間では不鮮明であるが(図3, レーン 3, 5)、48 時間で明らかであり(図3, レーン 7)、0.1 または 1 μ M のニブラジロールによって抑制された(図3, レーン 8、

【図1】 アポトーシス経路

サイトカインや温熱、紫外線やX線、増殖因子の除去などがアポトーシスの引き金となる。細胞内の情報伝達には Bax, Bclファミリー、FasL, Smac/DIABLO, カスケードを形成する一類のカパーゼ群が働いて染色体DNAがヒストンの単位で切断される。



【図2】 血清非添加培地におけるPC12細胞のアポトーシスとニブラジロールの効果
 a 血清添加培地におけるPC12細胞
 b 血清非添加培地によるPC12細胞死
 c 1 μ MニブラジロールによるPC12細胞死の抑制
 d 1 μ Mニブラジロールの効果。細胞死は抑制されない。
 (文献5)より引用)



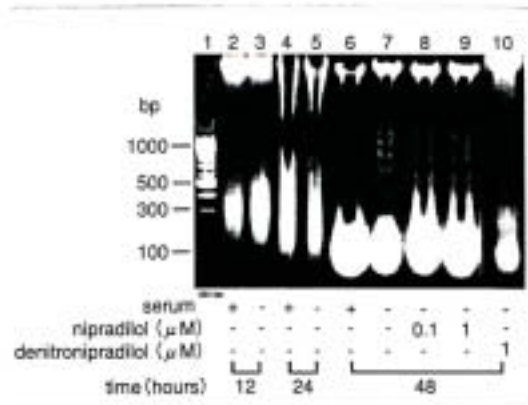
9). 脱ニトロ・ニブラジロールは、DNA ラダー形成を抑制しなかった(図3, レーン10)。Bax, Caspase-9 と Smac/DIABLO の遺伝子発現は血清非添加培地で12時間後に上昇し、ニブラジロールによって有意に低下したが、脱ニトロ・ニブラジロールは影響を及ぼさなかった。PC12細胞のNF- κ B活性は2時間後に血清非添加培地で低下し(図4, レーン2), ニブラジロールにより上昇した(図4, レーン3, 4)が、脱ニトロ・ニブラジロールは効果を示さなかった(図4, レーン5, 6)。脱ニトロ・ニブラジロールが何の効果も示さなかったことから、ニブラジロールのNO供与作用がNF- κ Bの活性化とアポトーシス関連分子の遺伝子発現の抑制を介したアポトーシスの抑制に重要な働きをしていると考えられる。

III 神経保護の今後

現在臨床で使用されているニブラジロールやカルテオロール、イソプロピルウノプロストン、あるいはドルゾラミド、プリソラミドなどで神経保護効果をもつことが示唆されている。また Alzheimer 病治療薬である神経細胞死抑制薬メマンチンの正常眼圧緑内障に対する有効性を検討するため欧米で試験が展開され、緑内障治療薬への応用が期待されている。網膜神経節細胞のアポトーシスの抑制は緑内障の治療に対する新しい戦略であると考えられる。

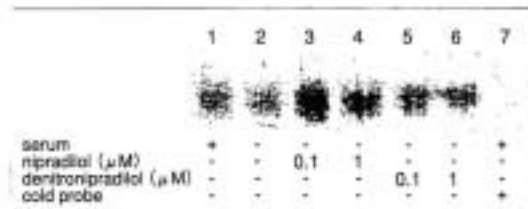
文献

- 1) Quigley, HA et al: Retinal ganglion cell death in experimental glaucoma and after axotomy occurs by apoptosis. *Invest Ophthalmol Vis Sci* 36: 774-786, 1995
- 2) Mizuno, K et al: Neuroprotective effect and intraocular penetration of nibradilol, a beta-blocker with nitric oxide donative action. *Invest Ophthalmol Vis Sci* 42: 688-694, 2001
- 3) Kashii, S et al: Dual actions of nitric oxide in N-methyl-D-aspartate receptor-mediated neurotoxicity in cultured retinal neurons. *Brain Res* 711: 93-101, 1996
- 4) Tomita, H et al: Nibradilol inhibits apoptosis by



【図3】 血清非添加培地におけるPC12細胞のDNAラダー形成とニブラジロールの効果

レーン1: DNAサイズマーカー。2, 4, 6: 血清添加培地で培養後12, 24, 48時間後。染色体DNAラダー形成はみられず。3, 5, 7: 血清非添加培地で培養後12, 24, 48時間後。48時間でPC12細胞の染色体DNAラダー形成がみられる。8, 9: 0.1および1 μ Mのニブラジロール添加。10: 1 μ Mの脱ニトロ・ニブラジロール添加。(文献4)より引用)



【図4】 血清非添加培地におけるPC12細胞のNF- κ B活性の阻害とニブラジロールの効果

electrophoresis mobility shift assay(EMSA)の結果

レーン1: 血清添加培地。2: 血清非添加培地。3, 4: 血清非添加培地+ニブラジロール。5, 6: 血清非添加培地+脱ニトロ・ニブラジロール。7: 非標識プローブを大量に添加したコントロール。(文献4)より引用)

preventing the activation of caspase-3 via S-nitrosylation and the cGMP-dependent pathway. *Eur J Pharmacol* 452: 263-268, 2002

- 5) Ando, A et al: Cytoprotection by nibradilol, an anti-glaucomatous agent, via down-regulation of apoptosis related gene expression and activation of NF- κ B. *Exp Eye Res* 80: 501-507, 2005

Chapter III

**PREVENTION OF APOPTOSIS BY DOWN-
REGULATION OF APOPTOSIS RELATED GENE
EXPRESSION OBTAINED BY NIPRADILOL VIA
NITRIC OXIDE DONATIVE ACTION**

Akira Ando^{1,}, Shiho Kaneko¹, Naoko Kiriyama¹, Sawako Unezaki²,
Emiko Okuda-Ashitaka², Tadayoshi Okumura², Tetsuya Nishimura¹,
Miyo Matsumura¹ and Seiji Ito²*

Departments of ¹Ophthalmology and ²Medical Chemistry, Kansai Medical University
10-15 Fumizono-cho, Moriguchi, Osaka 570-8507, Japan.

ABSTRACT

Apoptosis is a programmed cell death that plays an important role in the physiological process of development in animals and plants, and has also been reported to be involved in the pathogenesis and pathophysiology of various diseases. Glaucoma is a progressive optic neuropathy related to apoptosis that finally leads to blindness. Patients with the disease exhibit characteristic visual field loss and a large cupping of the optic nerve head due to glaucoma-specific deterioration of the retinal nerve fibers, which consist of retinal ganglion cell axons, in association with elevated intraocular pressure (IOP). It has also been reported that apoptosis of the retinal ganglion cells is a cause of the disease. The relationships between neuro-retinal tissue damage and apoptosis have been investigated and clarified in several experimental models, such as N-methyl-D-aspartate (NMDA)-induced retinal damage and secondary cell death caused by transection of the optic nerve, as well as in ocular hypertensive rats. Thus, the prevention of apoptosis in retinal ganglion cells is considered to be a novel strategy for treatment of

* Correspondence concerning this article should be addressed to Dr. Akira Ando, M.D., Ph. D. Department of Ophthalmology, Kansai Medical University 10-15 Fumizono-cho, Moriguchi, Osaka 570-8507, Japan. Tel: +81-6-6992-1001 (ext. 3324); Fax: +81-6-6993-2222.

glaucoma. Nipradilol [3,4-dihydro-8-(2-hydroxy-3-isopropyl-amino)-propoxy-3-nitroxy-2H-1-benzopyran] is a nonselective β - and selective α_1 - adrenoceptor antagonist that is used as an anti-glaucomatous agent due to its ability to lower IOP. Recently, it was reported that nipradilol had a cytoprotective effect toward neuronal cells by its nitric oxide (NO) donative action. NO has been shown to regulate apoptosis in both positive and negative directions in several experimental models, and many reports have shown that NO inhibits apoptosis by increasing caspase-3-like activity and cGMP-mediated mechanisms, as well as by inhibiting Bcl-2 cleavage and cytochrome *c* release *in vitro*. Further, the gene expressions of some apoptosis associated factors are also regulated by the activity of the transcription factor nuclear factor- κ B (NF- κ B). However, whether nipradilol regulates the expression of apoptosis associated genes and/or NF- κ B activity remains unclear. We found that nipradilol down-regulated Bax, Caspase-9, and Smac/DIABLO gene expression using a real-time polymerase chain reaction method, while increased levels of translocation of NF- κ B into nuclei were shown using an electrophoresis mobility shift assay of PC12 cells during apoptosis induced by serum deprivation. Activation of NF- κ B was seen prior to the alterations of gene expression, therefore, the down-regulation of some apoptosis related genes in PC12 cells by nipradilol may be the result of NF- κ B activation. Our results suggest that nipradilol regulates apoptosis associated gene expression as well as the translocation of NF- κ B into nuclei as a means of apoptosis prevention via NO donative activities. Control of apoptosis is expected to be an important goal of new therapies for apoptosis related diseases.

Keywords: nuclear factor- κ B, nitric oxide, cytoprotection, nipradilol, apoptosis

CLINICAL BACKGROUND

Apoptosis is a programmed cell death that plays important roles in the physiological process of development in animals and plants, and has also been reported to be involved in the pathogenesis and pathophysiology of various diseases. Various signals and factors contribute to apoptosis, and activation or inactivation of various molecules, including Bax, Bcl2, and caspases that form a complicated pathway, promotes or inhibits apoptosis. Control of apoptosis is expected to be an important goal of new therapies for apoptosis related diseases. In the field of ophthalmology, glaucoma is a progressive optic neuropathy that is associated with apoptosis in its pathophysiology, and has been associated with the mechanism of deterioration of the retinal nerve fiber and retinal ganglion cells in an experimental glaucoma model [1], as well as glaucoma patients [2,3]. This disease is a leading cause of blindness and the characteristic symptom is a progressive visual field defect due to damage of retinal nerve fibers accompanied by a decrease in glial tissue, which is observed as enlargement of cupping of the optic nerve head. The number of retinal nerve fibers in normal adults is approximately 1.2 million, and it has been reported that by the time an afflicted individual person notices a visual field defect, approximately half of the retinal nerve fiber bundles are already damaged [4]. Various factors are considered to be causes of the progression of neuro-retinal deterioration in glaucoma, with intraocular pressure (IOP) known to be closely related to disease progression. Abnormally elevated IOP causes deprivation of nutritional factors, mechanical compression, ischemic cellular damage to

retinal ganglion cells, and dysfunction of the glutamic acid transporter, after which the axon filaments of the retinal ganglion cells become damaged. Presently, the only effective treatment for glaucoma is IOP reduction, even in cases with normal tension glaucoma that exhibit IOP levels within the normal range. Therefore, anti-glaucomatous drugs are used to reduce IOP in order to protect the retinal nerve fibers and retinal ganglion cells. Relationships between neural retinal tissue disorders and apoptosis have been demonstrated in some experimental models, such as a retinal degenerative disease model using N-methyl-D-aspartate (NMDA) [5], a delayed retinal cell death model created by incision of the optic nerve [6], and an ocular hypertensive rat model [7]. However, no evidence supporting another therapy beside IOP reduction has been presented, therefore, a pharmaceutical glaucoma treatment that displays anti-apoptosis and neuroprotective actions is an important goal of research.

NEURO-PROTECTION AND NITRIC OXIDE

It has been reported that nitric oxide (NO) is involved in apoptotic signal transduction, as NO regulates the process of apoptosis under certain conditions. Nitric oxide synthase (NOS) and its activities have been observed in the optic nerve head of glaucoma patients [8], as well as in the retina and front part of the uvea in rabbits [9]. NO inhibits apoptosis by preventing increases in caspase activity [10,11] and via cGMP signaling [12-14], as well as by inhibition of Bcl-2 cleavage and cytochrome *c* release from mitochondria [15], suggesting that it has a cytoprotective effect. When inducible NOS (iNOS) activity was inhibited in a glaucomatous rat model, retinal ganglion cell damage was inhibited, while it was also suggested that excessive NO produced by iNOS promoted retinal ganglion cell damage [16]. On the other hand, it has also been reported that an increase in NO synthase by α -lipoic acid may be involved in retinal protection [17]. Other studies have shown that NO plays an important role in neuro-retinal degeneration, including conditions other than glaucoma, and also clarified that NO contributes to apoptosis by both inhibition and acceleration in some experimental models [18-20].

Nipradilol (3,4-dihydro-8-(2-hydroxy-3-isopropyl-amino) propoxy-3-nitroso-2H-1-beozopyran) (HYPADIL Kowa[®]) is a nonselective β - and selective α_1 -adrenoceptor antagonist [21,22], that has been used as an anti-glaucomatous drug in Japan since 1999, due to its IOP reduction effect that inhibits aqueous production and accelerates aqueous drainage via uveoscleral outflow [23,24]. Recently, a neuro-protective effect of nipradilol via NO donative action was reported [5,6,25,26] owing to its nitroso moiety [27]. In addition, NO increases the expression of Bcl-2, and has been shown to activate the transcription factor nuclear factor-kappaB (NF- κ B) and regulate the gene expression of apoptosis related molecules. Tomita et al. [26] reported that a decrease in caspase-3 activity by nipradilol via S-nitrosylation and a cGMP-dependent pathway was implied in the mechanisms of cytoprotection in PC12 cells. Apoptosis is easily induced in PC12 cells by serum deprivation, which has been used to study glaucomatous neuro-retinal degeneration, even though the PC12 cell line was originally established from a rat pheochromocytoma. Kim et al. [14] reported that NO inhibited apoptosis by decreasing caspase-3-like activity via cGMP-

mediated mechanisms in PC12 cells. However, it has also been shown that NO alters apoptosis associated gene expression during the inhibition of apoptosis by elevation of Bcl-2 expression in splenic B lymphocytes [28]. In addition, the gene expressions of some apoptosis associated factors are also regulated by the activities of NF- κ B [29-32].

TRANSCRIPTION FACTOR NF- κ B

NF- κ B regulates the expression of genes coding various kinds of protein, including apoptosis-related molecules, and its activity has been shown to regulate apoptosis related gene expression in an anti-apoptotic direction in several cancer cell lines [29-32]. In contrast, when NF- κ B is inactivated, Bax gene expression is up-regulated and Bcl-2, A1, and cIAP-2 gene expression is down-regulated, resulting in the induction of apoptosis [32]. From the results of experiments using a cancer cell line, suppression of NF- κ B activity was demonstrated during anoxia induced apoptosis, while NF- κ B was reactivated, the gene expression of Bcl-2 and Bcl-x was up-regulated, and Bax gene expression was down-regulated by reoxygenation [30]. Thus, NF- κ B contributes to apoptosis by controlling the gene expression of various molecules, though the mechanism remains to be elucidated.

EXPERIMENTAL BACKGROUND

It was previously reported that nipradilol and NO decreased the activity of caspase-3 with S-nitrosylation via a pathway by which the cGMP cascade inhibits apoptosis [26], though it remains unclear whether nipradilol regulates apoptosis related genes or NF- κ B activity. Therefore, we attempted to clarify the effects of nipradilol on the expression of apoptosis associated genes and activation of NF- κ B in PC12 cells during apoptosis induced by serum deprivation, a well-established *in vitro* model of apoptosis, in order to investigate the mechanism of the neuronal cytoprotective effect of nipradilol. We found that nipradilol inhibited the expression of apoptosis related genes via an NO donative action and activation of NF- κ B. Next, we added different concentrations of nipradilol and denitronipradilol, the latter which cancels the influence of NO donative action due to lack of nitroxy moiety, and incubated the cells for 12, 24, and 48 hours to examine the effects on cell viability as well as ladder formation of genomic DNA using agarose gel electrophoresis. In addition, we performed a quantitative real-time PCR assay and an electrophoresis mobility shift assay (EMSA) to investigate the gene expression of the apoptosis related molecules Bax, Bcl-2, Fas, FasL, Caspase-1, 2, 3 and 9, p53, and Smac/DIABLO, as well as the activity of transcription factor NF- κ B.

Cell Culture

The PC12 cell line, established from a rat pheochromocytoma, can be induced into apoptosis by culturing in serum-free culture media. Cells were cultured in RPMI1640

medium supplemented with 10% horse serum, 5% fetal bovine serum, 2 mM of L-glutamine, 100 U/ml of penicillin, and 100 mg/ml of streptomycin in an atmosphere of 5% CO₂/95% air at 37°C in a 75-cm² flask, and supplied with fresh medium every 3 days. When the cells reached sub-confluence, they were treated with 0.01% trypsin in a 0.002% EDTA solution, after which 1×10^5 cells were plated onto 6-well culture plates.

Cellular Viability Assay

To examine the effects of nipradilol on the viability of PC12 cells during serum-deprivation, the cells were incubated in serum-free medium for 12, 24, and 48 hours with or without 0.01, 0.1, 1, or 10 µM of nipradilol or denitronipradilol, after which the number of cells was counted using a hemocytometer.

Genomic DNA Ladder Formation Assay

Cells in another tube were lysed with 200 µl of lysis buffer (150 mM NaCl, 10 mM Tris-HCl, 10 mM EDTA, 0.1% SDS) and 20 µg of proteinase K for 2 hours at 55°C. DNA was extracted using 200 µl of neutralized phenol (pH 7.0) and treated with 10 µg of RNase A for 30 minutes at 37°C. DNA was extracted using neutralized phenol-chloroform-isoamyl alcohol (50:49:1), precipitated using isopropyl alcohol, and dissolved with 20 µl of Tris-EDTA buffer (pH 8.0). Genomic DNA was separated by electrophoresis on a 2% agarose gel to examine ladder formation.

Real-Time Polymerase Chain Reaction Method

The semi-quantitative real time polymerase chain reaction (PCR) method used was originally developed to quantitatively analyze and evaluate the gene expressions of various molecules [34]. With it, the intensity of SYBR green dye fluorescence is increased in proportion to the quantity of the product during a PCR reaction. The number of PCR reaction cycles during which the emission of fluorescence was strong was defined as the threshold cycle. We calculated the ratio to the threshold cycle using an internal standard that was ubiquitously and stably expressed without varying by condition, such as S16 or GAPD, and then evaluated the differences in threshold cycles between the samples. A difference of 1 cycle in the PCR reaction equaled a doubled gene expression between 2 samples. For example, Bax gene expression in PC12 cells cultured in serum-containing medium was 1, while it was doubled in cells cultured in serum-free medium and decreased by 1.08 times by culturing with 1 mM of nipradilol (Figure 5).

RNA Extraction and Real-Time Polymerase Chain Reaction for Apoptosis Related Genes

Cells were incubated in serum-free medium for 12, 24, or 48 hours with or without 0.1 or 1 μ M of nipradilol or denitronipradilol. After a brief washing with PBS 3 times, each sample was separated into 2 tubes. One tube was used for RNA extraction using TRIzol[®] according to the manufacturer's instructions. Briefly, cells were homogenized with 200 μ l of TRIzol[®], after which 40 μ l of chloroform was added and the mixture was shaken vigorously, followed by centrifugation at 12 000 rpm for 15 minutes. Total RNA was precipitated by isopropyl alcohol and then dissolved with 10 μ l of RNase-free water. The gene expressions of Bax, Bcl-2, Fas, FasL, Caspase-1, 2, 3, and 9, p53, and Smac/DIABLO were examined using a semi-quantitative real time PCR method. Total RNA (1 μ g) was reverse transcribed into cDNA. The first strand cDNA was amplified using Taq polymerase and anti-Taq antibody, with oligonucleotide primers specific for each molecule associated with apoptosis. The oligonucleotide primer sequences used for the PCR reactions are indicated in Table 1. The PCR conditions were as follows: hold at 94°C for 30 seconds, then 40 cycles of amplification (94°C for 1 minute, 60°C for 1 minute, 72°C for 1 minute) and a final extension at 72°C for 5 minutes. The presence of corresponding PCR products was determined by electrophoresis on a 2% agarose gel in 1x Tris-acetate-EDTA buffer.

Table 1. Primer sequences used for real-time PCR

Bax	forward 5'- TGCAGAGGATGATTGCTGAC -3' reverse 5'- GGAGGAAGTCCAGTGTCCAG -3'
Bcl-2	forward 5'- CGACTTTGCAGAGATGTCCA -3' reverse 5'- CATCCACAGAGCGATGTTGT -3'
Caspase-1	forward 5'- GTGGTTCCTCAAGTTTTGC -3' reverse 5'- TGCAGCAGCAACTTCATTTTC -3'
Caspase-2	forward 5'- CACCCTCTTCAAGCTTTTGG -3' reverse 5'- AACCTCTTGGAGCTGAAGCA -3'
Caspase-3	forward 5'- TACTCTACCGCACCCGGTTA -3' reverse 5'- CGGGATCTGTTTCTTTGCAT -3'
Caspase-9	forward 5'- TTTGAGGTGGCCTTCACTTC -3' reverse 5'- CAGGAACCGCTCTTCTTGTC -3'
Fas	forward 5'- CTCTTAGGGGGAACCTTTGC -3' reverse 5'- GACGGTCATCCCTCAAAGAA -3'
Fas-L	forward 5'- ATCATGAGCCAGATGGGAAG -3' reverse 5'- CTAAAAGACGGCCTCCTGTG -3'
p53	forward 5'- GTCTACGTCCCGCCATAAAA -3' reverse 5'- AGGCAGTGAAGGGACTAGCA -3'
Smac/DIABLO	forward 5'- CTCGGAGCGTAACCTTTCTG -3' reverse 5'- TCCTCATCAGTGCTTCGTTG -3'
S16	forward 5'- CACTGCAAACGGGAAATGG-3' reverse 5'- TGAGATGGACTGTCGGATGG

Electrophoresis Mobility Shift Assay (EMSA)

Translocation into nuclei of NF- κ B was examined using an EMSA according to the method reported by Schreiber et al. [33]. This method was used to visualize the translocation of NF- κ B in order to evaluate NF- κ B activity by electrophoresis using a polyacrylamide gel with a 32 P labeled NF- κ B consensus sequenced DNA probe. Briefly, PC12 cells were incubated for 2 hours with or without 0.1 or 1 μ M of nipradilol or denitronipradilol, followed by a brief washing with Tris-buffered saline (TBS, pH 7.4) 3 times on ice, after which they were collected with 0.5 ml of TBS. The cells were then lysed with 400 μ l of lysis buffer [10 mM HEPES-KOH (pH 7.9), 10 mM KCl, 0.1 mM ethylene diamine tetracetic acid (EDTA), 0.1 mM ethylene glycol tetracetic acid (EGTA), 500 U/ml Trasylol, 1 mM dithiothreitol (DTT), and 0.5 mM phenylmethylsulfonyl fluoride (PMSF)], after which 25 μ l of 10% Nonidet P-40 was added. The tubes were then shaken vigorously for 1 minute at room temperature, followed by centrifugation at 15 000 rpm for 1 minute. The nuclear pellet was dissolved with 75 μ l of lysis buffer (20 mM HEPES-KOH, 400 mM NaCl, 1 mM EDTA, 1 mM EGTA, 500 U/ml Trasylol, 1 mM DTT, 0.5 mM PMSF) and shaken vigorously for 20 minutes at 4°C. After centrifugation at 15 000 rpm for 5 minutes at 4°C, the nuclear extract was collected into a new tube. Each nuclear extract containing 4 μ g of protein was analyzed by electrophoresis on a 4.8% Tris-glycine-EDTA (TGE) polyacrylamide gel. For competition experiments, a cold NF- κ B probe (without 32 P labeling, 250-fold of 32 P-labeled probe) was added. The gels were dried using a gel dryer for 1 hour at 80°C and then exposed to X-ray film.

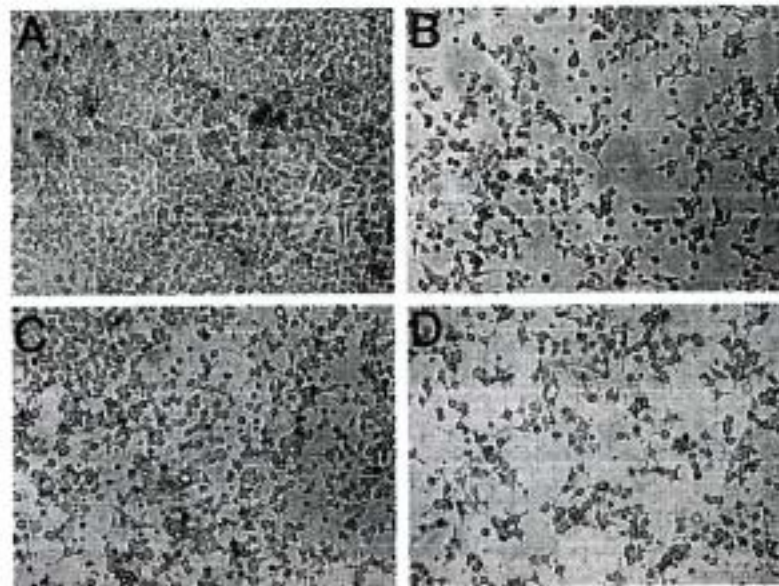


Figure 1. As compared to the serum-added control (A), PC12 cells were damaged and detached from the culture substrate of the dish at 48 hours after serum deprivation (B). The damage was limited by the addition of 0.1 μ M of nipradilol (C), while denitronipradilol (0.1 μ M) showed no effects (D). Phase-contrast photomicrographs, original magnification x 100.

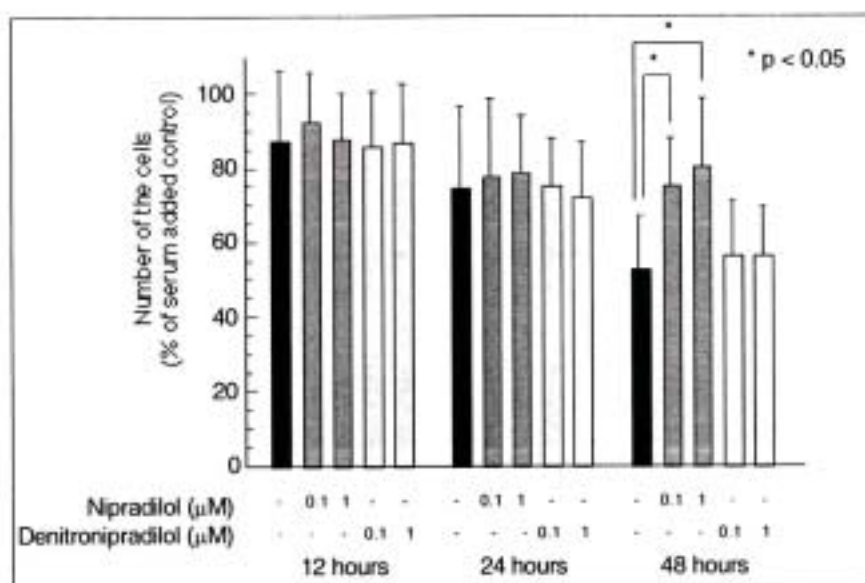


Figure 2. Following serum deprivation for 48 hours (closed column), the number of cells was reduced to approximately half that of the serum-added control. Nipradilol prevented the decrease in number of cells (hatched column) ($p = 0.0285$ at $0.1 \mu\text{M}$ and $p = 0.0235$ at $1 \mu\text{M}$), while denitronipradilol showed no effect (dotted column).

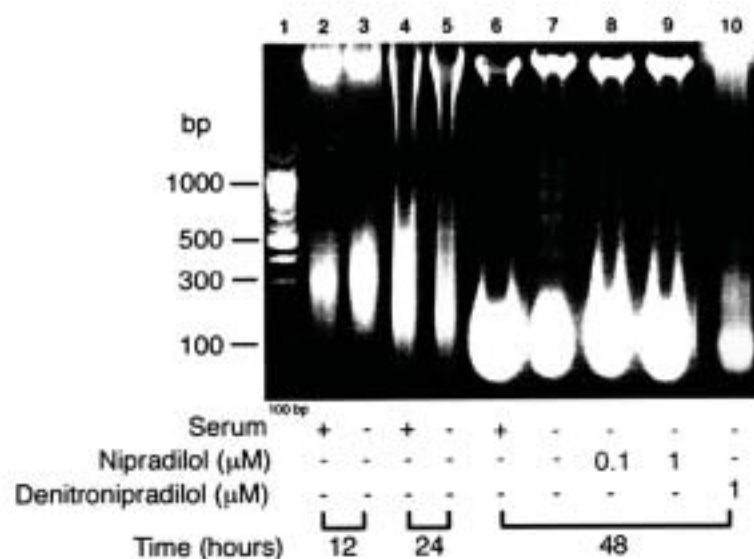


Figure 3. Genomic DNA ladder formation was clearly observed in PC12 cells at 48 hours after serum deprivation (lane 7), though not at 12 or 24 hours (lanes 3 and 5), or in the serum-added control (lanes 2, 4, and 6), as shown by 2% agarose gel electrophoresis. Nipradilol (0.1 and $1 \mu\text{M}$, lanes 8 and 9, respectively) decreased ladder formation at 48 hours, whereas denitronipradilol ($1 \mu\text{M}$, lane 10) did not. Lane 1 shows the 100-bp DNA size marker. Each image is representative of 3 independent experiments.

RESULTS

Nipradilol Restores PC12 Cells Induced to Apoptosis in by Serum Deprivation

After 48 hours, the number of cells in the serum-free samples (Figure 1B) was significantly lower as compared to the serum-added controls (Figure 1A). Nipradilol (0.1 μM) (Figure 1C), but not denitronipradilol (Figure 1D), increased the number of cells after 48 hours of incubation without serum ($p = 0.0285$ at 0.1 μM and $p = 0.0235$ at 1 μM) (Figure 2). Genomic DNA ladder formation was clearly observed between approximately 300 and 1200 bp at 48 hours (Figure 3, lane 7), though not at 12 or 24 hours (Figure 3, lanes 3 and 5), using 2% agarose gel electrophoresis, and was suppressed at 48 hours by the addition of 0.1 or 1 μM of nipradilol (Figure 3, lanes 8 and 9). Nipradilol (0.01 and 10 μM) did not exhibit a significant effect on PC12 cell viability or genomic DNA ladder formation (data not shown), while denitronipradilol showed no inhibitory effect toward DNA ladder formation (Figure 3, lane 10).

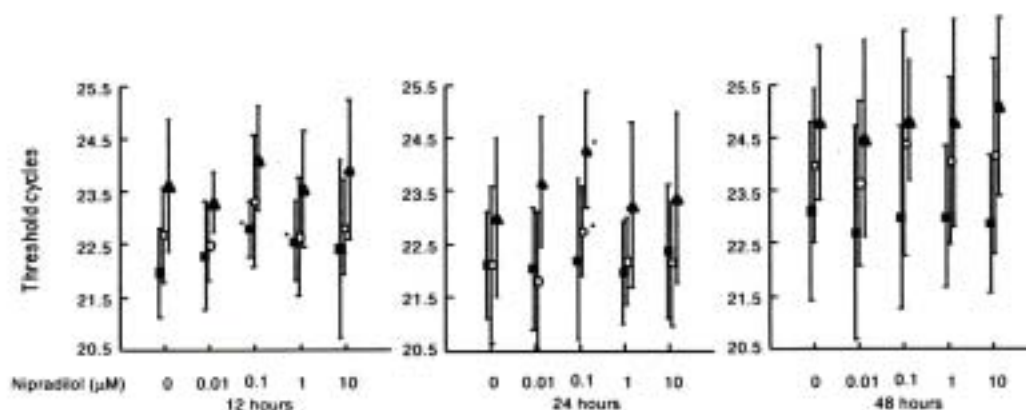


Figure 4. Comparison of threshold cycles using a real-time PCR method. Values were corrected by the S16 gene (internal control) in each experimental series. The number of threshold cycles that indicated Bax (■) gene expression in the cells was significantly increased with the addition of 0.1 and 1 μM of nipradilol in serum-free medium at 12 hours, while 0.1 μM of nipradilol in serum-free medium significantly increased that of Caspase-9 (○) and Smac/DIABLO (▲) at 24 hours (* $p < 0.05$).

Down-Regulation of Bax, Caspase-9, and Smac/DIABLO Gene Expression by Nipradilol

Figure 4 shows a comparison of threshold cycle values. Our results indicated that Bax gene expression was significantly increased ($p < 0.05$) in samples incubated with 0.1 and 1 μM of nipradilol in serum-free medium at 12 hours, and Caspase-9 and Smac/DIABLO gene expressions were also significantly increased ($p < 0.05$) in samples incubated with 0.1 μM of nipradilol in serum-free medium for 24 hours. Table 2 indicates the effects of nipradilol on apoptosis associated gene expression levels in PC12 cells during serum deprivation using

quantitative real time PCR. Each value shows the ratio of gene expression as compared to the serum-added controls. Nipradilol at 0.1 and 1 μM suppressed Bax gene expression to 0.96 and 1.07, respectively, as compared to the serum-free (1.88) and serum-added samples (1.00) after 12 hours (Table 2). Further, 0.1 μM of the agent suppressed Caspase-9 and Smac/DIABLO gene expressions to 0.77 and 0.52, respectively, compared to the serum-free (1.34 and 1.25, respectively) and serum-added samples (1.00) after 24 hours (Table 2). However, nipradilol did not exhibit any effects at the other concentrations and periods tested, and expressions of other genes examined in this experiment were not significantly affected (data not shown). In contrast, denitronipradilol did not have a statistically significant effect on the expressions of any of the genes examined in these experiments, including those that exhibited a significant change with nipradilol (Table 3).

Table 2. Effects of nipradilol on apoptosis associated gene expression (ratio to serum-free control, mean \pm SE).

Nipradilol (μM)	12 hours			24 hours			48 hours		
	0	0.1	1	0	0.1	1	0	0.1	1
Bax	1.88 ± 0.88	0.96* ± 0.34	1.07* ± 0.21	1.40 ± 0.99	1.06 ± 0.63	1.31 ± 0.58	1.16 ± 0.43	0.89 ± 0.13	1.19 ± 0.52
Bcl-2	1.25 ± 0.53	0.65 ± 0.38	0.78 ± 0.53	0.75 ± 0.43	0.71 ± 0.53	1.09 ± 0.72	0.68 ± 0.23	0.81 ± 0.51	0.62 ± 0.47
Caspase-1	1.06 ± 0.71	1.72 ± 1.23	1.20 ± 1.14	1.17 ± 1.52	0.89 ± 1.05	1.46 ± 1.68	1.94 ± 1.64	2.71 ± 3.56	2.98 ± 2.81
Caspase-2	1.15 ± 0.75	0.43 ± 0.41	0.86 ± 0.56	0.98 ± 0.63	0.72 ± 0.63	1.60 ± 1.23	1.33 ± 0.66	1.05 ± 0.58	0.59 ± 0.32
Caspase-3	0.76 ± 0.16	0.39 ± 0.25	0.72 ± 0.24	1.35 ± 0.62	0.71 ± 0.38	1.07 ± 0.71	1.52 ± 1.32	1.13 ± 0.42	1.66 ± 1.62
Caspase-9	0.82 ± 0.10	0.42 ± 0.25	0.86 ± 0.26	1.34 ± 0.42	0.77* ± 0.45	1.18 ± 0.54	1.08 ± 0.38	0.80 ± 0.28	0.87 ± 0.49
Fas	1.01 ± 0.68	1.38 ± 1.66	2.22 ± 2.12	1.65 ± 1.31	1.74 ± 1.37	2.47 ± 2.40	2.06 ± 1.44	0.84 ± 0.47	1.31 ± 1.16
FasL	0.72 ± 0.49	1.40 ± 1.87	0.97 ± 0.85	1.13 ± 1.15	1.05 ± 0.86	1.75 ± 1.05	1.48 ± 1.10	1.07 ± 0.73	1.32 ± 0.73
p53	1.36 ± 0.31	1.25 ± 0.58	1.32 ± 0.44	1.00 ± 0.20	0.79 ± 0.17	1.23 ± 0.46	1.11 ± 0.33	1.17 ± 0.23	1.58 ± 0.98
Smac/DIABLO	1.20 ± 0.51	0.71 ± 0.51	1.23 ± 0.59	1.25 ± 0.34	0.52* ± 0.25	1.06 ± 0.31	1.28 ± 0.51	1.14 ± 0.29	1.31 ± 0.79

(n=4, * p < 0.05, ANOVA)

Table 3. Effects of denitronipradilol on apoptosis associated gene expression (ratio to serum-added control, mean \pm SE).

Denitronipradilol (μM)	12 hours			24 hours		
	0	0.1	1	0	0.1	1
Bax	1.47 \pm 0.42	1.24 \pm 0.34	1.59 \pm 0.38	1.33 \pm 0.45	1.72 \pm 0.68	1.46 \pm 0.65
Caspase-9	0.79 \pm 0.12	0.79 \pm 0.20	0.85 \pm 0.27	0.90 \pm 0.18	0.84 \pm 0.40	1.09 \pm 0.57
Smac/DIABLO	0.89 \pm 0.27	0.90 \pm 0.2	0.71 \pm 0.35	0.86 \pm 0.22	0.61 \pm 0.35	0.80 \pm 0.27

(n=3)

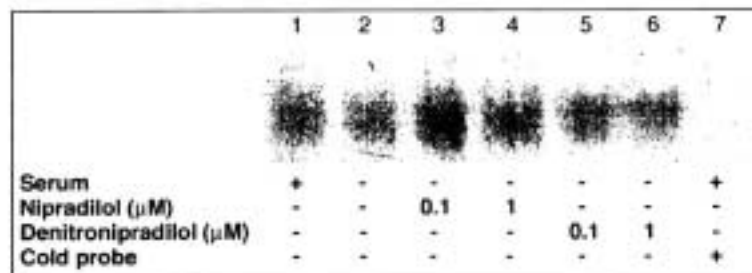


Figure 5. Results of electrophoresis mobility shift assays showing that the activity of NF- κ B was slightly suppressed by serum deprivation after 2 hours (lane 2), as compared to the serum-added sample (lane 1). Nipradilol (0.1 and 1 μM , lanes 3 and 4, respectively) increased NF- κ B activity, whereas denitronipradilol (0.1 and 1 μM , lanes 5 and 6, respectively) had no effect. Further, the band intensity was diminished by use of an excessive cold probe (lane 7). Each image is representative of 3 independent experiments.

Translocation into Nuclei of NF- κ B Increased by Nipradilol

Figure 5 shows the EMSA results, which indicate that constitutive NF- κ B activity in PC12 cells (lane 1) was slightly suppressed by serum deprivation after 2 hours (lane 2). Further, nipradilol (0.1 and 1 μM) increased the translocation into nuclei of NF- κ B (lane 3, 4) as compared to the serum-free controls at 2 hours (lane 2), whereas denitronipradilol had no effect (lanes 5, 6). Further, an excessive cold probe diminished the intensity of the band (lane 7).

CONCLUSION

Glaucoma patients exhibit visual field loss and a large cupping of the optic nerve head due to disease-specific deterioration of the retinal nerve fibers, which consist of axons of ganglion cells. Elevated IOP may be involved in the pathogenesis of glaucoma and might induce trophic factor deprivation, mechanical and/or ischemic lesions, as well as glutamate transporter dysfunction, finally resulting in apoptosis of ganglion cells. Recently, apoptosis was reported to be involved in the pathogenesis of glaucoma, which has been shown to cause damage to the retinal nerve fibers in an experimental glaucoma model and clinical investigations of glaucoma patients [1-3]. In addition, the relationship between neuro-retinal deterioration and apoptosis has been examined and clarified in several experimental models, such as with N-methyl-D-aspartate (NMDA)-induced retinal damage [5], secondary cell death caused by transection of the optic nerve [6], and ocular hypertensive rat models [7].

NO plays a crucial role in neuro-retinal degeneration, including that involved with glaucoma [8,16,34-36]. It has also been reported that NO regulated apoptosis in both positive and negative directions in several experimental models [18-20], while many authors found that NO inhibited apoptosis by decreasing caspase-3-like activity and cGMP-mediated mechanisms, as well inhibited Bcl-2 cleavage and cytochrome c release *in vitro* [10-15]. Nipradilol down-regulates Bax, Caspase-9, and Smac/DIABLO gene expressions, and

increases the translocation of NF- κ B into the nuclei of PC12 cells during apoptosis induced by serum deprivation [37]. Bax induces apoptosis by contributing to the breakdown of mitochondrial potential, through formation of an integral part of the anionic pores in the mitochondrial membrane [38]. Caspase-9, which is localized in the intermembrane space of mitochondria, appears to play a pivotal role in the downstream activation of other caspases [39]. Further, Smac/DIABLO is a mitochondrial protein that is released together with cytochrome c during apoptosis and promotes cytochrome c-dependent caspase activation by neutralizing the inhibitor of apoptosis proteins (IAPs) [40,41]. Together with the results of those previous studies, our findings suggest that nipradilol plays roles at various points of the apoptosis pathway, such as inhibition of Caspase-3 and gene expression, especially around the mitochondria.

NF- κ B exists ubiquitously in the cytoplasm of cells where it is combined with I κ B in an inactivated form. When an apoptosis signal comes to the cell surface, apoptotic signal transduction begins, and phosphorylation of I κ B disassembles the NF- κ B/I κ B combined construct and activated NF- κ B shifts to the nucleus. Activated NF- κ B regulates the transcription of messenger RNA that finally leads to protein production of various genes, which involves apoptosis-related genes that exist downstream of the signal transduction cascade. NF- κ B activity has been shown to regulate apoptosis related gene expression in an anti-apoptotic direction in several cancer cell lines [29-32]. Further, Poulaki et al. [32] reported that inhibition of constitutive NF- κ B activity up-regulated Bax, whereas it down-regulated Bcl-2, A1, and cIAP-2, resulting in apoptosis induction. It was also reported that activation and inhibition of NF- κ B down- and up-regulated, respectively, Bax gene expression in several cancer cell lines [31,32], while activation of NF- κ B up-regulated both Bcl-2 and Bcl-x during apoptosis induced by hypoxia followed by reoxygenation [30]. In the present study, activation of NF- κ B was seen prior to the alteration of gene expression, therefore, the down-regulation of some apoptosis related genes in PC12 cells by nipradilol might have been because of that activation. Also, NO may be located upstream of the process of activation of NF- κ B.

Our results suggest that the NO donative action of nipradilol is critical for the prevention of serum deprivation induced apoptosis, down-regulation of apoptosis related gene expression, and increase of translocation of NF- κ B into nuclei, whereas denitronipradilol did not exhibit any of those effects. Although further experiments are required, the present findings imply that nipradilol has an effect on apoptosis associated gene expression and translocation of NF- κ B into nuclei during the prevention of apoptosis via NO donative action.

ACKNOWLEDGEMENTS

This study was supported in part by a grant from Kowa Company, Ltd. (Nagoya, Japan).

REFERENCES

- [1] Quigley H.A., Nickells R.W., Kerrigan L.A., Pease M.E., Thibault D.J., Zack D.J., 1995. Retinal ganglion cell death in experimental glaucoma and after axotomy occurs by apoptosis. *Invest. Ophthalmol. Vis. Sci.* 36, 774-786.
- [2] Kerrigan L.A., Zack D.J., Quigley H.A., Smith S.D., Pease M.E., 1997. TUNEL-positive ganglion cells in human primary open-angle glaucoma. *Arch. Ophthalmol.* 115, 1031-1035.
- [3] Nickells R.W., 1999. Apoptosis of retinal ganglion cells in glaucoma: an update of the molecular pathways involved in cell death. *Surv. Ophthalmol.* 43 Suppl 1, S151-61.
- [4] Quigley H.A., Addicks E.M., Green W.R., Maumenee A.E., 1981. Optic nerve damage in human glaucoma. II. The site of injury and susceptibility to damage. *Arch. Ophthalmol.* 99, 635-649.
- [5] Mizuno K., Koide T., Yoshimura M., Araie M., 2001. Neuroprotective effect and intraocular penetration of nipradilol, a beta-blocker with nitric oxide donative action. *Invest. Ophthalmol. Vis. Sci.* 42, 688-694.
- [6] Nakazawa T., Tomita H., Yamaguchi K., Sato Y., Shimura M., Kuwahara S., Tamai M., 2002. Neuroprotective effect of nipradilol on axotomized rat retinal ganglion cells. *Curr. Eye Res.* 24, 114-122.
- [7] McKinnon S.J., Lehman D.M., Kerrigan-Baumrind L.A., Merges C.A., Pease M.E., Kerrigan D.F., Ransom N.L., Tahzib N.G., Reitsamer H.A., Levkovitch-Verbin H., Quigley H.A., Zack D.J., 2002. Caspase activation and amyloid precursor protein cleavage in rat ocular hypertension. *Invest. Ophthalmol. Vis. Sci.* 43, 1077-1087.
- [8] Neufeld A.H., Hernandez M.R., Gonzalez M., 1997. Nitric oxide synthase in the human glaucomatous optic nerve head. *Arch. Ophthalmol.* 115, 497-503.
- [9] Osborne N.N., Barnett N.L., Herrera A.J., 1993. NADPH diaphorase localization and nitric oxide synthetase activity in the retina and anterior uvea of the rabbit eye. *Brain Res.* 610, 194-198.
- [10] Kim Y.M., Talanian R.V., Billiar T.R., 1997. Nitric oxide inhibits apoptosis by preventing increases in caspase-3-like activity via two distinct mechanisms. *J. Biol. Chem.* 272, 31138-31148.
- [11] Thippeswamy T., McKay J.S., Morris R., 2001. Bax and caspases are inhibited by endogenous nitric oxide in dorsal root ganglion neurons in vitro. *Eur. J. Neurosci.* 14, 1229-1236.
- [12] Farinelli S.E., Park D.S., Greene L.A., 1996. Nitric oxide delays the death of trophic factor-deprived PC12 cells and sympathetic neurons by a cGMP-mediated mechanism. *J. Neurosci.* 16, 2325-2334.
- [13] Estevez A.G., Spear N., Thompson J.A., Cornwell T.L., Radi R., Barbeito L., Beckman J.S., 1998. Nitric oxide-dependent production of cGMP supports the survival of rat embryonic motor neurons cultured with brain-derived neurotrophic factor. *J. Neurosci.* 18, 3708-3714.
- [14] Kim Y.M., Chung H.T., Kim S.S., Han J.A., Yoo Y.M., Kim K.M., Lee G.H., Yun H.Y., Green A., Li J., Simmons R.L., Billiar T.R., 1999. Nitric oxide protects PC12

- cells from serum deprivation-induced apoptosis by cGMP-dependent inhibition of caspase signaling. *J. Neurosci.* 19, 6740-6747.
- [15] Kim Y.M., Kim T.H., Seol D.W., Talanian R.V., Billiar T.R., 1998. Nitric oxide suppression of apoptosis occurs in association with an inhibition of Bcl-2 cleavage and cytochrome c release. *J. Biol. Chem.* 273, 31437-31441.
- [16] Neufeld A.H., Kawai S., Das S., Vora S., Gachie E., Connor J.R., Manning P.T., 2002. Loss of retinal ganglion cells following retinal ischemia: the role of inducible nitric oxide synthase. *Exp. Eye Res.* 75, 521-528.
- [17] Chidlow G., Schmidt K.G., Wood J.P.M., Melena J., Osborne N.N., 2002. α -lipoic acid protects the retina against ischemia-reperfusion. *Neuropharmacology* 43, 1015-1025.
- [18] Lipton S.A., Choi Y.B., Pan Z.H., Lei S.Z., Chen H.S., Sucher N.J., Loscalzo J., Singel D.J., Stamler J.S., 1993. A redox-based mechanism for the neuroprotective and neurodestructive effects of nitric oxide and related nitroso-compounds. *Nature* 364, 626-632.
- [19] Kashii S., Mandai M., Kikuchi M., Honda Y., Tamura Y., Kaneda K., Akaike A., 1996. Dual actions of nitric oxide in N-methyl-D-aspartate receptor-mediated neurotoxicity in cultured retinal neurons. *Brain Res.* 711, 93-101.
- [20] Kim Y.M., Bombeck C.A., Billiar T.R., 1999. Nitric oxide as a bifunctional regulator of apoptosis. *Circ. Res.* 84, 253-256.
- [21] Uchida Y., Nakamura M., Shimizu S., Shirasawa Y., Fujii M., 1983. Vasoactive and β -adrenoceptor blocking properties of 3,4-dihydro-8-(2-hydroxy-3-isopropylamino)propoxy-3-nitroxy-2H-1-benzopyran (K-351), a new antihypertensive agent. *Arch. Int. Pharmacodyn. Ther.* 262, 132-149.
- [22] Ohira A., Wada Y., Fujii M., Nakamura M., Kasuya Y., Hamada Y., Shigenobu K., 1985. Effects of nipradilol (K-351) on alpha-adrenoceptor mediated responses in various isolated tissues. *Arch. Int. Pharmacodyn. Ther.* 278, 61-71.
- [23] Kanno M., Araie M., Tomita K., Sawanobori K., 1998. Effects of topical nipradilol, a beta-blocking agent with alpha-blocking and nitroglycerin-like activities, on aqueous humor dynamics and fundus circulation. *Invest. Ophthalmol. Vis. Sci.* 39, 736-743.
- [24] Kanno M., Araie M., Koibuchi H., Masuda K., 2000. Effects of topical nipradilol, a beta-blocking agent with alpha-blocking and nitroglycerin-like activities, on intraocular pressure and aqueous dynamics in humans. *Br. J. Ophthalmol.* 84, 293-299.
- [25] Kashiwagi K., Iizuka Y., Tsukahara S., 2002. Neuroprotective effects of nipradilol on purified cultured retinal ganglion cells. *J. Glaucoma* 11, 231-238.
- [26] Tomita H., Nakazawa T., Sugano E., Abe T., Tamai M., 2002. Nipradilol inhibits apoptosis by preventing the activation of caspase-3 via S-nitrosylation and the cGMP-dependent pathway. *Eur. J. Pharmacol.* 452, 263-268.
- [27] Adachi T., Hori S., Miyazaki K., Takahashi E., Nakagawa M., Udagawa A., Hayashi N., Aikawa N., Ogawa S., 1995. Rapid increase in plasma nitrite concentration following intravenous administration of nipradilol. *Eur. J. Pharmacol.* 286, 201-204.
- [28] Genaro A.M., Hortelano S., Alvarez A., Martinez C., Bosca L., 1995. Splenic B lymphocyte programmed cell death is prevented by nitric oxide release through mechanisms involving sustained Bcl-2 levels. *J. Clin. Invest.* 95, 1884-1890.

- [29] Wang C.Y., Mayo M.W., Baldwin Jr A.S., 1996. TNF- and cancer therapy-induced apoptosis: potentiation by inhibition of NF-kappaB. *Science* 274, 784-787.
- [30] Tamatani M., Mitsuda N., Matsuzaki H., Okado H., Miyake S., Vitek M.P., Yamaguchi A., Tohyama M., 2000. A pathway of neuronal apoptosis induced by hypoxia/reoxygenation: Roles of nuclear factor-kB and Bcl-2. *J. Neurochem.* 75, 683-693.
- [31] Bentires-Alj M., Dejardin E., Viatour P., Van Lint C., Froesch B., Reed J.C., Merville M.P., Bours V., 2001. Inhibition of the NF-kB transcription factor increases Bax expression in cancer cell lines. *Oncogene* 20, 2805-2813.
- [32] Poulaki V., Mitsiades C.S., Jousseaume A.M., Lappas A., Kirchoff B., Mitsiades N., 2002. Constitutive nuclear factor-kB activity is crucial for human retinoblastoma cell viability. *Am. J. Pathol.* 161, 2229-2240.
- [33] Schreiber E., Matthias P., Muller M.M., Schaffner W., 1989. Rapid detection of octamer binding proteins with 'mini-extracts', prepared from a small number of cells. *Nucleic Acids Res.* 17, 6419.
- [34] Goldstein I.M., Ostwald P., Roth S., 1996. Nitric oxide: a review of its role in retinal function and disease. *Vision Res.* 36, 2979-2994.
- [35] Vorwerk C.K., Hyman B.T., Miller J.W., Husain D., Zurakowski D., Huang P.L., Fishman M.C., Dreyer E.B., 1997. The role of neuronal and endothelial nitric oxide synthase in retinal excitotoxicity. *Invest. Ophthalmol. Vis. Sci.* 38, 2038-2044.
- [36] Neufeld A.H., Sawada A., Becker B., 1999. Inhibition of nitric-oxide synthase 2 by aminoguanidine provides neuroprotection of retinal ganglion cells in a rat model of chronic glaucoma. *Proc. Natl. Acad. Sci. USA.* 96, 9944-9948.
- [37] Ando, A et al: Cytoprotection by nipradilol, an anti-glaucomatous agent, via down-regulation of apoptosis related gene expression and activation of NF-kappaB. *Exp Eye Res* 80: 501-507, 2005
- [38] Antonsson B., Conti F., Ciavatta A., Montessuit S., Lewis S., Martinou I., Bernasconi L., Bernard A., Mermoud J.J., Mazzei G., Maundress K., Gambale F., Sadoul R., Martinou J.C., 1997. Inhibition of Bax channel-forming activity by BCL-2. *Science* 277, 370-372.
- [39] Slee E.A., Harte M.T., Kluck R.M., Wolf B.B., Casiano C.A., Newmeyer D.D., Wang H.G., Reed J.C., Nicholson D.W., Alnemri E.S., Green D.R., Martin S.J., 1999. Ordering the cytochrome c-initiated caspase cascade: hierarchical activation of caspases-2-3-6-7-8, and -10 in a caspase-9-dependent manner. *J. Cell Biol.* 144, 281-292.
- [40] Du C., Fang M., Li Y., Li L., Wang X., 2000. Smac, a mitochondrial protein that promotes cytochrome c-dependent caspase activation by eliminating IAP inhibition. *Cell.* 102, 33-42.
- [41] Verhagen A.M., Ekert P.G., Pakusch M., Silke J., Connolly L.M., Reid G.E., Moritz R.L., Simpson R.J., Vaux D.L., 2000. Identification of DIABLO, a mammalian protein that promotes apoptosis by binding to and antagonizing IAP proteins. *Cell.* 102, 43-53.

研究成果報告書

研究課題名	内耳有毛細胞の再生と機能回復に関する研究		
(英文)	Elucidation of the regeneration and the functional recovery of hair cells in the inner ear		
事業推進者	友田 幸一	E-mail	tomodak@hirakata.kmu.ac.jp
所属・職名	医学研究科・聴覚再生医学（耳鼻咽喉科学）講座・教授		
研究分担者名	八木 正夫、河本 光平、泉川 雅彦		
キーワード	内耳再生、有毛細胞、聴覚路、遺伝子導入		
<p>1. 概要</p> <p>感音難聴は主に内耳有毛細胞の消失による内耳障害によって起こるとされている。一旦失われた有毛細胞は自然に再生することができないため、有毛細胞消失による高度感音難聴は不可逆性であり半永久的に存続する。このような疾患は根治的治療が望めず、患者のQOLを著しく損なうことになる。そこで損失した聴力を回復させるには、聴覚機能を持つ有毛細胞を再生させる事が必要になると考えられる。本研究は内耳有毛細胞の再生と機能回復により感音難聴治療研究を推進することを目指す。</p> <p>2. 研究の背景と目的</p> <p>急性期の感音難聴は保存的治療にて回復するものもあるが、慢性期あるいは高度感音難聴に対しては有効な治療法は確立されていない。わが国では約 600 万人、世界中では約 5 億人が感音難聴であるとされている。高度感音難聴の原因は内耳から聴覚伝導路まで広範囲に障害を及ぼすことから生じることがあるが、多くはコルチ器に存在する蝸牛感覚細胞（内、外有毛細胞）の変性、消失による部分が大きいとされる。その原因は加齢、感染、音響外傷、耳毒性薬物投与など様々である。1980 年代後半より鳥類蝸牛の有毛細胞再生研究が進められてきた。鳥類などの蝸牛有毛細胞は障害後、自然に再生するが、哺乳類の失われた有毛細胞は自然に再生しないため、有毛細胞が消失した感音難聴は不可逆性である。そこで、有毛細胞再生の基礎的研究が注目されてきた。哺乳類において一旦損失した聴力を回復させるためには、能動的に感覚有毛細胞を再生させることが必要となるため、生体外から細胞を移植する（幹細胞移植術）、生体内の細胞増殖を促す、あるいは生体内に存在する細胞を形質変換させるなどの方法が考えられる。本研究は高齢化社会を迎える日本にあって増加する感音難聴の治療への発展に貢献できると思われる。特に本研究では内耳への遺伝子導入、有毛細胞再生、聴覚路の遺伝子発現変化・再生に焦点を当て、感音難聴の発症機序を解明し、診断・治療につながる臨床応用研究をすることを目的とする。</p> <p>3. 研究方法</p> <p>1) 内耳遺伝子導入法の検討</p> <ul style="list-style-type: none"> (1) Adeno-associated virus を用いて (2) Adenovirus を用いて (3) Non-viral vector を用いて <p>2) 蝸牛神経核および下丘における加齢による遺伝子発現変化</p> <ul style="list-style-type: none"> (1) 蝸牛神経核での検討 (2) 下丘での検討 <p>3) 下丘における幹細胞</p> <p>4) 内耳有毛細胞再生</p> <ul style="list-style-type: none"> (1) 遺伝子導入による再生 (2) 有毛細胞消失後の再生 (3) 機能回復についての検討 (4) 単離細胞による電気生理学的検討 (5) Atoh1 遺伝子以外による検討 			

4. これまでの成果

1) 内耳遺伝子導入法の検討

ハートレー系成熟モルモットの内耳へ enhanced green fluorescence protein (eGFP) を発現する AAV を局所投与し、コルチ器への遺伝子発現の分布を観察した。AAV はサイトメガロウィルス (CMV) プロモーターを有し、2 型をベースとした 2/1、2/2、2/5、2/7、2/8、2/9 のハイブリッド 6 種を使用した。内耳への投与方法は人工内耳手術に準じ、蝸牛基底回転の外リンパ腔内へ直接ベクターを投与した。eGFP を発現する Ad も同様の手技で投与し、遺伝子発現の分布を比較した。遺伝子発現の分布は各血清型でやや異なっているものの、全ての血清型で内毛細胞への発現が認められた。最も効率よく遺伝子導入可能であったのは AAV-2/2 であり、外毛細胞へは AAV-2/1、-2/2、-2/9 で遺伝子発現を認めた。AAV-2/1、-2/2、-2/7、-2/8、-2/9 においては Spiral limbus や Spiral ligament の線維芽細胞にも遺伝子発現を認めた。Ad 投与耳において遺伝子発現は外リンパ腔を裏打ちする細胞に局限していた。形態学的評価では AAV 投与後に有毛細胞の消失は認めず、また ABR においてもベクター投与前後において閾値変化は 4,8,16kHz のいずれの周波数においても 10dB 以下であった。これらはコントロール群においても同様の結果であった。遺伝子発現の分布は蝸牛の基底回転には強く、頂回転に向かうほど減衰する傾向にあった。

2) 蝸牛神経核および下丘における加齢による遺伝子発現変化

DNA マイクロアレイ法により若年モデルマウスと加齢モデルマウスの蝸牛神経核及び下丘における遺伝子発現の違いを比較した。若年モデル群に比して老年モデル群において発現強度の減少を認めた数種の遺伝子を認めた。その中で Glutamate receptor ionotropic NMDA zeta1 については in situ hybridization を行い下丘において老年モデルにおいて発現低下していることが示唆された。蝸牛神経核においてはデータにばらつきがあり再検討中である。

3) 聴覚伝導路 (下丘) における組織幹細胞の同定

下丘に存在する組織幹細胞を同定する目的で 3 日齢の C57BL/6 マウス背部皮下に BrdU を 2 回/day, 3 日間の連続投与を行い、16 週間後に幹細胞の可能性が示唆されている slow-cycling cell の同定を試みた。その結果、下丘に BrdU 陽性細胞を認め、さらに Bcrp1 にも陽性であったことから幹細胞がわずかながら存在することが明らかとなった。また、3 週齢のマウスから下丘を摘出後分散化し、Hoechst33342 にて染色後その陰性分画として Side Population (SP) 細胞として組織幹細胞の採取を試みた。その結果、SP 細胞は全体のおよそ 1% 存在しており、これらの分画は verapamil で処理すると消失した。さらに、採取した SP 細胞の発現する遺伝子を RT-PCR にて調査した結果、ABCG2(Bcrp1)、Sca-1、Oct4、Sox2 など幹細胞及び前駆細胞に共通に高発現している遺伝子が MP 細胞のそれと比較して高発現していることがわかった。

4) 内耳有毛細胞再生

聴覚閾値正常な成熟モルモットを使用した。アミノ配糖体の抗生物質であるカナマイシン (500mg/kg) を皮下投与し、その 2 時間後にケタミンおよびキシラジンで全身麻酔し、内頸静脈を確保しエタクリン酸 (50mg/kg) を静脈投与することにより内耳障害 (両耳の) モデルを作製した。その 3 日後に内耳障害の評価を ABR、免疫染色、そして電子顕微鏡 (電顕) にて行った。その翌日、左蝸牛の第 2 回転の内リンパ腔に Atoh1 遺伝子を組み込んだアデノウイルスベクター (Ad.Atoh1) あるいはアデノウイルスのみ (Ad.empty) を投与した。ベクター投与 4 日目に Atoh1 遺伝子の蝸牛内発現を観察し、さらにベクター投与 2 ヶ月後に細胞骨格を染色する phalloidin と有毛細胞特異的マーカーである myo7a を用いた免疫染色、電顕と光学顕微鏡 (光顕) による細胞形態の評価と ABR による聴覚閾値回復の評価を行った。Ad.Atoh1 投与 2 ヶ月後の再生した外毛細胞の切片像は外毛細胞の特徴である蓋板と stereocilia を持ち、さらには支持細胞の特徴である基底膜からコルチ器表層にまで伸展した細胞体と基底膜直上に核を持つ形態を示していた。有毛細胞特異的マーカーである myo7a を用いた免疫染色において、Ad.Atoh1 投与 2 ヶ月後の投与耳 (左耳) においてコルチ器内に多数の myo7a 陽性細胞が観察された。Ad.Atoh1 非投与耳 (右耳) と比較して、Ad.Atoh1 投与耳 (左耳) の平均 ABR 閾値は測定した全周波数において、有意に聴力の改善 (回復) を示していた。

5. これまでの進捗状況と今後の計画

研究計画に実験を重ねていくなかで、結果のでていない計画もあり、計画内容の一部変更を行いつつ進めている。新たなベクターでの遺伝子導入の検討、内耳遺伝子導入の効率化など課題がある。ただ予期しない結果から新たな学術的展開を期待している。さらに、臨床応用をめざした病態モデルや内耳再生による治療の基礎研究を進めている。

6. これまでの発表論文

(1) 発表論文

1) 原著論文

1. Kawamoto, K., Izumikawa, M., Beyer, L.A., Atkin, G.M. & Raphael, Y.
Spontaneous hair cell regeneration in the mouse utricle following gentamicin ototoxicity.
Hear. Res. in press 2008.
2. Konishi, M., Kawamoto, K., Izumikawa, M., Kuriyama, H. & Yamashita, T.
Gene transfer into guinea pig cochlea using adeno-associated virus vectors.
J. Gene Med. **10**, 610-618 (2008).
3. Izumikawa, M., Batts, S, Miyazawa, T., Swiderski, D. & Raphael, Y.
Response of the flat cochlear epithelium to forced expression of Atoh1.
Hear. Res. **240**, 52-56 (2008).
4. Raphael, Y., Kim, Y.H., Osumi, Y. & Izumikawa, M.
Non-sensory cells in the deafened organ of Corti: approaches for repair.
Int. J. Dev. Biol. **51**, 649-654 (2007).
5. Minoda, R., Izumikawa, M., Kawamoto, K., Zhang, H. & Raphael, Y.
Manipulating cell cycle regulation in the mature cochlea.
Hear. Res. **232**, 44-51 (2007).
6. Mustapha, M., Beyer, L., Izumikawa, M., Swiderski, D., Dolan, D., Raphael, Y. & Camper, S.
Whirler mutant hair cells have less severe pathology than shaker 2 or double mutants.
J. Assoc. Res. Otolaryngol. **8**, 329-337 (2007).
7. Abrashkin, K.A., Izumikawa, M., Miyazawa, T., Wang, C.H., Crumling, M.A., Swiderski, D.L., Beyer, L.A. & Raphael, Y.
The fate of outer hair cells after acoustic or ototoxic insults.
Hear. Res. **218**, 20-29 (2006).
8. Kanzaki, S., Beyer, L.A., Swiderski, D.L., Izumikawa, M., Stover, T., Kawamoto, K. & Raphael, Y.
p27(Kip1) deficiency causes organ of Corti pathology and hearing loss.
Hear. Res. **214**, 28-36 (2006).
9. Shen, J., Harada, N., Nakazawa, H., Kaneko, T., Izumikawa, M. & Yamashita, T.
Role of nitric oxide on ATP-induced Ca²⁺ signaling in outer hair cells of the guinea pig cochlea.
Brain Res. **1081**, 101-112 (2006).

2) 総説

1. 河本光平、小西将矢、栗山博道：
アデノ随伴ウィルスベクターを用いた内耳への遺伝子導入
逡信医学 **59**, 185-189 (2007).
2. 河本光平、小西将矢、栗山博道：内耳への遺伝子導入
逡信医学 **58**, 263-266 (2006).

(2) 学会発表

国際学会

3) 一般発表

1. Ooka, H., Kanda, S., Suzuki, H., Nishiyama, T. and Yamashita, T.
Identification of Tissue Specific Stem/progenitor Cells in Auditory Pathway.
ARO midwinter research meeting, Arizona, 2008.
2. Konishi, M., Kawamoto, K., Izumikawa, M., Yagi, M., Asako, M., Kuriyama, H. and Yamashita, T.
Gene Transfer Into Guinea Pig Cochlea Via Several Serotypes of AAV Vectors
ARO midwinter research meeting, Denver, 2007.

国内学会

2) シンポジウム講演

1. 泉川雅彦：遺伝子導入（内耳再生と聴覚回復）
シンポジウム1「内耳疾患の治療をめざして-基礎研究の最前線」
第109回日本耳鼻咽喉科学会、大阪、2008.
2. 小西将矢、河本光平、泉川雅彦、栗山博道、山下敏夫：AAVによる内耳への遺伝子導入
遺伝子デリバリー研究会シンポジウム、福岡、2006.
3. 河本光平、泉川雅彦、小西将矢、八木正夫、栗山博道、山下敏夫：
内耳への遺伝子導入の試み
遺伝子デリバリー研究会シンポジウム、福岡、2006.

3) 一般発表

1. 大岡久司、神田靖士、鈴木裕子、西山利正、山下敏夫：
聴覚伝導路における組織幹細胞の同定。
頭頸部自律神経研究会、大阪、2008.
2. 大岡久司、神田靖士、西山利正、山下敏夫：
聴覚伝導路における組織幹細胞の同定
日本耳鼻咽喉科学会、大阪、2008.
3. 大岡久司、山下敏夫：
聴覚伝導路における組織幹細胞の同定
日本耳科学会、神戸、2008.
4. 泉川雅彦、河本光平、八木正夫、栗山博道、Yehoash Raphael、山下敏夫：
高度難聴動物への Atoh1 遺伝子導入による蝸牛有毛細胞の再生と聴力閾値の改善
頭頸部自律神経研究会、大阪、2007.
5. 泉川雅彦、河本光平、八木正夫、栗山博道、山下敏夫：
高度聴覚障害動物への Atoh1 遺伝子導入による内耳有毛細胞の再生と聴覚閾値の改善
第51回日本聴覚医学会、山形、2006.
6. 泉川雅彦、河本光平、八木正夫、栗山博道、山下敏夫：
内耳障害の程度と Atoh1 遺伝子導入効果との相関性の検討
日本耳科学会、青森、2006.

7. これまでの成果の情報公開

ホームページ：耳鼻科学講座=<http://www3.kmu.ac.jp/~ent/>



Research paper

Response of the flat cochlear epithelium to forced expression of *Atoh1*Masahiko Izumikawa^{a,b}, Shelley A. Batts^a, Toru Miyazawa^{a,c}, Donald L. Swiderski^a, Yehoash Raphael^{a,*}^a Kresge Hearing Research Institute, The University of Michigan Medical School, Ann Arbor, MI 48109-5648, USA^b Department of Otolaryngology, Kansai Medical University, 2-3-1 Shinmachi, Hirakata, Osaka 573-1191, Japan^c Department of Otolaryngology, Kanazawa Medical University, 1-1 Daigaku, Uchinada, Ishikawa 920-0293, Japan

ARTICLE INFO

Article history:

Received 22 October 2007

Received in revised form 5 February 2008

Accepted 17 February 2008

Available online 7 March 2008

Keywords:

Cochlea
Deafness
Aminoglycosides
Neomycin
Adenovirus
Guinea pig
Atoh1
Gene transfer

ABSTRACT

Following hair cell elimination in severely traumatized cochleae, differentiated supporting cells are often replaced by a simple epithelium with cuboidal or flat appearance. *Atoh1* (previously *Math1*) is a basic helix–loop–helix transcription factor critical to hair cell differentiation during mammalian embryogenesis. Forced expression of *Atoh1* in the differentiated supporting cell population can induce transdifferentiation leading to hair cell regeneration. Here, we examined the outcome of adenovirus mediated over-expression of *Atoh1* in the non-sensory cells of the flat epithelium. We determined that seven days after unilateral elimination of hair cells with neomycin, differentiated supporting cells are absent, replaced by a flat epithelium. Nerve processes were also missing from the auditory epithelium, with the exception of infrequent looping nerve processes above the habenula perforata. We then inoculated an adenovirus vector with *Atoh1* insert into the scala media of the deafened cochlea. The inoculation resulted in upregulation of *Atoh1* in the flat epithelium. However, two months after the inoculation, *Atoh1*-treated ears did not exhibit clear signs of hair cell regeneration. Combined with previous data on induction of supporting cell to hair cell transdifferentiation by forced expression of *Atoh1*, these results suggest that the presence of differentiated supporting cells in the organ of Corti is necessary for transdifferentiation to occur.

© 2008 Elsevier B.V. All rights reserved.

1. Introduction

The cochlear sensory epithelium contains two types of differentiated epithelial cells: hair cells and supporting cells. When hair cells degenerate, supporting cells expand and replace them to maintain a confluent layer of cells lining the scala media and separating endolymph from perilymph. In some cases, supporting cells in lesioned ears remain differentiated and the organ of Corti maintains its tall appearance despite the lack of hair cells. However, in many cases the supporting cells that remain after hair cell loss do not maintain their differentiated state. As a result, the area of the organ of Corti becomes a flat or cuboidal simple epithelium with no patterned organization (Forge et al., 1998; Kim and Raphael, 2007). The condition of supporting cells in deaf ears will dictate the choice of therapy, once therapies such as hair cell regeneration or stem cell implantation become a reality.

The flat epithelium has been described after several types of trauma. For instance, ears that receive cochlear implants often exhibit a flat epithelium in both human and animal models (Nadol

et al., 1994). A variety of etiologies may lead to degeneration of the auditory epithelium to the flat state, including severe presbycusis (Bhatt et al., 2001), extremely severe ototoxic injury (Coco et al., 2007; Forge et al., 1998; Kim and Raphael, 2007) or hereditary cochlear pathologies (Webster, 1992). In many cases, the loss of hair cells does not initially involve supporting cell degeneration, but over time the non-sensory auditory epithelium is replaced by a flat epithelium. Because of the prevalence of this pathology in humans, the flat epithelium constitutes the substrate for potential future therapy in many clinical cases. It is therefore important to characterize the flat epithelium and determine how it responds to therapeutic manipulations.

In the present study, we have used the neomycin model to eliminate hair cells and induce transformation of supporting cells into the flat epithelium state. We tested the ability of the flat epithelium to be transduced with an adenovirus and whether forced expression of a developmental gene, *Atoh1*, in the flat epithelium can induce transdifferentiation of these cells into new hair cells. *Atoh1* is the mouse homolog of the *Drosophila* gene *atonal*, a basic helix–loop–helix transcription factor that acts as a ‘pro-hair cell gene’ (Jones et al., 2006). Forced expression of *Atoh1* in deaf ears with differentiated supporting cells can induce transdifferentiation of these supporting cells to new hair cells (Izumikawa et al., 2005; Shou et al., 2003).

Abbreviations: Green fluorescent protein (GFP); Scanning electron microscopy (SEM); Phosphate buffered solution (PBS); Figure (Fig)

* Corresponding author. Tel.: +1 734 936 9386; fax: +1 734 615 8111.

E-mail address: yoash@umich.edu (Y. Raphael).

We found that the adenovirus-mediated expression of a reporter gene in the flat epithelium was robust. However, forced expression of *Atoh1* did not induce noticeable changes in the morphology of the flat epithelium. The results point to the importance of designing ways to prevent supporting cell degeneration and indicate that once the auditory epithelium is flat, therapies other than *Atoh1* over-expression should be considered.

2. Materials and methods

2.1. Animals

All animal experiments were approved by the University of Michigan Institutional Committee on Care and Use of Animals (UCUCA) and performed using accepted veterinary standards. We used 72 young adult guinea pigs (Elm Hills Breeding Laboratory). At the beginning of the experiments, animals weighed 250–400 g and displayed normal Preyer's reflex. All animals were deafened unilaterally with neomycin (see below) and received one of the following treatments: Ad.*Atoh1* ($n = 33$), Ad.*Atoh1-GFP* ($n = 21$), Ad.*GFP* ($n = 3$), Ad.empty (adenovirus with no gene insert) ($n = 9$), artificial endolymph (NaCl 1 mM, KCl 126 mM, KHCO₃ 25 mM, MgCl₂ 0.025 mM, CaCl₂ 0.025 mM and K₂HPO₄ 1.4 mM) ($n = 2$) and deafening alone ($n = 4$).

2.2. Deafening and inoculation surgery

All animals were deafened unilaterally (left ear), with a single bolus injection of 60 μ l of 10% neomycin (Pharma-Tek, Huntington, NY) diluted in sterilized water. Neomycin was selected at this concentration because it leads not only to complete elimination of all hair cells in turns 1–3 of the guinea pig cochlea, but also to a drastic change in the morphology of supporting cells. The animals were anesthetized by the combination with Rompun (intramuscularly, xylazine, 10 mg/kg, Bayer, Shawnee Mission, KS, USA) and Ketalar (intramuscularly, ketamine HCl, 40 mg/kg, Parke Davis, Morris Plains, NJ, USA). We injected 1% lidocaine hydrochloride (subcutaneously, 0.5 ml) for local anesthesia in the postauricular region. The animals were placed at a prone position on a heated pad. An incision was made along the left postauricular region. The temporal bone was exposed and then opened by scalpel drilling and forceps to gain a view of the entire round window membrane. Using the bent tip of a 30 gauge needle and a 100 μ l Hamilton syringe, 60 μ l of 10% neomycin was injected into the scala tympani through the round window membrane, over 1 min. After the injection, the opening in the temporal bone was closed with carboxylate cement (Duleron) and the skin was sutured in two layers.

The vectors or artificial endolymph were inoculated into the scala media of left ear seven days after the deafening surgery, using the procedure described previously (Ishimoto et al., 2002) except that inoculation was into the second turn of the cochlea. Animals were sacrificed and prepared for morphological analysis (immunocytochemistry, plastic sections or SEM) six days after deafening, or two months after viral vector inoculation. In addition, a group of animals ($N = 4$) was used for immunocytochemical detection of *Atoh1* gene expression at a time point seven days after viral vector inoculation.

2.3. Adenoviral vectors

We used advanced generation replication-deficient recombinant adenoviral vectors with E1, E3 and partial E4 regions deleted (Brough et al., 1997). The vectors were Ad.*Atoh1*, Ad.*Atoh1-GFP*, Ad.*GFP* and Ad.empty. All vectors were provided by GenVec Inc. (Gaithersburg, MD, USA). The *Atoh1* gene insert was driven by

the human cytomegalovirus promoter and the *GFP* gene was driven by the chicken beta-actin promoter. We used undiluted vectors at a concentration of 1×10^{12} particles purified virus per ml. The viral suspensions were stored at -80°C until thawed for use.

2.4. Immunocytochemistry

Animals were deeply anesthetized with xylazine and ketamine as above, decapitated, and the temporal bones were removed. The inner ears were perfused with 4% paraformaldehyde in phosphate buffered saline (PBS) for 2 h. Further dissection was performed to remove the stria vascularis, Reissner's membrane and the tectorial membrane. Then the tissue was permeabilized with 0.3% Triton-X-100 in PBS for 10 min. Non-specific binding of secondary antibody was blocked with 5% normal goat serum in PBS for 30 min. Immunocytochemistry was performed using primary antibodies: a mouse monoclonal anti-neurofilament 200 kDa antibody (Sigma, St. Louis, MO, diluted 1:200) or mouse monoclonal anti-*Atoh1* (Hybridoma Core, University of Iowa), followed by a secondary antibody, a goat monoclonal anti-mouse conjugated to rhodamine (Jackson ImmunoResearch, West Grove, PA) for 30 min. To double stain for actin, we used FITC-conjugated phalloidin (Molecular Probes, Junction City, OR, diluted 1:200). The specimens were further dissected to separate individual cochlear turns and mounted on glass slides using CrystalMount (Biomedex, Foster City, CA). The samples were examined and photographed using a Leica DMRB epifluorescence microscope (Leica, Eaton, PA) with a Cooled SPOT-RT digital camera (Diagnostic Instruments, Sterling Heights, MI).

2.5. Scanning electron microscopy

Animals were deeply anesthetized (as described above) and perfused transcardially with 0.15 M cacodylate buffer, followed by 2% glutaraldehyde in the same buffer. Cochleae were removed and the otic capsule opened to continue fixation for 2 h. The tissues were postfixed using the osmium thiocarbonylhydrazide method (Osborne and Comis, 1991). The specimens were dehydrated with ethanol and dried by the critical point method with CO₂ in a SamDri-790 (Tousimis, Rockville, MD). The samples were fixed to stubs with silver paste and photographed digitally using a Philips XL30 Field Emission Gun scanning electron microscope (FEI, Hillsboro, OR).

2.6. Plastic sections

Animals were anesthetized and decapitated and the temporal bones removed and placed in 4% paraformaldehyde in PBS for 2 h. The otic capsule was dissected away and the modiolus along with the organ of Corti, were decalcified for a 2–3 days in 3% EDTA with 0.25% glutaraldehyde. Once tissues appeared soft, specimens were postfixed with 1% osmium tetroxide in phosphate buffer, dehydrated in ethanol and embedded in Embed 812 epoxy resin. Sections were obtained with glass knives and photographed using a Leica DMRB microscope.

3. Results

Morphological analysis reported here is based on observations in the first three turns of the cochlea. Little variation was seen among individuals. In normal ears that were not deafened, the combined staining with phalloidin and neurofilament shows presence of hair cells and nerves extending in the direction of the hair cells (Fig. 1a). In contrast, in animals sacrificed at six days after the deafening procedure, whole-mounts of the organ of Corti stained

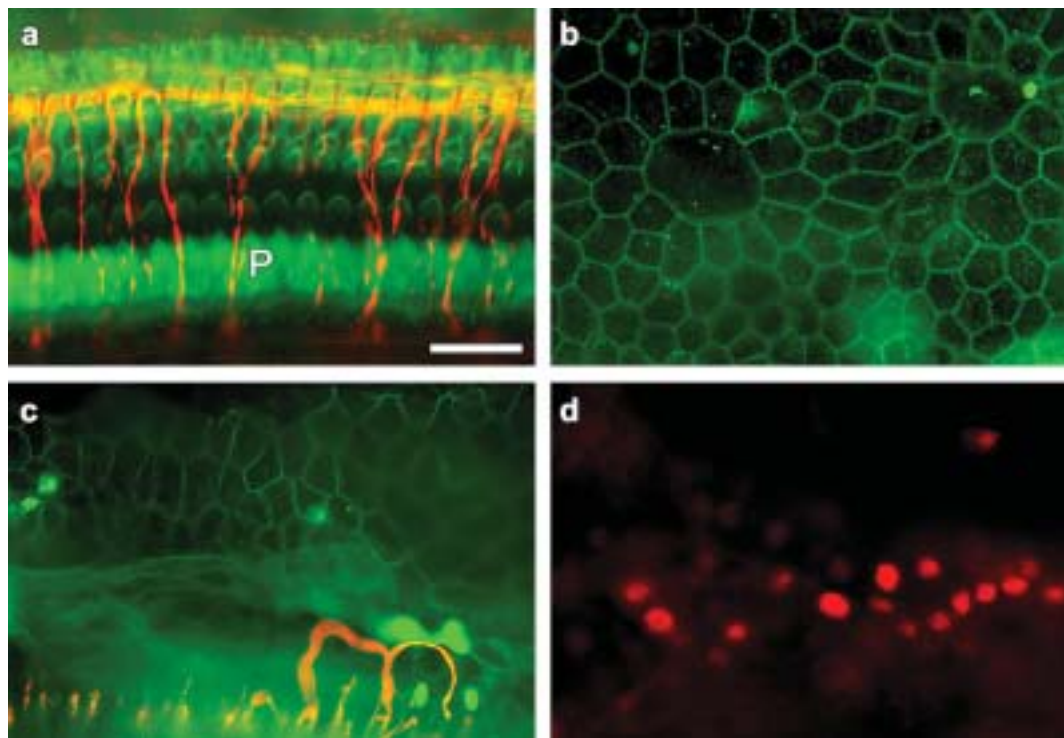


Fig. 1. Whole-mounts of the auditory epithelium stained with markers for neurofilament, actin or *Atoh1* and photographed with epifluorescence. (a) Fluorescent phalloidin (green) shows the distribution of actin in the normal auditory epithelium, depicting the outer pillar cells (P) and a normal array of hair cells and supporting cells. Co-localization with neurofilament (red) shows radial fibers extending towards the outer hair cell area and longitudinal fibers near the 3rd row outer hair cells. (b) Phalloidin staining six days after neomycin administration shows that hair cells are absent. The auditory epithelium consists of non-sensory cells with irregular apical junctional contours. (c) Double-staining with phalloidin and neurofilament antibody reveals absence of hair cells and lack of radial nerve fibers six days after neomycin. A small number of fibers extend and loop into the auditory epithelium. (d) A cochlea deafened with neomycin and inoculated with *Ad.Atoh1* seven days later. High efficiency of gene expression is detected by nuclear staining of *Atoh1*-specific antibody. Bar = 30 μm .

with phalloidin show that hair cells are absent and the reticular lamina lacks orderly organization (Fig. 1b). The typical organization of supporting cells in the organ of Corti is not present and rows of cells cannot be distinguished. Instead, irregular intercellular borders reveal an epithelium in which cell contour is variable and distinctively different from the normal organ of Corti.

Double-stained tissues in which phalloidin was applied in conjunction with the neurofilament antibody reveal that hair cells are absent, the remaining cells do not maintain the typical organization of the organ of Corti, and neuronal processes are not extending in the direction of the area where hair cells usually reside (Fig. 1c). Neurites are present medially of where the organ of Corti would have been, close to the habenula perforata. Occasionally, 1–2 neural processes are found looping into the sensory epithelium.

In animals that were deafened with neomycin, inoculated with *Ad.Atoh1* and sacrificed seven days later, high efficiency of *Atoh1* transgene expression is observed in non-sensory cells that remain in the auditory epithelium, as determined by use of *Atoh1*-specific antibodies (Fig. 1d). The density of *Atoh1*-positive nuclei was highest in the area adjacent to the inoculation site, where it exceeded 50% efficiency. The efficiency decreased with distance from the inoculation site. Control animals that were deafened and then inoculated with *Ad.empty* or not inoculated at all were negative for the *Atoh1* antibody (not shown).

Plastic sections of ears obtained six days after the deafening procedure show that no hair cells survive in the tissue, and also that supporting cells in a differentiated state are not found either (Fig. 2). The epithelium on the basilar membrane is simple, and cells appear cuboidal or flat. The sites of the habenula perforata and the vas spirale are visible. Supporting cells that are usually found in and around the organ of Corti are not identifiable.

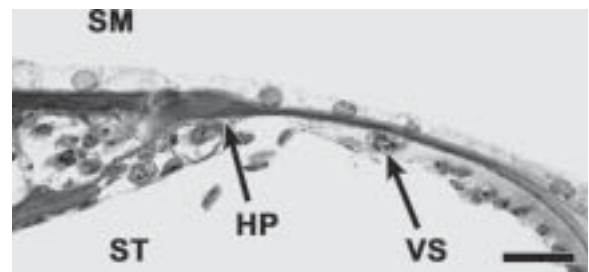


Fig. 2. A plastic cross section of the auditory epithelium six days after neomycin showing absence of hair cells and of differentiated supporting cells. The auditory epithelium consists of a monolayer of flat epithelial cells. The habenula perforata (HP) and vas spirale (VS) provide landmarks for localization in the tissue. The flat epithelium extends to areas flanking the original site of the organ of Corti. SM, scala media; ST, scala tympani. Bar = 20 μm .

SEM analysis of the cochlea at six days after the deafening showed complete absence of hair cells in the epithelium (Fig. 3a). In ears deafened with neomycin, inoculated with artificial endolymph a week later, and sacrificed two months after the inoculation (Fig. 3b), the morphology was similar to that seen in ears that were deafened with no further treatment. Hair cells were not seen and the apical contour of the auditory epithelium lacked an organized pattern. In deafened ears inoculated with *Ad.Atoh1* and sacrificed two months (Fig. 3c) or 10 weeks later (Fig. 3d) no hair cells could be identified and the morphology was similar to that seen in the deafened ears that received no further treatment (Fig. 3a). In all ears presented in Fig. 3, the non-sensory cells lacked regular organization and hair cells could not be found.

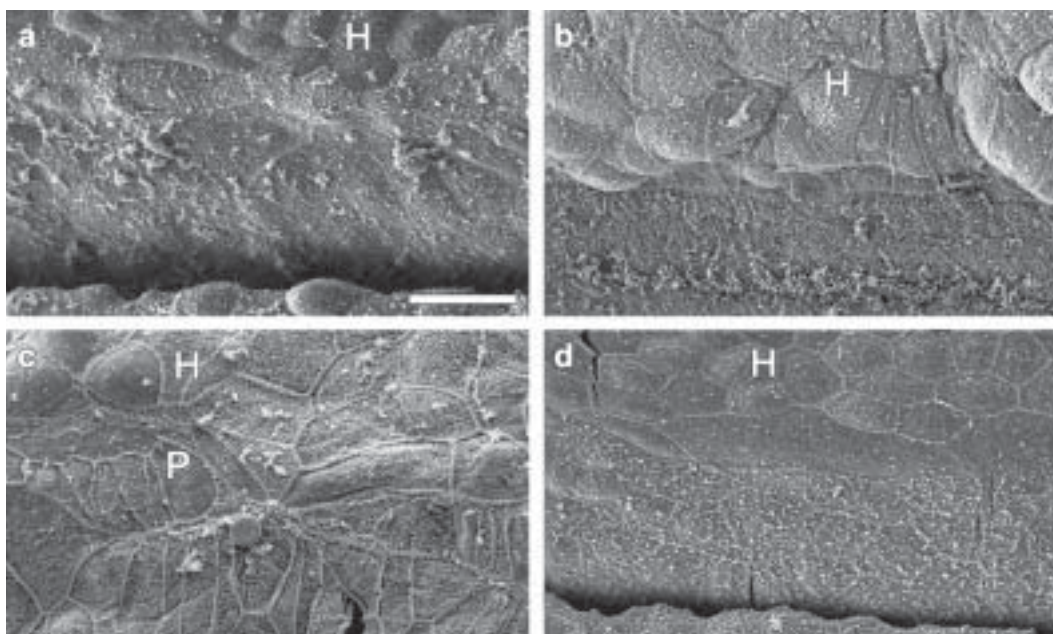


Fig. 3. SEM images of the surface of the auditory epithelium in ears treated with neomycin. (a) In a cochlea obtained six days after neomycin administration, the epithelium is completely devoid of hair cells. The apical contour of cells is disorganized and irregular but the border area with Hensen cell region (H) is visible. (b) A cochlea treated with neomycin, inoculated with artificial endolymph a week later and sacrificed two months after the inoculation showing similar surface morphology to that seen in (a). (c, d) In a deafened cochlea inoculated with Ad.Atoh1 and obtained two months (c) or 10 weeks later (d), no hair cells are seen. A few cells with apical morphology resembling pillar cells (P) are sometimes seen (c). The surface morphology is similar to deafened ears that received no Ad.Atoh1 (a, b). Bar = 20 μm.

4. Discussion

The data show that six days after placing neomycin in the perilymph neither hair cells nor differentiated supporting cells can be found. The rapid and devastating effect of this ototoxic regimen on hair cells has been described in the past (Jyung et al., 1989; Zappia and Altschuler, 1989). In this study, we show an equally devastating effect on supporting cells, such that the epithelium replacing the organ of Corti is flat and neuronal fibers are absent. We also show that this transformation has negative implications for adenovirus mediated therapeutic treatments. Adenovirus transduction of the tissue is substantial but less robust than in differentiated supporting cells. Forced expression of *Atoh1* in the flat epithelium does not lead to appearance of new hair cells.

The mechanism inducing transformation of differentiated supporting cells to an undifferentiated flat epithelium after hair cell removal is not clear. If kanamycin and ethacrynic acid are used to eliminate hair cells, supporting cells can remain differentiated for up to 10 weeks in the guinea pig model (Izumikawa et al., 2005) and perhaps longer. Presence of differentiated supporting cells in deaf ears with no hair cells was shown using other models (Sugawara et al., 2005). Together, these data suggest that the loss of hair cells is not sufficient to cause the loss of differentiated supporting cells. It may be that the supporting cells, themselves, are sensitive to extremely ototoxic aminoglycosides such as neomycin. Furthermore, this might not be the only reason for flattening of the auditory epithelium. In some experimental conditions, supporting cells become flat a long time after the ototoxic insult, suggesting that secondary degeneration may take place (Forge et al., 1998). This might be attributed to a mechanism that is distinct from the direct effects of the ototoxic drugs. Thus, several factors may determine the survival or degeneration of non-sensory cells in the auditory epithelium. Our results suggest that future reparative approaches will be more successful when differentiated supporting cells remain in the tissue, and therefore it will be important to

understand the transition to the flat epithelium and design ways to prevent it.

Phenotypic (immunocytochemical) characterization of the flat epithelium will help to determine the identity of these cells and facilitate attempts to manipulate these cells for therapeutic purposes. Several proteins have already been detected in this epithelium. For instance, these cells connect to each other with tight junctions, as determined by the presence of ZO-1 immunoreactivity, and express the supporting cell marker S-100 (Kim and Raphael, 2007). More complete molecular characterization will help determine whether these cells are de-differentiated supporting cells of the organ of Corti (such as Deiters, pillar or Hensen cells), and/or cells that have migrated from the flanking areas such as the inner or outer sulcus.

In birds, ototoxic lesions that deplete hair cells leave behind differentiated supporting cells and regeneration occurs spontaneously (Cotanche, 1999; Stone and Rubel, 2000; Stone et al., 1998). A more severe lesion that also influences the supporting cells has been accomplished with noise (Cotanche et al., 1995). In such cases, non-sensory cells that flank the basilar papilla can migrate into the sensory epithelium, as may be the case in the flat epithelium. These cells then become the therapeutic target for regenerative attempts or insertion of stem cells. Previous data show that cell migration is indeed possible in the auditory epithelium in mammals (Forge et al., 1998).

Better understanding of the biology of the flat epithelium will assist in advancing tasks such as integration of stem cells, enhancement of neuronal survival or induction of transdifferentiation to the hair cell phenotype. In mammals, the flat epithelium can undergo a robust proliferative phase (Kim and Raphael, 2007). This may be of help for designing therapies and inserting genes or stem cells. More work is necessary to characterize the origin of these cells, their general biology and their amenability to take up external molecules or vectors for gene delivery. It will be important to identify surface receptors on these cells that will allow the design

of gene transfer vectors that will have specificity to these cells. It will also be necessary to determine if these cells are heterogeneous in their origin and characteristics, as tentatively suggested by their pattern of transduction with adenovirus, with only a sub-population showing positive transgene expression.

The inability of *Atoh1* to induce transdifferentiation of flat non-sensory cells to new hair cells may be related to the state of differentiation of the epithelium. Specifically, the fate of developing cells that express *Atoh1* (in the inner ear and elsewhere) depends on the context determined by previous developmental gene expression in each of these tissues. The expression of *Atoh1* is usually a final step in differentiation. Thus, forced expression of *Atoh1* would be expected to exert different developmental outcomes depending on the developmental history of the cell. The current findings show that the flat epithelium fails to undergo transdifferentiation following forced expression of *Atoh1* and suggest that the flat epithelium has regressed to a very early state of differentiation and no longer presents the commitment to the hair cell or supporting cell phenotype. Based on the lack of response to *Atoh1*, it can be assumed that the flat epithelium is less differentiated than cells in the vicinity of the organ of Corti, such as interdental cells, where forced *Atoh1* expression induces ectopic hair cell formation (Kawamoto et al., 2003; Minoda et al., 2007).

These findings are important for conceptual and practical therapeutic approaches for hair cell regeneration. When considering transdifferentiation therapy, rebuilding the auditory epithelium may need to begin with inducing forced expression of early developmental genes, perhaps as early as otocyst specific genes that induce formation of the sensory areas, the epithelial ridges of the developing cochlear epithelium. Once expression of these early developmental genes recreates that epithelial ridge, *Atoh1* over-expression may be used as a final stage for inducing generation of new hair cells.

Better understanding and ability to manipulate the flat epithelium may also be of help for enhancing cochlear implant procedures. The present data show a complete lack of hair cells along with a near complete loss of nerve fibers in the auditory epithelium. However, we found that some nerves continued to meander in the epithelium despite the lack of hair cells, possibly looking for a target. Similar findings were reported in other models (Bohne and Harding, 1992; Strominger et al., 1995). The maintained ability of neurons to meander in the deafened epithelium, which appears to occur after several etiologies for hair cells loss, is important for the feasibility of innervating therapeutically-placed new hair cells or stem cells. However, the degree of neural survival may depend on the state of the supporting cells in the auditory epithelium (Sugawara et al., 2005). It would be important to characterize this correlation in human temporal bones, where deafferented spiral ganglion neurons tend to survive to a larger extent than in lab animals.

In conclusion, our data confirm that the neomycin model is an efficient method for creating a flat epithelium in the cochlea. We demonstrate that adenovirus is a useful gene carrier into the flat epithelium and *Atoh1* does not induce transdifferentiation of the flat epithelium into new hair cells. As such, it is necessary to design ways to prevent degeneration of supporting cells in ears depleted

of hair cells, and to direct specific therapies in cases where the flat epithelium does occur.

Acknowledgments

We thank Lisa Beyer for technical assistance. Viral vectors were kindly provided by Doug Brough (GenVec). Work was supported by the Taubman Institute, a gift from Berte and Alan Hirschfield, the R. Jamison and Betty Williams Professorship, a Research Grant from Kansai Medical University, and NIH/NIDCD Grants R01-DC01634, R01-DC05401, R01-DC03685, T32-DC00011 and P30-DC05188.

References

- Bhatt, K.A., Liberman, M.C., Nadol Jr., J.B., 2001. Morphometric analysis of age-related changes in the human basilar membrane. *Ann. Otol. Rhinol. Laryngol.* 110, 1147–1153.
- Bohne, B.A., Harding, G.W., 1992. Neural regeneration in the noise-damaged chinchilla cochlea. *Laryngoscope* 102, 693–703.
- Brough, D.E., Hsu, C., Kulesa, V.A., Lee, G.M., Cantolupo, L.J., Lizonova, A., Kovacs, I., 1997. Activation of transgene expression by early region 4 is responsible for a high level of persistent transgene expression from adenovirus vectors in vivo. *J. Virol.* 71, 9206–9213.
- Coco, A., Epp, S.B., Fallon, J.B., Xu, J., Millard, R.E., Shepherd, R.K., 2007. Does cochlear implantation and electrical stimulation affect residual hair cells and spiral ganglion neurons? *Hear. Res.* 225, 60–70.
- Cotanche, D.A., 1999. Structural recovery from sound and aminoglycoside damage in the avian cochlea. *Audiol. Neurootol.* 4, 271–285.
- Cotanche, D.A., Messana, E.P., Ofsie, M.S., 1995. Migration of hyaline cells into the chick basilar papilla during severe noise damage. *Hear. Res.* 91, 148–159.
- Forge, A., Li, L., Nevill, G., 1998. Hair cell recovery in the vestibular sensory epithelia of mature guinea pigs. *J. Comp. Neurol.* 397, 69–88.
- Ishimoto, S., Kawamoto, K., Kanzaki, S., Raphael, Y., 2002. Gene transfer into supporting cells of the organ of Corti. *Hear. Res.* 173, 187–197.
- Izumikawa, M., Minoda, R., Kawamoto, K., Abrashkin, K.A., Swiderski, D.L., Dolan, D.F., Brough, D.E., Raphael, Y., 2005. Auditory hair cell replacement and hearing improvement by *Atoh1* gene therapy in deaf mammals. *Nat. Med.* 11, 271–276.
- Jones, J.M., Montcouquiol, M., Dabdoub, A., Woods, C., Kelley, M.W., 2006. Inhibitors of differentiation and DNA binding (Ids) regulate *Math1* and hair cell formation during the development of the organ of Corti. *J. Neurosci.* 26, 550–558.
- Jyung, R.W., Miller, J.M., Cannon, S.C., 1989. Evaluation of eighth nerve integrity by the electrically evoked middle latency response. *Otolaryng. Head Neck* 101, 670–682.
- Kawamoto, K., Ishimoto, S., Minoda, R., Brough, D.E., Raphael, Y., 2003. *Math1* gene transfer generates new cochlear hair cells in mature guinea pigs in vivo. *J. Neurosci.* 23, 4395–4400.
- Kim, Y.H., Raphael, Y., 2007. Cell division and maintenance of epithelial integrity in the deafened auditory epithelium. *Cell Cycle* 6, 612–619.
- Minoda, R., Izumikawa, M., Kawamoto, K., Zhang, H., Raphael, Y., 2007. Manipulating cell cycle regulation in the mature cochlea. *Hear. Res.* 232, 44–51.
- Nadol Jr., J.B., Ketten, D.R., Burgess, B.J., 1994. Otopathology in a case of multichannel cochlear implantation. *Laryngoscope* 104, 299–303.
- Osborne, M.P., Comis, S.D., 1991. Preparation of inner ear sensory hair bundles for high resolution scanning electron microscopy. *Scanning Microsc.* 5, 555–564.
- Shou, J., Zheng, J.L., Gao, W.Q., 2003. Robust generation of new hair cells in the mature mammalian inner ear by adenoviral expression of *Hath1*. *Mol. Cell. Neurosci.* 23, 169–179.
- Stone, J.S., Rubel, E.W., 2000. Cellular studies of auditory hair cell regeneration in birds. *Proc. Natl. Acad. Sci. USA* 97, 11714–11721.
- Stone, J.S., Oesterle, E.C., Rubel, E.W., 1998. Recent insights into regeneration of auditory and vestibular hair cells. *Curr. Opin. Neurol.* 11, 17–24.
- Strominger, R.N., Bohne, B.A., Harding, G.W., 1995. Regenerated nerve fibers in the noise-damaged chinchilla cochlea are not efferent. *Hear. Res.* 92, 52–62.
- Sugawara, M., Corfas, G., Liberman, M.C., 2005. Influence of supporting cells on neuronal degeneration after hair cell loss. *J. Assoc. Res. Otolaryngol.* 6, 136–147.
- Webster, D.B., 1992. Degeneration followed by partial regeneration of the organ of Corti in deafness (dn/dn) mice. *Exp. Neurol.* 115, 27–31.
- Zappia, J.J., Altschuler, R.A., 1989. Evaluation of the effect of ototopical neomycin on spiral ganglion cell density in the guinea pig. *Hear. Res.* 40, 29–37.



NIH Public Access

Author Manuscript

Hear Res. Author manuscript; available in PMC 2008 October 1.

Published in final edited form as:

Hear Res. 2007 October ; 232(1-2): 44–51.

Manipulating cell cycle regulation in the mature cochlea

Ryosei Minoda^{a,b}, Masahiko Izumikawa^{a,c}, Kohei Kawamoto^{a,c}, Hui Zhang^d, and Yehoash Raphael^a

^aKresge Hearing Research Institute, The University of Michigan, MSRB 3, Rm. 9303, 1150 W. Medical Center Dr., Ann Arbor, MI 48109-0648, USA

^bDepartment of Otolaryngology- Head and Neck Surgery, Kumamoto University School of Medicine, 1-1-1 Honjo Kumamoto 860-8556, Japan.

^cDepartment of Otolaryngology- Head and Neck Surgery, Kansai Medical University, 10-15 Fumizono-cho, Moriguchi, Osaka 570-8506, Japan.

^dDepartment of Genetics, Yale University School of Medicine, 333 Cedar Street, P.O. Box 208005, New Haven, CT 06520-8005, USA

Abstract

Sensorineural hearing loss, which is often caused by degeneration of hair cells in the auditory epithelium, is permanent because lost hair cells are not replaced. Several conceptual approaches can be used to place new hair cells in the auditory epithelium. One possibility is to enhance proliferation of non-sensory cells that remain in the deaf ear and induce transdifferentiation of some of these cells into the hair cell phenotype. Several genes, including *p27^{Kip1}*, have been shown to regulate proliferation and differentiation in the developing auditory epithelium. The role of *p27^{Kip1}* in the mature ear is not well characterized. We now show that *p27^{Kip1}* is present in the nuclei of non-sensory cells of the mature auditory epithelium. We determined that forced expression of *Skp2* using a recombinant adenovirus vector, resulted in presence of BrdU-positive cells in the auditory epithelium. When *SKP2* over-expression was combined with forced expression of *Atoh1*, ectopic hair cells were found in the auditory epithelium in greater numbers than were seen with *Atoh1* alone. *Skp2* over-expression alone did not result in ectopic hair cells. These findings suggest that the *p27^{Kip1}* protein remains in the mature auditory epithelium and therefore *p27^{Kip1}* can serve as a target for gene manipulation. The data also suggest that induced proliferation, by itself, does not generate new hair cells in the cochlea.

Keywords

Adenovirus; gene transfer; *p27^{Kip1}*; *Atoh1*; *Skp2*; guinea pig; hair cell; supporting cell; BrdU

1. Introduction

The sensory epithelium of hearing in mammals consists of terminally differentiated epithelial cells: sensory hair cells and non-sensory supporting cells. These cells are quiescent in

Address for correspondence: Yehoash Raphael, MSRB-3, Rm. 9303, 1150 W. Med. Cntr. Dr., Ann Arbor, MI 48109-0648, USA Tel. (734) 36-9386, Fax: (734) 615-8111, E-mail: yoash@umich.edu.

Publisher's Disclaimer: This is a PDF file of an unedited manuscript that has been accepted for publication. As a service to our customers we are providing this early version of the manuscript. The manuscript will undergo copyediting, typesetting, and review of the resulting proof before it is published in its final citable form. Please note that during the production process errors may be discovered which could affect the content, and all legal disclaimers that apply to the journal pertain.

mammals. Therefore, hair cell degeneration is irreversible and leads to sensorineural hearing loss. One potential therapy for hearing loss is induction of hair cell regeneration in the organ of Corti, the sensory region of the auditory epithelium.

Recent data demonstrate that forced expression of genes encoding hair cell development can induce transdifferentiation of non-sensory cells into new hair cells in the developing (Woods et al., 2004; Zheng and Gao, 2000) and mature organ of Corti (Izumikawa et al., 2005; Kawamoto et al., 2003; Shou et al., 2003). As therapy, this procedure would be suboptimal because transdifferentiation of supporting cells into new hair cells does not involve mitosis in the tissue. Thus, formation of new hair cells would reduce the number of supporting cells and compromise the ability to restore normal cochlear structure and function. In birds, where hair cell regeneration leads to functional recovery (Dooling et al., 1997; Marean et al., 1995; Niemiec et al., 1994; Saunders et al., 1992), non-sensory cells divide after a lesion to the epithelium (Hashino and Salvi, 1993; Raphael, 1992; Stone and Cotanche, 1994). To induce proliferation in the mature organ of Corti as part of the reparative process, it may be necessary to manipulate expression of genes that regulate cell cycle.

Among the genes that regulate cell-cycle proteins in the developing inner ear are p27^{Kip1} (Chen and Segil, 1999; Lowenheim et al., 1999), Ink4d (Chen et al., 2003) and Rb1 (Sage et al., 2005). Cell proliferation past the normal developmental cessation of mitosis has been shown in these transgenic mice. The ability to remove the inhibition of cell cycle in the mature inner ear, in a cell or organ specific manner, may potentially be used for developing clinical therapy for hair cell regeneration. One important step for inducing proliferation in the mature auditory epithelium is to identify and localize the cell cycle regulating molecules that are present in the tissue. This set of experiments was designed to determine whether p27^{Kip1} is present in the mature guinea pig auditory epithelium and to test outcome of blocking this protein with Skp2.

p27^{Kip1} is a cyclin-dependent kinase-2 (cdk-2) inhibitor (Sherr and Roberts, 1999). p27^{Kip1} acts as a negative regulator of the G1–S transition of the cell cycle (Harper, 2001). Skp2 is an F-box protein and substrate of recognition component of Cullin 1 (CUL1) for SCF ubiquitin ligase (Nakayama et al., 2000). Skp2 induces the G1 to G0 transition of the cell cycle through ubiquitination of p27^{Kip1} and cyclin E (Nakayama KI, 2001). As such, it may be used to antagonize the inhibition exerted on cell cycle by p27^{Kip1}. During inner ear development in the mouse embryo, a down-regulation of *Skp2* expression was noted to coincide with onset of p27^{Kip1} expression in the non-sensory cells of the auditory epithelium (Dong et al., 2003).

Removal of inhibition on cell cycle in the auditory epithelium may not necessarily lead to formation of new hair cells. In birds and other non-mammalian vertebrates, the process of hair cell regeneration occurs spontaneously, with or without mitosis (Cotanche, 1997; Stone and Rubel, 2000). In mice with dysfunctional p27^{Kip1} supernumerary hair cells are formed (Chen and Segil, 1999; Kanzaki et al., 2006; Lowenheim et al., 1999). The outcome of inducing cell proliferation in the mature auditory epithelium is unknown. If new cells do not take up the hair cell phenotype, it may be necessary to induce transdifferentiation with forced expression of genes such as *Atoh1*. *Atoh1* (formerly *Math1*) is a basic helix-loop-helix (bHLH) transcription factor that is essential for generating hair cells in developing inner ear (Bermingham et al., 1999; Chen et al., 2002; Zine et al., 2001).

After maturation of hair cells in developing mammals, the expression of *Atoh1* is down-regulated (Zheng et al., 2000). However, over-expression of *Atoh1* (or its homologs) in cultures of developing or mature rat cochleae results in the production of ectopic hair cells derived from non-sensory epithelial cells (Shou et al., 2003; Zheng and Gao, 2000). Over-expression of *Atoh1* has also been shown to generate new hair cells in mature guinea pig cochleae *in vivo* (Izumikawa et al., 2005; Kawamoto et al., 2003). The goal of our experiments was to localize

p27^{Kip1} in the mature auditory epithelium, to determine if forced expression of *SKP2* can induce proliferation in the tissue and to assess the potential for generation of new ectopic hair cells by *SKP2* alone versus *SKP2* in combination with *Atoh1* over-expression. We demonstrate that p27^{Kip1} is present in numerous types of non-sensory cells in the mature auditory epithelium and that over-expressing *Skp2* can induce proliferation but no ectopic new hair cells are formed. Forced expression of *SKP2* in combination with *Atoh1* increases the number and alters the pattern of ectopic hair cell generation as compared with *Atoh1* alone.

2. Materials and methods

Animal care and use were approved by institutional UCUCA committee and conformed to National Institutes of Health guidelines.

Adenovirus vectors

The vectors Ad.*Atoh1* (5.2×10^{11} pfu/ml) and Ad.empty (5.1×10^{11} pfu/ml) were based on human adenovirus serotype 5 with E1, E3 and E4 regions deleted, as described previously (Brough et al., 1996). Ad.*SKP2* (1.0×10^{12} pfu/ml) was constructed using the AdEasy system (He et al., 1998). Expression of the transgene insert in each of these vectors was driven by the human cytomegalovirus promoter. The recombinant adenoviruses were amplified and propagated as described previously (Gervais et al., 1998).

Animals and inoculation surgery

We used adult guinea pigs weighing 300–500 g at the beginning of the experiment. We inoculated 5 μ l of the adenovirus vector or control solution into the 2nd turn scala media of the left ear, as previously described (Ishimoto et al., 2002). Briefly, animals were anesthetized with Rompun (i.m., xylazine, 10 mg/kg, Bayer, Shawnee Mission, KS) and Ketalar (i.m., ketamine HCl, 40 mg/kg, Parke Davis, Morris Plains, NJ). Chloramphenicol sodium succinate (i.m., 30 mg/kg) was administered as prophylaxis and 0.3 ml of 1% lidocaine HCl was injected subcutaneously in the post-auricular and neck areas, for local anesthesia. The animals were placed in a supine position on a thermo-regulated heated pad. Ventral skin was incised paramedially and the tympanic bulla was exposed. After opening the bony bulla, the lateral cochlea was revealed. A small perforation was made in the bone above the pigmented area of the stria vascularis using a fine surgical needle. A microcanula was inserted into the scala media through the perforation. The circumference of the inserted microcanula was sealed and covered with carboxylate cement (Durelon, 3M, St. Paul, MN).

To inoculate the fluid into the endolymph, we used a microcanula driven by an electromechanical infusion pump (Harvard Apparatus, Holliston, MA) operated at a rate of 1 μ l/ml over 5 min. To inoculate Ad.*SKP2* and Ad.*Atoh1* combined, the two vector solutions were combined at a volume ration of 1:1 resulting in 50% reduction in the concentration of each vector. Once the inoculation was complete, a layer of carboxylate cement was placed over the inoculation site to minimize the leak from the fenestration after removing the canula. The incision was closed in two layers.

Scanning electron microscopy

SEM was performed in order to determine the distribution and the number of ectopic hair cells. We used 8 animals for the group receiving both Ad.*SKP2* Ad.*Atoh1*, 5 animals for the *Atoh1* alone group, 5 animals for the *SKP2* alone group, 5 animals for the artificial endolymph group and 5 animals for the Ad.empty group. Animals were deeply anesthetized, exsanguinated and systemically perfused with glutaraldehyde (2% in phosphate buffer). Immediately following the perfusion, animals were decapitated, the temporal bones removed from the skull and the cochleae opened at the apical tip and the round and oval windows and immersed in fixative.

Two hours later, the bony wall at was removed along with the lateral wall tissues (stria vascularis and spiral ligament) to reveal the surface of the sensory epithelium. In all samples, SEM evaluation was performed in areas including (from medial to lateral) the interdental cell region, the inner sulcus and the organ of Corti. Images were collected from all cochlear turns.

SEM analysis was performed for localizing and counting ectopic hair cells. To be counted, hair cells had to be localized to an ectopic site in the interdental cell area or the inner sulcus, and exhibit two or more stereocilia on the apical surface. The area immediately adjacent to the site of inoculation was excluded from the statistical analysis, because tissue in this area may have responded to the mechanical trauma (of the inoculation) as well as the presence of the transgenes.

Immunohistochemistry

Whole mounts of the auditory sensory epithelium and surrounding tissues were used to localize p27^{Kip1}, Atoh1 and SKP2. To localize p27^{Kip1} in the auditory epithelium, we stained normal guinea pig cochleae from 4 animals with a monoclonal anti-mouse antibody specific to p27^{Kip1} (Neomarkers, Fremont, CA), diluted 1:200. To localize Atoh1 and SKP2 after combined Ad.*Atoh1* and Ad.*SKP2* inoculation, we obtained cochleae from 4 animals, 4 days after the inoculation. Contralateral ears served as controls. We fixed cochleae in 4% paraformaldehyde in phosphate buffer, pH 7.4, removed the spiral ligament, stria vascularis and tectorial membrane and then permeabilized the tissue with 0.3% Triton X-100 in PBS with 1% goat serum for 10 min. Nonspecific binding of secondary antibodies was blocked with 5% BSA in PBS for 20 min. Tissues were reacted with primary antibody, rinsed and incubated with the secondary antibody. Specimens were mounted on glass slides using Crystal Mount (Biomedex, Foster City, CA). To perform double staining of Atoh1 and SKP2, we used a primary anti-Atoh1 monoclonal antibody (1:4 dilution, University of Iowa Hybridoma Core) and a rabbit polyclonal anti-SKP2 antibody (1:300 dilution, Santa Cruz Biotechnology, Santa Cruz, CA). Secondary antibodies were TRITC-conjugated goat anti-mouse (diluted 1:200, Jackson ImmunoResearch, West Grove, PA) and FITC-conjugated goat anti-rabbit (diluted 1:300, Jackson ImmunoResearch). Samples were evaluated under a Leica DMRB epifluorescence microscope (Leica, Eaton, PA) using 40x and 100x oil objectives and a CCD-Cooled SPOT-RT digital camera (Diagnostic Instruments, Sterling Heights, MI).

BrdU study

This experiment was done to determine the uptake of BrdU by cells undergoing DNA synthesis. BrdU was given to 6 animals from the Ad.*SKP2* group and 4 animals that received Ad.empty. Contralateral ears of these 10 animals served as additional controls. BrdU was administered in the drinking water from day 1 to day 14 after the inoculation of the viral vector(s). Two weeks after the surgery, all animals were euthanized and their ears and gut (positive control) were prepared for immuno-staining with anti-BrdU antibody. The cochleae were fixed with 4% paraformaldehyde in phosphate buffer, pH 7.4, permeabilized in 0.3% Triton X-100, incubated with 3% hydrogen peroxide for 30 min, immersed in 2N HCl for 30 min, and then incubated with mouse monoclonal antibody against BrdU (Sigma, Saint Louis, MO) for 30 min. A peroxidase-conjugated secondary anti-mouse antibody (ABC kit, Vector Laboratories, Burlingame, CA) was used, followed by DAB. After completion of immuno-staining, specimens were decalcified in 3% EDTA for 7 days, embedded in JB-4 resin (Electron Microscopy Sciences, Hatfield, PA) and sectioned (5 μ m thickness). Every third section was collected, so that a given nucleus could only be counted once. Sections were mounted on glass slides and observed using light microscopy. The presence of BrdU-positive cells was assessed in 50 sections taken from serial sections of inoculated ears.

Data analysis

All analyses were performed using SPSS 13. Because of the small sample sizes, Fisher's exact test for the 2×2 contingency table comparing BrdU uptake between Ad.*SKP2* treated animals and controls. A one-sided t-test was used to test the hypothesis that treatment with both *Atoh1* and *SKP2* produced more ectopic hair cells than treatment with *Atoh1*, alone.

3. RESULTS

p27^{Kip1} is expressed in the mature auditory epithelium in and around the organ of Corti

We used antibodies to localize to p27^{Kip1} in whole-mounts of the normal mature auditory epithelium. The whole-mounts included tissues from the interdental cell layer (medially) to the outer sulcus (laterally). At a focal plane just above the basilar membrane, staining was detected in nuclei of Deiters and pillar cells within the sensory epithelium, and in Hensen cells (Fig. 1A). The staining intensity in Hensen cells was invariably higher compared to supporting cells in the sensory epithelium. At a slightly higher focal plane Hensen cell nuclei were strongly positive whereas hair cells were all negative (Fig. 1B). Other non-sensory cells that were p27^{Kip1} positive were inner sulcus cells and the interdental cells on the limbus (data not shown).

Over-expression of *Skp2* induces proliferation in the auditory epithelium

In animals that received BrdU for 2 weeks following the Ad.*SKP2* inoculation, and sacrificed 2 weeks later, several BrdU positive cells were found in the interdental cell area (Fig. 2) and the inner sulcus (data not shown). Some of the BrdU positive cells appeared in pairs. In the plastic sections we examined, cells within the organ of Corti did not exhibit BrdU staining. All 6 Ad.*SKP2* inoculated animals that received BrdU had BrdU-positive cells, whereas none of the 4 control animals that received BrdU, but not Ad.*SKP2*, had positive cells. Fisher's exact test of the corresponding 2×2 contingency table indicates this difference in BrdU uptake is significant ($p=0.005$). The number of BrdU positive cells in each section was between 5 and 10, suggesting that with extrapolation the total number per ear could have reached many hundreds.

Gene Expression of *Atoh1* and *Skp2*

The dual inoculation with Ad.*Atoh1* and Ad.*SKP2* was done by mixing equal amounts of each vector prior to inoculation. This leads to a dilution of each vector to half its original concentration and therefore to an overall reduction in the efficiency of gene expression. As such, the number of cells that are transduced by both vectors is limited. Cells expressing the *Atoh1* and *SKP2* transgenes are seen in the interdental cell region (Fig. 3A), in the organ of Corti, and in Hensen cell area (Fig. 3B). Staining for these transgenes was confined to the nucleus. The images were obtained at a focal plane immediately beneath the luminal surface. As expected, most transduced cells expressed only one transgene but dually transduced cells were found in all samples of the experimental group. Animals that received control inoculations did not show any positive staining with antibodies to these two proteins.

Ectopic hair cells

SEM analysis revealed numerous ectopic hair cells in ears inoculated simultaneously with Ad.*Atoh1* and Ad.*Skp2* (Fig. 4 A-C). Inoculation of Ad.*Atoh1* alone also induced generation of ectopic hair cells (Fig. 4B), but their number was smaller than that seen in the combined *Atoh1* and *SKP2* group. The mean number of ectopic hair cells \pm standard deviation in the 2nd turn of the 8 cochleae that received the combined (*Atoh1* and *SKP2*) inoculation was 17.8 ± 17.4 . In the group receiving the Ad.*Atoh1* alone (5 animals) the mean number of ectopic hair cells was 1.40 ± 1.67 . Thus the combined treatment produced more ectopic hair cells than did treatment with only *Atoh1* ($p=0.017$).

In the combined group, the highest number of ectopic hair cells was found near the site of inoculation. In this area, some of the ectopic hair cells existed in pairs (Fig. 4D). Some of the new hair cells exhibited a long and/or thick kinocilium-like projection in addition to the stereocilia (Fig. 4C and E). There were no ectopic hair cells in the cochleae of guinea pigs inoculated with the Ad.*SKP2* vector alone. Ad.empty or artificial endolymph inoculations did not lead to formation of ectopic hair cells either (data not shown).

4. DISCUSSION

Our data show that *p27^{Kip1}* is expressed in non-sensory cells flanking the organ of Corti of the mature guinea pig. We demonstrate that forced expression of *SKP2* leads to proliferation in non-sensory cells around the organ of Corti and that combined inoculation of Ad.*SKP2* and Ad.*Atoh1* enhances the number of newly generated ectopic hair cells as compared to over-expressing *Atoh1* alone.

The presence of *p27^{Kip1}* in non-sensory cells of the membranous labyrinth has previously been documented in the developing mouse cochlea (Chen and Segil, 1999; Dong et al., 2003; Lowenheim et al., 1999). The present study extends the finding to the guinea pig model and provides whole-mount analysis that allows for the detection of the protein in large experimental fields. The data reveal that *p27^{Kip1}* expression is maintained into adulthood in supporting cells of the organ of Corti as well as in areas outside the organ of Corti. Interestingly, the staining intensity appeared weaker in the supporting cells of the sensory epithelium (Deiters and pillar cells) as compared to Hensen cells which flank the sensory epithelium. The reason for this difference is unclear.

In *p27^{Kip1}* null mice, proliferation of non-sensory cells continues in the organ of Corti, leading to generation of supplementary hair cells (Chen and Segil, 1999; Lowenheim et al., 1999). In the mature guinea pig ears examined in this study, forced expression of *SKP2* did not cause a notable presence of BrdU-positive cells in the organ of Corti proper. BrdU-positive cells were localized in areas flanking the sensory epithelium. It is presently unclear why the localization of proliferation site differs between the two models.

The number of ectopic cells generated by *Atoh1* over-expression alone is limited (Izumikawa et al., 2005; Kawamoto et al., 2003). The ability of *SKP2* to increase the number of ectopic cells generated by *Atoh1* suggests that therapies for cell cycle enhancement and transdifferentiation can be combined. It also indicates that mature non-sensory cells that undergo cell division can respond to the developmental signals provided by *Atoh1*. The data suggest that in areas adjacent to the organ of Corti the expression of *SKP2* leads to proliferation of the non-sensory cells, which by itself is not sufficient for generating new hair cells. These findings are in agreement with the outcome of disrupted *p27^{Kip1}* in mice, where the number of hair cells is increased only in the organ of Corti and not in areas flanking the sensory epithelium (Chen and Segil, 1999; Kanzaki et al., 2006; Lowenheim et al., 1999), despite the fact that cell division continues in flanking areas (Chen and Segil, 1999). Our overall interpretation of these data is that *p27^{Kip1}* blocks proliferation in non-sensory cells in and around the organ of Corti, and that in the absence of this block, new cells that are generated in the organ of Corti proper can become new hair cells without further intervention. In ectopic areas, however, it is necessary to force expression of hair cells genes such as *Atoh1* to generate new hair cells.

The area immediately adjacent to the site of inoculation was excluded from the statistical analysis, because tissue in this area responded to the mechanical trauma (related to the inoculation) as well as the presence of the transgenes. Therefore the numbers presented here may represent an underestimate of the total number of newly generated hair cells. The area of

the organ of Corti was also excluded from the counting, because the procedure was performed on non-deafened guinea pigs. Many hair cells degenerate in response to the procedure of endolymphatic inoculation, and regenerated hair cells could have taken their place. However, we were unable to distinguish between original hair cells and possibly regenerated hair cells within the organ of Corti and therefore did not count hair cells in this area.

The increase in ectopic hair cell number and the presence of paired hair cells following the combined treatment with *SKP2* and *Atoh1* indicate that new hair cells may be generated via mitotic division followed by transdifferentiation. This finding has important implications for future clinical use of hair cell regeneration therapy. The fact that post-mitotic cells can attain the hair cell phenotype is encouraging in that these cells are less likely to continue dividing and form a tumor. It is also important to observe that non-sensory cells retain their responsiveness to *Atoh1* after division. This is not trivial, because these cells de-differentiate morphologically in order to divide. However, the data corroborate finding in vertebrates other than mammals, including avian species, where mitotic transdifferentiation is the main spontaneous route of hair cell regeneration.

Ectopic hair cells were not found following forced expression of *SKP2* alone, despite the presence of BrdU positive cells. This suggests that proliferation by itself is insufficient for inducing generation of new hair cells in the mature ear. This finding appears to contrast with the situation in the developing ear of mice with loss of function of *p27^{Kip1}* or *Rb1*, where the cell cycle regulation is disrupted and the phenotypic outcome is excessive number of hair cells (Chen and Segil, 1999; Lowenheim et al., 1999; Sage et al., 2005). It is possible that once an animal is mature, the addition of supernumerary hair cells due to the defect in cell cycle regulation is reduced, as seen in mature mice deficient for *p27^{Kip1}* (Kanzaki et al., 2006).

In this study, the forced expression of *SKP2* and *Atoh1* was accomplished by two different viral vectors, one for each gene. For several reasons, this approach leads to a small number of cells that are transduced by both vectors. First, mixing Ad.*Atoh1* and Ad.*SKP2* prior to inoculation dilutes the concentration of each vector by 50%, thereby lowering the overall efficiency of transgene expression. Second, the chance for a cell to be transduced by both vectors is further reduced. The timing of vector delivery may also matter for maximizing the effect on proliferation and transdifferentiation. In these experiments, the vectors were applied simultaneously, which may have further compromised production of a large number of new hair cells. The efficiency of generating new hair cells would likely be enhanced by utilization of a virus vector encoding both *Skp2* and *Atoh1*, which would increase the rate of cells simultaneously expressing both transgenes, and/or by optimized timing for sequential use of the vectors.

The presence of newly generated cochlear hair cells does not necessarily imply that hearing improves toward normal hearing. It is possible that tinnitus may also result from the new hair cells, and the presence of ectopic hair cells further complicates the physiological outcome. Interestingly, mice with deficient *p27^{Kip1}* expression have very poor hearing (Chen and Segil, 1999; Kanzaki et al., 2006; Lowenheim et al., 1999). It is currently unclear whether the functional quality of hair cells that arise due to *p27^{Kip1}* deficiencies is lacking in some way, or if other problems in these mice, in the ear and elsewhere, contribute to the deficiency. The next step in assessing the feasibility of the combined *SKP2* / *Atoh1* treatment would be histological and physiological assessment of such therapy in deafened mature mammals.

Manipulation of cell cycle regulation for therapeutic purposes is usually aimed at treating cancer, by stabilizing and enhancing *p27^{Kip1}* expression (Sumimoto et al., 2005; Supriatno et al., 2005). In contrast, our study looked at the effects of antagonizing *p27^{Kip1}* by over-expressing *SKP2*. This strategy is relevant to cases where adding new cells may contribute to

the therapeutic goals. Promoting cell cycle with SKP2 has also been attempted in cultured primary hepatocytes and in hepatocytes in vivo and resulted in mitosis in hepatocytes that were otherwise quiescent (Nelsen et al., 2001). Although this therapy is attractive, it would be important to improve the control of gene expression to ascertain that proliferation remains limited in place and time so as not to promote tumor formation.

In addition to p27^{Kip1}, enhanced proliferation in the post-mitotic organ of Corti has been shown with disruption of cell cycle regulatory gene *Rb1* (Sage et al., 2005). It is presently unclear if the two genes act on the same signaling cascade in regulating cell cycle arrest in non-sensory cells of the auditory epithelium. Based on studies in other tissue models, it is possible that Rb1 represses Skp2 resulting in stabilizing p27^{Kip1}, leading to arrest of the cell cycle (Ji and Zhu, 2005). Better understanding of the specific role of each gene in regulating proliferation in the auditory epithelium will help design robust yet well regulated means for increasing the number of cells in the tissue. This is important, because therapy for hair cell regeneration based on transdifferentiation of non-sensory cells requires that a large enough number of supporting cells remain in the deaf auditory epithelium.

The results we present do not provide evidence for a direct causative relationship between *SKP2* and p27^{Kip1}. It is possible that proliferation due to *SKP2* forced expression is accomplished by another signaling cascade, not directly involving p27^{Kip1}. Further work is necessary for elucidating the molecular signaling initiated by *SKP2* in non-sensory cochlear cells resulting in a proliferative response in these cells.

In conclusion, we determined that *p27^{Kip1}* is expressed in the mature auditory epithelium in the organ of Corti and in adjacent regions. Co-expression of Ad.*Atoh1* and Ad.*SKP2* enhances the number of ectopic hair cells compared to *Atoh1* over-expression alone. Forced expression of *SKP2* alone induces proliferation but does not enhance generation of new hair cells. These findings demonstrate that targeted enhancement of proliferation is by itself insufficient for inducing hair cell regeneration, but when combined with forced expression of *Atoh1*, regeneration in the mature auditory epithelium can be enhanced. The data suggest that therapies can be designed to induce proliferation in the auditory epithelium by removing the inhibition on cell cycle.

Acknowledgements

We thank Lisa Beyer for technical assistance and Don Swederski for help with statistics and manuscript preparation. We thank GenVec for providing the Ad.*Atoh1* and control vectors. The work is supported by the Williams Professorship, a gift from Berte and Alan Hirschfield, and by NIH/NIDCD Grants DC-01634, DC-05401, DC-03685 and DC05188.

References

- Bermingham NA, Hassan BA, Price SD, Vollrath MA, Ben-Arie N, Eatock RA, Bellen HJ, Lysakowski A, Zoghbi HY. Math1: an essential gene for the generation of inner ear hair cells. *Science* 1999;284:1837–1841. [PubMed: 10364557]
- Brough DE, Lizonova A, Hsu C, Kulesa VA, Kovesdi I. A gene transfer vector-cell line system for complete functional complementation of adenovirus early regions E1 and E4. *J. Virol* 1996;70
- Chen P, Segil N. p27(Kip1) links cell proliferation to morphogenesis in the developing organ of Corti. *Development* 1999;126:1581–1590. [PubMed: 10079221]
- Chen P, Johnson JE, Zoghbi HY, Segil N. The role of Math1 in inner ear development: Uncoupling the establishment of the sensory primordium from hair cell fate determination. *Development* 2002;129:2495–2505. [PubMed: 11973280]
- Chen P, Zindy F, Abdala C, Liu F, Li X, Roussel MF, Segil N. Progressive hearing loss in mice lacking the cyclin-dependent kinase inhibitor Ink4d. *Nat. Cell Biol* 2003;5:422–426. [PubMed: 12717441]

- Cotanche DA. Hair cell regeneration in the avian cochlea. *Annals Otol. Rhinol. Laryngol.- Suppl* 1997;168:9–15.
- Dong Y, Nakagawa T, Endo T, Kim TS, Iguchi F, Yamamoto N, Naito Y, Ito J. Role of the F-box protein Skp2 in cell proliferation in the developing auditory system in mice. *Neuroreport* 2003;14:759–761. [PubMed: 12692478]
- Dooling RJ, Ryals BM, Manabe K. Recovery of hearing and vocal behavior after hair-cell regeneration. *Proc. Natl. Acad. Sci. U. S. A* 1997;94:14206–14210. [PubMed: 9391178]
- Gervais JL, Seth P, Zhang H. Cleavage of CDK inhibitor p21(Cip1/Waf1) by caspases is an early event during DNA damage-induced apoptosis. *J. Biol. Chem* 1998;273:19207–19212. [PubMed: 9668108]
- Harper J. Protein destruction: adapting roles for Cks proteins. *Curr. Biol* 2001;11:R431–435. [PubMed: 11516665]
- Hashino E, Salvi RJ. Changing spatial patterns of DNA replication in the noise-damaged chick cochlea. *J. Cell Sci* 1993;105:23–31. [PubMed: 8360276]
- He TC, Zhou S, da Costa LT, Yu J, Kinzler KW, Vogelstein B. A simplified system for generating recombinant adenoviruses. *Proc. Natl. Acad. Sci. U. S. A* 1998;95:2509–2514. [PubMed: 9482916]
- Ishimoto S, Kawamoto K, Kanzaki S, Raphael Y. Gene transfer into supporting cells of the organ of Corti. *Hear. Res* 2002;173:187–197. [PubMed: 12372646]
- Izumikawa M, Minoda R, Kawamoto K, Abrashkin KA, Swiderski DL, Dolan DF, Brough DE, Raphael Y. Auditory hair cell replacement and hearing improvement by Atoh1 gene therapy in deaf mammals. *Nat. Med* 2005;11:271–276. [PubMed: 15711559]
- Ji P, Zhu L. Using kinetic studies to uncover new Rb functions in inhibiting cell cycle progression. *Cell Cycle* 2005;4:373–375. [PubMed: 15701969]
- Kanzaki S, Beyer LA, Swiderski DL, Izumikawa M, Stover T, Kawamoto K, Raphael Y. p27(Kip1) deficiency causes organ of Corti pathology and hearing loss. *Hear. Res* 2006;214:28–36. [PubMed: 16513305]
- Kawamoto K, Ishimoto S, Minoda R, Brough DE, Raphael Y. Math1 gene transfer generates new cochlear hair cells in mature guinea pigs in vivo. *J. Neurosci* 2003;23:4395–4400. [PubMed: 12805278]
- Lowenheim H, Furness DN, Kil J, Zinn C, Gultig K, Fero ML, Frost D, Gummer AW, Roberts JM, Rubel EW, Hackney CM, Zenner HP. Gene disruption of p27(Kip1) allows cell proliferation in the postnatal and adult organ of Corti. *Proc. Natl. Acad. Sci. U. S. A* 1999;96:4084–4088. [PubMed: 10097167]
- Marean GC, Cunningham D, Burt JM, Beecher MD, Rubel EW. Regenerated hair cells in the European starling: are they more resistant to kanamycin ototoxicity than original hair cells? *Hear. Res* 1995;82:267–276. [PubMed: 7775291]
- Nakayama K, Nagahama H, Minamishima YA, Matsumoto M, Nakamichi I, Kitagawa K, Shirane M, Tsunematsu R, Tsukiyama T, Ishida N, Kitagawa M, Hatakeyama S. Targeted disruption of Skp2 results in accumulation of cyclin E and p27(Kip1), polyploidy and centrosome overduplication. *EMBO J* 2000;19:2069–2081. [PubMed: 10790373]
- Nakayama KI HS, Nakayama K. Regulation of the cell cycle at the G1-S transition by proteolysis of cyclin E and p27Kip1. *Biochem. Biophys. Res. Commun* 2001;282:853–860. [PubMed: 11352628]
- Nelsen CJ, Hansen LK, Rickheim DG, Chen C, Stanley MW, Krek W, Albrecht JH. Induction of hepatocyte proliferation and liver hyperplasia by the targeted expression of cyclin E and skp2. *Oncogene* 2001;20:1825–1831. [PubMed: 11313930]
- Niemiec AJ, Raphael Y, Moody DB. Return of auditory function following structural regeneration after acoustic trauma: behavioral measures from quail. *Hear. Res* 1994;79:1–16. [PubMed: 7806472]
- Raphael Y. Evidence for supporting cell mitosis in response to acoustic trauma in the avian inner ear. *J. Neurocytol* 1992;21:663–671. [PubMed: 1403011]
- Sage C, Huang M, Karimi K, Gutierrez G, Vollrath MA, Zhang DS, Garcia-Anoveros J, Hinds PW, Corwin JT, Corey DP, Chen ZY. Proliferation of functional hair cells in vivo in the absence of the retinoblastoma protein. *Science* 2005;307:1114–1118. [PubMed: 15653467]
- Saunders JC, Adler HJ, Pugliano FA. The structural and functional aspects of hair cell regeneration in the chick as a result of exposure to intense sound. *Exp. Neurol* 1992;115:13–17. [PubMed: 1728559]
- Sherr CJ, Roberts JM. CDK inhibitors: positive and negative regulators of G1-phase progression. *Genes Dev* 1999;13:1501–1512. [PubMed: 10385618]

- Shou J, Zheng JL, Gao WQ. Robust generation of new hair cells in the mature mammalian inner ear by adenoviral expression of *Hath1*. *Mol. Cell. Neurosci* 2003;23:169–179. [PubMed: 12812751]
- Stone JS, Cotanche DA. Identification of the timing of S phase and the patterns of cell proliferation during hair cell regeneration in the chick cochlea. *J. Comp. Neurol* 1994;341:50–67. [PubMed: 8006223]
- Stone JS, Rubel EW. Cellular studies of auditory hair cell regeneration in birds. *Proc. Natl. Acad. Sci. U. S. A* 2000;97:11714–11721. [PubMed: 11050200]
- Sumimoto H, Yamagata S, Shimizu A, Miyoshi H, Mizuguchi H, Hayakawa T, Miyagishi M, Taira K, Kawakami Y. Gene therapy for human small-cell lung carcinoma by inactivation of *Skp-2* with virally mediated RNA interference. *Gene Ther* 2005;12:95–100. [PubMed: 15385954]
- Supriatno, Harada K, Yoshida H, Sato M. Basic investigation on the development of molecular targeting therapy against cyclin-dependent kinase inhibitor p27Kip1 in head and neck cancer cells. *Int. J. Oncol* 2005;27:627–635. [PubMed: 16077910]
- Woods C, Montcouquiol M, Kelley MW. *Math1* regulates development of the sensory epithelium in the mammalian cochlea. *Nat. Neurosci.* 2004
- Zheng JL, Gao WQ. Overexpression of *Math1* induces robust production of extra hair cells in postnatal rat inner ears. *Nat. Neurosci* 2000;3:580–586. [PubMed: 10816314]
- Zheng JL, Shou J, Guillemot F, Kageyama R, Gao WQ. *Hes1* is a negative regulator of inner ear hair cell differentiation. *Development* 2000;127:4551–4560. [PubMed: 11023859]
- Zine A, Aubert A, Qiu J, Therianos S, Guillemot F, Kageyama R, de Ribaupierre F. *Hes1* and *Hes5* activities are required for the normal development of the hair cells in the mammalian inner ear. *J. Neurosci* 2001;21:4712–4720. [PubMed: 11425898]

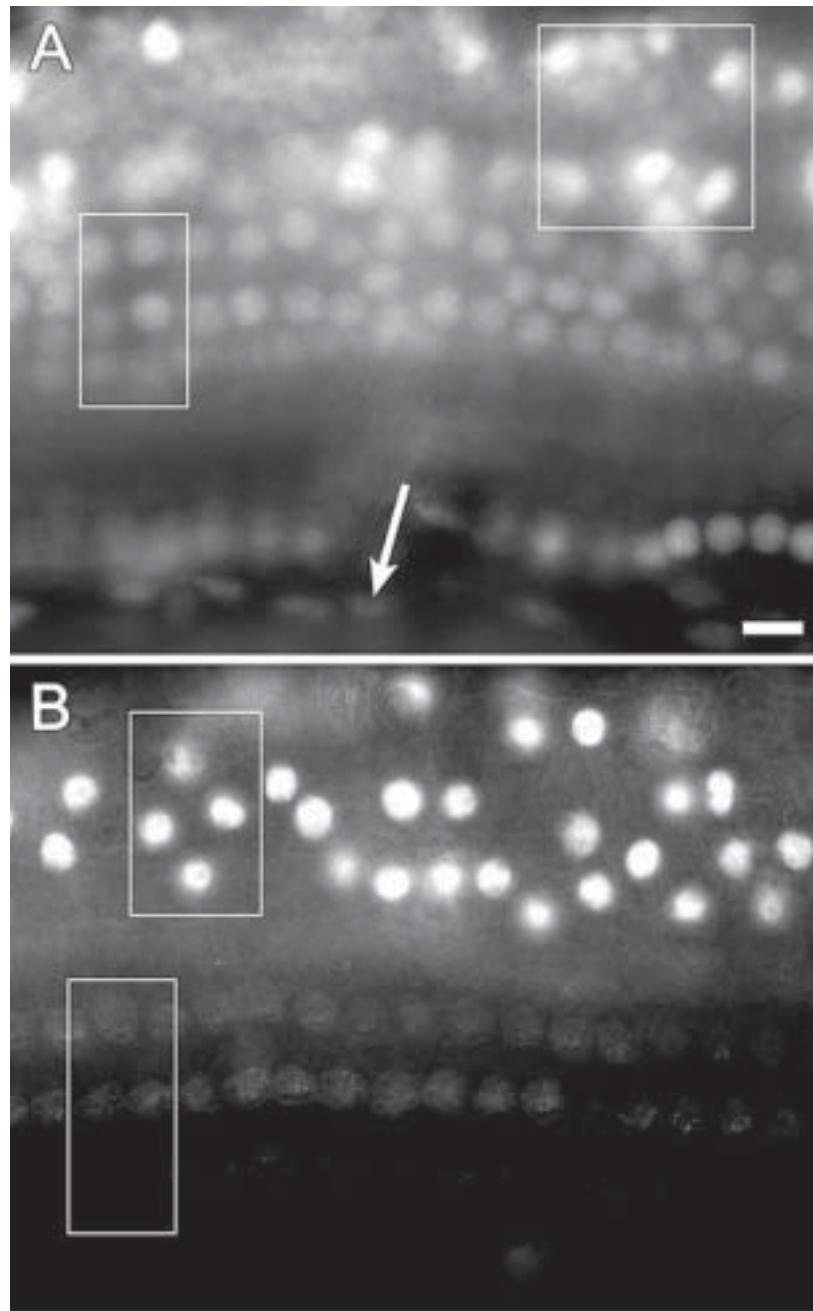


Figure 1. The normal distribution of p27^{Kip1} in mature guinea pig ears shown by immunofluorescence on whole-mounts of the auditory epithelium. A. At a focal plane immediately above the basilar membrane positive nuclei are found in Deiters cells (rectangle), Hensen cells (square) and inner pillar cells (round nuclei at bottom of image). Spindle shaped mesothelial cells located beneath the basilar membrane display background level staining (arrow). B. At a higher focal plane, p27^{Kip1} positive nuclei are found in Hensen cells (top rectangle) whereas nuclei of hair cells are at background staining level (bottom rectangle). Bar, 10 μ m for A and B.

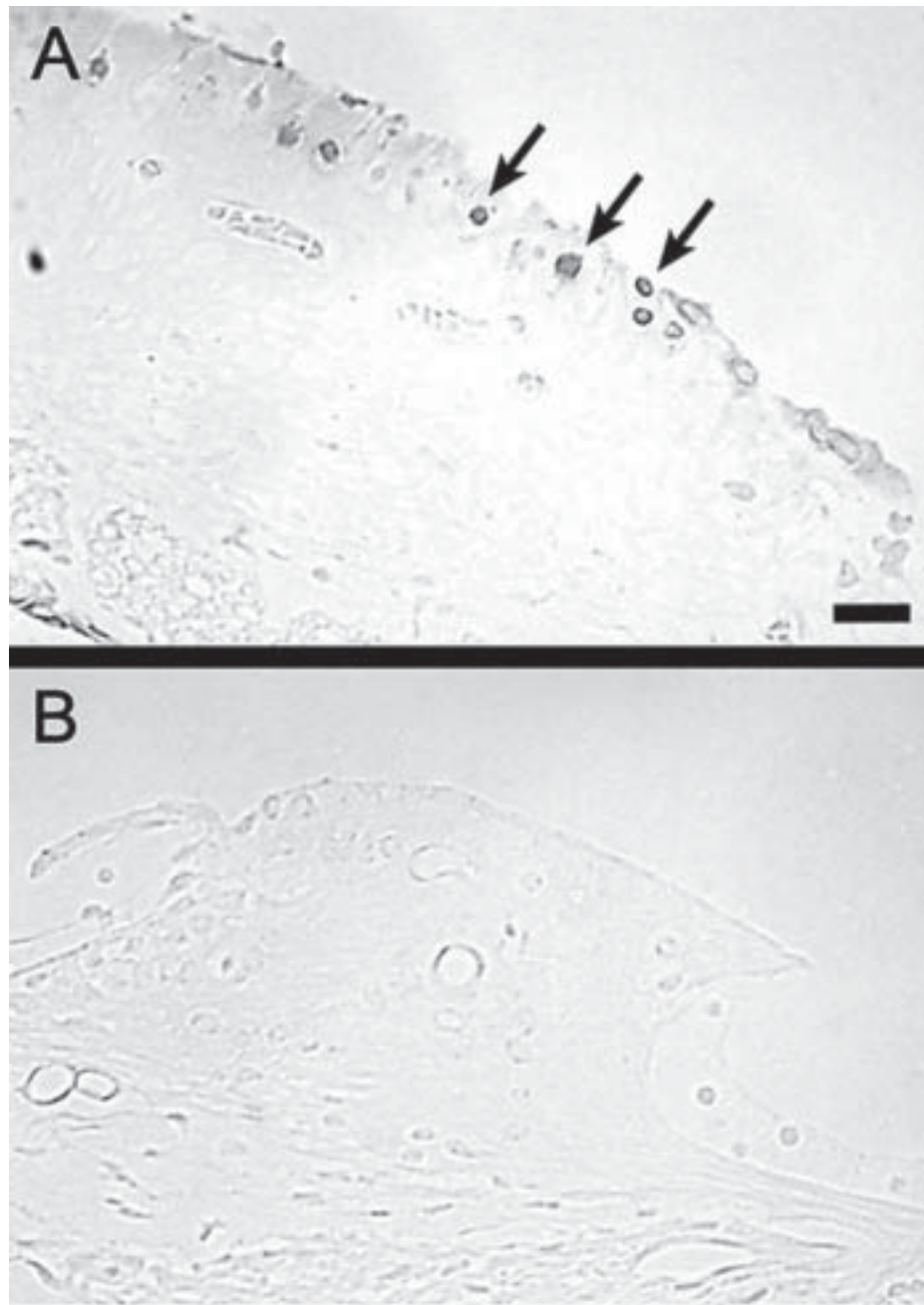


Figure 2. Plastic sections of the auditory epithelium of an Ad.*SKP2* treated ear (A) and an Ad.empty control ear (B) stained with antibody to BrdU. A. Numerous BrdU-positive cells are found in the interdental cell region (arrows). B. No BrdU-positive cells are seen in a control ear. Bar, 25 μ m for A and B.

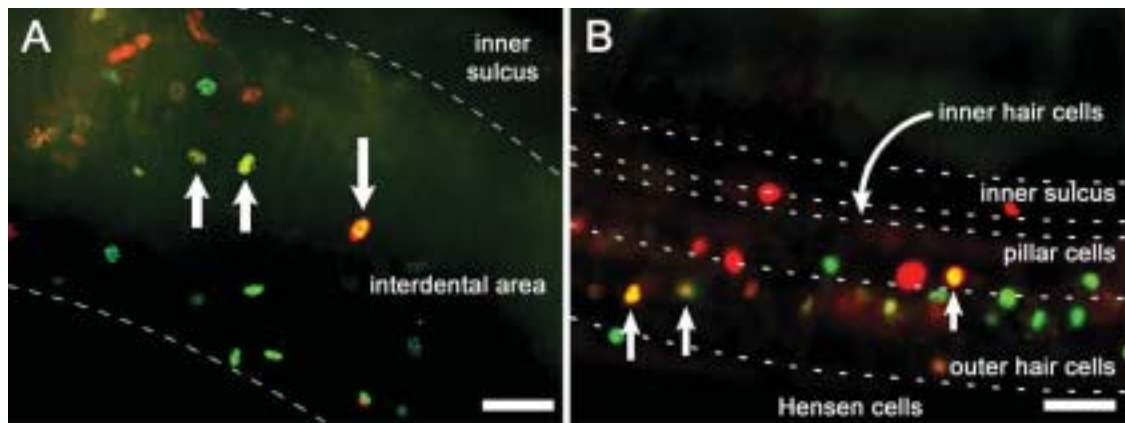


Figure 3.

Epi-fluorescence images of whole-mounts of the organ of Corti double immuno-labeled for *Atoh1* (green) and *SKP2* (red) 4 days after *Ad.Atoh1* and *Ad.SK2* inoculation. Images were obtained immediately beneath the luminal surface. A. In the interdentary cell region, numerous cells are stained for *Atoh1* or *SKP2*, and a small number of cells (yellow) express both proteins (arrows). B. In the organ of Corti and Hensen cell area, several cells (arrow) are yellow indicating dual expression of *SKP2* and *Atoh1* while others express either *Atoh1* (green) or *SKP2* (red). Dashed lines delimit regions within the tissue. Bar, 20 μ m.

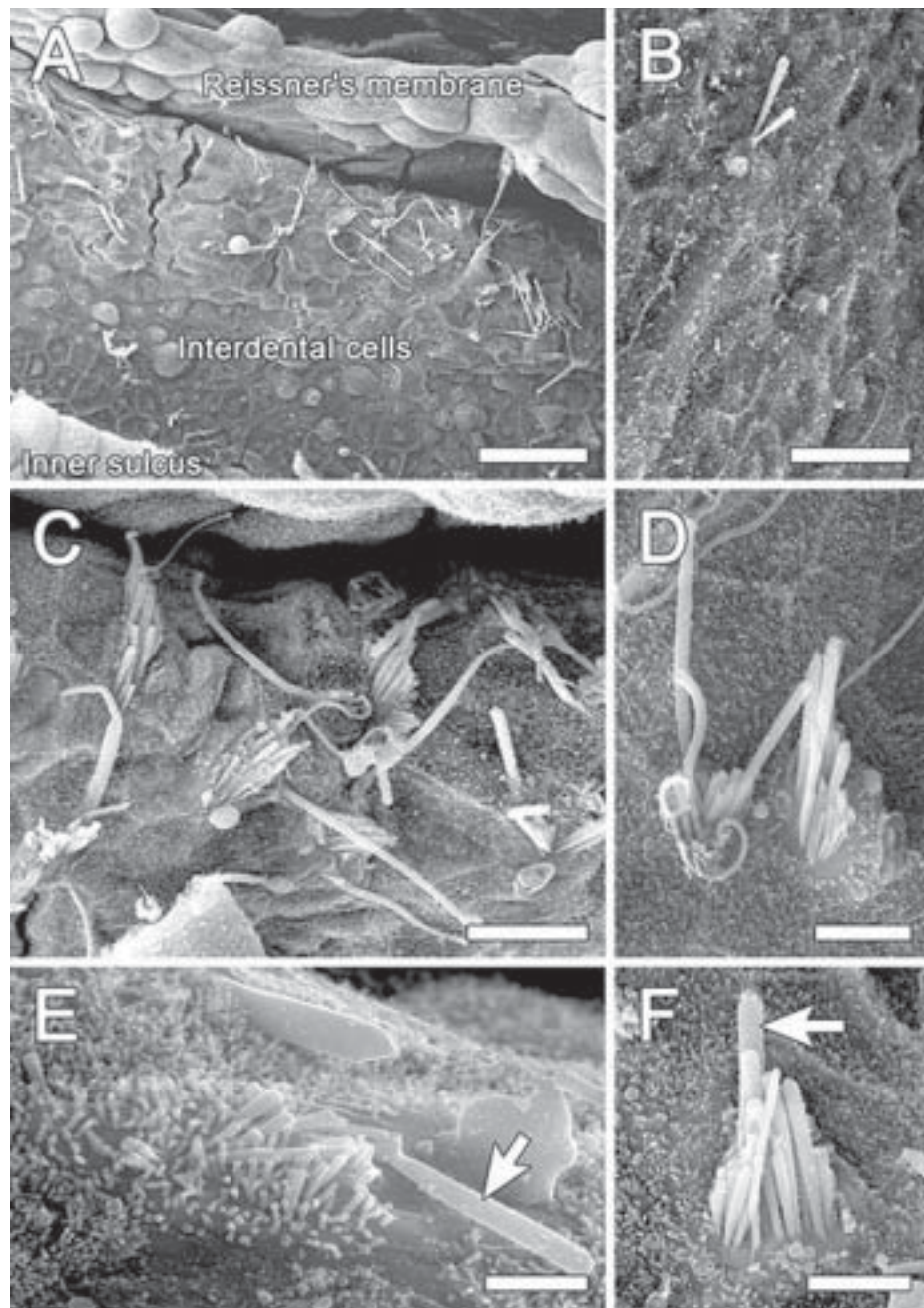
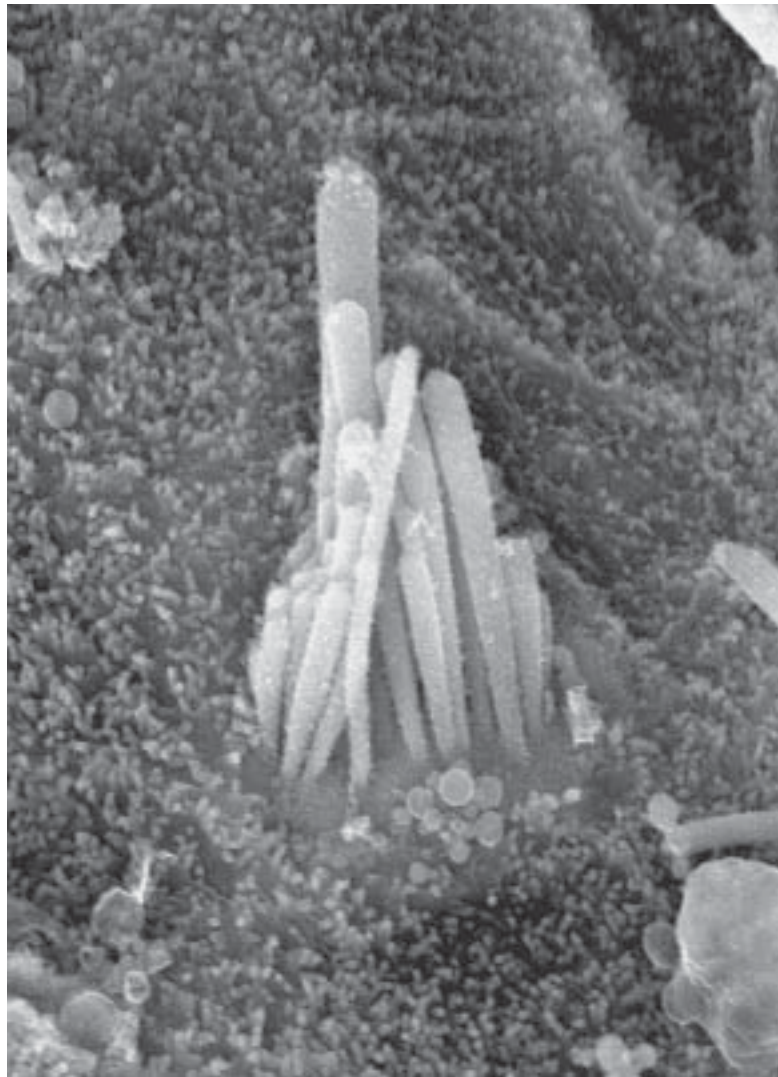


Figure 4. SEM images of interdigital cell area (2nd turn) 2 months after inoculation of *Ad.Atoh1* and *Ad.SK2* (A and C-F) or *Ad.Atoh1* alone (B). A. Numerous ectopic stereocilia bundles on the limbus, reaching to the area where Reissner's membrane is inserted. B. A single ectopic bundle among interdigital cells on the limbus. C. An enlarged area in (A) showing stereocilia bundles in an ectopic location on the limbus. Some bundles contain a graded array of stereocilia and others are rather disorganized. A kinocilium-like projection is seen on some of the bundles. D. Two ectopic hair cells appearing as a pair. E. Some ectopic hair cells appear like immature cells and exhibit a long and/or thick kinocilium-like protrusion (arrow). F. An ectopic hair cell

with a staircase organization of stereocilia and a projection that appears like a kinocilium (arrow). Bars, 30 μm in A, 10 μm in B, C, 5 μm in D, 2 μm in E, and 3 μm in F.



Suggested Cover Image.

SEM micrograph of an ectopic hair cell residing on the spiral limbus following inoculation of adenoviral vectors expressing *Atoh1* and *SKP2* into the cochlear endolymph of guinea pigs.



ELSEVIER

Available online at www.sciencedirect.com

SCIENCE @ DIRECT®

Hearing Research 218 (2006) 20–29

Hearing
Research

www.elsevier.com/locate/heares

Research paper

The fate of outer hair cells after acoustic or ototoxic insults

Karen A. Abrashkin, Masahiko Izumikawa, Toru Miyazawa, Chih-Hung Wang,
Mark A. Crumling, Donald L. Swiderski, Lisa A. Beyrer,
Tzy-Wen L. Gong, Yehoash Raphael *

Kresge Hearing Research Institute, Department of Otolaryngology, Rm. 9301 MSRB-3, Ann Arbor, MI 48109-0648, USA

Received 12 December 2005; received in revised form 7 April 2006; accepted 10 April 2006

Available online 14 June 2006

Abstract

In epithelial sheets, clearance of dead cells may occur by one of several routes, including extrusion into the lumen, phagocytic clearance by invading lymphocytes, or phagocytosis by neighboring cells. The fate of dead cochlear outer hair cells is unclear. We investigated the fate of the “corpses” of dead outer hair cells in guinea pigs and mice following drug or noise exposure. We examined whole mounts and plastic sections of normal and lesioned organ of Corti for the presence of prestin, a protein unique to outer hair cells. Supporting cells, which are devoid of prestin in the normal ear, contained clumps of prestin in areas of hair cell loss. The data show that cochlear supporting cells surround the corpses and/or debris of degenerated outer hair cells, and suggest that outer hair cell remains are phagocytosed by supporting cells within the epithelium.

© 2006 Elsevier B.V. All rights reserved.

Keywords: Guinea pig; Mouse; Prestin; Overstimulation; Ototoxicity; Outer hair cell; Supporting cell

1. Introduction

The process of cell death during development and in mature tissues has been extensively studied. Cells can be eliminated either by their neighbors or by professional scavengers such as macrophages. In both cases, specific molecules mediate cell–cell signaling associated with clearance of cell corpses, sending “find-me”, “eat-me” and “don’t-eat-me” signals (Lauber et al., 2004). In sheets of epithelial cells, the highly regulated process of cell elimination is particularly important because of the need to main-

tain structural and functional integrity of the luminal surface (Rosenblatt et al., 2001).

The organ of Corti is the auditory sensory epithelium of mammals. It consists of a highly organized mosaic of hair cells and supporting cells. The strictly organized pattern of the organ of Corti makes it a useful model for studying the process of cell death and elimination. One type of hair cell in the mosaic is the outer hair cell (OHC). OHCs enhance the sensitivity and frequency selectivity of the organ of Corti mainly through the action of the membrane motor protein prestin (Belyantseva et al., 2000; Dallos and Fakler, 2002; Zheng et al., 2000). OHC death in mammals leads to a hearing deficiency that is permanent, because lost hair cells do not spontaneously regenerate (Daudet et al., 1998; Engstrom et al., 1970; Hawkins, 1973; Spoendlin, 1976; Wang and Li, 2000; Yamasoba et al., 2003). When hair cells die, the adjacent supporting cells quickly expand in a highly regulated manner and quickly close the gap that would be left by damaged hair cells (Forge, 1985; Leonova

Abbreviations: OHC, outer hair cell; IHC, inner hair cell; GFP, green fluorescent protein; qRT-PCR, quantitative real-time polymerase chain reaction; Ad, adenovirus; SPL, sound pressure level; PBS, phosphate buffered saline; DAB, 3,3'-diaminobenzidine tetrahydrochloride; EDTA, ethylenediaminetetraacetic acid

* Corresponding author. Tel.: +1 734 936 9386; fax: +1 734 615 8111.

E-mail address: Yoash@umich.edu (Y. Raphael).

and Raphael, 1997; Raphael and Altschuler, 1991a,b). Sites of hair cell degeneration where supporting cells seal the luminal surface are called phalangeal scars. The fate of the damaged or dead hair cells remains unknown. In exploring how the “corpses” of hair cells are removed from the epithelium, it is important to consider whether injured or damaged hair cells are ejected from the organ of Corti and removed by the immune system, or whether they remain within the organ of Corti where they are engulfed by neighboring supporting cells or invading phagocytic cells.

The aim of this study was to investigate the fate of OHC corpses following cochlear insults that lead to hair cell degeneration. We used ototoxic drugs or acoustic overstimulation to induce hair cell death. The level of *prestin* mRNA in the cochlea decreased after the insult. Prestin, an OHC protein that is normally absent from supporting cells (Belyantseva et al., 2000; Dallos and Fakler, 2002; Zheng et al., 2000), was used as a marker to identify intact OHCs and remnants of damaged OHCs. Using whole mounts and transverse sections of the organ of Corti, we found that sites of hair cell loss consisted of scarring supporting cells and prestin aggregates. Overall, the data suggest that supporting cells phagocytose injured or dead hair cells and/or their debris.

2. Experimental procedures

2.1. Animals and deafening

All animal experiments were approved by the University Committee on Use and Care of Animals at the University of Michigan. We used young adult male guinea pigs (pigmented SPF animals from Elm Hill Breeding Labs, Chelmsford, MA) and 30–60-day old CD-1 mice of either sex (Charles River Breeding Labs, Wilmington, MA). In guinea pig experiments, hair cell lesions were induced by ototoxic insult or noise exposure. For ototoxic deafening, guinea pigs ($N = 11$) were given kanamycin (American Pharmaceutical Partners, Inc., Schaumburg, IL) and ethacrynic acid (Sodium Edecrin, Merck and Co., Inc., West Point, PA), as follows: a single dose of kanamycin (500 mg/kg, s.c.) was injected, followed 2 h later by ethacrynic acid (50 mg/kg, i.v.). Four of the 11 guinea pigs deafened with ototoxic drugs were inoculated with an adenoviral vector with a *GFP* gene insert (*Ad.GFP*) (GenVec, Gaithersburg, MD) 7 days after the deafening, to label supporting cells. These animals were sacrificed 4 days later and prepared for CFM analysis for prestin and GFP. For inducing acoustic lesions, guinea pigs ($N = 2$) were exposed for 4 h per day on two consecutive days to noise with a bandwidth of 1–20 kHz at an intensity of 120 dB SPL. Lesions in mice were produced by noise overstimulation. Eighteen mice ($N = 12$ for qRT-PCR and $N = 6$ for immunocytochemistry) were exposed to noise with a bandwidth of 1–20 kHz at an intensity of 120 dB SPL for 4 h. Animals with normal ears were used as controls ($N = 4$ guinea pigs,

$N = 3$ mice for histochemistry and $N = 8$ mice for qRT-PCR).

2.2. Inoculation of guinea pig cochlea with *Ad.GFP*

To enhance visualization of scarring supporting cells, we expressed GFP in these cells. Deafening was performed with kanamycin and ethacrynic acid as described above. Seven days later, *Ad.GFP* was inoculated into the endolymph of the left cochlea. The inoculation was performed as previously described (Ishimoto et al., 2002) except that the vector solution was inoculated into the scala media of the apical turn. The adenovirus vector was replication-deficient recombinant adenoviruses with deleted E1, E3, and E4 regions (Brough et al., 1997). We used undiluted vectors at a concentration of 1×10^{12} total particles purified virus per milliliter.

2.3. Tissue dissection and fixation for histology

Animals deafened with ototoxic drugs were sacrificed 2, 4 or 9 days after the insult. Animals exposed to noise were sacrificed 6–7 days after the insult. Animals (mice or guinea pigs) were anesthetized with ketamine (Ketaset, Fort Dodge Animal Health, Fort Dodge, IA) and xylazine (AnaSed, Shenandoah, IA), decapitated, and their temporal bones removed. Inner ears were dissected out and perfused with 4% paraformaldehyde in PBS. Temporal bones were then incubated for 1 h at room temperature in the same fixative. Tissues were rinsed with PBS and the bone surrounding the organ of Corti was removed. Tissues were rinsed several times in PBS to remove debris. One cochlea of each animal was stained for fluorescence analysis and prepared as a whole mount of the organ of Corti. The other cochlea was stained with antibodies and 3,3'-diaminobenzidine tetrahydrochloride (DAB, Sigma Chemical Co., St. Louis, MO) and embedded in plastic for sectioning.

2.4. Staining for fluorescence analysis of prestin, F-actin, GFP and DNA

Tissues were permeabilized with 0.3% Triton X-100 (Sigma Chemical Co., St. Louis, MO) for 1 h then rinsed thoroughly in PBS. To reduce non-specific antibody binding, tissues were incubated in a solution of 5% normal goat serum (Vector Laboratories, Inc., Burlingame, CA) and 2% bovine serum albumin (Sigma Chemical Co., St. Louis, MO) in PBS for 2 h, or 5% donkey serum (Jackson ImmunoResearch Laboratories, West Grove, PA) for 30 min. Tissues were then rinsed in PBS and incubated with a prestin-specific rabbit antibody (a kind gift of Dr. Bechara Kachar, NIH-NIDCD) at a concentration of 0.0023 $\mu\text{g}/\text{ml}$, or with a goat anti-prestin antibody (1:100; Santa Cruz sc-22692). After a 10 min PBS rinse, tissues were incubated for 30 min with a secondary antibody (goat anti-rabbit or donkey anti-goat, both rhodamine-conjugated, Jackson

ImmunoResearch Laboratories) diluted 1:200 in PBS and rinsed. Samples were then incubated for 30 min in fluorescein-conjugated phalloidin (Molecular Probes, Eugene, OR) diluted 1:100 in PBS. For a third stain, tissues were labeled with Hoechst 33342 (Molecular Probes) as described previously (Raphael, 1993). In ears inoculated with Ad.GFP, whole mounts were stained for prestin as described above, and then with GFP-specific mouse monoclonal antibody (MAB3580 diluted 1:200; Chemicon, Temecula, CA) followed by Alexa Fluor 488 conjugated secondary anti-mouse antibody (A21202 diluted 1:200; Molecular Probes). All incubations were done at room temperature.

After labeling, organ of Corti tissues were thoroughly rinsed in PBS, and carefully dissected away from the modiolus. Individual turns were mounted on slides in GelMount anti-fading medium (Biomedica Corp., Foster City, CA), cover slipped, and viewed with a Leica DMRB fluorescence microscope. Images were obtained with the appropriate filters using a digital monochrome Spot camera (Diagnostic Instruments, Inc., Sterling Heights, MI). Analysis of deafened ears inoculated with Ad.GFP was performed using an Olympus Fluoview 500 confocal laser scanning microscope (CFM) using a 40× oil objective and Fluoview Ver. 4.3 software (Olympus, Japan). GFP staining was scanned by Argon laser (488 nm), and prestin staining by HeNe(G) laser (543 nm). Optical sections were 1 μm thick.

2.5. Staining and preparation of plastic sections

We used a pre-embedding staining protocol. Fixation, permeabilization, blocking, and primary antibody staining were as described above. Tissues were then stained with rabbit IgG VectaStain ABC Kit (Vector Laboratories Inc., Burlingame, CA) followed by DAB. Tissues were incubated in anti-rabbit IgG biotinylated antibody diluted 1:200 in PBS for 45 min. After two PBS rinses, they were incubated in a solution consisting of two drops each of Solutions A and B in 10 mL PBS. Antibody detection was then achieved by placing the tissue in a DAB solution (20 mL PBS, 5 μL 30% H₂O₂, and one dissolved 10 mg DAB tablet) until a brown coloration appeared in the tissue (7–12 min). Then, cochleae were rinsed and decalcified in 3% EDTA with 1% glutaraldehyde until soft.

Decalcified cochleae were rinsed with phosphate buffer (pH 7.2), dehydrated in a series of increasing ethanol concentrations, and impregnated with increasing concentrations of Epon (Electron Microscopy Sciences, Fort Washington, PA) in propylene oxide (Electron Microscopy Sciences). Cochlear turns were cut apart, leaving the tectorial membrane intact. Samples were embedded in fresh Epon resin, and placed in a 60 °C oven for 2 days. Blocks were sectioned for light microscopy at a thickness of 1 μm on a Leica Ultracut R microtome. Sections were counterstained with toluidine blue, either lightly to gain optimal view of the prestin-specific immuno-staining pattern, or heavily, to enhance analysis of the cytoarchitecture of the

organ of Corti. Light microscope analysis and photomicrography were performed using a Leica DMRB upright photomicroscope. Samples were photographed on Kodak color slides which were digitized using a Polaroid Sprint-Scan 35 Plus scanner. Ultrathin sections were obtained using a diamond knife, stained lightly with uranyl acetate and lead citrate and observed with a Phillips CM 100 TEM equipped with a digital camera.

2.6. Image processing

Adjustment of image contrast, superimposition of images, and colorization of monochrome fluorescence images were performed using Adobe Photoshop.

2.7. RNA isolation and quantitative real-time polymerase chain reaction (qRT-PCR)

We used qRT-PCR to determine how *prestin* mRNA levels change upon OHC loss. Mice were exposed to noise and euthanized 6 or 7 days later. Cochlear tissues were obtained, the otic capsule removed and the soft tissues (modiolus, sensory epithelium, stria vascularis, and spiral ligament) dissected in cold PBS and transferred to a chilled lysis buffer. Tissues collected from two mice (four cochleae) were pooled together and frozen at –80 °C until RNA isolation was performed. A total of six pools of tissues were collected from 12 noise-exposed mice and four pools from eight non-exposed control mice.

Total RNA was isolated using a RNeasy Micro kit (Qiagen Inc. Valencia, CA) that included a DNase treatment to remove residual genomic DNA. RNA was eluted in DEPC-treated water and subjected to quality and quantity assessments using Agilent Bioanalyzer 2100 (Agilent Technologies; New Castle, DE). Total RNA (average 0.2 μg per pool) was reverse transcribed using RNase H-MMLV (SuperScript III, Invitrogen; Carlsbad, CA) and oligo (dT)_{12–18} (500 ng) at 50 °C for 1 h, followed by RNase H treatment to remove RNA templates. The synthesized first strand cDNAs were diluted 1:10 with water and subjected to qRT-PCR analysis using gene-specific primers and TaqMan probes for *prestin* and *Rps16* (Assays-on-Demand and Assays-by-Design, respectively; Applied Biosystems Inc). *Rps16* encodes ribosomal protein S16 and serves as an internal standard for normalization because its expression is relatively unchanged by noise trauma (our unpublished data). The thermocycling conditions were: 95 °C for 10 min to activate Taq polymerase, followed by 40 cycles of amplification at 95 °C for 15 s alternating with 60 °C for 1 min. Relative expression levels of *prestin* were first adjusted to *S16* mRNA levels within each sample. Fold change in *prestin* mRNA level between noise-exposed and non-exposed control mice was calculated based on the ratio of the adjusted prestin expression levels in the noise-exposed group to the average value of the controls. Fold change was subjected to statistical analysis by a two-tailed unpaired *t*-test.

3. Results

To demonstrate the specificity of the prestin staining procedure and to confirm the location of prestin in normal tissue, we examined transverse sections of organ of Corti tissues from untreated mice stained with prestin specific antibody and DAB (Fig. 1). The staining revealed the presence of normally organized hair cells in the organ of Corti and confirmed that prestin antibody staining was restricted to the plasma membrane of OHCs. Similar sections from the guinea pig organ of Corti (not shown) confirmed that prestin immuno-reactivity was restricted to OHCs.

Whole mounts of the normal guinea pig organ of Corti stained with three markers (prestins-specific antibody, phalloidin to identify actin, and Hoechst to identify nuclei) revealed normal cytoarchitecture with three rows of OHCs and nuclei (Fig. 2). At the apical (luminal) surface, circumferential actin rings that are associated with the adherens junctions delineated the intercellular borders. Because prestin is localized to the lateral membrane of the cylindrical OHCs, prestin appeared as a ring along these cells (Fig. 2C), as previously demonstrated (Belyantseva et al., 2000).

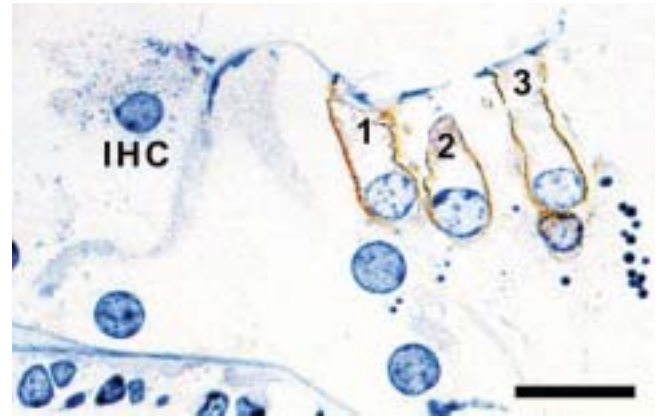


Fig. 1. Light microscope image of a plastic section cut at a near-mid modiolar plane of normal mouse organ of Corti stained with prestin specific antibody (DAB, brown) and counter-stained with toluidine blue. Inner hair cell (IHC) is prestin negative. 1, 2, 3 indicate first, second, and third rows of OHCs, respectively. Prestin localization is restricted to the baso-lateral membrane of OHCs. Scale bar = 15 μ m.

The fate of prestin in the organ of Corti after experimental lesion to the hair cells is presented first for ears exposed to an ototoxic insult, followed by ears exposed to noise

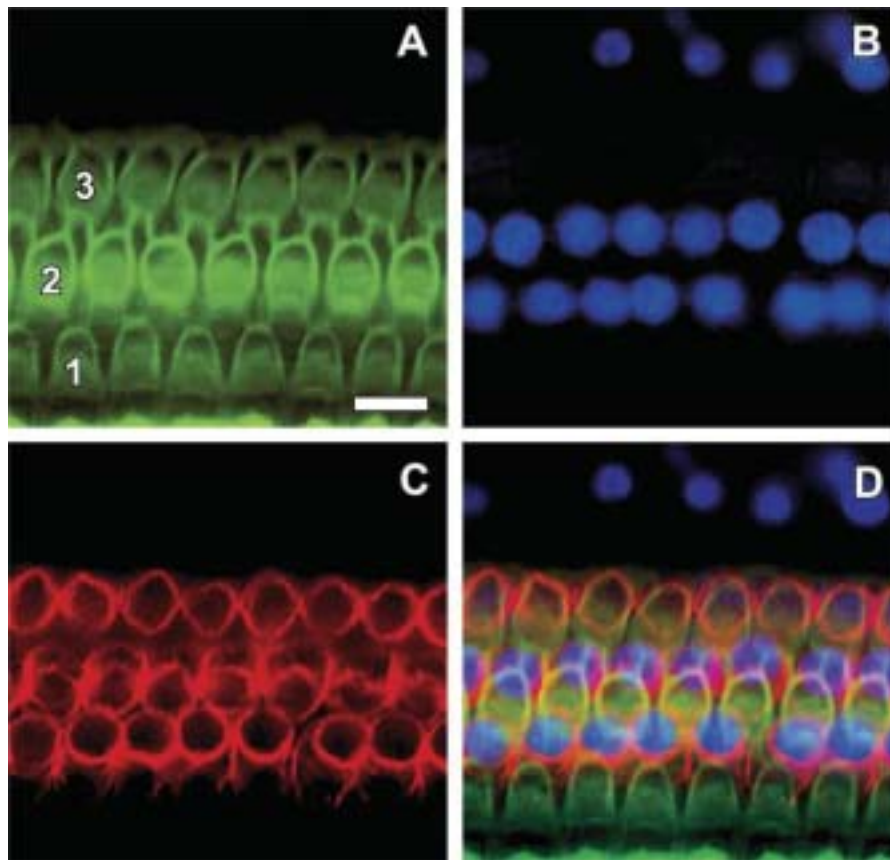


Fig. 2. Epi-fluorescence images showing actin (phalloidin stain, green), prestin (red) and nuclei (DNA stain, blue) in the OHC area of a whole mount of a normal guinea pig organ of Corti. (A) The reticular lamina (luminal border) of the auditory epithelium has three rows (1–3) of OHCs. Actin is abundant in the supporting cell-hair cell junction, depicting the normal cytoarchitecture at this plane, and in the cuticular plate of each hair cell. (B) Hoechst stain showing OHC nuclei at a slightly lower focal plane. The third row OHC nuclei are out of the focal plane. (C) At focal plane shown in (B), prestin is organized in complete rings delineating the peripheral membrane of each OHC. (D) Combined image of A–C. Note that focal plane of A is higher, to show the apical surface, and the mismatch between prestin and phalloidin is due to the slant of the OHCs (see Fig. 1). Scale bar = 10 μ m.

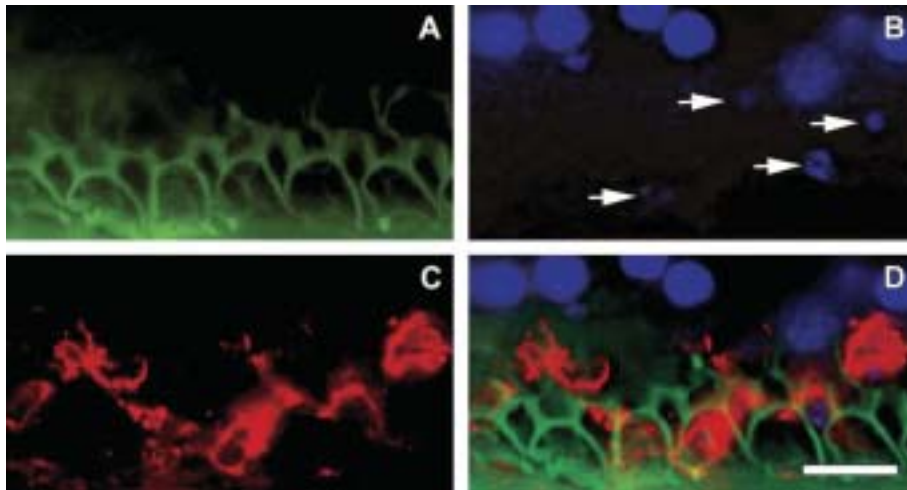


Fig. 3. Epi-fluorescence images of whole mount of the guinea pig organ of Corti 2 days after an ototoxic insult. (A) Phalloidin staining showing absence of cuticular plates and stereocilia bundles. A scar line is detected where expanded supporting cells seal the site of missing hair cells. (B) Hoechst staining at the focal plane where hair cell nuclei normally reside. A few fragmented nuclei are present (arrows) but most nuclei are missing. (C) Aggregates of protein that stain positive for prestin in areas where scarring supporting cells have filled the space left by degenerated hair cells. (D) Merged image (A–C) showing prestin immuno-reactivity in scarring supporting cells. Scale bar = 10 μ m.

overstimulation. Two days after deafening with kanamycin and ethacrynic acid, the guinea pig organ of Corti showed a complete loss of OHCs in the first three turns (Fig. 3A) and lack of intact nuclei in the OHC region (Fig. 3B). The distribution of actin at the luminal surface of the epithelium (Fig. 3A) was characteristic of the phalangeal scars formed by supporting cells (Raphael and Altschuler, 1991a). Some fragments of nuclear material were detected in the region of these scars (Fig. 3B). Irregularly-shaped aggregates containing prestin were detected in areas where supporting cells had expanded to fill spaces previously occupied by hair cells (Figs. 3C and D). The typical rings of prestin that are found in normal ears were not present in the traumatized organ of Corti (compare Figs. 3C and D to 2C and D).

Transverse sections of the guinea pig organ of Corti obtained 2 days after the ototoxic insult also showed that supporting cells had expanded to occupy the spaces of degenerated hair cells (Fig. 4). Aggregates of prestin were detected within the supporting cells in these scarred regions. Some of the prestin clumps appeared to be associated with cellular fragments, which may have been remnants of nuclei and/or other components of OHCs. These remnants had a shriveled appearance, and the prestin surrounding them followed the irregular contour of the fragments. Prestin aggregates were detected at various locations in the epithelium (Fig. 4A). Prestin positive areas were counter-stained with the cytoplasmic stain toluidine blue, suggesting an intracellular localization of these fragments, likely within supporting cells (Figs. 4A and B). Aggregates of prestin were also detected in the basal region of the epithelium, where only supporting cells reside (Fig. 4A). Toluidine blue counter staining showed co-localization of the prestin clumps within the cytoplasm of supporting cells (Fig. 4B), but the borders between scarring

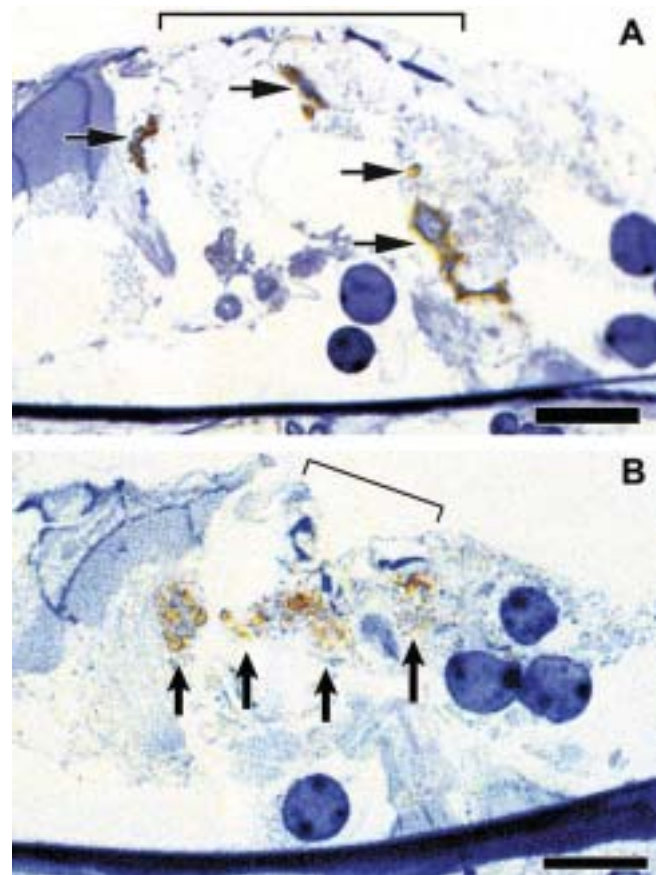


Fig. 4. Light microscope image of a plastic section (similar orientation to Fig. 1) of guinea pig organ of Corti 2 days after drug exposure. (A) Bracket indicates OHC region at the reticular lamina, where no hair cells survive. Prestin aggregates (arrows) are seen at different heights in the supporting cells that now occupy the sensory epithelium. Arrows show prestin aggregates in supporting cells that occupy former OHC spaces. (B) A section showing absence of OHCs (bracket) and presence of prestin aggregates (arrows) in supporting cells. Dense counter-stain shows that prestin-positive material is within cytoplasm of supporting cells. Scale bar = 15 μ m in A and 10 μ m in B.

supporting cells were difficult to follow and the traumatized auditory epithelium appeared like a syncytium.

Four days after drug treatment, whole mounts of guinea pig organ of Corti also revealed phalangeal scars generated by supporting cells, and a complete loss of OHCs and their nuclei (Fig. 5A). The scarring supporting cells contained aggregates of prestin, similar to those seen in tissues examined 2 days after ototoxic drug administration. Transverse sections of the organ of Corti 4 days after drug exposure (Fig. 5B) likewise appeared similar to those from 2 days after drug exposure, exhibiting prestin clumps in the cytoplasm of scarring supporting cells. Tissues examined 9 days after ototoxic drug administration showed complete lack of

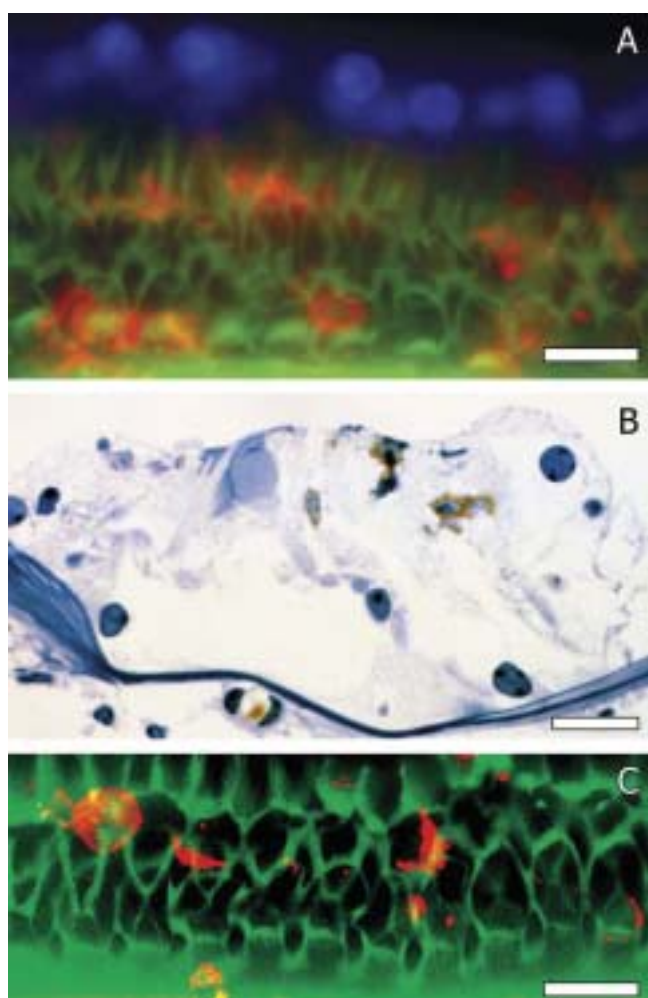


Fig. 5. Guinea pig organ of Corti tissues 4 (A,B) or 9 days (C) after drug exposure. (A) Whole mount showing OHC region where phalloidin (green) reveals complete scarring and absence of hair cells. Prestin immunoreactivity (red) is seen in scar area. Blue DNA stain shows nuclei in the Hensen cell area (top of figure) and lack of nuclei in the scarred region where OHCs are missing. (B) Transverse section of the organ of Corti showing complete lack of hair cells and the presence of prestin clumps (brown) in supporting cells that replaced missing OHCs. (C) Whole mount showing OHC region 9 days after the ototoxic insult. Phalloidin staining (green) shows complete scarring and loss of OHCs, whereas prestin staining (red) shows clumps of prestin in scars. Scale bars = 10 μ m in A and C, and 15 μ m in B.

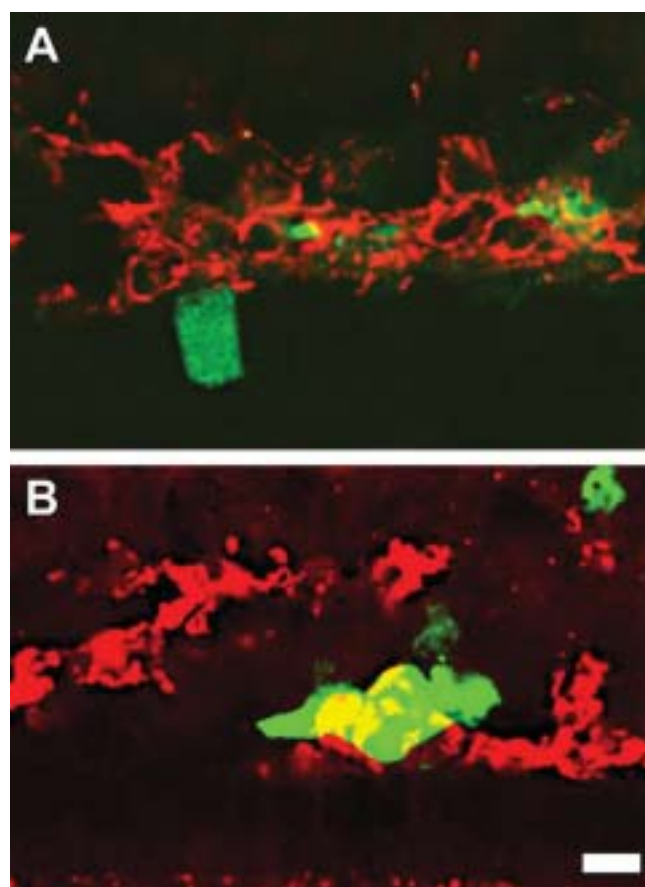


Fig. 6. CFM images of whole mounts of a deafened organ of Corti that was inoculated with Ad.GFP. (A) The area where OHCs usually reside is devoid of OHCs. A large number of prestin-positive clumps is found in the region. (B) The GFP-positive cytoplasm of supporting cells contains prestin clumps (red) resulting in yellow patches in the merged image. Scale bar = 10 μ m.

hair cells whereas prestin aggregates were present in the area of the scarring supporting cells (Fig. 5C). Co-localization of prestin with junctional F-actin immediately beneath the luminal surface strongly suggested that the prestin aggregates were within the cytoplasm of the scarring supporting cells (Fig. 5C).

Whole mounts of an organ of Corti that was deafened by ototoxic drugs and then inoculated with Ad.GFP were analyzed using CFM. The area where OHCs usually reside was devoid of OHCs and contained a large number of prestin-positive clumps (Fig. 6A). GFP was only seen in supporting cells and allowed for their identification. Some of the supporting cells that were GFP-positive contained prestin clumps (Fig. 6B). Co-localization of GFP and prestin indicates prestin is within the cytoplasm of these supporting cells and/or in pits surrounded by supporting cells.

TEM analysis of DAB-stained tissues revealed a dense granular stain representing prestin in the tissue (Fig. 7). Numerous clumps of prestin could be seen in areas with no surviving hair cells. In some cases, prestin clumps appeared to be trapped in the extra-cellular space between

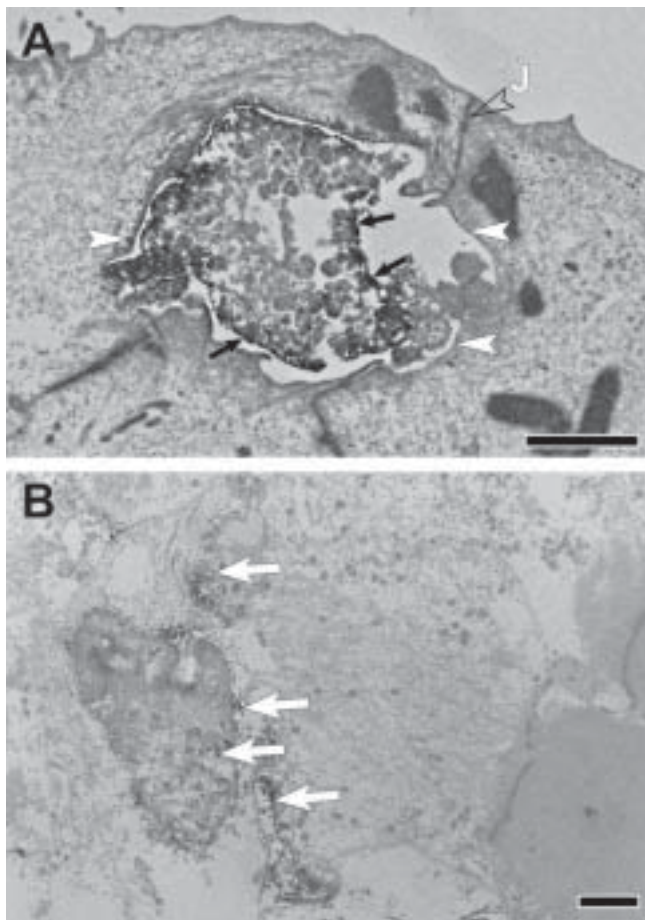


Fig. 7. TEM micrographs of DAB-stained organ of Corti showing electron-dense granules representing prestin-positive stain in areas with no surviving hair cells. (A) Prestin clumps appear engulfed between two supporting cells under the luminal surface. The amorphous prestin-rich mass (dark arrows) is surrounded by extra-cellular fluid. The membrane of the supporting cells is well defined (white arrowheads). An apical junction (J) seals the luminal surface. (B) Clusters of prestin-positive granules (arrows) are located in a scarring supporting cell. The aggregates appear to be enclosed in a phagosome. Scale bars = 2 μ m.

two supporting cells under the luminal surface (Fig. 7A). In other cases, the prestin clusters were enclosed by a membrane and located within the supporting cell body (Fig. 7B). The membrane-bound clusters of prestin appeared like phagosomes of several sizes (Fig. 7B). We could not determine if the membrane surrounding the cluster of prestin was the original OHC membrane or a phagosome membrane. Much of the prestin within this region was not associated with any type of plasma membrane.

In whole mounts of guinea pig organ of Corti examined 7 days after noise exposure, hair cells loss was extensive and clumps of prestin were seen in scars in the OHC region (Fig. 8A). Surviving OHCs found in the second and third turns had typical prestin rings and nuclei (not shown). In transverse sections obtained in areas devoid of hair cells, prestin clumps were seen within phalangeal scars that replaced OHCs (Fig. 8B). In some cases, aggregates of prestin were detected in the basal region of supporting

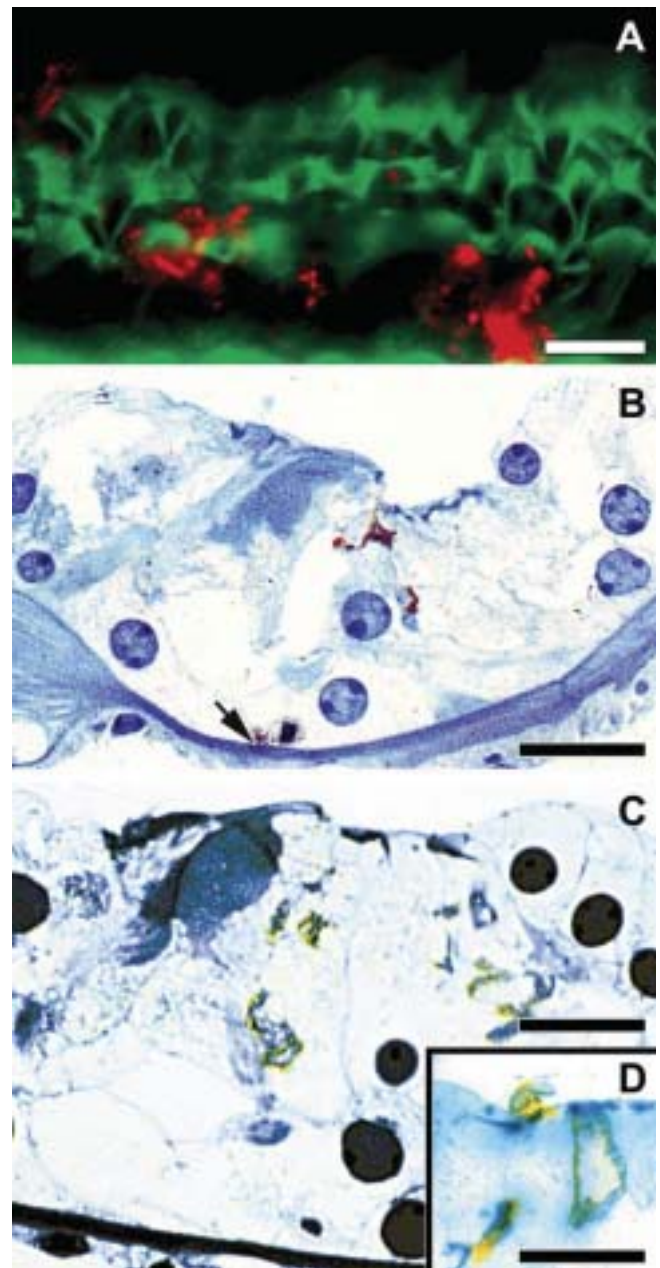


Fig. 8. Tissues from the guinea pig organ of Corti 7 days after noise exposure. (A) Epi-fluorescence showing phalloidin (green) in a complete scarring pattern with no remaining OHCs, and aggregates of prestin (red) in areas of scars made by Deiters and pillar cells. (B) A transverse section showing no remaining hair cells yet prestin immuno-reactive clumps (brown) aggregate in the upper, middle and lower (arrow) parts of the scarred area. (C) A densely counter-stained section showing that prestin (yellow-brown) is in supporting cell cytoplasm. The overlap of prestin and cytoplasm produces a green staining. (D) Inset showing the reticular lamina where a prestin-positive clump is seen on the luminal (endolymphatic) side of the epithelial surface (top left). Scale bars = 10 μ m in A and C, and 20 μ m in B and D.

cells, close to the basilar membrane. The prestin clumps in noise-exposed ears were similar in appearance to those seen in drug-deafened animals. In sections stained densely with toluidine blue, the clumps of prestin were seen to

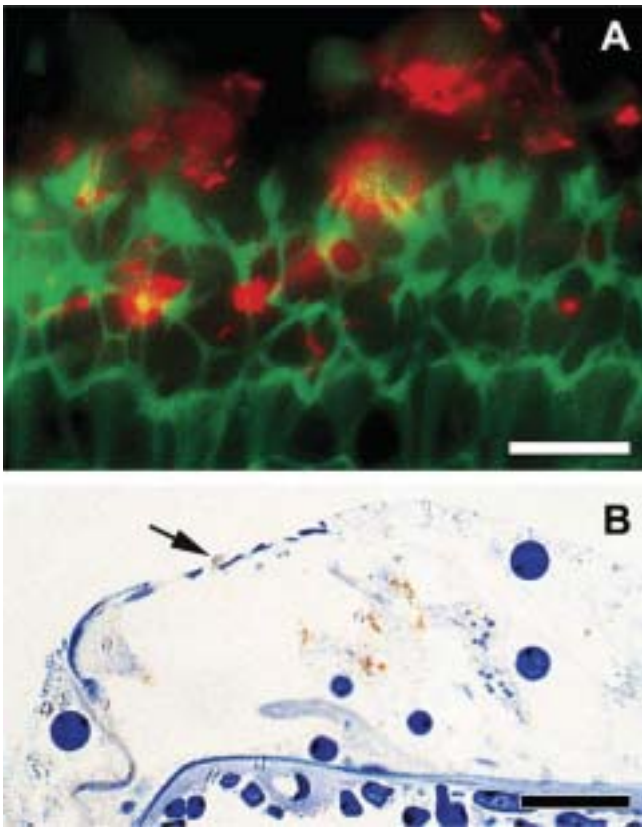


Fig. 9. Mouse organ of Corti tissues 4 (A) and 7 days (B) after noise exposure. (A) Whole mount showing the OHC region with severe scarring. The scarred area contains numerous aggregates of prestin. (B) A transverse section showing loss of OHCs with prestin aggregates in the scarring supporting cells. A small prestin clump is also found on the endolymphatic side of the reticular lamina (arrow). Scale bar = 10 μm in A and 15 μm in B.

reside in areas of supporting cell cytoplasm (Fig. 8C). Infrequently, clumps of prestin were seen on the endolymphatic side of the luminal border, suggesting that a portion of the hair cell was ejected into the lumen (Fig. 8D).

Like guinea pigs, mice subjected to noise overexposure exhibited extensive hair cell degeneration in the organ of Corti 4 days after the insult. Scarring cells in areas of OHC loss contained many prestin clumps (Fig. 9A). OHC elimination by the noise was incomplete and the surviving OHCs had typical prestin rings and nuclei (not shown). Inner ears obtained 7 days after noise exposure (Fig. 9B) appeared similar to those examined 4 days after noise exposure. Here too, a small prestin fragment was seen on the endolymphatic side of the luminal border (Fig. 9B, arrow). We did not observe entire hair cell bodies in the lumen in any of the sections we analyzed. Consistent with the observed loss of OHCs, mice subjected to noise overexposure exhibited decreased prestin mRNA in the cochlea. In 6 pools of cochlear RNA isolated from mice 6–7 days after noise exposure and analyzed with qRT-PCR, we observed a 4.9-fold decrease ($p < 0.05$) in *prestin* transcript level, compared to non-exposed controls.

Overall, the results in guinea pig and mouse ears appeared similar for both noise and ototoxic lesions. The data show that prestin clumps remain within or between supporting cells in the scarred areas of the auditory epithelium after OHCs die. These results suggest that supporting cells participate in the elimination of hair cell corpses.

4. Discussion

We show here that in the traumatized organ of Corti, prestin is detected in phalangeal scars created by supporting cells to replace degenerating or dead hair cells. Prestin remained in areas depleted of hair cells for at least 9 days after the insult to the organ of Corti. We demonstrate that in some cases, prestin immuno-positive material is located inside the supporting cell cytoplasm and in other cases it is trapped between supporting cells. These data indicate that supporting cells participate in the processing of corpses of dead hair cells and/or their debris.

Maintaining the continuity of the luminal surface is a major role of cells in most epithelial sheets. To that end, elimination of damaged epithelial cells is often orchestrated by neighboring cells so that the structural and functional integrity of the luminal border is maintained (Rosenblatt et al., 2001). In the cochlea, integrity of the luminal border (anatomically defined as the reticular lamina) is of particular importance because discontinuities in the epithelial sheet would result in leakage of endolymph into the epithelial layer, which would be detrimental to survival of any remaining hair cells. It is therefore imperative that death and removal of hair cells not disrupt the luminal surface.

There are at least two possible ways to accomplish cell corpse removal without compromising the integrity of the luminal surface. Corpses can potentially be eliminated either by extrusion into the lumen or by phagocytic activity within the epithelium. Phagocytic elimination of corpses within the epithelium could be performed by neighboring cells or by macrophages. In the avian auditory epithelium, there are reports of ejection of dying hair cells from the epithelial layer (Cotanche and Dopyera, 1990; Mangiardi et al., 2004). In the mammalian organ of Corti, however, ejection of entire hair cells is not typically found. Instead, it is more common that the stereocilia, cuticular plate, and possibly a small part of the apical portion of OHCs are ejected, while the bulk of the cell body remains within the epithelium (Forge, 1985; Raphael and Altschuler, 1991b). The present data provide additional support for this notion, and demonstrate that the apical portion of OHCs that is shed into the lumen may be large enough to include prestin.

The steps of cell death and removal of the corpses are closely related events regulated by a given set of genes depending on whether cell death occurs by apoptosis or necrosis (Chung et al., 2000; Lauber et al., 2004). Studies of cell death mechanisms in the inner ear showed that cochlear hair cells die via an apoptotic mechanism in mutants with abnormal inner ears (Wu et al., 2004), follow-

ing noise exposure (Nicotera et al., 2003) or after aminoglycoside drug treatment (Nakagawa et al., 2003; Wang et al., 2003). There is no clear evidence for a role of the immune system (macrophages) in removing the debris of degenerating hair cells, even when the lesion is substantial. In the absence of macrophages, the burden of eliminating OHC corpses falls on neighboring supporting cells. The relationship between the type of cell death and the timing of corpse removal by supporting cells is not currently known. It is possible that damaged (but still living) hair cells are surrounded by neighboring supporting cells prior to being phagocytosed, as seen with dying cells in other tissues such as the retina (Bok, 1993) and the liver (Dini et al., 2002).

We used several methods to determine that OHCs were missing from scar areas and to localize prestin in these areas. Phalloidin stained whole mounts showed the absence of cells with characteristic OHC features (e.g., stereocilia, cuticular plate) and a typical pattern of reorganized supporting cell boundaries in phalangeal scars. In addition, Hoechst staining revealed the absence of round nuclei in the scar area at a level where OHC nuclei typically are found. Transverse sections also showed the absence of cells with characteristic OHC features. Immunolabeling invariably found prestin in scarred areas but the morphology of the prestin was irregular and quite distinct from the normal pattern of prestin localization in OHCs. Prestin was detected within supporting cells or trapped between supporting cells, and in a few cases, small prestin clumps were found near the luminal surface. In some cases, prestin was found close to the basal end of the supporting cell, suggesting transport of the prestin clumps within the supporting cell. It is possible that elimination of hair cells is a multi-stage process involving phagocytosis of debris over time, perhaps with supporting cells surrounding the injured or dead hair cells and then gradually taking up their debris.

The finding of OHC material engulfed between two supporting cells is reminiscent of cultures of developing mouse organ of Corti, where a mechanically-induced lesion leads to injury of hair cells and their “hiding” under the luminal surface of the epithelium (Sobkowicz et al., 1996). Observations of injured hair cells with no luminal contact have not been reported in the mature ear in vivo. Our data show that supporting cells are able to seal the surface and trap remnants of OHCs, but do not support a mechanism where intact OHCs reside under the phalangeal scars in the mature living organ of Corti.

The lingering presence of prestin aggregates many days after the death of hair cells suggests that prestin is a very stable protein with very low turnover. The unusual stability of prestin may also explain the low level of *prestin* mRNA found in the normal cochlea. When expressed exogenously in epithelial cells of the LLC-PK1-CL4 porcine kidney line, prestin is efficiently targeted to the lateral and, to a lesser extent, the basal plasma membrane domains (James R. Bartles, Northwestern University Feinberg School of Medicine, personal communication). Likewise, we would assume that if supporting cells made prestin, they would

be able to target the protein to their lateral membranes. Instead, we found large prestin clumps with no apparent targeted localization, suggesting that supporting cells do not make prestin. Our finding of large aggregates of prestin is also consistent with recent observations on the hydrophobic nature of this protein and its tendency to clump once hair cells membranes are experimentally degraded (Jing Zheng, Northwestern University, personal communication). A longer term follow-up on the presence of prestin clumps in supporting cells will help determine the time-course of the disappearance of this protein from the cytoplasm of scarring supporting cells.

The demonstration of these findings in two different species (mouse and guinea pig) following two types of cochlear insults (drug toxicity and noise overstimulation) suggests that the ability of supporting cells to eliminate OHCs is a general phenomenon associated with OHC loss. Further studies are necessary to identify the signals that mediate the elimination of hair cell corpses by supporting cells. Specifically, the highly-organized scarring action by the supporting cells is probably initiated and directed by a set of signaling molecules. Native cells with phagocytic ability have been found in a variety of tissues, including epithelial layers (Cary et al., 1994; Nakajima et al., 1996; Sun et al., 1998; Suzuki et al., 1996), but the molecular signaling that triggers and controls the process of phagocytosis is not completely understood. In the auditory epithelium, the scarring activity of supporting cells is especially intriguing, as the volume of these cells seems to expand very quickly to fill the space previously occupied by OHCs.

Understanding the signaling that initiates and regulates the removal of hair cell corpses from the auditory epithelium would allow for the development of treatments to inhibit these processes and possibly rescue injured hair cells. A detailed ultrastructural analysis and time-course of the phagocytic process would also enhance understanding of the mechanism of OHC corpse removal. Interpretation of studies on OHC apoptosis would benefit from considering that some (or all) of the nuclear degradation may actually occur after OHCs are surrounded by supporting cells. Based on our observations in the organ of Corti and the pattern of epithelial cell elimination by neighboring cells in other tissues (Rosenblatt et al., 2001), we speculate that an injured hair cell sends an “eat-me” signal to its neighbors well before its death, and that its degradation is carried out by the surrounding supporting cells. As long as the risk of endolymph leakage is minimized, blocking this signal could be one strategy for enhancing OHC survival.

Acknowledgements

The adenovirus vector was a kind gift from GenVec. Research was supported by gifts from Berte and Alan Hirschfeld, the CHD, General Motors and the United Auto Workers Union, by the R. Jamison and Betty Williams Professorship (Y.R.), and by NIH/NIDCD Grants

R01-DC01634, R01-DC05401, R01-DC03685, T32-DC00011 and P30-DC05188.

References

- Belyantseva, I.A., Adler, H.J., Curi, R., Frolenkov, G.I., Kachar, B., 2000. Expression and localization of prestin and the sugar transporter GLUT-5 during development of electromotility in cochlear outer hair cells. *J. Neurosci.* 20, RC116.
- Bok, D., 1993. The retinal pigment epithelium: a versatile partner in vision. *J. Cell Sci. Suppl.* 17, 189–195.
- Brough, D.E., Hsu, C., Kulesa, V.A., Lee, G.M., Cantolupo, L.J., Lizonova, A., Kovessi, I., 1997. Activation of transgene expression by early region 4 is responsible for a high level of persistent transgene expression from adenovirus vectors in vivo. *J. Virol.* 71, 9206–9213.
- Cary, R.B., Klymkowsky, M.W., Evans, R.M., Domingo, A., Dent, J.A., Backhus, L.E., 1994. Vimentin's tail interacts with actin-containing structures in vivo. *J. Cell Sci.* 107, 1609–1622.
- Chung, S., Gumienny, T.L., Hengartner, M.O., Driscoll, M., 2000. A common set of engulfment genes mediates removal of both apoptotic and necrotic cell corpses in *C. elegans*. *Nat. Cell Biol.* 2, 931–937.
- Cotanche, D.A., Dopyera, C.E., 1990. Hair cell and supporting cell response to acoustic trauma in the chick cochlea. *Hear. Res.* 46, 29–40.
- Dallos, P., Fakler, B., 2002. Prestin, a new type of motor protein. *Nat. Rev. Mol. Cell Biol.* 3, 104–111.
- Daudet, N., Vago, P., Ripoll, C., Humbert, G., Pujol, R., Lenoir, M., 1998. Characterization of atypical cells in the juvenile rat organ of corti after aminoglycoside ototoxicity. *J. Comp. Neurol.* 401, 145–162.
- Dini, L., Pagliara, P., Carla, E.C., 2002. Phagocytosis of apoptotic cells by liver: a morphological study. *Microsc. Res. Techniq.* 57, 530–540.
- Engstrom, H., Ades, H.W., Bredberg, G. 1970. Normal structure of the organ of Corti and the effect of noise-induced cochlear damage. In: *Sensorineural Hearing Loss. Ciba Found. Symp.*, pp. 127–156.
- Forge, A., 1985. Outer hair cell loss and supporting cell expansion following chronic gentamicin treatment. *Hear. Res.* 19, 171–182.
- Hawkins Jr, J.E., 1973. Comparative otopathology: aging, noise, and ototoxic drugs. *Adv. Otorhinolaryngol.* 20, 125–141.
- Ishimoto, S., Kawamoto, K., Kanzaki, S., Raphael, Y., 2002. Gene transfer into supporting cells of the organ of Corti. *Hear. Res.* 173, 187–197.
- Lauber, K., Blumenthal, S.G., Waibel, M., Wesselborg, S., 2004. Clearance of apoptotic cells: getting rid of the corpses. *Mol. Cell* 14, 277–287.
- Leonova, E.V., Raphael, Y., 1997. Organization of cell junctions and cytoskeleton in the reticular lamina in normal and ototoxically damaged organ of Corti. *Hear. Res.* 113, 14–28.
- Mangiardi, D.A., McLaughlin-Williamson, K., May, K.E., Messina, E.P., Mountain, D.C., Cotanche, D.A., 2004. Progression of hair cell ejection and molecular markers of apoptosis in the avian cochlea following gentamicin treatment. *J. Comp. Neurol.* 475, 1–18.
- Nakagawa, T., Kim, T.S., Murai, N., Endo, T., Iguchi, F., Tateya, I., Yamamoto, N., Naito, Y., Ito, J., 2003. A novel technique for inducing local inner ear damage. *Hear. Res.* 176, 122–127.
- Nakajima, M., Yuge, K., Senzaki, H., Shikata, N., Miki, H., Uyama, M., Tsubura, A., 1996. Photoreceptor apoptosis induced by a single systemic administration of *N*-methyl-*N*-nitrosourea in the rat retina. *Am. J. Pathol.* 148, 631–641.
- Nicotera, T.M., Hu, B.H., Henderson, D., 2003. The caspase pathway in noise-induced apoptosis of the chinchilla cochlea. *J. Assoc. Res. Otolaryngol.* 4, 466–477.
- Raphael, Y., 1993. Reorganization of the chick basilar papilla after acoustic trauma. *J. Comp. Neurol.* 330, 521–532.
- Raphael, Y., Altschuler, R.A., 1991a. Scar formation after drug-induced cochlear insult. *Hear. Res.* 51, 173–183.
- Raphael, Y., Altschuler, R.A., 1991b. Reorganization of cytoskeletal and junctional proteins during cochlear hair cell degeneration. *Cell Motil. Cytoskel.* 18, 215–227.
- Rosenblatt, J., Raff, M.C., Cramer, L.P., 2001. An epithelial cell destined for apoptosis signals its neighbors to extrude it by an actin- and myosin-dependent mechanism. *Curr. Biol.* 11, 1847–1857.
- Sobkowicz, H.M., August, B.K., Slapnick, S.M., 1996. Post-traumatic survival and recovery of the auditory sensory cells in culture. *Acta Otolaryngol. (Stockh.)* 116, 257–262.
- Spoendlin, H., 1976. Anatomical changes following various noise exposures. In: Henderson, D. et al. (Eds.), *Effects of Noise on Hearing*, vol. 270. Raven Press, New York, pp. 69–90.
- Sun, W.B., Han, B.L., Peng, Z.M., Li, K., Ji, Q., Chen, J., Wang, H.Z., Ma, R.L., 1998. Effect of aging on cytoskeleton system of Kupffer cell and its phagocytic capacity. *World J. Gastroenterol.* 4, 77–79.
- Suzuki, Y., Takeda, M., Obara, N., Nagai, Y., 1996. Phagocytic cells in the taste buds of rat circumvallate papillae after denervation. *Chem. Senses* 21, 467–476.
- Wang, Z., Li, H., 2000. Microglia-like cells in rat organ of Corti following aminoglycoside ototoxicity. *Neuroreport* 11, 1389–1393.
- Wang, J., Van De Water, T.R., Bonny, C., de Ribaupierre, F., Puel, J.L., Zine, A., 2003. A peptide inhibitor of c-Jun N-terminal kinase protects against both aminoglycoside and acoustic trauma-induced auditory hair cell death and hearing loss. *J. Neurosci.* 23, 8596–8607.
- Wu, X., Gao, J., Guo, Y., Zuo, J., 2004. Hearing threshold elevation precedes hair-cell loss in prestin knockout mice. *Brain Res. Mol. Brain Res.* 126, 30–37.
- Yamasoba, T., Kondo, K., Miyajima, C., Suzuki, M., 2003. Changes in cell proliferation in rat and guinea pig cochlea after aminoglycoside-induced damage. *Neurosci. Lett.* 347, 171–174.
- Zheng, J., Shen, W., He, D.Z., Long, K.B., Madison, L.D., Dallos, P., 2000. Prestin is the motor protein of cochlear outer hair cells. *Nature* 405, 149–155.

研究成果報告書

研究課題名	ペインクリニックにおける新しい癌性疼痛治療法の臨床研究		
(英文)	Clinical investigation of a new approach for cancer pain in pain clinic		
事業推進者	新宮 興	E-mail	shingu@hirakata.kmu.ac.jp
所属・職名	医学研究科・侵襲反応制御学(麻酔科学)講座・教授		
研究分担者名	田口 仁士、中尾 慎一、増澤 宗洋		
キーワード	癌性疼痛、髄腔内、グルココルチコイド		
<p>1. 概要</p> <p>癌性疼痛は、癌の種類、発生部位、大きさ、転移病変などのため、患者により病態が著しく異なる。しかも病状が進行性で痛みも複雑であり、神経因性疼痛の病態を示す例もみられ、患者満足度の高い治療は容易ではない。腫瘍組織の縮小と共に破壊された組織の修復や再生を図りつつ鎮痛効果を得られないかについて検討しながら、新しいペインクリニックにおける治療法の開発を目指したい。</p> <p>2. 研究の背景と目的</p> <p>オピオイドによる癌性疼痛治療法が普及してきたにもかかわらず、激痛で苦しんでいる癌患者は少なくない。痛みを専門的に治療するペインクリニックには、オピオイドでは治療困難な癌性疼痛を持つ患者が多く紹介されてくる。我々はオピオイドや神経破壊薬を用いた神経ブロック法も取り入れて治療を行ってきたが、従来の方法では除痛できない癌の痛みを診ることが多くなった。</p> <p>今回の臨床研究は、1人の末期癌患者から激痛の苦しみを止めることを懇願され、くも膜下腔へのステロイド(ベタメタゾン)投与を行った結果、予想をはるかに越える優れた持続的な鎮痛効果がもたらされたことが発端となった。くも膜下腔へのステロイド投与は、一般的な鎮痛処置としては実施されておらず、その鎮痛効果や副作用・合併症についてほとんど不明である。そこで、癌性疼痛の患者に対してベタメタゾンを少量からくも膜下投与を行い、神経学的異常症状・所見などを確認しながら、鎮痛効果と副作用・合併症について検討した。今回は、特に骨転移におけるくも膜下ステロイドの鎮痛機序について、悪性腫瘍による骨破壊と骨新生に注目し、骨組織と神経の修復によってもたらされる鎮痛効果と運動機能の改善の可能性について検討したい。</p> <p>3. 研究方法</p> <p>1) 対象</p> <p>オピオイドによる通常の鎮痛法では除痛困難な癌性疼痛の患者を対象とした。オピオイドで疼痛コントロールが可能となった患者や全身状態悪化などで不適応と判断した患者は除外した。</p> <p>2) 患者への説明と同意</p> <p>合併症を含め治療法全体について口頭と文書で説明を行い、患者やその家族と十分協議をしながら治療を進めた。</p> <p>3) 処置前診察</p> <p>疼痛の原因となっている癌病変について診断し、疼痛の程度、性質、部位を観察した。また、現在までの治療と使用中の鎮痛薬を調べた。神経学的所見として、知覚および運動の障害を観察した。</p> <p>4) 手技</p> <p>くも膜下ベタメタゾン投与を、1週間に1回の頻度で行った。4回までの投与を原則としたが、合併症が観察されず鎮痛効果が期待できれば、5回以上の投与も可能とした。比較対象としての局所麻酔薬やオピオイドのくも膜下投与は、全身状態が悪化した進行癌患者において、低血圧、呼吸抑制、悪心・嘔吐等の副作用・合併症が生じる可能性が高いので行わなかった。</p>			

まず、患者のバイタルサインを観察して全身状態を評価したのち、側臥位で 25 または 27G ペンシルポイントスパイナル針を用い、腰部くも膜下穿刺を行った。投与薬液は、ベタメタゾン（リンデロン注射液；塩野義製薬）2-3 mg に生食水を混合して全量を 2-3ml としたものを使用した。薬液投与前に検査用として脳脊髄液を 3 ml 採取し、薬液は約 30 秒間で髄腔内投与を行った。

5) 鎮痛効果と症状・所見の観察

投与直前の疼痛を 100 とした Visual Analog Scale で、投与直後の鎮痛効果を 30 分間観察した。また、血圧測定と神経学的異常所見・症状の観察を行った。鎮痛効果については、帰宅後に患者自身が毎日記載する「痛み日誌」によって評価した。疼痛強度の評価はペインスコア（PS：0-10 の 11 段階）で行い、今回の痛みで最も強かった痛みを PS=10 とし、0 から 10 の数字で記録した。また、睡眠、食欲、気分、活動性の評価を患者自身で行った。

使用中の鎮痛薬については、定期投与のオピオイドの投与量は変更せず、NSAIDs やレスキューとして用いるオピオイドは変更可能とした。

癌病変に伴う症状と使用薬物による脊髄の神経毒性に関連して、下肢の知覚と運動異常、直腸・膀胱障害、会陰部違和感、頭痛、背部痛について観察した。

4. これまでの成果

鎮痛効果

30 名の癌性疼痛患者に対して、ベタメタゾン 2-3 mg のくも膜下投与を行った。約半数において、投与後 5-30 分における急性鎮痛効果がみられた。

優れた急性鎮痛が得られた例では、引き続いて長期間の鎮痛が得られる傾向がみられた。初回のベタメタゾンくも膜下投与後 1 週間において、7 日間の平均 PS が処置前と比較して 50%以下に減弱した者は、30 名中 13 名（43 %）であり、処置前から投与中のオピオイドと NSAIDs の増量はみられなかった。ベタメタゾンくも膜下投与を 4 回施行した 4 週間において、28 日間の平均 PS が処置前と比較して 50%以下に減弱した者は、30 名中 18 名（60 %）であった。特に脊椎転移の癌性疼痛において優れた鎮痛効果が得られた。

副作用・合併症

知覚・運動神経障害、精神・神経系の不快症状、血圧低下などはみられず、臨床的に神経毒性が疑われる合併症はまったく観察されなかった。

QOL 関連症状の変化

有効例では、睡眠、食欲、気分、活動性が有意に改善した。処置前にみられた運動障害などの神経症状の改善例が少なからずみられた。

脳脊髄液検査

髄液一般検査では、一部の髄腔内の癌播種例以外は、処置後の細胞数、糖、タンパクの異常はみられなかった。

髄液のサイトカイン類とプロスタグランジンの変化（13 名）をみると、くも膜下ベタメタゾン投与前と投与後において、有効例（疼痛の減弱が 50%以上、N=6）では IL-8 と PGE₂ が有意に低下した。また、IL-8 と PGE₂ は投与前値が高かった（183±21 pg/ml と 44±10 pg/ml）。TNFα、IL-1β、IL-6 は有意な変化がみられなかった。無効例（疼痛の減弱が 50%未満、N=7）では、いずれも有意な変化はみられなかった。

5. これまでの進捗状況と今後の計画

現在までの研究結果においては、通常の方法では鎮痛困難であっても、ベタメタゾンの少量くも膜下投与によって、副作用や合併症を生じることなく優れた長期間の鎮痛が半数近くの患者で得られることを示している。さらに、睡眠、食欲、気分、活動性の改善が得られたことは、鎮痛作用も含めて生活全般の改善が期待でき、身体及び精神の活動性への影響についてさらに検討したい。

くも膜下ベタメタゾンの神経障害の可能性については、治療法の安全性の点で十分に検討する必要がある。現在までの研究では観察されていないが、今後症例を増やして多数の患者における詳細な検討を行うつもりである。ただ、癌による処置前の運動障害が改善した例が少なからずみられており、神経機能全体の回復についても観察したい。

この治療は特に入院の必要がなく、外来通院にて実施が可能であり、比較的容易に実施できることが大きな特徴である。さらに安全で容易に実施できる工夫をしたいと考えている。

グルココルチコイドの作用については、リポコルチン産生によるホスホリパーゼ A2 の抑

制作用によりプロスタグランジンとロイコトリエンの産生が減少し、それにより生じる抗炎症作用が鎮痛作用に関係するとされている。優れた鎮痛効果が得られた例では、髄液中の IL-8 と PGE₂ が有意に低下したが、疼痛増強物質である PGE₂ の低下は、脊髄、後根神経節、神経根などでの疼痛伝達の抑制に何らかの影響を与えたと考えられる。しかし、急性の鎮痛効果がみられており、これは従来の考え方では説明がつかない。神経の細胞膜表面に存在する何らかの受容体に作用して、遺伝子発現を伴わない急性作用が生じることが推測される。

グリア細胞の活性化に伴うプロスタグランジンや炎症性サイトカインの産生が、難治性の疼痛に大きく関与している可能性がある。神経因性疼痛でグリア活性は著明に高まり、髄腔内と全身投与したメチルプレドニゾロンが、グリア活性と痛みを抑制したとの報告がある。末梢神経損傷で脊髄のマイクログリアが活性化されるとともに、脊髄損傷によってもマイクログリアが活性化され、慢性痛の維持にかかわっていることが考えられる。くも膜下腔へ投与されたグルココルチコイドがグリア細胞にどのような影響を及ぼすかについては、まだ不明な点が多く興味深い。

今回は特に癌の脊椎骨転移において、くも膜下ベタメタゾンの長期的な優れた鎮痛効果がみられた。くも膜下投与されたベタメタゾンが、脊椎骨の転移病巣に作用して骨破壊の抑制と骨新生の促進をもたらした可能性がある。骨転移においては破骨細胞の活性化が骨破壊に重要な役割を演じるとされるが、ステロイドが破骨細胞を抑制するならば骨および神経の修復が図られ、疼痛の減弱と運動機能の改善に結びつくことも考えられ、今後検討していきたい。

現在、癌と診断される患者数が年間 40 万人に達し、耐え難い痛みを経験する進行癌患者も増えている。今回の方法は、オピオイド治療が無効となった難治性の癌疼痛患者に対しても優れた鎮痛効果をもたらす可能性が高い。特に癌の脊椎転移などの治療困難な疼痛に対して効果があり、「癌の予防、治療、緩和ケア」が総合的に推進されている現在、緩和医療の発展にも役立つものと考えており、癌性疼痛に対する新しい治療法の開発を進めたい。

6. これまでの発表論文

(1) 発表論文

1. Inada, T., Kushida, A., Sakamoto, S., Taguchi, H. & Shingu, K.

Intrathecal betamethasone pain relief in cancer patients with vertebral metastasis: a pilot study. *Acta Anaesthesiol. Scand.* **51**, 490-494 (2007).

2. Taguchi, H., Oishi, K., Sakamoto, S. & Shing, K.

Intrathecal betamethasone for cancer pain in the lower half of the body: a study of its analgesic efficacy and safety. *Br. J. Anaesth.* **98** (3), 385-389 (2007).

(2) 学会発表

国際学会

Sakamoto, S., Inada, T., Shirane-Kushida, A., Taguchi, H. & Shingu K.

A possible mechanism of intractable pain relief using intrathecal steroid in patients with cancer. *Annual Meeting of American Society of Anesthesiologists*, Chicago, USA, 2006.

国内学会

1) 教育講演

田口仁士 :

ステロイドのくも膜下投与による鎮痛効果。

第 52 回日本麻酔科学会関西地方会、大阪、2006.

2) シンポジウム講演

田口仁士、増澤宗洋、大石敬子、新宮 興 :

「疼痛の臨床生理とペインクリニック」

癌性疼痛のくも膜下ステロイド投与による治療。第 44 回日本臨床生理学会、大阪、2007.

3) 一般発表

中尾浅香、田口仁士、増澤宗洋、大石敬子 :

腰椎転移による癌性疼痛に対して 2 年間で計 18 回のくも膜下ベタメタゾン投与を行った 1 例。日本ペインクリニック学会第 42 回大会、福岡、2008.

7. これまでの成果の情報公開

ホームページ：麻酔科学講座＝<http://www3.kmu.ac.jp/anesthw/>

Intrathecal betamethasone for cancer pain in the lower half of the body: a study of its analgesic efficacy and safety

H. Taguchi*, K. Oishi, S. Sakamoto and K. Shingu

Department of Anaesthesiology, Kansai Medical University, Osaka, Japan

*Corresponding author: Department of Anaesthesiology, Kansai Medical University, 10-15 Fumizono-cho, Moriguchi, Osaka 570-8506, Japan. E-mail: taguchi@takii.kmu.ac.jp

Background. Sufficient analgesia for cancer pain is sometimes difficult to achieve with conventional treatments. We aimed at investigating the analgesic efficacy and safety of intrathecal betamethasone in patients with uncontrollable cancer pain.

Methods. Betamethasone 1 mg mixed with saline was injected into the lumbar intrathecal space once a week in 10 patients with persistent cancer pain in the lower half of the body. During the 4-week study period, the analgesic efficacy and adverse effects related to intrathecal betamethasone were observed.

Results. Long-lasting analgesia (mean numerical pain score ≤ 5) for 7 days, after immediate analgesia within 10 min, was obtained without the need to increase the morphine dose in 5 of 10 patients. In almost all of the patients, not only pain, but also uncomfortable symptoms were improved. Adverse effects related to neurotoxicity of intrathecal betamethasone, such as sensory and motor dysfunctions, were not observed in any patients.

Conclusion. When conventional cancer pain treatments are not successful, intrathecal betamethasone may be useful, as it probably induces long-lasting analgesia without adverse effects and improves activities of daily living, especially in patients with vertebral bone metastases.

Br J Anaesth 2007; **98**: 385–9

Keywords: analgesics anti-inflammatory, steroid; analgesic techniques, subarachnoid; cancer; pain; toxicity, neurotoxicity

Accepted for publication: November 30, 2006

Despite advances in pain management, cancer pain is still often intractable.¹ In terminal cancer patients, glucocorticoids are given systemically to alleviate pain, anorexia, and malaise^{2,3} but are rarely used topically. It is thought that the effects of glucocorticoids are mediated by their anti-inflammatory or immunosuppressive actions. Recently, evidence for the involvement of various neurotransmitters and pain modulators in pain perception has been reported,^{4–6} and treatments that target this aspect of the pathogenesis of pain are being developed.⁷

The intrathecal use of glucocorticoid may be effective for the treatment of inflammatory or neuro-injury associated pain in the spinal cord and roots, as it has an inhibitory action on prostaglandins and other algogenic substances. However, adverse effects related to neurotoxicity of intrathecal glucocorticoid have been reported.⁸ We previously reported that intrathecal betamethasone produced long-lasting analgesia without any adverse effects in advanced pelvic and perineal cancer patients.⁹

Intrathecal injection of glucocorticoid may alleviate intractable pain caused by inflammation and sensitization without the development of neurotoxicity in the spinal cord and nerve roots, when the injection consists of a small dose of glucocorticoid that includes relatively safe preservatives.

Methods

This study was approved by the Research Ethics Committee of Kansai Medical University. After obtaining the patient's medical history and present illness, the vital signs were taken and a neurological examination was performed. Simple X-ray, CT, and MRI data were evaluated. Inclusion criteria consisted of the presence of advanced cancer, cancer pain located in the lower half of the body, and uncontrollable pain despite conventional analgesic therapies.

Ten patients who met the inclusion criteria were enrolled, and written informed consent was obtained from

Table 1 Patient characteristics

Patient no.	Age	Gender	Site of pain	Origin of cancer	Bone metastasis	Oral morphine dose (mg day ⁻¹)	Number of intrathecal betamethasone injections
1	54	M	r-Low back and lower limb	Lung	L3	120	2
2	71	F	r-Pelvis and bilateral lower limb	Liver	None	100	1
3	52	M	l-Pelvis and lower limb	Rectum	None	660	1
4	73	F	Low back	Liver	L4	90	1
5	74	M	Low back	Unknown	L2, 3	120	4
6	73	M	r-Pelvis and lower limb	Pelvis	Sacrum, ilium	40	3
7	30	F	Low back and lower limb	Uterus	L2	360	3
8	65	M	Perineum	Sigmoid colon	Sacrum	90	3
9	68	M	Back and low back	Pancreas	T12	60	2
10	62	M	Low back and low abdomen	Gallbladder	None	60	1

all of them. During the 4-week study period, intrathecal betamethasone was scheduled to be given once a week. The dose of slow-release oral morphine was to remain unchanged during the treatment, but rescue doses of oral morphine and NSAIDs, which were received 0–3 times a day before the treatment, could be given based on the patients' needs.

In the lateral decubitus position, a 25-gauge pencil-point spinal needle was inserted through the interlaminar space in the lumbar vertebrae to avoid the metastatic region. Betamethasone solution (Rinderon Injection, Shionogi Pharmaceuticals, Osaka, Japan), including 2 mg of betamethasone, 0.5 mg of sodium sulphite, and 15 mg of D-sorbitol in a volume of 0.5 ml, mixed with saline was injected into the lumbar subarachnoid space. The betamethasone dose was 1 mg (0.25 ml), and the total volume of the solution was 2 ml.

Immediately after intrathecal injection of betamethasone, the acute analgesic effect was examined at 5, 10, 20, and 30 min using the visual analogue scale (VAS). Analgesia was defined as a 50% or greater reduction in pain compared with the VAS score (100 mm) just before the treatment. The development of abnormal neurological signs and symptoms was observed for 1 h. During the 4-week study period, the patients themselves assessed their pain intensity; the daily pain assessment was done before going to sleep at night using the numerical pain score (PS; 0=no pain and 10=the worst pain in the 10 days before treatment). We used a PS as a pain relief scale after the treatment, considering the variability and multiple dimensions of cancer pain during the course of the disease. Potential adverse effects related to the neurotoxicity of betamethasone and the intrathecal injection procedure, such as headache, back pain, low back pain, numbness in the limbs, sensory weakness, motor weakness, gait disturbance, and recto-bladder dysfunction, were assessed weekly.

Results

The site of pain, cancer origin, bone metastasis, morphine dose, and the number of intrathecal betamethasone injections are shown in Table 1. Despite having been given anti-cancer therapies and systemic analgesic pharmacotherapies, the patients had severe and persistent pain in the low back, pelvis, perineum, or lower limb region. Before treatment, half of the patients were given small doses of morphine, because of their conditions or adverse effects such as nausea or somnolence.

Betamethasone was injected in the intrathecal space one to four times during the 4-week study period, depending on the patient's physical and mental condition. In four patients with bone metastasis in the lumbar vertebrae, the intrathecal approach was chosen to avoid the metastatic region. Injection failure, paresthesia, bleeding, and other technical difficulties were not seen in any of the patients.

Table 2 Analgesic effects during the first week of treatment. Acute analgesia was defined as a 50% or greater reduction in pain intensity compared with the pre-treatment VAS score (100 mm) after the first intrathecal injection of betamethasone. Daily pain intensity was assessed by the patients themselves using the numerical pain score (PS)

Acute analgesia in 30 min	Analgesia (everyday PS≤5) for 3 days	Analgesia (mean PS≤5) for 7 days
7/10	6/10	5/10

During the study period, three patients dropped out; of these three patients, two were transferred to another hospital, and one patient died.

Seven of 10 patients showed immediate analgesia (more than a 50% reduction in pain compared with the pre-treatment VAS) within 30 min after the first intrathecal injection of betamethasone (Table 2); five patients showed immediate and sufficient analgesia within 10 min. Abnormal symptoms and signs related to sensory and motor nerve dysfunction were not seen. Hypotension, bradycardia, headache, and recto-bladder dysfunction were not observed in the hour after betamethasone injection.

Long-lasting analgesia was maintained after immediate analgesia in many of the patients. During the first week of treatment, five patients (No. 1, 4, 5, 6, 8) had good analgesia (mean PS≤5) for 7 days without the need to increase their analgesics (Table 2). Good and long-lasting pain relief for 4 weeks was obtained in five of seven patients who completed the study. The rescue morphine dose had to be increased in three of the five patients without increasing the other analgesics, whereas two patients (No. 5, 6) had excellent analgesia without any need to increase their morphine or other analgesics in the 4-week study period. In patients with satisfactory pain relief, uncomfortable symptoms improved, and activities of daily living gradually recovered. Some patients could walk better; however, if vertebral bone stability could not be maintained, the patients had pain when walking and standing. Adverse effects related to neurotoxicity of intrathecal betamethasone, such as sensory and motor dysfunctions, did not occur in any of the patients (Table 3).

Discussion

We have previously reported on the achievement of long-lasting analgesia using intrathecal betamethasone with saline in three cancer patients.⁹ In the current study, the safety and analgesic efficacy of intrathecal betamethasone were investigated in 10 cancer patients who had not obtained sufficient analgesia despite conventional treatments. With intrathecal betamethasone treatment, none of the patients developed adverse effects such as neurological dysfunction, and about a half of the patients achieved sufficient analgesia against intractable pain. In the current study, we did not use a controlled design, as intrathecal injections of clonidine, midazolam, or opioids, which would be used in the control group, are often associated with uncomfortable adverse effects. Thus, it would be difficult to perform a controlled study of intrathecal analgesia in terminally ill patients.

Safety of intrathecal glucocorticoid

There are several arguments concerning the safety of intrathecal injection of steroids. Complications such as arachnoiditis and meningitis have been reported.¹⁰ Nelson and Landau¹¹ argued that the intrathecal administration of glucocorticoids is unsafe and indicated that intrathecal glucocorticoids could lead to the development of neurotoxicity in the spinal cord and meninges. However, the safety of intrathecal glucocorticoids has been advocated in some clinical and experimental studies. In the clinical study by Kotani and colleagues,¹² there were no complications in 89 patients with postherpetic neuralgia who received four doses of intrathecal methylprednisolone acetate (60 mg) containing propylene glycol. Langmayr and colleagues¹³ indicated that, after lumbar disc surgery, intrathecal betamethasone provided significant pain reduction without any disadvantageous effects. Latham and colleagues¹⁴ showed in sheep that repeated intrathecal administration of 5.7 mg (1 ml) betamethasone containing benzalkonium chloride did not result in pathological changes. However, large doses of betamethasone, such as 11.4 mg (2 ml) and more,

Table 3 Adverse effects during treatment. Symptoms related to neurotoxicity of intrathecal betamethasone and other adverse effects were not found in any of the patients during the 4-week study period. Motor nerve functions such as motor weakness and gait disturbance improved in some patients

Symptoms	Before treatment (n=10)	During the first 2 weeks of treatment (n=10)			During the last 2 weeks of treatment (n=7)		
		Newly developed	Unchanged	Improved	Newly developed	Unchanged	Improved
Headache	2	0	1	1	0	1	1
Back pain	2	0	1	1	0	1	1
Low back pain	5	0	0	5	0	0	4
Numbness	4	0	3	1	0	1	1
Sensory weakness	3	0	2	1	0	2	0
Motor weakness	5	0	2	3	0	2	2
Gait disturbance	5	0	2	3	0	1	3
Recto-bladder dysfunction	2	0	2	0	0	2	0
Other neural disorders	0	0	0	0	0	0	0

were associated with dose-dependent neurotoxicity. Furthermore, it has been found that intrathecal triamcinolone diacetate containing polyethylene glycol did not induce spinal neurotoxicity in rat model.¹⁵ It is believed that the chemicals responsible for neurotoxicity when glucocorticoids are administered intrathecally are not the glucocorticoids themselves, but the additives such as antioxidants, preservatives, and excipients that are present in the injected solution.¹⁶

We chose betamethasone as the glucocorticoid for intrathecal injection because of its water solubility, the presence of small dose additives in the solution, its safety in animal studies, and the fact that the intrathecal use of betamethasone is recommended for meningeal leukaemia, cerebrospinal meningitis, malignant lymphoma, etc. by the manufacturer of betamethasone. To avoid possible neural damage, we used a small dose (1 mg) and volume (0.25 ml) of betamethasone solution. The 0.5 ml volume of betamethasone solution used contains 2 mg of betamethasone, 0.5 mg of sodium sulphite, and 15 mg of D-sorbitol. The sulphites (Na_2SO_3 , NaHSO_3) act as antioxidants by combining with free oxygen at physiological pH.¹⁷ They are not neurotoxic in solution at physiological pH, but can be neurotoxic in low pH conditions through the production of SO_2 .¹⁸ The combination of betamethasone at pH 7.5–8.5 and saline at pH 4.5–8.0 used in the present study is not likely to provoke neurotoxicity as it has almost a physiological pH. Additionally, it has been reported that intrathecal bisulphite can reduce the neurotoxic damage induced by the intrathecal injection of local anaesthetic (chloroprocaine).¹⁹

In the current study, clinical neurotoxicity was not seen after intrathecal betamethasone injection. On the contrary, neurological symptoms such as motor weakness and gait disturbance improved, and activities of daily living gradually recovered in many patients. Nevertheless, the sample size of this study (10 patients) is too small to conclusively demonstrate the safety of intrathecal betamethasone; for this, a larger study is needed.

Analgesic effects of intrathecal glucocorticoid

Glucocorticoids have multipurpose use, offering symptomatic relief in the management of patients with cancer pain. Principally, the analgesic effect of glucocorticoids is assumed to occur in inflammatory conditions. Recently, the analgesic effects of intrathecal steroids have been observed in both human and animal studies.^{13 14 20} In patients with postherpetic neuralgia, the intrathecal injection of methylprednisolone with lidocaine induced excellent and long-lasting analgesia for burning pain, lancinating pain, and allodynia.

It is thought that the long-lasting analgesia that results from the intrathecal injection of betamethasone is achieved through a decrease in the inflammatory reactions in the injured nerves and a reduction in algogenic substances

such as prostaglandins, glutamate, and substance P in the spinal cord. The suppression of spinal glial activation and the inhibition of inflammatory cells and cytokines may accelerate analgesic effects.^{21 22} Almost all of the 10 patients studied showed an immediate analgesic effect within 30 min, which was followed by long-lasting analgesia; this was similar to the first observation in the previous three patients we reported. The effects of steroids are not expected to be immediate, as the changes in gene expression and synthesis of proteins take several hours.²³ In the traditional theory of steroid action, steroids bind to intracellular receptors and modulate nuclear transcription. Anti-inflammatory effects of glucocorticoids are induced by the inhibition of phospholipase A2 resulting from lipocortin production through the fundamental steroid pharmacology. However, this mechanism for the analgesic effect of intrathecal glucocorticoid does not explain the immediate analgesia that was seen. This rapid effect may be transmitted by specific membrane-bound receptors.^{24 25} Although a relationship between immediate and long-lasting analgesia is unknown, all of the patients with long-lasting analgesia had immediate analgesia after the first intrathecal betamethasone treatment. Given our findings, the mechanism of the analgesic effects of intrathecal glucocorticoid should be studied in greater depth in the future.

Treatments of cancer pain and intrathecal glucocorticoid

Opioids are widely used in the management of cancer pain, but sufficient pain relief without side-effects is sometimes difficult to obtain. Although intrathecal or epidural opioid injections may be a good option for cancer pain treatment, the patients develop side effects similar to oral opioids, and a catheter must be implanted for continuous opioid injection.²⁶ The intrathecal injection of neurolytic agents is a useful anaesthetic technique for treating some cancer pain, but there are practical difficulties with the procedure, and also as risks of neural complications.²⁷

Oral glucocorticoids are used palliatively for cancer pain treatment, especially in patients with bone metastases.²⁸ In the current study, small-dose betamethasone was used intrathecally once a week and sufficient pain relief was achieved in about a half of the patients, and no clinical complications were seen. Therefore, certain types of uncontrollable cancer pain can be better treated with intrathecal betamethasone, especially in patients with vertebral metastases whose pain is frequently difficult to control.

In contrast to epidural procedures, the intrathecal technique is easy and safe to perform in the lumbar region. Therefore, the intrathecal injection of betamethasone has a technical advantage over other anaesthetic procedures for the management of cancer pain.

Conclusions

When conventional treatments for cancer pain are not successful, intrathecal injection of small-dose betamethasone may be a useful approach, especially in patients with vertebral bone metastases. Intrathecal betamethasone may induce long-lasting analgesia without adverse effects. As a result, intrathecal betamethasone may be able to improve activities of daily living and quality of life in patients with cancer pain.

References

- 1 Portenoy RK, Lesage P. Management of cancer pain. *Lancet* 1999; **353**: 1695–700
- 2 Schell HW. Adrenal corticosteroid therapy in far advanced cancer. *Geriatrics* 1972; **27**: 131–41
- 3 Cherny NI, Portenoy RK. Practical issues in the management of cancer pain. *Anesthesiology* 1999; **91**: 1937–41
- 4 McCormack K. The spinal actions of nonsteroidal anti-inflammatory drugs and the dissociation between their anti-inflammatory and analgesic effects. *Drugs* 1994; **47**: 28–45
- 5 Ahlgren SC, Wang JF, Levine JD. C-fiber mechanical stimulus-response functions are different in inflammatory versus neuropathic hyperalgesia in the rat. *Neuroscience* 1997; **76**: 285–90
- 6 McMahon SB, Cafferty WB, Marchand F. Immune and glial cell factors as pain mediators and modulators. *Exp Neurol* 2005; **192**: 444–62
- 7 Rowbotham MC. Mechanisms of neuropathic pain and their implications for the design of clinical trials. *Neurology* 2005; **65**: 66–73
- 8 Nelson DA. Intraspinal therapy using methylprednisolone acetate. Twenty-three years of clinical controversy. *Spine* 1993; **18**: 278–86
- 9 Taguchi H, Shingu K, Okuda H, et al. Analgesia for pelvic and perineal cancer pain by intrathecal steroid injection. *Acta Anaesth Scand* 2002; **46**: 190–3
- 10 Roche J. Steroid-induced arachnoiditis. *Med J Aust* 1984; **140**: 281–4
- 11 Nelson DA, Landau WM. Intrathecal steroids. history, efficacy, accidentality, and controversy with review of United States Food and Drug Administration reports. *J Neurol Neurosurg Psychiatry* 2001; **70**: 433–43
- 12 Kotani N, Kushikata T, Hashimoto H, et al. Intrathecal methylprednisolone for intractable postherpetic neuralgia. *N Engl J Med* 2000; **343**: 1514–9
- 13 Langmayr JJ, Obwegeser AA, Schwarz AB, et al. Intrathecal steroids to reduce pain after lumbar disc surgery: a double-blind, placebo-controlled prospective study. *Pain* 1995; **62**: 357–61
- 14 Latham JM, Fraser RD, Moore RJ, et al. The pathologic effects of intrathecal betamethasone. *Spine* 1997; **22**: 1558–62
- 15 Abram SE, Marsala M, Yaksh TL. Analgesic and neurotoxic effects of intrathecal corticosteroids in rats. *Anesthesiology* 1994; **81**: 1198–205
- 16 Hodgson PS, Neal JM, Pollock JE, et al. The neurotoxicity of drugs given intrathecally (spinal). *Anesth Analg* 1999; **88**: 797–809
- 17 Feroci G, Fini A. Study of the antioxidant effect of the selenium and sulfur compounds. *J Trace Elem Med Biol* 1998; **12**: 96–100
- 18 Gissen AJ, Datta S, Lambert D. The chloroprocaine controversy. Is chloroprocaine neurotoxic? *Reg Anesth* 1984; **9**: 135–45
- 19 Taniguchi M, Bollen A, Drasner K. Sodium bisulfite: Scapegoat for chloroprocaine neurotoxicity? *Anesthesiology* 2004; **100**: 85–91
- 20 Takeda K, Sawamura S, Sekiyama H, et al. Effect of methylprednisolone on neuropathic pain and spinal glial activation in rats. *Anesthesiology* 2004; **100**: 1249–57
- 21 Hains BC, Waxman SG. Activated microglia contribute to the maintenance of chronic pain after spinal cord injury. *J Neurosci* 2006; **26**: 4308–17
- 22 Wieseler-Frank J, Maier SF, Watkins LR. Central proinflammatory cytokines and pain enhancement. *Neurosignals* 2005; **14**: 166–74
- 23 Cunningham FM, Lees P. Advances in anti-inflammatory therapy. *Br Vet J* 1994; **150**: 115–134
- 24 Jusko WJ. Receptor-mediated pharmacodynamics of corticosteroids. *Prog Clin Biol Res* 1994; **387**: 261–70
- 25 Wehling M. Specific, nongenomic actions of steroid hormones. *Annu Rev Physiol* 1997; **59**: 365–93
- 26 Mercadante S. Problems of long-term spinal opioid treatment in advanced cancer patients. *Pain* 1999; **79**: 1–13
- 27 Ferrer-Brechner T. Anesthetic techniques for the management of cancer pain. *Cancer* 1989; **63**: 2343–7
- 28 Twycross R. The risks and benefits of corticosteroids in advanced cancer. *Drug Safety* 1994; **11**: 163–78

Intrathecal betamethasone pain relief in cancer patients with vertebral metastasis: a pilot study*

T. INADA, A. KUSHIDA, S. SAKAMOTO, H. TAGUCHI and K. SHINGU
Department of Anesthesiology, Kansai Medical University, Osaka, Japan

Background: We have reported previously the usefulness of intrathecal betamethasone for pain relief in cancer patients who suffer from intractable pain caused by vertebral metastasis. The mechanism by which betamethasone relieves pain may be related to alterations in cerebrospinal fluid (CSF) concentrations of pro-inflammatory cytokines and prostanoids.

Methods: Thirteen cancer patients with intractable pain caused by vertebral metastasis received 2–3 mg betamethasone in the lumbar subarachnoid space. CSF concentrations of tumor necrosis factor- α (TNF- α), interleukin-1 β (IL-1 β), IL-6, IL-8 and prostaglandin E₂ (PGE₂) were measured with an enzyme-linked immunosorbent assay (ELISA) and a chemiluminescence enzyme immunoassay. Pain was measured using a numerical pain score (range, 0–10; 0, no pain; 10, worst pain imaginable).

Results: Intrathecal betamethasone was associated with a significant decrease in the pain score in six patients. In these cases, the

pain score decreased from 6.7 ± 0.5 (mean \pm standard error of the mean) to 3.3 ± 0.3 ($P < 0.05$), and the CSF concentrations of IL-8 and PGE₂ decreased significantly compared with pre-treatment levels (IL-8, 183.3 ± 21.2 to 116.5 ± 10.6 pg/ml; PGE₂, 43.8 ± 10.3 to 14.7 ± 3.0 pg/ml). There were no significant changes in the CSF concentrations of cytokines and PGE₂ in the remaining seven patients.

Conclusion: Pain relief with intrathecal betamethasone is related to decreases in the CSF concentration of IL-8 and PGE₂.

Accepted for publication 15 December 2006

Key words: cancer; cerebrospinal fluid; interleukin-8; intrathecal betamethasone; pain; prostaglandin E₂.

© 2007 The Authors
Journal compilation © 2007 Acta Anaesthesiol Scand

VERTEBRAL metastasis may cause severe pain in cancer patients (1). Although oral or systemic administration of opioids is the principal pain treatment for such patients, sufficient analgesia is sometimes difficult to achieve because of excessive sedation, pruritus and gastrointestinal side-effects (1). Previously, we have reported the usefulness of the intrathecal administration of betamethasone for pain relief (2), and we believe that it may provide an alternative to the administration of escalating doses of opioids.

The mechanism by which intrathecal betamethasone relieves pain is not known. Pain is associated with inflammation in the central nervous system (3–6), and betamethasone has anti-inflammatory effects (7). Therefore, the pain-relieving properties of betamethasone may be related to altered concentrations of pro-inflammatory cytokines and prostanoids

in the cerebrospinal fluid (CSF), including tumor necrosis factor- α (TNF- α), interleukin-1 β (IL-1 β), IL-6, IL-8 and prostaglandin E₂ (PGE₂), all of which have been implicated in inflammation and pain (3–6).

The aims of this study were to examine whether intrathecal betamethasone alters CSF concentrations of TNF- α , IL-1 β , IL-6, IL-8 and PGE₂, and to determine whether these alterations are associated with pain relief in cancer patients with vertebral metastasis.

Methods

Patients

Cancer patients with vertebral metastasis, who were referred to our department for pain management (because their pain was not controllable with conventional opioid therapy), were studied. Criteria for inclusion in the study were an advanced stage of cancer, presence of vertebral bone metastasis, uncontrollable pain despite conventional analgesic therapies and no ongoing chemotherapy or radiation therapy. Patients were studied consecutively from

*Presented in part at the Annual Meeting of the American Society of Anesthesiologists, October, 2006, Chicago, IL, USA.

February 2002 to December 2004. The study was approved by the Ethics Committee of Kansai Medical University, Osaka, Japan, and all patients gave written informed consent.

Protocol

Before the procedure, the intensity of pain was reported by patients using a numerical pain score (PS; range, 0–10; 0, no pain; 10, worst pain imaginable). In the lateral decubitus position, a 25G pencil-point spinal needle (Unisis, Tokyo, Japan) was inserted through the interlaminar space in the lumbar vertebrae of each patient, avoiding spaces adjacent to metastatic vertebral bone and sites of dural metastasis (assessed by computed tomography/magnetic resonance image), and a 3-ml control sample of CSF was obtained. Subsequently, betamethasone (Rinderson Injection 0.4%, Shionogi, Japan), 2–3 mg in saline in a volume of 3 ml, was injected. Patients evaluated their pain each day with the PS. Intrathecal betamethasone was scheduled to be given once a week without CSF procurement, except that a second CSF sample was obtained between the second and fourth intrathecal betamethasone injections (the time was determined at the discretion of the attending pain clinicians). The period between the first CSF sample (no intrathecal betamethasone) and the post-betamethasone CSF sample (7–28 days after the first intrathecal betamethasone injection) was the study period. We restricted the study to this short period in order to clarify the effect of intrathecal betamethasone and to minimize the background effect of relentlessly progressing vertebral metastasis-induced inflammation on the CSF pro-inflammatory molecules.

Evaluation of pain relief

We arbitrarily determined that successful pain relief was achieved if the PS value decreased to < 5 , as patients expressed considerable satisfaction when they described their pain as being $PS < 5$.

Measurement of TNF- α , IL-1 β , IL-6, IL-8 and PGE₂

CSF samples were immediately centrifuged at 3000 g for 10 min at 4 °C, and the supernatant was stored at –80 °C pending analysis. CSF concentrations of cytokines were measured with high-sensitivity enzyme-linked immunosorbent assay (ELISA). A Quantikine HS Kit (R & D Systems, Minneapolis, MN) was used to assay TNF- α , IL-1 β and IL-6. An Endogen Human IL-8 ELISA Kit (Pierce Biotechnology, Inc., Rockford, IL) was used to assay IL-8. PGE₂

was measured with a chemiluminescence enzyme immunoassay kit (Assay Designs Inc., Ann Arbor, MI). The lower limits of detection were 0.12 pg/ml for TNF- α , 0.10 pg/ml for IL-1 β , 0.039 pg/ml for IL-6, 2 pg/ml for IL-8 and 6.03 pg/ml for PGE₂. The intra- and inter-assay coefficients of variation for the ELISA and chemiluminescence kits were less than 10% and 14%, respectively. Measurements were performed in duplicate and the means were recorded.

Statistical analysis

Data are reported as the mean \pm standard error of the mean (SEM). Comparisons were made with the Wilcoxon signed-rank test or the Mann–Whitney *U*-test. $P < 0.05$ was considered to be significant.

Results

Thirteen patients were enrolled in the study (Table 1). In six patients, a successful decrease in pain intensity was measured at the time of post-betamethasone CSF sample procurement (effective group) (PS changed from 6.7 ± 0.5 to 3.3 ± 0.3 , $P < 0.05$). Intrathecal betamethasone was not associated with decreased pain in the remaining seven patients (non-effective group) (PS changed from 8.0 ± 0.6 to 7.5 ± 0.6 , $P = NS$). The patient characteristics were similar in the two groups, and the site of vertebral metastasis was not related to pain relief (Table 1). All patients (except for patients 1 and 6 in the effective group and patient 2 in the non-effective group) had a previous history of radiation to their metastatic lesions. Lytic bone destruction was noted in the vertebral metastases in all patients, and, in patient 5 in the effective group, osteogenic destruction was also observed. During the study period, the morphine dosage was decreased in one patient in the effective group, and increased in three patients in the non-effective group. The interval between obtaining the control CSF samples and the post-intrathecal betamethasone CSF samples (the patient follow-up period in this study) was 12 ± 2 days for the effective group and 15 ± 3 days for the non-effective group ($P = NS$).

The concentrations of IL-8 and PGE₂ in the control CSF samples were significantly higher ($P < 0.05$) in the effective group than in the non-effective group (Fig. 1). The CSF concentrations of IL-8 and PGE₂ decreased significantly ($P < 0.05$) following intrathecal betamethasone treatment in the effective group, whereas the concentrations of TNF- α , IL-1 β and IL-6 did not. There were no significant changes in the CSF concentrations of cytokines and PGE₂ following

Table 1

Patient characteristics and tumor and pain status.

Patient	Age (years)	Sex	Primary lesion	Spinal level of metastasis	Morphine (mg)	Control pain score	Pain score post-betamethasone†	Number of injections‡	Pain relief (days)§
Effective group									
1	61	M	Pharynx	Thoracic	40	7	4	1	7
2	49	F	Thyroid	Cervical, thoracic	10	8	4	2	7
3	59	M	Liver	Cervical, sacrum	380 → 0	8	2	2	12
4	74	M	Colon	Sacrum	105	6	3	2	5
5	68	M	Prostate	Thoracic, lumbar	480	6	4	2	8
6	72	M	Kidney	Thoracic	140	5	3	2	8
Mean ± SEM	64 ± 4				192 ± 78*	6.7 ± 0.5	3.3 ± 0.3¶		7.8 ± 0.9
Non-effective group									
1	64	M	Liver	Lumbar	30 → 40	9	7	2	
2	61	M	Esophagus	Thoracic	30	10	9	1	
3	55	M	Lung	Thoracic	20 → 40	8	6	1	
4	72	M	Thyroid	Thoracic, lumbar	40 → 160	6	6	1	
5	61	M	Rectum	Lumbar	110	6	9	3	
6	69	M	Liver	Lumbar, sacrum	20	9	10	2	
7	56	M	Pancreas	Thoracic, lumbar	250	8	6	3	
Mean ± SEM	63 ± 2				71 ± 32*	8.0 ± 0.6	7.5 ± 0.6		

SEM, standard error of the mean; →, change in morphine dose after intrathecal betamethasone.

*Before intrathecal betamethasone.

†Pain score measured at the time of post-betamethasone cerebrospinal fluid (CSF) sample collection.

‡Number of intrathecal betamethasone injections administered before collection of post-betamethasone CSF sample.

§Duration of pain relief (pain score < 5) at the time of post-betamethasone CSF sample collection.

¶ $P < 0.05$ vs. control pain score.

intrathecal betamethasone treatment in the non-effective group. The concentrations of PGE₂ after intrathecal betamethasone administration were significantly lower ($P < 0.01$) in the effective group than in the non-effective group.

Potential adverse effects related to the neurotoxicity of betamethasone and the intrathecal injection procedure, such as headache, low back pain, numbness in the limbs, sensory and motor weakness, and recto-bladder dysfunction, were not observed in any of the patients.

Discussion

In this study, pain relief was associated with significant decreases in the CSF concentrations of IL-8 and PGE₂ on intrathecal administration of betamethasone. Furthermore, responsive patients had higher CSF concentrations of IL-8 and PGE₂ than non-responsive patients prior to the intrathecal administration of betamethasone. These results suggest that intrathecal betamethasone exerts its effects by reducing the inflammatory component of pain, and is more effective in patients with considerable quantities of inflammatory components in the central nervous system.

IL-8 is associated with pain induced by an inflammatory reaction, and high CSF concentrations of IL-8

have been noted in patients with sciatic pain from disk herniation (3) and intractable post-herpetic neuralgia (PHN) (8). Furthermore, postmortem studies of patients with prolonged PHN have revealed marked inflammation around the spinal cord with massive accumulation of lymphocytes (9). The CSF concentration of IL-8 in our patients (effective group, 183.3 ± 21.2 pg/ml; non-effective group, 98.2 ± 20.5 pg/ml) was higher than that reported in PHN patients ($33\text{--}35 \pm 1.6\text{--}1.7$ pg/ml), and in patients without PHN or with other neurologic disorders (18 ± 1.0 pg/ml) (8). This suggests that cancer patients with vertebral metastasis have high CSF concentrations of IL-8. In the PHN study (8), methylprednisolone and lidocaine were given intrathecally to treat pain. The treatment was effective in alleviating pain, and pain relief was correlated significantly with a decrease in the CSF concentration of IL-8.

The PGE₂ concentrations in the effective group (43.8 ± 10.3 pg/ml) were considerably higher than those of normal controls (< 20 pg/ml) (10). PGE₂ is a potent mediator of inflammation. It produces prolonged dilatation of the arterioles and increases vascular permeability, leading to enhanced recruitment of leukocytes (11) and exaggerated inflammatory pain (5, 12). Increased CSF concentrations of PGE₂ are also implicated in the central sensitization of nociceptive processes (13–15).

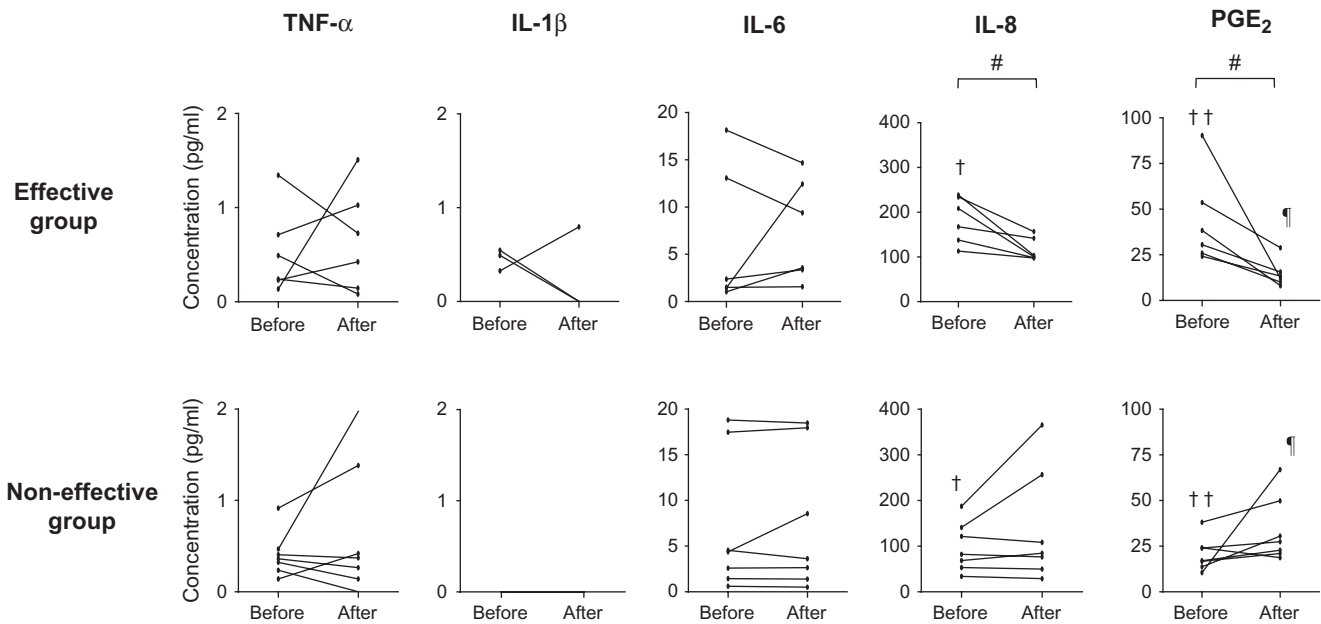


Fig. 1. Concentrations of tumor necrosis factor- α (TNF- α), interleukin-1 β (IL-1 β), IL-6, IL-8 and prostaglandin E₂ (PGE₂) in the cerebrospinal fluid (CSF) before and after intrathecal betamethasone. The effective group consists of patients whose pain scores (range, 0–10; 0, no pain; 10, worst pain imaginable) decreased to < 5 by betamethasone treatment at the time of post-betamethasone CSF sample collection. #P < 0.05 within groups. †P < 0.05, ††P < 0.01, between groups before intrathecal betamethasone. ¶P < 0.01 between groups after intrathecal betamethasone. Some IL-1 β data are hidden in the x-axis because of the absence of the cytokine in CSF before and after intrathecal betamethasone.

The origin of IL-8 and PGE₂ in CSF is not known, but tumor cells, osteoblasts, macrophages, astrocytes and microglia may be involved. It has been reported that metastasis-prone tumors often express high levels of IL-8 (16, 17) and cyclo-oxygenase (18), a key enzyme in PGE₂ production. Osteoblasts from deteriorating bone also produce PGE₂ (19). In addition, bone and tissue that are destroyed by tumors may be scavenged by macrophages and microglia that produce IL-8 and PGE₂ (20, 21). As a chemokine, IL-8 recruits neutrophils (which may produce IL-8 and PGE₂) to the inflammatory site, exacerbating the inflammation. This heightened *in situ* production of IL-8 and PGE₂ may be reflected by increased CSF concentrations of these molecules. The pro-inflammatory properties of IL-8 and PGE₂ increase pain transmission in neurons, resulting in inflammatory pain and creating a feed-forward pain cycle. We assume that intrathecal betamethasone, via its anti-inflammatory effects, interrupts the cycle and alleviates pain (7). However, other effects of steroids may also be involved, including stabilization of neuronal membranes and suppression of C-fiber discharges (22–24).

Some patients were unresponsive to intrathecal betamethasone treatment. There may be several explanations for this, including overwhelming tumors

(e.g. direct nerve invasion by tumors), an insufficient dose of betamethasone, a relatively small inflammatory contribution to the pain and the inefficient delivery of betamethasone to the site of inflammation.

The use of intrathecal steroids has been reported to be safe, although arachnoiditis and meningitis have been reported following their use (25, 26). In one study, four doses of intrathecal methylprednisolone (60 mg) were given to 89 PHN patients, and no complications were noted (8). The safe use of intrathecal betamethasone has been reported in patients after lumbar disk surgery (27) and in an animal experiment (28). Alternatively, additives, such as antioxidants and preservatives, that are present in the injected solution, rather than the steroids themselves, may cause neurotoxicity when administered intrathecally (29). The betamethasone solution used in this study contained the antioxidant sodium sulfite. Sodium sulfite can be neurotoxic at low pH as a result of the production of sulfur dioxide, but not at physiological pH (30). Thus, when combined with betamethasone (pH 7.0–8.0) in saline, it is not likely to be neurotoxic after intrathecal injection.

Intrathecal betamethasone treatment is simpler, less traumatic and has a more reproducible effect (31) than epidural blocks, which are often used to alleviate pain in cancer patients (32). Furthermore,

pain from metastasis at any level of the vertebral column can be an indication for betamethasone via the lumbar subarachnoid route. In addition, the duration of pain relief was sufficient such that intrathecal betamethasone needed to be administered only once a week. Thus, although not all patients are responsive, intrathecal betamethasone may be useful for the alleviation of pain in some terminal cancer patients. We are now conducting a study to determine the most effective doses of betamethasone to maximally alleviate pain, whilst minimizing the potential side-effects.

References

- Cleeland CS, Gonin R, Hatfield AK et al. Pain and its treatment in outpatients with metastatic cancer. *N Engl J Med* 1994; **330**: 592–6.
- Taguchi H, Shingu K, Okuda H, Matsumoto H. Analgesia for pelvic and perineal cancer pain by intrathecal steroid injection. *Acta Anaesthesiol Scand* 2002; **46**: 190–3.
- Brisby H, Olmarker K, Larsson K, Nutu M, Rydevik B. Proinflammatory cytokines in cerebrospinal fluid and serum in patients with disc herniation and sciatica. *Eur Spine J* 2002; **11**: 62–6.
- Alexander GM, van Rijn MA, van Hilten JJ, Perreault MJ, Schwartzman RJ. Changes in cerebrospinal fluid levels of pro-inflammatory cytokines in CRPS. *Pain* 2005; **116**: 213–9.
- Buvanendran A, Kroin JS, Berger RA et al. Upregulation of prostaglandin E2 and interleukins in the central nervous system and peripheral tissue during and after surgery in humans. *Anesthesiology* 2006; **104**: 403–10.
- Shi L, Smolders I, Umbrain V et al. Peripheral inflammation modifies the effect of intrathecal IL-1beta on spinal PGE2 production mainly through cyclooxygenase-2 activity. A spinal microdialysis study in freely moving rats. *Pain* 2006; **120**: 307–14.
- Manchikanti L. Role of neuraxial steroids in interventional pain management. *Pain Physician* 2002; **5**: 182–99.
- Kotani N, Kushikata T, Hashimoto H et al. Intrathecal methylprednisolone for intractable postherpetic neuralgia. *N Engl J Med* 2000; **343**: 1514–9.
- Watson CP, Deck JH, Morshead C, Van der Kooy D, Evans RJ. Post-herpetic neuralgia: further post-mortem studies of cases with and without pain. *Pain* 1991; **44**: 105–17.
- Almer G, Teismann P, Stevic Z et al. Increased levels of the pro-inflammatory prostaglandin PGE2 in CSF from ALS patients. *Neurology* 2002; **58**: 1277–9.
- Simmons DL, Botting RM, Hla T. Cyclooxygenase isozymes: the biology of prostaglandin synthesis and inhibition. *Pharmacol Rev* 2004; **56**: 387–437.
- Smith HS. Arachidonic acid pathways in nociception. *J Support Oncol* 2006; **4**: 277–87.
- Dirig DM, Yaksh TL. Hyperalgesia-associated spinal synthesis and release of prostaglandins. *Adv Exp Med Biol* 1997; **433**: 205–8.
- Baba H, Kohno T, Moore KA, Woolf CJ. Direct activation of rat spinal dorsal horn neurons by prostaglandin E2. *J Neurosci* 2001; **21**: 1750–6.
- Vanegas H, Schaible HG. Prostaglandins and cyclooxygenases in the spinal cord. *Prog Neurobiol* 2001; **64**: 327–63.
- Bendre MS, Gaddy-Kurten D, Mon-Foote T et al. Expression of interleukin 8 and not parathyroid hormone-related protein by human breast cancer cells correlates with bone metastasis in vivo. *Cancer Res* 2002; **62**: 5571–9.
- Bendre MS, Margulies AG, Walser B et al. Tumor-derived interleukin-8 stimulates osteolysis independent of the receptor activator of nuclear factor-kappaB ligand pathway. *Cancer Res* 2005; **65**: 11,001–9.
- Singh B, Berry JA, Shoher A, Lucci A. COX-2 induces IL-11 production in human breast cancer cells. *J Surg Res* 2006; **131**: 267–75.
- Ohshiba T, Miyaura C, Ito A. Role of prostaglandin E produced by osteoblasts in osteolysis due to bone metastasis. *Biochem Biophys Res Commun* 2003; **300**: 957–64.
- Lee YB, Nagai A, Kim SU. Cytokines, chemokines, and cytokine receptors in human microglia. *J Neurosci Res* 2002; **69**: 94–103.
- McMahon SB, Cafferty WB, Marchand F. Immune and glial cell factors as pain mediators and modulators. *Exp Neurol* 2005; **192**: 444–62.
- Hall ED. Glucocorticoid effects on central nervous excitability and synaptic transmission. *Int Rev Neurobiol* 1982; **23**: 165–95.
- Devor M, Govrin-Lippmann R, Raber P. Corticosteroids suppress ectopic neural discharge originating in experimental neuromas. *Pain* 1985; **22**: 127–37.
- Johansson A, Hao J, Sjolund B. Local corticosteroid application blocks transmission in normal nociceptive C-fibres. *Acta Anaesthesiol Scand* 1990; **34**: 335–8.
- Roche J. Steroid-induced arachnoiditis. *Med J Aust* 1984; **140**: 281–4.
- Nelson DA, Landau WM. Intraspinal steroids: history, efficacy, accidentality, and controversy with review of United States Food and Drug Administration reports. *J Neurol Neurosurg Psychiatry* 2001; **70**: 433–43.
- Langmayr JJ, Obwegeser AA, Schwarz AB, Laimer I, Ulmer H, Ortler M. Intrathecal steroids to reduce pain after lumbar disc surgery: a double-blind, placebo-controlled prospective study. *Pain* 1995; **62**: 357–61.
- Latham JM, Fraser RD, Moore RJ, Blumbergs PC, Bogduk N. The pathologic effects of intrathecal betamethasone. *Spine* 1997; **22**: 1558–62.
- Hodgson PS, Neal JM, Pollock JE, Liu SS. The neurotoxicity of drugs given intrathecally (spinal). *Anesth Analg* 1999; **88**: 797–809.
- Feroci G, Fini A. Study of the antioxidant effect of several selenium and sulphur compounds. *J Trace Elem Med Biol* 1998; **12**: 96–100.
- Bartynski WS, Grahovac SZ, Rothfus WE. Incorrect needle position during lumbar epidural steroid administration: inaccuracy of loss of air pressure resistance and requirement of fluoroscopy and epidurography during needle insertion. *Am J Neuroradiol* 2005; **26**: 502–5.
- Exner HJ, Peters J, Eikermann M. Epidural analgesia at end of life: facing empirical contraindications. *Anesth Analg* 2003; **97**: 1740–2.

Address:
T. Inada
Department of Anesthesiology
Kansai Medical University
10-15, Fumizono-cho
Moriguchi
Osaka, 570-8507
Japan
e-mail: takefumi@wd5.so-net.ne.jp

研究成果報告書

研究課題名	急性期脊髄損傷に対する培養自家骨髄間質細胞による脊髄再生治療		
(英文)	Spinal cord regeneration therapy with autologous bone marrow stromal cells for acute spinal cord injury		
事業推進者	中谷 壽男	E-mail	nakatant@takii.kmu.ac.jp
所属・職名	医学研究科・脊髄再生医学（救急医学科）講座・教授		
研究分担者名	村尾 佳則、岩瀬 正顕、平川 昭彦、前田 裕仁		
キーワード	脊髄損傷、脊髄再生、骨髄間質細胞、髄液内投与		
<p>1. 概要</p> <p>損傷された中枢神経系は回復することがないとの定説を覆し、脊髄損傷患者に対して脊髄再生を図ることを目的とした実験的、臨床的研究である。現在、基礎的実験、動物実験を経て脊髄損傷患者に培養自家骨髄間質細胞を髄液内投与する臨床試験をおこなっている。また、同時に動物実験により、欠損脊髄の機能を回復させるために最適の細胞、架橋物質、成長因子についての研究も行っている。</p> <p>2. 研究の背景と目的</p> <p>従来より、損傷された中枢神経系の機能を回復させる有効な治療法は無いとされ、治療が残った周辺の細胞の損傷を如何に抑制するか（二次損傷の防止）、損傷を免れた細胞の機能を如何に引き出すか（リハビリテーション）に、主眼が注がれていた。患者は生涯を車椅子やベッド上での生活が強いられ、時には人工呼吸器すら生涯を通じて外せない場合もある。そのため、本人はもとより、家族にとっても肉体的、精神的、金銭的負担は計り知れない。我が国では交通事故や転倒・転落により毎年5千人の患者が発生し、10万人を超える患者がいる。</p> <p>脊髄を再生させるために多くの研究がなされてきており、多くの研究者が努力しているが、たとえば幹細胞を用いる場合には、倫理的、免疫学的問題などクリアしなければ成らないハードルがある。本研究は、基礎実験、ラット、イヌでの動物実験、サルでの安全性試験を経て、財団法人先端医療センター臨床研究部と共同でプロトコルを作成し、試験実施施設、細胞培養・データ管理施設の倫理委員会承認され、既に2症例に実施済みである。現時点では安全性に主眼を置いた臨床試験Ⅰ-Ⅱ相であり、高度医療として定着させることを目的としている。</p> <p>3. 研究方法</p> <p>関西医科大学高度救命救急センターに搬入された脊髄損傷患者のうち、本臨床試験の対象となりうるか否かの選択基準（損傷程度、機能評価可能であること、72時間以内に手術が可能なこと、年齢、代諾者を含めインフォームドコンセントが可能なこと、など）や、除外基準（合併傷病、妊娠、感染症など）から患者を選択する。損傷した脊椎の固定手術に際し、欠損部位に充填するために腸骨を採取する。その際に同時に採取される海綿骨（骨髄組織）を先端医療センターに搬送し、骨髄間質細胞を分離し、2週間程度のうちに培養して所定の数に増殖させる。この間質細胞を関西医科大学に持ち帰り、腰椎麻酔の手技を用いて脳脊髄液に注入する。そのため、患者に対しては本臨床試験を実施するための特別な追加手術（細胞採取を目的とした手術や細胞移植を目的とした損傷部の再度の剥離・露出術）を必要とせず、腰椎穿刺と同等の侵襲で実施しうる点が特色である。</p>			

4. これまでの成果

これまで、2症例に本臨床試験を実施した。わずか2例ではあるが、ともに従来からの治療法に比べて、第1例はASIA分類Aであり、同様の損傷を受けた患者群の中で最良の程度の回復を示し、2年以上経過した現時点で、骨髄細胞による石灰化、腫瘍化なども含めて、問題は全く起きていない。特に第2症例はASIA分類Bであり、知覚は若干残存していたものの運動機能は全く見られていなかった。術後も約10日間に亘って何ら症状の改善が見られなかったものが、細胞移植の一週間程度の後から短期間に良好な回復を示しており、3ヶ月経過した現時点で起立が可能で歩行訓練を開始している。また、安全性には何ら問題は見られていない。

5. これまでの進捗状況と今後の計画

これまでの2症例は、ともに極めて良好な回復を示している。第2症例は6ヶ月まで安全性に関する追跡調査を実施する。

今後、症例を増やし、3症例を終えた時点で高度医療の申請を行い、他の機関でも治療として行い得るように準備を進めて行く。

一方で、骨髄細胞移植により間質細胞が有効に作用する機序を解明するために、基礎的研究を学外共同研究者と進めている。脊髄再生の効果を高めるには、再生を担う細胞、細胞を増殖・分化させる成長因子、細胞に再生の場を提供する足場の三者が一体となって初めて有効な組織再生が期待できると考えられる。損傷部を架橋する人工材料として、共同研究者らが開発したアミノ酸原料から3重らせん構造を有する人工コラーゲンに、アポトーシス抑制ペプチドを付加し、脊髄損傷ラットに対し標識神経幹細胞を移植して、その機能を研究している。

6. これまでの発表論文

(1) 発表論文

1) 原著論文

Saito, F., Nakatani, T., Iwase, M., Maeda, Y., Hirakawa, A., Murao, Y., Suzuki, Y., Onodera, R., Fukushima, M. & Ide, C. Spinal cord injury treatment with intrathecal autologous bone marrow stromal cell transplantation: The first clinical trial case report. *J. Trauma* **64**, 53-59 (2008).

2) 総説

1. 中谷壽男：脊髄再生. *Clinical Engineering* 印刷中 (2008).

2. 齊藤福樹、中谷壽男、岩瀬正顕：

急性期脊髄損傷に対する自家骨髄間質細胞移植. *Jpn. J. Rehabil. Med.* **45**, 349-364 (2008).

3. 中谷壽男：脊髄損傷の再生治療. *救急医学* **31**, 1785-1789 (2007).

4. 中谷壽男、鈴木義久、井出千束、福島雅典：

脊髄損傷の再生医療. *臨床スポーツ医学* **23**, 1081-1085 (2006).

(2) 学会発表

国際学会

3) 一般発表

1. Nakatni, T., Suzuki, Y., Ide, C., Saito, F., Iwase, M., Maeda, Y., Fujiwara, H., Hirakawa, A., Murao, Y., Onodera, R. & Fukushima, M.

Clinical trial of spinal cord regeneration with bone marrow stromal cell transplantation by lumbar puncture. Shanghai International Conference on Emergency Medicine and Trauma. Shanghai, 2007.

2. Saito, F., Nakatani, T. & Iwase, M.

Report of a half-year post-transplantation course of the first clinical case of spinal cord regeneration trial with a novel method of bone marrow stromal cell administration into cerebrospinal fluid by the lumbar puncture technique. Shanghai International Conference on Emergency Medicine and Trauma. Shanghai, 2007.

3. Nakatani, T., Saito, F., Iwase, M., Suzuki, Y., Hirakawa, A., Murao, Y. & Ide, C.

Spinal Cord Regeneration with Bone Marrow Stromal Cell Administration in the Cerebro-Spinal Fluid: Report of the First Case at 6 Months. 66th American Association for the Surgery of Trauma. Las Vegas, 2007.

4. Nakatani, T., Iwase, M., Saito, F., Maeda, Y., Fujiwara, H., Hirakawa, A., Murao, Y., Suzuki, Y., Ide, C., Fukushima, M. & Onodera, R.
Report of the first clinical trial of spinal cord injury treatment with autologous bone marrow stromal cells intrathecal transplantation. 2007 Annual Meeting of Korean Society of Emergency Medicine; Korea-Japan joint session. Seoul, 2007.
5. Nakatani, T., Iwase, M., Saito, F., Maeda, Y., Fujiwara, H., Kajimoto, S., Hashiba, M., Hirakawa, A., Murao, Y., Onodera, R., Suzuki, Y., Fukushima, M. & Ide, C.
Report of the First Clinical Trial of Spinal Cord Regeneration with Bone Marrow Stromal Cell Transplantation by Lumbar Puncture. The 8th Asia Pacific Conference on Disaster Medicine. Tokyo, 2006.

国内学会

1) 学会特別講演

中谷壽男：急性期脊髄損傷に対する培養自家骨髄間質細胞移植による脊髄再生臨床経験
第21回日本外傷学会、千葉、2007.

2) シンポジウム講演

1. 齊藤福樹、岩瀬正顕、中谷壽男、沖井 明、菅 俊光、吉田清和、柴田斉子、佐々木万弓：急性期脊髄損傷に対する培養自家骨髄間質細胞移植。
第44回日本リハビリテーション医学会、神戸、2007.
2. 齊藤福樹、岩瀬正顕、中谷壽男、前田裕仁、平川昭彦、藤原弘佳、前田敏樹、宮崎秀行、下戸 学、津田雅庸、村尾佳則：急性期脊髄損傷に対する培養自家骨髄間質細胞移植。第35回日本救急医学会、大阪、2007.

3) 一般発表

1. 鈴木義久、齋藤晋、井上由理、井出千束、中谷壽男、福島雅典、石川奈美子、太田正佳：自家骨髄間質細胞を用いた脊髄損傷に対する再生治療の現状。
第17回日本形成外科学会基礎学術集会、東京、2008.
2. 岩瀬正顕、齊藤福樹、前田裕仁、吉岡正太郎、中谷壽男、河本圭司：自家骨髄間質細胞移植による脊髄再生の開始。
第12回日本脳神経外科救急学会、東京、2007.
3. 鈴木義久、岩瀬正顕、中谷壽男、井出千束：骨髄細胞を用いた脊髄損傷治療。
第27回日本脳神経外科コンgres、仙台、2007.
4. 齊藤福樹、岩瀬正顕、平川昭彦、村尾佳則、前田裕仁、藤原弘佳、宮崎秀行、前田敏樹、杉本達哉、下戸学、中谷壽男：急性期脊髄損傷に対する自家骨髄間質細胞移植。
第16回河内救急医療懇話会、大阪、2007.2. 齊藤福樹、中谷壽男、岩瀬正顕：脊髄損傷に対する自家骨髄間質細胞移植による再生治療の試み：第1症例について。第15回近畿外傷フォーラム、枚方、2007.
5. 齊藤福樹、中谷壽男、岩瀬正顕、平川昭彦、村尾佳則：自家骨髄間質細胞移植による脊髄再生治療の開始。
第34回日本救急医学会、福岡、2006.
6. 岩瀬正顕、齊藤福樹、前田裕仁、平川昭彦、村尾佳則、中谷壽男：当科における頸髄損傷の治療成績。第16回近畿外傷フォーラム、橿原、2006.
7. 齊藤福樹、岩瀬正顕、中谷壽男：脊髄損傷に対する自家骨髄間質細胞移植による再生治療の試み -6ヶ月の長期経過-。
第16回近畿外傷フォーラム、橿原、2006.

7. これまでの成果の情報公開

ホームページ：救急医学科学講座=<http://www3.kmu.ac.jp/ecc/>

Spinal Cord Injury Treatment With Intrathecal Autologous Bone Marrow Stromal Cell Transplantation: The First Clinical Trial Case Report

Fukuki Saito, MD, Toshio Nakatani, MD, Masaaki Iwase, MD, Yuji Maeda, MD, Akihiko Hirakawa, MD, Yoshinori Murao, MD, Yoshihisa Suzuki, MD, Rie Onodera, MS, Masanori Fukushima, MD, and Chizuka Ide, MD

J Trauma. 2008;64:53–59.

Spinal cord injury often results in devastating dysfunction and disability. When a spinal cord is injured, various symptoms are presented depending on the segments of the damage and the degree. If cervical spinal damage is severe, tetraplegia results. If damage occurs at levels higher than C4, diaphragmatic movement will be impaired, and the patient has to live being connected with the ventilator on the bed. Patients will suffer from acute hyperesthesia or severe chronic pain, urinary and rectal dysfunction, and autonomic dystonia as well as motor and sensory deficits.

In Japan, there are more than 100,000 victims suffering from spinal injury, and a new 5,000 to 6,000 patients are added every year. In the United States, about 250,000 to 400,000 people are living with spinal cord injury, and there are about 11,000 to 13,000 new injuries every year. The number of incidence is increasing. The majority of them result from motor vehicle or sports injuries, violence, or falls.¹

An injured central nervous system never regenerates. This has long been thought as a medical common sense

terms. Therefore, the principal object for the treatment of spinal injury was mainly purposed how to minimize the progression of secondary injuries and maintain the remnant function of the spine. For the purpose of preventing secondary spinal cord injury, spine stabilization for the fracture or dislocation and rehabilitation were the main strategy in the treatment.

There has been no successful treatment for the severe spinal cord injury to recover the function satisfactorily.² However, if spinal cord damage is functionally improved even at the minimum, it will affect not only the physical, mental, and economic status of patients and their families, but also the medical resources of society. Recently, regenerative treatments with stem cells are in the limelight. However, there are some serious problems such as ethical ones to be solved for the study with stem cells. We reported significant recovery of motor function in rats with experimental spinal cord injury treated by transplanting bone marrow stromal cells (BMSCs) in the cerebrospinal fluid (CSF).^{3,4} Based on that study, we aimed at the clinical application of this treatment, and actually planned a clinical trial of spinal cord injury treatment by transplanting patient's autologous BMSCs into CSF in the acute phase after spinal cord injury, at Kansai Medical University Hospital. We have developed a detailed protocol for the clinical trial. The medical ethics committees of the institutions have approved the protocol officially. This clinical trial aims to treat a damaged spinal cord by a novel method of injecting BMSCs into CSF through the lumbar puncture, and assess the safety and efficacy of the procedure. Although we have experienced only a single case, a committee that monitors the data to assess the efficacy and safety of the trial with members independent of this study team has evaluated the safety of the trial in this case, approved to continue the study, and agreed to submit a report of the first case. In addition, Japan Spinal Cord Foundation strongly requested to disclose the course of the first case. Therefore, we would like to publish the report of the first case to enhance research work on the new strategy for the difficult treatment of spinal cord injury.

Submitted for publication July 6, 2007.

Accepted for publication September 18, 2007.

Copyright © 2008 by Lippincott Williams & Wilkins

From the Emergency and Critical Care Center (F.S., T.N., M.I., Y.M., A.H., Y.M.), Kansai Medical University, Osaka, Japan; Department of Plastic and Reconstructive Surgery (Y.S.), Kitano Hospital, Tazuke Research Institute, Osaka, Japan; Department of Clinical Trial Design and Management (R.O., M.F.), Translational Research Center, Kyoto University Hospital, Kyoto, Japan; Department of Occupational Therapy (C.I.), Faculty of Nursing and Rehabilitation, Aino University, Osaka, Japan.

This work was supported, in part, by a Grant-in-Aid for Scientific Research from Japan Society for the Promotion of Science, Japan.

Presented in part at the 8th Asian Pacific Conference on Disaster Medicine, November 22, 2006, Tokyo, Japan; at the Shanghai International Conference on Trauma and Emergency Medicine, May 13, 2006, Shanghai, China; and as a poster at the 66th Annual Meeting of the American Association for the Surgery of Trauma, September 27–29, 2007, Las Vegas, Nevada.

Address for reprints: Toshio Nakatani, MD, Emergency and Critical Care Center, Kansai Medical University, Osaka, Japan; email: nakatant@takii.kmu.ac.jp.

DOI: 10.1097/TA.0b013e31815b847d

Table 1 Symptoms and Signs at Admission

Consciousness	Clear
Vital signs	
Blood pressure (mm Hg)	131/68
Heart rate (min ⁻¹)	70
Body temperature (°C)	36.2
Respiratory rate (min ⁻¹)	18
Arterial blood gas analysis (under O ₂ 10 L/m with face mask)	
Paco ₂ (mm Hg)	41.3
Pao ₂ (mm Hg)	102
pH	7.390
Base excess (mmol/L)	0.2
HCO ₃ ⁻ (mmol/L)	24.2
Neurologic examination	
Motor	
C5 (biceps)	3/5 (MMT)
C6 and lower	0/5
Sensory	
C7 and lower	No sensation
Anal sphincter	(-), no sacral sparing
Priapism	(+)
American Spinal Injury Association Impairment Scale	A

MMT, muscle manual test.

CASE REPORT

A 35-year-old man fell down from about 7-m height during a dismantling construction site work in March 2006. He was transported with a complaint of quadriplegia by a ground ambulance to our Emergency and Critical Care Center.

Symptoms and signs at admission are shown in Table 1. Chief complaint was loss of sensation and movement below C5 level. Cervical spine radiograph revealed a fracture-dislocation of C5 on the lateral view (Fig. 1), and computerized axial tomography (Fig. 2A and B) revealed fractured 4th and 5th cervical vertebra. Figure 3 shows the T1- and T2-weighted magnetic resonance imaging (MRI) at admission. T2-weighted image (Fig. 3B) showed a low-intensity area at the level of C5 that was surrounded by high-intensity area. No other injury was found. He was admitted in intensive care unit. His respiration type was abdominal, but he did not need ventilatory assist. He remained on methylprednisolone protocol, and was administered a single bolus injection of 30 mg/kg methylprednisolone within 8 hours after injury followed by a continuous administration of 5.4 mg/kg/h for 23 hours according to the National Acute Spinal Cord Injury Study II.⁵ On the day of admission, he underwent installation of halo brace to prevent secondary injury caused by instability of the cervical spine. His neurologic function was evaluated according to the American Spinal Injury Association (ASIA) Scoring for Standard Neurologic Classification of Spinal Cord Injury (SNCSICI) as shown in Table 2.

As his case was indicated to the clinical trial, we informed his wife about the clinical trial spending several hours while the patient was sedated. Although we informed her of the whole process of the clinical trial, we intended to get the



Fig. 1. Cervical spine radiograph lateral view showed a fracture-dislocation of C5 at admission.

written consent from her in two steps. The first consent was only with collecting bone marrow during the operation for cervical stabilization, and to culture and multiply stromal cells. The first consent should be obtained before operation shortly after the injury occurs, but in this case the patient was sedated and his family was upset, and so we obtained a written consent not with the clinical trial but with only obtaining bone marrow for culture during the operation. The patient and family members could have their time for about a week to discuss whether they would accept the clinical trial, the BMSCs transplantation.

On day 3, the patient underwent anterior cervical stabilization of C4 through C6 with bone graft and instrumentation. Iliac bone pieces were obtained for grafting to the fractured spine. Simultaneously, cancellous bone of the ilium was collected. Postoperative cervical spine lateral view shows anterior cervical stabilization at C4 through C6 by instrumentation, with spinal canal space at C5 level being opened and maintained (Fig. 4). He needed ventilatory support for a few days after the operation. Rehabilitation pro-

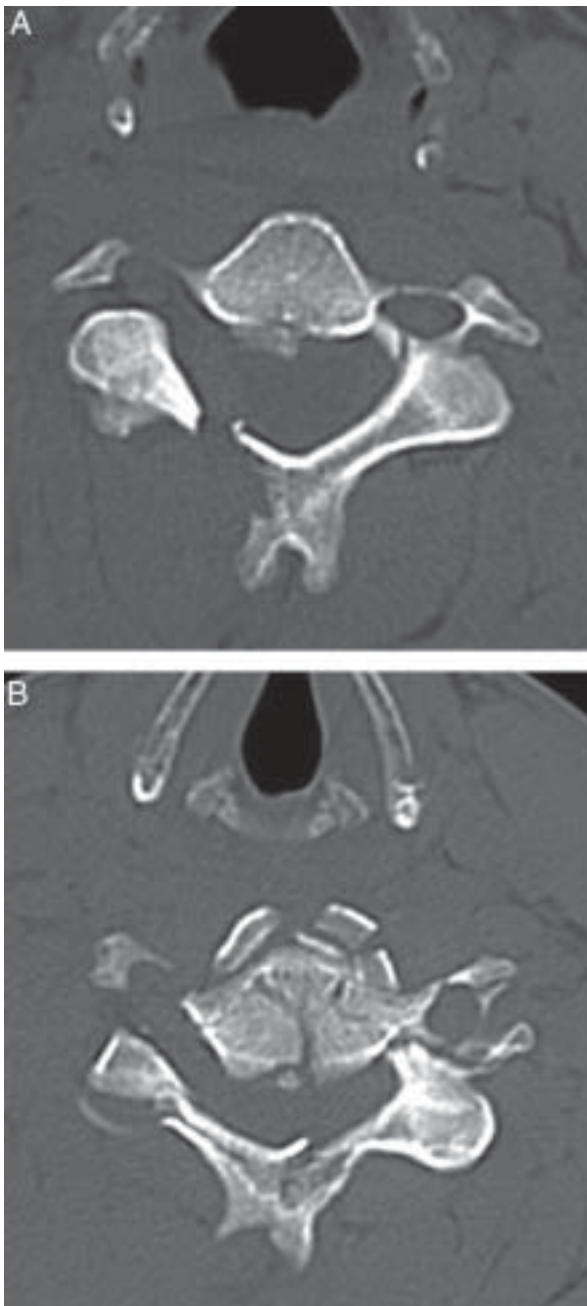


Fig. 2. Computed tomography at admission revealed the fractured 4th (A) and 5th (B) cervical vertebra.

gram was started shortly after the operation similarly for those with conventional treatment.

The cancellous bone was transported to a facility that meets the guideline for Good Manufacturing Practice of cell culture for clinical treatment in Japan, to isolate and culture stromal cells. Stromal cells were multiplied reaching a cell density of 10^6 after 10 days. We discussed again with his wife and the patient himself on the clinical trial at that point. He and his wife were willing to accept the cell transplantation therapy. On day 13, under written consent, 3.1×10^7 BMSCs, suspended in about 2 mL of saline, was transplanted

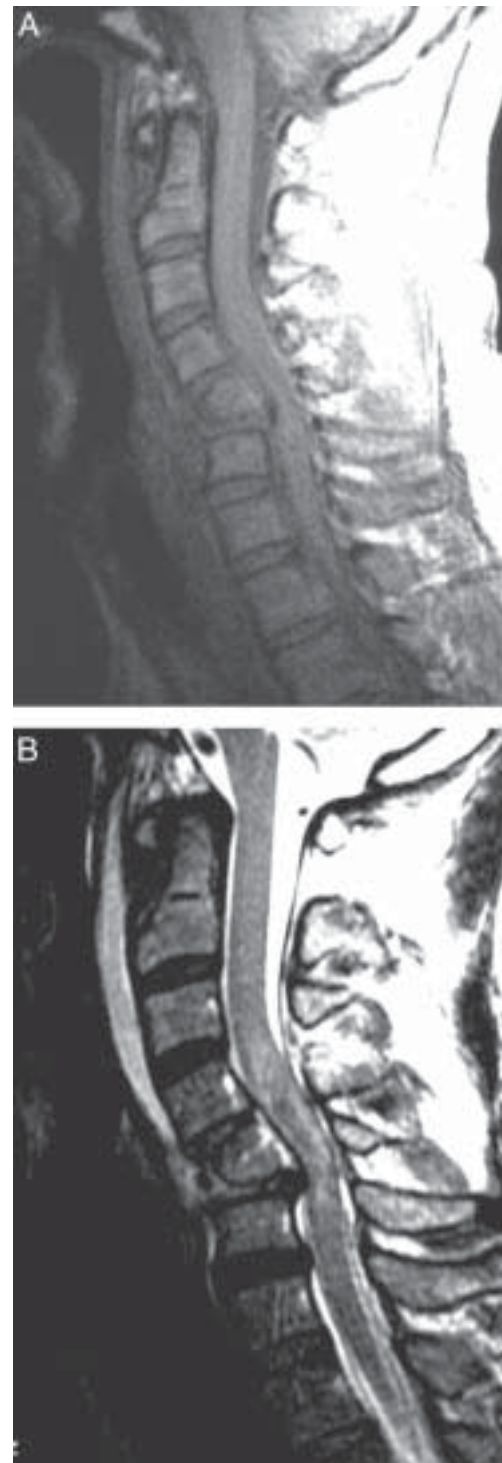


Fig. 3. MRI at admission. T1-weighted image (A) showed no remarkable change, but T2-weighted image (B) showed a low-intensity area at the level of C5 that was surrounded by high-intensity area.

into CSF through lumbar puncture technique. After transplantation, he had no sign of meningitis, such as fever or headache. His clinical course after the transplantation was uneventful and he left intensive care unit 22 days after the transplantation. A few weeks later, he once suffered from

Table 2 American Spinal Injury Association Scoring for Standard Neurologic Classification of Spinal Cord Injury

	Score			ASIA Impairment Scale
	Motor	Pinprick	Light Touch	
Normal (full)	100	112	112	E
Admission	6	16	16	A
Operation	8	20	17	A
1 mo	10	37	36	A
3 mo	16	34	43	A
6 mo	17	33	36	A

ASIA, American Spinal Injury Association.



Fig. 4. Cervical spine lateral view after the operation shows anterior cervical fusion at C4 through C6 by instrumentation, with spinal canal space at C5 level being opened and maintained.

urinary tract infection but no undesirable side effect of cell transplantation was observed throughout his course.

At 1, 3, and 6 months after the transplantation, neurologic function was evaluated in detail according to the SNCSCI of ASIA (Table 2). Motor and sensory scores gradually but apparently improved at 1 and 3 months compared with the scores before the transplantation. MRI at 3 months revealed a cavitation in the spinal cord (Fig. 5). Slight improvement was added to motor score, but no further improvement in the sensory score was observed at 6 months compared with that at 3 months. Changes in the score of key muscles at 6 months are shown in

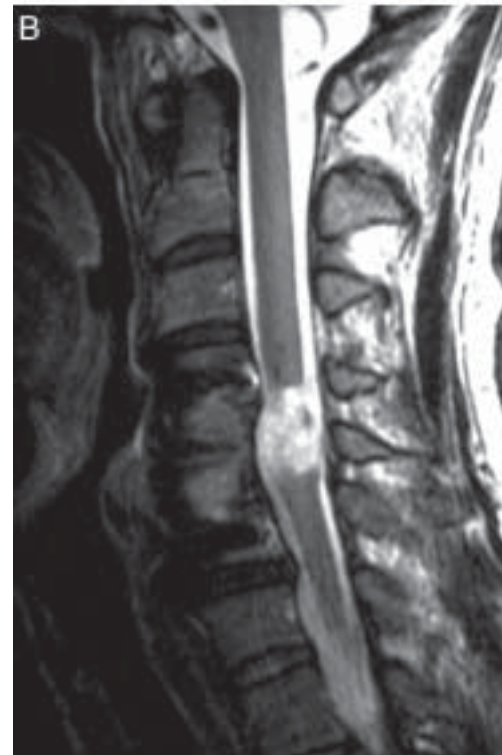


Fig. 5. Both T1-(A) and T2-weighted images (B) at 3 months after the transplantation shows a cavity formation at C5 level in the spinal cord.

Table 3. In addition to the gain in strength in the elbow flexors (C5), the gain in wrist extensors (C6) and elbow extensors (C7) motor levels elevated the motor score in the SNCSCI of ASIA.

Table 3 Changes in Key Muscles Motor Score

Level	Muscles	Motor Score			
		Before		6 M	
		R	L	R	L
C5	Elbow flexors	3	3	4	4
C6	Wrist extensors	0	0	0	3
C7	Elbow extensors	0	0	3	3
C8	Finger flexors	0	0	0	0

In the protocol of this clinical trial, our main endpoint is to evaluate the changes in motor scores at 6 months, and secondary endpoints are to evaluate the changes in sensory scores, anal functions, and ASIA impairment scale at 6 months. Our protocol does not call for quality of life as a main endpoint. However, we are continuing to observe his quality of life after the 6-month period. He is becoming able to sit on a wheelchair and drive slowly the wheelchair by himself. Further improvement in the scores and quality of life will be reported in our future study at a later time point.

In this clinical trial, patient data were registered and managed by an independent data center for the clinical trial. The efficacy and safety of the study should be discussed and evaluated in a committee with members outside of the study team. By far, the committee has evaluated the efficacy and safety of cell transplantation therapy in this first case. Although definite improvement in the score is obtained, we continue trials and increase the number of applied cases so that the efficacy and safety of this cell transplantation study can finally be evaluated in the committee.

DISCUSSION

Complete recovery of injured spinal cord is still a dream. It has long been thought that damaged central nervous system is fundamentally not recovered. It was reported from Vancouver Hospital that among 70 patients with complete spinal injury for minimum of 2-year complete follow-up, motor recovery did not occur below the zone of injury, although varying degrees of recovery can be expected within the zone of partial preservation.⁶ In the study of National Spinal Cord Injury Statistical Center, Alabama, only 5.6% of the 987 subjects with complete motor and sensory paralysis (ASIA grade A) at 1 year recovered to incomplete sensory or incomplete motor function at 5-year evaluation (ASIA grade B, C, or D).² Therefore, treatments for victims of spinal cord injury have been focused on preventing secondary damage and maintaining or maximally restoring preserved function by daily rehabilitation. Recently, various experimental or clinical studies with bioactive agents, growth factors, or cellular approaches are going on to inhibit inflammatory and degenerative responses or to enhance neural regeneration.⁷⁻¹⁴ Among them, clinical trials and animal experiments using stem cells,¹⁵⁻¹⁷ macrophages,¹⁸ olfactory ensheathing cells,^{2,19-23} and BMSCs²⁴⁻²⁶ are attracting a great deal of attention.

Among the cells, the BMSCs are of autologous origin and easy to obtain at the operation, and their incubation technique has been established. There will be no immunologic reaction, no ethical problem, and no uncontrollable proliferation as in the case of embryonic stem cells. BMSCs are considered to be realistic to use for the purpose of spinal cord injury treatment.

BMSCs make up approximately 0.125% of the total marrow cells.²⁷ BMSCs differentiate into osteoblasts, chondrocytes, adipocytes,^{28,29} skeletal muscle fibers,³⁰ cardiomyocytes,³¹ hepatocytes,³² and epithelial cells of liver, lung, intestinal tract, and skin.³³ BMSCs are reported to be capable of differentiating into Schwann cells in culture, and therefore would stimulate peripheral nerve regeneration.³⁴

Previously we investigated function of neurospheres derived from hippocampus or spinal cord cells in vitro and in vivo.^{35,36} We studied effects of transplantation of neurospheres in rats with Th8-9 level spinal cord contusion made using a New York University weight-drop device.³⁵ Considering clinical application, it is difficult to use neurosphere cells or neural stem cells from the standpoint of ethical problems. We, therefore, shifted to the study of BMSCs. In vitro, BMSCs exerted profound effects on neurite extension of co-cultured neurosphere cells, suggesting that BMSCs might have some potential regenerating influences to the spinal cord injury.³⁶ To avoid secondary injury on dissecting and injecting cells in the injured spinal cord, we administered BMSCs into CSF.^{37,38} We confirmed significant effects of BMSCs on the improvement of gait by using the open-field Basso, Beattie, and Bresnahan (BBB) scoring system³⁹ compared with control rats for up to 4 to 5 weeks.⁴ In this study, the cavity sizes were significantly smaller in the rats transplanted with BMSCs compared with those without BMSCs.^{3,4} After grafting, BMSCs were transported to the site of injury, attached to the injured neural tissue, then gradually decreased in number and disappeared within 3 weeks, promoting tissue repair in the injured spinal cord. This suggests that some trophic factors might be released from BMSCs to rescue neurons and glial cells from degeneration after the crush injury as well as to stimulate differentiation of neural stem cells in the recipient spinal cord.

On the basis of a series of in vitro and in vivo experiments, we planned a clinical trial of spinal cord injury treatment with a novel method. In this trial, only the patients who need operation for the spine stabilization are indicated. BMSCs can be obtained when iliac crest is harvested for grafting. No additional operation is necessary to obtain BMSCs. Multiplied BMSCs were transplanted into CSF by lumbar puncture technique. Therefore, reoperation is not necessary to open and dissect the lesion of the spinal cord as is needed for the direct cell infusion operation into spinal cord. Hence, secondary injury to the spinal cord can be avoided.

We made a protocol to transplant cells within 3 weeks after the injury. It is desired that cell transplantation can be

Table 4 Eligibility Criteria for the Preliminary Registration

1. Spinal cord injury is confirmed with MRI
2. ASIA Impairment Scale is A, B, or C
3. ISCSCI motor function score can be evaluated
4. Methylprednisolone therapy according to the NASCIS II study can be started within 8 h after the injury
5. BMSCs incubation can be started within 72 h after the injury
6. Age between 15 and 60
7. With the first informed consent of obtaining bone marrow

ASIA, American Spinal Injury Association (ASIA Impairment Scale: A, no motor or sensory function preserved in sacral segments; B, sensory but not motor function preserved in at least sacral segments; C, motor function preserved below the neurologic level and the majority of key muscle have motor score <3); ISCSCI, International Standard Classification of Spinal Cord Injury; NASCIS, National Acute Spinal Cord Injury Study; BMSC, bone marrow stromal cell.

Table 5 Exclusion Criteria

1. Complete disruption of spinal cord
2. Central spinal cord injury
3. Spinal canal stenosis before the injury
4. Brain or spinal cord disease before the injury
5. Multiple organ disease of SOFA score ≥ 12
6. Multiple trauma victim with injuries AIS ≥ 4 in more than 2 segments except for the spinal injury
7. Positive serologic test in at least one of the following; HBs antigen, HCV antibody, HIV antibody, or HTLV-1 antibody
8. Pregnancy

SOFA, sepsis-related organ failure assessment; AIS, Abbreviated Injury Score; HBs, hepatitis B surface antigen; HCV, hepatitis C virus; HIV, human immunodeficiency virus; HTLV, human T-cell leukemia virus.

performed as soon as possible after injury. However, BMSCs take about 7 to 10 days to proliferate to the cell density sufficient for transplantation. Based on the discussion for more than a year about the design of the clinical trial, we made the detailed protocol, which has been approved by the Ethics Review Board of our institutions.

In our protocol, candidates for the trial have to satisfy all the inclusion criteria listed in Table 4, and have no exclusion criteria listed in Table 5. They must be registered to an independent data center before the trial and checked again whether they meet all the inclusion and exclusion criteria. They also have to meet the eligibility criteria (Table 6) before transplantation. In this protocol, those with central spinal cord injury were omitted because they often recover spontaneously. Those with spinal canal stenosis before the injury for

Table 6 Eligibility Criteria for the Actual Registration

1. BMSCs $>10^6$ are obtained by the incubation
2. Transplantation can be performed <3 wk after the injury
3. ASIA impairment scale A, B, or C is confirmed within 3 d before transplantation
4. With second informed consent for transplantation

reasons such as ossification of posterior longitudinal ligament were also omitted because of a difficulty in evaluation.

In the study patient, although the findings of MRI (Fig. 3) after the injury suggest a poor prognosis of neural functional recovery, definite improvements were shown in motor and sensory functions up to 6 months. Although this clinical trial study has just started and this report is about only a single case, the safety of injecting autologous BMSCs into CSF has been confirmed in this first clinical case. The efficacy of this kind of cell transplantation should be evaluated by a committee with members outside this study team after a series of cases in accordance with the protocol.

In conclusion, to our knowledge, this is the first report of clinical trial for spinal cord injury treatment by transplanting BMSCs into CSF. As autologous BMSCs are used in our study, no ethical and immunologic problems develop. We are carefully observing the course of the present case. There is no adverse effect that might be caused by the administration of BMSCs into CSF. We have to accumulate in a number of cases so that the effectiveness and safety of BMSC transplantation through CSF can be evaluated on the more secured base in a committee.

REFERENCES

1. Lasfargues JE, Custis D, Morrone F, et al. A model for estimating spinal cord injury prevalence in the United States. *Paraplegia*. 1995; 33:62–68.
2. Lim PAC, Tow AM. Recovery and regeneration after spinal cord injury: a review and summary of recent literature. *Ann Acad Med*. 2007;36:49–57.
3. Bai H, Suzuki Y, Noda T, et al. Dissemination and proliferation of neural stem cells on the spinal cord by injection into the rat: a method for cell transplantation. *J Neurosci Methods*. 2003;124:181–187.
4. Ohta M, Suzuki Y, Noda T, et al. Bone marrow stromal cells infused into the cerebrospinal fluid promote functional recovery of the injured rat spinal cord with reduced cavity formation. *Exp Neurol*. 2004;187:266–278.
5. Bracken MB, Shepard MJ, Collins WF, et al. A randomized controlled trial of methylprednisolone or naloxone in the treatment of acute spinal cord injury: results of the Second National Acute Spinal Cord Injury Study. *N Engl J Med*. 1990;322:1405–1411.
6. Fisher CG, Noonan VK, Smith DE, et al. Motor recovery, functional status, and health-related quality of life in patients with complete spinal cord injuries. *Spine*. 2005;30:2200–2207.
7. Stirling DP, Khodarahmi K, Liu J, et al. Minocycline treatment reduces delayed oligodendrocyte death, attenuates axonal dieback, and improves functional outcome after spinal cord injury. *J Neurosci*. 2004;24:2182–2190.
8. Brines M, Cerami A. Emerging biological roles for erythropoietin in the nervous system. *Nat Rev Neurosci*. 2005;6:484–494.
9. Young W. Methylprednisolone and spinal cord injury. *J Neurosurg*. 2002;96(1 suppl):141–142.
10. Vitellaro-Zuccarello L, Mazzetti S, Madaschi L, et al. Erythropoietin-mediated preservation of the white matter in rat spinal cord injury. *Neuroscience*. 2007;144:865–877.
11. Ohori Y, Yamamoto S, Nagao M, et al. Growth factor treatment and genetic manipulation stimulate neurogenesis and oligodendrogenesis by endogenous neural progenitors in the injured adult spinal cord. *J Neurosci*. 2006;26:11948–11960.

12. Hagg T, Oudega M. Degenerative and spontaneous regenerative processes after spinal cord injury. *J Neurotrauma*. 2006;23:264–280.
13. Mandemakers WJ, Barres BA. Axon regeneration: it's getting crowded at the gates of TROY. *Curr Biol*. 2005;15:R302–R305.
14. Ha Y, Park HS, Park CW, et al. Granulocyte macrophage colony stimulating factor (GM-CSF) prevents apoptosis and improves functional outcome in experimental spinal cord contusion injury. *Clin Neurosurg*. 2005;52:341–347.
15. Liang P, Jin LH, Liang T, et al. Human neural stem cells promote corticospinal axons regeneration and synapse reformation in injured spinal cord of rats. *Chin Med J*. 2006;119:1331–1338.
16. Garbossa D, Fontanella M, Fronda C, et al. New strategies for repairing the injured spinal cord: the role of stem cells. *Neurol Res*. 2006;28:500–504.
17. Urdzikova L, Jendelova P, Glogarova K, et al. Transplantation of bone marrow stem cells as well as mobilization by granulocyte-colony stimulating factor promotes recovery after spinal cord injury in rats. *J Neurotrauma*. 2006;23:1379–1391.
18. Knoller N, Auerbach G, Fulga V, et al. Clinical experience using incubated autologous macrophages as a treatment for complete spinal cord injury: phase I study results. *J Neurosurg Spine*. 2005;3:173–181.
19. Boyd JG, Doucette R, Kawaja MD. Defining the role of olfactory ensheathing cells in facilitating axon remyelination following damage to the spinal cord. *FASEB J*. 2005;19:694–703.
20. Feron F, Perry C, Cochrane J, et al. Autologous olfactory ensheathing cell transplantation in human spinal cord injury. *Brain*. 2005;128(pt 12):2951–2960.
21. Barnett SC, Riddell JS. Olfactory ensheathing cells (OECs) and the treatment of CNS injury: advantages and possible caveats. *J Anat*. 2004;204:57–67.
22. Collazos-Castro JE, Muneton-Gomez VC, Nieto-Sampedro M. Olfactory glia transplantation into cervical spinal cord contusion injuries. *J Neurosurg Spine*. 2005;3:308–317.
23. Barnett SC, Riddell JS. Olfactory ensheathing cell transplantation as a strategy for spinal cord repair—what can it achieve? *Nat Clin Pract Neurol*. 2007;3:152–161.
24. Hofstetter CP, Schwarz EJ, Hess D, et al. Marrow stromal cells form guiding strands in the injured spinal cord and promote recovery. *Proc Natl Acad Sci U S A*. 2002;99:2199–2204.
25. Yoon SH, Shim YS, Park YH, et al. Complete spinal cord injury treatment using autologous bone marrow cell transplantation and bone marrow stimulation with granulocyte macrophage-colony stimulating factor (GM-CSF): phase I/II clinical trial. *Stem Cells*. 2007;25:2066–2073.
26. Nandoe RD, Hurtado A, Levi AD, et al. Bone marrow stromal cells for repair of the spinal cord: towards clinical application. *Cell Transplant*. 2006;15:563–577.
27. Mezey E, Chandross KJ. Bone marrow: a possible alternative source of cells in the adult nervous system. *Eur J Pharmacol*. 2000;405:297–302.
28. Prockop DJ. Marrow stromal cells as stem cells for nonhematopoietic tissues. *Science*. 1997;276:71–74.
29. Phinney DG, Kopen G, Righter W, et al. Donor variation in the growth properties and osteogenic potential of human marrow stromal cells. *J Cell Biochem*. 1999;75:424–436.
30. Ferrari G, Cusella-De Angelis G, Coletta M, et al. Muscle regeneration by bone marrow-derived myogenic progenitors. *Science*. 1998;279:1528–1530.
31. Orlic D. BM stem cells and cardiac repair: where do we stand in 2004? *Cytotherapy*. 2005;7:3–15.
32. Petersen BE, Bowen WC, Patrene KD, et al. Bone marrow as a potential source of hepatic oval cells. *Science*. 1999;284:1168–1170.
33. Krause DS, Theise ND, Collector MI, et al. Multi-organ, multi-lineage engraftment by a single bone marrow-derived stem cell. *Cell*. 2001;105:369–377.
34. Dezawa M, Takahashi I, Esaki M, et al. Sciatic nerve regeneration in rats induced by transplantation of in vitro differentiated bone-marrow stromal cells. *Eur J Neurosci*. 2001;14:1771–1776.
35. Wu S, Suzuki Y, Kitada M, et al. Migration, integration, and differentiation of hippocampus-derived neurosphere cells after transplantation into injured rat spinal cord. *Neurosci Lett*. 2001;312:173–176.
36. Wu S, Suzuki Y, Ejiri Y, et al. Bone marrow stromal cells enhance differentiation of cocultured neurosphere cells and promote regeneration of injured spinal cord. *J Neurosci Res*. 2003;72:343–351.
37. Wu S, Suzuki Y, Kitada M, et al. New method for transplantation of neurosphere cells into injured spinal cord through cerebrospinal fluid in rat. *Neurosci Lett*. 2002;318:81–84.
38. Wu S, Suzuki Y, Noda T, et al. Immunohistochemical and electron microscopic study of invasion and differentiation in spinal cord lesion of neural stem cells grafted through cerebrospinal fluid in rat. *J Neurosci Res*. 2002;69:940–945.
39. Basso DM, Beattie MS, Bresnahan JC. A sensitive and reliable locomotor rating scale for open field testing in rats. *J Neurotrauma*. 1995;12:1–21.

特集

脊髄損傷再生医学の最前線

脊髄損傷再生の研究動向—各施設から

脊髄損傷再生臨床試験について

関西医科大学高度救命救急センターから

中谷 壽男

脊椎脊髄ジャーナル

VOL. 20 NO. 12 別刷

2007年12月25日発行

三輪書店

脊髄損傷再生臨床試験について*

関西医科大学高度救命救急センターから

中谷 壽男**

はじめに

本号に脊髄損傷に対する再生医療の現状に関する特集が組まれた。進行中の脊髄損傷に対する臨床試験について、支障のない範囲での執筆依頼である。われわれの施設では、臨床試験「急性期脊髄損傷に対する培養自家骨髄間質細胞移植による脊髄再生治療の検討」が始まっている。臨床試験においては、その進行中に試験計画の詳細や、試験経過について公表することは差し控えるとするのが一般的である。しかしながら、本臨床試験については、患者団体などから注目されていること、概略を開示することにより症例の集積を図りたいこと、また臨床試験のデータ管理が外部にてなされ、外部委員による症例検討や効果・安全性評価委員会にて議論をいただきながら進行していることを明らかにするために、計画の概要について紹介したい。

損傷された中枢神経は再生することはない。これが従来の医学的常識であった。そのため、脊髄の二次損傷の防止と理学療法が治療の中心となっ

Key words

骨髄間質細胞 (bone marrow stromal cell)
髄内投与 (intrathecal administration)
脊髄損傷 (spinal cord injury)

ている。脊髄損傷が、再生医療によって完治とまでは望めなくとも、わずかでも機能が回復するならば、患者家族にとっての肉体的、精神的また経済的な負担の軽減ははかりしれない。

再生医療において幹細胞を使った治療が脚光を浴びている。しかし幹細胞を用いた研究には、倫理的問題など解決しなければならない点が残されている。骨髄間質細胞による細胞治療のメリットは、自らの細胞であるため拒絶反応、倫理的問題が生じないこと、容易に採取でき、培養技術が確立されていることなどである。今回の臨床試験は、骨髄間質細胞を神経細胞に分化させることを意図したものではなく、骨髄間質細胞の作用により、中枢神経系に残存している神経幹細胞の再生を促そうとするものであり、臨床再生医学に用いる細胞としては現実的なものと考えている。

臨床試験への準備

① 骨髄間質細胞とは

骨髄には大きく分けて2種類の細胞がある。血液細胞は血球に分化し、間質細胞は網状の構造をなして造血細胞を支持している。骨髄間質細胞は、種々の細胞に分化する能力を有しており、神経細胞や神経軸索を取り巻くシュワン細胞にも分化しうることから、神経の再生を刺激したり、細胞治

* Clinical Trial of Regeneration Treatment for Spinal Cord Injury at Kansai Medical University Emergency and Critical Care Center

** 関西医科大学救急医学科 (〒570-8507 守口市文園町10-15) / Toshio NAKATANI: Department of Emergency and Critical Care, Kansai Medical University

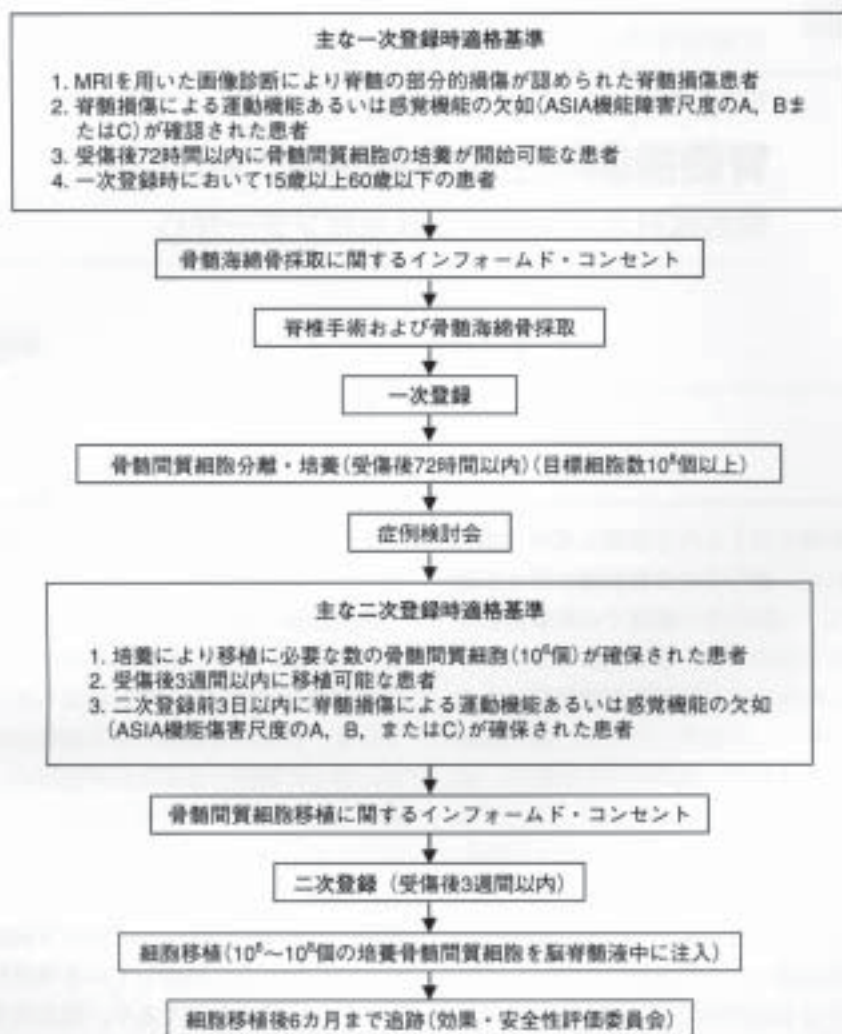


図1 臨床試験の流れ

療・臓器再生の細胞供給源として役立つと考えられている。

② 基礎となった実験の概要

鈴木、井出らは骨髄細胞が脊髄再生に有力と注目し、*in vitro*における種々の基礎実験を重ね⁹⁾、さらにラットの露出脊髄に一定の損傷を加え、直ちに損傷部に骨髄間質細胞を注入し、運動神経機能への回復と組織学的検討にて効果を確認した⁹⁾。

③ 脳脊髄液内投与

外国での臨床応用における細胞移植には、損傷

部位の脊椎の椎弓切除を行って脊髄実質内に直接に細胞を注入する方法がとられる⁹⁾。しかし、臨床例での直接注入は問題が多いため、髄液中へ間質細胞を注入することを検討し、次にはラット第4脳室内に注入して同様の効果を確認した¹⁰⁾。

④ 腰椎穿刺手技による移植

本臨床試験では、腰椎穿刺の手技を使って脳脊髄液中に細胞を投与する。そのため、諸外国の臨床試験と比較しても、患者への侵襲と危険性の少ない方法であると考えている。

表 1 一次登録適格基準

- 1) 脊髄損傷が MRI 画像により確認されている
- 2) ASIA スコアが A, B, C のいずれか
- 3) ISCSCI による運動機能の評価が可能であること
- 4) NASCIS II によるメチルプレドニゾン療法が受傷 8 時間以内に開始できる
- 5) 骨髄間質細胞の培養が受傷後 72 時間以内に開始できる
- 6) 年齢は 15~60 歳
- 7) 骨髄採取のための同意が書面で得られること

ASIA : American Spinal Injury Association

ISCSCI : international standard classification of spinal cord injury

NASCIS : national acute spinal cord injury study

表 2 除外基準

- 1) 脊髄の完全断裂
- 2) 中心性脊髄損傷
- 3) 受傷前に脊柱管狭窄症のあるもの
- 4) 受傷前に脳や脊髄疾患のあったもの
- 5) SOFA スコアが 12 点以上の多臓器障害
- 6) 脊髄損傷の他に、AIS 4 以上の損傷を体の 2 部位以上に受けた多発外傷患者
- 7) 血清の HBs 抗原, HCV 抗体, HIV 抗体, HTLV-1 抗体のいずれかが陽性のもの
- 8) 妊婦

SOFA : sepsis-related organ failure assessment, AIS : abbreviated injury score

HBs : hepatitis B surface antigen, HCV : hepatitis C virus

HIV : human immunodeficiency virus, HTLV : human T-cell leukemia virus

表 3 二次登録のための適格基準

- 1) 培養にて 10⁴以上の骨髄間質細胞が得られたもの
- 2) 受傷後 3 週間以内に移植が実施できる
- 3) 移植前 3 日以内に ASIA スコアが A, B, C であることが確認できたもの
- 4) 細胞移植のための第 2 回目の同意が文書で得られたもの

5 臨床応用へ向けての手続き

関西医科大学医学倫理委員会、および(財)先端医療センター臨床研究部の倫理委員会にて「急性期脊髄損傷に対する培養自家骨髄間質細胞移植による脊髄再生治療(第 I~II 相臨床試験)」の実施が承認され、患者説明会なども経て、京都大学での研究を基礎に先端医療センター、関西医科大学高度救命救急センターなどの協同で臨床試験が開始された。

臨床試験の実際

1 適用条件、除外条件と患者説明

図 1 に全体的な臨床試験の流れの概略を示し

た。

急性期脊髄損傷患者のうち、患者の一次登録に当たって表 1 に示した適格基準を満たし、かつ表 2 に示した除外基準に当てはまらないことを主たる対象とし、外部のデータセンターに患者の識別番号を登録する。患者の ID に関しては主治医のみが管理し、ほかはすべて識別番号で管理される。患者の感染症などの検査を行い、以後はデータセンターがデータ収集や適応条件などについて管理する。

初回のインフォームド・コンセントは、患者および患者家族の脊髄損傷に関する情報不足の中、また、精神的な動揺が大きい中で取得しなければ

ならないために、脊椎固定手術および補強のための腸骨採取に伴って骨髄海綿骨を採取することの同意を得るにとどめる。初回のインフォームド・コンセントにおいても、脊椎損傷の予後や臨床試験についての詳細な説明は行うものの、これらに関する同意を得ることをあえて控える。書面によるコンセントを得た場合に、患者の一次登録を行う。

細胞培養には、2週間程度を要するため、この間に、患者・家族はさまざまな方法を駆使して脊椎損傷の予後などに関する情報収集に当たることができ、またこれを促す。

細胞が順調に増殖し、表 3 の条件を満たす場合に、第 2 回目のインフォームド・コンセント、すなわち本臨床試験に参加することについて同意を得る。この頃には、家族も精神的に安定し、情報を収集し、患者本人にも病状を告知し、患者本人の意思を反映して同意を得ることが可能となる。書面にて第 2 回目の同意を得た場合に、患者の二次登録を行い、この時点での適応条件を満たしているかの再確認を行う。さらに、細胞培養液についてもエンドトキシンやウイルス抗体検査などを行ってクリアした場合に移植に供する。

なお、試験計画書、概要書などは 100 頁を遙かに超え、患者説明書だけでも A 4 判 20 頁に及び、数時間をかけてインフォームド・コンセントを得るための説明を行っている。

② 外部委員による管理・評価

対象にした培養自家骨髄間質細胞移植による脊椎再生治療の臨床効果および安全性は、本臨床研究チームに所属しない学内・学外の専門家から構成される効果・安全性評価委員会において経時的に評価される。主たるエンドポイントは ISCSCI-92 (international standards for neurological and functional classification of spinal cord injury 1992 version) の運動機能および知覚機能スコアの受傷直後から受傷後 6 カ月までの変化量であるが、当初は特に安全性を重視した追跡評価を行う。

③ 症例提示

症例については、先に述べた理由や二重投稿の

観点から、ここで詳細を報告したり、画像を供覧することはできないが、以下に概略のみを提示することで、ご容赦をいただきたい。

患者：35 歳、男性

臨床経過：高所より墜落し四肢麻痺を認めたため、当救命センターに搬送された。初診時、バイタルサインは安定しており徐脈を認めず、神経学的所見として徒手筋力テストでは、脊椎固定術から約 10 日を経過した細胞移植直前の運動機能では、三角筋・上腕二頭筋は 3/5 に低下、以下は 0/5 であった。すなわち、辛うじて肘関節の屈曲は可能であるものの、伸展や手関節の運動は不可能であった。知覚は第 5 頸髄領域から鈍麻、第 7 頸髄領域以下の完全脱失、ASIA (American Spinal Injury Association) 機能障害尺度は A であった。単純 X 線、CT にて第 4・5 頸椎に脱臼および骨折を認め、MRI では T2 強調画像で第 4~6 頸椎レベルに高信号と低信号の混在を認めた。第 3 病日に、第 4~6 頸椎前方除圧固定・自家骨移植術を施行し、細胞が順調に増殖したため、第 12 病日に髄液中に骨髄間質細胞移植を施行した。

移植後 6 カ月までの ASIA 機能障害評価法では、受傷 2 週目の移植時と比べて、感覚機能で 32 点、運動機能で 9 点の回復を示した。12 カ月を経過した現時点では、小さなものを握り所定の位置に収める作業や、三角筋の助けによるところが大きいものの、車いすを自分で押すことも可能であり、長時間の座位の保持が可能になっている。

移植前の症例検討会、移植後 1, 3, 6 カ月に外部委員からなる効果・安全性評価委員会を開催して、効果と安全性について評価をいただいている。現時点では、まだ初めての症例であり、機能は確実に回復しているものの、これが本臨床試験の効果によるものか否かについては言及するだけのデータや根拠がないため、われわれも委員会も、効果に関しては言及していない。しかしながら、安全性に関しては、細胞の髄内投与から 12 カ月以上が経過した現時点において、移植直後の髄膜炎や、長期経過後の異常増殖や石灰化などの不都合な問題はまったく発生していない。

おわりに

脊髄損傷が治癒するならば、これは夢のような話である。根治は望めなくとも、たとえ機能の一部だけでも回復すれば、神経学的な機能予後はおおいに改善し、生活の質は向上して、本人、家族の肉体的、精神的、経済的負担は軽減され、ひいては医療資源の節約、国民の保険負担の軽減など大きな社会的貢献が期待される場所である。その成否については現時点では不明であるが、臨床試験が、いま、ようやく始まったところである。

文献 (太字番号は重要文献)

- 1) Bai H, Suzuki Y, Noda T, et al : Dissemination and proliferation of neural stem cells on the spinal cord by injection into the fourth ventricle of the rat : A method for cell transplantation. *J Neurosci Methods* **124** : 181-187, 2003
- 2) Huang H, Chen L, Wang H, et al : Influence of patients'age on functional recovery after transplantation of olfactory ensheathing cells into injured spinal cord injury. *Chin Med J* **116** : 1488-1491, 2003
- 3) Ohta M, Suzuki Y, Noda T, et al : Bone marrow stromal cells infused into the cerebrospinal fluid promote functional recovery of the injured rat spinal cord with reduced cavity formation. *Exp Neurol* **187** : 266-278, 2004
- 4) Wu S, Suzuki Y, Ejiri Y, et al : Bone marrow stromal cells enhance differentiation of cocultured neurosphere cells and promote regeneration of injured spinal cord. *J Neurosci Res* **72** : 343-351, 2003
- 5) Wu S, Suzuki Y, Kitada M, et al : Migration, integration, and differentiation of hippocampus-derived neurosphere cells after transplantation into injured rat spinal cord. *Neurosci Lett* **312** : 173-176, 2001
- 6) Wu S, Suzuki Y, Kitada M, et al : New method for transplantation of neurosphere cells into injured spinal cord through cerebrospinal fluid in rat. *Neurosci Lett* **318** : 81-84, 2002



Mrs. Saito
三輪書店



三輪書店のホームページをご覧ください !!

<http://www.miwapubl.com>

- ◆ 会社案内
- ◆ 新刊案内
- ◆ 新刊雑誌のご案内
- ◆ 書籍のご案内
- ◆ ニューメディアのご案内
- ◆ 取扱い店一覧
- ◆ 購入のお申し込み
- ◆ OT募集広告

当社出版物の最新情報をご覧になれば、ネット上からご注文も可能です。



三輪書店

〒113-0033 東京都文京区本郷6-17-9 本郷編ビル4F
TEL:03-3816-7796 FAX:03-3816-8762



脊髄損傷の再生医療

Regenerative treatment for spinal cord injury

中谷 壽男*

Toshio Nabatani

◆key words : 骨髄間質細胞, 脊髄再生, 細胞移植, 脊髄損傷, 再生医療

はじめに

損傷された中枢神経は再生することはない、ということが従来の医学的常識であった。そのため脊髄損傷に対する治療方針は、脊椎骨折や脱臼に対する固定と、脊髄の二次損傷防止、そして理学療法が中心となってきた。患者は生涯を車椅子生活、ベッド上生活、あるいは人工呼吸器の補助を強いられる。脊髄損傷が、再生医療によって完治とまでは望めなくとも、わずかでも機能が回復するなら、患者や家族にとっての肉体的、精神的、経済的負担の軽減ははかりしれない。

世界中で多くの研究者が神経再生に取り組んでおり、再生医療において幹細胞を使った治療が脚光を浴びている。しかし幹細胞を用いた研究には、倫理的問題などの解決しなければならない点が残されている。京都大学の鈴木、井出らは、自己骨髄間質細胞を脳脊髄液中に投与することにより脊髄損傷ラットの機能を回復させる実験に成功し、筆者とともにその臨床応用を目指してきた。本稿では脊髄再生医療の概況と、関西医科大学における急性期脊髄損傷に対する培養自家骨髄間質細胞移植による脊髄再生臨床試験の概略を紹介したい。

脊髄再生の基礎的研究

1. 中枢神経系と末梢神経の差異

古くより、損傷された中枢神経系細胞は再生することがないが、末梢神経は再生することが知られてきた。中枢神経系と末梢神経では、軸索を囲むグリア細胞の種類と作用が大きく異なることが知られて

いる。

中枢神経系では、ニューロンを取り囲んで以下のグリア細胞が存在するが、これらが神経再生に抑制的に働くと考えられている。oligodendrocyteは髄鞘形成にかかわりミエリンを形成するが、損傷後はoligodendrocyteのapoptosisによるミエリンの脱失が続く。また、oligodendrocyte由来のミエリンに含まれる糖蛋白質には軸索の伸張を阻害する因子が含まれている。astrocyteは中枢神経系の栄養に関与して、oligodendrocyteによる再ミエリン化に必須のミエリン誘導物質を産生する。一方で損傷時には変性した神経組織に代わってastrocyteが肥大増殖し瘢痕を形成するだけでなく、軸索成長阻害作用のあるプロテオグリカンを生産して神経再生に抑制的に働くことが知られている。microgliaは免疫・マクロファージとして作用すると考えられている¹⁾。

一方、末梢神経系において、有髄線維ではミエリンが軸索を取り巻き、その外側をSchwann細胞が取り巻いている。無髄線維では軸索をSchwann細胞のみが取り巻いている。Schwann細胞はミエリンを形成し、このミエリンが神経再生を促進すると考えられてきた。末梢神経が損傷されると、それより遠位では軸索変性(ワラー変性)が起きる。Schwann細胞は軸索変性を受けて、髄鞘を形成する分化状態から未分化な状態に変化し、さまざまなサイトカインや促進因子を産生することによって、再生に適切な環境を作り出す。それらの促進因子は、ニューロトロフィン、毛様体神経栄養因子、線維芽細胞増殖因子などの栄養因子として同定され、損傷した神経線維の再生に作用し、ミエリンの再形成を図るなどの役目があるものと考えられている¹⁾。

脊髄損傷に対しては、血流改善、炎症抑制、再生阻害因子の阻止などの、種々の観点からの薬物療法

* 関西医科大学救急医学教授

表1 細胞治療に利用できる細胞

ES細胞 (胎児性幹細胞)
長所: 全能性を有し, すべての細胞を供与可能
短所: 量確保? 腫瘍化?
胎児組織からの同業系細胞
長所: 寿命長く, 十分な細胞数
短所: 倫理面
成人組織細胞
長所: 形成能および分化はもっとも優れている
短所: 寿命が短く増殖しない
骨髄間質細胞
長所: 採取容易, 培養技術確立, 拒絶反応ない自家移植
短所: 細胞数を増やすこと

(中谷壽男, 他: 骨髄損傷の再生医療, 臨床スポーツ医学 23: 1081-1085, 2006より引用)

が試みられているが, それらに関しては本特集の別項で述べられるので, 本稿においては以下に細胞治療のみを述べる。

2. 細胞を用いた再生医療

上記より, Schwann細胞は中枢神経系の再生も誘導できるのではないかと考えられている。中枢神経は再生しにくいと考えられてきたが, 神経細胞そのものは潜在的に再生能力を持っていることが知られており, 神経再生に阻害的な oligodendrocyte が主体をなす中枢神経系のグリアの環境を, 末梢神経の環境である Schwann細胞に置き換えることによって, 中枢神経系の再生を引き出すことが可能であると考えられる。すなわち, Schwann細胞は末梢神経だけでなく, 中枢神経の再生も誘導できると考えられている¹⁾。

近年, 中枢神経系の再生を支持する細胞としての Schwann細胞をはじめとして, 脳室の内面を覆う上皮細胞, 嗅神経鞘細胞, あるいは神経系の幹細胞などが, 神経線維の再生を引き出す機能があるとして注目され, 細胞を用いた再生医療の試みが急速に進展をみせている²⁾³⁾。それらの細胞と, それぞれの長所, 短所を表1に示した。

3. 骨髄間質細胞を用いた神経再生

骨髄間質細胞は, 多分化能を有することが知られてきた。たとえば, 骨髄中に存在する同業系骨芽細胞は, 脱メチル化薬を投与するなどの限定的な状況下にて *in vitro* で神経系細胞に転換することが知られてきた。このように従来の胚葉という既成概念を越えて組織が形成される可能性がわかってきた。胚

葉を越えて組織が分化するなら, 骨髄間質細胞が外胚葉由来である神経に分化する可能性もあると考えられ, これに注目がなされてきた。そこで入手が容易な骨髄間質細胞を採取し, これを継代培養し, そこへ β -メルカプトエタノール, 線維芽細胞増殖因子, その他の物質を添加することによって Schwann細胞と同形質の細胞を誘導する試みもなされてきた⁴⁾。

4. 骨髄間質細胞とは

骨髄間質細胞は, 網状の構造をなして造血細胞を支持している。一方, 骨細胞, 心筋細胞, 軟骨細胞, 腱細胞などへの分化能を有している骨髄間質細胞を, 細胞治療ならびに臓器再生の細胞供給源とすることができると考えられている。骨髄間質細胞による細胞治療のメリットは, 容易に採取でき, 培養技術が確立されていること, 自らの細胞であるため拒絶反応, 倫理的な問題が生じないことである。今回の臨床試験は, 骨髄間質細胞を神経細胞に分化させることを意図したのではなく, 骨髄間質細胞の作用により, 中枢神経系に残存している神経幹細胞の再生を促そうとするものであり, 臨床再生医学に用いる細胞としては現実的なものと考えている。

細胞による再生医療

1. 諸外国における試み

脊髄損傷治療として, 諸外国においては表2に挙げた細胞を用いた臨床試験が行われている。脳由来の神経幹細胞を用いた治療法では, 動物実験では移植細胞が神経系の細胞に分化したという報告があ

表2 諸外国における状況との比較

細胞の種類	脳由来神経幹細胞 (中絶胎児)	マクロファージ (自己)	嗅球鞘細胞 (OEG) (中絶胎児または自己)	骨髄間質細胞 (自己)	
開発 状況	動物実験中	イスラエルおよび米国で 臨床試験実施中	ポルトガル, オーストラ リア, 中国およびロシア で臨床試験実施中	臨床試験実施中	
特 徴	自家 移植	不可能。免疫抑制薬必要	可能	可能	可能
	細胞 採取	中絶胎児	末梢血	鼻粘膜および嗅球	骨髄
	細胞 培養	必要。ただし, 1 症例に つき複数の胎児が必要	マクロファージの活性化 が必要	必要	必要
	移植 手術	必要	必要	必要	不要
	体内 動態	長期残存	早期消失	長期残存	早期消失

(中谷壽男, 他: 脊髄損傷の再生医療, 臨床スポーツ医学 23: 1081-1085, 2006より引用)

る。しかし、臨床的な利用を考えると、本人からの中枢神経由来の幹細胞の採取は現実的には難しい。また、中絶ヒト胎児由来の幹細胞や胚性幹細胞 (ES cell) を利用する場合には倫理的な問題がある。他人の細胞である以上は拒絶反応の問題は避けられず、免疫抑制薬が必要となれば二次的な副作用も生じ得る。現在、患者自身のマクロファージを培養し、活性化してから骨髄損傷部へ直接移植する方法⁴⁾や、鼻粘膜より採取した嗅球の神経細胞を取り巻くグリア細胞、すなわち嗅神経鞘細胞 (olfactory ensheathing glia: OEG) を骨髄損傷部へ直接移植する方法⁵⁾が、実際にヒトへの臨床応用として行われている (表2)。

鼻の上皮細胞は感染によって破壊されるために、一生の間再生し続ける。すなわち、嗅神経は成体動物で継続的に再生する唯一の脳神経である。そこで、このように継続的に再生する嗅神経の軸索をミエリン鞘で包んでいる OEG を用いれば、神経再生が期待できるとの発想が浮かびあがる。すなわち、OEG は軸索再生に特化した遊走細胞であり、脳、脊髄に移植することによって機能的な神経再生を促進できるとの期待がもたれ、動物実験では脊髄は部分的に機能回復を示した。

OEG については中国ですでに多数の臨床試験が行われている。この治療法はまだ実験段階であり、有効性および安全性が検証されたものではなく、また胎児組織を用いるなど未解決の問題も多い⁶⁾。現在、移植のための OEG のソースとして成体嗅球 (自

家移植)、成体嗅粘膜 (自家移植)、胎児嗅球 (同種移植)、ヒト死体嗅球 (同種移植)、ブタ胎児嗅球 (異種移植) などが考えられているが、いずれも侵襲、免疫、倫理的な問題を抱えている。国内でも、嗅粘膜を用いた再生医療の準備が大阪大学において進行中である。

2. 骨髄間質細胞移植による臨床試験

京都大学で種々の基礎研究や動物実験を重ねたのち⁷⁻⁹⁾、臨床応用へ向けてのプロトコル作成や、患者団体への説明会などを経て、関西医科大学医学倫理委員会にて「急性期脊髄損傷に対する培養自家骨髄間質細胞移植による脊髄再生治療 (第 I ~ II 相臨床試験)」の実施が承認され、財団法人先端医療センター、臨床研究情報センター、関西医科大学高度救命救急センターの協同で臨床試験を行うことが承認された。本臨床試験については、現在進行中であり、そのプロトコルや臨床試験の経過の詳細を記載することは臨床試験実施のルールに反することになるために、ここでは概要を述べるに留めることをご容赦いただきたい。

本臨床試験の特徴は、脊髄損傷患者に対して脊椎固定手術を行うに際し、脊柱の補強のために腸骨稜を採取するが、その際に腸骨からわずかの海綿骨を追加採取し、これを培養施設において培養し増殖させる。すなわち、細胞を得るための追加処置は不要である。脊椎固定手術を要する ASIA (American Spinal Injury Association) 分類 A, B, C のみを

表3 第1回登録時の適格条件

1) 脊髄損傷が画像 (MRI) で確定診断されている
2) ASIA impairment scale の A, B, C であること
3) メチルプレドニゾロン療法が受傷 8 時間以内に開始されていること
4) 脊髄細胞の培養を受傷 72 時間以内に開始できること
5) 年齢 15~60 歳
6) 第 1 回インフォームド・コンセントが得られていること
7) その他、合併損傷、SOFA、運動・知覚評価可能、非妊娠、など

対象とし、かつ細胞投与のために再度の損傷部位の剥離手術を行わず、患者の脳脊髄液中に腰椎穿刺の手技を使って細胞を移植するため、臨床試験のための余計な侵襲を患者に加えないことを特徴としている。そのため、適用となる患者の状況には種々の制約がある。

脊髄の損傷部位を再度剥離しないために、脊髄の二次損傷を避け得る反面、脊髄損傷部にグリア細胞による瘢痕が形成されるまでに細胞を髄注しなければ、移植した細胞が脊髄損傷面に到達できない。そのため海綿骨採取と細胞培養を急ぐ必要があり、プロトコルにおいて、受傷後 72 時間以内に細胞培養を開始できる症例に限定している。この点は、症例を蓄積するに於ける最大のネックとなっている。一般に、患者やその家族はもちろんのこと、担当する医師にとっても日常的に遭遇する損傷ではないために、本臨床試験が実施できることを認識され、問い合わせをいただくのは、受傷後の時間制限をはるかに超えた後になるケースがほとんどである。表 3 に本臨床試験への第 1 回登録時適格条件を示したので、対象症例が発生した場合には、参考にしていただければ幸いであり、ご紹介いただけるとありがたい。ただし、このほかにも移植直前の第 2 回症例登録時の適格条件や除外条件 (省略) などの制約を満たした場合に臨床試験の対象となる。

3. 症例報告

上記の理由により、詳細を開示することができないので、概要を紹介することでご容赦いただきたい。

症例は、30 歳代男性で、7~8 m の高所より落下し、C5 以下の運動・知覚麻痺を主訴に搬入された。バイタルサインと意識レベルには異常なし。神経学的所見では運動機能は C5 は MMT (徒手筋力テスト) 3、C6 以下は MMT 0、知覚は C7 以下で脱失し、ASIA 分類で A であった。第 3 病日に前方固定術を実施し、海綿骨を採取して間質細胞の培養を開始。第 13 病日に 3.1×10^7 個の脊髄間質細胞

を腰椎穿刺にて髄液中へ投与した。髄注に伴う有害作用はいっさいなく、1 年以上を経過した現時点においても移植による合併症はまったく観察されていない。ASIA の Standard Neurological Classification Score では、運動機能は移植前と比較して 9 点 (満点は 100 点。受傷直後からは 11 点)、知覚機能では 32 点 (満点は 224 点。同じく 37 点) の回復を示している。具体的な運動状況は、移植直後に肘関節の屈曲が重力に抗してかろうじてできるのみで、手関節の運動や肘関節の伸展、手指の運動はまったくみられなかったが、現在では、動き得る筋肉を駆使すると、物をつかみ所定の場所に収納する動作や、車椅子にて坐位を保ち自力で病棟の廊下内を目的の場所まで移動することができるようになっている。

本症例は、自己培養脊髄間質細胞を腰椎穿刺にて髄液中に投与して脊髄再生を試みた世界最初の症例である。ASIA score でみた神経機能は、明らかな改善を示している。細胞移植に伴う副作用、合併症はみられていない。しかしながら、まだわずか 1 例を実施したにすぎず、効果と安全性については、一連の症例に実施した後に、外部委員による効果・安全性評価委員会で評価されることになっている。

おわりに

脊髄損傷が治癒するならば、これは夢のような話である。根治は望めなくとも、たとえ機能の一部だけでも回復すれば、神経学的な機能予後は大いに改善し、生活の質は向上して、本人、家族の肉体的、精神的、経済的負担は軽減され、ひいては医療資源の節約、国民の保険負担の軽減など大きな社会的貢献が期待される。いまだ臨床試験が始まったばかりであり、その成否については現時点では不明であるが、症例を重ねる必要があり、適格条件を満たす症例の紹介を受傷後ただちにいただければ幸いである。

【文 献】

- 1) 出澤真理：骨髄間質細胞を用いた神経再生への試み。実験医学 20：1312-1317, 2002.
- 2) Huang H, Chen L, Wang H, et al：Influence of patients' age on functional recovery after transplantation of olfactory ensheathing cells into injured spinal cord injury. Chin Med J 116：1488-1491, 2003.
- 3) Li Y, Field PM, Raisman G：Repair of adult rat corticospinal tract by transplants of olfactory ensheathing cells. Science 277：2000-2002, 1997.
- 4) Rapalino O, Lazarov-Spiegler O, Agranov E, et al：Implantation of stimulated homologous macrophages results in partial recovery of paraplegic rats. Nat Med 4：814-821, 1998.
- 5) Wu S, Suzuki Y, Kitada M, et al：Migration, integration, and differentiation of hippocampus-derived neurosphere cells after transplantation into injured rat spinal cord. Neurosci Lett 312：173-176, 2001.
- 6) Wu S, Suzuki Y, Kitada M, et al：New method for transplantation of neurosphere cells into injured spinal cord through cerebrospinal fluid in rat. Neurosci Lett 318：81-84, 2002.
- 7) Bai H, Suzuki Y, Noda T, et al：Dissemination and proliferation of neural stem cells on the spinal cord by injection into the fourth ventricle of the rat：A method for cell transplantation. J Neurosci Methods 124：181-187, 2003.
- 8) Ohta M, Suzuki Y, Noda T, et al：Bone marrow stromal cells infused into the cerebrospinal fluid promote functional recovery of the injured rat spinal cord with reduced cavity formation. Exp Neurol 187：266-278, 2004.
- 9) Wu S, Suzuki Y, Ejiri Y, et al：Bone marrow stromal cells enhance differentiation of cocultured neurosphere cells and promote regeneration of injured spinal cord. J Neurosci Res 72：343-351, 2003.

月刊「消化器外科」で大反響を呼んだ連載が、
読みやすい完全新訳版として今、蘇る！

すべての読者を感動させる医学ドキュメンタリー

外科医の世紀

近代医学のあけぼの

著：Jürgen Thorwald 訳：小川 道雄（熊本労災病院）

●定価3,780円（税込）送料420円 ●A5判・540ページ
ISBN978-4-89269-567-4

へるす出版 〒164-0001 東京都中野区中野2-2-3 TEL.03-3384-8035 FAX.03-3380-8645 <http://www.herusu-shuppan.co.jp>

急性脊髄損傷に対する再生医療

—臨床応用への取り組みの現状と課題—

Present Status and Problems for the Clinical Application of Regenerative Medicine for Acute Spinal Cord Injury

中谷 壽 男*

Toshio NAKATANI, MD

1. 脊髄損傷は毎年 5,000 人が受傷し、回復しない下半身麻痺、四肢麻痺に加えて直腸膀胱障害、褥瘡、自律神経障害などを生じ、本人は勿論、家族にとっても困難な状況をもたらしている。
2. 脊髄損傷に対する再生医療の試みが多くの研究者によってなされており、急性期脊髄損傷に対する培養自家骨髄間質細胞移植による脊髄再生治療（第Ⅰ～Ⅱ層臨床試験）の臨床試験が開始されようとしている。
3. 理学療法では、残された運動・知覚機能を最大限に引き出すべく、早期より開始し、障害の程度に応じた目標を定めて行うリハビリテーションが重要である。

はじめに

「損傷された中枢神経は再生することはない」—これが従来の医学的常識であった。そのため、脊髄損傷に対する治療は、残存している機能をいかに引き出すかという点に主眼が置かれ、脊椎の骨折や脱臼に対する固定と、脊髄の二次損傷の防止、そして理学療法が中心に行われていた。損傷部位より尾側の運動、知覚、自律の各神経が障害されるため、車椅子生活を生涯強いられ、損傷部位によってはベッド上での生活となったり、さらには人工呼吸器を手放すことができない症例も珍しくない。

そのような脊髄損傷が、再生医療により、完治までは望めなくとも、わずかでもその機能が回復するなら、患者・家族にとって、肉体的、精神的また経済的な負担の軽減は計り知れない。世界中で多くの研究者が神経再生に取り組んでおり、有効な治療方法が開発される日も遠くないと期待さ

れている。

最近、再生医療において幹細胞を使った治療が脚光を浴びている。しかし幹細胞を用いた研究には、倫理的問題など、解決しなければならない点が残されている。京都大学の鈴木、井出らは、自己の骨髄間質細胞を脳脊髄液中に投与することにより、脊髄損傷ラットの機能を回復させる実験に成功し、その臨床応用を目指してきた。彼らと筆者は関西医科大学において、「急性期脊髄損傷に対する培養自家骨髄間質細胞移植による脊髄再生治療（第Ⅰ～Ⅱ層臨床試験）」を計画し、臨床試験の準備を進めてきたが、このたび、医学倫理委員会において、臨床試験を実施することが承認され、臨床応用が始まろうとしている。

脊髄損傷の現状

Ⅰ 発生状況

わが国の脊髄損傷患者の累計は約 10 万人で、毎年約 5,000 人が新たに受傷している¹⁾。年齢分布は、若年層と中高年層にピークがある二極性ピークを示している。前者は主として交通事故とスポーツにより頸椎の他に胸・腰椎に受傷し、後者

*関西医科大学救急医学科
(〒570-8507 守口市文圃町 10-15)

は交通事故、墜落、転倒による場合が多く、頸髄損傷が圧倒的に多い²⁾。米国などでは、これに加えて戦傷による脊髄損傷が少なくない。

交通事故種別の内訳は、自動車事故によるものが半分弱、オートバイ、自転車などの二輪車による事故も半分弱を占め、残りわずかが歩行者である。スポーツ外傷としては、浅いプールに飛び込んでプールの底に頭を打撲する場合は最も多く、そのほか、スキー、ラグビーなどにより受傷する³⁾。

② 脊椎損傷と脊髄損傷

図に示すように、椎骨は椎体と椎弓が重なり合うことによって上下に長い脊柱管を形成し、この中に脊髄が走っている。上下の椎骨の間には椎間孔が形成され、ここから脊髄神経や血管が出入りしている³⁾。

脊椎が骨折や脱臼を来して脊髄が損傷される場合と、脊椎は損傷されないが、過度の屈曲や伸展により脊髄が損傷される場合とがある。特に後者は、加齢に伴う脊椎支持組織の骨化により脊柱管狭窄を来している場合に起こりやすい。脊椎骨折であっても、椎体のみの骨折や、棘突起、横突起のみの骨折の場合には脊髄損傷に至らないことも多く、脊椎骨折で脊髄損傷を招くのは10~20%である³⁾。

③ 脊髄損傷の症状

脊髄が損傷されると、損傷の部位や程度により、さまざまな症状を呈する。損傷した脊髄高位に一致した帯状の知覚過敏がみられ、損傷部以下では、弛緩性麻痺、表在知覚・深部知覚の脱失、膀胱・直腸障害、自律神経系症状がみられる。弛緩性麻痺は、やがて筋は廃用性萎縮に陥る。自律神経系の症状として発汗消失もみられる⁴⁾。

脊髄損傷患者では、交感神経系障害に伴う血管運動神経の弛緩のため血圧低下や徐脈がみられる(神経原性ショック)。さらに、脊髄損傷部位以下のすべての脊髄反射機能が一過性に消失する。

脊髄損傷の重症度については、American Spinal Injury Association (ASIA) が定めた麻痺の程度による機能障害尺度がある⁵⁾(表1)。

損傷された脊髄の横断面の部位別に、それぞれ特徴的な症状を呈する⁶⁾。横位診断による代表的な不完全型脊髄損傷の分類を表2に示した。

④ 受傷直後の治療

脊髄損傷患者が搬入された場合、まずは呼吸、循環に対する緊急処置を必要に応じて行う。頭頸損傷では横隔膜呼吸も障害されるため、ただちに人工呼吸を要する。また、高位脊髄損傷では血圧低下や徐脈がみられるため、循環管理も必要である。脊髄・脊椎以外の合併損傷に対する治療を優

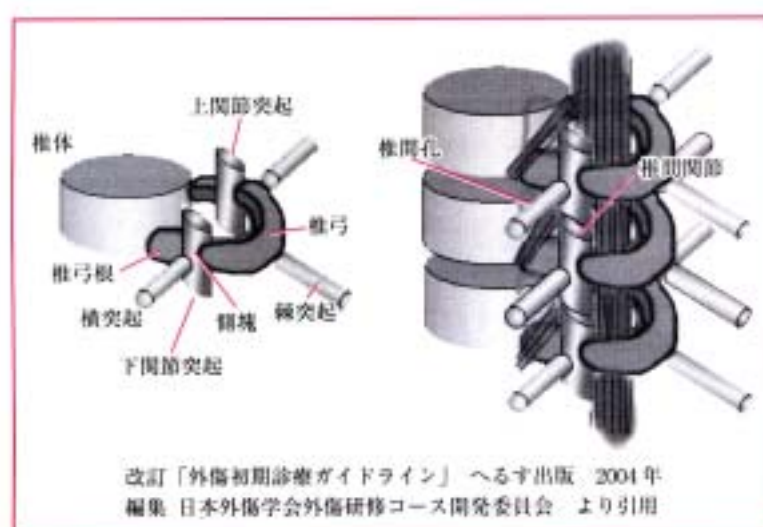


図 脊椎と脊髄の模式的解剖

表1 ASIA 機能障害尺度 (American Spinal Injury Association impairment scale)

- A) 完全麻痺 complete S4-5 領域の運動・知覚機能の完全喪失
 B) 不全麻痺 incomplete 神経学的高位より下位の運動は完全麻痺であり、知覚は S4-5 領域を含めて残存
 C) 不全麻痺 incomplete 神経学的高位より下位に運動機能が残存し、麻痺域の主要筋群の筋力 3*以上が半数未満
 D) 不全麻痺 incomplete 神経学的高位より下位に運動機能が残存し、麻痺域の主要筋群の筋力 3*以上が半数以上
 E) 正常 normal 運動・知覚機能とも正常

*筋力 3= 重力に抗して運動ができる (Manual Muscle Test)。

表2 不完全型脊髄損傷の横位診断

- 1) Brown-Sequard 症候群: 脊髄の半側全体の損傷
 2) 前脊髄型損傷: 脊髄の前部の損傷
 3) 中心性脊髄損傷: 脊髄の中心部のみの損傷
 4) 後方型損傷: 脊髄の後部の損傷

先しなければならない場合も少なくない。

脊髄そのものに対する治療としてステロイド大量療法が行われてきた。これは広く NASCIS II として知られているが、発症から 8 時間以内にメチルプレドニゾロン 30mg/kg を 15 分以内に静脈内投与し、その後 45 分間の間をおいてから 23 時間かけて 5.4mg/kg/h を持続点滴で投与するというものである²⁾。このステロイド大量療法については、有効な方法として紹介されて以来、脊髄損傷に対して広く国際的に取り入れられ、国によってはガイドライン化されていた。最近では、Evidence-based Medicine の観点から、その有効性に疑問を差し挟む声が高まってきている。わが国でも、日本外傷学会や日本救急医学会が主催する JATEC (外傷初期診療ガイドライン) ではこのステロイド大量療法をオプションとして主治医の判断に任せている³⁾。

⑧ 手術療法と保存療法

脊髄損傷患者は、脊椎の骨折や脱臼などにより脊椎の安定性が障害されている。保存的療法としては頸椎カラーやハローベストを用いた固定を行う。手術では、プレートなどを用いて脊椎を固定したり (前方固定術、後方固定術など)、時には緊急手術として脊髄への圧迫を除去する手術 (椎弓形成術) を行う⁴⁾。

⑨ 理学療法

脊髄損傷患者においては、脊髄の離断や挫滅だけでなく、浮腫や圧迫、血行障害などによっても

一過性の機能的な麻痺を生じている場合が多く、これらを放置すれば機能障害を残す。残された機能を少しでも引き出すためには、早期よりの積極的なリハビリテーションが非常に重要である。脊髄損傷の急性期には、局所の安静固定により二次的な脊髄損傷の広がりを防止しなければならない反面、早期からリハビリテーションを開始して残存機能を引き出す必要がある。

急性期のリハビリテーション^{5,6)}

脊椎手術後 1 週間以内には早期リハビリテーションを開始する。早期リハビリテーションはベッドサイド運動療法として行い、①合併症の予防、②残存筋力の維持と強化を目的に実施される。

リハビリテーションのプログラムは、部位 (筋肉、関節)、脊髄損傷の位置、重症度に応じて組み、

① 合併症の予防

頸髄損傷患者では呼吸障害が生じるため肺感染症の予防が重要である。その他の合併症として褥瘡、関節拘縮、筋萎縮、骨萎縮、体動時の血圧変動などを生じる恐れがある。

1) 肺理学療法

頸髄損傷患者では肋間筋の運動麻痺により胸式呼吸が抑制されるが、高位頸損患者ではこれに加えて横隔膜による腹式呼吸も障害されるため、肺理学療法が必要となる。胸壁可動性の改善を図り、呼吸筋の萎縮防止に努め、残存呼吸能力の強化、呼吸訓練、喀痰排出の介助と体位排痰を図る。脊椎の固定保持のためにハローベストを装着している場合には、これらを両立させながら実施する。

2) 褥瘡対策

好発部位は仙骨部、大転子部、踵骨部、坐骨結節部である。

① 2 時間毎の体位変換を行う。

② マットやクッションなどの予防具の併用を行う。

③ 1日1回以上の皮膚清拭を行い、乾燥させる。

④ 低蛋白血症の防止に留意する。

3) 関節拘縮対策

褥瘡による関節拘縮の好発部位は、肩関節、股関節、足関節、手指および足趾である。

① 諸関節の全可動域に及ぶ他動運動を毎日少なくとも1回実施する（関節可動域訓練）。

② 安静時の良肢位保持を行う。関節拘縮が生じた場合、以下の治療を行う。

③ 関節可動域訓練。

④ 理学療法（温熱療法など）。

⑤ 他動運動、ないし自動介助運動による徒手矯正、伸長運動などのリハビリテーション。

④ 残存筋力の維持・強化

1) 運動療法

筋力の評価に従って以下の運動療法を行う。MMT 0.1 ではマッサージ、他動運動により筋萎縮の防止を図る。

MMT 2 では重力や抵抗を排しての自動介助運動を行う。MMT 3 以上では徒手による自動運動から始め、体重や器具による抵抗運動へ移行する。

器具としては、各種のボール、ダンベルなどを使用する。体幹筋では等尺性運動を主体に実施する。筋力の回復に応じて、骨傷への悪影響を及ぼさない程度に徐々に抵抗運動を加えていく。

2) その他の理学療法

筋力の評価に応じて電気療法、特に低周波療法を実施する。

脊髄は再生できるか

古くより、損傷された中枢神経系の細胞は再生することがなく、脳や脊髄の損傷は治らないものと信じられてきた。一方、末梢神経は再生し、軸索が徐々に伸びていくことが知られてきた。しかも近年、末梢神経のみならず、中枢神経系においても、その再生を支持する細胞としてのシュワン細胞、嗅神経鞘細胞、あるいは神経系の幹細胞などが、神経線維の再生を引き出す機能があるとして注目されてきた。さらに近年、細胞を用いた再

表3 細胞治療に利用できる細胞

ES細胞（胎児性幹細胞）
長所：全能性を有し、すべての細胞を供与可能
短所：量確保？腫瘍化？
胎児組織からの間葉系細胞
長所：寿命長く、十分な細胞数
短所：倫理面
成人組織細胞
長所：形成能および分化は最も優れている
短所：寿命が短く増殖しない
骨髄間質細胞
長所：採取容易、培養技術確立、拒絶反応ない自家移植
短所：細胞数を増やすこと

生医療の試みが急速に進歩をみせている。それらの細胞と、それぞれの長所、短所を表3に示した。

④ 骨髄間質細胞とは

骨髄には大きく分けて2種類の細胞がある。血液細胞は血球に分化し、一方、間質細胞は網状の構造をなして造血細胞を支持している。骨髄間質細胞は、最近の研究によると種々の細胞に分化する能力を有しており、骨細胞、心筋細胞、軟骨細胞、腱細胞、脂肪細胞になり得るため、骨髄間質細胞を細胞治療ならびに臓器再生の細胞供給源として役立てることができると考えられている^{8,10)}。骨髄間質細胞による細胞治療のメリットは、容易に採取でき、培養技術が確立されていること、自らの細胞であるため拒絶反応や倫理的問題が生じないことである。今回の臨床試験は、骨髄間質細胞を神経細胞に分化させることを意図したものではなく、骨髄間質細胞の作用により、中枢神経系に残存している神経幹細胞の再生を促そうとするものであり、臨床再生医学に用いる細胞としては現実的なものと考えている。

④ 諸外国における試み

脊髄損傷治療として、諸外国においては表4に挙げた細胞を用いた臨床試験が行われている。脳由来の神経幹細胞を用いた治療法については、動物実験では移植細胞が神経系の細胞に分化したという報告がある。しかし、臨床的な利用を考えると、本人からの中枢神経由来の幹細胞の採取は現実的には難しい。また中絶ヒト胎児由来の幹細胞や胚性幹細胞（ES cell）を利用する場合には倫

表4 諸外国における状況

細胞の種類	脳由来神経幹細胞 (中絶胎児)	マクロファージ (自己)	嗅球神経細胞 (OEG) (中絶胎児または自己)	骨髄間質細胞 (自己)	
開発状況	動物実験中	イスラエルおよび米国で臨床試験実施中	ポルトガル、オーストラリア、中国およびロシアで臨床試験実施中	ヒトへ応用の倫理委員会承認	
特徴	自家移植	不可能、免疫抑制剤必要	可能	可能	
	細胞採取	中絶胎児	末梢血	鼻粘膜および嗅球	
	細胞培養	必要、ただし、1症例につき複数の胎児が必要	マクロファージの活性化が必要	必要	必要
	移植手術	必要	必要	必要	不要
	体内動態	長期残存	早期消失	長期残存	早期消失

理的な問題がある。他人の細胞である以上は拒絶反応の問題は避けられず、免疫抑制剤が必要となれば二次的な副作用も生じ得る。また、ウイルス、プリオンなどの感染の危険性もある。現在、患者自身のマクロファージを培養し活性化してから骨髄損傷部へ直接移植する方法¹¹⁾や、鼻粘膜より採取した嗅球の神経細胞を取り巻くグリア細胞(OEG)を骨髄損傷部へ直接移植する方法¹²⁾が、実際にヒトへの臨床応用として行われている(表4)。OEGについては中国で多数の臨床試験が行われているが、その治療法はまだ実験段階であり、有効性および安全性が検証されたものではなく、また胎児組織を用いるなど未解決の問題も多い¹³⁾。これらの細胞の移植には、損傷部位の脊椎の椎弓切除を行って損傷部の脊髄実質内に細胞を直接注入する方法がとられる。一方、われわれが試みる骨髄間質細胞の移植は、脳脊髄液中への培養細胞の投与が有効であるという京都大学の研究グループの研究結果¹⁴⁻¹⁶⁾を踏まえて、腰椎穿刺の手技を使って脳脊髄液中に細胞を投与する。そのため、諸外国で行われている臨床試験と比較しても患者への侵襲が少なく、より危険性の少ない方法であると考えている。

骨髄間質細胞移植の基礎的研究

1) in vitro の実験

骨髄間質細胞は骨髄細胞全体の約0.125%を構成する。骨髄の血液細胞とは、組織培養にあたり

プラスチックに付着することで分離が可能である。また、骨髄間質細胞は特殊な環境下において、骨芽細胞、軟骨細胞、脂肪細胞、心筋細胞、肝細胞、肺・腸管・皮膚の上皮細胞などに分化させ得ることが知られている。さらに間質細胞は、神経細胞や神経軸索を取り巻くアストロサイト、シュワン細胞にも分化し神経の再生を刺激し得ることから、鈴木、井出らは脊髄再生に有力と注目し、種々の基礎研究を重ねてきた¹⁴⁻¹⁶⁾。例えば、in vitroにおいてラットの胎児脊髄細胞だけを培養した場合には神経前駆細胞が徐々に発育し、neurosphereを形成するものの、突起を出さない。一方、骨髄間質細胞を脊髄細胞と共培養した場合には神経前駆細胞の急速な分化が誘発され、長い神経突起を伸ばし多様なネットワークを形成した¹⁶⁾。

2) 動物実験

4週ラットを用い、露出脊髄上に一定の損傷を加えられる装置を用いて脊髄を挫傷させ、ただちに損傷部に骨髄間質細胞培養液を注入し、運動神経機能の回復と、組織学的検討にて効果を確認した¹⁵⁻¹⁷⁾。さらに臨床応用に向けて、損傷部への直接注入は問題が多いため、脳脊髄液中へ間質細胞培養液を注入することを検討し、第4脳室内に注入して同様の効果を確認した。注入した骨髄間質細胞がやがて消失することから、幹細胞のように増殖に伴う合併症の可能性もないと考えられる。

3) 臨床応用へ向けて

関西医科大学医学倫理委員会にて「急性期脊髄損傷に対する培養自家骨髄間質細胞移植による脊髄再生治療（第Ⅰ～Ⅱ相臨床試験）」の実施が承認され、京都大学でなされた基礎研究を、財団法人先端医療センター、臨床研究情報センター、関西医科大学高度救命救急センターの協同で臨床試験を行うことが承認された。

救命救急センターと脊髄損傷

大阪における患者収容の実態

大阪府の中河内救命救急センターでは、2003年に府下の病院へ脊髄損傷患者の収容状況についてのアンケート調査を実施した。それによると、13の救命センターを含め、整形外科やリハビリテーション科を持つ255の病院のうち、回答を寄せた130施設の中で、脊髄損傷患者を年間に5人を超えて収容したのはわずかに数施設に過ぎず、2/3の施設が収容数ゼロという状況であった。また、患者のほぼ半数が130施設の中のわずか12の救命救急センターへ搬入されていることも明らかとなった。

厚生労働省の救命救急センター運営方針

厚生労働省に認可された救命救急センターは、厚生労働省の方針に沿って運営することを求められている。救命救急センターは重症患者診療の最後の砦であり、重症以上の救急患者受け入れの社会的使命がある。そのため、次に発生する重症患者に空床を確保する必要がある。生命危機が回避できた患者は完治に至らなくとも紹介元の病院などに転院させる必要がある。しかし、救急医にとっても家族にとっても転院先の確保は大問題であり、特に脊髄損傷患者のように長期間入院しリハビリテーションを受けなければならないケースについては、現在の医療制度の中で、容易ならざる問題である。このように救命救急センターの使命と脊髄損傷患者に対する長期的な治療は相容れない。これらを解決するためには、受傷の初期から慢性期のリハビリテーションまで、専門的施設において一貫した治療が行われることが望ましい。そのためにも、現在、わが国での整備が遅れている脊髄センターの設立が是非とも必要である。

慢性期における理学療法の課題

ゴール設定

損傷した脊椎の固定が確実なものとなり、急性期の治療が終了すれば、その後は残存している機能をフルに引き出し、筋肉、関節、骨などの萎縮の防止を図り、社会生活に向けてのリハビリテーションに移行する。リハビリテーションは理学療法士、作業療法士、看護師、また介護福祉士やソーシャルワーカーなど、さらには家族も協力して長期にわたって行われることになる。

この時期のリハビリテーションは、その患者の障害のレベルに応じて最終的な復帰の目標をどこに置くかを決定し、そのためのリハビリテーションを行うことになる。例えば高位頸髄損傷であれば、福祉機器をマウススティックで操作することになるので、首の周りの筋肉を鍛える必要がある。また、頸髄損傷による不全四肢麻痺の場合には、上半身の動きをできるだけ引き出すため、肩や肘などの関節の動きを円滑ならしめることを基本目標とする。さらに、胸腰髄の損傷による対麻痺の場合には車椅子で社会生活を送ることを目標にするため、車椅子への移動、トイレへの移動などが自力でできることを目指す。乗用車を手動で運転することを目標とすることも、レベルによっては可能となる。寝返りができる、ベッド上で起き上がることができる、車椅子に座りお尻を持ち上げることができる、自分で車椅子に移動できる、などの目標を定めてリハビリテーションに取り組むことがモチベーションを上げるために重要である。

その他の留意点

脊髄損傷患者では体動による血圧の低下が起りやすい。これは、自律神経の障害のために、血管運動神経が身体の動きについてこれないためである。これを最小限に押さえるためにも、早期から身体を動かすことが重要である。起立性低血圧を克服していくためには、寝返りやベッド上での起座など、姿勢を変えることから訓練を始めていく。骨の萎縮を防ぐために、体重や圧を骨に掛けることは意義があり、そのためにも身体を他動的

に動かす。患者を腹臥位にさせたり、他動的に立たせるなどの姿勢をとらせることも関節拘縮の予防効果がある。リハビリテーションで鍛える筋肉は下腿、大腿、四肢のみではなく、座位を維持するために体幹の筋肉も鍛えることも必要である。

このように慢性期のリハビリテーションではゴールの設定が重要であり、短期ゴールは、ベッドと車椅子の間の移動を自分でできる、装具と杖で自立歩行ができるなどであり、長期ゴールは、半年先、1年先にどのような生活ができているようにするかを目標を立てて行っていくこととなる。

おわりに

脊髄損傷が治癒するならば、これは夢のような話である。根治は望めなくとも、たとえ機能の一部だけでも回復すれば、神経学的な機能予後は大いに改善し、生活の質が向上して、本人・家族の肉体的、精神的、経済的負担は軽減され、ひいては医療資源の節約、国民の保険負担の軽減など大きな社会的貢献が期待される場所である。その成否については現時点では不明であるが、臨床試験が今始まろうとしている。

文 献

- 厚生労働省社会援護局障害保健福祉部：身体障害児・者実態調査結果(平成13年6月1日調査)、平成14年8月
- 新宮彦助：日本における脊髄損傷疫学調査 第3報 (1990-1992)、日本パラプレジア医学会雑誌 8：26-27, 1995
- 日本外傷学会外傷研修コース開発委員会：脊椎・脊髄外傷、改訂外傷初期診療ガイドライン JATEC (日本外傷学会外傷研修コース開発委員会編)、147-162。へるす出版、2004
- 国分正一：脊椎・脊髄損傷、標準整形外科学 第7版 (寺山和雄、辻陽雄監修)、675-693。医学書院、1999
- Ditunno JF Jr et al：The international standards booklet for neurological and functional classification of spinal cord injury, *Paraplegia* 32 (2)：70-80, 1994
- 遠藤重厚：脊椎・脊髄損傷、標準救急医学 第3版 (日本救急医学会監修)、351-352。医学書院、2001
- Bracken MB et al：A randomized controlled trial of methylprednisolone or naloxone in the treatment of acute spinal-cord injury：Results of the Second Acute Spinal Cord Injury Study, *N Engl J Med* 322：1405-1411, 1990
- 種市洋：脊髄損傷(リハビリテーションを含む)、今日の治療指針、724-725。医学書院、2004
- Mezey E et al：Turning blood into brain：Cells bearing neuronal antigens generated in vivo from bone marrow, *Science* 290：1779-1782, 2000
- Brazelton TR et al：From marrow to brain：Expression of neuronal phenotypes in adult mice, *Science* 290：1775-1779, 2000
- Rapalino O et al：Implantation of stimulated homologous macrophages results in partial recovery of paraplegic rats, *Nat Med* 4 (7)：814-821, 1998
- Huang H et al：Influence of patients' age on functional recovery after transplantation of olfactory ensheathing cells into injured spinal cord injury, *Chin Med J* 116 (10)：1488-1491, 2003
- Ying Li et al：Repair of adult rat corticospinal tract by transplants of olfactory ensheathing cells, *Science* 277：2000-2002, 1997
- Wu S et al：Migration, integration, and differentiation of hippocampus-derived neurosphere cells after transplantation into injured rat spinal cord, *Neurosci Lett* 312 (2)：173-176, 2001
- Wu S et al：New method for transplantation of neurosphere cells into injured spinal cord through cerebrospinal fluid in rat, *Neurosci Lett* 318 (2)：81-84, 2002
- Bai H et al：Dissemination and proliferation of neural stem cells on the spinal cord by injection into the fourth ventricle of the rat：A method for cell transplantation, *J Neurosci Methods* 124 (2)：181-187, 2003
- Ohta M et al：Bone marrow stromal cells infused into the cerebrospinal fluid promote functional recovery of the injured rat spinal cord with reduced cavity formation, *Exp Neurol* 187 (2)：266-278, 2004
- Wu S et al：Bone marrow stromal cells enhance differentiation of cocultured neurosphere cells and promote regeneration of injured spinal cord, *J Neurosci Res* 72 (3)：343-351, 2003

研究成果報告書

研究課題名	帯状疱疹後神経痛の機能分子の探索と臨床研究		
(英文)	Analysis of the cerebrospinal fluid of patients with postherpetic neuralgia		
事業推進者	南 敏明	E-mail	ane022@poh.osaka-med.ac.jp
所属・職名	大阪医科大学麻酔科学教室・教授		
研究分担者名	西村 渉、藤原 俊介、門野 紀子、荘園 雅子		
キーワード	帯状疱疹後神経痛、脳脊髄液、一酸化窒素		

1. 概要

神経因性疼痛では、自発痛、侵害性刺激に対する閾値が低下する痛覚過敏反応だけでなく、本来痛みを引き起こさない触覚刺激が痛覚となるアロディニアが惹起され、その発生には神経の可塑性が深く関与している。

今まで、マウスを用いた神経因性疼痛モデルの実験結果より、プロスタグランジン - グルタミン酸受容体 - 一酸化窒素が神経因性疼痛の発現・維持に重要な役割を果たしていることを明らかにしてきた。また、最近、毒茸ドクササコの成分であるアクロメリン酸をマウス脊髄腔内に投与しアロディニアを惹起させる神経因性疼痛モデルを確立した。

神経因性疼痛の代表疾患である帯状疱疹後神経痛患者から得られた脳脊髄液を解析することにより動物実験の結果と臨床患者との関係を明らかにすること、アクロメリン酸によるアロディニアモデルを用いて神経因性疼痛を抑制する化合物の検索を目指す。

2. 研究の背景と目的

臨床研究：神経因性疼痛である帯状疱疹後神経痛に対して、くも膜下局所麻酔薬およびステロイド注入療法が有効であると報告 (N Engl J Med 2000; 343: 1514-9) がされて以来、当施設でも種々の治療に抵抗を示す症例に施行している。くも膜下局所麻酔薬およびステロイド注入療法は、局所麻酔薬が有効なのか、ステロイドが有効なのか、また局所麻酔薬およびステロイドが有効なのかを検討すると共に、脳脊髄液を採取し、治療効果と脳脊髄液中のアミノ酸の関係を解析した。

基礎研究：毒茸のドクササコを摂取すると 4～5 日後に四肢末端に灼熱痛とアロディニアが出現し、1 ヶ月以上も持続する。ドクササコの成分であるアクロメリン酸に注目し、アクロメリン酸をマウス脊髄腔内に投与し触覚刺激を加えるとアロディニアが出現すること、アクロメリン酸によるアロディニアは長時間持続すること、アクロメリン酸は 10^{-15} g と非常に微量な用量でアロディニアを出現させることを明らかにしてきた。研究協力者の岐阜大学大学院医学系研究科再生医科学専攻の古田享史先生より、アクロメリン酸誘導体を提供していただき、アクロメリン酸によるアロディニアモデルだけでなく、神経損傷モデルの痛みの閾値を回復させる化合物を見出す。

3. 研究方法

臨床研究：発症 5 年以内の帯状疱疹および帯状疱疹後神経痛患者 65 名を対象とした。手術室で、脊椎くも膜下麻酔の手技に準じ、メチルプレドニゾロン 60mg を含む高比重リドカイン溶液を注入した。週に一度、4 回を 1 コールとし、初回のみ入院加療の上、施行した。効果判定は VAS (visual analogue scale) を用いて行い、治療開始時と治療終了時の VAS を比較検討した。

なお、倫理委員会の承認下に脳脊髄液を採取し解析を行った。

基礎研究：我々が確立したマウス脊髄腔内アクロメリン酸投与によるアロディニアモデルを指標にして、アクロメリン酸誘導体の分類を行い、アクロメリン酸誘発アロディニアに対する作動薬、拮抗薬を見出す。拮抗薬をスクリーニングした後、神経毒性がないかをマウス脊髄腔内投与による行動 (運動麻痺や痙攣等を惹起しないか) をチェックする。見出された拮抗薬に対して、神経因性疼痛モデル (Chung モデル) に対する効果を検討する。

4. これまでの成果

臨床研究: くも膜下局所麻酔薬およびステロイド注入療法は、発症 1 年以内の症例に効果があり、局所麻酔薬を除いてステロイドのみを投与しても効果が変わらないこと、帯状疱疹後神経痛患者の脳脊髄液は、変形性膝関節症やコントロールの患者に比較して有意にシトルリンが増加していた。脳脊髄液中の一酸化窒素を直接定量することは、一酸化窒素はガスであるため困難であるが、一酸化窒素合成酵素が活性化され、L-アルギニンから一酸化窒素とシトルリンが産生されることから、シトルリンが増加していることは、間接的に一酸化窒素の増加を意味する。このことは、マウスを用いた神経因性疼痛モデルの実験結果と一致することが明らかになった。

基礎研究: アクロメリン酸誘導体 150 化合物をアクロメリン酸によるアロディニアモデルを用いてスクリーニングした。その結果、アクロメリン酸によるアロディニアを用量依存性に抑制し、単独でアロディニアを惹起させず、神経毒性を有しない 2 化合物に絞れた。

5. これまでの進捗状況と今後の計画

痛みには個人差があり定量性に欠けるという点が、痛みの研究や治療を困難にしていたが、脳脊髄液をさらに解析することにより痛みを定量することが可能になることが期待できる。

アクロメリン酸誘導体 2 化合物を総合的に検討し、新規鎮痛薬として上市を目指す。

6. これまでの発表論文

(1) 発表論文

1) 原著論文

1. Takagi, K., Okuda-Ashitaka, E., Mabuchi, T., Katano, T., Onishi, T., Matsumura, S., Ohnaka, M., Kaneko, S., Abe, T., Hirata, T., Fujiwara, S., Minami, T. & Ito, S.
Involvement of stem cell factor and its receptor tyrosine kinase *c-kit* in pain regulation. *Neuroscience*. **153**, 1278-1288 (2008).
2. Sethuraman, R., Krishnamoorthy, M.G., Lee, T-L., Liu, E.H.C., Chiang, S., Nishimura, W., Sakai, M., Minami, T. & Tachibana, S. Simultaneous analysis of D- and L-Serine in cerebrospinal fluid by use of HPLC. *Clin. Chem.* **53**, 1489-1494 (2007).
3. Soen, M., Minami, T., Tatsumi, S., Mabuchi, T., Furuta, K., Maeda, M., Suzuki, M. & Ito, S. A synthetic kainoid, (2S,3R,4R)-3-carboxymethyl-4-(phenylthio) pyrrolidine-2-carboxylic acid (PSPA-1) serves as a novel anti-allodynic agent for neuropathic pain. *Eur. J. Pharmacol.* **575**, 75-81 (2007).
4. 藤原俊介、酒井雅人、西村 渉、近藤三鈴、南 敏明
難治性疼痛疾患に対するリドカイン軟膏の効果の検討
ペインクリニック **28**, 542-546 (2007).
5. Okuda-Ashitaka, E., Minami, T., Matsumura, S., Takeshima, H., Reinscheid, R.K., Civelli, O., & Ito, S. The opioid peptide nociceptin/orphanin FQ mediates prostaglandin E₂-induced allodynia, tactile pain associated with nerve injury. *Eur. J. Neurosci.* **23**, 995-1004 (2006).

2) 総説

1. 荘園雅子、南 敏明、伊藤誠二
アクロメリン酸と痛み
ペインクリニック **29**, 351-364 (2008).
2. 南 敏明、芦高恵美子、伊藤誠二
プロスタグランジンとノシセプチン
麻酔 **56 増刊**, S172-S178 (2007).
3. 西村 渉、南 敏明;
手術後痛と NMDA 受容体
CLINICAL NEUROSCIENCE **24**, 177-179 (2006).
4. 芦高恵美子、南 敏明、伊藤誠二:
脊髄におけるノシセプチン/オーファニン FQ を介したプロスタグランジンによる疼痛制

御ネットワーク

ペインクリニック **27**, 547-559 (2006).

5. 辰巳真一、南 敏明:
神経因性疼痛における Rho キナーゼの関与
ペインクリニック **27**, 578-591 (2006).
6. 南 敏明、伊藤誠二:
アロディニアのメカニズムとその制御
LiSA **13**, 826-828 (2006).

3) 著書

1. 南 敏明、荘園雅子、藤原俊介:
第2章 慢性疼痛研究 -臨床との関連を中心に-
「慢性疼痛研究 慢性疼痛の理解と医療連携」宮崎東洋, 北出利勝編 48-56, 真興交易、
東京 (2008).
2. 荘園雅子、南 敏明:
神経因性疼痛モデルの作成方法とその評価法
「痛み研究のアプローチ」河谷正仁編 27-35, 真興交易、東京 (2006).
3. 南 敏明、西村 渉:
周術期に末梢痛覚受容と情報伝達は変わるか
「麻酔科診察プラクティス 20」高崎真弓編 40-42, 文光堂、東京 (2006).

(2) 学会発表

国際学会

3) 一般発表

1. Minami, T., Soen, M., Tatsumi, S., Mabuchi, T., Shirae, A., Furuta, K., Suzuki, M. & Ito, S. A synthetic kainoid serves as a novel anti-allodynic agent for neuropathic pain. 12th World Congress on Pain, Glasgow, 2008.
2. Maeda, M., Furuta, K., Hirata, Y., Shibata, S., Kiuchi, K., Suzaki, M., Minami, T., Ito, S. & Suzuki, M. Design and synthesis of novel small molecules that regulate neuronal functions. The 21st Century COE-RCMS International Conference on Elucidation and Creation of Molecular Functions, January 10-11, Nagoya, 2007.
3. Sethuraman, R., Krishnamoorthy, M.G., Lee, T-L., Liu, E.H.C., Chiang, S., Nishimura, W., Sakai, M., Minami, T. & Tachibana, S. D-Serine and nitric oxide in cerebrospinal fluid of postherpetic neuralgia and chronic osteoarthritis patients. Tenth International Conference on the Mechanisms and Treatment of Neuropathic Pain, Salt Lake City, 2007.
4. Furuta, K., Maeda, M., Suzaki, M., Minami, T., Ito, S. & Suzuki, M. Design and synthesis of novel acromelic acid analogs that regulate allodynic responses. ICOB-5 & ISCNP-25 IUPAC International Conference on Biodiversity and Natural Products, Kyoto, 2006.
5. Okuda-Ashitaka, E., Minami, T., Matsumura, S., Takeshima, H., Reinscheid, R.K., Civelli, O., & Ito, S. Mediation by the opioid peptide nociceptin/orphanin FQ of prostaglandin E₂-induced allodynia, tactile pain associated with nerve injury. Society for Neuroscience 36th Annual Meeting, Atlanta, 2006.

国内学会

2) シンポジウム講演

1. 南 敏明、芦高恵美子、伊藤誠二
プロスタグランジンとノシセプチン
日本麻酔科学会第54回学術集会、札幌、2007.
2. 南 敏明
痛み治療の基礎と臨床
第36回日本慢性疼痛学会、京都、2007.

3. 南 敏明、西村 渉、酒井雅人
帯状疱疹後神経痛に対するくも膜下局所麻酔薬およびステロイド注入療法
第44回日本臨床生理学会総会、大阪、2007.
 4. 伊藤誠二、南 敏明
難治性疼痛の発症機構と診断・治療のバイオマーカーの探索
第44回日本臨床生理学会総会、大阪、2007.
 5. 辰巳真一、南 敏明
痛みの伝達における脊髄の Rho キナーゼの役割
日本麻酔科学会第53回学術集会、神戸、2006.
- 3) 一般発表
1. 金澤将勝、前田将秀、伊藤誠二、南 敏明、古田享史、鈴木正昭
抗アロディニア作用を示すアクロメリン酸類縁体の創製
日本化学会第88春季年会、東京、2008.
 2. 武田仁美、西村 渉、宮崎信一郎、森本賢治、藤原俊介、南 敏明
下肢帯状疱疹神経炎の発症を契機に腰椎椎間板ヘルニアの症状が増悪した2症例
日本ペインクリニック学会第42回大会、福岡、2008.
 3. 金澤将勝、須崎真史、前田将秀、伊藤誠二、南 敏明、古田享史、鈴木正昭
アロディニア誘発活性を示す新規アクロメリン酸類縁体の合成
日本化学会第87春季年会、大阪、2007.
 4. 前田将秀、古田享史、平田洋子、柴田翔子、木内一壽、南敏明、伊藤誠二、鈴木正昭
神経機能を制御する低分子化合物の創製
日本ケミカルバイオロジー研究会第2回年会、京都、2007.
 5. 荘園雅子、南 敏明、辰巳真一、古田享史、鈴木正昭、伊藤誠二
アクロメリン酸 A 誘導体は神経因性疼痛を抑制する
日本麻酔科学会第54回学術集会、札幌、2007.
 6. 間嶋 望、酒井雅人、西村 渉、近藤三鈴、村谷忠利、南 敏明
帯状疱疹後神経痛 (PHN) における治療効果の評価 - 疼痛範囲と Visual Analogue Scale (VAS)
日本麻酔科学会第54回学術集会、札幌、2007.
 7. 陸 景珊、片野泰代、南 敏明、裏出良博、伊藤誠二
プロテオミクスによる帯状疱疹後神経痛患者の脳脊髄液の解析
第30回日本分子生物学会年会・第80回日本生化学会大会 合同大会、横浜、2007.
 8. 森本賢治、西村 渉、村谷忠利、酒井雅人、南 敏明
帯状疱疹および帯状疱疹後神経痛に対するくも膜下ステロイド注入療法の効果
日本ペインクリニック学会第40回大会、神戸、2006.

7. これまでの成果の情報公開

ホームページ：大阪医科大学麻酔科学教室

<http://www.osaka-med.ac.jp/~ane000/Ane-index-J/>

資 料

関西医科大学ブレインメディカルリサーチセンター組織運営規則

(設置)

第1条 関西医科大学専門部にブレインメディカルリサーチセンター(Brain Medical Research Center) (以下「センター」という。)を置く。

(目的)

第2条 センターは、神経系疾患に関する基礎医学と臨床研究を行い、修復再生医学による新しい治療方法の開発・応用のための横断的トランスレーショナル研究を推進することを目的とする。

(部門)

第3条 センターに次の部門を置く。

- (1) 基礎・社会医学系部門
- (2) 臨床医学系部門

(職員)

第4条 センターの教職員は本学の教職員をもって充て、兼務とする。ただし、本学教職員以外の者を嘱託として委嘱することができる。

(センター長)

第5条 センターにセンター長を置く。

- 2 センター長は、センターを管理し、その運営にあたる。
- 3 センター長は、専門部教授会構成員の互選により選出する。
- 4 センター長の任期は2年とし、再任を妨げない。

(副センター長)

第6条 センターに副センター長を置く。

- 2 副センター長は、センター長を補佐し、センター長不在のときは、その職務を代行する。
- 3 副センター長は、専門部教授会構成員の互選により選出する。
- 4 副センター長の任期は2年とし、再任を妨げない。

(運営委員会)

第7条 センターに運営委員会を置く。

- 2 運営委員会は、次の者をもって構成する。
 - (1) センター長
 - (2) 副センター長
 - (3) 専門部教授会構成員の互選により選出された4名(基礎・社会医学系部門2名、臨床医学系部門2名)
 - (4) 学長が指名する委員 若干名
- 3 前項第1号及び第2号に掲げる委員の任期は、在任期間とする。
- 4 第2項第3号及び第4号に掲げる委員の任期は2年とする。ただし、再任を妨げない。
- 5 運営委員会は、センターの円滑な運営をはかるために、次の事項を審議する。
 - (1) センター長の諮問事項
 - (2) センターにおける研究の充実並びに促進に関する事項
 - (3) 研究の成果の活用に関する事項
 - (4) センターの施設利用に関する事項
 - (5) その他センター運営に関する事項
- 6 運営委員会は、必要に応じてセンター長がこれを招集し、議長となる。
- 7 運営委員会の庶務は、学部事務部研究課研究係において行う。

(規則の改廃)

第8条 この規則の改廃は、センター運営委員会の審議を経て、専門部教授会の承認を得なければならない。

附 則

この規則は、平成18年5月10日から施行する。

関西医科大学「ブレインメディカルリサーチセンター研究費」 運用内規について

研究費の使途内容については、別紙「ブレインメディカルリサーチセンター(以下、「センター」という。)の取扱いについて」(組織加入部門用)を参照のもと、次の主な事例をもとに運用のこと。

1. 消耗品費関係 加入部門が、センター研究に必要な抗体・動物又はその他の物品等の購入に要した費用。
2. 印刷製本費 加入部門が、センター実験や研究の成果に要した資料作成の製本費等。
3. 学会出張旅費関係

国内：センター併任教員が本研究に係わる学会等の参加時に要する旅費等、本学学会出張旅費規程に準じる。

国外：センター併任教員が本研究に係わる海外出張時に要する旅費等、本学教職員海外出張規程に準じる。

(但し、出張時には出張報告書(様式6)を必ず提出する。)

4. 修繕費関係 加入部門が、センターで整備した研究用機器備品にかかる修理費など。
5. 設備費関係 加入部門が、センター研究に関連する機器を整備した1個又は1組が20万円以上500万円未満の研究用機器備品。
6. その他留意事項

① 参考事例以外の取扱いについて

参考事例(1～5)以外にも、センターとして直接関係した研究経費であれば対象となるが、明瞭な理由が必要である。

② 飲食に関する経費は認められない。

③ 証拠書類の保管又は添付

研究経費の使途として、研究と関連付けが複雑であったり、高額な場合は経費を執行する理由書が必要である。

④ 会計検査院等の監査時の対応

センター加入部門における研究費総額の1/2(見込)は国庫補助金である。従って、研究経費の使途について、各加入部門が充分責任をもち、後の監査で説明を求められても対応できるようにすること。

⑤ 複雑な研究経費の取扱いについて

研究費の使途内容が複雑であったり、この運用内規以外の事項が発生した場合は、ブレインメディカルリサーチセンター運営委員会に諮り審議する場合がある。

この内規における運用開始は、平成18年6月14日からとする。

以 上

[追記]

なお、ブレインメディカルリサーチセンター研究費に係る明確なマニュアル等は所轄省庁等(日本私立学校振興・共済事業団)でも策定されておられません。従って、研究費の使途方法について各加入部門ともセンターに関係の経費に限定し、正確なる管理に努められますよう通知します。

平成18年6月14日

ブレインメディカルリサーチセンター長 伊 藤 誠 二

ブレインメディカルセンターに関する答申書（第2次）

平成20年5月26日

附属滝井病院

高橋 伯夫 病院長 殿

ブレイン・メディカル・センター

設置準備委員会委員長 日下 博文

平成10年4月 附属病院(当時) 8号館の1階に Brain Medical Service が設置され、脳神経外科、神経内科、心療内科、神経精神科の外来診療が集約された。「脳と心の臨床」を集約した全国にも例をみない中核医療体制として一定の成果を挙げることができた。しかし、当初からいくつかの問題があり、平成13年3月に、診察室の不足、Brain Medical Service の診療体制の附属病院内での再構成などを提案した要望書を 塚原 勇 理事長、日置紘士郎 学長（当時）へ提出した。平成15年12月にも上記4診療科で検討の上、改めて 新宮 興 病院長(当時)に要望書を提出したが具体的な解決には至らなかった。

平成18年1月、枚方病院開設に伴い、附属病院は、附属滝井病院として再構成された。一方、平成18年度私立大学学術フロンティア推進事業に本学が選定され、同年5月に研究組織ブレイン・メディカル・リサーチ・センター(センター長 伊藤誠二 教授)が設置された。これに呼応するかたちで、附属滝井病院 濱田 彰 病院長 (当時)によりブレイン・メディカル・センター設置準備室運営委員会が立ち上げられ、特色ある臨床を具現化し、ブレイン・メディカル・リサーチ・センターとの中期的将来連携、関係診療科の有機的連携を強化することを目的に、病院顧問 栗本匡久 教授を委員長のもとにこれまで7回開催された。その結果は 高橋伯夫 病院長に平成19年10月12日付けで 栗本匡久 委員長から答申された（資料1）。その後、栗本匡久 教授の病院顧問退任により、平成19年11月からは委員長 日下博文 のもとに4回開催された。栗本匡久 前委員長の答申内容と、香里病院開設に伴う附属滝井病院の再編を見据えて、具体的な議論を重ねた。その結果を以下に答申させていただきます。

附属滝井病院ブレイン・メディカル・センター(BMC)設置についての答申

1. 附属滝井病院 現ブレイン・メディカル・サービスの運営状況、歴史的経緯、実績に鑑み、関係診療科機能を8号館1階と2階に集約することが望まれる。
 - 1) 現ブレイン・メディカル・サービス関係診療科（脳神経外科、神経内科、心療内科、精神神経科）診察室、処置室、救急外来診察室（ストローク・ケア機能、精神科救急）。
 - 2) 小児心と体の発達支援センターの移設。
 - 3) 神経生理機能検査室（神経内科、整形外科）、精神生理機能検査室、心理療法

室など。

4) 学生臨床実習室。

以上を配置するために、できるだけ現状の診察体制を温存し、改修工事の負担を軽減することを考慮したフロア・プランを作成した（資料2）。

現在の外来患者数、診察室などへアクセスの利便性などを考慮して

a) 1階に脳神経外科、神経内科を配置する。

b) 2階に精神神経科、心療内科、発達支援センターを配置する。

救急搬送の数からみて、脳神経外科、神経内科は1階が適切と考える。救急診察室は共有であり、ストローク・ケアに近い診療連携を行う。従来からあるシールド・ルームは、移設の負担を避けて、そのまま電気生理検査室として主に神経内科・整形外科が使用する。精神神経科は患者数が最も多いが、この配置で、各階ともほぼ同数の外来患者数の配分になる。精神科は防音装置のある隔離の可能な部屋が必要である。一方、精神科受診患者と小児患者が同席するのを避けるために、2階の一番奥の部分に発達センターの待合を設ける。心療内科は外来診療、検査、治療が全て同一のフロアで行えるようになり効率的かつ実践的になる。2階の診察室は、1階に比べて奥行きが深く、すべての診察室が拡張される。さらに各科に予診室を設けることができるので、学生の臨床実習も円滑に行えるようになる。

受付に関しては、カルテ、フィルム、その他文書の管理上、それぞれの階に設ける必要がある。

待合スペースについては、1階、2階ともほぼ同じ大きさである。小児科のみ上記理由で、2階の奥に設置する。2階については精神科患者さんが利用するため、窓枠などに安全面での配慮が必要になると思われる。

2. 8号館1階、2階に関係診療科の機能が集約された場合に見込まれる今後の展望

診察室の不足が解消されることから、

- 1) 各科の一般外来患者数の増加がはかれる。
- 2) 各科、それぞれの特色を生かした専門外来が開設できる。
- 3) 心のケアと身体のケアを連携した診療サービスの提供が可能になる。
- 4) 臨床各科の連携によるさらなる臨床研究が容易になる。
- 5) 中期的にはブレイン・メディカル・リサーチ・センターとの連携によるより幅広い研究を行う基盤となる。

などが見込まれる。

詳細については、脳神経外科、神経内科、心療内科、精神神経科、小児科からの別途資料を参照いただきたい（資料3, 4, 5, 6, 7）。

ブレインメディカルセンターに関する答申書（第 1 次）

平成 19 年 10 月 12 日

附属滝井病院

高橋 伯夫 病院長殿

ブレイン メディカル センター設置準備委員会
同 委員長（設置準備室室長） 栗本 匡久

答 申 書

当ブレイン メディカル センター設置準備委員会では、〔附属滝井病院におけるブレイン
メディカル センターの設置〕について、検討した結果、以下の第 1 次答申を提出いたします。

附属滝井病院ブレイン メディカル センター（BMC）設置についての答申

- 1、特色ある附属滝井病院を具現化し、また関西医科大学ブレイン メディカル リサーチ
センターとの中期的将来連携、関係診療科の有機的連携を強化、容易にするため、附属滝
井病院 現ブレイン メディカル サービス部門を発展的に解消し、ブレイン メディカ
ル センターを附属滝井病院に開設する。
- 2、附属滝井病院 現ブレイン メディカル サービスの運営状況、歴史的経緯、実績に鑑み、
以下の関係診療機能を北館 1、2 階に集約することが望ましい。
 - 1) 現関係診療科（神経内科、心療内科、脳神経外科、精神科）診察室、処置室拡充。
脳神経外科、神経内科共有救急外来診察室、処置室。
精神科救急診察室。
 - 2) 小児心と体の発達支援センター移設。
 - 3) 神経内科、整形外科神経生理機能検査室（シールドルーム）、心理療法室移設、精神
生理機能検査室移設。
 - 4) 合同特殊外来診察室設置。（ブレイン メディカル リサーチ センター連携施設）
付言 1、ペイン医療、再生医療（移植医療）、てんかん外科、機能外科 等。
2、事前に、国内外での研修を通じ、人材を育成することが、急務である。
 - 5) ストローク ケアの拡充。
付言 神経画像診断機器運用の整備。
 - 6) 現 中央検査部 神経生理機能検査部門の移設。
付言 神経生理機能検査スクリーニング機能拡充。
臨床生理機能検査技師 2 名増員。
 - 7) 合同カンファレンス ルーム、学生臨床実習室設置。
- 3、ブレイン メディカル センター開設は、現附属滝井病院の病床削減、跡地利用、病棟再
編成の過程において、早急に実現を計る。
- 4、上記ブレイン メディカル センター計画の具体的設計（設計、改装費用概算等）、関係
部署調整、今後の運営は、第 2 次 BMC 設置準備委員会が当たり、第 2 次答申を病院長に
提出する。

資料3 【 脳神経外科 】

脳神経外科の今後の展望

マンパワーに限りがあるがブレインメディカルセンターの整備に伴い収益の向上や他科との連携について我々のできる事を列記する。

- 1) 外来診療の充実
 - ・セカンド オピニオン外来の新設
通常の診察時間にセカンド オピニオンを希望される患者さんに対応するのは時間の制約があり困難であるが、特殊外来の新設により、より良い患者サービスが行える。
 - ・ボトックス外来の充実
本年3月から開始しているが更に充実させる。
 - ・土曜日の外来の充実
これまでは2診であったが、3診で行うことを計画している。
外来名はつけないが診察室が3部屋確保されることにより、病状説明や手術の説明など時間のかかる患者・患者家族との面談に使用でき、より充実した患者サービスが可能となる。
- 2) 部屋数の確保により臨床実習生の医療面接が可能となりより充実した医学教育が可能となる。
現時点では空き部屋がなく医療面接をしてもらう機会はない。
- 3) 加速度脈波測定システムを積極的に活用し、血管老化度の診断や自律神経機能の評価を行う。臨床研究として、学内倫理委員会で承認されている「脂質異常症におけるスタチン投与前後の加速度脈波による血管年齢と自律神経状態の評価」を開始する。
- 4) 脳卒中の診療について
脳卒中については神経内科医と脳神経外科医、リハビリテーション医による総合的な診察、治療を行う事により早期の社会復帰をめざす取り組みをする。特に救急対応には神経内科との連携を密にしてストローク チームを作り万全の体制で一体化した治療を行う。
- 5) パーキンソン病の外科的治療について
パーキンソン病に対する深部電極埋め込み術を神経内科と協同して行い、術後の経過追跡にも参加する。
- 6) 難治性疼痛の外科的治療について
難治性疼痛について神経内科、整形外科と協同して脊髄硬膜外電気刺激術、大脳運動野刺激術や脳深部刺激術を行いたい。
- 7) てんかんの外科的治療について
てんかんの治療には神経内科、小児神経、精神科との連携が必要であるが、今後各科の協力を得て難治性てんかんに対する外科的治療を行いたい。
- 8) 機能的脊髄後根切断術について
小児神経科との協同で下肢痙性を軽減させる目的に機能的脊髄後根切断術を行いたい。

資料4 【神経内科】

神経内科の今後の展望

ブレイン・メディカル・センターの外来部門が整備されれば、神経内科としては毎日、3診察室が利用できる。その結果として以下のような診療が可能になると考える。

1. セカンドオピニオン外来の開設

神経難病など、初期の診断が困難である、あるいは、その診断の受容が難しい疾患がある。その結果、セカンドオピニオンが求められることが増えている。現在では、初診外来として対応しているが、診療、説明にかかる時間は、通常の初診にくらべて数倍かかる。そのための専用の時間枠が開設できると、より高い臨床サービスが提供できる。

2. 神経難病外来の開設

難病患者を診断から介護・福祉まで疾患の全経過に関わる医療が求められている。たとえば、午後の外来を週、数回難病の専門外来にするとよりニーズに見合った臨床サービスが提供できる。

3. パーキンソン病外来、

難病の中でもとりわけ多いパーキンソン病患者を対象とした外来を開設することで、深部刺激治療の適応患者をより多く見いだせる。

パーキンソン病患者の一部でみられる、高度の精神症状を示す患者への対応がより容易になり、電気刺激療法を協力して実施することが可能になる。

4. 神経免疫疾患センター

重症筋無力症、多発性硬化症、**Buillain-Barre** 症候群などの免疫神経疾患は現在、免疫修飾療法にて良好な治療効果をあげることが出来る。特にその急性期治療のさまざまなオプションに対応可能なインフラ、人材を整備し、良質の医療を提供できる施設となることが極めて重要である。

5. 心のケア

神経難病、遺伝性神経難病などの患者・家族に対して、精神科、心療内科と連携・協力して、より充実した心のケアを提供する。

根本的な治癒を望めない疾患の理解とその受容、長期的な介護の必要性の理解と受容、遺伝性疾患の理解と受容などを支援することができる。

6. てんかん治療

てんかんの診療には、小児科、神経内科、精神科の3領域の連携が必須である。

7. 脳卒中の診療

その救急対応には、神経内科と脳神経外科の連携が必須である。これは、神経内科の診療には整備されて当然の体制と言える。この体制が整備されなければ、神経疾患の診療施設として

8. 神経精神科と神経内科との共同研究について

近年、アルツハイマー病脳におけるA β 蛋白の沈着を、PETを用いて可視化できるようになってきた。今後、さまざまな蛋白の異常蓄積を可視化できるようになる可能性がある。一方、

病理学的に、 α シヌクレイン蛋白が脳に異常蓄積する疾患のうち、パーキンソン病では高率にうつ病を合併し、汎発性レビー小体病(DLBD)では幻覚が生じる。しかしこれらの病巣局在は明らかではない。また、トリプレットリピート病である筋緊張性ジストロフィーや球脊髄性筋萎縮症、ハンチントン病などでは、それぞれ特有の性格変化がみられる。そこで、神経内科と精神神経科が共同して、抑うつの診断や幻覚の基礎疾患除外、詳細な性格プロフィールの検討を行い、これらの症候と PET による異常蛋白蓄積部位との関連を検討して、精神症状や性格プロフィールの機能局在を明らかにする。

9. 脳神経外科と神経内科との共同研究

iPS 細胞をドパミン産生細胞や運動皮質 Betz 細胞、Purkinje 細胞などに分化誘導し、神経内科と脳神経外科の共同により、それぞれの適切な部位に定位脳手術の手法を用いて移植し、パーキンソン病や筋萎縮性側索硬化症、脊髄小脳変性症などの神経難病の治療を行う。

10. 心療内科、神経精神科、脳神経外科などとの共同研究

近年、functional brain imaging の手法が発達し、高磁場 MRI, fMRI, MRS, PET, SPECT, tensor MRI imaging などにより、脳の構造と機能をより詳細に検討できるようになった。これらにより、これまで脳内における局在が明らかでなかった psychosomatic および psychic symptom の局在が明らかにできる可能性が出てきている。BMS は organic lesion を対象とする脳神経外科・神経内科と、従来知見では局在が十分明らかではない functional disorder を対象とする精神科・心療内科が共同して診療・臨床研究にあたることことができる。この特長を生かし、4科が共同して脳機能をそれぞれの専門分野から解析すれば、total brain functional mapping を構築することができる、世界でも稀少な施設となりうる。

資料5 【心療内科】

心療内科の今後の展望

心療内科は以下のように考えています。よろしくお願ひします。

1) 各診療科の目指すところ

① これまで同様、心身医療の関西圏の中核診療施設として、重症の心身症患者、慢性疼痛症の診療と臨床研究、学生教育を行う。

② 今後の展開として、ブレインメディカルセンター主宰の合同カンファレンスの開催や、悪性疾患患者の全人医療カンファレンス、麻酔科・ペインクリニック、整形外科などとの重症疼痛患者の症例検討会などを通して滝井病院臨床各科との連携を強化し、相互の治療内容の充実に勤める。臨床他科専門医の短期のオプションなトレーニングも引き受ける。近年心療内科的トレーニングを希望する他科専門研修医に出会うことも度々あり、他の臨床科にとっても専門研修のオプションになりうる。

③ 予後不良の疾患や難治性疾患、また糖尿病などの生活習慣病の臨床現場では、医療サービスの質を高めるために、臨床心理士の介入が必要とされるようになっている。当科では、近年心理士の研修希望が増加しており、現在4名の非常勤心理士が研修中である。このようなマンパワーを生かして、精神科を中心としたブレインメディカルセンター内各科と協力して、将来的に臨床心理サービスを行うセンターとして機能することができる。

2) それを実現するための特色ある診療計画

何れもスペースとマンパワーが不足している。これが改善されるならば以下のような診療が可能になる。

① に関しての診療計画。

○ 当科の診療では科の特性上、診療時間当たりの患者数を増やすことはきわめて困難であり、また引き受けた患者は軽快するまで当科で治療する必要がある場合が大部分。したがって外来患者数は診察単位数で決定し、治療可能な新患者数も固定することになる。診察室に余裕があれば診察単位を現状のスタッフ数で数単位増やすことが可能であり、これにより月1,000人以上の診察患者数、1~2割り増しの新患者数を目指すことができる。

○ 心療内科の検査室が診察室と遠いため、医師の配置が重複し検査単位数が限られている。検査室が診察室に近くなれば、食道内圧(1,650点)、食道phモニタリング(650点)、腹部エコー(280-300点)、胆のう機能検査(280-300点)などの回数を増やすことが可能。

③ に関しての診療計画。

○ 集団療法室が単独で診察室近くに確保されれば、集団療法(自律訓練法、交流分析、いたみグループ療法、気功、ヨーガなど)を常時開催することができる。これらは保険診療のみでなく、保険外診療として自費での運営も可能。

○ 心理治療室が単独で確保できれば、自費でのカウンセリングが可能になる。

3) そこから予測される経済効果について

○ 診療患者数増加では、その比率に見合った収入増加、おそらく従来の1割から2割。自費でのカウンセリングや集団療法については、心理士の人件費以外はすべて病院収入になる。

○ 1)の②に関連して、心療内科も含めてブレインメディカルセンターがスペース的な改善から機能を強化することができれば、滝井病院の他の臨床各科と連携を強める基盤ができます。このことは滝井病院の他の診療科が特徴を強化することにつながり、ひいては滝井病院の機能強化につながると考えます。

附属滝井病院 ブレインメデイカルセンター (BMC) 設置準備委員会構成委員

《第1次答申案》

委員長 (BMC 準備室長)	栗本 匡久 (脳神経外科教授、滝井病院病院長顧問)
副委員長 (BMC 準備室副室長)	日下 博文 (神経内科部長、教授、滝井病院副病院長)
委 員	中井 吉英 (心療内科部長、教授、)
	山内 康雄 (脳神経外科部長、滝井病院教授)
	谷内 昇一郎 (小児科部長、滝井病院教授)
	齋藤 貴徳 (整形外科部長、滝井病院准教授)
	播磨 洋子 (放射線科部長、滝井病院教授)
	田口 仁士 (麻酔科部長、滝井病院教授)
	入澤 聡 (滝井病院精神科外来医長、講師)
	栗本 匡久 (脳神経外科教授、滝井病院病院長顧問)
	藤原 俊夫 (滝井病院 事務部長代理)
	川畑 ユミ子 (同 看護部副部長)
	宮内 清秀 (同 医事課課長)
	白川 大三 (同 管理課課長)
	山本 弘司 (同 管理課課長)
専門委員	伊藤 誠二 (医化学教授、副学長、BMRC センター長)
	正木 浩哉 (滝井病院臨床検査部部長、病院教授)
	宗像眞智子 (滝井病院臨床検査部管理技師長)

開催経過

第1回	平成 18 年 11 月 27 日	16 時—17 時 30 分
第2回	平成 18 年 12 月 22 日	16 時—17 時 30 分
第3回	平成 19 年 2 月 6 日	16 時—17 時 15 分
第4回	平成 19 年 4 月 23 日	16 時—17 時 30 分
第5回	平成 19 年 5 月 21 日	16 時—17 時 30 分
第6回	平成 19 年 8 月 28 日	17 時—18 時 30 分
第7回	平成 19 年 10 月 2 日	16 時—16 時 30 分

《第2次答申案》

委員長 (BMC 準備室長)	日下 博文 (神経内科部長、教授)
委 員	中井 吉英 (心療内科部長、教授、)
	山内 康雄 (脳神経外科部長、滝井病院教授)
	谷内 昇一郎 (小児科部長、滝井病院教授)
	齋藤 貴徳 (整形外科部長、滝井病院准教授)
	播磨 洋子 (放射線科部長、滝井病院教授)
	田口 仁士 (麻酔科部長、滝井病院教授)
	入澤 聡 (滝井病院精神科外来医長、講師)
	栗本 匡久 (脳神経外科教授、滝井病院病院長顧問)
	藤原 俊夫 (滝井病院 事務部長代理)
	川畑 ユミ子 (同 看護部副部長)
	宮内 清秀 (同 医事課課長)
	白川 大三 (同 管理課課長)
	山本 弘司 (同 管理課課長)

開催経過

第1回	平成 19 年 11 月 14 日	18 時—19 時 20 分
第2回	平成 19 年 12 月 6 日	18 時—18 時 50 分
第3回	平成 20 年 1 月 24 日	18 時—19 時 00 分
第4回	平成 20 年 2 月 21 日	18 時—19 時 00 分